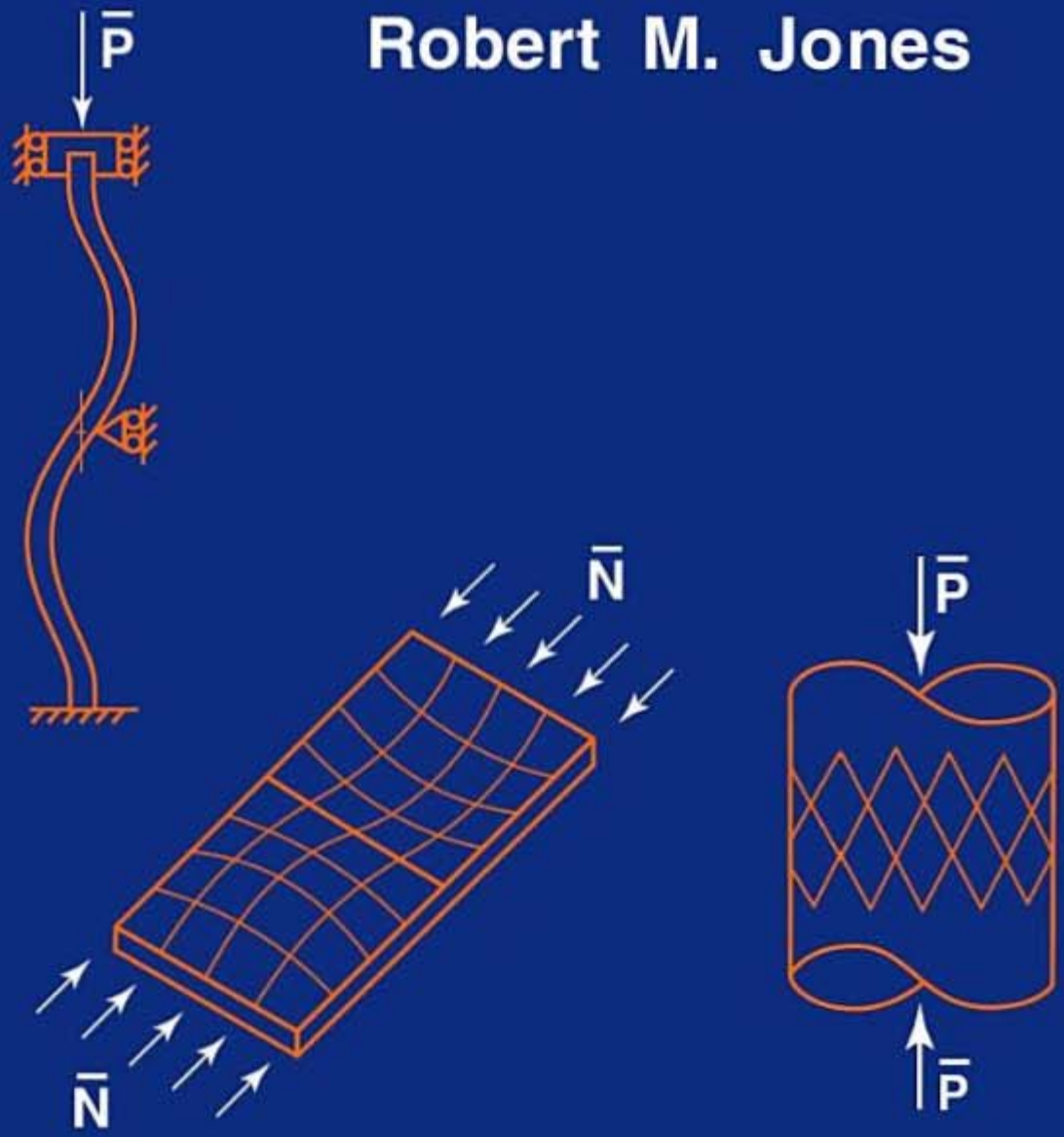
BUCKLING OF BARS, PLATES, AND SHELLS

Robert M. Jones



Éléments sous droits d'auteur

BUCKLING OF BARS, PLATES, AND SHELLS

ROBERT M. JONES

Éléments sous droits d'auteur

BUCKLING OF BARS, PLATES, AND SHELLS

ROBERT M. JONES

Professor Emeritus of Engineering Science and Mechanics
Virginia Polytechnic Institute and State University
Blacksburg, Virginia 24061-0219



Bull Ridge Publishing
Blacksburg, Virginia
United States of America

copyright © 2006 by Bull Ridge Publishing
all rights reserved

Éléments sous droits d'auteur

BUCKLING OF BARS, PLATES, AND SHELLS

Bull Ridge Publishing
Box 10698
Blacksburg, Virginia 24062-0698
United States of America
www.BullridgePublishing.com

Notice of Rights: copyright © 2006 by Bull Ridge Publishing. All rights reserved. Printed in the United States of America. Except as permitted under the United States Copyright Act of 1976, no part of this publication may be reproduced or distributed in any form or by any means, electronic or mechanical, including photocopying, microfilming, and recording, or stored in an information database or retrieval system, without the prior written permission of the publisher.

Notice of Liability: This book contains information from authentic and highly regarded sources. Reprinted material is used by permission where necessary, and sources are always cited. Reasonable efforts have been made to include reliable data and information. However, neither the publisher nor the author shall have any liability to any person or entity with respect to any loss or damage caused by or alleged to be caused directly or indirectly by the information contained in this book. This book is sold with the understanding that the publisher and the author are not engaged in rendering professional services. For professional advice, the services of a competent professional should be sought.

Production: This book was produced on the University of Connecticut computer in IBM Generalized Markup Language by Robert M. Jones and Karen S. Devens. The figures were designed by Robert M. Jones and executed in Adobe Illustrator by Beulah Prestrude and Ann Hardell. The cover was designed by Robert M. Jones and executed in Adobe Illustrator by Beulah Prestrude. The book was printed by Edwards Brothers, Ann Arbor, Michigan

1 2 3 4 5 6 7 8 9 0

The paper in this publication meets the requirements of the ANSI Standard Z39.48-1984 (Permanence of Paper).

Library of Congress Cataloging-in-Publication Data

Jones, Robert M. (Robert Millard Jones)
Buckling of Bars, Plates, and Shells / Robert M. Jones
848 p. cm.
Includes bibliographic references and index.
ISBN-13: 978-0-9787223-0-2 ISBN-10: 0-9787223-0-2 (hardcover : alk. paper)
1. Buckling. 2. Stability. 3. Bars. 4. Plates. 5. Shells. I. Title
Library of Congress Control Number 2006905767

ISBN-13: 978-0-9787223-0-2 ISBN-10: 0-9787223-0-2 (hardcover)

Éléments sous droits d'auteur

To the late Dr. James H. Starnes, Jr.,
Inspirational leader. mentor, and researcher
— the ultimate structural mechanics professional

Éléments sous droits d'auteur

Éléments sous droits d'auteur

CONTENTS

PREFACE xix

1 INTRODUCTION TO BUCKLING 1

1.1 FUNDAMENTAL DEFINITIONS OF MECHANICAL SYSTEMS BEHAVIOR 2

1.1.1 Stability 2
1.1.2 Instability 3
1.1.3 Buckling Load 5
1.1.4 Maximum Load 9
1.1.5 General Load-Deformation Behavior including Buckling 10

1.2 BOOK CONCENTRATION AND PHILOSOPHY 10

1.2.1 Introduction 10
1.2.2 Buckling of Bars 12
1.2.3 Buckling of Plates 14
1.2.4 Buckling of Shells 15
1.2.5 Summary 17

1.3 CLASSIFICATION OF TYPES OF BUCKLING AND POSTBUCKLING BEHAVIOR 18

1.3.1 Introduction 18
1.3.2 General Nature of Linear Eigenvalue Analysis 18
1.3.3 Types of Postbuckling Behavior 20
1.3.4 Initial Geometric Imperfections Effect on Postbuckling Behavior 22
1.3.5 Degree of Stability in Stable Postbuckling Behavior 24
1.3.6 Summary 25

1.4 IMPORTANCE OF EXPERIMENTAL RESULTS IN DEVELOPMENT OF THEORIES 26

1.4.1 Introduction 26
1.4.2 Comparison of Theoretical and Experimental Results 26
1.4.3 Experimental Results are Used More than 'Just' to Validate Theory 28
1.4.4 Experimental Results are the Very Basis of all Theoretical Models 30
1.4.5 Summary 32

1.5 SOME IMPORTANT DISTINCTIONS IN ENGINEERING ANALYSIS 33

1.5.1 Introduction 33
1.5.2 Presumption versus Assumption 33
1.5.3 Presumption versus Restriction 40
1.5.4 Misinterpretations and their Consequences 42
1.5.5 Summary 44

1.6 BOOK ROAD MAP 46

CHAPTER 1 REFERENCES 47

Éléments sous droits d'auteur

2 BUCKLING OF BARS 49

2.1 INTRODUCTION 49

2.2 EULER'S COLUMN EQUATION 50

2.2.1 Buckling of an Axially Compressed Pinned-Pinned Bar 50
2.2.2 Buckling of an Axially Compressed Fixed-Pinned Bar 56
2.2.3 Buckling of an Axially Compressed Fixed-Fixed Bar 57
2.2.4 Buckling of an Axially Compressed Fixed-Free Bar 58
2.2.5 Buckling of an Axially Compressed Pinned-Free Bar with Elastically Restrained Ends 59
2.2.6 Buckling of an Axially Compressed Pinned-Free Bar with an Elastic Translational Spring at the Free End 60
2.2.7 Buckling of an Axially Compressed Pinned-Pinned Bar with a Mid-Span Transverse Spring 62
2.2.8 Summary 66
Problem Set 2.2 66

2.3 AN ALTERNATIVE BAR BUCKLING DIFFERENTIAL EQUATION . 67

2.3.1 Derivation of an Alternative Differential Equation 67
2.3.2 Buckling of an Axially Compressed Pinned-Pinned Bar 69
2.3.3 Buckling of an Axially Compressed Fixed-Pinned Bar 70
2.3.4 Buckling of an Axially Compressed Fixed-Fixed Bar 71
2.3.5 Buckling of an Axially Compressed Fixed-Free Bar 72
2.3.6 Buckling of an Axially Compressed Fixed-Guided Bar 73
2.3.7 Buckling of an Axially Compressed Pinned-Guided Bar 75
2.3.8 The Effective Length Concept to Account for Boundary Conditions 76
2.3.9 Summary 76
Problem Set 2.3 78

2.4 LARGE DEFLECTIONS OF BUCKLED BARS — THE PROBLEM OF THE ELASTICA 79

2.4.1 Introduction 79
2.4.2 Exact Load-Deflection Behavior 80
2.4.3 Approximate Load-Deflection Behavior Just After Buckling 85
2.4.4 Other Large-Deflection Buckling Problems 90
2.4.5 Practical Significance of the Euler Buckling Load 91

2.5 BUCKLING OF BARS BY ENERGY PRINCIPLES 92

2.5.1 Basic Energy Principles 92
2.5.2 Application of Basic Energy Principles to Stability of a Spring-Supported Bar 95
2.5.3 Buckling Criteria 97
2.5.4 Derivation of Governing Differential Equation and Boundary Conditions for Bar Buckling by Energy Principles 100
2.5.5 Rigorous Derivation of the Differential Equation and Boundary Conditions for Bar Buckling by Energy Principles 106
2.5.5.1 Equilibrium Analysis 109
2.5.5.2 Buckling from a Straight Prebuckled Shape 111
2.5.5.3 Buckling from a Non-Straight Prebuckled Shape 115
Problem Set 2.5.5 117
2.5.6 Summary 118

Éléments sous droits d'auteur

2.6 APPROXIMATE BUCKLING LOADS BY ENERGY METHODS 119

2.6.1 Introduction 119
2.6.2 The Rayleigh Method 119
2.6.2.1 Strain Energy Integrals and Buckling Criteria 120
2.6.2.2 Boundary Conditions 123
2.6.2.3 Buckling of an Axially Compressed Pinned-Pinned Bar 127
2.6.2.4 Buckling of an Axially Compressed Fixed-Free Bar 130
2.6.2.5 Summary 134
Problem Set 2.6.2 135
2.6.3 The Rayleigh-Ritz Method 135
2.6.4 Buckling of a Bar under Its Own Weight 138
Problem Set 2.6.4 140
2.6.5 Buckling of Bars with Step Changes in Cross Section 140
Problem Set 2.6.5 142
2.6.6 Buckling of an Axially Compressed Pinned-Pinned Bar with a Mid-Span Transverse Spring 142
Problem Set 2.6.6 143
2.6.7 Summary 144

2.7 EFFECT OF TRANSVERSE SHEAR STIFFNESS 145

2.7.1 Introduction 145
2.7.2 Differential Equation Approach to Effect of Transverse Shear on Deflection of an End-Loaded Cantilever Beam 145
2.7.3 Energy Methods Approach to Effect of Transverse Shear on Deflection of an End-Loaded Cantilever Beam 149
2.7.4 Differential Equation Approach to Effect of Transverse Shear on Buckling of an Axially Compressed Fixed-Free Bar 152
2.7.5 Energy Methods Approach to Effect of Transverse Shear on Buckling of an Axially Compressed Pinned-Pinned Bar 154
2.7.6 Importance of Transverse Shear Stiffness on Buckling of Bars 155
Problem Set 2.7 155

2.8 EFFECT OF INITIAL GEOMETRIC IMPERFECTIONS 156

Problem Set 2.8 160

2.9 EFFECT OF RESTRAINED THERMAL EXPANSION 161

2.9.1 Introduction 161
2.9.2 Origins and Conditions of Thermal Stress and Thermal Strain 161
2.9.3 Fundamental Thermoelastic Relations 165
2.9.4 Bar Support Conditions 171
2.9.5 Thermal Buckling of an Axially Restrained Pinned-Pinned Bar subjected to a Uniform Temperature Change 174
2.9.6 Thermal Behavior of an Axially Restrained Bar subjected to a Linear Through-the-Thickness Temperature Change 178
2.9.7 Summary 184
Problem Set 2.9 186

2.10 PLASTIC BUCKLING OF BARS 187

2.10.1 Introduction 187
2.10.2 Reduced-Modulus Theory 189
2.10.3 Tangent-Modulus Theory 191
2.10.4 Transcendental Plastic Buckling Equation 191
2.10.5 Solution Strategy 193
2.10.6 Representation of the Nonlinear Stress-Strain Curve 196
2.10.7 Numerical Results 198

Éléments sous droits d'auteur

2.10.8 Comparison of Reduced-Modulus Theory with Tangent-Modulus Theory and Measured Buckling Loads 199
2.10.9 Summary 200
Problem Set 2.10 201

2.11 ASPECTS OF DESIGN OF BARS AGAINST BUCKLING 202

2.11.1 Introduction 202
2.11.2 Analysis versus Design 202
2.11.3 End and Lateral Support Conditions 207
2.11.4 Material Properties 211
2.11.4.1 Effect of Creep 211
2.11.4.2 Earthquakes 212
2.11.4.3 Environmental Effects for Fiber-Reinforced Composite Materials 213
2.11.5 Bar Cross-Sectional Shape 214
2.11.6 Design Codes and Their Development 215
2.11.7 Summary Remarks on Design 221

2.12 BUCKLING OF BARS SUMMARY 221

CHAPTER 2 REFERENCES 223

3 BUCKLING OF RECTANGULAR PLATES 227

3.1 INTRODUCTION 227

3.2 CONSISTENT DERVIVATION OF EQUILIBRIUM EQUATIONS, BUCKLING EQUATIONS, AND BOUNDARY CONDITIONS 230

3.2.1 Variation of a Double Integral with Three Dependent Variables 230
3.2.2 First Variation of a Double Integral 233
3.2.3 Equilibrium Differential Equations and Boundary Conditions for von Kármán Plate Theory 240
3.2.4 First Variation of the Second Variation of a Double Integral 249
3.2.5 Buckling Differential Equations and Energy Expressions for a Rectangular Plate with In-Plane Loads 255
3.2.6 Summary 262

3.3 CLASSICAL BUCKLING THEORY SOLUTIONS 264

3.3.1 Introduction 264
3.3.2 Buckling of Simply Supported Rectangular Plates under Uniform Compression N_x 264
3.3.2.1 The Buckling Differential Equation Approach 264
3.3.2.2 The Strain Energy Integral Approach 266
3.3.2.3 Results and Discussion 267
Problem Set 3.3.2 268
3.3.3 Buckling of Simply Supported Rectangular Plates under Uniform Biaxial Loading N_x and N_y 269
3.3.3.1 Basic Solution 269
3.3.3.2 Manner of Biaxial Load Introduction 270
3.3.3.3 General Nature of the Buckling Results 271
3.3.3.4 Results for Both N_x and N_y Compressive 273
3.3.3.5 Results for Tensile N_y and Compressive N_x 274
3.3.3.6 Behavior under Large Tensile Loads 274
3.3.3.7 Nonproportional Loading 275
3.3.3.8 Effect of Plate Aspect Ratio 277
3.3.3.9 Summary Remarks on Buckling under Biaxial Loading 279

Éléments sous droits d'auteur

Problem Set 3.3.3 279
3.3.4 Buckling of Simply Supported Rectangular Plates under Combined In-Plane Bending and Compression 279
Problem Set 3.3.4 285
3.3.5 Buckling of Simply Supported Rectangular Plates under In-Plane Shear N_{xy} 285
Problem Set 3.3.5 292
3.3.6 Buckling of Uniformly Compressed Rectangular Plates Simply Supported along Two Opposite Loaded Edges with Various Boundary Conditions along Two Unloaded Edges 292
3.3.6.1 One Edge Simply Supported and the Other Edge Free 294
3.3.6.2 One Edge Clamped and the Other Edge Free 297
Problem Set 3.3.6 298
3.3.7 Physical Restraints against Buckling 298
3.3.7.1 Examples for a Uniaxially Loaded Plate 299
3.3.7.2 Examples for a Biaxially Loaded Plate 300
3.3.7.3 Summary Remarks for Physical Restraint 300
Problem Set 3.3.7 300
3.3.8 Summary of Classical Buckling Results 301

3.4 POSTBUCKLING BEHAVIOR OF SIMPLY SUPPORTED RECTANGULAR PLATES UNDER UNIFORM COMPRESSION N_x 302

3.5 EFFECT OF INITIAL GEOMETRIC IMPERFECTIONS 308

3.5.1 Introduction 308
3.5.2 Analysis and Experimental Results 308
3.5.3 Consequences of Nonlinear Load-Deflection Behavior 315
3.5.4 Summary 319

3.6 EFFECT OF MULTIPLE FIBER-REINFORCED LAYERS 320

3.6.1 Introduction 320
3.6.2 Governing Equations for Buckling of Laminated Plates 322
3.6.2.1 Basic Restrictions, Assumptions, and Consequences 322
3.6.2.2 Equilibrium Equations for Laminated Plates 325
3.6.2.3 Buckling Equations for Laminated Plates 329
3.6.2.4 Solution Techniques 332
3.6.3 Buckling of Simply Supported Laminated Plates under In-Plane Loading 333
3.6.3.1 Specially Orthotropic Laminated Plates 335
3.6.3.2 Symmetric Angle-Ply Laminated Plates 337
3.6.3.3 Antisymmetric Cross-Ply Laminated Plates 339
3.6.3.4 Antisymmetric Angle-Ply Laminated Plates 342
3.6.4 General Remarks on Effects of Stiffnesses 346
3.6.5 Tow-Placed, Variable-Stiffness Plates 349
3.6.6 Summary 350
Problem Set 3.6 351

3.7 EFFECT OF RESTRAINED THERMAL EXPANSION 352

3.7.1 Introduction 352
3.7.2 Fundamental Thermoelastic Relations 355
3.7.3 In-Plane Loading and Restraint Conditions 365
3.7.3.1 What In-Plane Boundary Conditions can Result in Thermal and/or Mechanical Buckling? 365
3.7.3.1.1 Load versus Displacement in the Laboratory 366
3.7.3.1.2 Loading and Restraint Conditions in Engineering Practice 367

Éléments sous droits d'auteur

3.7.3.1.3 Elastic In-Plane Edge Restraint 368
3.7.3.1.4 Thermal Buckling without In-Plane Edge Restraint 369
3.7.3.2 In-Plane Displacement Notation 370
3.7.3.3 In-Plane Boundary Condition Notation 370
3.7.3.4 Compatibility of Boundary Conditions at Corners and on Adjacent Edges 372
3.7.3.5 Boundary Support and Thermal Loading Conditions Leading to Non-Classical Problems 376
3.7.3.6 Summary 376
3.7.4 Equivalent Mechanical Load Concept 377
3.7.5 Buckling under a Uniform Temperature Change of a Uniaxially In-Plane Restrained Simply Supported Plate 379
3.7.6 Buckling under a Uniform Temperature Change of a Biaxially In-Plane Restrained Simply Supported Plate 384
3.7.7 Buckling of a Partially In-Plane Restrained Plate under Uniform Temperature Change and Mechanical Load 387
3.7.7.1 Introduction 387
3.7.7.2 Manner of Load Introduction 387
3.7.7.3 Buckling Differential Equation and Solution 389
3.7.7.4 Results and Discussion 391
3.7.7.4.1 Behavior for Heating and Tensile N_x 392
3.7.7.4.2 Behavior for Heating and Compressive N_x 392
3.7.7.4.3 Behavior for Cooling and Compressive N_x 393
3.7.7.4.4 Nonproportional Loading 394
3.7.7.4.5 Effect of Poisson's Ratio 394
3.7.7.4.6 Effect of the Plate Aspect Ratio 395
3.7.7.4.7 Material-Property-Related Limitations 395
3.7.7.5 Summary of Thermal and Mechanical Buckling 395
3.7.8 Summary and Observations on Plate Thermal Buckling 396
3.7.9 Other Topics in Thermal Buckling of Plates 400
3.7.9.1 Various Edge Support Conditions 400
3.7.9.2 Nonuniform Heating 401
3.7.9.3 Time-Dependent Temperature Distributions 403
3.7.9.4 Limitations of the Linear Elastic Material Model 404
3.7.9.5 Temperature-Dependent Material Properties 404
3.7.9.6 Nonlinear Stress-Strain Behavior 405
3.7.9.7 Analogy between Temperature and Moisture Effects 406
3.7.9.8 Concluding Remarks 407
Problem Set 3.7 407

3.8 EFFECT OF PLASTIC DEFORMATION 408

3.8.1 Introduction 408
3.8.2 Derivation of Buckling Criterion 409
3.8.2.1 Fundamental Relations in J_2 Deformation Theory 409
3.8.2.2 Variations of Strains during Buckling 411
3.8.2.3 Variations of Stresses during Buckling 411
3.8.2.4 Variations of Forces and Moments during Buckling 413
3.8.2.5 Buckling Criterion 414
3.8.3 Solution Strategy 415
3.8.4 Numerical Results 417
3.8.5 Comparison of Theoretical and Experimental Results 419
3.8.6 Summary 421
Problem Set 3.8 421

Éléments sous droits d'auteur

3.9 ASPECTS OF DESIGN OF PLATES AGAINST BUCKLING 422
3.9.1 Introduction 422
3.9.2 Steps in the Structural Design Process 422
3.9.3 Design of an Isotropic Metal Plate 425
3.9.3.1 Design of an Isotropic Metal Plate Against Failure Caused by High Stresses 425
3.9.3.2 Design of an Isotropic Metal Plate Against Failure by Buckling 426
3.9.3.3 Design of a Stiffened Isotropic Metal Plate Against Failure by Buckling 429
3.9.4 Design of a Laminated Composite Plate 431
3.9.4.1 Design of a Laminated Composite Plate Against Failure Caused by High Stresses 431
3.9.4.2 Design of a Laminated Composite Plate Against Failure by Buckling 440
3.9.4.3 Design of a Stiffened Laminated Composite Plate Against Failure by Buckling 442
3.9.4.4 Genetic Algorithm Approach to Laminate Design 442
3.9.4.5 Summary of Design of a Laminated Composite Plate 447
3.9.5 Summary of Design of Plates Against Buckling 447
3.10 BUCKLING OF PLATES SUMMARY 448
3.10.1 General Problems 448
3.10.2 Review of Experimental Work 449
3.10.2.1 Consequences of Stable Postbuckling Behavior 449
3.10.2.2 Boundary Conditions in Experiments 450
3.10.3 Extensions of Present Coverage 451
3.10.3.1 Buckling of Plates of Nonlinear Composite Materials 451
3.10.3.2 Thermal Buckling of Cross-Ply Composite Plates 453
CHAPTER 3 REFERENCES 457

4 BUCKLING OF CIRCULAR CYLINDRICAL SHELLS 463
4.1 INTRODUCTION 463
4.2 DERIVATION OF EQUILIBRIUM AND BUCKLING EQUATIONS PLUS ASSOCIATED BOUNDARY CONDITIONS 467
4.2.1 Equilibrium Differential Equations for Moderately Large Deflections 467
4.2.2 Buckling Differential Equations and Energy Expressions for Combinations of Lateral Pressure, Axial Compression, and In-Surface Shear 478
Problem Set 4.2 489
4.3 CLASSICAL BUCKLING THEORY SOLUTIONS 490
4.3.1 Introduction 490
4.3.2 Batdorf's Classical Results 491
4.3.2.1 Axial Compression 491
4.3.2.2 Lateral Pressure 498
4.3.2.3 Hydrostatic Pressure 501
4.3.2.4 Comparison of Results for Axial Compression, Lateral Pressure, and Hydrostatic Pressure 502
4.3.2.5 Torsion 504
4.3.3 Use of Batdorf's Modified Donnell Equation for Axially Compressed Circular Cylindrical Shells

Éléments sous droits d'auteur

with Clamped Edge Buckling Boundary Condition C3 508
4.3.4 Use of All Three Buckling Differential Equations for Axially Compressed Circular Cylindrical Shells with Clamped Edge Buckling Boundary Condition C1 512
4.3.5 Summary for Classical Buckling Results 517
Problem Set 4.3 518

4.4 POSTBUCKLING BEHAVIOR 519

Problem Set 4.4 528

4.5 EFFECT OF PREBUCKLING DEFORMATIONS ON BUCKLING UNDER AXIAL COMPRESSION 529

Problem Set 4.5 533

4.6 EFFECT OF INITIAL GEOMETRIC IMPERFECTIONS 535

4.7 EFFECT OF ECCENTRIC STIFFENERS 540

4.7.1 Introduction 540
4.7.2 Derivation of Buckling Criterion 542
4.7.2.1 Variations of Stresses and Strains during Buckling 543
4.7.2.2 Variations of Forces and Moments during Buckling 544
4.7.2.3 Buckling Differential Equations 545
4.7.2.4 Buckling Criterion 545
4.7.3 Numerical and Experimental Results 547
4.7.4 The Stiffener Eccentricity Effect 550
4.7.5 Summary 554
Problem Set 4.7 554

4.8 EFFECT OF MULTIPLE FIBER-REINFORCED LAYERS 555

4.8.1 Introduction 555
4.8.2 Derivation of Buckling Criterion 557
4.8.2.1 Orthotropic Stress-Strain Relations 557
4.8.2.2 Variations of Stresses and Strains during Buckling 558
4.8.2.3 Variations of Forces and Moments during Buckling 559
4.8.2.4 Buckling Differential Equations 560
4.8.2.5 Buckling Criterion 561
4.8.3 Numerical Example 562
4.8.4 General k-Z Results for Antisymmetric Cross-Ply Laminates 564
4.8.4.1 Axial Compression 564
4.8.4.2 Lateral Pressure 567
4.8.4.3 Summary for Antisymmetric Cross-Ply Laminates 569
4.8.5 Results for Unsymmetric Cross-Ply Laminates 570
4.8.5.1 Axial Compression 570
4.8.5.2 Lateral Pressure 573
4.8.5.3 Summary for Unsymmetrically Laminated Shells 574
4.8.6 Summary for Laminated Shells 575
Problem Set 4.8 576

4.9 EFFECT OF RESTRAINED THERMAL EXPANSION 577

4.9.1 Introduction 577
4.9.2 Fundamental Thermoelastic Relations 581
4.9.3 In-Surface Loading and Restraint Conditions 591
4.9.3.1 What In-Surface Boundary Conditions can Result in Thermal and/or Mechanical Buckling of a Shell? 591
4.9.3.2 Load Versus Displacement Application in the Laboratory 592
4.9.3.3 Loading and Restraint Conditions

Éléments sous droits d'auteur

in Engineering Practice 593
4.9.3.4 Elastic In-Surface Edge Restraint 594
4.9.3.5 Thermal Buckling Without In-Surface Edge Restraint 595
4.9.4 Equivalent Mechanical Load Concept 596
4.9.5 Buckling of an Axially Restrained Circular Cylindrical Shell under a Uniform Temperature Change 598
4.9.5.1 Prebuckling Equilibrium Solution 599
4.9.5.2 Buckling Solution 601
4.9.5.3 Thermal Buckling Results 603
4.9.5.4 Correlation with Measured Buckling Temperature Change 605
4.9.6 Buckling of an Axially Restrained Circular Cylindrical Shell under a Uniform Temperature Change and Lateral Pressure 607
4.9.6.1 Prebuckling Equilibrium Solution 607
4.9.6.2 Buckling Solution 609
4.9.6.3 Thermal Buckling Results 613
4.9.7 Summary and Other Topics in Thermal Buckling of Shells 616
Problem Set 4.9 618

4.10 EFFECT OF PLASTIC DEFORMATION 619

4.10.1 Introduction 619
4.10.2 Derivation of Buckling Criterion for Single-Layered Shells 620
4.10.2.1 Fundamental Relations in J_2 Deformation Theory 620
4.10.2.2 Variations of Strains during Buckling 622
4.10.2.3 Variations of Stresses during Buckling 622
4.10.2.4 Variations of Forces and Moments during Buckling 624
4.10.2.5 Buckling Criterion 624
4.10.3 Solution of Buckling Criterion for Single-Layered Shells 626
4.10.4 Numerical Results for Single-Layered Shells 628
4.10.4.1 Single-Layered Circular Cylindrical Shell under Hydrostatic Pressure 628
4.10.4.2 Stiffened Large-Diameter Booster-Interstage Shell under Biaxial Loading 630
4.10.5 Derivation of Buckling Criterion for Multilayered Shells 633
4.10.5.1 Introduction 633
4.10.5.2 Fundamental Relations in J_2 Deformation Theory 634
4.10.5.3 Variations of Strains during Buckling 635
4.10.5.4 Variations of Stresses during Buckling 636
4.10.5.5 Variations of Forces and Moments during Buckling 638
4.10.5.6 Buckling Criterion 639
4.10.6 Solution of Buckling Criterion for Multilayered Shells 641
4.10.6.1 Introduction 641
4.10.6.2 Determination of the Yield Load 642
4.10.6.3 Determination of Layer and Stiffener Stresses, Strains, and Material Properties at an Estimated Buckling Load 644
4.10.6.4 Calculation of Absolute Minimum Buckling Load at an Estimated Buckling Load 648
4.10.6.5 Comparison of Estimated Buckling Load and Absolute Minimum Calculated Buckling Load 648
4.10.7 Numerical Results for Multilayered Shells 649
4.10.8 Summary 652
Problem Set 4.10 653

Éléments sous droits d'auteur

4.11 ASPECTS OF DESIGN OF SHELLS AGAINST BUCKLING 654
4.11.1 Introduction 654
4.11.2 The Importance of Experiments in the Development of Shell Buckling Analysis and Design 656
4.11.3 Knockdown Approach to Buckling-Critical Shell Design 657
4.11.4 Review of the NASA Shell Design Monographs 660
4.11.4.1 Enhanced Shell Analysis Capabilities 660
4.11.4.2 Sophisticated Experimental Measurements 661
4.11.4.3 Integration of Sophisticated Analyis and Sophisticated Experiments in the Design Process 662
4.11.4.4 Summary and What's to Come 662
4.11.5 High-Fidelity Analysis and Design of Buckling-Critical Shells 663
4.11.5.1 High-Fidelity Measurements and Experimental Procedures 663
4.11.5.2 Development of High-Fidelity Analyses 666
4.11.5.3 High-Fidelity Design Procedure 674
4.11.6 Design of Buckling-Critical Stiffened Isotropic Metal Shells 683
4.11.7 Design of Buckling-Critical Laminated Composite Shells 684
4.11.8 Summary Remarks on Shell Design Against Buckling 684
4.12 BUCKLING OF SHELLS SUMMARY 685
CHAPTER 4 REFERENCES 690

5 SUMMARY AND OTHER TOPICS 699
5.1 INTRODUCTION 699
5.2 DESIGN-RELATED PERSPECTIVE ON CONTRAST BETWEEN BAR, PLATE, AND SHELL BUCKLING BEHAVIOR 700
5.2.1 General Response 700
5.2.2 Design Considerations and Factor of Safety 702
5.2.3 Comparison with Experimental Results 704
5.3 OTHER CLASSICAL BUCKLING TOPICS 705
5.3.1 History of Buckling 705
5.3.2 Comments on Theoretical Derivations in this Book 705
5.3.3 Other Structural Elements and Structures 705
5.3.4 Solution Procedures for Buckling Problems 706
5.3.5 Other Structural Configurations 706
5.3.5.1 Sandwich Construction 705
5.3.5.2 Laminated Fiber-Reinforced Composite Structures 708
5.4 ADVANCED BUCKLING TOPICS 710
5.4.1 Introduction 710
5.4.2 Ziegler's Classification of Stability Problems 710
5.4.3 Nonconservative Systems 713
5.4.4 Stochastic Excitation 714
5.4.5 Dynamic Buckling 714
5.4.6 Chaos 714
5.5 ON THE TRANSITION TO COMPUTATIONAL APPROACHES 715
5.5.1 How to Learn Complex Buckling Behavior 715
5.5.2 Simple Analytical Approaches versus Numerical Approaches 717
5.5.3 Computational Tools Available 718
5.5.4 Replacement of Measured Behavior by Computer Simulation 720
5.5.5 Designing Structures 721

Éléments sous droits d'auteur

5.6 THE INCORRECT BENCHMARK PANEL BUCKLING SOLUTION AND COMPUTER PROBLEM-SOLVING LESSONS LEARNED 723
5.6.1 Introduction 723
5.6.2 General Characteristics of the Panel Buckling Problem 724
5.6.3 Characteristics of the Incorrect Benchmark Solution 725
5.6.4 Characteristics of the Correct Panel Buckling Solution 728
5.6.5 Common Difficulties in Engineering Problem Solving 733
5.6.6 Summary 734
5.7 SUMMARY REMARKS 735
CHAPTER 5 REFERENCES 735

APPENDIX A: MAXIMA AND MINIMA OF FUNCTIONS OF A SINGLE VARIABLE 738
APPENDIX A REFERENCE 742

APPENDIX B: ABSOLUTE MINIMUM OF A FUNCTION OF TWO VARIABLES 743
APPENDIX B REFERENCES 748

APPENDIX C: BEHAVIOR OF FIBER-REINFORCED LAMINATED COMPOSITE MATERIALS AND STRUCTURAL ELEMENTS 749
C.1 INTRODUCTION 749
C.2 FIBER-REINFORCED LAMINATED COMPOSITE MATERIALS 750
C.2.1 Introduction 750
C.2.2 Laminae 751
C.2.3 Laminates 752
C.2.4 Advantages 752
C.3 STRESS-STRAIN RELATIONS FOR ANISOTROPIC AND ORTHOTROPIC MATERIALS 756
C.4 STRESS-STRAIN RELATIONS FOR PLANE STRESS IN AN ORTHOTROPIC MATERIAL 761
C.5 STRESS-STRAIN RELATIONS FOR A LAMINA OF ARBITRARY ORIENTATION 763
C.6 CLASSICAL LAMINATION THEORY 767
C.6.1 Lamina Stress-Strain Behavior 768
C.6.2 Stress and Strain Variation in a Laminate 768
C.6.3 Resultant Laminate Forces and Moments 772
C.6.4 Summary 776
C.7 SPECIAL CASES OF LAMINATE STIFFNESSES 779
C.7.1 Single-Layered Configurations 780
C.7.2 Symmetric Laminates 782
C.7.3 Antisymmetric Laminates 789
C.7.4 Unsymmetric Laminates 793
C.7.5 Stacking-Sequence Notation 794
C.7.6 Balanced Laminates 795

Éléments sous droits d'auteur

C.7.7 Hybrid Laminates 795
C.8 SUMMARY REMARKS 795
APPENDIX C REFERENCES 796

APPENDIX D: ELEMENTS OF DESIGN PHILOSOPHY 797
D.1 INTRODUCTION 797
D.2 WHAT IS ENGINEERING DESIGN? 798
D.3 PHILOSOPHIES OVER THE AGES OF HOW TO ENSURE SAFE DESIGNS 801
D.4 THE ROLE OF PAST FAILURES IN UNDERSTANDING AND IMPROVING DESIGN PRACTICE 802
D.4.1 de Havilland Comet Fatigue Failures 803
D.4.2 Hyatt Regency Hotel Skywalk Failure 804
D.5 FAILURE MODES IN DESIGN 808
D.6 SUMMARY REMARKS 811
APPENDIX D REFERENCES 812

INDEX 813

Éléments sous droits d'auteur

PREFACE

Instability or buckling at a certain load as a potential failure mode of structural elements has received attention in the past several decades far beyond that accorded it previously. Although Leonhard Euler studied bar buckling in the mid-1700s, his work was not taken seriously until the 1800s. Before 1930, the primary buckling problems were associated with columns in buildings and plates in ship hulls. The advent of the stressed-skin airplane in the 1930s provided sharp impetus to the development of shell buckling analyses. More recently, ballistic missiles, reentry vehicles, and numerous space exploration vehicles have motivated even more complex bar, plate, and shell buckling analyses. A course on buckling has become virtually standard in graduate curriciula for aerospace engineering, mechanical engineering, civil engineering, and other studies of structural mechanics by whatever name. Timoshenko and Gere's *Theory of Elastic Stability* is accorded the distinction of being the primary reference book in the field. However, as is often the case, what amounts to a reference encyclopedia is at somewhat of a disadvantage in the classroom. Moreover, many important contemporary buckling topics are not treated because of the date (1961) of Timoshenko and Gere's second edition. This book was written in response to those needs.

The purpose of this book is to introduce graduate students and practicing engineers to the basic concepts of stability of structural elements and when they buckle. Bars, plates, and circular cylindrical shells are used as relatively simple examples to illustrate the fundamental concepts. Bars will be shown to carry, or sustain, just about the buckling load once buckling has occurred. Plates are seen to carry much more than the buckling load. Finally, some very common shells under some loading conditions carry much less than the buckling load after buckling occurs. Such comparison of the load-deformation behavior, including the postbuckling behavior, of these common structural elements yields a rationale for determining the practical usefulness of a calculated buckling load. Indeed, such comparisions reveal why buckling of structural elements can be the primary concern in many structural applications.

A minimum prerequisite for addressing the material in this book is an advanced mechanics of materials course in which elasticity, plates, and shells are introduced. More extensive coverage of these three topics in separate courses is desirable, but not essential. In addition, exposure to energy methods in applied mechanics would be helpful, but the motivated student can fill in the gaps in the author's presentation of energy concepts by self study. Of course, the more background that a reader has in these subjects, the more mature will be the structural mechanics base and the more overall perspective will be relied upon *and gained.*

Éléments sous droits d'auteur

The primary approach to the solution of buckling problems in this book involves the calculus of variations. *Leonhard Euler invented and developed the calculus of variations in the 1700s to study bar deflection and buckling problems!* Thus, use of the calculus of variations in this book seems to be a natural, historic manner in which to approach the buckling problem even now. For those readers who do not wish to pursue the derivation of the governing differential equations and associated boundary conditions by use of the calculus of variations, it is possible to study only the individual buckling problems in each applications section. Thus, this book is useful both to those who want to know where the equations and results come from (and how to derive them) and to those who want to know only how to use the equations and results.

The Introduction, Chapter One, includes a comprehensive definition of buckling of structural elements and a brief survey of historical developments in buckling analysis. Buckling of bars is addressed in Chapter Two. Numerous boundary conditions of the classical Euler buckling problem are treated, but many cases are left to be referred to in Timoshenko and Gere's fine book. Large deflections of axially loaded bars are investigated in order to appreciate the practical significance of the Euler buckling load. Other topics such as energy approaches, effect of shear, initial imperfections, restrained thermal expansion, plastic deformation, and design of bars against buckling complete Chapter Two. In Chapter Three, buckling of plates is introduced by the approach of first deriving the equilibrium differential equation and then the buckling differential equations by a consistent energy-based approach. In this manner, much of the mystery in the derivation of buckling equations is avoided. Classical solutions, large-deflection behavior, restrained thermal expansion, plastic deformation, and design of plates against buckling complete Chapter Three. In Chapter Four, Buckling of Circular Cylindrical Shells, in analogy to Chapter Three, consistent equilibrium and buckling differential equations are derived in addition to the associated boundary conditions and governing energy integrals. The equations are specialized for classical buckling theory and several solutions are presented. The postbuckling behavior is then investigated, followed by the effects of prebuckling deformations and initial imperfections. The contemporary topics of effect of eccentric stiffeners, laminated fiber-reinforced composite materials, restrained thermal expansion, and plastic deformation are then covered, followed by design of shells against buckling. Finally, all topics are brought into perspective through the mechanism of comparing the load-deformation behavior of the three structural elements in the Summary and Other Topics, Chapter Five. Advanced topics of structural stability are briefly described to whet the reader's interest in advancing beyond this book. Suggestions are made for how to progress from the theoretical aspects and approaches in this book to the necessarily more numerically oriented approaches to more general practical problems using computers, e.g., the finite element method.

Not all of what you will see in Chapter One will immediately 'sink in'. You will find, as you experience specific buckling and postbuckling ana-

Éléments sous droits d'auteur

lyses in each chapter, that going back and rereading Chapter One will develop and enhance your perspective of the various elements in buckling. When you reach Chapter Five, many concepts will have 'come together' so that you are ready to begin to appreciate the attractiveness of some new concepts as an extension of this book. You should then be ready to go beyond the topics in this book.

Continually emphasized throughout the book is the comparison of theoretical results with experimental measurements. Neither theory nor experiment is any real good without the other. Or, as my good friend, the late Dr. James H. Starnes, Jr., put it: "If you can't predict the behavior, then you don't understand it." He firmly believed in a combined theoretical and experimental approach to all structural mechanics problems.

Student exercises are given throughout the book. I expect graduate students to answer the 'unasked' questions in each exercise. Namely, what is the significance of the result(s) obtained, and how can they use these results in a practical manner? Moreover, they are expected to describe what they learned; perhaps plot the results to learn more even if not specifically requested in the problem statement; and add their observations and conclusions. That is, the stated exercises are but the heart or basic question to be addressed in the foregoing more comprehensive manner that leads to an in-depth understanding of the concepts.

In Timoshenko and Gere's book, the reader will find a rich assortment of classical bar, beam-column, and frame solutions for many loadings and structural configurations. Their book serves as a valuable reference for those who deal with special problems of those structural configurations. Their treatment of plates and shells is not as generous as that on bars, beam columns, and frames. Here, we concentrate on bar buckling and its fundamental statements of buckling criteria in order to 'leave room' for the more contemporary topics of plate and shell buckling including fiber-reinforced laminated plates and shells, thermal buckling, initial geometric imperfections, effect of boundary conditions, plastic buckling, etc. Problems such as torsional buckling of beams, frame stability, and similar problems are not treated in this book. Also, problems that require special numerical techniques such as finite difference and finite element methods or inherently complicated equations such as those for conical shells or for more general shells are avoided. Both classes of neglect are consistent with the basic premise of this book that the *fundamental concepts of buckling* are the main subject. Other problems and special numerical techniques can more appropriately be investigated after the basic concepts are well in hand. The author firmly believes that the basic philosophy of contrasting bars, plates, and shells better serves the purpose of illustrating basic concepts than does concentration on one class of problems such as one-dimensional buckling of bars and frames. A broad basis of understanding is built up by contrasting the behavior of bars, plates, and shells. What is left to study amounts to special cases and other problems that involve essentially nonconceptual details. The present book is limited to what Ziegler terms

Éléments sous droits d'auteur

nongyroscopic conservative systems, the most important class of problems from a practical standpoint.

The objective of the design sections at the end of each of the bars, plates, and shells chapters is to present some of the fundamentals of what is encountered in design. Design details usually found in design codes are left to those codes because they differ substantially from applications area to applications area, e.g., building construction as contrasted with aircraft design or nuclear power plant design. We can touch on the nature of design without being overwhelmed by the details. However, the old saying "The devil is in the details" applies most definitely to structural design! Many structural failures have occurred over the years because of lack of attention to crucial details.

The material in this book is designed to be presented in a one-semester course *only if selected applications topics are omitted*. That is, many more topics are included than can be addressed in a one-semester course. Thus, the instructor must 'pick and choose' those topics that are of primary interest to each class. For those schools on a quarter system, concentration on Chapters 2 and 3 (bars and plates) is recommended with Chapter 4 (shells) being covered in the first part of a follow-on course on advanced concepts of structural stability. There, a book such as Ziegler's *Principles of Structural Stability* or Bolotin's *Nonconservative Problems of the Theory of Elastic Stability* might be used in addition to the present book. Because more than a semester's worth of topics is provided in this book, some of the applied topics sections can be studied independently of each other. That is, the reader can chose which of the topics such as restrained thermal expansion, eccentric stiffening, or plastic buckling to address without reading the others because each applied topics section is complete enough to stand on its own. However, cross referencing between sections and chapters is provided. That cross referencing is generally to specific pages in order to speed the reader's access to information.

The major educational objective of this book is to make readers aware of all the fundamental principles necessary to solve relatively simple buckling problems in a complete manner with full understanding of all the concepts treated. More complex buckling problems are beyond the scope of this book, yet the reader must be well prepared to address them. Such contemporary techniques as finite elements as well as finite differences cannot be sensibly applied without full understanding of the fundamental buckling problem. Thus, we concentrate on the fundamentals and leave the details of more complex problems for later study.

Contemporary buckling problems are most commonly treated with numerical approaches such as finite element analysis or finite difference analysis. However, before effective use of current computer programs is possible, the fundamental nature of buckling analysis must be thoroughly understood. Without such understanding, computer programs will, in fact, be misused and are even dangerous to use (*for the end structure or machine user, not the analyst!*). Computer programs will be developed in this book in order to implement parts of various simple

Éléments sous droits d'auteur

solutions. However, such common engineering analysis computer programs as NASTRAN or PATRAN will emphatically *not* be addressed in this book. Rather, the fundamental educational issues of buckling theory and analysis will be addressed, and the training necessary to use such engineering analysis computer programs will be reserved for later. However, computer programs must be used with a firm understanding of what is happening. Too many people tend to do what my friend Jack Martinelli described in May 1984 as GIGO (which most people interpret as "Garbage in, Garbage out"), but his meaning or interpretation is "Garbage In, Gospel Out" — many tend to bless what comes out of the computer without attempting to test the output for plausibility or reasonableness. Another good friend, Dr. James G. Crose, said in May 1987 "If you don't know the answer to within 20% *without* the computer, then you're in never-never land *with* the computer." The bottom line is that we must have a firm grasp on the principles underlying every computer program and understand what the nature of the results must be in order to be able to intelligently use computer programs. Otherwise, we're kidding ourselves or we're even under delusions of control of the solution when we're actually out of control.

At various places in the book, I am pleased to provide occasional historical notes of some interest (at least to me and hopefully to you, too). Major or important authors (certainly a matter of opinion) are noted by their life dates (if known) where an author is first mentioned along with historical notes as seen noteworthy. The history of buckling and its interlocking with other developments in mechanics is quite engaging to me, and I hope to you, too. I therefore commend (not command, but your advisor might) all structural mechanicists to read Timoshenko's *History of Strength of Materials*, (McGraw-Hill, 1953, and Dover, 1983).

Tracking down the many references for this book was a major chore spread over the years during which I was developing this book. Library search engines and interlibrary loan at Virginia Tech were generally most helpful. I am also indebted to my good friend Valery V. Vasiliev of Moscow Aviation Technology University for many useful conversations and for giving me a copy of Ogibalov and Gribanov's *Thermal Stability of Plates and Shells*. That book (in Russian) is most interesting in its own right, but also led me to references of which I was not aware. Many of the NACA and NASA reports and other publications are available from NASA web sites (1) naca.larc.nasa.gov and (2) larc.nasa.gov.

Throughout this book, the masculine gender is deemed to include the feminine gender, so artificial 'person' constructions are not used. Reference numbers are given in square brackets for each citation. Author's names are cited exactly as written in the original work, not arbitrarily truncated to initials for so-called 'consistency' (which would actually be a violation of the quote of the author's name as published). Full journal titles are cited for reader's ease in obtaining the desired references hopefully without the difficulties that I had.

I am indebted to numerous classes at The Aerospace Corporation, Southern Methodist University, and Virginia Tech for struggling through

Éléments sous droits d'auteur

the inconsistencies and incompleteness of the various versions of this book. I also want to acknowledge numerous fruitful technical discussions with Sam Batdorf, Manny Stein, Bo Almroth and many others over the past forty years. In particular, Earl Thornton, Emeritus Professor of Aerospace Engineering at the University of Virginia and an old classmate of mine in 1960–61 at the University of Illinois (even if he doesn't remember me!), kindly reviewed the thermal buckling work on bars, plates, and shells as well as Chapters One and Two, and we engaged in many interesting conversations in the Fall of 1999 and the Spring and Summer of 2000. In addition, Dr. Michael P. Nemeth of NASA Langley Research Center was most helpful with references, solutions, and results from his work in thermal buckling during the Spring, Summer, and Fall of 2001, and he continues to provide references. He also provided exceptionally thoughtful, useful, extensive, and thorough comments on the first three chapters which led to significant improvements in the content and explanations. I am also indebted to Dr. Brian Wardle of the Massachusetts Institute of Technology for a prolonged series of email discussions on the incorrect benchmark panel buckling solution in Section 5.6. That section was written by heavy use of email alone, an example of the communications skills needed by engineers to solve contemporary problems. Other briefer conversations with Professors Charles Bert of the University of Oklahoma, Arthur Leissa of Ohio State University, and Theodore Tauchert of the University of Kentucky were most helpful. Their confidence and assistance are deeply appreciated.

Finally, I must express my sincere appreciation to the Computer Center of the University of Connecticut for being able to use their Document Composition Facility (DCF) to prepare much of the manuscript of this book. I began to use the UCONN capability in 2000 after VA Tech abandoned its state-of-the-art DCF capability in 1999.

Robert M. Jones
Blacksburg, Virginia
Summer 2006

Éléments sous droits d'auteur

Chapter 1

INTRODUCTION TO BUCKLING

We define the terms stability, instability, and buckling of structures under slowly applied loads (essentially static loading, not dynamic loading) to set the stage for the book. Then, the general book content and philosophy are described. We consider the fundamental buckling behaviors of three basic structural elements, bars, plates, and shells as in Figure 1-1. Our objective is to model those structural elements so we can predict the load at which they buckle (and the mode shape into which they buckle). When the behavior of those basic structural elements is well understood, we will be prepared to consider more complex structures. In this chapter, we also classify the possible types of buckling and initial postbuckling behavior, emphasize the importance of experimental results in the development of buckling theories, and describe some important distinctions that must be made in engineering analysis.

Be advised from the very beginning of this book that *the buckling problem is inherently nonlinear!* Specifically, *nonlinearities in the strain-displacement relations must be included in order to rigorously derive the proper buckling differential equations along with their associated boundary conditions and to clearly distinguish them from the equilibrium equations and their boundary conditions.* Indeed, some equations are linear, but they are derived in a consistent manner only from nonlinear considerations that some often ignore or use incorrect reasoning to obtain buckling equations that cannot be extended to problems with prebuckling deformations. Also, the practical significance of the buckling loads cannot be determined without solving a nonlinear equilibrium problem.

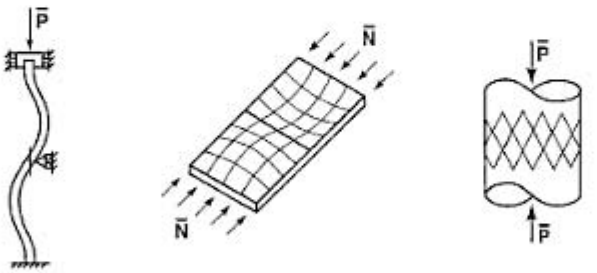


Figure 1-1 Structural Elements Treated

Éléments sous droits d'auteur

1.1 FUNDAMENTAL DEFINITIONS OF MECHANICAL SYSTEMS BEHAVIOR

We will address the definitions of stability, instability, buckling load, and maximum load plus the general load-deformation analysis procedure for mechanical systems, including structures and structural elements. All definitions are referenced from the equilibrium state or configuration in which the mechanical system is at rest. The *configuration* of a mechanical system is the geometric description of the simultaneous position of all the particles or 'material points' that constitute the system. Any movement of material points of a mechanical system, i.e., any change in configuration, constitutes a *displacement*. To fully describe the displacements also involves the concept of an immovable *constraint* on the system such as at the ends of a bar or the edges of a plate or shell, i.e., at the boundaries of the mechanical system, or more generally, anywhere in the mechanical system. The forces at a constraint do not do work. A coordinate system or reference frame is essential to all these descriptions. We consider only mechanical systems that are *conservative*, i.e., the work done by forces depends only on the initial and final configurations of the system, not on the path between the two configurations.

1.1.1 Stability

Definition: *An equilibrium state or configuration of a structural element, structure, or mechanical system is* ***stable*** *if every 'small' disturbance of the system results only in a 'small' response after which the structure always returns to its original equilibrium state. The term 'small' is a relative term to ensure that the behavior remains in the immediate vicinity of the equilibrium state.*

The simplest example of a *stable mechanical system* is a rigid ball in a valley as in Figure 1-2. The ball can be disturbed slightly such as by tapping on it, but the ball always returns to the bottom of the valley where the ball is in a state of *stable equilibrium*. However, if we give a big disturbance to the ball, then we cannot say precisely what will happen from the sketch in Figure 1-2. Perhaps the ball could even be displaced out of this valley, but we cannot say because we do not know anything about the topography of the surrounding hills and valleys.



Figure 1-2 Ball in a Valley

The simplest example of a *stable structural element* is a perfectly straight, axially loaded, pinned-ended bar that remains straight, but shortens in the axial direction by an amount, Δ, as the load, P, in Figure 1-3 increases slowly, i.e., in a quasi-static manner. The support mechanism for the pinned end at the top of the bar must move down as load increases (a pin that cannot move in the vertical direc-

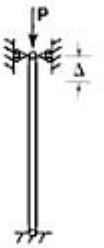


Figure 1-3 Axially Loaded Bar

Éléments sous droits d'auteur

tion at the top of the bar would not permit load to be introduced in the bar!). However, this stable behavior of bar in which the bar remains straight exists only if the load is small enough, as we will see.

The load, P, versus axial deflection, Δ, behavior for the straight axially loaded bar in Figure 1-3, i.e., without any disturbances, such as a periodic lateral force, is shown as the dashed line in Figure 1-4. Each point on each curve represents an equilibrium state, so the curves are *equilibrium paths*. When some form of a small lateral disturbance is applied to the bar in addition to the quasi-static increasing axial load, the load-deflection behavior is some equilibrium path near the pure axial load behavior shown as the solid line in Figure 1-4. That is, the effect of the lateral disturbances is only a small perturbation on the nature of the undisturbed axial load-deflection behavior. The axially loaded bar is stable and returns to its straight configuration after being disturbed just as the ball in Figure 1-2 returns to the bottom of the valley after being disturbed.

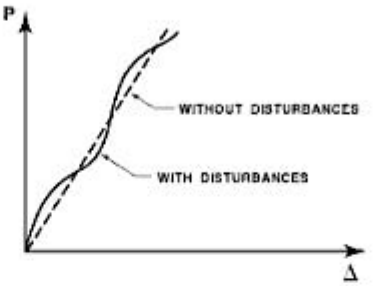


Figure 1-4 An Axially Loaded Bar under Small Disturbances

1.1.2 Instability

Definition: *An equilibrium state or configuration of a structural element, structure, or mechanical system is* ***unstable*** *if any 'small' disturbance of the system results in a sudden change in deformation mode or displacement value after which the system does not return to its original equilibrium state.*

The simplest example of an *unstable mechanical system* is a rigid ball perched precariously on the top of a hill as in Figure 1-5. If the ball is disturbed slightly (an infinitesimal disturbance suffices), the ball will immediately roll down the hill and will never return to the top of the hill. Thus, the ball is in a state of *unstable equilibrium* at the top of the hill.



Figure 1-5 Ball on a Hill

If the ball were in equilibrium at the bottom of a small valley surrounded first by hills and then by deeper valleys as in Figure 1-6, then the stability of the ball depends on the magnitude of the lateral disturbance applied to the ball. If the disturbance is large enough (i.e., a movement larger than dimension d in Figure 1-6), then obviously the ball is unstable in the small valley even though it is in equilibrium at the bottom of the small

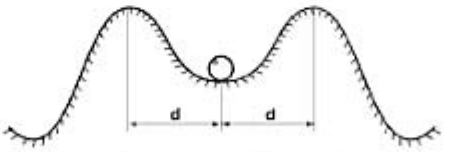


Figure 1-6 Ball in a Possibly Precarious Position

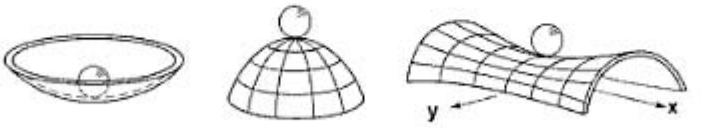
Éléments sous droits d'auteur

valley. If the disturbance is small enough (i.e., a movement smaller than dimension d in Figure 1-6), then the ball is stable in the equilibrium position. Thus, we call the ball at the equilibrium position at the bottom of the small valley *stable in the small,* but *unstable in the large.* Such an equilibrium position is sometimes called *metastable.*

The simplest example of an *unstable structural element* is the perfectly straight axially loaded bar in Figure 1-3 when the load is too high for the structure to always remain in the straight configuration shown. That is, the bar could be deforming in its straight (unstable) equilibrium configuration, but the slightest disturbance will cause the bar to suddenly bend laterally into the stable buckled equilibrium configuration just as the ball in Figure 1-5 rolls off the hilltop.

Note that the definitions of both stability and instability are 'local' definitions because they depend only on what happens in the immediate neighborhood of the equilibrium state (surrounded by an infinitesimal region). Thus, we address an *infinitesimal theory of stability* in this book. Of course, there could be other minima or maxima (valleys or hilltops) at some finite distance away from the equilibrium states being investigated. To study such cases, we would need a *finite theory of stability,* but that is usually not necessary for most engineering problems. Our usual objective is to determine the load at which the primary or first equilibrium state becomes unstable only because of small disturbances.

For a heavy ball rolling on a smooth, undulating surface, the total potential energy, V, is proportional to the elevation of the ball above some reference plane (plus an arbitrary constant). To generalize the stability concepts developed thus far in two dimensions to three dimensions such as in the topography of hills and valleys, consider the three equilibrium states in Figure 1-7. The location of the ball in each of the three cases is an equilibrium configuration, i.e., a stationary value of V exists there. The upward-facing bowl in Figure 1-7a represents a valley surrounded on all edges by hills. The ball at the bottom of the valley is obviously in stable equilibrium (at least 'in the small'), and the potential energy is a minimum. The downward-facing bowl in Figure 1-7b represents a hill surrounded on all edges by valleys. The ball on the top of the hill is obviously in unstable equilibrium, and the potential energy is a maximum. The third situation shown in Figure 1-7c represents a sort of low point on a long ridge in the x-direction which falls off in both the positive and negative y-directions. This situation is the so-called *minmax* or *saddle point* because V achieves a minimum in the lengthwise (x) direction of the saddle and simultaneously achieves a maximum in the cross-



a Valley b Hill c Saddle Point

Figure 1-7 Equilibrium Configurations for which Stability is at Issue

Éléments sous droits d'auteur

wise (y) direction of the saddle. That is, because V is the elevation-direction coordinate, $\partial^2 V/\partial x^2 > 0$ and $\partial^2 V/\partial y^2 < 0$ at the saddle point where, in addition, $\partial V/\partial x = 0$ and $\partial V/\partial y = 0$ are used to define the saddle point. Clearly, the ball at the saddle point is in *unstable equilibrium which is not accompanied by a maximum of potential energy* (except in the y-direction which is only a relative maximum in one direction, but not an absolute maximum in all directions). Conversely, we can conclude that an equilibrium position of a conservative mechanical system is not stable if the total potential energy is stationary, but not a minimum.

1.1.3 Buckling Load

Definition: *The **buckling load** is the load at which the current equilibrium state of a structural element or structure suddenly changes from stable to unstable, and is, simultaneously, the load at which the equilibrium state suddenly changes from that previously stable configuration to another stable configuration with or without an accompanying large response (deformation or deflection). Thus, the buckling load is the largest load for which stability of equilibrium of a structural element or structure exists in its original (or previous) equilibrium configuration.*

For some structural elements, the load versus buckling deflection behavior changes suddenly at the buckling load from a stable equilibrium configuration just below point A in Figure 1-8 shown schematically for a bar to an immediately adjacent different (buckled) stable equilibrium configuration just to the right of A. The load-deflection behavior is continuous with the loading path, O-A-B, being retraced in the opposite direction, B-A-O, when the structural element is unloaded.

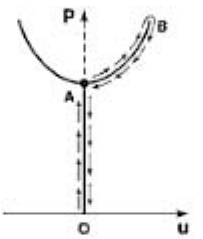


Figure 1-8 Buckling into an Adjacent Stable Equilibrium State

Other structural elements might have a load versus deflection behavior of the type illustrated in Figure 1-9 in which the load achieves a maximum at point C, called a *limit point*, but the load-deflection behavior falls off from C to D, so the structural element *'jumps'* from C to E under a fixed level of loading, $\bar{P}$. That is, the structural element *jumps* from one

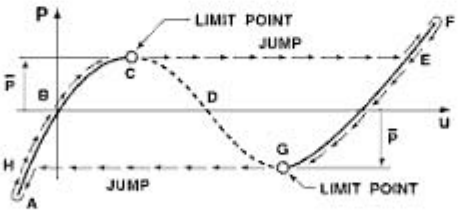


Figure 1-9 Buckling into a Non-Adjacent Stable Equilibrium State

Éléments sous droits d'auteur

stable equilibrium configuration to one that is *not adjacent*, and considerable deformation occurs accompanied by a 'snapping' or 'oil canning' sound. That is, the load-deflection behavior is discontinuous from C to E. Increasing the load from level P to that at, say, point F is possible. Upon unloading from F, another *limit point* is reached at G, so the structural element jumps from G to H. Again, a *jump* from one stable equilibrium configuration to another, but distant, stable equilibrium configuration. For both types of structural elements in Figures 1-8 and 1-9, buckling occurs suddenly, but in only the later case does the structural element actually *jump* from one configuration to another.

As a specific, practical example, a perfectly straight, axially loaded bar shortens in the axial direction as load increases and has a large sudden, both lateral and axial response to the slightest increase in load when the buckling load is reached as in Figure 1-10. That is, at the buckling load, the equilibrium of the straight bar becomes unstable, so the bar must seek another (now stable) equilibrium configuration, namely a bowed bar with substantial downward movement of the loaded end. For example, recall how you can buckle a 'yardstick' (meterstick) by standing it up vertically on one end and continuously increasing the force you exert on the top of the yardstick. This behavior is quite similar to that of a ball at the top of a hill which rolls off the hill if some disturbance is applied. The only difference is that with the yardstick we can see how the bar deforms to achieve equilibrium, whereas we don't know where the ball goes when it leaves the top of the hill.

As another example, we will see later that an in-plane loaded flat plate changes equilibrium states at the buckling load. However, the two equilibrium states are adjacent to one another, so no large response in deformation occurs. Moreover, we will see later that further buckling of a plate occurs at loads above the initial buckling load, i.e., many buckling loads exist at higher loads than the lowest load and do cause buckling (unlike the higher buckling loads for bars, only one of which causes buckling because of deformation constraints).

Thin straight or flat or circular cylindrical structural elements under slowly increasing loads typically remain straight or flat or circular cylindrical in shape until the buckling load is reached. At that load, the load-de-

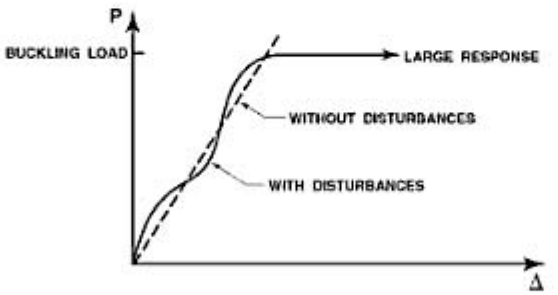


Figure 1-10 Response of an Axially Loaded Bar at the Buckling Load

Éléments sous droits d'auteur

formation behavior and shape changes quickly and sometimes drastically. The element is no longer straight or flat or circular cylindrical but has a bow or wrinkle or even a set of wrinkles depending on the type of structure. And, the structure might or might not be able to carry as much load as it did prior to buckling! For many structural elements, the deformations in the equilibrium configuration immediately make the structural element non-straight, non-flat, or non-circular-cylindrical, etc. That is, the structural element bows in some manner if only an infinitesimal load is applied, i.e., from the very beginning of load application, e.g., a warped (already bent) yardstick immediately bows as load is applied. Such behavior is *not* buckling because it is not sudden and is not a change in deformation configuration, but instead is ordinary deformation behavior in a non-straight, non-flat, or non-circular-cylindrical, etc. equilibrium configuration. At a particular load level, some structural elements suddenly deform into yet another shape, and this behavior *is* buckling.

Generally, we say a structural element has buckled if it ceases to deform in its original equilibrium shape and begins to deform in another equilibrium shape, i.e., the path on the load-deformation curve changes direction at the buckling load. The process of suddenly changing equilibrium shapes at the same load with or without drastic changes in deformation is called *bifurcation* because a bifurcation (or fork) exists between two separate equilibrium paths on the load-deformation curve. A trifurcation would have three possible paths, etc. The buckling load at bifurcation is often called the *bifurcation buckling load*, $\bar{P}$ (the overbar is used to denote the value of P at buckling). Leonhard Euler (1707–1783) was the first to study bifurcation buckling of a bar [1-1] *(References are denoted with square brackets and are found at the end of each chapter)*, so the buckling load of a bar is often called the Euler buckling load. Kurt O. Friedrichs (1901–1982) suggested that the bifurcation buckling load of any structural element be called the Euler buckling load [1-2] in Euler's honor, and that suggestion is followed in this book. The history of the Euler bar buckling equation is told by Stephen P. Timoshenko (1878–1972) [1-3] with more insights by Nicholas J. Hoff (1906–1997) [1-4].

Bifurcation buckling loads are shown in the context of load versus axial deformation behavior in Figures 1-11 and 1-12 for straight bars and

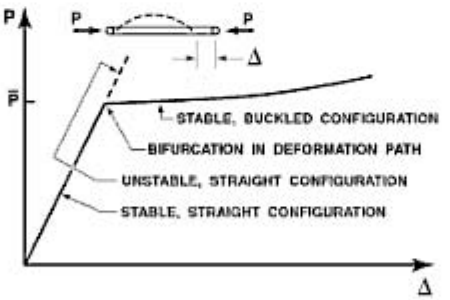


Figure 1-11 Load-Deformation Behavior for an Axially Loaded Bar

Éléments sous droits d'auteur

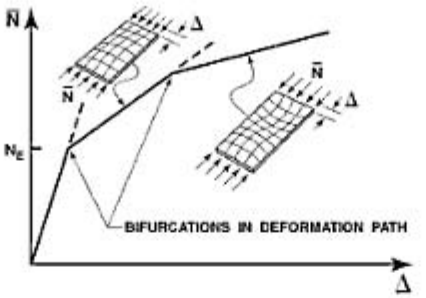


Figure 1-12 Load-Deformation Behavior for an In-Plane Loaded Plate

flat plates, respectively, along with the postbuckling behavior (i.e., load-deformation behavior after buckling has occurred) that we will derive in Chapters 2 and 3. As the load, P, increases, the bar deforms in the stable, straight equilibrium configuration in Figure 1-11 until the buckling load is reached. Then, the deformation path bifurcates with the bar not taking the unstable, straight configuration, but instead taking the stable, buckled configuration. Because of the sudden, large axial shortening caused by lateral bending at buckling in Figure 1-11, we can see that the Euler buckling load for a bar, $\bar{P}$ or P_E, is typically the end of the practical usefulness of a column in a building, i.e., the largest practical load the column can take. However, the Euler buckling load for a plate, $\bar{N}$ or N_E, in Figure 1-12 can easily be exceeded with only a small penalty of decreased stiffness (the slope of the load versus axial deformation curve). Note that several different bifurcation buckling loads exist for a plate, and each buckling load has a different buckling mode. For both an initially straight bar and an initially flat plate, the formerly applicable equilibrium path is shown as a dashed line above the bifurcation buckling load (of which there are usually at least two for plates!). Some of this bifurcation buckling phenomenon will be put into perspective of both the postbuckling behavior and the effect of initial geometric imperfections in Section 1.3, Classification of Types of Buckling and Postbuckling behavior. Other aspects must await definitive development of the theories underlying postbuckling behavior and the effect of initial geometric imperfections.

We identified the important attributes of the buckling phenomenon as

- Change in deflection mode shape
- Sudden occurrence (at a specific load)
- Change in path on the load-deformation curve

That is, somehow the structural element suddenly changes its mode of deformation, *whatever that mode might be.* For example, a buckled plate deforming stably in one mode shape along the load-deflection curve above $\bar{N}$ in Figure 1-12 might, at some specific load, buckle into another mode shape. Thus, more than one buckling load can occur as the load on a structural element is increased, i.e., some structural elements can

Éléments sous droits d'auteur

buckle more than once. Others buckle only once, and some structural elements have many possible buckling loads but buckle at only the lowest buckling load for given deflection constraints. Note especially that the definition of buckling does *not* require perfect initial (prebuckling) geometry (initial straightness of a bar, flatness of a plate, or perfect roundness of a circular cylindrical shell).

1.1.4 Maximum Load

Definition: *The **maximum load** of a structure or structural element is the largest load that can be carried by the structure without failure of any (meaningful or unacceptable) kind.*

This maximum load concept is of central importance in structural design. In design we seek to proportion or configure a structure to carry a specific loading with a prescribed factor of safety against failure. However, an obviously related concept is the determination of how much load a specific structure will carry without failure of any nature. These concepts are intimately related because *we must be able to analyze a structure before we can design it.*

The maximum load-carrying capacity of a structural element is not necessarily determined by the buckling load because *buckling is only one of several possible failure modes.* For example, failure could occur by fracture (material failure because of excessive stresses) or by yielding (a gross or mild material alteration—depending on the specific type of material—by virtue of the material achieving a certain combination of stresses). Or failure could occur if the deformations of a structure are too large to allow continued use of the structure. For example, a moving arm on a machine might bend so much under load that the arm contacts another part of the machine and jams to stop the machine. Thus, *the arm failed in its function* even though it did not break.

We will study the relation of the classical Euler buckling load to the maximum load of structural elements independently of the other failure modes. We want to know how much, if any, load can be carried by a structural element after it has buckled. We will (temporarily) ignore the possibility of failure in any other mode besides buckling in order to examine the large deflection behavior after buckling to gain a feeling for the practical significance of the calculated buckling load. A typical question might be: is the calculated buckling load at, above, or below the practical maximum load-carrying capacity of the structure? Of course, all possible failure modes must be considered in the design of a structure. That obvious fact seems to elude some designers as we will discuss later. The basic problem is one of imagining and identifying all 'things' that can happen to a structure. Some of us are lulled by the fact that a similar structure has already been built, and it has had no apparent problems. However, *if the design variables of the 'new' structure are sufficiently 'far enough' out of the range of those of the 'old' structure, then the experience of the 'old' structure is not fully applicable!* Many failures have occurred as a result of designers going beyond the applicability of the previous design variables into a region where an heretofore-not-encountered failure mode governs design.

Éléments sous droits d'auteur

1.1.5 General Load-Deformation Problem Including Bucking

For a defined loading on a structural element or a structure, we first determine the equilibrium configuration. That is, we establish the nature of the equilibrium configuration as a function of the applied load. That equilibrium configuration is stable up to a certain load. Then, we ask the question: Does another stable equilibrium configuration exist at some load? And what is that equilibrium configuration? That load is the buckling load. Of course, the existence of a new stable equilibrium configuration means that the old equilibrium configuration is no longer stable. This process of going up the load-deformation curve can, for some structural elements and structures, be carried out indefinitely. Of course, possible limitations on the behavior at every stage include (1) onset of plastic deformation that requires reformulation of the governing equations, (2) combinations of stresses that cause fracture, (3) excessive deflection that limits the practical usefulness of the structure, (4) damage accumulation that also limits the usefulness of the structure, etc. Sometimes the initial equilibrium configuration is seemingly trivial, e.g., a straight bar, a flat plate, etc. In other cases, the initial equilibrium configuration is more complex, e.g., a shell that deforms nonuniformly along its length.

After buckling, if the load is decreased below the buckling load, an undamaged elastic structure will return to its prebuckling equilibrium configuration, e.g., an initially straight bar that buckles will return to straightness. Of course, if the elastic limit has been exceeded in any part of the structure during buckling, then returning to the original equilibrium configuration is not possible, but the shape might be very close to the old shape unless substantial inelastic deformation or damage occurs.

The fundamental definitions just discussed are only a start in the definition of buckling of structural elements. Many buckling phenomena cannot be described in the simple terms used in this introductory chapter and are left to later in this book as described in the next section.

1.2 BOOK CONCENTRATION AND PHILOSOPHY

1.2.1 Introduction

Three structural elements will be addressed in this book: bars, plates, and shells. We will progress from one-dimensional bars to two-dimensional plates to three-dimensional shells as shown in Figure 1-13. Bars are one-dimensional because their principal dimension is length. Plates are two-dimensional because their principal dimensions are length and width. Finally, shells are three-dimensional because their dimensions exist in a three-dimensional volume (length, height, and width or length and cross-sectional area). For all these structural elements, the thickness is small compared to the other dimensions (as is the bar width). Thus, we treat the most different types of buckling phenomena possible in a one-semester course. Accordingly, the reader should be better prepared to study other buckling problems than if we had concentrated on one-dimensional problems such as linkages and frames at the expense of discussion of fundamental plate and shell problems. The premiere example of a buckling book that has all topics mentioned in Figure

Éléments sous droits d'auteur

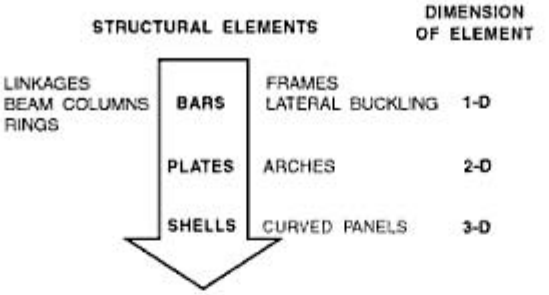


Figure 1-13 Thrust of Present Coverage

1-13 is Timoshenko and Gere's classic *Theory of Elastic Stability* [1-5]. However, many contemporary issues (such as composite structures, etc., outlined in Section 1.6) are necessarily, by virtue of the publication date, not covered in their book. Hence, the need for the present book.

The mathematical level in this book is kept as simple as possible. Numerical approaches will be used when necessary, but they will also be avoided when possible! That is, we will generally address only problems that can be solved in a very straightforward manner so that we see and control every aspect of the solution procedure without an intervening 'black box'. This viewpoint might surprise many who are familiar with the author's various computer programs including finite element analyses (see, e.g., [1-6]). However, the reason for this perhaps curious restriction is that we are studying the basic concepts of buckling in this book, not how to solve all possible buckling problems. This book is primarily a textbook, and textbooks are written to help instructors and students achieve a limited set of objectives within a relatively short period of time. The art of teaching has been described as choosing the topics in a subject in such a way as to avoid telling all you know so you can effectively present the essence of the subject in a class at the appropriate level without overwhelming detail. Thus, simplicity is preferred by the author.

The objective in this book is to understand the various phenomena of buckling. We address classical buckling results that serve as a firm basis for understanding the characteristics and nature of buckling. In addition, the results serve as check problems for computer programs that are designed to solve more complicated problems.

The author was educated in primarily analytical approaches with a classical grounding in fundamental concepts and quickly adapted to numerical approaches for solution of practical engineering problems. The value of a firm foundation in theory and experiment, e.g., that of buckling, has become painfully evident. Some engineers, having grown up using computers, *have a strong tendency to resort to the computer too quickly rather than preparing for that significant and essential step by carefully considering the expected behavior.* Instead, truly modern engineers use the basic understanding of a phenomenology in a thoughtful manner aided

Éléments sous droits d'auteur

further by computers to thoroughly address even more complex problems than their predecessors could! Merely preparing the input for a buckling computer program and reading the output is a rather dry, as well as dangerous, task. Dangerous not only in the sense of the proverbial 'garbage in, garbage out' (GIGO), but also in the sense that users of computer programs cannot properly interpret the results they get without a firm understanding of the theory on which the program is based along with understanding the phenomenon of buckling, the material behavior and characteristics, and the physical behavior of structural elements. From this observation has come the author's approach of presenting basic theory and simple illustrative results mostly without the use of computers to enable readers to fully understand the fundamentals of buckling in preparation for attacking more complicated problems for which computers are required.

We now preview the types of buckling behavior that we will investigate for bars, plates, and shells. For each structural element, the principal variables will be identified along with the buckling modes and the load-deformation behavior. Pioneering classical buckling work by Euler for bars, G. H. Bryan (1864–1928) for plates, and by Theodore von Kármán (1881–1963) and Hsue Shen Tsien (1911–), Lloyd Hamilton Donnell (1895–1997), Samuel Burbridge Batdorf (1914–), and several others for shells is used as the basis for a unified approach to buckling problems. Many important contributions by Stephen P. (Prokof'yevich) Timoshenko in all areas of buckling are included.

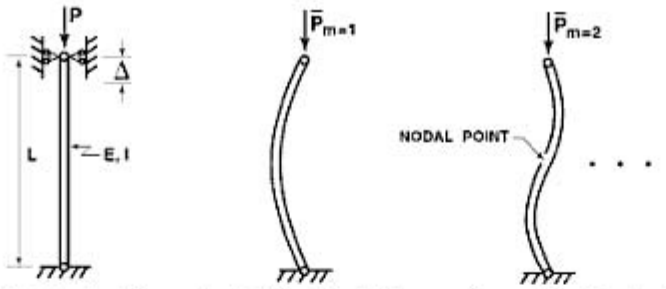
1.2.2 Buckling of Bars

A perfectly straight, axially loaded, simply supported bar with a cross section that is symmetric about at least one of the principal axes of the cross section has the straight initial configuration and the first two *buckling modes* shown in Figure 1-14 with the higher modes indicated with the ellipsis. The views in Figure 1-14 are from perpendicular to the plane in which buckling occurs. The buckling modes correspond to different values of m in the familiar Euler buckling load equation studied in elementary mechanics of materials (and re-derived in Chapter 2):

$$\bar{P} = P_E = P_{cr} = m^2\pi^2\frac{EI}{L^2} \qquad m = 1, 2, 3, \ldots \tag{1.1}$$

in which $\bar{P} = P_E = P_{cr}$ is the buckling load, m is the number of half-sine waves in the buckling mode, E is the Young's modulus of the bar material, I is the second moment of the bar cross-sectional area about the centroidal axis (often called the moment of inertia) and is a measure of how the geometrical distribution of material in the bar cross section resists bending, and L is the bar length. If m = 1, one half-sine wave is the first buckling mode in Figure 1-14b whereas m = 2 corresponds to two half-sine waves as the second buckling mode in Figure 1-14c. The *nodal point* marked in Figure 1-14c is the point that does not move laterally dur-

Éléments sous droits d'auteur



a Axially Loaded Bar b First Buckling Mode c Second Buckling Mode

Figure 1-14 Axially Loaded Bar and First Two Buckling Modes

ing buckling (although the point does move vertically before buckling because the axial load causes axial shortening of the bar). If some form of lateral support were placed at the nodal point, then the bar is prevented from buckling in the first mode and must buckle in the second mode with buckling load $P_{m=2}$. That is, the bar simply cannot buckle into the first mode because the structural constraint prevents such movement but does permit buckling into the second mode. We will later show this result to be valid for buckling in the plane of the page as shown in Figure 1-14. Accordingly, the I is about a principal axis of the bar cross section perpendicular to the plane of the paper.

In many common design problems, an engineer is required to find the buckling load for bars with the cross sections shown in Figure 1-15, among many others. The significant feature of those cross sections is the many different ways that exist to obtain an efficient cross section to resist buckling. i.e., with a high moment of inertia about a particular axis. All such bars have the characteristic load-deformation behavior with an almost horizontal response after buckling as shown in Figure 1-11. Thus, the Euler buckling load is a practical estimate of the maximum load a slender bar can support. Slightly larger loads can be supported, but at the considerable disadvantage of greatly increased axial shortening and

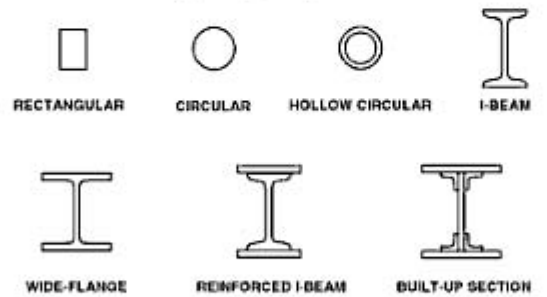


Figure 1-15 Typical Bar and Column Cross-Sectional Shapes

Éléments sous droits d'auteur

large lateral displacement that might not be acceptable in the structure.

Incidentally, the term *critical buckling load* is often used in buckling literature and must be explained. At first glance, the adjective 'critical' seems to be redundant. A structure with specified boundary or support conditions has a load at which it buckles first. That is, the load is increased from zero, and *we seek the first buckling event that occurs as the load is increased.* Higher buckling loads are also bifurcations in the load-deformation behavior (response curves as in Figure 1-11), but they are not possible to achieve without changing the bar support conditions. Some engineers use the word 'critical' to denote that lowest buckling load to the exclusion of the higher 'buckling loads'. Use of only the term 'buckling load', i.e., omission of the word 'critical', is quite adequate and is the general practice in this book for all structural elements.

1.2.3 Buckling of Plates

An in-plane compressed, simply supported (on all four edges) plate with a flat initial configuration has typical buckling modes of the general sinusoidal form displayed in Figure 1-16. Note that the buckling modes for plates have waviness in two dimensions. The *nodal line* in Figure 1-16 is an originally straight line on the plate middle surface which does not move perpendicular or parallel to the plate surface during buckling and is analogous to a nodal point for bars. The value of the buckling load, $\bar{N}_x$, will be shown in Chapter 3 to be dependent on plate geometry and material properties as well as on the buckling mode shape, i.e.,

$$\bar{N}_x = \bar{N}_x(a, b, t, E, \nu, m, n) \qquad (1.2)$$

in which $\bar{N}_x$ is positive in compression; a, b, and t are the plate length, width, and thickness, respectively; E is Young's modulus and ν is Poisson's ratio; and m and n are buckling wave numbers (number of half-sine waves in the buckling mode) in the x- and y- directions ($m = 2$, $n = 1$ in Figure 1-16). Plates that are initially flat have load-deformation behavior of the multi-linear character shown in Figure 1-12 on page 8. Thus, the Euler buckling load is not the largest load-carrying capacity of a plate, nor is a large deformation penalty paid to load the plate above the Euler load (although a plate is less stiff in the load direction above the Euler load, i.e., observe the lower second slope than the first slope of the load versus deflection diagram in Figure 1-12).

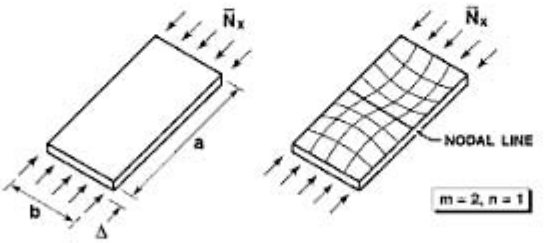


Figure 1-16 In-Plane Loaded Plate Before Buckling and Typical Buckling Mode

Éléments sous droits d'auteur

1.2.4 Buckling of Shells

A perfect circular cylindrical shell has the initial geometry and loading of axial force, torsion, and lateral pressure as shown in Figure 1-17. Prior to buckling, however, the shell surface has neither a circular nor even a cylindrical shape, as we will see in Chapter 4. The actual surface deformations are constrained by the shell edge supports, so the *prebuckling deformations* cannot be uniform along the shell length, although they are axisymmetric if the loading is axisymmetric. However, many classical theories are based on the presumption that a perfect circular cylindrical shape exists before buckling occurs, i.e., that bending near the edge supports is ignored. Those loadings in Figure 1-17 produce internal force resultants, N_x, N_{xy}, and N_y, respectively, but N_y from the lateral pressure loading cannot be shown because it is only an internal force resultant whereas N_x and N_{xy} are both internal and external force resultants.

An exaggerated, simplistic approximation to an axisymmetric buckling mode is shown in Figure 1-18 where the buckling mode is sinusoidal in the axial direction, but still axisymmetric, i.e., no buckles exist in the circumferential direction. However, the buckling mode can be sinusoidal in both the axial and circumferential directions, but the number of sine waves in the circumferential direction must be an integer to maintain deformation continuity. Actual shell buckling modes are much more complicated than the sinusoidal buckling waves of some bars and plates. Nevertheless, many solutions for simple shell problems have trigonometric functions in the buckling modes. One of the features of some shell buckling modes is the *nodal circles* (circles that do not move perpendicular to the shell surface during the buckling process, the shell analog of nodal points for bars and nodal lines for plates) shown in Figure 1-18.

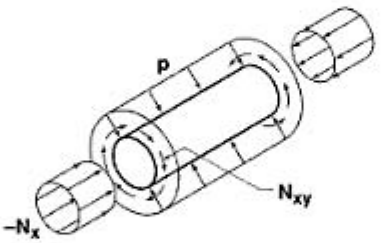


Figure 1-17 Circular Cylindrical Shell Geometry and Loading

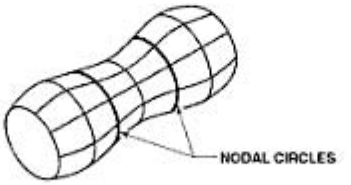


Figure 1-18 Circular Cylindrical Shell Axisymmetric Buckling Mode

Éléments sous droits d'auteur

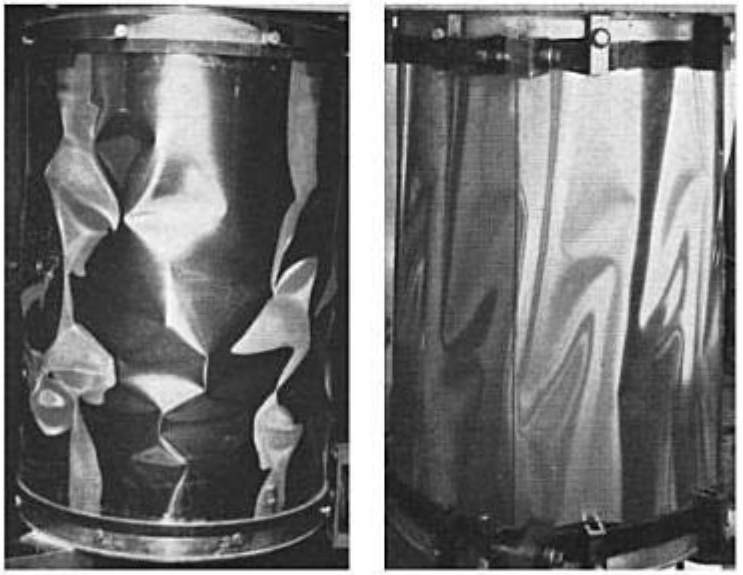
Buckled bars and plates have already been schematically depicted in Figures 1-14 and 1-16 on pages 13 and 14 with reasonable accuracy compared to their actual physical appearance. Buckled shells, however, are quite difficult to depict schematically. The book cover and Figure 1-1 on page 1 are very crude approximations to the actual buckle shape for a shell that has buckled under axial compression loading in Figure 1-19a. The shape of the buckles is more than difficult to describe in words, but the buckles resulting from axial compression are often referred to as 'diamond-shaped' buckles. For a shell under torsional loading as in Figure 1-19b, the buckles defy description in mere words (or equations).

Our objective in Chapter 4 will be to express the buckling loads as a function of the shell geometry, material properties, and buckling mode parameters, e.g., in functional form for only an axial load, N_x,

$$\bar{N}_x = \bar{N}_x(L, r, t, E, \nu, m, n) \tag{1.3}$$

in which L, r, and t are the shell length, radius, and thickness, respectively; E is Young's modulus and ν is Poisson's ratio; and m and n are the number of buckle waves in the axial and circumferential directions. Naturally, the loads, N_y and N_{xy}, for which we want to find buckling values could also be incorporated in an equation similar to Equation (1.3).

The load-deformation behavior for shells is strongly dependent on the loading and the shell geometry. For example, the postbuckling load-deformation curve of an axially loaded thin circular cylindrical shell lies



a Axial Compression b Torsion

Figure 1-19 Buckled Shells *(After Harris, Suer, and Skene [1-7])*

Éléments sous droits d'auteur

well below the Euler buckling load in Figure 1-20. Thus, such a shell can *snap through* or *'oil can'*, i.e., the shell rapidly buckles from the original shape to a grossly deformed shape at some load below the Euler buckling load usually accompanied by the same noise as snapping the top or bottom of an oil can from one deformation state to another. Buckling below the Euler load occurs, as we will see, because of the inevitable presence of geometric imperfections in the manufacture of shells. Making shells with a perfectly circular cross section along their length is just not possible—some degree of waviness will always exist. Under lateral pressure, circular cylindrical shells have a somewhat lower postbuckling behavior than the Euler load as in Figure 1-20, but not as pronounced as the axial load case. A modification of geometry to a cylindrical panel, i.e., a 'flat shell' (curved panel) in Figure 1-20, results in postbuckling behavior similar to that of a plate, as depicted in Figure 1-12 on page 8. For both lateral pressure loading and cylindrical panels, the shell buckling behavior is not particularly sensitive to manufacturing imperfections.

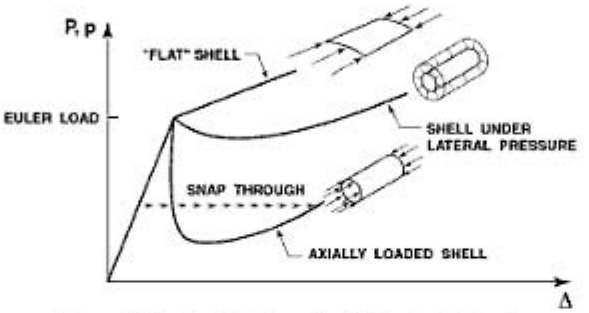


Figure 1-20 Load-Deformation Behavior for Shells

1.2.5 Summary

In the foregoing descriptions of bar, plate, and shell equilibrium and buckling behavior, the problems are relatively simple, and analytical solutions will be derived. However, the problems could be much more complicated. For example, the boundary conditions could be more complex resulting in non-closed-form solutions that cannot be easily understood. Or, the material properties could be generalized to represent the nonlinear stress-strain behavior of inelastic materials such as aluminum or the nonisotropic properties of a fiber-reinforced lamina and from there to the stiffnesses of a laminate (wherein the laminate *geometry* as well as the lamina material properties are essential factors) to treat structural elements made of fiber-reinforced composite materials. Loads could be more complex either in spatial distribution or by being time-dependent. However, only quasi-static loading is considered in this book because it is the logical starting point to understanding more complex loadings. Thus, we attempt to illustrate buckling behavior in the simplest possible manner, leaving the complications to future study.

Éléments sous droits d'auteur

1.3 CLASSIFICATION OF TYPES OF BUCKLING AND POSTBUCKLING BEHAVIOR

1.3.1 Introduction

Some of the characteristics of buckling and postbuckling behavior of structural elements are described in an introductory manner before we prove them later in this book. This section is a unifying effort to develop a framework of common understanding upon which we will build throughout the book. First, the bifurcation buckling load (the Euler buckling load) of a structural element is determined with a linear eigenvalue[1] analysis, but what do we actually learn from such an analysis? We will see that the shortcomings of a linear eigenvalue analysis mean that we must appeal to nonlinear postbuckling analysis to understand how to design structural elements.

Only with nonlinear postbuckling analysis can we begin to appreciate the physical significance in the design environment of the Euler buckling load for a specific structural element. That is, *what happens after the buckling load is reached?* Does the load-deflection behavior then go up, sideways, or down on a typical load-deformation plot? The answer determines whether the Euler buckling load for the structural element is (1) easily tolerated, (2) the limit on load-carrying capacity, or (3) well above the limit on load-carrying capacity, respectively. Thus, we must classify the types of postbuckling behavior that can occur to help us make that evaluation. We also determine the general nature of the influence of initial geometric imperfections in the manufactured structural element on the postbuckling behavior to further help us to evaluate the physical significance of the Euler buckling load in the design environment. Moreover, we characterize the nature of stable postbuckling behavior, i.e., what degrees such behavior can have in order to better understand the postbuckling behavior of some common structural elements.

1.3.2 General Nature of Linear Eigenvalue Analysis

We find the general nature of the results from a linearized model of behavior using linear eigenvalue analysis (as was done in the buckling analysis of an axially loaded bar in elementary mechanics of materials) in which the eigenvalue is the buckling load and the eigenvector is the buckling mode. Essential definitions for any structural element include: (1) λ is the loading parameter, (2) λ_B is the bifurcation buckling load (the eigenvalue) [(the Euler buckling load) from an originally straight (bar) or flat (plate) or circular cylindrical (circular cylindrical shell) equilibrium configuration to another equilibrium configuration], and (3) w_B is the amplitude of the buckling displacement. Below λ_B, buckling has not oc-

[1]The German word 'eigenwert' is usually translated into English as 'eigenvalue' and is synonymous with 'proper value' or 'characteristic value' in which proper and characteristic are possible English meanings of eigen. We are not honoring Eigen because there was no such person (or at least if there was, he didn't calculate buckling loads or vibration frequencies). For some unknown reason, the first translators kept the compound word form that is commonly used in German, leaving a mixed German-English word.

Éléments sous droits d'auteur

curred (i.e., the bar is still straight, etc.), so w_B is zero. Note that the buckling displacement, w_B, is normal to a bar axis, normal to the plane of a plate, or normal to a shell surface. That is, the mere appearance of w_B signifies that buckling has occurred as in Figure 1-21. When λ_B is reached, the structural element buckles, so the buckling mode (the eigenvector) appears with an *indeterminate amplitude* (e.g., the bar buckles, but we don't know the amplitude of the buckle wave). If we load a vertically oriented yardstick in the axial direction with one hand, the yardstick buckles at a sufficiently high load, and we see that the buckle amplitude has some limit (depending on how hard we push) because the bar does not simply keep bowing during buckling, but stops at some point. Obviously, there must be some final finite deflection for the bar buckling problem, but we can't find it with a linear eigenvalue analysis.

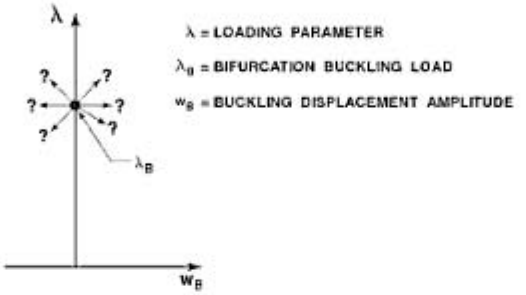


Figure 1-21 Linear Eigenvalue Analysis Results

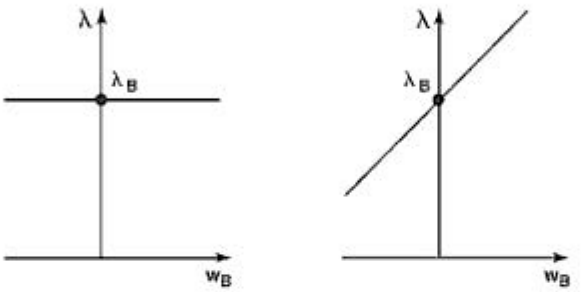
What have we really determined from this linear eigenvalue analysis? We know the bifurcation buckling load. We know the (initial) shape of the buckling mode (which can't be plotted on a figure of the type in Figure 1-21), but the amplitude of the buckling deflection is indeterminate as we will repeatedly see. We simply don't know what happens after buckling based only on the facts uncovered in the linear eigenvalue analysis! Therefore, we indicate with multi-directioned arrows away from the bifurcation buckling load that the postbuckling behavior goes in some unknown direction as in Figure 1-21. Moreover, we don't know the physical significance of the bifurcation buckling load without evaluating the postbuckling behavior. That is, we don't know how meaningful the calculated bifurcation buckling load is relative to the behavior around that load. Meaningful in the sense of how benign or how safe or how dangerous, i.e., can we approach the bifurcation buckling load or should we avoid it at all costs? What should the factor of safety be? Those questions can't be answered until the postbuckling behavior for the specific structural element is known from a nonlinear analysis. Nevertheless, the linear eigenvalue analysis will be our initial and primary approach to buckling problems. Then, the postbuckling behavior will be determined with a nonlinear analysis of the equilibrium configuration after buckling and differs in nature depending on the type of the structural element.

Éléments sous droits d'auteur

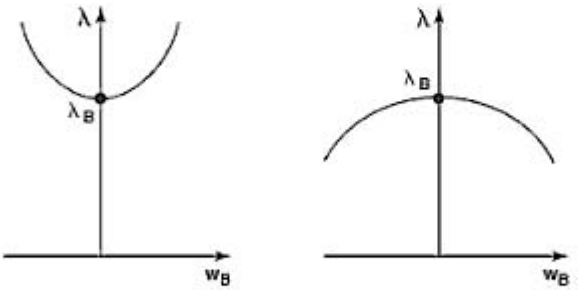
1.3.3 Types of Postbuckling Behavior

Postbuckling analysis is inherently nonlinear, so we obtain far more information than from linear eigenvalue analysis alone. The postbuckling behavior plots are not the conventional load-deflection plots involving deflection in the direction of the load such as in Figures 1-11 and 1-12 for bars and plates on pages 7 and 8, respectively, or in Figure 1-20 for shells on page 17. Instead, we get special load-deflection curves involving only the buckling deflection that is always zero before buckling and nonzero after buckling. For various structural elements, at least four types of postbuckling behavior after buckling at the bifurcation buckling load, λ_B, are possible:

- *Neutral Postbuckling Behavior* lies along a horizontal line extending to both the left and right of λ_B as in Figure 1-22a. Anywhere along the line, the structural element is in neutral equilibium because there is no lower or higher energy state that the structural element can assume. The structural element cannot carry load above λ_B where large deflections occur.



a Neutral Postbuckling Behavior b Unsymmetric Postbuckling Behavior



c Symmetric Stable Postbuckling Behavior

d Symmetric Unstable Postbuckling Behavior

Figure 1-22 Types of Postbuckling Behavior for Perfect Structural Elements

Éléments sous droits d'auteur

- *Unsymmetric Postbuckling Behavior* lies along a straight line that is inclined to the horizontal and extends to both the left and right of λ_B as in Figure 1-22b. The structural element can carry loads higher than λ_B if it is constrained so that it can buckle only to the right of λ_B. However, the structural element carries loads much less than λ_B if it is constrained so that it can buckle only to the left of λ_B as in Figure 1-22b.

- *Symmetric Stable Postbuckling Behavior* lies along a concave-upward curve extending to the left and right of λ_B as in Figure 1-22c. The degree of stability can be determined by using various derivatives of λ with respect to w_B as described in Section 1.3.5. Obviously, the structural element can carry load well in excess of λ_B.

- *Symmetric Unstable Postbuckling Behavior* lies along a concave-downward curve extending to the left and right of λ_B as in Figure 1-22d. Obviously, the structural element cannot safely carry λ_B.

We will see that straight bars have the type of postbuckling behavior that is both stable and also exceptionally close to the neutral type (see Chapter 2). Isotropic flat plates loaded axially in the plane of their middle surface will be seen to exhibit symmetric stable postbuckling behavior, i.e., the plate can buckle equally well either up or down (see Chapter 3). Finally, axially loaded perfect circular cylindrical shells have unstable postbuckling behavior in the immediate vicinity of λ_B (but we will see that such shells buckle only inward, so the behavior is not symmetric in w_B at λ_B) (see Chapter 4) as do externally pressurized spherical shells.

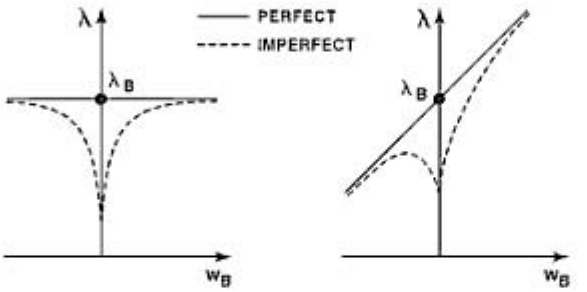
Koiter was the first to use asymptotic analysis to investigate the effects of the initial slope of the postbuckling curve on the buckling characteristics of perfect structural elements [1-8] and expanded his work in a more accessible reference [1-9]. Many others followed Koiter's pioneering work with increasingly refined consideration of more representative structures such as Hutchinson and Amazigo's work on shells with longitudinal and circumferential stiffeners [1-10]. Work on the initial postbuckling behavior of structural elements was later summarized by Hutchinson and Koiter [1-11]. Of course, we obtain more information if we determine the entire postbuckling behavior of a perfect structure, even if we only obtain the postbuckling behavior for a relatively short range of loads beyond the initial behavior at the bifurcation buckling load, λ_B. Note that the postbuckling behavior of a bar has been known since Euler's work in 1744 (see Section 2.4) so that full postbuckling behavior of at least one structural element dramatically predated Koiter's work, but we can be sure that known bar behavior gave Koiter a reference behavior against which he could test his proposed analysis. He addressed bars, plates, and shells, but, although some work had been done on the postbuckling behavior of plates and shells, the numerically definitive work was not done until the 1950s and 1960s. We will see proof of these stability concepts and actual evidence of the postbuckling curve in the chapters on bars, plates, and shells.

Éléments sous droits d'auteur

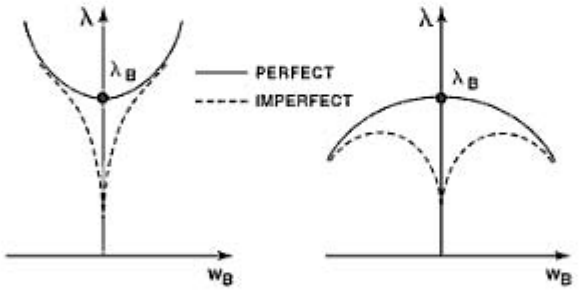
1.3.4 Initial Geometric Imperfections Effect on Postbuckling Behavior

The initial slope and, often, the initial curvature of the postbuckling curve at the bifurcation buckling load, λ_B, of a perfect structural element are closely related to the susceptibility to effects of inevitable initial geometric imperfections resulting from every manufacturing process. The postbuckling curves for perfect structural elements in Figure 1-22 and shown with a solid line in Figure 1-23 are modified to account for the effect of initial imperfections shown as the dashed line in Figure 1-23.

- If the initial slope is zero and the initial curvature is zero as in the *neutral* postbuckling behavior in Figure 1-23a, then the susceptibility to the effects of imperfections is 'moderate', i.e., a 'medium' deviation of the postbuckling curve of any imperfect structure from the postbuckling curve of the perfect structure. The practical load-carrying capacity of the imperfect structure is about the same as that of the perfect structure, i.e., about λ_B. We will see that this behavior is similar to, but not quite, the behavior of a bar in Chapter 2.



a Neutral Postbuckling Behavior b Unsymmetric Postbuckling Behavior



c Symmetric Stable Postbuckling Behavior

d Symmetric Unstable Postbuckling Behavior

Figure 1-23 Types of Postbuckling Behavior for Perfect and Imperfect Structural Elements

Éléments sous droits d'auteur

- If the initial slope is positive (increasing value of λ as we go away from λ_B) as in the right-hand side of the unsymmetric postbuckling behavior in Figure 1-23b, then the susceptibility to the effects of imperfections is 'small', i.e., 'not much' deviation of the postbuckling curve of any imperfect structure from the postbuckling curve of the perfect structure. The load-carrying capacity of the imperfect structure is about the same as that of the perfect structure, i.e., much higher than λ_B. This structural behavior is regarded as *stable*. Even if the initial curvature of the postbuckling curve for the perfect structure were negative, the load-carrying capacity of the imperfect structure would still be about the same as that of the perfect structure.

- If the initial slope is negative (decreasing value of λ as we go away from λ_B) as in the left-hand side of the unsymmetric postbuckling behavior in Figure 1-23b, then the susceptibility to the effects of imperfections is 'high', i.e., a 'very large' deviation of the postbuckling curve of any imperfect structure from the postbuckling curve of the perfect structure. The load-carrying capacity of the imperfect structure is far less than that of the perfect structure, i.e., far less than λ_B. This type of structural behavior is regarded as *highly unstable*. Only if the initial curvature of the postbuckling curve were positive might the load-carrying capacity be anywhere near that of the perfect structure. This behavior has similarities to that of axially loaded circular cylindrical shells as we will see in Chapter 4.

- If the initial slope is zero and the initial curvature is positive as in the *stable* postbuckling behavior in Figure 1-23c, then the susceptibility to the effects of imperfections is 'small', i.e., 'not much' deviation of the postbuckling curve of any imperfect structure from the postbuckling curve of the perfect structure. The load-carrying capacity of the imperfect structure is about the same as that of the perfect structure, i.e., well in excess of λ_B. We will see that this behavior is just about the behavior of a plate in Chapter 3 and has similarities to that of a bar in Chapter 2.

- If the initial slope is zero and the initial curvature is negative as in the symmetric *unstable* postbuckling behavior in Figure 1-23d, then the susceptibility to the effects of imperfections is 'high', i.e., a 'very large' deviation of the postbuckling curve of any imperfect structure from the postbuckling curve of the perfect structure. The load-carrying capacity of the imperfect structure is far less than that of the perfect structure. However, the load-carrying capacity of an inherently unstable structure is not a subject that makes much sense. We simply do not want to be near λ_B for such a structure. We will learn more about the load-carrying capacity of inherently unstable structures around λ_B such as axially loaded circular cylindrical shells in Chapter 4.

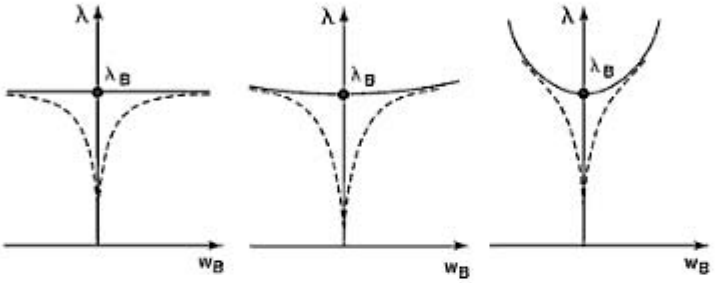
The degree to which the postbuckling behavior of an imperfect structure deviates from that of a perfect structure depends on the magnitude and nature of the imperfections (such as their distribution or shape).

Éléments sous droits d'auteur

1.3.5 Degree of Stability in Stable Postbuckling Behavior

The degree of stability of the stable postbuckled state at the bifurcation buckling load, λ_B, ranges from zero (neutral) to low to high in Figure 1-24. That degree depends on the nature of the postbuckling curve in the vicinity of λ_B. That nature, in turn, depends on the various derivatives of the loading parameter λ with respect to w_B of the postbuckling curve at λ_B above the first derivative which is, of course, zero at λ_B.

- For *neutral stability* in Figure 1-24a, all derivatives of the postbuckling curve at λ_B are zero and, indeed, are zero for all values of w_B.
- For a *low degree of stability* in Figure 1-24b, many of the lowest derivatives of the postbuckling curve at λ_B are zero or low, so the postbuckling curve gradually rises from the horizontal as w_B increases.
- For a *high degree of stability* in Figure 1-24c, the first derivative of the postbuckling curve at λ_B is zero, but the second derivative is positive.



a Neutral Stability b Low Degree of Stability c High Degree of Stability

Figure 1-24 Degree of Stability in Stable Postbuckling Behavior

The order of contact of a curve with a straight line depends directly on the degree of the polynomial representation of the curve (unless, of course, a polynomial representation is not possible in which case the order depends on the derivatives of the curve). For example, a polynomial of order two has an order of contact of two, and a polynomial of order four has an order of contact of four. The higher the order of contact, the flatter the curve is in the vicinity of the contact point. The flatness of a curve touching a horizontal straight line depends on how many of its derivatives at the point of contact are zero. We can use specific polynomial functions to describe many postbuckling curves. For example, if a curve $\lambda = w_B^2$ touches the horizontal axis at the origin, i.e., $w_B = 0$, as in Figure 1-25a, (where the first derivative is zero), the order of contact is lower than for a curve $\lambda = w_B^4$ as in Figure 1-25b (where the first three derivatives are zero) which, in turn, is even lower than for a curve $\lambda = w_B^{10}$ as in Figure 1-25c (where the first nine derivatives are

Éléments sous droits d'auteur

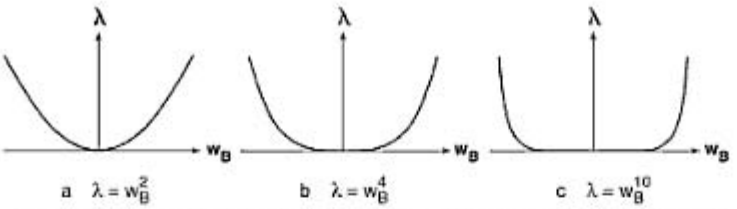


Figure 1-25 Polynomial Postbuckling Behavior with Various Orders of Contact

zero). A bar postbuckling curve has a very high order of contact with a straight line as in Figure 1-25c and resembles the low degree of stability curve in Figure 1-24b. In contrast, a plate postbuckling curve has a very low order of contact with a straight line as in Figure 1-25a and resembles the high degree of stability curve in Figure 1-24c. Note that the term 'order of contact of a curve with a straight line' is opposite to the term 'degree of stability' as we have used it in Figure 1-24, i.e., high for one term is low for the other and vice versa.

1.3.6 Summary

We will see in Chapter 2 that bars exhibit approximately the neutral (symmetric) postbuckling behavior in Figure 1-23a, but more accurately the very low degree of symmetric stable postbuckling behavior in Figure 1-24b with a moderate sensitivity to initial geometric imperfections. Then, plates are shown in Chapter 3 to have the symmetric highly stable postbuckling behavior in Figure 1-24c with a relatively small sensitivity to initial geometric imperfections. Finally, axially loaded circular cylindrical shells are shown in Chapter 4 on shells to have the unsymmetric postbuckling behavior in Figure 1-23b. We will see from experiments that shells buckle only inward from the original middle surface (toward the center of the shell) and not outward (whereas bars and plates can buckle in two directions from their axis or middle surface, respectively). Thus, the inward-buckling shell has the negative initial slope on the left-hand side of Figure 1-23b. The shell will not buckle outwardly, i.e., on the right-hand side of Figure 1-23b, because the shell obviously buckles more easily inward from the middle surface [because the path on the left-hand side of Figure 1-23b is the most attractive (easiest) of the two paths to follow]. The sensitivity of shells to initial geometric imperfections is very high with a potentially enormous reduction in load-carrying capacity if the negative slope is very large. All of these contentions will be demonstrated in the following chapters, but they are addressed now in a general way in order to prepare for later developments and to put all those later developments in a consistent framework of postbuckling analysis classification for structural elements. However, instead of relying upon a Koiter-type analysis of the initial postbuckling behavior, we will develop a postbuckling analysis to enable us to know what happens for a medium-sized range of deformations and loads after the buckling load of a structural element is reached.

Éléments sous droits d'auteur

1.4 IMPORTANCE OF EXPERIMENTAL RESULTS IN THE DEVELOPMENT OF THEORIES

1.4.1 Introduction

This section is not entitled '... Development and Validation of Theories' because *a theory is not developed until it is validated, so validation is an essential stage of development!* Many examples of very good agreement between theoretical predictions and experimental measurements of behavior of complicated structural and mechanical systems exist. That is, illustrations of the usual comparison between theory and experiment are plentiful. But, what more do we want? Can we perceive a stronger and more useful purpose for experimental measurements than 'just' validation of theory? Of course we can! To perform any theoretical prediction well, we must have a lot of information about the behavior of the widget (a generic name for a device or structure or mechanism) that we are investigating. Without that information, we are totally in the dark about how to model the widget. Or else we're kidding ourselves that we can construct a useful model without extensive fundamental *(experimental)* information. However, some people attempt to do just that! They seem to drastically oversimplify the problem so they can use a convenient overly simplistic mathematical model. These thoughts are addressed to those of us who are more rational and realize, if we only thought about it, that theoreticians need experimentalists much more than we might admit. This section has three major parts: (1) how experiments are used to validate theories, (2) how experiments are used more than 'just' to validate theory, and (3) how experiments are the very basis of the presumptions we make in every theory to effectively capture the essence of the observed behavior. Of course, our ultimate goal is to develop theories that agree with experimental results in every respect. But, if agreement does not exist, then the theory needs more development. As we derive various buckling theories, we will rely upon suitable experimental results to make crucial decisions in the development of our theories. We will expound upon that theme after lamenting that the present activity in experimental work is not what it should be, and, unfortunately, future experimental activity seems likely to be even less than today.

The over-riding theme of this section is the need for a high level of interaction and interdependence between theory and experiments. In fact, theory depends on experiment for definition of the qualitative and quantitative characteristics of a phenomenon that must be modeled. We must determine the minimum number of essential characteristics of behavior of a phenomenon in order to construct the simplest model. Less-essential features are addressed in higher-order models. Moreover, experimental results alone are quite difficult to utilize in design except in the immediate range of the important parametric values of the phenomenon in the experiment. In fact, determination of just what those parameters are is quite difficult from experiments alone. A major concern is that a theory is needed to relate the various aspects of the behavioral phenomenon in an understandable fashion. As the late James H. Starnes, Jr., (a major proponent of the high-fidelity analysis and design

Éléments sous droits d'auteur

of buckling-critical shells initiative at NASA Langley Research Center) put it: "If you can't predict the behavior, then you don't understand it." That is, neither experiment nor theory is sufficient, but a combination of both is required. Experiments provide the essential facts, and theory provides the essential framework for understanding the behavioral phenomenon. Only when a validated thoery exists can we claim that we fully understand the phenomenon. That is, then we can confidently predict behavior and expect those predictions to be correct because they are based on a validated theory that is, in turn, based on extensive and comprehensive experimental observations.

1.4.2 Comparison of Theoretical and Experimental Results

Never miss the opportunity to compare your theoretical predictions with experimental measurements! Then, you will be able to evaluate the importance and effectiveness of your theory. Just think where you would be as a theoretician with no knowledge of whether your theory has any factual basis in reality! If you haven't compared your theory with experimental results, then you are simply living in never-never land dreaming about things that don't matter!

If the agreement between theory and experiment is good, then you will have more confidence in your theory. If the agreement is not satisfactory (the more likely case if you are just starting to develop a theory), then you know you have more work to do. In either case, you will know far more than you did before the comparison.

If we don't get good agreement with experimental results, then our theory must not include modeling of some essential features of behavior. Accordingly, we must revert to the development stage and search for experimental evidence of what those features might be, so we can include them in our theory. In the current jargon, virtually every theory is a 'work in progress'. As such, the importance and usefulness of guidance from experimental results should be self-evident.

One of the attractive features of this book is the development of essentially parallel treatment of various effects that might need to be accounted for when developing a theory to describe a specific complex buckling problem. Those effects include:

- prebuckling deformations
- initial geometric imperfections
- higher order effects such as shear deformation
- large-deflection behavior (affecting strain-displacement relations)
- lamination characteristics
- stiffener eccentricities
- restraint of thermal expansion
- plastic deformation

Many effects require very sophisticated experimental measurements. Other effects besides those listed include different behavior under tension loading than under compression loading as described in Section 4.12. Perhaps only some effects must be included in an improved theory

Éléments sous droits d'auteur

for it to be sucessful, but sometimes many effects must be treated simultaneously to gain reasonable agreement with experimental evidence.

We can often get useful information from the nature of the difference between theoretical predictions and experimental measurements. For example, whether the predictions are too high or too low can be quite useful information if you can relate it to how the structure behaves.

(1) If a theory for plate deflection consistently under-predicts experimental measurements, then perhaps not all influences on stiffnesses have been taken into account (initial geometric imperfections, large deflection strain-displacement relations, plastic deformation, etc.).

(2) If a plate deflection theory over-predicts experimental measurements, then consider the possibility that the theory has an inherent flaw in its development such as a mathematical error or that the phenomenon has not been fully modeled to capture 'unexpected behavior' (such as ignoring bending-extension coupling in laminated plates as we will see in Chapter 3).

(3) If the theory and experiment agree for only a single value of the loading parameter, try higher and lower loads to make certain whether agreement still exists (you could have selected an initial load that just happened to be a crossing point between under- and over-prediction).

(4) Carefully examine the information you have from the comparison between theory and experiment. If plate deflections are being predicted as the *primary goal* and the predictions are too low, check a *secondary response parameter* such as the stresses. If the stresses are above the yield stress by use of some yield criterion, then plastic deformation surely must affect your problem. If the stresses are low compared to yielding, then you can probably eliminate consideration of plasticity effects and look for another cause for the disagreement.

Try to think for your particular problem whether there are similar characteristics to help you identify the cause of any deficiencies in your theory.

When very good agreement is finally achieved between theory and experiment, we have a truly mature theory in which all essential behavioral aspects are treated to a high level of accuracy. That theory is apparently capable of high-fidelity predictions of the response of our widget under challenging mechanical and perhaps thermal loading. Accordingly, we have achieved our goal of an effective theory.

Many might think this step of comparison between theory and experiment is the most important of all possible uses for experimental results. However, they overlook some other uses of experimental results that are, in the long-term view of theory development, perhaps far more important. Perhaps validation of theory is the ultimate goal with a theory because then a statement can be made that the theory apparently represents all aspects of the phenomenon correctly and accurately. However, development of theory to achieve this goal has been *guided by experimental evidence* ever since the first attempts at developing theory!

This goal of agreement between theory and experiment comes only after long hard work of addressing the various effects to develop theory

Éléments sous droits d'auteur

guided by information from experimental results (and perhaps developing new, more-sensitive experimental techniques to be able to measure more detailed information about the phenomenon than was previously possible). Those aspects of experiment that guide the development of theories are described in the next two sub-sections which are from the essence of a paper by Jones: Reflections on the Importance of Experimental Results to All Mechanicists, Especially Theoreticians [1-12].

1.4.3 Experimental Results are Used More than 'Just' to Validate Theory

An absolute need exists for experimental results to go beyond 'mere' validation of theory and for theory to extend the domain of usefulness of experimental results that obviously cannot be obtained for every conceivable circumstance. Both theory and experiment for many structural and mechanical problems have become refined enough that clearly superior results can be obtained, and they are in agreement. Here, we address further uses of experiment in the all-important theory-experiment interaction that must exist for mechanicists to make progress in developing theories to predict the behavior of structures (or widgets).

Daniel Drucker (1918–2001) (eminent plasticity thoeretician and experimentalist and later Dean of Engineering at the University of Illinois) hit the alarm bell in 1962 when he lamented that too many students were choosing to study theoretical approaches to mechanics problems rather than taking up the experimental reins. In fact, he was so upset that he said "Unless appreciable numbers of the most qualified students aim at combined experimental and theoretical research, the storehouse of physical information will be depleted by the tremendous emphasis on analysis and theory, and the theorist will be reduced to playing useless games. *Experiment is essential, it is vital, and it is creative* (italics added). Over the years, experiment provides the basis for the refinement of existing theory and the development of new theory" [1-13].

Josef Singer (1923–) (eminent shell buckling theorist and experimentalist) described eight motives for experiments in the specific or restricted area of shell buckling in 1980 [1-14] and 1982 [1-15]:

"(A) 'Better understanding of buckling and postbuckling behavior and the primary factors affecting it.

(B) To find new phenomena.

(C) To obtain better inputs for computations.

(D) To obtain correlation factors between analysis and test and for materials effects.

(E) To build confidence in multipurpose computer programs.

(F) To test novel ideas of construction or very complicated elements of a structure.

(G) For buckling under dynamic loading and in fluid-structure interaction problems.

(H) For certification tests of full-scale structures."

Éléments sous droits d'auteur

Interpretation of the motives should be fairly obvious in terms of applicability to buckling of other structural elements such as bars and plates or even more general mechanics topics. Singer and his coauthors, Arbocz and Weller, go on to explain each of the motives in their book *Buckling Experiments: Experimental Methods in Buckling of Thin-Walled Structures* [1-16]. We will refer more to that remarkable book later.

That these two luminaries of mechanics put so much emphasis on the importance of experimental work 'speaks volumes'. Drucker spoke those words in 1962, and his laments and cautions are probably more applicable today than when he first spoke them! Singer spoke nearly twenty years later, and addressed the still-needed work in experimental research, especially in shell buckling. The combination of those two points of view is a powerful commentary on the status of mechanics even today. Our focus on theory at the expense of experiment has 'led us down a garden path' to overreliance on the computer to solve our problems to the extent that we hardly appreciate experimental work, and that state of affairs is a real professional shame. Unfortunately, *experimental work might soon be an endangered species.* There is much to be learned in experimental work, and some theories will never be developed without sufficient experimental results.

1.4.4 Experimental Results are the Very Basis of all Theoretical Models

That experimental results are the fundamental basis of all theoretical models is a truism known to all who merely think about it, but is seemingly still a mystery to some. Actually, the idea is quite simple: *Engineers must always have a reason based on facts for doing whatever they do.* Obviously, *experimental results are the driving force for theory because experiments provide the essential facts!* Experiments should reveal new behavioral characteristics and motivate ever-advanced theory for a particular area of interest until all aspects of the phenomenon are both well understood and well modeled. In the theoreticians' world of curly overbars, underbars, various squiggles, bold-faced symbols, unusual characters, and other manifestations of what we often (questionably) regard as elegant, theoreticians must recognize that *experimental work provides the soul behind all theoretical work.* Experimental investigation is necessary to provide the *observations* of specific behavioral features or characteristics of a phenomenon that must be modeled with a theory. Without the observations, there is absolutely no basis for a model! That is, there must be a firm foundation of multiple observations of how a material or structure behaves under various loading conditions to serve as the evidence or phenomenon to be modeled. And there must be even more evidence that is independent of the information used to establish the theory so we can compare our theoretical predictions to that different (and necessarily independent) evidence to validate the theory.

Sometimes, conducting a proper experiment on a new behavioral issue is very difficult because of inadequate or severely challenged instrumentation, difficult-to-simulate events, or improbability or even im-

Éléments sous droits d'auteur

possibility of causing certain events to happen. Witness the severe trials of the astrophysicist who must rely on bits and pieces of information over a relatively short time span to construct or validate a theory involving motion of parts of the universe throughout the ages. Similarly, a structural mechanicist involved in analyzing and designing structures to withstand earthquakes has ground-motion spectra from past earthquakes to guide the loading definition, but little else except a few earthquake simulator 'tables' (large enough to carry major portions of structures!) to determine or confirm what happens to actual structures under such demanding and unusual conditions. Building and instrumenting an actual structure to test new structural concepts under actual earthquakes presupposes you know *where* an earthquake will occur and that it will occur *within the time period of your research grant!* Fat chance of either one of those two conditions happening! Moreover, in thermal buckling experiments on plates, (1) controlled heating in space and time as well as (2) precise support of plates at their edges have each in themselves been challenging topics in experimental structural mechanics for many years. Fortunately, many other structural mechanics simulations are more readily performable.

The reality of 'how things work' or 'what's happening' is quite difficult to determine in some cases. For example, shell buckling under axial compression loading occurs far too rapidly for the human eye to perceive all the events and stages of events that are happening. It took the amazing experiments and high-speed motion pictures of Almroth, Holmes, and Brush [1-17] to bring those facts to our attention and to help us understand how shells really buckle. Note that Almroth and Brush were primarily theorists, although Almroth would have considered himself a practical engineer. Bo Almroth (1921–1983) was an amazing individual who competed effectively with Ph.D. engineers and scientists even though he had less than the equivalent of a B.S. degree! And that formal education was not in mechanics!

An engineer must seek 'clues' in the form of revealing information from critical experiments to develop an appreciation for the nuances of the behavior of a particular type of mechanical or structural system. With that appreciation, an engineer is then prepared to attempt to model the behavior with the appropriate physical laws and principles to various levels of sophistication. If the model is good and the analysis correct, then the behavior might be predicted fairly well. However, if the model is lacking in essential features, then the behavior cannot be adequately predicted. The point is that the actual behavior provides modeling clues that must be addressed. *Thus, we must observe the behavior before we can attempt to model it!*

I am personally disappointed when I see some engineers try to develop a model with an obviously poor understanding of the phenomenon or phenomena addressed. In some cases, the apparent elegance of the mathematical approach is used to 'cover up' the fundamental reality that the theory has little basis in fact, namely *the fact of the actual behavior!* Some (fortunately few) theoreticians quite apparently choose to totally ignore most or all experimental data related to the phenomenon ad-

Éléments sous droits d'auteur

dressed with their theories! Seemingly, they do not use experimental results to justify their presumptions or even to use as a comparison for their theoretical results! How do they ever know if what they did has any meaning whatsoever? Or, was the work done in the context of the proverbial 'publish or perish' atmosphere, i.e., only an academic problem?

1.4.5 Summary

We are certainly aware of many cases of good agreement between theroretical predictions and experimental measurements of behavior for a wide variety of widgets (remember, a widget is the generic name for a device or structure or mechanism). But what do those cases of good agreement mean? They mean that we have been able to successfully perform two very challenging tasks: (1) develop a material model and a structural model that are capable of high-fidelity prediction of behavior or response and (2) measure behavior in a complex environment in which many behavioral aspects of our widget are excited. But is our sole interest obtaining validation of theoretical predictions by performing useful measurements? No! Absolutely not! Validation of theoretical predictions by achieving very good agreement with experimental measurements is the ultimate goal, but that final step is preceeded by the long effort of extensive development of the many aspects of the theory for representing the many aspects of the behavior of a specific phenomenon. We must have experiments to help us understand the behavior of our widget so that we can determine the very basis for any model we might develop for that widget. To properly do so, we must first establish the behavior and its characteristics, and then we'll see if we can develop useful approximations to capture the essence of the behavior of the widget. Those approximations must be both realistic and useful. The approximations are decidedly not 'assumptions' because they are not arbitrary as is inherent in the definition of the word assumption. The approximations must have a solid, reasonable basis in fact, so they are 'presumptions'. The distinction between assumptions and presumptions (and restrictions) is extremely important, yet tends to be glossed over by all too many as will be noted in Section 1.5.

The most important message to theoreticians is: *Seek and rely on experimental evidence to motivate, develop, validate, and extend your theories.* Work closely with an experimentalist to maximize your opportunity to capture and to understand the phenomenon addressed. Or, better yet, get involved with experimental work yourself! Some believe that a 'proper' investigator is a combination of a theorist and an experimentalist to enable the most rapid appreciation of the phenomenon. Remember, mere information is not knowledge. It takes much thoughtful work to mold information into a body of knowledge—it's called research! For some complex phenomena, there simply can't be enough information. Keep all these comments in mind (1) as we develop buckling theories in this book; (2) as we rely upon experimental results to help us develop those theories; and, finally, (3) as we compare those theories to other experimental results to see if our theories are valid.

Éléments sous droits d'auteur

1.5 SOME IMPORTANT DISTINCTIONS IN ENGINEERING ANALYSIS

1.5.1 Introduction

As we derive buckling equations, we must simplify our analysis in some way to find an effective solution without extraordinary effort. *Simplification is the very heart of the mechanics of materials approach to solving mechanics problems* (recall the famous 'plane sections remain plane' simplification). Too often, many say they make assumptions to simplify their approach, but they misinterpret the word 'assumption' to be applicable when it is actually not at all suitable for use in any engineering analysis! Why? Because to assume is "to take for granted; suppose (something) to be a fact" [1-18, p. 84]. The word 'suppose' is a direct invitation to be *arbitrary!* Thus, *an assumption is arbitrary, not fact.* However, **an arbitrary assumption has no place whatsoever in the logical derivation of an engineering result!** Note that use of both 'arbitrary' and 'assumption' is redundant because *the definition of assumption has no requirement for the assumption to be correct!* Thus, the word 'assumption' is incorrect and even confusing in engineering analysis. I will argue (reason) why the word 'presumption' is correct to use. When we firmly establish that 'presumption' is superior to 'assumption', we will also distinguish between 'presumption' and 'restriction' in the context of applying specific conditions to the familiar plate problem. Finally, we must encourage the precise use of words to reduce the possibility of our statements being misinterpreted with unfortunate, or even tragic, results.

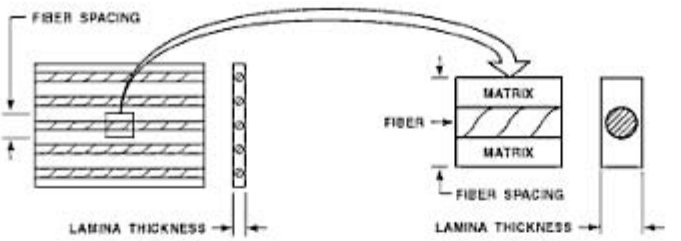
1.5.2 Presumption versus Assumption

The Problem

As I taught micromechanics using the text *Mechanics of Composite Materials* [1-19], I quickly became aware that many students regard an assumption in engineering analysis to be a *totally arbitrary* choice between two or more alternatives. Oh, could that be because arbitrary is the correct interpretation of the dictionary definition of 'assume'? We were discussing how to derive the mechanics of materials approximation to the effective modulus of a fiber-reinforced composite lamina perpendicular to the fiber direction, E_2, for the *representative volume element*[2] of the lamina in Figure 1-27a. Let's examine the analysis process.

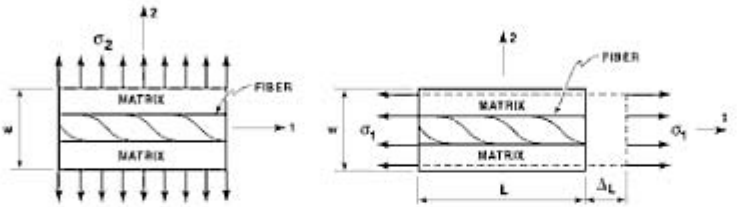
[2] A representative volume element (RVE) is the smallest region of material over which the stresses and strains can be regarded as *macroscopically uniform* and yet the volume still has the correct proportions of fiber and matrix, i.e., is still *representative* of the composite material and its constituents' proportions *by volume*. The original macroscopically homogeneous lamina is shown in Figure 1-26a. Microscopically, however, the stresses and strains are nonuniform because of the heterogeneity inherent to a composite material. Thus, the scale of the RVE is very important. Often, only a single fiber appears in an RVE, but more than one fiber can be required in the RVE to treat, e.g., woven fibers. The fiber spacing in a composite lamina with unidirectional fibers constitutes one dimension of the RVE, namely the width, w, in Figure 1-26b. One of the other two dimensions is the lamina thickness or the fiber spacing in the thickness direction of the lamina if the lamina is more than one fiber thick. The third dimension, the length in the fiber direction, is arbitrary.

Éléments sous droits d'auteur



a Macroscopically Homogeneous Lamina b Microscopically Heterogeneous Representative Volume Element

Figure 1-26 Representative Volume Element – Lamina with Unidirectional Fibers



a Load in the 2-Direction for E_2 b Load in the 1-Direction for E_1

Figure 1-27 The Representative Volume Element for a Fiber-Reinforced Composite Lamina with Unidirectional Fibers

In mechanics of materials analysis, the key concept is establishing a *useful simplifying approximation regarding the mechanical behavior of a loaded object or structure* in order to derive an effective solution in a relatively simple and straightforward manner[3]. Each approximation must be plausible, i.e., there must be a *reason* why the approximation *might* (should) be true (in mechanics, approximations cannot be arbitrary!). Of course, the simplifying approximation must satisfy the definition of the word approximation. First, 'approximate' means *"more or less correct or exact"* [1-18, p. 68]. Then, 'approximation' is "the act or state of approximating, or coming close" or "an estimate, guess, or mathematical result that is *approximately correct or close enough to exactness for a particular purpose"* [1-18, p. 68]. Thus, our objective is to find a useful approximation, i.e., a statement or condition that is nearly true and eases our solution efforts by dramatically simplifying the equations to be solved. Typically, in mechanics of materials, the simplifying approximation will be either related to kinematics or to kinetics, i.e., a statement about the deformations or the forces (or 'equivalently' stresses) in the problem ad-

[3]The alternative to the mechanics of materials approach is the elasticity approach in which all pertinent equations (equilibrium, compatibility, stress-strain relations, strain-displacement relations, etc.) are exactly satisfied simultaneously. However, those inherent complexities result in few problems actually being solved with the elasticity approach.

Éléments sous droits d'auteur

dressed. The most prominent deformation approximation is 'plane sections remain plane' in beam theory as well as its equivalents in plate and shell theory. Other approximations could be strictly mathematical such as truncating a series expansion or approximating $\sin\theta$ with θ for small angles. Many people call these simplifying approximations 'assumptions', and use of that misnomer is the main cause of problems to come. If the choice is to be made is truly an assumption, then the choice is indeed arbitrary, as we noted in the introduction to this section (1.5.1).

The first elastic modulus obtained with micromechanical analysis of a fiber-reinforced composite lamina is usually E_1, the modulus in the fiber-direction (the 1-direction in the RVE of Figure 1-27b). The simplifying approximation is that the strains in the fiber direction of a unidirectional fiber-reinforced composite material are the same in the fibers as in the matrix (a deformation or kinematic approximation), i.e.,

$$\varepsilon_{1f} = \varepsilon_{1m} \tag{1.4}$$

If the strains were not the same in the adjacent (parallel) constituents, then a fracture between the fibers and the matrix must exist because the fiber would be longer in the 1-direction than the matrix or vice versa. The equal-strains approximation is correct because portions of matrix and fibers that deform side-by-side (just like springs in parallel) must have the same strains at their interface if they are to remain part of an unfractured (continuous) body. The same can be said for parallel portions in the 1-direction within the fibers and within the matrix, so the strains are identical throughout the volume of the RVE. Thus, the equal-strains approximation has a very plausible, and even compelling, reason to be true. Note that cross sections normal to the 1-axis, which were plane before being stressed, remain plane after stressing, but they don't rotate as in ordinary beam theory. Also, with uniform strain in the RVE, the highest stress in the fiber because it has the highest modulus. The equal-strains approximation is used in the derivation of the modulus, E_1, which is the constant of proportionality in the one-dimensional relation between the macroscopic stress, σ_1, and the macroscopic strain, ε_1, that we develop from the microscopic deformations and stresses in the fiber and matrix of the (inhomogeneous) RVE.

$$\sigma_1 = E_1\varepsilon_1 \tag{1.5}$$

When we derive a simple expression for the elastic modulus, E_2, in the 2-direction of the lamina, a less-obvious situation arises. For the RVE in Figure 1-27a, the students were faced with having to decide whether the fibers and the matrix material have *equal strains* in the 2-direction (a kinematic approximation) or *equal stresses* in the 2-direction (a kinetic approximation), the only two options for a simplifying approximation. The modulus, E_2, is the constant of proportionality in the one-dimensional relation between the macroscopic stress, σ_2, and the macroscopic strain, ε_2, that we develop from the microscopic deformations and stresses in the fiber and matrix of the (inhomogeneous) RVE.

$$\sigma_2 = E_2\varepsilon_2 \tag{1.6}$$

Éléments sous droits d'auteur

Many students simply picked *either* equal strains in the 2-direction[4]

$$\varepsilon_{2f} = \varepsilon_{2m} \tag{1.7}$$

or equal stresses in the 2-direction[5]

$$\sigma_{2f} = \sigma_{2m} \tag{1.8}$$

as a simplifying approximation *without ever stating a reason as to why they made their choice! They were arbitrary even on an examination when they were required to 'derive E_2 and state all logical steps'.* That is, they skipped the logical step of describing *why* they chose their approximation or why their approximation was valid (and, by implication, why the other approximation is not valid). A simple coin toss would suffice if the word 'assume' is the correct description of what they were trying to accomplish (again, 'suppose' in the definition of assume is a direct invitation to be *arbitrary).* Those who chose equal strains[6] usually did not follow through in their problem solution to the stage where it is obvious that *their assumption of equal strains in the 2-direction in the derivation of E_2 violates equilibrium!* They essentially (and unwittingly) modified the concept of approximation to be the incorrect concept of assumption in which they were free to assume anything they pleased. I suspect that many others who chose the equal-stresses approach merely *remembered* that their choice was proper for finding E_2 rather than actually knowing the reason because they did not state the reason. That is, many just more or less *memorized* what to do in each of the four basic micromechanics problems of finding a practical, simple expression for E_1, E_2, ν_{12}, and G_{12}, the engineering constants for a lamina of fiber-reinforced composite material. *Memorization is not a valid approach to engineering analysis!* Thinking about the proper nature of their approximation is required. Their difficulty was lack of focus on a clear need to find a mechanics-based reason for the correct statement of approximation. Some of this difficulty is semantic in nature on their part (improper use of the word assumption) in addition to their not recognizing that *logic absolutely requires reasons.* Reasons come from the identification of physical evidence that helps us understand 'what is going on in the problem'. I often use the Spanish term 'Que Pasa?' (Que Pasa means "What's happening" or "What's going on") to ask what's going on in the problem as a gimmick to help students remember part of the analysis process and how to get started in an analysis. The connection between what is going on in the problem and a suitable approximation is often obvious *after* you determine what is actually going on.

---

[4]Note that the fiber and the matrix are not side-by-side in the load direction, i.e., not in parallel as springs, so there is no physical reason for their strains in the 2-direction to be equal. Hint: the strains are *not* equal.

[5]Note that the fiber and the matrix are in series in the load direction (just like springs in series). Thus, to satisfy equilibrium, the stresses must be equal because the areas on which the stresses act are equal. Accordingly, the RVE is in a state of approximately uniform stress, σ_2, and the highest strain is in the matrix because it has the lowest modulus.

[6]This approximation is correct for derivation of the modulus in the fiber direction, E_1, because portions of matrix and fibers that deform side-by-side in the load direction must have the same strains, but that fact has nothing to do with the derivation of E_2!

Éléments sous droits d'auteur

The Solution

Too often, a theoretician 'assumes' that a certain type of behavior exists and proceeds to develop a model and theory based on that assumption. That is, he ignores reality and simply makes a blind assumption that might not even be true. Then, he is not contributing to engineering because he is certainly not going to get a valid solution unless he is just plain lucky. However, the fundamental concept in analyses of mechanical behavior of materials and structures is not as simple as merely making an assumption because to assume is *"to take for granted; suppose (something) to be a fact"* [1-18, p. 84]. The word 'suppose' is a direct invitation to be arbitrary. Thus, *an assumption is arbitrary, not fact!* If a choice is truly arbitrary, then we might as well flip a coin! Accordingly, the word assumption leaves out entirely whether the (something) has any reason whatsoever to be considered. We in mechanics, and more generally in engineering, cannot be that illogical! We are not interested in arbitrarily taking something for granted! Our concern is with finding *why* we should consider some line of reasoning or approach.

To remedy this obvious problem for students of emphasizing the *reason* part of the approximation, I began searching for a word that would inherently have the two essential elements that must exist in a suitable approximation: (1) *what* to state as an approximation? and (2) *why* is that approximation reasonable and proper? My good friend Professor Paul Lagace of MIT says all engineering assumptions must have a reason associated with them. I cannot disagree with him (for he is far bigger than I am!). However, I wanted to go one step further and find a word that explicitly has the *two essential elements to help students remember the logic*. Preferably, I wanted something as explicit as the *yin and yang* of the simplifying approximation in which the yin is what is the approximation and the yang is why the approximation is plausible.

In the dictionary entry for 'assumption', I found a cross reference to 'presume': *"to take for granted; accept as true lacking proof to the contrary"* and "implies taking something for granted or accepting it as true, *usually on the basis of probable evidence in its favor and the absence of proof to the contrary"* [1-18, p. 1126]. *Bingo!* That single word, 'presume', has the two essential elements as an explicit part of its definition specifically without any hint of arbitrariness! Note that proof is required, or at least that *no proof to the contrary exists*. Thus, students now have a word to use that should remind them to (1) make a simplifying statement about the mechanics of the problem and (2) have a good reason why they make that statement! Accordingly, their ability to perform engineering analysis should be improved.

Presume (presumption) is a far stronger and, indeed, far more appropriate word for use in engineering analysis than *assume (assumption)*. For example, we could *assume* something that violates equilibrium, but certainly we cannot *presume* something that violates equilibrium! Assuming is poor practice, and violating equilibrium is unacceptable; the combination is simply not called engineering. An engineer should never make an arbitrary decision, i.e., one without a reason based in measur-

Éléments sous droits d'auteur

able fact. Instead, an engineer makes 'presumptions'. Clearly, the physical reason that is an essential part of every presumption must come from observation of the real behavior of the system addressed.

A crucial part of almost every mechanics of materials (or engineering) analysis is the *identification of the probable physical evidence that leads us to the correct presumption(s).* That is, the steps sometimes called 'assumptions' in a mechanics analysis are actually 'presumptions' because they are not *arbitrary* assumptions, but are presumptions that are based on evidence that we can examine and sometimes critically evaluate (although often not completely evaluate until after the analysis is finished). Our concern in the mechanics analyses in this book is with the probable evidence of material and structural behavior, so we deal with presumptions, not assumptions, and we must identify the probable behavior. That is, we must have a reason to justify our presumption, i.e., to make it plausible enough to consider. Thus, there are two elements in a presumption: (1) what? and (2) why? Or, (1) what is the presumption? and (2) why is the presumption believed to be true (lacking proof to the contrary)? (If we find proof to the contrary, then the presumption is obviously false). That is, what is the evidence to support the presumption? Without some form of evidence, we simply have no justification to make the presumption! *The obvious basis for every presumption is experimental fact!*

Note that another often-used word in engineering analysis, namely 'approximation', is not suitable as a replacement for 'assumption' because there is no explicit requirement for a reason in its definition. Again, 'approximate' means *"more or less correct or exact"* [1-18, p. 68]. Then, 'approximation' is "the act or state of approximating, or coming close" or "an estimate, guess, or mathematical result that is *approximately correct or close enough to exactness for a particular purpose"* [1-18, p. 68]. We are looking for the reason why we would make a specific approximation. Note that an incorrect statement cannot be an approximation because it would not be 'close enough to exactness'. *An incorrect approximation is a 'contradiction in terms'.* Thus, in the micromechanics derivation of E_2 in 'The Problem' part of Section 1.5.2, the approximation of equal strains for the fiber and matrix, which is not correct because equilibrium is violated, cannot be made. Note that the term 'correct approximation' is redundant. An approximation must be essentially correct, otherwise it is not a valid approximation. The word approximate has the inherent *quality* and *requirement* to be essentially correct (but not absolutely correct or precisely correct or else it would not be approximate!). That is, approximation has an *implicit* requirement of a reason why the approximation is correct. That implicit character is not quite good enough to provide a guideline word with built-in reminders of the process. Those reminders are, however, inherent to the definition of the word 'presumption'. However, the word 'approximation' is certainly far more suitable for use in engineering analysis than 'assumption'.

Just be careful when using either 'presumption' or 'approximation' in engineering analysis that your reason for the presumption or approximation you make is actually pertinent because an impertinent reason can

Éléments sous droits d'auteur

be a significant problem as evidenced by the following story. A farmer needed forty feet of rope to do a certain chore on his farm, so he asked a neighbor farmer if he could borrow that much rope. The second farmer said: "No, I need that rope to tie my milk." The first farmer said: "Hey, wait a minute! You can't tie milk with a rope!" The second farmer replied: "If you don't want to do something, one reason is as good as another." Watch out for such illogical approaches! Reasons must actually pertain to the problem addressed, not simply some random statement.

In all this insistence on a reason for making a presumption in engineering analysis, just remember that you must always have a reason for whatever you do as an engineer. If you follow that guidance, you will actually have a firmer understanding of engineering analysis! Keep thinking this way, and you will become a more effective engineering analyst. Much of what we do in this book relies upon our being aware of the suitability of the presumption we make; hence, the word 'presumption' is an especially convenient guide to keep us on the right path to success or to the right answer. Just having the 'right answer' is not the desired end result in engineering analysis. We must use *correct logic* throughout our entire analysis effort! Without correct logic, the fact that you arrived at the 'right answer' is mere coincidence and, in fact, meaningless. Moreover, logic requires using the correct words throughout every analysis.

Most engineers do not distinguish between 'assumption' and 'presumption' nor do they even use the word 'presume'. They typically use the word 'assume' (or assumption), but generally mean 'presume' (or presumption) because *good engineers always have a reason for doing anything* (as Paul Lagace says and as we must do). However, use of the word 'assume' is a mistake in semantics that is quite unfortunate because it can lead to serious misunderstanding with possibly tragic results.

The Example

The classical Euler-Bernoulli beam-bending hypothesis in elementary mechanics of materials is a good illustration of the two elements of a presumption. In accordance with that theory, we presume that (1) planes originally perpendicular to the neutral axis[7] of an undeformed beam remain perpendicular to the deformed neutral axis after bending because (2) we can see from the deformation of a rubber beam (a material that is easily and visibly deformable) that vertical lines drawn on the side of the beam of rectangular cross section in Figure 1-28a remain essentially straight during pure bending as in Figure 1-28b. Those vertical lines are traces in the plane of Figure 1-28 of planes that are perpendicular to the beam neutral axis. However, those originally vertical lines do rotate to a position such that, if extended, they all pass through a common point, namely the center of curvature. Thus, sections that are plane before pure bending remain plane after bending. During bending of the beam, the horizontal lines in Figure 1-28b below the neutral axis

[7]The neutral axis of a beam is the originally straight horizontal line that does not change length (strain) when pure bending moments are applied at each end of the beam. The neutral axis of a rectangular cross-section beam is at its mid-height.

Éléments sous droits d'auteur

stretch, and the horizontal lines above the neutral axis compress, describing arcs of circles with centers at the center of curvature through which the originally vertical lines pass after bending. Note that we are relying on the resolution capability of the unaided human eye in our observations. That is, at the resolution of our unaided eyes, we see that plane sections remain plane. However, if we were to bend a much deeper and shorter beam, we would observe that plane sections do not remain quite plane because shear deformation of the original planes is evidenced by some curvature of the deformed 'planes'. Alternatively, if we used a refined measurement technique such as Moiré interferometry, we would readily detect slight non-planeness of the deformed 'planes'.

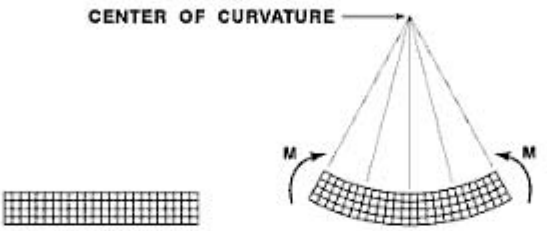


Figure 1-28 Deformations in Pure Bending of a Beam

1.5.3 Presumption versus Restriction

The dual terminology of 'restriction' and 'presumption' is used because the two terms have fundamentally different meanings, yet are often misused. *Restrictions* are limitations on the use of the theory which are *obviously* either satisfied or they are not. Thus, restrictions are concerned with the *known*. For example, a theory for square plates clearly does not apply to round plates; there is simply no doubt that a theory for square plates cannot be used for round plates! Thus, use of the theory is *restricted* to square plates. *Presumptions* are limitations on the theory which have a nature of *uncertainty* to them. That is, presumptions are concerned with the *unknown* because the reasons for the presumptions might not be totally accurate. For example, stresses perpendicular to the surface of a plate, but within the plate, are commonly presumed to be small enough to be regarded as zero because the stress normal to the surface, σ_z in the z-direction of Figure 1-29, is zero on an unloaded surface and the derivative of that normal stress with respect to z is also zero as established with the equilibrium equations. Thus, in a thin plate, we should not expect σ_z to grow much in the short distance (the half-thickness) it has to grow. However, we do not know for certain just how small the stresses are unless we appeal to a more accurate theory or compare with experimental results. Also, the displacements of a plate might be presumed to be small to enable certain approximations in the equations. However, whether the displacements actually are small or

Éléments sous droits d'auteur

not can be determined only when the final results are known. In summary, the difference between restrictions and presumptions is that restrictions involve the *known* (which we can observe) and presumptions involve the *unknown* (about which we wish to speculate). The validity of any restriction can be immediately determined. The speculation is quantified only when we are able to use the approximation and find results that can be compared with measured response (or with a more accurate theory).

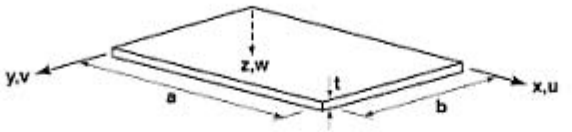


Figure 1-29 Plate Geometry, Coordinates, and Displacements

The following restrictions and presumptions provide further opportunity to clarify the difference between the two classifications for the common example of the plate in Figure 1-29. Recall that presumptions in engineering must be justified, i.e., we must know *why* we believe the presumption to be true from a physical standpoint.

Restrictions

- Each layer is isotropic, linear elastic, and of constant thickness (so the entire plate is of constant thickness).
- The plate thickness is very small compared to its length and width (such a configuration is commonly called a thin plate, although the name *plate* itself implies such a geometry).
- No body forces exist.

Presumptions

- Stresses acting in the x-y plane (the plane of the plate) dominate the plate behavior. Then, σ_z, τ_{xz}, and τ_{yz} are presumed to be zero such that an approximate state of *plane stress* is said to exist in which only σ_x, σ_y, and τ_{xy} are considered.
- The *Kirchhoff hypothesis* of negligible transverse shear strains, γ_{xz} and γ_{yz}, and negligible transverse normal strain, ε_z, constitutes a statement of nondeformable normals to the middle surface, but there is an inherent, but commonly ignored, conflict with the presumption of zero transverse normal stress, σ_z.
- Displacements u, v, and w are small compared to the plate thickness (generally indicative of small-deflection theory).
- Strains in the x-y plane, ε_x, ε_y, and γ_{xy}, are small compared to unity (small-strain theory).
- Rotatory inertia terms are negligible.

Éléments sous droits d'auteur

Clearly, we can determine precisely that each of the foregoing restrictions is correct (except that body forces might simply be quite small compared to the in-plane forces causing buckling and therefore negligible). However, we are not certain that each of the foregoing presumptions is perfectly true, and we cannot validate the presumptions without either a more accurate theory or, probably a more useful and practical basis, *experimental evidence!* What happens in the case of classical Kirchhoff plate theory when we presume that both σ_z and ε_z, the stress and strain normal to the plate, respectively, are zero? Clearly, one or the other can be zero, but certainly both cannot be zero because they are linked by the stress-strain relations that are violated if both are said to be zero. This is the common contradiction typical of a mechanics of materials analysis. The resulting theory is a very good approximation to the actual behavior of a plate, but the individual approximations can be contradictory of one another, although by themselves, each approximation is fine, i.e., plausible.

Some engineers *assume* something that can be clearly determined as fact or fallacy if they would just look at the phenomenon. For example, some engineers 'assume a rectangular plate' to start their analysis when all they have to do is look at the plate to determine whether it is rectangular or in fact some other shape. *There is no assumption involved!* Those engineers really mean they *restrict* their attention to a rectangular plate. That is, they confuse *restriction* with *assumption*. They certainly cannot 'presume' a rectangular plate because the essential reason behind a 'presumption' does not exist! Clearly, there is no need or place for such confusion. We must consistently use words or terms that cannot be misinterpreted, and we must not use words in an incorrect context.

1.5.4 Misinterpretations and their Consequences

Engineers are *responsible* for communicating their professional opinions, evaluations, designs, etc. in an absolutely precise and unambiguous manner. Otherwise, the possibility (or even probability) exists that what we said or wrote will be misinterpreted. The consequences of such misinterpretation range from mild to unfortunate to tragically serious.

An example of misinterpretation with only mild consequences is the Moscow Hotel which was designed in the 1930s to be built close to Red Square. The architect drew plans with two alternative exterior designs side-by-side as the (touching) left and right halves of a side of the hotel on the same sheet of paper. The drawing had no note to explain that a *choice* of exterior designs had to be made (with exterior choice A on the left-hand side and exterior choice B on the right-hand side of the drawing). However, the hotel was built exactly as shown on the plans. Nobody seems to know for certain how the misinterpretation actually occurred. One version of the story is that the architect was on vacation when the plans were approved, so he could not emphasize the need for making a choice before construction began. Another version is that Stalin himself just signed the plans, so of course no one would do anything except build precisely what was on the signed plans. This unusually nonsymmetric hotel stands in the spring of 2002 as shown in Figure

Éléments sous droits d'auteur



Figure 1-30 The Moscow Hotel Near Red Square
(Photograph by Professor Valery V. Vasiliev)

1-30 and is also featured schematically on the label of the Russian vodka Stolichnaya. In the summer of 2002, the Moscow city government decided to tear down and replace the Moscow Hotel sometime in the near future *because it is unsymmetrical! The moral of the story is that we engineers cannot afford to be ambiguous when presenting our results!* The misinterpreted result in this example was merely cosmetic in nature, but other misinterpretations could cause loss of value, serious injuries, or even deaths.

As an example of a more unfortunate consequence of misinterpretation, consider the following scenario. A young couple had just bought a new house and were now searching for landscaping. They wanted 50 bushes planted on each side of their long driveway for a total of 100 bushes and went shopping to find someone to provide and plant the bushes. One landscaper said he would plant 100 bushes for $2,000. A second landscaper said he would plant 50 bushes on either side of their driveway for $1,500. They chose the second landscaper's bid thinking it was the better deal of the two bids. However, after the second landscaper finished, they were very disappointed to see only 50 bushes planted on the left side of their driveway and *none on the right side!* They sued the second landscaper in small-claims court, but the judge ruled against the couple's claim pointing out that the first-listed definition of 'either' is "one or the other" (not both) [1-18, p. 447]. Thus, using 'either' when you mean 'both' is an invitation to problems! Unfortunately, this serious semantics error occurs in daily use of the English language. Common use of a word generally determines its meaning, so its meaning can, of course, change with the times. However, it is certainly not reasonable to expect the meaning of a word to transition to the **opposite**

Éléments sous droits d'auteur

of its original meaning! Or, if current society permits one word to have two meanings that are the opposite of one another, then *'either' is a horribly poor choice of words to ever use in any circumstance*, but especially in engineering where we must be absolutely precise and unambiguous or else lives can be lost. *There is nothing more ambiguous than a word with two meanings that are the opposite of one another!* Obviously, 'either' is a failed word because it has two conflicting meanings.

A third example with the most serious consequence of all misinterpretations discussed in this book is the Hyatt Regency Hotel skywalk collapse on 17 July 1981 in which 114 people died and more than 200 people were injured. The structural engineers' original design for the skywalk support system was modified by the building contractor whose shop drawings were then marked 'approved' by the architect and 'reviewed' by the structural engineers. The main problem hinges on the word 'reviewed' because the structural engineers did not fully investigate the shop drawings and allowed a faulty design to pass without challenge, much less a needed correction. Certainly, the structural engineers should have done more than 'review' the shop drawings, so their professional licenses were cancelled. Moreover, the situation is seriously compounded by the fact that the structural engineers' original design was unbuildable because the support rods were to be too long to be fabricated and installed. Thus, the design had to be modified (*prima facie* evidence of a design error—one of the cardinal rules of design is that it must be buildable, otherwise the design is worthless). The fact that the building contractors' shop drawings were faulty should not be unexpected. After all, building contractors are neither educated nor licensed to provide safe design of structures. Also, architects are neither educated nor licensed to provide safe design of structures, so their stamp of 'approved' on the contractor-modified plans is meaningless with respect to the safety of the structure. Had the structural engineers properly discharged their professional obligation instead of following their lawyer's advice to never 'approve' shop drawings but to merely mark them 'reviewed', this tragedy might not have occurred. This painfully distressing example is more fully discussed in Appendix D, Elements of Design Philosophy, with a suitable reference. Thus, misinterpreted words have clearly cost lives, and such tragedies will unfortunately happen again! Don't let them involve you!

We engineers cannot afford to underestimate the power and effect of our words, so we must choose our words carefully and properly with due attention to being absolutely precise and totally unambiguous. Otherwise, our professional work can (and often will) be misinterpreted with possibly dire consequences. Clearly, we must live up to our responsibility to the public, to our profession, and to ourselves.

1.5.5 Summary

We must have experiments to help us understand the behavior of our device or structure so that we can determine the very basis for any model we develop for that behavior for use in design of structures and devices. To properly do so, we must first establish the fundamental characteristics of the behavior, and then we will see if we can develop approx-

Éléments sous droits d'auteur

imations to capture the essence of the behavior of our device or structure. The approximations must be both realistic and useful. The approximations are decidedly not 'assumptions' because they are not arbitrary as is inherent in the definition of the word assumption. The approximations must have a solid basis in fact, so they are 'presumptions'. The significant distinction between 'assumptions' and 'presumptions' is extremely important, yet tends to be glossed over by far too many engineers. The word *presume (presumption)* is a much stronger and, indeed, an obviously much more appropriate word than *assume (assumption)* in engineering analysis.

An assumption is arbitrary, not fact! **An arbitrary assumption has no place whatsoever in the logical derivation of an engineering result!** *Logic absolutely requires reasons for each and every step of an engineering analysis.* What else justifies logic? To 'presume' is *"to take for granted; accept as true lacking proof to the contrary"* and *"implies taking something for granted or accepting it as true, usually on the basis of probable evidence in its favor and the absence of proof to the contrary"* [1-18, p. 1126]. A crucial part of almost every mechanics of materials (or engineering) analysis is the *identification of the probable physical evidence that leads us to the correct presumption.* Without some form of evidence, we simply have no justification to make the presumption! *The obvious basis for every presumption is experimental fact!* That is, the basis for any reason we use to establish our model must be *experimental results!* Throughout our analyses of bars, plates, and shells or anything else, we will always need to remain fully aware of any and all experimental measurements pertaining to our problem. Unfortunately, many (overly) theoretically oriented researchers seem quite willing to ignore the physical realities inherent to experimental results. Most engineers do not distinguish between assumptions and presumptions. They typically use the word assume (or assumption), but generally mean presume (or presumption) because *good engineers always have a reason for doing anything.* We further characterize experimental results as related to the development of theories in Section 1.4. Given that different dictionaries have different definitions of 'presume', some engineers might prefer to use 'approximation'. Indeed, approximation is a most suitable, but not perfect name for the concept. Irrespective of the various definitions, the word 'assume' is a totally unacceptable choice for engineers.

We also found that the word 'assumption' or even 'presumption' is often used when the writer or speaker really means 'restriction' (whether he realizes it or not!). The difference between restrictions and presumptions is that restrictions involve the *known* (which we can observe) and presumptions involve the *unknown* (about which we wish to speculate). The validity of any restriction can be immediately determined. The speculation is quantified only when we are able to use the approximation and find results that can be compared with measured response (or with a more accurate theory).

The distinctions between 'assumption' and 'presumption' as well as between 'restrictions' and 'presumptions' are very important. Misuse of words in writing and speaking can easily lead to serious problems when

Éléments sous droits d'auteur

a desired object is manufactured or built. In fact, by Murphy's law, such mistakes *will* lead to serious problems. Engineers simply must speak and write in totally precise and unambiguous terms! We are *responsible* for doing everything we can to ensure that the device or structure we design performs without failing. Trying to establish what possibly can 'go wrong' with a device or structure might appear to be the mark of a pessimist. That is, some people might accuse engineers of being pessimistic because they are always looking for the problems that could possibly cause difficulty with the device or structure they are designing. However, engineers must examine and identify all the 'bad things' that can happen to a device or structure[8] so they can design to *prevent those 'bad things' from causing serious problems*[9]. Another example of a system not being designed for all possible 'bad things' that did happen is the airport security system at Paris' Charles de Gaulle airport on 22 December 2001 when the 'shoe bomber' passed through security without challenge, boarded an airplane, and tried to ignite explosives hidden in his shoe while the plane was enroute to the United States. A French civil aviation authority official said: "All security systems in place worked perfectly. The problem is that we were confronted with a scenario that had never been considered" [1-21]. What a total fool he was to claim his system worked perfectly! Obviously, his system was not designed for all threats, yet he had the audacity to claim it worked perfectly. We simply cannot prevent 'something' unless we know what it is! Thus, engineers are not pessimists; they just do what they must to ensure public safety.

1.6 BOOK ROAD MAP

For each of the structural elements, namely bars, plates, and shells in Chapters 2, 3, and 4, respectively, we will derive the equilibrium differential equations and their associated boundary conditions for the stable prebuckling equilibrium behavior. More importantly, we will derive the buckling differential equations and their associated boundary conditions that govern the departure from the initial stable equilibrium state when the limit of that stable state is reached. These consistent derivations of distinctively different equation systems are enabled by use of energy principles and variational calculus in the manner of one of the author's professors, Henry Langhaar (1909–1992) [1-22]. The advantage of this approach is that often-confused differences between equilibrium and

[8]Prior to 11 September 2001, engineers and many others did not foresee the possibility of anyone deliberately flying a fully fueled airplane into a tall building to destroy it (although a B-25 did *accidently* crash into the Empire State Building in 1945 with only local damage). We were not that pessimistic about the attitudes of mankind. If someone attempts to design a tall building to resist such insane, unconscionable, and uncivilized assaults on innocent people, Henry Petroski points out that their proposed structure will be enormously expensive in order to provide a safe working place and will likely be without the visual amenities of windows with fantastic views, two reasons against building tall buildings ever again [1-20].

[9]The 'bad things' might happen, but they do not result in damage or failure of a well-designed structure, where 'well-designed' is relative only to those events considered in the design process. If a 'bad thing' that was not considered in the design process actually happens, the the structure or device is no longer 'well-designed".

Éléments sous droits d'auteur

buckling equations are made abundantly clear and distinct to the reader. Actually, the confusion originates by virtue of the actions of some who think they know how to 'get' buckling equations, but in fact do not understand the fundamentals of buckling and therefore make questionable and misleading statements to justify the equations they derive (which might be correct, but are not logically derived).

With the buckling differential equations and boundary conditions, we will examine the influence on the buckling load of the following factors:

- classical buckling and support conditions (first-order problems)
- prebuckling deformations
- large-deflection behavior (postbuckling behavior)
- shear deformation (bars only)
- initial geometric imperfections
- restrained thermal expansion
- eccentric stiffening (shells only)
- laminated fiber-reinforced composite materials (plates and shells)
- plastic deformation

Not all of the foregoing factors will be studied for each structural element. However, we will always find the influence of (large-deflection) postbuckling behavior to determine or assess the physical and practical significance of the Euler buckling load. Finally, we will address some significant aspects of design against buckling for each structural element.

The three fundamental book topics of bar, plate, and shell buckling will be put into a general perspective in Chapter Five. Also, some other buckling issues are raised in preparation for further study. Finally, our essentially analytical approach to the rather restricted behavior of the three basic structural elements will be related to current numerical techniques for finding buckling loads for structures with more complex geometry and loading than the simple elements in this book. In addition, appendices are provided on mechanics of composite materials and structures as well as on elements of design philosophy plus some essential mathematics related to minima of functions (such as buckling loads). You are reminded of the note in the preface to reread this chapter periodically as you work through the book so you will appreciate the unifying aspects of this chapter and understand buckling even better.

CHAPTER 1 REFERENCES

1-1 Leonhard Euler, On the Strength of Columns, *Academie Royale des Sciences et Belle Lettres Memoires*, Volume 13, p. 252, 1759. English translation by A. J. Van den Broek, Euler's Classic Paper 'On the Strength of Columns', *American Journal of Physics*, Volume 15, Number 4, July–August 1947, pp. 309–318.

1-2 K. O. Friedrichs, On the Minimum Buckling Load for Spherical Shells, *Theodore von Kármán Anniversary Volume*, California Institute of Technology, Pasadena, California, 11 May 1941, pp. 258–272.

1-3 Stephen P. Timoshenko, *History of Strength of Materials*, McGraw-Hill, New York, 1953, pp. 30–36. Reprinted by Dover Publications, New York, 1983.

1-4 N. J. Hoff, Buckling and Stability, The Forty-First Wilbur Wright Memorial Lecture, Fourth Anglo-American Aeronautical Conference, London, 14 September 1953, *Journal of the Royal Aeronautical Society*, Volume 58, Number 517, January 1954, pp. 3–52.

Éléments sous droits d'auteur

1-5 Stephen P. Timoshenko and James M. Gere, *Theory of Elastic Stability*, Second Edition, McGraw-Hill, New York, 1961.

1-6 James G. Crose and Robert M. Jones, *SAAS III, Finite Element Stress Analysis of Axisymmetric and Plane Solids with Different Temperature-Dependent Orthotropic Materials Properties in Tension and Compression*, The Aerospace Corporation, San Bernardino, California, TR-0059(S6816-53)-1, June 1971.

1-7 L. A. Harris, H. S. Suer, and W. T. Skene, Modal Investigations of Unstiffened and Stiffened Circular Shells, *Experimental Mechanics (Proceedings of the Society for Experimental Stress Analysis)*, Volume 18, Number 2, July 1961, pp. 1–9. See also Leonard A. Harris, Herbert S. Suer, William T. Skene, and Roland J. Benjamin, The Stability of Thin-Walled Unstiffened Circular Cylinders under Axial Compression Including the Effects of Internal Pressure, *Journal of the Aeronautical Sciences*, Volume 24, Number 8, August 1957, pp. 587–596.

1-8 Warner Tjardus Koiter, *Over de Stabiliteit van het Elastisch Evenwicht*, thesis, Technical Institute - Delft, H. J. Paris, Amsterdam, 1945. English translations, *On the Stability of Elastic Equilibrium*, available as NASA TT-F-10833, National Aeronautics and Space Administration, Washington, D. C., 1 March 1967 and as AFFDL-TR-70-25, Air Force Flight Dynamics Laboratory, Wright-Patterson Air Force Base, Ohio, February 1970.

1-9 W. T. Koiter, Elastic Stability and Post-Buckling Behavior, pp. 257–275, in *Nonlinear Problems*, Edited by Rudolph E. Langer, Proceedings of a Symposium Conducted by the Mathematics Research Center, 30 April–2 May 1962, Publication Number 8 of the Mathematics Research Center, United States Army, The University of Wisconsin, The University of Wisconsin Press, Madison, 1963.

1-10 John W. Hutchinson and John C. Amazigo, Imperfection Sensitivity of Eccentrically Stiffened Cylindrical Shells, *AIAA Journal*, Volume 5, Number 3, March 1967, pp. 392–401.

1-11 J. W. Hutchinson and W. T. Koiter, Postbuckling Theory, *Applied Mechanics Reviews*, Volume 23, Number 12, December 1970, pp. 1353–1356.

1-12 Robert M. Jones, Reflections on the Importance of Experimental Results to All Mechanicists, Especially Theoreticians, *Recent Advances in Experimental Mechanics - In Honor of Isaac M. Daniel*, Kluwer Academic Publishers, Amsterdam, 2002, pp. 537–550.

1-13 D. C. Drucker, On the Role of Experiment in the Development of Theory, *Proceedings of the 4th U. S. National Congress of Applied Mechanics*, 1962, pp. 15–33.

1-14 J. Singer, The Status of Experimental Buckling Investigations of Shells, *Buckling of Shells*, Proceedings of a State-of-the-Art Colloquium, 6–7 May 1982, Universität Stuttgart, edited by E. Ramm, Springer-Verlag, Berlin, Heidelberg, and New York, 1982, pp. 501–533.

1-15 J. Singer, Buckling Experiments on Shells—a Review of Recent Developments, presented at Euromech Colloquium Number 128, *Stability, Buckling and Postbuckling Behavior; Foundations and Analysis*, Delft, 30 March – 2 April 1980, *Solid Mechanics Archives*, Volume 7, Issue 3, Martinus Nijhoff, The Hague, 1982, pp. 213–313.

1-16 J. Singer, J. Arbocz, and T. Weller, *Buckling Experiments: Experimental Methods in Buckling of Thin-Walled Structures, Volume 1, Basic Concepts, Columns, Beams and Plates*, Wiley, Chichester, United Kingdom, 1998. *Volume 2, Shells, Built-up Structures, Composites and Additional Topics*, Wiley, New York, 2002.

1-17 B. O. Almroth, A. M. C. Holmes, and D. O. Brush, An Experimental Study of the Buckling of Cylinders Under Axial Compression, *Experimental Mechanics*, Volume 4, Number 9, September 1964, pp. 263–270.

1-18 *Webster's New World Dictionary*, Second College Edition, David B. Guralnik, Editor in Chief, Prentice Hall Press, 1984.

1-19 Robert M. Jones, *Mechanics of Composite Materials*, Second Edition, Taylor & Francis, Philadelphia, 1999, pp. 121–131.

1-20 Henry Petroski, The Fall of Skyscrapers, *American Scientist*, Volume 90, Number 1, January-February 2002, pp. 16–20.

1-21 Pierre Sparaco (a reporter), France, U. S. Probe CDG Passenger Screening, *Aviation Week & Space Technology*, Volume 156, Number 1, 7 January 2002, pp. 37–38.

1-22 Henry L. Langhaar, *Energy Methods in Applied Mechanics*, Wiley, New York, 1962. Reprinted by Krieger, Malabar, Florida, 1989.

Éléments sous droits d'auteur

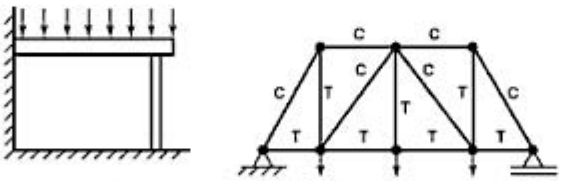
Chapter 2

BUCKLING OF BARS

2.1 INTRODUCTION

Slender axial-load-carrying members called bars or columns (the vertically upright form of a bar) occur in many forms in structures as shown in Figure 2-1. The building column in Figure 2-1a must be designed not to buckle because, as we will learn, the buckling load is the limit of the load-carrying capacity of the column. The top bars or struts in the truss in Figure 2-1b and the diagonal bars are in compression (C) and similarly limit the load-carrying capacity of the truss. The other bars in Figure 2-1b are in tension (T), so they do not buckle. Our objective is to determine how to find the maximum load-carrying capacity of bars that buckle so we can design practical structures that perform their function.

We will examine several approaches to calculating the buckling load of an initially straight bar. Some of the methods are deceptively simple because of the apparently simplistic nature of the bar buckling problem. However, plate and shell buckling problems are inherently more complex and thus require analysis procedures that enable us to treat those complexities effectively and clearly. Thus, we will use the bar buckling problem to explore methods to find an approach with the essential clarity and effectiveness to treat all buckling problems in an easily understood manner. That ultimate approach involves a nonlinearity and energy principles.



a Building Column b Truss Bars in Compression

Figure 2-1 Common Bars that Buckle

Éléments sous droits d'auteur

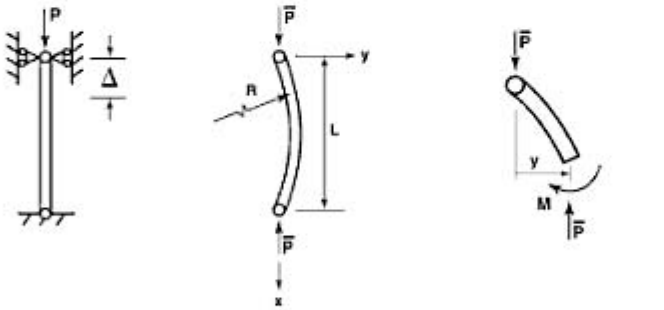
We start with the classical Euler column or bar buckling problem that is traditionally treated in introductory mechanics of materials courses. We also find how bars behave after buckling occurs to establish the significance of the bar buckling load in design applications. Then, energy concepts of buckling are introduced and used to derive a buckling differential equation with its consistent boundary conditions as well as energy integrals that are useful in approximate buckling analysis. In addition to studying the buckling of initially straight elastic bars, we will consider other important effects on bar buckling. The transverse shear force that develops during buckling is accounted for. If the bar is not straight prior to buckling, we must determine the influence of the initial geometric imperfections. The effect of restraining thermal expansion is also sought. If the material from which the bar is made can deform inelastically prior to buckling (i.e., a nonlinear stress-strain curve exists such as that for aluminum), then we find the effect of plastic deformation. Finally, we give some guidance for design of bars against buckling.

2.2 EULER'S COLUMN EQUATION

The fundamental solution to the bar buckling problem was obtained by Leonhard Euler (1707–1783) who investigated the mathematical problem of the stability of a flexible column or bar under axial end load [2-1]. Various boundary conditions are possible at the ends of the bar and will be examined to find their effect on the buckling load. Some aspects of this section were, perhaps, studied in a fundamental mechanics of materials course, but this treatment is at a higher level and involves definition of terms and concepts that will be explored in later problems.

2.2.1 Buckling of an Axially Compressed Bar with Pinned Ends

Consider the buckled axially loaded slender bar with simply supported (pinned) ends in Figure 2-2a. The bar has the usual pinned support at the bottom end. At the top end, the mechanism shown permits rotation, so is called a pinned end. However, to make the support not collapse, lateral movement is prevented by the two roller systems that permit only vertical movement. Without that vertical movement, no load



a Actual Support b Idealized Support c Free-Body Diagram

Figure 2-2 Axially Loaded, Pin-Ended, Initially Straight Bar

Éléments sous droits d'auteur

can be introduced in the bar nor can the bar buckle! That is, the bar can *not* be supported at the top with a pinned support like the one at the bottom of Figure 2-2a because *the bar could then not shorten or buckle* —all the applied load would be reacted at the top support, and no load would reach the bar! The bar cross section has two axes of symmetry: either the y-axis or the implied z-axis in Figure 2-2. Initially, we consider the bar to buckle in the plane of the paper, i.e., the x-y plane in Figure 2-2, but the arguments apply equally well to buckling in the x-z plane. We will see that the plane in which the bar actually buckles is determined by the least second moment of the area of the bar cross section.

Note that a beam is a structural member that bends under lateral loads whereas a bar is a structural member that extends or compresses under axial load. We focus on bars subjected to axially compressive load, so extension is not possible. A bar bends only *after* the buckling load, P, is reached (otherwise, it is a beam-column or beam-bar).

Initially, the bar is idealized as being perfectly straight, even under some low axial loading, P. We investigate the tendency of the bar, after bowing away from straightness, to return to the original straight equilibrium configuration. That is, we investigate the stability of the straight equilibrium configuration to find the load at which the bar buckles from the straight configuration to a nonstraight equilibrium configuration as in Figure 2-2b. In addition, we would like to determine the shape of the nonstraight equilibrium configuration. To achieve those two objectives, we determine the minimum load under which the bar remains in a nonstraight, i.e., bent or buckled, configuration described with some function y(x) in which y is the transverse deflection describing the buckled shape.

Note that the straight bar, when subjected to loads below the buckling load, merely shortens in the axial direction and has no transverse deflection, y. Thus, y(x) is a *buckling deflection* (a deviation from initial straightness) that occurs only after the buckling load is reached, and not a total displacement, although the buckling deflection and the total transverse displacement are identical for this initially perfectly straight bar (In more general situations, the total transverse deflection and the buckling deflection are not identical). Accordingly, we seek the solution to a very special type of problem, called an *eigenvalue problem*, in which the load, called the *eigenvalue* or *characteristic value*, at which the bar buckles into some buckled shape, called an *eigenvector*, only when the characteristic value of the load is reached. Below that characteristic load, the straight bar simply shortens in the axial direction as the load increases.

We examine the equilibrium of the bar in a bent configuration to see if that bent configuration can exist and is stable. We can *regard the buckling load as causing a disturbing moment to the bent bar.* The bar provides some inherent restoring moment caused by its bending stiffness (resistance to bending). If the restoring moment exceeds the disturbing moment, then the bar will return from the disturbed state to the straight equilibrium state. That is, the bar is in stable equilibrium when it is bent, but at a low enough load that the restoring moment returns the bar to straightness. If the load is large enough that the disturbing moment exceeds the restoring moment, then the bar is unstable and buckles (i.e.,

Éléments sous droits d'auteur

remains in the bent state). Next, we ask if the load gets large enough that the restoring moment just equals the disturbing moment, then what is the significance of that load? We call that load the buckling load. The point of this discussion is that we must have a physical reason for why we are solving a specific equation. That is, what led us to that equation in a logical, explainable manner? In this case, we explore the restoring moment and its relation to the disturbing moment.

The centerline of a bent bar has curvature, ρ, for which the exact expression in terms of the transverse (buckling) deflection $y(x)$ is

$$\rho = \frac{1}{R} = \frac{\pm y''}{\left[1 + (y')^2\right]^{3/2}} \tag{2.1}$$

in which R is the radius of curvature and the prime denotes a derivative with respect to x. If $y(x)$ is zero, then the column has not buckled! For small slopes, $(y')^2 << 1$, i.e., the square of a small quantity less than unity is even smaller than the small quantity itself. For example, if the slope were even as large as .1, then $(.1)^2 = .01$, so the square of the slope is quite negligible compared to unity (an error of only 1%). Thus, Equation (2.1) reduces to the linear approximation

$$\rho = \frac{1}{R} = \pm y'' \tag{2.2}$$

which is a most appropriate approximation because *we need only the slightest deviation from straightness for buckling to occur.* With only a slight deviation from initial straightness, the slope, y', is quite small.

For a beam under pure bending, i.e., in which the axial shortening, shearing deformations, and beam weight are neglected, the bending moment is related to the beam curvature by the well-known expression

$$\frac{M}{EI} = -\rho \tag{2.3}$$

which, if Equation (2.2) is substituted, becomes

$$EIy'' = \pm M \tag{2.4}$$

which is the differential equation for bending of a beam in which I is the second moment of the beam cross-sectional area (also called the moment of inertia) about the beam cross-sectional axis that is perpendicular to the plane of bending. The ambiguity in the sign of Equation (2.4) is resolved by determining whether a positive moment causes a positive or a negative curvature in the coordinates of the problem. In the first case, the sign of Equation (2.4) is positive and in the second case negative. Alternatively, a positive moment can be defined as one that is associated with positive curvature so the sign of Equation (2.4) is always positive. We choose the first approach and must always determine the sign of Equation (2.4) by examination.

For the present problem, with the sign convention in Figure 2-2, the moment at any point along the length of the bent bar is

$$M = Py \tag{2.5}$$

Thus, the disturbing moment is $\overline{Py}$, and the restoring moment is EIy'', so

Éléments sous droits d'auteur

the differential equation for buckling becomes

$$EIy'' = -\bar{P}y \tag{2.6}$$

in which I is the second moment of the bar cross-sectional area about the bar cross-sectional axis that is perpendicular to the plane of buckling. For problems, such as the present, in which the bar bends only after a certain load, $\bar{P}$, is reached, we seek the value of that specific load, called the buckling load, that causes the bending or buckling away from the straight bar shape. If we substitute

$$k^2 = \frac{\bar{P}}{EI} \tag{2.7}$$

then the differential equation becomes

$$y'' + k^2 y = 0 \tag{2.8}$$

Equation (2.8) is the eigenvalue equation or homogeneous differential equation in canonical form (the coefficient of the highest derivative is one) for the present problem. The differential equation is termed homogeneous because the right-hand side is zero. Also, the boundary conditions on the deflection function y have zero values, i.e., $y = 0$ (because the deflection is zero at the ends of the bar) and $y'' = 0$ (because the moment is zero at the ends). However, we do not use the fact that the moment is zero at the bar ends in the solution because the differential equation is of second order (no boundary condition can be applied that is of the same order as the highest derivative in the differential equation).

The general solution to the differential equation is

$$y = A \sin kx + B \cos kx \tag{2.9}$$

in which A and B are constants that are determined (qualitatively, but not quantitatively) from the boundary conditions. The boundary conditions of zero deflection at each end of the bar lead to

$$y(0) = 0 \quad \rightarrow \quad B = 0 \tag{2.10}$$

$$y(L) = 0 \quad \rightarrow \quad A \sin kL = 0 \tag{2.11}$$

Thus, either $A = 0$ or $\sin kL = 0$. However, A cannot be zero because B is already zero, so there would be no amplitude in the buckling deflection of Equation (2.9), i.e., the bar would not buckle. That solution is obviously uninteresting from the physical standpoint and is called the *trivial solution*. The solutions to the *characteristic equation* (the equation whose solution is the characteristic value or eigenvalue) $\sin kL = 0$ are

$$kL = n\pi \qquad n = 1, 2, \ldots \tag{2.12}$$

and are called the characteristic values or eigenvalues of the problem. Negative values of n are also a solution to Equation (2.11), but are not physical solutions to our problem. The characteristic equation results from substitution of the boundary conditions in the general solution to the differential equation. Thus, if k, Equation (2.7), is substituted, then the buckling loads, P_E or $\bar{P}$ (used interchangeably in this book), are

$$P_E = \bar{P} = n^2\pi^2 \frac{EI}{L^2} \qquad n = 1, 2, \ldots \tag{2.13}$$

Éléments sous droits d'auteur

Note that the buckling load is P_E, but do not refer to P_E as the 'critical' buckling load because that style of reference is redundant, hence improper. That is, P_E is the critical load *or* the buckling load, but *not* the critical buckling load. The lowest value of the infinite number of values of P_E occurs for $n = 1$, i.e.,

$$P_E = \pi^2 \frac{EI}{L^2} \qquad (2.14)$$

which is the *classical Euler column equation*. The buckling mode shapes for $n = 1$ and higher values of n, the number of half sine waves (buckles in this case), are shown in Figure 2-3. Recall that the mode shapes with $n = 2$ and higher are possible only if the column is physically constrained from buckling into all lower modes. For example, if a column cannot move transversely at its midlength, then the $n = 1$ buckling mode is not possible, and the column must buckle into the $n = 2$ buckling mode.

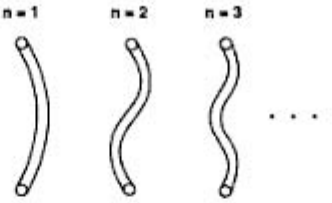


Figure 2-3 Buckling Mode Shapes

Note that the column mid-length location for $n = 2$ does not move transversely (but does, however, rotate). That point is called a *nodal point*. The nodal points for a column, e.g., for $n = 2$ and $n = 3$ (at the third points of the bar) in Figure 2-3, are theoretically possible from the solution, but are practically possible only if physical constraint against buckling in a lower mode is provided because the $n = 2$ mode occurs at a higher buckling load (by a factor of 4) than the $n = 1$ mode. Higher modes than for $n = 2$ occur at even higher buckling loads.

Some additional comments on the Euler solution are appropriate. The eigenvector corresponding to the lowest eigenvalue is

$$y = A \sin \frac{\pi x}{L} \qquad (2.15)$$

The constant A, the amplitude of the half-sine wave, in Equation (2.15) is indeterminate because we have no equation left from which we can calculate A. The indeterminate status of A is characteristic of all eigenvalue problems wherein we find the eigenvalue (buckling load) and the eigenvector (buckling mode shape), but we cannot find the amplitude of the buckling mode shape. Large-deflection equilibrium theory is required if the actual magnitude of deflection after buckling is desired (see Section 2.4). Here, buckling is defined as the sudden departure from the original stable equilibrium loading path at a well-defined load, e.g., the departure from initial straightness of the axially loaded bar. Thus, a small increment in load produces a large increment in transverse displacement.

The applicability of Euler's column equation is also limited by the maximum stress at buckling. That maximum stress must be in the elastic range of the material or else alternative methods must be used in which plastic deformation is considered. Thus, the Euler column equation must also be expressed in terms of stresses. To do so, we first define the *radius of gyration of the cross section, r*, to be

$$r = \sqrt{I/A} \qquad (2.16)$$

Éléments sous droits d'auteur

in which I is the second moment of the bar cross-sectional area (also called the moment of inertia) about the cross-sectional centroidal axis perpendicular to the plane of buckling and A is the area of the bar cross section. Physically, the radius of gyration is the distance from the bending axis that the area, A, is concentrated as a 'lump' to yield the second moment of the area, $I = Ar^2$, by the parallel-axis theorem of geometry. A structural interpretation is that r is a measure of the bending stiffness relative to the extensional stiffness of the bar cross section. That is, the higher the r, the more I is obtained from the same cross-sectional area. For example, the cross section of an I-beam has a much higher I than does a rectangular cross section of the same area. Thus, a bar with a higher r has an improved bending efficiency relative to its extensional efficiency, an important attribute for a bar subjected to axial loading because bending stiffness governs the buckling load in Equation (2.14). Then, with the radius of gyration definition, the Euler column equation can be written as

$$\sigma_E = \sigma_{cr} = \frac{P_E}{A} = \frac{\pi^2 E}{(L/r)^2} \tag{2.17}$$

Note that the buckling stress goes to zero as the slenderness ratio, L/r, increases, i.e., as the bar becomes more and more slender in Figure 2-4. As L/r decreases, i.e., as the bar becomes shorter and fatter, σ_E increases and is not valid for $\sigma_E > \sigma_y$ where σ_y is the yield stress of the material. The buckling load for stresses above the yield stress will be determined in Section 2.10. That is, slender columns or bars buckle elastically, whereas nonslender columns might buckle at stresses above the yield stress or could crush or deflect excessively in the axial direction.

Note that the force P throughout this section is stipulated to always remain vertical. Thus, the external forces are conservative, i.e., the work done while moving from configuration A to configuration B of a mechanical system is independent of path. If P were to always remain tangent to the end of the bar, then the work done would be path-dependent, and hence the loading would be nonconservative. This loading situation is called the follower-force problem, supposedly arises with non-gimballing rocket engines, and is briefly described in Chapter 5.

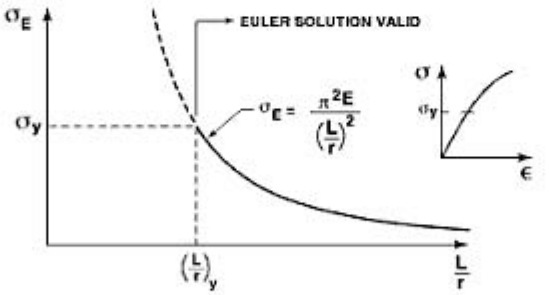


Figure 2-4 Buckling Stress versus Slenderness Ratio

Éléments sous droits d'auteur

2.2.2 Buckling of an Axially Compressed Fixed-Pinned Bar

Next, the support conditions of a bar are one end fixed with the other end pinned. The (upper) pinned end must be a special support that allows vertical movement to accept the axial load and also does not restrict rotation. If the pinned end did not permit axial movement, then no load could be developed in the bar! The reacting forces, R and P, and reacting moment, M_o, caused by applied load, $\bar{P}$, at the upper end (the origin) act as in Figure 2-5. The force R and moment M_o occur, of course, only after buckling. At any point along the bar, the disturbing moment is

$$M = \bar{P}y - Rx \qquad (2.18)$$

so the differential equation from Section 2.2.1 becomes

$$y'' + k^2 y = \frac{R}{EI}x = b^2 x \qquad (2.19)$$

in which $k^2 = \bar{P}/EI$ and $b^2 = R/EI$. The general solution is

$$y = A \sin kx + B \cos kx + Cx \qquad (2.20)$$

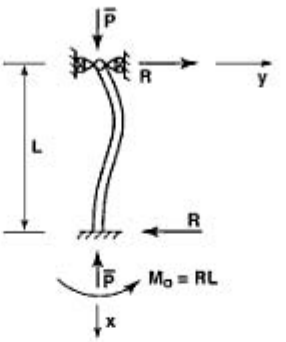


Figure 2-5 Axially Compressed Bar with One End Fixed and One End Pinned

in which $C = b^2/k^2$. Apply the three boundary conditions on y and y':

$$y(0) = 0 \quad \rightarrow \quad B = 0 \qquad (2.21)$$

$$y(L) = 0 \quad \rightarrow \quad A \sin kL + CL = 0 \qquad (2.22)$$

$$y'(L) = 0 \quad \rightarrow \quad Ak \cos kL + C = 0 \qquad (2.23)$$

A fourth apparent boundary condition of zero moment (thus, $y'' = 0$) at the pin cannot be used because the differential equation is second order. A nontrivial solution to the homogeneous simultaneous equations, Equations (2.22) and (2.23), exists only if the determinant of the coefficients of A and C is zero (A and C cannot be zero because then $y = 0$), so

$$kL = \tan kL \qquad (2.24)$$

which is a transcendental characteristic equation (i.e., the right-hand side is a function of the left-hand side, so a direct solution is not possible). By trial and error, the lowest value of kL is 4.493, so the eigenvalue is

$$\bar{P} = P_E = (4.493)^2 \frac{EI}{L^2} = 20.19 \frac{EI}{L^2} = 2.046\,\pi^2 \frac{EI}{L^2} \qquad (2.25)$$

and the eigenvector is

$$y = \frac{M_o}{\bar{P}}\left[\frac{x}{L} + 1.024 \sin\left(4.493 \frac{x}{L}\right)\right] \qquad (2.26)$$

in which the amplitude $M_o/\bar{P}$ is indeterminate as is the reaction R. Note the 105% increase in buckling load over the pinned lower end case in Section 2.2.1.

Éléments sous droits d'auteur

2.2.3 Buckling of an Axially Compressed Fixed-Fixed Bar

Next, a bar has both ends fixed against rotation, but the upper end is allowed to move vertically to accept the axial load. The reacting force, $\bar{P}$, and reacting moments, M_o, that develop after buckling caused by force $\bar{P}$ applied at the upper end are shown in Figure 2-6. At any point along the bar, the disturbing moment is

$$M = Py - M_o \qquad (2.27)$$

so the governing differential equation from Section 2.2.1 becomes

$$y'' + k^2 y = \frac{M_o}{EI} \qquad (2.28)$$

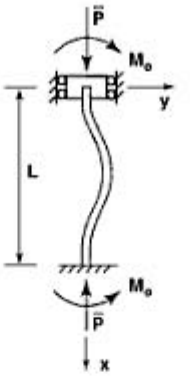


Figure 2-6 Axially Loaded Bar with Both Ends Fixed

with general solution

$$y = A \sin kx + B \cos kx + \frac{M_o}{EI}\frac{1}{k^2} \qquad (2.29)$$

Apply the boundary conditions on y and y' at each end of the bar to find the values of A, B, and M_o. At the upper end, x = 0,

$$y(0) = 0 \rightarrow B = -\frac{M_o}{EI}\frac{1}{k^2} \qquad (2.30)$$

$$y'(0) = 0 \rightarrow A = 0 \qquad (2.31)$$

At the lower end, x = L,

$$y(L) = 0 \rightarrow \cos kL = 1 \rightarrow k = \frac{n\pi}{L},\ n \text{ even} \qquad (2.32)$$

$$y'(L) = 0 \rightarrow \sin kL = 0 \rightarrow k = \frac{n\pi}{L},\ n \text{ even or odd} \qquad (2.33)$$

The value for n must satisfy both conditions in Equations (2.32) and (2.33), so the lowest buckling load occurs at n = 2. The eigenvalue is

$$\bar{P} = P_E = 4\pi^2 \frac{EI}{L^2} \qquad (2.34)$$

and the eigenvector is

$$y = B\left[\cos\frac{2\pi x}{L} - 1\right] \qquad (2.35)$$

Note that the buckle amplitude B is expressed in terms of M_o, an unknown, so the amplitude is indeterminate, as usual. Thus, replacing the upper pinned end in Section 2.2.2 with a fixed end results in nearly twice as great a buckling load (96% greater). Also, this buckling load is four times as great as when both ends are pinned as in Section 2.2.1.

Éléments sous droits d'auteur

2.2.4 Buckling of an Axially Compressed Fixed-Free Bar

Consider a bar with the lower end fixed against rotation, but the upper end is free. The reacting force, $\bar{P}$, and reacting moment, $M_o = \bar{P}\Delta$, that develops after buckling caused by the force P applied at the upper end are shown in Figure 2-7 along with the deflected shape with amplitude Δ. At any point along the bar, the disturbing moment can be shown to be

$$M = -Py + (M_o = P\Delta) = P\Delta - Py \quad (2.36)$$

so the differential equation governing buckling from Section 2.2.1 becomes

$$y'' + k^2 y = k^2 \Delta \quad (2.37)$$

with general solution

$$y = A \sin kx + B \cos kx + \Delta \quad (2.38)$$



Figure 2-7 Axially Compressed Bar with One End Fixed and One End Free

Apply the boundary conditions at each end of the bar to find the values of A, B, and Δ. At the lower end (x = 0),

$$y(0) = 0 \rightarrow 0 = A \sin 0 + B \cos 0 + \Delta \rightarrow B + \Delta = 0 \quad (2.39)$$

$$y'(0) = 0 \rightarrow Ak \cos 0 - Bk \sin 0 \rightarrow A = 0 \quad (2.40)$$

At the free end (x = L),

$$y(L) = \Delta \rightarrow \Delta = B \cos kl + \Delta \rightarrow B \cos kL = 0 \quad (2.41)$$

If B were zero, the bar would not buckle because then A, B, and Δ would all be zero in Equation (2.38) (the trivial solution). Thus, the nontrivial solution (the characteristic equation) is

$$\cos kL = 0 \quad (2.42)$$

which has solutions

$$kL = n\frac{\pi}{2} \quad n = 1, 3, 5, \ldots \quad (2.43)$$

with smallest solution $kl = \pi/2$, so that the buckling load (eigenvalue) is

$$\bar{P} = P_E = \frac{\pi^2}{4}\frac{EI}{L^2} \quad (2.44)$$

and the eigenvector is

$$y = \Delta\left[1 - \cos\frac{\pi x}{2L}\right] \quad (2.45)$$

in which Δ, the buckling amplitude, is indeterminate, as usual. This buckling load is the lowest that we have studied so far (1/4 of the pinned-pinned bar load). Of course, a free end should, intuitively, lead to a lower buckling load than an end with some (any) type of support.

Éléments sous droits d'auteur

2.2.5 Buckling of a Pinned-Free Axially Compressed Bar with Elastically Restrained Ends

In engineering practice, a bar or beam end that is perfectly free, perfectly pinned, or perfectly fixed is rarely, if ever, found. Those end support conditions are merely idealizations of situations that are only approximately true. Instead, structural members are typically fastened to other structural members (to make a structure!) so that, under applied load, the tendency of one member to rotate at its end that is fastened to another member is restrained to some extent by that other member. Similarly, the tendency of a structural member to translate at its end that is fastened to another member is restrained by that other member. Such conditions are usually modelled with rotational springs and translational springs, respectively. These springs are often linear for usual structural members (e.g., $F = kx$ or $M = k\theta$), but they can also be nonlinear (e.g., $F = kx^2$ or $M = k\theta^3$, etc.). We treat only linear elastic springs in this book.

Consider an axially loaded bar with its lower end pinned and upper end free, but the upper end is restrained from translation by a translational spring with spring constant α and the lower end is restrained from rotation by a rotational spring with spring constant β as in Figure 2-8. The rotational spring moment is, by statics,

$$M_\beta = \bar{P}\Delta - \alpha\Delta L \qquad (2.46)$$

in which Δ is the horizontal deflection of the upper end. At any point, x, along the bar, the disturbing moment is

$$M = \bar{P}(\Delta - y) - \alpha\Delta x \qquad (2.47)$$

so the differential (constitutive) equation of Section 2.2.1, Equation (2.4), becomes

$$y'' + k^2 y = k^2\left(\Delta - \frac{\alpha\Delta x}{\bar{P}}\right) \qquad (2.48)$$

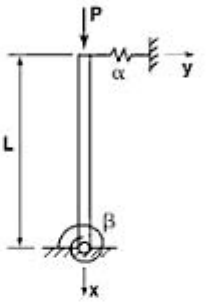


Figure 2-8 Pinned-Free Bar under Axial Compressive Load with a Rotational Spring and a Translational Spring

with general solution

$$y = A\sin kx + B\cos kx + \Delta - \frac{\alpha\Delta x}{\bar{P}} \qquad (2.49)$$

Apply the boundary conditions at each end of the bar to find the unknown constants of integration A, B, and Δ. At the upper end (x = 0),

$$y(0) = \Delta \;\rightarrow\; \Delta = A\sin 0 + B\cos 0 + \Delta \;\rightarrow\; B = 0 \qquad (2.50)$$

At the lower end (x = L),

$$y(L) = 0 \;\rightarrow\; 0 = A\sin kL + \Delta - \frac{\alpha\Delta L}{\bar{P}} \qquad (2.51)$$

$$y'(L) = \frac{M_\beta}{\beta} \;\rightarrow\; \frac{\bar{P}\Delta}{\beta} - \frac{\alpha\Delta L}{\beta} = Ak\cos kL - \frac{\alpha\Delta}{\bar{P}} \qquad (2.52)$$

or, after multiplying Equation (2.52) by β and rearranging, we get

Éléments sous droits d'auteur

$$A\beta k \cos kL + \alpha\Delta L - \bar{P}\Delta - \frac{\alpha\beta\Delta}{P} = 0 \qquad (2.53)$$

For a nontrivial solution to the two simultaneous homogeneous equations in A and Δ, Equations (2.51) and (2.53), (the third simultaneous equation, Equation (2.50), is satisfied trivially by B = 0), the determinant of the coefficients of A and Δ must be zero, i.e.,

$$\begin{vmatrix} \sin kL & 1 - \dfrac{\alpha L}{P} \\ \beta k \cos kL & \alpha L - \bar{P} - \dfrac{\alpha\beta}{P} \end{vmatrix} = 0 \qquad (2.54)$$

Simplify the determinant by multiplying the second column by P and then expand the determinant to get, after substituting $k^2 = P/EI$,

$$\sin kL \left[k^2 \alpha L EI - k^4 (EI)^2 - \alpha\beta\right] - \beta k \cos kL \left[k^2 EI - \alpha L\right] = 0 \qquad (2.55)$$

which is the characteristic equation of the title problem.

The effect of elastic rotational restraint must yield a buckling load which is between that for a pinned end and that for a fixed end. Similarly, the effect of elastic translational restraint must yield a buckling load which is between that for a free end and that for an end that is perfectly restrained from translation. Thus, we already know the upper and lower bounds on the solution of a problem with elastic restraints. Often, the lower-bound solution is used in design to conservatively estimate the actual capability (although this approach can be so overly conservative as to waste material in many cases) and to avoid the effort of estimating or evaluating the quantitative nature of the actual elastic restraint.

2.2.6 Buckling of a Pinned-Free Axially Compressed Bar with an Elastic Translational Spring at the Free End

Consider a special case of the bar with elastically restrained ends in Section 2.2.5, namely, an axially loaded bar pinned at one end and elastically restrained from motion transverse to the bar at the other end by a linear translational spring with stiffness, α, as in Figure 2-9. The characteristic equation is obtained from the more general result in Equation (2.55) by removing the rotational spring ($\beta = 0$):

$$\sin kL \left[k^2 \alpha L EI - k^4 (EI)^2\right] = 0 \qquad (2.56)$$

Next, divide by k^2 and EI, both of which are never zero, to get

$$\sin kL \,(\alpha L - \bar{P}) = 0 \qquad (2.57)$$

in which $k^2 = \bar{P}/EI$ is used. The characteristic equation root $\sin kL = 0$ with solution $kL = n\pi$ leads to the usual Euler bar buckling result

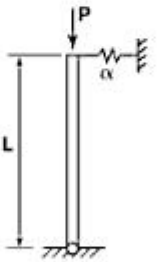


Figure 2-9 Pinned-Free Bar under Axial Compressive Load with a Translational Spring

Éléments sous droits d'auteur

$$\bar{P} = n^2\pi^2 \frac{EI}{L^2} \tag{2.58}$$

However, sin kL = 0 is not necessarily the lowest root of Equation (2.57)! We consider the bar properties to be specified and increase the spring stiffness, α, from zero. The lowest root of Equation (2.57) is

$$\bar{P} = \alpha L \tag{2.59}$$

Obviously, if no translational spring exists (i.e., if $\alpha = 0$), then the bar immediately rotates as a rigid body with no buckling load. Next, α can increase until P reaches the first Euler buckling load, namely,

$$\alpha L = \pi^2 \frac{EI}{L^2} \tag{2.60}$$

at which load the bar buckles equally well as an Euler column or bar with both ends pinned because the spring provides effectively rigid translational support (plus no rotational resistance).

Above a spring stiffness of $\alpha = P_E/L$, the lowest buckling load is still P_E *irrespective of any increase in spring stiffness* because then the lowest root of the characteristic equation is the usual Euler column result as in Figure 2-10 in which the normalized buckling load is plotted against the normalized spring stiffness. We call

$$\alpha = \pi^2 \frac{EI}{L^3} \tag{2.61}$$

the *critical spring stiffness* because that value is the minimum value to force buckling as a pinned-pinned bar. Again, that spring stiffness need not be exceeded—any increase is a waste of resources.

Thus, as α increases from zero, $\bar{P}$ increases linearly in Figure 2-10 until $\bar{P} = P_E$ when α has reached $\alpha = \pi^2 EI/L^3$. However, if α increases above $\pi^2 EI/L^3$, $\bar{P}$ is still only P_E because the bar then buckles into the pinned-pinned bar first buckling mode, i.e., a constant $\bar{P} = \pi^2 EI/L^2$. Thus, $\alpha_{cr} = \pi^2 EI/L^3$ is the minimum spring stiffness to cause this buckling mode change, so it is called the critical spring stiffness.

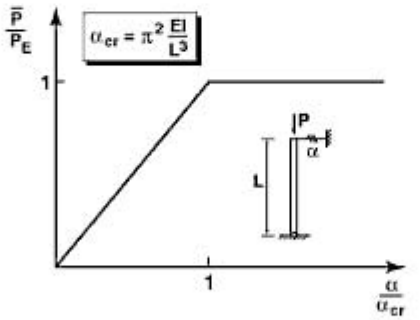


Figure 2-10 Effect of Translational Spring Constant on Buckling of an Axially Compressed Pinned-Free Bar

Éléments sous droits d'auteur

2.2.7 Buckling of a Pinned-Pinned Axially Compressed Bar with a Mid-Span Transverse Spring

Consider an axially loaded bar with pinned ends and a translational linear elastic spring with stiffness, α, restraining it at mid-span as in Figure 2-11. Given our knowledge of the effect of a translational spring from Section 2.2.6, find the critical spring stiffness for this problem.

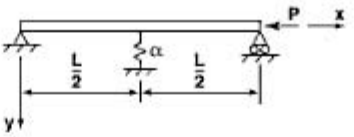


Figure 2-11 Pinned-Pinned Bar under Axial Compressive Load with a Mid-Span Transverse Spring

For a small spring stiffness, we presume that the bar will buckle in a *perturbed* symmetric half-sine-wave buckling mode shown in Figure 2-12 because the half-sine-wave shape is the buckling mode when no spring exists. We should also expect from Section 2.2.6 that if the spring is stiff enough, then it will completely restrain transverse movement at mid-span so that the bar buckles into the second (antisymmetric) mode of two half-sine waves. The minimum value of "stiff enough" is the critical spring stiffness that we seek.

For a small mid-span deflection, Δ, the spring force is $R = \alpha\Delta$ with resulting transverse reactions at each support of R/2. Thus, the moment at any point x for $0 < x < L/2$ is

$$M = \bar{P}y - \frac{R}{2}x \qquad (2.62)$$

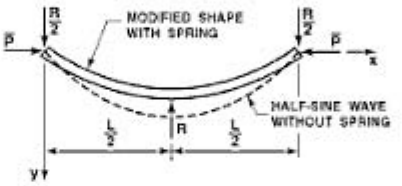


Figure 2-12 Free-Body Diagram of the Buckled Bar

so the constitutive relationship $M = -EIy''$ (the bar bends only if it has buckled) leads to the differential equation governing buckling:

$$EIy'' + \bar{P}y = \frac{R}{2}x \qquad 0 < x < \frac{L}{2} \qquad (2.63)$$

or in canonical form

$$y'' + k^2 y = \frac{R}{2EI}x \qquad (2.64)$$

(in which, as usual, $k^2 = \bar{P}/EI$) with a boundary condition of

$$y(0) = 0 \qquad (2.65)$$

and additional boundary conditions from the matching conditions for the solution to the differential equation in the region $L/2 < x < L$ of

$$y'(L/2) = 0 \qquad (2.66)$$

$$y(L/2) = \Delta \qquad (2.67)$$

The solution to the differential equation, Equation (2.64), is

$$y = A\sin kx + B\cos kx + \frac{1}{k^2}\frac{R}{2EI}x \qquad 0 < x < \frac{L}{2} \qquad (2.68)$$

Éléments sous droits d'auteur

Apply the boundary condition y(0) = 0:

$$0 = A \times 0 + B \times 1 + 0 \quad \rightarrow \quad B = 0 \tag{2.69}$$

so the deflected shape upon buckling is

$$y = A \sin kx + \frac{R}{2P} x \qquad 0 < x < \frac{L}{2} \tag{2.70}$$

which is a superposition of a linear buckling deflection term for the spring on the half-sine-wave shape of the buckled pinned-pinned bar. The effect of the linear term is largest at the center and decreases to zero as the left-hand end is approached as implied in Figure 2-12. This deflection effect is similar to that of a transverse force on *deflection* of a pinned-pinned *beam*, i.e., a bending problem, not a buckling problem. Then,

$$y' = Ak \cos kx + \frac{R}{2P} \tag{2.71}$$

so the solution-matching symmetry boundary condition y'(L/2) = 0 yields

$$0 = Ak \cos \frac{kL}{2} + \frac{R}{2P} \quad \rightarrow \quad A = -\frac{1}{k} \frac{R}{2P} \frac{1}{\cos \frac{kL}{2}} \tag{2.72}$$

leading to a deflection-during-buckling equation of

$$y = -\frac{1}{k} \frac{R}{2P} \frac{1}{\cos \frac{kL}{2}} \sin kx + \frac{R}{2P} x \tag{2.73}$$

Finally, apply the solution-matching boundary condition $y(L/2) = \Delta$ to get

$$-\frac{1}{k} \frac{R}{2P} \frac{1}{\cos \frac{kL}{2}} \sin \frac{kL}{2} + \frac{R}{2P} \frac{L}{2} = \Delta \tag{2.74}$$

but $R = \alpha\Delta$ and Δ is nonzero for buckling to occur, so divide by Δ to get

$$-\frac{1}{k} \frac{\alpha}{2P} \tan \frac{kL}{2} + \frac{\alpha}{2P} \frac{L}{2} = 1 \quad \rightarrow \quad \frac{\alpha}{2Pk} \left[\frac{kL}{2} - \tan \frac{kL}{2} \right] = 1 \tag{2.75}$$

Because $P = EI k^2$, we can write Equation (2.75) as

$$\frac{kL}{2} - 16 \frac{EI}{\alpha L^3} \left[\frac{kL}{2} \right]^3 = \tan \frac{kL}{2} \tag{2.76}$$

The roots of this transcendental characteristic equation, i.e., the values of kL/2 corresponding to a specified α, can be found numerically or graphically. We can plot each term in Equation (2.76) as a function of kL/2 to determine the solution. The first term, f(kL/2) = kL/2, is a straight line at 45° in Figure 2-13. The cubic term is a deviation downward from the straight line, and in combination with the linear term creates an upward rising then downward falling linear-cubic curve in Figure 2-13. Finally, the last term, f(kL/2) = tan kL/2, is a set of branches of curves of the same shape but offset from one another by period π. Only the cubic term is a function of α. The solution of the transcendental equation occurs where the left-hand side of Equation (2.76) (the linear-cubic curve) intersects the right-hand side (the tangent curves), and the intersection location depends on the value of α.

Éléments sous droits d'auteur

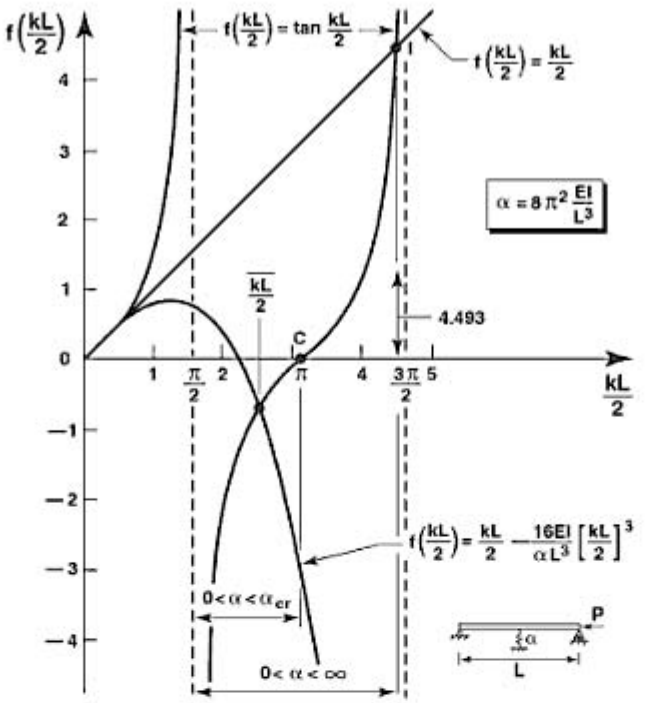


Figure 2-13 Graphical Representation of Solution Elements

Several categories of values of α are of interest:

1. If $\alpha = 0$, there is no spring and the coefficient of the cubic term is infinite so the cubic term of the linear-cubic expression on the left-hand side of Equation (2.76) dominates the behavior. The solution of $f(kL/2) = \tan kL/2 = -\infty$ is $kL/2 = \pi/2$ Thus, $k^2L^2 = \pi^2$ so we get the usual pinned-pinned bar without a spring result, namely $P = \pi^2 EI/L^2$.
2. As α increases, the cubic term in the linear-cubic expression decreases in importance, so the linear-cubic curve becomes less and less curved and approaches the linear term, $f(kL/2) = kL/2$.
3. For $\alpha = \infty$, the cubic term in the linear-cubic expression is zero, so the characteristic equation is

$$\frac{kL}{2} - 0 = \tan\frac{kL}{2} \tag{2.77}$$

with a root of $\overline{kL/2} = 4.493$ at point I in Figure 2-13 whereupon

$$\overline{P} = EIk^2 = EI\left[\frac{2}{L}4.493\right]^2 = 4 \times 4.493^2 EI/L^2 \tag{2.78}$$

Éléments sous droits d'auteur

However, if the spring were infinitely stiff, we would expect the mid-span immovability of the spring-supported bar to cause the bar to buckle into the second (antisymmetric) bar buckling mode (a full sine wave) (two half sine waves) at $\bar{P} = 4\pi^2 EI/L^2$ which is much lower than $P = 4(4.493^2)EI/L^2$. Obviously, the buckling behavior changes from the initial behavior in some manner at some α less than $\alpha = \infty$.

4. For the largest α that matters to us physically, i.e., the value of α necessary to force buckling into the second mode, the intersection occurs at point C in Figure 2-13. The intersection takes place where the bar buckles into the second mode for a pinned-pinned bar, i.e., $\bar{P} = 4\pi^2 EI/L^2$ or $kL/2 = \pi$. The corresponding α is found from

$$\left[\frac{kL}{2} = \pi\right] - \frac{16EI}{\alpha L^3}\left[\frac{kL}{2} = \pi\right] = \left[\tan\left[\frac{kL}{2} = \pi\right]\right] = 0 \qquad (2.79)$$

so the critical spring constant or stiffness is

$$\alpha_{cr} = 16\pi^2 \frac{EI}{L^3} \qquad (2.80)$$

If the spring stiffness α is α_{cr}, the bar buckles into the antisymmetric second mode. Increasing the spring stiffness α above α_{cr} will not change that basic fact and is a waste of material. That is, the spring stiffness α must be only α_{cr} to force that second-mode behavior.

5. For $\alpha = \alpha_{cr}/2 = 8\pi^2 EI/L^3$, the linear-cubic curve in Figure 2-13 intersects the tangent curve at $kL/2 = 2.519$ or $\bar{P} = 25.38EI/L^2$. This intersection is representative of all solutions for the problem.
6. The range of physically interesting values of α is $0 < \alpha < \alpha_{cr}$ between $kL/2 = \pi/2$ and $kL/2 = \pi$ for first-mode buckling in Figure 2-13.
7. Possible solutions of the transcendental equation are in the range $0 < \alpha < \infty$ as shown in Figure 2-13, but those above α_{cr} are not of practical importance because the bar buckles in the second mode.

The results of the solution process are presented in Figure 2-14. There, for $\alpha = 0$, the bar simply buckles as a pinned-pinned bar when P

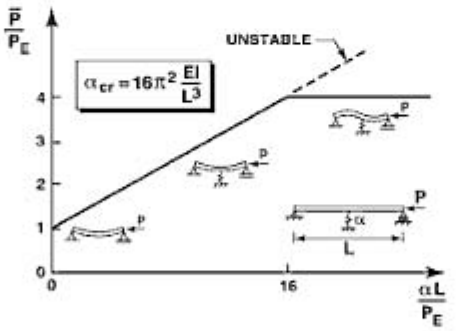


Figure 2-14 Buckling of a Pinned-Pinned Bar with a Mid-Span Transverse Spring

Éléments sous droits d'auteur

reaches $P_E = \pi^2 EI/L^2$. However, for increasing α, the buckling load increases in essentially a linear manner (the actual behavior is just a few percent above the straight line in Figure 2-14) with a diminished buckling mode amplitude until the critical spring constant is reached. Then, the bar buckles into the second mode at $\bar{P} = 4\pi^2 EI/L^2$ with no spring deflection irrespective of any increase in the value of α. That is, increasing α above the critical value α_{cr} has no effect on the buckling load.

Thus, a transverse support need not be perfectly rigid to force a bar to buckle into the second mode instead of the first mode. The support need only have the minimum or critical spring stiffness to raise the bar's axial buckling load. These considerations are significant in the assessment of, e.g., the buckling load of a two-story building column. There, the second floor need not be rigid in the horizontal plane but must exert only a relatively small horizontal resistance to force the vertical (pinned-pinned) column to sustain at least the second-mode buckling load of $4\pi^2 EI/L^2$ instead of the first-mode buckling load of $\pi^2 EI/L^2$. Of course, the actual end restraint condition for structural columns exceeds the pinned-end condition and thereby also increases the buckling load.

2.2.8 Summary

Some differential equation solutions in Section 2.2 might bother some readers. After all, we expect a second-order differential equation to have two constants of integration with two boundary conditions, yet we sometimes had three constants and three or four boundary conditions! The reason for this curious behavior is that the buckling problem inherently involves a fourth-order differential equation as we will see in the next section. Thus, some significant characteristics were masked when we based our analysis only on the constitutive equation $M = \pm Ely''$.

Problem Set 2.2

2.2.1 Rework the problem for the axially compressed fixed-fixed bar in Section 2.2.3 without assuming that the horizontal reactions are zero. Solve the resulting characteristic equation for the first three buckling loads. Determine the shapes into which the column buckles, i.e., find the buckling mode shapes, and plot them.

2.2.2 For the elastically restrained bar in Section 2.2.5, examine the special cases such as $\alpha = \infty$ which corresponds to perfect translational restraint, $\alpha = 0$ (no translational restraint), $\beta = \infty$ (perfect rotational restraint), and $\beta = 0$ (no rotational restraint). To which problems that we have studied do each of the special cases correspond? Derive the characteristic equation for each possible combination of special values of α and β and thereby find the buckling load for each combination.

2.2.3 Find the characteristic equation for a free-free bar with both elastic translational and rotational springs at each end. The translational springs are perpendicular to the bar, and one bar end has a fixed point to prevent rigid-body motion.

2.2.4 Find the "exact" (not from the linear approximation) buckling load of an axially compressed pinned-pinned bar with a mid-span transverse spring (in Section 2.2.7) with half the critical spring stiffness and compare with the linear approximation.

2.2.5 Find the characteristic equation for an axially compressed pinned-pinned bar with a transverse elastic translational spring at $x = L_1$ from the left end in a plot similar to Figure 2-11. Develop buckling load results as a function of the position of the load with L_1 varying from zero to L/2 by tenths crudely with further detail to clarify the behavior of the curves for various spring stiffnesses.

Éléments sous droits d'auteur

2.3 AN ALTERNATIVE BAR BUCKLING DIFFERENTIAL EQUATION

In the process of solving the buckling differential equation

$$EIy'' = \pm M \tag{2.81}$$

in Section 2.2.1, we must derive an expression for the moment at any point in the bar under consideration. As we have seen, we must be very careful to account for all reactive forces and moments (and their signs). In order to more straightforwardly treat bars with various end conditions that involve derivatives of the deflection, y, we must appeal to a differential equation of higher order than that used in Section 2.2.1.

2.3.1 Derivation of an Alternative Differential Equation

We derive the differential equation for behavior of a beam-column, a member subjected to both axial and transverse loads as in Figure 2-15. The relations between loads, q(x) and P; the shearing force, S; and the bending moment, M, are obtained from the equilibrium equations of the differential element of the deformed (buckled) beam-column in Figure 2-15. We still use the concept that the disturbing moment from the applied load must equal the restoring moment at the buckling load.

Sum the forces in the y-direction on the free-body diagram to get

$$-S + q\,dx + (S + dS) = 0 \tag{2.82}$$

so, upon elimination of S,

$$q = -\frac{dS}{dx} \tag{2.83}$$

Summation of moments about point n gives, for small angles dy/dx,

$$M + q\,dx\,\frac{dx}{2} + (S + dS)dx - (M + dM) + \bar{P}\,\frac{dy}{dx}\,dx = 0 \tag{2.84}$$

which, upon neglect of second-order terms, reduces to

$$S = \frac{dM}{dx} - \bar{P}\,\frac{dy}{dx} \tag{2.85}$$

Substitution of the relation between bar curvature and moment,

$$EI\,\frac{d^2y}{dx^2} = -M \tag{2.86}$$

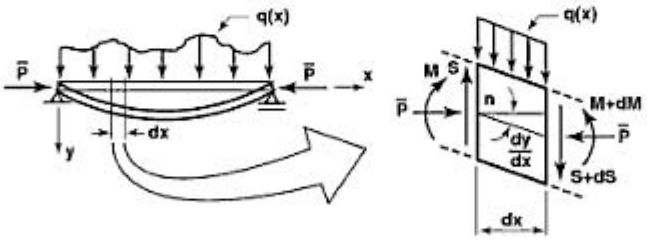


Figure 2-15 Beam-Column and Differential Element

Éléments sous droits d'auteur

in Equation (2.85) gives

$$EI\frac{d^3y}{dx^3}+\bar{P}\frac{dy}{dx}=-S \tag{2.87}$$

Then, differentiate Equation (2.87) and substitute the derivative of the shear force, S, from Equation (2.83) to get

$$EI\frac{d^4y}{dx^4}+\bar{P}\frac{d^2y}{dx^2}=q \tag{2.88}$$

When the axial force is zero, Equations (2.86)–(2.88) reduce to those for bending under transverse load only. When the transverse load is zero, Equations (2.86)–(2.88) apply to cases of buckling under axial load.

For buckling problems (q = 0), Equation (2.88) can be written as

$$y''''+k^2y''=0 \tag{2.89}$$

or

$$\left[y''+k^2y\right]''=0 \tag{2.90}$$

in which, as before,

$$k^2=\frac{\bar{P}}{EI} \tag{2.91}$$

Note that effectively the second derivative of the moment-curvature relation is inside Equation (2.90). That is, we see here that what we thought was the equation governing buckling in Section 2.2 is not complete in order of differentiation. In fact, there are two more derivatives and hence two more constants of integration than in Equation (2.9), i.e., what we thought was the general solution. Those two constants of integration was what we were getting in Section 2.2 when we dealt with moments and reactions, although we might have thought they were particular solutions (but they cannot be particular solutions because they involve unknown constants, not specific known functions as are required for particular solutions).

The general solution of Equation (2.89) [and (2.90)] is

$$y=A\sin kx+B\cos kx+Cx+D \tag{2.92}$$

Four constants, A, B, C, and D, occur in this solution as opposed to only two for the solution in Section 2.2.1. However, as mentioned before, now we need not explicitly determine the bending moment expression. The four constants are 'determined' by application of the boundary conditions. Now, the boundary conditions can involve derivatives of y up to the third order because the governing differential equation is of fourth order. The terms involving y and y' are referred to as the *geometric boundary conditions* whereas those involving y'' and y''' are referred to as *natural boundary conditions* because, as we will see, they are related to moment and shear, respectively. Note from Equation (2.87) that the shear boundary condition includes y' as well as y'''. Now, consider examples of variously supported bars including those studied in Section 2.2.

Éléments sous droits d'auteur

2.3.2 Buckling of an Axially Compressed Pinned-Pinned Bar

The boundary conditions for a bar with both ends pinned as in Figure 2-16 are zero deflection, $y = 0$, and zero moment at each of the two ends. Thus, $y'' = 0$ from the moment-curvature relation, Equation (2.4), in Section 2.2. Upon application of the boundary conditions to the general solution, Equation (2.43),

$$y = A \sin kx + B \cos kx + Cx + D \quad (2.93)$$

and its second derivative

$$y'' = -Ak^2 \sin kx - Bk^2 \cos kx \quad (2.94)$$

At the upper end, $y = 0$ and $M = 0$, so

$$y(0) = 0 \rightarrow B = -D \quad (2.95)$$

$$y''(0) = 0 \rightarrow B = 0 \quad (2.96)$$

so $D = 0$ by virtue of Equation (2.95). At the lower end, $y = 0$ and $M = 0$, so

$$y(L) = 0 \rightarrow A \sin kL + CL = 0 \quad (2.97)$$

$$y''(L) = 0 \rightarrow Ak^2 \sin kL = 0 \quad (2.98)$$

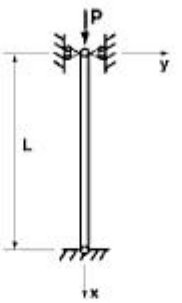


Figure 2-16 Pinned-Pinned Bar under Axial Compression

Because $A = 0$ would imply that the buckled shape is either linear ($C \neq 0$) or zero (no buckling), neither of which can be true, we are left with

$$\sin kL = 0 \quad (2.99)$$

as the characteristic equation, as in Section 2.2.1, with solutions

$$kL = n\pi \qquad n = 1, 2, \ldots \quad (2.100)$$

Furthermore, because $\sin kL = 0$ in Equation (2.97), $C = 0$. Finally,

$$\bar{P} = P_E = n^2 \pi^2 \frac{EI}{L^2} \quad (2.101)$$

from which the lowest buckling load occurs at $n = 1$:

$$\bar{P} = P_E = \pi^2 \frac{EI}{L^2} \quad (2.102)$$

which is the classical Euler buckling result. Higher values of P_E occur for $n > 1$. The first three buckling mode shapes are illustrated in Figure 2-17 from the eigenvector equation

$$y = A \sin \frac{n\pi x}{L} \quad (2.103)$$

There, n is the number of buckle half waves in the axial direction of the bar. Of course, the buckle amplitude, A, is indeterminate.

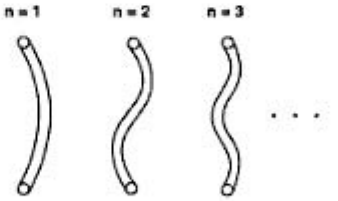


Figure 2-17 Buckling Mode Shapes

Éléments sous droits d'auteur

2.3.3 Buckling of an Axially Compressed Fixed-Pinned Bar

Consider a bar that is fixed at one end and pinned at the other end as shown in Figure 2-18. For this problem, we need not consider the reactive forces and moments as we did in Section 2.2.2. Here, we need only apply the boundary conditions to the general solution:

$$y = A \sin kx + B \cos kx + Cx + D \quad (2.104)$$

and to its derivatives

$$y' = Ak \cos kx - Bk \sin kx + C \quad (2.105)$$

$$y'' = -Ak^2 \sin kx - Bk^2 \cos kx \quad (2.106)$$

whereupon the two boundary conditions at the pinned end of the bar in Figure 2-18 ($y = 0$ and $M = 0$) lead to

$$y(0) = 0 \rightarrow B + D = 0 \quad (2.107)$$

$$y''(0) = 0 \rightarrow B = 0 \quad (2.108)$$

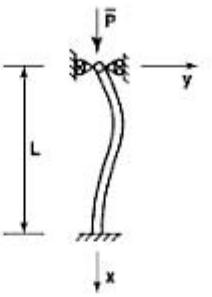


Figure 2-18 Axially Loaded Bar with One End Fixed and One End Pinned

and the two boundary conditions at the fixed end lead to

$$y(L) = 0 \rightarrow A \sin kL + B \cos kL + CL + D = 0 \quad (2.109)$$

$$y'(L) = 0 \rightarrow Ak \cos kL - Bk \sin kL + C = 0 \quad (2.110)$$

But $B = D = 0$ from Equations (2.107) and (2.108). All four boundary conditions are satisfied by the trivial solution $A = B = C = D = 0$, but the unacceptable and uninteresting implication of that trivial solution is that buckling does not occur! For a nontrivial solution to Equations (2.107)–(2.110), the determinant of the coefficients of A, B, C, and D in the set of homogeneous equations must be zero. An easier approach in this case is to simplify Equations (2.109) and (2.110) by use of the result $B = D = 0$ from Equations (2.107) and (2.108) and solve the resulting two equations in two unknowns to get

$$A(\sin kL - kL \cos kL) = 0 \quad (2.111)$$

which simplifies to the transcendental characteristic equation (transcendental because the left-hand side is a function of the right-hand side)

$$\tan kL = kL \quad (2.112)$$

from which $kL = 4.493$ by trial and error, so as in Section 2.2.2,

$$\bar{P} = P_E = (4.493)^2 \frac{EI}{L^2} = 20.19 \frac{EI}{L^2} = 2.046\,\pi^2 \frac{EI}{L^2} \quad (2.113)$$

The buckled shape or eigenvector can be shown to be

$$y = A\left[\sin(4.493 \frac{x}{L}) + .9778 \frac{x}{L}\right] \quad (2.114)$$

Of course, the buckle amplitude A is indeterminate.

Éléments sous droits d'auteur

2.3.4 Buckling of an Axially Compressed Fixed-Fixed Bar

The upper fixed or zero-slope end must move vertically in order to allow load to be introduced into the bar as in Figure 2-19, and we need not be concerned with the reactive forces and moments as we were in Section 2.2.3. Here, we need only apply appropriate boundary conditions to the general solution:

$$y = A \sin kx + B \cos kx + Cx + D \quad (2.115)$$

with

$$y' = Ak \cos kx - Bk \sin kx + C \quad (2.116)$$

to get

$$y(0) = 0 \rightarrow B + D = 0 \quad (2.117)$$

$$y'(0) = 0 \rightarrow Ak + C = 0 \quad (2.118)$$

$$y(L) = 0 \rightarrow A \sin kL + B \cos kL + CL + D = 0 \quad (2.119)$$

$$y'(L) = 0 \rightarrow Ak \cos kL - Bk \sin kL + C = 0 \quad (2.120)$$

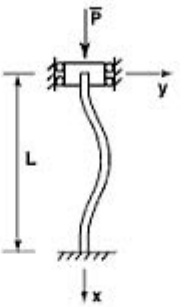


Figure 2-19 Axially Loaded Bar with Fixed Ends

We seek a nontrivial solution, i.e., one that allows buckling, to the set of Equations (2.117)–(2.120) which results from setting the determinant of the coefficients of A, B, C, and D equal to zero, i.e.,

$$\begin{vmatrix} 0 & 1 & 0 & 1 \\ k & 0 & 1 & 0 \\ \sin kL & \cos kL & L & 1 \\ k \cos kL & -k \sin kL & 1 & 0 \end{vmatrix} = 0 \quad (2.121)$$

Upon expansion of the determinant in Equation (2.121) according to the usual rules, we get the buckling criterion

$$2(\cos kL - 1) + kL \sin kL = 0 \quad (2.122)$$

Recognize that

$$\sin kL = 2 \sin \frac{kL}{2} \cos \frac{kL}{2} \quad (2.123)$$

$$\cos kL = 1 - 2 \sin^2 \frac{kL}{2} \quad (2.124)$$

so the buckling criterion becomes

$$\sin \frac{kL}{2} \left[\frac{kL}{2} \cos \frac{kL}{2} - \sin \frac{kL}{2} \right] = 0 \quad (2.125)$$

with one solution, the characteristic equation,

$$\sin \frac{kL}{2} = 0 \quad (2.126)$$

which implies $kL = 2n\pi$ in which $n = 1, 2, \ldots$, so the buckling load is

$$\bar{P} = P_E = 4n^2\pi^2 \frac{EI}{L^2} \qquad n = 1, 2, \ldots \quad (2.127)$$

Éléments sous droits d'auteur

for which the lowest buckling load corresponds to n = 1 and is

$$\bar{P} = P_E = 4\pi^2 \frac{EI}{L^2} \qquad (2.128)$$

i.e., the same result as obtained in Section 2.2.3. The mode shape for this buckling load is symmetric about the bar midpoint as in Figure 2-19. Equation (2.125) has another solution, the characteristic equation,

$$\tan \frac{kL}{2} = \frac{kL}{2} \qquad (2.129)$$

which is a transcendental expression with the lowest root of $kL/2 = 4.493$, so

$$\bar{P} = P_E = (8.986)^2 \frac{EI}{L^2} \qquad (2.130)$$

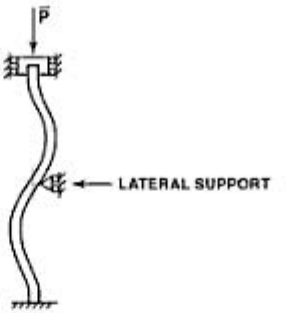


Figure 2-20 Buckling of an Axially Loaded Bar with Lateral Support

which is higher than Equation (2.128) but lower than for n = 2. The mode shape is antisymmetric (about the bar midpoint) as in Figure 2-20. The load in Equation (2.130) is realized only when a transverse support at the center exists as in Figure 2-20. Of course, the buckling amplitude is indeterminate.

2.3.5 Buckling of an Axially Compressed Fixed-Free Bar

The general solution to the governing differential equation for an axially loaded bar that is supported only at the base as in Figure 2-21 and its derivatives are

$$y = A \sin kx + B \cos kx + Cx + D \qquad (2.131)$$

$$y' = Ak \cos kx - Bk \sin kx + C \qquad (2.132)$$

$$y'' = -Ak^2 \sin kx - Bk^2 \cos kx \qquad (2.133)$$

$$y''' = -Ak^3 \cos kx + Bk^3 \sin kx \qquad (2.134)$$

The geometric boundary conditions at the lower (fixed) end of the bar lead to

$$y(0) = 0 \quad \rightarrow \quad B + D = 0 \qquad (2.135)$$

$$y'(0) = 0 \quad \rightarrow \quad Ak + C = 0 \qquad (2.136)$$

At the upper (free) end of the bar, the only boundary conditions are that the bending moment and shearing force must be zero, i.e., natural boundary conditions related to y'', y''', and y'. Thus, from the zero moment condition,

$$y''(L) = 0 \qquad (2.137)$$

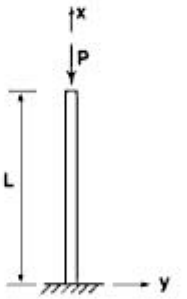


Figure 2-21 Axially Loaded Bar with One End Fixed and One End Free

Éléments sous droits d'auteur

and from Equation (2.87) for zero shear in Section 2.3.1 on page 68,

$$y'''(L) + k^2 y'(L) = 0 \tag{2.138}$$

The boundary conditions at the upper end of the bar result in

$$A \sin kL + B \cos kL = 0 \tag{2.139}$$

$$C = 0 \tag{2.140}$$

from which we also conclude that A = 0 because of Equation (2.136) and B cannot be zero, so we get the characteristic equation and its solutions

$$\cos kL = 0 \quad \rightarrow \quad kL = \frac{(2n-1)}{2}\pi \quad n = 1, 2, \ldots \tag{2.141}$$

Thus, the lowest buckling load occurs for n = 1:

$$\bar{P} = P_E = \frac{\pi^2}{4}\frac{EI}{L^2} \tag{2.142}$$

with eigenvector in which Δ is indeterminate as usual:

$$y = \Delta\left(1 - \cos\frac{\pi x}{2L}\right) \tag{2.143}$$

2.3.6 Buckling of an Axially Compressed Fixed-Guided Bar

The term 'guided' is used to describe a support that moves in the bar axial direction so that load can be applied, but does not allow the bar end to rotate, although the bar end can translate perpendicular to the bar axis as in Figure 2-22. That is, $y' = 0$, but $y \neq 0$, so there is no slope as with a fixed end, but the bar end can also deflect transverse to the bar axis quite unlike a fixed end, so the shear force at the end is zero. Fortunately, the shear force is addressed in the derivation of the fourth-order differential equation, Equation (2.88), as Equation (2.85), so

$$S = \frac{dM}{dx} - \bar{P}\frac{dy}{dx} \tag{2.144}$$

We consider the facts that S = 0 and $y' = 0$ at the upper end to get

$$\frac{dM}{dx} = 0 \tag{2.145}$$

but from Equation (2.81) we can re-express the moment as $\pm EIy''$, so

$$\frac{dM}{dx} = \frac{d}{dx}(\pm EIy'') = 0 \tag{2.146}$$

which reduces to the simple boundary condition $y''' = 0$ regardless of the moment sign. The support system in Figure 2-22 appears rather awkward, but it does satisfy the boundary conditions. We need not be con-

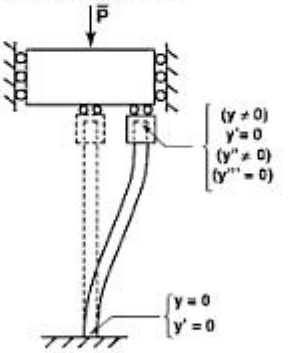


Figure 2-22 Axially Loaded Bar with Lower End Fixed and $y'|_{end} = 0$ but $y|_{end} \neq 0$

Éléments sous droits d'auteur

cerned with the magnitude of the displacement transverse to the bar axis because no deflections take place prior to buckling. At buckling, the deflections are not predictable with this kind of theory, but we might expect them to be at least moderate if not large.

The general solution to the governing differential equation for an axially loaded bar that is fixed at the base and guided at its top as in Figure 2-22 and its derivatives are

$$y = A \sin kx + B \cos kx + Cx + D \tag{2.147}$$

$$y' = Ak \cos kx - Bk \sin kx + C \tag{2.148}$$

$$y'' = -Ak^2 \sin kx - Bk^2 \cos kx \tag{2.149}$$

$$y''' = -Ak^3 \cos kx + Bk^3 \sin kx \tag{2.150}$$

The boundary conditions at the lower (fixed) end of the bar lead to

$$y(0) = 0 \quad \rightarrow \quad B + D = 0 \tag{2.151}$$

$$y'(0) = 0 \quad \rightarrow \quad Ak + C = 0 \tag{2.152}$$

At the upper (guided) end of the bar, the boundary conditions are that the slope and shearing force must be zero, i.e., a natural boundary condition related to y' and y'''. From the zero slope condition at the upper end and for the guided support condition of $y''' = 0$,

$$y'(L) = 0 \tag{2.153}$$

$$y'''(L) = 0 \tag{2.154}$$

so the boundary conditions at the upper (guided) end of the bar result in

$$Ak \cos kL - Bk \sin kL + C = 0 \tag{2.155}$$

$$-Ak^3 \cos kL + Bk^3 \sin kL = 0 \tag{2.156}$$

These four boundary condition equations in the four unknown constants, A, B, C, and D, have a nontrivial solution if and only if the determinant of the coefficients of A, B, C, and D is zero, i.e., if

$$\begin{vmatrix} 0 & 1 & 0 & 1 \\ k & 0 & 1 & 0 \\ k\cos kL & -k\sin kL & 1 & 0 \\ -k^3\cos kL & k^3\sin kL & 0 & 0 \end{vmatrix} = 0 \tag{2.157}$$

Expand the determinant to get the characteristic equation with solutions

$$\sin kL = 0 \quad \rightarrow \quad kL = n\pi \quad n = 1, 2, \ldots \tag{2.158}$$

Thus, the lowest buckling load occurs for n = 1:

$$\bar{P} = P_E = \pi^2 \frac{EI}{L^2} \tag{2.159}$$

which is the same result as for the bar with both ends pinned in Section 2.3.2. Derive and sketch the two buckled shapes to convince yourself!

Éléments sous droits d'auteur

2.3.7 Buckling of an Axially Compressed Pinned-Guided Bar

The general solution to the governing differential equation for an axially loaded bar that is pinned at the base and guided at its top as in Figure 2-23 and its derivatives are

$$y = A \sin kx + B \cos kx + Cx + D \quad (2.160)$$

$$y' = Ak \cos kx - Bk \sin kx + C \quad (2.161)$$

$$y'' = -Ak^2 \sin kx - Bk^2 \cos kx \quad (2.162)$$

$$y''' = -Ak^3 \cos kx + Bk^3 \sin kx \quad (2.163)$$

The boundary conditions at the lower (pinned) end of the bar lead to

$$y(0) = 0 \quad \rightarrow \quad B + D = 0 \quad (2.164)$$

$$y''(0) = 0 \quad \rightarrow \quad B = 0 \quad (2.165)$$

so $D = 0$. At the upper (guided) end of the bar, the boundary conditions are that the slope and shearing force must each be zero, i.e., a natural boundary condition related to y' and y'''. From the zero slope condition at the upper end and for the guided support condition of $y''' = 0$,

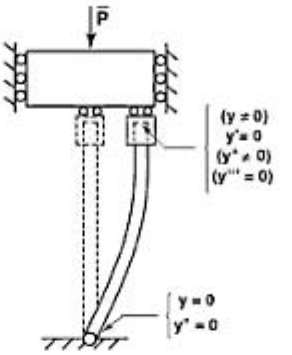


Figure 2-23 Axially Loaded Bar with Lower End Pinned and $y'|_{end} = 0$ but $y|_{end} \neq 0$

$$y'(L) = 0 \quad (2.166)$$

$$y'''(L) = 0 \quad (2.167)$$

so the boundary conditions at the upper (guided) end of the bar result in

$$Ak \cos kL - Bk \sin kL + C = 0 \quad (2.168)$$

$$-Ak^3 \cos kL + Bk^3 \sin kL = 0 \quad (2.169)$$

However, $B = 0$ from Equation (2.165), so Equations (2.167) and (2.169) are satisfied by the characteristic equation and its solutions

$$\cos kL = 0 \quad \rightarrow \quad kL = \frac{(2n-1)}{2}\pi \quad n = 1, 2, \ldots \quad (2.170)$$

because either $A = 0$ or $\cos kL = 0$ from Equation (2.169). However, if A were zero, then all coefficients, A, B, C, and D, would be zero, i.e., the trivial case of no buckling. The determinant approach would lead to the same result. Thus, the lowest buckling load occurs for n = 1:

$$\bar{P} = P_E = \frac{\pi^2}{4}\frac{EI}{L^2} \quad (2.171)$$

which is the same result as for the fixed-free bar in Section 2.3.5. Derive and sketch the two buckled shapes to convince yourself!

Éléments sous droits d'auteur

2.3.8 The Effective-Length Concept to Account for Boundary Conditions

A concept that is often useful in connection with various end-support conditions for bars in design is that of *effective length*. That is, bars with different boundary conditions at their ends can be viewed as having different lengths instead of their actual lengths. This approach is used to consolidate the characteristics of the support conditions and the different lengths into the single character of a fictitious or effective length.

The buckling load for each bar with the various bar support conditions that we have studied can be expressed in the form of some multiple, c^2, of the Euler buckling load for a pinned-pinned bar:

$$\bar{P} = P_E = c^2 \pi^2 \frac{EI}{L^2} \tag{2.172}$$

Note that $c = 1$ for the baseline pinned-pinned bar with an effective length of L, its real, physical length. Next, the result can be reformulated to incorporate c, the coefficient that depends on end support conditions, in the length by defining

$$L' = L_e = L_{effective} = \frac{L}{c} \tag{2.173}$$

so the buckling load for an arbitrary bar becomes

$$\bar{P} = P_E = \pi^2 \frac{EI}{L_e^2} \tag{2.174}$$

To use Equation (2.174), simply identify the boundary conditions for a bar in Table 2-1, determine L_e, and calculate P. For example, the fixed-free bar in Section 2.3.5 has a buckling load

$$\bar{P} = P_E = \frac{\pi^2}{4} \frac{EI}{L^2} = \frac{1}{4} \pi^2 \frac{EI}{L^2} = \pi^2 \frac{EI}{(2L)^2} \tag{2.175}$$

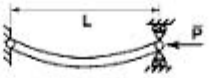
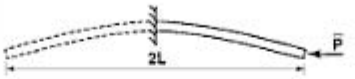
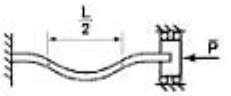
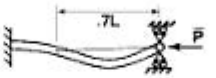
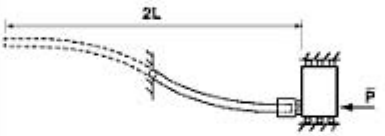
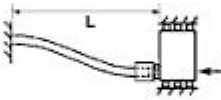
so $c^2 = 1/4$, $c = 1/2$, and $L_e = 2L$. The portion of the buckled shape that corresponds to the single half-sine wave buckle of a pinned-pinned bar is shown for each case in Table 2-1. With the effective length concept, the stress versus length over radius of gyration (L/r) plot in Figure 2-4 on page 55 can now be relabeled as *effective length over r* (L_e/r) or (L'/r) or ($L_{effective}/r$) and thereby generalized for practical use in design.

2.3.9 Summary

In all problems examined in Section 2.3, the fourth-order differential equation is homogeneous as are the four boundary conditions. Solution of the differential equation subject to the boundary conditions leads to a characteristic equation whose solution is the buckling load. Thus, the problem is termed an eigenvalue problem or proper-value problem or characteristic-value problem. In no problem were we able to determine the buckling deflection amplitude because of the inherent limitation of the problem formulation. The effective-length concept to incorporate the influence of boundary conditions on the buckling load in the length in the Euler equation was introduced for use in design.

Éléments sous droits d'auteur

Table 2-1 Bar Buckling Loads for Different Effective Lengths

Boundary Conditions*	Buckling Load	Buckled Shape and Relation to that of a Pinned-Pinned Bar	Effective Length
Pinned-Pinned	$\pi^2 \frac{EI}{L^2}$		L
Fixed-Free	$\frac{\pi^2}{4} \frac{EI}{L^2}$		2L
Fixed-Fixed	$4\pi^2 \frac{EI}{L^2}$		$\frac{L}{2}$
Fixed-Pinned	$2.04\pi^2 \frac{EI}{L^2}$		.7L
Pinned-Guided	$\frac{\pi^2}{4} \frac{EI}{L^2}$		2L
Fixed-Guided	$\pi^2 \frac{EI}{L^2}$		L

* 'Guidad' has the special definition in Sections 2.3.6 and 2.3.7 ($y' = 0$, but $y \neq 0$).

If we address the six cases considered in Section 2.3 in a different order from that in Table 2-1, we can more easily appreciate the relation of the cases to their end support or restraint conditions. Those conditions are the restraint of the deflection transverse to the bar axis at the bar end and the restraint of rotation about the bar end. The four types of end restraints that we have studied so far are:

1. Fixed: both deflection and slope restraint
2. Pinned: deflection restraint, but no slope restraint
3. Free: neither deflection nor slope restraint
4. Guided: no deflection restraint, but slope restraint

Éléments sous droits d'auteur

Of course, there could be elastic restraint of deflection and rotation at the bar ends caused by translation-resisting springs and rotation-resisting springs, respectively. The translation-resisting springs could be linear with a force-deflection relation of $F = kx$ or nonlinear such as $F = kx^3$. Similarly, the rotation-resisting springs could have a linear or nonlinear moment-rotation relationship. Such springs lead to lesser end stiffnesses and therefore smaller buckling loads than if perfect restraint existed.

We proceed from the highest buckling load to the lowest by successively removing various restraints to achieve the other end conditions using the fixed-fixed bar as the baseline result. The largest buckling load occurs when both ends are fixed, i.e., $P_E = 4\pi^2 EI/L^2$. We understand that both ends being fixed means that there is zero transverse deflection and zero slope at each end. That is, both deflection and slope are perfectly restrained to be zero at each end. If we remove the slope restraint at only one end, the bar becomes fixed-pinned with a somewhat smaller buckling load, i.e., $P_E = 2.04\pi^2 EI/L^2$. If we remove the slope restraint at the other end (in addition to that at the first end), the bar becomes pinned-pinned with the classical value $P_E = \pi^2 EI/L^2$. Alternatively, if we remove the deflection restraint but not the slope restraint at one end, then the fixed-guided bar also has $P_E = \pi^2 EI/L^2$. Next, if we remove both the deflection restraint and the slope restraint at one end creating a free end, the fixed-free bar has $P_E = 1/4\pi^2 EI/L^2$. Alternatively, if we remove the slope restraint at one end and the deflection restraint at the other end, the pinned-guided bar also has $P_E = 1/4\pi^2 EI/L^2$. Accordingly, we gain some feeling or appreciation for the importance of each restraint mechanism. For example, removing the transverse deflection restraint leads to lower buckling loads than if the slope restraint is relaxed. Recall that P and P_E are used interchangeably as the buckling load in this book.

Problem Set 2.3

2.3.1 Verify the two characteristic equations in Section 2.3.4 from the determinant condition in Equation (2.67).

2.3.2 Verify the characteristic equation in Section 2.3.6.

2.3.3 A bar is fixed at its base and loaded at its free end with a force P that is always directed toward the fixed point C in Figure 2-24. This force might be caused by a variable-tension cable (e.g., a cable with a turnbuckle) connecting C to the loaded end. Or, point C might be a metal ring through which a cable passes. Derive the characteristic equation for buckling of the bar. Then, solve the characteristic equation for several representative values of L_c/L and interpret the obvious special cases of L_c/L.

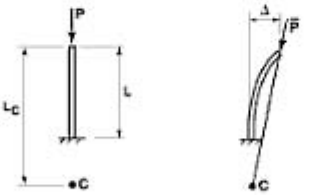


Figure 2-24 Axially Loaded Bar with a Restraining Cable

Éléments sous droits d'auteur

2.4 LARGE DEFLECTIONS OF BUCKLED BARS — THE PROBLEM OF THE ELASTICA

2.4.1 Introduction

In previous sections, we used an approximate curvature expression, Equation 2.2, to find the buckling load. However, we also found that the deflection at the buckling load is indeterminate in magnitude, although not in shape. We therefore dealt with an eigenvalue problem by virtue of the linearizing approximation of small deflections for the curvature expression. However, we want to determine the behavior of the bar at loads well in excess of the buckling load so that we can establish the physical significance of the buckling load itself, i.e., how a bar behaves at *and above* the buckling load. Thus, we must know the type of behavior in the vicinity of the buckling load and the potential danger of the act of buckling (catastrophic or benign). Thus, we must reject the small-deflection approximation for curvature, and are therefore led to the classical problem of the elastica.

The *Elastica* is the elastic line used to describe the shape of the axis of a deformed bar, i.e., the bar has no specific cross section transverse to its axis, but is represented only with a deformable or bendable line. This bendable line was first investigated by Leonhard Euler in the appendix *De Curvis Elasticis* of his 1744 book *Methodus Inveniendi Lineas Curvas Maximi Minimive Proprietate Gaudentes* [2-2][1] and was addressed further by J. L. Lagrange (1736–1813) [2-3]. More background on the large-deflection problem is available in Timoshenko's *History of Strength of Materials* [2-4]. Note that ordinary beam theory is essentially the theory of the elastica because we treat only the deformation of the beam axis and extend its deformation to the rest of the beam cross section by the Euler-Bernoulli hypothesis. The Euler-Bernoulli [Jacob Bernoulli (1654-1705)] hypothesis is that plane sections that are perpendicular to the beam axis before bending remain plane and perpendicular to the deformed beam axis during beam bending. This hypothesis is a usual mechanics of materials presumption that is justified by observing that vertical lines drawn on an undeformed rubber beam remain straight but rotate as the rubber beam bends.

The disadvantage of the approximate-curvature-based approach to buckling is that only the buckling load is determined and no information can be found about the load-deformation behavior after buckling. In particular, we would like to know the deflections and stresses just after buckling. In this section, we use the "exact" curvature expression to derive the load-deformation behavior up to and well beyond the actual buckling event. That exact approach naturally leads to the use of elliptic integrals. Then, we approximate the load-deformation behavior to study the nature and magnitude of deflections and stresses just after buckling of a fixed-free bar. We briefly extend the concepts to other bars, namely pinned-pinned bars. Finally, we use the derived results to establish the practical significance of the Euler buckling load for bars.

[1] An English translation of the appendix was published by W. A. Oldfather, C. A. Ellis, and D. M. Brown in *Isis*, Volume 20, Number 58, November 1933, p. 1 (reprinted in Bruges, Belgium). A German translation is available in *Ostwald's Klassiker*, Number 175.

Éléments sous droits d'auteur

2.4.2 Exact Load-Deflection Behavior

For a bar fixed at the base and free at the axially loaded upper end, the load P must be slightly greater than the Euler buckling load in order to cause the large deflection depicted in Figure 2-25. Note that the moving origin of coordinates is located at the loaded free end of the bar.

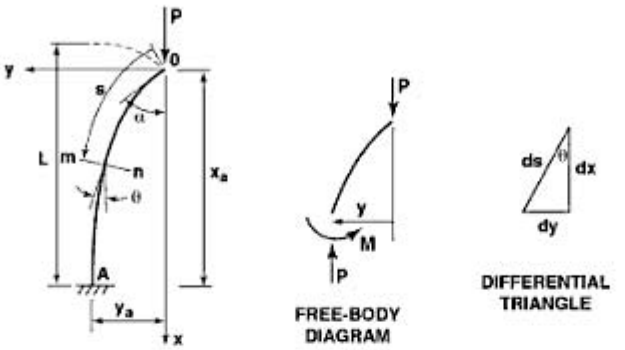


Figure 2-25 Axially Loaded Bar with One End Fixed and One End Free

We determine the shape of the elastica by solving the exact differential equation of the deflection curve. The exact differential equation is obtained by use of the exact expression for the curvature instead of an approximation thereto, i.e., the exact differential equation for pure bending is

$$EI\rho = -M \tag{2.176}$$

in which the exact curvature is

$$\rho = \frac{d\theta}{ds} \tag{2.177}$$

(the rate of change of slope with respect to arc length of the bar). Thus, the exact differential equation of the elastica is

$$EI\frac{d\theta}{ds} = -M = -Py \tag{2.178}$$

and can be written as

$$\frac{d\theta}{ds} + k^2 y = 0 \tag{2.179}$$

in which $k^2 = P/EI$. The differential equation, Equation (2.179), can be differentiated with respect to s and, upon recognition from the differential triangle in Figure 2-25 that

$$\frac{dy}{ds} = \sin\theta \tag{2.180}$$

we get

$$\frac{d^2\theta}{ds^2} + k^2 \sin\theta = 0 \tag{2.181}$$

Éléments sous droits d'auteur

Multiply Equation (2.181) by $d\theta$ and integrate to obtain

$$\int \frac{d^2\theta}{ds^2}\frac{d\theta}{ds}\,ds = -k^2\int \sin\theta\, d\theta \tag{2.182}$$

which can be written as

$$\frac{1}{2}\int \frac{d}{ds}\left[\frac{d\theta}{ds}\right]^2 ds = -k^2\int \sin\theta\, d\theta \tag{2.183}$$

and then integrated to obtain

$$\frac{1}{2}\left[\frac{d\theta}{ds}\right]^2 = k^2\cos\theta + C \tag{2.184}$$

in which C is a constant of integration that is determined from the boundary conditions at the loaded end of the bar. Because the moment at the loaded end is zero, the curvature is also zero, i.e.,

$$\left.\frac{d\theta}{ds}\right|_{x=0} = 0 \tag{2.185}$$

In addition, the angle at the loaded end is α, so finally,

$$C = -k^2\cos\alpha \tag{2.186}$$

Thus, the solution can be written as

$$\left[\frac{d\theta}{ds}\right]^2 = 2k^2(\cos\theta - \cos\alpha) \tag{2.187}$$

or

$$\frac{d\theta}{ds} = \pm\sqrt{2}\,k\sqrt{\cos\theta - \cos\alpha} \tag{2.188}$$

Note from the sketch of the loaded bar in Figure 2-25 that $d\theta/ds$ is always negative, so we drop the positive sign in Equation (2.188).

Solve Equation (2.188) for ds and integrate to obtain the bar length:

$$L = \int ds = \int_0^{\alpha} \frac{d\theta}{\sqrt{2}\,k\sqrt{\cos\theta - \cos\alpha}} \tag{2.189}$$

The total arc length S is not much different from the original bar length L. As we will see, the axial force in the bar does not differ much from the Euler load, so the bar lengths cannot be very different. Note that small strains in the axial direction do not result in significant changes in length [new length $= L(1+\varepsilon)$ in which ε is small]. That is, even though the transverse deflection y is large enough to require consideration of exact curvature, the axial deflection and hence the axial strain is still small. Thus, for a given α, we can solve for k to get P. However, some manipulations are required before the solution is in its most useful form.

First, use the trigonometric identity

$$\cos\beta = 1 - 2\sin^2\frac{\beta}{2} \tag{2.190}$$

and substitute θ and α for β to get

Éléments sous droits d'auteur

$$kL = \int_0^{\alpha} \frac{d\theta}{2\sqrt{\sin^2\frac{\alpha}{2} - \sin^2\frac{\theta}{2}}} \tag{2.191}$$

Now, at the loaded free end with slope α, use the substitution

$$p = \sin\frac{\alpha}{2} \tag{2.192}$$

and define a new variable ϕ such that

$$\sin\frac{\theta}{2} = p\sin\phi = \sin\frac{\alpha}{2}\sin\phi \tag{2.193}$$

Thus, as θ varies from 0 to α along the bar from the fixed end to the loaded free end, the quantity $\sin\phi$ varies from 0 to 1, so ϕ must vary from 0 to $\pi/2$. Differentiate Equation (2.193) to get

$$d\left[\sin\frac{\theta}{2}\right] = p\,d(\sin\phi) \tag{2.194}$$

so

$$\frac{1}{2}\cos\frac{\theta}{2}\,d\theta = p\cos\phi\,d\phi \tag{2.195}$$

or

$$d\theta = \frac{2p\cos\phi\,d\phi}{\cos\frac{\theta}{2}} = \frac{2p\cos\phi\,d\phi}{\sqrt{1-\sin^2\frac{\theta}{2}}} = \frac{2p\cos\phi\,d\phi}{\sqrt{1-p^2\sin^2\phi}} \tag{2.196}$$

Thus, upon substitution in the integral of Equation (2.191), we get

$$kL = \int_0^{\pi/2} \frac{1}{2\sqrt{p^2 - p^2\sin^2\phi}} \frac{2p\cos\phi\,d\phi}{\sqrt{1-p^2\sin^2\phi}} = \int_0^{\pi/2} \frac{d\phi}{\sqrt{1-p^2\sin^2\phi}} \tag{2.197}$$

which is a *complete elliptic integral of the first kind* and is tabulated as a function of $p = \sin\alpha/2$ in many handbooks (see, e.g., Jahnke and Emde [2-5]). Thus, with such numerical information, we can find the load P corresponding to any value of p (related to the slope at the free end), a much more direct process than finding α for a specified P.

For small deflections, α and p are small, so the term $p^2\sin^2\phi$ can be neglected in comparison to unity in Equation (2.197). Then,

$$kL = \int_0^{\pi/2} d\phi = \frac{\pi}{2} \tag{2.198}$$

so

$$P_E = \frac{\pi^2}{4}\frac{EI}{L^2} \tag{2.199}$$

which is the classical Euler buckling load for the end-loaded fixed-free bar. We will reference all large-deflection buckling solutions to this load.

Éléments sous droits d'auteur

The deflections of the bar are obtained from the differential triangle in Figure 2-25, i.e.,

$$dy = \sin\theta\, ds = -\frac{\sin\theta\, d\theta}{\sqrt{2}\, k\sqrt{\cos\theta - \cos\alpha}} \tag{2.200}$$

so the transverse deflection of the loaded free end of the bar is

$$y_a = \frac{1}{2k}\int_0^{\alpha} \frac{\sin\theta\, d\theta}{\sqrt{\sin^2\frac{\alpha}{2} - \sin^2\frac{\theta}{2}}} \tag{2.201}$$

which, upon substitution of relations derived earlier, can be written as

$$y_a = \frac{2p}{k}\int_0^{\pi/2} \sin\phi\, d\phi = \frac{2p}{k} \tag{2.202}$$

For a given k, p is determined from Equation (2.197) (or vice versa). Then, y_a is determined from Equation (2.202). Similarly, x_a is

$$x_a = \frac{2}{k}\int_0^{\pi/2} \sqrt{1 - p^2\sin^2\phi}\; d\phi - L = \frac{2}{k}E(p) - L \tag{2.203}$$

in which E(p) is the *complete elliptic integral of the second kind* and is also a tabulated function. Thus, the load and the coordinates of its deflected location are available from solution of Equations (2.202) and (2.203). The deflected shape is obtained by varying the upper limit in the integrals of Equations (2.202) and (2.203).

Load plus axial and transverse tip deflection results from Equations (2.197), (2.203), and (2.202), respectively, are given in Table 2-2. For example, a load only 1 1/2% higher than the Euler load leads to a transverse tip deflection, δ, of 22% of the bar length! Also, a load only 6% higher than the Euler load is required to get an α of 40°! The deformed shape of the bar can be obtained by use of elliptic integrals or numerical solution and is shown for various values of end angle α from Timoshenko and Gere's classical elliptic-integral-based results [2-6] in Figure 2-26 and various axial loads from Nemeth's extensive numerical results [2-7] in Figure 2-27. By cross reference between Figures 2-26 and 2-27 plus Table 2-2, it is obvious that very large deflections result from only slight increases in load over P_E. Moreover, note especially from Figure 2-27 that ever-increasing proportions of P are introduced as shear as opposed to axial load. In fact, in the vicinity of $P = 1.5 - 2\,P_E$, the vertical load P produces virtually all shear loading on the bar.

Table 2-2 Buckling Load and Deflections*

α	0°	20°	40°	60°	80°	100°	120°	140°
P/P_E	1	1.015	1.063	1.152	1.293	1.518	1.884	2.541
x_a/L	1	.970	.881	.741	.560	.349	.123	−.107
y_a/L	0	.220	.422	.593	.719	.792	.803	.750

*After Timoshenko and Gere [2-6], p. 79, reproduced by permission

Éléments sous droits d'auteur

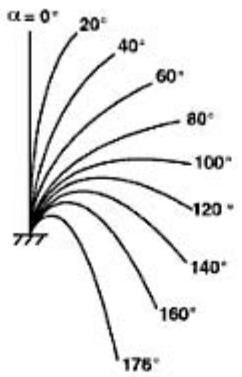


Figure 2-26 Deformed Bar
(After Timoshenko and Gere [2-6]) reproduced by permission

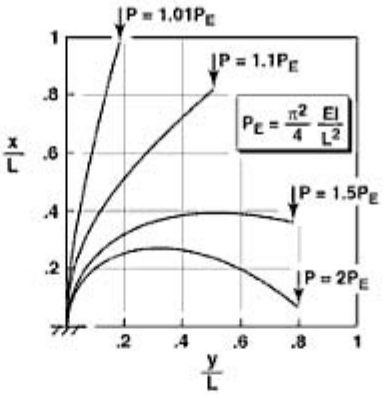


Figure 2-27 Deformed Bar under Various Axial Loads
(After Nemeth [2-7])

Another manner of plotting the large-deflection results is load versus relative bar tip horizontal deflection, δ/L, as in Figure 2-28. There, just as for bars studied with "small-deflection theory" in Sections 2.2 and 2.3, different buckling mode shapes occur at different levels of load. The load is normalized relative to the Euler buckling load, $P_E = (\pi^2/4)EI/L^2$. Results for the first three mode shapes $m = 1$, $m = 2$, and $m = 3$ of an infinite number are shown. The behavior for each mode shape is referred to as a branch. The branches for $m = 1$ and $m = 2$ appear to essentially coincide as P/P_E increases, but the branches can be shown not to actually intersect [2-7]. The principal observation for Figure 2-28 is that the load-deformation behavior is highly nonlinear. If $P < P_E$, the behavior is linear with the bar remaining straight (unbuckled) and is called the *primary equilibrium path*. Above P_E, the straight configuration of the bar is not stable, and the load path bifurcates such that the buckled bar is stable. That buckled load path $m = 1$ (shown in Figures 2-26 and 2-27) is called the *secondary load path* and is sometimes referred to as the *primary nonlinear solution branch*. The various nonlinear solution branches intersect the behavior for the straight bar at *bifurcation points* shown as circles in Figure 2-28. The corresponding buckling loads are called the *bifurcation buckling loads*. As seen for "small-deflection theory" in Sections 2.2 and 2.3, special constraints on bar buckling deformations must exist if the bar is to buckle into any mode except the $m = 1$ mode. This postbuckling behavior with a rising load path is stable-symmetric in the terminology of Section 1.3 starting on page 18. However, because the rise is so shallow and starts with a zero slope, the degree of stability is very low—virtually nonexistent for all practical purposes. Thus, P_E is the largest practical load that can be placed on a bar, and less must be carried for the sake of safety.

Éléments sous droits d'auteur

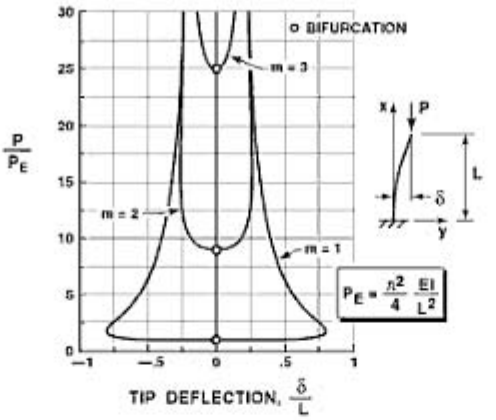


Figure 2-28 Load versus Tip Deflection Behavior for Many Loads
(After Nemeth [2-7])

2.4.3 Approximate Load-Deflection Behavior Just After Buckling

We now focus on the nature of the load-deformation behavior in the region of the first bifurcation buckling load in Figure 2-28 shown enlarged in Figure 2-29. For the ordinary fixed-free bar with no intermediate supports, buckling occurs at $P_E = (\pi^2/4)EI/L^2$ in the m = 1 mode. Clearly, the straight equilibrium shape is unstable above P_E as is denoted with the dashed line in Figure 2-29 unless special intermediate supports or con-

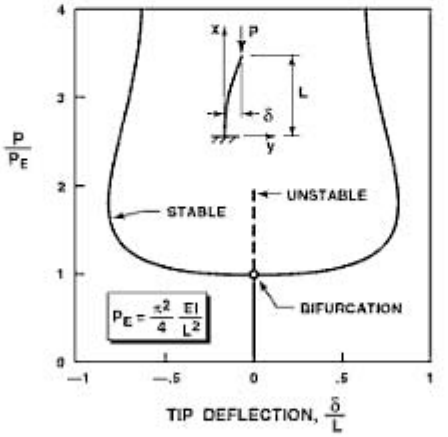


Figure 2-29 Load versus Tip Deflection Behavior Near the First Buckling Load
(After Nemeth [2-7])

Éléments sous droits d'auteur

straints on the bar exist (i.e., constraints that prevent the bar from buckling into the $m = 1$ mode). The stable behavior is buckling and subsequent large deformation into the mode $m = 1$ as shown with the solid curves in Figure 2-29. Note that the bar tip moves horizontally to the side by a maximum amount of 80% of the bar length at only about 50% above P_E, and then the tip horizontal deflection decreases as P increases. Note also that the tip horizontal deflection can never go above that maximum because the bar is fixed at its base, i.e., the bar must rise vertically from the base thereby limiting its horizontal displacement to some value less than L.

We must naturally question whether such large deflections might have other consequences or that they are even possible. Shear has already been pointed out as influencing the behavior, but its effect has not been considered in the derivation of the behavior presented.

In the vicinity of P_E, the load-deformation curve is very flat. In fact, the slope of the curve is zero at $P = P_E$. Thus, the increase in load for a small increase in deflection at $P = P_E$ is a quantity of second order, i.e., very, very small. (This demonstration that the axial force is essentially constant after buckling is the basis for the use of bars in space trusses in which a constant force is desired for practical considerations.) By virtue of the approximate curvature relation in small-deflection theory, that increase in load is neglected, so the horizontal or transverse tip deflection is indeterminate. However, we now know the nature of the actual deflections. Thus, we naturally turn to the stresses that are developed when such large deflections occur.

The approximate horizontal deflection (transverse to the original vertical axis) of an axially loaded fixed-free bar in the loading region just above buckling is

$$y_m = \frac{8L}{\pi}\left[\frac{P_E}{P}\left[\left[\frac{P}{P_E}\right]^{1/2} - 1\right]\right]^{1/2} \tag{2.204}$$

(in which P_E is the Euler load and P is the applied load) is reported by Frisch-Fay [2-8] and by Nemeth [2-7]. A similar result was supposedly derived by Grashof [2-9] according to Bleich [2-10]: however, I found no such expression in Grashof and Bleich's expression is too low by a factor of two. Such expressions are obtained by expanding the exact expression (involving elliptic integrals) in a series about P_E retaining only a few terms. Thus, the approximate expression is valid only near P_E, but not at very large deflections. From the form of Equation (2.204), we see that horizontal deflection can exist only if P_E has been exceeded (otherwise, the deflection is imaginary). Of course, that fact is consistent with our earlier observations. Specifically, from Equation (2.204), only a 1% increase in load above the Euler buckling load leads to a tip horizontal displacement of 18% of the length L!

To estimate the stresses that accompany the horizontal deflection of a fixed-free bar, we follow Gerard [2-11] and recast the deflection equation in terms of stresses by use of the simple expression, $\sigma = P/A$:

Éléments sous droits d'auteur

$$y_m = \frac{8L}{\pi}\left[\frac{\sigma_E}{\sigma_A}\left[\left[\frac{\sigma_A}{\sigma_E}\right]^{1/2} - 1\right]\right]^{1/2} \tag{2.205}$$

Again, the expression is applicable only for values of applied axial stress, σ_A, that are just above σ_E. Define the increase in stress above the Euler stress as

$$\Delta\sigma = \sigma_A - \sigma_E \tag{2.206}$$

Then, form the ratio of applied stress, σ_A, to the Euler stress in the following manner:

$$\frac{\sigma_A}{\sigma_E} = \frac{\sigma_E + \Delta\sigma}{\sigma_E} = 1 + \frac{\Delta\sigma}{\sigma_E} \tag{2.207}$$

Next, substitute the stress ratio in the deflection, Equation (2.205),

$$y_m = \frac{8L}{\pi}\left[\left[1 + \frac{\Delta\sigma}{\sigma_E}\right]^{-1}\left[\left[1 + \frac{\Delta\sigma}{\sigma_E}\right]^{1/2} - 1\right]\right]^{1/2} \tag{2.208}$$

Expand $(1 + \Delta\sigma/\sigma_E)^{1/2}$ and $(1 + \Delta\sigma/\sigma_E)^{-1}$ with the series

$$(1 + x)^n = 1 + nx + \frac{n(n-1)}{2!}x^2 + \ldots \tag{2.209}$$

and retain only the first two terms to get

$$y_m = \frac{8L}{\pi}\left[\left[1 - \frac{\Delta\sigma}{\sigma_E}\right]\frac{1}{2}\frac{\Delta\sigma}{\sigma_E}\right]^{1/2} \tag{2.210}$$

Then, retain only the highest order term to get

$$y_m = \frac{8L}{\pi}\left[\frac{\Delta\sigma}{2\sigma_E}\right]^{1/2} \tag{2.211}$$

Next, we examine the stresses in an axially loaded bent bar. On the concave side of the bent bar, the stress is highest because the compressive bending stress adds to the compressive axial stress, σ_A, i.e.,

$$\sigma_{maximum} = \sigma_{concave} = \sigma_A + \frac{Mc}{I} \tag{2.212}$$

in which c is the distance from the centroid to the most concave part of the bar cross section, but the bar-tip moment is Py_m, so

$$\sigma_{maximum} = \sigma_A + \frac{Py_m c}{I} \tag{2.213}$$

Substitute the maximum deflection, y_m in Equation (2.211), in the stress expression, Equation (2.213), to get

$$\sigma_{maximum} = \sigma_A + \frac{Pc}{I}\frac{8L}{\pi}\left[\frac{\Delta\sigma}{2\sigma_E}\right]^{1/2} \tag{2.214}$$

For a bar of rectangular cross section with width w and height 2c (in which $w > 2c$ in order to get buckling in the plane that includes the direction of the height because that plane involves the least second mo-

Éléments sous droits d'auteur

ment of the area of the bar cross section), $c/r = 3^{1/2}$ (recall that the radius of gyration is defined as $r^2 = I/A$), so

$$\frac{\sigma_{maximum}}{\sigma_A} = 1 + 3.12\,\frac{L}{r}\left[\frac{\Delta\sigma}{\sigma_E}\right]^{1/2} \tag{2.215}$$

The slenderness ratio, $(L/r)_y$, for σ_y at the boundary between elastic and plastic buckling behavior for a fixed-free bar comes from modification of Equation (2.44) on page 58 in the same manner as Equation (2.17) on page 55, i.e.,

$$\left[\frac{L}{r}\right]_y = \frac{\pi}{2}\sqrt{\frac{E}{\sigma_y}} \tag{2.216}$$

from which we easily calculate that $(L/r)_y = 50$ for mild steel[1], $(L/r)_y = 20$ to 30 for many aluminums[2], and $(L/r)_y = 100$ for high-modulus, low-yield-stress materials. Of course, a higher L/r than that at yielding merely signifies a more slender bar that will have higher bending stresses from Equation (2.215), but lower σ_A.

For a fixed-free bar of mild steel with $L/r = 50$, buckling occurs at yielding. If the load is increased by only .1% after buckling, then we see from Figure 2-30 that the maximum stress on the concave side of the bar is nearly 600% of the applied stress! Of course, for mild-steel bars with L/r less than 50, the buckling is plastic, so our elastic buckling predictions do not apply and we must appeal to the plastic buckling approach in Section 2.10. At $L/r = 100$, yielding of a mild steel bar does not occur before buckling, but the buckling stress is 1/4 of σ_y (note the hyperbolic nature of the buckling curve in Figure 2-4 on page 55). Then, if the applied load is increased by only .1% after buckling, the maximum stress on the concave side of the bar is nearly 12 times the original buckling stress or nearly 3 times the yield stress! However, mild steel cannot tolerate a stress above σ_y without developing very large strains, so a mild steel bar fails soon after buckling. Similar results can be observed for bars made of other materials such as aluminums. However, we will see later in Section 2.10 that the stress-strain-curve shapes for mild steel and aluminums are quite different, so different interpretations must be put on the significance of yielding of the two types of materials. In particular, aluminums with a nonlinear stress-strain curve can tolerate some stress above σ_y, but their stiffness decreases significantly. Nevertheless, irrespective of the bar material, the fundamental observation is that bending stresses increase enormously over the axial compressive stress at buckling after the imposition of only the slightest additional load beyond the buckling load. Obviously, such stresses cause fracture of brittle materials and yielding of those materials that yield as well as probable failure unless the material is exceptionally ductile. Apparently, the region of behavior beyond the immediate vicinity of σ_E is unreachable for practical purposes. That is, failure of the bar must occur shortly after the Euler load is reached because of excessive bending stresses.

[1] $E = 30\times10^6$ psi [207 GPa] and $\sigma_y = 30\times10^3$ psi [207 MPa].

[2] $E = 10\times10^6$ psi [70 GPa] and $\sigma_y = 30\times10^3$ psi [207 MPa] to nearly 60×10^3 psi [413 MPa].

Éléments sous droits d'auteur

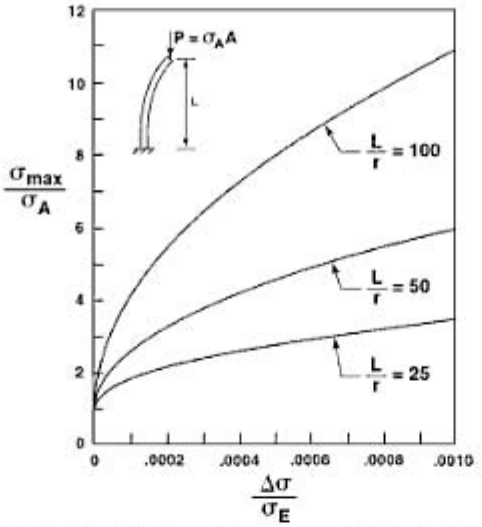


Figure 2-30 Relative Maximum Stress versus Relative Applied Stress

After we take into account the postbuckling bending stresses and their overwhelming influence on the total stresses, we schematically plot the relation between the load, P, and the horizontal bar tip deflection, δ, in Figure 2-31 from information in Table 2-2 and further calculations for the actual shape of the buckled bar. The load is normalized by P_E and the tip deflection is normalized by the bar length, L. The perfectly elastic load-deflection curve ABC from Figure 2-29 cannot actually be achieved because of the very high stresses that we just found are induced during buckling. When yielding begins at point B (or even closer to point A), the actual load-deflection curve is dashed downward toward point D rather than upward toward point C. Deformation after point D proceeds more rapidly than before to failure.

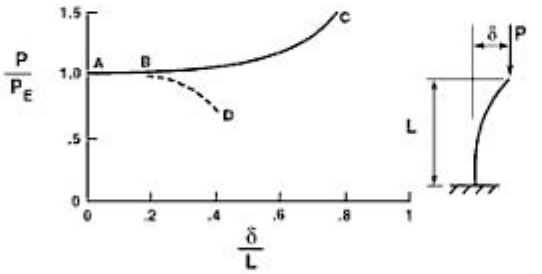


Figure 2-31 Load Versus Horizontal Tip Deflection of an Axially Loaded Bar

Éléments sous droits d'auteur

The main point of Figure 2-31 is that buckling of a bar at the Euler buckling load, P_E, is a nearly catastrophic event because of the sudden, very large outward bowing or buckling of the bar with subsequent yielding and failure. Also, for practical purposes, P_E represents the largest load that can be carried by a bar. Thus, the design significance of bar buckling is that the Euler buckling load must be avoided by use of a factor of safety that is appropriate for a catastrophic event.

Because the bar is bent over from the vertical so far after loads of even twenty percent above the Euler load in Figure 2-27, the need to include the effects of transverse shear on the bar deflection is quite obvious. Shear was ignored at the step, Equation (2.176), where the exact equation for bending was introduced. In addition, the bar was considered to be inextensible by virtue of the imposition of Equation (2.176) because only pure bending is considered. Of course, the bar must extend (actually contract) in order to accept axial load! These two inexact treatments render the Elastica solution somewhat dubious after only a small increase in load above the Euler buckling load. However, the solution of the Elastica in the vicinity of the Euler buckling load leads us to the correct conclusion that the Euler buckling load is the largest practical load that can be applied to a bar. Obviously, at the Euler load, the bar cannot accept any more load without undergoing large transverse (horizontal) deflections at the tip. Usually, there are many practical reasons why such large deflections are unacceptable in a practical structure.

2.4.4 Other Large-Deflection Buckling Problems

Note that the solution for the fixed-free bar enables us to immediately know the large-deflection buckling solution for the pinned-pinned bar. Just as we were able to accomplish the determination of buckling loads of bars with several different support systems in Table 2-1 on page 77, we can now do for large-deflection deformed shapes with different support systems. For example, we carefully consider the boundary conditions at the ends of the fixed-free bar as opposed to the boundary conditions at the ends and middle of the pinned-pinned bar Consider the second sketch in Table 2-1 on page 77 of a fixed-free bar with the buckle mode that is precisely half that of a pinned-pinned bar. Note that Table 2-1 has eigenfunctions for buckled shapes, i.e., the shapes at buckling, but not beyond. Moreover, the amplitude of the buckling deflection cannot be found in the eigenvalue problem. Obviously, there is a relationship between buckling of different bars with different support systems which does not depend on the curvature approximation used, but only on the boundary conditions. The boundary conditions are zero moment at the loaded tip and zero slope plus zero deflection at the fixed end of the fixed-free bar. And, the boundary conditions for the pinned-pinned bar are zero moment at each end, plus we observe zero slope in the middle of the bar. The two buckled bars are shown in Figure 2-32 in which the actual large-deflection deformed shapes, not just the eigenfunctions, are displayed. Of course, the Euler buckling loads are

Éléments sous droits d'auteur

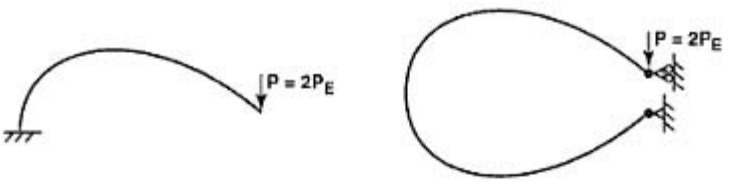


Figure 2-32 Similarity of Large-Deflection Buckling of Axially Loaded Fixed-Free and Pinned-Pinned Bars

different by a factor of four for the two different bars. These facts and symmetry plus some visual creativity allow us to establish the behavior (buckling load and actual deformation) of several other bars in various buckling modes under large loads beyond the Euler buckling load. However, just as for the fixed-free bar, all other bars quickly achieve enormous stresses just after buckling, so the large-deflection elastic solutions are not actually achievable.

2.4.5 Practical Significance of the Euler Buckling Load

Large horizontal deflections at the tip of a fixed-free bar are generally unacceptable in most engineering practice. We can easily imagine (especially after our proof) that large bending strains and stresses occur when a bar undergoes the deformations shown in Figure 2-27 for loads above the Euler buckling load. Those large stresses must be superimposed on the axial stresses from the axial load as well as the shearing stresses from the now off-axis nature of the 'axial' load. Such combined stresses surely must render the loaded bar subject to failure at some point before the bar accepts loads much higher than P_E. In fact, we have demonstrated that the stresses become enormous when the load increases by only .1%! The bending stresses compellingly dominate the axial stress in the behavior after buckling.

Thus, we now have a far better feeling or appreciation for the physical significance of the classical Euler buckling load. To wit, the classical Euler buckling load is a practical maximum load to which we can subject a bar without some desperately unattractive event happening (such as large deflection with only a small increase in load or stresses increasing to the level of failure of the material out of which the bar is made). This capping of the permissible behavior at the Euler buckling load constitutes an extremely effective and practical limit to the behavior. Popov [2-12] puts it very well: "for practical reasons, such enormous deflections can seldom be tolerated. Moreover, the material usually cannot resist the induced bending stresses. Therefore, real columns fail inelastically. In the vast majority of engineering applications, P_{cr} [P_E in the notation of this book] represents the ultimate capacity for a straight, concentrically loaded column." Those concise remarks summarize why we absolutely must limit the load-carrying capacity of all axially loaded bars to a fraction less than one of the Euler buckling load. That fraction is the inverse of the safety factor.

Éléments sous droits d'auteur

2.5 BUCKLING OF BARS BY ENERGY PRINCIPLES

Energy principles serve two main functions in structural mechanics: (1) they provide a tool for rational derivation of the differential equations and, simultaneously, the boundary conditions governing a problem and (2) they also provide techniques for direct solution of the problem without resort to the differential equations. The first function requires application of the calculus of variations which we will explore after introduction of the basic principles via the second function. Then, we will use energy principles to develop an understanding of buckling criteria in terms of potential energy. One criterion is used to derive the buckling differential equation and its boundary conditions governing buckling, and is used as the basic approach in the succeeding chapters. Two approaches will be investigated: (1) a more or less conventional approach in which the reader is misled into thinking that the reasoning is plausible and (2) a rigorous approach, not unknown before this book, in which the crucial nonlinearities are properly treated.

2.5.1 Basic Energy Principles

The *total potential energy* of a mechanical system is denoted by V and consists of two component energies:

$$V = U + \Omega \tag{2.217}$$

in which

U = strain energy
  = negative of work done by internal forces
Ω = potential energy of external forces
  = negative of work done by external forces

in which the internal and external forces are defined relative to a free-body diagram for the mechanical system. See Langhaar's book *Energy Methods in Applied Mechanics* [2-13] for a superb discussion of energy principles as most ably taught to the author by Professor Robert E. Miller. See also the book by Shames and Dym [2-14] and that by Reddy [2-15].

Consider the axially loaded rigid bar supported (held upright) by a linear rotational spring at its base as in Figure 2-33. There, the force P is external to the mechanical system, and the spring is the only internal element of the system. The U and Ω expressions for the spring and load are

$$U = \int_0^\theta k\theta \, d\theta = \frac{1}{2} k\theta^2 \tag{2.218}$$

$$\Omega = -P(L - L\cos\theta) \tag{2.219}$$

so

$$V = \frac{1}{2} k\theta^2 - PL(1 - \cos\theta) \tag{2.220}$$

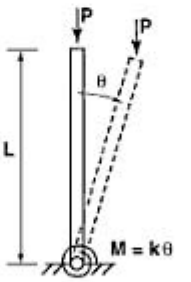


Figure 2-33 Axially Loaded Bar with a Rotational Spring Constraint

Éléments sous droits d'auteur

The *principle of stationary potential energy* is: *a mechanical system is in equilibrium if the first variation of the potential energy is zero,* i.e.,

$$\delta V = 0 \tag{2.221}$$

in which δ indicates a variation of the symbol that follows. A stationary value occurs at points where V has a horizontal tangent, i.e., a stationary value can be either a maximum, a minimum, or an inflection point of the function (see Appendix A now). For equilibrium of the example bar in Figure 2-33, we first note that the one-dimensional analogue of $\delta V = 0$ is

$$\frac{dV}{dx} = 0 \tag{2.222}$$

in which x is the independent variable. Then,

$$\frac{dV}{d\theta} = k\theta - PL \sin\theta = 0 \tag{2.223}$$

For equilibrium of the bar in Figure 2-33, we need only satisfy Equation (2.223) which is transcendental. However, we are usually interested only in the solution $\theta = 0$, i.e., the vertical equilibrium condition.

Although we know an equilibrium position or state of the bar, we must define the *character* of the equilibrium because satisfying the principle of stationary potential energy does not imply that *stable* equilibrium exists. The *types of equilibrium,* unstable, stable, and neutral, are defined in Figure 2-34 for virtual or infinitesimal displacements of a ball on a curved surface. We focus on problems for which the *infinitesimal theory of stability* suffices, i.e., only infinitesimal displacements are treated. Consider a single-degree-of-freedom system of a bead on a wire in Figure 2-35. The bead elevation is the total potential energy, V. If the bead is disturbed along the wire, apparently an infinitesimal theory is sometimes insufficient because some other stable states can be reached with

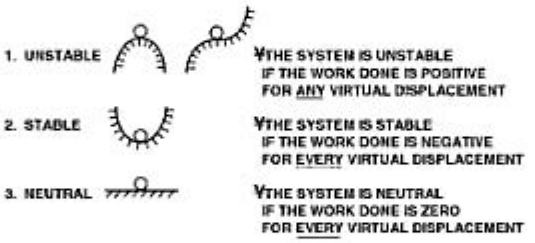


Figure 2-34 Types of Equilibrium

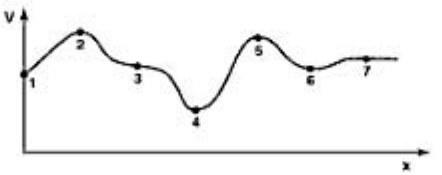


Figure 2-35 Total Potential Energy for a Single-Degree-of-Freedom System

Éléments sous droits d'auteur

finite displacements. Equilibrium occurs at a stationary point (a horizontal tangent), so V is stationary at points 2 through 7. Also, points 2, 3, and 5 are unstable; points 4 and 6 are stable (as is point 1 for which special consideration must be made because V is not stationary there); and point 7 is in neutral equilibrium. However, point 6 is not stable if large disturbances in x are permitted in which case point 6 is called *metastable*. Then, only point 4 is stable in the region depicted in Figure 2-35.

We now invoke the *principle of minimum potential energy: a mechanical system is in a stable equilibrium configuration if, and only if, the potential energy is a relative minimum for that equilibrium configuration.* Thus, although points 4 and 6 in Figure 2-35 satisfy the condition for stable equilibrium, evidently the principle of minimum potential energy as a stability criterion is not completely general. That is, if the horizontal disturbance of the system at point 4 exceeds the distance to point 5, then the system might seek a new stable equilibrium position at point 6. Alternatively, point 6 is quite apparently not a stable equilibrium point if the system is disturbed sufficiently; again, a metastable point. This type of situation is the fundamental basis for some of the snap-through buckling analyses for shells. The extension to continuous mechanical systems requires more than ordinary derivatives—partial derivatives are needed.

We can perturb a continuous mechanical system to get a change in potential energy, ΔV, that we can write in a Taylor series:

$$V + \Delta V = V + \delta V + \frac{1}{2!}\delta^2 V + \frac{1}{3!}\delta^3 V + \cdots \tag{2.224}$$

We saw that, for equilibrium,

$$\delta V = 0 \tag{2.225}$$

so the dominant term in ΔV is *presumably* $\delta^2 V$. Thus, for ΔV to be positive, i.e., for stable equilibrium,

$$\delta^2 V > 0 \tag{2.226}$$

when evaluated at the equilibrium state, i.e., where $\delta V = 0$. That is, the second variation of the total potential energy must be positive definite in order for the equilibrium configuration to be stable. Equation (2.226) serves as a stability criterion but often

$$\delta^2 V = 0 \tag{2.227}$$

is used to obtain the buckling load, i.e., the load at which equilibrium changes from stable to unstable because $\delta^2 V$ changes from positive to negative at $\delta^2 V = 0$. More precisely than Equation (2.227), we seek

$$\delta^2 V\Big|_{\delta V = 0} = 0 \tag{2.228}$$

because we are only interested in the stability of an equilibrium state. Alternatively, at the point at which ΔV changes from positive to negative, i.e., passes through zero, is where $\delta^2 V$ must be zero. If in Equation (2.224), $\delta^2 V \equiv 0$ and $\delta^3 V \equiv 0$ (as can happen in some problems), then we must examine $\delta^4 V$ to find the dominant term of ΔV in order to determine whether $\Delta V > 0$. Thus, $\delta^2 V > 0$ is not always a sufficient condition for stability (if $\delta^2 V$ doesn't even exist!), nor is $\delta^2 V = 0$ always a sufficient condition for buckling. Note that all variations above the first are only of

Éléments sous droits d'auteur

interest when evaluated at $\delta V = 0$, i.e., at an equilibrium state. That is, stability is *not* at issue when the mechanical system is not in equilibrium.

The spring-supported rigid bar in Figure 2-33 has energy in Equation (2.220), and the one-dimensional analog[1] of $\delta^2 V > 0$ is $d^2V/dx^2 > 0$, so

$$\left.\frac{d^2V}{d\theta^2}\right|_{\theta=0} = k - PL \quad \rightarrow \quad P_E = \frac{k}{L} \tag{2.229}$$

That is, the bar flops over from the upright position to an inclination of some angle, θ, when the load exceeds k/L.

2.5.2 Application of Basic Energy Principles to Stability of a Spring-Supported Rigid Bar

Find the angle θ for equilibrium of the spring-supported rigid bar system shown in Figure 2-36 if the configuration for which $\theta = 0$ corresponds to the unstretched spring. The total potential energy is

$$V = \frac{1}{2}k(a\sin\theta)^2 - W\frac{L}{2}\sin\theta \tag{2.230}$$

for a single-degree-of-freedom system, so the criterion $\delta V = 0$ corresponds to $dV/d\theta = 0$ or $V' = 0$. To find the possible equilibrium states, find V', equate it to zero, and solve for θ:

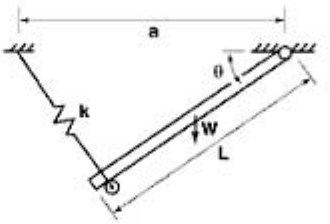


Figure 2-36 Spring-Supported Bar

$$V' = ka^2\sin\theta\cos\theta - \frac{WL}{2}\cos\theta = 0 \tag{2.231}$$

which can be written as

$$\cos\theta\left[ka^2\sin\theta - \frac{WL}{2}\right] = 0 \tag{2.232}$$

Thus, there are two equilibrium configurations. First,

$$\cos\theta = 0 \quad \rightarrow \quad \theta = \pi/2 \tag{2.233}$$

in which the bar is vertically upright and, second,

$$\theta = \text{Arcsin}\frac{WL}{2ka^2} \tag{2.234}$$

in which the bar is inclined at θ to the horizontal.

Now, investigate the nature of the equilibrium at the two equilibrium states by evaluating V" at each of the two equilibrium states and then examining its sign. First, note that

$$V'' = ka^2(-\sin^2\theta + \cos^2\theta) + \frac{WL}{2}\sin\theta \tag{2.235}$$

[1] Single-degree-of-freedom systems have a single variable, so ordinary derivatives are the equivalent of the variations.

Éléments sous droits d'auteur

$\cos\theta = 0$ Configuration:

Because $\sin\theta = 1$ when $\cos\theta = 0$,

$$V''\Big|_{\cos\theta = 0} = -ka^2 + \frac{WL}{2} \tag{2.236}$$

Thus, the equilibrium is stable if

$$\frac{WL}{2} > ka^2 \tag{2.237}$$

Apparently, the vertically upright bar becomes unstable at

$$\frac{WL}{2} = ka^2 \tag{2.238}$$

and instability occurs for all values of the parameters that do not satisfy Equation (2.237).

$\theta = \text{Arcsin } WL/2ka^2$ Configuration:

First, solve for $\cos^2\theta$ from $\cos^2\theta + \sin^2\theta = 1$, i.e.,

$$\cos^2\theta = 1 - \left[\frac{WL}{2ka^2}\right]^2 \tag{2.239}$$

Then

$$V''\Big|_{\theta = \text{Arcsin}\frac{WL}{2ka^2}} = ka^2\left[1 - 2\left[\frac{WL}{2ka^2}\right]^2\right] + \frac{W^2L^2}{4ka^2} = ka^2 - \frac{W^2L^2}{4ka^2} \tag{2.240}$$

Finally, the equilibrium is stable when

$$ka^2 - \frac{W^2L^2}{4ka^2} > 0 \tag{2.241}$$

Upon multiplication by ka^2, Equation (2.241) can be written as

$$(ka^2)^2 > \left[\frac{WL}{2}\right]^2 \tag{2.242}$$

or

$$ka^2 > \frac{WL}{2} \tag{2.243}$$

Upon comparison of the stability equations for the two foregoing equilibrium configurations, it is apparent that if $ka^2 > WL/2$, the spring is stiff enough to hold the bar in an inclined stable equilibrium state. However, if $ka^2 < WL/2$, the spring is flexible enough to allow the configuration to assume a vertical position that is stable. Thus, *there are two stable equilibrium configurations,* but not for the same values of the system parameters.

The condition $ka^2 = WL/2$ has not been explicitly examined. The equilibrium equation, $V' = 0$, can be written as

$$\cos\theta\left[\sin\theta - \frac{WL/2}{ka^2}\right] = 0 \tag{2.244}$$

Éléments sous droits d'auteur

or for this condition,

$$\cos\theta(\sin\theta - 1) = 0 \tag{2.245}$$

which has the same root for both $\cos\theta = 0$ and $\sin\theta = 1$, i.e., $\theta = \pi/2$. The stability of equilibrium is determined by examining the sign of V" in the equilibrium configuration. Upon substitution in Equation (2.235),

$$V''\Big|_{\theta = \pi/2} = -ka^2 + \frac{WL}{2} = 0 \tag{2.246}$$

Actually, then, the stability of equilibrium of the $\theta = \pi/2$ configuration cannot be assessed by examining the sign of V" because its value is zero. When V" = 0, the higher-order derivatives must be examined as in Appendix A until an even-order derivative has a nonzero value. Thus,

$$V''' = -4ka^2 \sin\theta\cos\theta + \frac{WL}{2}\cos\theta \tag{2.247}$$

$$\rightarrow \quad V'''\Big|_{\theta=\pi/2} = 0 \tag{2.248}$$

$$V'''' = -4ka^2\left(-\sin^2\theta + \cos^2\theta\right) - \frac{WL}{2}\sin\theta \tag{2.249}$$

$$\rightarrow \quad V''''\Big|_{\theta = \pi/2} = 4ka^2 - \frac{WL}{2} = 3ka^2 > 0 \tag{2.250}$$

Thus, the equilibrium of the $\theta = \pi/2$ (vertically upright bar) state is stable, and we see the need for not blindly relying on V" = 0 as a criterion for a boundary on instability but rather on fully investigating $\Delta V > 0$.

2.5.3 Buckling Criteria

We now know how to determine the stability of an equilibrium state by use of the principle of minimum potential energy. However, a common practical question is: what is the maximum load for which the mechanical system is stable? That is, what is the *limit* of stability? Or, at what load does the system *buckle*? Such a limit will be discussed within the restrictions of infinitesimal stability theory, i.e., for 'small' disturbances of the mechanical system.

Prior to the limit of stability, a mechanical system in equilibrium is, by definition, stable, i.e., $\delta V = 0$ and $\Delta V > 0$. Beyond the limit of stability, the system is, of course, unstable so that $\delta V = 0$, but $\Delta V < 0$. Obviously, then, buckling occurs when

$$\Delta V = 0 \tag{2.251}$$

at which situation neutral equilibrium is said to exist. That is, the structural element is free to take on one of several equilibrium configurations at precisely the same load and precisely the same total potential energy (because there is no change in total potential energy, i.e., $\Delta V = 0$). A specific criterion is desired for definition of the exact boundary between the two regimes of stability and instability, respectively. The condition $\Delta V = 0$ can be expanded in a Taylor Series as

$$\Delta V = \delta V + \frac{1}{2!}\delta^2 V + \frac{1}{3!}\delta^3 V + \cdots = 0 \tag{2.252}$$

Éléments sous droits d'auteur

which obviously does not constitute a practical criterion because of the infinite number of terms. We must, then, determine for which load an equilibrium configuration has $\Delta V = 0$ as the boundary between $\Delta V > 0$ (stable) and $\Delta V < 0$ (unstable). Such a condition is called a *buckling criterion*. Actually, there are several possible buckling criteria; we will discuss two such criteria in the following paragraphs.

We noted previously that $\delta^2 V$ is ordinarily the leading term in the expansion of ΔV in Equation (2.252) because $\delta V = 0$ in the equilibrium state for which we are investigating stability. Accordingly, $\delta^2 V > 0$ for stability and $\delta^2 V < 0$ for instability. A natural presumption might then appear to be that

$$\delta^2 V = 0 \tag{2.253}$$

for buckling. Actually, in the example of Section 2.5.2, the second variation of the total potential energy vanishes identically so it provides no information on the stability of the equilibrium. We were therefore forced to investigate higher order variations in the manner of Appendix A. However, for most practical mechanical systems, the loading grows from a value of zero, so an identically zero second variation is rather unlikely. Despite this unlikelihood, we must be cautious in applying $\delta^2 V = 0$ as a criterion for determining the buckling load. To denote that *the second variation must be evaluated at an equilibrium configuration*, a bar is put over the variational symbol to denote such an evaluation

$$\bar{\delta}^2 V = \delta^2 V \big|_{\delta V = 0} = 0 \tag{2.254}$$

which is known as the *neutral equilibrium method*.

An alternative buckling criterion is based on the concept of two infinitesimally close equilibrium states, i.e., two equilibrium configurations that are infinitesimally close to one another in configuration space. Pflüger [2-16] states this criterion as a form of the neutral equilibrium method:

'An equilibrium configuration is neutral if there is at least one neighboring state with unchanged loading for which the first variation of its potential energy disappears' (p. 67).

This form of the neutral equilibrium method is also known as the *adjacent equilibrium method*. If the reference configuration is denoted by subscript R and the adjacent configuration by subscript A and if both configurations are in equilibrium, then

$$\delta V_R = 0 \tag{2.255}$$

and

$$\delta V_A = 0 \tag{2.256}$$

But the reference energy plus its change under variation is

$$V_R + \Delta V_R = V_R + \delta V_R + \frac{1}{2!}\delta^2 V_R + \frac{1}{3!}\delta^3 V_R + \cdots \tag{2.257}$$

If the two states are infinitesimally close to one another,

$$V_A = V_R + \Delta V_R \tag{2.258}$$

Éléments sous droits d'auteur

Then, if we ignore $\frac{1}{3!}\delta^3 V_R$ and higher order terms,

$$V_A = V_R + \delta V_R + \frac{1}{2!}\delta^2 V_R \tag{2.259}$$

But, by Equation (2.255), Equation (2.259) reduces to

$$V_A = V_R + \frac{1}{2!}\delta^2 V_R \tag{2.260}$$

Now take the variation of both sides of Equation (2.160):

$$\delta V_A = \delta V_R + \frac{1}{2!}\delta(\delta^2 V_R) \tag{2.261}$$

But, because of Equations (2.255) and (2.256), we are left with

$$\delta(\delta^2 V_R) = 0 \tag{2.262}$$

i.e., $\delta^2 V_R$ is stationary (not necessarily a maximum or a minimum, but more likely an inflection point). Because $\delta^2 V_R$ is evaluated at the reference equilibrium state, we drop the subscript R and add a bar over the variational symbol to get the adjacent equilibrium buckling criterion

$$\delta(\bar{\delta}^2 V) = 0 \tag{2.263}$$

which is known as the Trefftz buckling criterion [2-17].

Although Equations (2.255) and (2.256) might appear to resemble one another, and indeed the variational operation δ is the same after $\delta^2 V$ is formed, the concept of each of the equations is totally different. Equation (2.255) is a description of equilibrium states through the principle of stationary potential energy. On the other hand, Equation (2.262) is a criterion for the load at which the equilibrium state changes character and at which another equilibrium state is possible through the principle of minimum potential energy.

Actually, both criteria are satisfied simultaneously, i.e., both $\bar{\delta}^2 V = 0$ and $\delta(\delta^2 V) = 0$, when buckling occurs as shown schematically in Figure 2-37 as Shen [2-18] points out. There, $\bar{\delta}^2 V$ achieves an inflection point precisely where its value changes from positive to negative with increasing P. Thus, both criteria are equally valid; both are used by many authors because both criteria lead to the same buckling equations.

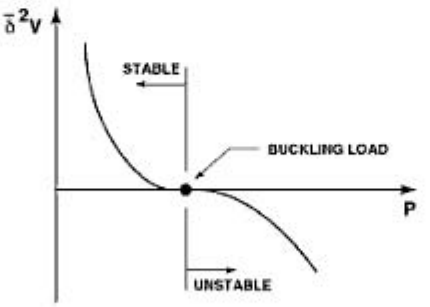


Figure 2-37 Second Variation of the Total Potential Energy in the Equilibrium State Versus Loading Parameter

Éléments sous droits d'auteur

2.5.4 Derivation of the Differential Equation and Boundary Conditions for Bar Buckling by Energy Principles

A major and too often neglected use for energy principles is the derivation of the differential equation and consistent associated boundary conditions governing a problem. The advantage of using energy principles is that the proper boundary conditions automatically result from the derivation as a part of the calculus of variations procedure. Thus, consistency of the boundary conditions is ensured. The various energy expressions must first be obtained. The total potential energy of the system is made up of the strain energy of bending during buckling and the potential energy of external forces during buckling.

The strain energy of bending of a bar is the negative of the work done by the internal forces. To a first-order approximation, from the bent bar element of differential length in Figure 2-38, the differential strain energy is

$$dU = \frac{1}{2} M\, d\theta \qquad (2.264)$$

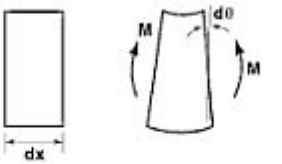


Figure 2-38 Differential Element of a Bar under Bending

in which M is the moment at a point along the bar and $d\theta$ is the differential of rotation at that point caused by M. Then, from elementary beam relations in Equations (2.176) and (2.177),

$$\frac{M}{EI} = \frac{1}{R} = \rho = \frac{d\theta}{ds} \qquad (2.265)$$

in which s is the arc length along the deformed bar. For small deflections, s is satisfactorily approximated by x, the axial coordinate. Thus,

$$d\theta = \frac{M}{EI}\, dx \qquad (2.266)$$

so from Equation (2.264),

$$dU = \frac{1}{2}\frac{M^2}{EI}\, dx \qquad (2.267)$$

Integrate the differential bending strain energy along the bar to get

$$U = \int_0^L \frac{1}{2}\frac{M^2}{EI}\, dx \qquad (2.268)$$

Note that M, E, and I can each be functions of x. An alternative bending strain energy expression is obtained by substituting the moment-curvature relation for small deflections, Equation (2.4) on page 52:

$$M = EIy'' \qquad (2.269)$$

(which is therefore consistent with other approximations already made) in Equation (2.268) to get

$$U = \int_0^L \frac{EI}{2}(y'')^2 dx \qquad (2.270)$$

Éléments sous droits d'auteur

in which E and I are functions of x as, of course, is y". We can show that the first form of U, i.e., Equation (2.268), leads to more accurate buckling loads than the second form in Equation (2.270) when approximate energy methods are used. However, there is no difference in the results when exact solution procedures are used. The second form, i.e., Equation (2.270), is convenient to use in what follows.

For an axially loaded bar, such as shown in Figure 2-39, the axial displacement of the moveable end is given by $L - L'$ when the change in length of the bar is neglected during buckling (i.e., there is no *change* in axial strain during the buckling process; however, the bar does have an axial strain prior to buckling corresponding to P/AE when under load P). An expression for $L - L' = \Delta$ is derived as follows. First, the bar length is

$$L = \int_0^L ds \tag{2.271}$$

Thus,

$$L' = \int_0^L \frac{dx}{ds}\, ds \tag{2.272}$$

But, with relations obtained from the differential triangle in Figure 2-39,

$$\frac{dx}{ds} = \left[1 - \left[\frac{dy}{ds}\right]^2\right]^{1/2} \tag{2.273}$$

At this point, we cannot ignore $(dy/ds)^2$ compared to one because if we did, then the bar would not deflect, i.e., no buckling could take place. Instead, expand the expression for dx/ds in Equation (2.273) by the binomial theorem to obtain a convenient, simplified representation of the nonlinear expression for dx/ds:

$$\frac{dx}{ds} = \left[1 - \left[\frac{dy}{ds}\right]^2\right]^{1/2} = 1 - \frac{1}{2}\left[\frac{dy}{ds}\right]^2 - \frac{1}{8}\left[\frac{dy}{ds}\right]^4 - \cdots \tag{2.274}$$

If we take only the first two terms as an approximation with the understanding that these terms represent the dominent nonlinear response,

$$L' \cong \int_0^L \left[1 - \frac{1}{2}\left[\frac{dy}{ds}\right]^2\right] ds \tag{2.275}$$

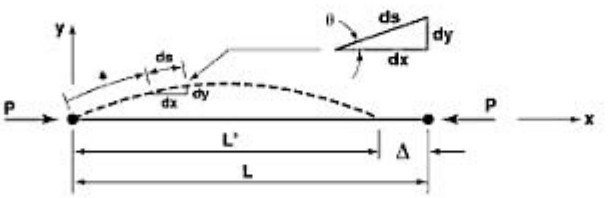


Figure 2-39 Deformed Elastic Line of a Bar

Éléments sous droits d'auteur

Then,

$$\Delta = L - L' = \int_0^L \frac{1}{2}\left[\frac{dy}{ds}\right]^2 ds \tag{2.276}$$

Thus, we note that the second term in the binomial expansion in Equation (2.274) becomes the first (and in this case only) term in the expression for the end shortening. The potential energy of external forces is then

$$\Omega = -\bar{P}\Delta = -\bar{P}\int_0^L \frac{1}{2}(y')^2 dx \tag{2.277}$$

in which for the last step we made the approximation dx = ds as with the expression for the strain energy and P has become $\bar{P}$, the buckling load.

Note that there is only axial shortening before the bar reaches the buckling load. Then, at the buckling load, the bar buckles, the end supporting the load moves toward the other end by some value Δ because of the bowing of the bar during buckling, and the work done during buckling is PΔ (not PΔ/2!) [the 1/2 in Equation (2.277) comes from the binomial expansion]. During buckling, the bar does not change its developed length because *the axial load does not change.*

An alternative derivation of Δ begins with the realization from the differential triangle in Figure 2-40 that, in turn, comes from Figure 2-39.

$$d\Delta = ds - dx \tag{2.278}$$

but

$$ds = \sqrt{dx^2 + dy^2} = \sqrt{1 + \left[\frac{dy}{dx}\right]^2}\, dx \tag{2.279}$$

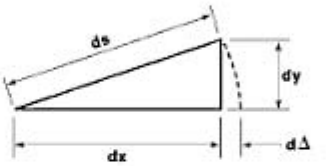


Figure 2-40 Differential Triangle of a Deformed Bar

then

$$\Delta = \int d\Delta = \int (ds - dx) = \int_0^{L'} \left[\sqrt{1 + \left[\frac{dy}{dx}\right]^2} - 1\right] dx$$
$$= \int_0^{L'} \left[\left[1 + \frac{1}{2}\left[\frac{dy}{dx}\right]^2 + \cdots\right] - 1\right] dx \cong \int_0^{L'} \frac{1}{2}\left[\frac{dy}{dx}\right]^2 dx \tag{2.280}$$

Now approximate L' by L (because L = L' + Δ and Δ is very small) to get

$$\Delta = \int_0^L \frac{1}{2}\left[\frac{dy}{dx}\right]^2 dx \tag{2.281}$$

We can now form the total potential energy

$$V = U + \Omega \tag{2.282}$$

or

Éléments sous droits d'auteur

$$V = \int_0^L \frac{EI}{2} (y'')^2 dx - \frac{\bar{P}}{2} \int_0^L (y')^2 dx \tag{2.283}$$

We should note at this point that the deflection y is actually a variation δy from the trivial equilibrium state of zero deflection. That is, the mere existence of a y implies that the bar has buckled. Because the derivatives of y appear to the second power in the foregoing integrals, *V is actually the second variation of the total potential energy because it is composed of second-order functions of the (variational) quantity y.* A usual buckling criterion for determining when stability no longer exists, i.e., the border between $\Delta V > 0$ and $\Delta V < 0$, is

$$\delta(\delta^2 V) = 0 \tag{2.284}$$

That is, the second variation, $\delta^2 V$, which must be positive (or zero when a higher order variation governs) for stable equilibrium, is made stationary. In the present case, we thus have

$$\delta V = 0 \tag{2.285}$$

as the buckling criterion because V in Equation (2.285) is the (second variation) quantity in Equation (2.283). This procedure will be clarified for bars in Section 2.5.5.2 (and for shells in Chapter 4 because they have a nontrivial prebuckled equilibrium shape which involves *variable deformations* along the shell normal to the shell after any loads that might cause buckling are applied).

In the normal calculus of variations approach (invented by Leonhard Euler while he worked on bar buckling and deformation problems!) to making an integral such as Equation (2.283) stationary, the deflection function y is given a variation δy (or arbitrary increment) such that

$$y \quad \rightarrow \quad y + \delta y = y + \varepsilon\eta \tag{2.286}$$

in which ε is an arbitrarily small number and η is an arbitrary nonzero function of x that satisfies the same boundary conditions as y. That is, ε is an arbitrary constant denoting the amplitude of $\eta(x)$. The function y(x) and its variation $y + \delta y$ are illustrated in Figure 2-41. Note that the variation $y + \delta y$ is arbitrary in the interval from $x = 0$ to $x = L$ (the length of the bar), but $y + \delta y$ also satisfies the same boundary conditions as y.

Note that when y is perturbed to $y + \delta y$, then V goes to $V + \Delta V$. And, because V is quadratic in y, ΔV contains terms only up to the fourth order. Then, the function $y + \varepsilon\eta$ can be differentiated and substituted in V to give $V + \Delta V$:

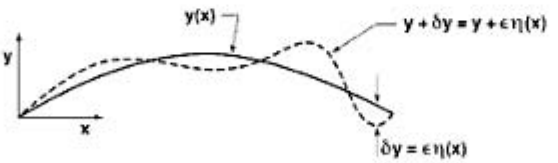


Figure 2-41 The Deflection and Its Variation

Éléments sous droits d'auteur

$$V + \Delta V = \int_0^L \frac{EI}{2}(y'' + \varepsilon\eta'')^2 dx - \frac{\bar{P}}{2}\int_0^L (y' + \varepsilon\eta')^2 dx$$

$$= \int_0^L \frac{EI}{2}\left[(y'')^2 + 2\varepsilon y''\eta'' + \varepsilon^2(\eta'')^2\right]dx$$

$$- \frac{\bar{P}}{2}\int_0^L \left[(y')^2 + 2\varepsilon y'\eta' + \varepsilon^2(\eta')^2\right]dx \qquad (2.287)$$

By definition, δV is composed of linear terms in the variational quantities, i.e., linear terms in ε:

$$\delta V = \varepsilon\left[\int_0^L EIy''\eta''dx - \bar{P}\int_0^L y'\eta'dx\right] = 0 \qquad (2.288)$$

As noted, δV is set equal to zero whereupon we observe that ε cannot be zero, so the integrals in the brackets must be zero. We now put the integrals in the form

$$\int_0^L F(x)\eta dx = 0 \qquad (2.289)$$

To do so, we integrate the second integral once by parts, i.e.,

$$-\bar{P}\int_0^L y'\eta'dx = -\bar{P}\left[y'\eta\Big|_0^L - \int_0^L y''\eta dx\right] \qquad (2.290)$$

and integrate the first integral twice by parts:

$$\int_0^L EIy''\eta''dx = EIy''\eta'\Big|_0^L - \int_0^L EIy'''\eta'dx$$

$$= EIy''\eta'\Big|_0^L - EIy'''\eta\Big|_0^L + \int_0^L EIy''''\eta dx \qquad (2.291)$$

Thus,

$$\int_0^L EIy''\eta''dx - \bar{P}\int_0^L y'\eta'dx =$$

$$EIy''\eta'\Big|_0^L - (EIy''' + \bar{P}y')\eta\Big|_0^L + \int_0^L (EIy'''' + \bar{P}y'')\eta dx = 0 \qquad (2.292)$$

Because $\eta(x)$ is an arbitrary function in the interval 0 to L, the term in parentheses under the last integral must be zero[2] for δV to be zero, i.e.,

$$EIy'''' + \bar{P}y'' = 0 \qquad (2.293)$$

which is the differential equation governing this problem. Equation (2.293) is identical to the differential equation that was derived in Section 2.3. The advantage to the present approach is that the boundary con-

[2] In accordance with the fundamental lemma of the calculus of variations [2-19], if all terms in a variational expression must be zero, then the integral of some function times an arbitrary function (in this case, δu) is zero if and only if the function itself is identically zero.

Éléments sous droits d'auteur

ditions are inherently a part of Equation (2.292). That is, because $\eta(x)$ is an arbitrary function except at the limits of the interval 0 to L, the two boundary terms in Equation (2.292) must each be zero, i.e.,

$$\begin{aligned}(EIy'')\eta'\Big|_0^L &= 0\\ (EIy''' + \bar{P}y')\eta\Big|_0^L &= 0\end{aligned} \tag{2.294}$$

The preceding equations are satisfied if either the geometric or natural boundary conditions are satisfied—the *geometric boundary conditions* are on slope and deflection (i.e., the variational quantities) and the *natural boundary conditions* are on shear and bending moment (Some authors use the terms forced, kinematic, or rigid for boundary conditions on displacements and slopes plus static and sometimes forced for boundary conditions on forces and moments). Thus, the four boundary conditions in Equations (2.295)–(2.298) are sufficient for solution of the homogeneous fourth-order differential equation in Equation (2.293):

Geometric		*Natural*	
$\eta(0) = 0$	or	$(EIy''' + \bar{P}y')\Big\|_{x=0} = 0$	(2.295)
$\eta(L) = 0$	or	$(EIy''' + \bar{P}y')\Big\|_{x=L} = 0$	(2.296)
$\eta'(0) = 0$	or	$(EIy'')\Big\|_{x=0} = 0$	(2.297)
$\eta'(L) = 0$	or	$(EIy'')\Big\|_{x=L} = 0$	(2.298)

Solution of the homogeneous differential equation subject to the homogeneous boundary conditions yields a buckling load as an eigenvalue.

For the simply supported bar that is depicted in Figure 2-39, the boundary conditions are

$$\eta(0) = 0 \tag{2.299}$$

$$\eta(L) = 0 \tag{2.300}$$

$$(EIy'')\Big|_{x=0} = 0 \tag{2.301}$$

$$(EIy'')\Big|_{x=L} = 0 \tag{2.302}$$

in which $\eta(x)$ has the same geometrically imposed boundary conditions as the function $y(x)$.

The common bar boundary conditions are depicted in Figure 2-42. The simply supported end has zero deflection and zero moment, and is often called pinned. The clamped end has zero deflection and zero slope at the supported, or fixed, end. A free end has no specified slope or deflection, but does have zero shear and moment (because it is 'free' of such loading). If linear elastic translational restraint is used to constrain the bar end, then the stiffness is k_q. Or if elastic rotational restraint is applied, then the stiffness is k_θ. These elastic restraint conditions are

Éléments sous droits d'auteur

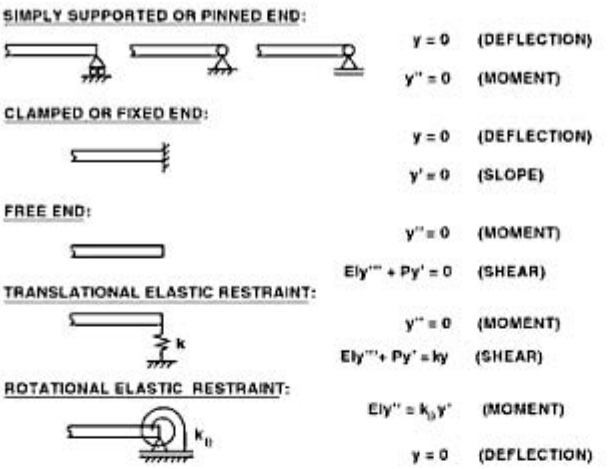


Figure 2-42 Common Bar Boundary Conditions

better studied by the approach in Section 2.5.5 (because the energy in the elastic restraints must be included in the total potential energy).

2.5.5 Rigorous Derivation of the Differential Equation and Boundary Conditions for Bar Buckling by Energy Principles

A more rigorous derivation than in Section 2.5.4 of the differential equations and boundary conditions governing bar equilibrium and buckling starts with the *nonlinear* strain-displacement relation for moderately large deformations (by omitting u_x^2 and w_x^2 from the exact strain expression)

$$\bar{\varepsilon}_x = u_x + \frac{1}{2} v_x^2 \tag{2.303}$$

in which $\bar{\varepsilon}_x$ is the strain at the bar middle surface, u is the axial displacement and v is the transverse displacement of the bar shown without supports in Figure 2-43. There, we have replaced the transverse coordinate y and transverse displacement or deflection y with y and v, respectively, to clearly separate the coordinate symbol from the displacement symbol. Moreover, the notation is subtle; $\bar{\varepsilon}_x$ is the value of ε in the x-direction at the middle surface, so that subscript x is a direction indicator; u_x is $\partial u/\partial x$; and v_x is $\partial v/\partial x$, so there the subscript x is a partial derivative indicator. Thus, the reader must take care to interpret a subscript as be-



Figure 2-43 Bar Coordinates x and y plus Displacements u and v

Éléments sous droits d'auteur

ing either a directional indicator or as a partial derivative indicator according to the context. Marguerre showed that this nonlinear strain-displacement term is necessary to rigorously treat buckling [2-20].

The Euler-Bernoulli [Jacob Bernoulli (1654–1705)] hypothesis is that plane sections that are perpendicular to the beam axis before bending remain plane and perpendicular to the deformed beam axis during beam bending. This hypothesis is a usual mechanics of materials presumption that is justified by observing that vertical lines drawn on an undeformed rubber beam remain straight but rotate as the rubber beam bends as in Figure 2-44. Thus, the strain at any point through the thickness of the beam or bar is

$$\varepsilon_x = \bar{\varepsilon}_x - y\kappa_x \tag{2.304}$$

in which κ_x is the linearized curvature of the bar middle surface

$$\kappa_x = v_{xx} \tag{2.305}$$

The stress in an axially loaded bar is a uniform one-dimensional state:

$$\sigma_x = E\varepsilon_x \tag{2.306}$$

although the possibility of a linear stress distribution through the bar thickness is provided because ε_x has a curvature term:

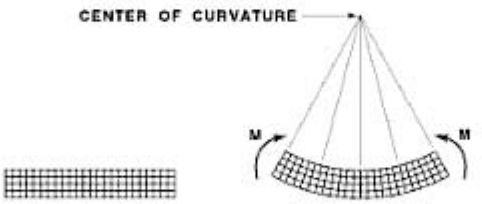
$$\sigma_x = E(u_x + \frac{1}{2} v_x^2 - y\, v_{xx}) \tag{2.307}$$

Moreover, not only the bar curvature v_{xx} will vary along the bar length, but so, of course, will the slope v_x. Thus, the bar force would appear to be a function of position along the length. However, by simple equilibrium, the bar axial force must be constant along the bar, so u_x, v_x, and v_{xx} must vary along the bar in such a manner that the bar force is constant at each point along the bar length. Thus, the resultant compressive axial force on a rectangular cross-section bar is

$$P = -\int \sigma_x dA = -E\int_{-h/2}^{h/2} (u_x + \frac{1}{2} v_x^2 - y\, v_{xx}) b dy \tag{2.308}$$

in which h is the height and b is the width of the rectangular bar cross section. However, the curvature term is linear in y, so that term integrates to zero with a resultant uniform force:

$$P = -Ebh(u_x + \frac{1}{2} v_x^2) \tag{2.309}$$



a Unloaded Beam b Loaded Beam

Figure 2-44 Bending Deformation of a Rubber Beam or Bar

Éléments sous droits d'auteur

Thus, we are not concerned with how v_{xx} varies along the bar length, but only with u_x and v_x. The negative sign in Equation (2.309) is applicable because *P is defined to be positive in compression* in this buckling environment (so the quantity we think most about is defined to be positive) and the displacements are, as always, positive in extension.

The strain energy of a three-dimensional body is

$$U = \int U_0 \, dVolume \tag{2.310}$$

in which U_0 is the strain energy density, i.e., the strain energy per unit volume. For a one-dimensional stress state, $U_0 = 1/2\sigma_x\varepsilon_x$, so

$$U = \frac{1}{2}\int \sigma_x\varepsilon_x \, dVolume \tag{2.311}$$

which becomes

$$\begin{aligned} U &= \frac{E}{2}\int\left(u_x + \frac{1}{2}v_x^2 - y\,v_{xx}\right)^2 dVolume \\ &= \frac{Eb}{2}\int_0^L\int_{-h/2}^{h/2}\left[\left(u_x + \frac{1}{2}v_x^2\right)^2 - 2yv_{xx}\left(u_x + \frac{1}{2}v_x^2\right) + y^2v_{xx}^2\right]dydx \end{aligned} \tag{2.312}$$

Integration through the bar thickness is straightforward and results in

$$U = \frac{Eb}{2}\int_0^L\left[\left(u_x^2 + u_xv_x^2 + \frac{1}{4}v_x^4\right)h + v_{xx}^2\frac{h^3}{12}\right]dx \tag{2.313}$$

The potential energy of external forces is $\Omega = +Pu\big|_{x=L}$, so

$$V = \frac{Eb}{2}\int_0^L\left[\left(u_x^2 + u_xv_x^2 + \frac{1}{4}v_x^4\right)h + v_{xx}^2\frac{h^3}{12}\right]dx + Pu\big|_{x=L} \tag{2.314}$$

Clearly, the bar is allowed both axial and transverse displacements, u and v, because it is a deformable body.

Now give a variation to the dependent variables u and v:

$$u \rightarrow u + \delta u \qquad v \rightarrow v + \delta v \tag{2.315}$$

The new energy after the variations is determined by substituting the variations, Equation (2.315), in the total potential energy expression, Equation (2.314):

$$\begin{aligned} V + \Delta V = \frac{Eb}{2}\int_0^L\Bigg[\Bigg[(u_x + \delta u_x)^2 + (u_x + \delta u_x)(v_x + \delta v_x)^2 + \frac{1}{4}(v_x + \delta v_x)^4\Bigg]h \\ + (v_{xx} + \delta v_{xx})^2\frac{h^3}{12}\Bigg]dx + P(u + \delta u)\big|_{x=L} \end{aligned} \tag{2.316}$$

Note that V is a quartic functional in the displacement derivatives. Thus, ΔV has the form $\Delta V = \delta V + 1/2!\,\delta^2V + 1/3!\,\delta^3V + 1/4!\,\delta^4V$ with no higher-order terms, i.e., $\delta^nV = 0$ for $n > 4$. And, we need only concentrate on δV and δ^2V. The indicated operations are performed, and we identify δV as those terms linear in the variations and δ^2V as those terms quadratic in the variations:

Éléments sous droits d'auteur

$$\delta V = \frac{Eb}{2}\int_0^L \left[(2u_x\delta u_x + \delta u_x v_x^2 + 2u_x v_x \delta v_x + v_x^3 \delta v_x)h + 2v_{xx}\delta v_{xx}\frac{h^3}{12} \right] dx + P\delta u\Big|_{x=L} \tag{2.317}$$

$$\frac{1}{2}\delta^2 V = \frac{Eb}{2}\int_0^L \left[(\delta u_x^2 + u_x \delta v_x^2 + 2\delta u_x v_x \delta v_x + \frac{3}{2} v_x^2 \delta v_x^2)h + \delta v_{xx}^2 \frac{h^3}{12} \right] dx \tag{2.318}$$

in which we note that $\delta^2 V$ has *no* contribution from the external force, i.e., *the second variation of the potential energy of external forces, $\delta^2\Omega$, is zero because Ω is a linear function of the displacement u, so no variation of Ω exists above the first.*

2.5.5.1 Equilibrium Analysis

For the equilibrium state, apply the principle of stationary potential energy, $\delta V = 0$, and integrate Equation (2.317) by parts to get

$$\delta V = \frac{Eb}{2}\left[h(2u_x + v_x^2)\delta u\Big|_0^L - \int_0^L (2u_{xx} + 2v_x v_{xx})\delta u\, h\, dx + h(2u_x v_x + v_x^3)\delta v\Big|_0^L + 2v_{xx}\delta v_x \frac{h^3}{12}\Big|_0^L - 2v_{xxx}\delta v \frac{h^3}{12}\Big|_0^L - \int_0^L \left[h\left[2(u_x v_{xx} + u_{xx} v_x)\delta v + 3v_x^2 v_{xx}\delta v \right] - \frac{h^3}{12}(2v_{xxxx}\delta v) \right] dx \right] + P\delta u\Big|_{x=L} = 0 \tag{2.319}$$

The multiplicand of δu in the integrand of the first integral must be 0[3], so

$$-\frac{Ebh}{2}(2u_{xx} + 2v_x v_{xx}) = 0 \tag{2.320}$$

which is the same as

$$N_{x,x} = 0 \tag{2.321}$$

in which N_x is the (constant!) axial force in the x-direction, but u and v can vary! In the same manner, the multiplicand of δv in the second integral of Equation (2.319) must be zero:

$$-\frac{Ebh}{2}\left[2(u_x v_{xx} + u_{xx} v_x) + 3v_x^2 v_{xx} \right] + \frac{Ebh^3}{12} v_{xxxx} = 0 \tag{2.322}$$

which because of Equation (2.320) reduces to

$$-\frac{Ebh}{2}(2u_x v_{xx} + v_x^2 v_{xx}) + \frac{Ebh^3}{12} v_{xxxx} = 0 \tag{2.323}$$

or

[3] In accordance with the fundamental lemma of the calculus of variations [2-19], if all terms in a variational expression must be zero, then the integral of some function times an arbitrary function (in this case, δu) is zero if and only if the function itself is identically zero.

Éléments sous droits d'auteur

$$N_x v_{xx} + M_{x,xx} = 0 \tag{2.324}$$

Equations (2.320) and (2.323) or (2.321) and (2.324) are moderately large-deflection equilibrium equations for a beam or bar (such as in Figure 2-39 on page 101 with a nontranslatable pin at $x = 0$ and a pin on rollers at $x = L$) with boundary conditions from Equation (2.319) as

$$\begin{aligned} Ebh(u_x + \frac{1}{2} v_x^2)\Big|_{x=0} = 0 \quad \text{or} \quad \delta u|_{x=0} = 0 \\ Ebh(u_x + \frac{1}{2} v_x^2)v_x - \frac{Ebh^3}{12} v_{xxx}\Big|_{x=0} = 0 \quad \text{or} \quad \delta v|_{x=0} = 0 \\ \frac{Ebh^3}{12} v_{xx}\Big|_{x=0} = 0 \quad \text{or} \quad \delta v_x|_{x=0} = 0 \end{aligned} \tag{2.325}$$

with similar boundary conditions at $x = L$ except for the force condition $-Ebh(u_x + v_x^2/2)|_{x=L} = P$. These boundary conditions can be written as

$$\begin{aligned} N_x|_{x=0} = 0 \quad \text{or} \quad \delta u|_{x=0} = 0 \\ N_x v_x + M_{x,x}|_{x=0} = 0 \quad \text{or} \quad \delta v|_{x=0} = 0 \\ M_x|_{x=0} = 0 \quad \text{or} \quad \delta v_x|_{x=0} = 0 \end{aligned} \tag{2.326}$$

i.e., as natural boundary conditions on the left in Equation (2.326) and geometric boundary conditions on the right. The natural boundary conditions are, of course, related to the derivatives of the displacements, so all boundary conditions are functions of the displacements. Also, note that the variational geometric boundary conditions after the 'or' in Equation (2.325) are each satisfied for constant values of u, v, and v_x at the ends of the bar. Thus, applied displacement or rotation boundary conditions are automatically satisfied.

Note that these equilibrium equations and boundary conditions are applicable for the equilibrium of a bar that has deformed in both the x- and y-directions, i.e., both u and v exist. Thus, these equations imply that the bar has deformed laterally (transversely) relative to its axis, although there is no implication of buckling because both the deformations u and v increase monotonically with increasing load. For these equations to be applied in an equilibrium state where the bar is straight before buckling, we must set $v = 0$ for all values of x, i.e., the bar is straight but shortens prior to buckling. Thus, the equilibrium equations and boundary conditions reduce to only the first equilibrium equation (all terms vanish in the second equilibrium equation)

$$-Ebh\, u_{xx} = 0 \quad [N_{x,x} = 0] \tag{2.327}$$

and the boundary conditions

$$Ebhu_x|_{x=0} = 0 \quad \left[N_x|_{x=0} = 0\right] \quad \text{or} \quad \delta u|_{x=0} = 0 \tag{2.328}$$

and $-Ebhu_x = P$ at $x = L$ because $\delta u \neq 0$ at $x = L$. All the other boundary conditions are automatically satisfied. This prebuckled state for a straight bar is a simple equilibrium state of uniform shortening under axial load. Such a state is often called the primary or fundamental equilibrium path

Éléments sous droits d'auteur

as a succession of straight (unbuckled) equilibrium configurations when axial load is applied in a monotonically increasing fashion.

Not all bars deform only in the shortening mode prior to buckling. Some bars also deform laterally or transversely, e.g., initially imperfect bars resulting from manufacturing defects or unsymmetrically laminated composite bars (such as the bimetallic strip in the common household thermostat as well as many structures of fiber-reinforced composite materials). For such non-straight bars, we must use the nonlinear equilibrium equations in Equations (2.320) and (2.323) plus the boundary conditions in Equation (2.325).

2.5.5.2 Buckling from a Straight Prebuckled Shape

To determine the buckling equations, apply the adjacent equilibrium (Trefftz) buckling criterion

$$\delta(\bar{\delta}^2 V) = 0 \tag{2.329}$$

from Equation (2.263). We will first address the special case in which the bar is perfectly straight prior to buckling, i.e., its prebuckling shape is straight, so recognize that prior to buckling $v \equiv 0$, hence $v_x \equiv 0$. Thus, the second variation in Equation (2.318) becomes the special second variation (evaluated in the primary equilibrium state)

$$\bar{\delta}^2 V = Eb\int_0^L \left[(\bar{\delta}u_x^2 + u_x\bar{\delta}v_x^2)h + \bar{\delta}v_{xx}^2 \frac{h^3}{12} \right] dx \tag{2.330}$$

in which the bars denote variations that are from the straight prebuckled equilibrium state determined from Equation (2.321) [with the appropriate terms eliminated because of the straight prebuckled equilibrium state of the bar (i.e., those terms involving v_x which is zero)]. Note that $\bar{\delta}^2 V$ can be written as

$$\bar{\delta}^2 V = \bar{\delta}^2 U_{m_1} + \bar{\delta}^2 U_{m_2} + \bar{\delta}^2 U_b \tag{2.331}$$

in which

$$\bar{\delta}^2 U_{m_1} = Ebh\int_0^L \bar{\delta}u_x^2\, dx \tag{2.332}$$

$$\bar{\delta}^2 U_{m_2} = Ebh\int_0^L u_x\,\bar{\delta}v_x^2\, dx \tag{2.333}$$

$$\bar{\delta}^2 U_b = \frac{Ebh^3}{12}\int_0^L \bar{\delta}v_{xx}^2\, dx \tag{2.334}$$

in which the subscript m denotes membrane effects and subscript b denotes bending effects, both occurring *during buckling*. Note that $\bar{\delta}^2 U_{m_1}$ depends only on $\bar{\delta}u$ whereas $\bar{\delta}^2 U_{m_2}$ and $\bar{\delta}^2 U_b$ depend on $\bar{\delta}v$. Thus, the value of $\bar{\delta}^2 U_{m_1}$ is totally independent of the values of $\bar{\delta}^2 U_{m_2}$ and $\bar{\delta}^2 U_b$ because $\bar{\delta}u$ and $\bar{\delta}v$ are independent variations.

Éléments sous droits d'auteur

Now give variations[4] to $\bar{\delta}u$ and $\bar{\delta}v$ noting that u_x is the equilibrium state value that remains constant during the variational process:

$$\bar{\delta}u \rightarrow \bar{\delta}u + \delta u \qquad \bar{\delta}v \rightarrow \bar{\delta}v + \delta v \tag{2.335}$$

That is, we give the special second variation $\bar{\delta}^2V$ another variation as indicated in the buckling criterion, Equation (2.329). Thus, we identify

$$\delta(\bar{\delta}^2V) = Eb\int_0^L \left[(2\bar{\delta}u_x\delta u_x + 2u_x\bar{\delta}v_x\delta v_x)h + 2\bar{\delta}v_{xx}\delta v_{xx}\frac{h^3}{12} \right] dx = 0 \tag{2.336}$$

Integrate by parts to obtain

$$Ebh\left[\bar{\delta}u_x\delta u\Big|_0^L - \int_0^L \bar{\delta}u_{xx}\delta u\,dx + u_x\bar{\delta}v_x\delta v\Big|_0^L + \bar{\delta}v_{xx}\delta v_x\frac{h^2}{12}\Big|_0^L - \bar{\delta}v_{xxx}\delta v\frac{h^2}{12}\Big|_0^L \right.$$
$$\left. - \int_0^L \left[u_{xx}\bar{\delta}v_x + u_x\bar{\delta}v_{xx} - \bar{\delta}v_{xxxx}\frac{h^2}{12} \right]\delta v\,dx \right] = 0 \tag{2.337}$$

The multipliers of δu and δv, respectively, in the integrands must be zero by the fundamental lemma of the calculus of variations, so

$$Ebh\bar{\delta}u_{xx} = 0 \tag{2.338}$$

$$Ebh(u_{xx}\bar{\delta}v_x + u_x\bar{\delta}v_{xx}) - \frac{Ebh^3}{12}\bar{\delta}v_{xxxx} = 0 \tag{2.339}$$

However, because v_x and v_{xx} are zero prior to buckling (because the bar is straight), the first equilibrium equation, Equation (2.327), results in

$$u_{xx} = 0 \tag{2.340}$$

whereupon Equation (2.339) reduces to

$$Ebhu_x\bar{\delta}v_{xx} - \frac{Ebh^3}{12}\bar{\delta}v_{xxxx} = 0 \tag{2.341}$$

Equations (2.338) and (2.341) can be written as

$$\delta N_{x,x} = 0 \tag{2.342}$$

$$\bar{N}_x\bar{\delta}v_{xx} + \delta M_{x,xx} = 0 \tag{2.343}$$

Note that Equations (2.342) and (2.343) have *variations* in forces and moments (from the prebuckling straight equilibrium state) as opposed to forces and moments themselves in the nonlinear equilibrium equations, Equations (2.321) and (2.324). This distinction is seldom explicitly stated by buckling investigators and is the cause of many misunderstandings, 'curious' explanations, and even misstatements in the buckling literature. From Equation (2.342) we get the somewhat trivial result that δN_x is constant or zero along the length. The term $\bar{N}_x$ in Equation (2.343) is, indeed, the value of the applied load that causes buckling, i.e., our objective. The boundary conditions from Equation (2.337) are:

[4]For buckling problems, the variations in Equation (2.335) might be the buckling displacements which must be visualized and interpreted as being quite different from the equilibrium displacements (which for many buckling problems are *zero*!).

Éléments sous droits d'auteur

$$\begin{aligned} Ebh\bar{\delta u}_x\Big|_{x=0} &= 0 \quad \text{or} \quad \delta u\Big|_{x=0} = 0 \\ Ebhu_x\bar{\delta v}_x - \frac{Ebh^3}{12}\bar{\delta v}_{xxx}\Big|_{x=0} &= 0 \quad \text{or} \quad \delta v\Big|_{x=0} = 0 \\ \frac{Ebh^3}{12}\bar{\delta v}_{xx}\Big|_{x=0} &= 0 \quad \text{or} \quad \delta v_x\Big|_{x=0} = 0 \end{aligned} \tag{2.344}$$

with analogous boundary conditions at $x = L$. The natural boundary conditions in Equation (2.344) can be written in terms of forces and moments and their variations as

$$\begin{aligned} \delta N_x\Big|_{x=0} &= 0 \quad \text{or} \quad \delta u\Big|_{x=0} = 0 \\ \bar{N}_x\bar{\delta v}_x + \delta M_{x,x}\Big|_{x=0} &= 0 \quad \text{or} \quad \delta v\Big|_{x=0} = 0 \\ \delta M_x\Big|_{x=0} &= 0 \quad \text{or} \quad \delta v_x\Big|_{x=0} = 0 \end{aligned} \tag{2.345}$$

Equations (2.342) and (2.343) are homogeneous differential equations with homogeneous boundary conditions in Equations (2.344) or (2.345). Thus, they constitute an eigenvalue problem and are solved accordingly. The eigenvalue is the value of N_x or the buckling load. The eigenvector is the shape of the buckled bar. Actually, there is no solution to Equation (2.342) because the eigenvalue is not involved, so, in fact, we can ignore Equation (2.342). Alternatively, we can argue that variations of u are independent of variations of v, so we need not solve the independent equation, Equation (2.342).

Note that we arrived at these equations without assuming the bar to be inextensible (as do some authors)! That is, the term $u_x\bar{\delta v}_x^2$ in $\bar{\delta}^2V$ arises *not* from external work, but from internal energy because external forces make *no* contribution to $\bar{\delta}^2V$. Thus, the 'usual' explanation of the energy approach as typified by much of the discussion in Section 2.5.4 is a *contrived falsehood*. *Contrived* because the explanations led to the correct equations to solve. *Falsehood* because incorrect statements about bar behavior are made (bars must contract axially during the loading prior to buckling; otherwise, they can have no load in them!). True, we had to work harder in Section 2.5.5 than in 2.5.4, but we obtained the correct equations with all the proper and correct explanations of bar buckling behavior, including what happens prior to buckling.

Alternatively, we could see that

$$\bar{\delta}^2V = \bar{\delta}^2U_{m_2} + \bar{\delta}^2U_b = Ebh\int_0^L u_x\,\bar{\delta v}_x^2\,dx + \frac{Ebh^3}{12}\int_0^L \bar{\delta v}_{xx}^2\,dx \tag{2.346}$$

in which we have ignored $\bar{\delta}^2U_{m_1}$ because it is expressed in terms of the variation of $\bar{u}$ ($\bar{\delta u}$) which is *independent* of the variation of $\bar{v}$ ($\bar{\delta v}$). That is, $\delta(\bar{\delta}^2U_{m_1})$ vanishes independently of $\delta(\bar{\delta}^2U_{m_2} + \bar{\delta}^2U_b)$. We saw that the differential equation from Equation (2.342) was irrelevant, and that the differential equation governing buckling came directly from the equation $\delta(\bar{\delta}^2U_{m_2} + \bar{\delta}^2U_b) = 0$. Rewrite Equation (2.346) by recognizing that

Éléments sous droits d'auteur

$$\bar{N}_x = Ebh\, u_x = -\bar{P} \tag{2.347}$$

$$\frac{Ebh^3}{12} = EI \tag{2.348}$$

in which $\bar{N}_x$ is positive in tension, but $\bar{P}$ is a compressive force, so

$$\bar{\delta}^2 V = \int_0^L EI\, \bar{\delta} v_{xx}^2\, dx - P \int_0^L \bar{\delta} v_x^2\, dx \tag{2.349}$$

which is the same as Equation (2.283) when we recognize that y in Equation (2.283) is clearly δv in Equation (2.349).

Thus, we use either the adjacent equilibrium (Trefftz) buckling criterion

$$\delta(\bar{\delta}^2 V) = 0 \tag{2.350}$$

or the neutral equilibrium buckling criterion

$$\bar{\delta}^2 V = 0 \tag{2.351}$$

With the $\bar{\delta}^2 V = 0$ buckling criterion, we are essentially setting

$$\bar{\delta}^2 U_b = -\bar{\delta}^2 U_{m_2} \tag{2.352}$$

because $\bar{\delta}^2 U_{m_1}$ vanishes independently of $\bar{\delta}^2 U_{m_2}$ and $\bar{\delta}^2 U_b$. Thus,

$$\int_0^L EI\, \bar{\delta} v_{xx}^2\, dx = P \int_0^L \bar{\delta} v_x^2\, dx \tag{2.353}$$

which Timoshenko [2-6] calls

$$\Delta U = \Delta T \tag{2.354}$$

in which Timoshenko refers to ΔU as the change in strain energy during buckling and ΔT as the work done by external forces during buckling. However, we know from Equation (2.316) that *there is no second variation of the potential energy of external forces, so* ΔT *must be something other than what Timoshenko calls it.* Considerable confusion has occurred as a result of Timoshenko's notation of a change in energy for the second variation of the total potential energy. The most confusion has resulted from his calling the second variation of part of the membrane strain energy $\bar{\delta}^2 U_{m_2}$ the change in potential energy of external forces. Timoshenko states that the bar is inextensible, but clearly (after the foregoing discussion) *that claim applies only to the bar at the buckling load during the process of buckling,* not before buckling in the necessarily deformable (extensible) equilibrium state[5]. Timoshenko's approach is most certainly not incorrect, but it is often misinterpreted and misunderstood by users, an unfortunate result from the work of as distinguished

[5]The statement by Timoshenko and Gere that a bar is inextensible (during buckling) is somewhat misleading and has seemingly come to mean that the bar is inextensible under all conditions. Actually, the bar is loaded and compresses axially because of that load. Then, during buckling, which takes place in an instant, the bar load does not change, so no additional axial strain occurs. Consequently, the bar is inextensible *only during buckling.* Thus, the bar is *always extensible,* but for an instant does not compress any more because the axial load does not change during buckling. Thereafter, with increasing load, the bar resumes compressing.

Éléments sous droits d'auteur

a scientist and engineer as Timoshenko who undoubtedly understood just what his words were intended to mean. Timoshenko's admirable objective of making the study of buckling easier for most engineers was fine when they were concerned only with buckling of straight bars. However, more contemporary engineering concerns such as laminated composite bars, plates, and shells with prestressed equilibrium states require us to adopt a more fundamental and explicitly precise terminology. We use the more explicit terminology in the remainder of this book.

2.5.5.3 Buckling from a Non-Straight Prebuckled Shape

To determine the buckling equations for the case in which the prebuckling shape of the bar is not straight, apply the adjacent equilibrium (Trefftz) buckling criterion

$$\delta(\bar{\delta}^2 V) = 0 \tag{2.355}$$

from Equation (2.263). However, we now consider the bar in a more general non-straight prebuckled equilibrium state described with the solution to the nonlinear equilibrium equations, Equations (2.320) and (2.323). Note that we are interested only in $\delta^2 V$ evaluated in the equilibrium state where $\delta V = 0$, i.e., we are concerned with $\bar{\delta}^2 V$, the special second variation. Thus, $\bar{\delta}^2 V$ can be written from Equation (2.318) as

$$\bar{\delta}^2 V = \bar{\delta}^2 U_{m_1} + \bar{\delta}^2 U_{m_2} + \bar{\delta}^2 U_{m_3} + \bar{\delta}^2 U_{m_4} + \bar{\delta}^2 U_b \tag{2.356}$$

in which

$$\bar{\delta}^2 U_{m_1} = Ebh \int_0^L \bar{\delta} u_x^2 \, dx \tag{2.357}$$

$$\bar{\delta}^2 U_{m_2} = Ebh \int_0^L u_x \, \bar{\delta} v_x^2 \, dx \tag{2.358}$$

$$\bar{\delta}^2 U_{m_3} = 2Ebh \int_0^L \delta u_x v_x \, \bar{\delta} v_x \, dx \tag{2.359}$$

$$\bar{\delta}^2 U_{m_4} = \frac{3}{2} Ebh \int_0^L v_x^2 \, \bar{\delta} v_x^2 \, dx \tag{2.360}$$

$$\bar{\delta}^2 U_b = \frac{Ebh^3}{12} \int_0^L \bar{\delta} v_{xx}^2 \, dx \tag{2.361}$$

in which the subscript m denotes membrane effects and b denotes bending effects, both occurring *during buckling*.

Now give variations to $\bar{\delta}u$ and $\bar{\delta}v$ from the equilibrium state noting that u_x and v_x are the equilibrium state values that remains constant during the variational process:

$$\bar{\delta}u \rightarrow \bar{\delta}u + \delta u \qquad \bar{\delta}v \rightarrow \bar{\delta}v + \delta v \tag{2.362}$$

Éléments sous droits d'auteur

That is, we give the special second variation $\bar{\delta}^2V$ in Equation (2.356) another variation as indicated in the buckling criterion, Equation (2.355). Thus, with the additional terms $\bar{\delta}^2U_{m_3}$ and $\bar{\delta}^2U_{m_4}$ in Equation (2.356) relative to the straight-bar case, we can identify

$$\delta(\bar{\delta}^2V) = Eb\int_0^L \left[\left(2\bar{\delta}u_x\delta u_x + 2u_x\bar{\delta}v_x\delta v_x + 2\bar{\delta}u_xv_x\delta v_x + 2v_x\bar{\delta}v_x\delta u_x + 3v_x^2\bar{\delta}v_x\delta v_x\right)h + 2\bar{\delta}v_{xx}\delta v_{xx}\frac{h^3}{12}\right]dx = 0 \tag{2.363}$$

Integrate by parts to obtain

$$\begin{aligned} Ebh\Bigg[&\left(\bar{\delta}u_x + v_x\bar{\delta}v_x\right)\delta u\Big|_0^L - \int_0^L\left(\bar{\delta}u_{xx} + v_x\bar{\delta}v_{xx} + v_{xx}\bar{\delta}v_x\right)\delta u\,dx \\ &+ u_x\delta v_x\delta v\Big|_0^L + \delta v_{xx}\delta v_x\frac{h^2}{12}\Big|_0^L + \left[\delta u_xv_x + \frac{3}{2}v_x^2\delta v_x - \delta v_{xxx}\frac{h^2}{12}\right]\delta v\Big|_0^L \\ &- \int_0^L\Bigg[\Big[u_{xx}\delta v_x + u_x\delta v_{xx} + \delta u_xv_{xx} + \delta u_{xx}v_x \\ &+ \frac{3}{2}v_x^2\bar{\delta}v_{xx} + 3v_xv_{xx}\bar{\delta}v_x\Big] - \bar{\delta}v_{xxxx}\frac{h^2}{12}\Bigg]\delta v\,dx\Bigg] = 0 \end{aligned} \tag{2.364}$$

The multipliers of δu and δv, respectively, in the integrands must be zero by the fundamental lemma of the calculus of variations, so

$$Ebh\left(\bar{\delta}u_{xx} + v_x\bar{\delta}v_{xx} + v_{xx}\bar{\delta}v_x\right) = 0 \tag{2.365}$$

$$Ebh\left[u_{xx}\bar{\delta}v_x + u_x\bar{\delta}v_{xx} + \bar{\delta}u_xv_{xx} + \bar{\delta}u_{xx}v_x + \frac{3}{2}v_x^2\bar{\delta}v_{xx} + 3v_xv_{xx}\bar{\delta}v_x\right] - \frac{Ebh^3}{12}\bar{\delta}v_{xxxx} = 0 \tag{2.366}$$

However, the first nonlinear equilibrium equation, Equation (2.320), can be written as

$$u_{xx} + v_xv_{xx} = 0 \tag{2.367}$$

whereupon Equation (2.366) simplifies to

$$Ebh\left[u_x\bar{\delta}v_{xx} + \bar{\delta}u_xv_{xx} + \bar{\delta}u_{xx}v_x + \frac{3}{2}v_x^2\bar{\delta}v_{xx} + 2v_xv_{xx}\bar{\delta}v_x\right] - \frac{Ebh^3}{12}\bar{\delta}v_{xxxx} = 0 \tag{2.368}$$

Finally, Equations (2.365) and (2.368) can be written in terms of forces and moments and their variations as

$$\delta N_{x,x} = 0 \tag{2.369}$$

Éléments sous droits d'auteur

$$\bar{N}_x \delta\bar{v}_{xx} + \delta N_x v_{xx} + \delta M_{x,xx} = 0 \tag{2.370}$$

Note that Equations (2.369) and (2.370) have *variations* in forces and moments (from the prebuckling equilibrium state) as opposed to forces and moments themselves in the nonlinear equilibrium equations, Equations (2.321) and (2.324). This distinction is seldom explicitly stated by buckling investigators and, again, is the cause of many misunderstandings, 'curious' explanations, and even misstatements in the buckling literature, especially in the case of bars that are not straight before buckling. The term $\bar{N}_x$ in Equation (2.370) is, indeed, the value of the applied load that causes buckling, i.e., our objective. The boundary conditions from Equation (2.364) are:

$$\begin{aligned}
Ebh(\bar{\delta u}_x + v_x \bar{\delta v}_x)\Big|_{x=0} = 0 \quad &\text{or} \quad \delta u\Big|_{x=0} = 0 \\
Ebh(u_x \bar{\delta v}_x + \bar{\delta u}_x v_x + \frac{3}{2} v_x^2 \bar{\delta v}_x) - \frac{Ebh^3}{12} \bar{\delta v}_{xxx}\Big|_{x=0} = 0 \quad &\text{or} \quad \delta v\Big|_{x=0} = 0 \\
\frac{Ebh^3}{12} \bar{\delta v}_{xx}\Big|_{x=0} = 0 \quad &\text{or} \quad \delta v_x\Big|_{x=0} = 0
\end{aligned} \tag{2.371}$$

with analogous boundary conditions at $x = L$. The natural boundary conditions in Equation (2.371) can be written in terms of forces and moments and their variations as

$$\begin{aligned}
\delta N_x\Big|_{x=0} = 0 \quad &\text{or} \quad \delta u\Big|_{x=0} = 0 \\
\bar{N}_x \bar{\delta v}_x + \delta N_x v_x + \delta M_{x,x}\Big|_{x=0} = 0 \quad &\text{or} \quad \delta v\Big|_{x=0} = 0 \\
\delta M_x\Big|_{x=0} = 0 \quad &\text{or} \quad \delta v_x\Big|_{x=0} = 0
\end{aligned} \tag{2.372}$$

Equations (2.369) and (2.370) are homogeneous differential equations with nonconstant coefficients (because of the obvious v_{xx} term and other derivatives of v) and homogeneous boundary conditions in Equations (2.371) or (2.372). Thus, they constitute an eigenvalue problem and are solved accordingly. The eigenvalue is the value of N_x or the buckling load. The eigenvector is the shape of the buckled bar. As with many buckling problems, the key is to understand not only (1) what happens during buckling, but (2) what happens before that crucial event.

Problem Set 2.5.5

2.5.5.1 Use linear strain-displacement relations in the derivation of equilibrium and buckling equations as in Section 2.5.5. What is unusual, if anything, about the buckling equations?

2.5.5.2 Use the buckling criterion $\bar{\delta}^2 V = 0$ instead of $\delta(\bar{\delta}^2 V) = 0$ in the derivation of Section 2.5.5 to obtain buckling equations. What differences do you detect from the final results of Section 2.5.5? Hint for solution: integration by parts is helpful. For example, in $\int \delta u_x^2 dx$, the integration by parts $\int pdq$ can include one part of the squared quantity in p and the other part in dq. Ultimately, recognize that δu is arbitrary in $\int \delta u\, f(x)\, dx = 0$, so $f(x) = 0$.

2.5.5.3 Complete all the individual steps in the equilibrium analysis in Section 2.5.5.1.

2.5.5.4 Complete all the individual steps in the buckling analysis for a straight prebuckling shape in Section 2.5.5.2.

Éléments sous droits d'auteur

2.5.5.5 Complete all the individual steps in the buckling analysis for a non-straight prebuckling shape in Section 2.5.5.3.

2.5.6 Summary

Many incorrect and misleading statements have been made in the literature about the formulation of the buckling problem. We tried to point out some of the fallacies in some of the usual derivations of buckling criteria and buckling equations. Hopefully, the consistent derivation in this section will 'put to rest' some of those unfortunate statements.

Much of the confusion comes from the overly simple nature of the problem of buckling of a straight bar. That straight bar has a trivial equilibrium state prior to buckling, i.e., straightness, so buckling displacements are unfortunately the only displacements that occur transverse to the bar. Of course, the bar has axial displacement in the equilibrium state because it is a deformable body carrying load. Then, we often see confusing statements such as the bar is inextensible (of course, it is not inextensible during equilibrium!) and the bar transverse displacements are a sinusoidal distribution when, in fact, the bar *buckling* transverse displacements are a sinusoidal distribution (and the equilibrium displacements are zero!). In the present consistent derivation, terminology or notation is introduced to clarify the distinction between equilibrium problems and buckling problems. Primarily, that notation is concerned with different notation for equilibrium displacements as opposed to buckling displacements. In addition, the equations used are clarified as opposed to simply saying the buckling equation comes from the large-deflection equilibrium equation by eliminating the transverse loading. Buckling is not an equilibrium problem despite the inference of those who state that they use "equilibrium equations" to find the buckling loads.

We developed a rational approach to buckling analysis based on energy principles, and that approach will be used throughout the book. In particular, the approach will be extended for plates and shells in Chapters 3 and 4, respectively. In the process of developing the rational approach to buckling analysis, we were able to clarify the essential differences between equilibrium differential equations and their boundary conditions as opposed to buckling differential equations and their boundary conditions. Recall that equilibrium differential equations and their boundary conditions constitute a boundary value problem in which we find the deflected shape of a beam for a prescribed loading. In contrast, the buckling differential equations and their boundary conditions constitute an eigenvalue problem in which we find the special load (the eigenvalue) such that the initial equilibrium configuration of the bar (whether straight or non-straight) is no longer stable, and the bar actually buckles into a new shape or configuration (the eigenvector). Use of this rigorous approach will help clarify what we must do when we address problems involving prebuckling deformations caused by thermal effects or initial geometric imperfections. Note that the rigorous approach inherently involves a nonlinear strain-displacement relation even to get the final linear equations, a fact that not all buckling investigators seem to be aware of.

Éléments sous droits d'auteur

2.6 APPROXIMATE BUCKLING LOADS BY ENERGY METHODS

2.6.1 Introduction

When the differential equation and boundary conditions governing a problem are too difficult to solve readily, direct energy methods are often used to find the approximate equilibrium deflections or an approximate buckling load. Two approximate direct energy methods will be discussed: the Rayleigh Method [2-21] and the Rayleigh-Ritz Method [2-22]. These methods are called direct because plausible deflection approximations are used to calculate the (approximate) components of the total potential energy directly (without using differential equations). Then, the principle of stationary potential energy is used to calculate the amplitudes of the approximate deflections for an equilibrium problem, and the principle of minimum potential energy is used to calculate the magnitude of the buckling load for a buckling problem. We will address only the direct methods for calculating the buckling load. These methods are also called direct methods of the calculus of variations as are the finite difference method and the finite element method.

The mechanical systems whose buckling loads we wish to find are usually continuous, i.e., they have an infinite number of degrees of freedom (the number of coordinates necessary to describe the configuration or position of the mechanical system at any time). The direct methods addressed differ in the number of degrees of freedom treated in their approximation of the real problem. Thus, convergence to the exact solution is a concern for multiple degree-of-freedom approaches.

The key to successfully employing direct approximate methods is selection of a suitable approximating buckling deflection function (or equilibrium deflection function). Some functions are simple and obvious; others are more complicated. We develop criteria for selection of plausible approximating functions as a major part of describing the process.

2.6.2 The Rayleigh Method

The Rayleigh Method was developed by Lord Rayleigh (John William Strutt) (1842–1919). His method is a simple, rapid way to calculate an approximate buckling load (or equilibrium deflection) with little effort. The general procedure is to choose a plausible approximate single-degree-of-freedom buckling deflection function, δv to distinguish it from the equilibrium transverse deflection function, v, which is zero for many buckling problems, calculate the corresponding total potential energy, and apply the principle of minimum potential energy to determine the buckling load. To be plausible, the approximate buckling deflection function must satisfy the geometric boundary conditions ($\delta v = 0$ and $\delta v_x = 0$) and have a shape between the ends which is approximately what the bar would assume upon buckling (implying that some differentiability conditions are imposed on the buckling deflection function by this shape requirement). Generally, the buckling deflection function will not satisfy the natural boundary conditions (i.e., those on variations in moment δM and variations in shear δS that involve higher derivatives of δv, i.e., the second and third as well as the first), and therein lies part of the reason for

Éléments sous droits d'auteur

the calculated buckling load being approximate. If the buckling deflection function satisfies the geometric boundary conditions, the natural boundary conditions, and the differential equations governing the problem, then it is the exact solution! But, that situation is far too much to realistically expect in general problems when single-degree-of-freedom approximations are used for continuous systems.

2.6.2.1 Strain Energy Integrals and Buckling Criteria

The procedure in the Rayleigh Method for buckling loads involves using the approximate buckling deflection function in the various strain energy integrals and applying a buckling criterion to those energy results. We use the notation *variation in transverse displacement, $\delta v(x)$, in order to emphasize the fact that we deal with the buckling displacement away from the equilibrium state,* i.e., we address a buckling problem, not an equilibrium problem. In addition, the boundary conditions are somewhat different for a buckling problem than for an equilibrium problem. The geometric boundary conditions appear similar (except that they are on variations of displacement, not displacement itself), but the natural boundary conditions are slightly more complicated for the buckling problem than for the equilibrium problem. In addition, to treat buckling, we must use the second variation of the total potential energy in one of two buckling criteria. First, we address the appropriate strain energy integrals.

For a bar that is perfectly straight before buckling, the special second variation of the total potential energy (evaluated in the primary equilibrium state that exists prior to buckling) is composed only of strain energy:

$$\bar{\delta}^2 V = \bar{\delta}^2 U_{m_1} + \bar{\delta}^2 U_{m_2} + \bar{\delta}^2 U_b \tag{2.373}$$

from Equation (2.331) on page 111 in which the factor of 1/2! on the second variation of V in the Taylor series expansion of V

$$V + \Delta V = V + \delta V + \frac{1}{2!}\bar{\delta}^2 V + \frac{1}{3!}\delta^3 V + \cdots \tag{2.374}$$

has been omitted because it appears in every term of Equation (2.373). Moreover, we disregard $\bar{\delta}^2 U_{m_1}$ because it vanishes independently of the other two terms in Equation (2.373) when a buckling criterion is applied, whether $\delta^2 V = 0$ or $\delta(\delta^2 V) = 0$ (see Section 2.5.5). Thus, we are left with

$$\bar{\delta}^2 V = \bar{\delta}^2 U_m + \bar{\delta}^2 U_b \tag{2.375}$$

in which $\bar{\delta}^2 U_m$ is the term $\bar{\delta}^2 U_{m_2}$ in Equation (2.373). Then, we recall from Equations (2.333) and (2.334) that

$$\bar{\delta}^2 U_m = Ebh \int_0^L u_x \, \bar{\delta} v_x^2 \, dx \tag{2.376}$$

$$\bar{\delta}^2 U_b = \frac{Ebh^3}{12} \int_0^L \bar{\delta} v_{xx}^2 \, dx \tag{2.377}$$

All overbars are a reference to variations from the equilibrium state. Now revert to notation of the variations of the displacements and their deriv-

Éléments sous droits d'auteur

atives from the primary equilibrium state being represented without an overbar for the sake of simplicity. Thus, we regard $\delta\bar{v}$, $\delta\bar{v}_x$, and $\delta\bar{v}_{xx}$ as δv, δv_x, and δv_{xx}, respectively, and rewrite the strain energy integrals as[1]

$$\bar{\delta}^2 U_m = \int_0^L Ebh\, u_x\, \delta v_x^2\, dx \tag{2.378}$$

$$\bar{\delta}^2 U_b = \int_0^L EI\, \delta v_{xx}^2\, dx \tag{2.379}$$

in which we recognize from Equation (2.347) that the quantity $Ebh\, u_x$ is the bar axial force N_x in the equilibrium state (positive in tension) or $-P$ in which P is a compressive force for buckling problems, so we can write

$$\bar{\delta}^2 U_m = -\int_0^L \bar{P}\, \delta v_x^2\, dx \tag{2.380}$$

so the buckling criterion is either the neutral equilibrium method:

$$\bar{\delta}^2 V = \bar{\delta}^2 U_m + \bar{\delta}^2 U_b = \int_0^L EI\, \delta v_{xx}^2\, dx - \int_0^L \bar{P}\, \delta v_x^2\, dx = 0 \tag{2.381}$$

or the adjacent equilibrium method (the Trefftz buckling criterion):

$$\delta(\bar{\delta}^2 V) = \delta\left[\bar{\delta}^2 U_m + \bar{\delta}^2 U_b = \int_0^L EI\, \delta v_{xx}^2\, dx - \int_0^L \bar{P}\, \delta v_x^2\, dx\right] = 0 \tag{2.382}$$

which for the single-degree-of-freedom Rayleigh Method is equivalent to

$$\frac{d}{da}\left[\bar{\delta}^2 V\right] = 0 \tag{2.383}$$

which is the one-dimensional analog of $\delta(\bar{\delta}^2 V) = 0$ if a is the single-degree-of-freedom parameter, usually the amplitude of the approximate deflection function. We will concentrate on the neutral equilibrium buckling criterion which has the simple result

$$\int_0^L EI\, \delta v_{xx}^2\, dx = \int_0^L \bar{P}\, \delta v_x^2\, dx \tag{2.384}$$

The left-hand side of Equation (2.384) is $\bar{\delta}^2 U_b$ involving the variation in curvature, δv_{xx}, and will be referred to as the variation-in-curvature bending strain energy integral.

Alternatively, the constitutive relation

$$M = EI\, v_{xx} \tag{2.385}$$

can be varied to get

$$\delta M = EI\, \delta v_{xx} \tag{2.386}$$

so we can write $\bar{\delta}^2 U_b$ as

[1] Observe that, because the bar is straight before buckling, any transverse displacement is a variation in displacement from the equilibrium state, but we will not rely on that coincidence to 'simplify' our work because that approach often leads to many unfortunate misinterpretations and misunderstandings, especially with plates and shells.

Éléments sous droits d'auteur

$$\bar{\delta}^2 U_b = \int_0^L \frac{(\delta M)^2}{EI}\, dx \tag{2.387}$$

which is called the variation-in-moment bending strain energy integral. Both forms of $\bar{\delta}^2 U_b$ have identical values if $\delta M = EI\, \delta v_{xx}$. However, when we approximate the buckling deflection δv, then the variation in curvature, δv_{xx}, also becomes approximate, and δM by statics involving δv also becomes approximate, but in a different manner or to a different degree of approximation than δv_{xx}. Thus, δM is no longer equal to $EI\, \delta v_{xx}$, so the two forms of bending strain energy integrals, namely the variation-in-curvature bending strain energy integral and the variation-in-moment bending strain energy integral do not yield identical results when δv is an approximate function.

In the Rayleigh method, *we are always approximating the buckling displacement*, so we get two different values of $\bar{\delta}^2 U_b$ from Equation (2.379) and (2.387) because the expression for variation in moment depends on an approximate δv, and the expression for the (approximate) variation in curvature, δv_{xx} is an approximation of higher order than for δ. Therefore, both the approximate δv and the approximate δv_{xx} are inherently of a different accuracy relative to the exact δv and δv_{xx}. That is, Equation (2.386) is *not satisfied by any approximate buckling deflection!* Of course, if we were so fortunate as to use the exact buckling deflection as an 'approximate deflection', then Equation (2.386) would be satisfied. Thus, we get different buckling loads when we use the approximate buckling deflections with the variation-in-moment-based $\bar{\delta}^2 U_b$ as opposed to the variation-in-curvature-based $\bar{\delta}^2 U_b$ as we will soon confirm.

Lang [2-23] shows the variation-in-moment bending strain energy integral approach to be inherently more accurate than the variation-in-curvature bending strain energy integral for the problem of buckling of an axially compressed strut (bar) with nonuniform stiffness [EI(x)] in which the variation in moment is directly proportional to the buckling deflection δv. Without even addressing his proof, we argue that his contention seems correct by using simple geometry-based concepts. The variation in moment involves the variation in deflection directly as a 'moment arm', and we can usually visualize what the variation in buckling deflection should be. However, the variation in curvature involves the *second derivative* of the variation in buckling deflection which is far more difficult to visualize, and therefore far more difficult to correctly approximate than the variation in buckling deflection itself.

The approximate buckling load calculated by use of the Rayleigh method is greater than the exact buckling load (except in the trivial case where the exact buckle mode shape is used). The reason for this result comes from the introduction of additional constraints on the real (continuous) system by using an approximate single-degree-of-freedom deflection. Thus, because the stable equilibrium configuration involves the least energy (by the principle of minimum potential energy), the approximate energy exceeds the exact energy, so, accordingly, the resulting approximate buckling load is higher than the exact buckling load. Finally, we can conclude that, of several approximate buckling loads, the lowest

Éléments sous droits d'auteur

is the closest to the exact solution because its energy is the closest to being correct. However, *we do not know how much higher the approximate buckling load is than the exact buckling load.*

2.6.2.2 Boundary Conditions

To determine or choose a deflection approximation, we might be guided somewhat by our knowledge of how beams deflect. That is, we might consider using the deflection equation for a beam under transverse load as a candidate approximation for a buckling problem. Why would we do that? Simply because the shape into which the beam deflects might *somewhat resemble the shape* into which a bar might buckle. Such equilibrium shapes are often polynomials or sinusoidal functions as we recall from solution of beam equilibrium problems.

Another tricky aspect to deal with is the possible symmetry or antisymmetry of deformation about the bar mid-length in a buckling problem. In contrast, in an equilibrium problem, a symmetrically loaded symmetric structure will deform only in a symmetrical manner. However, a symmetrically loaded symmetric structure can buckle either symmetrically or *antisymmetrically* depending on the buckling load and hence mode.

Yet another tricky aspect to deal with is the fact that the structure can buckle into many different buckle mode shapes with associated different buckling loads (just as there are many vibration frequencies and mode shapes). Thus, a specific deflection approximation might be to a higher mode than for the lowest buckling load we seek.

Caution is urged here! Deflection under transverse load is quite different from buckling deflection under axial load. For one thing, the natural boundary conditions to be fulfilled are entirely different. Of course, the differential equation is also entirely different! Thus, an approximate answer will be obtained, but that answer will be too high—in fact higher than our 'best effort' should be, in which our best effort is to use a deflection approximation that satisfies all the applicable boundary conditions and represents the deflection well between the ends.

In the Rayleigh Method, the geometric boundary conditions

$$\delta v\big|_{end} = 0 \tag{2.389}$$

$$\delta v_x\big|_{end} = 0 \tag{2.390}$$

must be satisfied by the approximating buckling deflection function or else an obviously different physical problem is treated than desired. However, the natural boundary conditions

$$\delta M\big|_{end} = EI\delta v_{xx}\big|_{end} = 0 \tag{2.391}$$

$$-\delta S\big|_{end} = EI\delta v_{xxx}\big|_{end} + \overline{P}\delta v_x\big|_{end} = 0 \tag{2.392}$$

need not be satisfied where they apply (although if they are not satisfied, then a 'slightly different' physical problem is implied). The reason for that claim is related to the fact that the natural boundary conditions are of higher order in terms of derivatives of the deflection than the geometric boundary conditions. However, if the natural boundary conditions are

Éléments sous droits d'auteur

satisfied, then the approximate buckling load will be closer to the exact buckling load than if they are not satisfied. This statement must be tempered by the realization that the buckling deflection must be well-approximated inside the boundaries. That is, the approximating function must be capable of representing the bar buckling deformation fairly well between the ends of the bar. Moreover, any energy methods solution is typically an approximation to the real physical problem (otherwise we would not be using energy methods!). Thus, any situation in which one or more boundary conditions, whether geometric or natural, is not satisfied constitutes a different physical problem than intended to a greater or lesser extent, respectively. The natural boundary conditions can be written as

$$\delta v_{xx}\big|_{end} = 0 \tag{2.393}$$

$$\delta v_{xxx}\big|_{end} + k^2 \delta v_x\big|_{end} = 0 \tag{2.394}$$

The zero variation-in-curvature boundary condition is easily satisfied with many deflection approximations. However, the second boundary condition, which is related to the variation in shear, can be satisfied only by the exact solution if δv_x and δv_{xxx} are not both zero. That is, satisfying the somewhat complicated variation-in-shear boundary condition is not possible unless the exact deflection and load are known because they both *interact* in that boundary condition. When $v_x = 0$, such as for the bar with a guided upper end[2] in Figure 2-45, a pure displacement derivative boundary condition results:

$$v_{xxx}\big|_{guide} = 0 \tag{2.395}$$

Only then can the second natural boundary condition $\delta S = 0$ be satisfied. Bars with guided supports are treated in Sections 2.3.6 and 2.3.7.

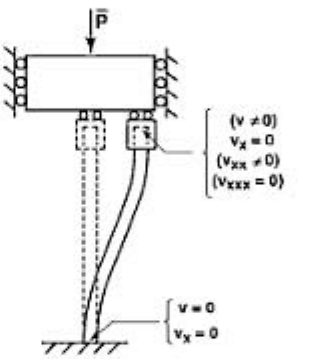


Figure 2-45 Axially Compressed Bar with Lower End Fixed and $v_x\big|_{guide} = 0$ but $v\big|_{guide} \neq 0$

Recall that the geometric boundary conditions for the buckling problem are identical to those of the equilibrium problem with the same support conditions, i.e., if $v = 0$, then $\delta v = 0$ and if $v_x = 0$, then $\delta v_x = 0$ because the variations in displacement must correspond to the same class of functions as the displacements themselves. Similarly, for the natural boundary conditions, if $M = 0$, then $\delta M = 0$ and if $S = 0$, then $\delta S = 0$ (although $\delta M = 0$ does not imply more than that M does not change during buckling). This realization helps us find plausible buckling deflection approximations because we can visualize and have experienced the

[2]The 'guided' bar end does not rotate, yet can translate perpendicular to the bar axis.

Éléments sous droits d'auteur

equilibrium deflection shapes of many beams under transverse loading. However, we must also recognize that transverse loading on a beam requires a shear force on at least one end of the bar whereas a buckled bar has no variation in shear. Such thoughts should be helpful in the process of identifying suitable buckling deflection approximations. For example, some equilibrium problems appear to have some, but not all, of the characteristics of a buckling problem. Thus, a known exact equilibrium deflection function might be of use to us in approximating a buckling deflection.

Note that the geometric boundary conditions involve derivatives to the zeroth and first order whereas the natural boundary conditions involve derivatives to the first, second, and third order. If we do not satisfy the geometric boundary conditions with a deflection approximation, then we *quite obviously* are not solving the correct physical problem. If we do not satisfy the natural boundary conditions, then it is less obvious that we are not solving the correct physical problem. That is, the subtleties of the higher-order boundary conditions are not obvious. Of course, failure to satisfy *all* the boundary conditions and the differential equation governing the problem always means that we are not solving the correct physical problem! We are attempting to solve physical problems in an approximate manner, so we must expect certain inconsistencies and inaccuracies in our procedure.

One of the pitfalls in our choice and assessment of a deflection approximation is our ability to visualize that deflection approximation in terms of the boundary conditions that it *must* satisfy (geometric), or in some cases only *should* satisfy (natural) to achieve a good solution. The human eye can easily perceive the deflection v and the slope v_x plotted for the structural element. However, we cannot visualize v_{xx} easily, and we simply cannot visualize v_{xxx} at all! Thus, our assessment of the validity of a specific deflection approximation must be based on whether the mathematically expressed boundary conditions are satisfied. That is, our first step with a candidate approximate deflection function must be to examine its consequences in terms of whether it satisfies the various boundary conditions. To do so, simply differentiate the deflection approximation as many times as necessary and compare each derivative with the respective boundary condition. Skipping this revealing step is overlooking one of the most important aspects of the Rayleigh method.

Although the usual form of geometric boundary condition is $v = 0$ or $\delta v = 0$ and/or $v_x = 0$ or $\delta v_x = 0$, a subtle form of a geometric boundary condition is, for example, that a deflection is non-zero or a slope is non-zero (thereby requiring imposition of the corresponding natural boundary condition). Suppose a candidate deflection approximation implies that a deflection (or slope) is zero at one end whereas in the real structural element the deflection (or slope) is *not* constrained to be zero at that end. Thus, the candidate deflection approximation corresponds to another physical problem, not the one you're trying to solve! Accordingly, you must make certain that every deflection approximation is valid by investigating the nature of the boundary conditions that it does satisfy, i.e., both the actual and implied boundary conditions.

Éléments sous droits d'auteur

Note that imposition of a transverse constraint someplace between the ends, for example at the center as in Figure 2-46a, is a geometric boundary condition that must be satisfied. If the geometric boundary conditions are not satisfied by a candidate deflection approximation, then that approximation corresponds to a different physical problem than the one you're trying to solve! Thus, we must regard all physical constraints as boundary conditions *even if they are not at the ends of the bar!* Think back to the problem of deflection of a two-span beam from elementary mechanics of materials in Figure 2-46b. To solve this statically indeterminate problem by a differential equation approach, we broke the beam into three intervals A-P, P-B, and B-C, integrated the three differential equations for the three intervals to obtain three general solutions (with integration constants) for the three intervals, applied the boundary conditions at the ends of the bar, and finally *applied the boundary conditions at the ends of each interval* (all of which had to match with those of the adjacent interval!) to determine all constants of integration. Thus, the zero deflection at a support such as B in Figure 2-46 is indeed a geometric boundary condition even though B is not at a bar end.

That a candidate deflection approximation function does not satisfy the natural boundary conditions is not unusual. Recall the three conditions on the deflection for the exact solution of a physical problem:

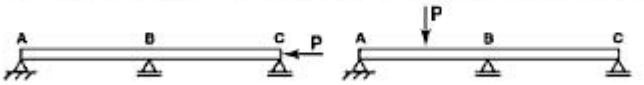
1. satisfies all geometric boundary conditions
2. satisfies all natural boundary conditions
3. satisfies the differential equation governing the phenomenon

In the Rayleigh Method, we do not even consider the solution of the differential equation. If the natural boundary conditions of the actual physical problem are not satisfied, then the candidate deflection approximation is also for a different physical problem, but not as much different as if the geometric boundary conditions are not satisfied. The difference between the two types of boundary conditions lies in the subtleties of the higher order derivatives (than in the geometric boundary conditions) in the natural boundary conditions (variations in moment and shear forces are related to second and third plus first derivatives, respectively).

A subtlety of natural boundary condition satisfaction is that the actual physical problem might have

$$\delta M\big|_{end} = EI\delta v_{xx}\big|_{end} \neq 0 \tag{2.388}$$

yet $\delta v_x\big|_{end}$ is not zero (of course, if $\delta v_x = 0$ there is a moment). Such a case can arise with a rotational spring constraint at the end where M is now proportional to the spring rotation, v_x. Thus, $\delta v_x\big|_{end} \neq 0$ in contrast to the simple fixed-end condition. Note that EI in the term $EI\delta v_{xx}$ cannot be zero at the bar end in buckling problems because an axial load cannot



a Buckling b Deflection

Figure 2-46 Buckling and Deflection of a Two-Span Bar or Beam

Éléments sous droits d'auteur

be applied to a bar with E = 0 or to a bar with a pointed end (I = 0) because a finite load on a zero-area end would result in infinite stresses! Note also that $\delta M = EI\delta v_{xx}$ is true only if the exact deflection is being used; otherwise, δM and $EI\delta v_{xx}$ are only approximately equal.

We next address two examples in the following manner:

1. The approximate buckling deflection function is selected and carefully examined to determine the boundary conditions that are satisfied and those that are not satisfied.
2. The variation-in-moment bending strain energy integral approach is used along with the variation-in-membrane strain energy integral to get a buckling load by the Rayleigh Method.
3. The variation-in-curvature bending strain energy integral approach is used along with the variation-in-membrane strain energy integral to get a buckling load by the Rayleigh Method to be contrasted with the result from step 2.

If an exact solution is available for special problems, the error in using the Rayleigh Method can be calculated. We hope from our study of various buckling problems for which an exact solution is available to be able to devise some guidelines for how to solve problems for which we don't know the exact solution. That is, we need guidelines for approximate solutions to problems that don't have exact solutions; otherwise, we would not be attempting to solve them approximately!

2.6.2.3 Buckling of an Axially Compressed Pinned-Pinned Bar

As an example, consider the axially compressed bar with pinned ends shown in Figure 2-47. The geometric boundary conditions are $\delta v = 0$ at $x = 0$ and $x = L$, and the natural boundary conditions are $\delta M = 0$, i.e., $\delta v_{xx} = 0$, at $x = 0$ and $x = L$. That is, only one type of natural boundary condition exists. We expect the lowest buckling mode to be symmetric about the mid-length of the bar based on our previous knowledge of this problem. Note that if we are wrong about a basic presumption such as the preceding, we will calculate an incorrect buckling load—however, it will be higher than the exact buckling load.

To test the Rayleigh Method, use the known exact buckling deflection function and find the buckling load to see if it agrees with the known exact solution. The buckling deflection function is

$$\delta v = \Delta \sin \frac{\pi x}{L} \qquad (2.396)$$

in which Δ is the unknown amplitude. That this δv satisfies both the geometric ($\delta v = 0$) and natural ($\delta v_{xx} = 0$) boundary conditions is readily veri-

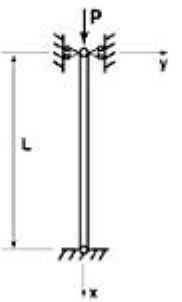


Figure 2-47 Axially Compressed Bar with Pinned Ends

Éléments sous droits d'auteur

fied (both boundary conditions involve the sine function evaluated at the ends x = 0 and x = L). The variation in moment along the bar is

$$\delta M = \bar{P}\delta v = \bar{P}\Delta \sin\frac{\pi x}{L} \tag{2.397}$$

The variation-in-moment bending strain energy integral leads to

$$\bar{\delta}^2 U_b = \int_0^L \frac{(\delta M)^2}{EI}\,dx = \frac{\bar{P}^2\Delta^2}{EI}\int_0^L \sin^2\frac{\pi x}{L}\,dx = \frac{\bar{P}^2\Delta^2}{EI}\frac{L}{2} \tag{2.398}$$

and the second variation of the membrane strain energy is

$$\bar{\delta}^2 U_m = -\int_0^L \bar{P}\,\delta v_x^2\,dx = -\bar{P}\Delta^2\frac{\pi^2}{L^2}\int_0^L \cos^2\frac{\pi x}{L}\,dx = -\bar{P}\Delta^2\frac{\pi^2}{2L} \tag{2.399}$$

Then, by the neutral equilibrium buckling criterion (see Section 2.5.5.2)[3] which can be written as $\bar{\delta}^2 V = \bar{\delta}^2 U_m + \bar{\delta}^2 U_b = 0$,

$$\bar{P} = \pi^2\frac{EI}{L^2} \tag{2.400}$$

which is, of course, the exact solution for the lowest buckling load of a pinned-pinned bar as we had hoped.

With the variation-in-curvature bending strain energy integral,

$$\bar{\delta}^2 U_b = \int_0^L EI\,\delta v_{xx}^2\,dx = EI\Delta^2\frac{\pi^4}{L^4}\int_0^L \sin^2\frac{\pi x}{L}\,dx = EI\Delta^2\frac{\pi^4}{2L^3} \tag{2.401}$$

so by the neutral equilibrium buckling criterion $\bar{P} = \pi^2 EI/L^2$. These two results for the buckling load are identical because δM is exactly equal to $EI\delta v_{xx}$ throughout the length of the bar, and therefore we simply have two forms of the exact solution to the buckling problem.

We could also use the adjacent equilibrium (or Trefftz) buckling criterion $\delta(\bar{\delta}^2 V) = 0$ which, in this single-degree-of-freedom case, is

$$\frac{d}{d\Delta}(\bar{\delta}^2 V) = 2\frac{\bar{P}^2\Delta}{EI}\frac{L}{2} - 2\bar{P}\Delta\frac{\pi^2}{2L} = 0 \tag{2.402}$$

which also leads to $\bar{P} = \pi^2 EI/L^2$ because Δ cannot be zero (no buckling).

Next, suppose as an approximate buckling deflection function we choose the quadratic function

$$\delta v = \Delta x(L - x) \tag{2.403}$$

in which Δ is the (unknown) amplitude of the buckle. The only obvious merit of this function is that $\delta v(x)$ satisfies the geometric boundary condition of $\delta v = 0$ at the ends x = 0 and x = L. The derivatives are

[3] Recall that because the deflection approximation is to the *buckling* deflection, the associated energy is actually the second variation of the total potential energy. In fact, there is no second variation of the potential energy of external forces (often a force times a displacement term). Instead, there is a term in the second variation of the *strain energy* (involving by equilibrium *internal* forces) that contains the loading. That term is decidedly *not* the potential energy of external forces, which should be quite apparent from the fact that the subject term is an integral term, not a boundary term!

Éléments sous droits d'auteur

$$\delta v_x = \Delta(L - 2x) \tag{2.404}$$

$$\delta v_{xx} = -2\Delta \tag{2.405}$$

The variation in slopes at each end are equal in magnitude and opposite in sign, a condition to be expected for a buckling deflection that is symmetric about the bar mid-length. That the second derivative is a constant signifies a constant variation in moment along the bar including at the ends where we know that the variation in moment must be zero because of the pinned ends. Moreover, we know the actual variation in moment has a maximum value at mid-span, so the variation in moment is improperly represented throughout the bar with this approximating function. The only failure to satisfy a natural boundary condition is the variation-in-moment condition, but there is indeed *only one natural boundary condition*, so we know we cannot possibly get the correct solution.

Substitute the derivatives of the deflection in the variation-in-curvature-based bending strain energy expression, Equation (2.379) to get

$$\bar{\delta}^2 U_b = \int_0^L EI\delta v_{xx}^2 \, dx = 4EI\,\Delta^2 \int_0^L dx = 4EIL\,\Delta^2 \tag{2.406}$$

The second variation in membrane strain energy during buckling is

$$\bar{\delta}^2 U_m = -\bar{P}\int_0^L \delta v_x^2 \, dx = -\bar{P}\,\Delta^2 \int_0^L (L^2 - 4Lx + 4x^2)dx = -\frac{\bar{P}L^3\Delta^2}{3} \tag{2.407}$$

Then, by the neutral equilibrium buckling criterion,

$$\bar{P} = 12\frac{EI}{L^2} \tag{2.408}$$

Alternatively, by the adjacent equilibrium buckling criterion $\delta(\bar{\delta}^2 V) = 0$,

$$\frac{d}{d\Delta}(\bar{\delta}^2 V) = 2\left[4EIL - \frac{\bar{P}L^3}{3}\right]\Delta = 0 \tag{2.409}$$

from which for nonzero Δ (zero Δ implies no buckling),

$$\bar{P} = 12\frac{EI}{L^2} \tag{2.410}$$

The two buckling criteria yield identical results in this example. The approximate buckling load is about 20% greater than the exact solution of

$$\bar{P} = \pi^2\frac{EI}{L^2} \tag{2.411}$$

The agreement with the exact solution might not be expected to be good in view of nonsatisfaction of the zero variation-in-curvature boundary conditions at each end. As a matter of fact, the chosen deflection function implies a constant variation in curvature and hence constant variation in moment along the bar! In addition to violation of the natural boundary condition of zero variation in moment at the ends, the deflection function obviously does not satisfy the governing differential equation. Nevertheless, the approximate buckling load is only 20% too high.

Éléments sous droits d'auteur

With the variation-in-moment bending strain energy integral

$$\bar{\delta}^2 U_b = \int_0^L \frac{(\delta M)^2}{EI}\,dx = \frac{\bar{P}^2\Delta^2}{EI}\int_0^L (L^2x^2 - 2Lx^3 + x^4)\,dx = \frac{\bar{P}^2L^5\Delta^2}{30EI} \qquad (2.412)$$

the neutral equilibrium buckling criterion leads to $\bar{P} = 10EI/L^2$ which is only 1.5% above the exact solution despite nonsatisfaction of the natural boundary condition.

So far, our anecdotal evidence has verified Lang's proof that the variation-in-moment bending strain energy integral leads to a more accurate buckling load than does the variation-in-curvature bending strain energy integral [2-23]. However, in this case, the variation-in-curvature integral was far easier to integrate than the variation-in-moment integral.

2.6.2.4 Buckling of an Axially Compressed Fixed-Free Bar

For an axially compressed bar fixed at its base and free at the loaded end as in Figure 2-48, a more complicated problem arises than for the pinned-pinned bar in the preceding section. Specifically, two natural boundary conditions are involved at the free end: $\delta M = 0$ and $\delta S = 0$ at $x = L$. Thus, there are more possible places to go wrong in the approximating buckling deflection function. The geometric boundary conditions are $\delta v = 0$ and $\delta v_x = 0$ at the fixed end ($x = L$). It should be no surprise that a buckling deflection approximation which is the exact solution, i.e.,

$$\delta v = \Delta\left[1 - \cos\frac{\pi x}{2L}\right] \qquad (2.413)$$

when substituted in the variation-in-energy integrals of the Rayleigh Method leads to the exact buckling load of $\bar{P} = (\pi^2/4)EI/L^2$ from Section 2.2.4 on page 58.

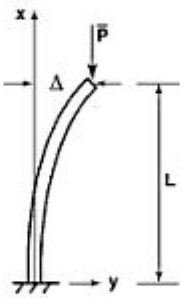


Figure 2-48 Axially Loaded Fixed-Free Bar

Next, we proceed to use a deflection approximation for a cantilever *beam* that is *transversely loaded at the free end (i.e., an equilibrium deflection, not a buckling deflection*, but hopefully the nature of the solutions is somewhat similar):

$$\delta v = \frac{\Delta x^2}{2L^3}(3L - x) \qquad (2.414)$$

in which Δ is the buckling deflection amplitude at the free end. The derivatives of the buckling approximation are

$$\delta v_x = \frac{3\Delta}{2L^3}(2xL - x^2) \qquad (2.415)$$

$$\delta v_{xx} = \frac{3\Delta}{L^3}(L - x) \qquad (2.416)$$

$$\delta v_{xxx} = -\frac{3\Delta}{L^3} \qquad (2.417)$$

Éléments sous droits d'auteur

whereupon we observe that the geometric boundary conditions at the fixed end ($x = 0$) are satisfied, as they must be for the approximation to be acceptable. Moreover, the natural boundary condition $\delta M = 0$ at the free end ($x = L$) is also satisfied. However, the other natural boundary condition of $\delta S = 0$ at the free end is not satisfied (nor should we have expected it to be satisfied because we chose as a deflection function one that comes from a transverse force being applied at the free end!).

If we evaluate the variation-in-curvature bending strain energy integral as well as $\bar{\delta}^2 U_m$ and apply the neutral equilibrium buckling criterion, then we find $\bar{P} = 2.50EI/L^2$ with an error of 1.3% above the exact solution of $\bar{P} = (\pi^2/4)EI/L^2$. Or, if we use the variation-in-moment bending strain energy integral, we get $\bar{P} = 2.4706EI/L^2$ with an error of only .13%.

If we use the quadratic buckling deflection approximation

$$\delta v = \frac{\Delta}{L^2} x^2 \tag{2.418}$$

we see that the derivatives are

$$\delta v_x = \frac{2\Delta}{L^2} x \tag{2.419}$$

$$\delta v_{xx} = \frac{2\Delta}{L^2} \tag{2.420}$$

$$\delta v_{xxx} = 0 \tag{2.421}$$

Again, the geometric boundary conditions at the fixed end are satisfied or we would not have addressed this approximation. At the free end, neither natural boundary condition is satisfied. In fact, the variation in moment is implied to be constant over the whole length of the bar, a fact in contradiction to simple statics for the fixed-free bar. However, this buckling deflection comes from the equilibrium solution for a fixed-free bar subjected to a moment at the free end, so $M \neq 0$ and hence $\delta M \neq 0$.

If we evaluate the variation-in-curvature bending strain energy integral as well as $\bar{\delta}^2 U_m$ and then apply the neutral equilibrium buckling criterion, we get $\bar{P} = 3EI/L^2$ which is 21.5% above the exact solution of $\bar{P} = (\pi^2/4)EI/L^2$. Alternatively, if we use the variation-in-moment bending strain energy integral, then we get $\bar{P} = 2.50EI/L^2$ which is only 1.3% high. Apparently, satisfying neither natural boundary condition leads to less accurate results than if we satisfy one of the two natural boundary conditions. With both buckling deflection approximations, the variation-in-moment bending strain energy integral always leads to better results than the variation-in-curvature bending strain energy integral.

Note that $M = EI\, v_{xx}$ is the differential equation governing the buckling disturbance approach that we first studied in Section 2.2. That is, we don't know v_{xx} until we *solve* the differential equation $M = EI\, v_{xx}$. However, if we make an approximation to the buckling deflection (usually and presumably) in the moment expression or to the curvature via differentiation of δv, then we make just such approximations in the Rayleigh Method, so δM is not equal to $EI\, \delta v_{xx}$ but is only an approximation.

Éléments sous droits d'auteur

The merits of the two 'variation-in-bending strain energy' integrals depend upon the characteristics of the deflection approximation over the length of the bar and its relation to the exact deflection. The variation-in-moment bending strain energy in Equation (2.387) involves a first-order quantity, the deflection, v, which is relatively easy to approximate well because we can 'see' v readily. And, we can always write a moment expression for a bar problem from statics. In contrast, the variation-in-curvature bending strain energy in Equation (2.379) involves a third-order quantity, the curvature, v_{xx}, which is far harder to approximate well than deflection because curvature, v_{xx}, is very difficult to visualize. For polynomials, the expression for the curvature approximation is less complicated than that for the deflection (although this statement is not true for sine functions). However, the expression for the moment is almost always more complicated than the deflection function. Thus, use of the variation-in-moment bending strain energy integral almost always involves more work to evaluate than does the variation-in-curvature bending strain energy integral. However, we easily see why the variation-in-moment bending strain energy integral, dependent only on the easily visualized deflection, v, leads to more accurate results than does the variation-in-curvature bending strain energy integral.

The results for the three different approximations (exact, cubic, and quadratic) for buckling of an axially compressed fixed-free bar are displayed for both the variation-in-moment bending strain energy approach and the variation-in-curvature bending strain energy approach in Table 2-3. There, we see the closer the buckling deflection approximation is to satisfying the two natural boundary conditions, the more accurate the buckling load regardless of the inherent accuracy of the variation in bending strain energy approach. Also, the variation-in-moment bending strain energy approach leads to a more accurate buckling load than does the variation-in-curvature bending strain energy approach.

Satisfying the geometric boundary conditions is required, but there is another aspect to the geometric boundary conditions. Suppose we find the variation in slope is zero for an approximation, but is not zero for the desired problem. Then, the approximation is related to another physical problem and cannot be used for the desired problem. That is, having the variation in slope *not* be zero is just as important as a specification that $\delta v_x = 0$. Similarly, we would not expect an approximation with $\delta v = 0$ to be for the right problem if δv is not zero for the desired problem.

Two approximations that each satisfy the same natural boundary conditions will not necessarily, or even likely, lead to the same buckling load by the Rayleigh Method because their characteristics (mainly shape) between the boundaries are different, so their evaluation in the variation-in-energy integrals is different. For a buckling problem with two different natural boundary conditions, e.g., the fixed-free bar, suppose two approximations are available, each satisfying only one of the two natural boundary conditions, but not the same one as the other approximation. No clear statement can be made about which of the two approximations leads to the more accurate buckling load. Perhaps satisfying the more complicated natural boundary condition ($\delta S = 0$) would lead to the better answer or perhaps the lower-order $\delta M = 0$ ($\delta v_{xx} = 0$) condition would.

Éléments sous droits d'auteur

Table 2-3 Approximate Solutions for Buckling of an Axially Compressed Fixed-Free Bar

Approximate Buckling Deflection	Factor c in $\overline{P} = cEI/L^2$ (Error)		Natural Boundary Conditions Satisfied?	
	Variation in Moment Approach $\overline{\delta^2 U_b} = \int_0^L \frac{(\delta M)^2}{EI}\,dx$	Variation in Curvature Approach $\overline{\delta^2 U_b} = \int_0^L EI(\delta v_{xx})^2 dx$	Variation in Moment at the Free End $\delta M\|_{end} = EI\delta v_{xx}\|_{end} = 0$	Variation in Shear at the Free End $-\delta S\|_{end} = EI\delta v_{xxx}\|_{end} + P\delta v_x\|_{end} = 0$
$\delta v = \Delta\left[1 - \cos\frac{\pi x}{2L}\right]$	$\frac{\pi^2}{4} = 2.4674$ (exact)	$\frac{\pi^2}{4} = 2.4674$ (exact)	yes	yes
$\delta v = \frac{\Delta x^2}{2L^3}(3L - x)$	2.4706 (.13%)	2.50 (1.3%)	yes	no
$\delta v = \frac{\Delta x^2}{L^2}$	2.50 (1.3%)	3 (21.5%)	no	no

Éléments sous droits d'auteur

2.6.2.5 Summary

This problem-solving procedure is useful for the Rayleigh Method:

1. Identify the geometric boundary conditions and natural boundary conditions of the buckling problem.
2. Select an approximating function that satisfies the most-possible natural boundary conditions (and, of course, satisfies all the geometric boundary conditions; otherwise, you are not working the correct physical problem). Carefuly examine each boundary condition associated with the approximating function, and compare the boundary condition of the approximation to that of the actual bar. If not all natural boundary conditions are satisfied, you are treating the wrong physical problem to a lesser degree than for the geometric boundary conditions. The more natural boundary conditions satisfied, the more accurate the solution (but even if all natural boundary conditions are satisfied, the answer is not precise unless the differential equation is also satisfied—an issue not addressed in the Rayleigh Method).
3. Use the variation-in-moment bending strain energy approach as being inherently more accurate than the variation-in-curvature approach. If you use a variation-in-curvature approach because the integral in the variation-in-moment approach is too difficult to evaluate, then realize that the error is sometimes significantly greater.
4. Make all possible reductions of the general problem you solve to compare with the exact solutions for subsets of the general problem. Each favorable comparison adds credence to the approximate solution to the general problem. Any non-favorable comparison is evidence that an error exists in the approximate solution to the general problem. This fourth piece of advice is applicable to every general problem you solve!

Note that we can assess the error in a Rayleigh Method solution *only if we already know the exact solution!* That is, we used the Rayleigh Method in a special situation in which we could evaluate its effectiveness and thereby learn about its characteristics. However, in general, we will not be in such an enviable position! Without knowing the exact solution, the only comments we can make on solution accuracy are that (1) a single Rayleigh approximation leads to a buckling load that is too high by an unknown amount (and therefore is unconservative when we are designing a bar). (2) the lowest buckling load we obtain from several Rayleigh approximations is the closest to the exact solution, and (3) the more natural boundary conditions satisfied, the more accurate the Rayleigh Method solution. Beyond those three comments, we have no assurances. Thus, we are well-motivated to make as many comparisons with known solutions as possible so we can learn more about how well the Rayleigh Method works. And, we can also use experiments to verify our analysis. Important characteristics and issues of the Rayleigh Method which we have discussed are summarized in Figure 2-49. Recall that in no case can we ever determine the buckle amplitude.

Éléments sous droits d'auteur

GIVEN:	**A CONTINUOUS MECHANICAL SYSTEM WITH AN INFINITE NUMBER OF DEGREES OF FREEDOM**
APPROXIMATION:	**APPROXIMATE THE BUCKLING DEFLECTION WITH A SINGLE DEGREE OF FREEDOM SHAPE (HENCE, MORE CONSTRAINT AND HIGHER ENERGY, SO THE STRUCTURE IS TOO STIFF, AND THE BUCKLING LOAD IS TOO HIGH)**
DRAWBACK:	**UNKNOWN ACCURACY (ABOVE THE EXACT BUCKLING LOAD)**
REQUIREMENTS:	**APPROXIMATE DEFLECTION MUST SATISFY THE GEOMETRIC BOUNDARY CONDITIONS (BUT SOLUTION IS MORE ACCURATE IF NATURAL BOUNDARY CONDITIONS ARE ALSO SATISFIED)**

Figure 2-49 Characteristics of the Rayleigh Method

Problem Set 2.6.2

2.6.2.1 Show that $P_E = 10\,EI/L^2$ for the axially compressed pinned-pinned bar in Figure 2-47 if the variation in bending strain energy is expressed in terms of the variation in moment and the buckling deflection approximation is $\delta v = \Delta x(L - x)$.

2.6.2.2 Verify that the (exact) buckling deflection function in Equation (2.413) leads to the exact buckling load for the axially compressed fixed-free bar in Figure 2-48.

2.6.2.3 Use the buckling deflection approximation $\delta v = (\Delta/2L^3)x^2(3L - x)$ for the axially compressed fixed-free bar in Figure 2-48. Use both the variation-in-curvature expression and the variation-in-moment expression for the bending strain energy. For what physical problem is this deflection approximation the exact solution?

2.6.2.4 Use the buckling deflection approximation $\delta v = \Delta x^2/L^2$ for the axially compressed fixed-free bar in Figure 2-48. Use both the variation-in-curvature and the variation-in-moment expression for the bending strain energy. For what physical problem is this deflection approximation the exact solution?

2.6.2.5 Use the variation-in-curvature expression for the bending strain energy and the buckling deflection approximation $\delta v = \Delta(x^2/L^4)(L - x)^2$ to determine the buckling load for the axially compressed fixed-free bar in Figure 2-48.

2.6.3 The Rayleigh-Ritz Method

A natural improvement of the accuracy of the approximate buckling loads is obtained by considering more than one buckle deflection approximation at a time. The Ritz Method was developed by Walther Ritz (1878–1909) who died of consumption at an early age. He proposed an infinite series of approximating deflection functions to treat a mechanical system with an infinite number of degrees of freedom [2-22]:

$$\delta v = \sum_{i=1}^{\infty} \Delta_i f_i(x) = \Delta_1 f_1(x) + \Delta_2 f_2(x) + \ldots \qquad (2.422)$$

in which the $f_i(x)$ satisfy the geometric boundary conditions but not necessarily the natural boundary conditions. The $f_i(x)$ could be trigonometric functions as in a Fourier sine series:

$$\delta v = \sum_{i=1}^{\infty} \Delta_i \sin\frac{i\pi x}{L} = \Delta_1 \sin\frac{\pi x}{L} + \Delta_2 \sin\frac{2\pi x}{L} + \ldots \qquad (2.423)$$

The approximating functions must be differentiable to be useable in the strain energy integrals. In contrast to the Rayleigh Method, information about the accuracy of the solution is available by considering more and more terms in the infinite set and observing the change in the

Éléments sous droits d'auteur

results. However, the infinite set of functions must be *complete*, i.e., it must be capable of representing the actual solution. Completeness guarantees uniform convergence and interchangeability of summation and integration as well as differentiability, all properties that we will use heavily. If the set is not complete (e.g., if not all terms of an infinite series are used), then apparent convergence to an incorrect answer is possible. Or, if an incomplete series is used, then termwise differentiation is not valid, so the wrong answer is obtained. For conditions on differentiation, integration, completeness, and convergence of Fourier series, consult Tolstov [2-24] or Brown and Churchill [2-25].

The procedure for the Rayleigh-Ritz Method is, except for one issue, identical to that for the Rayleigh Method. That is, we use an approximate buckling deflection function to calculate either the variation-in-moment-based bending strain energy change that occurs during buckling

$$\bar{\delta}^2 U_b = \int_0^L \frac{(\delta M)^2}{EI}\, dx \tag{2.424}$$

or else the variation-in-curvature-based bending strain energy change that occurs during buckling[4]

$$\bar{\delta}^2 U_b = \int_0^L EI\, \delta v_{xx}^2\, dx \tag{2.425}$$

and then add the second variation of the membrane strain energy change that occurs during buckling

$$\bar{\delta}^2 U_m = \int_0^L \bar{N}_x \delta v_x^2\, dx = -\int_0^L \bar{P} \delta v_x^2\, dx \tag{2.426}$$

to get the special second variation of the total potential energy, $\bar{\delta}^2 V$ (evaluated in the primary equilibrium state), and then make $\bar{\delta}^2 V$ either stationary in the adjacent equilibrium method (also the Trefftz criterion)

$$\delta(\bar{\delta}^2 V) = 0 \tag{2.427}$$

or zero in the neutral equilibrium method

$$\bar{\delta}^2 V = 0 \tag{2.428}$$

Recall from the Rayleigh Method and the discussion in Section 2.5.5.2 that the special second variation in membrane strain energy is most decidedly *not* the work done by external forces during buckling. Equation (2.426) is an integral expression, not a boundary term. There is no variation of the work done by external forces above the first, and that term is part of the equilibrium calculation, not the buckling calculation.

The essential difference between the Rayleigh Method and the Rayleigh-Ritz Method is in the approximating buckling deflection function. In the Rayleigh-Ritz Method, the approximate buckling deflection is a

[4]Again, the variation-in-moment-based and the variation-in-curvature-based bending strain energy changes that occur during buckling are equal if and only if δM is precisely equal to $EI\delta v_{xx}$, and those two terms are never equal unless the exact solution is used.

Éléments sous droits d'auteur

multiple-degree-of-freedom function of n variables, Δ_1, Δ_2, Δ_3, ..., so $\delta(\bar{\delta}^2 V) = 0$ means

$$\frac{\partial(\bar{\delta}^2 V)}{\partial \Delta_1} = \frac{\partial(\bar{\delta}^2 V)}{\partial \Delta_2} = \frac{\partial(\bar{\delta}^2 V)}{\partial \Delta_3} = \cdots = 0 \tag{2.429}$$

with the number of zero first partial derivatives equal to the number of degrees of freedom. Alternatively, $\delta^2 V = 0$ implies a set of homogeneous equations in number equal to the number of degrees of freedom.

Presumably, we would like to use approximating functions that converge to the exact solution as the number of degrees of freedom in the approximation increases. Unfortunately, the solution complexity increases as the number of degrees of freedom in the approximation increases because the number of equations to be solved is identical to the number of degrees of freedom. This practical complexity is a hinderance to the widespread use of the Rayleigh-Ritz Method for simple solutions suitable for use in preliminary design studies. Typically, the Rayleigh-Ritz Method is employed only when the structure has been configured in near-final form and more precise evaluations of capability are both required and justified to properly design the final configuration.

From Fourier series theory, it is known that the functions 1, cos x, cos 2x, ...; sin x, sin 2x, ... form a complete set in the interval of length 2π. That is, they are capable of representing any piecewise continuous function in the interval. It is important to note, however, that not every infinite sequence of functions is complete — if only one of the preceding trigonometric functions is missing, then the sequence is not complete. Thus, in theory, some of the terms in such a sequence cannot be used to obtain a solution without risk of failure to converge to the correct result. That is, part of an infinite sequence is not necessarily valid as an approximation. We often risk such an error by using only a few terms in a sequence because we obviously cannot take an infinite number of terms! Polynomials also constitute a complete set of functions.

First, the deflection approximation is substituted in the special second variation of the total potential energy expression (evaluated in the primary equilibrium state). Then, the special second variation of the total potential energy is made stationary relative to the a_i in the adjacent equilibrium buckling criterion or Trefftz criterion (or zero in the neutral equilibrium buckling criterion), and thus the buckling load is determined. As more terms are taken in the buckling deflection approximation, the approximate buckling load approaches the exact buckling load if the series of functions is uniformly convergent. Because a sine term expansion (Fourier series) is convergent and can represent an arbitrary function, given enough terms, it is commonly used when the boundary conditions are satisfied by the sine function. Other trigonometric functions are also used to advantage for other boundary conditions, e.g., Fourier series. However, as with the Rayleigh Method, we cannot determine the amplitude of the buckle wave amplitude components, Δ_i, in Equation (2.423).

As an example of the application of the Rayleigh-Ritz Method, do Problem 2.6.4.1 *after* examining the Rayleigh Method solution of the same problem (Buckling of a Bar under Its Own Weight) in Section 2.6.4.

Éléments sous droits d'auteur

The important characteristics and issues of the Rayleigh-Ritz Method which we have discussed are summarized in Figure 2-50. Contrast the Rayleigh-Ritz method with the analogous characteristics of the simpler Rayleigh Method in Figure 2-49 on page 135.

GIVEN:	**A CONTINUOUS MECHANICAL SYSTEM WITH AN INFINITE NUMBER OF DEGREES OF FREEDOM**
APPROXIMATION:	**APPROXIMATE THE BUCKLING DEFLECTION WITH A COMPLETE SET OF FUNCTIONS, BUT TRUNCATE THE SET (THUS, NOT COMPLETE) (HENCE, SYSTEM IS MORE CONSTRAINED AND HAS HIGHER ENERGY, SO STRUCTURE IS TOO STIFF, AND THE BUCKLING LOAD IS TOO HIGH)**
DRAWBACK:	**CONVERGENCE NOT GUARANTEED AND EVEN IF CONVERGENCE OCCURS, CORRECT ANSWER NOT GUARANTEED (EQUAL TO OR ABOVE EXACT BUCKLING LOAD)**
REQUIREMENTS:	**EACH TERM OF THE FUNCTION SET MUST SATISFY THE GEOMETRIC BOUNDARY CONDITIONS (FASTER CONVERGENCE IF THE NATURAL BOUNDARY CONDITIONS ALSO SATISFIED)**

Figure 2-50 Characteristics of the Rayleigh-Ritz Method

2.6.4 Buckling of a Bar under Its Own Weight

A bar in a vertical position can buckle under its own weight that is uniformly distributed along the bar length as in Figure 2-51 if it is heavy enough or tall enough. Greenhill treated trees, vertical poles, and masts [2-26]. Other examples of such bars include flagpoles and smokestacks.

The variation in moment in the bar at cross section mn caused by distributed load q (uniform weight per unit length) during buckling is

$$\delta M = \int_x^L \bar{q}(\eta - \delta v)\, d\xi \qquad (2.430)$$

in which η and ξ are dummy variables (η is like buckling displacement δv and ξ is like coordinate x). Then, for the buckling disturbance approach $\delta M = EI\, \delta v_{xx}$, we see that the integro-differential equation is

$$EI\, \delta v_{xx} = \int_x^L \bar{q}(\eta - \delta v)\, d\xi \qquad (2.431)$$

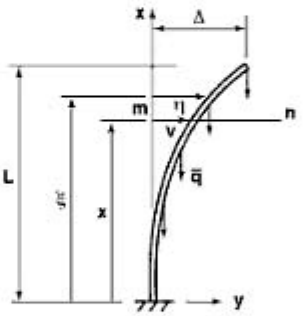


Figure 2-51 Buckling of a Vertical Bar under Its Own Weight

which can be differentiated and put into the form of Bessel's differential equation (see also Timoshenko and Gere [2-6, p. 101]) for which solutions are tabulated (e.g., Korn and Korn [2-27]). The final result is

$$(qL)_{cr} = 7.834\, \frac{EI}{L^2} \qquad (2.432)$$

and can be used to determine either a critical length or a critical weight.

Éléments sous droits d'auteur

We now use the Rayleigh Method to obtain an approximate solution, i.e., we use one buckling deflection approximation function

$$\delta v = \Delta\left[1 - \cos\frac{\pi x}{2L}\right] \tag{2.433}$$

which is the exact buckling deflection curve for a bar subjected to an *axial load* at the free end, i.e., *not the solution for this problem, but for a 'similar' problem.* Thus, the geometric boundary conditions at the fixed end and the natural boundary conditions at the free end are both satisfied, but we know that the solution is not correct because the buckling approximation function is not exact within the boundaries. Again, the variation in moment at any cross section mn in Figure 2-51 is

$$\delta M = \int_x^L \bar{q}(\eta - \delta v)\, d\xi \tag{2.434}$$

in which η and ξ are dummy variables (η is like δv and ξ is like x), so

$$\eta = \Delta\left[1 - \cos\frac{\pi\xi}{2L}\right] \tag{2.435}$$

and we can substitute η in the variation-in-moment expression to obtain

$$\begin{aligned}\delta M &= q\Delta\int_x^L \left[\left[1 - \cos\frac{\pi\xi}{2L}\right] - \left[1 - \cos\frac{\pi x}{2L}\right]\right] d\xi \\ &= \bar{q}\Delta\left[(L - x)\cos\frac{\pi x}{2L} - \frac{2L}{\pi}\left[1 - \sin\frac{\pi x}{2L}\right]\right]\end{aligned} \tag{2.436}$$

The variation-in-moment-based bending strain energy is

$$\bar{\delta}^2 U_b = \int_0^L \frac{(\delta M)^2}{EI}\, dx = \frac{\bar{q}^2\Delta^2 L^3}{EI}\left[\frac{1}{6} + \frac{9}{\pi^2} - \frac{32}{\pi^3}\right] \tag{2.437}$$

after substitution of the variation in moment and subsequent integration.

The bar force N_x at any section mn of the bar is the weight of the bar above mn, i.e.,

$$N_x = -\bar{q}(L - x) \tag{2.438}$$

so the second variation in membrane strain energy during buckling is

$$\begin{aligned}\bar{\delta}^2 U_m &= \int_0^L N_x \delta v_x^2\, dx = -\bar{q}\int_0^L (L - x)\delta v_{xx}^2\, dx \\ &= -\bar{q}\Delta^2\left[\frac{\pi}{2L}\right]^2\int_0^L (L - x)\left[\sin\frac{\pi x}{2L}\right]^2 dx \\ &= -\bar{q}\frac{\pi^2\Delta^2}{4}\left[\frac{1}{4} - \frac{1}{\pi^2}\right]\end{aligned} \tag{2.439}$$

Then, by the neutral equilibrium buckling criterion,

$$(qL)_E = 7.89\frac{EI}{L^2} \tag{2.440}$$

Éléments sous droits d'auteur

This approximate result is less than 1% (.7%) above the exact solution, $(qL)_E = 7.834EI/L^2$, in Equation (2.432). Obviously, this approximate result is quite adequate for use in design, but note that we cannot find Δ.

Alternatively, the variation-in-curvature-based bending strain energy expression yields

$$\bar{\delta}^2 U_b = \int_0^L EI\,\delta v_{xx}^2\,dx = EI\Delta^2\left[\frac{\pi}{2L}\right]^3\int_0^{\pi/2}\cos^2\left[\frac{\pi x}{2L}\right]d\left[\frac{\pi x}{2L}\right]$$

$$= \frac{EI}{2^3}\Delta^2\left[\frac{\pi}{L}\right]^3\frac{\pi}{4} = EI\frac{\Delta^2}{L^3}\frac{\pi^4}{4\times 2^3} \qquad (2.441)$$

after substitution of the variation-in-deflection approximation. Then, use the neutral equilibrium buckling criterion to get

$$(qL)_E = 8.29\frac{EI}{L^2} \qquad (2.442)$$

with an error of more than 5% (5.4%), so this solution might not be used in design, although it is suitable for preliminary design. Obviously, the variation-in-curvature-based bending strain energy approach is easier to calculate than the variation-in-moment-based bending strain energy approach, but yields less accurate results.

Problem Set 2.6.4

2.6.4.1 Use a two-term buckling deflection approximation, i.e., a Rayleigh-Ritz approach,

$$\delta v = \Delta_1(1 - \cos\frac{\pi x}{2L}) + \Delta_2(1 - \cos\frac{3\pi x}{2L})$$

to find the buckling load of a bar that is axially compressed by its own weight. That is, use the first two terms of a series for which the first term corresponds to the Rayleigh approximation we used in Section 2.6.4. Discuss the error in comparison to the Rayleigh approximation.

2.6.5 Buckling of Bars with Step Changes in Cross Section

The use of bars with constant cross section along their length is a waste of material in many applications, i.e., more material is used than is necessary. For example, at the loaded end of a vertical fixed-free bar, the moment-resisting capacity drastically exceeds that required (theoretically none!). A cross section that continuously varies (but not linearly) from zero at the loaded end to a maximum size at the fixed end can be shown to be an optimal use of material, but is quite difficult to manufacture. Thus, a step-wise change in bar cross section is often made to conserve material and to ease manufacturing difficulties. This change occurs usually by welding, bolting, or riveting additional plates on a bar that itself might be a standard structural shape. Thus, this approach is far more practical than a tapered bar in civil construction projects, but aircraft might still require use of a tapered bar to achieve the lightest possible structural member. As an approximate and practical first-step solution, consider the two-section bar in Figure 2-52. The moment of inertia of the upper segment is I_1 and that of the lower segment is I_2. The moduli of elasticity could also be different in the two segments.

Éléments sous droits d'auteur

The exact solution to the two-segment bar buckling problem involves matching the solutions to the differential equations for each bar segment at the boundary between the segments. That is, if subscripts 1 and 2 refer to the upper and lower segments, respectively, then the two differential equations are

$$EI_1\,\delta v_{1_{xx}} = P(\Delta - \delta v_1) \qquad (2.443)$$

$$EI_2\,\delta v_{2_{xx}} = P(\Delta - \delta v_2) \qquad (2.444)$$

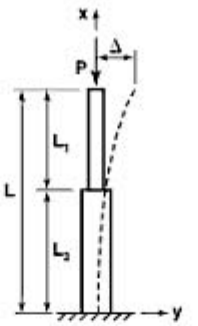


Figure 2-52 Axially Compressed Bar with a Change in Cross Section

for which, upon substitution of the constants $k_1^2 = P/EI_1$ and $k_2^2 = P/EI_2$, solution of the two differential equations, and use of the boundary conditions, the characteristic equation is

$$\tan k_1L_1 \tan k_2L_2 = k_1/k_2 \qquad (2.445)$$

which can be solved for various bar cross sections and lengths.

We can also use the Rayleigh Method to obtain an approximate solution. For example, use the exact deflection function for buckling of an axially compressed fixed-free bar of uniform cross section

$$\delta v = \Delta\left[1 - \cos\frac{\pi x}{2L}\right] \qquad (2.446)$$

as an approximation to the nonuniform-cross-section-bar problem. Thus, the geometric boundary conditions at the fixed end and the natural boundary conditions at the free end are both satisfied, but we know that the solution is not correct because the buckling approximation function is not exact within the boundaries.

The variation-in-moment bending strain energy is

$$\begin{aligned}\bar{\delta}^2U_b &= \int_0^{L_2}\frac{(\delta M^2)}{EI_2}\,dx + \int_{L_2}^{L}\frac{(\delta M^2)}{EI_1}\,dx \\ &= \frac{\bar{P}^2\Delta^2}{EI_2}\left[\int_0^{L_2}\cos^2\frac{\pi x}{2L}\,dx + \frac{I_2}{I_1}\int_{L_2}^{L}\cos^2\frac{\pi x}{2L}\,dx\right] \\ &= \frac{\bar{P}^2\Delta^2}{EI_2}\left[\frac{L_2}{2} + \frac{I_2}{I_1}\frac{L_1}{2} + \frac{L}{2\pi}\left[1 - \frac{I_2}{I_1}\right]\sin\frac{\pi L_2}{L}\right] \qquad (2.447)\end{aligned}$$

and the second variation in membrane strain energy during buckling is

$$\bar{\delta}^2U_m = -\int_0^{L}\bar{P}\,\delta v_x^2\,dx = -\frac{\bar{P}\Delta^2\pi^2}{4L^2}\int_0^{L}\sin^2\frac{\pi x}{2L}\,dx = -\frac{\pi^2\bar{P}\Delta^2}{8L} \qquad (2.448)$$

Finally, upon use of the neutral equilibrium buckling criterion, we get

Éléments sous droits d'auteur

$$P_E = \frac{\pi^2}{4}\frac{EI_2}{L^2}\frac{1}{\frac{L_2}{L}+\frac{L_1}{L}\frac{I_2}{I_1}-\frac{1}{\pi}\left[\frac{I_2}{I_1}-1\right]\sin\frac{\pi L_2}{L}} \tag{2.449}$$

which is an explicit expression for the buckling load in terms of the bar properties. The accuracy of this expression is quite good as long as the moments of inertia are not very dissimilar. Of course, the answer is exact if the moments of inertia are identical. Note that Δ is indeterminate.

Problem Set 2.6.5

2.6.5.1 Derive the characteristic equation for buckling of the axially compressed bar with a change in cross section as in Figure 2-52 as given in Equation (2.445). Compare the solution of this characteristic equation for $I_1/I_2 = .4$ and $L_2/L = .2$ and .6 with the Rayleigh solution in Equation (2.449).

2.6.5.2 Use the buckling deflection approximation of Equation (2.446) in the variation-in-curvature bending strain energy integral instead of the variation-in-moment bending strain energy integral. Compare the resulting accuracy with the variation-in-moment approach and the exact solution in the manner of Problem 2.6.5.1.

2.6.6 Buckling of a Pinned-Pinned Axially Compressed Bar with a Mid-Span Transverse Spring

Consider an axially loaded bar with pinned ends and a translational linear elastic spring with stiffness, α, restraining it at mid-span as in Figure 2-53. We found the exact solution for this problem in Section 2.2.7. Now, we will address approximate solutions that are easier to execute.

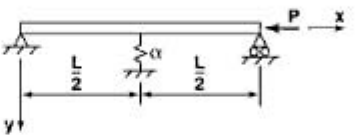


Figure 2-53 Pinned-Pinned Bar under Axial Compressive Load with a Mid-Span Transverse Spring

For a small spring stiffness, we presume that the bar will buckle in a *perturbed* symmetric half-sine-wave buckling mode shown in Figure 2-12 on page 62 because the half-sine-wave shape is the buckling mode when no spring exists. We should also expect from Section 2.2.6 that if the spring is stiff enough, then it will completely restrain transverse movement at mid-span so that the bar buckles into the second (antisymmetric) mode of two half-sine waves. The minimum value of "stiff enough" is the critical spring stiffness that we seek. However, we will first try the approximation of the sinusoidal shape as a single-degree-of-freedom Rayleigh approach as if the spring were not present:

$$\delta v = \Delta \sin\frac{\pi x}{L} \tag{2.450}$$

in which Δ is the amplitude of the buckle sine wave, i.e., the magnitude of the deflection of the mid-span spring. The variation-in-curvature bending strain energy is

$$\bar{\delta}^2 U_b = \int_0^L EI\,\delta v_{xx}^2\,dx = EI\Delta^2\frac{\pi^4}{L^4}\int_0^L \sin^2\frac{\pi x}{L}\,dx = EI\Delta^2\frac{\pi^4}{2L^3} \tag{2.451}$$

Éléments sous droits d'auteur

and the second variation in membrane strain energy during buckling is

$$\bar{\delta}^2 U_m = -\int_0^L \bar{P}\,\delta v_x^2\,dx = -\bar{P}\Delta^2\frac{\pi^2}{L^2}\int_0^L \cos^2\frac{\pi x}{L}\,dx = -\bar{P}\Delta^2\frac{\pi^2}{2L} \quad (2.452)$$

The second variation in spring internal energy is (see Problem 2.6.6.1)

$$\bar{\delta}^2 U_s = \alpha\Delta^2 \quad (2.453)$$

Then, by the neutral equilibrium buckling criterion,

$$\bar{\delta}^2 V = \bar{\delta}^2 U_m + \bar{\delta}^2 U_b + \bar{\delta}^2 U_s = 0 \quad (2.454)$$

we see that

$$EI\Delta^2\frac{\pi^4}{2L^3} - \bar{P}\Delta^2\frac{\pi^2}{2L} + \alpha\Delta^2 = 0 \quad (2.455)$$

so the buckling load is

$$\bar{P} = \frac{2L}{\pi^2}\left[EI\frac{\pi^4}{2L^3} + \alpha\right] = \pi^2\frac{EI}{L^2}\left[1 + \frac{2\alpha L^3}{\pi^4 EI}\right] \quad (2.456)$$

At what α does the buckling load equal the load at the second buckling mode, i.e., where the spring is so stiff that it prevents transverse movement, and hence the bar buckles in the second mode? The second-mode buckling load is $\bar{P} = 4\pi^2 EI/L^2$, so that condition occurs when

$$\frac{2\alpha L}{\pi^2} = 3\pi^2\frac{EI}{L^2} \quad (2.457)$$

and the critical value of the spring stiffness α is

$$\alpha_{cr} = \frac{3}{2}\pi^4\frac{EI}{L^3} \quad (2.458)$$

The critical spring constant calculated with this Rayleigh approximation is 7.5% below the exact value of $\alpha_{cr} = 16\pi^2 EI/L^3$ from Equation (2.80) on page 65. Thus, the results would be a dashed line in Figure 2-14 on page 65 starting from $\bar{P} = \pi^2 EI/L^2$ and going to a value of α less than the exact $\alpha_{cr} = 16\pi^2 EI/L^3$ at $\bar{P} = 4\pi^2 EI/L^2$. These approximate buckling loads are always higher than the exact results in Figure 2-14, as we would expect. Note that requiring α to be so high that the bar buckles into the second buckling mode means that the buckle shape is far from the half-sine wave that was initially assumed.

Problem Set 2.6.6

2.6.6.1 Derive the second variation of the strain energy of the transverse linear elastic spring with constant α, i.e., Equation (2.453).

2.6.6.2 Use the variation-in-moment bending strain energy approach to calculate an approximate buckling load and α_{cr} for the pinned-pinned bar with a mid-span transverse spring. Compare the results with those in Sections 2.2.7 and 2.6.6.

2.6.6.3 Use the Rayleigh-Ritz Method with a sinusoidal term and a linear term for the pinned-pinned bar with a mid-span transverse spring. What is δv_x at mid-span?

Éléments sous droits d'auteur

2.6.7 Summary

The direct energy methods of Rayleigh and Rayleigh-Ritz are extensively described and discussed to provide background for further problem solving in problems for which the differential equations and their boundary conditions are too formidable or too awkward to solve. In such cases, the variation in strain energy integrals are fairly easy and rapid to use, and can be accurate if certain guidelines are followed. The same energy integrals and buckling criteria are used in both methods, but the integrands are different because of the approximations involved. The Rayleigh Method involves a single-degree-of-freedom approximation to the bar buckling deflection whereas the Rayleigh-Ritz Method involves a multiple-degree-of-freedom approximation (from two degrees of freedom upward as more terms are taken in the set of functions chosen). The various guidelines involve the variation-in-moment versus the variation-in-curvature bending strain energy expressions, satisfaction of the geometric boundary conditions (if they are not satisfied, then you are treating the wrong physical problem), possible satisfaction of the natural boundary conditions (if they are satisfied, expect the Rayleigh approximation to be better and expect the convergence of the Rayleigh-Ritz Method to be faster). With both methods, the approximate load is always above the exact buckling load because the fewer number of degree of freedom in the approximations than in the real, continuous mechanical system with an infinite number of degrees of freedom provides an unnatural constraint on the system, hence higher energy.

Suppose we calculate several different approximate buckling loads by using several different Rayleigh buckling deflection approximations. Then, the lowest buckling load of the group is the closest to the exact solution and is therefore the approximation to use in design. Surely, no one is comfortable designing on the unconservative side, but there is simply no way to find a 'conservative Rayleigh buckling load'. However, we are still at a disadvantage in design because we don't know how much higher the approximate buckling load is than the exact solution. This circumstance of designing to an unconservative value of load is risky. If the bar is truly crucial in the structure being designed, an accurate evaluation is required. Thus, the Rayleigh-Ritz Method should be employed (or solve the differential equation subject to the boundary conditions, or use a numerical technique such as finite elements) wherein a sequence of approximation functions used gives an indication of convergence to the exact buckling load if enough terms are used. Although the Rayleigh-Ritz load is still above the exact buckling load, i.e., unconservative, it should be suitable for use in design because it is close to the exact buckling load. Note that the Rayleigh Method might be quite suitable when designing a bar at the preliminary design stage of a structure (with improved calculations undertaken at a later stage in design).

Several specific problems are treated with the Rayleigh Method to illustrate the procedure as well as to view some significant results. Some of the problems solved are useful in developing criteria or guidelines for problem solving with both approximate methods.

Éléments sous droits d'auteur

2.7 EFFECT OF TRANSVERSE SHEAR STIFFNESS ON BUCKLING OF BARS

2.7.1 Introduction

In previous sections, the effect of the transverse shear stiffness on the buckling process was neglected. We will examine the influence of transverse shear stiffness on beam deflection and, then, on bar buckling loads first by a differential equation approach and then by an energy approach. We should anticipate increased beam deflections and decreased bar buckling loads when transverse shear effects are included.

2.7.2 Differential Equation Approach to Effect of Transverse Shear on Deflection of an End-Loaded Cantilever Beam

The deflections of transversely loaded slender beams are more than adequately treated by use of bending theory alone. However, if the beam is not slender, e.g., the beam is short and deep (thick), shear deformations can even dominate the total beam deflections. Of course, a bending moment causes curvature of the neutral surface of a beam such that

$$EI\,M = y_b'' \tag{2.459}$$

We will investigate the deflection of the end-loaded cantilever beam in Figure 2-54 caused by both bending moment, – Px, and shear force, P.

The bending deformation of the beam under the usual presumption that plane cross sections remain plane under the linearly varying moment is shown in Figure 2-55a. Note that the curvature is highest at the fixed support where the moment is largest, and both curvature and moment go to zero as the beam end is approached. For a cantilever beam subjected to transverse force, P, the shear force is constant, and the resulting deformation is shown in Figure 2-55b. Note that there is no shear stress, hence, no shear strain at the top and bottom of the beam. The shear stress, hence, shear strain, is known to vary through the depth of the beam, and they both achieve a maximum at the centroid of the beam cross section (the center of a rectangular or circular cross section) to which we refer all shearing deformations (and bending deformations) as we reduce the treatment to a one-dimensional theory. The total deformation (combined bending and shearing) is shown in Figure 2-55c. Note that, because of the shear stress and shear strain, cross sections that were plane before loading actually warp out of plane during loading.

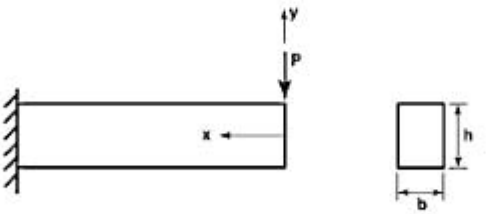


Figure 2-54 End-Loaded Cantilever Beam

Éléments sous droits d'auteur

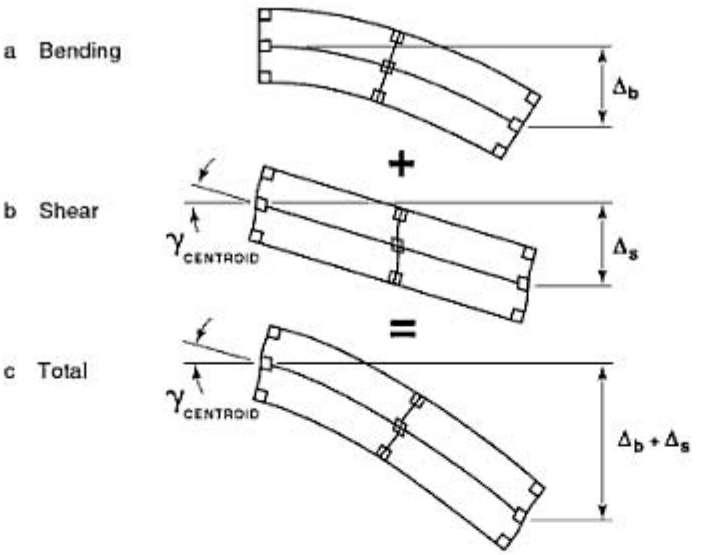


Figure 2-55 Deformation of an End-Loaded Cantilever Beam

We can identify the slope at the neutral axis of the beam-like member in Figure 2-55b as the shearing strain, i.e.,

$$\frac{dy_s}{dx} = \gamma\Big|_{\text{neutral axis}} = \frac{\tau}{G}\Big|_{\text{neutral axis}} \qquad (2.460)$$

but we know from basic mechanics of materials that the shear stress at any point y on a general beam cross section as in Figure 2-56 is

$$\tau = \frac{SQ}{It} \qquad (2.461)$$

in which S is the shear force, Q is the first moment of the cross-sectional area above y in Figure 2-56 about the centroidal axis (i.e., $A'y_1$), I is the second moment of the cross-sectional area about the centroidal axis, and t is the width of the cross section at y in Figure 2-56. The shear stress at the centroid can then be expressed in terms of the average shear stress as

$$\tau = k\frac{S}{A} \qquad (2.462)$$

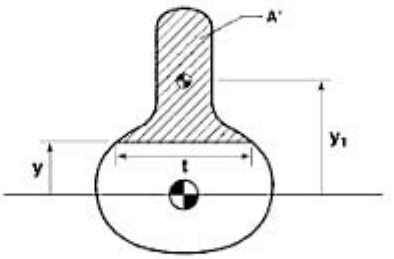


Figure 2-56 Beam Cross Section

Éléments sous droits d'auteur

i.e., k is the multiplier of the average shear stress, S/A, so

$$k = \frac{QA}{It} \tag{2.463}$$

which is a function of the shape of the beam cross section. For a rectangular-cross-section beam, k = 3/2 whereas for a circular-cross-section beam, k = 4/3. Finally, we can write

$$\frac{dy_s}{dx} = k\frac{S}{AG} \tag{2.464}$$

If we superimpose the deflections causing bending and shear, we get

$$y = y_b + y_s \tag{2.465}$$

from which we see that

$$y'' = y_b'' + y_s'' \tag{2.466}$$

But

$$y_b'' = \frac{M}{EI} = -\frac{Px}{EI} \tag{2.467}$$

so

$$y_b' = -\frac{Px^2}{2EI} + C_1 \tag{2.468}$$

Also

$$y_s' = k\frac{S}{AG} = k\frac{P}{AG} \tag{2.469}$$

so

$$y_s'' = k\frac{1}{AG}\frac{dS}{dx} = 0 \tag{2.470}$$

Thus,

$$y' = y_b' + y_s' = \left[-\frac{Px^2}{2EI} + C_1\right] + k\frac{P}{AG} = -\frac{Px^2}{2EI} + k\frac{P}{AG} + C_1 \tag{2.471}$$

Apply the slope boundary condition $y' = \gamma$ at $x = L$:

$$y' = k\frac{P}{AG} \tag{2.472}$$

to get

$$C_1 = \frac{PL^2}{2EI} \tag{2.473}$$

Thus,

$$y = -\frac{Px^3}{6EI} + k\frac{P}{AG}x + \frac{PL^2}{2EI}x + C_2 \tag{2.474}$$

and apply the deflection boundary condition $y = 0$ at $x = L$ to get

$$C_2 = -\frac{PL^3}{3EI} - k\frac{PL}{AG} \tag{2.475}$$

Éléments sous droits d'auteur

Finally, the total beam deflection caused by bending and shearing is

$$y = -\frac{P}{6EI}(x^3 - 3L^2x + 2L^3) + k\frac{P}{AG}(x - L) \tag{2.476}$$

At the loaded end of the beam,

$$y|_{x=0} = -\frac{PL^3}{3EI} - k\frac{PL}{AG} \tag{2.477}$$

in which the first term is the deflection due to bending and the second term is the deflection due to transverse shearing. Moreover, the slope at the 'fixed end' is

$$y'|_{x=L} = k\frac{P}{AG} \tag{2.478}$$

i.e., the shear strain at the neutral axis (centroid). We see that a 'fixed end' does not have zero slope if shear deformations are considered. However, two possible 'fixed end' conditions exist in the elasticity solution, both of which are described by Timoshenko and Goodier [2-28]. The actual condition at the 'fixed end' can be either a rotation, γ, of the neutral surface or a rotation, γ, of the line originally perpendicular to the neutral surface (with a different deflection at the loaded end). The present solution agrees with the elasticity solution in which the neutral surface rotates as sketched in Figure 2-55b. Without the shear correction, the deflection in Equation (2.479) agrees with the elasticity solution in which the line originally perpendicular to the neutral surface rotates. Actually, neither 'fixed end' support condition is perfectly attained, so both solutions are approximations of reality.

For a rectangular-cross-section beam with $\nu = .25$ (reasonable for steel), the end deflection is

$$y = -\frac{PL^3}{3EI}\left[1 + k\frac{3EI}{GAL^2}\right] = -\frac{PL^3}{3EI}\left[1 + \frac{15}{16}\left[\frac{h}{L}\right]^2\right] \tag{2.479}$$

If L/h, which is a measure of beam slenderness, exceeds 10 (perhaps even 5), we see in Table 2-4 that the influence of shear deformation is negligible, i.e., less than 1% at L/h = 10 (and less than 4% at L/h = 5). Thus, for slender beams, bending deformation is a very adequate prediction of beam behavior. However, if L/h is less than 1 (hardly what we would call a beam because the beam is so short in length and simultaneously so deep), the influence of shearing deformation is dominant over the influence of bending deformation! A solution for bending of a uniformly loaded, simply supported beam is given by Timoshenko and Young [2-29]. For a solution for bending of a uniformly loaded cantilever beam, see Shames and Pitarresi [2-30].

Table 2-4 Deflection of an End-Loaded Cantilever Beam

$\frac{L}{h}$	.5	1	2	5	10	20	∞
$\frac{y}{y_b}$	4.75	1.938	1.234	1.038	1.009	1.002	1

Éléments sous droits d'auteur

2.7.3 Energy Methods Approach to Effect of Transverse Shear on Deflection of an End-Loaded Cantilever Beam

Before we apply energy concepts to bar buckling with transverse shear stiffness effects, we study a simple beam-bending problem to determine how the shear stresses lead to an energy component in addition to that due to bending. Moreover, we will see the circumstances under which the shearing contribution is important and where it is not important.

The derivation of the strain energy due to shearing deformations starts with the shearing strain energy per unit volume:

$$U_0 = \int \tau \, d\gamma \tag{2.480}$$

Substitute the shear stress – shear strain relation to get

$$U_0 = \int G\gamma \, d\gamma = \frac{G\gamma^2}{2} \tag{2.481}$$

with an alternative formulation of

$$U_0 = \frac{\tau^2}{2G} \tag{2.482}$$

as obtained by use of the stress-strain relation. However, from mechanics of materials, the shear stress at any point, y, above the centroidal axis on a beam cross section in Figure 2-56 is:

$$\tau = \frac{SQ}{It} \tag{2.483}$$

Accordingly, the total shearing strain energy in the beam is

$$U_S = \int_0^L \int_A U_0 \, dA \, dx = \int_0^L \int_A \left[\frac{SQ}{It} \right]^2 \frac{dA}{2G} \, dx$$

$$= \int_0^L \frac{S^2}{2GA} \left[\frac{A}{I^2} \int_A \frac{Q^2}{t^2} \, dA \right] dx = \int_0^L \frac{\alpha S^2}{2GA} \, dx \tag{2.484}$$

in which

$$\alpha = \frac{A}{I^2} \int_A \frac{Q^2}{t^2} \, dA \tag{2.485}$$

is a dimensionless constant that is a function of the shape of the beam cross section. *Note especially that α is not the same as k in Equation (2.463)!* They are not of the same form nor do they have the same function. Here, α is defined to make the strain energy of a uniform shear stress on the beam cross-sectional area equal to the strain energy of the actual shear stress distribution that occurs in accordance with Equation (2.483) on the same cross-sectional area. In contrast, k is the magnification factor of the shear stress at the neutral axis compared to the average shear stress on the cross section. The difference between the values of the constants for rectangular and circular cross sections ranges from 15% to 25%.

Éléments sous droits d'auteur

The constant α can be shown to have a value of 6/5 for a rectangular cross section, 10/9 for a circular cross section, $1.2\ A/A_f$ for an I-beam bending about its x-x axis as in Figure 2-57, and A/A_w for an I-beam bending about its y-y axis as in Figure 2-57. A wide-flange beam has values of α calculated with the same expressions as for an I-beam. Values of $1.2\ A/A_f$ are typically 1.4 to 2.8 whereas values of A/A_w are typically 2 to 6. Values of α for solid cross sections are lower than those for other sections. Values of α for beams with built-up sections having lacing bars or cover plates are even higher than for I-beams.

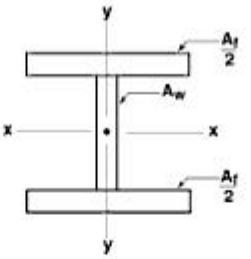


Figure 2-57 I-Beam Cross Section

Consider the deformation of the end-loaded cantilever beam with a rectangular cross section in Figure 2-58. There, the deflection due to shearing is y_s and the deflection due to bending is y_b. The objective is to find the ratio of the *bending* strain energy to the shearing strain energy. This example is obviously *not* a buckling problem. The moment of inertia of the cross section is $(1/12)bh^3$, and the area is bh.

The section constant α for a rectangular cross section is:

$$\alpha = \frac{A}{I^2}\int_A \frac{Q^2}{t}\,dy \tag{2.486}$$

because $dA = t\,dy$. Substituting I and A, recognizing that t = b, we get

$$\alpha = \frac{2}{b}\,\frac{bh}{\left[\frac{1}{12}bh^3\right]^2}\int_0^{\frac{h}{2}} Q^2 dy = \frac{288}{b^2h^5}\int_0^{\frac{h}{2}}\left[\frac{b}{2}\left(\frac{h}{2}+y\right)\left(\frac{h}{2}-y\right)\right]^2 dy = \frac{6}{5} \tag{2.487}$$

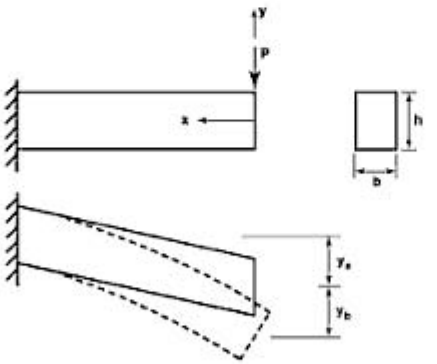


Figure 2-58 Deformation of an End-Loaded Cantilever Beam

Éléments sous droits d'auteur

Thus, if G = .4E (when ν = .25), then

$$\frac{U_b}{U_s} = \frac{\int_0^L \frac{M^2}{2EI}\,dx}{\int_0^L \frac{\alpha S^2}{2GA}\,dx} = \frac{\int_0^L \frac{P^2x^2}{2EI}\,dx}{\int_0^L \frac{\alpha P^2}{2GA}\,dx} = \frac{\frac{L^3/3}{E\,\frac{1}{12}\,bh^3}}{\frac{6/5\,L}{.4\,E\,bh}} = \frac{4}{3}\left[\frac{L}{h}\right]^2 \tag{2.488}$$

This strain energy ratio is calculated for various length-to-depth ratios, L/h, in Table 2-5. The bending energy dominates the total energy to engineering accuracy for slender beams (L/h > 6). However, for short, deep beams, the strain energy of shear can make significant contributions to the total deflection.

Table 2-5 Energy Ratio versus Length-to-Depth Ratio for Beam Bending

$\frac{L}{h}$	30	15	9	6	3	1
$\frac{U_b}{U_s}$	1200	300	108	48	12	4/3

We use Castigliano's theorem

$$\Delta = \frac{\partial U}{\partial P} \tag{2.489}$$

in which Δ is the deflection of the elastic system at the point of application of the load P in the direction of P. The strain energy is

$$\begin{aligned} U = U_b + U_s &= \int_0^L \frac{M^2}{2EI}\,dx + \int_0^L \frac{\alpha S^2}{2GA}\,dx \\ &= \int_0^L \frac{P^2x^2}{2EI}\,dx + \int_0^L \frac{\alpha P^2}{2GA}\,dx = \frac{P^2L^3}{6EI} + \frac{\alpha}{2}\,\frac{P^2L}{AG} \end{aligned} \tag{2.490}$$

and thus the end deflection is

$$\frac{\partial U}{\partial P} = \frac{PL^3}{3EI} + \alpha\,\frac{PL}{AG} = \Delta_{end} \tag{2.491}$$

With α = 6/5, as calculated from Equation (2.485) for a rectangular cross section, this deflection result in Equation (2.491) is about 20% less than the elasticity solution in Timoshenko and Goodier [2-28]. If we arbitrarily use k from Equation (2.463) instead of α, the influence of shear on end deflection is precisely that listed in Table 2-4, and, as noted in Section 2.7.2, in agreement with one version of the elasticity solution.

The Rayleigh method (see Section 2.6.1) cannot be used to calculate approximate beam deflections because the strain energy of shear does not depend on the deflection or its derivatives (and thus would be a constant in the energy expression, so that term would vanish in the first variation of the total potential energy).

Éléments sous droits d'auteur

2.7.4 Differential Equation Approach to Effect of Transverse Shear on Buckling of an Axially Compressed Fixed-Free Bar

We should readily anticipate from a simple free-body diagram as in Figure 2-59 that the transverse shear force, S, is a destabilizing influence because the shear force causes a destabilizing moment about the upper end of the bar. Thus, the buckling loads must be lower when transverse shear is taken into account than when transverse shear is ignored. We use the disturbance approach to buckling analysis studied in Section 2.2.

The transverse shear force, S, is related to the applied axial buckling force, $\bar{P}$, from equilibrium of the free body in Figure 2-59 by

$$S = \bar{P}\frac{dy}{dx} \tag{2.492}$$

when only small angles are considered as is appropriate for the onset of buckling. In addition, use the result from mechanics of materials that the effect of transverse shear force on deformation is to increase the slope at the neutral axis by the amount in Equation (2.464), i.e.,

$$\frac{dy_s}{dx} = \frac{kS}{AG} \tag{2.493}$$

in which k is the cross-section shape factor defined in Equation (2.463) (3/2 for rectangular cross sections and 4/3 for circular cross sections), S is the transverse shear force at the point along the bar being considered, A is the cross-sectional area, and G is the shear modulus of the material.

The buckling deflection can be thought of as being composed of two parts; that due to bending and that due to shearing:

$$y = y_b + y_s \tag{2.494}$$

as in Figure 2-59 whereupon we can differentiate Equation (2.494) to get

$$y'' = y_b'' + y_s'' \tag{2.495}$$

but, from bending considerations, i.e., the fundamental constitutive relation in Equation (2.4),

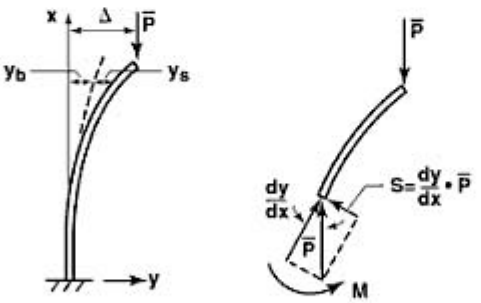


Figure 2-59 Buckled Bar and Free-Body Diagram

Éléments sous droits d'auteur

$$y''_b = +\frac{M}{EI} = \frac{\bar{P}(\Delta - y)}{EI} \tag{2.496}$$

and

$$y''_s = \frac{k}{AG} S' = \frac{k\bar{P}}{AG} y'' \tag{2.497}$$

Thus,

$$y'' = \frac{\bar{P}(\Delta - y)}{EI} + \frac{k\bar{P}}{AG} y'' \tag{2.498}$$

which can be written as

$$y'' + (k')^2 y = (k')^2 \Delta \tag{2.499}$$

in which

$$(k')^2 = \frac{\bar{P}}{EI\left[1 - \dfrac{k\bar{P}}{AG}\right]} \tag{2.500}$$

The general solution of Equation (2.499) is

$$y = A \sin k'x + B \cos k'x + \Delta \tag{2.501}$$

in which the constants A, B, and Δ are determined from the boundary conditions (actually only the relation *between* the constants is obtained because this is an eigenvalue problem, so the buckling amplitude, Δ, at the free end is indeterminate).

Apply the boundary conditions:

$$y(0) = 0 \quad \rightarrow \quad B + \Delta = 0 \tag{2.502}$$

$$y'(0) = 0 \quad \rightarrow \quad Ak' = 0 \quad \rightarrow \quad A = 0 \tag{2.503}$$

$$y(L) = \Delta \quad \rightarrow \quad B \cos k'L + \Delta = \Delta \tag{2.504}$$

$$\rightarrow \quad B \cos k'L = 0 \tag{2.505}$$

Thus, $A = 0$, $B \cos k'L = 0$, and $\Delta = -B$. However, B cannot be zero in Equation (2.505) because with $A = 0$ from Equation (2.503) then there would be no buckling deflection in Equation (2.501). Thus, the characteristic equation is

$$\cos k'L = 0 \tag{2.506}$$

with solutions

$$k'L = \left[\frac{2n-1}{2}\right]\pi \qquad n = 1, 2, \ldots \tag{2.507}$$

and then

$$\bar{P} = \left[(2n-1)\frac{\pi}{2L}\right]^2 EI\left[1 - \frac{k\bar{P}}{AG}\right] \qquad n = 1, 2, \ldots \tag{2.508}$$

which achieves its lowest value for $n = 1$, i.e.,

Éléments sous droits d'auteur

$$\bar{P} = \frac{\pi^2}{4}\frac{EI}{L^2}\left[1 - \frac{k\bar{P}}{AG}\right] \tag{2.509}$$

The coefficient on the term in brackets in Equation (2.509) is merely

$$P_E = \frac{\pi^2}{4}\frac{EI}{L^2} \tag{2.510}$$

which is the Euler buckling load (in which transverse shear stiffness is neglected), so the results can be written as

$$\bar{P} = \frac{P_E}{1 + kP_E/AG} \tag{2.511}$$

which is one of the few places in this book where $\bar{P} \neq P_E$. The effect of transverse shear stiffness is to reduce the buckling load from P_E by the fraction multiplying P_E in Equation (2.511). This fraction is very nearly unity for solid columns. For other cross sections, the effect of transverse shear stiffness can reduce buckling loads by up to 50%.

2.7.5 Energy Methods Approach to Effect of Transverse Shear on Buckling of an Axially Compressed Pinned-Pinned Bar

The Rayleigh Method is used to find the effect of transverse shear stiffness on buckling of pinned-pinned bars as in Figure 2-60. The buckling deflection approximation used is the exact solution for a pinned-pinned bar without transverse shear stiffness effects:

$$\delta v = \Delta \sin\frac{\pi x}{L} \tag{2.512}$$

in which Δ is the buckling amplitude. The variation-in-moment bending strain energy for the axially compressed bar is, from Equation (2.387),

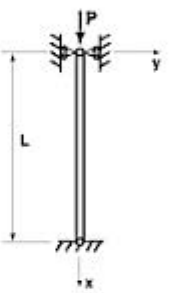


Figure 2-60 Axially Loaded Bar with Pinned Ends

$$\bar{\delta}^2 U_b = \int_0^L \frac{M^2}{EI}\,dx = \frac{\bar{P}^2}{EI}\int_0^L \delta v^2\,dx = \frac{\bar{P}^2 L\Delta^2}{2EI} \tag{2.513}$$

The second variation of the strain energy of shearing during buckling can be shown from Equation (2.484) to be

$$\bar{\delta}^2 U_s = \int_0^L \frac{\alpha S^2}{AG}\,dx = \frac{\alpha\bar{P}^2}{AG}\int_0^L \delta v_x^2\,dx = \frac{\alpha\bar{P}^2\pi^2\Delta^2}{2AGL} \tag{2.514}$$

The second variation of the membrane strain energy during buckling is, from Equation (2.380),

$$\bar{\delta}^2 U_m = -\int_0^L \bar{P}\,\delta v_x^2\,dx = -\frac{\bar{P}\pi^2\Delta^2}{2L} \tag{2.515}$$

Éléments sous droits d'auteur

Finally, upon application of the neutral equilibrium buckling criterion, from Equation (2.381),

$$\bar{\delta}^2 V = \bar{\delta}^2 U_b + \bar{\delta}^2 U_s + \bar{\delta}^2 U_m = 0 \tag{2.516}$$

we find the transverse-shear-affected buckling load to be

$$\bar{P} = \frac{P_E}{1 + \alpha P_E/AG} \tag{2.517}$$

in which $P_E = \pi^2 EI/L^2$, i.e., the Euler buckling load for this pinned-pinned bar without transverse shear effects. Of course, the buckling amplitude, Δ, in Equation (2.512) is indeterminate.

2.7.6 Importance of Transverse Shear Stiffness on Buckling of Bars

For both cases studied in Sections 2.7.4 and 2.7.5, we see that the transverse-shear-affected buckling load can be expressed as

$$P = \frac{P_E}{1 + \beta P_E/AG} \tag{2.518}$$

in which β is either k or α for all bar buckling problems with the only problem being the difference between the value of k (from the differential equation approach) and the value of α (from the energy approach). Because k is always greater than α, the most conservative (lowest) and perhaps more accurate buckling load is obtained by using $\beta = k$. That is, recall from Section 2.7.2 that k provides better agreement with the elasticity solution for deflection of an end-loaded cantilever beam than does α for which the deflection is underestimated. By examining the terms in Equation (2.518) and the definition of P_E, we can conclude that the influence of transverse shear stiffness on bar buckling is primarily caused by a cross-section-shape function (β I/A) rather than a material properties function (E/G) because the E/G term depends, for an isotropic material, only on Poisson's ratio, ν, which does not vary enough (−1 to +1/2, but usually between 1/4 and 1/2) to have significant effect on $\beta P_E/AG$. The reduction in buckling load in Equation (2.518) is negligible for solid cross-section bars, but can approach 50% for some open cross-section bars.

Problem Set 2.7

2.7.1 Derive the second variation of the shear strain energy in Equation (2.514) starting from Equation (2.484).

2.7.2 Calculate and plot P/P_E for a simply supported steel ($\nu = .3$) bar with a rectangular cross section of height h and width b against L/h in which L is the bar length. Below what value of L/h is the influence of shear deformation greater than 5%?

2.7.3 Calculate and plot P/P_E for a simply supported W 14 × 82 (U. S.) steel column ($\nu = .3$) against the length, L, in inches. Tables of properties of rolled-steel cross sections are found in many basic mechanics of materials textbooks [e.g., 2-29]. The column is restrained such that buckling occurs first in the plane perpendicular to the plane of the web. Use the approximation $\alpha \cong A/A_w$ where A is the cross-sectional area of the column and A_w is the area of the column web. Below what value of L/h is the influence of shear deformation greater than 5%?

Éléments sous droits d'auteur

2.8 EFFECT OF INITIAL GEOMETRIC IMPERFECTIONS

Actual bars always have deviations from straightness called *initial geometric imperfections* that result from inaccuracies in the manufacturing process. An actual bar might resemble Figure 2-61 in which the geometric imperfections are *grossly exaggerated* on both a local and a global scale. The imperfections remove the initial perfect straightness of a bar that we have considered to be the prebuckling equilibrium state for perfectly straight bars, and are represented by a known function $y_i(x)$. Considering their effect on bar behavior, and even on *whether the bar will buckle at all*, requires only minor escalation in mathematical modeling complexity.

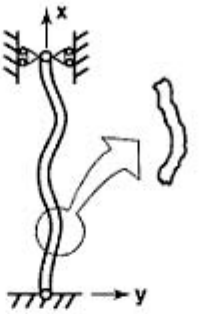


Figure 2-61 Unloaded Bar with *Exaggerated Imperfections*

A sinusoidal initial geometric imperfection of the bar in the transverse direction,

$$y_i = a \sin \frac{\pi x}{L} \qquad (2.519)$$

corresponds to a simple bowing of the bar in the shape of the lowest buckling mode of a perfect bar. This shape is argued to be the most damaging to an axially loaded bar in the sense that the buckling load should be more strongly affected than if the geometric imperfection were tiny random wiggles not related to a buckle mode shape. That is, if the bar is already deformed into the shape into which it tends to buckle, then its buckling load should be less than the Euler load, or at least some substantial change occurs. Some would argue that such already deformed bars never buckle, but we will see that for small enough geometric imperfections, the behavior of such bars does *resemble* buckling.

An axial force on the bar will result in additional transverse deflection y_t even if the load is nearly zero. The total deflection is the summation:

$$y(x) = y_i(x) + y_t(x) \qquad (2.520)$$

in which only $y_i(x)$ is known initially and $y_t(x)$ is the additional transverse displacement. From the free-body diagram in Figure 2-62, the disturbing moment at any cross section at position x is

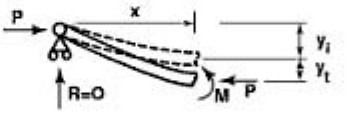


Figure 2-62 Free-Body Diagram of an Axially Loaded Imperfect Bar

$$M = P(y_i + y_t) \qquad (2.521)$$

But, for bending from an equilibrium state, the differential equation is

$$EIy'' = -M \qquad (2.522)$$

in which we take y'' to be y_t'' because the initial curvature does not require a moment to exist. Thus, the bending differential equation becomes

$$EIy_t'' = -P(y_i + y_t) \qquad (2.523)$$

or, group the unknown y_t on the left and leave the known y_i on the right:

Éléments sous droits d'auteur

$$EIy_t'' + Py_t = -Py_i \tag{2.524}$$

[which can be differentiated twice to obtain the moderately large deflection equilibrium equation, Equation (2.324), if the axial equilibrium equation, Equation (2.321), is considered] or

$$y_t'' + k^2 y_t = -k^2 a \sin \frac{\pi x}{L} \tag{2.525}$$

in which, as in the Euler buckling problem,

$$k^2 = \frac{P}{EI} \tag{2.526}$$

although by use of such a term we do not imply Euler buckling occurs.

The general solution to the differential equation in Equation (2.525) consists of the homogeneous solution

$$y_h = A \sin kx + B \cos kx \tag{2.527}$$

as in the Euler problem plus the particular solution because Equation (2.525) is not homogeneous (Thus, this is not an eigenvalue problem):

$$y_p = \frac{1}{\frac{1}{k^2}\frac{\pi^2}{L^2} - 1} a \sin \frac{\pi x}{L} = \frac{1}{\frac{1}{\alpha} - 1} a \sin \frac{\pi x}{L} = \frac{\alpha}{1-\alpha} a \sin \frac{\pi x}{L} \tag{2.528}$$

in which

$$\alpha = \frac{k^2 L^2}{\pi^2} = \frac{P}{\pi^2 \frac{EI}{L^2}} = \frac{P}{P_E} \tag{2.529}$$

i.e., the ratio of the load P to its value at Euler buckling P_E. Thus, the complete solution to the differential equation is

$$y_t = A \sin kx + B \cos kx + \frac{\alpha}{1-\alpha} a \sin \frac{\pi x}{L} \tag{2.530}$$

The boundary conditions are zero deflection at each end, i.e.,

$$y_t(0) = 0 = A \times 0 + B \times 1 + \frac{\alpha}{1-\alpha} a \times 0 \tag{2.531}$$

$$y_t(L) = 0 = A \sin kL + \frac{\alpha}{1-\alpha} a \times 0 \tag{2.532}$$

Thus, $B = 0$ and $A \sin kL = 0$. If we do not allow A to be zero, then we get the Euler solution from the characteristic equation $\sin kL = 0$ which implies that there is no effect of initial geometric imperfections. However, unlike the Euler solution for the perfect bar, here both A and B can be zero without trivializing the buckling deflection. Thus, the general solution for the transverse deflection caused by load P reduces to

$$y_t = \frac{\alpha}{1-\alpha} a \sin \frac{\pi x}{L} \tag{2.533}$$

Thus, the total transverse deflection of the imperfect bar is

$$y = y_i + y_t = a \sin \frac{\pi x}{L} + \frac{\alpha}{1-\alpha} a \sin \frac{\pi x}{L} = \frac{1}{1-\alpha} a \sin \frac{\pi x}{L} \tag{2.534}$$

Éléments sous droits d'auteur

For an initial geometric imperfection amplitude, a, the mid-length transverse deflection is plotted in Figure 2-63 in proportion to a and increases rapidly as P approaches P_E. Each curve is mapped from another by changing the amplitude and the horizontal scale by use of Equation (3.534). For example, at $\alpha = P/P_E = .5$, for amplitude a, y_t is $2.00 \times a$ whereas for amplitude a/2, y_t is $1.00 \times a$, and for amplitude a/10, y_t is $.20 \times a$. Note that these points are actually all the same! That is, y_t is always twice the imperfection amplitude! For fractions of a fixed amount of a as imperfection amplitudes, the transverse deflection is increasingly smaller as the amplitude decreases and tends toward that of a perfect bar that buckles at P_E. If a very small load is applied, then the mid-length transverse deflection increases by a factor of $1/(1 - \alpha)$. As the load approaches P_E, the mid-length transverse deflection becomes unbounded because $\alpha = 1$ is approached. Obviously, the imperfect bar can be said to also buckle at P_E, but its mid-length transverse deflection is dramatically affected by the imperfection at loads well below P_E whereas the perfect bar is unaffected.

The practical maximum load that can be carried is still P_E. The difference from the perfect to the imperfect bar is that the imperfect bar has significant bowing prior to buckling and the perfect bar does not. A perfect column or bar can buckle transversely either to the right or to the left. However, the sinusoidally imperfect bar can bow only in the direction of the imperfection (if large enough). As the imperfection amplitude decreases, the load-deflection curve approaches the behavior of the perfect bar which is zero transverse deflection until Euler buckling occurs.

The axial load, P, versus axial (end) deflection, Δ_E (the end deflection at the Euler load), response of a bar with an arbitrary cross section that is symmetric about its centroidal axes can be shown to have the shapes shown in Figure 2-64 for various amplitudes of a half-sine-wave imperfection. The bar cross section is fully characterized with the radius of gyration, r, so the family parameter of the curves is

$$k = \frac{a}{r} \tag{2.535}$$

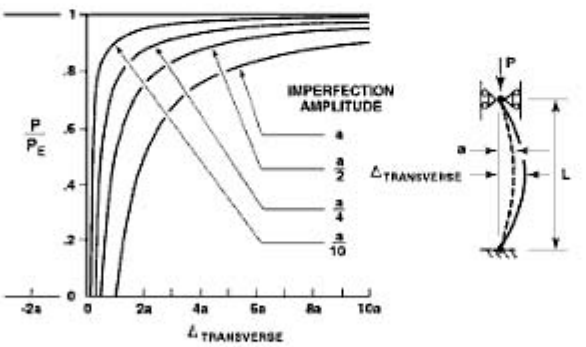


Figure 2-63 Load versus Total Transverse Deflection at Bar Mid-Length

Éléments sous droits d'auteur

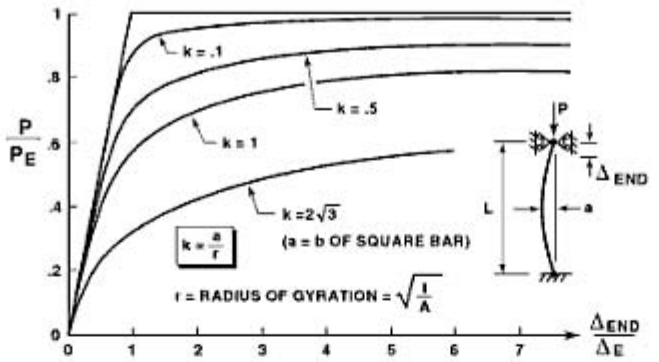


Figure 2-64 Axial Load versus Axial (End) Deflection of a Bar with an Arbitrary Cross Section (Symmetric about Centroidal Axes) and a Half-Sine-Wave Imperfection of Amplitude = a

(in which a = geometric imperfection amplitude) because both the bar cross section and the imperfection amplitude are represented with k. For a square bar of side length b with a = b, we get the $k = 2\sqrt{3}$ curve (which could also be the behavior of a rectangular cross-section bar with base, b, and height, h, perpendicular to the axis of bending if a = h irrespective of b). The behavior for a circular cross-section bar of radius, R, is the k = 1 curve if a = R/2 and the k = .1 curve if a = R/20. The behavior for all other bars is obtained by calculating their radii of gyration, calculating k from r and a, and plotting the k curve from the equation for the transverse deflection obtained in Problem 2.8.2. The behavior is characteristic of an equilibrium or boundary value problem, not a buckling or eigenvalue problem. That is, no distinct bifurcation occurs unless the bar is perfect. However, the geometrically imperfect bar deformation problem and the perfect bar buckling problem have in common the fact that no additional load can be supported at P_E without encountering large deflections. Thus, P_E is the limiting load for both problems. However, imperfect bars might deflect so much prior to buckling load P_E that their performance would be suspect or too large for the design application.

Next, consider the stresses in a square cross-section bar of side b with amplitude a of half-sine-wave imperfection. The maximum moment in the bar is at mid-length with value from Equations (2.521) and (2.534):

$$M_{max} = P(y_i + y_t)\Big|_{max} = P\,\frac{1}{1-\alpha}\,a \sin\frac{\pi x}{L}\Bigg|_{max} = \frac{P}{1-\alpha}\,a \qquad (2.536)$$

so the usual superposition of axial stress and bending stress is

$$\sigma_{max} = \frac{P}{A} + \frac{Mc}{I} = \frac{P}{A} + \left[\frac{P}{1-\alpha}\,a\right]\frac{b/2}{b^4/12} = \frac{P}{A}\left[1 + \frac{1}{1-\alpha}\,\frac{6a}{b}\right] \qquad (2.537)$$

Éléments sous droits d'auteur

We now compare σ_{max} to $\sigma_A = P/A$, the nominal axial stress on the bar. For a small imperfection amplitude a of .1b (k = .35 in Equation (2.535) which is closely above the curve k = .5 in Figure 2-64), σ_{max} is $2 \times \sigma_A$ at $P = .4P_E$, $3 \times \sigma_A$ at $P = .7P_E$, and $7 \times \sigma_A$ at $P = .9P_E$. For a larger imperfection amplitude of a = b (the curve $k = 2\sqrt{3}$ in Figure 2-64), σ_{max} is $10 \times \sigma_A$ at $P = P_E/3$, $20 \times \sigma_A$ at $P = .7P_E$, and $60 \times \sigma_A$ at $P = .9P_E$! Thus, no longer can we simply compare P/A to σ_y to determine whether yielding occurs or to a failure stress to determine whether failure occurs. The induced bending stresses can be quite significant and can lead to failure, whether by yielding or by fracture, for loads well below the Euler buckling load, P_E. For very small geometric imperfections, the bending stresses are not large until extremely high values of α are reached. Then, however, the Euler buckling load is the obvious limiting load value anyway. We have found that we must avoid the Euler buckling load —whether for large deflections because of initial geometric imperfections below P_E or because of large deflections of perfect bars just above P_E. The result in both cases is the same: P_E is a limiting load value above which we cannot allow a structure to go (and must use an adequate factor of safety in design to avoid this load at which a catastrophic failure occurs).

In summary, perfectly straight bars remain straight until they buckle whereas imperfect bars are initially bent in some manner and begin to bend even more as axial load is applied, but do not buckle. This bending deflection (and axial deflection) increases very slowly at low axial loads, but then increases very rapidly as the load approaches the Euler buckling load of a perfect bar. In fact, the Euler buckling load is asymptotically approached as the load increases, but at quite large, in fact unbounded, transverse and axial deflections. An imperfect bar always carries less than the Euler load no matter how small the imperfection. As the imperfection amplitude gets larger, so does the deflection, whether transverse or axial, at any load. The results are normalized as imperfection amplitude over the radius of gyration of an arbitrary bar cross section that is symmetric about its centroidal axes (rather than a/L for a specific cross section—here length is implicit in P_E). Induced bending stresses can exceed the nominal axial stress of P/A by large amounts leading to fracture or yielding at loads well below the Euler buckling load of a perfect bar. Other forms of initial geometric imperfections are much more difficult to treat than the sinusoidal imperfection. For example, the actual imperfections of a specific rolled-steel column could be measured, and that shape used in an analysis. However, a numerical technique would be essential unless an effective approximation to the imperfections distribution could be obtained by, for example, a Fourier series approach.

Problem Set 2.8

2.8.1 Plot the load versus the total transverse mid-span deflection due to axial load on a bar with a half-sine-wave geometric imperfection, i.e., include the initial geometric imperfection component of deflection to plot Figure 2-63.

2.8.2 Derive the expression for the axial deflection of a sinusoidally imperfect bar used to plot Figure 2-64 and then calculate and plot a figure like Figure 2-64.

2.8.3 Verify the stress calculations and bending stress magnitudes in the last example for half-sine-wave amplitudes a = .1b and a = b. Also investigate a = .01b.

Éléments sous droits d'auteur

2.9 EFFECT OF RESTRAINED THERMAL EXPANSION

2.9.1 Introduction

Thermal effects on structures are of at least two types: (1) change of material properties under elevated or lowered temperatures (i.e., many material properties are temperature dependent) and (2) thermal stresses can be induced by temperature gradients in an unrestrained body as well as by uniform or nonuniform temperature changes in restrained bodies. Thermal stresses, whether with or without mechanical stresses, can be high enough to cause failure. Compressive thermal stresses can be high enough to cause buckling of structural members if restraints to thermal expansion exist. For a bar, if no axial restraints prevent thermal expansion, then no thermal force can occur to cause buckling. For plates and shells, we will see that structural restraints are not always necessary to cause buckling. To cope with these effects, we (1) carefully select materials that can withstand the design thermal environment and (2) design structures and other bodies with shapes that keep thermal stresses from causing failure and will not buckle under thermal loading.

We will address (1) how thermal strains and stresses develop, (2) fundamental thermoelastic relations, (3) bar support conditions, (4) thermal buckling of a bar under a uniform temperature change, and (5) the deformation response of an axially constrained bar under a linear temperature gradient through the thickness plus a constant temperature. The second solution (5) reduces to the first solution (4) as the linear temperature gradient goes to zero in the same manner that the imperfect bar deformation response problem in Section 2.8 (half-sine-wave imperfection) reduces to Euler buckling as the imperfection amplitude goes to zero.

2.9.2 Origins and Conditions of Thermal Stress and Thermal Strain

An unrestrained body subjected to uniform temperature increase will simply expand (or contract if the temperature decreases) with what is called *free thermal strain* in all directions as in Figure 2-65. *Free* is a reference to the lack of restraint on movement of the body; *thermal* is a reference to the change in temperature origin of the induced deformation; and *strain* is obviously a reference to the deformation per unit length of the body. No stresses accompany the free thermal strain because the body is not restrained. Choice of a reference state for such deformations is arbitrary and is usually chosen for physical significance or for convenience in the problem addressed. For example, if a body is manufactured at room temperature, then we naturally choose room temperature as the reference temperature for any subsequent temperature excursions for the body and as the base state for any body dimensional changes when

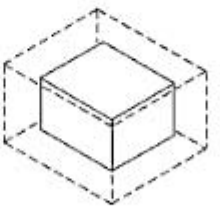


Figure 2-65 Free Thermal Expansion of a Uniformly Heated Body

Éléments sous droits d'auteur

temperature increases or decreases. Metals are created at very high temperatures and then cooled to room temperature, but are often 'heat-treated' to change their properties. Thus, the reference temperature that you use depends on the point in the history of the material or of the body you are addressing. The free thermal strains on a uniformly heated three-dimensional body in rectangular coordinates are

$$\varepsilon_x = \alpha\Delta T \qquad \varepsilon_y = \alpha\Delta T \qquad \varepsilon_z = \alpha\Delta T \tag{2.538}$$

in which α is the coefficient of thermal expansion of the material out of which the body is made (and is, like virtually all material properties, a function of temperature) and ΔT is the change in temperature from the reference temperature at which we regard the deformations as a reference state of 'zero deformation' or zero thermal strain. That is, we define $\Delta T = T - T_{reference}$. However, if we reduce the temperature from that so-called reference state, then the body would have different dimensions, so the reference temperature, and hence the reference deformation state are somewhat arbitrarily defined, so the reference temperature is almost an arbitrary initial condition for the problem. Finally, we note that *thermal strain* is, in general, a reference to a strain induced in some manner by thermal loading, whether uniform or in gradient form.

The body that is subjected to a uniform temperature rise, but is not restrained from movement in any direction as in Figure 2-65 undergoes simple expansion, hence thermal strains, yet no thermal stress accompanies those thermal strains: *a case of thermal strain without thermal stress.* If a uniformly heated body with free thermal strains in Equation (2.538) is subjected to a set of mechanical stresses, then the final strain state is a superposition of the mechanical strains

$$\begin{aligned}
\varepsilon_x &= \frac{\sigma_x}{E} - \frac{\nu}{E}\sigma_y - \frac{\nu}{E}\sigma_z \\
\varepsilon_y &= -\frac{\nu}{E}\sigma_x + \frac{\sigma_y}{E} - \frac{\nu}{E}\sigma_z \\
\varepsilon_z &= -\frac{\nu}{E}\sigma_x - \frac{\nu}{E}\sigma_y + \frac{\sigma_z}{E} \\
\gamma_{xy} &= \frac{\tau_{xy}}{G} \qquad \gamma_{xz} = \frac{\tau_{xz}}{G} \qquad \gamma_{yz} = \frac{\tau_{yz}}{G}
\end{aligned} \tag{2.539}$$

on the free thermal strain state of Equation (2.538) resulting in

$$\begin{aligned}
\varepsilon_x &= \frac{\sigma_x}{E} - \frac{\nu}{E}\sigma_y - \frac{\nu}{E}\sigma_z + \alpha\Delta T \\
\varepsilon_y &= -\frac{\nu}{E}\sigma_x + \frac{\sigma_y}{E} - \frac{\nu}{E}\sigma_z + \alpha\Delta T \\
\varepsilon_z &= -\frac{\nu}{E}\sigma_x - \frac{\nu}{E}\sigma_y + \frac{\sigma_z}{E} + \alpha\Delta T \\
\gamma_{xy} &= \frac{\tau_{xy}}{G} \qquad \gamma_{xz} = \frac{\tau_{xz}}{G} \qquad \gamma_{yz} = \frac{\tau_{yz}}{G}
\end{aligned} \tag{2.540}$$

Clearly, we see the mechanical loading contribution to the strains as well as the thermal loading contribution. This superposition is valid because the mechanical stresses are applied in such a manner that all surfaces

Éléments sous droits d'auteur

of the body move (but are not subject to any displacement restraint except for a single point preventing rigid-body movement). Mechanical stresses exist, but no thermal stresses. Both mechanical strains and free thermal strains exist. The difficulty begins when either a structural restraint or a thermal gradient is imposed.

Thermal stress is a stress that is *induced* when the temperature of a body changes in some manner, yet is restrained from the free movement of the case of free thermal strains. (Or thermal stress can be induced by a nonlinear temperature gradient on an unrestrained body[1]). That is, a thermal stress is associated with thermal loading in contrast to a mechanical stress that is associated with mechanical loading. Actually, there is no such thing as thermal stress, but only a *thermally induced stress*. Nevertheless, we use the term thermal stress with the understanding that we mean thermally induced stress. The simplest example of thermal stress is a bar subjected to a uniform temperature rise, yet is restrained from any axial movement at its ends as in Figure 2-66. Thus, thermal stresses arise because the bar tends to expand axially with a free thermal strain of $\alpha\Delta T$ (and transversely, but there is no transverse restraint, so the bar does expand freely in the transverse directions), but the restrained ends prevent any axial expansion, so the bar is compressed from what it would have become without axial restraint to what it must be with axial restraint thereby generating an axial stress. The axial stress is the amount of stress necessary to compress the bar by a strain of $\alpha\Delta T$, and for the bar that stress for full axial restraint is

$$\sigma = -E\alpha\Delta T \tag{2.541}$$

Because of the axial restraint and associated lack of axial movement, there is no axial strain: *a case of thermal stress without thermal strain.*

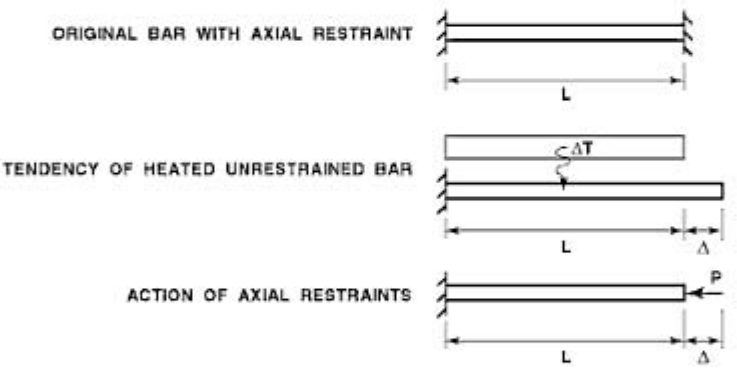


Figure 2-66 Axially Restrained Bar with Uniform Temperature Increase

[1]Thornton [2-31, pp. 166–167] shows that a nonlinear temperature gradient on an unrestrained isotropic elastic body with constant material properties causes thermal stresses, thermal strains, and displacements. However, a linear temperature gradient causes no thermal stresses, but there are thermal strains and displacements.

Éléments sous droits d'auteur

As a more complicated example, if an unrestrained body is subjected to a temperature gradient, then different parts of the body tend to expand different amounts. However, all parts of the body must be in equilibrium with each other and must have compatible strains to remain a continuous body. Hence, a system of equilibrating stresses and compatible strains is induced by the temperature gradient. The stresses are called thermal stresses, and the strains are called thermal strains. However, these thermal strains are not as large as free thermal strains, and these thermal stresses are not as large as the case in which the body is fully restrained from movement. Thornton shows that a linear temperature gradient on an unrestrained isotropic elastic body with constant material properties causes no thermal stresses, but there are thermal strains and displacements [2-31, pp. 166–167]. Accordingly, we apply a nonlinear temperature gradient on the rectangular body (that is thin in the direction perpendicular to the rectangular area shown) in Figure 2-67 by rapid heating of the top of the rectangle (or the material has low heat conductivity, but the heating rate is slow). Thus, there is a nonlinear temperature gradient from the top to the bottom of the rectangle. (If the heating is applied slowly enough, the heat will 'soak through' the entire body, so the temperature will soon become uniform throughout the entire body). The top tends to expand because of the heating, but the bottom by itself has no reason to expand because it is not heated. However, both the top and the bottom are attached to the middle of the rectangle which has a lower tendency to expand than the top because of lower heating than the top and yet a higher tendency to expand than the bottom because of higher heating than the bottom. Those three 'parts' of the body must deform in a continuously varying manner to maintain continuity of the body. The resulting stress field in the body ranges from compressive stress at the top (because the top is 'held back' by the middle) to tensile stress at the bottom (because it is 'pulled' by the middle) with zero stress somewhere in the middle of the body. The stress field must be *self-equilibrating* because no mechanical loading is applied. The strain field is an extension

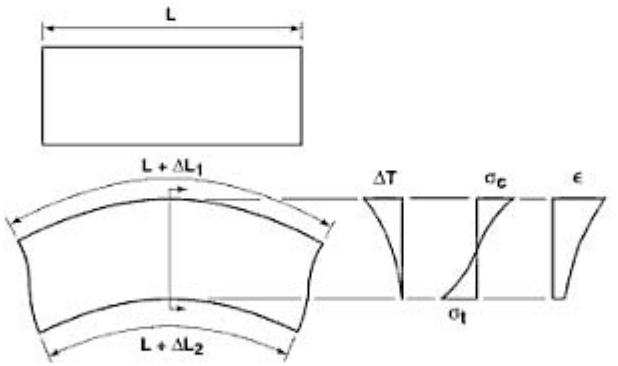


Figure 2-67 A Rectangular Body Subjected to a Temperature Gradient

Éléments sous droits d'auteur

at the top which is less than the free thermal strain $\alpha\Delta T$ corresponding to the ΔT of the top and an extension at the bottom which is more than the zero strain which would otherwise result from the zero temperature change. Note that the entire body is extended because of the heating. No part of the body contracts.

Most heated bodies have both thermal stress and thermal strain by virtue of movement restraints and/or temperature gradients being applied. The thermal stresses are usually less than the thermal stresses in a perfectly restrained body, and the thermal strains are less than the free thermal strains of an unrestrained body. However, we cannot easily identify the relative magnitudes of the thermal stresses and mechanical stresses or of the thermal strains and mechanical strains. The situation is complicated by the fact that, in addition to the stress-strain relations, all points in the body must satisfy the force equilibrium equations and the strain compatibility conditions as part of a well-posed thermoelasticity problem. We will concentrate in this section on one-dimensional bars under various thermal loadings. Two-dimensional flat plates and three-dimensional shells are treated in Chapters 3 and 4, respectively.

2.9.3 Fundamental Thermoelastic Relations

We consider a long, slender, straight bar of isotropic elastic material with the reference axis (x-axis) through the centroid of the bar cross section. Transverse deformations (bending) are permitted, but shearing deformations are neglected. Thus, the stress state is uniaxial and we impose some form of temperature-change distribution over the bar volume. The thermoelastic strain-stress relation at a point is obtained by superimposing a mechanical strain on a free thermal strain:

$$\varepsilon_x = \frac{\sigma_x}{E} + \alpha\,\Delta T \tag{2.542}$$

in which ε_x is the total strain, σ_x/E is the mechanical strain, and $\alpha\,\Delta T$ is the free thermal strain resulting from the temperature change at any point in the bar volume as a function of time, namely $\Delta T = T(x,y,z,t) - T_{ref}$ in which T_{ref} is a reference temperature as an arbitrary and convenient baseline configuration of 'zero strain' or zero thermal stress. We will not address the time dependence of the temperature gradient except for remarks in the summary section (2.9.7). The thermoelastic stress-strain relation is, by inversion of Equation (2.542),

$$\sigma_x = E(\varepsilon_x - \alpha\,\Delta T) \tag{2.543}$$

in which $\varepsilon_x - \alpha\Delta T$ is apparently the mechanical strain.

In a typical structural mechanics problem, we impose conditions (1) on the total strain (such as, e.g., $\varepsilon_x = 0$ on a heated bar between two immovable walls as in Figure 2-68a) which can be regarded as a displacement-type boundary condition, e.g., u = 0 at the ends of the bar or (2) on the stress (such as, e.g., $\sigma_x = 0$ on the free end of a heated cantilever bar as in Figure 2-68b), i.e., a stress-type boundary condition. Support conditions will be addressed in more detail in Section 2.9.4.

Éléments sous droits d'auteur



a Bar between Walls b Cantilever Bar

Figure 2-68 Two Bar Support Conditions

We might think from the preceding derivation that we have mechanical stress on the left-hand side of Equation (2.543), but we would be wrong part of the time. We have to regard Equation (2.543) as simply *a constitutive equation relating stress of whatever origin to strain of whatever origin* at that point. We examine two bar restraint conditions to clarify that contention:

1. If there is no axial restraint such as in the cantilever bar of Figure 2-68b and $\Delta T = 0$, then $\varepsilon_{total} \neq 0$ because one end must move in order for the bar to accept applied stress. Then, Equation (2.543) reduces to $\sigma_x = E\varepsilon_x$, so σ_x is *mechanical stress* as we probably thought or expected.
2. If there is full axial restraint such as in the bar between walls in Figure 2-68a and a uniform ΔT is imposed, then $\varepsilon_{total} = 0$ because neither end can move and Equation (2.543) reduces to $\sigma_x = -E\alpha\Delta T$ and here the same symbol σ_x from the same stress-strain relation now means *thermal stress*, not mechanical stress as it meant in the no axial restraint case.

Although we initially brought σ into the problem as a mechanical stress generating a mechanical strain, σ simply means just the stress at a point that results when the loading and restraint are taken into account. Thus, we must be very careful when we try to attribute the characteristics of mechanical or thermal as adjectives on stresses or strains.

By the Bernoulli-Euler beam-bending hypothesis, the total strain varies linearly through the bar thickness (the y-direction):

$$\varepsilon_x = \bar{\varepsilon}_x - y\,\kappa_x \tag{2.544}$$

in which $\bar{\varepsilon}_x$ is the strain at the centroidal axis of the bar and κ_x is the bar centroidal-axis curvature

$$\kappa_x = v_{xx} \tag{2.545}$$

Also, the nonlinear centroidal-axis strain-displacement relation for moderately large deformation is

$$\bar{\varepsilon}_x = \frac{\partial u}{\partial x} + \frac{1}{2}\left[\frac{\partial v}{\partial x}\right]^2 = u_x + \frac{1}{2}v_x^2 \tag{2.546}$$

in which u and v are centroidal-axis displacements, i.e., $\bar{\varepsilon}_x$ is the nonlinear bar centroidal-axis strain. Note that the Bernoulli-Euler hypothesis is applicable only to the total strains that result from application of pure bending, i.e., the only loading is a bending moment at each end of the bar, although presence of an axial force does not change the validity of the hypothesis (plane sections originally perpendicular to the bar axis still remain plane after deformation). We simply substitute the centroidal-axis

Éléments sous droits d'auteur

strain, Equation (2.544) in the one-dimensional stress-strain relation, Equation (2.543), to get

$$\sigma_x = E\,(\bar{\varepsilon}_x - y\,\kappa_x - \alpha\,\Delta T) \tag{2.547}$$

The axial force in a homogeneous bar (constant E, ν, and α) is

$$\begin{aligned} N_x &= \int_A \sigma_x\,dA \\ &= E\int_A (\bar{\varepsilon}_x - y\,v_{xx} - \alpha\,\Delta T)\,dA \\ &= E\,\bar{\varepsilon}_x \int_A dA - E\,v_{xx}\int_A y\,dA - E\,\alpha\int_A \Delta T\,dA \\ &= E\,A\,\bar{\varepsilon}_x - E\,\alpha\int_A \Delta T\,dA \\ &= E\,A\,\bar{\varepsilon}_x - N_x^T \end{aligned} \tag{2.548}$$

in which the middle integral in the third step is zero because $\int_A y\,dA$ is the definition of the first moment of the area which is zero at the centroidal axis. Also, N_x^T is the thermal force that depends on the temperature-change distribution over the bar cross-sectional area, i.e.,

$$N_x^T = E\,\alpha\int_A \Delta T\,dA \tag{2.549}$$

Note that the term $EA\bar{\varepsilon}_x$ in Equation (2.548) is not the mechanical force as contrasted with the thermal force, N_x^T just as we cannot identify σ_x in Equation (2.543) as either a thermal or mechanical stress until the restraint conditions are imposed. If we substitute the nonlinear strain-displacement relation, Equation (2.546), the force becomes

$$N_x = E\,A\left[u_x + \frac{1}{2}\,v_x^2\right] - N_x^T \tag{2.550}$$

Similarly, the moment on a homogeneous bar is

$$\begin{aligned} M_x &= \int_A \sigma_x\,y\,dA \\ &= E\int_A (\bar{\varepsilon}_x - y\,v_{xx} - \alpha\,\Delta T)\,y\,dA \\ &= E\int_A \bar{\varepsilon}_x\,y\,dA - E\int_A y\,v_{xx}\,y\,dA - E\,\alpha\int_A \Delta T\,y\,dA \\ &= -E\,v_{xx}\int_A y^2\,dA - E\,\alpha\int_A \Delta T\,y\,dA \\ &= -E\,I\,v_{xx} - M_x^T \end{aligned} \tag{2.551}$$

in which the first integral in the third line of Equation (2.551) vanishes because $\bar{\varepsilon}_x$ does not vary over the bar cross-sectional area and the origin is at the centroid, so $\int_A y\,dA = 0$. Also, M_x^T is the thermal moment that depends on the temperature-change distribution over the bar cross-sectional area, i.e.,

Éléments sous droits d'auteur

$$M_x^T = E\,\alpha \int_A \Delta T\, y\, dA \tag{2.552}$$

In a similar manner to the reasoning for the force equation, Equation (2.548), the term $EI\,v_{xx}$ in Equation (2.551) is not the mechanical moment as contrasted with the thermal moment, M_x^T.

The moderately large-deflection equilibrium differential equations and associated boundary conditions as well as the buckling differential equations and associated boundary conditions can be derived with the fundamental energy approach used in Sections 2.5.5.1 and 2.5.5.2. Simply include the thermal effects in the strain energy density expression (strain energy per unit volume[2]) of Equation (2.311) on page 108:

$$U_o = \frac{E}{2}\sigma_x^2 = \frac{E}{2}(\varepsilon_x - \alpha\Delta T)^2 = \frac{E}{2}(\varepsilon_x^2 - 2\varepsilon_x\,\alpha\Delta T + \alpha^2\Delta T^2) \tag{2.553}$$

in which the ε_x^2 term is the usual strain energy density term (and the only term) when thermal effects are not present and the term $\alpha^2\Delta T^2$ is merely an additive constant to U_o and therefore does not affect the results when the principles of stationary potential energy and minimum potential energy are applied [because $\delta(\text{constant}) = 0$]. Thus, the only additional term in the strain energy density beyond that caused by mechanical effects is $2\varepsilon_x\,\alpha\Delta T$. Recall that in general $\Delta T = \Delta T(x,y,z,t)$, but has no variations because it is not a function of displacements which are varied. The variational process leads to the nonlinear equilibrium and linear buckling differential equations and their associated boundary conditions in this section (verification is left as exercises in Problem Set 2.9).

From Section 2.5.5.1, the moderately large-deflection bar equilibrium equations without explicit thermal effects and without body forces are

$$N_{x,x} = 0 \tag{2.554}$$

$$N_x v_{xx} + M_{x,xx} = 0 \tag{2.555}$$

in which the force and moment can be a function of thermal effects such as in Equations (2.548) and (2.551) so can be written as

$$EA\frac{\partial \bar{\varepsilon}_x}{\partial x} - \frac{\partial N_x^T}{\partial x} = 0 \tag{2.556}$$

$$EI\frac{\partial^4 v}{\partial x^4} - EA\bar{\varepsilon}_x\frac{\partial^2 v}{\partial x^2} + N_x^T\frac{\partial^2 v}{\partial x^2} + \frac{\partial^2 M_x^T}{\partial x^2} = 0 \tag{2.557}$$

For a bar with uniform ΔT through the thickness, h, $v = 0$ in the equilibrium state prior to buckling (provided the bar was perfectly straight before loading); otherwise, $v \neq 0$.

The associated equilibrium boundary conditions for a bar of general cross section are

[2]Recall from Section 2.5.5 that the strain energy density results from the work of the stresses internal to a body or mechanical system and can be expressed alternatively in terms of strains, stresses, or stresses and strains by use of the stress-strain relations.

Éléments sous droits d'auteur

$$\left[EA\left(u_x + \frac{1}{2}v_x^2\right) - N_x^T\right]\Big|_{x=0} = 0 \quad \text{or} \quad \delta u|_{x=0} = 0$$

$$\left[\left[EA\left(u_x + \frac{1}{2}v_x^2\right) - N_x^T\right]v_x - \left[EIv_{xx} - M_x^T\right]_{,x}\right]\Big|_{x=0} = 0 \quad \text{or} \quad \delta v|_{x=0} = 0$$

$$\left[EIv_{xx} - M_x^T\right]\Big|_{x=0} = 0 \quad \text{or} \quad \delta v_x|_{x=0} = 0 \tag{2.558}$$

with similar boundary conditions at $x = L$ except for the force condition

$$\left[-EA(u_x + v_x^2/2) + N_x^T\right]\Big|_{x=L} = P \tag{2.559}$$

Note that these boundary conditions can be written as

$$\begin{aligned} N_x|_{x=0} &= 0 \quad \text{or} \quad \delta u|_{x=0} = 0 \\ N_x v_x + M_{x,x}|_{x=0} &= 0 \quad \text{or} \quad \delta v|_{x=0} = 0 \\ M_x|_{x=0} &= 0 \quad \text{or} \quad \delta v_x|_{x=0} = 0 \end{aligned} \tag{2.560}$$

i.e., as natural boundary conditions on the left in Equation (2.560) and geometric boundary conditions on the right in which the force and moment are the total quantities including thermal effects implicitly through Equations (2.548) and (2.551), respectively.

For buckling problems, the variations in force and moment are

$$\delta N_x = \int_A \delta\sigma_x \, dA \tag{2.561}$$

$$\delta M_x = \int_A \delta\sigma_x \, y \, dA \tag{2.562}$$

in which

$$\delta\sigma_x = E\delta\varepsilon_x \tag{2.563}$$

and $\delta\varepsilon_x$ has a variation in terms of the variations in u and v. Note that the $\alpha\,\Delta T$ term in σ_x, Equation (2.543), does not have a variation, i.e., both α and ΔT are constant when displacements are varied as is the load, P, because none are a function of displacements. As a consequence, $\delta N_x^T = 0$ and $\delta M_x^T = 0$ because these thermal loadings, like the mechanical loadings, are constant in the variational process and affect only the prebuckling equilibrium stress state.

The usual bar buckling equations without explicit thermal terms (or body forces) from Section 2.5.5.2 are

$$\delta N_{x,x} = 0 \tag{2.564}$$

$$N_x \bar{\delta} v_{xx} + \delta M_{x,xx} = 0 \tag{2.565}$$

in which $\bar{\delta}$ is the special variation from the prebuckling equilibrium state. We seek the value of the prebuckling force N_x that yields a solution to Equation (2.565), i.e., the eigenvalue of the equation, N_x. When only mechanical loading is considered, $N_x = EAu_x$.

Éléments sous droits d'auteur

The bar buckling equations, including thermal terms, depend on the variations of the force and the moment, but recall that the first variations of the thermal force and thermal moment are zero. Thus, the bar thermoelastic buckling equations become

$$\delta N_{x,x} = 0 \tag{2.566}$$

$$E I \frac{\partial^4 \delta v}{\partial x^4} - N_x \frac{\partial^2 \delta v}{\partial x^2} = 0 \tag{2.567}$$

in which

$$N_x = E A \frac{\partial u_0}{\partial x} - N_x^T \tag{2.568}$$

which is the eigenvalue we seek in the thermoelastic buckling problem because, for a perfectly straight bar, the transverse deflection, v, in the prebuckling equilibrium state is zero (as are its derivatives) and u_0 is the prebuckling centroidal-axis displacement. The nature of N_x in Equation (2.568) must be determined prior to buckling from the solution of the equilibrium boundary value problem. The two terms in N_x could each be a function of x as long as the equilibrium equation, Equation (2.556) is satisfied. That is, if one of the two terms increases, then the other term must decrease in order for N_x to satisfy Equation (2.556). At any rate, Equation (2.567) can be a differential equation with nonconstant coefficients and therefore often difficult to solve.

The associated buckling boundary conditions are

$$\begin{aligned} EA\bar{\delta}u_x\big|_{x=0} &= 0 \quad \text{or} \quad \delta u\big|_{x=0} = 0 \\ \left[EAu_x\bar{\delta}v_x - EI\bar{\delta}v_{xxx} - N_x^T\bar{\delta}v_x\right]\Big|_{x=0} &= 0 \quad \text{or} \quad \delta v\big|_{x=0} = 0 \\ EI\bar{\delta}v_{xx}\big|_{x=0} &= 0 \quad \text{or} \quad \delta v_x\big|_{x=0} = 0 \end{aligned} \tag{2.569}$$

with analogous boundary conditions at x = L or

$$\begin{aligned} \delta N_x\big|_{x=0} &= 0 \quad \text{or} \quad \delta u\big|_{x=0} = 0 \\ N_x\bar{\delta}v_x + \delta M_{x,x}\big|_{x=0} &= 0 \quad \text{or} \quad \delta v\big|_{x=0} = 0 \\ \delta M_x\big|_{x=0} &= 0 \quad \text{or} \quad \delta v_x\big|_{x=0} = 0 \end{aligned} \tag{2.570}$$

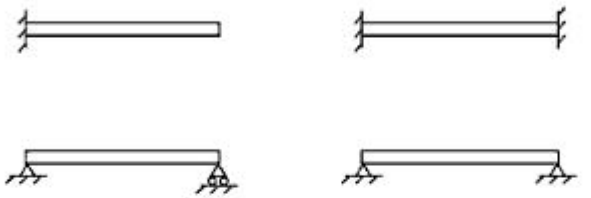
Equations (2.566) and (2.567) are homogeneous differential equations with homogeneous boundary conditions in Equations (2.569) or, alternatively, (2.570). Thus, they constitute an eigenvalue problem and are solved accordingly. The eigenvalue is the value of N_x, the buckling load or ΔT, the thermal buckling load. The eigenvector is the shape of the buckled bar. Actually, there is no physically interesting solution to Equation (2.564) because the eigenvalue is not involved, so we can ignore Equation (2.564). Variations of u are independent of variations of v, so we need not solve the independent differential equation, Equation (2.564).

We will use these fundamental thermoelastic relations in problems involving equilibrium and buckling after we have further explored the issue of bar support conditions as related to axial restraint in Section 2.9.4.

Éléments sous droits d'auteur

2.9.4 Bar Support Conditions

Bar end support conditions are crucial to the nature of the problem. If bars are free to expand axially under a temperature change as in Figure 2-69a, then no thermal buckling can occur because no compressive thermal stresses can develop. If bars are not free to expand or contract axially under a temperature change as in Figure 2-69b, then compressive or tensile thermal stresses develop. Obviously, only compressive thermal stresses cause buckling of a bar. The bottom bars in Figure 2-69 are both called pinned-pinned, but the key difference between them is no axial restraint versus perfect axial restraint. That is, the pinned ends in Figure 2-69b cannot move in the axial direction whereas the right-hand pinned end in Figure 2-69a can move because it is on rollers.



a Without Axial Restraint b With Axial Restraint

Figure 2-69 Bars Without and With Axial Restraint

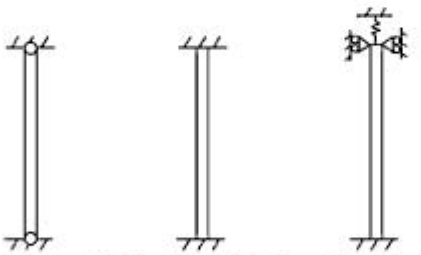
The rotational and translational restraints of a bar affect the level of the thermal buckling load, just as they affect the level of the mechanical buckling load that we studied for various support conditions in previous sections in this chapter. However, unlike mechanical buckling load problems, thermal buckling load problems do not require movement between the bar ends to cause load that leads to buckling. In fact, *thermal buckling problems require that some restriction on movement occur between the bar ends!* That is, either no movement can occur because the ends cannot move relative to one another or an elastic restraint exists against movement such as an axially oriented spring. Note that the free expansion of a heated bar will exceed the contraction of the spring thereby developing an axial prebuckling force that is less than what would be developed if the end were immovable.

All of the loaded ends of the bars in preceding sections are free to move in the axial direction just as are the bars in Figure 2-69a. That is, all of the support mechanisms permit axial movement in order for the bar to accept mechanical load. Without the possibility of axial deformation, the bars cannot be loaded with a mechanical load. However, those supports do not permit thermal buckling under a constant ΔT throughout the bar because no thermal force can develop without axial restraint. Even if the temperature change varies in the axial direction, the effect is only to lengthen the bar, not to buckle it. Linear temperature gradients through the thickness of the bars in Figure 2-69a merely result in bar bending in proportion to the magnitude of the gradient and bar extension in proportion to the average temperature rise of the bar.

Éléments sous droits d'auteur

Accordingly, we define some bar end support or restraint conditions that can lead to thermal buckling. Both end supports cannot move toward one another in Figure 2-70a and b, although the spring-supported upper end in Figure 2-70c can move away from the lower end if the temperature increases and can rotate during buckling (a rotation-preventing support could be provided similar to the block on rollers at the top of the bar in Figure 2-6 on page 57). Thus, a uniform temperature increase, ΔT, throughout any of the bars in Figure 2-70 leads to compressive thermal stresses that can be high enough to cause the bar to buckle outward in either direction transverse (perpendicular) to the bar axis. However, before that buckling condition occurs, the bar merely develops compressive thermal stress *without any axial strain whatsoever* (with a uniform ΔT throughout the bar), except in the spring-supported-end case in Figure 2-70c. If ΔT is a function of axial coordinate, x, along the bar, then both the displacements and strains are also a function of x, i.e., $u = u(x)$ and $\varepsilon_x = \varepsilon_x(x)$. Both a uniform ΔT and an axially varying ΔT lead to compressive thermal forces that can cause buckling. However, for the simply supported and fixed-fixed bars in Figures 2-70a and b, there is no net displacement of one end relative to the other end irrespective of whether the temperature change varies in the axial direction or not. For the fixed-spring supported bar, the net force comes from the integrated effect of the variable temperature change. Similarly, the guided-fixed and guided-pinned bars of Figures 2-22 and 2-23 on pages 73 and 75, respectively, could have their load holders (the box with side wheels under the load) fixed in vertical position so the bars have no net displacement of one end relative to the other end. Note that axial restraint is the sole determining factor for the prebuckling thermal force in the bar, i.e., any rotational restraint is immaterial (except, of course, when determining the buckling load). Thus, for the same heating condition, each of the bars in Figure 2-70a and b as well as in Figures 2-22 and 2-23 has the same prebuckling thermal force. Only the axial-spring-supported bar has a different prebuckling thermal force than the other four bars because the spring permits a limited amount of axial movement in proportion to the force developed prior to buckling.

If a bar has been shortened by a deformation-controlled device such as in a screw-type load frame as opposed to a hydraulic load frame, then



a Simply Supported b Fixed-Fixed c Fixed-Spring Supported

Figure 2-70 Bars with Axial Restraint

Éléments sous droits d'auteur

a mechanical load has been introduced with an axial restraint now in position. The screw-type load frame is a way of introducing load by applying a displacement to shorten a bar or other object. Essentially, the upper end of the bar in Figure 2-71 screws down applying a load but remaining in position to resist any thermal expansion if heating occurs. Subsequently, a thermal loading can be applied, so the buckling load is the result of thermal loading on a bar that is prestressed with mechanical load. Thus, buckling under nearly simultaneous thermal and mechanical loading is possible. In many more ordinary cases, bars cannot be supported in a manner such that *both* buckling due to mechanical loads and buckling due to thermal loads occur. That is, both thermal and mechanical loads are quite difficult to simultaneously develop in a one-dimensional structural member such as a bar because they generally require contradictory, i.e., mutually exclusive, support mechanisms that are not likely to be achieved in practice.

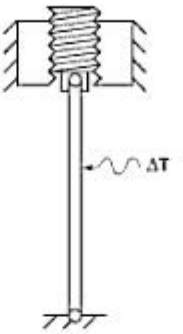


Figure 2-71 Displacement Loading of a Bar

Consider the spring-supported bar in Figure 2-72. If the bar is mechanically loaded with force P on the freely movable load holder (the box with the side wheels in Figure 2-72), then the bar buckles at the Euler buckling load, $P = \pi^2 EI/L^2$. If the bar is heated as well as mechanically loaded, then it expands in the axial direction moving both the spring and the load holder upward. However, the spring force between the load holder and the bar end does not change, i.e., it remains P. Thus, no thermal buckling can occur for this bar in contrast to the fact that the spring-supported bar in Figure 2-70c can buckle under thermal load. However, if the load holder is actually a deformation-controlled device such as in a screw-type load frame described in the previous paragraph, the spring force between the load holder and the bar changes as the temperature increases. Thus, both mechanical and thermal load can be introduced in such a support system thereby opening the possibility of both mechanical and thermal buckling.

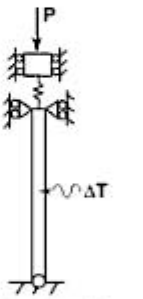


Figure 2-72 Combined Thermal and Mechanical Loading

In all support cases, we do not address any heat transfer from the bar to the supports. Instead, we expect the associated heating analysis to take into account any heat transfer to the supports as part of defining the heating of the bar as well as its support system. That thermal loading can, however, cause buckling only if there is axial restraint of the bar.

Éléments sous droits d'auteur

2.9.5 Thermal Buckling of an Axially Restrained Pinned-Pinned Bar subjected to a Uniform Temperature Change

How do we solve thermal buckling problems? As for many other mechanics problems, we can break the overall problem into workable parts and then superpose them (as long, of course, as every part has *linear* behavior). Alternatively, we could formulate and solve a governing differential equation and boundary conditions, i.e., solve an eigenvalue problem. We first use superposition for this simple problem.

Consider a bar with both ends pinned a constant distance apart and subjected to a uniform ΔT throughout the bar volume as in Figure 2-73a. Initially, the bar is perfectly straight (i.e., no imperfections are considered). Superposition of the free thermal expansion problem in Figure 2-73b and the thermal restraining force problem in Figure 2-73c is subject to the requirement that the total deformation is zero, i.e., that the free thermal expansion precisely equals the thermal restraining force contraction (i.e., we seek the compressive force that will exactly eliminate the free thermal expansion):

$$(\Delta_{FTE} = \alpha\, \Delta T\, L) = (\Delta_{TRF} = \frac{PL}{AE}) \tag{2.571}$$

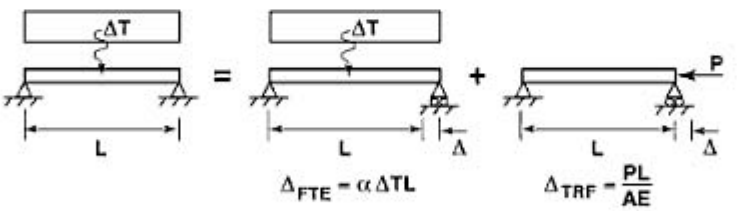
in which α is the coefficient of thermal expansion of the bar material. This condition leads to a compressive thermal stress of magnitude

$$\sigma = -\frac{P}{A} = -\frac{E}{L}\, \alpha\, \Delta T\, L = -E\, \alpha\, \Delta T \tag{2.572}$$

The implication is that free thermal expansion leads to a deformation that must be suppressed by a compressive "mechanical" force P, the induced thermal restraining force P in Figure 2-73c (defined to be positive although it is a compressive force), which causes stresses in the bar. We seek the value of $\overline{P}$ or σ, hence $\overline{\Delta T}$, that will cause buckling.

However, we already know the value of the mechanical force $\overline{P}$ that causes buckling! Our work in previous sections of Chapter Two is for just such problems. That is, we can rearrange Equation (2.572) to get the thermal buckling load:

$$\overline{\Delta T} = \frac{\overline{P}}{A\, E\, \alpha} \tag{2.573}$$



a Thermal Buckling Problem

b Free Thermal Expansion Problem

c Thermal Restraining Force Problem

Figure 2-73 Superposition of Loading Cases

Éléments sous droits d'auteur

For a simply supported bar, as in Figure 2-73c, $\bar{P} = \pi^2 EI/L^2$, so

$$\overline{\Delta T} = n^2\pi^2 \frac{EI}{L^2}\frac{1}{AE\alpha} = n^2\pi^2 \frac{I}{A}\frac{1}{L^2}\frac{1}{\alpha} \tag{2.574}$$

We could write I/A as r^2 where r is the radius of gyration of the bar cross section. The lowest buckling load always occurs at n = 1, i.e.,

$$\overline{\Delta T} = \pi^2 \frac{I}{A}\frac{1}{L^2}\frac{1}{\alpha} = \pi^2 r^2 \frac{1}{L^2}\frac{1}{\alpha} = \pi^2 \frac{1}{\alpha(L/r)^2} \tag{2.575}$$

from which we observe that

1. Thermal buckling is independent of the bar material's modulus of elasticity, E (E is a *mechanical* property of the material).

2. Thermal buckling is inversely dependent on the bar material's coefficient of thermal expansion, α (α is a *thermal* property of the material). That is, the higher the α of the bar, the lower the ΔT.

3. Of course, as with buckling under mechanical loading, the thermal buckling load is inversely proportional to the square of the bar length, so that long bars buckle under far lower ΔT than do short bars.

4. The more efficient the cross section is in the sense of a higher value of $r^2 = I/A$, the higher the thermal (and mechanical) buckling load.

The predicted $\overline{\Delta T}$ can range from several degrees to hundreds of degrees. In the latter case, we should suspect that the material properties surely must have changed over such a large temperature range, and, in addition, that the prebuckling stresses are high enough that inelastic effects might be important. Both effects lead to significantly smaller ΔT than predicted with linear elastic, room temperature properties (both material stiffnesses and α) as demonstrated for bars by Jones [2-32].

We can directly substitute the mechanical buckling load P for all mechanical buckling load cases that we solved in previous sections of this chapter in Equation (2.573) to get the thermal buckling load *as long as we recognize that the bar ends are now unable to move away from one another.* That is, the actual end support conditions for the two problems, mechanical buckling and thermal buckling, are quite different, but the two solutions are identical. Of course, all free-end mechanical buckling solutions have no such use.

We would expect that the initial postbuckling behavior of the uniformly heated bar would look similar to that for segment AB of Figure 2-31 on page 89. However, for higher temperatures, the postbuckling behavior should look similar to that in Figure 2-29 on page 85 in Section 2.4 for the elastica as long as the bar material remains elastic and has the same properties as it had at initial loading (and has the correct length relative to the fixed-free bar of Section 2.4). Of course, the higher the temperature, the less likely that the bar will remain elastic with undiminished properties. That is, an increased temperature is likely to lead to both inelastic behavior as well as decreased material properties.

Éléments sous droits d'auteur

We found bifurcation buckling from the straight equilibrium state to a buckled state in the foregoing derivation. Thornton [2-31] uses a differential equation approach to solve the same eigenvalue problem[3]. He solves the buckling differential equation (in present notation)

$$E\,I\frac{\partial^4(\delta v)}{\partial x^4} - N_x\frac{\partial^2(\delta v)}{\partial x^2} = 0 \tag{2.576}$$

in which the variation in the thermal moment does not appear. Of course, the thermal moment, M_x^T,

$$M_x^T = E\,\alpha\int_A \Delta T\, y\, dA \tag{2.577}$$

is itself zero because the ΔT is uniform leaving an even integral in y which is always zero. Also,

$$N_x = -P \tag{2.578}$$

i.e., the axial force is the force developed at the immovable end supports (simple supports that do not translate, but do allow rotation). Thus, we can rearrange Equation (2.576) to read

$$\frac{\partial^4(\delta v)}{\partial x^4} + \lambda^2\frac{\partial^2(\delta v)}{\partial x^2} = 0 \tag{2.579}$$

in which

$$\lambda^2 = \frac{P}{E\,I} \tag{2.580}$$

The boundary conditions are for displacements:

$$\delta v(0) = 0 \qquad \delta v(L) = 0 \tag{2.581}$$

and for moments:

$$\begin{aligned} \delta M(0) &\sim \frac{\partial^2(\delta v)}{\partial^2 x}(0) = 0 \\ \delta M(L) &\sim \frac{\partial^2(\delta v)}{\partial^2 x}(L) = 0 \end{aligned} \tag{2.582}$$

The general solution to the governing differential equation is

$$\delta v = c_1 + c_2 + c_3 \sin\lambda x + c_4 \cos\lambda x \tag{2.583}$$

Application of the boundary conditions at $x = 0$ leads to

$$[\delta v(0) = 0] \quad 0 = c_1 + c_4 \tag{2.584}$$

$$[\delta M(0) = 0] \quad 0 = -c_4\lambda^2 \tag{2.585}$$

whereupon c_1 and c_4 are both zero (because λ cannot be zero and have the bar buckle). Then, the boundary conditions at $x = L$ lead to

[3]Note that the superposition of thermal and mechanical effects inherently involves the solution of an eigenvalue problem to begin with for the mechanical buckling problem.

Éléments sous droits d'auteur

$$[\delta v(L) = 0] \quad 0 = c_2 L + c_3 \sin \lambda L \tag{2.586}$$

$$[\delta M(L) = 0] \quad 0 = -c_3 \lambda^2 \sin \lambda L \tag{2.587}$$

but, again, $\lambda = 0$ is not a physically meaningful solution, so

$$0 = c_3 \sin \lambda L \tag{2.588}$$

must be the solution to the last boundary condition. There are now two possible solutions. First, $c_2 = c_3 = 0$ which is a physically uninteresting trivial solution from which we conclude there can be no buckling because then $\delta v = 0$, i.e., the bar remains straight. The second, more interesting, solution to Equations (2.586) and (2.588) is

$$c_2 = 0 \tag{2.589}$$

$$\sin \lambda L = 0 \quad \text{implies} \quad \lambda_n L = n\pi \tag{2.590}$$

in which n is an integer, (n = 1, 2, 3, ...). This second solution leads to

$$\overline{P} = n^2 \pi^2 \frac{E I}{L^2} \tag{2.591}$$

which is the familiar Euler buckling load for a simply supported bar in the manner of Figure 2-70a (i.e., without axial restraint). Because the present bar is axially restrained as in Figure 2-71a, a thermal force, N_x^T, is developed and is equal to P in Equation (P), i.e.,

$$N_x^T = E \alpha A \Delta T \tag{2.592}$$

so that

$$\overline{\Delta T} = \frac{\overline{P}}{E \alpha A} = n^2 \pi^2 \frac{I}{A} \frac{1}{L^2} \frac{1}{\alpha} \tag{2.593}$$

which is the same result as Equation (2.574). As in other eigenvalue problems, we cannot find the amplitude, c_n, of the buckling deflection

$$\delta v_n(x) = c_n \sin \frac{n\pi x}{L} \tag{2.594}$$

but the initial postbuckling behavior is shown in Figure 2-31 on page 89.

Irrespective of whether a bar is loaded by mechanical or thermal means (or both), the total buckling load remains the same. For example, if the preload of thermal load due to temperature change is one-third of the Euler load, then an additional mechanical load of two-thirds of the Euler load can be imposed before buckling occurs *as long as the support conditions permit both thermal and mechanical loading, an important restriction that is not satisfied in most problems.*

Many similar buckling problems can be solved with either the superposition approach or the differential equation approach. The solution key is to find the prebuckling thermal loading state that is consistent with the support system. The free thermal expansion of an axially restrained bar is the same irrespective of whether the restraining support is pinned, fixed, or guided. The thermal buckling load for different support systems is found by equating the force necessary to suppress the free thermal expansion to the mechanical buckling load for that support system.

Éléments sous droits d'auteur

2.9.6 Thermal Behavior of an Axially Restrained Bar subjected to a Linear Through-the-Thickness Temperature Change

When heating is applied in a nonuniform manner through the thickness of a bar, a thermal moment is developed. This thermal moment causes bending of the bar from the very start of thermal loading when only the slightest change of temperature (an infinitesimal amount) is applied. Thus, the bar bends like a beam (even if it is initially straight) and cannot suddenly buckle in the classical Euler sense from initially straight to buckled. We will investigate the general bending response of such a bar that is pinned at both ends, yet with axial constraint so that a thermal force in the axial direction also is developed. That is, the bar is subjected to both (1) a thermal force that can cause buckling at the Euler load if applied by itself (which it is not) and (2) a thermal moment that causes bending immediately. These two problems cannot be superimposed because they are both nonlinear problems. Thus, we use the boundary-value problem approach to this equilibrium problem.

For a change in temperature that is linear through the bar thickness and constant along the bar length,

$$\Delta T = \Delta T_{avg} + \Delta T_h \frac{y}{h} \tag{2.595}$$

in which ΔT_{avg} is the average bar temperature change and ΔT_h is the temperature change from one surface of the bar to the other surface in the y-direction as shown in Figure 2-74. Of course, the temperature changes could be regarded as a function of time, t, but we will not address those problems in this book. The remainder of this sub-section is modeled after Thornton's investigation of this problem [2-31].

The thermal moment is

$$M_x^T = E\,\alpha \int_A \Delta T\, y\, dA \tag{2.596}$$

in which E and α are constant (although they can each be temperature dependent). Upon evaluation, the integral can be shown to be

$$M_x^T = \frac{E\,\alpha\, I}{h}\,\Delta T_h \tag{2.597}$$

This thermal moment causes bar bending even if ΔT_{avg} is zero.

The thermal force is

$$N_x^T = E\,\alpha \int_A \Delta T\, dA \tag{2.598}$$

which for a linear ΔT through the thickness as in Equation (2.455) reduces to

$$N_x^T = E\,\alpha\,\Delta T_{avg}\,A \tag{2.599}$$

and can, by itself (i.e., without the presence of a thermal moment), cause the bar to buckle as in Section 2.9.5.

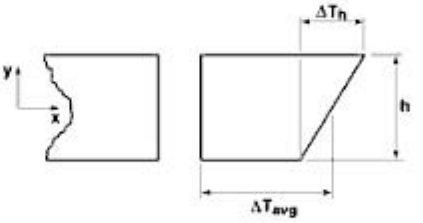


Figure 2-74 Linear Temperature Distribution Through the Bar Thickness

Éléments sous droits d'auteur

The problem now is to determine the bar response under the influence of both M_x^T and N_x^T in the manner of Thornton [2-31]. He noted that the character of the problem changes from the bifurcation buckling problem in Section 2.9.5 to a bending or bowing problem. That is, the bar bends as the M_x^T is applied and increased. Of course, the N_x^T causes an axial force, P, that will cause buckling or buckling-like behavior if the temperature change is large enough and if N_x^T is applied by itself (which it is not). Specifically, as the average temperature change increases, the bar mid-span transverse deflection, v, in Figure 2-75 increases until it grows without limit as ΔT_{avg} approaches the value ΔT_{cr} from Section 2.9.5. Thus, the relationship between the thermal loading inputs ΔT_{avg} and ΔT_h and the bar response is highly nonlinear. Thornton obtained that relationship for the elastic behavior of a bar subjected to a wide range of temperatures in the following manner [2-31].

The axial force N_x does not vary with axial position x because of the nonlinear equilibrium equation

$$\frac{\partial N_x}{\partial x} = 0 \tag{2.600}$$

Thus, we can set N_x equal to $-P$, an axial force caused by restrained thermal expansion and affected by transverse deflection. The force P is developed at the immovable end supports when the supports are removed and replaced with the forces they exert. However, unlike the axial force in the uniformly heated bar of Section 2.9.5, the reactive force P is less than N_x^T because the transverse deflection, v(x), of the bar *during* heating decreases the axial force at the supports. That is, the bar bends away from its original straight configuration and relieves some of the force at the immovable ends. Thus, a free-body diagram of the beam is as represented in Figure 2-75. It should be intuitively obvious that the force P would be higher if the bar stayed straight instead of bending. Note that the known N_x^T is greater than the unknown P which we must find. Thus, P is a derived quantity, not a controlled quantity. The controlled quantity is the thermal loading, and the response quantity is the mid-span transverse deflection of the bar.

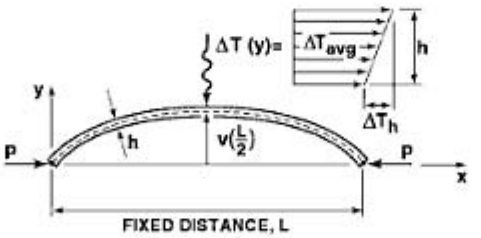


Figure 2-75 Free-Body Diagram of Bar with Linear Temperature Change

Éléments sous droits d'auteur

The force-strain relation

$$N_x = E A \left[\frac{\partial u_o}{\partial x} + \frac{1}{2} \left[\frac{\partial v}{\partial x} \right]^2 \right] - N_x^T \tag{2.601}$$

can be written as

$$\frac{\partial u_o}{\partial x} = \frac{N_x^T - P}{E A} - \frac{1}{2} \left[\frac{\partial v}{\partial x} \right]^2 \tag{2.602}$$

which we can integrate over the length of the bar subject to the boundary conditions that the ends are fully restrained from moving in the axial direction, i.e., $u_o(0) = 0$ and $u_o(L) = 0$:

$$(N_x^T - P) \frac{L}{E A} - \frac{1}{2} \int_0^L \left[\frac{\partial v}{\partial x} \right]^2 dx = 0 \tag{2.603}$$

which is applicable for the entire loading range for the bar (although we will see that the load cannot exceed the buckling load from Section 2.9.5). Equation (2.603) is a "constraint equation expressing the condition that the overall change in displacement between the (end) supports must be zero because the supports are immovable" [2-31].

Next, solve the moderately large-deflection equilibrium equation

$$E I \frac{\partial^4 v}{\partial x^4} - N_x \frac{\partial^2 v}{\partial x^2} + \frac{\partial^2 M_x^T}{\partial x^2} = 0 \tag{2.604}$$

[which is Equation (2.224) in Section 2.5.5.1. with an added thermal term] which is also Equation (2.557) subject to the condition that M_x^T is independent of x, so Equation (2.604) reduces to

$$\frac{\partial^4 v}{\partial x^4} + \lambda^2 \frac{\partial^2 v}{\partial x^2} = 0 \tag{2.605}$$

in which

$$\lambda^2 = \frac{P}{E I} = -\frac{N_x}{E I} \tag{2.606}$$

The displacement boundary conditions are

$$v(0) = 0 \qquad v(L) = 0 \tag{2.607}$$

and the moment boundary conditions are

$$\begin{aligned} M(0) &= -E I \frac{\partial^2 v}{\partial x^2}(0) - M_x^T = 0 \\ M(L) &= -E I \frac{\partial^2 v}{\partial x^2}(L) - M_x^T = 0 \end{aligned} \tag{2.608}$$

The general solution to the governing differential equation is

$$v = C_1 + C_2 x + C_3 \sin \lambda x + C_4 \cos \lambda x \tag{2.609}$$

Éléments sous droits d'auteur

With the four boundary conditions, the four integration constants lead to

$$v(x) = \frac{M_x^T}{P}\left[\left[\frac{1-\cos\lambda L}{\sin\lambda L}\right]\sin\lambda x + \cos\lambda x - 1\right] \qquad (2.610)$$

Of course, we don't know the value of λ in Equation (2.610) because it is related to the unknown load P. However, we do know that the deflection v(x) must satisfy the constraint relationship, Equation (2.603). Hence, we substitute the deflection v(x) in the constraint condition to get (after some simplification)

$$(N_x^T - P)\frac{L}{AE} - \frac{(M_x^T)^2\lambda^2}{2P^2}\left[\frac{(1-\cos\lambda L)^2}{\sin^2\lambda L}\left[\frac{L}{2} + \frac{\sin 2\lambda L}{4\lambda}\right] - (1-\cos\lambda L)\frac{\sin\lambda L}{\lambda} + \left[\frac{L}{2} - \frac{\sin 2\lambda L}{4\lambda}\right]\right] = 0 \qquad (2.611)$$

Computational difficulties occur in Equation (2.611) as λL approaches π, so use trigonometric identities to revise one term:

$$\frac{(1-\cos^2\lambda L)}{\sin^2\lambda L} = \frac{(1-\cos^2\lambda L)}{1-\cos^2\lambda L} = \frac{(1-\cos^2\lambda L)}{(1-\cos\lambda L)(1+\cos\lambda L)} = \frac{(1-\cos\lambda L)}{(1+\cos\lambda L)} \qquad (2.612)$$

Note that for zero M_x^T, Equation (2.611) reduces to $N_x^T = P$, i.e., the solution for the uniformly heated bar problem in Section 2.9.5.

If we prescribe the thermal loading condition via the temperature change expression in Equation (2.595), we will get the known value of N_x^T and M_x^T. Thus, the only unknown in Equation (2.611) is λ (P can be eliminated by use of the definition $\lambda^2 = P/EI$ in Equation (2.606)). We then solve the highly nonlinear transcendental equation, Equation (2.611), for λ at a pair of values of ΔT_{avg} and ΔT_h to determine the relationship between the load P and the transverse deflection v.

Consider an initially straight, rectangular-cross-section, simply supported, 7075-T6 aluminum bar subjected to a linear temperature change distribution through the bar thickness with total axial restraint of the simple supports. For 7075-T6 aluminum, $E = 10.4\times10^6$ lb/in^2 (72 GPa) and $\alpha = 13.1\times10^{-6}$/°F ($23.6\times10^{-6}$/°C). The bar is .1 in (2.54 mm) thick, 1.00 in (25.4 mm) wide, and 4 in (101.6 mm) long. Thus, we easily calculate the axial buckling load as

$$\bar{P} = \pi^2\frac{EI}{L^2} = 534 \text{ lb } (120 \text{ N}) \qquad (2.613)$$

and the critical ΔT_{avg} for thermal buckling with no thermal moment is

$$\Delta T_{avg} = \frac{\bar{P}}{E\alpha A} = 39.2°\text{F } (21.8 °\text{C}) \qquad (2.614)$$

as well as N_x^T and M_x^T as a function of ΔT:

Éléments sous droits d'auteur

$$N_x^T = E\,\alpha\,\Delta T_{avg}\,A = 13.62\,\Delta T_{avg}\ \text{lb/°F}\ (109.6\,\Delta T_{avg}\ \text{N/°C}) \qquad (2.615)$$

$$M_x^T = E\,\alpha\,I\,\frac{\Delta T_h}{h} = .1135\,\Delta T_h\ \text{lb in/°F}\ (.02320\,\Delta T_h\ \text{N m/°C}) \qquad (2.616)$$

The results of solving Equation (2.611) for λ as a family of curves each for a fixed value of ΔT_h with increasing ΔT_{avg} to get the load-deflection response curves (P versus mid-span transverse deflection, v(L/2)) are shown in Figure 2-76. There, the curves each start at a small value of mid-span transverse deflection for zero load (caused by the thermal moment) and bend over to asymptotically approach $\bar{P}$ as ΔT_{avg} increases. The curves with larger ΔT_h, hence a higher thermal moment, bend over more than those with smaller ΔT_h. Also, as ΔT_h approaches zero, the curves approach the behavior of an axially restrained bar with only ΔT_{avg}, i.e., a bifurcation thermal buckling problem with no transverse deflection until the critical temperature has been reached. The response curve for ΔT_h = 1°F (.6°C) fits up near the upper left-hand corner of the response plot so that it is nearly the ΔT_h = 0 curve, i.e., the simple uniform temperature heating buckling load response. As a measure of the magnitude of the transverse deflection, note that the maximum deflection plotted in Figure 2-76 is the bar thickness. Note also the resemblance of Figure 2-76 to the analogous results for the nonlinear equilibrium problem of bending of an imperfect bar in Figure 2-63 on page 158.

All curves should asymptotically approach P = 534 lb (120 N) as the mid-span transverse deflection, v(L/2), goes to infinity. However, some

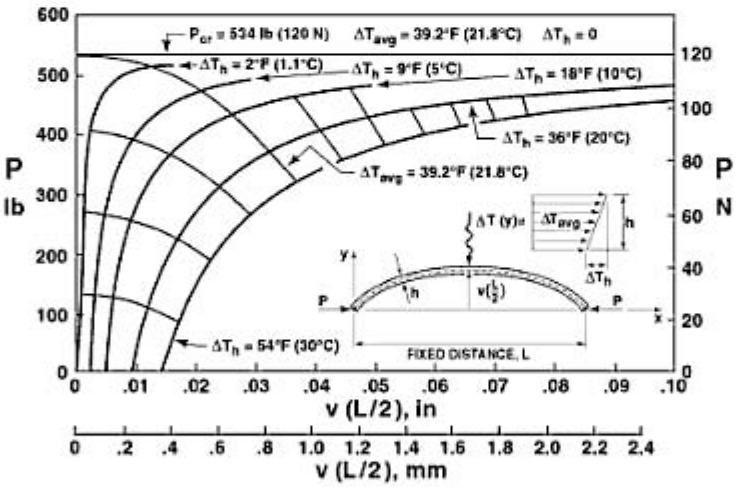


Figure 2-76 Response of an Axially Loaded 7075-T6 Aluminum Bar to a Linear Through-the-Thickness Temperature Distribution

Éléments sous droits d'auteur

of the terms in the expressions for λ and v(L/2), Equations (2.611) and

$$v(L/2) = \frac{M_x^T}{P}\left[\frac{1-\cos\lambda L}{\sin\lambda L}\sin\frac{\lambda L}{2} + \cos\frac{\lambda L}{2} - 1\right] \qquad (2.617)$$

approach infinity, so the complete curves in the range of values shown in Figure 2-76 cannot be obtained with Mathematica®. That is, the equations in the formulation are inherently ill-conditioned for solution in some range of variables. Hence, only the portions of the curves that can be calculated with Mathematica® are shown.

The set of lines essentially orthogonal to the constant ΔT_h lines in Figure 2-76 is a set of constant ΔT_{avg} lines with magnitude, from lower left to upper right, 10°F (5.6°C), 20°F (11.1°C), 30°F (16.7°C), 40°F (22.2°C), 50°F (27.8°C), 60°F (33.3°C), 70°F (38.9°C), 80°F (44.4°C), 90°F (50°C), and 100°F (55.6°C). One specific curve, namely ΔT_{avg} = 39.2°F (21.8°C), goes to the uniform temperature thermal buckling load of 534 lb (120 N) with zero v(L/2) as ΔT_h goes to zero. Numerical results for curves ΔT_h = 9°F (5°C) and ΔT_h = 54°F (30°C) are given in Table 2-6 for those who wish to check similar calculations. Note that the calculations were done in U. S. Standard Units, so the values reported in SI Units are necessarily approximate.

The stress at buckling under uniform temperature heating is

$$\sigma = \frac{P}{A} = \frac{534\text{ lb}}{.1\text{ in}^2} = 5{,}340\text{ psi (36.8 MPa)} \qquad (2.618)$$

which is far below the yield stress of 73 ksi (500 MPa). More importantly, even when a thermal moment exists and ΔT_{avg} is high as at the right-hand end of the ΔT_h = 54°F (30°C) curve with ΔT_{avg} = 153°F (85°C), the largest stress determined from the usual P/A±Mc/I is well below one-quarter of the yield stress. Thus, the behavior shown in Figure 2-76 is always elastic.

Table 2-6 Response of an Axially Loaded 7075-T6 Aluminum Bar to a Linear Through-the-Thickness Temperature Distribution

ΔT_h	ΔT_{avg}	P	v(L/2)
9°F (5°C)	10°F (5.6°C)	134.7 lb (599.2 N)	.003176 in (.0807 mm)
	20°F (11.1°C)	268.6 lb (1195 N)	.004811 in (.1222 mm)
	30°F (16.7°C)	394.8 lb (1756 N)	.009225 in (.2343 mm)
	40°F (22.2°C)	473.1 lb (2104 N)	.02108 in (.5354 mm)
54°F (30°C)	10°F (5.6°C)	87.09 lb (387.4 N)	.01698 in (.4313 mm)
	20°F (11.1°C)	189.8 lb (844.2 N)	.02216 in (.5629 mm)
	30°F (16.7°C)	269.3 lb (1198 N)	.02694 in (.7351 mm)
	40°F (22.2°C)	324.0 lb (1441 N)	.03658 in (.9291 mm)
	50°F (27.8°C)	360.0 lb (1601 N)	.04422 in (1.123 mm)
	60°F (33.3°C)	384.3 lb (1709 N)	.05145 in (1.307 mm)
	70°F (38.9°C)	401.5 lb (1786 N)	.05815 in (1.477 mm)
	80°F (44.4°C)	414.3 lb (1843 N)	.06439 in (1.636 mm)
	90°F (50°C)	424.2 lb (1887 N)	.07019 in (1.783 mm)
	100°F (55.6°C)	432.1 lb (1922 N)	.07564 in (1.921 mm)

Éléments sous droits d'auteur

The temperature change difference through the thickness, ΔT_h, has the analogous role for a thermally loaded, axially restrained bar as the amplitude of a sinusoidal initial geometric imperfection, a, does on a mechanically loaded bar in Section 2.8. That is, both ΔT_h and initial geometric imperfection amplitude, a, cause a moment that bends the bar from the instant any load, whether thermal or mechanical, is applied. Also, the average temperature change, ΔT_{avg}, has the analogous role for a thermally loaded, axially restrained bar as the axial load, P, does on a mechanically loaded, imperfect bar in Section 2.8. Both ΔT_{avg} and P cause increased bending and have the limiting value of the Euler buckling temperature or the Euler buckling load, respectively. The bar curvature is

$$\frac{d^2v}{dx^2}(x) = -\frac{M_x^T}{E\,I}\left[\left[\frac{1-\cos\lambda L}{\sin\lambda L}\right]\sin\lambda x + \cos\lambda x\right] \qquad (2.619)$$

because $P = \lambda^2 E\,I$. Note that the curvature at the simply supported ends is *not* zero! The curvature is always negative which means the bar bends concave downward as shown in Figures 2-75 and 2-76. This result can also be seen from the relation

$$M = -EI\frac{\partial^2 v}{\partial x^2} - M_x^T \qquad (2.620)$$

in which at a simple support M = 0, so

$$EI\frac{\partial^2 v}{\partial x^2} = -M_x^T \neq 0 \qquad (2.621)$$

We observed the highly nonlinear behavior of an axially restrained pinned-pinned bar with a linear temperature gradient through the thickness. The temperature change causes the bar to immediately bow into an ever increasingly concave downward configuration in Figure 2-75. Because of the bowing, the bar never buckles, but merely increases the bowing. If the temperature gradient were eliminated leaving a constant temperature change through the thickness of the bar and along its length, the present solution would reduce to that of Section 2.9.5. Note also the striking similarity of the present solution to the analogous effect of a sinusoidal initial geometric imperfection on bar behavior in Section 2.8.

2.9.7 Summary

When heated uniformly, most bodies tend to expand in all directions. If the bodies are not restrained from movement, then the resulting expansion is called a free thermal strain and is not accompanied by any stresses. If the body is restrained when heated, but without mechanical loading, then stresses are induced that we call thermal stresses and no strains accompany them. Also, if a body is heated with a nonlinear temperature gradient and/or with movement restraints, then both thermal stresses and thermal strains are induced. However, the thermal stresses are not as high as in bars with an axial restraint, and the thermal strains are not as high as the free thermal strains.

Éléments sous droits d'auteur

We treated thermal buckling of axially restrained bars by both a superposition and a differential equation approach. A key observation: *For thermal buckling of a bar, there must be axial restraint to enable development of compressive stresses that resist free thermal expansion under temperature increase; otherwise, the bar will merely expand without danger of buckling.* The main challenge in solving these problems is determining the prebuckling loading state consistent with the support system for the bar. The differential equation that governs thermal and mechanical buckling can have non-constant coefficients often leading to somewhat complicated solutions. However, many problems have temperature change distributions and material properties for which the coefficients are constant and hence the differential equation is easily solved.

For narrow ranges of temperature change, most materials have essentially constant mechanical and thermal properties. However, over broader ranges of temperature change, the material properties do vary. Hence, if a body with temperature-dependent material properties is subjected to a large-enough temperature range, the body becomes inhomogeneous with respect to material properties. Treatment of such problems would probably require a finite element approach.

We addressed a simple thermal buckling problem of an axially restrained, perfectly straight bar subjected to a uniform temperature change. For that problem, we found the critical value of the (uniform) temperature change to cause buckling. The problem is more complicated if the temperature change is not uniform through the bar thickness. In that case, a thermal moment is developed which causes the bar to bend immediately. Then, we see that classical bifurcation buckling from an initially straight configuration does not happen. Instead, bar bending increases until a maximum load-carrying capability is reached which corresponds to the simple thermal buckling load (temperature!) for a uniformly heated bar. Other problems could be addressed such as a temperature change distribution that is sinusoidal along the bar length or, for example, a distribution that is sinusoidal along the bar length *and* linear through the thickness. Or, other through-the-thickness temperature change distributions could be examined. Note that lengthwise (i.e., axial) temperature change distributions or variable α on an axially restrained bar with uniform through-the-thickness heating and α should have an effect of

$$\Delta_{FTE} = \text{Free Thermal Expansion} = \int_0^L \alpha(x)\Delta T(x)\, dx \qquad (2.622)$$

to be used in Equation (2.571) to calculate the ΔT at buckling. Thus, hot spots and cold zones can occur along the bar, and their net effect is an attempted elongation which creates a thermal expansion that must be countered with a force that can cause buckling if the force (and expansion) is high enough. The need for such a variety of temperature-change distribution problems depends on the design environment for a bar.

Treating the temperature gradient, $\Delta T(x, y, z)$, as a function of time, i.e., $\Delta T(x, y, z, t)$, is a realistic physical problem because the thermal conductivity in most engineering materials is high. Thus, the ΔT distrib-

Éléments sous droits d'auteur

ution is likely to change quite rapidly with time. Alternatively, we could examine a sequence of quasi-static problems with different ΔT to model the actual ΔT distributions that occur with time. Generally, because of thermal soaking (total absorption of heat) of a body, the temperature gradient decreases with time. For thermal buckling problems, we are usually concerned with the largest temperature gradient rather than the behavior with time. Thus, ignoring the change in temperature gradient with time, but seeking the largest temperature gradient, is appropriate.

Some fiber-reinforced composite materials, namely some polymer matrix materials and even some fibers, can absorb water from environmental contact or direct contact. This absorbed moisture causes the polymer materials to expand or swell just as most materials expand or swell when they are heated. Note, however, that absorbed moisture in a structural element is likely to be quite inhomogeneously distributed through the thickness of even a thin structural element. Only with prolonged exposure, usually measured in months and even years, will the moisture distribution become uniform through the thickness. Thus, deformation caused by restrained expansion after absorption of moisture from only one side of the bar is likely to be of the continuous bending nature of the problem of thermal behavior of an axially restrained bar subjected to a linear through-the-thickness temperature change in Section 2.9.6 rather than a classical buckling problem. However, if moisture is absorbed from both sides of the bar, then there is no moment, and the bar buckles in the usual manner. Restrained moisture expansion with a coefficient of moisture expansion, β, can be treated in the same manner as restrained thermal expansion with a coefficient of thermal expansion, α. However, the moisture diffusion coefficient is about six orders of magnitude lower than the thermal diffusion coefficient for many engineering materials. Thus, the time scale of deformation that occurs because of moisture expansion is about six orders of magnitude slower than deformation because of thermal expansion.

Problem Set 2.9

2.9.1 Use variational techniques to derive the moderately large-deflection equilibrium differential equations and their associated boundary conditions for a bar with thermal and mechanical loading effects.

2.9.2 Use variational techniques to derive the bucking differential equations and their associated boundary conditions for a bar with thermal and mechanical loading effects.

2.9.3 Find the thermal buckling load of a bar that has a spring-supported, pinned upper end with spring constant k and a pinned lower end as in Figure 2-70c on page 172. A superposition approach should suffice.

2.9.4 Find the thermal buckling load, ΔT, of a fixed-fixed bar subjected to a uniform ΔT.

2.9.5 Find the thermal buckling load, ΔT, of a fixed-fixed bar subjected to a step loading of $2\Delta T$ on the left half of the bar and ΔT on the right half of the bar as contrasted with the uniform distribution in Figure 2-73a on page 174. In the prebuckling equilibrium state, does the mid-point of the bar move? If so, which way and how much?

2.9.6 Find the thermal buckling load, ΔT, of a fixed-fixed bar subjected to a loading that varies from $+\Delta T$ at the left end of the bar to $-\Delta T$ at the right end as contrasted with the uniform distribution in Figure 2-73a on page 174. In the prebuckling equilibrium state, does the mid-point of the bar move? If so, which way and how much?

2.9.7 A pinned-pinned bar has a translational spring with constant k at one end as in Figure 2-70c on page 172. Find the uniform temperature change, ΔT, that causes buckling. Hint: address the movement of the spring base. Use the known limits of behavior $k = 0$ and $k = \infty$ to check your solution.

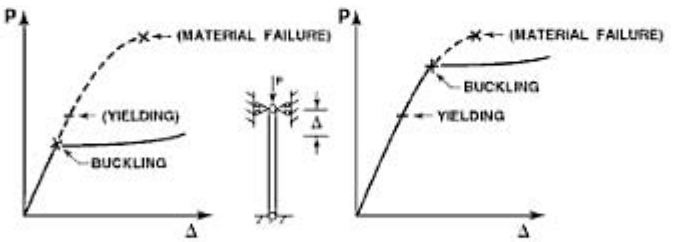
Éléments sous droits d'auteur

2.10 PLASTIC BUCKLING OF BARS

2.10.1 Introduction

For nearly one hundred years, Euler's 1759 contribution to buckling [2-1] was disregarded because his theoretical predictions were always much higher than measured bar buckling loads. Unfortunately for him, the tests were performed on the typically short, thick bars of those days for which the axial stress before buckling exceeded the yield stress, and often even equalled the crushing strength. Thus, most of the bars commonly used during his life did not buckle. Later, when compression tests were performed on long, slender bars, Euler's predictions were closely realized. The essential restriction of Euler's theory is that the stresses must remain elastic, but this fact was not recognized for many years.

Buckling is a phenomenon that is a characteristic failure mode of compressively loaded thin structural members, especially bars, plates, and shells. Thus far, we have been concerned only with bars made of linear elastic materials, but now we want to investigate the buckling of bars made of materials with nonlinear stress-strain behavior such as aluminum. Note that the uniform stress state in a compressed bar necessarily leads to a load-deflection behavior with the same shape as the material stress-strain curve because the two curves differ only by simple scaling factors relating stress to axial load ($\sigma = P/A$) and strain to axial deformation ($\varepsilon L = \Delta$). Thus, the load-deflection curves for an axially loaded, simply supported bar in Figure 2-77 are identical in shape, until buckling occurs, to the bar material's (dashed) stress-strain curve which has a yield point and an ultimate stress level (material failure in compression). If the bar is thin enough or long enough, buckling can happen elastically even for bars made of materials with nonlinear stress-strain curves as seen in Figure 2-77a, i.e., before nonlinear stress-strain behavior. There, the capability of the material exceeds that of the structure, i.e., the bar fails by buckling at a stress well below that which would cause yielding, much less material failure. If the bar is thicker (higher I) or shorter than the bar for Figure 2-77a, then the bar first yields at a yield load and then buckles after experiencing some nonlinear behavior as in Figure 2-77b, but does not have a high enough stress to experience material failure. Thus, the bar is said to buckle plastically, i.e., at a stress



a Elastic Buckling b Plastic Buckling

Figure 2-77 Buckling versus Yielding versus Material Failure Events

Éléments sous droits d'auteur

above the yield stress of the material. If the bar is even thicker or shorter, then the bar material first yields and then fails in compression, i.e., a material failure without buckling. Thus, we see that the order of possible events, namely the independent events of buckling, yielding, and material failure, depends on the geometry of the bar (I and L) as well as on the material properties (E, σ_y, $\sigma_{ultimate}$, and the stress-strain curve shape). If buckling is predicted to occur at a stress above the material failure stress, then obviously material failure occurs, not buckling. We are concerned in this section with bars that are thick enough and/or short enough that elastic buckling is not possible, so plastic buckling occurs (unless the stress level is so high that material failure occurs first, and that failure mode must be independently investigated).

The objective of this section is to derive an equation for plastic buckling of bars, i.e., buckling of bars that are so short and so thick that the elastic buckling stress exceeds the yield stress of the material. However, the theory is not applicable to bars that are so short that they do not buckle at all, but instead simply crush. Because of misunderstanding of the proper formulation of the plastic buckling problem, controversy raged for about sixty years over the various solutions that were derived.

Two main approaches to the plastic buckling problem and a discussion of their respective merits and interpretations are addressed in the following two subsections (2.10.2 and 2.10.3). In both approaches, we now seek a definition for the modulus $\overline{E}$ in the usual buckling expression

$$\overline{P} = \pi^2 \frac{\overline{E}I}{(L')^2} \qquad (2.623)$$

in which $\overline{E}$ is an unknown modulus that is lower than E because yielding reduces the modulus of the material, I is the second moment of the bar cross-sectional area, and L' is the effective length defined in Section 2.3.8 on page 76. Divide by A to get buckling stress:

$$\overline{\sigma} = \frac{\pi^2 \overline{E}}{(L'/r)^2} \qquad (2.624)$$

a useful formulation when dealing with the stress-strain curve and in which r is the radius of gyration of A ($r^2 = I/A$).

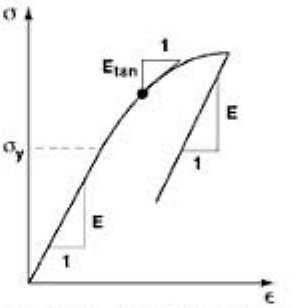


Figure 2-78 Stress-Strain Curve Typical of Aluminum

For materials that readily deform in a plastic manner, the representative stress-strain curve in Figure 2-78 serves to define the important characteristics. The slope of the stress-strain curve is E below σ_y, the yield stress. The slope upon unloading (whether from above or below yielding) is usually idealized as E. The local slope above σ_y is

$$E_{tan} = \frac{d\sigma}{d\varepsilon} \qquad (2.625)$$

in which E_{tan} is the tangent modulus at the point under consideration. Below σ_y, E_{tan} is simply E. We seek in the next two sub-sections to demonstrate how these basic stress-strain curve definitions can be used to find a value (actually more than one value) for E in Equation (2.623).

Éléments sous droits d'auteur

Beyond the modulus-related considerations, the equation governing buckling is formulated in Section 2.10.4 and solved in Section 2.10.5. In both sections, the tangent modulus is deemed the most appropriate modulus to use. Then, we address the issue of how to represent nonlinear stress-strain curves in equation form for ease of use in the solution process. Numerical results are next obtained for square-cross-section bars. Then, results for both the reduced-modulus and tangent-modulus approaches are contrasted with experimental results in Section 2.10.8 to solidify the decision to use the tangent-modulus approach. Finally, conclusions about plastic buckling are summarized in Section 2.10.9.

2.10.2 Reduced-Modulus Theory

If buckling is to take place as a sudden deflection transverse to the bar at a specific axial load, then bending must simultaneously take place. For an axial load that is constant during the buckling process, the simultaneous occurrence of bending implies that some stresses increase while other stresses decrease to maintain axial equilibrium. Specifically, the axial stresses on the concave side of the bent bar increase whereas the axial stresses on the convex side of the bent bar decrease as in Figure 2-79. Hence, some strains reverse upon buckling. If, at a given axial load, some stresses increase, then the modulus associated with the increasing stresses is E_{tan} whereas the modulus for the decreasing stresses is merely E in accordance with the unloading portion of the stress-strain curve in Figure 2-78. Thus, two moduli are involved which is why this theory is also called the double-modulus theory, a more accurate name than reduced modulus because *all $\bar{E}$ are reduced from E.*

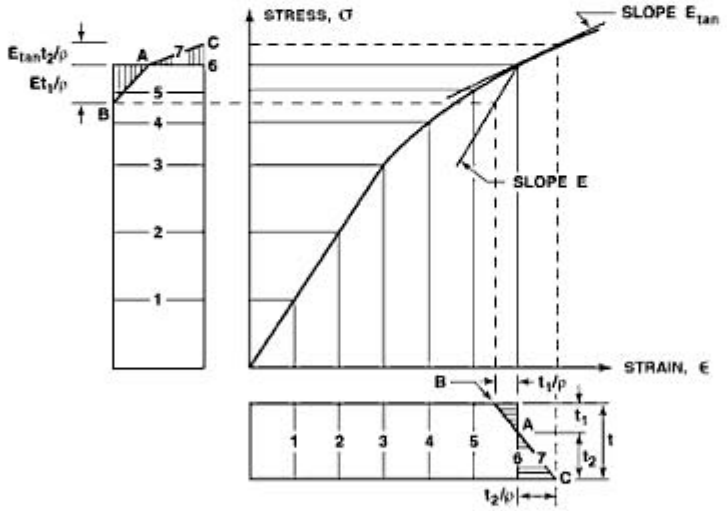


Figure 2-79 Stress and Strain Increments during Buckling

Éléments sous droits d'auteur

Bending strains are related to the curvature, ρ, of the bar in proportion to the distance from the surface of zero bending strain (i.e., plane sections remain plane under bending), so the stresses and strains can be related as shown in Figure 2-79. The bending strains are t_2/ρ and t_1/ρ. If t_1 is the location of the position of zero bending stress, then equilibrium of the forces associated with bending of a rectangular cross section of thickness t and width b requires that

$$\frac{1}{2}\left[\frac{Et_1}{\rho}\right]t_1 b = \frac{1}{2}\left[\frac{E_{tan}t_2}{\rho}\right]t_2 b \tag{2.626}$$

whereupon, because $t_1 + t_2 = t$,

$$\frac{t_1}{t} = \frac{E_{tan}^{1/2}}{E^{1/2} + E_{tan}^{1/2}} \tag{2.627}$$

The bending moment is

$$M = \left[\frac{1}{2}\left[\frac{Et_1}{\rho}\right]t_1 b\right]\frac{2}{3}t = \frac{1}{3}\frac{E}{\rho}t_1^2 tb \tag{2.628}$$

But substitute for t_1 in terms of t from Equation (2.627) to get

$$M = \frac{1}{3}\frac{E}{\rho}t^3 b\frac{E_{tan}}{\left(E^{1/2} + E_{tan}^{1/2}\right)^2} = \frac{4EE_{tan}}{\left(E^{1/2} + E_{tan}^{1/2}\right)^2}\frac{I}{\rho} \tag{2.629}$$

in which $I = bt^3/12$ for a rectangular cross section. Compare Equation (2.629) with the usual moment-curvature expression $M = \bar{E}I/\rho$ to get

$$\bar{E} = \frac{4EE_{tan}}{\left[E^{1/2} + E_{tan}^{1/2}\right]^2} = E_r \tag{2.630}$$

The reduced-modulus result has a controversial history that took nearly sixty years to resolve. Engesser proposed in 1889 that $\bar{E}$ simply be the tangent modulus E_{tan} [2-33]. Also in 1889, Considère suggested the basic double-modulus idea that because of unloading on the convex side of a buckled bar $\bar{E}$ is some combination of E and E_{tan}, but did not offer an equation [2-34]. In 1895, Jasinski noted Considère's work and pointed out that the compressive stresses on the convex side of the buckled bar should be governed by the unloading modulus E [2-35]. Accordingly, Engesser retracted his original claim in 1895 [2-36] and derived the reduced-modulus expression. In 1910, von Kármán rederived Equation (2.490) and accompanied it with experimental work [2-37], so the reduced-modulus approach became accepted. In 1946, Shanley [2-38 & 2-39] pointed out that real bars are not perfect, so strain reversal does not occur at buckling, going back to Engesser's original claim of $\bar{E} = E_{tan}$ with von Kármán's full approval. Buckling loads predicted with E_r are higher than those predicted with E_{tan} because $E > E_r > E_{tan}$. Further discussion of buckling loads calculated with the reduced modulus is deferred to Section 2.10.8 where results from the two theories are compared with each other and with measured buckling loads.

Éléments sous droits d'auteur

2.10.3 Tangent-Modulus Theory

The fundamental premise of tangent-modulus theory is that *no strain reversal occurs at buckling.* Strains are presumed to continuously increase, even though the strain on one side of the bar (the concave side of the buckled bar) increases more rapidly than on the other side (the convex side) caused by bending, whereupon the modulus relating bending strains to bending stresses is the tangent modulus, E_{tan}. That is, bending takes place *simultaneously* with imposing the last increment of load as the buckling load is reached.

In a manner similar to that used to derive reduced-modulus theory, the stress distribution for the *last increment of load* is shown in Figure 2-80. Thus, resistance to bending with this theory depends only on the tangent modulus. The moment is

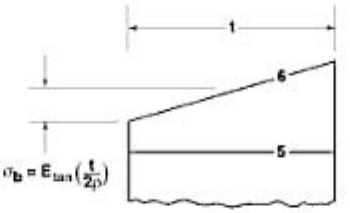


Figure 2-80 Stress Increments during Buckling

$$M = E_{tan}\left[\frac{t}{2\rho}\right]\frac{1}{2}\frac{t}{2}\frac{2}{3}tb = \frac{E_{tan}I}{\rho} \qquad (2.631)$$

so, as suggested by Engesser in 1889 [2-33] and clarified by Shanley in 1946 [2-38 & 2-39], $\bar{E} = E_{tan}$ in the equations governing buckling, Equations (2.623) and (2.624).

2.10.4 Transcendental Plastic Buckling Equation

For the pinned-pinned bar in Figure 2-81, the plastic buckling equation is a straight-forward modification of the Euler equation, namely,

$$\bar{P} = \pi^2 \frac{E(\bar{P})I}{L^2} \qquad (2.632)$$

in which Young's modulus is a function of buckling load, i.e., $E(\bar{P})$. Obviously, the left-hand side of Equation (2.632), $\bar{P}$, is a function of the right-hand side. However, the right-hand side is a function of the left-hand side because Young's modulus is a function of load. Thus, the plastic buckling equation is *transcendental.*

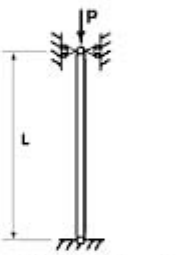


Figure 2-81 Buckling of a Pinned-Pinned Bar

The solution of such a transcendental equation involves the following searching procedure. First, estimate a buckling load and hence a buckling stress. Then, find the modulus, $E(\bar{P})$, for that stress level. Next, calculate the buckling load from Equation (2.632) corresponding to the material property implied in the first step. Now compare the calculated buckling load with the estimated buckling load. If the calculated buckling load is bigger than the estimated buckling load, then the estimated buckling load was too low. This conclusion is easily reached when you recognize that $E(\bar{P})$ *always decreases* as stress increases. From Equation (2.632), if $E(\bar{P})$ is too high, then $P_{calculated}$ will be too high. This relationship will

Éléments sous droits d'auteur

be referred to as the *special relationship* between the estimated and calculated buckling loads (or stresses). For example, if the elastic Young's modulus is selected, the first estimated buckling load, λ_{1e}, is, by implication, the load at yielding or lower. However, buckling does not necessarily take place at yielding. In fact, the material can yield but not buckle until a considerably higher stress level is reached. That is, buckling and yielding are two *independent* physical events. Buckling can occur at stresses below yielding, and, in that case, the buckling is elastic. In contrast, yielding can occur at stresses below buckling, and, in that case, the buckling is called plastic buckling.

The tangent modulus is used as E(P) in Equation (2.632) in accordance with Shanley's arguments [2-39]. That is, we deal with the infinitesimal displacements that occur only during the buckling process. Those infinitesimal displacements are related to infinitesimal strains and to infinitesimal stresses through an infinitesimal stress-strain relation

$$\delta\sigma = E_{tan}\delta\varepsilon \tag{2.633}$$

which comes from the definition for the slope of a stress-strain curve,

$$\frac{d\sigma}{d\varepsilon} = E_{tan} \tag{2.634}$$

For obvious reasons, this approach to plastic bar buckling is known as the tangent-modulus approach.

The so-called double-modulus approach to calculation of the bar buckling load is based on the supposition that the bar partially unloads on one side as it buckles. That unloading behavior is governed by the elastic modulus whereas the loading behavior on the other side of the bar is governed by the tangent modulus; hence, the term double modulus. The buckling loads predicted with the double-modulus (or reduced-modulus) approach are above both the tangent-modulus predictions and measured buckling loads as we will soon see. Thus, the double-modulus approach is not appropriate for use in design.

Let us recast the governing equation from the form of Equation (2.632) by dividing both sides by the cross-sectional area A to get

$$\frac{P}{A} = \pi^2 \frac{E_{tan}(I/A)}{L^2} \tag{2.635}$$

Then, we define I/A as the usual square of the radius of gyration of the bar cross section, r, and identify P/A as the stress at buckling to get

$$\bar{\sigma} = \pi^2 \frac{E_{tan}}{(L/r)^2} \tag{2.636}$$

known as the critical stress or the buckling stress (but not the redundant term 'critical buckling stress'). The quantity L/r is known as the slenderness ratio. Thus, a bar with a high L/r is very long and slender whereas a bar with a low L/r is short and thick. Generally, bars with a high L/r buckle elastically, whereas bars with a low L/r buckle plastically (or can even have a material failure as in Figure 2-77 on page 187).

The load-deformation curve for a bar will be identical to the (scaled) shape of the stress-strain curve for the material. That is, if axial load is

Éléments sous droits d'auteur

plotted versus axial shortening of the bar, the shape of the curve will be identical to the shape of the stress-strain curve. This observation follows from the fact that a single uniaxial stress, σ, occurs in Equation (2.636), so the relation between load and deformation is a special version of the relation between stress and strain.

2.10.5 Solution Strategy

If, in fact, the bar buckles plastically, then the first estimated buckling load λ_{1e} is less than the corresponding calculated buckling load λ_{1c} in Figure 2-82. Because of the basic concave downward nature of the stress-strain curve for most materials, the same relation exists between all estimated and calculated buckling loads. The estimated buckling load is less than the actual buckling load for the first three estimated buckling loads in Figure 2-82. The fourth estimated buckling load leads to a calculated load that is below the estimated buckling load because the estimate is above the actual buckling load. Only when the estimated buckling load is the actual buckling load do the estimated, calculated, and actual buckling loads coincide.

The *special relationship* between the estimated, calculated, and actual buckling loads is the basis for a simple strategy to determine the actual buckling load of a bar. That is, if a buckling load is estimated and a buckling load calculated, then we know whether to increase or decrease the next estimate to get closer to the actual buckling load.

The next question is *how much* to increase the second estimated buckling load above the first estimated buckling load, if the buckling is plastic. The known special relationship between estimated, calculated, and actual buckling loads does not determine the magnitude of the next estimated buckling load. Thus, we must resort to simply guessing in an educated manner, and then we can rely upon the known special relationship to determine the sign of the next adjustment.

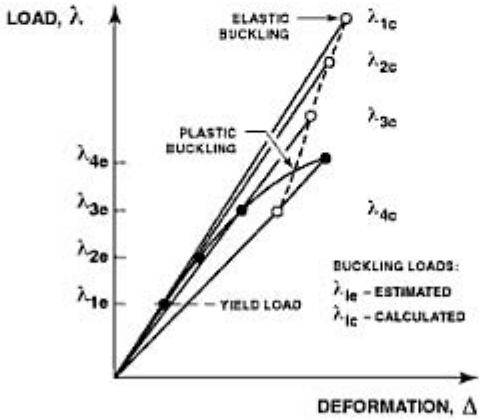


Figure 2-82 Estimated and Calculated Buckling Loads

Éléments sous droits d'auteur

Thus, we simply march up the stress-strain curve or the load-deformation curve as in Figure 2-82 until the known special relationship dictates that we have increased the estimated buckling load to too high a level. *Then, we know two estimated loads that bracket the actual buckling load.* For example, λ_{3e} is too low and λ_{4e} is too high. Thus, λ_{actual} must lie between λ_{3e} and λ_{4e}.

Now that we have bracketed the actual buckling load, how do we find that load? Again, we have no quantitative way of choosing the next estimated buckling load. Thus, we must again rely upon the known *special relationship* and adopt a special searching strategy. That special searching strategy could take several forms. The strategy could be to drop back to the estimated buckling load that is below the actual buckling load and march up the load-deformation curve at increments of, say, one-tenth the load difference between λ_{3e} and λ_{4e}. That is, split the bracket into ten parts (i.e., interval tenthing) and find which of the ten segments is a closer bracket on the actual buckling load than the original bracket. That closer bracket can subsequently be split into ten parts to get an even closer bracket. The splitting and searching procedure is repeated until a bracket with sufficient accuracy is found. That is, the upper bound and lower bound on the bracket can be averaged to obtain an estimate of the actual buckling load. The error in that estimate is related to the deviation of the bounds on the bracket from the average of the bounds. Thus, the smaller the bracket, the higher the accuracy of the calculated buckling load.

Another numerical technique for searching for the solution of a transcendental equation is the *interval-halving* or *binomial-search* procedure. Instead of dividing the segment between the upper and lower bounds into ten parts as in the preceding method, we merely halve the segment. The ends of each half segment are examined to find new upper and lower bounds to the solution (one is actually an old bound). Then, the half segment that provides the new upper and lower bounds is investigated. Its half that gives yet another more refined set of upper and lower bounds is split in two, and so on. This interval-halving technique is far more efficient, i.e., quicker, than the interval-tenthing procedure. Thus, interval halving will be applied in the solution of transcendental equations.

The interval-halving solution procedure logic is depicted schematically in Figure 2-83. There, the initial estimate of the buckling load, λ_{1e}, is the yield load, λ_y. Of course, if the calculated buckling load, λ_c, is less than λ_y, then the buckling is elastic, and no further computations are necessary. If $\lambda_c > \lambda_y$, then we must search for the correct value of λ_c that corresponds to the correct material properties. The initial search increment size, $\Delta\lambda_c$, is arbitrarily set as one-tenth the yield load. Then, the material property, in this case the tangent modulus, is calculated or found graphically at the estimated buckling load. Next, the buckling load is calculated from Equation (2.632) using the tangent modulus just determined. Then, the calculated buckling load, λ_c, is compared to the estimated buckling load, λ_e. The special relation between the calculated, estimated, and actual buckling loads is used to determine the next step.

Éléments sous droits d'auteur

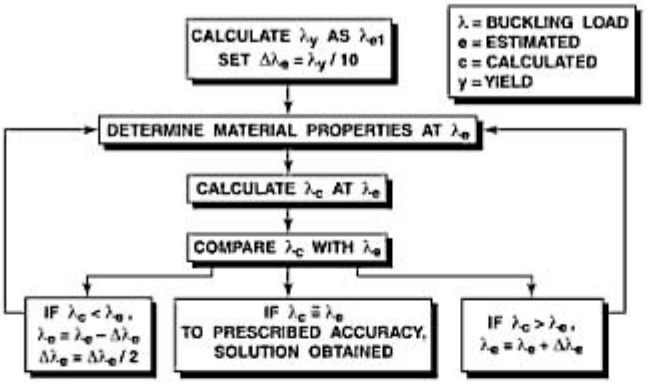


Figure 2-83 Interval-Halving Solution Procedure Logic

If the calculated buckling load exceeds the estimated buckling load, then the estimated buckling load is increased by the interval-halving increment in estimated load. That change in estimated load requires returning to the material property determination step in Figure 2-83.

If the calculated buckling load is less than the estimated buckling load, then the estimated buckling load is too high and must be reduced. The estimated buckling load is reduced by the interval-halving increment to return to the previous estimated buckling load that we already know to be too low. This redundant calculation[1] is made to always maintain our awareness of the upper and lower bounds on the buckling load. Simultaneously, the estimated load increment is halved for all subsequent calculations. Accordingly, the distance between the bounds is always decreased as the number of calculations increases.

This interval-halving search procedure is further illustrated in Figure 2-84 where estimated points e_3 and e_4 represent λ_{3e} and λ_{4e} from Figure 2-83, respectively. Similarly, calculated points c_3 and c_4 represent λ_{3c} and λ_{4c}, respectively. Thus, λ_{3e} represents a lower bound on λ, and λ_{4e} represents an upper bound. We found those values by always going around the right-hand side of the logic flow chart in Figure 2-83. The last value, λ_{4c}, is less than λ_{4e} so we exit the comparison step to the left in Figure 2-83. We drop back from λ_{4e} to $\lambda_{5e} = \lambda_{3e}$ and, in accordance with the interval-halving procedure, we halve $\Delta\lambda$, i.e., we go from $\lambda_y/10$ to $\lambda_y/20$. We already know that $\lambda_{5c} > \lambda_{5e}$ (but we recalculate anyway), so we know we will move up the stress-strain curve. However, we do not move up the curve as much as before, i.e., only to λ_{6e}. Suppose $\lambda_{6c} > \lambda_{6e}$. Then, we increase λ_{6e} by $\Delta\lambda$ to get to λ_{7e} where we have al-

[1]This redundant calculation is quickly performed and is therefore preferable to 'remembering' the result of each past calculation. However, for problems in which the calculation is very time consuming, 'remembering' the result of each past calculation is more efficient.

Éléments sous droits d'auteur

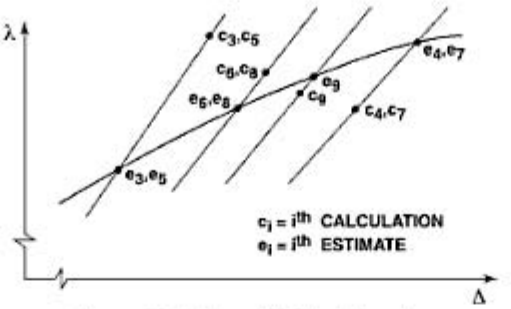


Figure 2-84 Interval-Halving Example

ready calculated $\lambda_{4c} = \lambda_{7c}$. Next, we move up by another halved increment to λ_{9e} which we see is another upper bound that is lower than $\lambda_{7e} = \lambda_{4e}$.

We have narrowed the upper and lower bounds from $\lambda_{3e} < \lambda < \lambda_{4e}$ to $\lambda_{8e} < \lambda < \lambda_{9e}$. The latter bounds are one-fourth the amount of load apart that the original bounds were. Naturally, this procedure can continue until the bounds are close enough that we can say λ_c is equal to λ_e to whatever prescribed accuracy we desire. At that point, the solution for the buckling load has been obtained.

2.10.6 Representation of the Nonlinear Stress-Strain Curve

So far, we implicitly assumed that we can effectively use the stress-strain curve to calculate the tangent modulus at any point. However, the task associated with that assumption is not easily performed. The most desirable situation is to have an equation to represent the stress-strain curve so we can directly and simply calculate E_{tan} instead of having to perform difference calculations between test data points when no suitable equation for the curve is available.

The Nadai stress-strain curve [2-40] is a four-parameter model of nonlinear stress-strain behavior. The curve is formulated in two regions, below and above yielding:

$$\varepsilon = \frac{\sigma}{E} \qquad \sigma \le \sigma_y \tag{2.637}$$

$$\varepsilon = \frac{\sigma}{E} + \varepsilon_{oy}^{P}\left[\frac{\sigma - \sigma_y}{\sigma_{oy} - \sigma_y}\right]^n \qquad \sigma > \sigma_y \tag{2.638}$$

in which σ_{oy} is the offset yield stress at a specific permanent strain ε_{oy}^{P} in Figure 2-85 and n is an exponent that need not be an integer. We

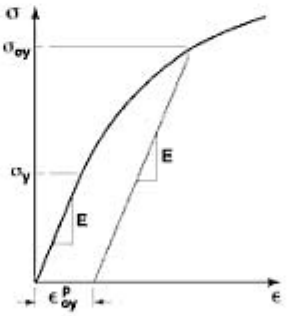


Figure 2-85 Nadai Stress-Strain Curve

Éléments sous droits d'auteur

can see in Equation (2.638) that the strain above yielding is separated into elastic strain plus plastic strain. Thus, $\varepsilon^P_{\sigma y}$ is easily shown to be the plastic strain at $\sigma_{\sigma y}$, i.e., the permanent strain used to determine $\sigma_{\sigma y}$. A common value used for $\varepsilon^P_{\sigma y}$ is .002 for both steel and aluminum.

The Nadai stress-strain curve equation exponent n cannot be determined with a direct approach from Equation (2.638). The Nadai stress-strain curves for various values of n are displayed in Figure 2-86 for specific values of σ_y, $\sigma_{\sigma y}$, $\varepsilon^P_{\sigma y}$, and E. Integer values of n are shown, but n will likely be a noninteger value when the equation is used to represent actual stress-strain data.

Actually, five parameters, E, $\varepsilon^P_{\sigma y}$, σ_y, $\sigma_{\sigma y}$, and n, appear in Equation (2.638), not four as claimed. However, not all five parameters are independent because Equation (2.638) can be written as

$$\varepsilon = \frac{\sigma}{E} + K(\sigma - \sigma_y)^n \qquad \sigma > \sigma_y \tag{2.639}$$

in which we note only four parameters. Equation (2.639) is a generalization of the three-parameter Ramberg-Osgood stress-strain curve that does not have an initial linear portion [2-41]. Note that the units of K must change as the exponent changes. In contrast, all quantities in Equation (2.638) have obvious physical significance with no change in dimensions as n changes. However, we can show that

$$K = \varepsilon^P_{\sigma y}(\sigma_{\sigma y} - \sigma_y)^{-n} \tag{2.640}$$

The Nadai stress-strain curve in the form of Equation (2.639) is more easily used than Equation (2.638) because n can be directly calculated, i.e., no curve-fitting or trial and error work is necessary to find n.

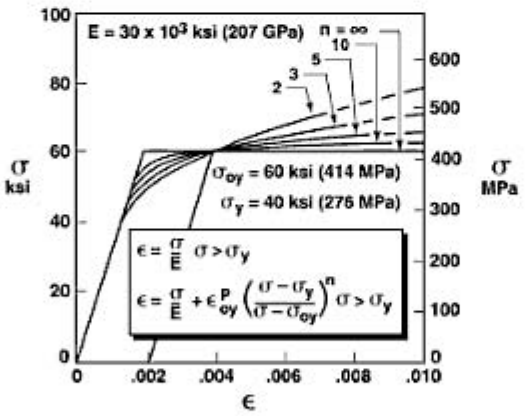


Figure 2-86 Nadai Stress-Strain Curves for Various n

Éléments sous droits d'auteur

The question now is the significance of three versus four parameters in the various stress-strain curve equations. Actually, the number is not as important as the character of the individual curves. For example, the Nadai stress-strain curve with its defined elastic region is physically more attractive than stress-strain curve models with no elastic region. However, we must not lose sight of the physical reality that nonlinear stress-strain curves are generally curved perceptibly from the zero stress level and hence do not necessarily have a well-defined yield stress with a corresponding linear elastic region below and nonlinear region above. Moreover, we cannot lose sight either of the fact that we have gone to a great deal of trouble to idealize the nonlinear stress-strain behavior in such a way that it is mathematically tractable. To abandon that useful idealization would negate our considerable efforts thus far. Thus, we should choose the stress-strain curve equation that is consistent with our mathematical idealization, namely the Nadai stress-strain curve.

2.10.7 Numerical Results

Consider bars made of 2024-T4 aluminum for which the stress-strain curve is shown in Figure 2-87. That curve has the following parameters when expressed in the form of a four-parameter Nadai stress-strain curve model:

$\sigma_y = 27$ ksi (186 MPa) $\quad n = 2.409$

$\sigma_{oy} = 45$ ksi (310 MPa) $\quad K = .18939 \times 10^{-5} (\text{ksi})^{-n}$

$E = 10.8 \times 10^3$ ksi (74.5 GPa)

for which the two measured stress-strain curve points used to determine n are $[\sigma_1 = 37.5$ ksi (258 MPa), $\varepsilon_1 = .0040]$ and $[\sigma_2 = 45$ ksi (310 MPa), $\varepsilon_2 = .0061]$, and the offset yield strain is $\varepsilon_{oy}^P = .002$.

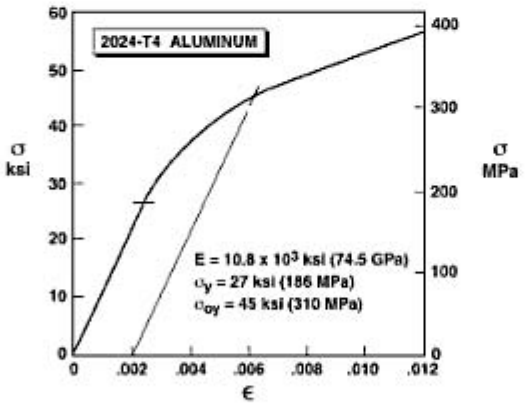


Figure 2-87 Stress-Strain Curve for 2024-T4 Aluminum

Éléments sous droits d'auteur

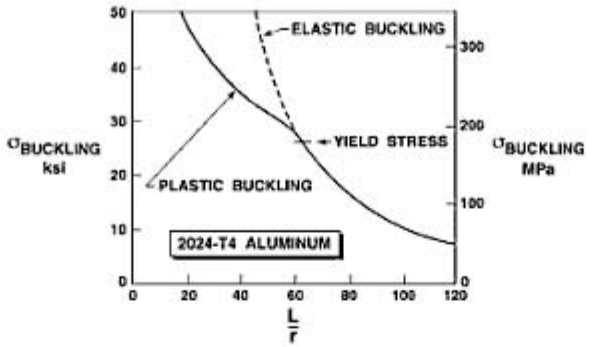


Figure 2-88 Square-Cross-Section Bar Buckling Results

The calculation of the elastic buckling load for various values of L/r (in which r is the radius of gyration of the bar cross section) for square-cross-section bars is quite simple and leads to the parabolic curve labeled elastic buckling in Figure 2-88. The plastic buckling results were obtained by use of the interval-halving technique described in Section 2.10.5. Obviously, the two curves deviate from one another at the value of L/r = 63 where the buckling stress is the yield stress. For bars with L/r less than 63, the plastic buckling loads or stresses are substantially below the elastic buckling results.

2.10.8 Comparison of Reduced-Modulus Theory with Tangent-Modulus Theory and Measured Buckling Loads

The key consideration in determining whether reduced-modulus theory or tangent-modulus theory leads to an adequate prediction of plastic buckling is whether the bar bends *before* or *after* the buckling stress is reached. For perfect bars, there seems to be agreement that no bending occurs before the buckling stress, and thus their behavior is governed by reduced-modulus theory. However, imperfect bars do bend prior to buckling so their behavior is governed by tangent-modulus theory. Because no bar is truly perfect, the tangent-modulus buckling load is commonly accepted as the lowest load for which bending can occur with increasing load. Thus, the tangent-modulus buckling load is now regarded as the practical buckling load even by von Kármán [2-37] who refined the reduced-modulus approach!

This conclusion is borne out by buckling tests conducted by Templin, Sturm, Hartman, and Holt [2-42] on solid circular cross-section 17S-T aluminum bars. Note that the measured values in Figure 2-89 fall on or very close to the tangent-modulus theory curve except for the point corresponding to the shortest, squatest bar (lowest L'/r in which L' is the effective length of the bar as defined in Section 2.3.8 on page 76). Thus, over a wide range of L'/r, the tangent-modulus theory is a good prediction

Éléments sous droits d'auteur

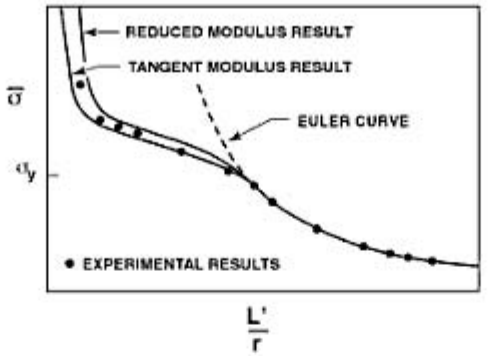


Figure 2-89 Buckling Stress Versus Effective Slenderness Ratio *(After Templin, Sturm, Hartman, and Holt [2-42])*

of the plastic buckling behavior. Thus, experimental buckling results are in substantial agreement with the theoretical results, both elastic for slender bars and plastic where applicable.

As an alternative to the general approach just discussed (which will also be used for plates and shells in Chapters 3 and 4, respectively), the following approach is useful for the bar buckling analysis problem. Recast the buckling equation, Equation (2.623), in the transcendental form

$$\sigma = \frac{\pi^2 E(\sigma)}{(L/r)^2} \tag{2.641}$$

and rearrange Equation (2.641) to obtain

$$\left[\frac{L}{r}\right]^2 = \pi^2 \frac{E(\sigma)}{\sigma} \tag{2.642}$$

or

$$\frac{L}{r} = \pi\sqrt{\frac{E(\sigma)}{\sigma}} \tag{2.643}$$

Thus, for a specified σ, the value of E(σ) is easily calculated if the equation for the appropriate stress-strain curve is known. Then, obviously the L/r (or L'/r) can be found, so curves such as Figure 2-89 can be determined directly instead of going through the process of solving a transcendental equation. This procedure is not useful for design, however, because the unknown area that is related to r, the radius of gyration, is also on the right-hand side of Equation (2.643) implicitly in definition of the stress (σ = P/A).

2.10.9 Summary

We developed an approach to finding the buckling load of a bar when the applied stress exceeds the yield stress. That is, the bar has

Éléments sous droits d'auteur

yielded, and we ask: what then is its buckling stress or load? Shanley convinced us that the tangent modulus is the most appropriate modulus to use in the buckling equation [2-39]. After we made that choice, formulation of the transcendental buckling equation was straightforward. However, the solution of the transcendental equation involves a strategy that is based on a simple fact: we know whether the estimated load is above the buckling load or it is below the buckling load. That fact enables us to develop a simple solution strategy. We also faced the problem of finding equations to represent the nonlinear stress-strain curves typical of structural materials. Then, we obtained some numerical results for buckling of bars made of a typical structural-grade aluminum. Finally, we were able to demonstrate that the buckling load predictions using the tangent-modulus approach are indeed quite close to experimental results. And, in contrast, the reduced-modulus results are well above the experimental results. Note that nowhere have we determined the buckle amplitude because this plastic buckling problem, too, is an eigenvalue problem.

Problem Set 2.10

2.10.1 Derive E_{tan} and E_{sec} for the Nadai stress-strain curve in the form of Equation (2.639).

2.10.2 Derive an equation for n in the Nadai stress-strain curve in the form of Equation (2.639) when the stress-strain curve is passed through two arbitrary points. Then, calculate n and K for the stress-strain data of 7075-T6 aluminum. Plot the data as dots along with the Nadai stress-strain curve you calculate. Also, plot the calculated Poisson's ratio versus stress ($\nu_{elastic} = .32$) if $\nu(\sigma)$ is

$$\nu = \frac{1}{2} - \frac{E_{sec}}{E}\left[\frac{1}{2} - \nu_{elastic}\right]$$

Table P2.10.2 Stress-Strain Data for 7075-T6 Aluminum

σ ksi (MPa)	ε	σ ksi (MPa)	ε	σ ksi (MPa)	ε
55.0* (379)	.00524	61.5 (424)	.00611	68.0 (469)	.00755
55.5 (383)	.00530	62.0 (427)	.00620	68.5 (472)	.00770
56.0 (386)	.00536	62.5 (431)	.00629	69.0 (476)	.00785
56.5 (390)	.00542	63.0 (434)	.00639	69.5 (479)	.00800
57.0 (393)	.00548	63.5 (438)	.00649	70.0 (483)	.00816
57.5 (396)	.00554	64.0 (441)	.00659	70.5 (486)	.00832
58.0 (400)	.00560	64.5 (445)	.00669	71.0 (490)	.00848
58.5 (403)	.00566	65.0 (448)	.00680	71.5 (493)	.00865
59.0 (407)	.00572	65.5 (452)	.00691	72.0 (496)	.00883
59.5 (410)	.00579	66.0 (455)	.00703	72.5 (500)	.00902
60.0 (414)	.00587	66.5 (459)	.00715	73.0 (503)	.00922
60.5 (417)	.00595	67.0 (462)	.00728	73.5 (507)	.00943
61.0 (421)	.00603	67.5 (465)	.00741		

2.10.3 Recall the Nadai stress-strain curve model previously developed in Problem 2.10.2 for 7075-T6 aluminum along with the expression for E_{tan} derived in Problem 2.10.1. Use those results along with the bar buckling equation, Equation (2.632), and the interval-halving procedure to obtain elastic and plastic buckling curves for L/r values up to 70. Below what value of L/r is buckling plastic?

Éléments sous droits d'auteur

2.11 ASPECTS OF DESIGN OF BARS AGAINST BUCKLING

2.11.1 Introduction

From the general Euler bar buckling equation in the form

$$\overline{P} = P_E = \pi^2 \frac{EI}{(L')^2} = \pi^2 \frac{EI}{L_e^2} = \pi^2 \frac{EI}{L_{effective}^2} \qquad (2.644)$$

we see the principal analysis factors that influence the buckling behavior and hence must be carefully addressed in design against buckling:

- $L' = L_e = L_{effective}$: to account for support conditions at the bar ends and along the bar length (see Section 2.3.8 on page 76)
- E: material properties — elastic (constant with load level) or inelastic (variable with load level) as well as other factors that cause E to change, namely creep, temperature, loading rate, sometimes moisture, etc.
- I: geometrical distribution of bar cross-sectional area property in which I is the second moment of the bar area about the axis that is perpendicular to the plane in which buckling occurs

Of course, we regard the actual bar length, L, as a known or controlled quantity that is changed only under restrictive design circumstances. For example, a bar used as a building column typically has a length equal to the building story height unless the connection to a mid-column-height floor is so flexible as to be able to exert an influence on the column in only one plane (shown later in Section 2.11.3). Then, the column length is considered to be at least two stories. In other applications such as a space truss, the bar length could be a design variable because the truss size and configuration is variable (unlike a building of fixed story height).

We will examine the principal analysis and design factors in Section 2.11.3 on end and lateral support conditions, Section 2.11.4 on material properties, and Section 2.11.5 on cross-sectional shapes. Comments on the applicability of design codes are offered in Section 2.11.6. First, let us put analysis and design into perspective relative to each other.

2.11.2 Analysis versus Design

We will first contrast analysis, with which you are presumably quite familiar, and the philosophical concepts of design. Analysis is viewed in Figure 2-90 in this manner: *analysis is the determination of the behavior that a specific structural configuration exhibits under specific loads.* That is, what load does the structure take? Or, how much does the structure deflect at a certain crucial point? Analysis is a one-way street. We start with a specific structure, and ask: how good is this structure, how much stress can it take, or how much overall load can it take without violating any stress limitations, deflection limitations, or any other performance limitations? What is the load at which the structure buckles? What are

Éléments sous droits d'auteur

- **ANALYSIS**

  THE DETERMINATION OF THE BEHAVIORAL RESPONSE EXHIBITED BY A PARTICULAR STRUCTURAL CONFIGURATION UNDER SPECIFIC LOADS (WHAT LOAD DOES THE STRUCTURE TAKE?)

- **DESIGN**

  THE PROCESS OF ALTERING DIMENSIONS, SHAPES, AND MATERIALS TO FIND THE BEST (OPTIMUM) STRUCTURAL CONFIGURATION TO CARRY SPECIFIC LOADS AND PERFORM SPECIFIC TASKS (WHAT IS THE 'BEST' STRUCTURE TO TAKE THE LOAD?)

Figure 2-90 Analysis versus Design

its vibration frequencies? Thus, *analysis is an overall assessment of the response and capabilities of the structure*. We start with one structural configuration and uniquely determine all the pertinent response characteristics such as deflections, stresses, buckling loads, vibration frequencies, etc. This process is generally a collection of either boundary-value problems or eigenvalue problems. Accordingly, analysis is a *deterministic* approach to solving a very narrow set of problems. We think of analysis as a very broad process of various features, but, relative to design, analysis is actually a quite narrow and restricted process.

Many analysts tend to believe that design is merely a sequence of analyses. They also tend to think that finite element analysis is the foremost design tool in the world. Some people know me best as a finite element specialist, and yes, I did imply that finite elements are not the 'be all and end all' or the penultimate tool! Certainly finite element analysis is an indispensable and major *part* of most design practice for complicated structures. However, *the driving soul behind design is the* ***logic*** *for how to change the design variables in the configuration to meet the design requirements*. That is, design is *behavior modification* of a structure! Design can be automated to some extent; the danger is that if all failure modes are not included in the automated process, then the possibility of failure in some other mode is totally ignored.

In contrast to analysis, *design is the process of altering all the dimensions, the shapes, and perhaps the materials that are involved in a structural configuration to enable that configuration to carry specific loads, perform specific tasks, cost the least, weigh the least, or satisfy some other criterion for 'goodness'*. That is, we turn the problem around from analysis in one respect. We are saying: we do not know the structural configuration, but we know only the loads. What structure will carry these loads? *This problem does not have a unique answer!* We can find many different structures that will carry the desired loading. The process of design is trying to determine, under the constraints or guidelines for the particular object we want to design, what is the *best structure* to carry those loads. Therefore, *design is not a deterministic process*. Instead, design is an iterative procedure of selecting a configuration and seeing how close its capabilities are to satisfying the design requirements, and then making changes that we hope will lead toward satisfaction of all the

Éléments sous droits d'auteur

design requirements. Typically included in the design process is a statement that cost must be as low as possible and that weight must be as low as possible, if in fact those factors are considerations.

A key element of a rational design process is establishing a set of mechanistic relationships that relate the structural configuration to its performance. Use of mechanistic relationships is what distinguishes the structural designer from a dress designer (who has no such relations).

Philosophically, *design is much more than just the inverse of analysis*. Analysis versus design is not a mathematical inverse problem: it is far more as seen in Figure 2-91. We have fundamentally changed from a deterministic analysis problem to a nondeterministic design problem. The design problem has many decisions that must be made, and those decisions make design very complicated as well as nondeterministic. The other major distinguishing element of the design process is the *logic* for making the required decisions. Moreover, the end result of the design process is not a even unique solution to the design specifications! That is, many possible configurations might meet the design performance requirements. And, there are also usually requirements on cost and often on weight. The final question then becomes: which of the possible configurations is the 'best'? Defining the 'best' is often very difficult. Sometimes, we don't ever seek the 'best', but are satisfied to merely have made it through the design process once, much less to have iterated through the design process many times to achieve the 'best' design.

As an example of the contrast between analysis and design, consider the bar buckling problem. To analyze the buckling resistance of a simply supported, axially loaded bar, we use the Euler buckling equation,

$$\overline{P} = \frac{\pi^2 EI}{L^2} \tag{2.645}$$

in which $\overline{P}$ is the buckling load, E is the modulus of elasticity of the material, I is the second moment of the bar cross-sectional area, and L is

- **ANALYSIS**
  - **EVALUATE RESPONSE OF A SPECIFIC STRUCTURE**
  - **DETERMINISTIC PROCESS**
  - **BOUNDARY VALUE PROBLEMS AND EIGENVALUE PROBLEMS**
- **DESIGN**
  - **FIND THE NONUNIQUE STRUCTURE THAT SATISFIES REQUIREMENTS**
    - **FUNCTION**
    - **COST**
    - **WEIGHT**
  - **NONDETERMINISTIC PROCESS**
  - **LOGIC FOR CHANGING THE STRUCTURAL CONFIGURATION CRUCIAL**
  - **WHAT IS THE 'BEST' STRUCTURAL CONFIGURATION?**

Figure 2-91 Design is More than Just the 'Inverse' of Analysis

Éléments sous droits d'auteur

the unsupported length of the bar. A typical analysis problem consists of finding the buckling load for a specific bar. Hence, E, I, and L are known, so the problem obviously is deterministic. That is, all the variables on the right-hand side of the single governing equation are known, so the equation can readily be evaluated.

In contrast to the analysis problem, suppose we must design a bar to resist buckling under a prescribed load. Therefore, we seek the bar properties E, I, and L knowing only the buckling load $\bar{P}$, i.e., the load that must be carried without buckling. However, we have three unknowns, one known, and only one governing equation, so the problem obviously is *not deterministic!* That is, knowing $\bar{P}$ *does not lead to* ($\not\rightarrow$) values for E, I, and L. Even if we know the column length as in a typical column design problem for a building, we still do not have a tractable problem. We make the problem partially tractable by selecting the column from a specified set of possible materials, say steel, concrete, wood, or aluminum for an ordinary building column as in Figure 2-92. That is, if we know L and E for a desired design load $\bar{P}$, we can solve for I from Equation (2.645) as if we were dealing with an analysis problem:

$$I = \frac{\bar{P}L^2}{\pi^2 E} \tag{2.646}$$

However, four different moments of inertia for each of the four different materials (hence different moduli of elasticity) are obtained from Equation (2.646). Moreover, *knowing the moment of inertia of a bar does not tell us the shape or dimensions of a bar!* We usually select a bar that has a moment of inertia at least as great as that determined from Equation (2.646). However, that selection process usually results in considering quite a few bar cross sections that meet the design requirements. Thus, we must exercise some other criterion besides avoiding buckling in order to select the actual bar cross section. That is, many bar cross sections can have the same required moment of inertia, so how do we decide which bar is 'best'? Perhaps cost is an appropriate basis on which to

- **BUCKLING LOAD ANALYSIS**

  $\bar{P} = \pi^2 \frac{EI}{L^2}$ E, I, L $\rightarrow$ $\bar{P}$

- **DESIGN AGAINST BUCKLING**
  - $\bar{P}$ DESIRED $\not\rightarrow$ E, I, L
  - IF L KNOWN, $\bar{P}$, L $\not\rightarrow$ E, I
  - IF L KNOWN AND MATERIAL SELECTED, $\bar{P}$, L, E $\rightarrow$ I
  - OR IF L KNOWN AND MATERIAL SELECTED FROM STEEL, CONCRETE, WOOD, AND ALUMINUM,

    $\bar{P}, L, E_S, E_C, E_W, E_A \not\rightarrow I_S, I_C, I_W, I_A$

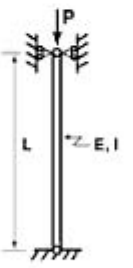


Figure 2-92 Buckling Design versus Analysis Example

Éléments sous droits d'auteur

compare the various bars, so we would select the material and cross section that correspond to the least-cost column. Or, perhaps weight is the *design driver*, so we would select the least-weight column. For structural steel, cost and weight are very nearly synonymous. That is, least-cost and least-weight criteria result in the same design because the cost of a steel member depends on its weight. At any rate, the complexity of the design problem as opposed to the analysis problem is suitably illustrated in this example as summarized in Figure 2-92.

An even more difficult problem occurs if the bar is not prismatic, i.e., if the area and moment of inertia are not constant along the length. We must then solve for I(x) where x is the axial coordinate of the bar. This optimization of cross-section distribution has been addressed only for problems with fixed E and L, not the general bar design problem.

The term *trade-off* arises frequently in discussions of the design process. When conflicting objectives are encountered, some compromise must be achieved between the conflicts. To trade-off means to exchange (or trade) one achievement for another. For example, aircraft weight increases can be accommodated by shortening the range, decreasing the payload, increasing the fuel consumption, or some combination of all three possibilities. The appropriate trade-off of these consequences can be arrived at only by examining the requirements for successful operation of the aircraft and deciding what combination of factors is the 'best', i.e., the most meaningful for the application of the aircraft. Trade-offs are confined to the nonunique design process because of the existence of many possible solutions to the design problem. Trade-offs do not exist in analysis because there we deal with an already-defined configuration, so changes are not possible.

The final concept of design that must be addressed is the multiplicity of possible failure modes that a structure can experience. Buckling is but one of the possible failure modes. Failure inherently limits the maximum load-carrying capability of a structure as in Figure 2-93. All possible failure modes must be investigated to be assured of a safe structure. And, we cannot investigate failure modes without suitable analyses.

- **THE MAXIMUM LOAD-CARRYING CAPABILITY OF A STRUCTURE IS OF CENTRAL IMPORTANCE IN DESIGN**
- **MUST CONFIGURE A STRUCTURE TO CARRY A SPECIFIED LOADING**
- **MUST KNOW HOW MUCH LOAD A STRUCTURE WILL CARRY WITHOUT FAILURE**
- **A STRUCTURE CAN FAIL IN SEVERAL *INDEPENDENT* FAILURE MODES, E.G.,**
  - **FRACTURE**
  - **BUCKLING**
  - **EXCESSIVE DEFLECTION**
  - **FATIGUE**
- ***ALL* FAILURE MODES MUST BE INVESTIGATED IN DESIGN**
- **DESIGN AND THE MAXIMUM LOAD ARE CLOSELY RELATED BECAUSE *WE MUST BE ABLE TO ANALYZE A STRUCTURE BEFORE WE CAN DESIGN IT!***

Figure 2-93 Maximum Load Considerations

Éléments sous droits d'auteur

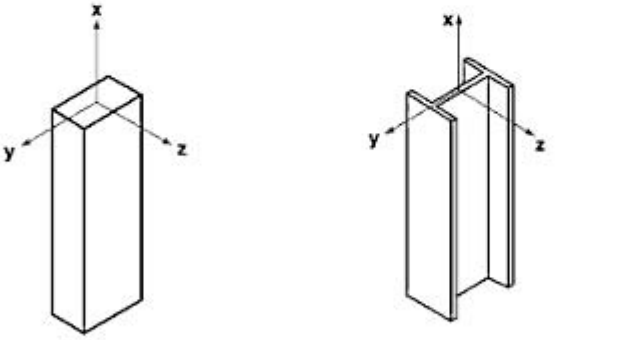
2.11.3 End and Lateral Support Conditions

One of the presumptions or default conditions of the discussion of bar buckling up until this point in the book is that bars buckle only in the plane of the book page because that is what was easiest to draw and to discuss. Thus, the I in the buckling equations is about a cross-sectional axis that is perpendicular to the plane in which buckling occurs, namely perpendicular to the book page. However, *in design, we must be prepared to consider the possibility of buckling in any plane that includes the bar longitudinal axis.*

We will restrict our attention here to bars that have two principal planes of cross-sectional symmetry and therefore two moments of inertia about two cross-sectional plane axes. Such a bar is shown in Figure 2-94a where the x,y,z axes are principal axes for the rectangular-cross-section bar. This bar, if supported identically in the x-y plane as in the x-z plane, buckles in the x-z plane because I_z is obviously greater than I_y. A more common building column is a rolled-steel wide-flange cross section as in Figure 2-94b. Because $I_z > I_y$, the wide-flange column buckles in the x-z plane if supported at the ends in the same manner in the x-z plane as in the x-y plane. Of course, if the end support conditions are different in the x-y plane from those in the x-z plane, the conclusion as to which plane buckling occurs in could be different.

In which plane of two planes, x-y and x-z, in Figure 2-94 does a general bar buckle? The answer depends on three factors: (1) the moment of inertia (second moment of the cross-sectional area) about each axis of the cross-sectional area, (2) the end support conditions for buckling in each plane containing one of the transverse-to-the-bar axes and the longitudinal axis of the bar, and (3) the transverse support conditions along the bar axis in the y and z directions in Figure 2-94.

For example, consider a bar with a cross-sectional area in the y-z plane which has a different I about the y-axis than about the z-axis and also different support conditions for buckling in the x-z plane than for buck-



a Rectangular-Cross-Section Bar b Rolled-Steel Wide-Flange Column

Figure 2-94 Principal Axes for Bars

Éléments sous droits d'auteur

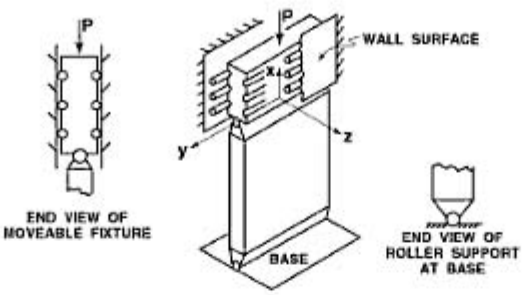


Figure 2-95 A Bar with Different Conditions in the Principal Planes

ling in the x-y plane as in Figure 2-95. For buckling in the x-z plane, for which the I (I_y) is the lowest, the ends are simply supported. For buckling in the x-y plane, for which the I (I_z) is the highest, the ends are fixed. Note that higher I leads to higher buckling loads, and simply supported bars buckle at lower loads than fixed-end bars. At the top of the bar, the rollers are somewhat recessed in the moveable fixture and roll on the vertical wall surface on each side of the fixture (see Figure 2-96 for more details of a possible construction scheme). At the bottom of the bar, the roller is captured in the end of the bar and rotates in a groove in the base. Note that the least I corresponds to simply supported ends whereas the largest I corresponds to fixed ends. Thus, the conclusion of which plane the bar buckles in is obviously the x-z plane.

We can imagine many possible support mechanisms, but all of them will likely have some important flaws that make them not work precisely as we would like. A simple support is essentially a pinned connection that permits free rotation of a structural member about the pin. However, the rotation is never perfectly free because of always-present friction. If the simple support is to be at the top of a column (or the end of any bar), then the support must also move freely in the vertical direction (or along

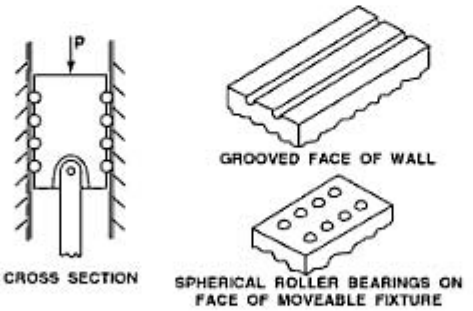


Figure 2-96 Possible Mechanism to Allow
Free Vertical Movement of the Loading Head

Éléments sous droits d'auteur

the bar) in order to introduce the axial load. This vertical movement can be accommodated by the moveable pinned-end fixture shown in Figure 2-96. Spherical ball bearings are captured in a spherical cavity in the movable fixture attached to the top of the bar in Figure 2-96. The bearings roll in a vertical round-bottom groove in the fixed wall. Or, ball bearings could be avoided by heavily greasing a sliding contact between the moveable fixture and the vertical wall. Of course, adapting this kind of fixture for a fixed end (rotation-free, but still moveable in the vertical direction) is relatively simple.

Consider a two-story-high, wide-flange column with two beams fastened to it at mid-height as in Figure 2-97. This situation might arise if a steel framework were built to enclose a two-story open area (the beams are required to support windows and the exterior wall). The column is continuous in the vertical direction, but the beams fit between columns, so are not continuous. Imagine the connections are welded, so the figure is essentially correct (except for four carry-through plates to 'extend the beam flanges through the column'). Other types of connections, e.g., riveted or bolted angles, could be used instead of welding. Our principal observation is that the connection in Figure 2-97 permits movement in the y direction, but restrains movement in the z direction.

Despite the fact that the connections in Figure 2-97 appear to provide a fixed end for the beams, i.e., prevent rotation of the connected member, building designers generally regard them more conservatively as simply supported. Thus, we will also regard all connections as simply supported. The column in Figure 2-97 has similar connections at its top and bottom. Moreover, the top of the column is fastened to beams in both the y and z directions. Thus, the column cannot move in either the y direction or the z direction at its top and bottom.

Now consider buckling of the column in Figure 2-97 in the x-z plane and in the x-y plane. In the x-z plane, the column is simply supported at the top and bottom of its two-story length (2L) and is restrained from movement in the z direction at its mid-height (L). Thus, the column is constrained to buckle into the second mode ($m = 2$ with two half-sine waves in Figure 2-98) in the x-z plane. In the x-y plane, the column in Figure 2-97 is simply supported at the top and bottom of its two-story

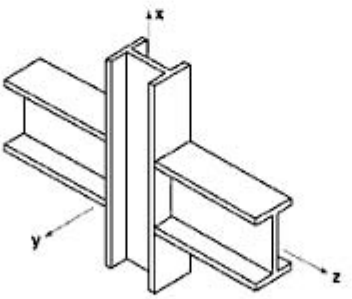


Figure 2-97 A Column with Different Support Conditions in the Principal Planes

Éléments sous droits d'auteur

length (2L) with no transverse support along its entire length. Thus, the buckling loads in the two planes are

$$\bar{P}_{xz} = 4\pi^2 \frac{E I_y}{(2L)^2}$$

$$\bar{P}_{xy} = \pi^2 \frac{E I_z}{(2L)^2} \qquad (2.647)$$

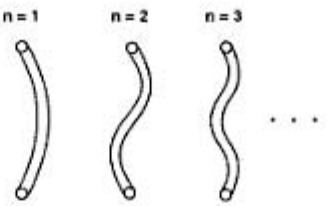


Figure 2-98 Buckling Mode Shapes

But $I_y > I_z$ for a wide-flange section, so the column always buckles in the x-y plane because that plane corresponds to the lowest buckling load. If the column were rotated 90° about the x axis, then $I_z > I_y$, and then we cannot determine the lowest buckling load and the corresponding plane of buckling without substituting the actual I values in the equations and comparing the results. This second orientation would be more efficient use of the rolled-steel wide-flange shape.

The concept of a simple support, i.e., a support that permits free rotation, but does not allow lateral (transverse) movement in one or both directions, is only a very idealized situation. Most practical support conditions provide more restraint than the ideal simple support, e.g., at least a modest amount of rotational restraint is provided by the attachment fixtures used to fasten a bar or column to the rest of the structure!

For example, a column can be fastened to an overlying beam by the use of riveted or bolted angles as shown in Figure 2-99. Not all the reinforcement details are shown in Figure 2-99 because the principal attachments are the main message. Even if the column is welded to the overlying beam, the full rotational restraint of a "fixed end" cannot be achieved because the overlying beam is elastic and can itself rotate somewhat at the connection. Thus, an upper bound on the buckling load is a fixed end for the column whereas a lower bound is a simply supported end. Then, because the fixed-end condition is unconservative (associated with a higher buckling load than can actually be achieved), designers naturally choose the conservative approach. Thus, we have no particular difficulty in ignoring the impracticality of achieving an actual

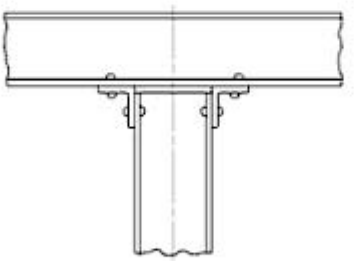


Figure 2-99 Representative Connection of a Column to a Beam

Éléments sous droits d'auteur

simple support *unless we try to measure buckling loads for real structures and need to have workable, practical supports to correspond to the supposed supports in our analyses.*

2.11.4 Material Properties

We addressed the influence of plastic deformation on buckling loads in Section 2.10. There, we found the effect of decreasing the modulus of elasticity as load increases. The plastic buckling load is always lower than the elastic buckling load by an amount that depends on the level of plastic deformation. Other material characteristics and environmental effects change the modulus of elasticity in the Euler equation in some manner and are described in this subsection.

2.11.4.1 Effect of Creep

Creep is the phenomenon in which a material continuously and increasingly deforms with time as a constant load is applied (as opposed to having a constant, unique, time-constant deformation for a specific load which situation occurs for most structural materials under ordinary conditions). Creep rupture is the characteristic of a material which has first increased deformation under constant stress with time and then fractures at a stress well below the static strength of the material. Such material behavior is common for plastics at moderately elevated temperatures and even for most structural metals when they are exposed to elevated temperatures such as in supersonic flight of an aircraft or even higher speeds for a missile. Moreover, most fiber-reinforced composite materials can exhibit similar behavior at somewhat lower temperatures than those of supersonic flight.

Creep buckling is the progressive deformation and finally collapse of axially loaded bars made of materials that creep. Hoff states that creep buckling can only occur for bars that are not initially perfectly straight nor is their axial load applied in a perfectly centric manner [2-43]. Thus, the creep buckling problem has some of the same fundamental conditions as the buckling of imperfect bars in Section 2.8. Hoff describes the creep buckling of such bars as taking place in the following manner: 'The curvature of the initially imperfect bar increases slowly at first under the action of the constant load. Then, as time increases, the lateral deflections become more and more noticeable. Finally, the bar collapses, i.e., is unable to carry the load to which it has been subjected up until this critical time'. That is, even though a bar might not be highly enough loaded to buckle immediately, the long-time application of load (that would be withstood statically!) still can result in creep buckling. The critical time for creep buckling must exceed the expected design life of the structure. That design life might be minutes for a missile, many hours for an aircraft, or years for a more ordinary structure.

The reader is cautioned in the design process to ask whether the materials being considered are susceptible to creep. If they are, then creep deformation and creep buckling must be considered in design. Further discussion of creep and creep buckling in Kraus' book [2-44].

Éléments sous droits d'auteur

2.11.4.2 Effect of Earthquakes

Some reinforced-concrete columns are susceptible to great damage during earthquakes. The susceptibility stems from the nearness of axial or vertical steel reinforcement (that forms a major part of the second moment of the transformed cross-sectional area, i.e., moment of inertia, of the column) to the exterior surface of the column in many typical designs. Earthquake motions cause forces that induce spalling of the unrestrained (except by the inherent strength of the unreinforced concrete) outer layer of concrete away from the axially oriented steel reinforcing bars. Then, that axial reinforcement is unsupported and buckles as in Figure 2-100. There, a column that supported an approach to the San Francisco – Oakland Bay Bridge is shown after the October 1989 Loma Prieta earthquake. Such actions can lead to severe degradation of the columns and subsequent collapse of the structure supported by the columns. We recall that the Oakland end of the bridge approach structure did collapse!

One solution to this susceptibility for already-built columns is to circumferentially wrap them with high-strength, high-stiffness, fiber-reinforced composite material layers (For a study of the mechanics of composite materials, see Jones [2-45]. With that reinforcement, the columns have far higher resistance to spalling, so column integrity (specifically the integrity of the axially oriented steel reinforcing bars) is maintained to be able to withstand higher levels of earthquakes than at present. Similar approaches could be effectively used for newly designed columns.



Figure 2-100 Earthquake-Damaged Reinforced-Concrete Column Supporting the San Francisco – Oakland Bay Bridge (Photo courtesy of Dr. James R. Martin)

Éléments sous droits d'auteur

2.11.4.3 Environmental Effects for Fiber-Reinforced Composite Materials

Composite materials have applications to structures that buckle ranging from earthquake-resistant reinforced-concrete columns to space trusses for the International Space Station. However, such materials have susceptibilities to certain environmental effects not found in more usual structural materials.

Elevated moisture and temperature effects on polymer-matrix materials were addressed by Browning, Husman, and Whitney [2-46]. Moisture absorption for many, but not all epoxies causes swelling, plasticization, and decrease in glass-transition temperature. Plasticization is the increase in spacing between molecules, so molecular mobility increases, and hence stiffness decreases. The glass-transition temperature, T_g, is the temperature at which a polymer changes from a hard, glassy solid to a soft, rubbery solid with associated decreases in stiffness and strength. Actually, this transition takes place not at a specific temperature, but over a relatively small temperature range. Such physical changes for the matrix of a polymer-matrix composite material cause the matrix-dominated properties to be most affected (degraded) and the fiber-dominated properties to be least affected. Browning, Husman, and Whitney present absorbed moisture profiles through the thickness of AS-3501-5 graphite-epoxy composite laminates with associated mechanical properties as a function of moisture and temperature.

The effects of environmental factors that cause expansional strains were studied by Whitney and Ashton for laminated plate buckling [2-47]. Such factors include temperature rise and matrix swelling due to water vapor or sudden expansion of absorbed gases. Temperature rises and matrix expansion can cause degradation of material properties. However, Whitney and Ashton held the material properties constant and treated only the effects of temperature and swelling on structural response. Both phenomena cause buckling; thus, buckling caused by thermal expansion was assessed directly. Swelling resulted in reduced buckling loads. These effects are all significant enough to warrant attention in composite structures design-analysis.

Composite materials in space, such as in orbiting space stations, are subject to an environment of hard vacuum, thermal cycling because of passing in and out of the sun's rays, as well as ultraviolet, electron, and proton radiation. The effects of those environmental factors include: (1) vacuum causes outgassing and migration of low-molecular-weight components from matrix materials such as polymers, so the properties of the polymers change with time; (2) thermal cycling can cause significant dimensional changes in such dimension-sensitive instruments as space telescopes; and (3) radiation causes damage because of competing effects of polymer chain-cutting and enhanced cross-linking. The latter effects change the melting point, hardness, strength, and stiffness as well as the dimensional stability of polymers.

Éléments sous droits d'auteur

2.11.5 Bar Cross-Sectional Shapes

In many common design problems, an engineer is required to find the buckling load for bars with the cross sections shown in Figure 2-101, among many others. The distinctive feature of those cross sections is the different ways to obtain an efficient cross section to resist buckling. i.e., with a high moment of inertia about a particular axis for a small amount of material. The largest I for the least area (hence, least amount of material) is the design objective. The value I/A is otherwise known as the square of the radius of gyration (defined earlier in Section 2.8). All such bars have the characteristic load-deformation behavior with an almost horizontal response after buckling as shown in Figure 1-11 on page 7. Thus, the Euler buckling load is a practical estimate of the maximum load a bar can support. Somewhat larger loads can be supported, but at the considerable disadvantage of greatly increased axial shortening and substantial lateral displacement.

Ordinarily, solid cross sections such as the square, rectangle, or circle are not efficient. That is, their I is too small for the amount of material used. Hollow cross sections such as the hollow circle or hollow square are far more efficient. Hollow circular cross sections are typically used in all space trusses because of the extraordinarily high cost of boosting the truss members into space.

Many possible cross-sectional shapes exist for a bar as seen in Figure 2-101. However, in a specific design environment, say an office building, only certain shapes or types of shapes might be desirable. In the office building example, a mixture of hollow circular cross-section members and rolled-steel wide-flange cross-section members would likely create enormous compatibility (attachment) problems between structural elements. For many reasons, compatibility included, circular cross sections would not likely be used, unless the architect wanted to 'make a statement' and had a large budget. Thus, common rolled-steel cross sections would likely be used. And, although many rolled-steel sections are available, that number is obviously finite, so the choices in a specific design are quite limited. An I-beam (sometimes called an S section) has a high second moment of the cross-sectional area about one axis (the hor-

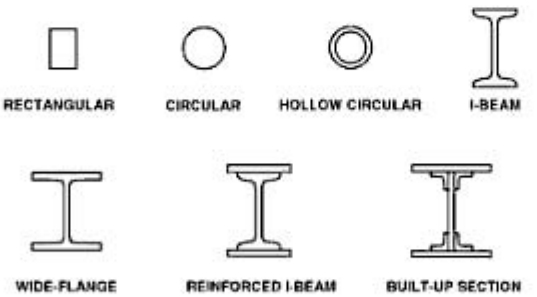


Figure 2-101 Typical Bar and Column Cross Sections

Éléments sous droits d'auteur

izontal in Figure 2-101) and a much smaller I about the other axis, a range of ratios of I from 50 to 10. In contrast, a wide-flange section (also called a W section) has a range of ratios from 35 to 3 with many column sizes in the range of 3 to 10. The more I-balanced wide-flange sections are inherently better suited for columns that might buckle about either axis. Beams are often made of I-beam sections, but I-beams and wide-flange section columns are relatively easy to attach to one another, as seen in Figures 2-97 on page 209 and 2-99 on page 210. When standard structural rolled-steel sections are not adequate, the first approach usually is to reinforce the standard sections with a 'cover plate', i.e., a flat steel plate placed in a position as far as possible from the neutral axis to give the largest contribution to I for the weight added as for the reinforced I-beam in Figure 2-101. When standard sections are not desirable, custom-made sections can be constructed by building up webs and flanges from plates with various angle sections used as connections for the built-up section as in Figure 2-101. Even if the I-beam sections are reinforced with cover plates as in the bottom center of Figure 2-101, the attachments can be made without great difficulty. In contrast, attaching circular cross-section columns to any other structural element is quite involved and expensive.

Many other possible cross sections and column constructions have been used over the years. See structural steel design books for such applications, e.g., Gaylord, Gaylord, and Stallmeyer [2-48].

2.11.6 Design Codes and Their Development

In addition to all the design aspects mentioned so far, there are design codes for certain segments of the engineering community. Various building design codes exist in the United States, Europe, and elsewhere in the world. These codes are a prescription of how the wide variety of bars and columns used in structures are to be analyzed and designed. Such codes are developed over a long period of time by interaction between structural behavior researchers, structural designers, and public officials in a committee environment to hopefully achieve the required balance between the responsible parties in order to serve the public safely and economically. The details of these design codes will not be examined in this book, but are left to the concern of those readers in various parts of the world who are guided and governed by the codes. Other engineers are not bound by building design codes: for example, aircraft designers are essentially independent of any influence of building codes. The aerospace structures community generally has no such codified design rules because their structures are far less conventional and repetitive. Moreover, their designs are not governed by any usual structures design authority except for governmental aircraft certifiers. However, aerospace structural designers do pay very special attention to practices that would appear to be helpful to their goals of safe aircraft. The concern in this book is with the general nature of design without all the (variable) details and without the often conflicting practices of some of the various design codes.

Éléments sous droits d'auteur

One aspect that must be addressed in any design procedure is the factor of safety to be used. The factor of safety depends on a myriad of factors including whether the structure is man-rated or unmanned, the nature of the potential failure (benign or catastrophic), the uncertainty of the analysis accuracy, etc. The key factor to recognize in design of a bar against buckling is the relatively catastrophic nature of bar buckling as shown in Figure 2-31 on page 89, i.e., the buckling deflections are rather large and usually unacceptable in a structure (certainly in a building!). Thus, we expect factors of safety for bar buckling to be in the upper range of usual values.

Two components of engineering are used to enable the effective and appropriate design of bars: (1) experiments on typical bars to determine fundamental behavior as the basis for analyses and their verification and (2) analyses to unify and extend the experiments. The analyses must generally include both elastic and plastic behavior as seen in Section 2.10. Also, such effects as residual stresses and initial geometric imperfections, both caused by imperfect manufacturing processes, must be addressed because they reduce the bar buckling load. All these factors are taken under consideration by various technical committees first to establish a common understanding of how, for example, bars or columns behave under compressive loads. Then, other technical committees establish suitable design rules, equations, or curves to be used in their specific area of practice taking into account an appropriate factor of safety. In what follows, we examine those two aspects of (1) a common understanding of bar behavior and (2) a design equation for bars used as columns in buildings, bridges, and other structures.

As a practical behavioral issue of how real bars or columns behave and how we design them, we examine some pertinent experimental results for welded and rolled columns. Tall very nicely summarized the behavior of practical axially compressed columns in a comprehensive survey article [2-49]. He addressed many issues and details that are important practical considerations, but we will focus on only a few.

In general, the load-carrying capacity of a bar depends on how it is made, supported, and loaded. The following discussion is primarily applicable to ordinary structural steel and the processes used to make columns for building construction, namely rolled-steel columns and welded columns from plate stock. Welding induces both geometric changes as well as residual stresses in columns. Rolling does induce some residual stresses, but they are generally much less than in welded columns, and out-of-straightness is much less of a problem. Tall states "Welded columns tend to have a greater out-of-straightness than rolled columns, and even though all columns are straightened to minimum tolerances, the combined effect of the out-of-straightness and the large magnitudes of residual stress is so great that out-of-straightness must be considered with welded columns, where it is normally neglected with rolled columns" [2-49, p. 20]. Also, "The residual stress distribution ... in a cross section due to welding may be vastly different from that ... in a rolled shape due to cooling" [2-49, p. 19]. Accordingly, we should expect higher column strengths for rolled columns as opposed to welded columns. Moreover,

Éléments sous droits d'auteur

because of the high residual stresses, a column could fail by having stresses that exceed the strength of the material, i.e., by being overstressed instead of buckling. However, if a welded column is annealed, its strength improves substantially (because residual stresses are reduced by annealing, a form of heat treatment).

Consider the buckling strength of bars with 'small' rolled and welded cross sections (H and box). Plot the maximum load as a fraction of the yield load (P_{max}/P_y) versus the so-called slenderness ratio, in which

$$\lambda = \frac{1}{\pi}\frac{L}{r}\sqrt{\frac{\sigma_y}{E}} \tag{2.648}$$

for pinned-pinned bars in Figure 2-102. Note that λ is dimensionless. Of course, the effective-length factor, c, could be used to divide L to get results for other boundary conditions in accordance with Equation (2.173) on page 76. Note that λ is a measure both of the column geometrical slenderness and of the material properties, σ_y and E. Thus, steel columns with higher strength than mild steel can supposedly be evaluated, as can aluminum columns, in addition to columns made of other metals, although the nonlinearities in some materials are then not properly treated. The quantity λ is often called the slenderness ratio, but obviously two material properties are involved. If they are fixed, e.g., for a specific material, then λ is truly a geometric slenderness ratio.

Three curves are shown in Figure 2-102 in addition to the experimental data, namely the limiting yield curve, the Euler buckling curve, and the Column Research Council (CRC) (now known as the Structural Stability Research Council) behavior curve. The limiting yield curve represents a cut-off of yielding of the material irrespective of the slenderness ratio. The Euler buckling curve in Figure 2-102 is, of course, the hyper-

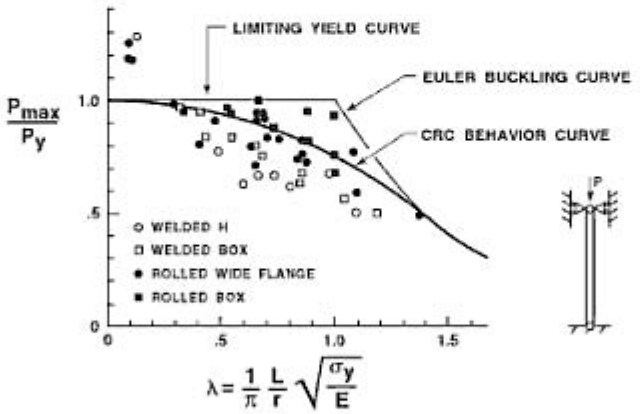


Figure 2-102 Buckling Results for Small Rolled and Welded Cross Sections including Theoretical, Experimental, and Representative Results *(After Tall [2-49])*

Éléments sous droits d'auteur

bolic elastic buckling behavior of a column as calculated by Euler. The CRC parabolic behavior curve in Figure 2-102 is an agreement by committee of what represents the actual behavior of real, as-manufactured, rolled-steel columns, so it is not surprising that the CRC curve passes through the middle of the rolled-steel column data in Figure 2-102. The equation for the CRC curve has two parts: (1) the behavior for the range in which the slenderness ratio is low and (2) the behavior for the range in which the slenderness ratio is high (and the results coincide with the Euler buckling curve) [2-50, page 32].

$$\frac{P_{max}}{P_y} = 1 - \frac{\lambda^2}{4} \quad \text{for } \lambda \le \sqrt{2}$$
$$\frac{P_{max}}{P_y} = \frac{1}{\lambda^2} \quad \text{for } \lambda \ge \sqrt{2} \tag{2.649}$$

Note that the CRC behavior curve meets the Euler buckling curve at values $P_{max}/P_y = 1/2$ and $\lambda = \sqrt{2}$. If a column were perfectly straight, free of residual stresses, supported on frictionless pins, and loaded in a perfectly centric manner, then all data would presumably fall on either the limiting yield curve or on the Euler buckling curve.

Welded steel columns typically have lower buckling loads than do equivalent rolled-steel columns as seen in Figure 2-102 for 'small' welded and rolled cross sections (H and box) as we expected because of the characteristics of welded elements mentioned previously in this section. The H welded cross section and the wide-flange rolled cross section are equivalent, but not identical. The wide-flange sections must have tapered flanges to allow rolling, whereas the H section is made with constant-thickness plates as flanges. Also, H-cross-section columns are weaker than box-cross-section columns for both welded and rolled construction.

The horizontal curve in Figure 2-102, i.e., the limiting yield curve, is the limit of the yield stress, σ_y, for the typical mild steel that is used in building construction. The idealized stress-strain curve for the early stress-strain behavior of such steels is shown in Figure 2-103 where we see an initial elastic portion followed by perfectly plastic yielding. This behavior is termed elastic – perfectly plastic behavior, and is notable for the unending yielding that takes place at σ_y in Figure 2-103.

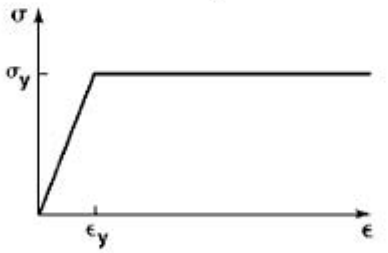


Figure 2-103 Idealized Elastic – Perfectly Plastic Stress-Strain Behavior

Éléments sous droits d'auteur

The behavior of the materials for which Figure 2-103 is appropriate is representative of the early stress-strain behavior of mild steels used for building construction with an extensive yield-strain range before the stress-strain curve again rises to the ultimate stress and failure of the material as in Figure 2-104. The horizontal or yield range is about twenty times the elastic strain to the yield stress, and that is the range of strains modeled with the elastic – perfectly plastic stress-strain curve of Figure 2-103. Many high-strength steels that are also used in building construction have a stress-strain behavior similar to the nonlinear stress-strain behavior of aluminum in Figure 2-78 on page 188. However, columns made of those materials are designed as if σ_y were the maximum stress they could bear at buckling. Note that σ_y for such steels is artificially defined as σ_{oy}, the offset yield stress, by the intersection of the stress-strain curve with a line parallel to the initial slope E from the point ε^p_{oy} (amount of permanent strain at σ_{oy}) on Figure 2-85 on page 196, not by the proportional limit. Thus, a nonnegligible amount of nonlinear behavior occurs prior to 'yielding' for these 'high-strength' steels. We should expect the design curves for structures made of mild steel as opposed to aluminum and other nonlinear stress-strain curve materials to have different shapes because of the different shapes of the respective stress-strain curves (Figure 2-103 versus Figure 2-78 on page 188).

More general buckling experimental results are shown for many types of column cross sections, manufacturing processes, and steels in Figure 2-105. The open-circle symbols shown are for all column conditions, and merely indicate scatter of the extensive measurements made. Consult Tall for the various conditions that are actually represented [2-49]. Obviously, the CRC behavior curve passes through the heart of the data if not a bit on the high side. Three curves in Figure 2-105 are identical to those in Figure 2-102, namely the limiting yield curve, the Euler buckling curve, and the CRC behavior curve. However, an additional curve, the AISC (American Institute of Steel Construction) design curve, is added to guide building and bridge designers who use doubly symmetric shapes with elements that meet certain minimum width-to-thickness ratios. The AISC design curve equations are obtained by dividing the two CRC behavior curves by a factor of safety:

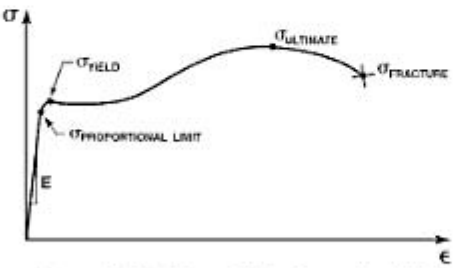


Figure 2-104 Stress-Strain Curve for Mild Steel

Éléments sous droits d'auteur

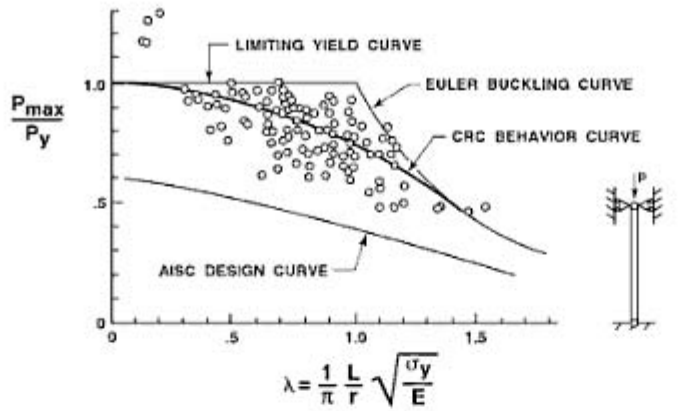


Figure 2-105 Experimental, Theoretical, and Design Buckling Results for Various Column Cross Sections and Steels *(After Tall [2-49])*

$$\frac{P_{max}}{P_y} = \frac{1 - \frac{\lambda^2}{4}}{\frac{5}{3} + \frac{3}{8\sqrt{2}}\lambda - \frac{1}{16\sqrt{2}}\lambda^3} \quad \text{for } \lambda \le \sqrt{2} \qquad (2.650)$$

$$\frac{P_{max}}{P_y} = \frac{\frac{1}{\lambda^2}}{\text{factor of safety}} \quad \text{for } \lambda \ge \sqrt{2}$$

For $\lambda \le \sqrt{2}$, the factor of safety depends on λ and varies from 1.67 at $\lambda = 0$ to 1.92 at $\lambda = \sqrt{2}$, and, for $\lambda > \sqrt{2}$, the factor of safety remains at 1.92 [2-50].

The AISC design equations are intended to represent a safe allowable load for a real structure, i.e., a factor of safety is included, whereas the CRC behavior curve is intended to represent the actual buckling behavior without a factor of safety. The factor of safety is, at minimum, on the order of 1.20, not large at all, relative to the lowest of the data plotted in Figure 2-105. Another very different design approach called Load and Resistance Factor Design [2-51] has replaced the AISC design equation in Equation (2.650), but our explanation of the design process related to the behavior facts is better exemplified by the 'old method'.

For bars made of materials with ever-rising stress-strain curves such as for aluminum in Figure 2-78 on page 188, there is no limiting yield curve as occurs in Figures 2-102 and 2-105. That is, there is no yield stress cut-off curve because the stress-strain behavior goes beyond yielding. Thus, buckling occurs above σ_y which is not a limit of stress-strain behavior for these highly nonlinear materials as it is for elastic – perfectly plastic materials. That the actual buckling load occurs above the yield load is shown for aluminum bars in Figure 2-89 on page 200.

Éléments sous droits d'auteur

2.11.7 Summary Remarks on Design

The *Guide to Stability Design Criteria for Metal Structures* is a rich source of information on many structural elements that are not covered in this book [2-52]. For example, some of the chapters are laterally supported beams; box girders; beam-columns; tapered structural members; composite columns; columns with lacing, battens, or perforated cover plates; members with elastic lateral restraints; frame stability; and arches. C. E. Massonnet chaired the European technical committee on rules for design of structures against buckling for Eurocode 3 (steel) and presented unofficial comments on the committee's considerations [2-53].

All design rules are based on accumulated research data and on vast practical experience with various column loading, support, and construction types. In design, taking advantage of, or copying, someone else's design that was successful is most appropriate behavior, certainly not plagiarism! In research and analysis, plagiarism is a grave offense. In design, by contrast, remember the words of Tom Lehrer's character, the great Russian mathematician Nickolai Ivanovich Lobachevsky[†]:

"In one word he told me secret of success in mathematics: Plagiarize!
Plagiarize,
Let no one else's work evade your eyes
Remember why the good lord made your eyes,
So don't shade your eyes,
But plagiarise, plagiarise, plagiarise -
Only be sure always to call it please *research*"

(copyright © 1952 and 1953 by Tom Lehrer).

2.12 BUCKLING OF BARS SUMMARY

The disturbing moment versus restoring moment approach to finding the buckling load of a bar seems straightforward. However, this method is very difficult to adapt to more general problems than those for which it was demonstrated in Sections 2.2 and 2.3. The various energy approaches developed in Sections 2.5 and 2.6 have the advantage of simplicity, yet *some* are hampered by terminology that inherently confuses the method of attack. We finally settled on the consistent energy approach based on the calculus of variations starting from the nonlinear strain-displacement relation. Note that Euler actually developed the calculus of variations to solve the bar buckling problem [2-2]! That approach can be used in either of two manners: (1) use of the variation in energy integrals to obtain the governing differential equation along with its associated boundary conditions or (2) use of the variation in energy integrals in the direct methods of the calculus of variations, namely, the Ray-

[†]Of course, Lehrer never met Lobachevski (1792–1856) because Lehrer wasn't born until 1928, but it makes an amusing song. Lobachevski actually was a renowned mathematician with a famous work in non-Euclidian geometry, Lobachevski space, Lobachevski's constant, and a crater on the far side of the moon named after him. However, Lobachevski's most famous book [2-54] has no such advice as 'Plagiarise'. For more information on Lehrer, go on the web at www.hometown.aol.com/sillysongbook/LEHRER.htm

Éléments sous droits d'auteur

leigh Method, the Rayleigh-Ritz Method, etc. or obviously the contemporary method of finite elements. Both of these manners of employing energy principles will be used to study the buckling behavior of plates in Chapter 3 and shells in Chapter 4.

Buckling of bars was treated with approaches ranging from the simplest that is typical of an introductory mechanics of materials course to an energy approach that is easily interpreted. Effects of bar end conditions, distributed load, changes in cross section, shear stiffness, and initial geometric imperfections were considered along with the effects of plastic deformation plus thermal expansion and constraint. In all cases, the buckling loads were readily expressed in the form

$$\bar{P} = c^2 \frac{E(\bar{P})I}{L^2} \tag{2.651}$$

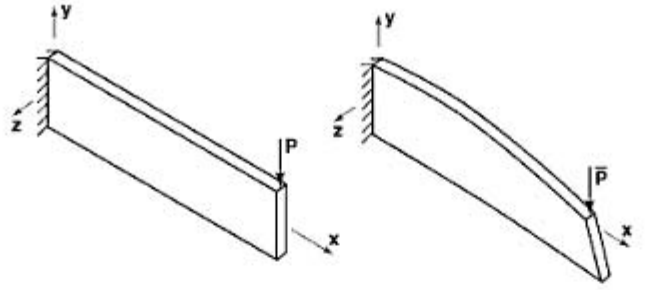
in which c is some factor peculiar to the boundary conditions of the specific problem and E(P) is the elastic modulus if the behavior is elastic, i.e., E(P) = E; otherwise, E(P) is some plastic modulus, preferably the tangent modulus. Although buckling load tests are difficult to perform accurately, reasonable experimental verification of the theories presented was found. Finally, design guidance was given in Section 2.11.

Some readers might wonder about the seeming obsession of most buckling researchers with the simply supported end boundary condition for bars. We most often consider a simply supported bar because of two factors. The most important factor is that the buckling load for a simply supported structural member is a lower bound on the buckling loads for all other support conditions except an end without any support, i.e., a free end. Such a consideration is quite important in design where support conditions are often difficult to model or even to determine with reasonable confidence. The second factor is that the procedure to calculate the buckling load for a simply supported structural member is nearly always easier than the calculation for another end condition.

Another bar buckling problem not addressed in this book, but deserving of mention, is lateral buckling of a transversely loaded beam with a narrow rectangular cross section as in Figure 2-106. There, an end-loaded cantilever beam will initially just deflect as usual in the negative y direction as in Figure 2-106a as long as the transverse load, P, is small enough. However, at some value of P, the normal downward deflection mode of the beam becomes becomes unstable, so the beam also deforms out of its original x-y plane, i.e., it buckles laterally as in Figure 2-106b. Prandtl [2-55] studied buckling of such a strip as his Ph.D. thesis in Munich, and Michell also addressed this problem [2-56]. Timoshenko [2-57] extended Prandtl's work to lateral buckling of a structural I beam as his Ph.D. dissertation under Prandtl. They all addressed issues of both essentially one-dimensional beam behavior as well as two-dimensional plate-like behavior.

von Kármán in his Ph.D. thesis under Prandtl in the early years of the 20th Century [2-37] performed highly sensitive column buckling experiments with great attention to support conditions and load eccentrici-

Éléments sous droits d'auteur



a Beam Deflection b Lateral Buckling

Figure 2-106 Lateral Buckling of a Transversely Loaded Beam

ties, and he also developed a theory of plastic buckling of columns. Those experiments and many others are admirably described by Singer, Arbocz, and Weller in a lucid review and discussion of many buckling research efforts in a two-volume book [2-58]. Included topics of special interest relative to this chapter on bar buckling are Roorda's experiments on bars, trusses, and frames from the 1960s [2-59]; the development of the Southwell plot in the 1930s for interpretation of experimental buckling results [2-60]; and generalizations and extensions of the Southwell plot by Lundquist [2-61] and Donnell [2-62].

I think it's very interesting that one now world-famous solid mechanician, Timoshenko, and another now world-famous aerodynamicist and structural mechanicist, von Kármán, started their professional careers with graduate work at the start of the twentieth century under another now world-famous fluid mechanician, Prandtl, and *all were working on buckling problems!* Thus, at least two fluid mechanicians started their professional careers as honest men.

Remember this very important message: experiments are used to uncover the fundamental behavior of a structure or structural element as well as to provide verification of theoretical predictions. That is, we must use experiments to determine the essential features of structural behavior as the very basis for developing a suitable theoretical model for use in design. Such philosophizing about the importance of experimental work is a significant contribution of the extremely useful book by Singer, Arbocz, and Weller [2-58], and I strongly suggest you consult it.

Other essentially one-dimensional buckling problems such as linkages, beam columns, frames, and rings are found in such sources as Timoshenko and Gere [2-6], Chajes [2-63], Brush and Almroth [2-64], Simitses [2-65], and Alfutov [2-66]. Hoff describes many aspects of the history, experimentation, and solution of buckling problems in his classic Wilbur Wright Memorial Lecture [2-67].

Éléments sous droits d'auteur

CHAPTER 2 REFERENCES

2-1 Leonhard Euler, On the Strength of Columns, *Academie Royale des Sciences et Belle Lettres Memoires*, Volume 13, p. 252, 1759. English translation by J. A. Van den Broek, Euler's Classic Paper 'On the Strength of Columns', *American Journal of Physics*, Volume 15, Number 4, July–August 1947, pp. 309–318.

2-2 Leonhard Euler, *Methodus Inveniendi Lineas Curvas Maximi Minimive Proprietate Gaudentes*, Marcum Michaelum Bousquet, Lausanne and Geneva, 1744.

2-3 J. L. Lagrange, Sur La Figure des Colonnes, *Misc. Taurinensia*, Volume 5, 1770–1773. Lagrange's work is also available in *Oeuvres de Lagrange*, Volume 2, pp. 125–170, Gauthier-Villars, Paris, 1868.

2-4 Stephen P. Timoshenko, *History of Strength of Materials*, McGraw-Hill, New York, 1953, pp. 30–36. Reprinted by Dover Publications, New York, 1983.

2-5 Eugene Jahnke and Fritz Emde, *Tables of Functions with Formulae and Curves*, 4th Edition, Dover Publications, New York, 1945.

2-6 Stephen P. Timoshenko and James M. Gere, *Theory of Elastic Stability*, 2nd Edition, McGraw-Hill, New York, 1961.

2-7 M. P. Nemeth, *The Elastica Problem*, unpublished lecture notes on *Buckling of Structures*, NASA Langley Research Center, Hampton, Virginia, 2001.

2-8 R. Frisch-Fay, *Flexible Bars*, Butterworths, Washington, 1962, p. 23.

2-9 F. Grashof, *Theorie der Elasticität und Festigkeit mit Bezug auf ihre Anwendungen in der Technik*, Second Edition, Gaertner, Berlin, 1878, p. 168 (according to Bleich, but no such equation appears directly in the reference).

2-10 Friedrich Bleich with the collaboration of Commander Lyle B. Ramsey, USN, edited by Hans H. Bleich, *Buckling Strength of Metal Structures*, McGraw-Hill, New York, 1952, p. 6.

2-11 George Gerard, *Introduction to Structural Stability Theory*, McGraw-Hill, New York, 1962, pp. 7–9.

2-12 E. P. Popov, *Mechanics of Materials*, 2nd Edition, Prentice-Hall, Englewood Cliffs, New Jersey, 1976, p. 465.

2-13 Henry L. Langhaar, *Energy Methods in Applied Mechanics*, Wiley, New York, 1962. Reprinted by Krieger, Malabar, Florida, 1989.

2-14 Irving H. Shames and Clive L. Dym, *Energy and Finite Element Methods in Structural Mechanics*, Taylor & Francis, Washington, D. C., 1985.

2-15 J. N. Reddy, *Energy and Variational Methods in Applied Mechanics*, Wiley, New York, 1984.

2-16 A. Pflüger, *Stabilitätsprobleme der Elastostatik*, Springer-Verlag, 2nd Edition, Berlin, 1964. See also NASA Technical Translation TT F-9777, National Aeronautics and Space Administration, Washington, D. C., March 1966.

2-17 E. Trefftz, Zur Theorie der Stabilität des elastischen Gleichgewichts, *Zeitschrift für angewandte Mathematik und Mechanik*, Volume 13, Number 2, April 1933, pp. 160–165.

2-18 M. K. Shen, Note on the Static Criterion of Elastic Stability, *Zeitschrift für Angewandte Mathematik*, Volume 48, Number 5, July 1968, pp. 356–357.

2-19 R. Courant and D. Hilbert, *Methods of Mathematical Physics*, Volume I, Interscience, New York, 1953, p. 185.

2-20 Karl Marguerre, Über die Anwendung der energetischen Methode auf Stabilitätsprobleme, Deutschen Versuchsanstalt für Luftfahrt Jahrbuch 1938, pp. 252–262. Also translated as *On the Application of the Energy Method to Stability Problems*, NACA Technical Memorandum TM 1138, National Advisory Committee on Aeronautics, Washington, D. C., October 1947.

2-21 Lord Rayleigh (John William Strutt), *The Theory of Sound*, First edition: Volume I, 1877, Volume II, 1878, Macmillan, London. First American edition, Dover Publications, New York, 1945.

2-22 Walther Ritz, Über eine neue Methode zur Lösung gewisser Variationsprobleme der Mathematischen Physik, *Journal für die Reine und Angewandte Mathematik* (also known as *Crelle's Journal* and *Borchardt's Journal für Mathematik*), Volume 135, Number 1, 1909, pp. 1–61. Also *Gesammelte Werke Walther Ritz Oeuves*, Gauthier-Villars, Paris, 1911, pp. 192–250.

2-23 H. A. Lang, Note on Rayleigh's Method and the Non-Uniform Strut, *Quarterly of Applied Mathematics*, Volume 5, Number 4, January 1948, pp. 510–511.

2-24 Georgi P. Tolstov, *Fourier Series*, translated by Richard A. Silverman, Dover, New York, 1976.

Éléments sous droits d'auteur

2-25 James Ward Brown and Ruel V. Churchill, *Fourier Series and Boundary Value Problems*, 5th edition, McGraw-Hill, New York, 1993.
2-26 A. G. Greenhill, Determination of the Greatest Height Consistent with Stability that a Vertical Pole or Mast can be Made, and of the Greatest Height to which a Tree of Given Proportions can Grow, *Proceedings of the Cambridge Philosophical Society*, Volume 4, Part II, 1881, pp. 65–73.
2-27 Granino A. Korn and Theresa M. Korn, *Mathematical Handbook for Scientists and Engineers*, 2nd Edition, McGraw-Hill, New York, 1968, Section 21.8.
2-28 S. P. Timoshenko and J. N. Goodier, *Theory of Elasticity*, McGraw-Hill, New York, 1970, pp. 41–46.
2-29 S. Timoshenko and D. H. Young, *Elements of Strength of Materials*, 5th edition, D. Van Nostrand, Princeton, New Jersey, 1968, pp. 224–230.
2-30 Irving H. Shames and James M. Pitarresi, *Introduction to Solid Mechanics*, 3rd Edition, Prentice Hall, Upper Saddle River, New Jersey, 2000, pp. 462–464.
2-31 Earl A. Thornton, *Thermal Structures for Aerospace Applications*, American Institute of Aeronautics and Astronautics, Reston, Virginia, 1996, Chapter Ten, pp. 397–406.
2-32 Robert M. Jones, Plastic Thermal Buckling of Uniformly Heated Bars with Temperature-Dependent Material Properties, AIAA Paper 2004-1709, *Proceedings of the 45th AIAA/ASME/ASCE/ AHS/ASC Structures, Structural Dynamics and Materials Conference*, 19-22 April 2004, Palm Springs, California, AIAA, Reston, Virginia.
2-33 Fr. Engesser, Ueber die Knickfestigkeit gerade Stäbe, *Zeitschrift des Architecten- und Ingenieur-Vereins zu Hannover*, Volume 35, 1889, pp. 455–462.
2-34 A. Considère, Résistance des Pièces Comprimés, Congrès International des Procédés de Constructions, Paris, 9-14 September 1889, *Comptes Rendus des Séances et Visites du Congrès*, Paris, Baudry et cie, Volume 3, 1891, Annexe, pp. 371–397. Librairie Polytechnique, Paris. OCLC 6974087.
2-35 F. Jasinski, Noch ein Wort zu den "Knickfragen", *Schweizerische Bauzeitung*, Volume XXV, Number 25, 23 June 1895, pp. 172–175.
2-36 Fr. Engesser, Ueber Knickfragen, *Schweizerische Bauzeitung*, Volume XXVI, Number 4, 27 July 1895, pp. 24–26.
2-37 Theodore von Kármán, Untersuchengen über Knickfestigkeit, *Mitteilungen über Forschungsarbeiten, Verein Deutscher Ingenieure*, Heft 81, Berlin, 1910, pp. 1–44. Reprinted in *Collected Works of Theodore von Kármán*, Butterworths, London, 1956, Volume I, 1902–1913, pp. 90–140.
2-38 F. R. Shanley, The Column Paradox, *Journal of the Aeronautical Sciences*, Volume 13, Number 12, December 1946, p.678.
2-39 F. R. Shanley, Inelastic Column Theory, *Journal of the Aeronautical Sciences*, Volume 14, Number 5, May 1947, pp. 261–268, including discussion by Theodore von Kármán.
2-40 J. L. Holmquist and A. Nadai, A Theoretical and Experimental Approach to the Problem of Collapse of Deep-Well Casing, *Drilling and Production Practice*, 1939 (American Petroleum Institute, 1940), pp. 392–420.
2-41 Walter Ramberg and William R. Osgood, *Description of Stress-Strain Curves by Three Parameters*, NACA Technical Note 902, National Advisory Committee on Aeronautics, Washington, D.C., July 1943.
2-42 R. L. Templin, R. G. Sturm, E. C. Hartmann, and M. Holt, Column Strength of Various Aluminum Alloys, Aluminum Research Laboratory Technical Paper Number 1, Aluminum Company of America, Pittsburgh, 1938. See also William R. Osgood and Marshall Holt, *The Column Strength of Two Extruded Aluminum-Alloy H-Sections*, NACA Report Number 656, National Advisory Committee on Aeronautics, Washington, D. C., 1939.
2-43 N. J. Hoff, Creep Buckling, *The Aeronautical Quarterly*, Volume VII, February 1956, pp. 1–20.
2-44 Harry Kraus, *Creep Analysis*, Wiley-Interscience, New York, 1980.
2-45 Robert M. Jones, *Mechanics of Composite Materials*, 2nd Edition, Taylor & Francis, Philadelphia, 1999.
2-46 C. E. Browning, G. E. Husman, and J. M. Whitney, Moisture Effects in Epoxy Matrix Composites, in *Composite Materials: Testing and Design (Fourth Conference)*, J. G. Davis, Jr. (Chairman), Valley Forge, Pennsylvania, 3–4 May 1976, ASTM STP 617, American Society for Testing and Materials, 1977, pp. 481–496.

Éléments sous droits d'auteur

2-47 J. M. Whitney and J. E. Ashton, Effect of Environment on the Elastic Response of Layered Composite Plates, *AIAA Journal*, Volume 9, Number 9, September 1971, pp. 1708–1713.
2-48 Edwin H. Gaylord, Jr., Charles N. Gaylord, and James E. Stallmeyer, *Design of Steel Structures*, 3rd edition, McGraw-Hill, New York, 1992.
2-49 Lambert Tall, Centrally Compressed Members, in *Axially Compressed Structures: Stability and Strength*, Edited by R. Narayanan, Elsevier Applied Science Publishers, London, 1982, pp. 1–40.
2-50 *Specification for the Design, Fabrication and Erection of Structural Steel for Buildings*, American Institute of Steel Construction, New York, 1978, p. 17.
2-51 *Load and Resistance Factor Design, Volume I, Structural Members Specifications & Codes*, 2nd Edition, American Institute of Steel Construction, New York, 1995.
2-52 Theodore V. Galambos, Editor, *Guide to Stability Design Criteria for Metal Structures*, sponsored by the Structural Stability Research Council (formerly the Column Research Council), John Wiley & Sons, New York, 1988.
2-53 C. E. Massonnet, The Collapse of Struts, Trusses and Frames: A Survey of Up-to-date Problems, pp. 183–208 in *Collapse: The Buckling of Structures in Theory and Practice*, Proceedings of the International Union of Theoretical and Applied Mechanics Symposium, London, 31 August through 3 September 1982, Edited by J. M. T. Thompson and G. W. Hunt, Cambridge University Press, Cambridge, 1983.
2-54 Nicolai Lobachevski, *Geometrical Researches on the Theory of Parallels*, Berlin, 1840. Also translated by George Bruce Halsted, Open Court Publishing, Chicago, 1914.
2-55 Ludwig Prandtl, Kipperscheinungen, thesis, Munich, 1899. Reprinted in *Ludwig Prandtl Gesammelte Abhandlungen zur angewandten Mechanik, Hydro- und Aerodynamik*, 3 Volumes, Springer-Verlag, Berlin/Göttingen/Heidelberg, 1961, Volume I, pp. 10–74.
2-56 A. G. M. Michell, Elastic Stability of Long Beams under Transverse Forces, *The London, Edinburgh, and Dublin Philosophical Magazine and Journal of Science*, Volume 48, Series 6, 1899, pp. 298–309.
2-57 S. P. Timoshenko, On Stability of the Lateral Form of Bending of an I-Beam under Forces acting in the Plane of its Maximum Stiffness, *Izvestiya S.-Peterburgskogo Politekhnicheskogo Instituta (Bulletin of the Polytechnical Institute of St. Petersburg*, Volume 4, Numbers 3 & 4, pp. 151–219, 1905; Volume 5, Numbers 1 & 2, pp. 3–34, 1906; and Volume 5, Numbers 3 & 4, pp. 263–292, 1906. Reprinted in *Stability of Beams, Plates, and Shells*, Fitzmatgiz, Moscow, 1971.
2-58 J. Singer, J. Arbocz, and T. Weller, *Buckling Experiments: Experimental Methods in Buckling of Thin-Walled Structures, Volume 1, Basic Concepts, Columns, Beams and Plates*, Wiley, Chichester, United Kingdom, 1998, *Volume 2, Shells, Built-up Structures and Additional Topics*, Wiley, New York, 2002.
2-59 J. Roorda, Instability of Imperfect Elastic Structures, Ph.D. Thesis, University of London, 1965.
2-60 R. V. Southwell, On the Analysis of Experimental Observations in Problems of Elastic Stability, *Proceedings of the Royal Society of London. Series A, Containing Papers of a Mathematical and Physical Character*, Volume 135, Issue 828, 1 April 1932, pp. 601–616.
2-61 E. E. Lundquist, Generalized Analysis of Experimental Observations in Problems of Elastic Stability, NACA Technical Note 658, National Advisory Committee on Aeronautics, Washington, D.C., July 1938.
2-62 L. H. Donnell, On the Application of Southwell's Method for the Analysis of Buckling Tests, *Contributions to the Mechanics of Solids dedicated to Stephen Timoshenko on the occasion of his sixtieth birthday anniversary*, MacMillan, New York, 1938, pp. 27–38.
2-63 Alexander Chajes, *Principles of Structural Stability Theory*, Prentice-Hall, Englewood Cliffs, New Jersey, 1974.
2-64 Don O. Brush and Bo O. Almroth, *Buckling of Bars, Plates, and Shells*, McGraw-Hill, New York, 1975.
2-65 George J. Simitses, *An Introduction to the Elastic Stability of Structures*, Prentice-Hall, Englewood Cliffs, New Jersey, 1976.
2-66 N. A. Alfutov, *Stability of Elastic Structures*, Springer, Berlin, 2000.
2-67 N. J. Hoff, Buckling and Stability, The Forty-First Wilbur Wright Memorial Lecture, Fourth Anglo-American Aeronautical Conference, London, 14 September 1953, *Journal of the Royal Aeronautical Society*, Volume 58, Number 517, January 1954, pp. 3–52.

Éléments sous droits d'auteur

Chapter 3

BUCKLING OF RECTANGULAR PLATES

3.1 INTRODUCTION

A plate is an essentially planar structural element with two large dimensions, a and b, in the plane of the plate as in Figure 3-1 and a much smaller dimension in the direction perpendicular to the plane of the plate (the thickness, t). The plate is loaded only in its plane. In buckling analyses, the plate is generally modeled as being perfectly flat, i.e., the initial transverse deflection, w, is zero over the entire surface of the plate. Therefore, the slopes, w_x and w_y, and the curvatures, w_{xx}, w_{xy}, and w_{yy}, are all initially zero. However, no restrictions are placed on the in-plane displacements u and v. Such solely in-plane deformations are possible only if the loads are in the plate mid-plane (except, as we will see, for plates that are unsymmetrically laminated about their mid-plane). That is, loads that are applied transverse to the plane of the plate do not cause buckling. As the in-plane load increases, the in-plane deformations increase until suddenly the plate undergoes a deviation from the flat state to a state that is bowed in the z-direction. Then, the transverse deflection, slopes, and curvatures become nontrivial, i.e., they aquire nonzero values. More generally, the plate undergoes a deviation from some not necessarily, but nearly, flat equilibrium state to a state that is (more) bowed in the z-direction. Evaluation of the quasi-static load at which this change in behavior occurs, i.e., the buckling load, is the principal objective of this chapter. Another important objective is to determine the nature of the behavior following buckling so we can assess the practical importance of the calculated buckling load.

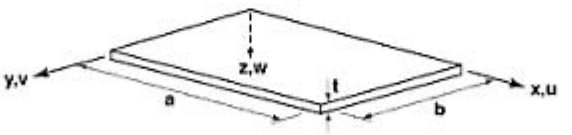


PLATE ASPECT RATIO = $\frac{a}{b}$

Figure 3-1 Plate Geometry

Éléments sous droits d'auteur

The forces and moments on a plate element are defined in Figures 3-2 and 3-3, respectively. Actually, in our analyses, we will use forces per unit width and moments per unit width of the plate edge on which they act instead of forces P_x, etc. in the various directions in order to reduce our approach to a two-dimensional theory. Those average forces per unit width are calculated as

$$N_x = \frac{P_x}{b} \quad N_y = \frac{P_y}{a} \quad N_{xy} = \frac{P_{shear_x}}{a} = \frac{P_{shear_y}}{b}$$

Note that K_x is the shear force transverse to the plate per unit width (the Kirchhoff shear force). However, we will call the forces per unit width and moments per unit width simply forces and moments for convenience of reference. The forces are positive in tension, so all buckling loads are negative (unless locally redefined). If a moment about the z-axis were applied on the edges $x = 0$ and $x = a$ in Figure 3-1, then N_x would be nonuniformly distributed along the edges in order to obtain the proper resultant moment. Of course, an axial force P_x could also be applied leading to a more complex distribution of N_x along the edges.

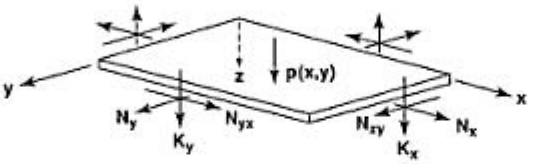


Figure 3-2 Plate Forces

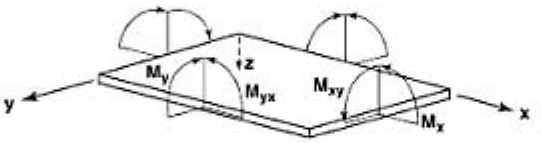


Figure 3-3 Plate Moments

Buckling of rectangular plates appears to have been first investigated by Bryan [3-1] for portions of ship plating under various loading conditions as in Figure 3-4 in which the compressive buckling forces, N_x and N_y, are shown, i.e., $N_x = -N_x$ and $N_y = -N_y$. Obviously, many boundary conditions must be considered as well in such applications. Other motivations for study of plate buckling problems include local buckling of long plate-type elements found in various structural shapes such as I-beams, angles, etc. as in the flanges shown in Figure 3-5. The webs of structural shapes are also susceptible to buckling. In fact, the actual design of the cross-sectional dimensions of both rolled and built-up structural shapes depends on buckling analysis. Practical applications of plates that can buckle are common in everyday engineering practice. For example,

Éléments sous droits d'auteur

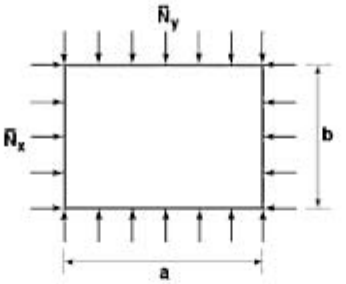


Figure 3-4 Representative Piece of Ship Plating Subjected to In-Plane Forces

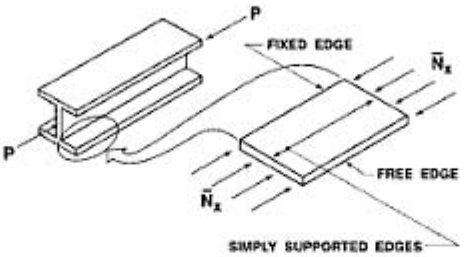


Figure 3-5 Local Buckling of a Beam

- flanges and webs of rolled or built-up beams and columns
- aircraft wing, tail, and rudder panels
- aircraft fuselage panels
- vehicle body panels in a collision
- shear walls in a building

After our experience with deriving bar buckling equations from several points of view, we now know the best and most effective approach in which the differences between equilibrium and buckling equations are revealed. Thus, we use that best approach to derive plate buckling equations along with their consistent boundary conditions. Part of the derivation will be devoted to the equilibrium differential equations in clarification of the difference between equilibrium and buckling equations. The subsequent sections are devoted to solution of various classical buckling problems with different loading and boundary conditions. In addition, postbuckling behavior results are displayed to gain perspective into the usefulness of the derived classical Euler buckling solutions. Next, the influence of multiple orthotropic layers, i.e., a laminated composite plate, on buckling is evaluated. Then, the effects of restrained thermal expansion on the buckling load are determined. Also, the effect of plastic deformation on the buckling load is investigated. Finally, some of the elements of design of both isotropic metal plates and fiber-reinforced laminated composite plates are addressed.

Éléments sous droits d'auteur

3.2 CONSISTENT DERIVATION OF EQUILIBRIUM EQUATIONS, BUCKLING EQUATIONS, AND BOUNDARY CONDITIONS

The differential equations governing equilibrium and buckling will be derived along with the associated boundary conditions. The appropriate energy expressions will be derived in the course of application of the governing equations to plate equilibrium and buckling problems.

The total potential energy can be varied (or expanded in a Taylor's series) about an equilibrium state to obtain

$$V + \Delta V = V + \delta V + \frac{1}{2!}\delta^2 V + \frac{1}{3!}\delta^3 V + \cdots \tag{3.1}$$

Equilibrium is expressed by use of the principle of stationary potential energy as we saw in Chapter 2 as

$$\delta V = 0 \tag{3.2}$$

and stability of that equilibrium state is expressed by

$$\bar{\delta}^2 V > 0 \tag{3.3}$$

(in which $\bar{\delta}^2 V = \delta^2 V|_{\delta V = 0}$) according to the principle of minimum potential energy. Equilibrium equations are obtained through the calculus of variations from $\delta V = 0$ and buckling equations from $\delta(\delta^2 V) = 0$. By making $\delta^2 V$ stationary, we determine where it can achieve a minimum. Alternatively, we could use $\bar{\delta}^2 V = 0$ to obtain the equations of neutral equilibrium, but we choose the former approach.

3.2.1 Variation of a Double Integral with Three Dependent Variables

Consider the integral

$$V = \iint_R F(x, y, u, u_x, u_y, v, v_x, v_y, w, w_x, w_y, w_{xx}, w_{xy}, w_{yy})dxdy \tag{3.4}$$

over the region R in which F is a function of three dependent variables, u, v, and w (and their derivatives for a total of twelve dependent variables) and two independent variables, x and y. Courant and Hilbert show that continuous partial derivatives of all dependent variables must exist in the region up to and including the fourth order, e.g., w_{xxxx} where subscripts x and y denote partial differentiation [3-2]. For a physical problem in which the dependent variables represent deflections of a plate, the deflection functions themselves must be continuous, as must their first derivatives, in order not to imply fracture of the body.

In the variational process, the three dependent variables, u, v, and w, are given the variations $\alpha\xi(x,y)$, $\beta\eta(x,y)$, and $\gamma\zeta(x,y)$, respectively. The functions ξ, η, and ζ are of the same class as u, v, and w, respectively, i.e., they have the same boundary conditions. The constants α, β, and γ are arbitrarily small. With these variations, V becomes

$$\begin{aligned} V + \Delta V = \iint_R F\Big(&x, y, u + \alpha\xi, u_x + \alpha\xi_x, u_y + \alpha\xi_y, v + \beta\eta, v_x + \beta\eta_x, \\ &v_y + \beta\eta_y, w + \gamma\zeta, w_x + \gamma\zeta_x, w_y + \gamma\zeta_y, \\ &w_{xx} + \gamma\zeta_{xx}, w_{xy} + \gamma\zeta_{xy}, w_{yy} + \gamma\zeta_{yy}\Big)dxdy \end{aligned} \tag{3.5}$$

Éléments sous droits d'auteur

Next, ΔV can be isolated from $V + \Delta V$ in Equation (3.5) by expanding Equation (3.5) and subtracting V. We see that ΔV is composed of variations involving the powers of α, β, and γ and is represented as

$$\Delta V = \delta V + \frac{1}{2!}\delta^2 V + \frac{1}{3!}\delta^3 V + \frac{1}{4!}\delta^4 V + \cdots \tag{3.6}$$

in which δV involves linear functions of α, β, and γ, $\delta^2 V$ involves quadratic functions of α, β, and γ, etc. The function F can be expanded in a Taylor's series, and the first and second variations can be identified as

$$\begin{aligned}
\delta V = {} & \alpha \iint \left[\xi \frac{\partial F}{\partial u} + \xi_x \frac{\partial F}{\partial u_x} + \xi_y \frac{\partial F}{\partial u_y} \right] dxdy \\
& + \beta \iint \left[\eta \frac{\partial F}{\partial v} + \eta_x \frac{\partial F}{\partial v_x} + \eta_y \frac{\partial F}{\partial v_y} \right] dxdy \\
& + \gamma \iint \left[\zeta \frac{\partial F}{\partial w} + \zeta_x \frac{\partial F}{\partial w_x} + \zeta_y \frac{\partial F}{\partial w_y} \right. \\
& \qquad \left. + \zeta_{xx} \frac{\partial F}{\partial w_{xx}} + \zeta_{xy} \frac{\partial F}{\partial w_{xy}} + \zeta_{yy} \frac{\partial F}{\partial w_{yy}} \right] dxdy
\end{aligned} \tag{3.7}$$

$$\begin{aligned}
\delta^2 V = {} & \alpha^2 \iint \left[\xi^2 \frac{\partial^2 F}{\partial u^2} + \xi_x^2 \frac{\partial^2 F}{\partial u_x^2} + \xi_y^2 \frac{\partial^2 F}{\partial u_y^2} \right. \\
& \qquad \left. + 2 \left[\xi \xi_x \frac{\partial^2 F}{\partial u \partial u_x} + \xi \xi_y \frac{\partial^2 F}{\partial u \partial u_y} + \xi_x \xi_y \frac{\partial^2 F}{\partial u_x \partial u_y} \right] \right] dxdy \\
& + \beta^2 \iint \left[\eta^2 \frac{\partial^2 F}{\partial v^2} + \eta_x^2 \frac{\partial^2 F}{\partial v_x^2} + \eta_y^2 \frac{\partial^2 F}{\partial v_y^2} \right. \\
& \qquad \left. + 2 \left[\eta \eta_x \frac{\partial^2 F}{\partial v \partial v_x} + \eta \eta_y \frac{\partial^2 F}{\partial v \partial v_y} + \eta_x \eta_y \frac{\partial^2 F}{\partial v_x \partial v_y} \right] \right] dxdy \\
& + \gamma^2 \iint \left[\zeta^2 \frac{\partial^2 F}{\partial w^2} + \zeta_x^2 \frac{\partial^2 F}{\partial w_x^2} + \zeta_y^2 \frac{\partial^2 F}{\partial w_y^2} + \zeta_{xx}^2 \frac{\partial^2 F}{\partial w_{xx}^2} + \zeta_{xy}^2 \frac{\partial^2 F}{\partial w_{xy}^2} \right. \\
& \qquad + \zeta_{yy}^2 \frac{\partial^2 F}{\partial w_{yy}^2} + 2 \left[\zeta \zeta_x \frac{\partial^2 F}{\partial w \partial w_x} + \zeta \zeta_y \frac{\partial^2 F}{\partial w \partial w_y} + \zeta \zeta_{xx} \frac{\partial^2 F}{\partial w \partial w_{xx}} \right. \\
& \qquad + \zeta \zeta_{xy} \frac{\partial^2 F}{\partial w \partial w_{xy}} + \zeta \zeta_{yy} \frac{\partial^2 F}{\partial w \partial w_{yy}} + \zeta_x \zeta_y \frac{\partial^2 F}{\partial w_x \partial w_y} \\
& \qquad + \zeta_x \zeta_{xx} \frac{\partial^2 F}{\partial w_x \partial w_{xx}} + \zeta_x \zeta_{xy} \frac{\partial^2 F}{\partial w_x \partial w_{xy}} + \zeta_x \zeta_{yy} \frac{\partial^2 F}{\partial w_x \partial w_{yy}} \\
& \qquad \left. \left. + \zeta_y \zeta_{xx} \frac{\partial^2 F}{\partial w_y \partial w_{xx}} + \zeta_y \zeta_{xy} \frac{\partial^2 F}{\partial w_y \partial w_{xy}} + \zeta_y \zeta_{yy} \frac{\partial^2 F}{\partial w_y \partial w_{yy}} \right] \right] dxdy
\end{aligned}$$

Éléments sous droits d'auteur

$$+\zeta_{xx}\zeta_{xy}\frac{\partial^2 F}{\partial w_{xx}\partial w_{xy}}+\zeta_{xx}\zeta_{yy}\frac{\partial^2 F}{\partial w_{xx}\partial w_{yy}}$$

$$+\zeta_{xy}\zeta_{yy}\frac{\partial^2 F}{\partial w_{xy}\partial w_{yy}}\Bigg]\Bigg]dxdy$$

$$+2\alpha\beta\iint\Bigg[\xi\eta\frac{\partial^2 F}{\partial u\partial v}+\xi\eta_x\frac{\partial^2 F}{\partial u\partial v_x}+\xi\eta_y\frac{\partial^2 F}{\partial u\partial v_y}$$

$$+\xi_x\eta\frac{\partial^2 F}{\partial u_x\partial v}+\xi_x\eta_x\frac{\partial^2 F}{\partial u_x\partial v_x}+\xi_x\eta_y\frac{\partial^2 F}{\partial u_x\partial v_y}$$

$$+\xi_y\eta\frac{\partial^2 F}{\partial u_y\partial v}+\xi_y\eta_x\frac{\partial^2 F}{\partial u_y\partial v_x}+\xi_y\eta_y\frac{\partial^2 F}{\partial u_y\partial v_y}\Bigg]dxdy$$

$$+2\alpha\gamma\iint\Bigg[\xi\zeta\frac{\partial^2 F}{\partial u\partial w}+\xi\zeta_x\frac{\partial^2 F}{\partial u\partial w_x}+\xi\zeta_y\frac{\partial^2 F}{\partial u\partial w_y}+\xi\zeta_{xx}\frac{\partial^2 F}{\partial u\partial w_{xx}}$$

$$+\xi\zeta_{xy}\frac{\partial^2 F}{\partial u\partial w_{xy}}+\xi\zeta_{yy}\frac{\partial^2 F}{\partial u\partial w_{yy}}+\xi_x\zeta\frac{\partial^2 F}{\partial u_x\partial w}+\xi_x\zeta_x\frac{\partial^2 F}{\partial u_x\partial w_x}$$

$$+\xi_x\zeta_y\frac{\partial^2 F}{\partial u_x\partial w_y}+\xi_x\zeta_{xx}\frac{\partial^2 F}{\partial u_x\partial w_{yy}}+\xi_x\zeta_{xy}\frac{\partial^2 F}{\partial u_x\partial w_{xy}}$$

$$+\xi_x\zeta_{yy}\frac{\partial^2 F}{\partial u_x\partial w_{yy}}+\xi_y\zeta\frac{\partial^2 F}{\partial u_y\partial w}+\xi_y\zeta_x\frac{\partial^2 F}{\partial u_y\partial w_x}+\xi_y\zeta_y\frac{\partial^2 F}{\partial u_y\partial w_y}$$

$$+\xi_y\zeta_{xx}\frac{\partial^2 F}{\partial u_y\partial w_{xx}}+\xi_y\zeta_{xy}\frac{\partial^2 F}{\partial u_y\partial w_{xy}}+\xi_y\zeta_{yy}\frac{\partial^2 F}{\partial u_y\partial w_{yy}}\Bigg]dxdy$$

$$+2\beta\gamma\iint\Bigg[\eta\zeta\frac{\partial^2 F}{\partial v\partial w}+\eta\zeta_x\frac{\partial^2 F}{\partial v\partial w_x}+\eta\zeta_y\frac{\partial^2 F}{\partial v\partial w_y}+\eta\zeta_{xx}\frac{\partial^2 F}{\partial v\partial w_{xx}}$$

$$+\eta\zeta_{xy}\frac{\partial^2 F}{\partial v\partial w_{xy}}+\eta\zeta_{yy}\frac{\partial^2 F}{\partial v\partial w_{yy}}+\eta_x\zeta\frac{\partial^2 F}{\partial v_x\partial w}+\eta_x\zeta_x\frac{\partial^2 F}{\partial v_x\partial w_x}$$

$$+\eta_x\zeta_y\frac{\partial^2 F}{\partial v_x\partial w_y}+\eta_x\zeta_{xx}\frac{\partial^2 F}{\partial v_x\partial w_{xx}}+\eta_x\zeta_{xy}\frac{\partial^2 F}{\partial v_x\partial w_{xy}}$$

$$+\eta_x\zeta_{yy}\frac{\partial^2 F}{\partial v_x\partial w_{yy}}+\eta_y\zeta\frac{\partial^2 F}{\partial v_y\partial w}+\eta_y\zeta_x\frac{\partial^2 F}{\partial v_y\partial w_x}+\eta_y\zeta_y\frac{\partial^2 F}{\partial v_y\partial w_y}$$

$$+\eta_y\zeta_{xx}\frac{\partial^2 F}{\partial v_y\partial w_{xx}}+\eta_y\zeta_{xy}\frac{\partial^2 F}{\partial v_y\partial w_{xy}}+\eta_y\zeta_{yy}\frac{\partial^2 F}{\partial v_y\partial w_{yy}}\Bigg]dxdy \tag{3.8}$$

and so on with equations of increasing complexity for higher order variations. The foregoing equations are utilized in the following sections.

Éléments sous droits d'auteur

3.2.2 First Variation of a Double Integral

Motivated by the principle of stationary potential energy, we equate the first variation of the double integral to zero, i.e., in Equation (3.7), set $\delta V = 0$. Then, because α, β, and γ are arbitrary, the following three integrals must be zero:

$$\iint \left[\xi \frac{\partial F}{\partial u} + \xi_x \frac{\partial F}{\partial u_x} + \xi_y \frac{\partial F}{\partial u_y} \right] dxdy = 0 \tag{3.9}$$

$$\iint \left[\eta \frac{\partial F}{\partial v} + \eta_x \frac{\partial F}{\partial v_x} + \eta_y \frac{\partial F}{\partial v_y} \right] dxdy = 0 \tag{3.10}$$

$$\iint \left[\zeta \frac{\partial F}{\partial w} + \zeta_x \frac{\partial F}{\partial w_x} + \zeta_y \frac{\partial F}{\partial w_y} + \zeta_{xx} \frac{\partial F}{\partial w_{xx}} + \zeta_{xy} \frac{\partial F}{\partial w_{xy}} + \zeta_{yy} \frac{\partial F}{\partial w_{yy}} \right] dxdy = 0 \tag{3.11}$$

In analogy to the situation already considered for bars in Chapter 2, we must do something like integrate by parts to be able to draw appropriate conclusions about the foregoing integrals. Integration by parts is usually written in the form

$$\int_A^B udv = uv\Big|_A^B - \int_A^B vdu \tag{3.12}$$

but can be written in the form

$$\int_A^B (udv + vdu) = uv\Big|_A^B \tag{3.13}$$

in which we convert an integral over an interval to a function of its constituent functions at the ends of the interval (the boundary). The two-dimensional analog of the one-dimensional integration by parts is called Green's Theorem in which an integral over a two-dimensional region R is converted to an integral around the boundary of the region, i.e.,

$$\iint_R \left[\frac{\partial v}{\partial x} - \frac{\partial u}{\partial y} \right] dxdy = \oint_C (udx + vdy) \tag{3.14}$$

in which C is the boundary of region R (see, e.g., Sokolnikoff and Redheffer [3-3]). The boundary integration is carried out in the clockwise direction when looking in the positive z-direction in Figure 3-1 on page 227.

Consider the special case of Green's Theorem in which $v = \phi\psi$ and $u = 0$ to obtain

$$\iint_R \phi \frac{\partial \psi}{\partial x} dxdy = -\iint_R \psi \frac{\partial \phi}{\partial x} dxdy + \oint_C \phi\psi dy \tag{3.15}$$

Similarly, when $v = 0$ and $u = \phi\psi$,

Éléments sous droits d'auteur

$$\iint_R \phi \frac{\partial \psi}{\partial y}\, dxdy = -\iint_R \psi \frac{\partial \phi}{\partial y}\, dxdy - \oint_C \phi\psi dx \tag{3.16}$$

Thus, we can obtain

$$\iint_R \xi_x \frac{\partial F}{\partial u_x}\, dxdy = -\iint_R \xi \frac{\partial}{\partial x}\left[\frac{\partial F}{\partial u_x}\right] dxdy + \oint_C \xi \frac{\partial F}{\partial u_x}\, dy \tag{3.17}$$

$$\iint_R \xi_y \frac{\partial F}{\partial u_y}\, dxdy = -\iint_R \xi \frac{\partial}{\partial y}\left[\frac{\partial F}{\partial u_y}\right] dxdy - \oint_C \xi \frac{\partial F}{\partial u_y}\, dx \tag{3.18}$$

Finally, Equation (3.9) can be written as

$$\iint_R \left[\frac{\partial F}{\partial u} - \frac{\partial}{\partial x}\left[\frac{\partial F}{\partial u_x}\right] - \frac{\partial}{\partial y}\left[\frac{\partial F}{\partial u_y}\right]\right] \xi\, dxdy + \oint_C \xi \frac{\partial F}{\partial u_x}\, dy - \oint_C \xi \frac{\partial F}{\partial u_y}\, dx = 0 \tag{3.19}$$

The following reasoning is used to obtain the differential equation and boundary conditions. First, because the function $\xi(x,y)$ is arbitrary, the double integral over the region can be made to vanish irrespective of the value of ξ on the boundary. Thus, we are left with the boundary integrals

$$\oint_C \xi \frac{\partial F}{\partial u_x}\, dy - \oint_C \xi \frac{\partial F}{\partial u_y}\, dx = 0 \tag{3.20}$$

For the special, but extremely common and useful, case of coincidence of coordinate lines with the boundaries of the region (such as the rectangle of a rectangular plate), the integrals in Equation (3.20) become

$$\begin{aligned} \oint_C \xi \frac{\partial F}{\partial u_x}\, dy &= \oint_{C_x} \xi \frac{\partial F}{\partial u_x}\, dy + \oint_{C_y} \xi \frac{\partial F}{\partial u_x}\, dy \\ \oint_C \xi \frac{\partial F}{\partial u_y}\, dx &= \oint_{C_x} \xi \frac{\partial F}{\partial u_y}\, dx + \oint_{C_y} \xi \frac{\partial F}{\partial u_y}\, dx \end{aligned} \tag{3.21}$$

in which C_x are lines of constant x coordinate lines and C_y are lines of constant y coordinate lines. Together, $C_x + C_y = C$. However, $dx = 0$ on C_x and $dy = 0$ on C_y, so we are left with

$$\oint_{C_x} \xi \frac{\partial F}{\partial u_x}\, dy - \oint_{C_x} \xi \frac{\partial F}{\partial u_y}\, dx = 0 \tag{3.22}$$

However, values of ξ on C_x are independent of values of ξ on C_y. Thus, the boundary integrals must vanish separately; this result can happen only if their integrands are identically zero. In summary, the following conditions must be satisfied. First, because ξ is arbitrary in region R;

$$\frac{\partial F}{\partial u} - \frac{\partial}{\partial x}\left[\frac{\partial F}{\partial u_x}\right] - \frac{\partial}{\partial y}\left[\frac{\partial F}{\partial u_y}\right] = 0 \quad \text{in R} \tag{3.23}$$

Éléments sous droits d'auteur

Then, from the separate vanishing of the boundary integrals;

$$\xi\left[\frac{\partial F}{\partial u_x}\right] = 0 \quad \text{on lines } x = \text{constant} \tag{3.24}$$

$$\xi\left[\frac{\partial F}{\partial u_y}\right] = 0 \quad \text{on lines } y = \text{constant} \tag{3.25}$$

in which Equation (3.23) is the Euler equation for the dependent variable u and Equations (3.24) and (3.25) are boundary conditions on that Euler equation. For example, if $u = 0$ on lines of $x = \text{constant}$, then ξ must also be zero and Equation (3.24) is satisfied identically. If, however, $u \neq 0$ on lines of $x = \text{constant}$, then $\xi \neq 0$ and we are left with $\partial F/\partial u_x = 0$.

For Equation (3.10), the Euler equation and boundary conditions analogous to Equations (3.23)–(3.25) are

$$\frac{\partial F}{\partial v} - \frac{\partial}{\partial x}\left[\frac{\partial F}{\partial v_x}\right] - \frac{\partial}{\partial y}\left[\frac{\partial F}{\partial v_y}\right] = 0 \quad \text{in R} \tag{3.26}$$

$$\eta\left[\frac{\partial F}{\partial v_x}\right] = 0 \quad \text{on lines } x = \text{constant} \tag{3.27}$$

$$\eta\left[\frac{\partial F}{\partial v_y}\right] = 0 \quad \text{on lines } y = \text{constant} \tag{3.28}$$

For Equation (3.11) in w and ζ, repeated applications of Equations (3.15) and (3.16) are necessary to obtain

$$\iint_R \zeta_{xx}\frac{\partial F}{\partial w_{xx}}\,dx\,dy = \iint_R \zeta\frac{\partial^2}{\partial x^2}\left[\frac{\partial F}{\partial w_{xx}}\right]dx\,dy + \oint_{C_x}\zeta_x\frac{\partial F}{\partial w_{xx}}\,dy - \oint_{C_x}\zeta\frac{\partial}{\partial x}\left[\frac{\partial F}{\partial w_{xx}}\right]dy \tag{3.29}$$

$$\iint_R \zeta_{yy}\frac{\partial F}{\partial w_{yy}}\,dx\,dy = \iint_R \zeta\frac{\partial^2}{\partial y^2}\left[\frac{\partial F}{\partial w_{yy}}\right]dx\,dy - \oint_{C_y}\zeta_y\frac{\partial F}{\partial w_{yy}}\,dx + \oint_{C_y} + \int_{C_y}\zeta\frac{\partial}{\partial y}\left[\frac{\partial F}{\partial w_{yy}}\right]dx \tag{3.30}$$

$$\begin{aligned}\iint_R \zeta_{xy}\frac{\partial F}{\partial w_{xy}}\,dx\,dy &= \iint_R \zeta\frac{\partial^2}{\partial x\partial y}\left[\frac{\partial F}{\partial w_{xy}}\right]dx\,dy + \oint_{C_y}\zeta\frac{\partial}{\partial x}\left[\frac{\partial F}{\partial w_{xy}}\right]dx + \oint_{C_x}\zeta_y\frac{\partial F}{\partial w_{xy}}\,dy \\ &= \iint_R \zeta\frac{\partial^2}{\partial x\partial y}\left[\frac{\partial F}{\partial w_{xy}}\right]dx\,dy - \oint_{C_x}\zeta\frac{\partial}{\partial y}\left[\frac{\partial F}{\partial w_{xy}}\right]dy - \oint_{C_y}\zeta_x\frac{\partial F}{\partial w_{xy}}\,dx\end{aligned} \tag{3.31}$$

Éléments sous droits d'auteur

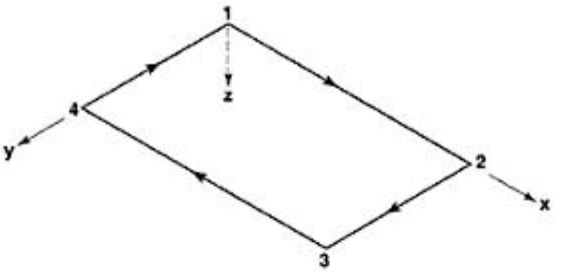


Figure 3-6 Integration over a Rectangular Region

Because of the appearance of two possible forms of Equations (3.31), i.e., the 'integration by parts' of the mixed derivative w_{xy}, further transformation is necessary. For a region bounded by lines of constant x and lines of constant y (coordinate lines), the boundary integrals can be integrated by parts once more. The region is illustrated in Figure 3-6, and the troublesome integrals are

$$\oint_{C_x} \zeta_y \frac{\partial F}{\partial w_{xy}}\,dy = \int_2^3 \zeta_y \frac{\partial F}{\partial w_{xy}}\,dy + \int_4^1 \zeta_y \frac{\partial F}{\partial w_{xy}}\,dy$$

$$= \zeta \frac{\partial F}{\partial w_{xy}}\bigg|_2^3 - \int_2^3 \zeta \frac{\partial}{\partial y}\left[\frac{\partial F}{\partial w_{xy}}\right]dy + \zeta \frac{\partial F}{\partial w_{xy}}\bigg|_4^1 - \int_4^1 \zeta \frac{\partial}{\partial y}\left[\frac{\partial F}{\partial w_{xy}}\right]dy$$

$$= \left[\zeta \frac{\partial F}{\partial w_{xy}}\right]\bigg|_1 - [\ ]|_2 + [\ ]|_3 - [\ ]|_4 - \oint_{C_x} \zeta \frac{\partial}{\partial y}\left[\frac{\partial F}{\partial w_{xy}}\right]dy \tag{3.32}$$

in which the blank terms in brackets are identical to the preceding term.

$$\oint_{C_y} \zeta_x \frac{\partial F}{\partial w_{xy}}\,dx = -\left[\zeta \frac{\partial F}{\partial w_{xy}}\right]\bigg|_1 + [\ ]|_2 - [\ ]|_3 + [\ ]|_4 - \oint_{C_y} \zeta \frac{\partial}{\partial x}\left[\frac{\partial F}{\partial w_{xy}}\right]dx \tag{3.33}$$

Finally,

$$\iint_R \zeta_{xy} \frac{\partial F}{\partial w_{xy}}\,dx\,dy = \iint_R \zeta \frac{\partial^2}{\partial x\,\partial y}\left[\frac{\partial F}{\partial w_{xy}}\right]dx\,dy + \oint_{C_y} \zeta \frac{\partial}{\partial x}\left[\frac{\partial F}{\partial w_{xy}}\right]dx$$

$$- \oint_{C_x} \zeta \frac{\partial}{\partial y}\left[\frac{\partial F}{\partial w_{xy}}\right]dy + \left[\zeta \frac{\partial F}{\partial w_{xy}}\right]\bigg|_1 - [\ ]|_2 + [\ ]|_3 - [\ ]|_4 \tag{3.34}$$

Éléments sous droits d'auteur

With the foregoing 'integrations by parts', Equation (3.11) becomes

$$\begin{aligned}
&\iint_R \left[\frac{\partial F}{\partial w} - \frac{\partial}{\partial x}\left[\frac{\partial F}{\partial w_x}\right] - \frac{\partial}{\partial y}\left[\frac{\partial F}{\partial w_y}\right] \right. \\
&\qquad \left. + \frac{\partial^2}{\partial x^2}\left[\frac{\partial F}{\partial w_{xx}}\right] + \frac{\partial^2}{\partial x \partial y}\left[\frac{\partial F}{\partial w_{xy}}\right] + \frac{\partial^2}{\partial y^2}\left[\frac{\partial F}{\partial w_{yy}}\right] \right] \zeta \, dx dy \\
&+ \oint_{C_x} \left[\frac{\partial F}{\partial w_x} - \frac{\partial}{\partial x}\left[\frac{\partial F}{\partial w_{xx}}\right] - \frac{\partial}{\partial y}\left[\frac{\partial F}{\partial w_{xy}}\right] \right] \zeta \, dy \\
&- \oint_{C_y} \left[\frac{\partial F}{\partial w_y} - \frac{\partial}{\partial y}\left[\frac{\partial F}{\partial w_{yy}}\right] - \frac{\partial}{\partial x}\left[\frac{\partial F}{\partial w_{xy}}\right] \right] \zeta \, dx \\
&- \oint_{C_y} \frac{\partial F}{\partial w_{yy}} \zeta_y dx + \oint_{C_x} \frac{\partial F}{\partial w_{xx}} \zeta_x dy \\
&+ \zeta \frac{\partial F}{\partial w_{xy}}\bigg|_1 - \zeta \frac{\partial F}{\partial w_{xy}}\bigg|_2 + \zeta \frac{\partial F}{\partial w_{xy}}\bigg|_3 - \zeta \frac{\partial F}{\partial w_{xy}}\bigg|_4 = 0
\end{aligned} \tag{3.35}$$

By reasoning developed previously, the term in brackets in the double integral must be zero as must *each* of the boundary terms. That is, the Euler equation for the dependent variable w is

$$\begin{aligned}
&\frac{\partial F}{\partial w} - \frac{\partial}{\partial x}\left[\frac{\partial F}{\partial w_x}\right] - \frac{\partial}{\partial y}\left[\frac{\partial F}{\partial w_y}\right] \\
&+ \frac{\partial^2}{\partial x^2}\left[\frac{\partial F}{\partial w_{xx}}\right] + \frac{\partial^2}{\partial x \partial y}\left[\frac{\partial F}{\partial w_{xy}}\right] + \frac{\partial^2}{\partial y^2}\left[\frac{\partial F}{\partial w_{yy}}\right] = 0 \quad \text{in R}
\end{aligned} \tag{3.36}$$

and the boundary conditions are obtained from

$$\left[\frac{\partial F}{\partial w_x} - \frac{\partial}{\partial x}\left[\frac{\partial F}{\partial w_{xx}}\right] - \frac{\partial}{\partial y}\left[\frac{\partial F}{\partial w_{xy}}\right] \right] \zeta = 0 \quad \text{on lines x = constant} \tag{3.37}$$

$$\left[\frac{\partial F}{\partial w_y} - \frac{\partial}{\partial y}\left[\frac{\partial F}{\partial w_{yy}}\right] - \frac{\partial}{\partial x}\left[\frac{\partial F}{\partial w_{xy}}\right] \right] \zeta = 0 \quad \text{on lines y = constant} \tag{3.38}$$

$$\left[\frac{\partial F}{\partial w_{xx}}\right] \zeta_x = 0 \quad \text{on lines x = constant} \tag{3.39}$$

$$\left[\frac{\partial F}{\partial w_{yy}}\right] \zeta_y = 0 \quad \text{on lines y = constant} \tag{3.40}$$

$$\left[\frac{\partial F}{\partial w_{xy}}\right] \zeta = 0 \quad \text{at } (x_1, y_1), (x_2, y_2), (x_3, y_3), (x_4, y_4) \tag{3.41}$$

in which (x_i, y_i) denotes the i^{th} corner of the region in Figure 3-6.

The Euler equations and boundary conditions to make the first variation of Equation (3.4) zero (i.e., to make Equation (3.4) stationary) have

Éléments sous droits d'auteur

been derived as Equations (3.23)–(3.25), (3.26)–(3.28), and (3.36)–(3.41). The geometric boundary conditions involve u, v, w, w_x, and w_y and hence ξ, η, ζ, ζ_x, and ζ_y because they must be of the same class. If all these quantities are zero, then there are no natural boundary conditions because the foregoing boundary conditions are satisfied identically. However, if any of the foregoing quantities is nonzero, then the corresponding natural boundary condition is obtained from the foregoing boundary conditions. If F in Equation (3.4) is used to describe a plate, then a clamped plate has all geometric boundary conditions. A simply supported plate has w = 0 (so $\zeta = 0$) and might or might not have u = 0 and v = 0 (and $\xi = 0$ with $\eta = 0$). Or, for an applied deformation in a load frame, u(0, y) = 0 at the base and u(a, y) = Δ at the top, so $\delta u = \delta\Delta = 0$ ($\xi = 0$) because Δ is fixed in magnitude. Thus, natural boundary conditions from the foregoing boundary condition equations must be invoked. Note that, for a plate, the last boundary condition, Equation (3.41), is related to the corner reaction. However, in order to explicitly show the corner reaction, the in-plane force boundary conditions, and the moment boundary conditions for a plate, the work of those quantities must be included in a boundary integral added to Equation (3.4). Addition of boundary integrals to Equation (3.4) does not affect the Euler equations because in principle they are already included by transformation into the region, R, from the boundary, C. The following work terms are important in practical problems.

If the work of an applied corner force, R,

$$\sum_{i=1}^{4} R_i w_i \tag{3.42}$$

were added to Equation (3.4), the variational process obviously leads to the boundary condition

$$\sum_{i=1}^{4} \left[R_i - \left[\frac{\partial F}{\partial w_{xy}} \right]_i \right] \zeta_i = 0 \tag{3.43}$$

whereupon the natural boundary condition (if $\zeta_i \neq 0$) is

$$R_i = \left[\frac{\partial F}{\partial w_{xy}} \right]_i \tag{3.44}$$

The work of pressure, p, transverse to the plate surface can be included in Equation (3.4) in its present form because

$$W_{e_p} = \iint_R p\, w\, dx\, dy \tag{3.45}$$

The work of edge moments is

$$W_{e_m} = -\oint_{C_x} \overline{M}_x w_x\, dy + \oint_{C_y} \overline{M}_y w_y\, dx \tag{3.46}$$

and has a first variation

Éléments sous droits d'auteur

$$\delta W_{e_m} = -\oint_{C_x} \bar{M}_x \zeta_x \, dy + \oint_{C_y} \bar{M}_y \zeta_y \, dx \tag{3.47}$$

and then the boundary conditions, Equations (3.39) and (3.40), become

$$\left[\bar{M}_x + \frac{\partial F}{\partial w_{xx}} \right] \zeta_x = 0 \quad \text{on lines } x = \text{constant} \tag{3.48}$$

$$\left[\bar{M}_y + \frac{\partial F}{\partial w_{yy}} \right] \zeta_y = 0 \quad \text{on lines } y = \text{constant} \tag{3.49}$$

The work of the in-plane forces (note that $N_{xy} = N_{yx}$ and also that $M_{xy} = -M_{yx}$ because $\tau_{xy} = \tau_{yx}$) is

$$W_{e_F} = -\oint_{C_y} (\bar{N}_y v + \bar{N}_{xy} u) dx + \oint_{C_x} (\bar{N}_x u + \bar{N}_{xy} v) dy \tag{3.50}$$

so Equations (3.24), (3.25), (3.27), and (3.28) become

$$\xi \left[\frac{\partial F}{\partial u_x} - \bar{N}_x \right] = 0 \quad \text{on lines } x = \text{constant} \tag{3.51}$$

$$\xi \left[-\frac{\partial F}{\partial u_y} + \bar{N}_{xy} \right] = 0 \quad \text{on lines } y = \text{constant} \tag{3.52}$$

$$\eta \left[\frac{\partial F}{\partial v_x} - \bar{N}_{xy} \right] = 0 \quad \text{on lines } x = \text{constant} \tag{3.53}$$

$$\eta \left[-\frac{\partial F}{\partial v_y} + \bar{N}_y \right] = 0 \quad \text{on lines } y = \text{constant} \tag{3.54}$$

Note that a force that is applied eccentrically relative to the plate reference surface can be resolved into a force and a moment. Thus, such a force can be treated within the context of the foregoing equations.

The work of distributed edge forces in the z-direction such as the Kirchhoff shear force is

$$W_{e_K} = -\oint_{C_y} \bar{K}_y w \, dx + \oint_{C_x} \bar{K}_x w \, dy \tag{3.55}$$

so that the boundary conditions, Equations (3.37) and (3.38), become

$$\left[\frac{\partial F}{\partial w_x} - \frac{\partial}{\partial x} \left[\frac{\partial F}{\partial w_{xx}} \right] - \frac{\partial}{\partial y} \left[\frac{\partial F}{\partial w_{xy}} \right] - \bar{K}_x \right] \zeta = 0 \text{ on lines } x = \text{constant} \tag{3.56}$$

$$\left[\frac{\partial F}{\partial w_y} - \frac{\partial}{\partial y} \left[\frac{\partial F}{\partial w_{yy}} \right] - \frac{\partial}{\partial x} \left[\frac{\partial F}{\partial w_{xy}} \right] - \bar{K}_y \right] \zeta = 0 \text{ on lines } y = \text{constant} \tag{3.57}$$

The Kirchhoff shear force was first identified by Kirchhoff [3-4] as the consistent boundary condition for plate theory. Previously, a nonconsistent shear boundary condition derived by observation caused great controversy because there were too many boundary conditions for the order of the differential equation.

Éléments sous droits d'auteur

3.2.3 Equilibrium Differential Equations and Boundary Conditions for von Kármán Plate Theory

We know from bar buckling theory in Chapter 2 that we must start with an equilibrium theory with moderately large-deflection terms in the strain-displacement relations. In von Kármán plate theory [3-5], as contrasted with classical plate theory, deflections are large enough that in-plane forces and displacements must be considered. Specifically, the strain-displacement relations for the middle surface of a plate are

$$\begin{aligned} \bar{\varepsilon}_x &= u_x + \frac{1}{2} w_x^2 \\ \bar{\varepsilon}_y &= v_y + \frac{1}{2} w_y^2 \\ \bar{\gamma}_{xy} &= v_x + u_y + w_x w_y \end{aligned} \tag{3.58}$$

in which the second-order terms are caused by moderate deformations (and the first-order terms exist by themselves for small deformations). The Kirchhoff presumption of a linear strain variation through the plate thickness [3-4] is invoked and signifies that

$$\begin{aligned} \varepsilon_x &= \bar{\varepsilon}_x + z\kappa_x \\ \varepsilon_y &= \bar{\varepsilon}_y + z\kappa_y \\ \gamma_{xy} &= \bar{\gamma}_{xy} + z\kappa_{xy} \end{aligned} \tag{3.59}$$

in which ε_x, ε_y, and γ_{xy} are the strains at any point through the thickness, z is the thickness coordinate measured from the reference surface, and κ_x, κ_y, and κ_{xy} are the middle-surface curvatures:

$$\begin{aligned} \kappa_x &= -w_{xx} \\ \kappa_y &= -w_{yy} \\ \kappa_{xy} &= -2w_{xy} \end{aligned} \tag{3.60}$$

An alternative description of the Kirchhoff hypothesis involves the following physical argument. If a line element that is originally perpendicular to the plate middle surface remains straight and perpendicular as well as inextensional under deformation of the plate, then straightness of the line element implies

$$\gamma_{yz} = 0 \qquad \gamma_{xz} = 0 \tag{3.61}$$

and the inextensional character of the line element implies

$$\varepsilon_z = 0 \tag{3.62}$$

We now make some observations about the geometry of the Kirchhoff hypothesis. First, a plane perpendicular to any line in the plate middle surface remains perpendicular after deformation that consists of bending (perceptible in Figure 3-7) and stretching (*not* perceptible in Figure 3-7). Thus, 'plane sections remain plane', but now we must simultaneously consider two perpendicular planes, i.e., the x-z plane and the y-z plane in Figure 3-7, and their intersection, the z-axis.

Éléments sous droits d'auteur

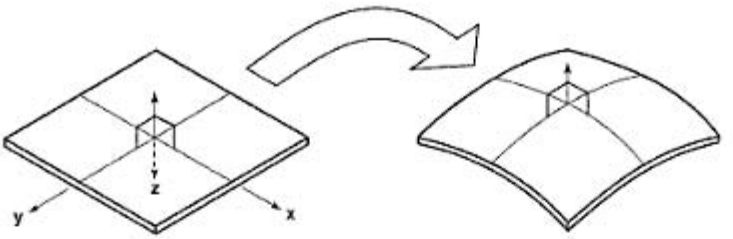


Figure 3-7 Deformation of a Plate

Simultaneously, the transverse stress is presumed to be zero:

$$\sigma_z = 0 \tag{3.63}$$

However, ε_z and σ_z cannot both be zero in any exact solution; thus, a contradiction exists. This type of contradiction is entirely consistent with fundamental mechanics of materials approaches in which a vastly simplifying presumption is made about the hypothesized behavior of a mechanical system. This contradiction is the crux of the Kirchhoff hypothesis; through use of the contradiction, an important and very effective approximation in structural mechanics is obtained. Part of the hypothesis is that a state of plane stress exists with nonzero stresses σ_x, σ_y, and τ_{xy} remaining in addition to the approximate state of plane strain with nonzero strains ε_x, ε_y, and γ_{xy}.

The strains are related to the stresses in an isotropic elastic material:

$$\begin{aligned}
\sigma_x &= \frac{E}{1-\nu^2}(\varepsilon_x + \nu\varepsilon_y) \\
\sigma_y &= \frac{E}{1-\nu^2}(\varepsilon_y + \nu\varepsilon_x) \\
\tau_{xy} &= \frac{E}{2(1+\nu)}\gamma_{xy}
\end{aligned} \tag{3.64}$$

in which E is the elastic modulus and ν is Poisson's ratio.

By definition, the strain energy for an isotropic elastic material with $\sigma_z = 0$, $\tau_{xz} = 0$, and $\tau_{yz} = 0$ is

$$U = \frac{1}{2E}\iint_R \left[\int_{-t/2}^{t/2}\left[\sigma_x^2 + \sigma_y^2 - 2\nu\sigma_x\sigma_y + 2(1+\nu)\tau_{xy}^2\right]dz\right]dxdy \tag{3.65}$$

in which Equations (3.59), (3.60), and (3.64) can be substituted and the result integrated through the thickness to obtain

$$U = U_m + U_b \tag{3.66}$$

in which U_m is the membrane strain energy,

$$U_m = \frac{Et}{2(1-\nu^2)}\iint_R \left[\bar{\varepsilon}_x^2 + \bar{\varepsilon}_y^2 + 2\nu\bar{\varepsilon}_x\bar{\varepsilon}_y + \frac{1}{2}(1-\nu)\bar{\gamma}_{xy}^2\right]dxdy \tag{3.67}$$

Éléments sous droits d'auteur

and U_b is the bending strain energy,

$$U_b = \frac{Et^3}{24(1-\nu^2)} \iint_R \left[w_{xx}^2 + w_{yy}^2 + 2\nu w_{xx} w_{yy} + 2(1-\nu) w_{xy}^2 \right] dx dy \quad (3.68)$$

The membrane strain energy is associated with deformations that take place primarily as stretching or contraction of the plate middle surface as if the plate were a thin piece of rubber (a membrane) that has no bending resistance but has good in-plane resistance. The bending strain energy is associated with deformations that take place as bending of the plate without any extension or contraction of the middle surface. Note that these two types of deformation and strain energy are separable for isotropic plates. However, for laminated composite plates and shells, such separation of deformations and energies does not always exist!

The potential energy of the external forces consists of that caused by transverse pressure, p, on the surface of the plate:

$$\Omega_p = -\iint_R p\, w\, dx\, dy \quad (3.69)$$

that caused by applied in-plane forces, $\bar{N}_x$ $\bar{N}_y$, and $\bar{N}_{xy}$:

$$\Omega_N = +\oint_{C_y} (\bar{N}_y v + \bar{N}_{xy} u) dx - \oint_{C_x} (\bar{N}_x u + \bar{N}_{xy} v) dy \quad (3.70)$$

that caused by applied edge moments, $\bar{M}_x$ and $\bar{M}_y$:

$$\Omega_M = +\oint_{C_x} \bar{M}_x w_x dy - \oint_{C_y} \bar{M}_y w_y dx \quad (3.71)$$

that caused by applied Kirchhoff shearing forces:

$$\Omega_K = +\oint_{C_y} \bar{K}_y w\, dx - \oint_{C_x} \bar{K}_x w\, dy \quad (3.72)$$

and that caused by applied corner forces

$$\Omega_R = \sum_{i=1}^{4} \bar{R}_i w_i \quad (3.73)$$

Next, substitute Equation (3.58) in Equations (3.67) and (3.68) and identify F in Equation (3.4) as

$$F = \frac{A}{2}\left[\left[u_x + \frac{1}{2} w_x^2 \right]^2 + \left[v_y + \frac{1}{2} w_y^2 \right]^2 + 2\nu \left[u_x + \frac{1}{2} w_x^2 \right] \left[v_y + \frac{1}{2} w_y^2 \right] + \left[\frac{1-\nu}{2} \right] (v_x + u_y + w_x w_y)^2 \right] + \frac{D}{2}\left[w_{xx}^2 + w_{yy}^2 + 2\nu w_{xx} w_{yy} + 2(1-\nu) w_{xy}^2 \right] - pw \quad (3.74)$$

in which $A = Et/(1-\nu^2)$ and $D = Et^3/[12(1-\nu^2)]$. Usually, A is called the extensional stiffness and D the bending stiffness because of the strain energy integrals with which those terms are associated. Sometimes the symbol B is used in place of A. Apparently, F is a quartic function in w_x

Éléments sous droits d'auteur

and w_y, and only Ω_p contributes to F. Note also that a bar over a symbol in the potential energy of external force terms denotes the applied force or moment at a boundary rather than an internal force or moment.

In the process of substitution of Equation (3.74) in the Euler equations and boundary conditions in Section 3.2.2, the following first partial derivatives of F are needed:

$$\frac{\partial F}{\partial u} = 0 \qquad \frac{\partial F}{\partial u_x} = A\left[(u_x + \frac{1}{2}w_x^2) + \nu(v_y + \frac{1}{2}w_y^2)\right] \qquad \frac{\partial F}{\partial v} = 0$$

$$\frac{\partial F}{\partial u_y} = \frac{A}{2}[(1-\nu)(v_x + u_y + w_x w_y)] \qquad \frac{\partial F}{\partial v_x} = \frac{A}{2}[(1-\nu)(v_x + u_y + w_x w_y)]$$

$$\frac{\partial F}{\partial v_y} = A\left[(v_y + \frac{1}{2}w_y^2) + \nu(u_x + \frac{1}{2}w_x^2)\right] \qquad \frac{\partial F}{\partial w} = -p$$

$$\frac{\partial F}{\partial w_x} = A\left[w_x(u_x + \frac{1}{2}w_x^2) + \nu w_x(v_y + \frac{1}{2}w_y^2) + \frac{(1-\nu)}{2}w_y(v_x + u_y + w_x w_y)\right]$$

$$\frac{\partial F}{\partial w_y} = A\left[w_y(v_y + \frac{1}{2}w_y^2) + \nu w_y(u_x + \frac{1}{2}w_x^2) + \frac{(1-\nu)}{2}w_x(v_x + u_y + w_x w_y)\right]$$

$$\frac{\partial F}{\partial w_{xx}} = D(w_{xx} + \nu w_{yy}) \qquad \frac{\partial F}{\partial w_{xy}} = 2D(1-\nu)w_{xy} \qquad \frac{\partial F}{\partial w_{yy}} = D(w_{yy} + \nu w_{xx}) \tag{3.75}$$

Substitute the $\partial F/\partial u_i$, Equation (3.75), in the Euler equations and boundary conditions of Section 3.2.2 to get the equilibrium equations

$$\frac{\partial}{\partial x}\left[(u_x + \frac{1}{2}w_x^2) + \nu(v_y + \frac{1}{2}w_y^2)\right] + \frac{1-\nu}{2}\frac{\partial}{\partial y}(v_x + u_y + w_x w_y) = 0 \tag{3.76}$$

$$\frac{1-\nu}{2}\frac{\partial}{\partial x}(v_x + u_y + w_x w_y) + \frac{\partial}{\partial_y}\left[(v_y + \frac{1}{2}w_y^2) + \nu(u_x + \frac{1}{2}w_x^2)\right] = 0 \tag{3.77}$$

$$-A\frac{\partial}{\partial x}\left[w_x\left[(u_x + \frac{1}{2}w_x^2) + \nu(v_y + \frac{1}{2}w_y^2)\right] + \frac{1-\nu}{2}w_y(v_x + u_y + w_x w_y)\right]$$

$$-A\frac{\partial}{\partial y}\left[w_y\left[(v_y + \frac{1}{2}w_y^2) + \nu(u_x + \frac{1}{2}w_x^2)\right] + \frac{1-\nu}{2}w_x(v_x + u_y + w_x w_y)\right]$$

$$+D\left[\frac{\partial^2}{\partial x^2}(w_{xx} + \nu w_{yy}) + 2(1-\nu)\frac{\partial^2}{\partial x \partial y}(w_{xy}) + \frac{\partial^2}{\partial y^2}(w_{yy} + \nu w_{xx})\right] = p \tag{3.78}$$

and the boundary conditions

$u = 0$ or $A\left[(u_x + \frac{1}{2}w_x^2) + \nu(v_y + \frac{1}{2}w_y^2)\right] = \bar{N}_x$ on lines x = constant

$v = 0$ or $A\left[(v_y + \frac{1}{2}w_y^2) + \nu(u_x + \frac{1}{2}w_x^2)\right] = \bar{N}_y$ on lines y = constant

$u = 0$ or $\frac{1-\nu}{2}A(v_x + u_y + w_x w_y) = \bar{N}_{xy}$ on lines y = constant

$v = 0$ or $\frac{1-\nu}{2}A(v_x + u_y + w_x w_y) = \bar{N}_{xy}$ on lines x = constant

Éléments sous droits d'auteur

$$w = 0 \text{ or } A\left[w_x\left[(u_x + \frac{1}{2}w_x^2) + \nu(v_y + \frac{1}{2}w_y^2)\right] + \frac{1-\nu}{2}w_y(v_x + u_y + w_x w_y)\right]$$
$$- D\left[\frac{\partial}{\partial x}(w_{xx} + \nu w_{yy}) + \frac{\partial}{\partial y}[2(1-\nu)w_{xy}]\right] = \bar{K}_x$$
$$\text{on lines } x = \text{constant}$$

$$w = 0 \text{ or } A\left[w_y\left[(v_y + \frac{1}{2}w_y^2) + \nu(u_x + \frac{1}{2}w_x^2)\right] + \frac{1-\nu}{2}w_x(v_x + u_y + w_x w_y)\right]$$
$$- D\left[\frac{\partial}{\partial y}(w_{yy} + \nu w_{xx}) + \frac{\partial}{\partial x}[2(1-\nu)w_{xy}]\right] = \bar{K}_y$$
$$\text{on lines } y = \text{constant}$$

$$w_x = 0 \text{ or } -D(w_{xx} + \nu w_{yy}) = \bar{M}_x \qquad \text{on lines } x = \text{constant}$$

$$w_y = 0 \text{ or } -D(w_{yy} + \nu w_{xx}) = \bar{M}_y \qquad \text{on lines } y = \text{constant}$$

$$w = 0 \text{ or } 2(1-\nu)Dw_{xy} = \bar{R} \quad \text{at corners} \tag{3.79}$$

The last condition at corners also applies at discontinuities in the integrand of the boundary integral.

An interesting situation arises for simply supported edges if the applied moment is zero, e.g., $\bar{M}_x = 0$ in the moment-curvature relation from Equation (3.79)

$$-D(w_{xx} + \nu w_{yy}) = \bar{M}_x \qquad \text{on lines } x = \text{constant}$$

If $w = 0$ along an edge with $x = \text{constant}$, then w_y and w_{yy} are necessarily zero, so $w_{xx} = 0$ because $\bar{M}_x = 0$. A similarly curious result occurs along edges $y = \text{constant}$ (w_x, w_{xx}, and $w_{yy} = 0$).

The foregoing equations can be simplified considerably if the following force-strain and moment-curvature relations are used in conjunction with the strain-displacement relations in Equation (3.58) and the curvature-displacement relations in Equation (3.60):

$$N_x = \int_{-t/2}^{t/2} \sigma_x \, dz = A(\bar{\varepsilon}_x + \nu\bar{\varepsilon}_y)$$
$$N_y = \int_{-t/2}^{t/2} \sigma_y \, dz = A(\bar{\varepsilon}_y + \nu\bar{\varepsilon}_x)$$
$$N_{xy} = \int_{-t/2}^{t/2} \tau_{xy} \, dz = \frac{1-\nu}{2}A\bar{\gamma}_{xy} \tag{3.80}$$

$$M_x = \int_{-t/2}^{t/2} \sigma_x \, z \, dz = D(\kappa_x + \nu\kappa_y)$$
$$M_y = \int_{-t/2}^{t/2} \sigma_y \, z \, dz = D(\kappa_y + \nu\kappa_x)$$
$$M_{xy} = \int_{-t/2}^{t/2} \tau_{xy} \, z \, dz = \frac{(1-\nu)}{2}D\kappa_{xy} \tag{3.81}$$

If the first two equilibrium equations are used to simplify the third equilibrium equation, the resulting equilibrium equations are

$$\frac{\partial N_x}{\partial x} + \frac{\partial N_{xy}}{\partial y} = 0 \tag{3.82}$$

Éléments sous droits d'auteur

$$\frac{\partial N_{xy}}{\partial x} + \frac{\partial N_y}{\partial y} = 0 \tag{3.83}$$

$$D\nabla^4 w - N_x w_{xx} - N_y w_{yy} - 2N_{xy} w_{xy} = p \tag{3.84}$$

in which

$$\nabla^4 w = \frac{\partial^4 w}{\partial x^4} + 2\frac{\partial^4 w}{\partial x^2 \partial y^2} + \frac{\partial^4 w}{\partial y^4} \tag{3.85}$$

The boundary conditions then become identities, e.g., $N_x = \bar{N}_x$, etc. Note that all displacements u,v,w are of the plate middle surface. Thus, boundary conditions are stipulations only along the edges of the middle surface itself, not on the entire thickness of the plate.

These moderately large-deflection equilibrium equations were first derived by von Kármán [3-5]. He applied them to equilibrium problems in which deformations were large enough that the membrane or in-plane forces provide a significant portion of the plate resistance. With the associated boundary conditions, we have a boundary-value problem.

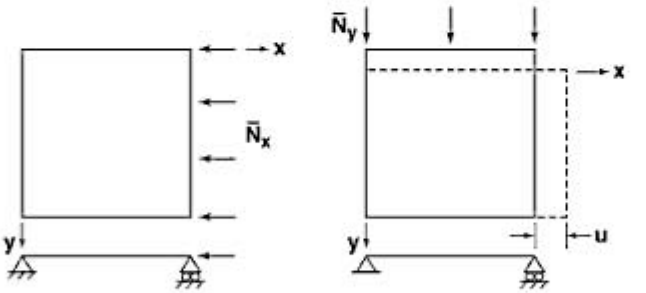
The statement after Equation (3.85) that the boundary conditions become identities, e.g., $N_x = N_x$ (the internal force N_x is equal to the applied external force $\bar{N}_x$ at the boundary), etc. requires further explanation. Actually, several possible interpretations occur for the boundary condition

$$\xi(N_x - \bar{N}_x) = 0 \text{ on } C_x \tag{3.86}$$

i.e., one of the following three possibilities for a particular problem:

1. When applied external force $\bar{N}_x$ is nonzero, i.e., when a load that does work is applied such as in Figure 3-8a, then $N_x = \bar{N}_x$ and $u \neq 0$ or
2. When $\bar{N}_x$ is zero, then either $\xi = 0$ whereupon $u = 0$ and N_x is equal to a reaction that does not do work or
3. $N_x = 0$, so the edge is free to move in the x-direction as in Figure 3-8b.

Similar explanations can be developed for the other boundary conditions.



a Plate Loaded in the x-direction b Plate Free to Deform in x-direction

Figure 3-8 Different In-Plane Boundary Conditions for the x-direction

Éléments sous droits d'auteur

A consistent and attractive notation for the various cases of simply supported and clamped edges was introduced for shells by Almroth [3-6]. We adapt that notation for plates:

Simply Supported Edges:

$$\begin{array}{lllll} \text{S1:} & w = 0 & M_n = 0 & u_n = \bar{u}_n & u_t = \bar{u}_t \\ \text{S2:} & w = 0 & M_n = 0 & N_n = \bar{N}_n & u_t = \bar{u}_t \\ \text{S3:} & w = 0 & M_n = 0 & u_n = \bar{u}_n & N_{nt} = \bar{N}_{nt} \\ \text{S4:} & w = 0 & M_n = 0 & N_n = \bar{N}_n & N_{nt} = \bar{N}_{nt} \end{array} \tag{3.87}$$

Clamped Edges:

$$\begin{array}{lllll} \text{C1:} & w = 0 & w_{,n} = 0 & u_n = \bar{u}_n & u_t = \bar{u}_t \\ \text{C2:} & w = 0 & w_{,n} = 0 & N_n = \bar{N}_n & u_t = \bar{u}_t \\ \text{C3:} & w = 0 & w_{,n} = 0 & u_n = \bar{u}_n & N_{nt} = \bar{N}_{nt} \\ \text{C4:} & w = 0 & w_{,n} = 0 & N_n = \bar{N}_n & N_{nt} = \bar{N}_{nt} \end{array} \tag{3.88}$$

The subscripts n and t denote the directions in the plane of the plate normal and tangential to the edge under consideration as in Figure 3-9. An overbar denotes an applied or a prescribed displacement, force, or moment value. Mostly, however, we use overbars to denote a buckling load or buckling displacement, so be careful with the overbar.

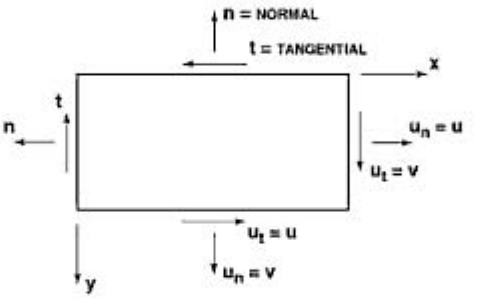


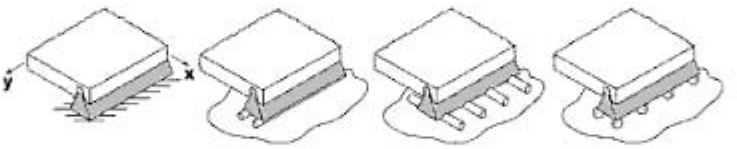
Figure 3-9 Boundary Condition Notation

A rectangular plate can be characterized as having any one of the eight conditions in Equations (3.87) and (3.88) on each of its four edges. The range of possibilities is, therefore, quite large [twelve possible conditions on each of the four edges if the free-edge conditions are included along with the simply supported and clamped or fixed edges in Equations (3.87) and (3.88)]. The simplest cases to analyze naturally involve like types of boundary conditions on opposite, if not all, edges. The emphasis in this book is on plates with four simply supported edges, so cases are chosen from those in Equation (3.87). Note that simply supported edges have no rotational restraint, but when this simplified terminology of simply supported edges is used, the specific in-plane conditions are not determined. Obviously, the totality of boundary conditions including in-plane conditions must be specified by stating, for example, that a solution is obtained for S1 boundary conditions. Failure to completely specify the boundary conditions leads only to confusion (instances in the literature can be cited!).

Éléments sous droits d'auteur

Consider the four possible simply supported edge support mechanisms, schematically illustrated in Figure 3-10, which are for easily understanding how the various supports *could* work. Only the reader can decide what support conditions are applicable to a specific structure. For all simply supported plate edges, the principal support mechanism in Figure 3-10 is a triangular prism with a circular-cross-section prismatic pivot on top as a schematic mechanism for the usual so-called knife-edge support for free rotation about the plate middle surface, i.e., $M_x = 0$. The end view of the triangular prism looks similar to the usual beam support, but with more realistic mechanisms that permit various movements. The pivot is a bearing that permits (limited) rotation about the y-axis through the center of the pivot which is located at the middle surface of the plate (although not precisely at the edge of the plate). The pivot fits in a cavity in the plate such that rotation around a y-direction axis is possible, but movement transverse to the plate surface is prevented ($w = 0$) and translation along a y-direction axis of the triangular prism is not permitted. The four manners of supporting the triangular prism are:

(1) For the S1 condition, the triangular prism is fastened to a horizontal surface so the prism cannot translate in either the x- or y-directions. Thus, $u = 0$ and $v = 0$. Hence, forces N_x and N_{xy} must exist.
(2) For the S2 condition, the triangular prism is supported on partially embedded y-direction roller bearings that permit translation in the x-direction, but translation cannot occur in the y-direction, so $u \neq 0$ and $v = 0$. Hence, force N_x must be zero, but N_{xy} must exist.
(3) For the S3 condition, the triangular prism is supported on partially embedded x-direction roller bearings that permit translation in the y-direction, but translation cannot occur in the x-direction, so $u = 0$ and $v \neq 0$. Hence, force N_x must exist, but N_{xy} must be zero.
(4) For the S4 condition, the triangular prism is supported on partially embedded spherical bearings that permit translation in any direction in the x-y plane. Thus, $u \neq 0$ and $v \neq 0$, so both forces N_x and N_{xy} must be zero.

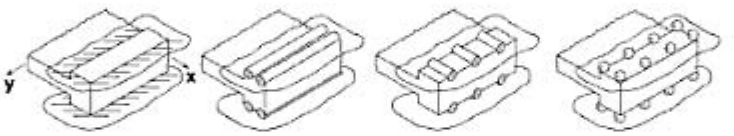


S1	S2	S3	S4
$w = 0$	$w = 0$	$w = 0$	$w = 0$
$M_x = 0$	$M_x = 0$	$M_x = 0$	$M_x = 0$
$u = 0$	$N_x = 0$	$u = 0$	$N_x = 0$
$v = 0$	$v = 0$	$N_{xy} = 0$	$N_{xy} = 0$

Figure 3-10 Simply Supported Edge Equilibrium Boundary Conditions

Éléments sous droits d'auteur

The analogous four boundary conditions for clamped edges are a little more difficult to perceive. The first impression for what constitutes a clamped edge might be the C1 condition of no displacements, u, v, and w, and no rotation, $\partial w/\partial x$. However, a clamped edge is commonly interpreted to mean only that the transverse displacement, w, and the edge rotation, $\partial w/\partial x$, are both zero *without specifying any in-plane displacement conditions*. Accordingly, the boxy mass that constitutes the clamping fixture in Figure 3-11 restrains both transverse displacement, w, and edge rotation, $\partial w/\partial x$. The way the clamping fixture is itself supported determines the in-plane boundary conditions. Thus, if the clamping fixture cannot move in the x-y plane, then u = 0 and v = 0 for the C1 condition. Only the C1 condition is truly clamped in every respect, i.e., entirely without displacement or rotation. The other clamped-edge conditions all have some form of in-plane movement permitted because various rollers are present. That is, the term clamped is interpreted to mean only that all boundaries have complete edge rotation restraint and no displacement occurs transverse to the plate surface. If the clamping fixture can roll in the x-direction, then $N_x = 0$, but v = 0 because no displacement occurs in the y-direction for the C2 boundary condition. Next, if the clamping fixture can roll in the y-direction but not in the x-direction, then $N_{xy} = 0$ and u = 0. Finally, if the clamping fixture can roll in both the x- and y-directions as if supported on frictionless balls, then the in-plane forces must be zero, i.e., $N_x = 0$ and $N_{xy} = 0$. The specific characteristics of these idealized models of support mechanisms are very difficult to achieve in practice.



C1	C2	C3	C4
$w = 0$	$w = 0$	$w = 0$	$w = 0$
$w_{,x} = 0$	$w_{,x} = 0$	$w_{,x} = 0$	$w_{,x} = 0$
$u = 0$	$N_x = 0$	$u = 0$	$N_x = 0$
$v = 0$	$v = 0$	$N_{xy} = 0$	$N_{xy} = 0$

Figure 3-11 Clamped-Edge Equilibrium Boundary Conditions

If the plate equilibrium equations, Equations (3.82), (3.83), and (3.84), are linearized, i.e., the nonlinear terms in the strain-displacement relations, Equation (3.58), are ignored, then the first two equilibrium equations, Equations (3.82) and (3.83), are decoupled from the last equilibrium equation, Equation (3.84). Accordingly, the boundary conditions on u and v are decoupled from those on w. Thus, the boundary conditions simplify to simply supported ($w = 0$ and $w_{,nn} = 0$) and clamped ($w = 0$ and $w_{,n} = 0$) for many transverse loading problems for plates.

Éléments sous droits d'auteur

3.2.4 First Variation of the Second Variation of a Double Integral

Buckling equations and associated boundary conditions will be derived by use of the principle of minimum potential energy expressed as

$$\delta(\bar{\delta}^2 V) = 0 \tag{3.89}$$

in which $\bar{\delta}^2 V$ is simply $\delta^2 V$ evaluated at $\delta V = 0$, i.e., at the equilibrium state that has already been determined. Equation (3.89) is the adjacent equilibrium buckling criterion or Trefftz buckling criterion described in Section 2.5.3 [3-7]. In order to obtain δV, a variation was given to the displacements, u_i, of the equilibrium state, i.e.,

$$u_i \rightarrow u_i + \delta u_i \tag{3.90}$$

in which the δu_i are the displacements away from the equilibrium state. By definition, δV is that part of the change in V that is linear in the variational displacements, δu_i. Similarly, $\delta^2 V$ is that part of the change in V that is quadratic in the δu_i.

We will emphasize the fact that the displacements *from* the equilibrium state, δu_i, are separate from the displacements *of* the equilibrium state, u_i, by relabeling the δu_i as $\bar{u}_i$. All quantities with variational symbols are associated with the physical act of buckling. These variations have no relation to what happens in the equilibrium state leading up to the buckling load. Then, if V was originally expressed in terms of the integral of a functional F of the displacements and their derivatives,

$$\delta^2 V = \iint_R \left[(\delta u)^2 \frac{\partial^2 F}{\partial u^2} + (\delta u_x)^2 \frac{\partial^2 F}{\partial u_x^2} + \cdots + (\delta u)(\delta v) \frac{\partial^2 F}{\partial u \partial v} + \cdots \right] dx dy \tag{3.91}$$

becomes

$$\bar{\delta}^2 V = \iint_R \left[\bar{u}^2 \frac{\partial^2 F}{\partial u^2} + \bar{u}_x^2 \frac{\partial^2 F}{\partial u_x^2} + \cdots + \bar{u}\,\bar{v} \frac{\partial^2 F}{\partial u \partial v} + \cdots \right] dx dy \tag{3.92}$$

in which the $\partial^2 F / \partial u_i \partial u_j$ are evaluated for equilibrium-state displacements.

Next, employ the notation

$$\bar{\delta}^2 V = \iint_R H \, dx dy \tag{3.93}$$

in which H is defined as the integrand in Equation (3.92). Then, a statement that $\bar{\delta}^2 V$ must be stationary according to the principle of minimum potential energy results in

$$\delta(\bar{\delta}^2 V) = \iint_R \left[\delta\bar{u} \frac{\partial H}{\partial \bar{u}} + \delta\bar{u}_x \frac{\partial H}{\partial \bar{u}_x} + \cdots \right] dx dy = 0 \tag{3.94}$$

Satisfaction of Equation (3.94) signifies that stability has ceased to exist in the original equilibrium state. However, the new equilibrium state is immediately adjacent, so the buckling load is stable and exists at a *stable symmetric bifurcation point* as on pages 20–21 in Section 1.3. The new functional H is treated in Equation (3.94) just as F was when the Euler

Éléments sous droits d'auteur

equations for $\delta V = 0$ were sought. Note, however, that the boundary conditions are now homogeneous because the second variations of the boundary integrals are all zero (the variations of the work done by applied loads do not contribute to $\delta^2 V$). Thus, the magnitude of the displacements of the buckled state from the equilibrium state is indeterminate.

For a solution to the buckling problem, the equilibrium state just before buckling must be known, i.e., the $\partial^2 F/\partial u_i \partial u_j$ must be known in Equation (3.92). In many simple cases, such as uniform in-plane loading of a plate without any cutouts (holes), the solution for the prebuckling equilibrium state is taken to be a membrane state, i.e., idealized as a pure expansion or contraction in the plane of the plate without any bending. However, the membrane solution is obviously not a rigorous solution. The membrane solution is paradoxical because its boundary conditions are entirely unrelated to the normal concepts of simply supported or clamped edges because, by definition, the membrane solution signifies no bending near the edges. Apparently, a rigorous buckling analysis must include a realistic equilibrium (prebuckling) solution which is some cases such as a plate with a cutout can be quite complicated. However, we can show that almost negligible accuracy is sacrificed by use of buckling analyses based on a membrane prebuckling solution.

Because of its relation to the second variation of V, H is a quadratic function of the $\bar{u}_i$ and their derivatives. Consequently, the differential equations resulting from the variational process are linear. Then, the first variation involving H can be determined explicitly in terms of $\bar{u}_i$ and $\partial^2 F/\partial u_i \partial u_j$ where the latter terms are evaluated in the equilibrium state. For a membrane prebuckling solution, the $\partial^2 F/\partial u_i \partial u_j$ are constants, i.e., not a function of x and y. Hence, the buckling differential equations have constant coefficients. Because the $\partial^2 F/\partial u_i \partial u_j$ are functions of x and y for other than a membrane prebuckling shape, the resulting buckling differential equations have nonconstant coefficients. The latter equations are solvable only by numerical techniques.

From a general viewpoint, the buckling problem appears to be a linear eigenvalue problem because the characteristic values (buckling loads) are sought for linear differential equations with homogeneous boundary conditions. Further classification and ease in solution depends on whether the coefficients in the differential equation are constant or nonconstant.

In accordance with the foregoing discussion, Equation (3.8) can be written in the notation of Equation (3.92) as

$$\bar{\delta}^2 V = \iint \left[\left[\bar{u}^2 \frac{\partial^2 F}{\partial u^2} + \bar{u}_x^2 \frac{\partial^2 F}{\partial u_x^2} + \bar{u}_y^2 \frac{\partial^2 F}{\partial u_y^2} + 2 \left[\bar{u}\,\bar{u}_x \frac{\partial^2 F}{\partial u \partial u_x} + \bar{u}\,\bar{u}_y \frac{\partial^2 F}{\partial u \partial u_y} + \bar{u}_x \bar{u}_y \frac{\partial^2 F}{\partial u_x \partial u_y} \right] \right] + \left[\bar{v}^2 \frac{\partial^2 F}{\partial v^2} + \bar{v}_x^2 \frac{\partial^2 F}{\partial v_x^2} + \bar{v}_y^2 \frac{\partial^2 F}{\partial v_y^2} \right.$$

Éléments sous droits d'auteur

$$+2\left[\bar{v}\,\bar{v}_x\frac{\partial^2 F}{\partial v\partial v_x}+\bar{v}\,\bar{v}_y\frac{\partial^2 F}{\partial v\partial v_y}+\bar{v}_x\bar{v}_y\frac{\partial^2 F}{\partial v_x\partial v_y}\right]\Bigg]$$

$$+\left[\bar{w}^2\frac{\partial^2 F}{\partial w^2}+\bar{w}_x^2\frac{\partial^2 F}{\partial w_x^2}+\bar{w}_y^2\frac{\partial^2 F}{\partial w_y^2}+\bar{w}_{xx}^2\frac{\partial^2 F}{\partial w_{xx}^2}+\bar{w}_{xy}^2\frac{\partial^2 F}{\partial w_{xy}^2}\right.$$

$$+\bar{w}_{yy}^2\frac{\partial^2 F}{\partial w_{yy}^2}+2\left[\bar{w}\,\bar{w}_x\frac{\partial^2 F}{\partial w\partial w_x}+\bar{w}\,\bar{w}_y\frac{\partial^2 F}{\partial w\partial w_y}\right.$$

$$+\bar{w}\,\bar{w}_{xx}\frac{\partial^2 F}{\partial w\partial w_{xx}}+\bar{w}\,\bar{w}_{xy}\frac{\partial^2 F}{\partial w\partial w_{xy}}+\bar{w}\,\bar{w}_{yy}\frac{\partial^2 F}{\partial w\partial w_{yy}}$$

$$+\bar{w}_x\bar{w}_y\frac{\partial^2 F}{\partial w_x\partial w_y}+\bar{w}_x\bar{w}_{xx}\frac{\partial^2 F}{\partial w_x\partial w_{xx}}+\bar{w}_x\bar{w}_{xy}\frac{\partial^2 F}{\partial w\partial w_{xy}}$$

$$+\bar{w}_x\bar{w}_{yy}\frac{\partial^2 F}{\partial w_x\partial w_{yy}}+\bar{w}_y\bar{w}_{xx}\frac{\partial^2 F}{\partial w_y\partial w_{xx}}+\bar{w}_y\bar{w}_{xy}\frac{\partial^2 F}{\partial w_y\partial w_{xy}}$$

$$+\bar{w}_y\bar{w}_{yy}\frac{\partial^2 F}{\partial w_y\partial w_{yy}}+\bar{w}_{xx}\bar{w}_{xy}\frac{\partial^2 F}{\partial w_{xx}\partial w_{xy}}+\bar{w}_{xx}\bar{w}_{yy}\frac{\partial^2 F}{\partial w_{xx}\partial w_{yy}}$$

$$\left.+\bar{w}_{xy}\bar{w}_{yy}\frac{\partial^2 F}{\partial w_{xy}\partial w_{yy}}\right]\Bigg]+2\left[\bar{u}\,\bar{v}\frac{\partial^2 F}{\partial u\partial v}+\bar{u}\,\bar{v}_x\frac{\partial^2 F}{\partial u\partial v_x}\right.$$

$$+\bar{u}\,\bar{v}_y\frac{\partial^2 F}{\partial u\partial v_y}+\bar{u}_x\bar{v}\frac{\partial^2 F}{\partial u_x\partial v}+\bar{u}_x\bar{v}_x\frac{\partial^2 F}{\partial u_x\partial v_x}+\bar{u}_x\bar{v}_y\frac{\partial^2 F}{\partial u_x\partial v_y}$$

$$\left.+\bar{u}_y\bar{v}\frac{\partial^2 F}{\partial u_y\partial v}+\bar{u}_y\bar{v}_x\frac{\partial^2 F}{\partial u_y\partial v_x}+\bar{u}_y\bar{v}_y\frac{\partial^2 F}{\partial u_y\partial v_y}\right]$$

$$+2\left[\bar{u}\,\bar{w}\frac{\partial^2 F}{\partial u\partial w}+\bar{u}\,\bar{w}_x\frac{\partial^2 F}{\partial u\partial w_x}+\bar{u}\,\bar{w}_y\frac{\partial^2 F}{\partial u\partial w_y}+\bar{u}\,\bar{w}_{xx}\frac{\partial^2 F}{\partial u\partial w_{xx}}\right.$$

$$+\bar{u}\,\bar{w}_{xy}\frac{\partial^2 F}{\partial u\partial w_{xy}}+\bar{u}\,\bar{w}_{yy}\frac{\partial^2 F}{\partial u\partial w_{yy}}+\bar{u}_x\bar{w}\frac{\partial^2 F}{\partial u_x\partial w}+\bar{u}_x\bar{w}_x\frac{\partial^2 F}{\partial u_x\partial w_x}$$

$$+\bar{u}_x\bar{w}_y\frac{\partial^2 F}{\partial u_x\partial w_y}+\bar{u}_x\bar{w}_{xx}\frac{\partial^2 F}{\partial u_x\partial w_{xx}}+\bar{u}_x\bar{w}_{xy}\frac{\partial^2 F}{\partial u_x\partial w_{xy}}$$

$$+\bar{u}_x\bar{w}_{yy}\frac{\partial^2 F}{\partial u_x\partial w_{yy}}+\bar{u}_y\bar{w}\frac{\partial^2 F}{\partial u_y\partial w}+\bar{u}_y\bar{w}_x\frac{\partial^2 F}{\partial u_y\partial w_x}+\bar{u}_y\bar{w}_y\frac{\partial^2 F}{\partial u_y\partial w_y}$$

$$\left.+\bar{u}_y\bar{w}_{xx}\frac{\partial^2 F}{\partial u_y\partial w_{xx}}+\bar{u}_y\bar{w}_{xy}\frac{\partial^2 F}{\partial u_y\partial w_{xy}}+\bar{u}_y\bar{w}_{yy}\frac{\partial^2 F}{\partial u_y\partial w_{yy}}\right]$$

$$+2\left[\bar{v}\,\bar{w}\frac{\partial^2 F}{\partial v\partial w}+\bar{v}\,\bar{w}_x\frac{\partial^2 F}{\partial v\partial w_x}+\bar{v}\,\bar{w}_y\frac{\partial^2 F}{\partial v\partial w_y}+\bar{v}\,\bar{w}_{xx}\frac{\partial^2 F}{\partial v\partial w_{xx}}\right.$$

Éléments sous droits d'auteur

$$+\bar{v}\,\bar{w}_{xy}\frac{\partial^2 F}{\partial v\partial w_{xy}}+\bar{v}\,\bar{w}_{yy}\frac{\partial^2 F}{\partial v\partial w_{yy}}+\bar{v}_x\bar{w}\frac{\partial^2 F}{\partial v_x\partial w}+\bar{v}_x\bar{w}_x\frac{\partial^2 F}{\partial v_x\partial w_x}$$
$$+\bar{v}_x\bar{w}_y\frac{\partial^2 F}{\partial v_x\partial w_y}+\bar{v}_x\bar{w}_{xx}\frac{\partial^2 F}{\partial v_x\partial w_{xx}}+\bar{v}_x\bar{w}_{xy}\frac{\partial^2 F}{\partial v_x\partial w_{xy}}$$
$$+\bar{v}_x\bar{w}_{yy}\frac{\partial^2 F}{\partial v_x\partial w_{yy}}+\bar{v}_y\bar{w}\frac{\partial^2 F}{\partial v_y\partial w}+\bar{v}_y\bar{w}_x\frac{\partial^2 F}{\partial v_y\partial w_x}+\bar{v}_y\bar{w}_y\frac{\partial^2 F}{\partial v_y\partial w_y}$$
$$+\bar{v}_y\bar{w}_{xx}\frac{\partial^2 F}{\partial v_y\partial w_{xx}}+\bar{v}_y\bar{w}_{xy}\frac{\partial^2 F}{\partial v_y\partial w_{xy}}+\bar{v}_y\bar{w}_{yy}\frac{\partial^2 F}{\partial v_y\partial w_{yy}}\Bigg]\Bigg]dxdy \tag{3.95}$$

Next, $\bar{\delta}^2V$ can be made stationary by use of Equation (3.94). The details of the procedure are the same as in the derivation of the Euler equations for equilibrium in Section 3.2.2, so the Euler equations for buckling are

$$\frac{\partial H}{\partial \bar{u}}-\frac{\partial}{\partial x}\left[\frac{\partial H}{\partial \bar{u}_x}\right]-\frac{\partial}{\partial y}\left[\frac{\partial H}{\partial \bar{u}_y}\right]=0 \tag{3.96}$$

$$\frac{\partial H}{\partial \bar{v}}-\frac{\partial}{\partial x}\left[\frac{\partial H}{\partial \bar{v}_x}\right]-\frac{\partial}{\partial y}\left[\frac{\partial H}{\partial \bar{v}_y}\right]=0 \tag{3.97}$$

$$\frac{\partial H}{\partial \bar{w}}-\frac{\partial}{\partial x}\left[\frac{\partial H}{\partial \bar{w}_x}\right]-\frac{\partial}{\partial y}\left[\frac{\partial H}{\partial \bar{w}_y}\right]+\frac{\partial^2}{\partial x^2}\left[\frac{\partial H}{\partial \bar{w}_{xx}}\right]+\frac{\partial^2}{\partial x\partial y}\left[\frac{\partial H}{\partial \bar{w}_{xy}}\right]+\frac{\partial^2}{\partial y^2}\left[\frac{\partial H}{\partial \bar{w}_{yy}}\right]=0 \tag{3.98}$$

and the boundary conditions are

on lines x = constant: $\bar{u}=0$ or $\frac{\partial H}{\partial \bar{u}_x}=0$ (3.99)

on lines y = constant: $\bar{u}=0$ or $\frac{\partial H}{\partial \bar{u}_y}=0$ (3.100)

on lines x = constant: $\bar{v}=0$ or $\frac{\partial H}{\partial \bar{v}_x}=0$ (3.101)

on lines y = constant: $\bar{v}=0$ or $\frac{\partial H}{\partial \bar{v}_y}=0$ (3.102)

on lines x = constant:

$$\bar{w}=0 \text{ or } \frac{\partial H}{\partial \bar{w}_x}-\frac{\partial}{\partial x}\left[\frac{\partial H}{\partial \bar{w}_{xx}}\right]-\frac{\partial}{\partial y}\left[\frac{\partial H}{\partial \bar{w}_{xy}}\right]=0 \tag{3.103}$$

Éléments sous droits d'auteur

on lines y = constant:

$$\bar{w} = 0 \quad \text{or} \quad \frac{\partial H}{\partial \bar{w}_y} - \frac{\partial}{\partial y}\left[\frac{\partial H}{\partial \bar{w}_{yy}}\right] - \frac{\partial}{\partial x}\left[\frac{\partial H}{\partial \bar{w}_{xy}}\right] = 0 \tag{3.104}$$

on lines x = constant:

$$\bar{w}_x = 0 \quad \text{or} \quad \frac{\partial H}{\partial \bar{w}_{xx}} = 0 \tag{3.105}$$

on lines y = constant:

$$\bar{w}_y = 0 \quad \text{or} \quad \frac{\partial H}{\partial \bar{w}_{yy}} = 0 \tag{3.106}$$

at corners:

$$\bar{w} = 0 \quad \text{or} \quad \frac{\partial H}{\partial \bar{w}_{xy}} = 0 \tag{3.107}$$

The foregoing boundary conditions are homogeneous because all static equilibrium considerations (boundary conditions) are, by definition, taken care of (satisfied) in the equilibrium state. Often, the potential energy of external forces is a linear function of the displacements; hence, $\delta^2\Omega = 0$ and only $\delta^2 U$ remains in $\delta^2 V$. This observation was made by Trefftz [3-7] and results in a buckling criterion of $\delta(\delta^2 U) = 0$.

From inspection of Equation (3.95), the following index notation is convenient:

$$H = \bar{u}_i \bar{u}_j \frac{\partial^2 F}{\partial u_i \partial u_j} \tag{3.108}$$

in which repeated subscripts indicate summation; $\bar{u}_i$ represents the various buckling displacements and their derivatives, i.e., $\bar{u}_i = (\bar{u}, \bar{u}_x, \bar{u}_y, \bar{v}, \bar{v}_x, \bar{v}_y, \bar{w}, \bar{w}_x, \bar{w}_y, \bar{w}_{xx}, \bar{w}_{xy}, \bar{w}_{yy})$; and u_i represents the various equilibrium displacements and their derivatives, i.e., $u_i = (u, u_x, u_y, v, v_x, v_y, w, w_x, w_y, w_{xx}, w_{xy}, w_{yy})$. The subscript i ranges from 1 to 12, i.e., $u_{12} = w_{yy}$. Then, the partial derivatives of H with respect to the $\bar{u}_i$ are

$$\frac{\partial H}{\partial \bar{u}_i} = 2\bar{u}_j \frac{\partial^2 F}{\partial u_i \partial u_j} \tag{3.109}$$

in which the $\dfrac{\partial^2 F}{\partial u_i \partial u_j}$ are known from the equilibrium solution and, for example

$$\begin{aligned}\frac{\partial H}{\partial \bar{u}} = 2\Bigg[& \bar{u}\frac{\partial^2 F}{\partial u^2} + \bar{u}_x \frac{\partial^2 F}{\partial u \partial u_x} + \bar{u}_y \frac{\partial^2 F}{\partial u \partial u_y} + \bar{v}\frac{\partial^2 F}{\partial u \partial v} + \bar{v}_x \frac{\partial^2 F}{\partial u \partial v_x} + \bar{v}_y \frac{\partial^2 F}{\partial u \partial v_y} \\ & + \bar{w}\frac{\partial^2 F}{\partial u \partial w} + \bar{w}_x \frac{\partial^2 F}{\partial u \partial w_x} + \bar{w}_y \frac{\partial^2 F}{\partial u \partial w_y} \\ & + \bar{w}_{xx}\frac{\partial^2 F}{\partial u \partial w_{xx}} + \bar{w}_{xy}\frac{\partial^2 F}{\partial u \partial w_{xy}} + \bar{w}_{yy}\frac{\partial^2 F}{\partial u \partial w_{yy}} \Bigg]\end{aligned} \tag{3.110}$$

With the index notation, the Euler equations for buckling become

Éléments sous droits d'auteur

$$\bar{u}_j \frac{\partial^2 F}{\partial u \partial u_j} - \frac{\partial}{\partial x}\left[\bar{u}_j \frac{\partial^2 F}{\partial u_x \partial u_j}\right] - \frac{\partial}{\partial y}\left[\bar{u}_j \frac{\partial^2 F}{\partial u_y \partial u_j}\right] = 0 \tag{3.111}$$

$$\bar{u}_j \frac{\partial^2 F}{\partial v \partial u_j} - \frac{\partial}{\partial x}\left[\bar{u}_j \frac{\partial^2 F}{\partial v_x \partial u_j}\right] - \frac{\partial}{\partial y}\left[\bar{u}_j \frac{\partial^2 F}{\partial v_y \partial u_j}\right] = 0 \tag{3.112}$$

$$\bar{u}_j \frac{\partial^2 F}{\partial w \partial u_j} - \frac{\partial}{\partial x}\left[\bar{u}_j \frac{\partial^2 F}{\partial w_x \partial u_j}\right] - \frac{\partial}{\partial y}\left[\bar{u}_j \frac{\partial^2 F}{\partial w_y \partial u_j}\right] + \frac{\partial^2}{\partial x^2}\left[\bar{u}_j \frac{\partial^2 F}{\partial w_{xx} \partial u_j}\right] + \frac{\partial^2}{\partial x \partial y}\left[\bar{u}_j \frac{\partial^2 F}{\partial w_{xy} \partial u_j}\right] + \frac{\partial^2}{\partial y^2}\left[\bar{u}_j \frac{\partial^2 F}{\partial w_{yy} \partial u_j}\right] = 0 \tag{3.113}$$

and the boundary conditions become

$$\bar{u} = 0 \text{ or } \bar{u}_j \frac{\partial^2 F}{\partial u_x \partial u_j} = 0 \quad \text{on lines } x = \text{constant} \tag{3.114}$$

$$\bar{u} = 0 \text{ or } \bar{u}_j \frac{\partial^2 F}{\partial u_y \partial u_j} = 0 \quad \text{on lines } y = \text{constant} \tag{3.115}$$

$$\bar{v} = 0 \text{ or } \bar{u}_j \frac{\partial^2 F}{\partial v_x \partial u_j} = 0 \quad \text{on lines } x = \text{constant} \tag{3.116}$$

$$\bar{v} = 0 \text{ or } \bar{u}_j \frac{\partial^2 F}{\partial v_y \partial u_j} = 0 \quad \text{on lines } y = \text{constant} \tag{3.117}$$

$$\bar{w} = 0 \text{ or } \bar{u}_j \frac{\partial^2 F}{\partial w_x \partial u_j} - \frac{\partial}{\partial x}\left[\bar{u}_j \frac{\partial^2 F}{\partial w_{xx} \partial u_j}\right] - \frac{\partial}{\partial y}\left[\bar{u}_j \frac{\partial^2 F}{\partial w_{xy} \partial u_j}\right] = 0$$

$$\text{on lines } x = \text{constant} \tag{3.118}$$

$$\bar{w} = 0 \text{ or } \bar{u}_j \frac{\partial^2 F}{\partial w_y \partial u_j} - \frac{\partial}{\partial y}\left[\bar{u}_j \frac{\partial^2 F}{\partial w_{yy} \partial u_j}\right] - \frac{\partial}{\partial x}\left[\bar{u}_j \frac{\partial^2 F}{\partial w_{xy} \partial u_j}\right] = 0$$

$$\text{on lines } y = \text{constant} \tag{3.119}$$

$$\bar{w}_x = 0 \text{ or } \bar{u}_j \frac{\partial^2 F}{\partial w_{xx} \partial u_j} = 0 \quad \text{on lines } x = \text{constant} \tag{3.120}$$

$$\bar{w}_y = 0 \text{ or } \bar{u}_j \frac{\partial^2 F}{\partial w_{yy} \partial u_j} = 0 \quad \text{on lines } y = \text{constant} \tag{3.121}$$

$$\bar{w} = 0 \text{ or } \bar{u}_j \frac{\partial^2 F}{\partial w_{xy} \partial u_j} = 0 \quad \text{at corners} \tag{3.122}$$

An example of the application of the foregoing general equations to obtain buckling differential equations is given in Section 3.2.5.

Éléments sous droits d'auteur

3.2.5 Buckling Differential Equations and Energy Expressions for a Rectangular Plate with In-Plane Loads

We begin with the same strain-displacement relations for moderately large displacements as in Section 3.2.3 and use the same total potential energy expression except that we discard all potential energy of external forces terms except those caused by compressive in-plane forces, $\bar{N}_x$ and $\bar{N}_y$ plus shear force, $\bar{N}_{xy}$, that cause buckling and are depicted in Figure 3-12. Note that N_x is positive in tension, so $N_x = -\bar{N}_x$.

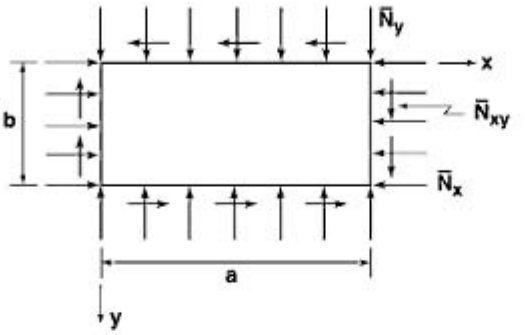


Figure 3-12 Simply Supported Rectangular Plate with In-Plane Loads

To find the second variation of the total potential energy, the following partial derivatives are first obtained from Equation (3.75):

$$\frac{\partial^2 F}{\partial u_x^2} = A \quad \frac{\partial^2 F}{\partial u_x \partial u_y} = 0 \quad \frac{\partial^2 F}{\partial u_x \partial v_x} = 0 \quad \frac{\partial^2 F}{\partial u_x \partial v_y} = \nu A \quad \frac{\partial^2 F}{\partial u_x \partial w} = 0$$

$$\frac{\partial^2 F}{\partial u_x \partial w_x} = Aw_x \quad \frac{\partial^2 F}{\partial u_x \partial w_y} = \nu Aw_y \quad \frac{\partial^2 F}{\partial u_x \partial w_{xx}} = 0 \quad \frac{\partial^2 F}{\partial u_x \partial w_{xy}} = 0$$

$$\frac{\partial^2 F}{\partial u_x \partial w_{yy}} = 0 \quad \frac{\partial^2 F}{\partial u_y^2} = \frac{1-\nu}{2} A \quad \frac{\partial^2 F}{\partial u_y \partial v_x} = \frac{1-\nu}{2} A \quad \frac{\partial^2 F}{\partial u_y \partial v_y} = 0$$

$$\frac{\partial^2 F}{\partial u_y \partial w} = 0 \quad \frac{\partial^2 F}{\partial u_y \partial w_x} = \frac{1-\nu}{2} Aw_y \quad \frac{\partial^2 F}{\partial u_y \partial w_y} = \frac{1-\nu}{2} Aw_x \quad \frac{\partial^2 F}{\partial u_y \partial w_{xx}} = 0$$

$$\frac{\partial^2 F}{\partial u_y \partial w_{xy}} = 0 \quad \frac{\partial^2 F}{\partial u_y \partial w_{yy}} = 0 \quad \frac{\partial^2 F}{\partial v_x^2} = \frac{1-\nu}{2} A \quad \frac{\partial^2 F}{\partial v_x \partial v_y} = 0 \quad \frac{\partial^2 F}{\partial v_x \partial w} = 0$$

$$\frac{\partial^2 F}{\partial v_x \partial w_x} = \frac{1-\nu}{2} Aw_y \quad \frac{\partial^2 F}{\partial v_x \partial w_y} = \frac{1-\nu}{2} Aw_x \quad \frac{\partial^2 F}{\partial v_x \partial w_{xx}} = 0 \quad \frac{\partial^2 F}{\partial v_x \partial w_{xy}} = 0$$

$$\frac{\partial^2 F}{\partial v_x \partial w_{yy}} = 0 \quad \frac{\partial^2 F}{\partial v_y^2} = A \quad \frac{\partial^2 F}{\partial v_y \partial w} = 0 \quad \frac{\partial^2 F}{\partial v_y \partial w_x} = \nu Aw_x \quad \frac{\partial^2 F}{\partial v_y \partial w_y} = Aw_y$$

Éléments sous droits d'auteur

$$\frac{\partial^2 F}{\partial v_y \partial w_{xx}} = 0 \quad \frac{\partial^2 F}{\partial v_y \partial w_{xy}} = 0 \quad \frac{\partial^2 F}{\partial v_y \partial w_{yy}} = 0 \quad \frac{\partial^2 F}{\partial w^2} = 0 \quad \frac{\partial^2 F}{\partial w \partial w_x} = 0$$

$$\frac{\partial^2 F}{\partial w \partial w_y} = 0 \quad \frac{\partial^2 F}{\partial w \partial w_{xx}} = 0 \quad \frac{\partial^2 F}{\partial w \partial w_{xy}} = 0 \quad \frac{\partial^2 F}{\partial w \partial w_{yy}} = 0$$

$$\frac{\partial^2 F}{\partial w_x^2} = \frac{A}{2}\left[2\left(u_x + \frac{1}{2}w_x^2\right) + 2w_x^2 + 2\nu\left(v_y + \frac{1}{2}w_y^2\right) + (1-\nu)w_y^2\right]$$

$$\frac{\partial^2 F}{\partial w_x \partial w_y} = \frac{A}{2}\left[2\nu w_x w_y + 2(1-\nu)w_x w_y + (1-\nu)(v_x + u_y)\right]$$

$$\frac{\partial^2 F}{\partial w_x \partial w_{xx}} = 0 \quad \frac{\partial^2 F}{\partial w_x \partial w_{xy}} = 0 \quad \frac{\partial^2 F}{\partial w_x \partial w_{yy}} = 0$$

$$\frac{\partial^2 F}{\partial w_y^2} = \frac{A}{2}\left[2\left(v_y + \frac{1}{2}w_y^2\right) + 2w_y^2 + 2\nu\left(u_x + \frac{1}{2}w_x^2\right) + (1-\nu)w_x^2\right]$$

$$\frac{\partial^2 F}{\partial w_y \partial w_{xx}} = 0 \quad \frac{\partial^2 F}{\partial w_y \partial w_{xy}} = 0 \quad \frac{\partial^2 F}{\partial w_y \partial w_{yy}} = 0 \quad \frac{\partial^2 F}{\partial w_{xx}^2} = D \quad \frac{\partial^2 F}{\partial w_{xx} \partial w_{xy}} = 0$$

$$\frac{\partial^2 F}{\partial w_{xx} \partial w_{yy}} = \nu D \quad \frac{\partial^2 F}{\partial w_{xy}^2} = 2(1-\nu)D \quad \frac{\partial^2 F}{\partial w_{xy} \partial w_{yy}} = 0 \quad \frac{\partial^2 F}{\partial w_{yy}^2} = D \tag{3.123}$$

Then, Equation (3.95) for the second variation becomes

$$\begin{aligned}
\bar{\delta}^2 V = A\iint\Bigg[&\bar{u}_x^2 + \frac{1-\nu}{2}\bar{u}_y^2 + \frac{1-\nu}{2}\bar{v}_x^2 + \bar{v}_y^2 \\
&+ \left[\left[u_x + \frac{1}{2}w_x^2\right] + w_x^2 + \nu\left[v_y + \frac{1}{2}w_y^2\right] + \frac{1-\nu}{2}w_y^2\right]\bar{w}_x^2 \\
&+ \left[\left[v_y + \frac{1}{2}w_y^2\right] + w_y^2 + \nu\left[u_x + \frac{1}{2}w_x^2\right] + \frac{1-\nu}{2}w_x^2\right]\bar{w}_y^2\Bigg]\,dxdy \\
+ D\iint&\left[\bar{w}_{xx}^2 + 2(1-\nu)\bar{w}_{xy}^2 + \bar{w}_{yy}^2 + 2\nu\bar{w}_{xx}\bar{w}_{yy}\right]dxdy \\
+ 2A\iint&\Bigg[\left[\frac{1-\nu}{2}(v_x + u_y) + w_x w_y\right]\bar{w}_x\bar{w}_y + \nu\bar{u}_x\bar{v}_y + \frac{1-\nu}{2}\bar{u}_y\bar{v}_x \\
&+ w_x\bar{u}_x\bar{w}_x + \nu w_y\bar{u}_x\bar{w}_y + \frac{1-\nu}{2}w_y\bar{u}_y\bar{w}_x + \frac{1-\nu}{2}w_x\bar{u}_y\bar{w}_y \\
&+ \frac{1-\nu}{2}w_y\bar{v}_x\bar{w}_x + \frac{1-\nu}{2}w_x\bar{v}_x\bar{w}_y + \nu w_x\bar{v}_y\bar{w}_x + w_y\bar{v}_y\bar{w}_y\Bigg]\,dxdy
\end{aligned} \tag{3.124}$$

in which we recall that $\bar{u}_x$, ..., $\bar{v}_x$, ..., $\bar{w}_x$, ... are actually δu_x, ..., δv_x, ..., δw_x, ..., the various derivatives of the variational displacements *from* the equilibrium state. Also, u_x, ..., v_x, ..., w_x, ..., etc., are the derivatives of the displacements *of* the equilibrium state.

Éléments sous droits d'auteur

We find it convenient to rewrite Equation (3.124) as

$$\bar{\delta}^2 V = \bar{\delta}^2 U_{m_1} + \bar{\delta}^2 U_{m_2} + \bar{\delta}^2 U_{m_3} + \bar{\delta}^2 U_{m_4} + \bar{\delta}^2 U_b \tag{3.125}$$

in which

$$\bar{\delta}^2 U_{m_1} = A\iint\left[\bar{u}_x^2 + \bar{v}_y^2 + 2\nu\bar{u}_x\bar{v}_y + \frac{1-\nu}{2}(\bar{u}_y + \bar{v}_x)^2\right] dxdy \tag{3.126}$$

$$\bar{\delta}^2 U_{m_2} = A\iint\left[(u_x + \nu v_y)\bar{w}_x^2 + (v_y + \nu u_x)\bar{w}_y^2 + (1-\nu)(v_x + u_y)\bar{w}_x\bar{w}_y\right] dxdy \tag{3.127}$$

$$\bar{\delta}^2 U_{m_3} = 2A\iint\left[(\bar{u}_x + \nu\bar{v}_y)w_x\bar{w}_x + (\bar{v}_y + \nu\bar{u}_x)w_y\bar{w}_y + \frac{1-\nu}{2}(\bar{u}_y + \bar{v}_x)(w_y\bar{w}_x + w_x\bar{w}_y)\right] dxdy \tag{3.128}$$

$$\bar{\delta}^2 U_{m_4} = \frac{A}{2}\iint(3w_x^2\bar{w}_x^2 + 3w_y^2\bar{w}_y^2 + w_x^2\bar{w}_y^2 + \bar{w}_x^2 w_y^2 + 4w_x w_y\bar{w}_x\bar{w}_y)\, dxdy \tag{3.129}$$

$$\bar{\delta}^2 U_b = D\iint\left[\bar{w}_{xx}^2 + \bar{w}_{yy}^2 + 2\nu\bar{w}_{xx}\bar{w}_{yy} + 2(1-\nu)\bar{w}_{xy}^2\right] dxdy \tag{3.130}$$

in which the subscript m denotes membrane and b denotes bending effects. Note that $\bar{\delta}^2 V = \bar{\delta}^2 U$ because $\bar{\delta}^2\Omega \equiv 0$! That is, the interpretation by Timoshenko and others that a ΔT exists is incorrect [3-8]. He relates the double integral, Equation (3.127), to work of external forces during buckling whereas the integrand is actually a quantity defined *inside* the boundaries of the plate. This kind of misinterpretation is quite common in the theory of buckling because of the general lack of sound basic understanding of how buckling is quite different from equilibrium.

For a plate with initial perfect flatness which is subjected to in-plane loads, deformation occurs only in the plane of the plate prior to buckling. That is, the plate deforms as a membrane prior to buckling. Thus, w_x and w_y vanish in Equations (3.128) and (3.129) and, in fact, those entire integrals vanish as a consequence. For initially imperfect plates, neither w_x nor w_y vanish in Equations (3.128) and (3.129).

Substitute the second partial derivatives in the Euler equations for buckling of initially perfectly flat plates subject to $w_x = 0$ and $w_y = 0$ in the buckling differential equations, Equations (3.111)–(3.113), to get

$$\frac{\partial}{\partial x}(\bar{u}_x + \nu\bar{v}_y) + \frac{1-\nu}{2}\frac{\partial}{\partial y}(\bar{u}_y + \bar{v}_x) = 0 \tag{3.131}$$

$$\frac{1-\nu}{2}\frac{\partial}{\partial x}(\bar{u}_y + \bar{v}_x) + \frac{\partial}{\partial y}(\bar{v}_y + \nu\bar{u}_x) = 0 \tag{3.132}$$

$$D\nabla^4\bar{w} - \bar{w}_{xx}A(u_x + \nu v_y) - \bar{w}_{yy}A(v_y + \nu u_x) - \bar{w}_{xy}A(1-\nu)(v_x + u_y) = 0 \tag{3.133}$$

The foregoing buckling differential equations can be rewritten upon realization that, in analogy to Equations (3.80) and (3.81), the variations in forces and moments during buckling can be written as

Éléments sous droits d'auteur

$$\delta N_x = A(\bar{u}_x + \nu\bar{v}_y) \quad \delta N_y = A(\bar{v}_y + \nu\bar{u}_x) \quad \delta N_{xy} = \frac{(1-\nu)}{2} A(\bar{u}_y + \bar{v}_x) \quad (3.134)$$

$$\delta M_x = -D(w_{xx} + \nu w_{yy}) \quad \delta M_y = -D(w_{yy} + \nu w_{xx}) \quad \delta M_{xy} = -(1-\nu)Dw_{xy} \quad (3.135)$$

Thus, when Equations (3.134), (3.135), and (3.80) are substituted in Equations (3.131), (3.132), and (3.133), we get

$$\frac{\partial}{\partial x}(\delta N_x) + \frac{\partial}{\partial y}(\delta N_{xy}) = 0 \quad (3.136)$$

$$\frac{\partial}{\partial x}(\delta N_{xy}) + \frac{\partial}{\partial y}(\delta N_y) = 0 \quad (3.137)$$

$$\frac{\partial^2}{\partial x^2}(\delta M_x) + 2\frac{\partial^2}{\partial x \partial y}(\delta M_{xy}) + \frac{\partial^2}{\partial y^2}(\delta M_y) + N_x\bar{w}_{xx} + N_y\bar{w}_{yy} + 2N_{xy}\bar{w}_{xy} = 0 \quad (3.138)$$

or with a symbol following a comma denoting partial differentiation and replacing N_x, N_y, and N_{xy} which are positive in tension with $-\bar{N}_x$, $-\bar{N}_y$, and $-\bar{N}_{xy}$ in which N_x and N_y are positive in compression because of our principal interest in finding the compressive forces that cause buckling.

$$\delta N_{x,x} + \delta N_{xy,y} = 0 \quad (3.139)$$

$$\delta N_{xy,x} + \delta N_{y,y} = 0 \quad (3.140)$$

$$\delta M_{x,xx} + 2\delta M_{xy,xy} + \delta M_{y,yy} - \bar{N}_x w_{,xx} - \bar{N}_y w_{,yy} - 2\bar{N}_{xy} w_{,xy} = 0 \quad (3.141)$$

in which $\bar{N}_x$, $\bar{N}_y$, and $\bar{N}_{xy}$ can be functions of x and y. The boundary conditions for the buckling equations, Equations (3.139)–(3.141), are

$$\bar{u} = 0 \quad \text{or} \quad \delta N_x = 0 \quad \text{on lines } x = \text{constant} \quad (3.142)$$

$$\bar{v} = 0 \quad \text{or} \quad \delta N_{xy} = 0 \quad \text{on lines } x = \text{constant} \quad (3.143)$$

$$\bar{u} = 0 \quad \text{or} \quad \delta N_{xy} = 0 \quad \text{on lines } y = \text{constant} \quad (3.144)$$

$$\bar{v} = 0 \quad \text{or} \quad \delta N_y = 0 \quad \text{on lines } y = \text{constant} \quad (3.145)$$

$$\bar{w}_{,x} = 0 \quad \text{or} \quad \delta M_x = 0 \quad \text{on lines } x = \text{constant} \quad (3.146)$$

$$\bar{w}_{,y} = 0 \quad \text{or} \quad \delta M_y = 0 \quad \text{on lines } y = \text{constant} \quad (3.147)$$

$$\bar{w} = 0 \quad \text{or} \quad \delta K_x = 0 \quad \text{on lines } x = \text{constant} \quad (3.148)$$

$$\bar{w} = 0 \quad \text{or} \quad \delta K_y = 0 \quad \text{on lines } y = \text{constant} \quad (3.149)$$

$$\bar{w}_i = 0 \quad \text{or} \quad \delta R_i = 0 \quad \text{at corners} \quad (3.150)$$

Note that, at first glance, the buckling differential equations, Equations (3.136)–(3.138), do *resemble* the equilibrium differential equations, Equations (3.82)–(3.84). However, in the buckling equations, we deal with δN_x, etc. *instead* of the N_x, etc. in the equilibrium equations. Also, we deal with δw (the buckling displacement) *instead* of w (the equilibrium displacement). These essential differences are too seldom recognized.

Éléments sous droits d'auteur

In many presentations and derivations, the equilibrium equations are simply 'modified' without sufficient interpretation to make it clear that a boundary-value problem is being 'converted' to an eigenvalue problem. Even worse, some people refer to the buckling equations as equilibrium equations! True, the buckling equations could be called neutral equilibrium equations, but they are *not* equilibrium equations! You would certainly think that the fundamental difference between equilibrium problems which are boundary-value problems and buckling problems which are eigenvalue problems would be perfectly obvious and quite distinctive.

The forces N_x, N_y, and N_{xy} are the equilibrium forces in the plate at buckling, and we seek their values in order to determine the buckling load. That is, we seek the eigenvalues $\bar{N}_x$, $\bar{N}_y$, and $\bar{N}_{xy}$ which are the values of the compressive equilibrium forces at buckling. Ordinarily, the equilibrium forces are known to be a trivial membrane state prior to buckling because the plate is flat. For example, in a plate loaded in the x-direction, N_x is uniform throughout the plate and we seek its (negative) value $\bar{N}_x$ at buckling.

In regard to the notation N_x and δN_x that arises in the buckling equations, Equations (3.139), (3.140), and (3.141), consider the following logic. First, rewrite the in-plane forces, N_x, N_y, and N_{xy}, from Equation (3.80) and Equation (3.58) as

$$\begin{aligned} N_x &= A\left[(u_x + \frac{1}{2}w_x^2) + \nu(v_y + \frac{1}{2}w_y^2)\right] \\ N_y &= A\left[(v_y + \frac{1}{2}w_y^2) + \nu(u_x + \frac{1}{2}w_x^2)\right] \\ N_{xy} &= \frac{1-\nu}{2}A(v_x + u_y + w_x w_y) \end{aligned} \tag{3.151}$$

Then, give u, v, and w variations δu, δv, and δw such that

$$\begin{aligned} N_x + \Delta N_x &= A\left[\left[u_x + \delta u_x + \frac{1}{2}(w_x + \delta w_x)^2\right] + \nu\left[v_y + \delta v_y + \frac{1}{2}(w_y + \delta w_y)^2\right]\right] \\ N_y + \Delta N_y &= A\left[\left[v_y + \delta v_y + \frac{1}{2}(w_y + \delta w_y)^2\right] + \nu\left[u_x + \delta u_x + \frac{1}{2}(w_x + \delta w_x)^2\right]\right] \\ N_{xy} + \Delta N_{xy} &= \frac{1-\nu}{2}A[v_x + \delta v_x + u_y + \delta u_y + (w_x + \delta w_x)(w_y + \delta w_y)] \end{aligned} \tag{3.152}$$

Thus, upon collecting terms linear in the displacement variations,

$$\begin{aligned} \delta N_x &= A[\delta u_x + w_x \delta w_x + \nu(\delta v_y + w_y \delta w_y)] \\ \delta N_y &= A[\delta v_y + w_y \delta w_y + \nu(\delta u_x + w_x \delta w_x)] \\ \delta N_{xy} &= \frac{1-\nu}{2}A(\delta v_x + \delta u_y + w_x \delta w_y + w_y \delta w_x) \end{aligned} \tag{3.153}$$

which, for flat plates with $w_x = 0$ and $w_y = 0$ in the prebuckling equilibrium state when only in-plane loads are considered, reduces to

Éléments sous droits d'auteur

$$\begin{aligned}\delta N_x &= A(\delta u_x + \nu \delta v_y)\\ \delta N_y &= A(\delta v_y + \nu \delta u_x)\\ \delta N_{xy} &= \frac{1-\nu}{2} A(\delta v_x + \delta u_y)\end{aligned} \tag{3.154}$$

which are indeed the same as Equation (3.134) when $\delta u_x = \bar{u}_x$, etc., is substituted. The relations for the variations in the moments, Equation (3.135), are obtained in a straight-forward manner as illustrated by

$$M_x = D(\kappa_x + \nu\kappa_y) = -D(w_{xx} + \nu w_{yy}) \tag{3.155}$$

being given variations in w to obtain

$$M_x + \Delta M_x = -D[(w_{xx} + \delta w_{xx}) + \nu(w_{yy} + \delta w_{yy})] \tag{3.156}$$

whereupon, by definition,

$$\delta M_x = -D(\delta w_{xx} + \nu \delta w_{yy}) \tag{3.157}$$

and so on to obtain Equation (3.135).

The boundary conditions for simply supported and clamped-edge plates for the buckling problem analogous to those for the equilibrium problem in an adaptation of Almroth's notation [3-6] for shells are:

Simply Supported Edges:

$$\begin{array}{llllll} \text{S1:} & \delta w = 0 & \delta M_n = 0 & \delta u_n = 0 & \delta u_t = 0\\ \text{S2:} & \delta w = 0 & \delta M_n = 0 & \delta N_n = 0 & \delta u_t = 0\\ \text{S3:} & \delta w = 0 & \delta M_n = 0 & \delta u_n = 0 & \delta N_{nt} = 0\\ \text{S4:} & \delta w = 0 & \delta M_n = 0 & \delta N_n = 0 & \delta N_{nt} = 0 \end{array} \tag{3.158}$$

Clamped Edges:

$$\begin{array}{llllll} \text{C1:} & \delta w = 0 & \delta w_{,n} = 0 & \delta u_n = 0 & \delta u_t = 0\\ \text{C2:} & \delta w = 0 & \delta w_{,n} = 0 & \delta N_n = 0 & \delta u_t = 0\\ \text{C3:} & \delta w = 0 & \delta w_{,n} = 0 & \delta u_n = 0 & \delta N_{nt} = 0\\ \text{C4:} & \delta w = 0 & \delta w_{,n} = 0 & \delta N_n = 0 & \delta N_{nt} = 0 \end{array} \tag{3.159}$$

Subscripts n and t denote directions in the plane of the plate that are normal and tangential to the edge under consideration in Figure 3-13. Note that all the boundary conditions are homogeneous. Thus, because the differential equations are also homogeneous, we have an eigenvalue problem. Just as in the case of equilibrium, the buckling bound-

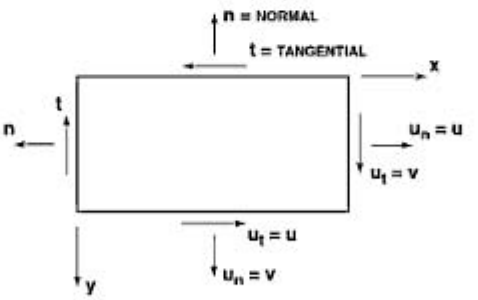


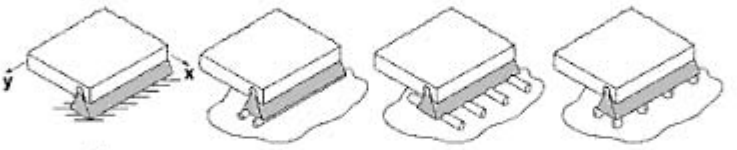
Figure 3-13 Boundary Condition Notation

Éléments sous droits d'auteur

ary conditions are depicted in Figures 3-14 and 3-15. The physical mechanisms for plate edge support are identical to those described for the equilibrium problem on pages 247–248.

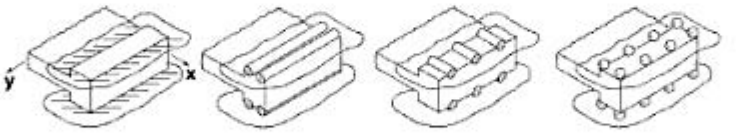
Buckling boundary conditions are similar to equilibrium boundary conditions, but in a possibly deceptive manner. In both buckling boundary conditions S2 and S4 for simply supported edges in Equation (3.158), $\delta N_n = 0$ appears. In the equilibrium boundary conditions, the seemingly analogous term $N_n = 0$ appears and signifies that no such force exists in the n-direction at the edge. In contrast for buckling, $\delta N_n = 0$ signifies that a force N_n *can exist*, but that N_n *does not change (vary) at the buckling load!* Alternatively, the displacement u_n exists, but does not change during buckling ($\delta u_n = 0$). Analogous statements can be made about the other boundary condition differences between equilibrium and buckling. Accordingly, *buckling boundary conditions have to do with how the loads and displacements are applied, not what they are.*

The three buckling equations for classical plate buckling theory for single-layered plates, Equations (3.139), (3.140), and (3.141), are *decoupled* such that the two in-plane equations, Equations (3.139) and (3.140), do not contain the desired buckling loads, but the third out-of-



S1	S2	S3	S4
$\delta w = 0$	$\delta w = 0$	$\delta w = 0$	$\delta w = 0$
$\delta M_x = 0$	$\delta M_x = 0$	$\delta M_x = 0$	$\delta M_x = 0$
$\delta u = 0$	$\delta N_x = 0$	$\delta u = 0$	$\delta N_x = 0$
$\delta v = 0$	$\delta v = 0$	$\delta N_{xy} = 0$	$\delta N_{xy} = 0$

Figure 3-14 Simply Supported Edge Buckling Boundary Conditions



C1	C2	C3	C4
$\delta w = 0$	$\delta w = 0$	$\delta w = 0$	$\delta w = 0$
$\delta w_{,x} = 0$	$\delta w_{,x} = 0$	$\delta w_{,x} = 0$	$\delta w_{,x} = 0$
$\delta u = 0$	$\delta N_x = 0$	$\delta u = 0$	$\delta N_x = 0$
$\delta v = 0$	$\delta v = 0$	$\delta N_{xy} = 0$	$\delta N_{xy} = 0$

Figure 3-15 Clamped-Edge Buckling Boundary Conditions

Éléments sous droits d'auteur

plane equation, Equation (3.141), does contain the buckling loads. That out-of-plane equation also contains terms only in δw, the variational transverse (out-of-plane) displacement (during buckling), but none in δu and δv, the variational in-plane displacements (during buckling). Thus, the boundary conditions on the variational in-plane displacements, δu and δv, and their derivatives do not affect the plate buckling load! An exception occurs for laminated plates in Section 3.6. Accordingly, the edge boundary conditions 'reduce' to concerns about the values of δw, $\delta w_{,n}$, and $\delta w_{,nn}$, where n is the in-plane direction normal to the edge. For example, if $\delta w = 0$ and $\delta w_{,n} = 0$, then the plate edge is clamped or fixed. If $\delta w = 0$, $\delta w_{,n} \neq 0$, and $\delta w_{,nn} = 0$ ($\delta M_n = 0$), then the plate edge is simply supported (sometimes called pinned). Finally, if $\delta w \neq 0$ and $\delta w_{,n} \neq 0$, then the plate edge is called free.

3.2.6 Summary

Two principal approaches are used for calculating buckling loads: (1) the differential equation approach and (2) the energy integral approach.

In the differential equation approach, the buckling differential equations in displacement form, Equations (3.131)–(3.133) or in variational force and moment form, Equations (3.139)–(3.141), i.e., with δw instead of $\bar{w}$ for variation in displacement from the equilibrium state during buckling (the form we will use from here on):

$$\delta N_{x,x} + \delta N_{xy,y} = 0 \tag{3.160}$$

$$\delta N_{xy,x} + \delta N_{y,y} = 0 \tag{3.161}$$

$$\delta M_{x,xx} + 2\delta M_{xy,xy} + \delta M_{y,yy} - \bar{N}_x \delta w_{,xx} - \bar{N}_y \delta w_{,yy} - 2\bar{N}_{xy} \delta w_{,xy} = 0$$

or

$$D\nabla^4(\delta w) + \bar{N}_x \delta w_{,xx} + \bar{N}_y \delta w_{,yy} + 2\bar{N}_{xy} \delta w_{,xy} = 0 \tag{3.162}$$

are solved subject to the boundary conditions in Equations (3.87), (3.88), or other applicable boundary conditions. Note in Equation (3.162) that $\bar{N}_x$, $\bar{N}_y$, and $\bar{N}_{xy}$, the compressive buckling forces, can be functions of x and y. Thus, Equation (3.162) can be a partial differential equation with nonconstant coefficients that is much more difficult to solve than a differential equation with constant coefficients. Moreover, transverse shear is not included in these equations, so they cannot be regarded as exact.

Many authors are so overwhelmed by the similarity in form of the buckling equation, Equation (3.162), and the large-deflection equilibrium equation, Equation (3.84), that *they overlook the essential differences of form and origin of the various terms* and state that they obtain the buckling equation from the large-deflection equilibrium equation. The notation used here of δw versus w and δM versus M emphasizes the differences in form and origin of each term so that buckling equations cannot be mistaken for large-deflection equilibrium equations. After all, *buckling is an eigenvalue problem and equilibrium is a boundary-value problem!*

Éléments sous droits d'auteur

In the energy integral approach, Rayleigh or Rayleigh-Ritz deflection approximations are used in the various variations in strain energy integrals defined in Equations (3.125)–(3.130). That is, for a plate with a flat prebuckled shape, the variations in strain energy integrals for $\bar{\delta}^2 V$ are

$$\bar{\delta}^2 V = \bar{\delta}^2 U_{m_1} + \bar{\delta}^2 U_{m_2} + \bar{\delta}^2 U_b \tag{3.163}$$

in which

$$\bar{\delta}^2 U_{m_1} = A\iint\left[\delta u_x^2 + \delta v_y^2 + 2\nu\delta u_x\delta v_y + \frac{1-\nu}{2}(\delta u_y + \delta v_x)^2\right]dxdy \tag{3.164}$$

$$\bar{\delta}^2 U_{m_2} = -\iint\left[\bar{N}_x\delta w_x^2 + \bar{N}_y\delta w_y^2 + 2\bar{N}_{xy}\delta w_x\delta w_y\right]dxdy \tag{3.165}$$

$$\bar{\delta}^2 U_b = D\iint\left[\delta w_{xx}^2 + \delta w_{yy}^2 + 2\nu\delta w_{xx}\delta w_{yy} + 2(1-\nu)\delta w_{xy}^2\right]dxdy \tag{3.166}$$

in which δw is the buckling displacement *from* the prebuckling equilibrium state and N_x, N_y, and N_{xy} are buckling forces (positive in compression).

We use the neutral equilibrium buckling criterion $\bar{\delta}^2 V = 0$ with Equation (3.163) and see that Equation (3.164) has only δu and δv whereas Equations (3.165) and (3.166) have only δw. Then, because δu and δv are independent of δw (variations from the equilibrium state), Equation (3.163) reduces to two equations:

$$\bar{\delta}^2 U_{m_1} = 0 \tag{3.167}$$

$$\bar{\delta}^2 U_{m_2} + \bar{\delta}^2 U_b = 0 \tag{3.168}$$

Equation (3.168) is equivalent to Timoshenko and Gere's Equation (9.5) on page 350 [3-8]. Note that $\bar{\delta}^2 U_{m_2}$ is clearly derived from the strain energy and not from the potential energy of external forces as so many authors erroneously state. Equation (3.167) has variations in the in-plane displacements δu and δv alone and no prebuckling equilibrium state, so can be disregarded for now. Moreover, Equation (3.168) has variations in transverse buckling displacement δw alone (i.e., separately from δu and δv) along with the prebuckling equilibrium state (values of N_x, N_y, and N_{xy} at buckling). We will illustrate the power of the direct method of the calculus of variations, i.e., in our case the Rayleigh-Ritz method. We choose buckling deflections δw that must satisfy the geometric boundary conditions (and hopefully satisfy the natural boundary conditions) and then find buckling loads that satisfy Equation (3.168).

We will concentrate in Section 3.3 on classical plate buckling problems in which we need to solve only the third (out-of-plane) buckling equation with buckling boundary conditions of simply supported (pinned), clamped (fixed), or free edges. For laminated composite plates in Section 3.6, we will find that the three buckling equations are irretrievably coupled if the plate is not laminated symmetrically about its middle surface, so we must use the buckling boundary conditions in Equations (3.158) and (3.159) depicted in Figures 3-14 and 3-15.

Éléments sous droits d'auteur

3.3 CLASSICAL BUCKLING THEORY SOLUTIONS

3.3.1 Introduction

Solutions to plate buckling problems without considering such effects as prebuckling deformations were first obtained in 1891 by Bryan [3-1]. Such solutions are called classical solutions primarily because they were the first, the simplest, and for the most basic loadings. The procedure for calculating plate buckling loads is the two-dimensional analog of Euler's approach to bar buckling; hence, classical plate buckling loads are often called Euler buckling loads in Euler's honor. The general group of classical solutions is important as a baseline for discussion of all other solutions. Classical solutions with simply supported edge conditions are typically used as lower-bound estimates of capability in design, especially when boundary conditions are not known with certainty.

Classical solutions and results for plates with all edges simply supported are described for uniaxial loading, biaxial loading, combined in-plane bending and compression, and in-plane shear. Possible physical restraints that limit or restrict the modes into which a plate can buckle are also examined. Finally, boundary conditions other than all four edges simply supported are briefly addressed. Thermal buckling of plates, in analogy to the concentration in this section on buckling under mechanical loads, is separately treated in Section 3.7.

3.3.2 Buckling of Simply Supported Rectangular Plates under Uniform Compression N_x

Consider a simply supported rectangular plate uniformly compressed by a force (per unit width) N_x as shown in Figure 3-16. We will find the buckling load for these rectangular plates by (1) the buckling differential equation approach and (2) the strain energy integral approach.

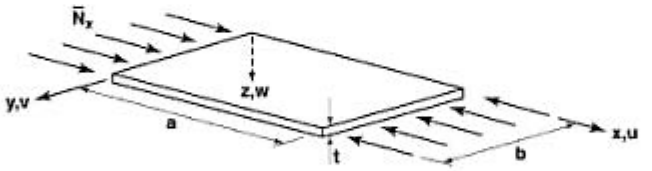


Figure 3-16 Simply Supported Rectangular Plate with Load in the x-Direction

3.3.2.1 The Buckling Differential Equation Approach

If a rectangular plate subjected to in-plane loads has no out-of-plane deflections prior to buckling, i.e., the plate is flat, then the plate is said to have a membrane prebuckled shape. We need not be concerned with the buckling differential equations for δu and δv because there is no interaction of those equations with the equation for δw, Equation (3.162). Because of the membrane prebuckled shape, $w = 0$ for equilibrium. The

Éléments sous droits d'auteur

prebuckling force state within the plate is, by inspection, $N_x(x,y) = -\bar{N}_x$, $N_y(x,y) = 0$, and $N_{xy}(x,y) = 0$.

For the solution to the differential equation governing buckling, we then 'mysteriously' choose the sinusoidal buckling displacement function (Actually, this is almost a form of the semi-inverse method in the theory of elasticity in which we use a possible solution and find what problem it solves. However, in this case we are simply guessing at what might be a solution to a rather simple partial differential equation).

$$\delta w = \tilde{w} \sin \frac{m\pi x}{a} \sin \frac{n\pi y}{b} \tag{3.169}$$

in which $\tilde{w}$ is the amplitude of the deflection and see whether the boundary conditions and the buckling differential equation are satisfied. First, we observe that the geometric boundary conditions of

$$\delta w = 0 \quad \text{along lines } x = \text{constant and lines } y = \text{constant} \tag{3.170}$$

are satisfied by Eq. (3.169) as are the natural boundary conditions

$$\delta M_x = 0 \quad \text{along lines } x = \text{constant} \tag{3.171}$$

$$\delta M_y = 0 \quad \text{along lines } y = \text{constant} \tag{3.172}$$

when the definitions for δM_x and δM_y in Equation (3.135) are used. The buckling differential equation, Equation (3.162), which is simplified for the present loading as

$$D\nabla^4(\delta w) + \bar{N}_x \delta w_{,xx} = 0 \tag{3.173}$$

is easily seen to be precisely satisfied for the δw in Equation (3.169) if

$$\bar{N}_x = \frac{D\left[(m\pi/a)^4 + 2(m\pi/a)^2(n\pi/b)^2 + (n\pi/b)^4\right]}{(m\pi/a)^2} \tag{3.174}$$

Note that Equation (3.174) is called the characteristic equation and that the buckling amplitude $\tilde{w}$ is indeterminate as in bar buckling problems.

The word 'mysteriously' is used in the reference to the selection of a buckling displacement function because only by experience can we explain how to make such a choice. Basically, we choose a trial function by experience because it works. We are fortunate that such a simple expression is the solution to the governing partial differential equation.

Equation (3.174) can be simplified to read

$$\bar{N}_x = \frac{\pi^2 a^2 D}{m^2}\left[\left[\frac{m}{a}\right]^2 + \left[\frac{n}{b}\right]^2\right]^2 \tag{3.175}$$

Both the geometric and the natural boundary conditions are satisfied as well as the buckling differential equation, so Equation (3.175) is the exact solution to Equation (3.173) and the associated boundary conditions. However, recall that Equation (3.162) does not include shear deformation so is not itself exact. Discussion of the differential equation solution follows the alternative derivation by the use of the strain energy integrals.

Éléments sous droits d'auteur

3.3.2.2 The Strain Energy Integral Approach

The appropriate strain energy integrals that must be satisfied for buckling to occur are given by Equations (3.168), (3.165), and (3.166). For the given in-plane loading condition,

$$\begin{aligned} N_x &= A(u_x + \nu v_y) = -\bar{N}_x \\ N_y &= A(v_y + \nu u_x) = 0 \\ N_{xy} &= A\frac{(1-\nu)}{2}(u_y + v_x) = 0 \end{aligned} \tag{3.176}$$

the strain energy integrals in Equation (3.168) reduce to

$$\begin{aligned} 0 = &-\int_0^b\int_0^a \bar{N}_x(\delta w_x)^2 dxdy \\ &+ D\int_0^b\int_0^a \left[(\delta w_{xx})^2 + (\delta w_{yy})^2 + 2\nu\delta w_{xx}\delta w_{yy} + 2(1-\nu)(\delta w_{xy})^2\right]dxdy \end{aligned} \tag{3.177}$$

As an approximation to the buckled shape, let the deflection δw from the flat prebuckled shape be given by the double Fourier series[1]

$$\delta w = \sum_{m=1}^{\infty}\sum_{n=1}^{\infty} \tilde{w}_{mn} \sin\frac{m\pi x}{a}\sin\frac{n\pi y}{b} \tag{3.178}$$

in which $\tilde{w}_{mn}$ is the amplitude of the individual $\sin(m\pi x/a)\sin(n\pi y/b)$ deflection shapes, each of which satisfies both the natural and geometric boundary conditions and the Fourier sine series can represent any δw within the boundaries. Upon substitution of Equation (3.178), the first term in Equation (3.177) becomes

$$\int_0^b\int_0^a \bar{N}_x(\delta w_x)^2 dxdy = \frac{\pi^2 b}{4a}\bar{N}_x\sum_{m=1}^{\infty}\sum_{n=1}^{\infty} m^2\tilde{w}_{mn}^2 \tag{3.179}$$

and the second term becomes

$$\bar{\delta}^2 U_b = \frac{\pi^4 ab}{4} D\sum_{m=1}^{\infty}\sum_{n=1}^{\infty}\left[\left[\frac{m}{a}\right]^2 + \left[\frac{n}{b}\right]^2\right]^2\tilde{w}_{mn}^2 \tag{3.180}$$

whereupon

$$\bar{N}_x = \pi^2 a^2 D\frac{\displaystyle\sum_{m=1}^{\infty}\sum_{n=1}^{\infty}\left[\left[\frac{m}{a}\right]^2 + \left[\frac{n}{b}\right]^2\right]^2\tilde{w}_{mn}^2}{\displaystyle\sum_{m=1}^{\infty}\sum_{n=1}^{\infty} m^2\tilde{w}_{mn}^2} \tag{3.181}$$

Note that $\bar{\delta}^2 U$ can be written in the form

[1] For conditions on differentiation, integration, completeness, and convergence of Fourier series, consult Tolstov [3-9] or Brown and Churchill [3-10].

Éléments sous droits d'auteur

$$\bar{\delta}^2 U = \frac{\pi^2}{4} \sum_{m=1}^{\infty} \sum_{n=1}^{\infty} \left[\pi^2 abD \left[\left[\frac{m}{a} \right]^2 + \left[\frac{n}{b} \right]^2 \right]^2 + \frac{b}{a} \bar{N}_x m^2 \right] \tilde{w}_{mn}^2 \quad (3.182)$$

Only if each coefficient of $\tilde{w}_{mn}^2$ is positive is $\bar{\delta}^2 U$ positive definite in Equation (3.182). Then, buckling occurs when any coefficient is zero, i.e.,

$$\bar{N}_x = \frac{\pi^2 a^2 D}{m^2} \left[\left[\frac{m}{a} \right]^2 + \left[\frac{n}{b} \right]^2 \right]^2 = k \frac{\pi^2 D}{b^2} \quad (3.183)$$

which is the same characteristic equation as Equation (3.175) except that the normalized loading parameter k is introduced. The factor k depends on the aspect ratio, a/b, of the rectangular plate and its bending stiffness, D, on the buckle mode shape numbers, m and n, and, of course, on the buckling load. As usual, the buckle amplitude $\tilde{w}$ is indeterminate.

3.3.2.3 Results and Discussion

Irrespective of the approach, the buckling load for a simply supported rectangular plate subjected to a compressive force per unit width N_x is Equation (3.183). The load $\bar{N}_x$ is applied in a monotonically increasing manner starting from zero. Thus, the lowest value of $\bar{N}_x$ that satisfies Equation (3.183) is the buckling load. To find the lowest buckling load, we might be tempted to use calculus to find where the partial derivatives of $\bar{N}_x$ with respect to m and n are zero (although this approach is clearly *not* a sufficient condition for a minimum). However, $\bar{N}_x$ is *not* a continuous function of m and n, a necessary condition for minimization by calculus to be valid. In fact, the buckle mode shape numbers, m and n, must be integers to satisfy the plate boundary conditions. Thus, we must minimize a function of discrete variables as described in Appendix B. However, in this case, the minimization is actually quite simple. The minimum buckling load always occurs for n = 1 and various values of m because $\bar{N}_x$ in Equation (3.183) always increases for increasing n. That is, the plate always buckles with a single half wave in the y-direction and a variety of values of m as shown for m = 2 in Figure 3-17 along with the flat prebuckled shape. There, see again the nodal

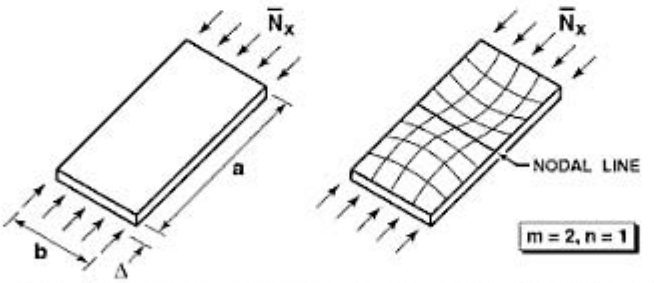


Figure 3-17 In-Plane Loaded Plate Before Buckling and Typical Buckling Mode

Éléments sous droits d'auteur

line that does not move during buckling. Note that n = 0 corresponds to the plate buckling like a wide column (i.e., without supports along the edges parallel to the x-direction) because Equation (3.183) reduces to the Euler column result for $\nu = 0$. However, such a plate does not have simple supports on all four edges so is not part of the title problem.

Values of $\bar{N}_x$ are plotted as festooned curves in Figure 3-18 for a range of plate aspect ratios, a/b. The lowest buckling load for the governing mode shape is plotted with festooned solid curves that intersect at 'cusps' where the buckle mode shape changes as the plate length, a, increases. The dashed curves represent buckling loads in modes that do not correspond to buckling unless some physical restraint forces the plate to buckle in a higher mode shape (see Section 3.3.7). If buckle mode shape changes are ignored, k for a long plate is always 4 as we can easily conclude by inspection of Figure 3-18.

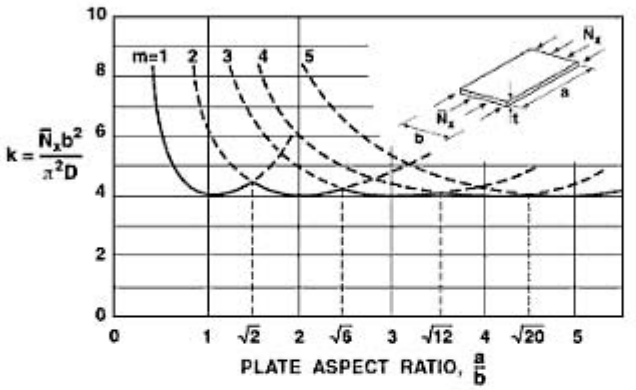


Figure 3-18 Normalized Buckling Load k for Rectangular Plates with Various Plate Aspect Ratios

Problem Set 3.3.2

3.3.2.1 Verify that the buckling differential equation, Equation (3.173), is satisfied for the sinusoidal buckling displacement in Equation (3.169) if N_x is the expression in Equation (3.175).

3.3.2.2 Verify Equation (3.179).

3.3.2.3 Verify Equation (3.180).

3.3.2.4 Prove that the cusps at mode-shape changes in Figure 3-18 occur at the locations $a/b = \sqrt{2}, \sqrt{6}, \sqrt{12}$, etc.

3.3.2.5 Ignore the fact that m, the number of buckle half-waves in the x-direction, must be an integer and use simple calculus to find the minimum value of N_x. What value of $k = (\bar{N}_x b^2)/(\pi^2 D)$ do you get? Discuss the implications of ignoring the essential integer character of m. Compare the result for k with the simply supported column buckling result in Chapter 2 and with Figure 3-18. Explain why and prove analytically that k approaches 4 for long plates, i.e., for high a/b in Figure 3-18.

3.3.2.6 Demonstrate that setting the number of lateral buckle half waves, n, equal to zero in Equation (3.183) leads to the wide-column buckling problem if $\nu = 0$.

Éléments sous droits d'auteur

3.3.3 Buckling of Simply Supported Rectangular Plates under Uniform Biaxial Loading N_x and N_y

3.3.3.1 Basic Solution

Consider a simply supported rectangular plate that is uniformly compressed by forces per unit length $\bar{N}_x$ and $\bar{N}_y$ in two directions as in Figure 3-19. Of course, one of the biaxial loads could be tensile and buckling could still occur. However, if both loads are tensile, then no buckling occurs. We will explore the whole spectrum or range of biaxial loading in which buckling occurs. The prebuckling equilibrium state within the plate is, by inspection, $N_x(x,y) = -\bar{N}_x$, $N_y(x,y) = 0$, and $N_{xy}(x,y) = 0$ if biaxial compression exists. If, for example, the loading is a compressive $\bar{N}_x$ and a tensile N_y, then the prebuckling equilibrium state within the plate is, by inspection, $N_x(x,y) = -\bar{N}_x$, $N_y(x,y) = N_y$, and $N_{xy}(x,y) = 0$.

The differential equation governing buckling, Equation (3.162), reduces for biaxial compression loading to

$$D\nabla^4(\delta w) + \bar{N}_x \delta w_{,xx} + \bar{N}_y \delta w_{,yy} = 0 \tag{3.184}$$

For other biaxial loading, $\bar{N}_x$ changes to $-N_x$ or $\bar{N}_y$ changes to $-N_y$. Irrespective of the loading, the exact solution to Equation (3.184) is

$$\delta w = \tilde{w} \sin \frac{m\pi x}{a} \sin \frac{n\pi y}{b} \tag{3.185}$$

just as for the case in which only $\bar{N}_x$ is applied in Section 3.3.1.1. That is, both the geometric and natural boundary conditions are satisfied as well as the differential equation. The resulting characteristic equation analogous to Equation (3.176) is

$$\bar{N}_x\left[\frac{m\pi}{a}\right]^2 + \bar{N}_y\left[\frac{n\pi}{b}\right]^2 = D\left[\left[\frac{m\pi}{a}\right]^2 + \left[\frac{n\pi}{b}\right]^2\right]^2 \tag{3.186}$$

Again, the buckle amplitude $\tilde{w}$ is indeterminate.

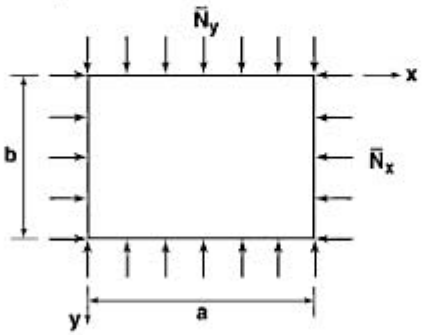


Figure 3-19 Simply Supported Rectangular Plates with Compressive Load in the x- and y-Directions

Éléments sous droits d'auteur

Numerical results for the buckling criterion in Equation (3.186) cannot be presented in a single general format in the manner of the uniaxial load, $\bar{N}_x$, results in Section 3.3.2 which depend only on plate aspect ratio, a/b, and the buckling mode shape parameter, m. Buckling of biaxially loaded plates is more complicated and depends on the relative values of the biaxial loads, N_x and N_y, the buckling mode shape parameters, m and n, and the plate aspect ratio, a/b. Finding the buckling load requires minimizing Equation (3.186), a function of two integer variables, m and n, for some prescribed plate aspect ratio, a/b, and some prescribed loading ratio, s, of applied N_y to applied N_x, i.e.,

$$s = \frac{N_y}{N_x} \tag{3.187}$$

or with either $\bar{N}_x$ or $\bar{N}_y$ specified or in some more complex manner.

We will consider two practical buckling problems: (1) what are the buckling loads, $\bar{N}_x$ and $\bar{N}_y$ if the plate is loaded with N_x and N_y in a fixed loading ratio, $s = N_y/N_x$, and the loads are steadily increased until buckling occurs? and (2) what is $\bar{N}_y$ if $\bar{N}_x$ is specified? Alternatively, what is $\bar{N}_x$ if $\bar{N}_y$ is specified? The first problem can be handled analytically by using the loading ratio, s, in the buckling criterion and solving for a single eigenvalue, N_x. Understanding of both problems is simplified by next considering the nature of how the biaxial loading is applied.

3.3.3.2 Manner of Biaxial Load Introduction

We want to study how plates buckle under biaxial mechanical loading, so let's examine a generic concept for applying such loads to a plate until it buckles. Consider a rectangular plate under the action of an axial force (per unit width), N_x, and a lateral force (per unit width), N_y, both loads either tensile (+) or compressive (-) (but obviously both loads cannot be tensile if buckling is to occur). The ultimate objective is to determine the specific shape and location of the *buckling boundary*, i.e., the interaction curve (actually segments of straight lines) between N_x and N_y. The buckling boundary is the envelope of a collection of intersecting straight lines each of which corresponds to buckling in a different mode shape. Only a portion of each straight line corresponds to buckling at the lowest buckling load. The remaining portion of each straight line corresponds to a higher buckling load than the lowest. The buckling boundary of a biaxially loaded plate is similar to the festooned solid curves in the uniaxial buckling results of Figure 3-18 on page 268.

We can apply the two biaxial forces simultaneously or we can apply them in a sequence, but in the latter case *the order of load application is crucial.* Simultaneous application of the two biaxial loads in a constant proportion to one another throughout the entire load-application process is usually called 'radial loading' or 'proportional loading'. For example, load radially with N_x and N_y in some fixed proportion, $s = N_y/N_x$, as in load path OB in Figure 3-20. Note that the value of N_x at B is above the buckling load for N_x alone. Thus, if the loading is not radial or proportional, then we cannot load from O to A' (anticipating a next load path in

Éléments sous droits d'auteur

the sequence of A' to B) because the plate buckles at the buckling load for no lateral load applied and, hence, cannot reach point A'. Alternatively, we can load from O to A without difficulty (no buckling occurs under lateral tension) and from A to B also without difficulty. Of course, we could load in any path from O to B provided that, for every load step in the sequence of loading, we have not imposed a load that would cause buckling at the end of that load step until the last load step. The basis for this restriction is that we can't have premature buckling in a *valid* load path. The basis for this latitude in loading ability is the fact that applying axial or lateral tension to the plate increases the ability of the plate to withstand forces that would otherwise cause buckling.

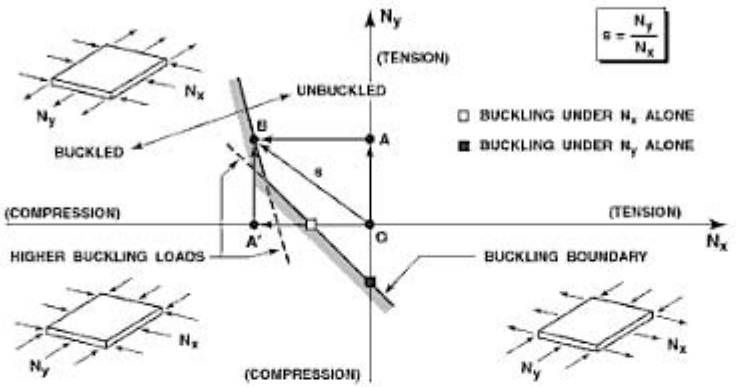


Figure 3-20 Proportional and Nonproportional Biaxial Mechanical Loading

3.3.3.3 General Nature of the Buckling Results

The buckling results are plotted on normalized loading axes, namely $N_y b^2/\pi^2 D$ and $N_x b^2/\pi^2 D$, as is done for the uniaxial buckling load in Section 3.3.2. Buckling occurs in a variety of doubly sinusoidal mode shapes, each with different values of m and n. The buckling mode that corresponds to the lowest set of $\bar{N}_x$ and $\bar{N}_y$ for a specified ratio, s, of N_y to N_x governs buckling. All other modes correspond to higher buckling loads that do not govern unless some physical restraint forces the plate to buckle in a higher mode (see Section 3.3.7). However, the buckling mode shape changes as s is varied and as the plate aspect ratio, a/b, changes. We simplify the problem by first considering only square plates, i.e., a/b = 1. Then, the lines representing the buckling mode that corresponds to the lowest set of $\bar{N}_x$ and $\bar{N}_y$ for many values of s are shaded on the buckled plate side of the solid buckling mode line. The shaded lines are collectively called the *buckling boundary*. The buckling boundary in the results shown schematically in Figure 3-21 consists of many different lines corresponding to different mode shapes and represents the boundary between a buckled plate and an unbuckled plate.

Éléments sous droits d'auteur

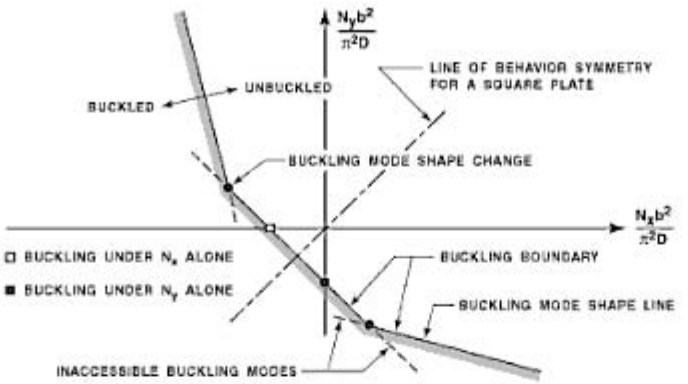


Figure 3-21 General Nature of the Results for Buckling under Biaxial Loading

To start the process of finding the buckling behavior, we know the uniaxial buckling loads, N_x and N_y, from Section 3.3.2. We also know the plate will buckle at some value of the biaxial loads. Moreover, we know there must be interaction between the two biaxial loads such that

- Presence of two compressive loads perpendicular to each other results in buckling before either of the two applied loads reaches its uniaxial buckling value. That is, the plate is *reduced in stiffness against buckling* by the additional compressive load.
- Presence of a *tensile* load and a perpendicular compressive load should result in buckling at a *higher* compressive load than the uniaxial load. That is, the plate is *stiffened against buckling* (but *not prevented* from buckling) by the tensile load.

We speculate that the collective set of mode shape lines governing buckling, i.e., the buckling boundary, is concave toward the origin (the point of zero biaxial loads). This speculation is justified by observing that even though a tensile load exists, a compressive load in the perpendicular direction is required to cause buckling, and that tensile load must increase more rapidly than the compressive load as we move away from the origin because buckling is a compressive-load-dominated process. All of the foregoing elements are present in Figure 3-21 in a schematic manner, i.e., the uniaxial buckling loads, the reduction in biaxial compression buckling loads from the uniaxial values, the increase in compressive buckling load in biaxial tension and compression because of the perpendicular tensile loading, and the concavity of the buckling boundary toward the origin of loading. In addition, buckling mode shape changes occur at intersections of straight-line segments of the buckling boundary. Moreover, some buckling modes are inaccessible for certain combinations of buckling loads. For square plates, the buckling behavior is symmetric about the line $s = 1$. Next, we address specific buckling results.

Éléments sous droits d'auteur

3.3.3.4 Results for Both $\bar{N}_x$ and $\bar{N}_y$ Compressive

The buckling results for a square plate with both $\bar{N}_x$ and $\bar{N}_y$ compressive are shown in the third quadrant of Figure 3-22. Recall that $\bar{N}_x$ and $\bar{N}_y$ are *compressive loads*, so they have signs opposite to N_x and N_y. Values of both loadings are specified in the form $\bar{N}_x = N$ ($N_x = -N$) in which N is the compressive load. The relation between $\bar{N}_x$ and $\bar{N}_y$ for a fixed plate aspect ratio and a specified plate bending stiffness, D, is linear as long as buckling occurs in the same buckling mode (i.e., the same values of m and n)—a valid statement in all quadrants. Different straight lines result for different mode shapes for a square plate in Figure 3-22 in which *all the biaxial behavior is symmetric about the line s = 1.* Three modal lines, m = 1, n = 1; m = 2, n = 1; and m = 3, n = 1, for the lowest buckling loads are shown as shaded solid lines, i.e., the buckling

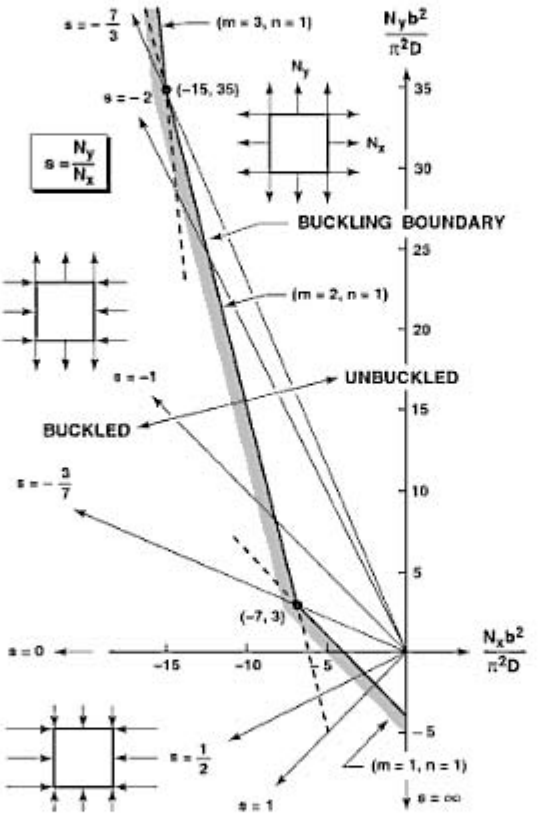


Figure 3-22 Buckling of a Square Plate under Biaxial Loading $\bar{N}_x$ and $\bar{N}_y$

Éléments sous droits d'auteur

boundary, in Figure 3-22. The dashed lines represent behavior in mode shapes with higher buckling loads than at the shaded solid lines and are therefore beyond the buckling boundary, i.e., on the buckled side. The value of $\bar{N}_x$ for $\bar{N}_y = 0$ ($s = 0$), i.e., the uniaxial buckling load, is the same as was obtained in Section 3.3.2 ($4\pi^2 D/b^2$). Also, the value of the other uniaxial buckling load, $\bar{N}_y$ for $\bar{N}_x = 0$ ($s = \infty$), is the same ($4\pi^2 D/b^2$) as it must be because both are the uniaxial buckling load for a *square* plate. Various proportional loading lines each with different slope $s = N_y/N_x$ are also shown. Under radial loading from the origin, the intersection with the buckling boundary corresponds to the lowest buckling load. If we proceed on the radial path $s = 1$ ($N_x = N_y$), we first encounter the buckling mode $m = 1$, $n = 1$, next $m = 2$, $n = 1$ and $m = 1$, $n = 2$, then $m = 3$, $n = 1$ and $m = 1$, $n = 3$, etc. However, the buckling boundary for $m = 1$, $n = 1$ is encountered first with buckling loads $\bar{N}_x b^2/\pi^2 D = 2$ ($N_x b^2/\pi^2 D = -2$) and $\bar{N}_y b^2/\pi^2 D = 2$ ($N_y b^2/\pi^2 D = -2$). If we proceed on the radial path $s = 1/2$ ($N_y = 1/2\ N_x$), we first encounter the buckling mode with $m = 1$, $n = 1$, next $m = 2$, $n = 1$, then $m = 1$, $n = 2$, etc. However, the buckling boundary for $m = 1$, $n = 1$ is encountered first with the buckling loads $\bar{N}_x b^2/\pi^2 D = 8/3$ ($N_x b^2/\pi^2 D = -8/3$) and $\bar{N}_y b^2/\pi^2 D = 4/3$ ($N_y b^2/\pi^2 D = -4/3$).

3.3.3.5 Results for Tensile N_y and Compressive $\bar{N}_x$

If tensile N_y is applied, then the compressive $\bar{N}_x$ required to cause buckling exceeds the uniaxial buckling load $\bar{N}_x$ as seen in the second quadrant of Figure 3-22. That is, a plate that is compressed in one direction and pulled on in the perpendicular direction has a far higher compressive buckling load than the same plate subjected to uniaxial compression. Thus, applying a lateral tensile load is a powerful and effective way to raise the buckling load, i.e., to stiffen a plate against buckling. Buckling does occur, but at a higher compressive load than without the lateral tensile load. For radial loading along the line $s = -1$, the plate buckles first into the $m = 2$, $n = 1$ mode at $\bar{N}_x b^2/\pi^2 D = 8\ 1/3$ ($N_x b^2/\pi^2 D = -8\ 1/3$) and $N_y b^2/\pi^2 D = +8\ 1/3$ [calculations from Equation (3.186)]. Thus, in this biaxial loading case, the compressive buckling load is more than twice the uniaxial compressive buckling load! For radial loading along the line $s = -2$, the plate also buckles first into the $m = 2$, $n = 1$ mode at the loads $\bar{N}_x b^2/\pi^2 D = 12.5$ ($N_x b^2/\pi^2 D = -12.5$) and $N_y b^2/\pi^2 D = +25$. Thus, in this biaxial loading case, the compressive buckling load is more than three times the uniaxial buckling load!

3.3.3.6 Behavior under Large Tensile Loads

Now we address what happens when the tensile load component becomes very large (but a compressive load component still exists in the perpendicular direction). Note that the buckling boundary for each buckling mode shape in the second quadrant of Figure 3-22, as $\bar{N}_y$ increases

Éléments sous droits d'auteur

in the positive (tensile) sense and $\bar{N}_x$ gets larger in the negative (compressive) sense, can never rise with a slope to the right of vertical because that slope would imply (1) buckling under only tensile $\bar{N}_y$ at some very large value of $\bar{N}_y$, a physical impossibility and (2) cross over into the biaxial tension quadrant where buckling cannot occur. Similarly, the buckling boundary in the fourth quadrant (which is not shown, but we know the behavior in the fourth quadrant because the buckling results for a square plate are symmetric about the proportional loading line $s = 1$). There, as $\bar{N}_y$ increases in the negative sense (compressive) and $\bar{N}_x$ becomes larger in the positive (tensile) sense, the behavior in the fourth quadrant can never have a slope that is above the horizontal (for the same reason as in the second quadrant). Both buckling boundaries must approach an asymptote that is vertical in the second quadrant and horizontal in the fourth quadrant, respectively. Approaching the asymptote signifies the effective end of stiffening the plate against buckling by applying a tensile load in a perpendicular direction to the compressive load. Note, of course, that another mode of failure aside from buckling might 'stop' the plate (i.e., cause failure in a different mode than buckling) before it buckles. For example, tensile fracture might occur because of the high tensile stresses.

3.3.3.7 Nonproportional Loading

We can address two practical problems for buckling of biaxially loaded plates, as noted in Section 3.3.3.1. First, we used proportional loading in Sections 3.3.3.4–3.3.3.6. Now, for the second problem of nonproportional loading, a further two typical problems arise. The first and simplest problem is two nonproportional loading steps, one in the x-direction and the other in the y-direction, to reach the buckling boundary. The second problem is loading with many load steps of various sizes to reach the buckling boundary. We must expect that the order of such variously sized load steps is crucial to the process of determining the loads at which buckling occurs.

The nonproportional loading problem of one load step in each of the two directions to the buckling boundary is addressed first. If we load the plate nonproportionally such as by fixing the value of $\bar{N}_y$ and varying N_x to seek N_x, then the buckling load occurs where the new loading path first crosses a shaded solid modal line (the buckling boundary) in Figure 3-22. For example, if $N_y b^2/\pi^2 D$ is prescribed to be 23 (tensile), no solid modal line exists to the right of that value on the $N_y b^2/\pi^2 D$ axis, so we must go to the left to the $m = 2$, $n = 1$ modal buckling line to get $\bar{N}_x b^2/\pi^2 D = 12$ ($N_x b^2/\pi^2 D = -12$) (three times the uniaxial buckling load!). Note that the equations of the modal lines are easily found because we can readily verify that the buckle mode shape changes from $m = 1$, $n = 1$ to $m = 2$, $n = 1$ at normalized load coordinates (–7, 3) and from $m = 2$, $n = 1$ to $m = 3$, $n = 1$ at (–15, 35). Of course, we get the same buckling result irrespective of whether we do proportional or nonproportional loading, i.e.,

Éléments sous droits d'auteur

both approaches are equally valid. For example, radial loading at s = −2 leads to (−12 1/2, 25) whereas going to $N_y b^2/\pi^2 D = 25$ and then over to the m = 2, n = 1 modal line also results in $N_x b^2/\pi^2 D = -12\ 1/2$. However, although the two approaches are equivalent in buckling load, they are not equivalent in load-application sequence. Note that the stiffening tensile load must be applied *before* the compressive load, otherwise the plate would buckle at $N_x b^2/\pi^2 D = -4$ and never reach the compressive buckling load of $N_x b^2/\pi^2 D = -12\ 1/2$. That is, the order of application of the load steps is crucial.

The second practical nonproportional loading problem of many loading steps to the buckling boundary is treated now. That every proportional loading path touches the buckling boundary at a unique point is easy to see in Figure 3-22. However, nonproportional loading is far more complicated and consists, in general, of a sequence of many loading steps (increments of loading or unloading in either the x- or y-directions or both in some proportion). Unless *all* steps are proportional loading, the total load path is nonproportional loading. That is, if *any* step is nonproportional loading, then the overall loading path is nonproportional. The load path is theoretically free to exploit every portion of the unbuckled plate side of the buckling boundary (because the plate material is considered to be elastic), loading and unloading in various directions until finally the path touches the buckling boundary. Thus, every path must stay within the buckling boundary except for the last step which just touches the buckling boundary and causes buckling. The point is that wherever the nonproportional loading path touches the buckling boundary for the first time is the buckling load. Thus, the loading sequence is quite path-sensitive.

The loading paths shown in Figure 3-23 are not all-inclusive of the types of paths that are possible for the second nonproportional loading problem. However, they are representative of most paths of practical interest. Path 1 from normalized load coordinates (0, 0) to (0, −2) to (−2, −2) is two loading steps that are equivalent in buckling loads to the proportional loading path s = 1 in Figure 3-22. Path 2 from (0, 0) to (−1, 0) to (−1, −1) to (−1, −3) is simply three loading steps that culminate in buckling. Path 3 from (0, 0) to (−2, 3) is proportional loading, but not to buckling. The path continues to (−7, 3) where buckling occurs. Although part of the path is proportional loading, the entirety of the path must be called nonproportional loading. This path has the same buckling loads as the proportional loading path s = −3/7. Path 4 from (0, 0) to (−3, 0) to (−3, 5) to (−7 1/2, 5) is simply three loading steps culminating in buckling. Path 5 from (0, 0) to (−1, 9) to (−5, 9) to (−5, 8) to (−4, 8) to (−4, 7) to (−8, 7) has three steps of unloading prior to a final load step to buckling. Path 6 from (0, 0) to (−1, 0) to (−1, 10) to (−8, 10) to (−8, 7) has one step of unloading (in tension) just prior to a final load step to buckling. That is, *the plate actually buckles while being unloaded!*

Éléments sous droits d'auteur

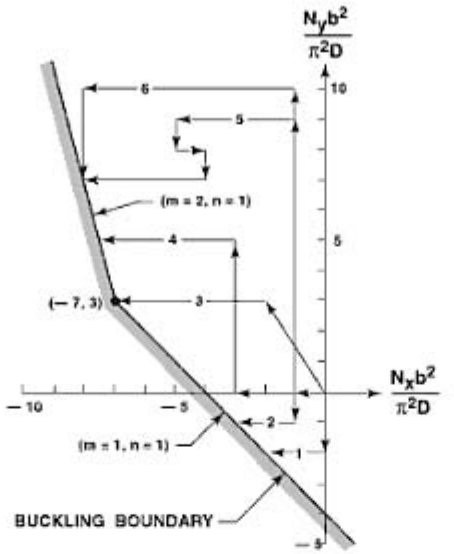


Figure 3-23 Schematic of Loading Near the Buckling Boundary

3.3.3.8 Effect of Plate Aspect Ratio

The plate aspect ratio, a/b, is unity (a square plate) in the numerical results of Figure 3-22, and those results are symmetric about the proportional loading slope of $s = 1$. For other plate aspect ratios, figures analogous to Figure 3-22 would be quite different and, in particular, would not exhibit symmetry about the proportional loading line, $s = 1$. Specifically, the locations of the points where mode shapes change would be different as would be the slopes of the mode shape lines.

Another facet of buckling of biaxially loaded plates is depicted in Figure 3-24 where normalized buckling loads are plotted versus the plate aspect ratio. The loading is equal biaxial compression ($N_x = N_y$, not equal forces), and all buckling occurs in the $m = 1$, $n = 1$ mode. If we examine the loading parameter $\bar{N}_x b^2/(\pi^2 D)$, we see that the buckling load approaches infinity as the plate aspect ratio approaches zero. In this case, the primary load is in the x-direction because $N_x b > N_y a$. Simultaneously, the loading parameter $\bar{N}_y a^2/(\pi^2 D)$ approaches unity as a/b approaches zero. This effect can be explained by first observing, with the aid of Figure 3-25, that for such values of a/b the force in the y-direction is negligible. Thus, because all four edges are simply supported, the buckling load for this plate is higher than for a column, i.e.,

Éléments sous droits d'auteur

$$\bar{N}_x b > \frac{\pi^2 EI}{a^2} \tag{3.188}$$

However, the right-hand side of Equation (3.188) approaches infinity as a, the plate length, approaches zero. For a plate aspect ratio of unity, $\bar{N}_x b^2/(\pi^2 D) = \bar{N}_y a^2/(\pi^2 D) = 2$. For large plate aspect ratios, the inverse of the small plate aspect ratio problem occurs. That is, as a/b approaches infinity, so does $\bar{N}_y a^2/(\pi^2 D)$, but $\bar{N}_x b^2/(\pi^2 D)$ approaches unity.

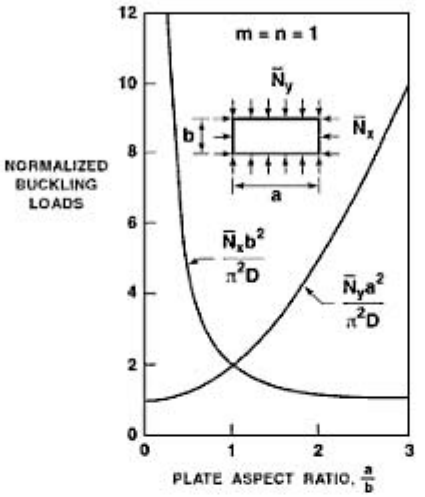


Figure 3-24 Normalized Buckling Loads for Rectangular Plates under Equal Biaxial Compression

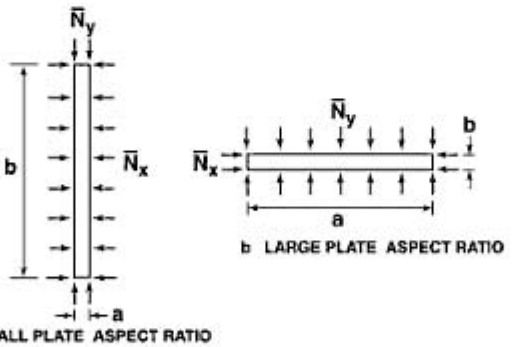


Figure 3-25 Rectangular Plates Under Uniform Biaxial Compression

Éléments sous droits d'auteur

3.3.3.9 Summary Remarks on Buckling under Biaxial Loading

We just addressed the most complicated buckling problem thus far in this book. Biaxial loading itself is complex enough, but the number of required variables for the buckling part of the problem is larger than for any problem so far. Issues of both tensile and compressive loading affect buckling as well as how loads are introduced, including nonproportional loading. The concept of the buckling boundary, which is comprised of all the buckling mode shape lines that correspond to the lowest buckling loads, is introduced and exploited in this study. Once the buckling boundary is established, then analysis of buckling problems is straightforward. Note that some buckling mode shapes are not accessible (i.e., are outside the buckling boundary) for some combinations of buckling loads. The loading of a plate must stay within the buckling boundary in Figure 3-22 on page 273, or any other buckling results diagram, unless there are physical restraints that prevent the plate from buckling into the indicated mode. If such restraints exist (see the discussion in Section 3.3.7), then the buckling boundary will move away from the loading origin to encompass the new buckling boundary. Finally, the effect of the plate aspect ratio, a/b, is studied for the special case of equal biaxial compression ($\bar{N}_x = \bar{N}_y$, not equal forces).

Problem Set 3.3.3

3.3.3.1 Derive the buckling criterion in Equation (3.186).

3.3.3.2 Calculate the coordinates of all buckling mode shape intersections and the slopes of the buckling boundary segments in each mode shape in Figure 3-22.

3.3.3.3 Plot the buckling results for m = 2, n = 2 in the manner of Figure 3-22. Why are we not interested in this result?

3.3.3.4 Plot $N_x b^2/\pi^2 D$ for equal biaxial compression against a/b from a/b = .5 to a/b = ∞. What is the limiting value of k for a long plate?

3.3.3.5 A rectangular plate of plate aspect ratio, a/b = 2, and simply supported on all four edges is subjected to biaxial loading. Plot the buckling results in a manner analogous to Figure 3-22.

3.3.3.6 A simply supported rectangular plate subjected to N_x is restrained from in-plane movement in the y-direction on the edges y = 0 and y = b. Plot $N_x b^2/\pi^2 D$ for v = 0, .1, 1/6, 1/5, 1/4, .3, 1/3, .4, and 1/2 from a/b = .5 to 5. Discuss the results in comparison to previous results.

3.3.4 Buckling of Simply Supported Rectangular Plates under Combined In-Plane Bending and Compression

Rolled and built-up structural sections must have flanges and webs that do not buckle under the imposed load. The web of a beam that is subjected to pure bending has a free-body diagram as shown in Figure 3-26 if shear stresses are ignored. The fact that the beam must bend implies that the web is subjected to bending in its plane. If, in addition, axial force is imposed upon the beam, the web has a superimposed load in the x-direction. The effect of shear on the web will be addressed later. Thus, we seek to solve the buckling problem of a plate subjected to in-plane bending and compression wherein the load is described as

$$N_x(x,y) = N_o\left[1 - \alpha \frac{y}{b}\right] \tag{3.189}$$

Éléments sous droits d'auteur

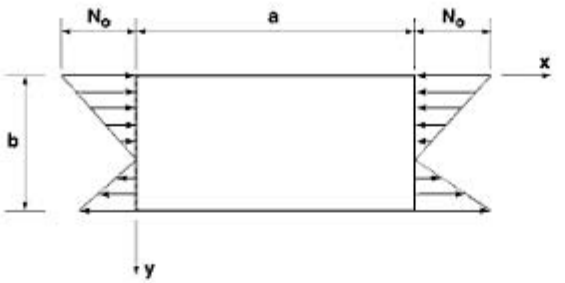


Figure 3-26 Rectangular Plate Subjected to In-Plane Bending and Compression

in which N_o is the force per unit width at the edge $y = 0$. The factor α is a constant that represents the type of in-plane loading. For example, $\alpha = 0$ for pure in-plane compression and $\alpha = 2$ for pure in-plane bending as in Figure 3-27. For values of α less than two, the loading is in-plane bending plus compression. On the other hand, for values of α greater than two, the loading is tension superimposed on the in-plane bending. We will obtain results only for $\alpha < 2$. This problem was first addressed by Timoshenko [3-11] and later by Johnson and Noel [3-12].

The plate edges are simply supported as a lower-bound type of approximation to the actual web support conditions. We can look at the problem from a purely theoretical standpoint: we solve the buckling problem of a simply supported rectangular plate subjected to in-plane bending and compression. Then, we can apply that 'exact' result as an approximation to the actual physical problem of structural shape analysis.

The differential equation, Equation (3.162), has non-constant coefficients because of the loading. Thus, we adopt an approximate strain energy integral approach to the problem and note that the double Fourier series[2] for the variation of deflection (buckling deflection)

$$\delta w = \sum_{m=1}^{\infty} \sum_{n=1}^{\infty} \bar{w}_{mn} \sin \frac{m\pi x}{a} \sin \frac{n\pi y}{b} \tag{3.190}$$

satisfies both the geometric and the natural boundary conditions on all edges and can represent any deflection within the plate boundaries. The

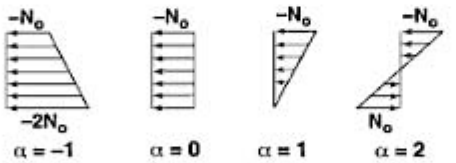


Figure 3-27 Force Intensity Distributions for Various Values of α

[2]For conditions on differentiation, integration, completeness, and convergence of Fourier series, consult Tolstov [3-9] or Brown and Churchill [3-10].

Éléments sous droits d'auteur

variation of deflection does not, however, satisfy the differential equation governing buckling. Realize that this deflection function is the exact solution to the buckling differential equation for pure compression, so it cannot be the exact solution for the present problem. Moreover, as with previous problems, the buckling deflection component amplitudes $\tilde{w}$ are indeterminate. The two variation in strain energy expressions that must be evaluated for this deflection approximation are given by Equations (3.165) and (3.166) which for this problem can be written as

$$\bar{\delta}^2 U_{m_2} = -\int_0^a \int_0^b N_o(1 - \alpha y/b)\delta w_x^2 dxdy \tag{3.191}$$

$$\bar{\delta}^2 U_b = D\int_0^a \int_0^b \left[\delta w_{xx}^2 + \delta w_{yy}^2 + 2\nu\delta w_{xx}\delta w_{yy} + 2(1-\nu)\delta w_{xy}^2\right]dxdy \tag{3.192}$$

Because the axial force per unit width is a function of y, integration of Equation (3.191), after substitution of the deflection approximation in Equation (3.190), requires the following special integration results:

$$\int_0^b y \sin\frac{i\pi y}{b}\sin\frac{j\pi y}{b}dy = \begin{cases} \dfrac{b^2}{4} & \text{for } i = j \\ 0 & \text{for } i \neq j \text{ and } i \pm j \text{ an even number} \\ -\dfrac{4b^2}{\pi^2}\dfrac{ij}{(i^2-j^2)^2} & \text{for } i \neq j \text{ and} \\ & i \pm j \text{ an odd number} \end{cases} \tag{3.193}$$

With Equation (3.193), we can show that

$$\bar{\delta}^2 U_{m_2} = -N_o\frac{ab}{4}\sum_{m=1}^{\infty}\sum_{n=1}^{\infty}\tilde{w}_{mn}^2\frac{m^2\pi^2}{a^2} + N_o\frac{\alpha a}{2b}\sum_{m=1}^{\infty}\frac{m^2\pi^2}{a^2}\left[\frac{b^2}{4}\sum_{n=1}^{\infty}\tilde{w}_{mn}^2 - \frac{8b^2}{\pi^2}\sum_{n=1}^{\infty}\sum_{i}^{\infty}\frac{\tilde{w}_{mn}\tilde{w}_{mi}ni}{(n^2-i^2)^2}\right] \tag{3.194}$$

wherein $n \pm i$ is always odd. Also, we can easily show that

$$\bar{\delta}^2 U_b = D\frac{ab\pi^4}{4}\sum_{m=1}^{\infty}\sum_{n=1}^{\infty}\tilde{w}_{mn}^2\left[\frac{m^2}{a^2} + \frac{n^2}{b^2}\right]^2 \tag{3.195}$$

Thus, we can now apply the buckling criterion

$$\delta\left(\bar{\delta}^2 V\right) = \delta\left(\bar{\delta}^2 U_{m_2} + \bar{\delta}^2 U_b\right) = 0 \tag{3.196}$$

which is formally

$$\frac{\partial}{\partial\tilde{w}_{mn}}\left(\bar{\delta}^2 V\right) = 0 \tag{3.197}$$

an infinite set of linear algebraic equations in an infinite number of unknowns:

Éléments sous droits d'auteur

$$-2N_o\frac{ab}{4}\tilde{w}_{mn}\frac{m^2\pi^2}{a^2}+N_o\frac{\alpha a}{2b}\frac{m^2\pi^2}{a^2}\left[\frac{b^2}{4}2\tilde{w}_{mn}-\frac{8b^2}{\pi^2}\sum_i^{\infty}\frac{\tilde{w}_{mi}ni}{(n^2-i^2)^2}\right]$$

$$+D\frac{ab}{4}\pi^4 2\tilde{w}_{mn}\left[\frac{m^2}{a^2}+\frac{n^2}{b^2}\right]^2=0 \quad n\pm i \text{ odd} \tag{3.198}$$

Naturally, we restrict our attention to a finite subset of those characteristic equations. First, however, we note that the infinite set of characteristic equations is divided into subgroups of equations for which each subgroup has a single value of m, but an infinite number of values of n. That is, each of the sets of equations as represented by one value of m in Equation (3.198) is independent of all the other sets. That is, buckling occurs in an integer number of half-waves in the x-direction according to the equation (a simplification of Equation (3.198)):

$$\tilde{w}_{mn}\left[\left[m^2+n^2\frac{a^2}{b^2}\right]^2-N_o\frac{m^2a^2}{\pi^2D}\left[1-\frac{\alpha}{2}\right]\right]$$

$$-8N_o\alpha\frac{m^2a^2}{\pi^4D}\sum_i^{\infty}\frac{\tilde{w}_{mi}ni}{(n^2-i^2)^2}=0 \tag{3.199}$$

wherein m and n take on values from one to infinity. We would have arrived at the same characteristic equation had we initially *assumed* the variation in deflection function (buckling deflection)

$$\delta w=\sin\frac{m\pi x}{a}\sum_{n=1}^{\infty}\tilde{w}_{mn}\sin\frac{n\pi y}{b} \tag{3.200}$$

which is sinusoidal in the x-direction and complete in the y-direction, so it can represent any function in the y-direction. We have just verified that such an assumption is indeed appropriate, but its validity was not obvious.

In order to satisfy the characteristic equations, Equation (3.199), the determinant of the coefficients of $\tilde{w}_{mn}$ must be zero for a nontrivial solution to exist. However, the determinant is still infinite so we must successively approximate the exact solution by taking more and more terms in the governing equation and thereby obtaining a larger and larger determinant. For example, if m = 1 (a single half-wave in the x-direction), the characteristic equations are

$$\tilde{w}_{1n}\left[\left[1+n^2\frac{a^2}{b^2}\right]^2-N_o\frac{a^2}{\pi^2D}(1-\alpha/2)\right]-8N_o\alpha\frac{a^2}{\pi^4D}\sum_i^{\infty}\frac{\tilde{w}_{1i}ni}{(n^2-i^2)^2}=0 \tag{3.201}$$

and you will recall that $n\pm i$ must be an odd number in the last term of Equation (3.201). Then, the first approximation to the characteristic equation involves only $\tilde{w}_{11}$:

Éléments sous droits d'auteur

$$\tilde{w}_{11}\left[\left[1+\frac{a^2}{b^2}\right]^2-\frac{N_o a^2}{\pi^2 D}(1-\alpha/2)\right]=0 \tag{3.202}$$

whereupon because $\tilde{w}_{11}$ cannot be zero (or buckling would not occur!)

$$N_o=\frac{\pi^2 D}{a^2}\left[1+\frac{a^2}{b^2}\right]^2\frac{1}{1-\alpha/2} \tag{3.203}$$

or

$$N_o=\frac{\pi^2 D}{b^2}\left[\frac{b}{a}+\frac{a}{b}\right]^2\frac{1}{1-\alpha/2} \tag{3.204}$$

This one-term approximation is invalid for the pure bending case where $\alpha=2$ because of the last term in Equation (3.204). However, the approximation does reduce to the exact solution when $\alpha=0$ [uniform axial compression for a square plate which has the buckling mode of $m=1$ and $n=1$ as in Equation (3.176)] as expected. Thus, the first approximation is valid only for very small values of α with buckling near $m=1$ and $n=1$. Accordingly, we must seek other approximations as α increases above small values near zero.

The second approximation to the characteristic equations involves only $\tilde{w}_{11}$ and $\tilde{w}_{12}$:

$$\tilde{w}_{11}\left[\left[1+\frac{a^2}{b^2}\right]^2-\frac{N_o a^2}{\pi^2 D}(1-\alpha/2)\right]-8N_o\alpha\frac{a^2}{\pi^4 D}\frac{2}{9}\tilde{w}_{12}=0 \tag{3.205}$$

$$-8\alpha\frac{N_o a^2}{\pi^4 D}\frac{2}{9}\tilde{w}_{11}+\left[\left[1+4\frac{a^2}{b^2}\right]^2-\frac{N_o a^2}{\pi^2 D}(1-\alpha/2)\right]\tilde{w}_{12}=0 \tag{3.206}$$

for which the criterion that the determinant of the coefficients of $\tilde{w}_{11}$ and $\tilde{w}_{12}$ in the homogeneous equation set must be zero to avoid the trivial solution ($\tilde{w}_{11}=\tilde{w}_{12}=0$) requires that

$$\left[\frac{N_o a^2}{\pi^2 D}\right]^2\left[(1-\alpha/2)^2-\left[\frac{8\alpha}{\pi^2}\frac{2}{9}\right]^2\right]+\left[1+\frac{a^2}{b^2}\right]^2\left[1+4\frac{a^2}{b^2}\right]^2$$
$$-\frac{N_o a^2}{\pi^2 D}(1-\alpha/2)\left[\left[1+\frac{a^2}{b^2}\right]^2+\left[1+4\frac{a^2}{b^2}\right]^2\right]=0 \tag{3.207}$$

from which the second approximation to N_o is obtained. Again, the accuracy of this approximation decreases as α approaches 2 (the inaccuracy can be shown to be about 8% in the pure bending case).

Éléments sous droits d'auteur

The third approximation to the characteristic equations involves $\bar{w}_{11}$, $\bar{w}_{12}$, and $\bar{w}_{13}$ and is used only when $\alpha = 2$ (pure bending) because the second approximation suffices for lesser values of α. The three characteristic equations are

$$\left[1 + \frac{a^2}{b^2}\right]^2 \bar{w}_{11} - 16\frac{N_o a^2}{\pi^4 D}\frac{2}{9}\bar{w}_{12} = 0 \tag{3.208}$$

$$-16\frac{N_o a^2}{\pi^4 D}\frac{2}{9}\bar{w}_{11} + \left[1 + 4\frac{a^2}{b^2}\right]^2 \bar{w}_{12} - 16\frac{N_o a^2}{\pi^4 D}\frac{6}{25}\bar{w}_{13} = 0 \tag{3.209}$$

$$-16\frac{N_o a^2}{\pi^4 D}\frac{6}{25}\bar{w}_{12} + \left[1 + 9\frac{a^2}{b^2}\right]^2 \bar{w}_{13} = 0 \tag{3.210}$$

from which a buckling equation is obtained if the determinant of the coefficients of $\bar{w}_{11}$, $\bar{w}_{12}$, and $\bar{w}_{13}$ is equated to zero. Timoshenko and Gere [3-8] note that a fourth approximation differs from the third approximation by about one-third of one percent.

The overall results can be expressed as

$$N_o = k\frac{\pi^2 D}{b^2} \tag{3.211}$$

in which the value of k depends on the type of loading (the value of α) and the plate aspect ratio, a/b, as in Table 3-1 for m = 1. All results are obtained by use of the second approximation to the characteristic equations except for the pure bending results for which the third approximation was used. For pure bending ($\alpha = 2$), the smallest buckling load occurs for a/b = 2/3. For smaller α, the a/b for the smallest buckling load increases to unity which is the value for a plate subjected to N_x only. The values of k for the pure bending case are plotted in Figure 3-28 for various numbers of half waves in the x-direction. The results are obtained for m = 2, m = 3, etc., by varying m in Equation (3.200).

Table 3-1 Buckling Coefficient k for Simply Supported Rectangular Plates Subjected to In-Plane Bending and Compression Buckling in the m = 1 Mode*

α	Plate Aspect Ratio, a/b								
	.4	.5	.6	.667	.75	.8	.9	1.	1.5
2	29.1	25.6	24.1	23.9	24.1	24.4	25.6	25.6	24.1
4/3	18.7		12.9		11.5	11.2		11.0	11.5
1	15.1		9.7		8.4	8.1		7.8	8.4
4/5	13.3		8.3		7.1	6.9		6.6	7.1
2/3	10.8		7.1		6.1	6.0		5.8	6.1

After Timoshenko and Gere [3-8], p. 377, reproduced by permission

Éléments sous droits d'auteur

The axial stress varies from compressive to tensile as we go from top to bottom in the sketch in Figure 3-28. Thus, we expect buckles to occur in the upper portion of the plate (with increasing amplitude toward the top), but no buckles to occur in the lower portion (or at least smaller-amplitude buckles because of their suppression or flattening by tensile stress in that region). This shape of buckling deflection would not have been modelled correctly without the complete nature of the sine series in the y-direction of the variation in deflection in Equation (3.200).

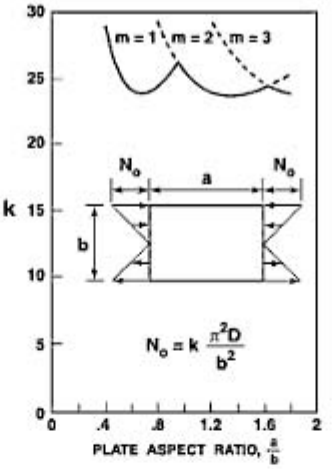


Figure 3-28 Buckling under Pure In-Plane Bending of Simply Supported Rectangular Plates *(Inspired by Timoshenko and Gere [3-8])*

Problem Set 3.3.4

3.3.4.1 Verify the strain energy expressions in Equations (3.194) and (3.195).
3.3.4.2 Verify the infinite set of characteristic buckling equations in Equation (3.198).
3.3.4.3 Verify the subset of characteristic buckling equations in Equation (3.199).
3.3.4.4 Verify the infinite set of characteristic buckling equations in Equation (3.201).
3.3.4.5 Verify the first approximation to the characteristic equations, Equation (3.204).
3.3.4.6 Verify the second approximation, Equations (3.205)–(3.207).
3.3.4.7 Verify the third approximation, Equations (3.208)–(3.210).
3.3.4.8 Evaluate the second approximation, Equation (3.207), for uniaxial compression ($\alpha = 0$). What is the significance of the results?
3.3.4.9 Plot the results for the first and second approximations for a square plate as α goes from 0 toward 2.

3.3.5 Buckling of Simply Supported Rectangular Plates under In-Plane Shear N_{xy}

Consider the simply supported rectangular plate in Figure 3-29 subjected to uniform in-plane shearing forces, $\bar{N}_{xy}$. Such a problem is a partial representation of the web of a structural shape such as an I-beam that is subjected to pure shear loading perpendicular to the beam axis.

The equilibrium state prior to buckling is $N_x(x,y) = 0$, $N_y(x,y) = 0$, and $N_{xy}(x,y) = N_{xy}$. No exact solution is known for the differential equation governing buckling which, by reduction from Equation (3.162), is

$$D\nabla^4(\delta w) + 2\bar{N}_{xy}\delta w_{,xy} = 0 \qquad (3.212)$$

Éléments sous droits d'auteur

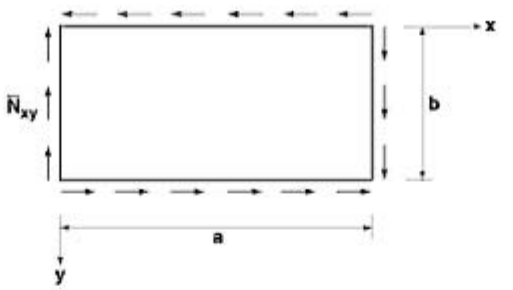


Figure 3-29 Simply Supported Rectangular Plate Subjected to In-Plane Shear

Stein and Neff [3-13] used a strain energy approach with the buckle deflection approximation in the form of a double Fourier sine series

$$\delta w = \sum_{m=1}^{\infty} \sum_{n=1}^{\infty} \tilde{w}_{mn} \sin \frac{m\pi x}{a} \sin \frac{n\pi y}{b} \tag{3.213}$$

which satisfies the simply supported edge boundary conditions on all edges. The strain energy integrals to be evaluated are

$$\bar{\delta}^2 U_{m_2} = 2N_{xy} \int_0^a \int_0^b \delta w_{,x} \delta w_{,y} \, dx dy \tag{3.214}$$

$$\bar{\delta}^2 U_b = D \int_0^a \int_0^b \left[(\delta w_{,xx} + \delta w_{,yy})^2 - 2(1-\nu)(\delta w_{,xx} \delta w_{,yy} - \delta w_{,xy}^2) \right] dx dy \tag{3.215}$$

These integrals are, of course, summed to obtain $\bar{\delta}^2 V$ which is subsequently made stationary to determine the buckling load. The evaluation of the first strain energy integral, Equation (3.214), requires the special integration result

$$\int_0^a \sin \frac{m\pi x}{a} \cos \frac{p\pi x}{a} \, dx = \begin{cases} 0, & \text{if } m \pm p \text{ is an even number} \\ \dfrac{2a}{\pi} \dfrac{m}{m^2 - p^2}, & \text{if } m \pm p \text{ is an odd number} \end{cases} \tag{3.216}$$

Thus, with the already known evaluation of $\bar{\delta}^2 U_b$ for this deflection approximation, the second variation of the total potential energy is

$$\bar{\delta}^2 V = 8N_{xy} \sum_m \sum_n \sum_p \sum_q \tilde{w}_{mn} \tilde{w}_{pq} \frac{mnpq}{(m^2 - p^2)(q^2 - n^2)} + \frac{\pi^4 abD}{4} \sum_{m=1}^{\infty} \sum_{n=1}^{\infty} \tilde{w}_{mn}^2 \left[\frac{m^2}{a^2} + \frac{n^2}{b^2} \right]^2 \tag{3.217}$$

Éléments sous droits d'auteur

in which, because of the special integration result in Equation (3.216), $m \pm p$ and $n \pm q$ are odd integers.

Buckling of the plate occurs when

$$\delta(\bar{\delta}^2 V) = 0 \tag{3.218}$$

which, for a finite degree of freedom system, is equivalent to

$$\frac{\partial}{\partial \tilde{w}_{mn}}(\bar{\delta}^2 V) = 0 \tag{3.219}$$

which is an infinite set of homogeneous characteristic equations in the unknowns $\tilde{w}_{mn}$ and can be written as

$$\tilde{w}_{mn} M_{mn} + \sum_{p=1}^{\infty} \sum_{q=1}^{\infty} \tilde{w}_{pq} \frac{mnpq}{(m^2 - p^2)(q^2 - n^2)} = 0 \tag{3.220}$$

in which

$$M_{mn} = \frac{\pi^2}{32 k_s \left[\frac{a}{b}\right]^3} \left[m^2 + n^2 \left[\frac{a}{b}\right]^2 \right]^2 \tag{3.221}$$

in which k_s is the coefficient in the shear buckling load expression:

$$\bar{N}_{xy} = k_s \frac{\pi^2 D}{b^2} \tag{3.222}$$

A nontrivial solution to the set of characteristic equations, Equation (3.220), results when the determinant of the coefficients of $\tilde{w}_{mn}$ is zero. However, observe that the determinant can be separated into two subdeterminants because the corresponding set of characteristic equations has two subsets, one having $\tilde{w}_{mn}$ with $m + n$ an odd number and the other having $\tilde{w}_{mn}$ with $m + n$ an even number. This conclusion can be reached by use of the following logic: because $m + p$ is odd and $n + q$ is odd, then $m + p + n + q$ must be even; also, if $m + n$ is even, then $p + q$ must be even; finally, if $m + n$ is odd, then $p + q$ must also be odd. The first set of characteristic equations ($m + n$ odd) is associated with buckling deflections that are antisymmetric about a central point of inversion symmetry, i.e., the deformations are antisymmetric about the midpoint of the plate in a polar sense (with an even number of buckle halfwaves in the longest direction of the plate). The antisymmetry is not about a nodal line. The second set ($m + n$ even) has buckling deflections that are symmetric about a central point of inversion symmetry, i.e., the deformations are symmetric about the midpoint of the plate in a polar sense (with an odd number of buckle halfwaves).

The determinant can be separated into two subdeterminants in the following manner. First, write the set of characteristic equations as

$$\begin{aligned} &C_{11}\tilde{w}_{11} + C_{22}\tilde{w}_{22} + \ldots + C_{rs}\tilde{w}_{rs} = 0 \\ &C_{12}\tilde{w}_{12} + C_{21}\tilde{w}_{21} + \ldots \\ &\quad\vdots \end{aligned} \tag{3.223}$$

which has a nontrivial solution for the $\tilde{w}_{ij}$ if

Éléments sous droits d'auteur

$$\begin{vmatrix} C_{11} & 0 & C_{22} & 0 & C_{44} & 0 & C_{24} & \cdots & C_{1s} \\ 0 & C_{12} & 0 & C_{21} & 0 & & & & \\ \cdot & & & & & & & & \\ \cdot & & & & & & & & \\ \cdot & & & & & & & & \end{vmatrix} = 0 \qquad (3.224)$$

However, the individual rows and columns can be successively interchanged until the determinant is rearranged in the form

$$\left|\begin{array}{ccccc|ccccc} S_{11} & S_{12} & S_{13} & \cdots & S_{1n} & & & & & \\ S_{12} & & & & & & & & & \\ \vdots & & & & \vdots & & & \text{zero} & & \\ S_{1n} & \cdots & & & S_{nn} & & & & & \\ \hline & & & & & A_{11} & A_{12} & A_{13} & \cdots & A_{1n} \\ & & & & & A_{12} & & & & \\ & & \text{zero} & & & \vdots & & & & \vdots \\ & & & & & A_{1n} & \cdots & & & A_{nn} \end{array}\right| = 0 \qquad (3.225)$$

Finally, by a theorem from the theory of determinants (a determinant is zero if any of its subdeterminants are zero), we see that

$$\begin{vmatrix} S_{11} & S_{12} & S_{13} & \cdots & S_{1n} \\ S_{12} & & & & \\ \cdot & & & & \cdot \\ \cdot & & & & \cdot \\ \cdot & & & & \cdot \\ S_{1n} & \cdots & & & S_{nn} \end{vmatrix} = 0 \qquad (3.226)$$

which governs symmetric buckling and

$$\begin{vmatrix} A_{11} & A_{12} & A_{13} & \cdots & A_{1n} \\ A_{12} & & & & \\ \cdot & & & & \cdot \\ \cdot & & & & \cdot \\ \cdot & & & & \cdot \\ A_{1n} & \cdots & & & A_{nn} \end{vmatrix} = 0 \qquad (3.227)$$

Éléments sous droits d'auteur

which governs antisymmetric buckling.

The two infinite sets of linear algebraic characteristic equations are solved by taking successively more terms in each set until satisfactory convergence is achieved. For example, if only the first two terms are taken in the set for which m+n is even (symmetric buckling), the following buckling load is obtained by equating the determinant of the coefficients of $\tilde{w}_{11}$ and $\tilde{w}_{22}$ to zero:

$$\bar{N}_{xy} = \pm \frac{9}{32} \pi^2 \frac{\left[1 + \left[\frac{a}{b}\right]^2\right]^2}{\left[\frac{a}{b}\right]^3} \frac{\pi^2 D}{b^2} \tag{3.228}$$

from which it is apparent that buckling occurs irrespective of the sign of N_{xy}. This numerical result can be shown to be about 15% too high for square plates and even higher for plates with larger plate aspect ratios, a/b [3-8]. Thus, more terms must be taken in the two governing determinants. Stein and Neff [3-13] took ten terms in each determinant (actually 10×10 determinants):

m+n even (symmetric buckling):

	$\tilde{w}_{11}$	$\tilde{w}_{13}$	$\tilde{w}_{22}$	$\tilde{w}_{31}$	$\tilde{w}_{15}$	$\tilde{w}_{24}$	$\tilde{w}_{33}$	$\tilde{w}_{42}$	$\tilde{w}_{51}$	$\tilde{w}_{35}$
m = 1, n = 1	M_{11}	0	$-\frac{4}{9}$	0	0	$-\frac{8}{45}$	0	$-\frac{8}{45}$	0	0
m = 1, n = 3	0	M_{13}	$\frac{4}{5}$	0	0	$-\frac{8}{7}$	0	$\frac{8}{25}$	0	0
m = 2, n = 2	$-\frac{4}{9}$	$\frac{4}{5}$	M_{22}	$\frac{4}{5}$	$\frac{20}{63}$	0	$\frac{36}{25}$	0	$\frac{20}{63}$	$-\frac{4}{7}$
m = 3, n = 1	0	0	$\frac{4}{5}$	M_{31}	0	$\frac{8}{45}$	0	$-\frac{8}{7}$	0	0
m = 1, n = 5	0	0	$\frac{20}{63}$	0	M_{15}	$\frac{40}{27}$	0	$\frac{8}{63}$	0	0
m = 2, n = 4	$-\frac{8}{45}$	$-\frac{8}{7}$	0	$\frac{8}{25}$	$\frac{40}{27}$	M_{24}	$\frac{72}{35}$	0	$\frac{8}{63}$	$-\frac{8}{3}$
m = 3, n = 3	0	0	$-\frac{36}{25}$	0	0	$\frac{72}{35}$	M_{33}	$\frac{72}{35}$	0	0
m = 4, n = 2	$-\frac{8}{45}$	$\frac{8}{25}$	0	$-\frac{8}{7}$	$\frac{8}{63}$	0	$\frac{72}{35}$	M_{42}	$\frac{40}{27}$	$\frac{120}{147}$
m = 5, n = 1	0	0	$\frac{20}{63}$	0	0	$\frac{8}{63}$	0	$\frac{40}{27}$	M_{51}	0
m = 3, n = 5	0	0	$-\frac{4}{7}$	0	0	$-\frac{8}{3}$	0	$\frac{120}{147}$	0	M_{35}

(3.229)

Éléments sous droits d'auteur

m+n odd (antisymmetric buckling):

	$\tilde{w}_{12}$	$\tilde{w}_{21}$	$\tilde{w}_{23}$	$\tilde{w}_{32}$	$\tilde{w}_{41}$	$\tilde{w}_{43}$	$\tilde{w}_{52}$	$\tilde{w}_{61}$	$\tilde{w}_{54}$	$\tilde{w}_{63}$
m = 1, n = 2	M_{12}	$\frac{4}{9}$	$-\frac{4}{5}$	0	$\frac{8}{45}$	$-\frac{8}{25}$	0	$\frac{4}{35}$	0	$-\frac{36}{175}$
m = 2, n = 1	$\frac{4}{9}$	M_{21}	0	$-\frac{4}{5}$	0	0	$-\frac{20}{63}$	0	$-\frac{8}{63}$	0
m = 2, n = 3	$-\frac{4}{5}$	0	M_{23}	$\frac{36}{25}$	0	0	$\frac{4}{7}$	0	$-\frac{40}{49}$	0
m = 3, n = 2	0	$-\frac{4}{5}$	$\frac{36}{25}$	M_{32}	$\frac{8}{7}$	$-\frac{72}{35}$	0	$\frac{4}{9}$	0	$-\frac{4}{5}$
m = 4, n = 1	$\frac{8}{45}$	0	0	$\frac{8}{7}$	M_{41}	0	$-\frac{40}{27}$	0	$-\frac{16}{27}$	0
m = 4, n = 3	$-\frac{8}{25}$	0	0	$-\frac{72}{35}$	0	M_{43}	$\frac{8}{3}$	0	$-\frac{80}{21}$	0
m = 5, n = 2	0	$-\frac{20}{63}$	$\frac{4}{7}$	0	$-\frac{40}{27}$	$\frac{8}{3}$	M_{52}	$\frac{20}{11}$	0	$-\frac{36}{11}$
m = 6, n = 1	$\frac{4}{35}$	0	0	$\frac{4}{9}$	0	0	$\frac{20}{11}$	M_{61}	$\frac{8}{11}$	0
m = 5, n = 4	0	$-\frac{8}{63}$	$-\frac{40}{49}$	0	$-\frac{16}{27}$	$-\frac{80}{21}$	0	$\frac{8}{11}$	M_{54}	$\frac{360}{77}$
m = 6, n = 3	$-\frac{36}{175}$	0	0	$-\frac{4}{5}$	0	0	$-\frac{36}{11}$	0	$\frac{360}{77}$	M_{63}

(3.230)

Stein and Neff obtained the numerical results shown in Table 3-2 and plotted in Figure 3-30. Note that symmetric (about the midpoint in a polar sense) buckling deformation occurs for a/b less than about 2.1 and greater than about 3.5; in between, the buckling deformation is antisymmetric about the midpoint in a polar sense. The behavior is asymptotic to $k_s = 5.34$. The theoretical buckling deformations that occur for a/b = 1.5 (symmetric) and a/b = 2.5 (antisymmetric) are shown in Figure 3-31 and Figure 3-32, respectively. There, note the two curved nodal lines (marked with 0) for symmetric buckling and the single curved nodal line (marked with 0) for antisymmetric buckling. Budiansky and Connor used the Lagrangian multiplier method to obtain shear buckling loads for plates with clamped edges [3-14].

Table 3-2 Values of k_s for Buckling of Simply Supported Rectangular Plates under In-Plane Shear*

a/b	1.0	1.2	1.5	2.0	2.5	3.0	4.0
$k_{symmetric}$	9.35	8.00	7.07	6.59	6.29	6.04	5.67
$k_{antisymmetric}$	11.63	9.70	7.97	6.61	6.06	5.89	5.77

After Stein and Neff [3-13]

Éléments sous droits d'auteur

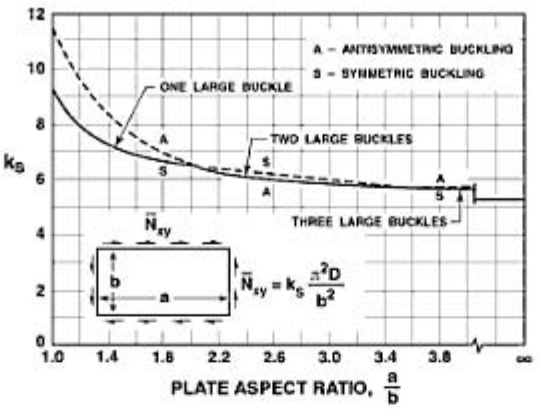


Figure 3-30 Buckling Loads of Simply Supported Rectangular Plates Subjected to In-Plane Shear *(After Stein and Neff [3-13])*

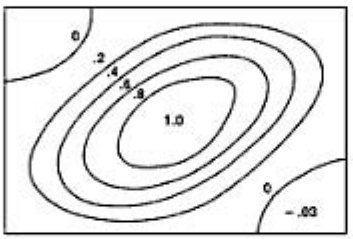


Figure 3-31 Polar Symmetric about Midpoint Buckle Mode of Simply Supported Rectangular Plates with a/b = 1.5 Subjected to In-Plane Shear *(After Stein and Neff [3-13])*

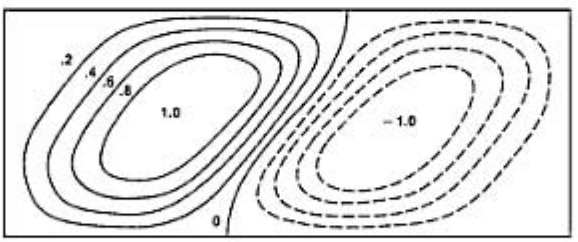


Figure 3-32 Polar Antisymmetric about Midpoint Buckle Mode of Simply Supported Rectangular Plates with a/b = 2.5 Subjected to In-Plane Shear *(After Stein and Neff [3-13])*

Éléments sous droits d'auteur

Problem Set 3.3.5

3.3.5.1 Derive the second variations of the membrane and bending strain energies, Equations (3.214) and 3.215), respectively.
3.3.5.2 Derive the second variation of the total potential energy, Equation (3.217), for the buckling displacement in Equation (3.213).
3.3.5.3 Verify that the use of the buckling criterion $\delta(\overline{\delta^2 V}) = 0$ leads to Equation (3.220).
3.3.5.4 Derive the two-term approximation to the in-plane shear buckling load of plates that buckle symmetrically, Equation (3.228), a simplified version of Equation (3.229).
3.3.5.5 Derive the two-term approximation to the in-plane shear buckling load of plates that buckle antisymmetrically, a simplified version of Equation (3.230).
3.3.5.6 Calculate the symmetric and antisymmetric shear buckling loads for a square plate using the results of Exercises 3.3.5.4 and 3.3.5.5. Compare the results with each other and with the results in Table 3-2.

3.3.6 Buckling of Uniformly Compressed Rectangular Plates Simply Supported Along Two Opposite Loaded Edges with Various Boundary Conditions Along Two Unloaded Edges

Irrespective of the boundary conditions, the buckling differential equation, Equation (3.173), governs for the title problem [3-11, 3-15], i.e.,

$$D\nabla^4(\delta w) + \bar{N}_x \delta w_{,xx} = 0 \tag{3.231}$$

The plate loading and support configuration is shown in Figure 3-33. If all edges are simply supported, we note in Section 3.3.2 that the exact solution for the shape of δw is

$$\delta w = \delta w(x, y) = \tilde{w} \sin \frac{m\pi x}{a} \sin \frac{n\pi y}{b} \tag{3.232}$$

For simply supported edges only when $x = 0$ and $x = a$, Timoshenko retains the character of Equation (3.232) in the x-direction, but allows an arbitrary function in the y-direction by considering a function of the form:

$$\delta w = \delta w(x, y) = \tilde{w}\, f(y) \sin \frac{m\pi x}{a} \tag{3.233}$$

in which $\tilde{w}$ is the (indeterminate) amplitude of the buckling displacement and $f(y)$ is a function of y alone that will be determined. That is, we seek a separated-variables solution. We can easily verify that the expression for δw in Equation (3.233) satisfies the geometric boundary conditions

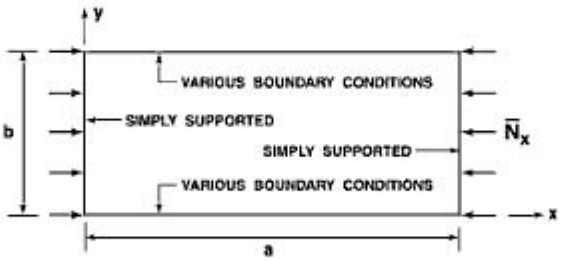


Figure 3-33 Variously Supported Rectangular Plate under Load in the x-Direction

Éléments sous droits d'auteur

$$\delta w = 0 \text{ at } x = 0 \text{ and } x = a \tag{3.234}$$

and the natural boundary conditions

$$\delta M_x = -D(\delta w_{,xx} + \nu \delta w_{,yy}) \text{ at } x = 0 \text{ and } x = a \tag{3.235}$$

Upon substitution of the expression for δw, Equation (3.233), in the differential equation governing buckling, Equation (3.231), we get

$$\left[\frac{d^4 f}{dy^4} - 2\left[\frac{m\pi}{a} \right]^2 \frac{d^2 f}{dy^2} + \left[\left[\frac{m\pi}{a} \right]^4 + \frac{\bar{N}_x}{D} \left[\frac{m\pi}{a} \right]^2 \right] f \right] \tilde{w} \sin \frac{m\pi x}{a} = 0 \tag{3.236}$$

in which $\tilde{w}$ is an arbitrary amplitude of deformation that cannot be determined and will hereafter be ignored. Note that $\sin(m\pi x/a)$ is not zero at all points interior to the region boundary (i.e., within the plate edges). Thus, for Equation (3.236) to be satisfied, the term in the largest brackets must be zero, i.e., the differential equation governing buckling becomes

$$\frac{d^4 f}{dy^4} - 2\left[\frac{m\pi}{a} \right]^2 \frac{d^2 f}{dy^2} + \left[\left[\frac{m\pi}{a} \right]^4 + \frac{\bar{N}_x}{D} \left[\frac{m\pi}{a} \right]^2 \right] f = 0 \tag{3.237}$$

in which the character of the term in large brackets must be investigated in order to solve the differential equation. If the term is positive, a different solution results than when the term is negative.

First, we restrict ourselves to consideration of plates that have at least one of the two lateral edges supported in some manner. Then, we know that the case of no support along two edges, i.e., a wide column, provides a lower bound on the buckling load of the present configuration (there is no lower constraint boundary condition set). The buckling load of a wide column is

$$\bar{P} = \bar{N}_x b = m^2 \pi^2 \frac{EI}{L^2} = \frac{m^2 \pi^2 E}{a^2} \left[\frac{1}{12} bt^3 \right] \tag{3.238}$$

whereupon

$$\bar{N}_x = \frac{m^2 \pi^2}{a^2} \left[\frac{Et^3}{12} \right] \tag{3.239}$$

but the term in brackets is D evaluated at $\nu = 0$, so we write

$$\frac{\bar{N}_x}{D} = \left[\frac{m\pi}{a} \right]^2 \tag{3.240}$$

and recognize that D is actually more than $Et^3/12$. Finally, when at least one edge is supported,

$$\frac{\bar{N}_x}{D} < \left[\frac{m\pi}{a} \right]^2 \tag{3.241}$$

Thus, the term on f in Equation (3.237) is always positive.

Because of the condition in Equation (3.241), the general solution to Equation (3.237) is

Éléments sous droits d'auteur

$$f(y) = C_1 e^{-\alpha y} + C_2 e^{\alpha y} + C_3 \cos \beta y + C_4 \sin \beta y \tag{3.242}$$

in which

$$\alpha = \left[\left[\frac{m\pi}{a} \right]^2 + \left[\frac{-\bar{N}_x}{D} \left[\frac{m\pi}{a} \right]^2 \right]^{1/2} \right]^{1/2} \tag{3.243}$$

$$\beta = \left[-\left[\frac{m\pi}{a} \right]^2 + \left[\frac{-\bar{N}_x}{D} \left[\frac{m\pi}{a} \right]^2 \right]^{1/2} \right]^{1/2} \tag{3.244}$$

The C_i must be found for the edge conditions at $y = 0$ and $y = b$.

3.3.6.1 One Edge Simply Supported and the Other Edge Free

If the edge at $y = 0$ is simply supported, the appropriate geometric boundary condition is

$$\delta w = 0 \text{ at } y = 0 \tag{3.245}$$

and the natural boundary condition is

$$\delta M_y = -D(\delta w_{,yy} + \nu \delta w_{,xx}) = 0 \text{ at } y = 0 \tag{3.246}$$

Then, for a free edge at $y = b$, the natural boundary conditions are

$$\delta K_y = -D[\delta w_{,yyy} + (2 - \nu)\delta w_{,xxy}] = 0 \text{ at } y = b \tag{3.247}$$

$$\delta M_y = -D(\delta w_{,yy} + \nu \delta w_{,xx}) = 0 \text{ at } y = b \tag{3.248}$$

Apparently, certain derivatives of Equation (3.233), the expression for δw, are required:

$$\begin{aligned}
\delta w &= \tilde{w} f(y) \sin \frac{m\pi x}{a} \\
\delta w_{,x} &= \frac{m\pi}{a} \tilde{w} f(y) \cos \frac{m\pi x}{a} \\
\delta w_{,xx} &= -\left[\frac{m\pi}{a} \right]^2 \tilde{w} f(y) \sin \frac{m\pi x}{a} \\
\delta w_{,xxx} &= -\left[\frac{m\pi}{a} \right]^3 \tilde{w} f(y) \cos \frac{m\pi x}{a} \\
\delta w_{,y} &= \tilde{w} f'(y) \sin \frac{m\pi x}{a} \\
\delta w_{,yy} &= \tilde{w} f''(y) \sin \frac{m\pi x}{a} \\
\delta w_{,yyy} &= \tilde{w} f'''(y) \sin \frac{m\pi x}{a} \\
\delta w_{,xxy} &= -\left[\frac{m\pi x}{a} \right]^2 \tilde{w} f'(y) \sin \frac{m\pi x}{a}
\end{aligned} \tag{3.249}$$

in which the prime denotes differentiation with respect to y. The derivatives of f(y) are

Éléments sous droits d'auteur

$$\begin{aligned} f(y) &= C_1 e^{-\alpha y} + C_2 e^{\alpha y} + C_3 \cos \beta y + C_4 \sin \beta y \\ f'(y) &= -\alpha C_1 e^{-\alpha y} + \alpha C_2 e^{\alpha y} - \beta C_3 \sin \beta y + \beta C_4 \cos \beta y \\ f''(y) &= \alpha^2 C_1 e^{-\alpha y} + \alpha^2 C_2 e^{\alpha y} - \beta^2 C_3 \cos \beta y - \beta^2 C_4 \sin \beta y \\ f'''(y) &= -\alpha^3 C_1 e^{-\alpha y} + \alpha^3 C_2 e^{\alpha y} + \beta^3 C_3 \sin \beta y - \beta^3 C_4 \cos \beta y \end{aligned} \tag{3.250}$$

Then, by virtue of the geometric boundary condition in Equation (3.245),

$$C_1 + C_2 + C_3 = 0 \tag{3.251}$$

whereas from the natural boundary condition in Equation (3.246),

$$\left[\alpha^2 C_1 + \alpha^2 C_2 - \beta^2 C_3\right] - \nu\left[\frac{m\pi}{a}\right]^2 (C_1 + C_2 + C_3) = 0 \tag{3.252}$$

Use of Equation (3.251) in Equation (3.252) yields

$$\alpha^2 (C_1 + C_2) - \beta^2 C_3 = 0 \tag{3.253}$$

which, because α and β are independent, has solution

$$C_1 = -C_2 \tag{3.254}$$

$$C_3 = 0 \tag{3.255}$$

Now the function f(y) and its derivatives can be written as

$$\begin{aligned} f(y) &= A \sinh \alpha y + B \sin \beta y \\ f'(y) &= \alpha A \cosh \alpha y + \beta B \cos \beta y \\ f''(y) &= \alpha^2 A \sinh \alpha y - \beta^2 B \sin \beta y \\ f'''(y) &= \alpha^3 A \cosh \alpha y - \beta^3 B \cos \beta y \end{aligned} \tag{3.256}$$

in which A and B are new constants that must be determined from the boundary conditions. The boundary condition in Equation (3.247) yields

$$\begin{aligned} &\alpha^3 A \cosh \alpha b - \beta^3 B \cos \beta b \\ &\quad - (2 - \nu)\left[\frac{m\pi}{a}\right]^2 (\alpha A \cosh \alpha b + \beta B \cos \beta b) = 0 \end{aligned} \tag{3.257}$$

whereas the boundary condition in Equation (3.248) yields

$$\left[\alpha^2 A \sinh \alpha b - \beta^2 B \sin \beta b\right] - \nu\left[\frac{m\pi}{a}\right]^2 (A \sinh \alpha b + B \sin \beta b) = 0 \tag{3.258}$$

Equations (3.257) and (3.258) are two simultaneous homogeneous characteristic equations in the two unknown constants A and B. For a nontrivial solution (i.e., A and B not zero), the determinant of the coefficients of A and B in Equations (3.257) and (3.258) must be zero, i.e.,

$$\beta\left[\alpha^2 - \nu\left[\frac{m\pi}{a}\right]^2\right]^2 \tanh \alpha b = \alpha\left[\beta^2 + \nu\left[\frac{m\pi}{a}\right]^2\right]^2 \tan \beta b \tag{3.259}$$

which follows directly from Equations (3.257) and (3.258) when we realize that from Equations (3.243) and (3.244)

Éléments sous droits d'auteur

$$\alpha^2 = \beta^2 + 2\left[\frac{m\pi}{a}\right]^2 \tag{3.260}$$

In the solution of the transcendental characteristic equation, Equation (3.259), the m = 1 buckling mode corresponds to the lowest buckling load, $\bar{N}_x$, which can be expressed as

$$\bar{N}_x = k\frac{\pi^2 D}{b^2} \tag{3.261}$$

in which the factor k is laboriously obtained from Equation (3.259) for a specific Poisson's ratio, ν, and plate aspect ratio, a/b. The results for ν = .25 are shown in Figure 3-34 and Table 3-3. Note that for long plates, $\bar{N}_x/D$ is indeed always greater than the wide-column result as expected.

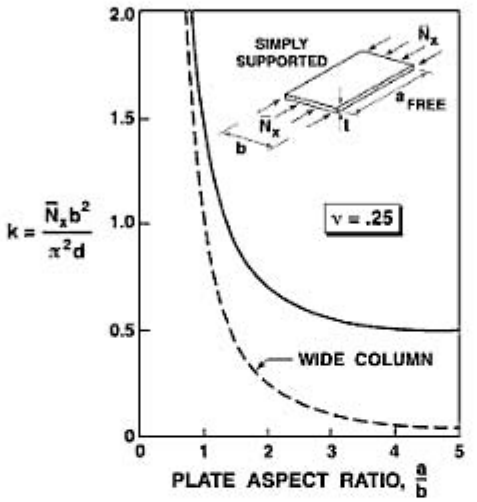


Figure 3-34 Buckling of an Axially Compressed Rectangular Plate Simply Supported Along Two Opposite Loaded Edges with One Unloaded Edge Simply Supported and the Other Free

Table 3-3 Buckling Coefficient k for an Axially Compressed Rectangular Plate Simply Supported Along Two Opposite Loaded Edges with One Unloaded Edge Simply Supported and the Other Free*

	$\frac{a}{b}$										
	.5	1.0	1.2	1.4	1.6	1.8	2.0	2.5	3.0	4.0	5.0
k	4.40	1.440	1.135	.952	.835	.755	.698	.610	.564	.516	.506

*After Timoshenko and Gere [3-8], p. 362, reproduced by permission

Éléments sous droits d'auteur

3.3.6.2 One Edge Clamped and the Other Edge Free

If the unloaded edge at $y = 0$ in Figure 3-30 is clamped, then the appropriate geometric boundary conditions are

$$\delta w = 0 \text{ at } y = 0 \tag{3.262}$$

$$\delta w_{,y} = 0 \text{ at } y = 0 \tag{3.263}$$

For a free edge at $y = b$, the natural boundary conditions are

$$\delta K_y = -D[\delta w_{,yyy} + (2 - \nu)\delta w_{,xxy}] = 0 \text{ at } y = b \tag{3.264}$$

$$\delta M_y = -D(\delta w_{,yy} + \nu \delta w_{,xx}) = 0 \text{ at } y = b \tag{3.265}$$

By application of the foregoing boundary conditions to the general solution, a characteristic equation can be derived with the results shown in Figure 3-35 and Table 3-4. To compare the effect of boundary conditions, observe the differences between the results for k in Sections 3.3.1, 3.3.4.1, and Figure 3-35.

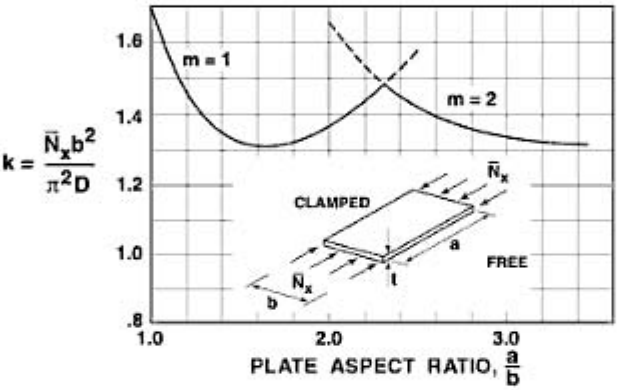


Figure 3-35 Buckling of an Axially Compressed Rectangular Plate Simply Supported Along Two Opposite Loaded Edges with One Unloaded Edge Clamped and the Other Free *(Inspired by Timoshenko and Gere [3-8], p. 364)*

Table 3-4 Buckling Coefficient k for an Axially Compressed Rectangular Plate Simply Supported Along Two Opposite Loaded Edges with One Unloaded Edge Clamped and the Other Free*

	$\frac{a}{b}$												
	1.0	1.1	1.2	1.3	1.4	1.5	1.6	1.7	1.8	1.9	2.0	2.2	2.4
k	1.70	1.56	1.47	1.41	1.36	1.34	1.33	1.33	1.34	1.36	1.38	1.45	1.47

**After Timoshenko and Gere [3-8], p. 364, reproduced by permission*

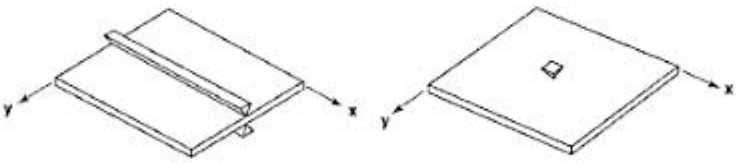
Éléments sous droits d'auteur

Problem Set 3.3.6

3.3.6.1 Substitute the separated-variables buckling displacement of Equation (3.233) in the differential equation governing buckling, Equation (3.231), to get Equation (3.236).
3.3.6.2 Derive the general solution, Equation (3.242), to the ordinary differential equation governing buckling, Equation (3.237).
3.3.6.3 Derive the transcendental buckling criterion, Equation (3.259), for one unloaded edge simply supported and the other unloaded edge free.
3.3.6.4 Derive the transcendental buckling criterion when one unloaded edge is clamped and the other unloaded edge is free.
3.3.6.5 Derive the buckling criterion when both unloaded edges are simply supported.
3.3.6.6 To make certain that N_x for one unloaded edge fixed is greater than N_x for one unloaded edge simply supported, as our intuition tells us, compare the problems in Sections 3.3.6.1 and 3.3.6.2.

3.3.7 Physical Restraints Against Buckling

Suppose physical restraints *within* the boundary of the plate, i.e., *not on* the boundary of the plate, prevent buckling in a specific mode that corresponds to the lowest buckling load for an unrestrained plate. Then that mode is not active in the buckling boundary, and another mode replaces it, generally pushing the buckling boundary farther from the origin of loading, i.e., raising the buckling load. The buckling boundary can be that for biaxial loading in Figure 3-22 on page 273, the festooned buckling curves for uniaxial loading in Figure 3-18 on page 268, or any other representation of buckling loads in this section. Recall that if a lateral support or restraint is placed at the mid-length of an axially loaded, pinned-end bar as in Figure 2-20 on page 72, then the bar cannot buckle in the first mode, but must buckle in the second mode thereby raising the buckling load by a factor of four over that of an unrestrained bar. Similarly, if a plate has a physical restraint of a transverse, rotation-free line support along one of its centerlines as in Figure 3-36a, i.e., a line restraint, in addition to the simply supported edges, then the plate cannot buckle in the $m = 1$, $n = 1$ mode. The physically possible buckling modes are limited to those that satisfy the physical restraints, namely any integer values of m and only even integer values of n. That is, the plate still buckles into one of its natural modes, but only into the lowest mode that also satisfies the additional restraint condition. Another type of restraint is the transverse, rotation-free point restraint in Figure 3-36b. That point restraint can be applied anywhere on the surface of the plate.



a Line Restraint b Point Restraint

Figure 3-36 Surface Physical Restraints on Plates within the Plate Edges (Edge Supports are not Shown)

Éléments sous droits d'auteur

The physically possible buckling modes are much easier to determine for a simply supported plate with a restraint that is effectively another simple support apparatus at the centerline of the plate or some other parallel location than for any other kind of restraint. Other types of physical restraints on plates, whether simply supported or not at the edges, are often much more difficult to analyze. Those restraints can be straight or curved and can occur in various multiple groups to create a very complicated problem. Moreover, the restraints could restrain rotation or consist of various springs as an elastic restraint instead of just restraining displacement.

An alternative way to treat a plate with a straight physical restraint might be to divide the plate at the restraint and consider the boundary conditions on both parts of the plate. If the straight line restraint is precisely at the middle of the plate, then the resulting half plate would have simply supported edge boundary conditions on all four edges and therefore is an easy and obvious plate solution to obtain. However, if the restraint were a point restraint at the center, no such easy subdivision is possible unless quarter plates, each of which is simply supported, satisfy the restraints and the boundary conditions. Often, subdivision of the plate could lead to a plate for which the solution is not readily available. Such a solution might then be obtained by numerical techniques such as the finite element method. Please study the section in Chapter 5 on cautionary notes when using numerical procedures, especially 'canned' computer programs.

Examples are now addressed for restraint on the simplest cases of plates with all edges simply supported. Accordingly, we consider simple situations for which the reader can easily work out the calculations from the pertinent equations already displayed and marvelously and comprehensively digested by now.

3.3.7.1 Examples for a Uniaxially Loaded Plate

For a plate with uniaxial load N_x, a line restraint in the y-direction as in Figure 3-36a at the middle of the plate prevents the plate from buckling into the usual $m = 1$, $n = 1$ mode for an unrestrained plate and forces the plate into the $m = 2$, $n = 1$ mode. If the plate is square, then we can see from Figure 3-18 on page 268 that the buckling load with the restraint is about 50% higher than without the restraint!

A line restraint in the x-direction at the middle of the plate as in Figure 3-36a prevents the plate from buckling into any mode with $n = 1$ (on which Figure 3-18 is based). Hence, the plate is forced into the $m = 1$, $n = 2$ mode. If the plate is square, then we can show that the buckling load with the restraint is 25/4 times the magnitude without the restraint!

A point restraint at the center of a square plate as in Figure 3-36b makes the usual $m = 1$, $n = 1$ mode shape for an unrestrained plate not possible (nor is any mode shape with an odd integer number of buckle waves in either direction). Then the lowest possible buckling mode is $m = 2$, $n = 2$. Then, the buckling load of the point-restrained plate can be shown to be sixteen times the buckling load of the unrestrained plate!

Éléments sous droits d'auteur

3.3.7.2 Examples for a Biaxially Loaded Plate

For a line restraint in the y-direction as in Figure 3-36a on a plate under equal biaxial compression, the line restraint prevents buckling into the $m = 1$, $n = 1$ mode and forces buckling to occur in the $m = 2$, $n = 1$ mode. In Figure 3-22 on page 273, both modes are shown, but the buckling boundary for an unrestrained plate occurs in the $m = 1$, $n = 1$ mode. Thus, we must determine the buckling load by use of Equation (3.186) on page 269. The resulting value can be shown to be $N_x b^2/\pi^2 D = 5$ along with the same value for the normalized $\bar{N}_y$, i.e., 2 1/2 times the buckling load of the unrestrained plate. Note that the buckling boundary is no longer symmetric about the $s = 1$ loading line because the physical restraint interrupts the symmetry of the problem.

In the case of a point restraint at the center of a plate as in Figure 3-36b, the $m = 1$, $n = 1$ mode shape is not possible, nor is any mode possible in which either $m = 1$ or $n = 1$ (or any odd integer). Only mode shapes with m and n even integers are physically possible. As the ratio of biaxial loads decreases from 1 toward negative infinity in quadrants three and two of Figure 3-22, the plate buckling mode will change from $m = 2$, $n = 2$ to $m = 4$, $n = 2$ to $m = 2$, $n = 4$ to $m = 4$, $n = 4$ which constitutes a totally different buckling boundary than in Figure 3-22.

3.3.7.3 Summary Remarks on Physical Restraints

For sinusoidal buckling modes, straight restraints, which are quite common in engineering practice, can cause readily discernible buckling mode changes because the restraints coincide with nodal lines in the buckling mode shape. They also cause a higher buckling load for the restrained plate than for the unrestrained plate.

For plates with buckling modes that are not periodic such as plates under in-plane shear, straight restraints interrupt the fundamental buckling mode in Figure 3-31 on page 291, as well as the next buckling mode in Figure 3-32 on page 291. Thus, restraints on plates with naturally complicated buckling modes nearly always cause far higher buckling loads than if the restraints did not exist. However, thier buckling loads and modes are quite difficult to predict.

The fundamental conclusion is that physical restraints within the boundaries of a plate load to a much higher buckling load than if the restraints did not exist. The magnitude of the buckling load increase depends on the nature of the restraint and on the buckling behavior of the unrestrained plate.

Problem Set 3.3.7

3.3.7.1 For a uniaxially loaded simply supported plate with a centerline restraint in the x-direction, verify that the buckling load with the restraint is 25/4 times the buckling load without the restraint.

3.3.7.2 For a uniaxially loaded simply supported plate with a point restraint at the plate center, verify that the buckling load with the restraint is 16 times the buckling load without the restraint.

3.3.7.3 For a simply supported plate under equal biaxial compression with a point restraint at the plate center, verify that the buckling load with the restraint is 2 1/2 times the buckling load without the restraint.

Éléments sous droits d'auteur

3.3.8 Summary of Classical Buckling Results

We solved the classical plate buckling problem for six cases of practical importance. First, buckling caused by uniaxial loading was studied to learn some of the basic characteristics of a (two-dimensional) plate buckling problem such as buckle mode shapes and cusps in the results when buckling load is plotted versus plate aspect ratio, a/b. Next, a biaxial loading state was addressed to see how two loads can work together or against one another in the buckling process. Then, variable in-plane load was combined with uniaxial loading to create in-plane bending plus varying amounts of compression. Buckling under in-plane shear loading was also evaluated. All previous cases are for plates that have all four edges simply supported. Finally, for a unlaxially loaded plate, the boundary conditions were taken as simply supported on the two opposite loaded edges with solutions obtained for various boundary conditions on the other two opposite edges that were not loaded. The important limiting case of the other two opposite edges being not supported, i.e., the wide-column problem, was also addressed. For all classical buckling results, the buckling deflection amplitudes are indeterminate just as for bar buckling problems, although buckling mode shapes can be determined. Many important cases of various buckling loads and conditions were omitted and left to the resources of the reader (see, for example, Timoshenko and Gere [3-8] and Reddy [3-16]). Extensive experimental methods and results are described by Singer, Arbocz, and Weller [3-17].

Solving buckling problems can be thought of as a two-step process:

(1) Solve the plane elasticity problem to determine the stress distribution in the prebuckling equilibrium state under the prescribed loading.
(2) Use the prebuckling stresses from step (1) as the equilibrium state stress distribution in the buckling problem to determine the magnitude of the loading that causes buckling.

In each of the buckling problems studied in this section, the prebuckling equilibrium state involved a uniform, easily determined set of stresses. Because the prebuckling stresses are uniform throughout the plate, the buckling differential equations have constant coefficients. In more complicated loadings, the prebuckling equilibrium stresses are not uniform throughout the plate, so the buckling differential equations have nonconstant coefficients and are not easily solved.

Comparison of predicted and measured plate buckling loads will be deferred to Section 3.5, Effect of Initial Geometric Imperfections, after identification of key fundamental postbuckling behavior characteristics in Section 3.4. In those sections, we will recognize that plate buckling has a significantly different physical nature and importance than bar buckling. Thus, the interpretation of the buckling load must also be different. The physical significance of the classical buckling loads is that generally the calculated buckling load can be exceeded by a large margin without undue concern as implied in Figure 1-12 on page 8. There, the plate axial stiffness decreases somewhat after buckling, but the load still increases. We will study the basis for this perhaps curious exceedence of the buckling load in Section 3.4 on postbuckling behavior.

Éléments sous droits d'auteur

3.4 POSTBUCKLING BEHAVIOR OF SIMPLY SUPPORTED RECTANGULAR PLATES UNDER UNIFORM COMPRESSION $\bar{N}_x$

We must investigate the postbuckling behavior of rectangular plates to appreciate the practical significance of the classical buckling loads predicted in Section 3.3. Unlike the differential equations governing the postbuckling behavior of bars (the problem of the elastica in Section 2.4), the equilibrium differential equations for plates cannot be solved exactly. However, postbuckling behavior of plates is a complicated large-deflection equilibrium problem that can be solved approximately.

The moderately large-deflection equilibrium equations for a plate with no transverse load [Equations (3.82)–(3.84) on pages 170–171] were derived by von Kármán [3-5] as

$$\begin{aligned} N_{x,x} + N_{xy,y} &= 0 \\ N_{xy,x} + N_{y,y} &= 0 \\ D\nabla^4 w - (N_x w_{,xx} + N_y w_{,yy} + 2N_{xy} w_{,xy}) &= 0 \end{aligned} \tag{3.266}$$

in which the forces per unit length are expressed in terms of the middle-surface strains as

$$\begin{aligned} N_x &= A(\bar{\varepsilon}_x + \nu\bar{\varepsilon}_y) \\ N_y &= A(\bar{\varepsilon}_y + \nu\bar{\varepsilon}_x) \\ N_{xy} &= \frac{(1-\nu)}{2} A\bar{\gamma}_{xy} \end{aligned} \tag{3.267}$$

and the middle-surface strains are expressed in terms of the middle-surface displacements as

$$\begin{aligned} \bar{\varepsilon}_x &= u_{,x} + \frac{1}{2} w_{,x}^2 \\ \bar{\varepsilon}_y &= v_{,y} + \frac{1}{2} w_{,y}^2 \\ \bar{\gamma}_{xy} &= u_{,y} + v_{,x} + w_{,x} w_{,y} \end{aligned} \tag{3.268}$$

Stein [3-18] solved the three nonlinear partial differential equations in Equation (3.266) for plates loaded with N_x as in Figure 3-37 by expanding each of the middle-surface displacements in a power series in terms of a small parameter ε about the displacements that occur at buckling:

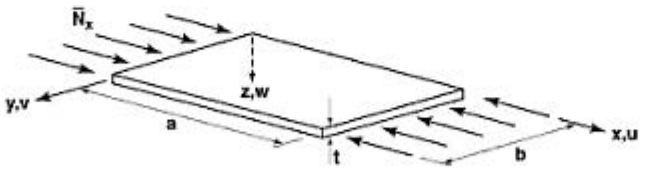


Figure 3-37 Simply Supported Rectangular Plate with Load in the x-Direction

Éléments sous droits d'auteur

$$u = \sum_{n=0,2,\ldots}^{\infty} u^{(n)}\varepsilon^n$$
$$v = \sum_{n=0,2,\ldots}^{\infty} v^{(n)}\varepsilon^n \qquad (3.269)$$
$$w = \sum_{n=1,3,\ldots}^{\infty} w^{(n)}\varepsilon^n$$

in which $u^{(n)}$, $v^{(n)}$, and $w^{(n)}$ are functions of x and y only. Stein chose the arbitrary parameter ε in terms of the resultant end compressive force P such that

$$\varepsilon^2 = \frac{P - P_E}{P_E} \qquad (3.270)$$

i.e., $\varepsilon = 0$ at the buckling load, P_E or $\bar{P}$. The terms in the series were chosen with the following reasoning. Before buckling, u and v take on their determinate values based on simple in-plane equilibrium of the plate. At the same time, w is zero by definition because buckling has not occurred, i.e., the plate is still flat. Note from its definition that ε can be either positive or negative for a given load. Thus, the next term in the series for u and v must involve ε^2 because u and v must be the same values irrespective of whether the plate buckles up or down from the initially flat middle surface. Similarly, the first term in the series for w must be a power of ε alone in order that w represents either buckling up or buckling down in Figure 3-37 because both buckling deformations are equally possible. This reasoning leads to the conclusion that all terms in the series for u and v must contain only even powers of ε whereas the series for w must contain only odd powers of ε.

The primary characteristic of Stein's procedure is that the three nonlinear partial differential equations are replaced by an infinite sequence of linear partial differential equations that fortunately can be solved for the present problem. The solution to the problem is approximated by taking more and more terms in the infinite sequence of equations. The linear partial differential equations are obtained as follows.

Upon substituting the displacement expansions, Equations (3.269), in the force-strain and strain-displacement relations, we get

$$N_x = \sum_{n=0,2,\ldots}^{\infty} N_x^{(n)}\varepsilon^n + \sum_{m=1,3,\ldots}^{\infty}\sum_{n=1,3,\ldots}^{\infty} N_x^{(mn)}\varepsilon^{m+n}$$
$$N_y = \sum_{n=0,2,\ldots}^{\infty} N_y^{(n)}\varepsilon^n + \sum_{m=1,3,\ldots}^{\infty}\sum_{n=1,3,\ldots}^{\infty} N_y^{(mn)}\varepsilon^{m+n} \qquad (3.271)$$
$$N_{xy} = \sum_{n=0,2,\ldots}^{\infty} N_{xy}^{(n)}\varepsilon^n + \sum_{m=1,3,\ldots}^{\infty}\sum_{n=1,3,\ldots}^{\infty} N_{xy}^{(mn)}\varepsilon^{m+n}$$

in which

Éléments sous droits d'auteur

$$N_x^{(n)} = \frac{Et}{1-\nu^2}\left[u_{,x}^{(n)} + \nu v_{,y}^{(n)}\right]$$
$$N_y^{(n)} = \frac{Et}{1-\nu^2}\left[v_{,y}^{(n)} + \nu u_{,x}^{(n)}\right] \tag{3.272}$$
$$N_{xy}^{(n)} = \frac{Et}{2(1+\nu)}\left[u_{,y}^{(n)} + v_{,x}^{(n)}\right]$$

$$N_x^{(mn)} = \frac{Et}{2(1-\nu^2)}\left[w_{,x}^{(m)}w_{,x}^{(n)} + \nu w_{,y}^{(m)}w_{,y}^{(n)}\right] = N_x^{(nm)}$$
$$N_y^{(mn)} = \frac{Et}{2(1-\nu^2)}\left[w_{,y}^{(m)}w_{,y}^{(n)} + \nu w_{,x}^{(m)}w_{,x}^{(n)}\right] = N_y^{(nm)} \tag{3.273}$$
$$N_{xy}^{(mn)} = \frac{Et}{2(1+\nu)}w_{,x}^{(m)}w_{,y}^{(n)}$$

Next, the force-displacement relations are substituted along with the series for w in the nonlinear partial differential equations of equilibrium, Equation (3.266). The result is three power series in ε which, because ε is an arbitrary parameter, must have zero coefficients on the powers of ε if each of the series is to vanish in order to satisfy the differential equations. Accordingly, because the following sequence of linear partial differential equations are coefficients of powers of ε, they must vanish:

$$N_{x,x}^{(0)} + N_{xy,y}^{(0)} = 0$$
$$N_{xy,x}^{(0)} + N_{y,y}^{(0)} = 0 \tag{3.274}$$

$$D\nabla^4 w^{(1)} - \left[N_x^{(0)}w_{,xx}^{(1)} + N_y^{(0)}w_{,yy}^{(1)} + 2N_{xy}^{(0)}w_{,xy}^{(1)}\right] = 0 \tag{3.275}$$

$$N_{x,x}^{(2)} + N_{xy,y}^{(2)} = -\left[N_{x,x}^{(11)} + N_{xy,y}^{(11)}\right]$$
$$N_{xy,x}^{(2)} + N_{y,y}^{(2)} = -\left[N_{xy,x}^{(11)} + N_{y,y}^{(11)}\right] \tag{3.276}$$

$$\begin{aligned} D\nabla^4 w^{(3)} - \left[N_x^{(0)}w_{,xx}^{(3)} + N_y^{(0)}w_{,yy}^{(3)} + 2N_{xy}^{(0)}w_{,xy}^{(3)}\right] &= \left[N_x^{(2)} + N_x^{(11)}\right]w_{,xx}^{(1)} + \left[N_y^{(2)} + N_y^{(11)}\right]w_{,yy}^{(1)} \\ &\quad + 2\left[N_{xy}^{(2)} + N_{xy}^{(11)}\right]w_{,xy}^{(1)} \end{aligned} \tag{3.277}$$

$$N_{x,x}^{(4)} + N_{xy,y}^{(4)} = -\left[2N_{x,x}^{(13)} + N_{xy,y}^{(13)} + N_{xy,y}^{(31)}\right]$$
$$N_{xy,x}^{(4)} + N_{y,y}^{(4)} = -\left[2N_{y,y}^{(13)} + N_{xy,x}^{(13)} + N_{xy,x}^{(31)}\right] \tag{3.278}$$

$$\begin{aligned} D\nabla^4 w^{(5)} - \left(N_x^{(0)}w_{,xx}^{(5)} + N_y^{(0)}w_{,yy}^{(5)} + 2N_{xy}^{(0)}w_{,xy}^{(5)}\right) &= \left(N_x^{(2)} + N_x^{(11)}\right)w_{,xx}^{(3)} + \left(N_y^{(2)} + N_y^{(11)}\right)w_{,yy}^{(3)} \\ &\quad + 2\left(N_{xy}^{(2)} + N_{xy}^{(11)}\right)w_{,xy}^{(3)} + \left(N_x^{(4)} + 2N_x^{(13)}\right)w_{,xx}^{(1)} \\ &\quad + \left(N_y^{(4)} + 2N_y^{(13)}\right)w_{,yy}^{(1)} + 2\left(N_{xy}^{(4)} + N_{xy}^{(13)} + N_{xy}^{(31)}\right)w_{,xy}^{(1)} \\ &\quad \vdots \end{aligned} \tag{3.279}$$

Éléments sous droits d'auteur

Equations (3.274) are the small-deflection in-plane equilibrium equations which for the simply supported edge boundary conditions

$$N_{xy} = w = M_n = 0 \tag{3.280}$$

$$\int_0^b N_x \Big|_{x=0,a} dy = -\bar{P} \tag{3.281}$$

$$\int_0^a N_y \Big|_{y=0,b} dx = 0 \tag{3.282}$$

(in which M_n is the moment normal to each edge) have the solution

$$u^{(0)} = -\frac{\bar{P}^{(0)}}{Etb}\left[x - \frac{a}{2}\right]$$
$$v^{(0)} = \frac{\nu \bar{P}^{(0)}}{Etb}\left[y - \frac{b}{2}\right] \tag{3.283}$$

The first equation of Equation (3.283) represents the linear load-shortening behavior in the x-direction prior to buckling, and the second equation represents the corresponding Poisson lateral deformation effect.

Equation (3.275) is the usual linear buckling differential equation which has known solutions from Section 3.3.2:

$$w^{(1)} = w_1 \sin\frac{m\pi x}{a} \sin\frac{n\pi y}{b} \tag{3.284}$$

$$\bar{P}^{(0)} = Db\frac{\left[\left[\frac{m\pi}{a}\right]^2 + \left[\frac{n\pi}{b}\right]^2\right]^2}{\left[\frac{m\pi}{a}\right]^2} \tag{3.285}$$

in which $n = 1$ always yields the lowest value of $\bar{P}^{(0)}$ and the value of m for the lowest $\bar{P}^{(0)}$ depends on the plate aspect ratio, a/b, as has already been plotted in Figure 3-18 on page 268. Recall that w_1 is an undetermined coefficient, i.e., only the buckling mode shape is known, and the magnitude of the buckling deformation is indeterminate as of Section 3.3.2. However, if further terms are taken in Stein's power series for the displacements, then w_1 can be determined just as the postbuckling deflections of a bar were found.

Equations (3.276) have right-hand sides that can be expressed in terms of w_1. Subsequently, they can be solved by inspection for $u^{(2)}$ and $v^{(2)}$ in terms of w_1 (the solutions are too long to repeat here). Then, we can show that Equation (3.277) has a solution only if

$$w_1^2 = \frac{16\bar{P}^{(2)}}{Etb}\frac{\left[\frac{m\pi}{a}\right]^2}{\left[\frac{m\pi}{a}\right]^4 + \left[\frac{n\pi}{b}\right]^4} \tag{3.286}$$

Éléments sous droits d'auteur

which, in conjunction with $u^{(2)}$ and $v^{(2)}$, is a first approximation to the load-shortening behavior of a rectangular plate. Note that the first approximation contains up through second powers in ε. Similar and more tedious work leads to a second approximation to the load-shortening behavior wherein up through fourth powers in ε are retained.

The theoretical load-shortening results are plotted along with the general nature of experimental results obtained by Stein for a/b = 1 in Figure 3-38 and for a/b = ∞ in Figure 3-39. For both aspect ratios and indeed for every integer aspect ratio, the lowest buckling load is

$$\bar{N}_x = \frac{\bar{P}}{b} = \frac{4\pi^2 D}{b^2} \tag{3.287}$$

so, in the normalized curves of Figures 3-38 and 3-39, the load-shortening behavior changes significantly at

$$\frac{\bar{P}b}{4\pi^2 D} = 1 \tag{3.288}$$

In Figure 3-38, an m = 2 buckling mode curve (recall that n is always 1 for this problem) deviates from the linear load-deflection curve at

$$\frac{\bar{P}b}{4\pi^2 D} = 1.5 \tag{3.289}$$

which corresponds to

$$\bar{N}_x = \frac{6\pi^2 D}{b^2} \tag{3.290}$$

which, in turn is observed as well in Figure 3-18. Above a normalized load of about twice the buckling load, the m = 2 mode provides the lowest equilibrium load. There, the postbuckling behavior of the plate must ex-

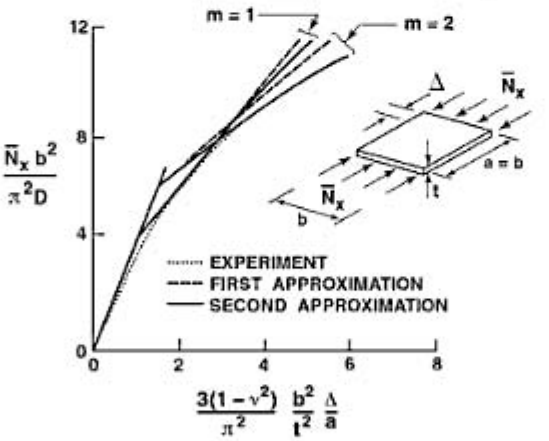


Figure 3-38 Load Versus Shortening for a/b = 1 *(After Stein [3-18], p. 11)*

Éléments sous droits d'auteur

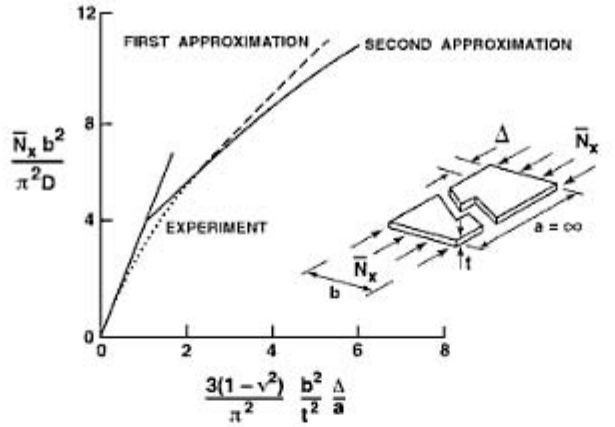


Figure 3-39 Load Versus Shortening for a/b = ∞ *(After Stein [3-18], p. 12)*

hibit a change in mode shape (secondary buckling). Changes in mode shape are not immediately apparent for a/b = ∞. However, they do occur, although more in a continuous manner rather than abruptly.

Note in Figures 3-38 and 3-39 that both the possibility of a stress-type failure and yielding are ignored. That is, either event could terminate or modify the curves shown when some failure event aside from buckling occurs. Note also that, unlike the classical buckling results, the amplitudes of the deflections are determinate because the postbuckling problem is an equilibrium problem (a boundary-value problem).

Experimental results generally fall only somewhat below the theoretical load-shortening curves primarily because plates cannot be made perfectly flat. Stein [3-18] obtained slightly stiffer load-shortening curves for long plates (a/b about five) with clamped edges rather than simply supported edges shown later in Figure 3-42 on page 311. However, the mere length (high a/b) of the plates signifies that the actual boundary conditions at the loaded ends of the plate are not particularly important.

The major conclusion to be reached from this study is that plates are capable of carrying significant loads well above the buckling load at the expense of much increased deformation. That is, the buckling loads calculated in Section 3.3 are indicators not of gross failure but of merely a decrease in axial stiffness of the plate. Loads above the Euler plate buckling load can be tolerated in some structures as long as the resulting larger deformations do not violate the design objectives of the structure. Recall that the bar buckling load is a measure of the practical maximum load for a bar because a perfect bar would undergo very large deflections with only a slight increase in load above the buckling load. Thus, a significant difference between the behavior of plates and bars has been identified. This plate load-deflection behavior near buckling is clearly stable, symmetric bifurcation behavior with a high degree of stability as in Figure 1-24c on page 24. In contrast, although bar load-deflection behavior is stable symmetric, it has a very low degree of stability.

Éléments sous droits d'auteur

3.5 EFFECT OF INITIAL GEOMETRIC IMPERFECTIONS

3.5.1 Introduction

Perfectly flat plates simply do not exist in practice because manufacturing processes are never perfect. Various flattening devices nearly always lead to nonflat surfaces. Plate rolling machines, despite their objective of creating flat plates, cause surface waves and even overall bows in the surface plus nonuniform thickness. Fastening with rivets or bolts induces geometric distortions. Also, welding induces geometric distortions and residual stresses because of necessarily uneven heating.

The approach to analysis of imperfect plates is similar to that for analysis of imperfect bars in Section 2.7. That is, the most detrimental or influential imperfection is presumed to be one with the shape of a buckling mode of a perfect plate. Of course, as with imperfect bars, *imperfect plates do not actually buckle*, they *bow* gradually without changing shape from an initial imperfect (bowed) shape. Often, large increases in out-of-plane deflections occur at loads near the bifurcation buckling load. However, imperfect plates can buckle from the bowed shape to another buckling mode at higher loads than the Euler buckling load of a perfect plate. Recall that, unlike bars, plates can carry higher loads than the Euler load after buckling as we have clearly seen from Stein's results in Section 3.4. Now, we want to find how plate imperfections modify Stein's results.

We will show that geometrically imperfect plates have a stable, but softening (decreasing in slope), nonlinear load-deflection behavior without a well-defined buckling load. This objective is accomplished by describing some available analyses and their results along with pertinent experimental results in Section 3.5.2, Analysis and Experimental Results. Then, we study some of the consequences of the typical nonlinear load-deflection behavior in Section 3.5.3, namely the difficulty in deciding upon a *so-called* (artificial) buckling load to be used in design studies. That is, some key behavioral characteristics must be identified to evaluate the merits (or rank) of competitive designs.

3.5.2 Analysis and Experimental Results

Uniaxially loaded, imperfect rectangular plates with simple supports along the loaded edges x = 0 and x = a and various supports along the unloaded edges y = 0 and y = b in Figure 3-40 were addressed by Rhodes

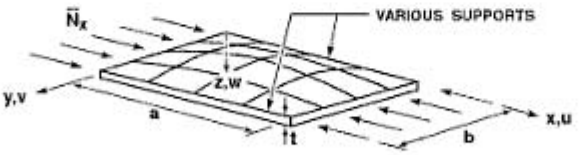


Figure 3-40 Axially Compressed Imperfect Rectangular Plate with Simply Supported Loaded and Variously Supported Unloaded Edges

Éléments sous droits d'auteur

and Harvey [3-19]. The unloaded edges are free to 'wave in-plane', i.e., to deform without restraint in-plane as is typical of the S2 or S4 boundary condition in Figure 3-10 on page 247. The geometric imperfection in Figure 3-40 is a sine-sine shape valid only for plates with all edges simply supported. For other boundary conditions, *shapes that satisfy the boundary conditions and are buckling modes are presumed to be the most detrimental.* The choice of the presumably most detrimental imperfection shape in a design implies that all other imperfections are less detrimental. Thus, the design would be conservative (have a higher load-deflection curve) relative to all but the most detrimental imperfection (and, in that case, the design would be appropriate).

The initial geometric imperfections of the plate are taken to be

$$w_o = A_o Y(y) \sin \frac{m\pi x}{a} \tag{3.291}$$

in which the $\sin m\pi x/a$ term in Equation (3.291) satisfies the imposed simply supported edge boundary condition in the x-direction (the load direction) and the Y(y) are the deflections across the plate between the variously supported edges $y = 0$ and $y = b$ for the first mode of buckling of a perfect plate and are expressed in series form as

$$Y(y) = \sum_{n=1}^{N} A_n Y_n(y) \tag{3.292}$$

in which the $Y_n(y)$ are algebraic shape functions of the form

$$Y_n(y) = \left[\left[\frac{y}{b} \right] + d_{1n} \left[\frac{y}{b} \right]^2 + d_{2n} \left[\frac{y}{b} \right]^{a_n} + d_{3n} \left[\frac{y}{b} \right]^{b_n} \right] \tag{3.293}$$

in which a_n and b_n are integers with different values for different values of n and d_{1n}, d_{2n}, and d_{3n} are determined by satisfying the plate boundary conditions. Alternatively, the $Y_n(y)$ could be written as

$$Y_n(y) = \sum_{p}^{p=r} c_{pn} \left[\frac{y}{b} \right]^p \tag{3.294}$$

The use of these $Y_n(y)$ is described by Rhodes and Harvey [3-20].

The initial shape of the imperfect plate is amplified in magnitude as load increases from zero. Although the initial shape is specified to be that of one or more buckle modes of a perfect plate, that initial shape must not be called a buckle because *buckling has not occurred!* That is, no sudden deformation mode shape change has occurred. The initial shape is a *bow* in the surface of the imperfect plate, and that bow grows in amplitude as load is increased.

Rhodes and Harvey's approach appears to be somewhat similar to the solutions in Section 3.3.5 for the classical (Euler) buckling problem of simple support on the loaded edges and various boundary conditions on the unloaded edges. However, here, although the deflection functions are similar, the governing equations are quite different. This is a moderately large-deflection equilibrium problem leading to the definition of the load-deflection behavior for a wide range of loads, and the problem in

Éléments sous droits d'auteur

Section 3.3.5 is a classical buckling problem leading to an Euler buckling load. Then, unlike Stein's solution of a sequence of approximating differential equations in Section 3.4, Rhodes and Harvey use an energy approach first satisfying von Kármán's compatibility equation exactly for the deflection functions and then using the principle of stationary potential energy to find the full load-deflection behavior of an imperfect plate.

The results for imperfect square plates with all edges simply supported are plotted as normalized load $N_x b^2/\pi^2 D$ (in the manner of Sections 3.3 and 3.4) versus the net plate transverse deflection, $w - w_0$, at the center normalized by the plate thickness, t. Results for four different values of the imperfection amplitude, .02 t, .05 t, .10 t, and t, are shown in Figure 3-41 [3-21]. Obviously, the smaller the imperfection amplitude, the closer the load-delection behavior of an imperfect plate is to that of a perfect plate. For the three small imperfection amplitudes, the load-deflection curve is different from the curve for a perfect plate only in the region near the Euler buckling load, $N_x b^2/\pi^2 D = 4$. Both below and above the Euler buckling load, all three curves are fairly close to the behavior of a perfect plate. For a very large imperfection with an amplitude of the plate thickness, the load-deflection response is quite markedly different from the curve for a perfect plate for all loads (except one trivial case at the crossing of the curves, but even a stopped clock is correct twice a day!). Note that Rhodes, Harvey, and Fok's results [3-21] are for elastic material behavior and that plastic deformation certainly must influence the load-deflection behavior at large loads.

The behavior in Figure 3-41 is somewhat reminiscent of the behavior of perfect and imperfect bars in Section 2.7. However, the postbuckling curve for a perfect plate always rises from the point of buckling, whereas

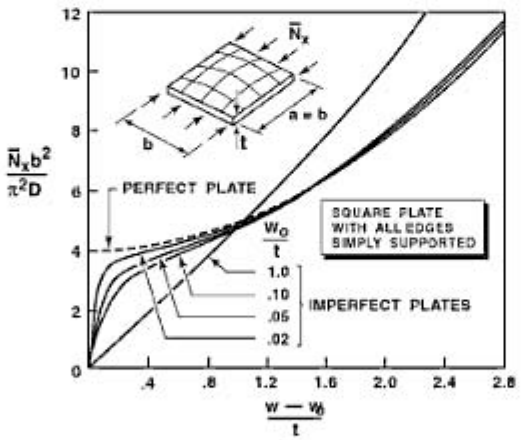


Figure 3-41 Load-Deflection Behavior of Axially Loaded Square Plates with Simply Supported Edges and Various Geometric Imperfections *(After Rhodes, Harvey, and Fok [3-21])*

Éléments sous droits d'auteur

the postbuckling curve for a bar is essentially horizontal. The significance of the rising is that plate behavior is stable in the postbuckling regime whereas bar behavior is unstable because the bar postbuckling curve is essentially horizontal in Figure 2-29 on page 85 and Figure 2-63 on page 158, but barely rising. These statements signify a higher degree of stability for a plate than a bar as described in Section 1.3 (more upward curvature in Figure 1-24 on page 24). The fundamental interpretation of the stable postbuckling behavior for plates is that substantial loads can be sustained well beyond the Euler buckling load (whereas the Euler buckling load of a bar is essentially the maximum sustainable load in practice). Of course, such a result was predicted and measured by Stein [3-18] and others for plates with all edges simply supported.

The stable postbuckling behavior with its accompanying lack of a well-defined buckling load has many interesting characteristics. Both the out-of-plane and in-plane boundary conditions are important because of the necessarily large deflections that include membrane stresses that excite the in-plane boundary conditions. Moreover, the prolonged loading and deformation include multiple changes of buckling mode called *secondary buckling* observed by Stein theoretically in Figure 3-38 on page 306 for perfect, square plates after the initial buckling event and experimentally in Figure 3-42 for imperfect plates with a/b of 5 [3-18]. Note the changes in buckle mode shape of imperfect plates from 5 to 6 to 7 to 8 as load increases in Figure 3-42. The initial buckling mode is m = 5, and the subsequent mode shape changes are called *secondary buckling* or *change in buckle pattern (mode)*. Secondary buckling is not observed in Rhodes and Harvey's results because they do not investigate the stability of the large-deflection equilibrium behavior shown in Figure 3-41. Stein's theoretical results in Figure 3-42 are for elastic, infinite-length plates for which secondary buckling does not occur. Note also

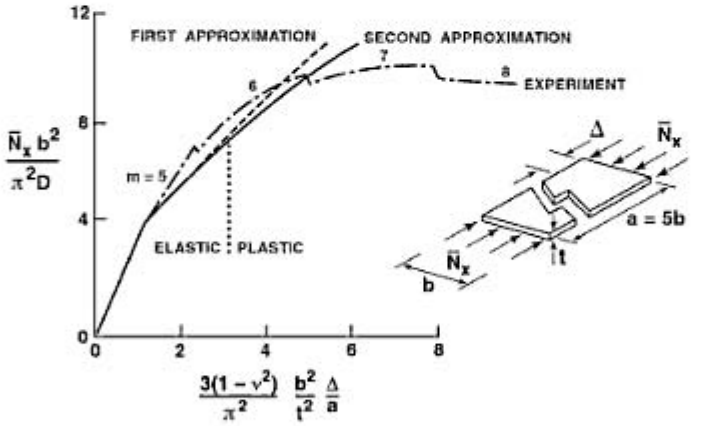


Figure 3-42 Load Versus Shortening for a/b = 5 *(After Stein [3-18], p. 14)*

Éléments sous droits d'auteur

also in Figure 3-42 the approximate boundary between elastic and plastic behavior delineated with a dotted vertical line at which point strain gage readings at the crest of a buckle went from elastic to plastic strains. However, all theoretical results are for elastic behavior only.

Initial geometric imperfections (or initial out-of-flatness) do not significantly affect the buckling load or the ultimate load as seen in Rhodes and Harvey's results in Figure 3-41 [3-21]. There, although perfect and imperfect plates start their load-deflection behavior in a different manner, they soon essentially join paths. From experiments, we know that the effects of imperfections on plate behavior are largest in the vicinity of the Euler buckling load for the corresponding perfect plate which is indicative of the onset of strong interaction between membrane stresses and out-of-plane deformations. The effects are smaller both above and below the Euler buckling load.

Additional results for perfect and imperfect rectangular plates with a/b = 2 and simply supported loaded edges are plotted as normalized load (in the manner of Sections 3.3 and 3.4) versus the net plate center transverse deflection ($w - w_o$) normalized by the plate thickness in Figure 3-43. Results are shown for three different sets of boundary conditions on the unloaded edges (1) both fixed, (2) both simply supported, and (3) one simply supported and one free [3-19]. All these imperfect plates have an imperfection amplitude of $w_o = .1\,t$.

The effect of initial geometric imperfections on plate buckling is quite similar to that on bars in Section 2.7. That is, a sharp buckling load is sometimes, but not always, observed in either an imperfect bar or an imperfect plate. Here, with plates having various edge support conditions

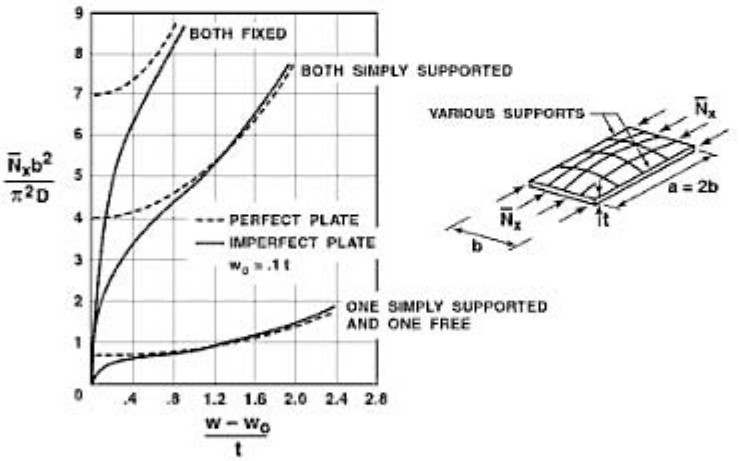


Figure 3-43 Load-Deflection Behavior of Axially Loaded Rectangular Plates with Simply Supported Loaded Edges and Variously Supported Unloaded Edges
(After Rhodes and Harvey [3-19])

Éléments sous droits d'auteur

in Figure 3-43, the significant behavior is that large loads and deflections can be obtained that are well above the Euler buckling load (the intersection of each dashed curve with the vertical axis in Figure 3-43) as was demonstrated for simply supported plates by Stein [3-18] in Section 3.4. Here, the same conclusions apply for plates with opposite unloaded edges that are (1) fixed and (2) simply supported on one edge and free on the other edge. Note that the value of normalized buckling load, $N_x b^2/\pi^2 D$, for each support case is available, except for the fixed edge case. That is, the normalized buckling load for a plate with all edges simply supported and a plate aspect ratio of 2.0 is exactly 4 in Figure 3-18 on page 268, and Rhodes and Harvey get 4.00171 with two terms and 4.00000 with four terms. The normalized buckling load for the one edge simply supported and one edge free case is .698 in Table 3-3 on page 296 whereas Rhodes and Harvey get .668 (a 4% error) [3-19]. Finally, the normalized buckling load for the both-unloaded-edges-fixed case is 6.97 for $\nu = .3$, and Reddy obtains 6.972 for $\nu = .25$ from an exact solution [3-14].

Rhodes and Harvey compare their theoretical results with their own experimental results [3-21] and those of Walker [3-22] However, in no case were the actual geometric imperfections measured. Thus, when they compared theory with experiment, they adjusted the imperfection amplitude so that the theoretical and experimental load-deflection behaviors matched at low load levels. The resulting curves are quite impressive in their agreement over the entire range of behavior, but, of course, it would be preferable to actually measure the initial geometric imperfections and then compare the theoretical and experimental results in a more independent fashion. Just because the predicted and measured load-deflection curves can be made to align with each other in magnitude and shape after adjusting the amount of the initial geometric imperfection does not mean correlation exists between predicted behavior and measured behavior *under the same conditions*. In fact, the measured results could have been for plates with a higher amplitude of initial deflection, but a mode shape that was not the most detrimental. We simply do not know because the initial geometric imperfections were not measured. Until specific imperfection shapes and amplitudes are created and the behavior measured, there is no firm basis for stating that theory and experiment are in good agreement.

A well-defined, obvious buckling stress or load for an imperfect plate cannot exist in any formal sense because of the nature of the stable postbuckling behavior in Figure 3-43. That lack of definiteness is certainly not convenient for any engineer trying to analyze and design a challenging structure using various competitive design concepts. Thus, Hu, Lundquist, and Batdorf stated "However, just as a defined yield stress has been found useful for materials that have no actual yield stress, so a defined buckling or critical stress for a plate can convey much meaning to a practicing engineer" [3-23]. That is, although a practicing engineer might understand that a buckling stress is hard to define, that engineer still needs some quantitative measure to 'get his or her teeth into' for various comparative purposes in design studies.

Éléments sous droits d'auteur

Uemura and Byon obtained finite element results and performed experiments on square plates clamped on all four edges to investigate the secondary buckling phenomenon and to compare theoretical and experimental results [3-24]. Their one-term approximation to the initial geometric imperfection is

$$w_o = \frac{A_{11}}{4}\left[1 - \cos\frac{2\pi x}{a}\right]\left[1 - \cos\frac{2\pi y}{b}\right] \tag{3.295}$$

The initial geometric imperfection profile of the plate was measured with a dial gage sliding on a cruciform frame. Axial shortening was measured with strain gages on both sides of the plate near the unloaded edges.

A 2 mm (.079 in) thick Duralumin plate has the measured geometric imperfection profiles along the plate centerlines in both the x-direction and the y-direction shown in Figure 3-44 (at a scale five times that of the other deflections plotted) with $A_{11}/t = .08$ and $b/t = 150$. The deformation mode of the initial geometric imperfection shape (one wave in the load direction) snaps through at P = 2,420 kg (5,340 lb) to two waves in the load direction, i.e., secondary buckling is observed. Above that secondary buckling load, the amplitude of the two buckle waves increases. In the direction transverse to the loading direction, the initial geometric imperfection increases in amplitude with increasing load. However, at the secondary buckling load, the deformation snaps through in the direction opposite to which it had been deforming! Thus, secondary buckling did actually occur and is an example of bifurcation from the nonlinear load-deformation state. During unloading, the plate snaps back into its original shape in almost the opposite of the order of events that occurred during

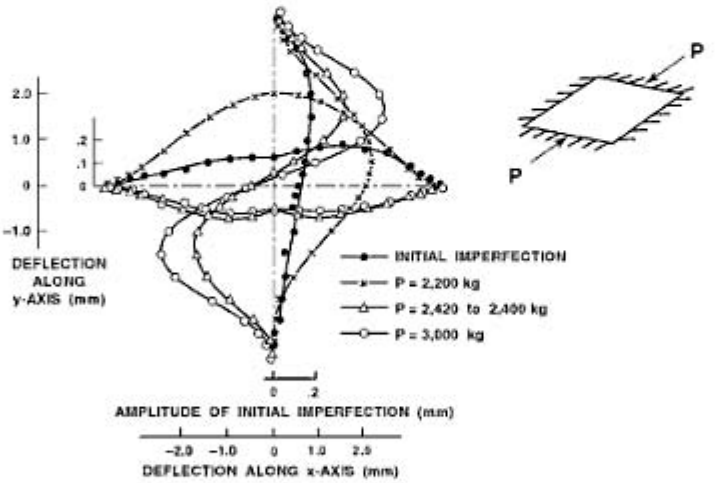


Figure 3-44 Deformation Profiles Below and Above Secondary Buckling of an Imperfect, Clamped, Square Plate
(After Uemura and Byon [3-24])

Éléments sous droits d'auteur

loading. Specifically, first, the plate snaps through from two waves in the x-direction to one wave, and, then, at a somewhat lower load, the plate snaps through again in the y-direction back to its original configuration of an imperfect plate. That is, the snap-through events during unloading occur at two different loads in contrast to the single snap-through load during loading.

3.5.3 Consequences of Nonlinear Load-Deflection Behavior

A part of the stable postbuckling behavior characteristic is the problem of determining just what load to report as the buckling load for an actual, imperfect plate that is, of course, both imperfectly supported and imperfectly loaded. The loading can be displacement-controlled or load-controlled including dead-weight loading. Displacement measurements have progressed over the years from rulers and shim gages to dial gages to displacement transducers to the moiré shadow technique to speckle interferometry.

The characteristic load-deflection behavior of an imperfect plate seen in Figures 3-41 or 3-43 is a rounded-over path without a well-defined buckling load (because such a plate does not buckle—it starts with an initial bow and the amplitude of the bowing increases until secondary buckling occurs). The problem then is defining some sort of measure of a buckling load so one plate can be compared with another in a design environment. The unfortunate aspect is that we are trying to quantify an obviously ill-defined *nonevent!*

The results of load-deflection experiments are interpreted here by using two different methods of identifying crucial quantities that might indicate 'buckling', although buckling of course does not occur. One method is 'strain-reversal' which is a local measure of buckling and the other is the 'top-of-the-knee' which is a global measure of buckling.

Strain-Reversal Method Two strains are considered: (1) ϵ_1 which is the 'extreme-fiber' compressive strain in the x-direction on the concave side of the bow crest in Figure 3-45 and (2) ϵ_2 which is the 'extreme-fiber'

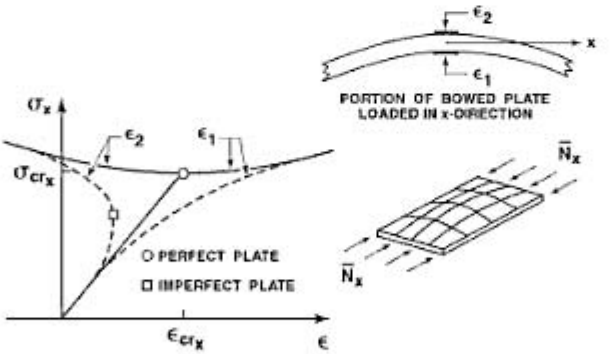


Figure 3-45 Strain Reversal at 'Buckling'

Éléments sous droits d'auteur

compressive strain in the x-direction on the convex side of the bow crest in Figure 3-45, i.e., back-to-back strain gages. As the in-plane load is increased, both ε_1 and ε_2, which are by nature compressive strains, increase in compression. The critical stress by the strain-reversal method is the stress at which the extreme-fiber strain ε_2 stops increasing in compression and begins to decrease in compression, i.e., a vertical tangent to the σ_x versus ε_2 curve must be estimated (a somewhat subjective task subject to small differences of opinion between various observers). The bow crest (mistakenly called the buckle crest by some) is in the center of the plate for the symmetric deformations considered. Of course, the calculated strain state at the center of the plate is used to determine the so-called critical stress or buckling stress at the open-square symbol in Figure 3-45. For the limiting case of a perfect plate, the two strains, ε_1 and ε_2, diverge at the Euler buckling stress, σ_{cr_E}, because only there does bending caused only by buckling occur.

Top-of-the-Knee Method The knee on a load-deformation curve is so-named because of the resemblence to the human knee when the leg is bent. That is, the knee is the portion of the leg that when looked at from the side connects the upper and lower portions of the leg as in the sketch in Figure 3-46. In such a view, quite unlike a two sticks with a hinge situation, the human knee occupies a lot of space. In analogy, the knee of the load-deformation curve is the curved transition region from the lower portion of the load-deflection curve to the upper portion. In that vague region, the rate of increase of lateral or transverse deflection with respect to load goes from low to high (the slope of the load-deflection curve goes from high to low) as in Figure 3-46. However, the slope is never infinite or zero in the extreme, so judging the location of the knee, much less its top, is quite subjective and highly dependent on the observer's eye. Identifying precisely where the human knee starts and stops is not an easy task (except in total-knee replacement where the surgeon's cuts precisely, but artificially, define the starting and stopping points—I know because I have one! Thank you, Dr. Diduch!). You still can't find the end points of the replaced knee without an x-ray or some

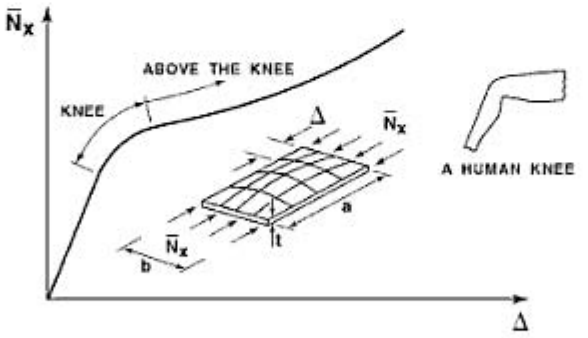


Figure 3-46 Top of the Load-Deflection Curve 'Knee'

Éléments sous droits d'auteur

other inspection technique besides the naked eye. The tops of the lower leg and of the upper leg are virtually straight lines as in the sketch in Figure 3-46, yet the limits of the human knee are still difficult to determine. The load-deflection curve for an imperfect plate is not straight either below or above the knee, so the knee of the plate load-deflection curve is even more difficult to define than the human knee. The 'buckling' stress is essentially, but vaguely, defined to be the stress corresponding to the 'top' of the knee of a curve of stress versus transverse deflection (σ versus w). If the transverse deflections cannot be readily measured, then any other quantity that increases in about the same manner can be plotted instead. One such quantity is $\varepsilon_1 - \varepsilon_2$, the difference in strains in the load direction on the two sides of the bow crest. That difference will be small at low loads, large near the Euler buckling load of a perfectly flat plate, and small again well above that Euler buckling load. Obviously, the top-of-the-knee stress for a perfectly flat plate is well-defined as in Figure 3-41 on page 310 because the knee occurs at a point. However, as the size of the imperfection amplitude is increased, the appearance of the 'knee' is no longer well-defined, and becomes even less well-defined as the imperfection amplitude becomes larger. Visual determination of the location of the top of the knee of the load-deformation curve by an individual observer is far more subjective than estimating the vertical tangent in the strain-reversal method and hence prone to significantly different interpretations by different observers. We apply these definitions of 'buckling', namely strain reversal and top-of-the-knee, to theoretical results obtained by Hu, Lundquist, and Batdorf.

Hu, Lundquist, and Batdorf use von Kármán large-deflection plate theory suitably modified for treatment of initial geometric imperfections to calculate stress, strain, and deflection results that are then regarded as 'simulated test data' to make judgements about the load-deflection behavior of simply supported, imperfectly flat plates [3-23]. See their Appendix A for the long derivation and Appendix B for the specialization to square plates. The essence of the derivation is that the deflection, w, is represented with the double Fourier series

$$w = \sum_{m=1}^{\infty} \sum_{n=1}^{\infty} w_{mn} \sin \frac{m\pi x}{a} \sin \frac{n\pi y}{b} \tag{3.296}$$

and the initial geometric imperfection, w_o, is similarly represented with

$$w_o = \sum_{m=1}^{\infty} \sum_{n=1}^{\infty} w_{o_{mn}} \sin \frac{m\pi x}{a} \sin \frac{n\pi y}{b} \tag{3.297}$$

Only the first six components of the series with odd subscripts are considered. Symmetrical initial curvature and symmetrical deformation (*bowing*, not buckling) are assumed to occur. Thus, the antisymmetric initial geometric imperfection with $m = 2$ and $n = 1$ is not considered because it makes no contribution to the center deflection of the plate. The geometric imperfections can be written as

$$w_o = t \sum_{m=1}^{} \sum_{n=1}^{} K_{o_{mn}} \sin \frac{m\pi x}{a} \sin \frac{n\pi y}{b} \tag{3.298}$$

Éléments sous droits d'auteur

(for a perfectly flat plate, $K_{o_{mn}} = 0$). The first buckling mode of a perfectly flat plate is

$$w = t\,K_{11} \sin\frac{\pi x}{a} \sin\frac{\pi y}{b} \tag{3.299}$$

and, as load increases, the next symmetric buckling mode is

$$w = t\,K_{31} \sin\frac{3\pi x}{a} \sin\frac{\pi y}{b} \tag{3.300}$$

so the most important initial deviations from flatness of a square plate are

$$\begin{aligned} w_o &= t\,K_{o_{11}} \sin\frac{\pi x}{a} \sin\frac{\pi y}{b} \\ w_o &= t\,K_{o_{31}} \sin\frac{3\pi x}{a} \sin\frac{\pi y}{b} \end{aligned} \tag{3.301}$$

The resulting equations are solved in the manner of Levy [3-25], and then the results are interpreted in the following as if they were *simulated test data* instead of theoretical results.

The load as a fraction of the Euler buckling load of a perfect square plate versus the net center transverse deflection increase (center deflection minus the imperfection center deflection, $w - w_o$, over the plate thickness, t, is plotted in Figure 3-47. Hu, Lundquist, and Batdorf study various combinations and values of the imperfection amplitudes in Equation (3.301), $K_{o_{11}}$ and $K_{o_{31}}$, as displayed in Figure 3-47. As the loads or stresses increase well beyond the 'buckling stress' determined by any observation method, the effect of the type and amplitude of the imperfection decreases to the point where imperfections have no influence on

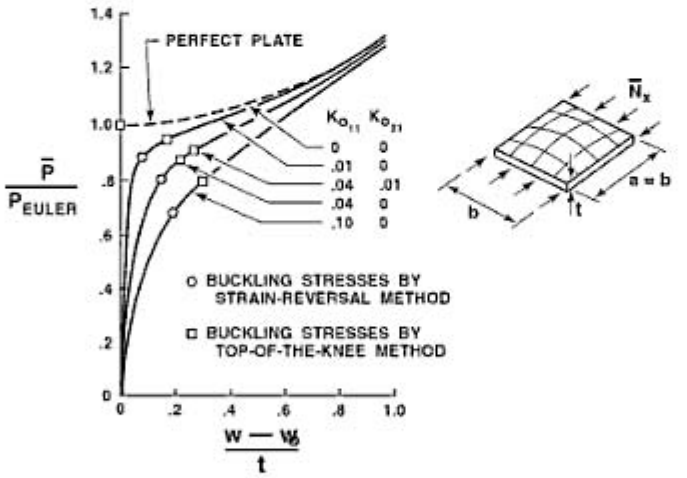


Figure 3-47 Buckling Stresses by Methods of Strain-Reversal and Top-of-the-Knee *(After Hu, Lundquist, and Batdorf [3-23])*

Éléments sous droits d'auteur

the large-load center deflection behavior in Figure 3-47. Similar behavior occurs for low loads or stresses. Only near the Euler buckling load for perfect plates do the geometric imperfections have significant influence.

The buckling stresses determined with both methods are shown in Figure 3-47. Both methods lead to buckling stresses that are more or less on the knee of the stress-deflection curve with the strain-reversal stress always being lower than the top-of-the-knee stress. Both methods lead to reported results that are considerably lower than the theoretical buckling loads for perfect plates as seen in Figure 3-47 where we note that the buckling load using the strain-reversal method is always lower than the top-of-the-knee buckling load. Given the ambiguity of the top-of-the-knee location, those buckling stresses could be plotted even higher than they are in Figure 3-47.

Other definitions of the experimental buckling load were suggested by Hoff, Boley, and Coan in 1948 [3-26]. In addition, the Southwell plot has been adopted for plates and modified to accommodate the large in-plane deflections. Singer, Arbocz, and Weller describe a total of ten methods, eight of which they rank better than the earlier-developed top-of-the-knee and strain-reversal methods [3-17]. That is, there are far better concepts available to determine a so-called buckling load, but they are left to further study.

3.5.4 Summary

Several approaches to evaluating the effect of initial geometric imperfections on plate buckling have been examined. Rhodes and Harvey [3-19] [3-21] derived analyses for treating geometric imperfections for four different boundary conditions on rectangular plates. They compared their predictions with their own experiments and to those of Walker [3-22], but in neither case were geometric imperfections measured to make the comparison completely satisfying and convincing, although the agreement over a large range of loads and deformations is quite impressive. Rhodes and Harvey did not observe secondary buckling either in their experiments or in their theory. Stein both predicted and measured secondary buckling [3-18] as did Uemura and Byon [3-24].

One of the significant problems in interpreting both predicted and measured load-deflection response of geometrically imperfect plates is that a well-defined buckling load does not exist in most situations. (Other significant sources of discrepancies include imperfect boundary conditions relative to the analysis idealization and variations in plate thickness). That is, there is usually no sharp break in the curve as is seen for perfect plates. However, from a design standpoint, an easy-to-use comparative measure is needed to assess competitive design concepts. Thus, many attempts have been made to construct a simple logic to assign a so-called buckling load based on various criteria. Two such methods, strain-reversal and top-of-the-knee, were described, but others that are better are left to further study. Many extensive experimental methods and results are described by Singer, Arbocz, and Weller [3-17].

Éléments sous droits d'auteur

3.6 EFFECT OF MULTIPLE FIBER-REINFORCED LAYERS

3.6.1 Introduction

Laminated plates are one of the simplest and most widespread practical applications of composite laminates and display well the unique two-dimensional capabilities and characteristics of composite laminates that have elements of orthotropy and inhomogeneity. These composite materials analysis topics are addressed by Jones in his *Mechanics of Composite Materials* [3-27]. The conditions for a laminate are given in this book's Appendix C which should be studied if the reader is not familiar with mechanics of composite materials.

The objective in this section is to demonstrate the effect of the various laminated plate coupling stiffnesses (A_{16}, A_{26}, B_{ij}, D_{16}, and D_{26}) on the buckling behavior of laminated plates. That is, the basic questions of laminated plate analysis are: (1) what are the conditions for a set of laminae to act together as a laminate? (2) how does a laminate respond to imposed forces and moments? and (3) what are the buckling loads of laminated plates as in Figure 3-48? The objective does not include a complete study of laminated plate theory. Instead, some of the important laminated plate theory results are examined so that the physical significance of the effects of the stiffnesses are appreciated. The theory of laminated plates with associated solution techniques is a very suitable topic for further study. A more complete cataloging and classification of laminated plate problems than here is found in books by Whitney [3-28], Vinson and Sierakowski [3-29], Vasiliev [3-30], and Reddy [3-31].

The theoretical considerations underlying the basic theory of laminated plates are discussed in Section 3.6.2 based on pioneering work in the 1940s and 1950s by Ambartsumyan [3-32] and further work in the 1960s by Pister and Dong [3-33] as well as by Reissner and Stavsky [3-34]. Then, the differential equations and associated boundary conditions governing the buckling behavior of laminated plates are displayed along with a brief discussion of possible solution techniques. Next, solutions for the various special laminate configurations that are described in Appendix C are displayed in Section 3.6.3. Finally, some general observations on the effects of laminate stiffnesses on buckling loads are addressed in Section 3.6.4.

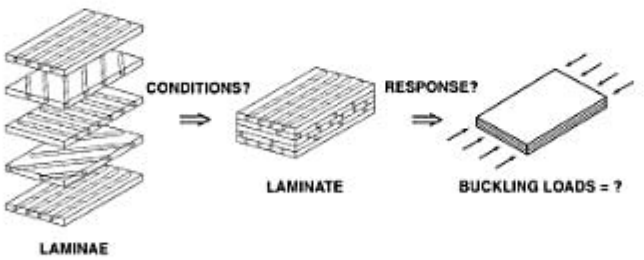


Figure 3-48 Basic Questions of Laminated Plate Analysis

Éléments sous droits d'auteur

A simply supported rectangular plate is used consistently in all subsections to illustrate the kinds of results that can be obtained, i.e., the influence of the various stiffnesses on laminated plate behavior. In addition, only the simplest types of loading will be studied in order to avoid the solution difficulties inherent to complex loadings. Accordingly, in the interest of simplicity, just the bare thread of basic laminated plate results will be presented.

Specially orthotropic plates, i.e., plates with multiple specially orthotropic layers that are symmetric about the plate middle surface have, as is noted in Appendix C, force and moment resultants in which there is no bending-extension coupling nor any shear-extension or bend-twist coupling, that is, if ε_x°, ε_y°, γ_{xy}°, and κ_x, κ_y, and κ_{xy} are middle-surface strains and curvatures,

$$\begin{bmatrix} N_x \\ N_y \\ N_{xy} \end{bmatrix} = \begin{bmatrix} A_{11} & A_{12} & 0 \\ A_{12} & A_{22} & 0 \\ 0 & 0 & A_{66} \end{bmatrix} \begin{bmatrix} \varepsilon_x^\circ \\ \varepsilon_y^\circ \\ \gamma_{xy}^\circ \end{bmatrix} \tag{3.302}$$

$$\begin{bmatrix} M_x \\ M_y \\ M_{xy} \end{bmatrix} = \begin{bmatrix} D_{11} & D_{12} & 0 \\ D_{12} & D_{22} & 0 \\ 0 & 0 & D_{66} \end{bmatrix} \begin{bmatrix} \kappa_x \\ \kappa_y \\ \kappa_{xy} \end{bmatrix} \tag{3.303}$$

For plate problems, whether the specially orthotropic laminate has a single layer or multiple layers is essentially immaterial; the laminate need only be characterized by D_{11}, D_{12}, D_{22}, and D_{66} in Equation (3.303). That is, because there is no bending-extension coupling, the force-strain relations, Equation (3.302), are not used in plate analysis for transverse loading causing only bending. However, note that force-strain relations are needed in shell analysis because of the differences between deformation characteristics of plates as opposed to shells (shells have initial curvature that is inherently coupled to forces).

Often, because specially orthotropic laminates are virtually as easy to analyze as isotropic plates, other laminates are regarded as, or approximated with, specially orthotropic laminates. This approximation will be studied by comparison of results for each type of laminate with and without the various stiffnesses that distinguish it from a specially orthotropic laminate. Specifically, the importance of the bend-twist coupling terms D_{16} and D_{26} will be examined for symmetric angle-ply laminates. Then, bending-extension coupling will be analyzed for antisymmetric cross-ply and antisymmetric angle-ply laminates and compared with the specially orthotropic approximation in which the B_{ij} are ignored. These comparisons will be made for buckling of symmetrically and antisymmetrically laminated simply supported plates in Section 3.6.3. Finally, the engineering significance of the various coupling stiffnesses is summarized in Section 3.6.4.

Éléments sous droits d'auteur

3.6.2 Governing Equations for Buckling of Laminated Plates

3.6.2.1 Basic Restrictions, Presumptions, and Consequences

Most of the restrictions and presumptions on which laminated plate theory is based are developed in Appendix C. However, for completeness, they will be reiterated here in a slightly different manner. The seemingly dual terminology of restrictions and presumptions is used because the terms have fundamentally different meanings. *Restrictions* are limitations on the use of the theory that are *obviously* either satisfied or they are not. Thus, restrictions are concerned with the *known*. For example, a theory for square plates does not apply to round plates. *Presumptions* are limitations on the theory that have a nature of uncertainty to them. That is, presumptions are concerned with the *unknown*. For example, stresses perpendicular to the surface of a plate are commonly presumed to be small enough to be regarded as zero, or presumed to be zero; however, we do not know for certain just how small the stresses are unless we appeal to a more accurate theory. Also, displacements might be presumed to be small to enable certain approximations. However, whether the displacements actually are small can be determined only when the final results are known. In summary, the difference between restrictions and presumptions is that restrictions involve the *known* and presumptions involve the *unknown* (about which we wish to speculate). Thus, we certainly do not 'presume a rectangular plate', but instead we 'restrict our attention to rectangular plates'.

The following restrictions and presumptions for laminated plates are further opportunity to clarify the difference between the two classifications, but mainly to build a firm foundation for the study of laminated plate theory. Note especially that presumptions in engineering must be justified, i.e., we must know *why* we believe the presumption to be true from a physical standpoint. The key feature of any mechanics of materials (or mechanics of deformable bodies) approach to a problem is that certain *simplifying presumptions* must be made regarding the mechanical behavior of the object in order to get a workable or tractable solution. Each presumption must be plausible, i.e., there must be a *reason* why the presumption *might* actually be true (in mechanics, presumptions cannot be arbitrary!). The most prominent presumption in common beam bending problems is that plane sections remain plane. That is, the famous Bernoulli-Euler hypothesis is that plane sections that are perpendicular to the beam axis before bending remain plane and perpendicular to the deformed beam axis during beam bending. This hypothesis is a usual mechanics of materials presumption that is justified by observing that vertical lines drawn on an undeformed rubber beam remain straight (*to the resolution level of our 'naked' eyes*) but rotate as the rubber beam bends as in Figure 2-44 on page 107. *Any* and *every* presumption in engineering must be an assumption *plus a reason why the assumption might be true!* See Section 1.5 for more discussion of presumptions.

Éléments sous droits d'auteur

In classical plate buckling theory, we ignore the prebuckling deformation by presuming or requiring the plate to be flat before the buckling load is reached. Note that in the case of laminated plates with bending-extension coupling that the prebuckling state is not at all flat, but can be highly curved as in Figure C-22 (there, no boundary conditions are applied in contrast to the plate buckling theory results in which all edges have some form of simple support). The author is not aware of a solution for plate buckling in which rigorous prebuckling deformations are accounted for, although Jones and Hennemann [3-35] found up to a 15% percent lowering of the actual buckling load from the classical result for laminated circular cylindrical shells. Nevertheless, most theories have the inherent approximation of a flat prebuckled plate.

The geometry, forces, and moments for a plate are shown in Figures 3-49, 3-50, and 3-51, respectively. Note in Figure 3-49 that the plate aspect ratio, a/b, is merely a common way of quantitatively describing the shape of a rectangular plate. Recall that N_x, N_y, N_{xy} and M_x, M_y, M_{xy} are the forces and moments per unit width of the plate. New are the Kirchhoff shear forces K_x and K_y in Figure 3-50 as well as the distributed transverse loading, p(x,y). Recall that the laminate geometry is defined in Figure C-16.

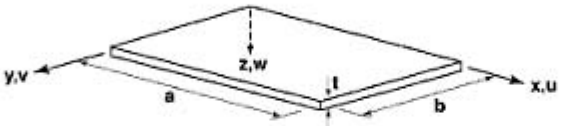


PLATE ASPECT RATIO, $\frac{a}{b}$

Figure 3-49 Plate Geometry and Displacements

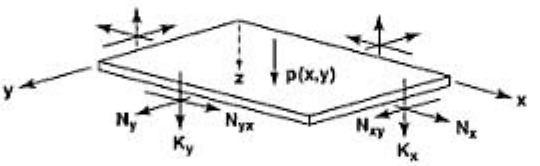


Figure 3-50 Plate Forces

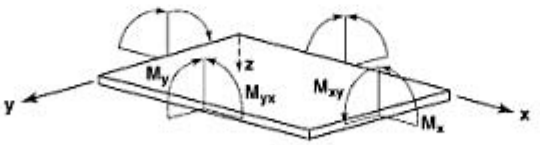


Figure 3-51 Plate Moments

Éléments sous droits d'auteur

Restrictions

- Each layer is orthotropic (but the principal material directions of each layer need not be aligned with the plate axes), linear elastic, and of constant thickness (so the entire plate is of constant thickness).
- The plate thickness is very small compared to its length and width (such a configuration is commonly called a thin plate, although the name *plate* itself implies such a geometry).
- No body forces exist.

Presumptions

- Stresses acting in the x-y plane (the plane of the plate) dominate the plate behavior. Then, σ_z, τ_{xz}, and τ_{yz} are presumed to be zero (or negligible relative to the other stresses) such that an approximate state of *plane stress* is said to exist (wherein only the stresses σ_x, σ_y, and τ_{xy} are considered).
- The *Kirchhoff hypothesis* of negligible transverse shear strains, γ_{xz} and γ_{yz}, and negligible transverse normal strain, ε_z, constitutes a statement of nondeformable normals to the middle surface although there is an inherent, but commonly ignored, conflict with the presumption of zero transverse normal stress, σ_z [3-4].
- Displacements u, v, and w are small compared to the plate thickness (generally, although not necessarily, indicative of small-deflection theory).
- Strains, ε_x, ε_y, and γ_{xy}, are small compared to unity (small-strain theory).
- Rotatory inertia terms are negligible.

Consequences

- If transverse shear strains are ignored or are presumed to be zero, then transverse shear stresses are also zero throughout the plate by virtue of the stress-strain relations. However, even if nothing is said about the transverse shear strains, we still know that the transverse shear stresses are zero on both the upper and lower plate surfaces if there is no shear loading. Commonly, in classical plate theory, the transverse shear strains are regarded as zero, yet transverse shear stresses are calculated from equilibrium considerations. Such procedures will be ignored in this book for the sake of simplicity in presenting only a demonstration of the effect of the various coupling stiffnesses.
- By virtue of the Kirchhoff hypothesis, the remaining strains, ε_x, ε_y, and γ_{xy}, as well as the displacements, u and v, are a linear function of the transverse coordinate z. Moreover, the stresses are accordingly a linear, but discontinuous, function of the transverse coordinate z. Both of these results are shown schematically in Figure 3-52.
- As the restriction to thin plates is relaxed, i.e., as the plate becomes thicker, the plane stress presumption, $\sigma_z = \tau_{xz} = \tau_{yz} = 0$, becomes less accurate.

Éléments sous droits d'auteur

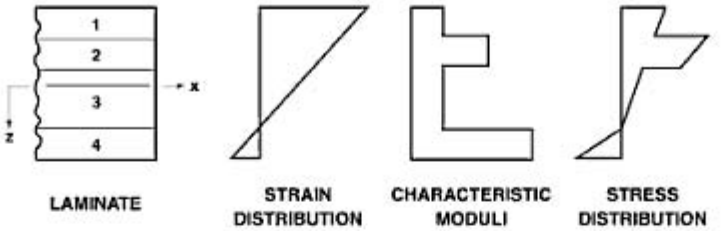


Figure 3-52 Stress and Strain Distribution through the Laminate Thickness

Note that no presumptions involve fiber-reinforced composite materials explicitly. Instead, only the restriction to orthotropic materials at various principal material direction orientations is significant because we treat the macroscopic behavior of an individual orthotropic lamina (easily extended to an anisotropic lamina). Therefore, what follows is essentially a classical plate theory for laminated materials. Actually, interlaminar stresses cannot be entirely disregarded in laminated plates, but that refinement will not be treated in this book.

3.6.2.2 Equilibrium Equations for Laminated Plates

The equilibrium differential equations in terms of the force and moment resultants derived in Section 3.2.3 [linearized versions of the von Kármán plate equilibrium equations, Equations (3.82–3.84)] and the transverse loading p(x,y) are

$$N_{x,x} + N_{xy,y} = 0 \tag{3.304}$$

$$N_{xy,x} + N_{y,y} = 0 \tag{3.305}$$

$$M_{x,xx} + 2M_{xy,xy} + M_{y,yy} = -p \tag{3.306}$$

in which a comma denotes differentiation of the principal symbol with respect to the subscript that follows the comma. In this form, the equilibrium equations are merely those of classical plate theory as derived from the equilibrium of a differential element or as in Section 3.2.3. When the stipulation of a laminated plate is introduced by the explicit use of the force and moment resultants in Equations (C.53) and (C.54) and the strain and change of curvature definitions in Equations (C.45) and (C.46), then the equilibrium equations, Equations (3.304) to (3.306), become (upon dropping the zero subscript used to denote middle-surface displacements)

$$\begin{aligned} &A_{11}u_{,xx} + 2A_{16}u_{,xy} + A_{66}u_{,yy} + A_{16}v_{,xx} + (A_{12} + A_{66})v_{,xy} + A_{26}v_{,yy} \\ &\quad - B_{11}w_{,xxx} - 3B_{16}w_{,xxy} - (B_{12} + 2B_{66})w_{,xyy} - B_{26}w_{,yyy} = 0 \end{aligned} \tag{3.307}$$

Éléments sous droits d'auteur

$$A_{16}u_{,xx} + (A_{12} + A_{66})u_{,xy} + A_{26}u_{,yy} + A_{66}v_{,xx} + 2A_{26}v_{,xy} + A_{22}v_{,yy} - B_{16}w_{,xxx} - (B_{12} + 2B_{66})w_{,xxy} - 3B_{26}w_{,xyy} - B_{22}w_{,yyy} = 0 \tag{3.308}$$

$$D_{11}w_{,xxxx} + 4D_{16}w_{,xxxy} + 2(D_{12} + 2D_{66})w_{,xxyy} + 4D_{26}w_{,xyyy} + D_{22}w_{,yyyy} - B_{11}u_{,xxx} - 3B_{16}u_{,xxy} - (B_{12} + 2B_{66})u_{,xyy} - B_{26}u_{,yyy} - B_{16}v_{,xxx} - (B_{12} + 2B_{66})v_{,xxy} - 3B_{26}v_{,xyy} - B_{22}v_{,yyy} = p \tag{3.309}$$

Obvious and sometimes drastic simplifications occur when the laminate is symmetric about the middle surface ($B_{ij} = 0$), specially orthotropic (all the terms with 16 and 26 subscripts vanish in addition to the B_{ij}), homogeneous ($B_{ij} = 0$ and $D_{ij} = A_{ij}t^2/12$), or isotropic. In all those cases, Equations (3.307) and (3.308) are coupled to each other, but uncoupled from Equation (3.309). That is, Equation (3.309) contains derivatives of the transverse displacement w only, and Equations (3.307) and (3.308) contain both u and v but not w. Accordingly, only Equation (3.309) must be solved to determine the transverse deflections of a plate with the aforementioned simplifications; the in-plane displacements can be found from the solution of Equations (3.307) and (3.308). The more general case of unsymmetrical laminates requires the simultaneous solution of the three coupled equations, Equations (3.307)–(3.309) for the transverse and in-plane displacements.

Boundary conditions used to be thought of as a choice between simply supported, clamped, or free edges if all classes of elastically restrained edges are neglected. The real situation for laminated plates is more complex than for isotropic plates because now there are actually *four* types of boundary conditions that can be called simply supported edges. These more complicated boundary conditions arise because now we must consider u, v, and w instead of just w alone. Similarly, there are four kinds of clamped edges. These boundary conditions can be concisely described as a displacement or derivative of a displacement or, alternatively, a force or moment is equal to some prescribed value (often zero) denoted by an overbar at the edge:

$$\begin{aligned} u_n &= \bar{u}_n \quad \text{or} \quad N_n = \bar{N}_n \\ u_t &= \bar{u}_t \quad \text{or} \quad N_{nt} = \bar{N}_{nt} \\ w_{,n} &= \bar{w}_{,n} \quad \text{or} \quad M_n = \bar{M}_n \\ w &= \bar{w} \quad \text{or} \quad M_{nt,t} + Q_n = \bar{K}_n \end{aligned} \tag{3.310}$$

in n and t coordinates in which n is the direction normal to the edge and t is the direction tangent to the edge as in Figure 3-53. Also, Q_n is the shear force and K_n is the well-known Kirchhoff shear force of classical plate theory (see Timoshenko and Woinowsky-Krieger [3-36]). For example, on the edge x = 0 in Figures 3-49 and 3-50 on page 323.

$$u = 0 \quad \text{or} \quad N_x = 0 \tag{3.311}$$

Éléments sous droits d'auteur

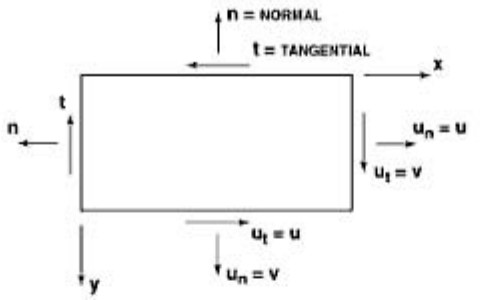


Figure 3-53 Boundary Condition Notation

The eight possible types of simply supported (prefix S) and clamped-edge (prefix C) boundary conditions [combinations of the conditions in Equation (3.310)] are commonly classified as (see Almroth [3-6]):

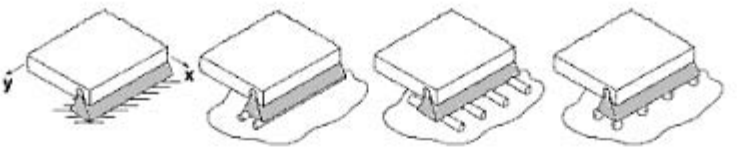
$$\begin{aligned}
&\text{S1:}\quad w=0 \quad M_n=0 \quad u_n=\bar{u}_n \quad u_t=\bar{u}_t\\
&\text{S2:}\quad w=0 \quad M_n=0 \quad N_n=\bar{N}_n \quad u_t=\bar{u}_t\\
&\text{S3:}\quad w=0 \quad M_n=0 \quad u_n=\bar{u}_n \quad N_{nt}=\bar{N}_{nt}\\
&\text{S4:}\quad w=0 \quad M_n=0 \quad N_n=\bar{N}_n \quad N_{nt}=\bar{N}_{nt}
\end{aligned} \tag{3.312}$$

$$\begin{aligned}
&\text{C1:}\quad w=0 \quad w_{,n}=0 \quad u_n=\bar{u}_n \quad u_t=\bar{u}_t\\
&\text{C2:}\quad w=0 \quad w_{,n}=0 \quad N_n=\bar{N}_n \quad u_t=\bar{u}_t\\
&\text{C3:}\quad w=0 \quad w_{,n}=0 \quad u_n=\bar{u}_n \quad N_{nt}=\bar{N}_{nt}\\
&\text{C4:}\quad w=0 \quad w_{,n}=0 \quad N_n=\bar{N}_n \quad N_{nt}=\bar{N}_{nt}
\end{aligned} \tag{3.313}$$

whereupon a rectangular plate can be characterized as having any one of the eight conditions in Equations (3.312) and (3.313) on each of its four edges. The range of possibilities is, therefore, quite large (twelve possible conditions on each of the four edges if the free-edge conditions are included). The simplest cases to analyze naturally involve like types of boundary conditions on opposite, if not all, edges. The emphasis in this book is on plates with four simply supported edges, so cases are chosen from those in Equation (3.312). Note that simply supported edges have no rotational restraint, but when this simplified terminology of simply supported edges is used, the specific in-plane conditions are not determined. Obviously, the totality of boundary conditions including in-plane conditions must be specified by stating, for example, that a solution is obtained for S1 boundary conditions.

To better appreciate the four possible simply supported edge boundary conditions, consider the support system for the edge of a plate illustrated in Figure 3-54 in near-physical terms with mechanisms that the reader can easily understand (repeated here from Section 3.2.3 because

Éléments sous droits d'auteur



(S1)	(S2)	(S3)	(S4)
$w = 0$	$w = 0$	$w = 0$	$w = 0$
$M_x = 0$	$M_x = 0$	$M_x = 0$	$M_x = 0$
$u = 0$	$N_x = 0$	$u = 0$	$N_x = 0$
$v = 0$	$v = 0$	$N_{xy} = 0$	$N_{xy} = 0$

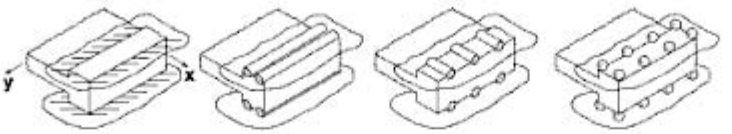
Figure 3-54 Simply Supported Edge Equilibrium Boundary Conditions

of the special importance for laminated plates). Note that the support mechanisms depicted are only for understanding how the various supports *could* work. Only the reader can decide what support conditions are applicable to a specific structure of interest. For a simply supported plate edge, the principal support mechanism in Figure 3-54 is a triangular prism with a circular-cross-section prismatic protrudance on top as a realistic mechanism for the usual so-called knife-edge support for free rotation, i.e., $M_x = 0$. The end view of the triangular prism looks similar to the usual beam support, but with more realistic mechanisms that permit the motion required. For a plate, the protrudance is a bearing that permits (limited) rotation about the y-axis through the center of the protrudance which is located at the middle surface of the plate (but not precisely at the edge of the plate). The protrudance fits in a cavity in the plate such that rotation around the y-axis is possible, but motion transverse to the plate surface is prevented ($w = 0$) and translation along the y-axis of the circular prism is not permitted. The four manners of supporting the triangular prism are:

(1) For the S1 condition, the triangular prism is fastened to a horizontal surface so that the prism cannot translate in either the x- or y-directions. Thus, $u = 0$ and $v = 0$. Hence, forces N_x and N_{xy} must exist.
(2) For the S2 condition, the triangular prism is supported on partially embedded y-direction roller bearings that permit translation in the x-direction, but translation cannot occur in the y-direction, so $u \neq 0$ and $v = 0$. Hence, force N_x must be zero, but N_{xy} must exist.
(3) For the S3 condition, the triangular prism is supported on partially embedded x-direction roller bearings that permit translation in the y-direction, but translation cannot occur in the x-direction, so $u = 0$ and $v \neq 0$. Hence, force N_x must exist, but N_{xy} must be zero.
(4) For the S4 condition, the triangular prism is supported on partially embedded spherical bearings that permit translation in any direction in the x-y plane. Thus, $u \neq 0$ and $v \neq 0$, so both forces N_x and N_{xy} must be zero.

Éléments sous droits d'auteur

For a clamped-edge plate, the principal support mechanism is a boxy mass that restrains rotation about the edge of the plate ($w_{,x} = 0$) and motion transverse to the plate surface ($w = 0$). The four ways of supporting the boxy mass to attain this goal are analogous to the four ways to support a simply supported edge and are shown in Figure 3-55. Recall the discussion of Figure 3-11 on page 248.



C1	C2	C3	C4
$w = 0$	$w = 0$	$w = 0$	$w = 0$
$w_{,x} = 0$	$w_{,x} = 0$	$w_{,x} = 0$	$w_{,x} = 0$
$u = 0$	$N_x = 0$	$u = 0$	$N_x = 0$
$v = 0$	$v = 0$	$N_{xy} = 0$	$N_{xy} = 0$

Figure 3-55 Clamped-Edge Equilibrium Boundary Conditions

3.6.2.3 Buckling Equations for Laminated Plates

A plate buckles when the in-plane compressive load gets so large that the originally flat equilibrium state is no longer stable, and the plate deflects into a nonflat (wavy) configuration. The load at which the departure from the flat state takes place is called the buckling load. The flat equilibrium state has only in-plane forces and undergoes only extension, compression, and shear. Thus, the flat equilibrium state is often called the membrane prebuckled state and consists of only in-plane deformations. More comprehensively, the load at which the plate deformed configuration *suddenly* changes into a *different configuration* is called the buckling load. Note that with bending-extension coupling, an originally flat plate (when without load) under axial in-plane compression *bends* at all loads prior to bifurcation buckling.[1] Thus, a membrane (flat and uniformly stressed) prebuckled state is not actually possible. However, a first-order approximation to the bifurcation buckling load is made by ignoring the prebuckling out-of-plane deflections. Jones and Hennemann studied this approximation for laminated shells and found that the bifurcation buckling loads for a shell with bending-extension coupling induced prebuckling deformations are as much as 15% lower than a shell with such prebuckling deformations ignored [3-35].

Analysis of plates buckling under in-plane loading involves solution of an eigenvalue problem as opposed to the boundary-value problem of equilibrium analysis. The distinctions between boundary-value problems

[1]Bifurcation buckling occurs at the load at which the load path forks into two load paths, the new one stable and the other, the continuation of the old path, unstable, irrespective of the type of deformation path prior to buckling (linear or nonlinear).

Éléments sous droits d'auteur

and eigenvalue problems are too involved to treat here. Instead, the buckling differential equations governing the buckling behavior from a membrane prebuckled state (prebuckling out-of-plane deformations are ignored) are, from Equations (3.160)–(3.162) on page 262,

$$\delta N_{x,x} + \delta N_{xy,y} = 0 \tag{3.314}$$

$$\delta N_{xy,x} + \delta N_{y,y} = 0 \tag{3.315}$$

$$\delta M_{x,xx} + 2\delta M_{xy,xy} + \delta M_{y,yy} - \bar{N}_x \delta w_{,xx} - 2\bar{N}_{xy}\delta w_{,xy} - \bar{N}_y \delta w_{,yy} = 0 \tag{3.316}$$

in which δ denotes a variation of the principal symbol from its value in the prebuckled equilibrium state. Thus, the terms δN_x, ... δM_x, ... are variations of forces and moments, respectively, from their values in a membrane prebuckling equilibrium state. The terms δw and, by implication, δu and δv are variations in displacement from the same flat prebuckled state. In appearance, the buckling differential equations *resemble* the equilibrium differential equations except for the all-important variational notation and the fact that the right-hand sides of the buckling differential equations are zero. Note that if the prebuckling state is a membrane, then $\delta w = w$ because there is no prebuckling out-of-plane displacement. Also note that the in-plane buckling loads $\bar{N}_x$, $\bar{N}_y$, and $\bar{N}_{xy}$ enter the mathematical formulation of the eigenvalue problem as coefficients of the variations in curvatures rather than as 'loads' on the right-hand side of the equilibrium equation. The essence of the eigenvalue problem is to determine the smallest applied loads, $\bar{N}_x$, etc., that cause buckling. An important consequence of this type of problem is that the magnitude of the deformations after buckling cannot be determined without resort to a large-deflection analysis; i.e., the deformation amplitudes are indeterminate when only Equations (3.314) to (3.316) are considered.

The variations in force and moment resultants are obtained by varying the force and moment resultants in Appendix C, Equation (C.53) on page 775. Note that the A, B, and D matrices are constant during the variational process.

$$\begin{bmatrix} \delta N_x \\ \delta N_y \\ \delta N_{xy} \end{bmatrix} = \begin{bmatrix} A_{11} & A_{12} & A_{16} \\ A_{12} & A_{22} & A_{26} \\ A_{16} & A_{26} & A_{66} \end{bmatrix} \begin{bmatrix} \delta\varepsilon_x^\circ \\ \delta\varepsilon_y^\circ \\ \delta\gamma_{xy}^\circ \end{bmatrix} + \begin{bmatrix} B_{11} & B_{12} & B_{16} \\ B_{12} & B_{22} & B_{26} \\ B_{16} & B_{26} & B_{66} \end{bmatrix} \begin{bmatrix} \delta\kappa_x \\ \delta\kappa_y \\ \delta\kappa_{xy} \end{bmatrix} \tag{3.317}$$

$$\begin{bmatrix} \delta M_x \\ \delta M_y \\ \delta M_{xy} \end{bmatrix} = \begin{bmatrix} B_{11} & B_{12} & B_{16} \\ B_{12} & B_{22} & B_{26} \\ B_{16} & B_{26} & B_{66} \end{bmatrix} \begin{bmatrix} \delta\varepsilon_x^\circ \\ \delta\varepsilon_y^\circ \\ \delta\gamma_{xy}^\circ \end{bmatrix} + \begin{bmatrix} D_{11} & D_{12} & D_{16} \\ D_{12} & D_{22} & D_{26} \\ D_{16} & D_{26} & D_{66} \end{bmatrix} \begin{bmatrix} \delta\kappa_x \\ \delta\kappa_y \\ \delta\kappa_{xy} \end{bmatrix} \tag{3.318}$$

in which the variations in in-plane strains and changes in curvature are related to the variations in displacements by

Éléments sous droits d'auteur

$$\delta\varepsilon_x^\circ = \delta u_{,x} \qquad \delta\varepsilon_y^\circ = \delta v_{,y} \qquad \delta\gamma_{xy}^\circ = \delta u_{,y} + \delta v_{,x} \tag{3.319}$$

$$\delta\kappa_x = -\delta w_{,xx} \qquad \delta\kappa_y = -\delta w_{,yy} \qquad \delta\kappa_{xy} = -2\delta w_{,xy} \tag{3.320}$$

The buckling differential equations can be expressed in terms of the variations in displacements by substituting the variations in in-plane strains and curvatures, Equations (3.319) and (3.320), in the variations in force and moment resultants, Equations (3.317) and (3.318), and subsequently in the buckling differential equations in terms of the variations of forces, moments, and displacements during buckling, i.e., Equations (3.314) to (3.316). The resulting equations take a form similar to the corresponding equilibrium equations, Equations (3.307) to (3.309). Just as for equilibrium problems, buckling of generally laminated plates has bending-extension coupling. However, some special laminates exhibit no bending-extension coupling; hence, their buckling loads are obtained by solution of only Equation (3.316) or its variation of deflections equivalent.

The boundary conditions for buckling problems are applied only to the buckling deformations because the prebuckling deformations are assumed to be a membrane state (even if bending-extension coupling does exist). That is, we ignore the prebuckling deformations just as we ignore initial geometric imperfections. One of the distinguishing features of an eigenvalue problem is that all the boundary conditions are homogeneous, i.e., zero. Thus, during buckling, the boundary conditions are

Simply Supported Edges:

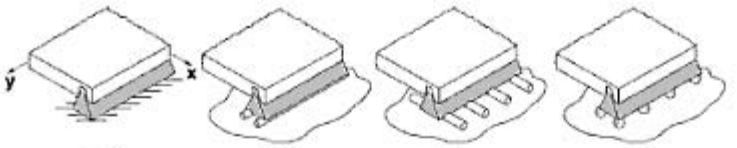
$$\begin{array}{llllll} \text{S1:} & \delta w = 0 & \delta M_n = 0 & \delta u_n = 0 & \delta u_t = 0 \\ \text{S2:} & \delta w = 0 & \delta M_n = 0 & \delta N_n = 0 & \delta u_t = 0 \\ \text{S3:} & \delta w = 0 & \delta M_n = 0 & \delta u_n = 0 & \delta N_{nt} = 0 \\ \text{S4:} & \delta w = 0 & \delta M_n = 0 & \delta N_n = 0 & \delta N_{nt} = 0 \end{array} \tag{3.321}$$

Clamped Edges:

$$\begin{array}{llllll} \text{C1:} & \delta w = 0 & \delta w_{,n} = 0 & \delta u_n = 0 & \delta u_t = 0 \\ \text{C2:} & \delta w = 0 & \delta w_{,n} = 0 & \delta N_n = 0 & \delta u_t = 0 \\ \text{C3:} & \delta w = 0 & \delta w_{,n} = 0 & \delta u_n = 0 & \delta N_{nt} = 0 \\ \text{C4:} & \delta w = 0 & \delta w_{,n} = 0 & \delta N_n = 0 & \delta N_{nt} = 0 \end{array} \tag{3.322}$$

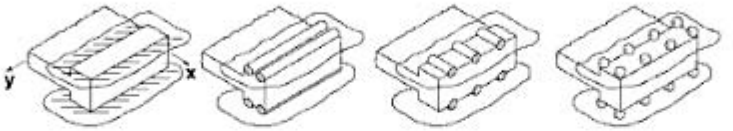
The boundary conditions could be different for each edge of a plate, so the number of combinations of possible boundary conditions is quite large as it was with equilibrium problems. The possible simply supported edge boundary conditions and the clamped-edge boundary conditions *during buckling* are shown in physical terms in Figures 3-56 and 3-57.

Éléments sous droits d'auteur



S1	S2	S3	S4
$\delta w = 0$	$\delta w = 0$	$\delta w = 0$	$\delta w = 0$
$\delta M_x = 0$	$\delta M_x = 0$	$\delta M_x = 0$	$\delta M_x = 0$
$\delta u = 0$	$\delta N_x = 0$	$\delta u = 0$	$\delta N_x = 0$
$\delta v = 0$	$\delta v = 0$	$\delta N_{xy} = 0$	$\delta N_{xy} = 0$

Figure 3-56 Simply Supported Edge Boundary Conditions during Buckling



C1	C2	C3	C4
$\delta w = 0$	$\delta w = 0$	$\delta w = 0$	$\delta w = 0$
$\delta w_{,x} = 0$	$\delta w_{,x} = 0$	$\delta w_{,x} = 0$	$\delta w_{,x} = 0$
$\delta u = 0$	$\delta N_x = 0$	$\delta u = 0$	$\delta N_x = 0$
$\delta v = 0$	$\delta v = 0$	$\delta N_{xy} = 0$	$\delta N_{xy} = 0$

Figure 3-57 Clamped-Edge Boundary Conditions during Buckling

3.6.2.4 Solution Techniques

Many techniques exist for solution of the buckling problems formulated in the preceding subsections. The techniques range from fortuitous exact solutions that are obtained essentially by 'observation' through numerical approximations such as finite element and finite difference approaches to the various approximate energy methods such as those of Rayleigh-Ritz and Galerkin as well as complex potential functions. Because the objective here is to demonstrate the importance of the various coupling stiffnesses, only those solution techniques necessary for fruitful illustrations are used.

A prominent part of many of the techniques is separation of variables. In that method, the buckling deflection variables, or the variation in deflection variables, are arbitrarily separated into functions of plate coordinate x alone times functions of y alone. Wang [3-37] determined that separation of variables leads to exact solutions for some classes of plate problems, but does not for many others, i.e., the buckling deflections are not always separable.

Éléments sous droits d'auteur

3.6.3 Buckling of Simply Supported Laminated Plates under In-Plane Load

Consider the general class of laminated rectangular plates that are simply supported along edges $x = 0$, $x = a$, $y = 0$, and $y = b$ and subjected to uniform in-plane force in the x-direction as in Figure 3-58. Other more complicated loads and boundary conditions could be treated. However, the importance of the various stiffnesses in buckling problems is well-illustrated with this simple loading. More comprehensive treatment of plate buckling in general is given by Timoshenko and Gere [3-8] and by Reddy [3-14] and of laminated plate buckling in particular is given by Whitney [3-28] and by Reddy [3-31].

When columns buckle, a lateral deformation develops along the column length, as is well known. When plates buckle, the deformation transverse to the plane of the plate has a two-dimensional wavy nature. Moreover, that two-dimensional nature has multiple sine waves in the load direction, as shown for the example of two buckle waves in Figure 3-59. Generally, if the plate is very long in the load direction, many sine waves develop. Note that the nodal line in Figure 3-59 does not move during buckling.

The load-deformation behavior of plates is more complicated than that of columns. First, as load increases, the plate simply shortens in the load direction while remaining flat. Then, the plate buckles at N where the deformation path bifurcates (takes one of two paths) from the flat shape to the buckled shape in Figure 3-60. After buckling, the plate can

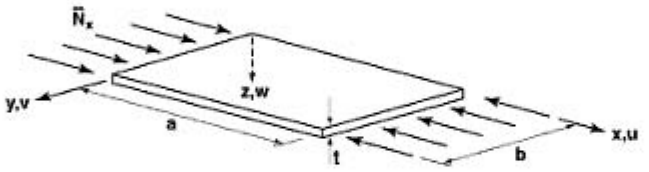


Figure 3-58 Simply Supported Laminated Rectangular Plate under Uniform Uniaxial In-Plane Compression

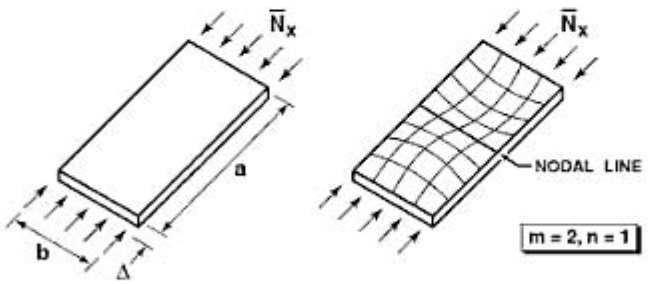


Figure 3-59 In-Plane Loaded Plate Before Buckling and Typical Buckling Mode

Éléments sous droits d'auteur

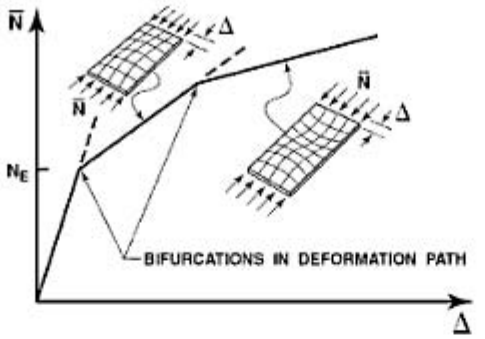


Figure 3-60 Load-Deformation Behavior for an In-Plane Loaded Plate

actually support increased load over the buckling load, but at decreased stiffness as in Figure 3-60. In contrast, columns cannot support any load higher than the buckling load. Thus, the two structural elements have a very different meaning for their buckling loads; one (the column) is the maximum load, the other (the plate) is only an interruption in the load-deformation behavior (a change in slope called a knee).

This knee in the load-deformation curve for a plate occurs only for a plate that is perfectly flat before loading. For plates with increasing magnitudes of initial geometric imperfections, the knee is rounded over, and the load-deformation curve decreases as in Figure 3-61.

The buckling load will be determined for plates with various laminations: specially orthotropic, symmetric angle-ply, antisymmetric cross-ply, and antisymmetric angle-ply. The results for the different lamination types will be compared to find the influence of bend-twist coupling and bending-extension coupling. Different simply supported edge boundary conditions will be used in the several problems addressed for convenience of illustration.

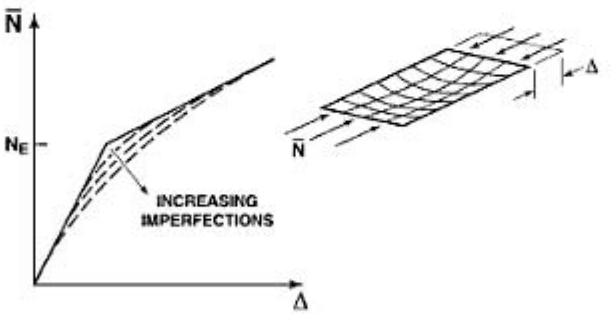


Figure 3-61 Behavior of Plates with Initial Geometric Imperfections

Éléments sous droits d'auteur

3.6.3.1 Specially Orthotropic Laminated Plates

A specially orthotropic laminate has either a single layer of a specially orthotropic material or multiple specially orthotropic layers that are symmetrically arranged about the laminate middle surface (to form a symmetric cross-ply laminate). In both cases, the laminate stiffnesses consist solely of A_{11}, A_{12}, A_{22}, A_{66}, D_{11}, D_{12}, D_{22}, and D_{66}. That is, neither shear-extension or bend-twist coupling nor bending-extension coupling exists. Then, for plate problems, the buckling loads are determined from only one buckling differential equation:

$$D_{11}\delta w_{,xxxx} + 2(D_{12} + 2D_{66})\delta w_{,xxyy} + D_{22}\delta w_{,yyyy} + \bar{N}_x \delta w_{,xx} = 0 \quad (3.323)$$

subject to the simply supported edge boundary conditions

$$\begin{aligned} x = 0, a: \quad & \delta w = 0 \quad \delta M_x = -D_{11}\delta w_{,xx} - D_{12}\delta w_{,yy} = 0 \\ y = 0, b: \quad & \delta w = 0 \quad \delta M_y = -D_{12}\delta w_{,xx} - D_{22}\delta w_{,yy} = 0 \end{aligned} \quad (3.324)$$

Note that because of the absence of the variations in in-plane displacements, δu and δv, the boundary conditions are much simpler than the general case in Equation (3.321).

The solution to this fourth-order partial differential equation and associated homogeneous boundary conditions is simple. The boundary conditions are satisfied by the variation in transverse displacement (for plates, δw actually is the physical buckle displacement because $w = 0$ in the membrane prebuckling state; however, δu and δv are variations from a nontrivial equilibrium state. Hence, we retain the more rigorous variational notation consistently):

$$\delta w = \tilde{w}_{mn} \sin \frac{m\pi x}{a} \sin \frac{n\pi y}{b} \quad (3.325)$$

in which m and n are the number of buckle half wavelengths in the x- and y-directions, respectively, and $\tilde{w}$ is the indeterminate buckling deflection amplitude. In addition, the governing differential equation is satisfied by Equation (3.325) if

$$\bar{N}_x = \pi^2 \left[D_{11}\left[\frac{m}{a}\right]^2 + 2(D_{12} + 2D_{66})\left[\frac{n}{b}\right]^2 + D_{22}\left[\frac{n}{b}\right]^4 \left[\frac{a}{m}\right]^2 \right] \quad (3.326)$$

The smallest value of $\bar{N}_x$ obviously occurs when $n = 1$, so the buckling load expression further reduces to

$$\bar{N}_x = \pi^2 \left[D_{11}\left[\frac{m}{a}\right]^2 + 2(D_{12} + 2D_{66})\frac{1}{b^2} + D_{22}\left[\frac{1}{b^4}\right]\left[\frac{a}{m}\right]^2 \right] \quad (3.327)$$

The smallest value of $\bar{N}_x$ for various m is not obvious, but varies for different values of the stiffnesses and the plate aspect ratio, a/b.

For example, if $D_{11}/D_{22} = 10$ and $(D_{12} + 2D_{66})/D_{22} = 1$ (representative values for boron-epoxy, then Equation (3.327) becomes

Éléments sous droits d'auteur

$$\bar{N}_x = \pi^2 D_{22}\left[10\left[\frac{m}{a}\right]^2 + \frac{2}{b^2} + \left[\frac{a}{m}\right]^2 \frac{1}{b^4}\right] \tag{3.328}$$

which is plotted in Figure 3-62 versus the plate aspect ratio. There, for small plate aspect ratios (that is, $a/b < 2.5$), the plate buckles into a single half-wave in the x-direction. For example, the buckling load of a square plate is

$$\bar{N}_x = \frac{13\pi^2 D_{22}}{b^2} \tag{3.329}$$

As the plate aspect ratio increases, the plate buckles into more and more buckle half-waves in the x-direction and has an N_x versus a/b curve that gets even flatter and, in fact, approaches

$$\bar{N}_x = \frac{8.32456\pi^2 D_{22}}{b^2} \tag{3.330}$$

For other materials, other families of curves such as in Figure 3-62 are obtained with correspondingly different buckling loads and different points of change from one buckling mode to another.

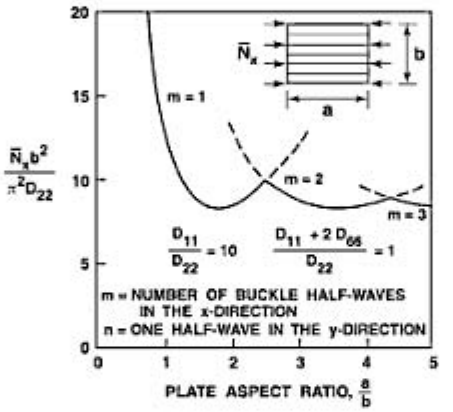


Figure 3-62 Buckling of Rectangular Specially Orthotropic Laminated Plates under Uniform Compression, N_x

Consider two rectangular plates that are simply supported on all four edges, of the same thickness, and made of the same fiber-reinforced material as in Figure 3-63. One plate consists of all unidirectional material with fibers in the load direction. The other plate has the same layers, but alternately arranged in the form of a symmetric cross-ply laminate. Many might think or expect that the plate with the most fibers in the load direction would have the highest buckling load. However, that position is based on the premise that the buckling load depends primarily

Éléments sous droits d'auteur

on the bending resistance in the load direction. However, *the plate buckling load is a function of all four bending stiffnesses* D_{11}, D_{12}, D_{22}, and D_{66}, as is clear from Equation (3.327). Thus, it should not be surprising that the cross-ply plate has a higher buckling load than the unidirectionally reinforced plate. In fact, the support on all four edges of a plate signifies that a plate cannot simply deform as a wide column (as a plate supported on only the two loaded edges would be). The behavior of a wide column would, of course, be dominated by the bending stiffness in the direction of the load.

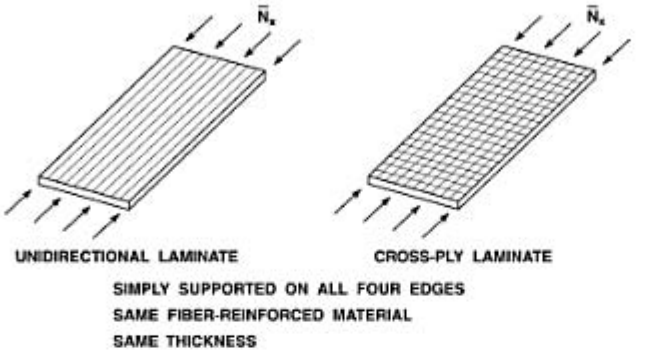


Figure 3-63 Which Plate Has the Highest Buckling Load?

3.6.3.2 Symmetric Angle-Ply Laminated Plates

Symmetric angle-ply laminates are found in Appendix C to be characterized by a full matrix of extensional stiffnesses as well as bending stiffnesses, but not to have bending-extension coupling. The principal difference between these laminates and specially orthotropic laminates is the introduction here of the bend-twist coupling stiffnesses D_{16} and D_{26} (the shear-extension coupling stiffnesses A_{16} and A_{26} are immaterial for buckling of a symmetrically laminated plate because the three governing differential equations are uncoupled). Accordingly, the governing buckling differential equation is

$$\begin{aligned} D_{11}\delta w_{,xxxx} + 4D_{16}\delta w_{,xxxy} + 2(D_{12} + 2D_{66})\delta w_{,xxyy} \\ + 4D_{26}\delta w_{,xyyy} + D_{22}\delta w_{,yyyy} + \bar{N}_x\delta w_{,xx} = 0 \end{aligned} \tag{3.331}$$

subject to the simply supported edge boundary conditions

$$\begin{aligned} x = 0, a: \quad & \delta w = 0 \quad \delta M_x = -D_{11}\delta w_{,xx} - D_{12}\delta w_{,yy} - 2D_{16}\delta w_{,xy} = 0 \\ y = 0, b: \quad & \delta w = 0 \quad \delta M_y = -D_{12}\delta w_{,xx} - D_{22}\delta w_{,yy} - 2D_{26}\delta w_{,xy} = 0 \end{aligned} \tag{3.332}$$

The presence of D_{16} and D_{26} in the governing differential equation and boundary conditions makes a closed-form solution impossible. That is, the variation in transverse displacement, δw, cannot be separated into a function of x alone times a function of y alone as in Equation (3.325).

Éléments sous droits d'auteur

However, an approximate Rayleigh-Ritz solution was obtained by Ashton and Waddoups [3-38] (or equivalently a Galerkin solution as presented by Chamis [3-39]) by substituting the variation in transverse displacement expression

$$\delta w = \sum_{m=1}^{\infty} \sum_{n=1}^{\infty} \bar{w}_{mn} \sin \frac{m\pi x}{a} \sin \frac{n\pi y}{b} \tag{3.333}$$

in the expression for the second variation of the total potential energy and subsequently making it stationary relative to the $\bar{w}_{mn}$. Note that Equation (3.333) satisfies the geometric boundary conditions of the problem ($\delta w = 0$ on all edges), but not the natural boundary conditions ($\delta M_n = 0$ on all edges) or the differential equations, so the results probably converge slowly toward the actual solution. As with previous buckling problems, the buckling deflection component amplitudes, $\bar{w}_{mn}$, are indeterminate.

The actual solution procedure is only incidental to the present objectives, so we are satisfied to report the results for several laminates of boron-epoxy with $E_1/E_2 = 10$, $G_{12}/E_2 = .3$, and $\nu_{12} = .3$. Normalized buckling loads for three laminates, 20 layers at $+\theta$, 20 layers alternating at $\pm\theta$, and the specially orthotropic approximation, are plotted in Figure 3-64. The Rayleigh-Ritz curves are for 49 terms ($m = 7$ and $n = 7$). Experimental results by Mandell [3-40] are also shown in Figure 3-64; obviously, the agreement between theory and experiment is very satisfactory. Apparently, bend-twist coupling is just as important for buckling problems as it is for bending problems. The principal influence of bend-twist coupling is to lower the buckling load from what would be obtained with the specially orthotropic approximation. Thus, the specially orthotropic approximation is unconservative in design applications. The author is not aware of any skew plate analogy results for plate buckling as do exist for the anisotropic plate bending problem (see Ashton [3-41]).

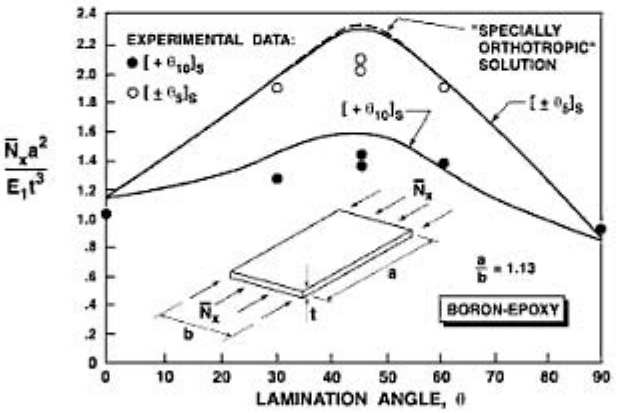


Figure 3-64 Buckling Loads for Rectangular Symmetric Angle-Ply Plates under Uniform Compression, N_x *(After Whitney [3-28])*

Éléments sous droits d'auteur

3.6.3.3 Antisymmetric Cross-Ply Laminated Plates

Antisymmetric cross-ply laminates are found in Appendix C to have extensional stiffnesses A_{11}, A_{12}, $A_{22} = A_{11}$, and A_{66}; bending-extension coupling stiffnesses B_{11} and $B_{22} = -B_{11}$; and bending stiffnesses D_{11}, D_{12}, $D_{22} = D_{11}$, and D_{66}. The new terms here in comparison to a specially orthotropic laminate are B_{11} and B_{22}. Because of this bending-extension coupling, the three buckling differential equations are coupled:

$$A_{11}\delta u_{,xx} + A_{66}\delta u_{,yy} + (A_{12} + A_{66})\delta v_{,xy} - B_{11}\delta w_{,xxx} = 0 \tag{3.334}$$

$$(A_{12} + A_{66})\delta u_{,xy} + A_{66}\delta v_{,xx} + A_{11}\delta v_{,yy} + B_{11}\delta w_{,yyy} = 0 \tag{3.335}$$

$$\begin{aligned} D_{11}(\delta w_{,xxxx} + \delta w_{,yyyy}) + 2(D_{12} + 2D_{66})\delta w_{,xxyy} \\ - B_{11}(\delta u_{,xxx} - \delta v_{,yyy}) + \bar{N}_x \delta w_{,xx} = 0 \end{aligned} \tag{3.336}$$

Jones solved this problem for the simply supported edge boundary condition S2 [3-42]:

$$x = 0, a: \quad \delta w = 0 \quad \delta M_x = B_{11}\delta u_{,x} - D_{11}\delta w_{,xx} - D_{12}\delta w_{,yy} = 0 \tag{3.337}$$

$$\delta v = 0 \quad \delta N_x = A_{11}\delta u_{,x} + A_{12}\delta v_{,y} - B_{11}\delta w_{,xx} = 0 \tag{3.338}$$

$$y = 0, b: \quad \delta w = 0 \quad \delta M_y = -B_{11}\delta v_{,y} - D_{12}\delta w_{,xx} - D_{11}\delta w_{,yy} = 0 \tag{3.339}$$

$$\delta u = 0 \quad \delta N_y = A_{12}\delta u_{,x} + A_{11}\delta v_{,y} + B_{11}\delta w_{,yy} = 0 \tag{3.340}$$

and found that the variations in displacements (with indeterminate amplitudes $\tilde{u}$, $\tilde{v}$, and $\tilde{w}$)

$$\begin{aligned} \delta u &= \tilde{u} \cos \frac{m\pi x}{a} \sin \frac{n\pi y}{b} \\ \delta v &= \tilde{v} \sin \frac{m\pi x}{a} \cos \frac{n\pi y}{b} \\ \delta w &= \tilde{w} \sin \frac{m\pi x}{a} \sin \frac{n\pi y}{b} \end{aligned} \tag{3.341}$$

satisfy both the boundary conditions and the differential equations exactly if the buckling load is

$$\bar{N}_x = \left[\frac{a}{m\pi}\right]^2 \left[T_{33} + \frac{2T_{12}T_{23}T_{13} - T_{22}T_{13}^2 - T_{11}T_{23}^2}{T_{11}T_{22} - T_{12}^2}\right] \tag{3.342}$$

in which

$$\begin{aligned} T_{11} &= A_{11}\left[\frac{m\pi}{a}\right]^2 + A_{66}\left[\frac{n\pi}{b}\right]^2 \\ T_{12} &= (A_{12} + A_{66})\left[\frac{m\pi}{a}\right]\left[\frac{n\pi}{b}\right] \\ T_{13} &= -B_{11}\left[\frac{m\pi}{a}\right]^3 \end{aligned} \tag{3.343, continued}$$

Éléments sous droits d'auteur

$$T_{22} = A_{11}\left[\frac{n\pi}{b}\right]^2 + A_{66}\left[\frac{m\pi}{a}\right]^2$$

$$T_{23} = B_{11}\left[\frac{n\pi}{b}\right]^3 \qquad \text{(3.343, concluded)}$$

$$T_{33} = D_{11}\left[\left[\frac{m\pi}{a}\right]^4 + \left[\frac{n\pi}{b}\right]^4\right] + 2(D_{12} + 2D_{66})\left[\frac{m\pi}{a}\right]^2\left[\frac{n\pi}{b}\right]^2$$

Note that if no bending-extension coupling exists, i.e., $B_{11} = 0$, then T_{13} and T_{23} are also zero, so Equation (3.342) reduces to the specially orthotropic plate solution, Equation (3.326), if $D_{11} = D_{22}$. Because T_{11}, T_{12}, T_{22}, and T_{33} are functions of both m and n, no simple conclusion can be drawn about the value of n at buckling as was done for specially orthotropic laminated plates for which n had to be one. Instead, Equation (3.342) is a complicated function of both m and n.

One of the major complications in the plate buckling solution is the need to investigate the influence of buckle mode shape on the buckling load. That is, the plate buckling load in Equation (3.342) is a function of the buckling mode shape parameters m and n (the number of buckle half wavelengths in the x- and y-directions) as well as the laminated plate stiffnesses. In contrast, the column buckling load can, of course, be expressed in terms of the buckle mode shape parameter m, i.e.,

$$\bar{P} = P_E = m^2\pi^2\frac{EI}{L^2} \qquad (3.344)$$

However, because we are usually interested only in the lowest buckling load for a column, m is always one. For plates, both m and n enter the buckling equation as well as the plate aspect ratio, a/b, so the lowest buckling load does not typically occur for $m = 1$ and $n = 1$ (but it can occur). Thus, we must find the absolute minimum of the values of the buckling load, $\bar{N}_x$, or more generally, λ, for a wide range of integer m and n values. See Appendix B for a generic description of a search procedure by Jones [3-43] for how to find the absolute minimum buckling load for some range of *integer* values of m and n (*not* by equating to zero the first partial derivatives of N_x with respect to m and n!).

We want to study the effect of the number of layers on laminate performance. The fair comparison is to keep the total laminate thickness constant to consider only equal-weight laminates. Then, we vary the number of layers by dividing the laminate into more and more layers. That is, we construct the sequence of antisymmetric cross-ply laminates with an increasing number of layers but of constant thickness as in Figure 3-65. Accordingly, the effect of the number of layers on the buckling load is found by dividing a constant-thickness, equal-weight cross-ply laminate into more and more (thinner) alternating 0° and 90° laminae as in Figure 3-65 (where only the fiber cross sections that are cut are shown). Results for graphite-epoxy antisymmetric cross-ply laminated plates with properties $E_1/E_2 = 40$, $G_{12}/E_2 = .5$, and $\nu_{12} = .25$ are shown in Figure 3-66. There, the buckling load is normalized with respect to the plate width b and plate stiffness D_{22} for various rectangular plate aspect ratios and for various numbers of layers. The solution for an infinite number of layers (a specially orthotropic laminated plate) is shown as a limiting

Éléments sous droits d'auteur

case of no bending-extension coupling. The coupling is extremely significant for a small number of layers. For two layers at a plate aspect ratio of one, the overestimate of buckling resistance is 183% if the specially orthotropic approximation is made. From another point of view, the actual resistance is 65% less than calculated by use of the specially orthotropic approximation. For four layers, the analogous numbers are 19% overestimate and 16% reduction, respectively. For six layers, the numbers drop to 8% overestimate and 7% reduction. Obviously, the effect of bending-extension coupling dies out very rapidly as the number of layers increases for an antisymmetric laminate. However, for fewer than six layers, the effect cannot be ignored.

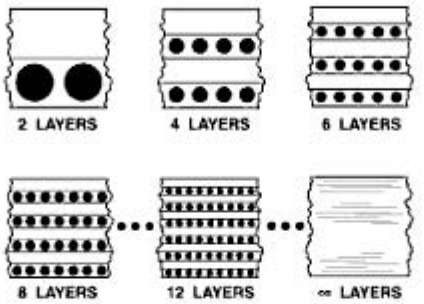


Figure 3-65 Antisymmetric Cross-Ply Laminate Example

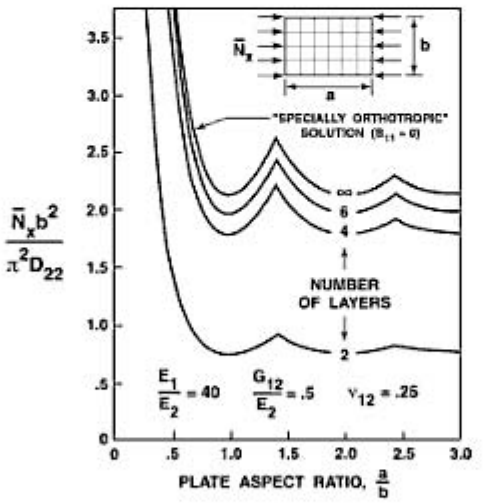


Figure 3-66 Buckling Loads for Antisymmetric Cross-Ply Laminated Plates under Uniform Uniaxial Compression N_x *(After Jones [3-42])*

Éléments sous droits d'auteur

When other composite materials are considered, the effect of bending-extension coupling on the buckling load depends essentially on the orthotropic modulus ratio, E_1/E_2, as shown in Figure 3-67. There, the buckling load is normalized by the buckling load of a specially orthotropic square plate ($B_{11} = 0$). Values of G_{12}/E_2 and ν_{12} are fixed because they do not vary significantly and their influence on the buckling load is small compared to that of E_1/E_2. As the modulus ratio decreases from the graphite-epoxy value of 40, the influence of bending-extension coupling decreases slowly. As noted before, the reduction in buckling load of a square two-layered graphite-epoxy plate from the specially orthotropic plate is about 65%. For a square boron-epoxy plate, the reduction is about 43%. From the design-analysis point of view, the specially orthotropic plate solution is too high by 183% for a graphite-epoxy plate and by 74% for an analogous boron-epoxy plate. Obviously, bending-extension coupling is extremely important when the plate has only two layers. However, the influence of coupling dies out quite rapidly as the number of layers increases. For example, the reduction in buckling load for a six-layered graphite-epoxy plate is only about 7% and about 5% for a boron-epoxy plate.

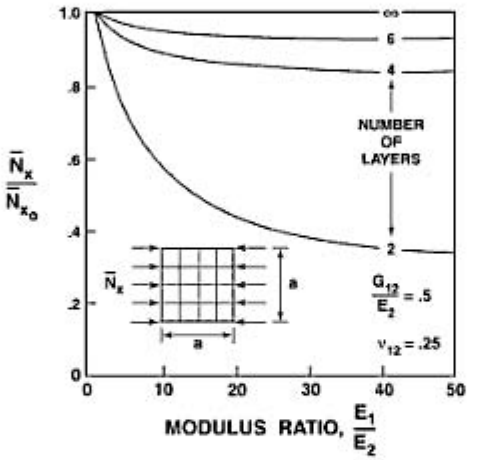


Figure 3-67 Relative Uniaxial Buckling Loads of Square Antisymmetric Cross-Ply Laminated Plates *(After Jones [3-42])*

3.6.3.4 Antisymmetric Angle-Ply Laminated Plates

Antisymmetric angle-ply laminates are found in Appendix C to have extensional stiffnesses A_{11}, A_{12}, A_{22}, and A_{66}; bending-extension coupling stiffnesses B_{16} and B_{26}; and bending stiffnesses D_{11}, D_{12}, D_{22}, and D_{66}. Thus, this type of laminate exhibits a very different kind of bending-extension coupling than does the antisymmetric cross-ply lami-

Éléments sous droits d'auteur

nate examined in Section 3.6.3.3. The coupled buckling differential equations are

$$A_{11}\delta u_{,xx} + A_{66}\delta u_{,yy} + (A_{12} + A_{66})\delta v_{,xy} - 3B_{16}\delta w_{,xxy} - B_{26}\delta w_{,yyy} = 0 \quad (3.345)$$

$$(A_{12} + A_{66})\delta u_{,xy} + A_{66}\delta v_{,xx} + A_{22}\delta v_{,yy} - B_{16}\delta w_{,xxx} - 3B_{26}\delta w_{,xyy} = 0 \quad (3.346)$$

$$D_{11}w_{,xxxx} + 2(D_{12} + 2D_{66})\delta w_{,xxyy} + D_{22}\delta w_{,yyyy} - B_{16}(3\delta u_{,xxy} + \delta v_{,xxx}) - B_{26}(\delta u_{,yyy} + 3\delta v_{,xyy}) + \bar{N}_x\delta w_{,xx} = 0 \quad (3.347)$$

Whitney solved this problem for the simply supported edge boundary condition S3 [3-44 and 3-45] (note that this boundary condition differs significantly from the S2 condition used for buckling of antisymmetric cross-ply laminated plates in Section 3.6.3.3)):

$$x = 0, a: \quad \delta w = 0 \quad \delta M_x = B_{16}(\delta v_{,x} + \delta u_{,y}) - D_{11}\delta w_{,xx} - D_{12}\delta w_{,yy} = 0 \quad (3.348)$$

$$\delta u = 0 \quad \delta N_{xy} = A_{66}(\delta v_{,x} + \delta u_{,y}) - B_{16}\delta w_{,xx} - B_{26}\delta w_{,yy} = 0 \quad (3.349)$$

$$y = 0, b: \quad \delta w = 0 \quad \delta M_y = B_{26}(\delta v_{,x} + \delta u_{,y}) - D_{12}\delta w_{,xx} - D_{22}\delta w_{,yy} = 0 \quad (3.350)$$

$$\delta v = 0 \quad \delta N_{xy} = A_{66}(\delta v_{,x} + \delta u_{,y}) - B_{16}\delta w_{,xx} - B_{26}\delta w_{,yy} = 0 \quad (3.351)$$

He observed that the variations in displacements (with indeterminate amplitudes $\tilde{u}$, $\tilde{v}$, and $\tilde{w}$)

$$\begin{aligned} \delta u &= \tilde{u} \sin\frac{m\pi x}{a}\cos\frac{n\pi y}{b} \\ \delta v &= \tilde{v} \cos\frac{m\pi x}{a}\sin\frac{n\pi y}{b} \\ \delta w &= \tilde{w} \sin\frac{m\pi x}{a}\sin\frac{n\pi y}{b} \end{aligned} \quad (3.352)$$

satisfy the boundary conditions and also satisfy the differential equations exactly if the buckling load is

$$\bar{N}_x = \left[\frac{a}{m\pi}\right]^2 \left[T_{33} + \frac{2T_{12}T_{23}T_{13} - T_{22}T_{13}^2 - T_{11}T_{23}^2}{T_{11}T_{22} - T_{12}^2}\right] \quad (3.353)$$

in which

$$\begin{aligned} T_{11} &= A_{11}\left[\frac{m\pi}{a}\right]^2 + A_{66}\left[\frac{n\pi}{b}\right]^2 \\ T_{12} &= (A_{12} + A_{66})\left[\frac{m\pi}{a}\right]\left[\frac{n\pi}{b}\right] \\ T_{13} &= -\left[3B_{16}\left[\frac{m\pi}{a}\right]^2 + B_{26}\left[\frac{n\pi}{b}\right]^2\right]\left[\frac{n\pi}{b}\right] \\ T_{22} &= A_{22}\left[\frac{n\pi}{b}\right]^2 + A_{66}\left[\frac{m\pi}{a}\right]^2 \end{aligned} \quad (3.354, \text{continued})$$

Éléments sous droits d'auteur

$$T_{23} = -\left[B_{16}\left[\frac{m\pi}{a}\right]^2 + 3B_{26}\left[\frac{n\pi}{b}\right]^2\right]\left[\frac{m\pi}{a}\right] \qquad \text{(3.354, concluded)}$$

$$T_{33} = D_{11}\left[\frac{m\pi}{a}\right]^4 + 2(D_{12} + 2D_{66})\left[\frac{m\pi}{a}\right]^2\left[\frac{n\pi}{b}\right]^2 + D_{22}\left[\frac{n\pi}{b}\right]^4$$

When B_{16} and B_{26} are zero, then T_{13} and T_{23} are also zero, so Equation (3.353) reduces to the specially orthotropic plate solution, Equation (3.326). The character of Equation (3.353) is the same as that of Equation (3.342) for antisymmetric cross-ply laminated plates, so the remarks on finding the buckling load in Section 3.6.3.3 are equally applicable here.

To study the effect of number of layers on laminate performance, we construct a sequence of equal-weight (constant thickness) angle-ply laminates with an increasing number of layers as in Figure 3-68. That is, the effect of the number of layers on the buckling load is found by dividing a constant-thickness, equal-weight angle-ply laminate into more and more (thinner) alternating $+\theta$ and $-\theta$ laminae as in Figure 3-68 (where the fiber cross sections are elliptical because they are cut at an angle to the fiber axis). Numerical results for graphite-epoxy composite material with $E_1/E_2 = 40$, $G_{12}/E_2 = .5$, and $\nu_{12} = .25$ in square plates are shown as a function of lamination angle in Figure 3-69. The influence of bending-extension coupling is to reduce the buckling load for two-layered plates from the many layered result (which is the specially orthotropic plate solution of Section 3.6.3.1). At $\theta = 45°$, the reduction is by about a factor of 2/3; perhaps more significant is the fact that use of the specially orthotropic approximation leads to a predicted buckling load that is three times the actual buckling load! The specially orthotropic approximation is obviously very unconservative for antisymmetric angle-ply laminates with less than six layers. For six layers, the error in the buckling load is about 7%. Thus, the bending-extension coupling effect dies out very rapidly as the number of layers increases. Alternatively, the fewer the number of layers, the higher the actual buckling curve and the bigger the change in buckling load from the specially orthotropic solution. Both conclusions are valid for other materials as represented in Figure 3-70 in the manner of Section 3.6.3.3.

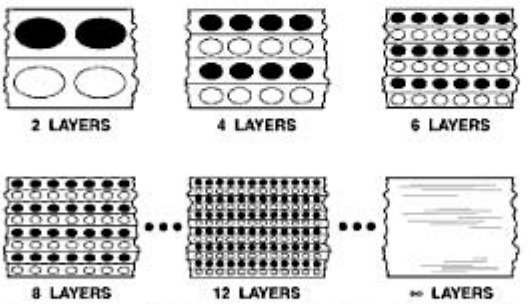


Figure 3-68 Antisymmetric Angle-Ply Laminate Example

Éléments sous droits d'auteur

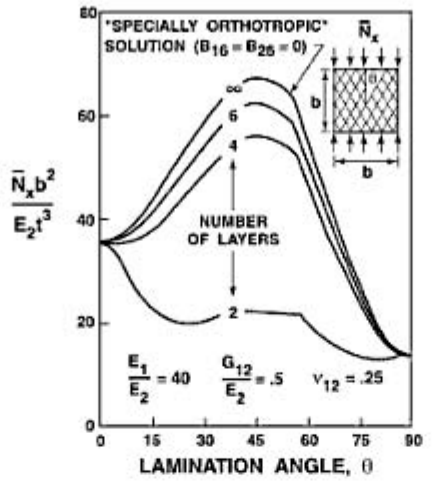


Figure 3-69 Buckling of Square Antisymmetric Angle-Ply Laminated Plates under Uniform Uniaxial Compression, $\bar{N}_x$
(After Jones, Morgan, and Whitney [3-46])

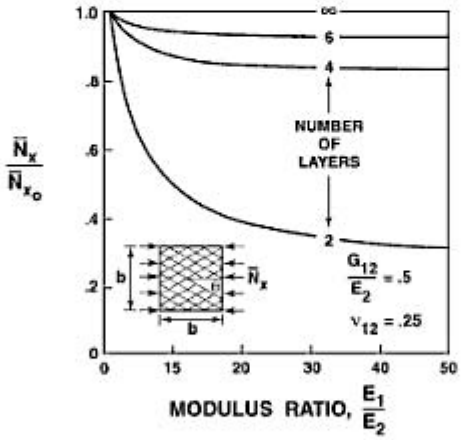


Figure 3-70 Relative Uniaxial Buckling Loads of Square Antisymmetric Angle-Ply Laminated Plates
(After Jones [3-27])

Éléments sous droits d'auteur

3.6.4 General Remarks on Effects of Stiffnesses

The presence of bending-extension coupling in a laminated plate generally increases deflections. Hence, coupling decreases the effective bending stiffnesses of a laminate. At the same time, this coupling reduces buckling loads and vibration frequencies significantly as would be expected for plates with effectively lower bending stiffnesses.

Similarly, for laminated plates with bend-twist coupling, the deflections are increased, the buckling loads decreased, and the vibration frequencies decreased. In both cases of bending-extension coupling and bend-twist coupling, the effect on deflections, buckling loads, and vibration frequencies for a fixed-thickness antisymmetric or symmetric laminate, respectively, dies out rapidly as the number of layers increases. For more general laminates, specific investigation is required. That is, *there is simply no guarantee or even any reason to expect that conclusions reached for many layered antisymmetric laminated plates have any validity whatsoever for more general unsymmetrically laminated plates.*

A somewhat more general class of laminates, unsymmetric cross-ply laminates, was discussed by Jones [3-42] as well as Jones and Morgan [3-47]. All geometric and material property symmetry requirements of the preceding sections are relaxed. Still, the restriction to cross-ply laminates (of arbitrary layer thickness and 0° and 90° stacking sequence) enables a simple exact solution to be obtained. However, because of the infinite complexity of this class of laminates, general results are impossible. Instead, consider the cross sections of the contrived, but representative unsymmetric laminate example in Figure 3-71. There, the fibers in the second layer from the bottom are always oriented at 90°, and the fibers in all other layers are oriented at 0° to the plate x-axis. Thus, for a constant-thickness laminate, the 90° layer gets thinner and moves toward the bottom of the laminate as the number of layers increases. This example is probably never encountered in engineering practice, but it is a simple, straightforward example of unsymmetric laminates that is amenable to comprehensive parametric study. The results obtained serve as a very simple proof by contradiction that the structural effects of bending-extension coupling do not necessarily die out rapidly as the number of layers increases (contrary to the results for antisym-

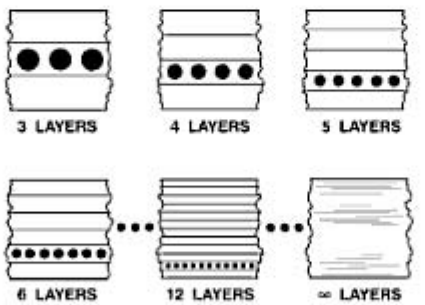


Figure 3-71 Unsymmetric Cross-Ply Laminate Example *(After Jones [3-42])*

Éléments sous droits d'auteur

metric cross-ply and angle-ply laminated plates). The applicable theory is already available in Section 3.6.3.

Normalized buckling loads for graphite-epoxy unsymmetric cross-ply laminated rectangular plates are shown in Figure 3-72. The plate aspect ratio is 2, a value for which the results are the most strikingly different from baseline results. One of the baseline comparison values is the buckling load for a laminate with all 0° layers. The other comparison case is an unsymmetric laminate for which bending-extension coupling is ignored ($B_{ij} = 0$). Results for the actual unsymmetric laminate, for which coupling is considered, are labeled exact solution. The actual laminate has, not surprisingly, less buckling resistance than a laminate with $B_{ij} = 0$. On the other hand, the actual laminate has more buckling resistance than a laminate with all 0° layers. This curious result is a consequence of the relative values of the bending stiffnesses in the x- and y-directions as well as the plate aspect ratio. As will be seen subsequently, D_{11} is decreased somewhat by the presence of a 90° layer, but simultaneously D_{22} is increased by factors of up to an order of magnitude. The influence of D_{22} is most easily examined for a three-layered plate that is, of course, symmetric. Thus, the exact solution corresponds to the specially orthotropic plate solution ($B_{ij} = 0$); for example, see the horizontal tick mark at three layers in Figure 3-72 where the two curves coincide. At that point, the specially orthotropic solution for a plate with an aspect ratio of 2 which buckles into the m = 1, n = 1 mode is

$$\bar{N}_x L^2 = \pi^2 \left[\frac{D_{11}}{4} + 2(D_{12} + 2D_{66}) + 4D_{22} \right] \tag{3.355}$$

which is readily obtained from Equation (3.344). The term in Equation (3.355) involving D_{11} decreases by less than 4% when the actual lami-

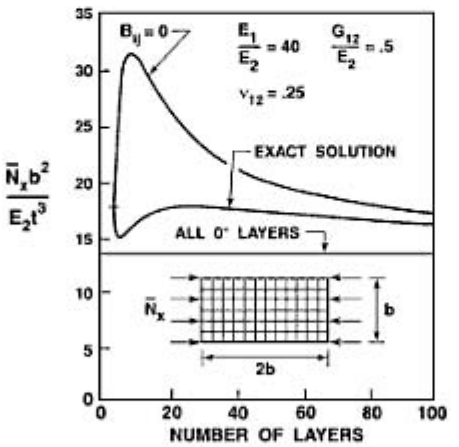


Figure 3-72 Uniaxial Buckling Loads of Graphite-Epoxy Unsymmetric Cross-Ply Laminated Rectangular Plates *(After Jones [3-42])*

Éléments sous droits d'auteur

nate is considered as opposed to the all-0°-layer laminate. The net result is a normalized buckling load that is 33% bigger for the actual laminate than for the all-0°-layer laminate.

The differences between the exact, specially orthotropic, and all-0°-layer predictions in Figure 3-72 range from 48% less than the specially orthotropic solution at 6 layers to 18% less at 40 layers to 6% less at 100 layers. In addition, the exact results range from about 30% more than the all-0°-layer laminate results at 30 layers to about 18% more at 100 layers. Again, such differences are well within the consideration of usual engineering design practice.

We will see that the unsymmetric laminate has far more bending stiffness in the y-direction than the all-0°-layer laminate and almost as much bending stiffness in the x-direction. Thus, the center deflection of the unsymmetrically laminated plate *should* exceed that of the all-0°-layer laminated plate. However, we are already aware that bending-extension coupling increases deflections, so the center deflection of the unsymmetric laminate *should* exceed that of the orthotropic laminated plate.

The real point of this example is that the deflection effects just discussed are very significant for numbers of layers that, in our studies of antisymmetric laminates earlier in this chapter, we concluded that bending-extension coupling had disappeared! Here, the exact solution exceeds the orthotropic solution by 165% at 6 layers, 165% at 10 layers, 90% at 20 layers, and 30% at 50 layers. Even at 100 layers, the discrepancy is still 11%. These differences are well within the consideration of usual engineering design practice. These discrepancies exist for many more layers than bending-extension coupling was believed to be important. That belief (by some, not all) was established on the basis of extrapolating antisymmetric cross-ply and antisymmetric angle-ply results like those in Sections 3.6.3.3 and 3.6.3.4. Obviously, such extrapolation is invalid. However, truly no one had any better basis except to remain skeptical and try to find out what actually happens for unsymmetric laminates.

As an aid to understanding the buckling behavior in Figure 3-72, the normalized extensional, bending-extension coupling, and bending stiffnesses are plotted versus the number of layers in Figure 3-73. The stiffnesses in the x-direction (with which most fibers are aligned), A_{11} and D_{11}, are nearly independent of the number of layers. However, the 90° layer causes the stiffnesses in the y-direction, A_{22} and D_{22}, to deviate by up to an order of magnitude from the values for the all-0°-layer laminate (which are the same as for an infinite number of layers). These discrepancies die out very, very slowly as the number of layers increases. Moreover, the normalized stiffness for bending-extension coupling, which can be shown to be

$$\frac{B_{11}}{Q_{11}t^2} = \frac{1}{2N^2}\left[1 - \frac{E_2}{E_1}\right](N-3) \tag{3.356}$$

(where N is the number of layers) and which appears in Equation (3.342) and thereby enables stiffnesses A_{22} and D_{22} to influence the buckling

Éléments sous droits d'auteur

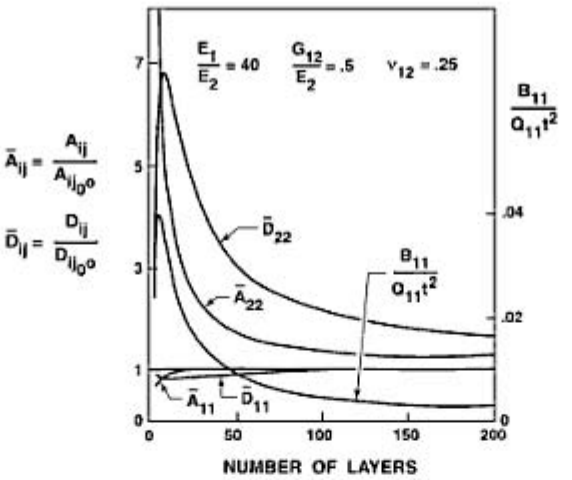


Figure 3-73 Normalized Stiffnesses of Example Unsymmetric Cross-Ply Graphite-Epoxy Laminate *(After Jones [3-42])*

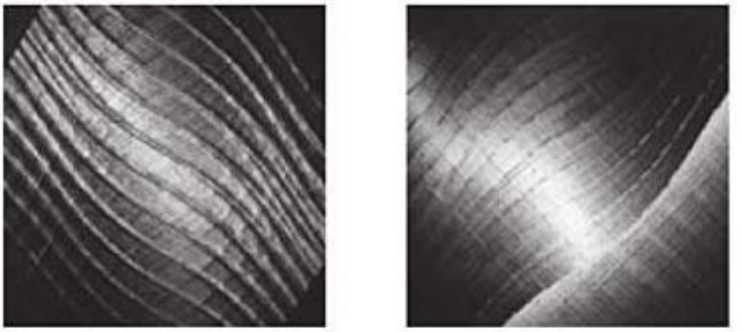
load, also dies out very slowly. The maximum bending-extension coupling occurs for this unsymmetric laminate at N = 6. Do not attempt to compare the magnitudes of, for example, the terms D_{22} and $B_{11}/(Q_{11}t^2)$ quantitatively. They do not have the same base for normalization (B_{11} cannot be normalized relative to its value for an all-0°-layer laminate because in that case its value is zero). Thus, the effect of a single unsymmetrically placed 90° layer on the deflection dies out very slowly as the number of layers increases.

3.6.5 Tow-Placed, Variable-Stiffness Plates

A recent innovation in fiber-reinforced composite structures is the use of multiple-degree-of-freedom, computer-driven, tow-placement machines to create plates with stiffnesses that vary over the plane of the plate as the tows change direction in parallel or non-parallel curvilinear paths. A tow is a flat bundle of thousands of parallel fibers that are impregnated with matrix material. Bands of multiple (12–24 or more) tows are dispensed by the tow-placement machines which evolved from the filament-winding machine and the tape-laying machine.

Consider a simply supported square plate with parallel tows oriented at ± 30° to the vertical axis near the left and right edges of the plate in Figure 3-74a. The ± 30° tow paths at the edges are morphed to ± 60° paths in the middle of the plate. The plate has the highest axial stiffness at the left and right edges that are supported against buckling and the lowest axial stiffness in the unsupported middle distant from the edges.

Éléments sous droits d'auteur



a Variable Thickness b Constant Thickness

Figure 3-74 Vertically Loaded, Tow-Placed, Variable-Stiffness Square Plates

Thus, under constant-displacement loading, vertical load is borne mainly near the plate edges, but very little is borne in the plate middle which is naturally susceptible to buckling. Gürdal and Olmedo predicted that such plates carry 80% more buckling load than a baseline plate with the optimum straight-fiber laminae orientation of $\pm 45°$ over the whole plate [3-48]! If each band has the same number of parallel tows over its entire length, then the band edges must periodically overlap and create the bumpy surface in Figure 3-74a. Such plates have a 10% weight penalty over the baseline [$\pm 45°$] plate, but actually carry three times the buckling load as shown by Wu, Gürdal, and Starnes [3-49]. If some of the parallel fiber tows are periodically cut and dropped from each band to decrease the band width, then no overlap occurs and a smooth, flat plate results, as in Figure 3-74b, with no weight penalty and a buckling load twice that of the baseline plate [3-49]. Part of a layer is missing from the lower right-hand corner of Figure 3-74b (taken during manufacturing), and gaps between two band edges appear as barely visible white dashed lines.

3.6.6 Summary

A theory for buckling of laminated fiber-reinforced plates was developed to address contemporary needs for using composite materials and applied to several classes of laminates as learning exercises. None of the laminate classes is applicable in many practical applications, but all help us understand the response of various laminates. The symmetric cross-ply laminate is an introduction to orthotropy whereas the symmetric angle-ply is an introduction to bend-twist coupling. The antisymmetric cross-ply laminate and the antisymmetric angle-ply laminates are an introduction to bending-extension coupling. The unsymmetric cross-ply laminate is an introduction to bending-extension coupling in a more general sense. Of course, there are many very practical reasons for not using laminates that exhibit either bend-twist coupling or bending-extension coupling, namely that their mechanical response to loading might be quite undesirable.

Éléments sous droits d'auteur

Some coupling effects seem to die out as the number of layers increases under very special circumstances (e.g., laminate antisymmetry, a usually impractical laminate), yet do *not* have this special behavior in general for practical laminates (e.g., unsymmetric laminates). However, in some applications, the unusual characteristic of bend-twist coupling can be quite advantageous, such as preventing divergence of aircraft forward-swept wings. Also, the basic principle by which the ordinary household thermostat works is bending-extension coupling!

Plates can have stiffeners attached on their surfaces to increase the bending stiffness and hence the deflection resistance, buckling load, and vibration frequencies. The influence of such stiffeners on buckling of circular cylindrical shells is studied in Section 4.7. The differences seen there between having stiffeners on the inside versus the outside of the shell are not applicable to plates because plates do not have the same prejudicial inside versus outside that a shell does (plates have a top and a bottom surface, but the effect of putting the stiffeners on the top is identical to putting them on the bottom).

Many other plate buckling topics are of interest. For the 1970–1995 time period, Turvey and Marshall [3-50] edited a summary of research on laminated plates that are made of long-fiber reinforced plastics such as carbon or glass fibers in an epoxy matrix. Many topics beyond what is covered here are addressed in that reference. Also, see the Chapter Summary, Section 3.10, for a description of a combination of this section's study of laminated plates with that of Section 3.8 on plastic buckling of plates. Moreover, Whitney and Ashton addressed the effect of temperature change and moisture change on the buckling of laminated composite plates [3-51]. They found that both increases in temperature and increases in moisture caused expansional strains that can lead to buckling at lower loads than if the heating and moisture were not present. The plate thermal buckling problem is treated in the next section. Leissa surveyed the laminated composite plate and shell panel research literature as of 1985 [3-52]. Also consult the extensive compendium of composite materials and structures books, review papers, conference proceedings, ASTM STPs (Special Technical Publications), and journals by Bogdanovich and Sierakowski [3-53].

Problem Set 3.6

3.6.1 Derive the analogy of Equations (3.307)–(3.309) for the buckling differential equations, Equations (3.314)–(3.316).

3.6.2 Derive Equation (3.326).

3.6.3 Consider a symmetric cross-ply laminated plate and a unidirectionally reinforced plate as in Figure 3-59. Both plates have three graphite-epoxy layers each of thickness t, simple supports on all four edges, and N_x applied. Demonstrate that the bending stiffnesses have the inequalities: $D_{11UD} > D_{22UD}$ (UD = unidirectional), $D_{11UD} > D_{11CP}$ (CP = cross-ply), and $D_{22CP} > D_{22UD}$. Express all laminate bending stiffnesses in terms of that of a single 0° layer, i.e., $E_1t^3/12(1 - \nu_{12}\nu_{21})$. Use these stiffness results to calculate the buckling load in Equation (3.327) to explore the importance of D_{22} (as well as D_{12} and D_{66}) in the calculation for a/b = 2 and m = 1. Describe the importance of the second two terms in Equation (3.327) as (1) a/b increases and (2) m increases. What happens to m as a/b increases?

3.6.4 Derive Equation (3.342). Hint: for a set of homogeneous equations to have a nontrivial solution, the determinant of the coefficients must be zero.

3.6.5 Derive Equation (3.353). See hint in Problem 3.6.4.

Éléments sous droits d'auteur

3.7 EFFECT OF RESTRAINED THERMAL EXPANSION

3.7.1 Introduction

We wish to determine the influence that thermal expansion caused by spatially uniform temperature change has on the stress state of a plate which has suitable restraint against thermal expansion and, further, what effect that restrained thermal expansion has on plate buckling. The plate thermal buckling problem is much more general than that restricted problem, and we will allude to some features of the more general problem. This section should not be studied without first fully understanding Section 2.9 on bar buckling caused by restrained thermal expansion.

Recall some of the fundamental origins of thermal stresses and thermal strains that are discussed in Section 2.9.2 as a preliminary to treating thermal buckling of bars. The stresses that we call thermal stresses are actually *thermally induced stresses* because a stress is just a stress irrespective of its origin (and all stresses are a figment of our imagination as well!). However, for the sake of convenience in this book, we will refer to thermally induced stresses as simply thermal stresses. Recall that one-dimensional bars must have some form of axial restraint in order to develop thermal stresses under uniform through-the-thickness thermal loading. Two-dimensional plates do develop thermal stresses if restrained in their plane, e.g., between two opposite boundaries of a rectangular plate. However, two-dimensional plates do *not* require external or boundary restraint to develop thermal stresses.

Plates can, under certain special circumstances, *self-impose* thermal stresses by means of inherent internal elastic restraints. For example, if a locally concentrated temperature increase (a hot spot) is imposed on a plate, then the surrounding colder regions of the plate provide elastic restraint against expansion of the hotter region (just as the bar with a nonlinear temperature gradient in Section 2.9.2 develops thermal stresses and thermal strains). Note that the thermal stresses must be self-equilibrating if no external restraint is provided. The compressive thermal stresses in the hot region could get high enough to cause thermal buckling. The tensile thermal stresses in the cold region do not suppress buckling, but, in fact, drive buckling by inducing compressive thermal stresses when the cold region 'declines' to expand as much as the hot region 'wants' it to. Such problems are not simple because the prebuckling equilibrium stress state is highly nonuniform (a significant thermoelasticity problem by itself), and the buckling differential equation therefore has nonconstant coefficients, so it is not easy to solve. We will address only the simpler boundary restraints that cause thermal buckling under uniform heating and leave the internal restraints and self-equilibrating stress fields to further study.

Just as axial restraint was the key factor in determining the prebuckling load for bars, in-plane boundary restraints are the key factor for determining the prebuckling load for plates that are uniformly heated. For both bars and plates, rotational restraints at the ends do not affect the prebuckling forces, but do strongly influence the bar or plate buckling loads. The most important characteristic to identify in plate thermal buck-

Éléments sous droits d'auteur

ling problems with uniform spatial temperature change is the specific nature of the prebuckling in-plane restraint to free thermal expansion. If there is no restraint, then a spatially uniform increase in temperature merely leads to free thermal expansion with no accompanying stresses in an isotropic plate, and no thermal buckling can occur. However, with restraint, thermal forces that can cause buckling do develop. We must be especially careful to determine the nature of the restraint to define what thermal loads exist to cause thermal plate buckling. For plates, such restraint must occur in the plane of the plate. Thus, we can have a simply supported plate almost in the 'usual' sense except for the nature of the in-plane restraint. We can also have a clamped-edge plate that restrains edge rotation, but with a variety of in-plane restraint conditions. Even with the same in-plane restraint, the clamped-edge plate has a higher thermal buckling load than a simply supported plate because of higher resistance to out-of-plane deformation of the clamped-edge plate.

Plates are two-dimensional in character (we effectively eliminate the dimension perpendicular to the plate surface by using the Kirchhoff hypothesis [3-4]), so the *possibility* of combined thermal and mechanical loading exists. Therefore, both thermal buckling and buckling due to mechanical loads can occur under certain circumstances, but not in others. For example, if all four edges of a rectangular plate are simply supported but are fixed against movement in the plane of the plate as in Figure 3-75a (in which *the terms "fixed" and "free" are descriptive of only the in-plane displacement characteristics* of the plate, *not including the edge rotation characteristics*), then only thermal buckling can occur under uniform heating because mechanical loading cannot be accepted by the plate (unless screw-type loading is applied). Or, if two adjacent edges can move in-plane and two other adjacent edges cannot move in-plane (and therefore accept mechanical loads) as in Figure 3-75b, then only mechanical buckling can occur because thermal expansion is not restrained. However, if three edges are immovable, but the fourth is free to move in-plane and therefore accept mechanical loads as in Figure 3-75c, then the plate can buckle under a combination of thermal and mechanical loads! Note that the thermal and mechanical forces are perpendicular to each other, i.e., not in the same direction (unless screw-type loading is applied). We study the plate in-plane boundary conditions and how loads are applied in more detail in Section 3.7.3.

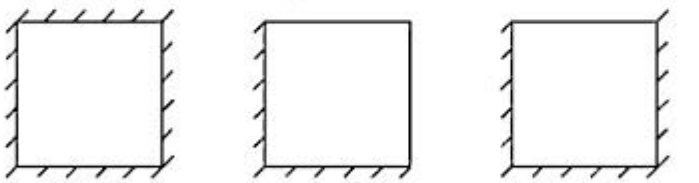


Figure 3-75 Some In-Plane Boundary Conditions for Rectangular Plates (Fixed means fixed against in-plane movement only)

Éléments sous droits d'auteur

Recall from Section 2.9 that for a bar, the axial restraint at the bar ends determines whether thermal load can be developed (and without axial restraint, there is no thermal load), but the rotational restraint (or lack thereof) at the bar end determines how high the thermal load can get until buckling occurs. For example, the thermal load is $E\alpha\Delta TA$ for both pinned-pinned bars and fixed-fixed bars that have both ends perfectly restrained against axial movement. However, that thermal load grows only to the value π^2EI/L^2 for pinned-pinned bars before buckling whereas the thermal load can grow to $4\pi^2EI/L^2$ for fixed-fixed bars with a ΔT four times higher than that for pinned-pinned bars.

For a plate, the in-plane restraint at the plate edges determines whether the uniform thermal load can be developed in the direction perpendicular to the in-plane restraint (and without that restraint there is no thermal load), but the rotational restraint (or lack thereof) at each plate edge determines how high the thermal load can get until buckling occurs. The plate problem is more complicated than the bar problem because of the two-dimensional nature of a plate. For example, a plate could have in-plane restraint in one or both perpendicular directions relative to the (rectangular) plate edges. In addition, the Poisson effect complicates the calculations. You are advised to review the discussion of plates with biaxial mechanical loads in Section 3.3.3 before proceeding to address problems of plates with combined mechanical and thermal load.

In this section, we will first develop the fundamental plate thermoelastic relations including the buckling differential equations and their associated boundary conditions in Section 3.7.2. Next, we will describe and discuss possible plate boundary conditions extensively in Section 3.7.3 because the specific nature of the boundary conditions determines the nature of the thermal forces that cause buckling under uniform heating. Then in Section 3.7.4, we will address an equivalent mechanical loading concept to treat some thermal loading problems, although the approach is limited to simple problems. Next, in Sections 3.7.5 through 3.7.7 we will solve several plate thermal buckling problems. We do not address the possibility of temperature changes through the thickness as is addressed for bars in Section 2.9.6. Then, the present plate thermal buckling solutions are summarized in Section 3.7.8. Finally, other plate thermal buckling topics are discussed in Section 3.7.9. Those other topics involve effects or material characteristics beyond what we are able to treat simply. Included are nonuniformities in spatial temperature distribution, variation of pertinent material properties with temperature and with stress, and other boundary support conditions than the simply supported edges we treat.

The reader can delve into plate thermal buckling to various levels of detail. For example, if you are interested only in thermal buckling results for simply supported plates under uniform temperature change, you could proceed directly to Sections 3.7.5 to 3.7.7. Or, if you want more description of the bases for those solutions, you could study Sections 3.7.2 to 3.7.4. For problems beyond thermal buckling of simply supported plates under uniform temperature change, go to Section 3.7.9 for an introductory glimpse at the nature of some other important problems.

Éléments sous droits d'auteur

3.7.2 Fundamental Thermoelastic Relations

For an isotropic elastic plate subjected to a biaxial state of (plane) stress and some form of temperature-change distribution over the plate volume, the two-dimensional thermoelastic strain-stress relations at a point are

$$\begin{aligned} \varepsilon_x &= \frac{\sigma_x}{E} - \frac{\nu}{E}\sigma_y + \alpha\Delta T \\ \varepsilon_y &= -\frac{\nu}{E}\sigma_x + \frac{\sigma_y}{E} + \alpha\Delta T \\ \gamma_{xy} &= \frac{\tau_{xy}}{G} \end{aligned} \tag{3.357}$$

in which (1) ε_x, ε_y, and γ_{xy} are the total strains, (2) σ_x/E, σ_y/E, and τ_{xy}/G are mechanical strains and (3) $\alpha\Delta T$ is the free thermal strain resulting from the temperature change at any point in the plate volume as a function of time, namely $\Delta T = T(x,y,z,t) - T_{ref}$, where T_{ref} is the arbitrary and convenient reference temperature at which no strain is observed in a baseline configuration of 'zero strain' or zero thermal stress. We will not address the time dependence of the temperature change in this section except in Section 3.7.9. Note that an isotropic body only expands (contracts) upon heating (cooling) and does not exhibit any shearing deformation caused solely by thermal loading.

The corresponding two-dimensional thermoelastic stress-strain relations are, by inversion of Equation (3.357),

$$\begin{aligned} \sigma_x &= \frac{E}{1-\nu^2}(\varepsilon_x - \alpha\Delta T) + \frac{\nu E}{1-\nu^2}(\varepsilon_y - \alpha\Delta T) \\ \sigma_y &= \frac{\nu E}{1-\nu^2}(\varepsilon_x - \alpha\Delta T) + \frac{E}{1-\nu^2}(\varepsilon_y - \alpha\Delta T) \\ \tau_{xy} &= G\gamma_{xy} \end{aligned} \tag{3.358}$$

in which ε_x, ε_y, and γ_{xy} are the total strains, $\alpha\Delta T$ is the free thermal strain, and $\varepsilon_x - \alpha\Delta T$ and $\varepsilon_y - \alpha\Delta T$ are apparently the mechanical strains.

In a typical structural mechanics problem, we impose conditions (1) on the total strain (such as, e.g., $\varepsilon_x = 0$ on a heated bar between two immovable walls as in Figure 3-76a) which can be regarded as a displacement-type boundary condition, e.g., $u = 0$ at the ends of the bar or (2) on the stress (such as, e.g., $\sigma_x = 0$ on the free end of a heated cantilever bar as in Figure 3-76b), i.e., a stress-type boundary condition. Plate support conditions will be addressed in more detail in Section 3.7.3 where we will see conditions analogous to those for bars in Figure 3-76.



a Bar between Walls b Cantilever Bar

Figure 3-76 Two Bar Support Conditions

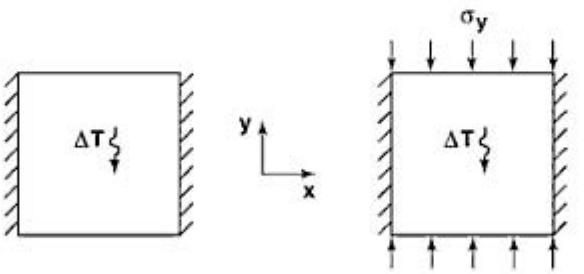
Éléments sous droits d'auteur

Consider the plate that is restrained from in-plane movement in the x-direction but not restrained in the y-direction in Figure 3-77. If only thermal loading is applied as in Figure 3-77a, then the total strains are $\varepsilon_x = 0$ and $\varepsilon_y \neq 0$ [see if you can prove that $\varepsilon_y = (1 - \nu)\alpha\Delta T$] whereas the stresses are $\sigma_x = -E\alpha\Delta T$ and $\sigma_y = 0$. Obviously, σ_x is a thermal stress (a stress of thermal origin) and there is no mechanical stress. If both thermal and mechanical loading are applied as in Figure 3-77b, then the total strains are $\varepsilon_x = 0$ because of the perfect restraint and $\varepsilon_y \neq 0$ because mechanical load σ_y is applied as well as ΔT. The resulting stresses are somewhat involved. First, σ_x has one component caused by restraint of thermal expansion and another component caused by restraint of the Poisson expansion. Thus, σ_x is both a thermal and a mechanical stress. Also, σ_y is a mechanical stress. However, both stresses have the same symbol, σ, i.e., are indistinguishable from each other in the stress-strain relations, Equation (3.358). Thus, unlike strains, *stresses cannot necessarily be simply labeled as mechanical or thermal stresses because their specific identity depends on the support and loading conditions.*

By the Kirchhoff plate deformation hypothesis [3-4], lines originally normal to the undeformed middle surface remain normal after deformation and do not change length as in Figure 3-7 on page 241, i.e.,

$$\gamma_{xz} = \gamma_{yz} = 0 \qquad \varepsilon_z = 0 \tag{3.359}$$

which is a state of plane strain. We have implied a state of plane stress and simultaneously a state of plane strain, an unacceptable fundamental contradiction of elasticity theory. However, ordinary plate theory is not elasticity theory but is a mechanics of materials approach in which vastly simplifying presumptions are made based on apparent physical reasons related to the nature of the behavior (e.g., we say plane sections remain plane for beams because we can see that lines drawn on the side of a beam before bending in Figure 2-44 on page 107 remain straight after deformation *to the resolution level of our 'naked' eyes!*) and are simply part of the necessarily approximate and imperfect problem-solving process. Of course, with heating or cooling, the plate thickness changes (hence, there actually is a transverse strain, ε_z), but we do not address that out-of-plane behavior in this book.



a Uniform Thermal Load b Uniform Thermal and Mechanical Load

Figure 3-77 Plate Restrained in the x-Direction

Éléments sous droits d'auteur

Consequently, the total strains are observed to vary in an approximately linear manner through the plate thickness:

$$\begin{aligned} \varepsilon_x &= \bar{\varepsilon}_x + z\,\kappa_x \\ \varepsilon_y &= \bar{\varepsilon}_y + z\,\kappa_y \\ \gamma_{xy} &= \bar{\gamma}_{xy} + z\,\kappa_{xy} \end{aligned} \tag{3.360}$$

in which the terms $\bar{\varepsilon}_x$, $\bar{\varepsilon}_y$, and $\bar{\gamma}_{xy}$ are nonlinear moderately large-deflection middle-surface strains in the manner of von Kármán [3-5].

$$\begin{aligned} \bar{\varepsilon}_x &= \frac{\partial u_o}{\partial x} + \frac{1}{2}\left[\frac{\partial w_o}{\partial x}\right]^2 \\ \bar{\varepsilon}_y &= \frac{\partial v_o}{\partial y} + \frac{1}{2}\left[\frac{\partial w_o}{\partial y}\right]^2 \\ \bar{\gamma}_{xy} &= \frac{\partial u_o}{\partial y} + \frac{\partial v_o}{\partial x} + \frac{\partial w_o}{\partial x}\frac{\partial w_o}{\partial y} \end{aligned} \tag{3.361}$$

in which u_o and v_o are in-plane displacements of the plate middle surface, w_o is the transverse deflection of the plate middle surface, z is the through-the-thickness coordinate from the middle surface, and κ_x, κ_y, and κ_{xy} are the middle-surface curvatures

$$\kappa_x = -\frac{\partial^2 w_o}{\partial x^2} \qquad \kappa_y = -\frac{\partial^2 w_o}{\partial y^2} \qquad \kappa_{xy} = -2\frac{\partial^2 w_o}{\partial x \partial y} \tag{3.362}$$

However, we presume $\varepsilon_z = 0$, so w_o cannot be distinguished from w at any point through the thickness, and the curvatures can be written as

$$\kappa_x = -\frac{\partial^2 w}{\partial x^2} \qquad \kappa_y = -\frac{\partial^2 w}{\partial y^2} \qquad \kappa_{xy} = -2\frac{\partial^2 w}{\partial x \partial y} \tag{3.363}$$

so we will use w in the following derivations instead of w_o as well as simply u and v, and for all such symbols we mean middle-surface values.

The Kirchhoff hypothesis is applicable only to strains that result from pure bending, i.e., the only loading is moments M_x and M_y as in Figure 3-3 on page 228. To account for the free thermal expansion of a plate, we merely add the free thermal expansion to the mechanical strains to get the total strains and invert the result to get the stress-strain relations

$$\begin{aligned} \sigma_x &= \frac{E}{1-\nu^2}(\bar{\varepsilon}_x - z\,w_{xx} - \alpha\Delta T) + \frac{\nu E}{1-\nu^2}(\bar{\varepsilon}_y - z\,w_{yy} - \alpha\Delta T) \\ &= \frac{E}{1-\nu^2}\left[(\bar{\varepsilon}_x - \nu\bar{\varepsilon}_y) - z(w_{xx} + \nu w_{yy}) - (1+\nu)\alpha\Delta T\right] \\ \sigma_y &= \frac{\nu E}{1-\nu^2}(\bar{\varepsilon}_x - z\,w_{xx} - \alpha\Delta T) + \frac{E}{1-\nu^2}(\bar{\varepsilon}_y - z\,w_{yy} - \alpha\Delta T) \\ &= \frac{E}{1-\nu^2}\left[(\bar{\varepsilon}_y - \nu\bar{\varepsilon}_x) - z(w_{yy} + \nu w_{xx}) - (1+\nu)\alpha\Delta T\right] \\ \tau_{xy} &= G\bar{\gamma}_{xy} \end{aligned} \tag{3.364}$$

Éléments sous droits d'auteur

in which $\bar{\varepsilon}_x$, $\bar{\varepsilon}_y$, and $\bar{\gamma}_{xy}$ contain in Equation (3.361) nonlinear terms that are essential for buckling analysis, but we will keep those nonlinear terms within the middle-surface strains, $\bar{\varepsilon}_x$, $\bar{\varepsilon}_y$, and $\bar{\gamma}_{xy}$, for the present.

The in-plane forces (per unit width by convention used throughout this book) on a unit width of a plate are

$$N_x = \int \sigma_x \, dz = \frac{E}{1-\nu^2} \int (\bar{\varepsilon}_x + \nu \bar{\varepsilon}_y) \, dz - \frac{E(1+\nu)}{1-\nu^2} \int \alpha \, \Delta T \, dz$$

$$= \frac{E}{1-\nu^2} \int (\bar{\varepsilon}_x + \nu \bar{\varepsilon}_y) \, dz - \frac{E}{1-\nu^2} \int (w_{xx} + \nu w_{yy}) \, z \, dz - \frac{E}{1-\nu} \int \alpha \, \Delta T \, dz$$

$$= \frac{E}{1-\nu^2} (\bar{\varepsilon}_x + \nu \bar{\varepsilon}_y) \int dz - \frac{E}{1-\nu^2} (w_{xx} + \nu w_{yy}) \int z \, dz - \frac{E}{1-\nu} \int \alpha \, \Delta T \, dz$$

$$= \frac{E\,t}{1-\nu^2} (\bar{\varepsilon}_x + \nu \bar{\varepsilon}_y) - \frac{E}{1-\nu} \int \alpha \, \Delta T \, dz = A(\bar{\varepsilon}_x + \nu \bar{\varepsilon}_y) - N^T$$

$$N_y = \frac{E\,t}{1-\nu^2} (\bar{\varepsilon}_y + \nu \bar{\varepsilon}_x) - \frac{E}{1-\nu} \int \alpha \, \Delta T \, dz = A(\bar{\varepsilon}_y + \nu \bar{\varepsilon}_x) - N^T$$

$$N_{xy} = G\,t\,\bar{\gamma}_{xy} = \frac{1-\nu}{2} A \bar{\gamma}_{xy} \tag{3.365}$$

in which the extensional stiffness is $A = Et/(1-\nu^2)$ as defined on page 242 and we define the thermal force (per unit width) as

$$N^T = \frac{E}{1-\nu} \int \alpha \, \Delta T \, dz \tag{3.366}$$

which depends on how the temperature change and α vary through the plate thickness.

The moments (per unit width) are

$$M_x = \int \sigma_x \, z \, dz = \frac{E}{1-\nu^2} \int (\bar{\varepsilon}_x + \nu \bar{\varepsilon}_y) \, z \, dz - \frac{E(1+\nu)}{1-\nu^2} \int \alpha \, \Delta T \, z \, dz$$

$$= \frac{E}{1-\nu^2} \left[\int (\bar{\varepsilon}_x + \nu \bar{\varepsilon}_y) \, z \, dz - \int (w_{xx} + \nu w_{yy}) \, z^2 \, dz \right] - \frac{E}{1-\nu} \int \alpha \, \Delta T \, z \, dz$$

$$= \frac{E}{1-\nu^2} \left[(\bar{\varepsilon}_x + \nu \bar{\varepsilon}_y) \int z \, dz - (w_{xx} + \nu w_{yy}) \int z^2 \, dz \right] - \frac{E}{1-\nu} \int \alpha \, \Delta T \, z \, dz$$

$$= -\frac{E\,t^3}{12(1-\nu^2)} (w_{xx} + \nu w_{yy}) - \frac{E}{1-\nu} \int \alpha \, \Delta T \, z \, dz = -D(w_{xx} + \nu w_{yy}) - M^T$$

$$M_y = -\frac{E\,t^3}{12(1-\nu^2)} (w_{yy} + \nu w_{xx}) - \frac{E}{1-\nu} \int \alpha \, \Delta T \, z \, dz = -D(w_{yy} + \nu w_{xx}) - M^T$$

$$M_{xy} = -G \frac{t^3}{6} w_{xy} = -\frac{E}{1+\nu} \frac{t^3}{12} w_{xy} = -(1-\nu) D w_{xy} \tag{3.367}$$

Éléments sous droits d'auteur

in which the bending stiffness is $D = Et^3/\left[12(1-\nu^2)\right]$ and we define the thermal moment (per unit width) as

$$M^T = \frac{E}{1-\nu}\int \alpha\,\Delta T\, z\, dz \tag{3.368}$$

which depends on how the moment of the temperature change and α vary through the plate thickness.

For a plate, the in-plane forces (per unit width) written with obvious nonlinear terms are

$$N_x = \frac{Et}{1-\nu^2}\left[\left[\frac{\partial u_o}{\partial x}+\frac{1}{2}\left[\frac{\partial w}{\partial x}\right]^2\right]+\nu\left[\frac{\partial v_o}{\partial y}+\frac{1}{2}\left[\frac{\partial w}{\partial y}\right]^2\right]\right]-N^T$$

$$N_y = \frac{Et}{1-\nu^2}\left[\left[\frac{\partial v_o}{\partial y}+\frac{1}{2}\left[\frac{\partial w}{\partial y}\right]^2\right]+\nu\left[\frac{\partial u_o}{\partial x}+\frac{1}{2}\left[\frac{\partial w}{\partial x}\right]^2\right]\right]-N^T$$

$$N_{xy} = \frac{Et}{1+\nu}\left[\frac{\partial u_o}{\partial y}+\frac{\partial v_o}{\partial x}+\frac{\partial w}{\partial x}\frac{\partial w}{\partial y}\right] \tag{3.369}$$

or in more compact notation realizing that all terms exist only on the middle surface

$$\begin{aligned} N_x &= A\left[(u_x+\frac{1}{2}w_x^2)+\nu(v_y+\frac{1}{2}w_y^2)\right]-N^T \\ N_y &= A\left[(v_y+\frac{1}{2}w_y^2)+\nu(u_x+\frac{1}{2}w_x^2)\right]-N^T \\ N_{xy} &= (1-\nu)A(u_y+v_x+w_xw_y) \end{aligned} \tag{3.370}$$

The moderately large-deflection equilibrium differential equations and associated boundary conditions as well as the buckling differential equations and associated boundary conditions can be derived in the manner of the fundamental energy approach used in Section 3.2. Simply include the thermal effects in the strain energy density expression (strain energy per unit volume) by subtracting the free thermal strains from the total strains to get the mechanical strains that cause energy to be stored:

$$\begin{aligned} U_o &= \frac{E}{2(1-\nu^2)}\left[(\varepsilon_x-\alpha\Delta T)^2+(\varepsilon_y-\alpha\Delta T)^2\right. \\ &\qquad \left.+2\nu(\varepsilon_x-\alpha\Delta T)(\varepsilon_y-\alpha\Delta T)+\frac{1-\nu}{2}\gamma_{xy}^2\right] \\ &= \frac{E}{2(1-\nu^2)}\left[\varepsilon_x^2-2\varepsilon_x\alpha\Delta T+(\alpha\Delta T)^2+\varepsilon_y^2-2\varepsilon_y\alpha\Delta T+(\alpha\Delta T)^2\right. \\ &\qquad \left.+2\nu\varepsilon_x\varepsilon_y-2\nu\varepsilon_x\alpha\Delta T-2\nu\varepsilon_y\alpha\Delta T+2\nu(\alpha\Delta T)^2+\frac{1-\nu}{2}\gamma_{xy}^2\right] \\ &= \frac{E}{2(1-\nu^2)}\left[(\varepsilon_x^2+\varepsilon_y^2+2\nu\varepsilon_x\varepsilon_y+\frac{1-\nu}{2}\gamma_{xy}^2)\right. \\ &\qquad \left.-2(1+\nu)(\varepsilon_x+\varepsilon_y)\alpha\Delta T+2(1+\nu)(\alpha\Delta T)^2\right] \end{aligned} \tag{3.371}$$

Éléments sous droits d'auteur

[which reduces to the strain energy density for a bar, Equation (2.553) on page 168, if $\varepsilon_y = 0$, $\gamma_{xy} = 0$, and $\nu = 0$] in which the sum of the quadratic terms in the strains constitutes the mechanical strain energy density, the sum of the linear terms in the strain and in ΔT constitutes the coupling between the mechanical and thermal effects portion of the strain energy density, and the quadratic term in ΔT is the constant thermal term that is irrelevant in the subsequent variational process when the principle of stationary potential energy is applied [because $\delta(\text{constant}) = 0$]. Thus, the only relevant additional term in the strain energy density expression beyond mechanical effects is

$$(U_c)_T = -\frac{E}{(1-\nu)} \alpha \Delta T (\varepsilon_x + \varepsilon_y) \tag{3.372}$$

in which ΔT can be a function of x, y, and z (and time). The results of the variational process lead to the nonlinear equilibrium differential equations and linear buckling differential equations and their associated boundary conditions just as in Section 3.2. Here, we show only the results and leave verification to exercises in Problem Set 3.7.

The moderately large-deflection nonlinear plate equilibrium equations are

$$\begin{aligned}
&\frac{\partial}{\partial x}\left[A\left[(u_x + \frac{1}{2}w_x^2) + \nu(v_y + \frac{1}{2}w_y^2)\right] - N^T\right] + \frac{1-\nu}{2} A \frac{\partial}{\partial y}(v_x + u_y + w_x w_y) = 0 \\
&\frac{1-\nu}{2} A \frac{\partial}{\partial x}(v_x + u_y + w_x w_y) + \frac{\partial}{\partial y}\left[A\left[(v_y + \frac{1}{2}w_y^2) + \nu(u_x + \frac{1}{2}w_x^2)\right] - N^T\right] = 0 \\
&-\frac{\partial}{\partial x}\left[w_x\left[A\left[(u_x + \frac{1}{2}w_x^2) + \nu(v_y + \frac{1}{2}w_y^2)\right] - N^T\right] + \frac{1-\nu}{2} A w_y (v_x + u_y + w_x w_y)\right] \\
&-\frac{\partial}{\partial y}\left[w_y\left[A\left[(v_y + \frac{1}{2}w_y^2) + \nu(u_x + \frac{1}{2}w_x^2)\right] - N^T\right] + \frac{1-\nu}{2} A w_x (v_x + u_y + w_x w_y)\right] \\
&+ D\left[\frac{\partial^2}{\partial x^2}(w_{xx} + \nu w_{yy}) + 2(1-\nu)\frac{\partial^2}{\partial x \partial y}(w_{xy}) + \frac{\partial^2}{\partial y^2}(w_{yy} + \nu w_{xx})\right] + \nabla^2 M^T = p
\end{aligned} \tag{3.373}$$

and the associated boundary conditions are

$$u = 0 \quad \text{or} \quad A\left[(u_x + \frac{1}{2}w_x^2) + \nu(v_y + \frac{1}{2}w_y^2)\right] - N^T = \bar{N}_x \quad \text{on edges } x = 0,a$$

$$v = 0 \quad \text{or} \quad A\left[(v_y + \frac{1}{2}w_y^2) + \nu(u_x + \frac{1}{2}w_x^2)\right] - N^T = \bar{N}_y \quad \text{on edges } y = 0,b$$

$$u = 0 \quad \text{or} \quad \frac{1-\nu}{2} A(v_x + u_y + w_x w_y) = \bar{N}_{xy} \quad \text{on edges } y = 0,b$$

$$v = 0 \quad \text{or} \quad \frac{1-\nu}{2} A(v_x + u_y + w_x w_y) = \bar{N}_{xy} \quad \text{on edges } x = 0,a$$

$$\begin{aligned}
w = 0 \quad \text{or} \quad & w_x\left[A\left[(u_x + \frac{1}{2}w_x^2) + \nu(v_y + \frac{1}{2}w_y^2)\right] - N^T\right] + \frac{1-\nu}{2} A w_y (v_x + u_y + w_x w_y) \\
& - \left[D\frac{\partial}{\partial x}(w_{xx} + \nu w_{yy}) + M^T + D\frac{\partial}{\partial y}[2(1-\nu)w_{xy}]\right] = \bar{K}_x \\
& \qquad \text{on edges } x = 0,a
\end{aligned}$$

Éléments sous droits d'auteur

$$w = 0 \text{ or } w_y\left[A\left[(v_y + \frac{1}{2}w_y^2) + \nu(u_x + \frac{1}{2}w_x^2)\right] - N^T\right] + \frac{1-\nu}{2}Aw_x(v_x + u_y + w_xw_y)$$
$$-\left[D\frac{\partial}{\partial y}(w_{yy} + \nu w_{xx}) + M^T + D\frac{\partial}{\partial x}[2(1-\nu)w_{xy}]\right] = \bar{K}_y$$
$$\text{on edges } y = 0,b$$

$$w_x = 0 \text{ or } -D(w_{xx} + \nu w_{yy}) - M^T = \bar{M}_x \qquad \text{on edges } x = 0,a$$

$$w_y = 0 \text{ or } -D(w_{yy} + \nu w_{xx}) - M^T = \bar{M}_y \qquad \text{on edges } y = 0,b$$

$$w = 0 \text{ or } 2(1-\nu)Dw_{xy} = \bar{R} \quad \text{at corners} \tag{3.374}$$

The last condition at corners also applies at discontinuities in the integrand of the boundary integral. Thus, we have the differential equations and boundary conditions for the thermoelastic equilibrium problem.

For buckling problems, the variations in forces and moments during buckling are

$$\delta N_x = \int \delta\sigma_x\, dz \qquad \delta N_y = \int \delta\sigma_y\, dz \qquad \delta N_{xy} = \int \delta\tau_{xy}\, dz \tag{3.375}$$

$$\delta M_x = \int \delta\sigma_x\, z\, dz \qquad \delta M_y = \int \delta\sigma_y\, z\, dz \qquad \delta M_{xy} = \int \delta\tau_{xy}\, z\, dz \tag{3.376}$$

in which the variations in stresses during buckling are

$$\begin{aligned}
\delta\sigma_x &= \frac{E}{1-\nu^2}(\delta\varepsilon_x + \nu\delta\varepsilon_y) \\
\delta\sigma_y &= \frac{E}{1-\nu^2}(\delta\varepsilon_y + \nu\delta\varepsilon_x) \\
\delta\tau_{xy} &= \frac{E}{2(1+\nu)}\delta\gamma_{xy}
\end{aligned} \tag{3.377}$$

Note that the $\alpha\,\Delta T$ terms in the thermoelastic stress-strain relations, Equation (3.358), *do not have a variation*, i.e., both α and ΔT are constant during buckling, just as is the mechanical load when the displacements are varied. Thus, all variations of thermal forces and moments are zero because these thermal loadings, like the mechanical loadings, are constant in the variational process.

The variations in strains are

$$\begin{aligned}
\delta\varepsilon_x &= \delta\bar{\varepsilon}_x + z\,\delta\kappa_x \\
\delta\varepsilon_y &= \delta\bar{\varepsilon}_y + z\,\delta\kappa_y \\
\delta\gamma_{xy} &= \delta\bar{\gamma}_{xy} + z\,\delta\kappa_{xy}
\end{aligned} \tag{3.378}$$

Then, after elimination of the subscript zero for the middle surface, the variations in middle-surface strains are

$$\begin{aligned}
\delta\bar{\varepsilon}_x &= \delta u_x + w_x\delta w_x \\
\delta\bar{\varepsilon}_y &= \delta v_y + w_y\delta w_y \\
\delta\bar{\gamma}_{xy} &= \delta v_x + \delta u_y + w_x\delta w_y + w_y\delta w_x
\end{aligned} \tag{3.379}$$

which for an initially flat plate with $w_x = w_y = 0$ become

Éléments sous droits d'auteur

$$\delta\bar{\varepsilon}_x = \delta u_x$$
$$\delta\bar{\varepsilon}_y = \delta v_y \qquad (3.380)$$
$$\delta\bar{\gamma}_{xy} = (\delta v_x + \delta u_y)$$

Also, the variations in middle-surface curvatures are

$$\delta\kappa_x = -\delta w_{xx} \qquad \delta\kappa_y = -\delta w_{yy} \qquad \delta\kappa_{xy} = -2\delta w_{xy} \qquad (3.381)$$

Thus, the variations in in-plane forces are

$$\delta N_x = \int \sigma_x \, dz = \frac{E}{1-\nu^2}\int (\delta\varepsilon_x + \nu\delta\varepsilon_y)\, dz$$
$$= \frac{E}{1-\nu^2}\int (\delta\bar{\varepsilon}_x + \nu\delta\bar{\varepsilon}_y)\, dz - \frac{E}{1-\nu^2}\int (\delta w_{xx} + \nu\delta w_{yy})\, z\, dz$$
$$= \frac{E}{1-\nu^2}(\delta\bar{\varepsilon}_x + \nu\delta\bar{\varepsilon}_y)\int dz - \frac{E}{1-\nu^2}(\delta w_{xx} + \nu\delta w_{yy})\int z\, dz$$
$$= \frac{E\,t}{1-\nu^2}(\delta\bar{\varepsilon}_x + \nu\delta\bar{\varepsilon}_y) = A(\delta\bar{\varepsilon}_x + \nu\delta\bar{\varepsilon}_y) = A(\delta u_x + \nu\delta v_y)$$
$$\delta N_y = \frac{E\,t}{1-\nu^2}(\delta\bar{\varepsilon}_y + \nu\delta\bar{\varepsilon}_x) = A(\delta v_y + \nu\delta u_x)$$
$$\delta N_{xy} = G\,t\,\delta\bar{\gamma}_{xy} = \frac{1-\nu}{2}A\delta\bar{\gamma}_{xy} = \frac{1-\nu}{2}A(\delta u_y + \delta v_x) \qquad (3.382)$$

and the variations in moments are

$$\delta M_x = \int \delta\sigma_x\, z\, dz = \frac{E}{1-\nu^2}\int (\delta\varepsilon_x + \nu\delta\varepsilon_y)\, z\, dz$$
$$= \frac{E}{1-\nu^2}\left[\int (\delta\bar{\varepsilon}_x + \nu\delta\bar{\varepsilon}_y)\, z\, dz - \int (\delta w_{xx} + \nu\delta w_{yy})\, z^2\, dz\right]$$
$$= \frac{E}{1-\nu^2}\left[(\delta\bar{\varepsilon}_x + \nu\delta\bar{\varepsilon}_y)\int z\, dz - (\delta w_{xx} + \nu\delta w_{yy})\int z^2\, dz\right]$$
$$= -\frac{E\,t^3}{12(1-\nu^2)}(\delta w_{xx} + \nu\delta w_{yy}) = -D(\delta w_{xx} + \nu\delta w_{yy})$$
$$\delta M_y = -\frac{E\,t^3}{12(1-\nu^2)}(\delta w_{yy} + \nu\delta w_{xx}) = -D(\delta w_{yy} + \nu\delta w_{xx})$$
$$\delta M_{xy} = -G\,\frac{t^3}{6}\,\delta w_{xy} = -\frac{E}{1+\nu}\,\frac{t^3}{12}\,\delta w_{xy} = -(1-\nu)D\delta w_{xy} \qquad (3.383)$$

The in-plane forces for a plate that is flat before buckling (so $w_x = 0$ and $w_y = 0$) become

Éléments sous droits d'auteur

$$N_x = A(u_x + \nu v_y) - N^T$$
$$N_y = A(v_y + \nu u_x) - N^T \tag{3.384}$$
$$N_{xy} = Gt(u_y + v_x) = \frac{1-\nu}{2} A(u_y + v_x)$$

The compressive in-plane forces at buckling are $\bar{N}_x$, $\bar{N}_y$, and $\bar{N}_{xy}$:

$$\bar{N}_x = -N_x = -A(u_x + \nu v_y) + N^T$$
$$\bar{N}_y = -N_y = -A(v_y + \nu u_x) + N^T \tag{3.385}$$
$$\bar{N}_{xy} = -\frac{1-\nu}{2} A(u_y + v_x)$$

Note that the moments do not appear in the buckling equations, only the *variations in moments* which have been shown to be

$$\delta M_x = -D(\delta w_{xx} + \nu \delta w_{yy})$$
$$\delta M_y = -D(\delta w_{yy} + \nu \delta w_{xx}) \tag{3.386}$$
$$\delta M_{xy} = -(1-\nu) D \delta w_{xy}$$

The variations in in-plane forces have been shown to be

$$\delta N_x = A(\delta u_x + \nu \delta v_y)$$
$$\delta N_y = A(\delta v_y + \nu \delta u_x) \tag{3.387}$$
$$\delta N_{xy} = \frac{1-\nu}{2} A(\delta v_x + \delta u_y)$$

in which we note that $\delta N^T = 0$ by inspection of the expression for N^T in Equation (3.366).

The process of making the second variation in strain energy stationary can be used to get the buckling differential equations and boundary conditions as was done in Section 3.2. Specifically, we supplement the second variation in energy integrals, Equations (3.164), (3.165), and (3.166) on page 263, with

$$\delta^2 U_{\bar{T}} = -\iint N^T (\delta w_x^2 + \delta w_y^2) dx dy \tag{3.388}$$

which can easily be shown to come from varying the integral of the strain energy density of the coupled mechanical and thermal terms, Equation (3.372) on page 360, over the area of the plate.

The plate buckling equations (without body forces) are identical to the equations from Section 3.2.5, i.e., Equations (3.160)–(3.162) on page 262:

$$\delta N_{x,x} + \delta N_{xy,y} = 0 \tag{3.389}$$

$$\delta N_{xy,x} + \delta N_{y,y} = 0 \tag{3.390}$$

$$\delta M_{x,xx} + 2\delta M_{xy,xy} + \delta M_{y,yy} - \bar{N}_x \delta w_{xx} - 2\bar{N}_{xy} \delta w_{xy} - \bar{N}_y \delta w_{yy} = 0 \tag{3.391}$$

or

$$D\nabla^4 \delta w + \bar{N}_x \delta w_{xx} + 2\bar{N}_{xy} \delta w_{xy} + \bar{N}_y \delta w_{yy} = 0 \tag{3.392}$$

in which we seek the values of the applied compressive in-plane me-

Éléments sous droits d'auteur

chanical and thermal forces at buckling, $\bar{N}_x$, $\bar{N}_y$, and $\bar{N}_{xy}$ that yield a solution to Equation (3.391) or (3.392). The nature (distribution) of those forces is obtained from the prebuckling equilibrium solution to the plate problem. Note that the first variations of the thermal forces and thermal moments are zero. The thermal force, N^T, is implicitly included in $\bar{N}_x$ and/or $\bar{N}_y$ to account for the thermal loading. Note that the thermal moment, M^T, does not appear in the buckling equation because such a moment would cause the plate to bend immediately upon imposition of the slightest ΔT rather than buckle at an elevated ΔT. That is, those loadings that create a thermal moment do not cause buckling

The associated buckling boundary conditions for the buckling problem analogous to those for the equilibrium problem in an adaptation to plates of Almroth's notation [3-6] for shells are:

Simply Supported Edges:

$$\begin{array}{llllll} \text{S1:} & \delta w = 0 & \delta M_n = 0 & \delta u_n = 0 & \delta u_t = 0 \\ \text{S2:} & \delta w = 0 & \delta M_n = 0 & \delta N_n = 0 & \delta u_t = 0 \\ \text{S3:} & \delta w = 0 & \delta M_n = 0 & \delta u_n = 0 & \delta N_{nt} = 0 \\ \text{S4:} & \delta w = 0 & \delta M_n = 0 & \delta N_n = 0 & \delta N_{nt} = 0 \end{array} \tag{3.393}$$

Clamped Edges:

$$\begin{array}{llllll} \text{C1:} & \delta w = 0 & \delta w_{,n} = 0 & \delta u_n = 0 & \delta u_t = 0 \\ \text{C2:} & \delta w = 0 & \delta w_{,n} = 0 & \delta N_n = 0 & \delta u_t = 0 \\ \text{C3:} & \delta w = 0 & \delta w_{,n} = 0 & \delta u_n = 0 & \delta N_{nt} = 0 \\ \text{C4:} & \delta w = 0 & \delta w_{,n} = 0 & \delta N_n = 0 & \delta N_{nt} = 0 \end{array} \tag{3.394}$$

in which n and t are normal and tangential directions and δM_n and δN_n do not include M^T or N^T variations because they are zero. Note that these boundary conditions are on the variations in forces and variations in moments, not on the forces and moments, so the prebuckling boundary conditions have nothing to do with the buckling boundary conditions. Observe the graphic depiction of the simply supported edge buckling boundary conditions in Figure 3-14 on page 261 as well as for clamped edges in Figure 3-15 on page 261. Equations (3.389), (3.390), and (3.391) (or 3.392) are homogeneous differential equations with homogeneous boundary conditions in Equations (3.393) or, alternatively, (3.394). Thus, they constitute an eigenvalue problem and are solved accordingly. The eigenvalue is the value of $\bar{N}_x$ ($\bar{N}_y$), i.e., the buckling load, or within $\bar{N}_x$ ($\bar{N}_y$) the value of ΔT, the thermal buckling load. The eigenvector is the shape of the buckled plate. Actually, there is no physically interesting solution to Equations (3.389) and (3.390) because the eigenvalue is not involved; in fact, we can ignore them except when we consider unsymmetrically laminated composite plates for which all three differential equations are coupled (see Section 3.6).

We will use these fundamental thermoelastic relations in problems involving buckling after we have further explored the issue of plate support conditions as related to in-plane restraint in Section 3.7.3.

Éléments sous droits d'auteur

3.7.3 In-Plane Loading and Restraint Conditions for Plates

Only the *change in temperature* from some reference state affects the buckling load, although absolute temperature determines the properties of the material involved. And that change in temperature, if uniform throughout the volume, must take place while some form of appropriate restraint exists on bar, plate, or shell movement. That is, the uniformly distributed temperature could increase from a low temperature for some time while the bar, plate, or shell is not restrained in any manner, so only free thermal expansion would take place. Then, if some type of in-plane restraint were introduced, the amount of temperature change to cause buckling would be sought. However, that temperature change does not include the temperature at any time prior to application of the restraint condition, but only the change in temperature from the instant the restraint was imposed. In addition, the temperature change need not be constant over the volume of the structural element. Thus, we are concerned with how a structural element develops thermal forces from variously distributed thermal loadings under various deformation restraint conditions. We will also describe how thermal buckling can occur without restraint but with spatially nonuniform changes in temperature.

Some combinations of in-plane edge restraint and distributions of temperature change produce plate buckling when a certain level of temperature change is reached. For example, if the temperature change is constant through the thickness of a plate, buckling occurs from the flat state at a specific temperature change (long after the first increment of temperature change is applied). However, other combinations of in-plane edge restraint and temperature change distributions produce only bending, bowing, or curling from the instant that the first increment of temperature change is applied. If the temperature change distribution varies through the thickness of a plate in a manner that is not symmetric about the plate middle surface, then the plate will not remain flat as the temperature change is increased in amplitude, i.e., the plate will bend, bow, or curl at the instant when the first increment of temperature change is imposed, i.e., no buckling occurs unless into a different mode at a higher ΔT. The simplest case of thermal loading for us to consider is a spatially uniform temperature change distribution, and we will concentrate on that case in this book. However, from time to time, we will also address nonuniform temperature change distributions.

3.7.3.1 What In-Plane Boundary Conditions can Result in Thermal and/or Mechanical Buckling?

The principal in-plane restraint necessary in order for thermal buckling to occur under a *spatially uniform or nonuniform temperature change* distribution is on the in-plane displacement normal to the edge on *two opposite edges* of a rectangular plate. That normal in-plane displacement must be restrained in some manner to resist free thermal expansion of the plate in order to develop in-plane compressive forces that cause thermal buckling to occur when a sufficiently high temperature change is

Éléments sous droits d'auteur

reached. Also realize that full restraint of the in-plane displacement normal to the plate edge on two opposite edges permits no mechanical forces to be applied in the in-plane direction perpendicular to those two opposite edges because in-plane movement under load cannot occur; thus, buckling under mechanical loading cannot take place (except as in the next subsection). The in-plane displacement tangential to a plate edge can also be restrained to not allow free thermal expansion along the edge and, hence, the restraint would cause thermal stresses that in turn could cause thermal buckling if the stresses are high enough. The alternative to buckling is bowing, curling, or bending that begins at the first instant that temperature change is applied, i.e., no (sudden) buckling event occurs. Loading and support conditions in engineering laboratories and in engineering practice are contrasted in the following to address their influence on buckling under both thermal and mechanical loading.

3.7.3.1.1 Load Versus Displacement Application in the Laboratory

If a displacement, in contrast to a load, is mechanically applied, then a structural element has axial or in-plane boundary restraint in addition to a mechanical load in the direction of the displacement. Displacements can be applied with a screw-type loading machine whereas loads are applied by dead-weight loading or hydraulic loading machines. Turning the screws on a screw-type loading machine or load frame as in Figure 3-78 moves the head to a new position and the screws keep the head in that position (which is why this form of loading is called displacement loading or displacement control). The head compresses the object, straining it, thereby stressing it, and thus introducing mechanical load. When the screws stop turning, the applied displacement is held relatively constant by the position of the loading head on the screws. Most load frames currently in laboratories are hydraulically operated with very sophisticated programmable load-application controls. Those controls are capable of applying load, displacement, or strain. Although displacements can be applied, many current loading machines are not stiff enough to remain perfectly in position when a thermal load is applied in addition to the mechanical load that is being held (these machines have a large load capacity, but relatively small stiffness). That is, heating the specimen could move the supposedly "fixed" head. A load frame with four screws (two on each side of the plate) is typically stiffer than one with only two screws. That enhanced stiffness is important for plate thermal buckling experiments. Machines with lesser stiffness have a tendency for the heads to move when a thermal load is applied.

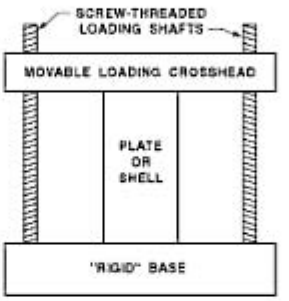


Figure 3-78 Screw-type Load Frame

Éléments sous droits d'auteur

For a plate, edge displacement can be applied with a loading machine that has at least two threaded screw shafts as in Figure 3-78. Applying a thermal loading to an object as wide and as stiff as a plate can be quite difficult. If only a bar is being loaded, then a small heating box can be placed around the bar so the heat does not get to the load frame. A heating box encloses the specimen and has heating coils to apply heat to the specimen and unavoidably to the load frame to some extent. However, the heating box for a plate must be much larger than for a bar, and the inevitable heat loss to the load frame must be accounted for. Heating the load frame usually results in diminished mechanical loading because the load frame tends to expand and therefore release some of the mechanical load by movement of the loading head.

After a displacement has been applied and held, a temperature change can be applied and if it *and* the load corresponding to the applied displacement are high enough, the plate will buckle. That is, the buckling load can be composed of a mechanical component as well as a thermal component in a wide variety of possible proportions of the two components. If the mechanical load is small, the thermal load causing buckling is large and vice versa. The complex methods of ensuring that various types of simply supported or clamped edges are effectively modeled on plates in the laboratory is left to the descriptions of experimental work in Singer, Arbocz, and Weller [3-17].

3.7.3.1.2 Loading and Restraint Conditions in Engineering Practice

Whether the loading and restraint conditions available in the engineering laboratory are specifically applicable in engineering practice is questionable and a matter of engineering judgement. The important issue is to recognize the types of restraint that are possible and their effects and then to be able to identify the actual restraint conditions that exist in engineering practice. For example, consider the set of frames, spars, stringers, and ribs of different stiffnesses in different directions on a wing panel for an aircraft wing or in a stiffened fuselage panel in Figure 3-79. The biaxially stiffened plate is fastened to unequal-stiffness stiffeners in the two directions at the plate edges. One set of stiffeners is called 'heavy' and the other 'light' in Figure 3-79. The heavy stiffeners do not respond quickly in the y-direction to temperature change. Thus, the heavy stiffeners (nearly) prevent thermal expansion of the panel in the y-direction. The light stiffeners have so little stiffness that the panel expands (almost) freely in the x-direction. Mechanical load can be accepted in the x-direction because movement can take place in the x-direction. In this case, the frames in one direction, the y-direction, are so stiff as to be approximated by rigid restraint but in the perpendicular x-direction, the restraint is so small as to be negligible. Such approximations are always necessary in engineering practice unless analyses for more precise evaluations are available *and* the actual stiffnesses are known to some degree of precision or accuracy.

Examples of this type of loading and restraint include aircraft wing panels and fuselage panels as in Figure 3-79. Wing panels react wing

Éléments sous droits d'auteur

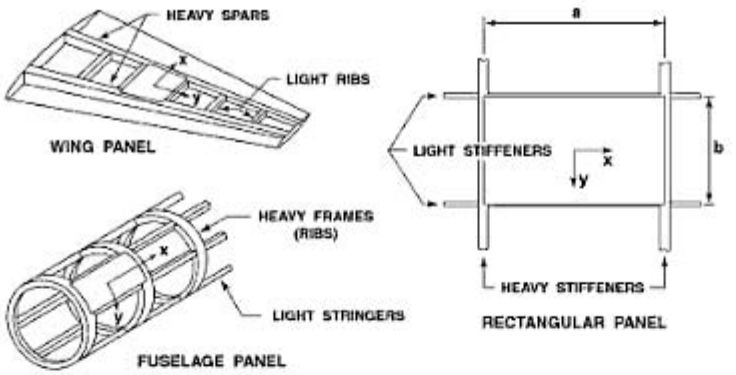


Figure 3-79 Practical Examples of Mechanically and Thermally Loaded Panels *(Inspired by Parkes [3-54])*

bending moments by y-direction forces (compression in the top panels and tension in the bottom panels or vice versa). Fuselage panels react body bending moments by variable x-direction forces. Simultaneously, the heavy spars in wings and the heavy frames (also called ribs) in fuselage structures prevent thermal expansion in the y-direction. The thermal loading comes from heating during supersonic aircraft flight, reentry of spacecraft into the atmosphere, or movement of spacecraft in and out of the sun. Mechanical loading is caused by wing and fuselage bending and twisting in addition to fuselage pressurization. Hoff [3-55] reviews motivations for treating thermal buckling.

3.7.3.1.3 Elastic In-Plane Edge Restraint

The in-plane normal-to-the-edge-displacement restraint can be complete, i.e., fixed to be zero, or partial, e.g., elastic restraint in which the restraining force is proportional in some manner to the normal displacement of the edge. Accordingly, if linear translational springs are placed normal to the edge of the plate in its plane to restrain the edge as in Figure 3-80, then the restraining force is linearly proportional to the normal displacement of the edge. More complex load-deformation characteristics of the in-plane springs (elastic restraints) can result in a

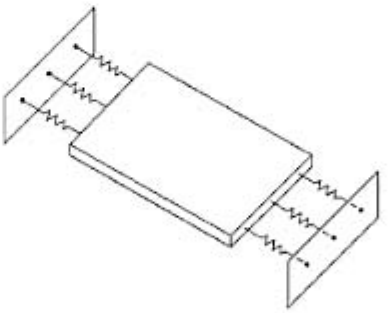


Figure 3-80 Plate with In-Plane Spring Restraint

Éléments sous droits d'auteur

nonlinear relationship between the restraining force and the edge normal displacement. The thermal buckling load is highest for 'rigid' in-plane springs and decreases as the in-plane, normal-to-the-edge springs decrease in stiffness until, in the limit of zero-stiffness in-plane springs, no restraint exists, so thermal buckling cannot occur. Rotational-edge-restraint springs are also possible (in addition to essential in-plane restraint of some type to develop thermal forces) as shown in Figure 3-81. The 'infinitely stiff' limit for the rotational springs corresponds to the usual clamped-edge condition with a high ΔT. Successively decreasing the stiffness of the rotational springs leads to the lower simply supported edge plate value of $\overline{\Delta T}$ for zero-stiffness rotational springs. The in-plane translational springs affect the nature and magnitude of the prebuckling thermal load, whereas the rotational springs have no effect on the prebuckling thermal load, but do affect the level of the thermal buckling load.



Figure 3-81 Side View of Plate with Rotational Spring and In-Plane Restraint

3.7.3.1.4 Thermal Buckling without In-Plane Edge Restraint

Thermal buckling can occur for a *spatially nonuniform temperature change* even in the absence of restraint of the in-plane displacement normal (or tangential) to the edge. That is, no edge restraints whatever are needed for thermal buckling to occur if the temperature distribution is nonuniform because then self-equilibrating tensile and *compressive stresses will develop* inside the plate area even without boundary restraint. Thus, a central "hot spot" in a plate could cause buckling in the following manner. The hot spot tends to expand, but is restrained by deformation compatibility with the surrounding colder region that tends to expand less leading to a complex self-equilibrating stress field of compressive stresses in the hot spot and tensile stresses in the colder region. If the temperature change is uniform through the thickness, then at some level of temperature change, as the hot spot gets hotter, the compressive stresses in the hot spot cause the region of the hot spot to buckle. If the temperature change is not uniform through the thickness, then the hot spot will simply bulge or bow from the very first instant that the temperature change is applied.

A spatially uniform temperature change is the most common situation in engineering practice. Yes, spatial temperature gradients do exist in many practical problems because of heat conduction that occurs at different rates for different materials. Also, spatial temperature gradients exist for aerodynamic problems such as airflow over a wing (leading to wing panels with nonuniform in-plane temperature distributions). Of course, spatial temperature distributions are the most complicated and interesting (Remember the Chinese curse: may you live in interesting times!) to treat, but they are out of the scope of this book (except for the through-the-thickness temperature variation for a bar in Section 2.9.5).

Éléments sous droits d'auteur

3.7.3.2 In-Plane Displacement Notation

In most buckling problems, we seem to be primarily concerned with whether a plate has simply supported or clamped edges, i.e., the lack or presence of rotational restraint of the edges. However, now with thermal buckling we are also interested in the in-plane displacement restraints because they, too, have a strong influence on buckling because they determine the nature of the prebuckling in-plane stresses that cause buckling. Of course, the rotational restraint, or lack thereof, also still strongly influences the actual buckling load, but, for now, we will concentrate on physically describing the in-plane displacement restraints. We consider the in-plane displacements of the plate with the aid of the following definition. The subscripts n and t denote the *directions in the plane of the plate normal and tangential to the edge* under consideration as in Figure 3-82. The in-plane displacement normal to the edge, u_n, is often, but not always, the key displacement in a thermal buckling problem and can be fixed to be zero, elastically restrained, or free. The in-plane displacement tangential to the edge, u_t, is, for simple problems with a membrane prebuckling equilibrium state, often merely unrestrained in any manner (except for an essential fixed point somewhere to prevent rigid-body motion), although restraint of u_t can lead to buckling. The tangential displacement, u_t, could also be either elastically restrained or fixed to be zero, but those conditions usually, but not always, result in more complex prebuckling equilibrium states than the simple membrane stress states of the unrestrained tangential displacement case.

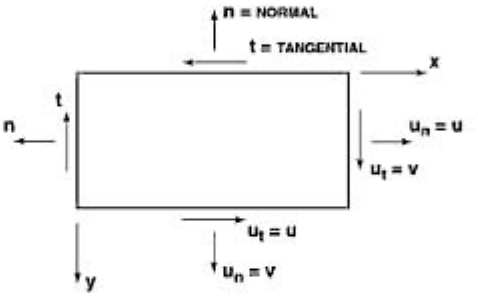


Figure 3-82 In-Plane Displacement Notation

3.7.3.3 In-Plane Boundary Condition Notation

We address only combinations of perfect fixed or free (non-elastic) restraints on the in-plane (IP) displacements. For each of the two in-plane displacements, u_n and u_t, there are two choices of conditions:

1. ZM (Zero Movement)
2. NR (Not Restrained)

We have excluded consideration of the elastic restraint possibilities, so we are concerned with only four possible in-plane displacement conditions (each with simply supported or clamped edge rotation conditions if only the zero transverse-to-the-plate-surface displacement condition, $w = 0$, and the zero transverse-to-the-plate buckling displacement condi-

Éléments sous droits d'auteur

Table 3-5 Possible In-Plane Displacement Restraint Conditions

Type	u_n	u_t
IP1	ZM	ZM
IP2	NR	ZM
IP3	ZM	NR
IP4	NR	NR

tion, $\delta w = 0$, is addressed) in Table 3-5. If elastic in-plane restraint is present such as with springs as in Figure 3-80, then a third category ER (Elastic Restraint) must be added to Table 3-5 increasing the number of possible restraint combinations on each edge to nine (3^2). This notation corresponds to the adaptation of Almroth's shell boundary conditions [3-6] for plates in Equations (3.87) and (3.88) on page 246 in which the prescribed values of displacements and forces are always zero. That is, NR corresponds to no restraint or force being applied in that direction (NR = Not Restrained) and ZM to a restraint causing no displacement in that direction (ZM = Zero Movement). Each of these numbers in the IP designation is identical to the in-plane boundary conditions of simply supported or clamped edge conditions in Figures 3-10 and 3-11 on pages 247 and 248, respectively. This notation enables us to concentrate on only the in-plane boundary conditions that affect the prebuckling equilibrium forces without the nuisance of considering the irrelevant issue (at this equilibrium stage) of whether each edge is simply supported or clamped. That is, we consider only the in-plane displacement boundary conditions to obtain the membrane prebuckled equilibrium state (if it exists). The out-of-plane rotational or transverse to the plate surface conditions do, of course, strongly affect the value of both the thermal and mechanical buckling loads. However, those buckling loads cannot be calculated until the prebuckling equilibrium stress state is established.

Note that a plate with IP4 (NR-NR) boundary conditions on four opposite edges does not buckle thermally for a uniform temperature change because there is no in-plane restraint. That is, the plate is free to move in its plane with those IP4 boundary conditions, so application of a change in temperature merely results in free thermal expansion of the plate in the directions normal to the four edges.

The various in-plane boundary conditions are depicted looking from a point of view perpendicular to the plane of the plate in Figure 3-83. For IP1, the edge can't move in either the n- or t-direction. For IP2, a roller can move in the n-direction, but not in the t-direction. For IP3, the rollers can

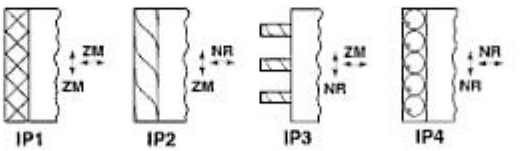


Figure 3-83 Schematic of In-Plane Boundary Conditions

Éléments sous droits d'auteur

move in the t-direction, but not in the n-direction. Finally, for IP4, the spherical balls can roll in both the n- and t-directions. These in-plane boundary conditions are applicable to both simply supported as well as clamped (fixed) edges. Simply superimpose the in-plane boundary conditions on either the simply supported or the clamped edge boundary conditions. Somehow, this in-plane boundary condition depiction is 'overlaid' with a depiction of fixed or simply supported edges, i.e., an edge-rotation condition. Alternatively, we simply appeal to Figures 3-10 or 3-11 on pages 247 and 248, respectively, for depiction of the various simply supported edge conditions or various clamped edge conditions, respectively, including the in-plane conditions.

3.7.3.4 Compatibility of Boundary Conditions at Corners and on Adjacent Edges

The boundary condition corner-compatibility condition is

The two displacements on each of the two adjacent (intersecting) edges at an enclosed corner of a plate must be compatible with each other at the corner. The tangential displacement u_t along edge A must be compatible with the normal displacement u_n on adjacent edge B at corner A-B. Also, the normal displacement u_n on edge A must be compatible with the tangential displacement u_t along adjacent edge B at corner A-B.

Corner compatibility and adjacent-edge compatibility in which the corner-compatibility condition is extended to the entirety of the two adjacent edges are part of the two-dimensional nature of plates as opposed to the one-dimensional nature of bars. We have defined corner compatibility first, and now, for uniform temperature changes, we will address adjacent-edge compatibility.

The boundary condition adjacent-edge-compatibility condition is

Under conditions of uniform temperature change over the plate area, the consequences of the boundary condition corner-compatibility condition are automatically extended to the entirety of one edge from the corner and possibly to the entirety of both adjacent edges.

If a ΔT is applied that is uniform in the y-direction, then a plate tends to expand (contract) in the y-direction uniformly at every point in the y-direction irrespective of any constraint in the y-direction. However, having an edge constraint of zero net movement in the y-direction because of the ZM-NR condition (IP3) on edges B and D in Figure 3-84 implies that the actual movement of the plate in the y-direction must be zero at every point in the plate. Thus, *effectively*, the boundary conditions on edges A and C are IP1 as shown in Figure 3-85.

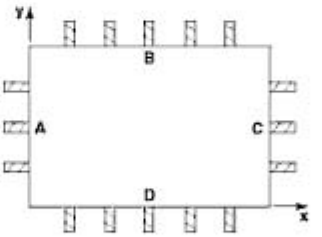


Figure 3-84 Plate with IP3 on all Edges

Éléments sous droits d'auteur

Those effective boundary conditions are not realized for a nonuniform ΔT in the y-direction because at any point in the plate the movement could be different from that of any other point. For the now-implied nonuniform ΔT in the x-direction (because we have not restricted the nature of ΔT in the x-direction), any point in the plate can have a displacement in the x-direction except at edges A and C.

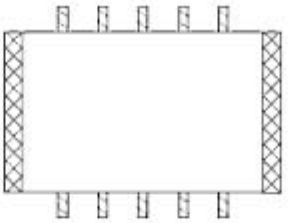


Figure 3-85 Plate with Conditions IP3 on Two Opposite Edges and IP1 on the Other Two Opposite Edges



Figure 3-86 Plate with IP1 on all Edges

If the applied ΔT is also uniform in the x-direction as well as in the y-direction, then the tendency of the plate to deform the same at every point implies that the movement of the plate in the x-direction must be zero at every point in the plate. Thus, *effectively*, the boundary conditions are zero movement in both the x- and y-directions along all four edges, i.e., boundary condition IP1 in Figure 3-86 with associated lack of in-plane movement at all points in the plate. These *effective* boundary conditions are not realized for a nonuniform ΔT in the x-direction because, at any point in the plate, movement can differ from that of any other point, i.e., the original plate boundary conditions of IP3 on all four edges govern because the corner compatibility condition then does not extend to edge compatibility.

If two opposite edges of a uniformly heated plate are fixed against in-plane movement in any direction (IP1), then there is no expansion along or normal to those two edges. If the other two edges are not restrained against in-plane movement (IP4), movement can occur parallel to the restrained edges except, of course, at the restrained edges themselves (by the edge-compatibility condition). The heated plate widens in the direction parallel to the restrained edges, but gets wider at the center than near the restrained ends. The center portion of the plate could expand freely in the direction parallel to the restrained edges if the center is 'far enough away' from the restrained ends and achieve its free thermal expansion width value of $(1 + \alpha\Delta T)b$. A nonuniform temperature-change distribution might enhance or diminish that widening effect.

Consider the in-plane temperature-change distribution that is nonuniform in the special, restricted manner of an antisymmetric distribution (about a line through the middle of the plate) with an equal amount and spatial distribution of positive temperature change as well as negative temperature change. Then, the net expansion of the plate perpendicular to the line of antisymmetry is zero, but, along the edge or any line per-

Éléments sous droits d'auteur

pendicular to the line of antisymmetry, the movement is sometimes an expansion and sometimes a contraction. Thus, only at the corner does the edge-compatibility issue arise. The real special case is uniform temperature change that 'converts' the corner-compatibility condition into a condition on two adjacent edges (the edge-compatibility condition) and indeed all four edges, in their entirety.

If the in-plane temperature-change distribution is nonuniform, then in-plane movement can and will take place in different amounts at different positions in the plate. However, the *net* expansion or contraction of the plate in a particular specified direction is constrained to be zero if there are boundary conditions of zero normal movement on the two opposite edges that are perpendicular to that specified direction. Consider a sinusoidal temperature-change distribution in the x-direction on a plate that is fully restrained in-plane along the y-direction edges. Before the temperature-change distribution is applied, the x-direction cross section of the plate appears as in Figure 3-87a, the initial unloaded condition. There, no movement is allowed in the x-direction because the boundary conditions on the two edges $y = 0$ and $y = b$ are either IP1 or IP3. Now apply a temperature change that is nonuniform in the x-direction, say $\Delta T = \Delta T_o \sin \pi x/a$. The plate deforms a different amount at different x positions in accordance with the x-direction ΔT distribution. Local movement of the plate depends on the local temperature change *if the edges are unrestrained in the x-direction*. Note that the strain in the x-direction is distributed sinusoidally in the x-direction just as the change in temperature is distributed (because the free-thermal expansion strain is $\varepsilon = \alpha\Delta T$). Thus, the plate freely expands in the x-direction in an amount obtained by integration of the variable strain ε_x over the length a to get the free-thermal-expansion condition shown in Figure 3-87b.

$$\Delta_T = \int \varepsilon_x dx = \int \alpha \Delta T dx = \alpha \Delta T_o \int_0^a \sin \frac{\pi x}{a} dx = \frac{2}{\pi} a \alpha \Delta T_o \qquad (3.395)$$

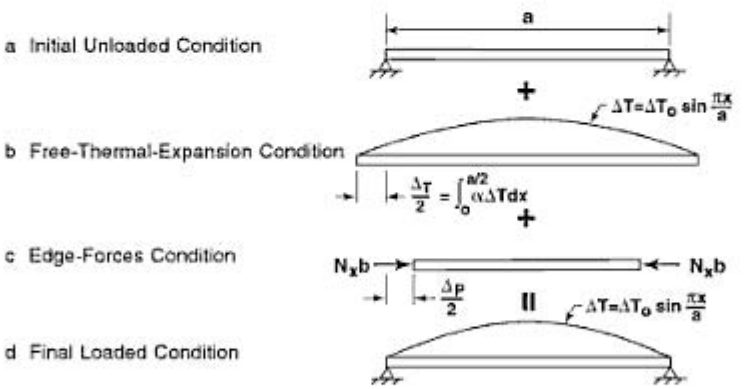


Figure 3-87 Effect of Nonuniform Temperature Change on In-Plane Movement

Éléments sous droits d'auteur

However, because *the edges are actually constrained in the x-direction,* we must superimpose this end-restraint condition on the thermal-expansion condition in the form of the edge-forces condition in Figure 3-87c. That is, thermally induced forces must act at the restrained edges to push the expanded plate back to the original (restrained) support condition.

$$\Delta_P = \frac{PL}{AE} = \frac{(N_x b)a}{(b\,t)E} = \frac{N_x a}{t\,E} \tag{3.396}$$

This action causes a uniform strain (and stress) to be superimposed on the sinusoidal distribution of free thermal strain (with no stress) to attain the final (loaded) condition such that the plate regains its original length in Figure 3-87d in which the supports have compressive forces to enforce the zero-displacement boundary condition because of the two supports. Those thermal forces are obtained by equating Δ_T to Δ_P to get

$$N_x^T = \frac{2}{\pi} E\alpha\Delta T_o\, t \tag{3.397}$$

Although each of the two adjacent edges in Figure 3-88 can be called ZM-NR (IP3), the adjacent-edge boundary compatibility requirement leads to the same deformation condition as if each edge were ZM-ZM (IP1) for simple thermal loadings, e.g., uniform temperature rise (For more complex thermal loadings, the u_t could vary along the edge B, but the corner conditions remain valid). Note that u_t on one edge corresponds to u_n on the other edge, and u_n on one edge corresponds to u_t on the other edge. That is, the complete restraint of u_n for edge A implies that u_t for adjacent edge B must be zero at the corner. Similarly, complete restraint of u_n on edge B implies that u_t on adjacent edge A must be zero at the corner. Thus, the in-plane boundary conditions on adjacent edges cannot be specified independently.

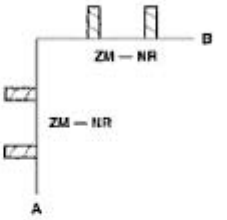


Figure 3-88 Boundary Conditions at a Corner

Consider another set of boundary conditions on edges A, B, and C in Figure 3-89. Edge A (ZM-NR) (IP3) and edge B (NR-NR) (IP4) are apparently compatible at the corner A-B, but note that the tangential in-plane displacement of edge B is not fully specified merely by this corner condition. Actually, at the corner between A and B, the u_t of edge B must be zero. What u_t is for the rest of edge B depends on the in-plane boundary conditions for edge C and on the ΔT distribution in the direction along edge B. If edge C is ZM-NR (IP3) and the ΔT distribution in the direction of edge B is uniform, then u_t for edge B must be zero everywhere along edge B leaving edge B with the effective boundary condition of NR-ZM (IP2). If edge C is ZM-NR (IP3) and the ΔT distribution in the x-direction is nonuniform, then edge B can have NR-NR (IP4) boundary conditions. If edge C is NR-NR (IP4), then adjacent edge B

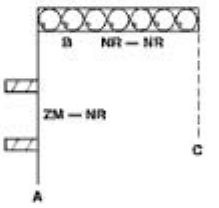


Figure 3-89 Boundary Conditions at Adjacent Corners

Éléments sous droits d'auteur

can be NR-NR (IP4), but no thermal buckling could occur for uniform areal ΔT distribution because there is no restraint in the plate! However, the plate might buckle for a nonuniform ΔT distribution.

3.7.3.5 Boundary Support and Thermal Loading Conditions Leading to Non-Classical Problems

Consider a plate with two adjacent edges fixed against both normal and tangential in-plane movement in Figure 3-90. The two IP1 edges are compatible with each other at their intersection. However, they place in-plane restraint on the two free edges at each intersection of an IP1 edge with a free edge (IP4 edge) whereas there is no in-plane restraint at the intersection of the two free edges. As the temperature change increases, say in a uniform distribution throughout the volume of the plate for the simplest case, the plate tends to expand, but cannot do so in a uniform manner because of the in-plane restraint that is nonuniform. A uniform ΔT distribution leads to a state of biaxial compression at the two fixed edges, ranging to uniaxial compression at the intersection of a fixed edge with a free edge, and finally to zero stress at the intersection of the two free edges. The stress distribution is symmetric about the diagonal line from the intersection of the fixed edges to the intersection of the free edges. Thus, a change in temperature that causes buckling can be calculated. If the ΔT distribution is not uniform over the surface of the plate or symmetric about the diagonal line, stress distribution symmmetry does not exist, so bending, bowing, or curling will occur, not buckling.



Figure 3-90 Plate with Two Adjacent Edges Fixed against In-Plane Movement

3.7.3.6 Summary

We examined only the in-plane boundary conditions on a plate edge, but perfect rotational restraint or lack thereof or elastic rotational restraint remain to be considered. The thermal buckling loads associated with each edge rotational restraint condition are different, but the prebuckling *distributions* of stresses are identical for the same in-plane boundary conditions. The in-plane boundary conditions determine the distribution of the in-plane stresses whereas the rotational boundary conditions determine the buckling load, i.e., the *magnitude* of the stress distribution. That is, the magnitudes of the stress distribution to cause buckling vary depending on the nature of the rotational restraint, but the stress distributions themselves do not vary. Thus, this sub-section forms the basis for many different thermal buckling problems. We now revert to the complete description of the boundary conditions including both in-plane and rotational specifications for simply supported edges in Figure 3-10 on page 247 and for clamped edges in Figure 3-11 on page 248. We will address three solutions for uniform thermal loading of simply supported plates after we introduce the equivalent mechanical loading concept.

Éléments sous droits d'auteur

3.7.4 Equivalent Mechanical Load Concept

In some thermal loading problems, a mechanical load that is equivalent in action caused to the prescribed thermal load can be found, i.e., causes the same prebuckling equilibrium stresses. This *equivalent mechanical load concept* can be used to thoughtfully extend the applicability of some problems of buckling under mechanical loading to buckling under thermal loading. For many simple thermal loading problems, this process has long been used implicitly, i.e., without a name and without a general description of its applicability and only on a case-by-case basis for a few cases.[1] In the following, we will describe and develop the *equivalent mechanical load concept* for thermal buckling problems.

We implicitly made use of the equivalent mechanical load concept in our study of thermal buckling of bars in Section 2.9. There, we immediately visualized an axially restrained bar as having an end mechanical force that arose from restraint of thermal expansion in the axial direction (see Figure 2-73 on page 174). We found the logic of a mechanical force needed to 'push back' the free thermal expansion compellingly obvious and easy to understand. The general situation for thermally loaded bars was fairly simple: (1) either a mechanical force or a thermal force could exist (at the ends), although both could exist under certain conditions; (2) either an end was restrained or it was free to move; (3) the bar could be subjected to uniform ΔT or one that varied along the length of the bar (if ΔT varied through the bar thickness in a manner not symmetric about the bar axis, we found that a thermal moment develops causing bending, curling, or bowing, not thermal buckling).

For plates, the equivalent mechanical load concept is more involved than for bars because there are potentially two forces or loadings, one in each perpendicular direction of a rectangular plate. For example, uniform temperature change on an unrestrained plate causes free thermal expansion in *both* the x- and y-directions. Restraint can be in one or the other or both directions in the simplest cases. However, recall that a force applied in one direction on a two-dimensional object to eliminate the deformation in that direction to simulate restraint actually causes a change in dimension of the object in the perpendicular direction because of the Poisson effect. Thus, although temperature change causes free thermal expansion in two directions, how each of those two directions is, or is not, restrained can lead to somewhat complicated equations for the state of the in-plane forces in a plate. We must include the Poisson effect in any analysis by use of the two-dimensional strain-displacement relations and the stress-strain-change-in-temperature relations.

The process of establishing an equivalent mechanical load is centered on identifying the stresses in the prebuckling equilibrium state of a thermally loaded plate and then hopefully finding a mechanically loaded plate with the same stresses. That is, the key element in the process is the prebuckling equilibrium stresses because if the prebuckling stresses

[1] For example, Burgreen addresses how an equivalent mechanical stress problem can be developed for a three-dimensional thermal stress equilibrium problem with specializations for two-dimensional and one-dimensional problems [3-56].

Éléments sous droits d'auteur

in two problems are identical, then the buckling loads are identical because the origin of the prebuckling stresses in a buckling problem is immaterial. By 'stresses' is meant the totality of the distribution of prebuckling stresses within the plate and on its boundary.

Are the prebuckling deformations the same for the thermal loading problem as for the equivalent mechanical loading problem? No. Recall that deformation restraint is essential to develop thermal force whereas deformation is essential to develop or accept mechanical load. For thermal buckling of bars, axial restraint forced the axial deflection to be zero to develop an axial thermal force whereas, in contrast, axial deflection must exist to develop and accept mechanical load. For thermal loading of plates, required in-plane restraint causes at least one in-plane deflection to be zero to develop an in-plane thermal force whereas in-plane deflection must be non-zero in one direction to have a mechanical loading. However, those deflections are quite small in comparison to the major structural element dimensions, namely the bar length or the plate length and width.

To find the prebuckling stresses from the thermal loading, we must first consider the deformation restraints, if any, on the plate edges because these restraints are irretrievably associated with the development of thermal stresses on the plate boundary. However, thermal stresses can develop wholly within the plate without any stresses existing on the boundary; in this class of thermal buckling problems, no equivalent mechanical load exists. That is, without deformation restraints on the boundary, there is no distribution of prebuckling stresses on the boundary, and we know of no *simple* buckling problem for mechanical loading without prebuckling boundary stresses, i.e., load on the boundary.

To find the equivalent mechanical loading for any structural element, we must simultaneously consider the three conditions of

- stress-strain-change-in-temperature (σ-ε-ΔT) relations
- equilibrium in the prebuckled state
- boundary support conditions

The boundary support conditions, especially (1) along the axis of a bar at the end or (2) in the plane of a plate at the edges or (3) in the surface of a circular cylindrical shell along the edges at each end, are crucial to the (proper) determination of the prebuckling thermal forces and hence to the definition of the equivalent mechanical loads and finally to the proper solution of thermal buckling problems.

The equivalent mechanical load concept will be developed for three straightforward thermal buckling of simply supported plates problems in the process of solving those problems in the next three sub-sections. All three problems involve uniform temperature change but different boundary support conditions: one-dimensional in-plane deformation restraint and two-dimensional in-plane deformation restraint. Also, combined uniform temperature change and mechanical loading is addressed in which a lateral in-plane mechanical force develops because of the Poisson effect and the one-dimensional in-plane deformation restraint.

Éléments sous droits d'auteur

3.7.5 Buckling under Uniform Temperature Change of a Uniaxially In-Plane Restrained Simply Supported Plate

Consider a rectangular plate that is simply supported on all four edges, but in different manners as in Figure 3-91. There, restraint of in-plane movement exists only in the x-direction with S3 boundary conditions on edges $x = 0$ and $x = a$. Thus, a compressive thermal force is developed in the x-direction when heat is applied. However, the plate is supported with S2 boundary conditions on edges $y = 0$ and $y = b$. Thus, no mechanical force, N_x, can be applied (unless by screw-type loading followed by heating) nor can any thermal force develop in the y-direction from heating. Although N^T appears in the equation for N_y, no force can

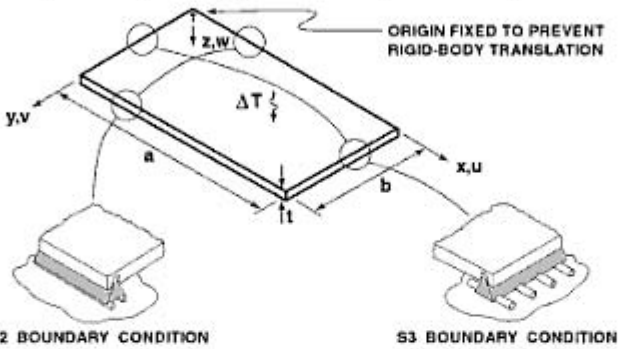


Figure 3-91 A Uniaxially In-Plane Restrained Simply Supported Rectangular Plate Subjected to Uniform Temperature Change

develop in the y-direction. Also, N_{xy} does not exist. Another, perhaps more direct, yet incomplete, manner of perceiving the in-plane plate support conditions is depicted in Figure 3-92 where the permissible in-plane movements are shown. Thus, ΔT causes force but no displacement in the x-direction and displacement but no force in the y-direction. The in-plane boundary conditions are IP3 on $x = 0$ and $x = a$ plus IP2 on $y = 0$ and $y = b$. Thus, a plate with fixed edges C3 and C2 on the respective sides has the same in-plane movement and, thus, the same prebuckling force distributions, but a higher $\overline{\Delta T}$ at buckling.

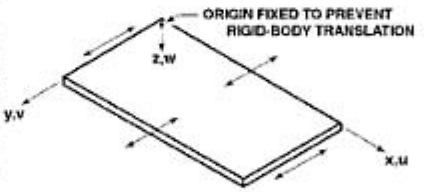


Figure 3-92 Possible In-Plane Movement of a Uniaxially In-Plane Restrained Simply Supported Rectangular Plate

First, we must find the linear prebuckling (equilibrium) force state. The force-strain and force-displacement relations are

Éléments sous droits d'auteur

$$N_x = A(\varepsilon_x + \nu\varepsilon_y) - N^T = A(u_x + \nu v_y) - N^T$$
$$N_y = A(\varepsilon_y + \nu\varepsilon_x) - N^T = A(v_y + \nu u_x) - N^T \tag{3.398}$$

in which N_x and N_y are positive in tension and

$$N^T = \frac{E}{1-\nu}\int \alpha\,\Delta T\,dz = \frac{E}{1-\nu}\,\alpha\,\Delta T\,t \tag{3.399}$$

for the case of a uniform temperature change through the plate thickness (positive ΔT for heating leading to compressive N_x and N_y). Moreover, ΔT and hence N^T are constant over the plate area. The boundary conditions are $u = 0$ at $x = 0$ and $x = a$, as well as for all x (and y), in addition to $v = 0$ at $y = 0$, but v is unrestrained (and a function of ΔT) at $y = b$. Thus, $N_y = 0$ at $y = 0$ and $y = b$. Then, the force-strain relations become

$$N_x = A\nu v_y - N^T \tag{3.400}$$

$$0 = Av_y - N^T \tag{3.401}$$

so that from Equation (3.401)

$$v_y = \frac{N^T}{A} \tag{3.402}$$

Thus, with substitution of Equation (3.402) in Equation (3.400), the prebuckling in-plane forces are

$$N_x = A\nu\frac{N^T}{A} - N^T = -(1-\nu)N^T = -E\alpha\Delta T\,t$$
$$N_y = 0 \tag{3.403}$$

so the condition of zero force in the y-direction coexists with a compressive force for a positive ΔT (heating) in the x-direction plus no displacement in the x-direction and some expansion in the y-direction. Note that N_x is reduced by the factor $1 - \nu$ from the nominal thermal force N^T.

The buckling differential equation for a uniformly heated plate that remains flat until buckling occurs (no thermal moment) is

$$D\nabla^4\delta w + N_x\delta w_{,xx} + N_y\delta w_{,yy} + 2N_{xy}\delta w_{,xy} = 0 \tag{3.404}$$

However, for this plate, the prebuckling force is (positive in compression)

$$\bar{N}_x = E\,\alpha\,t\,\bar{\Delta T} \tag{3.405}$$

plus $\bar{N}_y = 0$ and $\bar{N}_{xy} = 0$, so the differential equation becomes

$$D\nabla^4\delta w + E\,\alpha\,t\,\bar{\Delta T}\,\delta w_{,xx} = 0 \tag{3.406}$$

subject to the buckling displacement boundary conditions

$$\delta w(0,y) = \delta w(a,y) = 0$$
$$\delta w(x,0) = \delta w(x,b) = 0 \tag{3.407}$$

and to the variation in curvature boundary conditions from the variation in moment boundary conditions

$$\delta w_{,xx}(0,y) = \delta w_{,xx}(a,y) = 0$$
$$\delta w_{,yy}(x,0) = \delta w_{,yy}(x,b) = 0 \tag{3.408}$$

Éléments sous droits d'auteur

The buckling displacement with indeterminate amplitude, $\bar{w}$,

$$\delta w = \bar{w} \sin \frac{m\pi x}{a} \sin \frac{n\pi y}{b} \tag{3.409}$$

satisfies both the homogeneous differential equation and the homogeneous boundary conditions (which constitute an eigenvalue problem) if

$$E \alpha t \frac{\overline{\Delta T}}{D} = \frac{\pi^2}{\left[\frac{m}{a}\right]^2} \left[\left[\frac{m}{a}\right]^2 + \left[\frac{n}{b}\right]^2 \right]^2 \tag{3.410}$$

in the same manner as $\bar{N}_x$ for a uniaxially loaded plate was found in Section 3.3.1. Note that Equation (3.410) always is of least value when $n = 1$ (by observation of the form of Equation (3.410). Thus, the plate always buckles in one half-sine wave in the y-direction), and Equation (3.410) can then be rearranged to read

$$k_T = \frac{12}{\pi^2} (1 - \nu^2) \alpha \overline{\Delta T} \left[\frac{b}{t}\right]^2 = \left[m \frac{b}{a} + \frac{1}{m} \frac{a}{b} \right]^2 \tag{3.411}$$

These results are shown in abbreviated form for square plates by Parkes [3-54] and for rectangular plates by Boley and Weiner [3-57]. The results for Equation (3.411) are plotted in Figure 3-93 as a function of the plate aspect ratio, a/b. Obviously, from the left-hand side of Equation (3.411), the higher the coefficient of thermal expansion for a material, the lower the change in temperature to cause thermal buckling. Also, the thinner the plate, the lower the thermal buckling load. These conclusions are in agreement with our intuition. Figure 3-93 is identical to the mechanical buckling load result for N_x in Figure 3-18 on page 268 when k_T is set equal to k. That is, the same festooned curves exist for various values of m. The lower limit of both behaviors is $k_T = 4$ and $k = 4$ at integer values of a/b. Both $k_T = 4$ and $k = 4$ are reasonable lower bounds to use

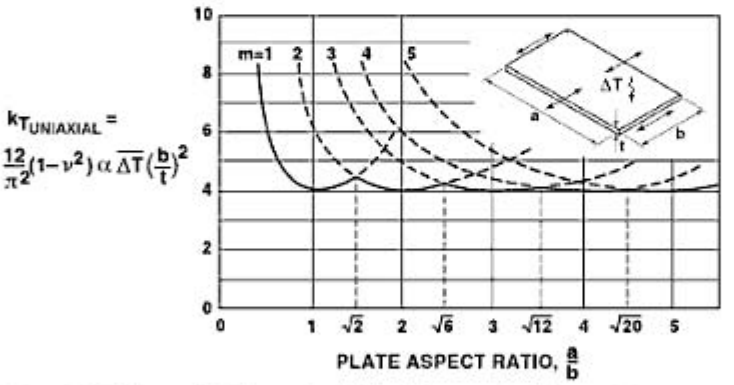


Figure 3-93 Thermal Buckling under Uniform Temperature Change of a Uniaxially In-Plane Restrained Simply Supported Rectangular Plate with Variable Plate Aspect Ratio, a/b

Éléments sous droits d'auteur

for the buckling loads in design (any slight increase in buckling load for noninteger values of a/b is hardly justifiable to rely upon when the behavior is obviously very close to $k_T = 4$ and $k = 4$).

Wilcox and Clemmer addressed simply supported plates with in-plane springs normal to each edge and no tangential restraint as in Figure 3-94, i.e., in-plane normal spring restraint on all four edges instead of on just two edges as in Figure 3-80 on page 368 [3-58]. Their thermal buckling load for the mode m = 1 and, of course, n = 1 is

$$\alpha\overline{\Delta T} = \frac{\dfrac{\pi^2}{12(1-\nu^2)}\left[\dfrac{t}{a}\right]^2\left[1+\left[\dfrac{a}{b}\right]^2\right]^2\left[\left[1+\dfrac{2E}{k_x a}\right]\left[1+\dfrac{2E}{k_y b}\right]-\nu^2\right]}{\left[1+\left[\dfrac{a}{b}\right]^2\right](1+\nu)+\dfrac{2E}{k_y b}+\left[\dfrac{a}{b}\right]^2\dfrac{2E}{k_x a}} \qquad (3.412)$$

For normal springs only in the x-direction ($k_y = 0$) and with those springs having infinite stiffness, $k_x = \infty$, to achieve perfect in-plane x-direction restraint, Equation (3.412) reduces to the present solution, Equation (3.411). Thus, Equation (3.411) agrees with the results of Wilcox and Clemmer for the m = 1, n = 1 buckling mode [3-58], but they do not obtain results for higher buckling modes, i.e., higher values of m are necessary for their results to be valid beyond $a/b = \sqrt{2}$ in Figure 3-93.

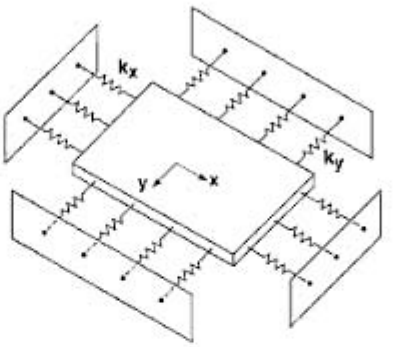


Figure 3-94 Plate with In-Plane Normal Springs on all Edges and No Tangential Restaint

The ordinate of Figure 3-93 (the left side of Equation (3.411)), k_T, is four (from the right-hand side of Equation (3.411)) when the plate aspect ratio, a/b, is any integer (including infinity) and m = a/b. As a numerical example, we solve for $\overline{\Delta T}$ from Equation (3.411) for integer a/b for a 6061-T6 aluminum plate with material properties $E = 10\text{x}10^6$ psi (70 GPa), $\alpha = 13.1\text{x}10^{-6}/°F$ ($23.6\text{x}10^{-6}/°C$), $\nu_e = .32$, and $\sigma_y = 35\text{x}10^3$ psi (240 MPa) (note that σ_y is the yield stress of the material, not the stress in the y-direction). For these room-temperature material properties, we get

$$\overline{\Delta T} = \frac{4}{\dfrac{12}{\pi^2}(1-\nu^2)\alpha\left[\dfrac{b}{t}\right]^2} = 2.798\text{x}10^5\ °F\ (1.554\text{x}10^5\ °C)\left[\frac{t}{b}\right]^2 \qquad (3.413)$$

Nemeth's results for infinitely long, laminated composite plates with thermal restraint only in the x-direction can be shown to reduce to this

Éléments sous droits d'auteur

solution, i.e., Equation (3.413) [3-59]. Numerical results are displayed to three or four significant figure accuracy even though the accuracy of the input data do not warrant such high implied accuracy. The variation of $\overline{\Delta T}$ with plate side-length-to-thickness ratio, b/t, for integer a/b is shown in Figure 3-95. For b/t = 100, the $\overline{\Delta T}$ for buckling is 28.0°F (15.6°C). However, it is unlikely that a plate that thin would be truly flat before thermal loading, so the plate would probably have an imperfection that would mean the plate is bent prior to any heating. Thus, the plate would behave in a manner similar to the nonuniformly heated bar in Section 2.9.4, i.e., the plate would immediately bend, bow, or curl with the imposition of any heat whatsoever. For b/t = 50, the $\overline{\Delta T}$ for buckling is 111.9°F (62.17°C). Finally, for b/t = 10, the $\overline{\Delta T}$ for buckling is 2798°F (1554°C). Such a thick plate would certainly require a very significant correction for the influence of material property degradation with elevated temperature and for the influence of extensive plastic deformation, not to mention the fact that the plate has long since melted with such a large $\overline{\Delta T}$ (so some correction must be made)! The compressive stress in the x-direction corresponding to $\overline{\Delta T}$ is $\sigma_x = -E\alpha\overline{\Delta T}$ with no stress in the y-direction. Thus, at yielding, $\overline{\Delta T}$ takes on the value

$$\overline{\Delta T}_y = \frac{\sigma_y}{E\alpha} = 267°F\ (148°C) \tag{3.414}$$

at b/t = 32.4. Above this value of $\overline{\Delta T}$, the thermal buckling results must be modified to account for plastic deformation (see Section 3.8, Effect of Plastic Deformation) and to account for decreasing E with increasing temperature, not to mention changing ν and α. Below $\overline{\Delta T}_y$, the elastic behavior is nearly valid. For example, for a plate with b/t = 60, $\overline{\Delta T}$ = 77.7°F (43.2°C).

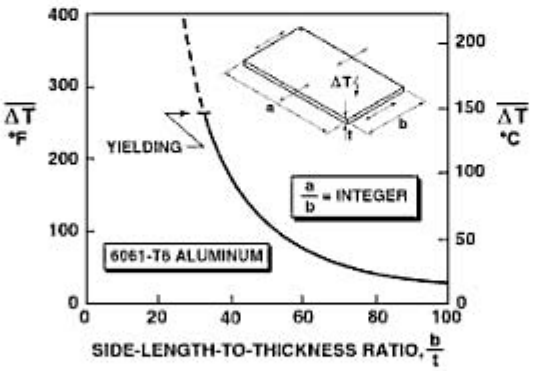


Figure 3-95 Thermal Buckling under Uniform Temperature Change of a Uniaxially In-Plane Restrained Simply Supported Rectangular Plate with Variable Side-Length-to-Thickness Ratio, b/t

Éléments sous droits d'auteur

3.7.6 Buckling under Uniform Temperature Change of a Biaxially In-Plane Restrained Simply Supported Plate

Consider a rectangular plate that is simply supported at all four edges with boundary condition S1 as in Figure 3-96. Alternatively, all four edges could have boundary condition S3 with a single fixed point to prevent rigid-body movement. Because of the complete in-plane restraint, the plate develops compressive in-plane forces in the x- and y-directions when heated uniformly throughout its volume. The plate is immovable in its plane, i.e., the plate cannot expand in area. However, the plate has freedom to rotate about its edges when it bends or buckles.

First, we must find the linear prebuckling (equilibrium) force state. No movement is permited in either the x- or y-direction, so heating causes compressive thermal stresses in both directions. The equilibrium stress and displacement solution is easily obtained as

$$\sigma_x = \sigma_y = -\frac{E}{1-\nu}\alpha\Delta T$$
$$u = v = w = 0 \qquad (3.415)$$

so that as heating increases, the compressive stresses increase. However, the strains and displacements are identically zero. The forces are

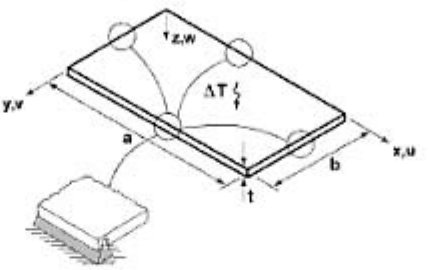


Figure 3-96 A Biaxially In-Plane Restrained Simply Supported Rectangular Plate Subjected to Uniform Thermal Loading

$$N_x = A(\varepsilon_x + \nu\varepsilon_y) = A(u_x + \nu v_y) - N^T$$
$$N_y = A(\varepsilon_y + \nu\varepsilon_x) = A(v_y + \nu u_x) - N^T \qquad (3.416)$$

in which

$$N^T = \frac{E}{1-\nu}\int \alpha\,\Delta T\,dz = \frac{E}{1-\nu}\,\alpha\,\Delta T\,t \qquad (3.417)$$

for the case of a uniform temperature change through the plate thickness. Moreover, N^T is constant over the plate area. The boundary conditions are $u = 0$ at $x = 0$ and $x = a$ (as well as for all x and y) in addition to $v = 0$ at $y = 0$ and $y = b$ (as well as for all x and y). Thus, $u_x = v_y = 0$, so

$$N_x = -N^T$$
$$N_y = -N^T \qquad (3.418)$$

The buckling differential equation for a uniformly loaded plate is

$$D\nabla^4\delta w + \bar{N}_x\delta w_{,xx} + \bar{N}_y\delta w_{,yy} + 2\bar{N}_{xy}\delta w_{,xy} = 0 \qquad (3.419)$$

However, the compressive prebuckling in-plane forces are

$$\bar{N}_x = \bar{N}_y = -N_x = -N_y = \frac{E\,\alpha\,t}{1-\nu}\,\Delta T \qquad (3.420)$$

Éléments sous droits d'auteur

and $\bar{N}_{xy} = 0$, so the buckling differential equation becomes

$$D\nabla^4 \delta w + \frac{E\,\alpha\,t}{1-\nu}\,\overline{\Delta T}\,[\delta w_{,xx} + \delta w_{,yy}] = 0 \tag{3.421}$$

subject to the buckling displacement boundary conditions

$$\begin{aligned} \delta w(0,y) &= \delta w(a,y) = 0 \\ \delta w(x,0) &= \delta w(x,b) = 0 \end{aligned} \tag{3.422}$$

and to the variation in curvature boundary conditions (obtained from the variation in moment boundary conditions)

$$\begin{aligned} \delta w_{,xx}(0,y) &= \delta w_{,xx}(a,y) = 0 \\ \delta w_{,yy}(x,0) &= \delta w_{,yy}(x,b) = 0 \end{aligned} \tag{3.423}$$

The buckling displacement with indeterminate amplitude, $\bar{w}$,

$$\delta w = \bar{w} \sin\frac{m\pi x}{a} \sin\frac{n\pi y}{b} \tag{3.424}$$

satisfies both the homogeneous differential equation and the homogeneous boundary conditions (which constitute an eigenvalue problem) if

$$\frac{E\,\alpha\,t}{1-\nu}\,\frac{\overline{\Delta T}}{D} = \pi^2\left[\left[\frac{m}{a}\right]^2 + \left[\frac{n}{b}\right]^2\right] \tag{3.425}$$

which can be rearranged as

$$\frac{12(1+\nu)}{\pi^2}\,\alpha\,\overline{\Delta T}\left[\frac{b}{t}\right]^2 = m^2\left[\frac{b}{a}\right]^2 + n^2 \tag{3.426}$$

for which the lowest buckling load occurs at $m = 1$, $n = 1$ (all higher mode buckling occurs at far higher values of the right-hand side and hence a higher ΔT). These results are shown in abbreviated form for square plates by Parkes [3-54] and for rectangular plates by Boley and Weiner [3-57] as well as in more extensive form by Thornton [3-60]. Equation (3.426) agrees with Wilcox and Clemmer's results when their in-plane elastic spring constants are set to infinity in Equation (3.412) on page 382 [3-58]. For plates that are infinitely long in the x-direction, Equation (3.426) with right-hand side equal to one also agrees with Nemeth's results [3-61]. The results for Equation (3.426) are plotted in Figure 3-97 as a function of the plate aspect ratio, a/b. Obviously, from the left-hand side of Equation (3.426), the higher the coefficient of thermal expansion for a material, the lower the change in tem-

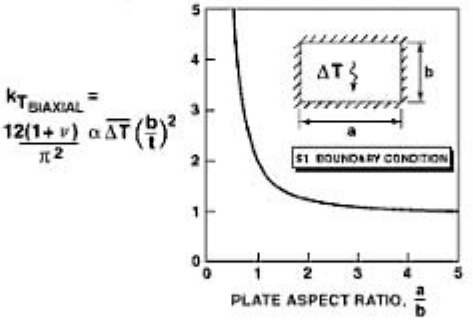


Figure 3-97 A Biaxially In-Plane Restrained Simply Supported Rectangular Plate with Variable Plate Aspect Ratio, a/b under Uniform Temperature Change

Éléments sous droits d'auteur

perature needed to cause thermal buckling. Also, the thinner the plate, the lower the thermal buckling load in agreement with our intuition.

As a numerical example, consider a square 6061-T6 aluminum plate with properties $\alpha = 13.1\text{x}10^{-6}/°\text{F}$ $(23.6\text{x}10^{-6}/°\text{C})$ and $\nu = .32$ with various side-length-to-thickness ratios. Solve for $\overline{\Delta T}$ from Equation (3.426):

$$\overline{\Delta T} = \frac{2}{\frac{12}{\pi^2}(1+\nu)\,\alpha\left[\frac{b}{t}\right]^2} = 9.513\text{x}10^{4}\ °\text{F}\ (5.285\text{x}10^{4}\ °\text{C})\left[\frac{t}{b}\right]^2 \qquad (3.427)$$

The variation of $\overline{\Delta T}$ with plate width-to-thickness ratio, b/t, is shown in Figure 3-98. For b/t = 100, $\overline{\Delta T}$ is 9.5°F (5.3°C). However, it is unlikely that a plate that thin would be truly flat before thermal loading, i.e., the plate would probably have an imperfection that would cause the plate to be bent prior to any heating. Thus, the plate would behave in a manner similar to the nonuniformly heated bar in Section 2.9.5, i.e., the plate would bow, bend, or curl with the imposition of the slightest heating. For b/t = 50, $\overline{\Delta T}$ is 38.0°F (21.1°C). For the biaxial stress state in Equation (3.415) on page 384, the stress intensity $\sigma_i = \left[\sigma_x^2 + \sigma_y^2 - \sigma_x\sigma_y + 3\tau_{xy}^2\right]^{1/2}$ from Equation (3.452) on page 409 in Section 3.8 on effect of plastic deformation takes on the value $\sigma_i = E\alpha\Delta T/(1-\nu)$, so

$$\overline{\Delta T}_y = \frac{1-\nu}{E}\,\frac{\sigma_y}{\alpha} = 181.7°\text{F}\ (100.9°\text{C}) \qquad (3.428)$$

which corresponds to b/t = 22.9 and which is about 70% of the yield temperature if the plate is only uniaxially restrained. Above the yielding $\overline{\Delta T}$ (and below the yielding b/t), inelastic effects, changes in material properties such as E, α, and ν, plus changes in state such as melting must be considered. Finally, for b/t = 10, $\overline{\Delta T}$ is 951°F (528°C) for which the aluminum is above yielding and surely must verge upon melting, so the present elastic calculation is not reliable.

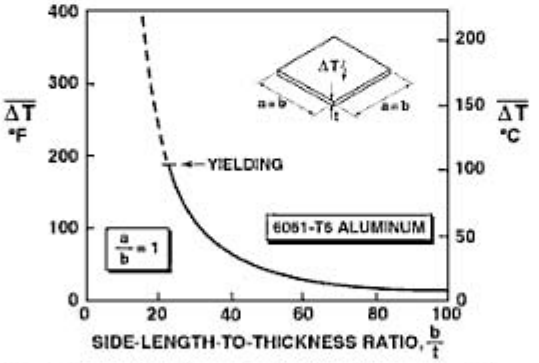


Figure 3-98 Thermal Buckling under Uniform Temperature Change of a Biaxially In-Plane Restrained Simply Supported Square Plate with Variable Side-Length-to-Thickness Ratio, b/t

Éléments sous droits d'auteur

3.7.7 Buckling of a Uniaxially In-Plane Restrained Plate under Uniform Temperature Change and Mechanical Load

3.7.7.1 Introduction

Loading on a plate can be uniaxial or biaxial mechanical loading as discussed in Section 3.3.3 or essentially mechanical in one direction and thermal in the perpendicular direction as we saw for aircraft panels in Section 3.7.3. Or, with screw-type mechanical loading, both thermal and mechanical loading can co-exist in the same direction. We will address only the problem of mechanical loading in one direction and thermal loading in the perpendicular direction because simultaneous mechanical and thermal loading is easily treated given that their total value (sum) in one direction is identical to the buckling load for that direction.

A plate under biaxial mechanical loading can buckle when the compressive load in one direction is more than the uniaxial buckling load in that direction if the load in the direction transverse to the compressive load is tensile. That is, tensile loading in one direction has a stiffening effect against buckling of the plate that is compressively loaded in the transverse direction as we see in Section 3.3.3. Similarly, cooling of an appropriately restrained plate has a stiffening effect against buckling of a plate under uniaxial compressive load. The key factor is the boundary conditions on all four edges including the in-plane restraint provided in addition to the obvious influence of the edge rotational restraint for a clamped-edge plate or lack thereof for a simply supported plate. The buckling criterion for biaxial loading of a simply supported plate is

$$\bar{N}_x\left(\frac{m\pi}{a}\right)^2+\bar{N}_y\left(\frac{n\pi}{b}\right)^2=D\left[\left(\frac{m\pi}{a}\right)^2+\left(\frac{n\pi}{b}\right)^2\right]^2 \qquad (3.429)$$

in which $\bar{N}_x$ and $\bar{N}_y$ are positive in compression is well known (see Timoshenko and Gere [3-8] and Section 3.3.3). The approach for thermal buckling problems is to identify the plate in-plane edge boundary conditions, determine the prebuckling equilibrium state, N_x and N_y, that is consistent with the boundary conditions, and finally to find the plate buckling load from Equation (3.429). The prebuckling equilibrium state, N_x and N_y, arises from either thermal or mechanical loading or both. The specific process will be described for buckling under combined thermal and mechanical loading with uniaxial in-plane restraint such that a thermally induced in-plane force is developed. These results were obtained by Jones [3-62, 3-63].

3.7.7.2 Manner of Load Introduction

To study how plates buckle under combined thermal and mechanical loading, let's first examine a generic concept for how a plate is loaded. We expect to be able to apply both in-plane mechanical forces as well as temperature changes that induce in-plane forces on plates because of various restraint conditions that prevent or diminish free thermal expansion, e.g., immovable in-plane supports or springs, respectively. We can sometimes treat the two types of loading somewhat independently,

Éléments sous droits d'auteur

although we must be certain that we do not violate any conditions or constraints on the problem.

Consider a rectangular plate to which is applied an in-plane force (per unit width), N_x, and a uniform temperature change, ΔT. We can apply the two loadings simultaneously, or sometimes we can apply them in sequence, but the order of load application in that sequence is often crucial. The simultaneous application of the two loads in a constant proportion to one another throughout the entire load-application process is usually called 'radial loading' or 'proportional loading'. For example, suppose we load radially with N_x and ΔT in some fixed proportion,

$$s = \frac{\Delta T}{N_x} \tag{3.430}$$

as in load path OB in Figure 3-99. Note that the value of $\overline{N}_x$ at B is above the buckling load for ΔT alone, i.e., entirely without N_x. Thus, if the loading is not radial or proportional, then we cannot load from O to A' (anticipating a next load path of A' to B) because the plate buckles at the buckling temperature change for no axial load applied and, hence, cannot reach point A'. Alternatively, we can load from O to A without difficulty (no buckling occurs under axial tension) and then from A to B by adding heat also without difficulty until buckling occurs at B. Of course, we could load along any path from O to B as long as we do not impose a load that would cause buckling by itself, i.e., that would cross the buckling boundary (as defined on pages 270–271), before B is reached. The basis for this observation is the fact that applying axial tension to the plate increases the ability of the plate to withstand forces that would otherwise cause buckling. This concept was demonstrated for biaxial mechanical loading by Timoshenko and Gere [3-8] and more extensively in Section 3.3.3 with information about the buckling boundary and mode shape changes.

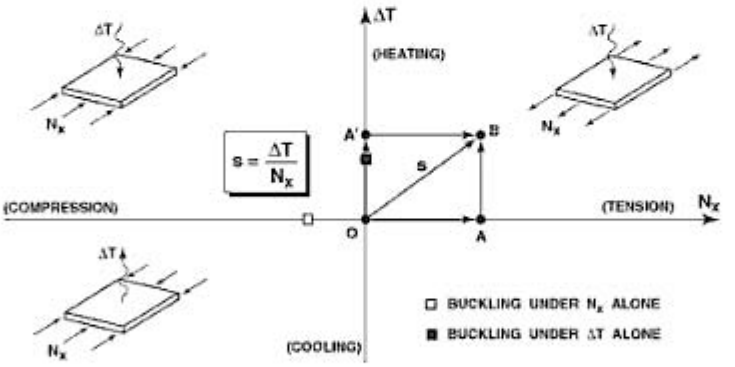


Figure 3-99 Buckling under Proportional and Nonproportional Simultaneous Thermal and Mechanical Loading

Éléments sous droits d'auteur

3.7.7.3 Buckling Differential Equation and Solution

Consider a rectangular plate that is simply supported at all four edges with boundary condition S3 on two opposite edges $y = 0$ and $y = b$, boundary condition S1 on the edge $x = 0$, and boundary condition S2 on the edge $x = a$ as shown in Figure 3-100. Restraint of movement exists only in the y-direction (in addition to the obvious lack of movement at $x = 0$), so the plate develops in-plane thermal force in the y-direction when heated uniformly throughout its volume. Moreover, in-plane compressive force, $N_x = -N$, a mechanical force, is applied in the x-direction

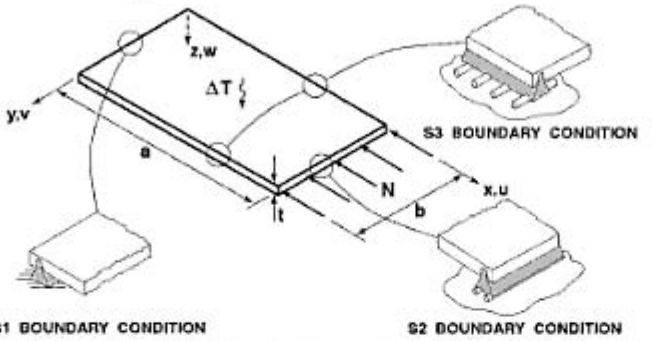


Figure 3-100 A Uniaxially In-Plane Restrained Simply Supported Rectangular Plate Subjected to Uniform Thermal Loading and N_x

and, because of the Poisson effect and in-plane y-direction restraint, causes a lateral in-plane force, $N_y = \nu N_x = -\nu N$. Another, perhaps more direct yet incomplete, manner of perceiving the in-plane plate support conditions is depicted in Figure 3-101 where the permissible in-plane movements are clearly shown.

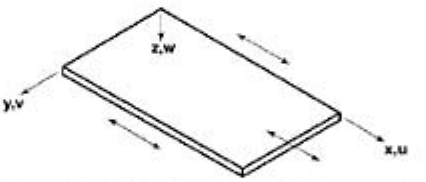


Figure 3-101 Possible In-Plane Movement of a Uniaxially In-Plane Restrained Simply Supported Rectangular Plate

First, we must find the linear prebuckling (equilibrium) force state noting that ΔT is constant throughout the plate volume. The thermal loading ΔT causes force but no strain in the y-direction and strain but no force in the x-direction. The applied compressive mechanical load, N, causes compressive force in the x-direction and, again by virtue of the Poisson effect and the restraint in the y-direction, compressive force in the y-direction. The force-strain relations are

$$\begin{aligned} N_x &= A(\varepsilon_x + \nu\varepsilon_y) = A(u_x + \nu v_y) - N^T \\ N_y &= A(\varepsilon_y + \nu\varepsilon_x) = A(v_y + \nu u_x) - N^T \end{aligned} \tag{3.431}$$

Éléments sous droits d'auteur

in which

$$N^T = \frac{E}{1-\nu}\int \alpha\,\Delta T\,dz = \frac{E}{1-\nu}\,\alpha\,\Delta T\,t \tag{3.432}$$

for the case of uniform temperature change through the plate thickness. Moreover, ΔT, and hence N^T, is constant over the plate area. The boundary conditions are $u = 0$ at $x = 0$, $u =$ unspecified at $x = a$ (with $N_x = -N$) along with $v = 0$ at $y = 0$ and $v = 0$ at $y = b$, and, indeed, $v = 0$ for all x and y. Thus, $v_y = 0$, so

$$-N = Au_x - N^T \tag{3.433}$$

$$N_y = Av u_x - N^T \tag{3.434}$$

Solve for u_x from Equation (3.433):

$$u_x = \frac{1}{A}(-N + N^T) \tag{3.435}$$

so from Equations (3.434) and (3.435),

$$N_y = Av\left[\frac{1}{A}(-N + N^T)\right] - N^T = -\nu N - (1-\nu)N^T \tag{3.436}$$

in which we see that both terms in N_y are compressive as they must be if ΔT is positive (heating). Finally, the prebuckling state of loading with positive compressive force, N, is

$$\begin{aligned} N_x &= -N \\ N_y &= -\nu N - (1-\nu)N^T \end{aligned} \tag{3.437}$$

The buckling differential equation for a uniformly loaded plate that remains flat prior to buckling is

$$D\nabla^4\delta w + \bar{N}_x\delta w_{,xx} + \bar{N}_y\delta w_{,yy} + 2\bar{N}_{xy}\delta w_{,xy} = 0 \tag{3.438}$$

However, for this plate,

$$\bar{N}_x = -N_x = N \qquad \bar{N}_y = -N_y = \nu N + (1-\nu)N^T = \nu N + E\alpha\Delta T t \tag{3.439}$$

plus $\bar{N}_{xy} = 0$, so the buckling differential equation becomes

$$D\nabla^4\delta w + \bar{N}_x\delta w_{,xx} + (\nu N + E\,\alpha\,\Delta T\,t)\delta w_{,yy} = 0 \tag{3.440}$$

subject to the buckling displacement boundary conditions

$$\begin{aligned} \delta w(0,y) &= \delta w(a,y) = 0 \\ \delta w(x,0) &= \delta w(x,b) = 0 \end{aligned} \tag{3.441}$$

and to the equivalent of the variation in moment buckling boundary conditions (the variation in curvature buckling boundary conditions)

$$\begin{aligned} \delta w_{,xx}(0,y) &= \delta w_{,xx}(a,y) = 0 \\ \delta w_{,yy}(x,0) &= \delta w_{,yy}(x,b) = 0 \end{aligned} \tag{3.442}$$

The buckling displacement (with indeterminate amplitude, $\tilde{w}$)

$$\delta w = \tilde{w}\sin\frac{m\pi x}{a}\sin\frac{n\pi y}{b} \tag{3.443}$$

satisfies both the homogeneous differential equation and the homogeneous boundary conditions (which constitute an eigenvalue problem) if

Éléments sous droits d'auteur

$$\frac{\bar{N}_x b^2}{\pi^2 D}\left[\frac{m}{a}\right]^2+\frac{\nu N+E\alpha\overline{\Delta T}t}{\pi^2 D}n^2=b^2\left[\left[\frac{m}{a}\right]^2+\left[\frac{n}{b}\right]^2\right]^2 \tag{3.444}$$

which, if $\nu = 0$ (to eliminate N from the term on n^2), can be rearranged to

$$\frac{\bar{N}_x b^2}{\pi^2 D}\left[\frac{b}{a}\right]^2 m^2+\frac{12}{\pi^2}\alpha\overline{\Delta T}\left[\frac{b}{t}\right]^2 n^2=\left[\left[\frac{b}{a}\right]^2 m^2+n^2\right]^2 \tag{3.445}$$

The complicating factor of the Poisson's ratio in Equation (3.444) signifies that a mechanical load in the x-direction causes a reactive force in the y-direction even when there is no temperature change in the plate (see problem 3.3.3.6 on page 279). In the present numerical results for the special case in which $\nu = 0$, that reactive force does not exist, so only part of the general topic problem is addressed. However, this approach enables us to study the heart of the problem without the detailed complexities of the reactive force in the y-direction caused by mechanical load. Equation (3.445) reduces to (1) Equation (3.183) on page 267 for uniaxial mechanical loading with no lateral restraint because $\nu = 0$ and to (2) Equation (3.410) on page 381 for thermal buckling with uniaxial restraint and $\nu = 0$.

From the left-hand side of Equation (3.445), obviously the higher the coefficient of thermal expansion for a material, the lower the change in temperature must be to cause thermal buckling. Also, the thinner the plate, the lower the thermal buckling load. Moreover, if the plate is cooled, then the value of N_x under combined mechanical and thermal loading exceeds N_x when N acts alone! In addition, a tensile N_x increases the amount of heating a plate can withstand without buckling. These conclusions are consistent with our intuition.

3.7.7.4 Results and Discussion

All results are for square plates made of a material with $\nu = 0$ [to eliminate N from the term on n^2 in Equation (3.444)] and subjected to spatially uniform temperature change, ΔT, and uniform load per unit width in the x-direction, N_x. The results are conveniently separated into those predominantly in the first quadrant of a normalized ΔT versus N_x plot (with results also in the second quadrant) and those predominantly in the third quadrant of a normalized ΔT versus N_x plot. The normalization is $E\alpha\Delta T t b^2/\pi^2 D$ for ΔT and the usual $N_x b^2/\pi^2 D$ for N_x. The slope of a proportional or radial loading line on the normalized plot is therefore

$$s=\frac{E\alpha\Delta T t}{N_x} \tag{3.446}$$

in a similar manner to that for buckling of plates under biaxial mechanical loading. All buckling behavior is symmetric about the loading line with slope $s = -1$. Note that buckling cannot occur for thermal and mechanical loading in the fourth quadrant of the normalized ΔT versus N_x plot because biaxial in-plane tension does not cause buckling.

Éléments sous droits d'auteur

3.7.7.4.1 Behavior for Heating and Tensile N_x

In the first quadrant of a normalized ΔT versus N_x plot, applying a tensile N_x enables the plate to withstand significantly higher temperatures without buckling than without any N_x as shown in Figure 3-102. This stiffening effect of axial tension is well-known from the study of biaxial mechanical loading. Ever greater values of tensile N_x are required to achieve the tensile N_x stiffening effect against buckling as the buckling mode shape, (m,n), changes with increasing n. The buckling mode shape changes from (m = 1, n = 1) to (m = 1, n = 2) to (m = 1, n = 3) to ... as N_x and ΔT increase. For the proportional loading slope of s = 1, ΔT is positive (heating) and N_x is also positive (tension) such that we get $E\alpha\Delta Tt = N_x$. The buckling mode shape changes from (m = 1, n = 1) to (m = 1, n = 2) at coordinates (3, 7) at a loading slope of s = 7/3. Further, the buckling mode shape changes from (m = 1, n = 2) to (m = 1, n = 3) at coordinates (35, 15) at a loading slope of s = 3/7.

3.7.7.4.2 Behavior for Heating and Compressive N_x

In the second quadrant, the buckling behavior varies from that of a uniaxially compressed square plate at the proportional loading slope of s = 0 (the negative $N_x b^2/\pi^2 D$ axis) to that of a uniaxially restrained, heated plate at the loading slope of $s = \infty$ (the positive $E\alpha\Delta Tb^2/\pi^2 D$ axis) in Figure 3-102. Between the two limits, the buckling mode shape is always (m = 1, n = 1) (one-half sine buckle wave in each direction), so the interaction curve is linear. For the loading slope of s = – 1, ΔT is positive (heating) and N_x is negative (compression) such that $E\alpha\Delta Tt = -N_x$.

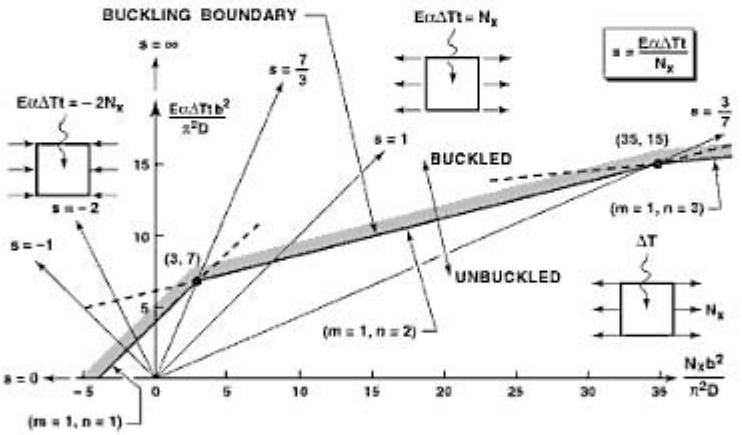


Figure 3-102 Buckling of a Square Plate Restrained from Movement in the y-Direction under Combined Axial Force N_x and Temperature Change ΔT with Poisson's Ratio: ν = 0
Quadrant I: Tensile Force and Heating;
Quadrant II: Compressive Force and Heating

Éléments sous droits d'auteur

3.7.7.4.3 Behavior for Cooling and Compressive N_x

In the third quadrant of a normalized ΔT versus N_x plot, cooling enables the plate to withstand significantly higher compressive force N_x without buckling than without any temperature change as shown in Figure 3-103. This stiffening effect of cooling is analogous to the well-known stiffening effect of lateral tension from the study of biaxial mechanical loading in Section 3.3.3. Ever greater values of cooling are required to achieve the cooling stiffening effect against buckling as the buckling mode shape, (m,n), changes with increasing m. The buckling mode shape changes from (m = 1, n = 1) to (m = 2, n = 1) to (m = 3, n = 1) to ... as N_x gets larger in compression ($-N_x$) and ΔT decreases (cools). The buckling

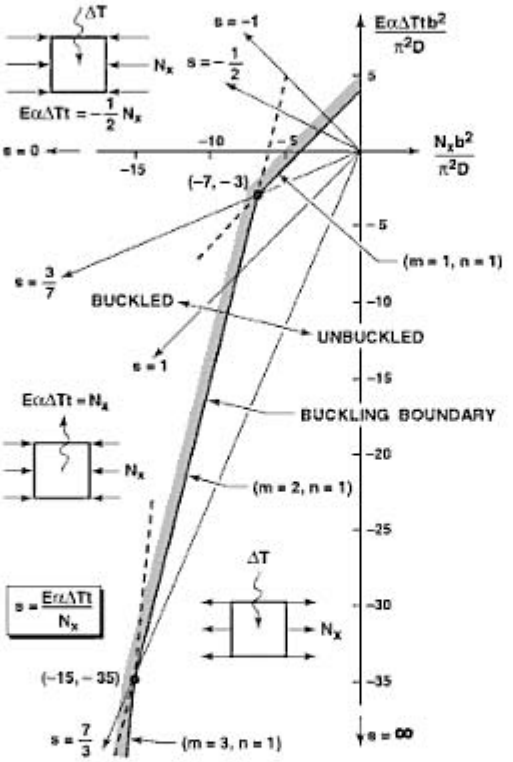


Figure 3-103 Buckling of a Square Plate Restrained from Movement in the y-Direction under Combined Axial Force N_x and Temperature Change ΔT with Poisson's Ratio: $\nu = 0$
Quadrant II: Compressive Force and Heating;
Quadrant III: Compressive Force and Cooling

Éléments sous droits d'auteur

mode shape changes from (m = 1, n = 1) to (m = 2, n = 1) at coordinates (−7, −3) at a proportional loading slope of s = 3/7. Further, the buckling mode shape changes from (m = 2, n = 1) to (m = 3, n = 1) at coordinates (−15, −35) at a loading slope of s = 7/3.

3.7.7.4.4 Nonproportional Loading

Nonproportional loading for combined thermal and mechanical loading is possible just as it is for buckling under biaxial mechanical loading as in Section 3.3.3. First, a compressive force that is either more or less than the uniaxial force necessary to cause buckling can be specified. Then, the corresponding cooling or heating, respectively, necessary to cause buckling under combined thermal and mechanical loading can be found. Alternatively, a temperature change that is either more or less than that necessary to cause thermal buckling alone can be specified. Then, the uniaxial force necessary to cause buckling under combined thermal and mechanical loading can be found.

For example, if a normalized axial force of $N_x b^2/\pi^2 D = -2$ (axial compression) is specified, then $E\alpha\Delta T t b^2/\pi^2 D$ is found to be +2 (heating). If a normalized axial force of $N_x b^2/\pi^2 D = -7$ (axial compression) is specified, then $E\alpha\Delta T t b^2/\pi^2 D$ is found to be −3 (cooling). If a normalized temperature change of $E\alpha\Delta T t b^2/\pi^2 D = +15$ (heating) is specified, then the axial force $N_x b^2/\pi^2 D$ is found to be +35 (axial tension). These values can be confirmed by first forming the fraction of axial loading

$$\eta = \frac{N_x}{\bar{N}_x} \tag{3.447}$$

in which N_x is the applied uniaxial loading, $\bar{N}_x$ is the uniaxial loading that causes buckling, and η is the fraction relating the two. The objective is to find the fraction ϕ of the temperature change necessary to cause buckling under combined thermal and mechanical loading over the temperature change necessary to cause buckling under thermal loading only, i.e.,

$$\phi = \frac{\Delta T}{\overline{\Delta T}} \tag{3.448}$$

in which $\overline{\Delta T}$ is the temperature change necessary to cause buckling under thermal loading only. The temperature change is different for uniaxial restraint than for biaxial restraint, but for biaxial restraint no mechanical loading is possible unless screw-type loading is applied.

3.7.7.4.5 Effect of Poisson's Ratio

For $\nu = 0$, the mechanical and thermal buckling interaction results are identical in mode shapes and coordinates of mode shape changes to those for the biaxial mechanical load interaction curve because N_y has been reinterpreted in terms of ΔT via the equivalent mechanical loading concept, i.e.,

$$N_y = -E\alpha\Delta T t \tag{3.449}$$

Éléments sous droits d'auteur

If the Poisson's ratio, ν, is not zero as is the case for most isotropic materials, then the nature of the numerical results changes somewhat. Specifically, the mode shape changes occur at different coordinates than in Figures 3-102 and 3-103 because of the complicating factor of νN in the N_y term of the buckling criterion, i.e., the term on n^2 in Equation (3.444). That is, a lateral (y-direction) mechanical reaction is caused by virtue of the Poisson effect. For compressive N_x and $0 < \nu < .5$, compressive N_y develops even without heating because the plate is laterally restrained. If $-1 < \nu < 0$ (a possible range of values from thermodynamic considerations), then tensile N_y develops if there is no heating. Heating the plate merely adds to the inherent $N_y = \nu N_x$, and cooling subtracts from N_y as seen in Equation (3.439). The proportional loading slope, s, and coordinates of the buckling mode shape changes are affected by the value of ν. Accordingly, numerical results must be obtained for each specific value of ν. See problem 3.7.6 on page 407.

3.7.7.4.6 Effect of the Plate Aspect Ratio

The plate aspect ratio, a/b, is unity (a square plate) in the numerical results of Figures 3-102 and 3-103, and those results are symmetric about the proportional loading slope of $s = -1$. For other plate aspect ratios, figures analogous to Figures 3-102 and 3-103 would be quite different and, in particular, would not exhibit the symmetry about the proportional loading slope of $s = -1$ seen in Figures 3-102 and 3-103. If both the plate aspect ratio is changed from unity and Poisson's ratio is changed from zero, both the proportional loading slopes to mode shape changes (Poisson's ratio effect) are different and asymmetry of the N_x versus ΔT curves (plate aspect ratio effect) results.

3.7.7.4.7 Material-Property-Related Limitations

The limitations on the present analysis cannot be specified without a numerical example as done in the preceding sub-sections, but there is no material with $\nu = 0$. Thus, we address the limitations in a general manner. As heating increases, the material properties must degrade in the inevitable downfall toward melting with the opposite effect upon cooling. Also, the implied stress, σ_y, that is associated with ΔT can easily exceed the yield stress leading to inelastic behavior. More will be addressed on these topics in Section 3.7.9.

3.7.7.5 Summary of Thermal and Mechanical Buckling

The buckling behavior of a simply supported rectangular plate under uniform temperature change (heating or cooling) and uniaxial mechanical loading (compressive or tensile) is addressed. The plate has a uniaxial in-plane restraint along two opposite edges to prevent free thermal expansion so that in-plane thermal load develops in the direction perpendicular to the restrained edges. However, the plate movement is not restrained in-plane in the direction perpendicular to the uniaxial in-plane restraint, so mechanical loading can also be applied (mechanical loading

Éléments sous droits d'auteur

can be applied in a screw-type load frame in the direction perpendicular to the restrained edges). The plate buckles into different buckling modes at different loads depending on the ratio of the thermal load to the mechanical load, the plate aspect ratio (ratio of the length to width of the plate), and on the Poisson's ratio. Numerical results are presented for a wide range of ratios of thermal to mechanical loading for the very special case of a square plate made of isotropic material with a Poisson's ratio of zero. Similar numerical results would be obtained for other plate aspect ratios because the effects of the appropriate terms in the solution are readily apparent. For other Poisson's ratios, the shifts in buckling mode shapes would occur at different loads than for those shown for zero Poisson's ratio. For biaxial mechanical loading, if a lateral tensile force is applied to a plate, then the axial buckling force exceeds the uniaxial buckling load, as is well known. Similarly, for combined thermal and mechanical loading, an axial tensile load enables the plate to withstand higher temperatures without buckling than if no mechanical loading were present. Also, cooling the plate enables a higher uniaxial compressive mechanical load to be sustained without buckling than if the plate temperature were not changed. For this biaxial loading case, we can either specify the applied N and seek $\overline{\Delta T}$ or specify ΔT and seek $\overline{N}$. Nonproportional loading is also possible.

3.7.8 Summary and Observations on Plate Thermal Buckling

Solving plate thermal buckling problems is a two-step process that is almost the same as for any plate buckling problem:

(1) Solve the plane *thermo*elasticity problem to determine the two-dimensional in-plane stress or force *distribution* in the prebuckling equilibrium state under the prescribed *thermal* (and mechanical) loading.
(2) Use the prebuckling stresses from step (1) as the prebuckling equilibrium state stress or force distribution in the buckling partial differential equation to determine the *magnitude* of the *thermal* and/or mechanical loading that causes buckling.

The first step in calculating a thermal buckling load is to determine the prebuckling stress state in the plate from the change-in-temperature distribution and the mechanical loading, if any. That is, we solve the thermal stress problem in step one. The plane thermoelasticity problem can be simple, such as from spatially uniform thermal loading, or complex, such as from spatially nonuniform thermal loading. In either event, whether the prebuckling stresses arise from mechanical or thermal loading is totally immaterial; actually, they are just stresses, no matter how they arise. Some prebuckling stress states are quite simple and easy to determine. For example, uniform change in temperature with some edge restraint often readily leads to a simple uniform prebuckling stress state as we have seen in this section. Other change in temperature distributions lead far less directly to complicated prebuckling stress distributions that have severe implications in step two.

Éléments sous droits d'auteur

The second step in calculating a thermal buckling load is to actually solve the buckling partial differential equation to find the magnitude of the buckling load (temperature change). The nature and solvability of the partial differential equation is highly dependent upon the individual terms that appear in the partial differential equation as well as on the *coefficients* of the terms. As an example of terms appearing, the solution of a partial differential equation with, as opposed to without, the in-plane shear force, N_{xy}, is quite different. That is, the presence of certain terms in a partial differential equation can enormously complicate its solution. The coefficients of the various terms are of considerable interest in thermal buckling problems because the coefficients which come from the prebuckling solution (step one) directly determine the degree of difficulty of solution of the partial differential equation. If the change in temperature distribution is uniform, then the coefficients on the terms of the partial differential equation are constant in many cases, and, as is well-known, the solution of a partial differential equation with constant coefficients is often straightforward. If the change in temperature distribution is nonuniform, then the coefficients on the terms of the partial differential equation are nonconstant, and, as is equally well-known, the solution of a partial differential equation with nonconstant coefficients is often difficult, certainly more difficult than if the coefficients are constant.

In general, the essential condition for plate thermal buckling to occur is that *the plate must remain flat as the magnitude of the temperature change increases* until the in-plane forces in the plate become so large that buckling occurs, just as for in-plane mechanical loading.[1] Otherwise, the plate simply bends immediately and in an increasing amplitude under thermal loading. However, an equilibrium state can involve bending and then buckle at some elevated load level. For example, circular cylindrical shells have a rather bending-intensive, axially varying prebuckling deformation state near each end, yet have an eigenvalue (buckling load) when the load gets high enough (as we will see in Section 4.5). Thus, a flat or membrane prebuckling state is not always essential to develop a buckling problem. We will consider here that a flat prebuckling state is necessary to achieve a plate thermal buckling problem. Certain conditions involving the spatial distribution of the change in temperature in the plate and the in-plane restraints on movement of the plate affect whether the plate can stay flat. The change in temperature distribution must be uniform through the thickness as the simplest case or, in general, symmetric about the plate middle surface. The in-plane restraints must be applied at the plate middle surface in order to avoid eccentric restraint that would cause plate bending, bowing, or curling, i.e., movement from flatness that precludes buckling in many problems.

Two aspects of the change in temperature (ΔT) spatial distribution in the plate affect whether and how plate buckling occurs. The three-dimensional spatial distribution consists of two geometric components:

[1]However, just as for mechanical buckling problems, secondary buckling, i.e., changes in buckling modes at higher loads or higher temperatures than at initial buckling, can certainly occur. That is, plate buckling does not always occur from a flat prebuckled state.

Éléments sous droits d'auteur

1. through-the-thickness ΔT distribution
2. areal (over the plate middle-surface *area*) ΔT distribution

For the two through-the-thickness ΔT distribution possibilities:

1. If the through-the-thickness distribution of ΔT is uniform or symmetric about the plate middle surface, then only in-plane forces develop in the plate and increase with increasing ΔT until buckling occurs. That is, no moment develops that would cause the plate to bend away from flatness as the magnitude of the ΔT increases.
2. If the through-the-thickness distribution of ΔT is not uniform or symmetric about the plate middle surface, then bending moments develop causing the plate to bend, bow, or curl from the very instant that ΔT is applied, so no buckling occurs.

For the areal distribution of ΔT (with a through-the-thickness ΔT distribution that is uniform or symmetric about the plate middle surface):

1. If the areal distribution of ΔT is uniform and no in-plane restraints exist, then no in-plane forces develop in the plate and the plate merely expands freely as the magnitude of ΔT increases. Thus, no buckling occurs.
2. If the areal distribution of ΔT is uniform and in-plane restraints exist, then in-plane forces develop in the plate and increase with increasing magnitude of ΔT until buckling occurs.
3. If the areal distribution of ΔT is nonuniform and no in-plane restraints exist, then self-equilibrating in-plane forces can develop in the plate and the compressive forces increase with increasing magnitude of ΔT until buckling occurs, e.g., a "hot spot" in an unrestrained plate can buckle if hot enough.
4. If the areal distribution of ΔT is nonuniform and in-plane restraints exist, then in-plane forces develop in the plate and increase with increasing magnitude of ΔT until buckling occurs.

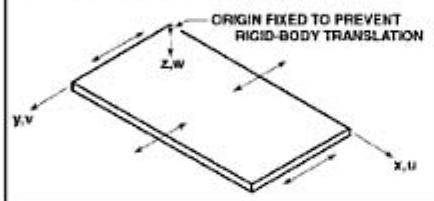
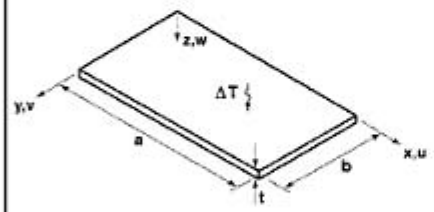
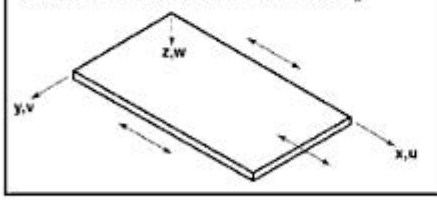
Thus, the through-the-thickness ΔT distribution must be uniform or symmetric about the plate middle surface for buckling to be possible. That is, the areal ΔT distribution and the in-plane restraints are immaterial unless the through-the-thickness distribution is such that only in-plane forces can develop. Problems with uniform through-the-thickness and uniform areal ΔT distributions are the easiest to solve. Problems with either symmetric-about-the-middle-surface ΔT distributions or nonuniform areal ΔT distributions (or both) are the most difficult to solve.

In summary, we derived the fundamental thermoelastic force and moment relations for equilibrium including the equilibrium differential equation (step one in the solution process) as well as the variations in forces and moments during buckling including the buckling differential equation (step two) in Section 3.7.2. Then, we investigated the types of in-plane loading as well as the in-plane restraint conditions and their implications and interactions. Next, we identified an equivalent mechanical load for the thermal loading in certain restricted cases that enables us to

Éléments sous droits d'auteur

use known solutions to buckling problems under mechanical loading to solve thermal buckling problems. That is, there is no need to distinguish between prebuckling stresses that arise from thermal loading and those that arise from mechanical loading. However, a firm understanding of how thermal stresses arise from temperature-change distributions and restraint conditions is essential to the determination of the prebuckling stresses. Then, we studied three simple plate thermal buckling problems in which the temperature change is uniform throughout the volume, so the prebuckling equilibrium state involved a uniformly distributed, easily determined set of stresses. The prebuckling stresses are uniform throughout the plate, so the buckling differential equation has constant coefficients and is easily solved for the buckling load. Each of the three problems is represented in Table 3-6 along with its equivalent mechanical loads, N_x and N_y, as well as the buckling coefficient, k_T. The values of

Table 3-6 Plate Thermal Buckling Results

Uniform ΔT Loading of Simply Supported Plates with In-Plane Movement Restrictions	Prebuckling Forces, N_x and N_y, and Buckling Coefficient, k_T
Uniaxial In-Plane Restraint with ΔT 	$N_x = -E\alpha\Delta T t$ $N_y = 0$ $k_T = \frac{12}{\pi^2}(1-\nu^2)\alpha\overline{\Delta T}\left(\frac{b}{t}\right)^2$
Biaxial In-Plane Restraint with ΔT 	$N_x = -\frac{E}{1-\nu}\alpha\Delta T t$ $N_y = -\frac{E}{1-\nu}\alpha\Delta T t$ $k_T = \frac{12}{\pi^2}(1+\nu)\alpha\overline{\Delta T}\left(\frac{b}{t}\right)^2$
Uniaxial In-Plane Restraint with ΔT and N_x 	$N_x = -N$ $N_y = -\nu N - E\alpha\Delta T t$ $k_T = \frac{12}{\pi^2}\alpha\overline{\Delta T}\left(\frac{b}{t}\right)^2$ (for $\nu = 0$) $k = \frac{N_x b^2}{\pi^2 D}$

Éléments sous droits d'auteur

k_T vary with plate aspect ratio, but have limiting values for long plates of four for uniaxial restraint and one for biaxial restraint. In addition, the uniaxial restraint k_T is four for all integer values of a/b. Note that the uniaxial restraint k_T has a factor $(1-\nu^2)$ whereas the biaxial restraint k_T has a factor $(1+\nu)$. That difference comes from the respective values of N_x and N_y. The third problem of combined ΔT and N_x cannot be simply represented unless we examine the special case in which $\nu = 0$ (not a typical material by any means) to decouple the problem somewhat. The biaxial loading in the third problem has the interesting aspect that cooling a plate can increase its mechanical load-carrying capacity before buckling just as heating can decrease that capacity.

3.7.9 Other Topics in Thermal Buckling of Plates

The other topics addressed in the remainder of this section include various boundary support conditions including elastic restraints, nonuniform heating, time-dependent temperature distributions, limitations of the linear elastic material model, temperature-dependent material properties, nonlinear stress-strain behavior, the analogy between temperature and moisture effects, and general remarks. These topics are addressed to extend the reader's awareness from the present simple analyses to the more complex problems that naturally occur.

3.7.9.1 Various Edge Support Conditions

One of the key important issues to address in thermal buckling problems is how thermal stresses or forces are developed as a result of in-plane restraints on deformation. Those restraints or boundary support conditions influence the prebuckling stresses and forces. General concepts of the many varieties of in-plane restraint are developed in Section 3.7.3 to introduce the reader to the complexities of how thermal stresses are developed. Simple specific examples are addressed in Sections 3.7.5 to 3.7.7 to relate those thermal stress distributions to thermal buckling loads for simply supported plates. For plates with rotational edge restraint (fixed plates) or with free edges, the same prebuckling stresses exist as for simply supported edges *if the in-plane restraints are identical.* However, the rotational edge restraint for fixed edges and the lack of transverse restraint for free edges lead to *different levels of buckling load* than for simply supported plates (higher for fixed edges and lower for free edges).

Nemeth noted that the increase in buckling load for an infinitely long, clamped-edge plate over the infinitely long simply supported edge plate is approximately 3.76 for mechanical loading of biaxially in-plane restrained plates [3-61]. Thus, the present results in Section 3.7.6 for thermally loaded, infinitely long, simply supported edge plates could be multiplied by 3.76 to get reasonable clamped-edge plate buckling results.

Plates can have elastic restraints at the edges of two types: in-plane and rotational (or both). If the elastic restraint is in-plane, then the in-plane thermal forces are affected (the prebuckling in-plane loading) and are less than if the edges were totally prevented from in-plane move-

Éléments sous droits d'auteur

ment. If the elastic restraint is rotational (about a line along the plate edge at the middle surface), then the in-plane thermal forces have the same nature (i.e., distribution) as if the elastic rotational restraint did not exist. However, the thermal buckling load (the temperature change or value of the in-plane thermal forces at which buckling occurs) is raised from the value for a free-rotation edge (any simple support) toward, but not achieving, the value for a no-rotation edge (some form of clamped or fixed support) as the rotational elastic restraint increases in magnitude.

3.7.9.2 Nonuniform Heating

Nonuniform heating conditions can include nonuniform spatial temperature-change distributions that are constant in time as well as nonuniform temperature-change distributions with time. We address only nonuniform spatial temperature-change distributions in this book.

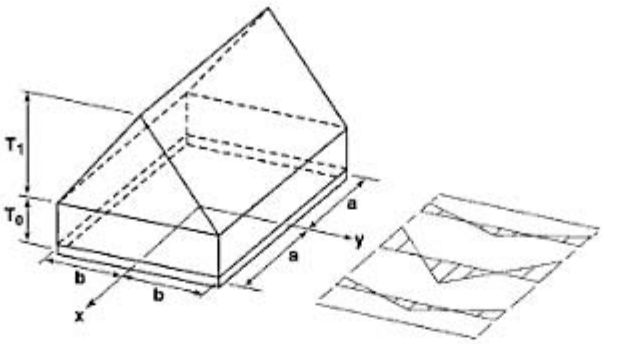
Possible spatial temperature-change distributions include variable distributions over the plate area (areal ΔT distributions) such as Klosner and Forray's expression for arbitrary temperature distributions that are symmetric about both centerlines of the plate [3-64]:

$$\Delta T = \Delta T_1 + \Delta T_2 + \sum_{i=0}^{\infty}\sum_{j=0}^{\infty} \cos\frac{i\pi x}{a}\cos\frac{j\pi y}{b} \qquad (3.450)$$

in which ΔT_1 is the difference between the average temperature of the supporting structure and room temperature and ΔT_2 is the difference between the temperature at the edge of the plate and the average temperature of the supporting structure. That is, the plate is supported at its edges on an elastic assembly that can have a different temperature than both room temperature and the plate edges. Klosner and Forray treat a parabolic temperature-change distribution as an example. However, their specific procedure was not clear, and their references were missing or not accurate.

Another significant practical application of plate thermal buckling problems is an areal distribution of temperature change simulating the heating conditions on aircraft wing panels in supersonic flight. As a first step, an areal distribution should be investigated that is simple enough to readily permit experimental verification of theoretical predictions. A typical such problem involves the "tent-like" temperature distribution studied by Heldenfels and Roberts [3-65] which is depicted in Figure 3-104a. The tent-like temperature distribution is generated by a heating strip placed along the longitudinal centerline of the plate parallel to the x-axis and cooling pipes along the two longitudinal edges parallel to the x-axis. The surfaces and ends of the plate are insulated to restrict heat losses. After thermal equilibrium is reached, the tent-like distribution results from heating to $T_0 + T_1$ at the ridge of the tent and the cooling pipes are adjusted to reduce the temperature at the plate edges (tent side walls) to T_1. The plate is not restrained in its plane (although the edges are simply supported in some manner which can be represented with simple support boundary condition S4 in Figure 3-10 on page 247). The nonuniform temperature distribution in combination with the free-edge

Éléments sous droits d'auteur



a Temperature Distribution b Distribution of σ_x

Figure 3-104 A "Tent-Like" Temperature Distribution and Distribution of σ_x on an Unrestrained Rectangular Plate *(After Heldenfels and Roberts [3-65])*

boundary condition leads to a complex state of mixed tensile and compressive in-plane stresses. Of course, the thermal stresses must be self-equilibrating because the edges are not restrained. The prebuckling equilibrium stress distribution is approximated with the solution for σ_x in an infinitely long plate (by a method in Timoshenko and Goodier [3-66] on pages 433–434) with determination of the other stresses, σ_y and τ_{xy}, from equilibrium considerations for a finite-length plate. The resulting distribution of σ_x across the plate is shown in Figure 3-104b at several longitudinal locations. The magnitude of the stress distribution is highest at the longitudinal center of the plate and decreases toward zero as the ends are approached because all edges are stress-free. Note that there is always compressive stress in a central zone along the longitudinal axis except at the very ends of the plate. The compressive stresses are equilibrated by the tensile stresses near the longitudinal edges because thermal stresses must be self-equilibrating. Moreover, σ_y is also compressive in the central zone of the plate leading to a state of biaxial compression (σ_x, σ_y) in the central zone. This state of biaxial compression, if high enough, can lead to thermal buckling.

For plates with the areal "tent-like" temperature distribution in Figure 3-104a, Gossard, Seide, and Roberts developed a thermal buckling solution, a postbuckling behavior analysis, and a large-deflection equilibrium solution to the deformation of a plate with initial geometric imperfections [3-67]. The constant temperature, T_0 (tent side wall), does not cause or even contribute to thermal buckling because T_0 causes only free thermal expansion of the in-plane-unrestrained edges. They predicted a buckling temperature $\bar{T}_1$ for the perfect plate of

$$\bar{T}_1 = 5.39\frac{\pi^2 D}{b^2 E\alpha t} = 4.43\frac{1}{(1-\nu^2)\alpha}\left[\frac{t}{b}\right]^2 \qquad (3.451)$$

Éléments sous droits d'auteur

Note that the compressive stresses in the hottest zone cause the perfect plate to buckle *even without external edge restraint!* Gossard, Seide, and Roberts heated a 24-inch x 36-inch x 1/4-inch thick (9.45-cm x 14.2-cm x .098-cm) 7057-T6 aluminum plate to three different values of T_1 [60°F (33°C), 100°F (55°C), and 152°F (84°C)] [also, T_0 = 100°F (27°C), and the initial temperature was 80°F (27°C) as stated in [3-65]]. Instead of thermal buckling, they observed the highly nonlinear thermal load-deformation behavior for a geometrically imperfect plate with initial center deflection of .045 in. (.11 cm) in Figure 3-105. In contrast, the thermal buckling temperature is T_1 = 193°F (107°C) from Equation (3.451) with their calculated postbuckling behavior shown as the dashed line in Figure 3-105. The geometric imperfections in the plate prevent thermal buckling and cause a large-deflection equilibrium problem to exist just as geometric imperfections prevent buckling under mechanical loading in Section 3.5. That is, the plate bends, bows, or curls in the form of the initial geometric imperfection from the first instant that temperature is applied. And, the magnitude of the center deflection is quite high, reaching the plate thickness by the temperature at buckling of a perfect plate.

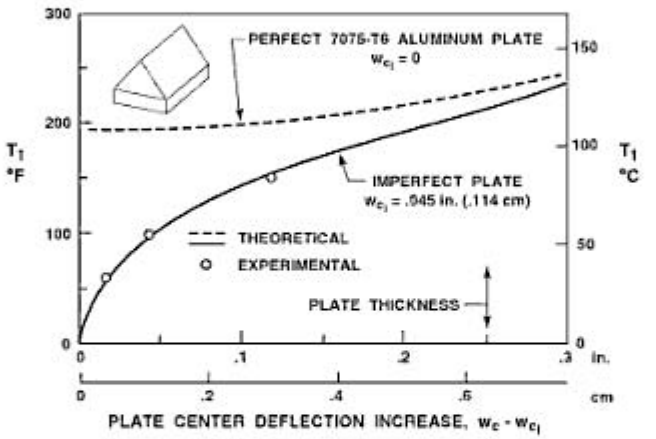


Figure 3-105 Theoretical versus Experimental Plate Center Deflection *(After Gossard, Seide, and Roberts [3-67])*

3.7.9.3 Time-Dependent Temperature Distributions

Treating $\Delta T(x, y, z)$ as a function of time, i.e., $\Delta T(x, y, z, t)$, is a realistic physical problem because the thermal conductivity in most engineering materials is quite high. Thus, the ΔT distribution is likely to change quite rapidly with time. Alternatively, we could examine a sequence of quasi-static problems with different ΔT to model the actual ΔT distributions that occur with time. Generally, because of thermal soaking (total absorption and distribution of heat) of a body, the temper-

Éléments sous droits d'auteur

ature gradient decreases with time. For thermal buckling problems, we are usually concerned with the largest temperature gradient that occurs at any instant rather than the behavior with time. Thus, ignoring the change in temperature gradient with time, but seeking the largest temperature gradient at any instant, is often appropriate.

3.7.9.4 Limitations of the Linear Elastic Material Model

The deformation behavior of bodies under mechanical and thermal loading has many aspects, some relatively simple, others far more complex. We most often address linear elastic behavior characterized by mechanical properties: Young's modulus, E, Poisson's ratio, ν, and strength plus thermal properties: coefficient of thermal expansion, α, and coefficient of thermal conductivity, k. Mechanical stresses are a function of E and ν as well as, of course, the mechanical loading. Thermal stresses are functions of E, ν, and α, as well as the thermal loading as influenced by k. That is, the thermal conductivity affects the distribution of the temperature in the body under thermal loading, and then with that temperature distribution we can calculate thermal stresses with E, ν, and α. The most common end to linear elastic behavior occurs when the stress level reaches the strength of the material (determined with a failure criterion for multiaxial stress states). The elastic characterization is not sufficient to address materials with viscous or quasi-viscous (time-dependent) behavior (characterized with a coefficient of viscosity, η) as evidenced by various creep and other phenomena called viscoelastic behavior. Moreover, another limit of linear elastic behavior is called the elastic limit or yield stress, σ_y, which is followed by perfectly plastic behavior for a few materials or by nonlinear stress-strain behavior for most materials. Viscoplastic behavior is the result of combining the quasi-viscous character with the nonlinear stress-strain behavior.

3.7.9.5 Temperature-Dependent Material Properties

We have implicitly ignored the fact that the properties of most materials vary significantly with temperature. However, we are faced with large temperature ranges because of the large buckling temperature changes that are often predicted with elastic material properties at room temperature. Such variable properties include stiffness or modulus, strength, Poisson's ratio, yield stress, and coefficient of thermal expansion, not to mention thermal conductivity which influences time-dependent problems. In addition, these same properties can be time-dependent, e.g., modulus and strength in creep and creep rupture problems.

The Young's modulus, E, is perhaps least affected by temperature of all properties except that Poisson's ratio, ν, has a limited range of variation because of an upper bound of 1/2 for incompressibility of isotropic materials. As temperature increases, modulus and strength typically decrease. However, some materials such as polycrystalline graphite have increasing stiffness and strength over a wide temperature range between room temperature and just below the graphitization temperature, but, after that temperature of creation, they soften.

Éléments sous droits d'auteur

The coefficient of thermal expansion, α, generally increases with temperature. Freudenthal suggested the very rough approximation of

$$\alpha = \alpha_o + \Delta\alpha\sqrt{\frac{T}{T_m}} \tag{3.452}$$

in which α_0 is the initial coefficient of thermal expansion at $T = 0$ and $\Delta\alpha$ is the total range of variation between $T = 0$ and T_m, the melting temperature [3-68]. Others have used a linear increase in α with temperature. Use of only initial values of the coefficient of thermal expansion must lead to underestimates of thermal stresses at elevated temperatures because there the thermal expansion is much higher, therefore driving stresses higher (but E should get lower causing the opposite effect). Hilton observed that using the actual temperature variation of material properties (E and α) over the temperature range resulted in appreciable decreases in maximum thermal stresses and slight increases in maximum thermal strains for a thick-walled circular cylinder [3-69]. For example, using the room temperature values of E and α over some temperature range would lead to overestimates of the true peak stresses and underestimates of the peak strains for many problems.

The coefficient of thermal conductivity increases with temperature for some materials, but decreases for others, so no general statement can be made. At any rate, the heat conduction problem is generally separated from the stress analysis problem, so is beyond the scope of this book.

Treatment of viscoelastic or viscoplastic behavior is also beyond the scope of this book. However, we note that viscoelastic materials are inherently very temperature-sensitive. The coefficient of viscosity changes fairly rapidly with temperature; in fact, it is the most temperature-sensitive mechanical property of all that we have addressed.

3.7.9.6 Nonlinear Stress-Strain Behavior

The driving force in thermal stress problems is generally proportional to $E\alpha\Delta T$, and the material properties, E and α, can both be nonlinear. We have already noted that E generally, but not always, decreases with increasing temperature (and α generally increases). However, we have not accounted for the additional decrease of E with increasing stress level for materials with nonlinear stress-strain curves. In addition to relatively straightforward variation of material properties with temperature, the high temperatures generally cause softening of a material and significantly increased nonlinearity of the stress-strain curve. That is, the shape of the nonlinear stress-strain curve characteristic of most materials changes quite rapidly with temperature, becoming more and more nonlinear as T increases. The nonlinear stress-strain behavior is first and foremost a stress-dependent behavior or characteristic, but also varies significantly with temperature and can be a function of strain rate, i.e., viscoplastic effects. For aluminum, the stress-strain curves are nonlinear and decrease in E and σ_y and the nonlinearity increases rapidly as temperature increases as in the results of Mathauser and Brooks for 7075-T6 aluminum in Figure 3-106 [3-70]. The offset yield stress (the inclined tick marks in Figure 3-106) decreases much faster with increasing tempera-

Éléments sous droits d'auteur

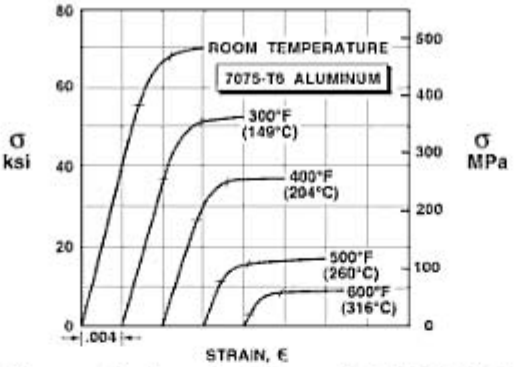


Figure 3-106 Compressive Stress-Strain Curves for 7075-T6 Aluminum as a Function of Temperature *(After Mathauser and Brooks [3-70])*

ture than does the initial modulus. The yield stress (the horizontal tick marks in Figure 3-106) decreases even faster with increasing temperature than does the offset yield stress. Those two relative decreases are consistent with (and the cause of) the increasing nonlinearity of the stress-strain curves with increasing temperature. This behavior is typical for aluminums and might be true for other materials with nonlinear stress-strain curves. Of course, nonlinear stress-strain behavior exists even at room temperature, so inelastic treatment of buckling is essential even without the complications of temperature variations.

If large changes in temperature to cause buckling, ΔT, are predicted (large being several hundred degrees), we simply must be suspicious that the material properties surely must have changed over such a large temperature range and, in addition, that inelastic effects might be important. Both effects lead to significantly smaller ΔT than predicted with linear elastic, room-temperature material properties (both stiffnesses and α) as demonstrated for plates by Jones [3-71]. Incorporation of this variability in material properties including inelastic effects is necessary to treat the thermal buckling problem realistically.

These many variations in material properties with temperature coupled with the complexities of aerodynamic heating in flight structures can lead to extremely difficult and involved problems. Usually, we must make several simplifying approximations to reach a solvable and understandable problem.

3.7.9.7 Analogy between Temperature and Moisture Effects

Some materials can absorb moisture to the extent that they expand with added moisture and contract when moisture is decreased, just as most materials expand with added temperature and contract with decreased temperature. Polymer-matrix-based composite materials often are affected in that manner by moisture, and their structural behavior depends strongly on analysis of the resulting effects. The role of the

Éléments sous droits d'auteur

thermal expansion coefficient in thermal buckling is mirrored by the role of the moisture expansion coefficient in moisture-induced buckling for those materials that are affected by moisture. For many such materials, different thermal and moisture expansion coefficients exist in different principal material directions. The formulations of the thermal buckling and moisture-induced buckling problems are analogous, but the details are beyond the scope of this book, so see Ashton and Whitney [3-51].

3.7.9.8 Concluding Remarks

More plate thermal buckling and thermal bending problems are summarized by Thornton in a review paper [3-72] and in his thermal structures book [3-60]. See also the earlier review paper by Tauchert [3-73]. Of significant interest is the thermal buckling of plates and shells book by Ogibalov and Gribanov [3-74].

Extensive results for buckling of many long fiber-reinforced composite laminated plates have been obtained by Nemeth in a series of papers and reports [3-59, 3-61, and 3-75 to 3-79]. Included are both thermal and mechanical buckling, so the work represents combination of this section and the previous on laminated composite plates. The variety of laminates treated is representative of current design practice. The analysis results in those papers are a significant aid to our understanding how such plates behave and how to design them.

Problem Set 3.7

3.7.1 Demonstrate that the thermal force per unit width of a plate is

$$N_x^T = -\frac{E\alpha}{1-\nu}\int_{-t/2}^{t/2} \Delta T \, dz$$

by using the plane stress condition $\sigma_z = 0$ in the three-dimensional stress-strain relations including thermal expansion terms.

3.7.2 Use variational techniques to derive the moderately large-deflection equilibrium differential equations and their associated boundary conditions for a plate with thermal effects. Be sure to clarify precisely where the thermal effects enter the problem.

3.7.3 Use variational techniques to derive the buckling differential equations and their associated boundary conditions for a plate with thermal effects. Be sure to clarify precisely where the thermal effects enter the problem.

3.7.4 Consider a rectangular plate restrained from any in-plane deformation at the edges $x = 0$ and $x = a$ with S1 simply supported edge boundary conditions and unrestrained on the edges $y = 0$ and $y = b$ with S4 simply supported edge boundary conditions. Characterize the nature of the prebuckling stress and deformation state as well as the buckling differential equations that must be solved.

3.7.5 Calculate the coordinates of all mode shape intersections and the slopes of the buckling boundary in each mode shape for Poisson's ratio $\nu = 0$ in Figures 3-102 and 3-103.

3.7.6 Find the thermal and mechanical buckling loads for the plate in Section 3.7.7 (hence the equivalents of Figures 3-102 and 3-103) for the case of Poisson's ratio $\nu = .3$.

3.7.7 Determine the equivalent mechanical loading for a plate that is simply supported on all four edges with a change in temperature distribution that varies linearly in the y-direction from 0 to ΔT_0 and is constant in the x-direction. The plate cannot deform in-plane in the x-direction on the edges $x = 0$ and $x = a$ (but is free to deform in the y-direction along those edges). The plate is free to deform in-plane in both the x- and y-directions along the edges $y = 0$ and $y = b$. Then, use a mechanical loading problem treated earlier in the book to find the value of ΔT_0 at thermal buckling.

Éléments sous droits d'auteur

3.8 EFFECT OF PLASTIC DEFORMATION

3.8.1 Introduction

Plastic deformation generally reduces bar buckling loads as we saw in Section 2.10. We now address plastic buckling of rectangular plates loaded with arbitrary combinations of axial and lateral forces, N_x and N_y, as in Figure 3-107, that can be high enough to cause plastic deformation before buckling. Classical buckling theory, by which is implied a flat or membrane prebuckled equilibrium state, is used for simply supported edge boundary conditions on all four edges.

The essential complexity of plastic buckling of rectangular plates over that of bars is the presence of a biaxial stress state as opposed to a uniaxial stress state. Moreover, the energy in biaxial loading might be higher than in uniaxial loading and thus lead to a more pronounced effect of plasticity. Another difference between the two problems is the partial differential equation for the plate problem (because a plate is essentially two-dimensional) as opposed to the ordinary differential equation for a bar (because a bar is essentially one-dimensional).

Simple J_2 deformation theory of plasticity (also called maximum octahedral shear stress theory, maximum energy of distortion theory, etc.) as described by Nadai [3-80] and Jones [3-81] is used in spite of the fact that incremental theory is more valid for general loading histories. Incremental and deformation theories lead to identical results for proportional loading equilibrium problems because, for that class of problems, deformation theory is merely incremental theory integrated along a single, straight load path. However, Budiansky [3-82] shows that deformation theory is consistent with accepted incremental theory conditions even for some range of nonproportional loading about the proportional loading condition. The permissible bounds on the degree of nonproportionality of loading are not necessarily satisfied by the deformations *during* buckling. However, experimental bar, plate, and shell buckling results are in good agreement with deformation theory predictions whereas predictions with incremental theory are well above measured buckling loads. Nevertheless, more experimental evidence is required to fully substantiate the applicability of deformation theory to plastic buckling problems.

The present solution for rectangular plates by the author is a reduction to plates from the shell analysis of Jones [3-83] which in turn is an extension of Stowell's plates work [3-84] and that of Ilyushin [3-85]. Stowell, just like Shanley [3-86], presumed that unloading does not occur

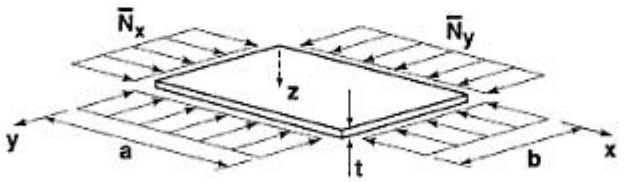


Figure 3-107 Rectangular Plate Under Biaxial In-Plane Load

Éléments sous droits d'auteur

during buckling. In contrast to the constant Poisson's ratio ($\nu = 1/2$) employed by Stowell and Ilyushin, a variable Poisson's ratio here provides a smooth transition from the elastic compressible state to the plastic incompressible state with increasing stresses. The present secant-modulus theory for a biaxial configuration, i.e., a plate or shell, reduces to tangent-modulus theory when the biaxial terms are reduced to uniaxial terms in a consistent manner. The plate buckling differential equation is used to derive a *transcendental* buckling criterion in terms of the geometry and unknown material properties *at buckling*. The technique for solving this type of buckling criterion is discussed, numerical examples are given to illustrate application of the theory, and the theoretical buckling predictions are compared with measured buckling results.

3.8.2 Derivation of Buckling Criterion

By use of simple J_2 deformation theory of plasticity, expressions are obtained for the variations of the biaxial stresses during buckling in terms of the variations of strains and material properties during buckling of a plate made of an isotropic material with a nonlinear stress-strain curve. The variations in biaxial stresses are then integrated through the plate thickness to obtain expressions for the variations in forces and moments during buckling. Finally, the variations in forces and moments are substituted in the buckling differential equation that is solved to obtain a closed-form, but transcendental, buckling criterion in terms of the geometry and nonlinear stress-strain behavior of the plate material *at buckling*. The criterion is applicable for arbitrary combinations of uniform in-plane forces in the x- and y-directions of the plate as in Figure 3-107.

3.8.2.1 Fundamental Relations in J_2 Deformation Theory

Simple J_2 deformation theory of plasticity is used to relate the biaxial stresses to the plastic deformation (see Nadai [3-80] and Jones [3-81]). The fundamental quantities in J_2 deformation theory for isotropic materials are the stress intensity, σ_i, ($\sigma_i = 3\,\tau_o/\sqrt{2}$ in which τ_o is the octahedral shear stress) as a function of the biaxial stresses:

$$\sigma_i = \sqrt{\sigma_x^2 + \sigma_y^2 - \sigma_x\sigma_y + 3\tau_{xy}^2} \tag{3.452}$$

the strain intensity, ε_i, ($\varepsilon_i = 3\gamma_o/[2\sqrt{2}\,(1+\nu)]$ in which γ_o is the octrahedral shear strain) as a function of the biaxial strains:

$$\varepsilon_i = \frac{1}{1-\nu^2}\sqrt{\left[1-\nu+\nu^2\right]\left[\varepsilon_x^2+\varepsilon_y^2\right] - \left[1-4\nu+\nu^2\right]\varepsilon_x\varepsilon_y + \frac{3}{4}(1-\nu)^2\gamma_{xy}^2} \tag{3.453}$$

(This strain intensity expression is apparently due to Lunchick [3-87] and is a continuous function of ν, so ν can vary from the elastic value to the plastic value of 1/2 rather than being restricted to 1/2 at all stress levels as is the expression by Ilyushin [3-85]—set $\nu = 1/2$ in Equation (3.453)),

Éléments sous droits d'auteur

and the stress-strain relations, with general nonlinear material properties, E_{sec} and ν,

$$\sigma_x = \frac{E_{sec}}{1-\nu^2}(\varepsilon_x + \nu\varepsilon_y)$$
$$\sigma_y = \frac{E_{sec}}{1-\nu^2}(\varepsilon_y + \nu\varepsilon_x) \qquad (3.454)$$
$$\tau_{xy} = \frac{E_{sec}}{2(1+\nu)}\gamma_{xy}$$

that relate the stress intensity to the strain intensity, i.e., $\sigma_i = E_{sec}\varepsilon_i$. In addition, certain material properties are defined in terms of the stress and strain intensities on a stress-intensity versus strain-intensity curve. However, the problem is enormously simplified by the following result. For a uniaxial stress state (σ_x plus ε_x and $\varepsilon_y = -\nu\varepsilon_x$), the stress intensity is simply $\sigma_i = \sigma_x$ and the strain intensity can be shown to be $\varepsilon_i = \varepsilon_x$ (see Problem 3.8.1 on page 421). Thus, *the stress-intensity versus strain-intensity curve is simply the uniaxial stress-strain curve for an isotropic material.* This powerful identity enables us to directly use the usual uniaxial stress-strain curve as the stress-intensity versus strain-intensity curve, so no special stress-intensity versus strain-intensity curve need be measured. Thus, we define three variable material properties on the *nonlinear uniaxial stress-strain curve* in Figure 3-108. First, the secant modulus, E_{sec}, is the slope of a line from the origin of the stress-strain curve to the active stress point (the stress level being considered):

$$E_{sec} = \frac{\sigma_i}{\varepsilon_i} = \frac{\sigma}{\varepsilon} \qquad (3.455)$$

Second, the tangent modulus, E_{tan}, is the stress-strain curve slope at the active stress point:

$$E_{tan} = \frac{d\sigma_i}{d\varepsilon_i} = \frac{d\sigma}{d\varepsilon} \qquad (3.456)$$

Third, Poisson's ratio, ν, is

$$\nu = -\frac{\varepsilon_y}{\varepsilon_x} \qquad (3.457)$$

for an applied uniaxial σ_x and is derived by Gerard and Wildhorn [3-88] to be

$$\nu = \frac{1}{2} - \left(\frac{1}{2} - \nu_e\right)\frac{E_{sec}}{E} \qquad (3.458)$$

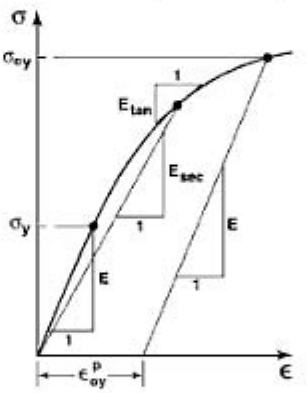


Figure 3-108 Nonlinear Stress-Strain Curve

in which ν_e is the elastic Poisson's ratio and E is the elastic Young's modulus. Thus, a smooth transition is provided between the elastic compressible state and the plastic incompressible state of the material as opposed to Stowell's and Ilyushin's assumption that ν is always the plastically incompressible state Poisson's ratio ($\nu = \nu_e = \nu_p = 1/2$).

Éléments sous droits d'auteur

3.8.2.2 Variation of Strains during Buckling

During buckling, the strains vary from their prebuckling values. Let the variation be denoted by δ. Then,

$$\begin{aligned}\delta\varepsilon_x &= \delta\varepsilon_x^o - z\delta\kappa_x\\ \delta\varepsilon_y &= \delta\varepsilon_y^o - z\delta\kappa_y\\ \delta\gamma_{xy} &= \delta\gamma_{xy}^o - z\delta\kappa_{xy}\end{aligned} \tag{3.459}$$

in which the plate middle surface is the reference surface; $\delta\varepsilon_x^o$, $\delta\varepsilon_y^o$, $\delta\gamma_{xy}^o$ are the variations in middle-surface strains,

$$\begin{aligned}\delta\varepsilon_x^o &= \delta u_{,x}\\ \delta\varepsilon_y^o &= \delta v_{,y}\\ \delta\gamma_{xy}^o &= \delta u_{,y} + \delta v_{,x}\end{aligned} \tag{3.460}$$

$\delta\kappa_x$, $\delta\kappa_y$, $\delta\kappa_{xy}$ are the variations in middle-surface curvatures from an initially flat plate,

$$\begin{aligned}\delta\kappa_x &= \delta w_{,xx}\\ \delta\kappa_y &= \delta w_{,yy}\\ \delta\kappa_{xy} &= 2\delta w_{,xy}\end{aligned} \tag{3.461}$$

and δu, δv, δw are the variations in the middle-surface displacements that occur during buckling.

3.8.2.3 Variation of Stresses during Buckling

During buckling, the stresses and the nonlinear material properties, E_{sec} and ν, in Equation (3.454) vary from their prebuckling values, e.g.,

$$\begin{aligned}\delta\sigma_x = {} & \frac{E_{sec}}{1-\nu^2}(\delta\varepsilon_x + \nu\delta\varepsilon_y) + (\varepsilon_x + \nu\varepsilon_y)\frac{\delta E_{sec}}{1-\nu^2}\\ & + \varepsilon_x E_{sec}\delta\left[\left(1-\nu^2\right)^{-1}\right] + \varepsilon_y E_{sec}\delta\left[\nu\left(1-\nu^2\right)^{-1}\right]\end{aligned} \tag{3.462}$$

That is, each term in the equations for the stresses is a function of stress level. Accordingly, the following variations are required:

$$\delta E_{sec} = -\frac{E_{sec}^2}{\sigma_i}\left[1 - \frac{E_{tan}}{E_{sec}}\right]\delta\varepsilon_i \tag{3.463}$$

$$\delta\left[\left(1-\nu^2\right)^{-1}\right] = \left[2\nu/\left(1-\nu^2\right)^2\right]\delta\nu \tag{3.464}$$

$$\delta\left[\nu\left(1-\nu^2\right)^{-1}\right] = \left[\left(1+\nu^2\right)/\left(1-\nu^2\right)^2\right]\delta\nu \tag{3.465}$$

From the fundamental relation for Poisson's ratio, Equation (3.458), and the variation in E_{sec}, Equation (3.463),

$$\delta\nu = (1-2\nu)\frac{E_{sec}}{2\sigma_i}\left[1 - \frac{E_{tan}}{E_{sec}}\right]\delta\varepsilon_i \tag{3.466}$$

Éléments sous droits d'auteur

so that all variations of the material properties are expressed in terms of $\delta\varepsilon_i$ which, in turn, can be obtained from ε_i [Equation (3.453)] as

$$\delta\varepsilon_i = \frac{1}{2H\sigma_i(1-\nu^2)}\Big[[(2-\nu)\sigma_x - (1-2\nu)\sigma_y]\delta\varepsilon_x + [(2-\nu)\sigma_y - (1-2\nu)\sigma_x]\delta\varepsilon_y + 3(1-\nu)\tau_{xy}\delta\gamma_{xy}\Big] \tag{3.467}$$

in which

$$H = 1 - \frac{1-2\nu}{2(1-\nu^2)}\left[1 - \frac{E_{tan}}{E_{sec}}\right] \times \left[2\nu + \frac{1}{2\sigma_i^2}\left[-(1+2\nu)(\sigma_x^2+\sigma_y^2) + 2(2+\nu)\sigma_x\sigma_y - 6(1+\nu)\tau_{xy}^2\right]\right] \tag{3.468}$$

Finally, the relation for $\delta\sigma_x$, Equation (3.462), becomes

$$\delta\sigma_x = \frac{E_{sec}}{1-\nu^2}\left[\delta\varepsilon_x + \nu\delta\varepsilon_y + \left[1 - \frac{E_{tan}}{E_{sec}}\right]\frac{1}{2H\sigma_i^2} \times \left[-\sigma_x + \frac{(1-2\nu)}{2(1-\nu^2)}(\sigma_y + \nu\sigma_x)\right]\Big[[(2-\nu)\sigma_x - (1-2\nu)\sigma_y]\delta\varepsilon_x + [(2-\nu)\sigma_y - (1-2\nu)\sigma_x]\delta\varepsilon_y + 3(1-\nu)\tau_{xy}\delta\gamma_{xy}\Big]\right] \tag{3.469}$$

The expressions for $\delta\sigma_y$ and $\delta\tau_{xy}$ are obtained in the same manner as is $\delta\sigma_x$, and all the expressions for the variations in stresses during buckling in terms of the variations in strains, membrane prebuckling stresses, and prebuckling material properties can be written. For the present loading condition of only combinations of N_x and N_y, $\tau_{xy} = 0$, so the stress variations simplify from Jones' more general treatment [3-83] to

$$\begin{aligned}\delta\sigma_x &= \frac{E_{sec}}{1-\nu^2}(K_{11}\delta\varepsilon_x + \nu K_{12}\delta\varepsilon_y)\\ \delta\sigma_y &= \frac{E_{sec}}{1-\nu^2}(\nu K_{12}\delta\varepsilon_x + K_{22}\delta\varepsilon_y)\\ \delta\tau_{xy} &= \frac{E_{sec}}{1-\nu^2}K_{33}\delta\gamma_{xy}\end{aligned} \tag{3.470}$$

in which

$$\begin{aligned}K_{11} &= 1 - \frac{K}{4(1-\nu^2)}[(2-\nu)\sigma_x - (1-2\nu)\sigma_y]^2\\ K_{12} &= 1 - \frac{K}{4\nu(1-\nu^2)}[(2-\nu)\sigma_y - (1-2\nu)\sigma_x][(2-\nu)\sigma_x - (1-2\nu)\sigma_y]\\ K_{22} &= 1 - \frac{K}{4(1-\nu^2)}[(2-\nu)\sigma_y - (1-2\nu)\sigma_x]^2\\ K_{33} &= (1-\nu)/2\end{aligned} \tag{3.471}$$

Éléments sous droits d'auteur

in which

$$K = \frac{1}{H\sigma_i^2}\left[1 - \frac{E_{tan}}{E_{sec}}\right] \tag{3.472}$$

For elastic behavior, $E_{sec} = E_{tan} = E$ and $K = 0$, so the K_{ij} reduce to unity, and the variations of stresses, Equation (3.470), are identical to the variations in elastic stresses for isotropic materials.

3.8.2.4 Variation of Forces and Moments during Buckling

The variations of the forces per unit width during buckling are obtained by integrating the variations of the biaxial stresses through the plate thickness, e.g.,

$$\delta N_x = \int_{-t/2}^{t/2} \delta\sigma_x dz \tag{3.473}$$

Then, the variations in forces during buckling can be written as

$$\begin{aligned} \delta N_x &= A_{11}\delta\varepsilon_x^o + A_{12}\delta\varepsilon_y^o \\ \delta N_y &= A_{12}\delta\varepsilon_x^o + A_{22}\delta\varepsilon_y^o \\ \delta N_{xy} &= A_{33}\delta\gamma_{xy}^o \end{aligned} \tag{3.474}$$

in which the A_{ij}

$$A_{ij} = K_{ij}\frac{E_{sec}t}{1-\nu^2},\ i = j \qquad A_{12} = \nu K_{12}\frac{E_{sec}t}{1-\nu^2} \tag{3.475}$$

are the plate extensional stiffnesses (no longer the same as for isotropic materials because $K_{11} \neq K_{22} \neq 1$ and $K_{12} \neq 1$ thereby effectively creating an orthotropic material when yielding has occurred).

The variations of the moments per unit width during buckling are obtained by integrating the moment of the variations of the biaxial stresses through the plate thickness, e.g.,

$$\delta M_x = \int_{-t/2}^{t/2} \delta\sigma_x z dz \tag{3.476}$$

Then, the variations in moments during buckling can be written as

$$\begin{aligned} \delta M_x &= D_{11}\delta\kappa_x + D_{12}\delta\kappa_y \\ \delta M_y &= D_{12}\delta\kappa_x + D_{22}\delta\kappa_y \\ \delta M_{xy} &= D_{33}\delta\kappa_{xy} \end{aligned} \tag{3.477}$$

in which the D_{ij}

$$D_{ij} = K_{ij}\frac{E_{sec}t^3}{12(1-\nu^2)},\ i = j \qquad D_{12} = \nu K_{12}\frac{E_{sec}t^3}{12(1-\nu^2)} \tag{3.478}$$

are the plate bending stiffnesses (no longer the same as for isotropic materials because $K_{11} \neq K_{22} \neq 1$ and $K_{12} \neq 1$ thereby effectively creating an orthotropic material when yielding has occurred).

Éléments sous droits d'auteur

3.8.2.5 Buckling Criterion

The buckling differential equation for flat rectangular plates under biaxial in-plane loading, Equation (3.162) on page 262, can be written as

$$-\delta M_{x,xx} + 2\delta M_{xy,xy} - \delta M_{y,yy} + \bar{N}_x \delta w_{,xx} + \bar{N}_y \delta w_{,yy} = 0 \qquad (3.479)$$

Upon substitution of the expressions for the variations in moments during buckling from Equations (3.477), and the expressions for the variations of the middle-surface curvatures from Equation (3.461), the buckling differential equation, Equation (3.479), becomes

$$D_{11}\delta w_{,xxxx} + 2(D_{12} + 2D_{33})\delta w_{,xxyy} + D_{22}\delta w_{,yyyy} + \bar{N}_x \delta w_{,xx} + \bar{N}_y \delta w_{,yy} = 0 \qquad (3.480)$$

We seek the solution to the buckling differential equation for the simply supported edge boundary conditions

$$\begin{aligned} &\delta w = 0 \text{ along all edges} \\ &\delta M_x = 0 \text{ along edges } x = \text{constant} \\ &\delta M_y = 0 \text{ along edges } y = \text{constant} \end{aligned} \qquad (3.481)$$

The following buckling displacement satisfies the boundary conditions, Equation (3.481) (but, of course, has indeterminate amplitude, $\tilde{w}$):

$$\delta w = \tilde{w} \sin \frac{m\pi x}{a} \sin \frac{n\pi y}{b} \qquad (3.482)$$

in which the values m and n are the (integer) number of axial and lateral half-waves in the sinusoidal buckle patterns of the plate. The buckling displacement is shown in Figure 3-109 for $m = 2$ and $n = 1$, i.e., two half-waves in the x-direction and a single half-wave in the y-direction. Note the nodal line in the middle of the plate where no buckling displacement occurs. The buckling displacement is substituted in the buckling differential equation, Equation (3.480). For a nontrivial solution to the resulting equation, the coefficient of $\tilde{w} \sin(m\pi x/a) \sin(n\pi y/b)$ must be zero, and the following buckling criterion results:

$$\begin{aligned} &(m\pi/a)^2 \bar{N}_x + (n\pi/b)^2 \bar{N}_y \\ &= D_{11}(m\pi/a)^4 + 2(D_{12} + 2D_{33})(m\pi/a)^2 (n\pi/b)^2 + D_{22}(n\pi/b)^4 \end{aligned} \qquad (3.483)$$

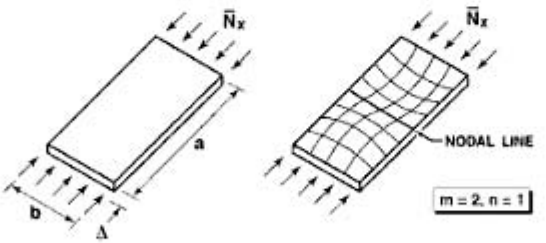


Figure 3-109 In-Plane Loaded Plate Before Buckling and Typical Buckling Mode

Éléments sous droits d'auteur

in which the bending stiffnesses on the right-hand side are a function of the buckling loads on the left-hand side, so Equation (3.483) is a transcendental relationship that must be solved by trial and error for the plastic buckling load. Because of the many parameters, the need to examine a large range of buckling modes (values of m and n) to find the mode for the lowest buckling load, and the search procedure for the transcendental equation, a computer is essential for practical numerical work (see Jones [3-89]). The solution represented by Equation (3.483) reduces to Stowell's plastic buckling solution if $\nu = 1/2$ [3-84] and to the classical Euler load for elastic plates by Bryan [3-1].

3.8.3 Solution Strategy

The general procedure for solving the transcendental equation governing plastic buckling for plates, Equation (3.483), is essentially the same as for the plastic bar buckling problem in Section 2.10. A similar logic flow chart applies, i.e., Figure 3-110. However, for a plate, the material properties are a much more complicated function of the load level than for a bar. This added complexity is caused by the biaxial state of stress in the plate and the need to relate that state of stress to the material properties. Also, the buckling criterion for plates is a much more complicated function to evaluate than for bars.

One of the major complications in the plate solution is the need to investigate the influence of buckle mode shape on the buckling load itself within the overall solution strategy in Figure 3-110. That is, the plate buckling load in Equation (3.483) is a function of the buckling mode shape parameters m and n. In contrast, the column buckling load can, of course, be expressed in terms of the single buckle mode shape parameter, m, i.e.,

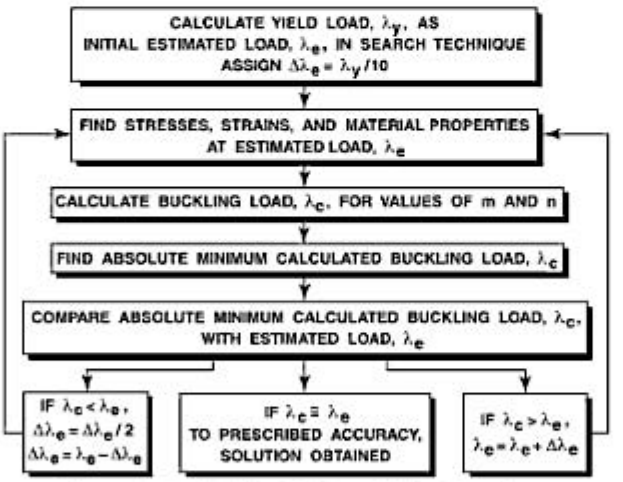


Figure 3-110 Buckling Criterion Solution Procedure

Éléments sous droits d'auteur

$$\bar{P} = m^2 \pi^2 \frac{E(P)I}{L^2} \tag{3.484}$$

However, because we are usually interested only in the lowest buckling load, m is always one. For plates, both m and n enter the equation as well as the plate aspect ratio, a/b, in a complicated-enough fashion that the lowest buckling load does not usually occur for m = 1 and n = 1, although it does for nearly square plates. Thus, we must find the absolute minimum of the values of the calculated buckling load, λ_c, for a wide range of m and n values. See Appendix B for a generic description of a buckling mode shape search procedure and also a FORTRAN subroutine, MINIMA, for how to find the absolute minimum buckling load for some prescribed range of integer values of m and n.

If the plate buckles plastically, then the first estimated buckling load λ_{1e} at the yield load is less than the corresponding calculated buckling load λ_{1c} in Figure 3-111. Because of the concave downward nature of the stress-strain curve for most materials, *a special relation exists between all estimated and calculated buckling loads.* If the estimated buckling load, λ_e, is too low, then the calculated buckling load, λ_c, is too high because the material properties are too high. Conversely, if λ_e is too high, then λ_c is too low because the material properties are too low. This special relationship between λ_e and λ_c is the key to knowing whether to increase or decrease λ_e in the search procedure as we observed in Section 2.10. The estimated buckling load is less than the actual buckling load for the first three estimated buckling loads in Figure 3-111. The fourth estimated buckling load leads to a calculated load that is below the estimated buckling load because the estimate is above the actual buckling load. The rest of the search strategy, including its convergence to the actual buckling load, is described in Section 2.10.5, Solution Strategy, on pages 193–196.

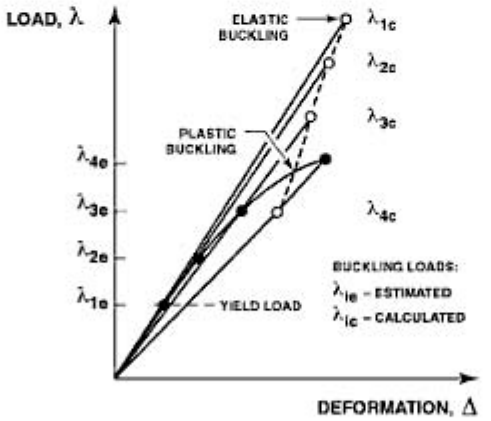


Figure 3-111 Estimated and Calculated Buckling Loads

Éléments sous droits d'auteur

3.8.4 Numerical Results

Consider plates made of 7075-T6 aluminum for which the nonlinear stress-strain curve is shown in Figure 3-112. The plate material is represented with the Nadai stress-strain curve [3-90] which is described in Section 2.10.6 starting on page 196.

$$\sigma \le \sigma_y : \quad \varepsilon = \frac{\sigma}{E}$$

$$\sigma > \sigma_y : \quad \varepsilon = \frac{\sigma}{E} + .002\left[\frac{\sigma - \sigma_y}{\sigma_{oy} - \sigma_y}\right]^n \tag{3.485}$$

in which σ_y is the yield stress, σ_{oy} is the offset yield stress at $\varepsilon^p_{oy} = .002$ as in Figure 3-108 on page 410, and n is a material parameter that determines the shape of the stress-strain curve. That aluminum has the following values of the Nadai stress-strain curve model parameters:

σ_y = 55 ksi (380 MPa) E = 10.5x10^3 ksi (72.4 GPa)

σ_{oy} = 72 ksi (500 MPa) n = 2.16

for which the measured stress-strain curve points used to determine n are (σ_1 = 63.5 ksi (438 MPa), ε_1 = .00649) and (σ_2 = 72 ksi (500 MPa), ε_2 = .00883). The elastic Poisson's ratio is ν_e = .32.

Use of a plates version of the BOPS computer program [3-89] to obtain buckling loads is straightforward. The program is merely the implementation of the buckling criterion in Equation (3.483) embedded in the solution strategy of Section 3.8.3 for a specified range of buckle mode values. For a plate of thickness t = .37 in (.94 cm), length a = 10 in (25.4 cm), and variable width, the elastic and plastic buckling forces are shown in Figure 3-113 as the usual festooned curves with various buckling mode shapes that change at cusps. The plate always buckles into one lateral half-sine wave, i.e., n = 1, with a variable number of axial half-sine waves, m. The yield load is 20,350 lb/in (3.564 MN/m) and corresponds

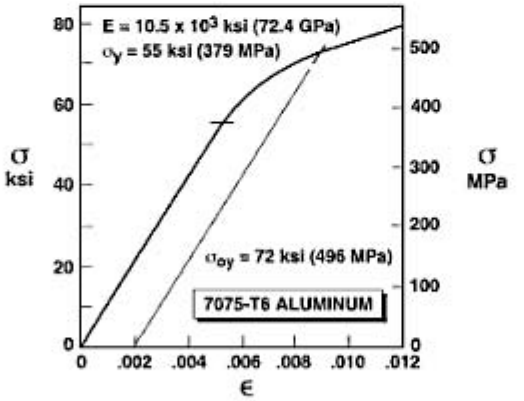


Figure 3-112 Stress-Strain Curve for 7075-T6 Aluminum

Éléments sous droits d'auteur

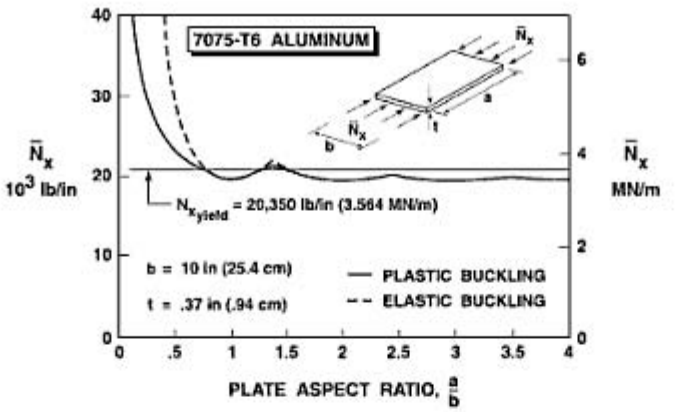


Figure 3-113 Plastic Buckling of Plates [t = .37 in (.94 cm)]

to an axial (yield) stress of 55 ksi (380 MPa). If the plate is longer than a/b = 1.5, then buckling is always elastic. Below a/b = .6, very large reductions from elastic to plastic buckling load are observed. In the intermediate range of a/b from .6 to 1.5, sometimes the buckling is elastic and sometimes plastic. In the vicinity of a/b = 1.4, plastic buckling occurs, but on each side of a/b = 1.4, the buckling is elastic.

For a thicker plate, buckling is always plastic, and even larger reductions from the elastic buckling loads are seen for t = .40 in (1.02 cm) in Figure 3-114 than in Figure 3-113. For a thinner plate, all buckling is elastic except at very low plate aspect ratios. That is, only in the vicinity of t = .37 in (.94 cm) is a transition from elastic to plastic buckling observed with varying plate aspect ratio, a/b. Also note in Figure 3-114 that

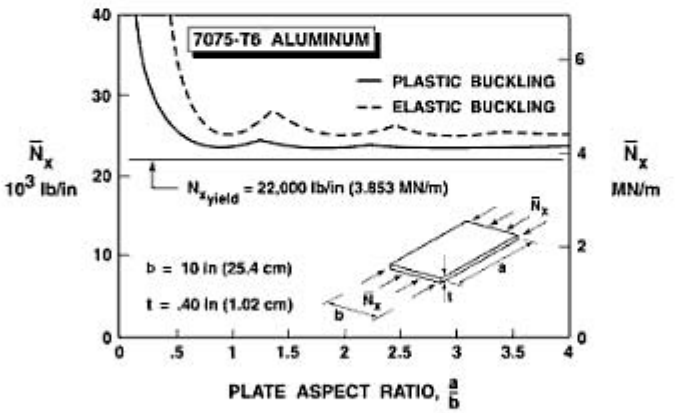


Figure 3-114 Plastic Buckling of Plates [t = .40 in (1.02 cm)]

Éléments sous droits d'auteur

buckle mode shape changes (the cusps) occur at lower values of a/b for plastic buckling than for elastic buckling. The cusps in the plastic buckling results migrate from coincidence with the cusps in the elastic buckling results for thin plates toward lower values of a/b than for the elastic buckling results as the plate thickness increases. Thus, the plate that buckles plastically behaves as if it were longer than the elastic plate.

3.8.5 Comparison of Theoretical and Experimental Results

To establish confidence in the plastic buckling of plates analysis, we examine predicted and measured stresses for uniaxial loading. Definitive plastic versus elastic buckling experiments are quite difficult to perform with plates. Actually creating the simply supported edge boundary conditions on all four edges of a plate to which the present theory applies is quite difficult, if not nearly impossible, to precisely accomplish under conditions of in-plane loading. For a plate with flat edges under axial compression between the platens of a loading frame, the real boundary conditions at the loaded ends are somewhere between simply supported and fixed (clamped) because the flat edges cannot rotate freely against the platens. The principal problem is loading the plate and simultaneously permitting both the loaded edges and the non-loaded edges to freely rotate. Certainly, in any practical loading condition, the theoretical approximations to the actual boundary conditions can be quite crude.

Pride and Heimerl [3-91] measured buckling stresses for uniaxially loaded simply supported rectangular plates of 14S-T6 aluminum (now known as 2014-T6). Simply supporting all four edges and also applying load up to the buckling load is a very difficult experimental problem, as just discussed. Pride and Heimerl largely avoided that difficulty by employing a technique suggested by Timoshenko [3-8] (Figure 9-3, p. 356). He observed that it is possible to reduce the influence of the boundary conditions along the two non-loaded lateral edges of a plate by axially loading thin-walled square-cross-section tubes and then interpreting each side or wall of the tube as a simply supported plate as in Figure 3-115. There, each adjacent side or wall of the tube rotates at the adjoining edges such that no restraining moment occurs. Hence, the four sides or walls of the tube are effectively four simply supported plates *if the loaded edges of the tube are simply supported.*

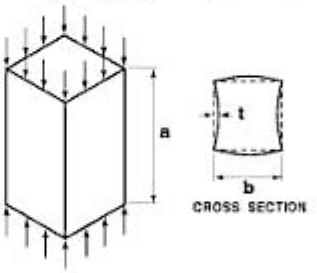


Figure 3-115 Timoshenko's Tube-as-Four-Plates Experiment for Simply Supported Edges

Use of thin-walled square-cross-section tubes is not the perfect solution to the simply supported edge boundary condition problem because the loaded edges at each end of the tube are certainly not simply supported. Instead, each tube end was machined flat so that it mounted evenly against each platen of a load frame. Thus, the edges at each end

Éléments sous droits d'auteur

are somewhere between fixed and simply supported. However, the longer the tube, the lower the influence the end conditions have on the buckling load. If the tube is too short, each tube wall (plate) is affected by end effects as if it were partially clamped on at least one end edge, so the buckling stress exceeds that of a simply supported plate. In addition, the tube must be short enough that local buckling of the tube walls as plates as in Figure 3-115 occurs before buckling of the long tube as a column or bar. Pride and Heimerl determined that the tube length must be at least four times the tube width, i.e., $a/b > 4$, before a minimum buckling load is achieved in order to avoid the influence of end effects. In contrast, the theoretical results for a simply supported elastic plate have equal minima of the buckling stresses at all integer values of a/b, including low values of $a/b = 1, 2, 3, \ldots$, as shown in Figure 3-113.

We compare predicted and measured buckling stresses on the basis of the important plate geometric parameters width-to-thickness ratio, b/t, and aspect ratio, a/b. Pride and Heimerl varied the plate aspect ratio, a/b, and the plate width-to-thickness ratio, b/t, by using different lengths and cross sections of commercially available drawn tubes. They observed that the material properties changed somewhat from specimen to specimen as did the thicknesses as well as other dimensions. Pride and Heimerl's results [3-91] for $a/b = 4.5$ (long enough that end effects are small) and various b/t are shown as circles in Figure 3-116. There, two experimental results are shown for each of four b/t ratios. The two measured elastic buckling results are in excellent agreement with the predicted elastic buckling curve (with the usual hyperbolic shape). Also, the six measured plastic buckling results agree very well with the predicted plastic buckling curve obtained with use of the Nadai stress-strain curve model [3-90] by Jones [3-71]. If the somewhat lower material properties of the two specimens at $b/t = 22.5$ were adjusted as if they were made of the same material as for the other data points (as is sug-

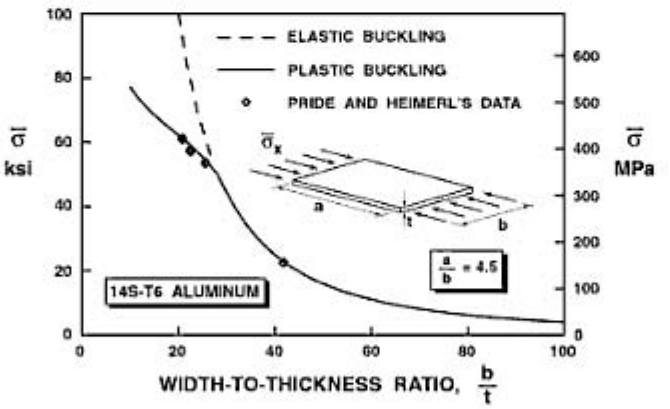


Figure 3-116 Buckling of Uniaxially Loaded Simply Supported Plates *(After Jones [3-71])*

Éléments sous droits d'auteur

gested by Pride and Heimerl), those two points would rise by about 1 ksi making the agreement between the measured and predicted buckling stresses excellent. Pride and Heimerl reported other buckling results that were primarily elastic, but all were at a/b values other than 4.5, so they are not comparable to results for a/b = 4.5 in Figure 3-116. Agreement between measured and predicted results in Figure 3-116 gives us confidence that the present plastic buckling analysis is essentially correct.

Plastic buckling stresses for mechanical loading generally can also be plotted as a function of the plate aspect ratio, a/b, as for the elastic results in Figure 3-113, so we can learn even more about the transition from elastic buckling to plastic buckling. Pride and Heimerl's results could not be effectively plotted against a/b because the tube a/b had to be four or greater to avoid the influence of end effects. Moreover, each plot of $\bar{\sigma}$ versus a/b must be for a specific plate-width-to-thickness ratio, b/t. Only one group of their measured results could be plotted, namely at a/b = 4.5 with variable b/t. Of course, if the data agree well with the theory for constant a/b and variable b/t as in Figure 3-116, then we would certainly expect them to also agree for constant b/t and variable a/b (except any tube data for a/b < 4).

3.8.6 Summary

A solution for the plastic buckling of flat rectangular plates subjected to uniform in-plane forces, N_x and N_y, is derived by use of a deformation theory of plasticity for simply supported edge boundary conditions. The theory includes a continuously variable Poisson's ratio as plastic deformation increases from the elastic regime toward a fully plastic regime. The Nadai stress-strain curve is used to successfully model a reasonably nonlinear material, namely aluminum. Numerical results are obtained for plates with two different thicknesses as a function of plate aspect ratios. Plastic effects are found to be more broadly applicable and influential for low-aspect-ratio, thick plates than for high-aspect-ratio, thin plates. Loading the plate above the proportional limit of the material significantly lowers the buckling load from the elastic value, as we would expect.

The present simply supported edge plastic buckling solution is a lower bound on the true solution if initial geometric imperfections and prebuckling deformations are ignored (no prebuckling deformations should exist without initial geometric imperfections). For long plates (a/b > 4), the present theory is in very good agreement with the experimental results of Pride and Heimerl [3-91].

Problem Set 3.8

3.8.1 Demonstrate for a uniaxial stress state (σ_x plus ε_x and $\varepsilon_y = -\nu\varepsilon_x$) that the stress intensity is $\sigma_i = \sigma_x$ and the strain intensity is $\varepsilon_i = \varepsilon_x$.

3.8.2 Derived the variation of σ_x, Equation (3.462).

3.8.3 Start from the definition of E_{sec}, Equation (3.455), and derive the expression for δE_{sec} in Equation (3.463).

3.8.4 Start from the biaxial stress-strain relations, Equation (3.454), and show, for a uniaxial state of stress as in the bar buckling problem, that the equation for the variation in σ_x during buckling, i.e., the uniaxial version of Equation (3.462), reduces to $\delta\sigma_x = E_{tan}\,\delta\varepsilon_x$, i.e., the tangent-modulus relation used by Shanley [3-85].

Éléments sous droits d'auteur

3.9 ASPECTS OF DESIGN OF PLATES AGAINST BUCKLING

3.9.1 Introduction

Much of the discussion of bar design is also applicable to plates, so please review Section 2.11, Aspects of Design of Bars Against Buckling, before addressing plates design. There, fundamental design versus analysis issues are treated as well as support conditions, material properties, and other characteristics affecting design. We will focus here on those factors that distinguish plates from bars with concentration on generic design procedures. Both isotropic plates and laminated fiber-reinforced composite plates will be addressed including stiffened plates of both types. First, we examine several general structural design considerations of high interest and direct applicability.

3.9.2 Steps in the Structural Design Process

In structural design, we start with a set of design requirements in order to define our objectives. The *design requirements* are merely a statement of what we want the structure to do and/or be. The three principal *design objectives* are function, cost, and weight. *Function* is the set of performance requirements or design requirements that the structure must meet or be able to do. *Cost* is the life-cycle cost of the structure, i.e., the initial purchase price plus the operating and maintenance costs over the life of the structure less any scrap value at the end of the structure's life. *Weight* is obviously the structural weight and might or might not be important. For aircraft, low weight is obviously crucial. For spacecraft, low weight is all-important. For buildings, weight is not usually a significant factor, although the structure weight certainly does affect individual member sizing. Note that function often has many sub-objectives, whereas cost and weight are each single objectives.

The structure can be optimized, i.e., designed, for any one, two, or all three design objectives. That is, the design objectives might be to have the lowest weight aircraft for a specified set of functions that must be performed. Or, the highest speed aircraft might be the most important objective with cost being allowed to rise in order to achieve the desired speed. Perhaps the cost might be minimized with certain compromises made for performance or weight. In all cases, every design must be measured against fundamental design objectives expressed in terms of function, cost, and weight.

The structural design process is depicted by means of a schematic flow chart in Figure 3-117. That is, the flow chart is not a precisely defined computer program flow chart, but is instead a flow chart of ideas, concepts, and procedures, i.e., the *all-important logic* of the design process. We start presumably knowing the loads that must be carried and what materials might possibly be considered for our design. Through some process, we then choose an initial configuration for our structure. That configuration might be very crude, but constitutes a start to the *necessarily iterative design process*. At this point, we might have a significant problem because if our structure is an airplane, we do not know

Éléments sous droits d'auteur

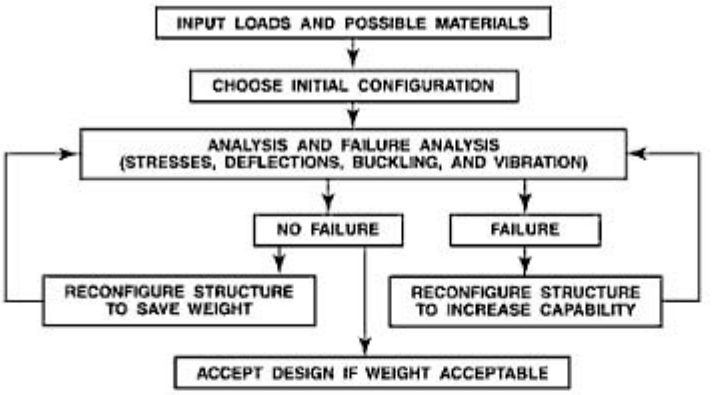


Figure 3-117 The Structural Design Process

the precise aerodynamic loads without knowing the actual structural configuration. Thus, sometimes there is a lot of interplay between choosing the initial configuration and determining the loads used in design. Accordingly, the design process is often not as simple as portrayed here. However, once we have the initial configuration, some knowledge of the loads, and some idea of what materials we might like to use, then we can begin the actual structural design process.

We go next to the analysis and failure analysis block in Figure 3-117. That is, we consider the initial configuration with a particular material or set of materials. Then, for the prescribed loads, we perform a set of structural analyses to get the various structural response parameters such as stresses, displacements, buckling loads, natural frequencies, etc. Those analyses are all deterministic processes. That is, within the limits of accuracy of the available analysis techniques, we are able to predict a specific set of responses for a particular structural configuration. We must know how a particular structural configuration behaves so we can compare the actual behavior with the desired behavior, i.e., with the design requirements in the context of the design objectives.

Reconfiguration of a structure simply means to change some or all of the design variables such as thicknesses, fiber directions, stiffener sizes, etc. to achieve a more suitable structure than the current configuration. Note that the term 'more suitable' has two possible meanings. If the structure has too little capability relative to the loads and conditions we place on it, then the structure is underdesigned, and we must reconfigure the structure to *increase* its capability. However, if the structure has too much capability, then it is overdesigned, and we must reconfigure the structure to actually *decrease* its capability. Both alternatives will be discussed. Recognize that *structural reconfiguration is the very heart of structural design*, and the logic to accomplish reconfiguration is the key to the design process.

Éléments sous droits d'auteur

Suppose we perform the failure evaluation for the current structural configuration and find some kind of a failure, i.e., a violation of one or more of the design requirements (not necessarily a fracture!). Thus, the current structure is underdesigned, so its capacity must be increased. Accordingly, we must move to the next box labeled *reconfigure the structure to increase capability*. The word *capability* is used here in a very broad sense. Increasing the capability could mean increasing the stiffness to change the deflection conditions. That is, increasing capability could mean decreasing deflections if that was the violated design requirement. Increasing capability could also mean increasing buckling loads or increasing vibration frequencies. That is, somehow we must *reconfigure the structure to increase the basic structural capabilities*. Under some circumstances, we might actually want to decrease the stiffness to avoid an exciting frequency that could drive the structure into resonance.

If the current design in the iterative design process depicted in Figure 3-117 did not fail, then the structure is overdesigned. Accordingly, we must change the structure, i.e., reconfigure the structure, so that it will carry the same load but at a lower weight. And at that lower weight we must reevaluate the structural performance. Thus, we must go through some process to *reconfigure the structure to save weight*. After reconfiguration, we proceed back up on the flow chart in Figure 3-117 to the analysis and failure analysis box because we now have a new configuration to evaluate. We must go through the process all over again of determining the structural response parameters and comparing them with their allowable values.

With the newly reconfigured structure, we go back to the analysis and failure analysis block in Figure 3-117 and evaluate the new configuration. We keep cycling around the diagram (figuratively speaking) between failures and no failures until the design is refined to the point where it has the least weight and satisfies all the design functional requirements, i.e., does not fail in any of the possible ways. Those conditions are what is meant by the design not violating any of the design requirements in general. Then, we would accept that design if the weight is acceptable. Perhaps, from other analyses, we have determined that the airplane being designed cannot weigh more than a certain amount. Otherwise, for various propulsion requirements, we cannot make the plane travel at the required speed or have the required range and so on (those issues are design requirements, too). After all the design requirements are satisfied and the weight is as small as possible, then the design is declared to be satisfactory. The same kind of overall design process can be performed with a governing parameter other than weight. The other design parameter could be cost, or it could be various performance-related objectives, or some combination thereof.

The extent to which we try to optimize the structure depends on the relative value and characteristics of the structure. If the structure is not crucial or weight-critical, then we might be satisfied with only enough iterations to achieve a design that merely works, but is not the 'best' design. On the other hand, if the structure is quite crucial including perhaps weight-sensitive and/or cost-sensitive, then we must iterate to the 'best' solution within the constraints of time and money.

Éléments sous droits d'auteur

3.9.3 Design of an Isotropic Plate

Let's start by examining in a quantitative manner the design process for isotropic plates. First, we'll address design against high stresses, and then we'll consider design against buckling. In both cases, we will examine the attributes of the pertinent analysis equations to see if they can be used directly in the design process. Unlike a column or bar with its variability in cross-sectional shape, an isotropic plate has a simple fixed shape that is easier to design than a bar. That is, a plate has only one design variable, the thickness, if the material is known. Of course, if the material can be changed, then the number of design variables is doubled. One of the principal observations based on the bar design process already described in Section 2.11 is that we must pay attention to the number of knowns and the number of unknowns to determine our design procedure. That is, is the procedure deterministic or nondeterministic? Obviously, any nondeterministic process is far more complex and involved than a deterministic process.

3.9.3.1 Design of an Isotropic Plate Against Failure Caused by High Stresses

For an isotropic plate under extensional loading, N_x only as in Figure 3-118, the load (which could be tensile) is related to the strains by

$$N_x = \frac{E\,t}{(1-\nu^2)}(\varepsilon_x^\circ + \nu\varepsilon_y^\circ)$$
$$N_y = \frac{E\,t}{(1-\nu^2)}(\varepsilon_y^\circ + \nu\varepsilon_x^\circ) = 0 \qquad (3.486)$$

Then, from the lateral force condition that $N_y = 0$,

$$\varepsilon_y^\circ = -\nu\varepsilon_x^\circ \qquad (3.487)$$

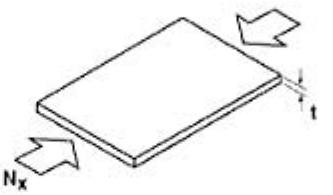


Figure 3-118 Plate under N_x only

the applied force becomes

$$N_x = E\,t\,\varepsilon_x^\circ \qquad (3.488)$$

Thus, for a prescribed allowable strain, we can solve for the plate thickness necessary to avoid failure caused by high stresses:

$$t_{required} = \frac{\text{Factor of Safety} \times N_x}{E\,\varepsilon_{allowable}} \qquad (3.489)$$

The factor of safety is explicitly stated in Equation (3.489), but could be implicit in the value of the allowable strain. Note that different thicknesses result from Equation (3.489) for different materials with their different characteristic values of E and $\varepsilon_{allowable}$. That is, the design problem has only one answer if the material is specified, i.e., is deterministic, but many answers exist if the material is not specified, i.e., the design problem is nondeterministic. Thus, a different thickness results for each candidate material considered, so we must choose among the candidate

Éléments sous droits d'auteur

designs on the basis of least weight, least cost, or some other design merit consideration.

In a similar manner, if a bending moment, M_x only, is applied as in Figure 3-119, the moment is related to the curvatures by

$$M_x = \frac{E t^3}{12(1-\nu^2)}(\kappa_x + \nu\kappa_y)$$
$$M_y = \frac{E t^3}{12(1-\nu^2)}(\kappa_y + \nu\kappa_x) = 0 \qquad (3.490)$$

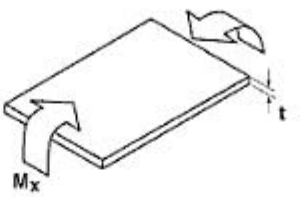


Figure 3-119 Plate under M_x only

Then, from the lateral moment condition ($M_y = 0$),

$$\kappa_y = -\nu\kappa_x \qquad (3.491)$$

Thus, the applied moment becomes

$$M_x = \frac{E t^3}{12}\kappa_x \qquad (3.492)$$

However, from the linear strain distribution through the plate thickness,

$$\varepsilon_x = \varepsilon_x^0 + z\,\kappa_x \qquad (3.493)$$

For pure bending ($\varepsilon_x^0 = 0$), the largest strain is at $z = \pm t/2$, so

$$\kappa_{x_{max}} = \frac{2}{t}\varepsilon_{x_{max}} \qquad (3.494)$$

Accordingly, the required thickness is

$$t_{required} = \left[\frac{6 \times \text{Factor of Safety} \times M_x}{E\,\varepsilon_{allowable}}\right]^{1/2} \qquad (3.495)$$

Again, the factor of safety could be explicit as in Equation (3.495) or implicitly in the definition of the allowable strain.

Thus, for both extensional loading and pure bending of isotropic metal plates, the required thickness to support a specific loading can be determined directly by an inverse of the analysis equations, i.e., the design process is *deterministic* as long as the material is specified. However, the design problem is nondeterministic if the material is not known or specified.

3.9.3.2 Design of an Isotropic Plate Against Failure by Buckling

We now ask how can we use the attributes of the bar buckling equations in the design process? One of the principal observations based on the bar design process already described in Section 2.11 is that we must pay close attention to the number of unknowns and the number of unknowns to determine the nature of our design procedure.

Plate design against buckling, unlike bar design, is deterministic if a plate material is selected prior to finding the required thickness. That is, there is no cross-sectional shape issue to resolve in plate design as there is in bar design. The key design parameter is $D = Et^3/12(1-\nu^2)$, the

Éléments sous droits d'auteur

plate bending stiffness, which involves only the material properties, E and ν, plus the geometrical factor, t, the thickness. As in bar design in which we usually know the bar length, L, we also usually know the plate in-plane dimensions, a and b. Thus, we need only solve for t (again, if we know the material we will use in the design).

We found the buckling equation for a simply supported, axially loaded rectangular plate to be Equation (3.183) on page 267.

$$\bar{N}_x = \frac{\pi^2 a^2 D}{m^2}\left[\left[\frac{m}{a}\right]^2 + \left[\frac{n}{b}\right]^2\right]^2 = k\frac{\pi^2 D}{b^2} \tag{3.496}$$

Now, in addition to wanting to know the thickness, t, we must find t for several values of m to find the minimum buckling load and hence the correct t. Thus, if the plate must support a specific $\bar{N}_x$ and the material is known as well as the desired plate dimensions a and b, then

$$t_{required} = \text{Minimum of}\left[\frac{\frac{12(1-\nu^2)}{E} \times \text{Factor of Safety} \times \frac{\bar{N}_x m^2}{\pi^2 a^2}}{\left[\left[\frac{m}{a}\right]^2 + \left[\frac{1}{b}\right]^2\right]^2}\right]^{\frac{1}{3}} \tag{3.497}$$

with respect to m. A few calculations of Equation (3.497) for several values of m should quickly lead to the correct answer.

Note that Equation (3.496) can be rearranged as

$$\frac{\bar{N}_x b^2}{\pi^2 D} = k = \left[\frac{b}{a}\right]^2 \frac{1}{m^2}\left[m^2 + \left[\frac{a}{b}n\right]^2\right]^2 \tag{3.498}$$

The value of k in Equation (3.498) is independent of D, i.e., independent of E, ν, and t. Thus, for a fixed plate aspect ratio, a/b (because we presumably know a and b for the design condition), we must find the minimum of the term in brackets. Fortunately, we have already done so graphically in the form of Figure 3-18 on page 268 repeated here as Figure 3-120. Recall that n always is 1 to obtain the least buckling load. We can plot further results for higher plate aspect ratios if needed, or we can make the conservative approximation that k = 4 for plate aspect ratios above 5. For large a/b (a long plate),

$$t_{required} = \left[\frac{3}{\pi^2}\frac{(1-\nu^2)}{E} \times \text{Factor of Safety} \times \bar{N}_x b^2\right]^{\frac{1}{3}} \tag{3.499}$$

That is, for a given plate aspect ratio, we observe the ordinate of the lowest curve (the solid portion, not the dashed portion) and then solve for the required thickness (for the candidate material).

Éléments sous droits d'auteur

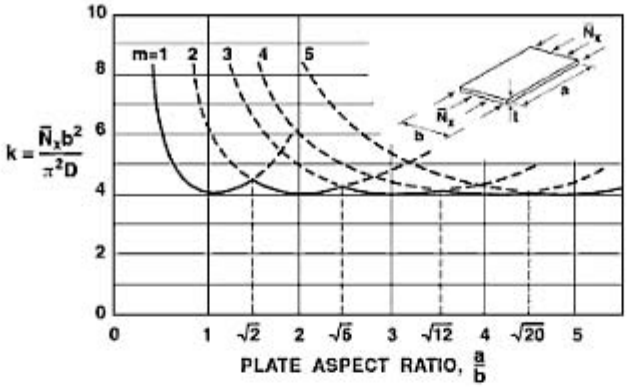


Figure 3-120 Normalized Buckling Load k for Rectangular Plates with Various Plate Aspect Ratios

If the material is not known, then the plate design problem is nondeterministic, although not as seriously as bar design with its required cross-sectional shape selection. We would determine the required plate thickness for each candidate material, and then we must choose among the candidate designs based on weight, cost, or some other design merit consideration.

If we do not know the plate dimensions, a and b, *à priori*, then the plate design problem is even more nondeterministic than if we do not know the material to be used. Of course, such free form in geometry is a complex design problem anyway. The plate dimensions, a and b, are presumably, although not always, influenced and determined by other design considerations anyway, i.e., often some other constraint determines a and b.

Consideration of plates with boundary conditions other than simply supported and/or with other loadings than axial compression N_x is possible in the manner just described only if the governing buckling equation is known in closed form. That is, without an analytic solution, there can be no 'design equation' in the manner we have just seen. For example, for axially compressed plates with various boundary conditions along the unloaded edges, we found a transcendental equation in Section 3.3.5 for the buckling load. Obviously, no closed-form solution exists, so the available tabular results must be used in the design process.

For buckling under in-plane shear, the two-term approximation for symmetric buckling in Equation 3.228) is readily solved for the thickness if a factor of safety and the material are specified. Recall, however, that this equation is about 15% too high for square plates and even more inaccurate for plates with higher a/b. Also, antisymmetric buckling with its own two-term approximation is possible for some ranges of a/b.

If no 'design equation' is possible, then we must use whatever analysis tool that is available to find the buckling load in some form of iterative

Éléments sous droits d'auteur

design procedure. For example, suppose the buckling load of the desired plate with its particular edge support conditions and loading can be found only with an approximate numerical procedure such as the finite element method. Then, that numerical solution procedure must be 'nested' inside a sequence of logical steps to use the analysis in a design mode (somehow you vary the plate thickness and determine the structural response numerically until either the stresses or the buckling load satisfy the design requirements). However, such an approach does not involve the clarity of what we just examined for a simply supported plate with N_x applied. The logic can be quite complex to 'drive' the design approach toward finding the necessary thickness of a plate to resist buckling with the specified edge support conditions and loading.

Of course, any credible design must satisfy all possible loading conditions. Thus, the design thicknesses from high stresses caused by extensional loading, from high stresses caused by moment loading, and from prevention of buckling, plus any other design condition, must simultaneously be considered. Obviously, the largest thickness of the set just described satisfies all design conditions.

3.9.3.3 Design of a Stiffened Isotropic Plate Against Failure by Buckling

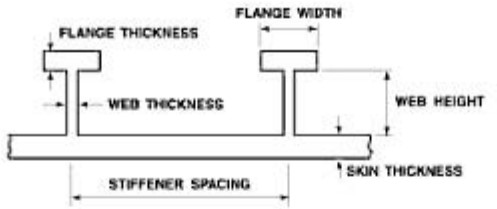
Plates are stiffened to increase their buckling load (which is dominated by the bending stiffnesses) with less weight than merely increasing the plate thickness. Stiffening concepts for two-dimensional structures are described in Section 4.7 with special emphasis on shells.

The process of describing appropriate stiffeners for plates begins with the definition of a design driver, continues with examination of typical stiffeners, and concludes with a hint of how to design stiffened plates.

A *design driver* is a design variable that, when changed, strongly influences the performance of the design. A design driver can also be a design condition that strongly influences which design variables govern the design. One of the early objectives in the design process is to identify the design drivers and concentrate on manipulating them as opposed to changing variables that do not strongly influence the design. Thus, for aircraft, we would make many decisions based on how we can get each part of the structural job done with the least amount of weight because of its strong influence on range, economy, and performance. Similarly, spacecraft have a least-weight objective because of the design driver of high cost to boost the spacecraft into space. Accordingly, it is not at all surprising that we use high-stiffness – low-weight materials such as composite materials to achieve the design objective of least weight. Cars are also weight-sensitive, in general, but some parts are especially sensitive to strength and stiffness. Trusses are stiffness-sensitive because of the tendency of compression members to buckle.

A specific example of strong and weak design drivers is developed by examining the bending resistance of the stiffened panel in Figure 3-121. There, the stiffener web height is a strong influence on the panel bending resistance because the stiffener moment of inertia is strongly

Éléments sous droits d'auteur



ALL FACTORS AFFECT PANEL BENDING RESISTANCE, BUT

- STRONG DESIGN DRIVERS
  - FLANGE THICKNESS
  - STIFFENER SPACING
  - FLANGE WIDTH
  - WEB HEIGHT
- WEAK DESIGN DRIVERS
  - WEB THICKNESS
  - SKIN THICKNESS

Figure 3-121 Anatomy of a Stiffened Panel

affected and, in turn, has a large influence on the bending resistance. However, stiffener web thickness is not a strong design driver because web thickness has little influence on bending resistance. We conclude through similar reasoning that flange thickness, flange width, and stiffener spacing are strong design drivers in Figure 3-121 and that skin thickness is a weak design driver. We must be conscious of the type of design drivers at each stage of design.

Stiffeners can have a wide variety of cross-sectional shapes, some of which are shown in Figure 3-122. For metal stiffeners, some of the shapes are typically rolled sections that are then fastened to the panel, e.g., tee, I, z, hat, or channel shapes. Fastening could be mechanical, bonding, or welding. Other more unusual shapes or thickness distributions over the cross section are typically machined integrally with the panel from material that is at least as thick as the stiffener height plus the panel thickness, e.g., inverted tee, blade, or J shapes. That machining is either mechanical, i.e., chip producing, or chemical, known as chem milling. Both machining processes are quite expensive.

To solve the stiffened plate design problem, we must include the stiffener variables in the analysis and in the design logic for reconfiguration of the structure. Further detail is beyond the scope of this book.

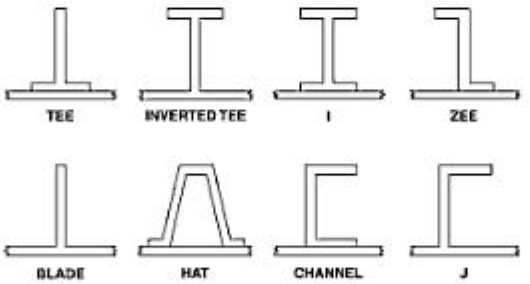


Figure 3-122 Nominal Stiffener Cross-Sectional Shapes

Éléments sous droits d'auteur

3.9.4 Design of a Laminated Composite Plate

Let's consider the structural design problem of a laminated fiber-reinforced composite plate. Obviously, we now must include more parameters than in the isotropic plate design problem, namely parameters related to the fiber-reinforced lamina material properties (engineering constants), E_1, E_2, ν_{12}, and G_{12} (which we probably would probably consider known in the design process, although we can repeat the process for several candidate materials with specific properties) and to the laminate characteristics of individual lamina thicknesses and lamina principal material direction orientations (see Jones [3-27]). You have seen claimed as attractive advantages of composite structures the fact that we can orient the laminae in a laminate to our heart's content to try to get the most efficient structure. This characteristic is totally unlike what is possible with structures made of isotropic materials. This laminae orientation flexibility is certainly an advantage, but how do we use it?

3.9.4.1 Design of a Laminated Composite Plate Against Failure Caused by High Stresses

We consider first a simple laminate that is not even practical, but will serve to illustrate an important point. For a simple symmetric cross-ply laminated plate subjected to in-plane force N_x only, as in Figure 3-118 on page 425, the force-strain relations are

$$\begin{bmatrix} N_x \\ N_y \end{bmatrix} = \begin{bmatrix} A_{11} & A_{12} \\ A_{12} & A_{22} \end{bmatrix} \begin{bmatrix} \varepsilon_x^0 \\ \varepsilon_y^0 \end{bmatrix} = \begin{bmatrix} N_x \\ 0 \end{bmatrix} \tag{3.500}$$

From the lateral force condition ($N_y = 0$),

$$0 = A_{12}\varepsilon_x^0 + A_{22}\varepsilon_y^0 \tag{3.501}$$

we get

$$\varepsilon_y^0 = -\frac{A_{12}}{A_{22}}\varepsilon_x^0 \tag{3.502}$$

Thus, the applied force becomes

$$N_x = (A_{11} - \frac{A_{12}^2}{A_{22}})\varepsilon_x^0 \tag{3.503}$$

However, recall that the extensional stiffnesses are

$$A_{ij} = \sum_{k=1}^{N} (\overline{Q}_{ij})_k t_k \tag{3.504}$$

in which the $\overline{Q}_{ij}$ are known functions of Q_{11}, Q_{12}, Q_{22}, and Q_{66} (which are defined in terms of the engineering constants in Equation (C.19) on page 762); α_k, the fiber orientation of the k^{th} layer; and the laminae thicknesses, t_k. However, we cannot solve for the laminae thicknesses,

Éléments sous droits d'auteur

number of layers, and laminae angles from a *single* (force-strain) equation. Thus, even the simplest laminate design problem is *indeterminate* or *nondeterministic* That fact creates a particularly big problem when we would actually like to optimize the laminate design, and we have trouble determining a single laminate design, much less the 'best' design.

For general laminated composite plates, the relations between forces, moments, middle-surface strains, and middle-surface curvatures,

$$\begin{bmatrix} N_x \\ N_y \\ N_{xy} \\ M_x \\ M_y \\ M_{xy} \end{bmatrix} = \begin{bmatrix} A_{11} & A_{12} & A_{16} & B_{11} & B_{12} & B_{16} \\ A_{12} & A_{22} & A_{26} & B_{12} & B_{22} & B_{26} \\ A_{16} & A_{26} & A_{66} & B_{16} & B_{26} & B_{66} \\ B_{11} & B_{12} & B_{16} & D_{11} & D_{12} & D_{16} \\ B_{12} & B_{22} & B_{26} & D_{12} & D_{22} & D_{26} \\ B_{16} & B_{26} & B_{66} & D_{16} & D_{26} & D_{66} \end{bmatrix} \begin{bmatrix} \varepsilon_x \\ \varepsilon_y \\ \gamma_{xy} \\ \kappa_x \\ \kappa_y \\ \kappa_{xy} \end{bmatrix} \tag{3.505}$$

are such complicated functions of the number of layers and the stacking sequence that no direct solution exists in the same manner as for isotropic plates. That is, there are no solutions for the required thickness of a laminated plate that are analogous to Equations (3.489) and (3.495). The problem is that we seek more than one unknown, i.e., the thickness *and* the laminae orientations, but we have only one equation! Or, at most, six equations from Equation (3.505).

The solution to this laminate design problem with more design variables than loading parameters is nontrivial. Without a direct solution, we must appeal to an indirect solution approach. One such indirect approach is described in Section 7.7.2.4 on optimization methods in Jones' *Mechanics of Composite Materials* [3-27]. There, a brute-force, try-many-possible-combinations scheme is used to find a laminate that satisfies the design requirements. Another approach is Tsai's laminate-ranking procedure [3-92], which is not a true design approach, but instead is a sequence of evaluations of different predetermined laminates under specified loading with subsequent ordering of the chosen set of laminates with respect to their ability to bear the prescribed load. The best laminate is chosen from those examined, so the actual best laminate could be missed. However, Tsai's method has the advantage that searching can be limited to those laminates or laminate families that are of interest. For example, attention might be restricted to laminates for which fatigue data are available or which are readily made.

The fundamental laminate problem is: given the overall loading and a rough idea of the shape that we want, what is the optimum set of laminae orientations that constitute this laminate? Here, we must get quantitative and outline a specific approach to laminate design. First, we do not even know *how many* laminae we need! Our basic objective

Éléments sous droits d'auteur

is that we want to carry a certain set of loads. The design process is not simply finding a thickness as with a metal plate, it is finding a thickness and *what goes into that thickness*, namely the number and orientation of the laminae as in Figure 3-123. That basic process for composite laminates is much more complicated than that for metal structures where we must determine only one variable — the thickness.

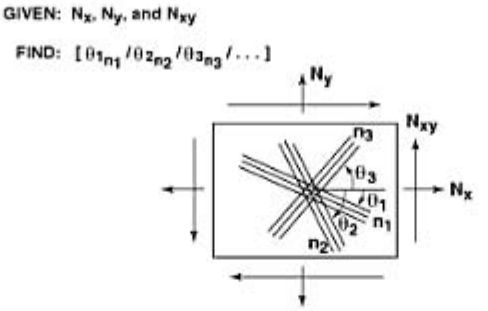


Figure 3-123 The Fundamental Laminate Design Problem

Evaluating the load-carrying capacity of a specific laminate (including the load-deformation behavior) is a straightforward deterministic process and is described in Section 4.5 of Jones' *Mechanics of Composite Materials* [3-27]. For example, a 20-layered laminate has a certain load-carrying capacity for one type of loading (and a different capacity for a different type of loading). In contrast, the same specified load-carrying capacity can be achieved with perhaps a 20-, 30-, 40-, or 50-layered laminate or with many other laminates. All those laminates meet the load-carrying requirement, so *the process of laminate design is inherently nondeterministic*. If each lamina is of the same material, then the laminate weight is directly proportional to the number of laminae. Obviously, the 20-layered laminate weighs the least of the several just mentioned. When laminate weight is considered, we have a quantifiable means of distinguishing between the various possible answers to the laminate design question. That is, with a merit function such as weight, we can *rank* the laminates as to how well they satisfy the design requirements. Note that strength is *not* a merit function because strength is a *constraint* on the laminate design.

In general, we might like to consider all possible laminae orientations for the laminate, but that approach is impossible. That is, if we were to try to evaluate all the corresponding laminates, an infinite number of solutions is possible, so that approach is obviously not realistic. Considering a totally arbitrary set of orientations for most laminates is also unrealistic simply because for manufacturing reasons you do not want to specify that one layer must be at 67.3° and the next at 52.7°. Such refined specification of laminae angles cannot be achieved in manufacturing, nor is it necessary or desirable. A far more practical approach is to

Éléments sous droits d'auteur

think in terms, at the most refined stage, of allowing the laminae to be oriented at 5° increments. That restriction on laminae angular orientation drastically cuts down the number of possible laminates. That restriction, however, still leaves an enormously large number of possible laminae orientations in a laminate.

An even more practical approach is to restrict the acceptable laminae angles to certain combinations, such as 0°, 90°, and ±45° laminae. I am not suggesting that we build only quasi-isotropic laminates because I did not say that you must have the same number of 90° laminae as 0° laminae as +45° laminae as −45° laminae. Let the numbers of laminae, the proportions of those various types of layers, change. The design parameters that we then search for are the values of three parameters, L, M and N, the numbers of 0°, 90°, and ±45° laminae, respectively. We would be searching for many more numbers if we drop back one stage and let the layers be oriented at 5° increments as possible orientations. The mathematical nature of the design optimization problem is changed very drastically when we cut down the number of design variables or restrict the possible values of the design variables.

Structural optimization techniques for composite structures as described by Schmit [3-93] and by Gürdal, Haftka, and Hajela [3-94]. can be used to provide a decision-making process for variation of laminate design parameters. Optimization is particularly well suited to composite structures design because both the *possibility and necessity* exists to tailor the structure to meet requirements to a degree not seen for isotropic materials. The invariant laminate stiffness concepts developed by Tsai and Pagano [3-95 and 3-96] and further described by Jones [3-27, pp. 85–87] are useful in laminate design.

The objective in effective laminate design is to resist both the *magnitude* and the *directional nature* of the loads without overdesign. That is, the laminate is tailored to *just meet* specific requirements. Structures made of isotropic materials are usually inefficient, i.e., overdesigned, because excess strength and stiffness are inevitably available in some direction. By appropriate consideration of the load magnitudes and their directions, a laminate can be constructed of individual laminae in such a manner as to just resist those loads and no more (with, of course, a suitable factor of safety).

Laminate design is a much more complex process than isotropic plate design. Under a specified loading for a metal plate, the only design variable is the thickness of the plate (unless the plate material is not specified). Even for a simple loading, laminate design involves finding the number of laminae and the orientations of each lamina (even if the material is specified). Thus, many more design variables must be determined for a laminate than for an isotropic plate. Moreover, laminate design involves issues of stiffness, strength, and energy absorption (the area under the load-deformation curve) as depicted implicitly in Figure 3-124 along with fatigue life that cannot be depicted. Also shown is the potentially large number of failure events (all relatively benign until laminate failure) that occur during laminate loading and influence the suitability of a particular laminate for specific design requirements.

Éléments sous droits d'auteur

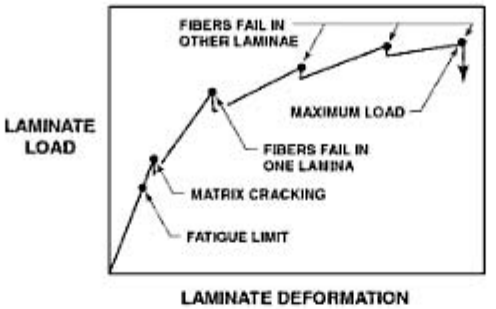


Figure 3-124 Possible Events during Laminate Loading

In this sub-section, a generic concept for laminate design will be outlined. That is, the general nature of laminate design and how to alter a laminate to better achieve the design objectives expressed in terms of stiffness, strength, energy absorption, and fatigue life will be addressed. The generic approach is based on obtaining a laminate with a load-deformation curve (or curves) to failure that satisfies the fundamental laminate design requirements expressed in terms of stiffness, strength, energy absorption, and fatigue life. This four-fold requirement is far more complex than the situation for many laminates with simple design requirements. However, we will address this general case to complete our overview of the laminate design process.

The nature of laminate behavior can range from very brittle to very ductile. A typical brittle behavior to a particular uniaxial failure load is shown as curve A (laminate A) in Figure 3-125. More ductile behaviors in the sense of larger deformations to failure are shown as laminates B, C, and D. The principal difference between the four behaviors to the same failure load is the amount of energy absorbed, but the initial slope of each load-deflection curve also varies. The combination of the highest initial slope and highest energy absorption is laminate B. Laminate C has a significant energy absorption but also a very low first-ply failure

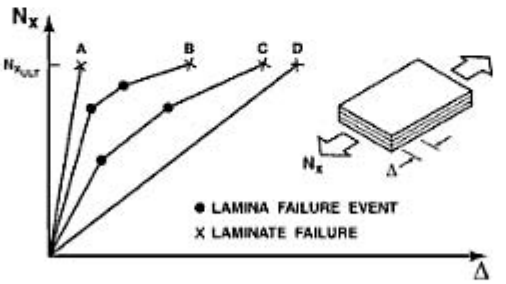


Figure 3-125 Possible Laminate Behaviors

Éléments sous droits d'auteur

load. Thus, under fatigue loading, laminate C would not be a good choice because the operating load must likely be less than the relatively low first-ply failure load. The presence of these different laminate behaviors is an additional complication in design over and above the nature of metal structures. However, the different behaviors also present additional opportunity for latitude in design.

The different laminate behaviors can be changed by changing the laminate stacking sequence and the number of layers. Discussion of the behavioral aspects, stiffnesses, strengths, energy absorption, and fatigue life, is simplified by considering only a simple uniaxial loading N_x in Figure 3-126. The stiffnesses are principally dependent on the stacking sequence, i.e., the individual laminae orientations, with some dependence on the number of layers. The strengths are principally dependent on the number of layers, although stacking sequence is also important. The energy absorption and fatigue life depend on both the stacking sequence and the number of laminae. Changing those variables also changes the first-ply failure load.

The laminate design problem is to find a laminate that will meet the design performance goals expressed in terms of strength, stiffness, energy absorption, fatigue life, plus other structural response measures as in Figure 3-127. Those goals are attained by changing the stacking sequence and/or the number of layers to change the laminate behavior until the desired structural response is obtained.

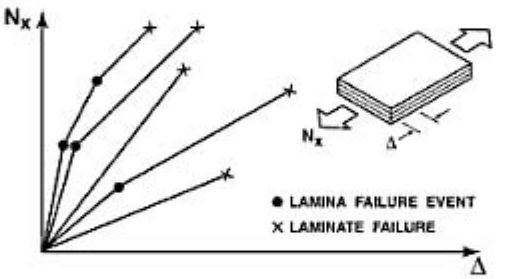


Figure 3-126 Effect of Changing Laminate Stacking Sequence

OBJECTIVE: FIND A LAMINATE THAT WILL MEET THE DESIGN PERFORMANCE GOALS EXPRESSED IN TERMS OF, E.G.,

- STRENGTHS
- STIFFNESSES
- ENERGY ABSORPTION
- FATIGUE LIFE

APPROACH: CHANGE THE STACKING SEQUENCE AND/OR THE THICKNESS TO CHANGE THE BEHAVIOR UNTIL THE DESIRED RESPONSE IS OBTAINED

Figure 3-127 The Laminate Design Problem

Éléments sous droits d'auteur

That is, the fundamental laminate design problem can be expressed as: given the loading N_x, N_y, and N_{xy}, find the laminate stacking sequence in Figure 3-123 on page 433. That is, what are the laminae orientations $\theta_1, \theta_2, \theta_3, \ldots$, and how many of each orientation are needed, i.e., what are $n_1, n_2, n_3, \ldots$?

From a practical standpoint, the layers that are added in the process of designing a laminate cannot have purely arbitrary fiber orientation. If the fiber orientations were unlimited, then the design process would sometimes lead to laminates quite unlike any previously built. Thus, the strength, and especially the fatigue life, would not be predictable or known with the necessary confidence. That is, considerable risk is involved in proposing a totally new laminate. Moreover, the cost of evaluating the strength and fatigue life for a new laminate is certainly not trivial. Thus, the addition of layers with often-used fiber orientations keeps design practice in the familiar territory of families of often-used laminates whose characteristics are relatively well-known so we can design with confidence and low cost in money and time.

Laminate design can be approached in flow-chart form as in Figure 3-128. There, some initial laminate is arbitrarily selected to start the procedure. Then, the laminate load-deflection behavior is evaluated by use of the laminate strength analysis procedure described in Section 4.5 of Jones' *Mechanics of Composite Materials* [3-27]. The next step is to evaluate the laminate fatigue life, and that behavior must be measured, although progress is being made with laminate life-prediction techniques. At this stage, we examine the strength, stiffness, fatigue life, and energy absorption characteristics of the candidate laminate. If they are either too high or too low, then we must change the stacking sequence and/or the number of layers until the response meets the required goals.

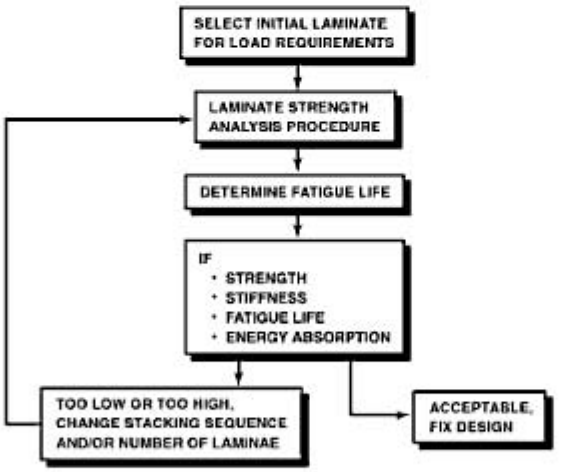


Figure 3-128 Laminate Design Procedure

Éléments sous droits d'auteur

Under the best of circumstances, the laminate at this iteration of the design process has known fatigue behavior. Under slightly less desirable circumstances, the laminate is close in stacking sequence to laminates with known fatigue behavior. Finally, under awkward, at best, circumstances, the laminate's fatigue behavior is totally unknown. In such a case, that laminate must either (1) be rejected from the design process as being an unknown entity or (2) have its fatigue behavior assessed. Obviously, the first choice is disappointing and the second choice is expensive and time-consuming, unlike the situation for the design of metal structures. The only helpful aspect is the fact that composite structures typically have longer fatigue lives than metal structures.

Consider an example to illustrate the foregoing concepts. Suppose the initial laminate choice is $[0°/90°_5]_S$ with the load-deflection behavior as in Figure 3-129. This laminate would appear to be obviously unsuited to the loading because most of the laminae have fibers in the wrong direction. However, we treat this example as being representative of the usual design circumstance in which each structural element is subjected to many different types of loadings. Some of those loadings are not critical or design-limiting for each structural element as is the case with this loading. That is, some loadings are easily accepted by the structural element. This laminate would obviously accept more load in the y-direction (transverse to the load direction), but we investigate its capability in the x-direction. The 90° layers fail by cracking parallel to the fibers (perpendicular to the predominant loading). Simultaneously with, or immediately after, matrix cracking in the 90° layers, the 0° layers also fail by cracking parallel to the fibers, as shown by Tsai [3-97]. However, the two 0° layers are still capable of carrying significant load in the x-direction. In fact, the ultimate load is several times the first-ply failure load. Note that this laminate also is still capable of carrying significant load in the y-direction even after matrix cracking in the 90° layers because the 90° layers still have unbroken fibers, but that issue is not addressed.

Suppose we replace the 90° layers with $\pm\alpha$ laminae in an attempt to increase the initial axial stiffness and to increase the first-ply failure load

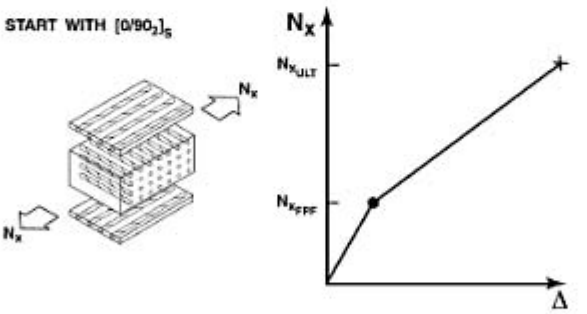


Figure 3-129 Initial Laminate Choice

Éléments sous droits d'auteur

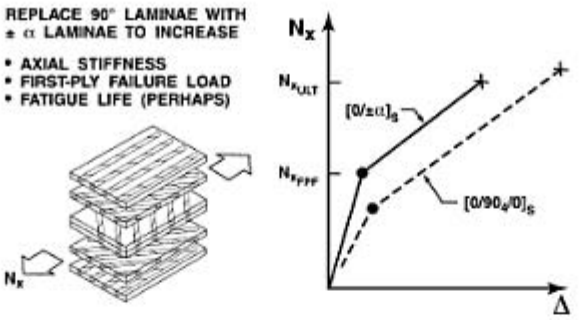


Figure 3-130 Second Laminate Choice

as in Figure 3-130. The load-deflection curve slope after first-ply failure also increases when $\pm\alpha$ laminae replace the 90° layers. However, the energy absorption decreases with such a stacking sequence change. The associated fatigue lives are not known unless both laminates are made and subjected to fatigue loading.

The general laminate design procedure is to continue to change the stacking sequence and/or the number of laminae to obtain required levels of strength, stiffness, fatigue life, and energy absorption. However, we must recognize that the design procedure has a very important limitation—the fatigue life can be determined only by measurement, not by prediction.

A possible adjunct to the laminate design procedure is a specific laminate failure criterion that is based on the maximum strain criterion. In such a criterion, all lamina failure modes are ignored except for fiber failure. That is, matrix cracking is regarded as unimportant. The criterion is exercised by finding the strains in the fiber directions of each layer. When these strains exceed the fiber failure strain in a particular type of layer, then that layer is deemed to have failed. Obviously, more laminae of that fiber orientation are needed to successfully resist the applied load. That is, this criterion allows us to preserve the identity of the failing lamina or laminae so that more laminae of that type (fiber orientation) can be added to the laminate to achieve a positive margin of safety.

The allowable stresses and/or strains in the design process for laminated composite plates are affected by many factors:

- stress concentrations due to holes
- hot, wet conditions
- notches
- free edges
- required factor of safety

That is, prudent structural design must address the 'what ifs' which are all the possible 'bad things' that could happen to a structure in practice.

Éléments sous droits d'auteur

3.9.4.2 Design of a Laminated Composite Plate Against Failure by Buckling

We would now essentially repeat the design process of the preceding sub-section for design against high stresses, except now we address buckling resistance instead of stiffness, strength, fatigue life, energy absorption, etc. However, all characteristics of candidate laminate designs must be known in order to use them effectively in practice. Not investigating all possible failure modes is totally unacceptable in design practice. Although always thinking about failure might seem an enormous negative attitude to some, realize that *preventing failure is our responsibility as engineers*, so we are professionally obliged to think of all possible manners a structure or machine might fail. Only with that knowledge can we act to prevent failure.

To resist a specified buckling load, a laminated composite plate must survive until the buckling load is reached in the manner of design of a laminated composite plate against failure caused by high stresses in Section 3.9.4.1. Furthermore, the laminate stiffnesses at the buckling load must be high enough to resist the buckling load, but those stiffnesses might have been reduced on the way up to the buckling load by various laminate degradation mechanisms discussed in Section 3.9.4.1. The specific governing buckling differential equation depends on the type of laminate, but a general form of the buckling differential equation to treat arbitrarily laminated plates can be obtained.[1] However, the difficulty would be in solving such a formulation. Of course, a finite element approach could be taken leading to results in numerical form, but we will not attempt such an approach initially (although it is open for the future).

Even if we restrict the design to regular laminates, i.e., laminates with equal-thickness laminae, we are still left with questions of how many layers of those equal-thickness laminae do we need (including the lamina thickness which probably is known if the material is known) *and what are the orientations of the individual laminae?*

The isotropic plate design problem at this point had only one unknown, the plate thickness, but here for the laminated composite plate problem we even have an unknown number of unknowns! Thus, whereas the isotropic plate design problem is deterministic, the laminated composite plate design problem is highly nondeterministic.

We approach the laminated composite plate design problem in a sequential manner with some simplified (not general) laminate classes such as regular cross-ply laminates or regular angle-ply laminates and then proceed to more complicated laminates with their more complicated design process. For a regular cross-ply laminate with alternating 0° and 90° layers, we must use an odd number of layers in order to avoid laminate antisymmetry that would decrease the buckling load as we saw in

[1]Hybrid composite laminated plates present special additional problems of variability that must be addressed in a very restricted manner. That is, the very nature of a hybrid composite with different materials in different layers means that we must consider many variations on a stacking sequence to find the least-weight laminate.

Éléments sous droits d'auteur

Section 3.6. The only unknown is the number of layers, so the problem is deterministic. Accordingly, we can solve for the number of equal-thickness layers of each of a $[0°/90°/ \ldots /90°/0°]$ stacking sequence and a $[90°/0°/ \ldots /0°/90°]$ stacking sequence. Then, we would choose the laminate of the two with the least number of layers because it would weigh the least and therefore cost the least of the two choices (both obviously meet the load-carrying capability requirement). Recall from Figure 3-63 on page 337 that it is not always desirable to put all the fibers in the loaded direction of a laminated plate. Of course, we must have an integer number of layers. For equal biaxial compressive loading, the two stacking sequences would have identical behavior, but their behavior would be different for other loadings. We just examined a very special case of a laminate, namely a cross-ply laminate, and it was not one that would generally be used in practice, so we have not yet considered a practical design problem.

The next least-complicated laminate is a regular angle-ply laminate that again must be symmetric to avoid a reduced buckling load. However, we are faced with the choice of whether the first layer is a $+\alpha$ or a $-\alpha$ orientation, so we would appear to need to examine both possibilities. Moreover, we do not know the value of α! Thus, the problem is nondeterministic to the first degree. We could approach solving the problem in a searching manner such as specifying a value of α and then finding which of the $[+\alpha/-\alpha/ \ldots /-\alpha/+\alpha]_S$ or, alternatively and necessarily, $[-\alpha/+\alpha/ \ldots /+\alpha/-\alpha]_S$ laminates have the least number of layers to resist the design buckling load. This procedure is essentially a repeat of the cross-ply laminate design problem wherein the laminae orientation angles were known. Of course, that problem would have to be repeated for many different values of α until we find a regular symmetric angle-ply laminate that satisifies the required design load (with an appropriate factor of safety) and has least weight, or least cost, etc. And we still do not have what would be considered to be a practical laminate.

Another yet more complicated laminate to consider is the $[0°/90°/\pm45°]_S$ which is regarded as practical in comparison to the cross-ply and the angle-ply laminates. Perhaps even more practical is the $[0°_m/90°_n/\pm45°_p]_S$ in which m, n, and p are integers. Obviously, variants of these two laminate classes exist and must be investigated to find a suitable laminate. Moreover, more than one laminate will satisfy the design requirements, so some discriminatory design merit condition must be applied (such as least weight, least cost, etc.).

Not all laminates need be investigated because you will be able to detect trends (if you can observe all the laminates being investigated along with their performance) and hence the 'direction' to go. Sometimes those trends will be manifested only in the form of system derivatives as in gradient-search techniques. Only if you can 'see' the candidate laminates can you absorb the trends and act based on them. Otherwise, you must rely on the mathematical operations in the computer program to work correctly because you will not have any feeling for how the design is progressing.

Éléments sous droits d'auteur

Of course, the most general laminated composite plate design problem must involve the most general laminate $[\alpha_m/\beta_n/\theta_p/\phi_q/ \ldots]$. A description of how to approach such a general laminate is not yet available.

3.9.4.3 Design of a Stiffened Laminated Composite Plate Against Failure by Buckling

With all the practical design problems involving such weight-sensitive structures such as aircraft and spacecraft, it is not at all surprising that we use high-stiffness-low-weight materials such as composite materials to achieve the design objective of least weight.

For composite stiffeners as in Figure 3-122 on page 430, all shapes are builtup from individual layers of material. Of course, some stiffener shapes can be produced by roll forming or pultrusion, for example, and then fastened to panels. Or, the stiffened panel could be made in a single operation involving the placement, usually by hand, of individual laminae of various dimensions in positions such that a builtup structure results. Stiffeners can be fastened to panels by bonding, stitching, or mechanical fastening.

Standard shapes for composite stiffeners are not likely to occur for most aerospace applications. There, the value and function of the structure warrant optimizing the stiffener design. In contrast, for more everyday applications such as scaffolding, stairways, and walkways in chemical plants, competitive pressures lead to a situation where compromises in stiffener efficiency are readily accepted (overdesign) in order to achieve lower cost than would be associated with optimum design.

To solve the stiffened laminated composite plate design problem, we must include the many stiffener variables, including those in the laminated composite stiffeners themselves, in the analysis and in the design logic for reconfiguration of the structure. Further detail is beyond the scope of this book.

3.9.4.4 Genetic Algorithm Approach to Laminate Design

Genetic algorithms emulate biological evolution as is evident from the word 'genetic' which is a reference to the 'branch of biology that deals with heredity and variation in similar or related plants or animals' [3-98]. Moreover, the mathematical process is incorporated in the formulation of an 'algorithm' or mathematical procedure in which the concepts of probability are included. In short, genetic algorithms are a way of modeling the evolutionary process including Darwin's principle of survival of the fittest[1] [3-99]. Biological species evolve over time, and presumably those members of the species with the hardiest characteristics are more likely to breed and pass on those hardy characteristics, i.e., the natural selection process in action. Those genetic characteristics are embedded in the DNA string for each member of a species. Thus, we are con-

[1] Cannon said *'On the Origin of Species* is more often cited than read, and more often read than understood' [3-100].

Éléments sous droits d'auteur

cerned with how those DNA strings are changed in an evolutionary manner for each species.

Genetic algorithms are a probabilistic optimization method or guided random-search technique. They do not rely on gradient-based information as do many search techniques. The disadvantage of gradient-based techniques is that they can easily converge to a local minimum of the merit function and perhaps miss the global minimum unless the search starting point is close to the global minimum. Genetic algorithms are more robust and are essentially insensitive to the complexity of the design space, e.g., capable of handling discontinuous (discrete or disjointed) design spaces in addition to continuous design spaces. The robustness, however, comes at the expense of an increased number of analyses which are highly sensitive to the number of design variables in the problem. Discontinous (disjointed or disconnected) design space is where genetic algorithms have a major advantage over gradient-based techniques (there is no advantage for continous design spaces). For example, laminated composite materials are composed of *discrete* layers that individually can have different orientations, if not completely different material properties. Further, genetic algorithms are well adaptable to parallel computation.

Our application of genetic algorithms to any structural optimization problem has the objective of achieving certain design goals such as the 'best' structure with the lowest weight (or some other criterion or criteria). The survival of the fittest in such an application means the lightest or strongest or the most buckling-resistant laminate among a succession of laminates that are considered in the hereditary process. Actually, we do not specifically address heredity, but we do simulate the process of evolution by considering various laminates in a heirarchical fashion based on manipulation of the characteristics of laminates as if they were a chain of laminates in a 'family' over time. That is, we search for the 'best' laminate over 'time', but we only simulate the passage of time by examining the evolutionary process in a mathematical iterative fashion. We compress the evolutionary process in time by using genetic algorithms to search for an optimum solution to a structural mechanics problem, i.e., we address a form of genetic engineering.

Fiber-reinforced composite laminates in structures have the dual characteristics of (1) fixed lamina thicknesses for a specific composite material and (2) our strong motivation to use only a few specific lamina orientations (e.g., $0°, 90°, \pm 45°$ at the least) to simplify the design and manufacturing process. Both characteristics involve *discrete variables*, so a composite laminate can be described with a bit-string representation, the laminate equivalent of the DNA string. For example, the bit string could have a {0,1,2,3,4}-bit alphabet to model a laminate stacking sequence which has empty laminae (to model variable-thickness laminates that are adjacent), $0°, +45°, -45°$, and $90°$ laminae as in Figure 3-131. The higher the number of elements (possible fiber orientations in a laminate) in the alphabet, the larger the population of laminates that must be considered, hence the longer the potential calculation time. Also, the more layers in a laminate, the longer the calculation time.

Éléments sous droits d'auteur

[0/1/1/2/3/4/3/2/1/1/0]

0 = EMPTY LAMINA
1 = 0° LAMINA
2 = + 45° LAMINA
3 = – 45° LAMINA
4 = 90° LAMINA

Figure 3-131 Bit-String Representation of a Laminate

The process typically starts by random creation of a population of possible laminate designs. (If you have some information on the nature of a possible design solution, then you can 'seed' the population with that information). Then, we evaluate the performance of each design and assign a 'fitness' value corresponding to that performance. Next, the designs with the highest level of fitness are presumed to be the 'best breeders', i.e., most likely to carry on the favorable characteristics to the next generation.

Most search procedures are concerned with various points in design-variable space, but genetic algorithms are concerned with an entire population of bit strings. This population consideration enables us to have a better chance of finding the global optima in a problem. That is, keeping the whole population in our region of concern enables us to distinguish between mere local minima and the far more important global minima of a function.

The basic operators of a genetic algorithm search procedure are:

- Selection
- Crossover
- Mutation
- Permutation

All these genetic operators are simple random changes or exchanges of locations of numbers in the bit string used to represent the design variables of a laminate and are described in the following paragraphs.

Selection After random generation of the initial population of laminates, a series of genetic operators is used to produce a 'new generation' which replaces the initial population of laminates with some exceptions that might involve cloning of some of the initial population, so there is a Dolly the lam(inate)! Those members of the initial population with a higher 'fitness' level have, via Darwin's principle, a higher probability of breeding to produce new generations. That higher probability is embodied in the fact that a higher portion of the area of a roulette wheel is assigned to the higher fitness designs, and the now-biased roulette wheel is spun (figuratively speaking) to generate the new population. Typically, we use an elitist selection scheme wherein we always retain laminates with the best fitness values. The process continues for successive generations until some convergence criterion is met.

Crossover In the evolutionary process, parents beget children. In the genetic algorithm process, the parents are in the population of the current 'generation', and the children share certain characteristics with

Éléments sous droits d'auteur

their parents. How these characteristics are passed onto children from their parents involves a random process called *crossover*. A single-point crossover location in the bit string is randomly generated in each of the parents' bit strings (more complex crossovers are possible). For a bit string with length 9 and crossover point 5 (five bits from the left), two symmetric laminate parents with possible 'child' designs are shown in Figure 3-132.

Parent 1:	0 0 1 2 1	3 1 1 1	$[0°/45°/0°/-45°/0°_3]_S$
Parent 2:	0 0 0 0 1	2 3 4 1	$[0°/45°/-45°/90°/0°]_S$
Child 1:	0 0 1 2 1	2 3 4 1	$[0°/45°/0°/45°-45°/90°/0°]_S$
Child 2:	0 0 0 0 1	3 1 1 1	$[0°/-45°/0°_3]_S$

Figure 3-132 Crossover Operator

The crossover point is the dividing line between parts of the parents' bit strings that are cut and reassembled to form the children's bit strings. That is, the left side of parent 1's bit string is combined with the right side of parent 2's bit string to create one child, and the right side of parent 1's bit string is combined with the left side of parent 2's bit string to create the other child. Although both parents are balanced laminates (see Section C.7.6 for the definition of 'balanced'), neither child is balanced. Another restriction to laminates that eliminates unbalanced laminates is to use $\pm 45°$ laminae as an inseparable pair represented by a single digit in the bit string. The crossover operation is implemented with a high probability (on the order of probability of .9 or even 1). If crossover is not implemented, then one of the parent laminates is 'cloned' into the next generation! At any rate, the next generation of laminates has the same number of laminates as the previous generation.

Mutation Mutation is the occasional random alteration of a bit string. Because the initial population was selected randomly, not all possible characteristics are necessarily represented in the initial population. Mutation enables the introduction of new characteristics that are not included in the initial population.

Permutation Permutation is a specific mutation operator that changes the stacking sequence without changing the constituents of the laminate. Thus, permutation changes the bending stiffnesses of the laminate, but not the extensional stiffnesses. Such an operator is useful when constraints on both the extensional behavior and on the bending behavior exist. Actually, permutation must involve two mutation operators simultaneously, an event with a very low probability of occurrence in the natural scheme, but extremely practical for composite laminates. Thus, specific permutation operators have been developed. One such operator is called 'lamina swap' or ply swap in which two laminae are simply interchanged in the stacking sequence (the order of two bits is inverted between two randomly assigned points in the bit string). The target laminae are shown in bold in Figure 3-133.

Éléments sous droits d'auteur

Before Lamina Swap:

2 3 1 4 4 1 2 1 1 3 $[45°/-45°/0°/90°_2/0°/45°/0°_2/-45°]_S$

After Lamina Swap:

2 3 2 4 4 1 1 1 1 3 $[45°/-45°/+45°/90°_2/0°_4/-45°]_S$

Figure 3-133 Lamina Swap Operator

Termination The genetic algorithm procedure is terminated when a prescribed maximum number of generations has been considered without improvement in the best design. Termination is a form of convergence.

The computational cost of using genetic algorithms can be quite high. The design-space size and how constraints limit movement in the design space are primary cost determiners. Obviously, we try to restrict the design-space size and the number of constraints to achieve a workable, yet practical problem. Certain restrictions on laminate choices are typical: (1) only balanced laminates are considered, i.e., the number of $+45°$ laminae equals the number of $-45°$ laminae to avoid shear-extension coupling and (2) the laminates are symmetric to avoid bending-extension coupling. However, bend-twist coupling is *not* eliminated with these restrictions. Both restrictions reduce the number of bits used in the string, which, in turn, requires fewer individuals in the population. Thus, fewer laminates are considered, so we decrease the calculation time and ease the manufacturing process.

Genetric algorithms were first applied to composite laminates by Callahan and Weeks [3-101] and by Le Riche and Haftka [3-102]. More extensive applications and theory including the history of genetic algorithms are described by Gürdal, Haftka, and Hajela [3-94]. Of course, the use of genetic algorithms is far more involved than discussed here. Many nuances of the laminate states require detailed treatment of specific problems that is beyond the scope of this book. The overall topic of genetic algorithms is itself evolving as we learn more about it.

The genetic algorithm approach was extended to the very practical problem of blending different laminate stacking sequences in different regions of, for example, an airplane wing to decrease manufacturing problems and costs by Soremekum, Gürdal, Kassapoglu, and Toni [3-103]. Blending is the process of providing continuity of some laminae across the boundaries of regions in which different laminate stacking sequences are individually optimum. If no blending were done, then manufacturing an airplane wing would have lots of starts and stops of individual laminae at various orientations in different regions—a sure bet for increasing manufacturing problems and cost. Moreover, the thicknesses would vary discontinuously from region to region over the area of the wing—an unacceptable feature from the aerodynamic point of view. Finally, the discontinuity of laminates at the region boundaries is unacceptable from local strength and stiffness considerations.

Éléments sous droits d'auteur

We're searching for the 'ultimate' laminate for a prescribed loading, i.e., the evolutionary version of the Einstein of laminates for each problem, but there's a uniquely different Einstein in each case! Moreover, each laminate is typically subjected to a variety of different loading conditions in a design application. For example, an airplane wing has different loading conditions for each maneuver expected for the airplane in flight. Those loading conditions are further expanded by considerations of different environmental conditions such as temperature or wind gusts. In addition, remember that the optimum laminate to achieve the highest axial buckling load $\bar{N}_x$ is *not* composed of all 0° fibers in the load direction (see Figure 3-63 on page 337 and surrounding discussion) because of the two-dimensional nature of the plate buckling problem and indeed for all plate problems. When all of these factors are considered, we observe that genetic algorithms can be used for multi-objective and multiple-load-case designs, a very practical objective.

3.9.4.5 Summary of Design of a Laminated Composite Plate

Some of the essential attributes of the laminated plate design process with optimization concepts were described in general terms. The process is indeterminate, unlike that for some metal plates. A logical iterative procedure must be used to guide a design toward satisfaction of the design requirements with simultaneous consideration of design merit factors such as least weight, least cost, etc. Application of the genetic algorithm approach to laminate design was introduced and briefly described. This approach is relatively new (1992) and is rapidly developing.

The PASCO (Panel Analysis and Sizing COde) structural optimization program was developed by Stroud and Anderson to design axially loaded prismatic rectangular laminated composite stiffened panels with a balanced symmetric laminate [3-104]. The laminated composite stiffeners can have many different cross sections, including both closed and open cross sections, and there can be imperfections in the panel geometry. The design conditions are to achieve specified stiffness, strength, buckling resistance, and vibration frequencies, all at lowest weight. The analysis element is the VIPASA (Vibration and Instability of Plate Assemblies including Shear and Anisotropy) program developed by Wittrick and Williams [3-105]. The optimization element is CONMIN (for constrained minimization), a nonlinear programming approach by Vanderplaats [3-106].

3.9.5 Summary of Design of Plates Against Buckling

The design process can rarely be simple and can even be quite complicated if the desired design variables are nondeterministic. The key is to determine the logical steps that will lead to the 'best' nonunique design that satisfies all the design requirements with simultaneous consideration of design merit factors such as least weight, least cost, etc. Of course, some form of safety factor must be applied against each type of failure possible. And, the values of the safety factors depend on the manner, result, and danger of failing.

Éléments sous droits d'auteur

3.10 BUCKLING OF PLATES SUMMARY

A wide range of plate buckling problems has been addressed starting with classical buckling from a flat prebuckled shape. As with bars, the nature of the postbuckling response was investigated to determine the practical design significance of the Euler buckling load. Also, as with bars, the effect of initial geometric imperfections on plate buckling was treated with both of the last two topics revealing some surprises relative to bar behavior. Unlike for bars, we did not address the effect of transverse shear on plate buckling loads. Consult Reddy for an excellent study of these shear effects [3-16, Chapter Ten] and also Wang, Reddy, and Lee [3-107, Chapter Eleven]. Next, the characteristics of buckling of fiber-reinforced laminated composite plates were investigated. Then, the influence of restrained thermal expansion on buckling was described. Subsequently, the influence of plastic deformation on plate buckling was considered. Finally, some basic design aspects of both isotropic metal plates and fiber-reinforced laminated composite plates were introduced.

3.10.1 General Problems

For treatment of plate buckling problems not addressed in this Chapter, consult Szilard [3-108], Bulson [3-109], Allen and Bulson [3-110], Reddy [3-16], and Bloom and Coffin [3-111] in addition to the buckling books mentioned in the summary of Chapter Two on page 223.

Some readers might wonder about the seeming obsession of most buckling researchers with the simply supported edge boundary condition for plates. We most often consider a simply supported plate because of two factors. The most important factor is that the buckling load for a simply supported structural member is a lower bound on the buckling loads for all other support conditions except for an edge without any support, i.e., a free edge. The second factor is that the effort to calculate the buckling load by classical analysis techniques for a simply supported structural member is fortunately nearly always less than the calculation for another edge condition. The fact that a simply supported edge is a lower bound to actual support conditions is responsible for the primary concern seen in Section 3.10.2 for simulating working simple supports for plate problems. In practice, we certainly would not want to overestimate the buckling resistance of a structure, and the simply supported edge boundary condition gives us assurance that we are calculating a buckling load that we expect the capacity of the actual structure to exceed thereby achieving a conservatively designed structure.

Some general considerations that are advisable to include in the evaluation of plate buckling are addressed in the NASA Space Vehicle Design Criteria (Structures) document Buckling Strength of Structural Plates by Gallagher [3-112]. Included are not only isotropic plates but also corrugated, stringer-stiffened, waffle-stiffened, sandwich, and fiber-reinforced plates. The format is description of effects with reference to procedures and analyses covered in 132 specific papers, reports, and books.

Éléments sous droits d'auteur

3.10.2 Review of Experimental Work

Singer, Arbocz, and Weller's book on buckling experiments is a rich source of information about plate buckling experiments [3-17] for which there are two significant classes of problems. First, plates exhibit a stable postbuckling behavior in that they can be loaded well beyond the theoretical buckling load, so the problem is deciding upon what is the buckling load for a real, imperfect plate. Second, attempting to provide loaded and unloaded edges with some form of simple support or clamping results in various intricate, yet robust, support mechanisms.

3.10.2.1 Consequences of Stable Postbuckling Behavior

The load-deflection behavior obtained by Rhodes and Harvey [3-19] in Figure 3-134 is somewhat reminiscent of the behavior of perfect and imperfect bars in Section 2.8 except that the post-buckling curve for a perfect plate always rises from the point of buckling. The significance of the rising is that the plate behavior is stable in the postbuckling regime whereas bar behavior is unstable because the bar postbuckling curve is essentially horizontal in Figure 2-29 on page 85, albeit barely rising. The fundamental interpretation of the stable postbuckling behavior for plates is that substantial loads can be sustained well above and beyond the Euler buckling load, whereas the Euler buckling load of a bar is essentially the maximum sustainable load in practice.

The stable postbuckling behavior with its accompanying lack of a well-defined buckling load has many interesting characteristics. Both the out-of-plane and in-plane boundary conditions are important because of

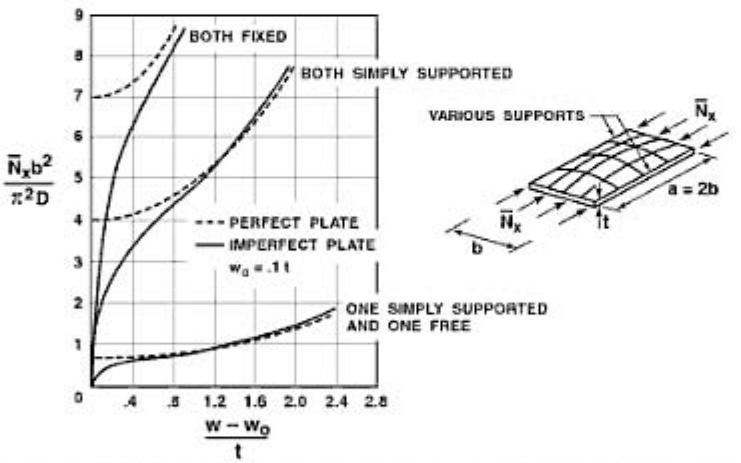


Figure 3-134 Load-Deflection Behavior of Perfect and Imperfect Axially Loaded Rectangular Plates with Simply Supported Loaded Edges and Variously Supported Unloaded Edges
(After Rhodes and Harvey [3-19])

Éléments sous droits d'auteur

the necessarily large deflections that include membrane stresses that excite the in-plane boundary conditions. Moreover, the prolonged loading and deformation include multiple changes of buckling mode called *secondary buckling*. And, initial geometric imperfections (or initial out-of-flatness) do not significantly affect the buckling load or the ultimate load as seen in Rhodes and Harvey's results in Figure 3-134 [3-19]. There, although perfect and imperfect plates start their load-deflection behavior in a different manner, they soon essentially join paths.

The effect of initial geometric imperfections on plate buckling is quite similar to that on bars in Section 2.8. That is, a sharp buckling load is not observed in either an imperfect bar or an imperfect plate. Here, with plates having various edge support conditions in Figure 3-134, the significant behavior is that large loads and deflections can be obtained that are well above the Euler buckling load (the intersection of each dashed curve with the vertical axis in Figure 3-134) as was demonstrated for simply supported plates by Stein [3-18] in Section 3.4. Here, the same conclusions apply for plates with opposite unloaded edges that are (1) fixed and (2) simply supported on one edge and free on the other edge.

Obviously, there cannot be a well-defined, obvious buckling stress or load for an imperfect plate in any formal sense because of the continuously rising nature of the stable postbuckling behavior in Figure 3-134. That lack of definiteness is not convenient for any engineer trying to analyze and design a challenging structure by assessing and comparing competing design concepts. A part of the stable postbuckling behavior characteristic is the problem of determining just what load to report as the 'buckling load' for an actual, imperfect plate that is imperfectly supported and loaded.

A buckled plate on an aircraft wing or fuselage surface will degrade aerodynamic performance. However, buckled plates in interior parts of the structure are generally acceptable, so advantage can be taken of the substantial load-carrying capacity above the buckling load. Note that plate buckling could lead directly to buckling of a larger structure (of which the plate is an integral part) because of load redistribution in the larger structure after buckling of a single plate.

3.10.2.2 Boundary Conditions in Experiments

Singer, Arbocz, and Weller review an extensive collection of plate buckling experiments starting with Fairbairn's in 1845 for the Britannia and Conway Tubular Railway bridges [3-17]. The main issue seems always to be how can so-called simple supports be realized for actual plates. The concept of a simply supported plate is easy to formulate, but very difficult to achieve in a laboratory. The idealization or schematics of the four kinds of simple support in Figure 3-10 on page 247 are nice to look at and state as objectives. However, creating *real* supports that allow different in-plane movement at different positions along the edge of a plate leads to a variety of mechanisms that typically challenge even a superb machinist! A major part of the problem is creating a mechanism that functions well beyond the small-deflection range on into the large-

Éléments sous droits d'auteur

deflection range at high loads. Accordingly, support mechanisms must move to follow the in-plane motion of the plate. Moreover, those mechanisms must move different amounts at different positions along the plate edge in order to accommodate the non-uniform plate stresses and hence deflections along each edge.

The described experiments include those at the U. S. Bureau of Standards in 1930; Hoff, Boley, and Coan at Brooklyn Polytechnic Institute in 1948 [3-26]; by Kollbrunner at ETH Zürich in the 1940s and 1950s; by Stein at NACA Langley in the 1950s [3-18]; the David Taylor Model Basin work in the 1960s; the Cambridge University tests of the 1960s through the 1980s; plus the 1970s work by Uemura and Byon of the University of Tokyo [3-24]. Those tests are mentioned to reveal the breadth of the investigators in both time and country. For specific citations and additional discussion, see Singer, Arbocz, and Weller [3-17].

In the various descriptions of the many different approaches to supporting a plate 'properly', many different specific techniques are noted. For example, to get a rotation-free restraint that varies along a plate edge, needles and roller bearings are mounted on multiple individual fingers along the edge. About the only criticism of the many experiments that have been run is that so far no one has used duct tape (duck tape, sic), although teflon tape is quite popular as a friction reducer.

Singer, Arbocz, and Weller [3-17] discuss not only buckling of plates but of shear panels that are typical of aircraft wing and fuselage panels plus webs in large bridge and building girders. Also, web crippling which is the local instability of a thin web of a plate girder under very localized loading is described. Finally, biaxial loading of plates is briefly treated.

3.10.3 Extensions of Present Coverage

Other modifications to the basic problems treated in this chapter include truly nonlinear independent non-isotropic stress-strain curve behavior typical of most fiber-reinforced composite laminae. That is, the stress-strain curves in the principal material directions are independent of each other so that some are more nonlinear than others. Also treated is thermal buckling of composite plates with an unusual result.

3.10.3.1 Buckling of Plates of Nonlinear Composite Materials

Most fiber-reinforced composite materials have at least one significant stress-strain curve nonlinearity. For example, boron-epoxy and graphite-epoxy have linear stress-strain behavior in the fiber direction, slightly nonlinear behavior transverse to the fibers, and a fairly strong nonlinearity in shear as shown schematically in Figure 3-135. Metal-matrix composite materials such as boron-aluminum have strong E_2 and G_{12} nonlinearities, but a mild E_1 nonlinearity. Three-dimensionally fiber-reinforced composite materials such as carbon-carbon have nonlinearities in all principal material directions. These stress-strain curve nonlinearities are large enough that not including them in buckling analyses of laminated plates can lead to unconservative buckling load predictions.

Éléments sous droits d'auteur

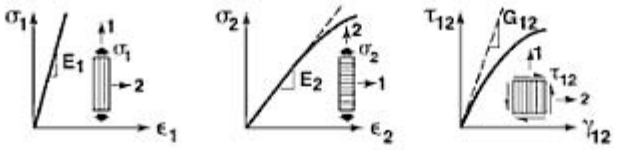


Figure 3-135 Typical Stress-Strain Behavior of Fiber-Reinforced Composite Materials

These nonlinear fiber-reinforced composite materials are made in the form of laminated plates, and their buckling loads are evaluated as a combination of laminated plate theory and inelastic behavior by Morgan and Jones [3-113]. They found that the influence of the nonlinearity in the transverse-to-the-fibers direction for boron-epoxy and graphite-epoxy, materials with only a single stress-strain curve nonlinearity (E_2) in the 2-direction (except for an always-present shear nonlinearity), is approximately ten to twenty percent. In contrast, for boron-aluminum, a material with nonlinearities in all principal material direction stress-strain curves (including in the fiber direction, i.e., E_1) and in shear, the effect of the multiple nonlinearities can be as high as an eighty percent reduction in buckling load (although this prediction does not include processing stresses and is not yet substantiated by experiments) as seen in Figure 3-136. The buckling loads are less than the corresponding linear elastic loads by significant amounts for boron-aluminum (up to 80%) and by much less significant amounts for boron-epoxy and graphite-epoxy.

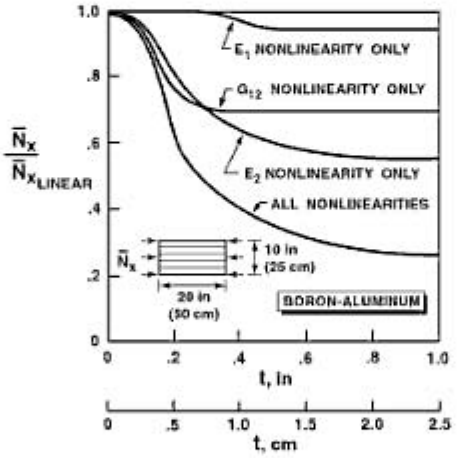


Figure 3-136 Relative Buckling Loads for Unidirectional 0° Boron-Aluminum Laminates *(After Morgan and Jones [3-113])*

Éléments sous droits d'auteur

3.10.3.2 Thermal Buckling of Cross-Ply Composite Plates

Three intriguing cases for thermal buckling of simple unidirectional and symmetric fiber-reinforced cross-ply laminated composite plates under uniaxial in-plane restraint as in Figures 3-91 and 3-92 on page 379 are investigated by Jones [3-114]: (1) unidirectionally reinforced laminated plates with fibers in the direction of the restraint, (2) unidirectionally reinforced laminated plates with fibers perpendicular to the direction of the restraint, and (3) symmetric cross-ply laminated plates with fibers both parallel and perpendicular to the restraint.

(1) Unidirectionally Laminated Plates with Fibers in the Direction of Restraint

When the fibers of all layers are in the x-direction (the in-plane restraint direction), Jones showed the buckling temperature change from the stress-free temperature to be [3-114]

$$\overline{\Delta T} = \frac{\pi^2}{12(1-\nu_{12}\nu_{21})\alpha_1} \times \left[m^2 \left(\frac{b}{a}\right)^2 + 2\left[\nu_{21} + 2(1-\nu_{12}\nu_{21})\frac{G_{12}}{E_1}\right] + \frac{E_2}{E_1}\left(\frac{a}{b}\right)^2 \frac{1}{m^2} \right] \left(\frac{t}{b}\right)^2 \tag{3.506}$$

which depends on ratios of the engineering constants and reduces for isotropic materials to the equivalent of Equation (3.411), as it must, in which $\overline{\Delta T}$ is independent of E. Some reinforcing fibers have a pronounced negative α in their axial direction. Thus, because α_1 is a fiber-dominated property, some fiber-reinforced laminae have a negative α_1. Other laminae have a more 'normal' positive α_1. Thus, from Equation (3.506), if α_1 is positive, then $\overline{\Delta T}$ is positive (heating is required to buckle the laminated plate) and if α_1 is negative, then $\overline{\Delta T}$ is negative (cooling is required to buckle the laminated plate). The smallest value of $\overline{\Delta T}$ for various m is not obvious, but varies with different relative values of the engineering constants and with the plate aspect ratio, a/b. The value of $\overline{\Delta T}$ depends directly on the square of the inverse of the width-to-thickness ratio, b/t.

The buckling temperature changes from the stress-free temperature, $\overline{\Delta T}$, are plotted for different b/t values as a function of plate aspect ratio, a/b, for high-modulus graphite-epoxy in the bottom pair of curves in Figure 3-137. The results are the typical festooned buckling-mode-shape-dependent curves. However, note especially that a plate made of high-modulus graphite-epoxy with its negative α_1 must be cooled, not heated, to buckle. The laminated plates with fibers parallel to the restraint direction in Figure 3-137 act as very short plates in comparison to the isotropic plates in Figure 3-93. That is, the number of axial buckle half-waves, m, is only 1, 2, or 3 up to a/b = 5 in Figure 3-137, whereas isotropic plates reach m = 5 by a/b = 5 in Figure 3-93. Thus, the buckling temperature change for laminated plates with fibers in the restraint direction is still highly dependent on a/b even beyond a/b = 5 and does not approach its constant minimum value until relatively high a/b.

Éléments sous droits d'auteur

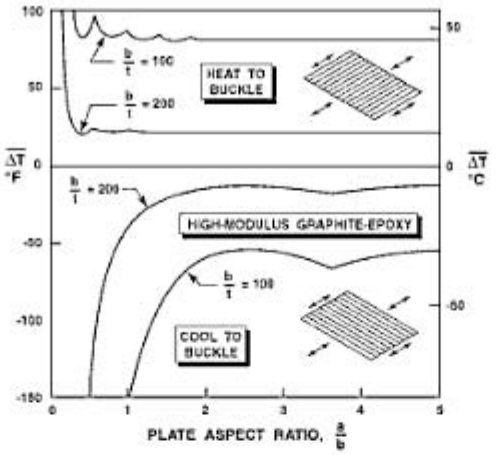


Figure 3-137 Thermal Buckling of Uniaxially In-Plane Restrained High-Modulus Graphite-Epoxy Unidirectionally Laminated Composite Plates *(After Jones [3-114])*

Whitney and Ashton addressed thermal buckling of $\pm\theta$ angle-ply laminated rectangular plates clamped on two opposite edges and free on the other two edges [3-51]. They found that a $\theta = 0°$ (unidirectional) angle-ply laminate, when made of high-modulus graphite-epoxy, with fibers in the direction of restraint actually buckles under cooling, not heating, a result analogous to the present results.

(2) Unidirectionally Laminated Plates with Fibers Perpendicular to the Direction of Restraint

When the fibers of all layers are in the y-direction (perpendicular to the in-plane restraint direction), the buckling temperature change from the stress-free temperature can be shown to be quite similar to Equation (3.411) except with α_2 in place of α_1. Thus, because of the fact that α_2 is always positive for fiber-reinforced composite laminae, clearly ΔT is always positive, so such laminated plates must always be heated to buckle. The smallest value of ΔT for various m is not obvious, but varies with different relative values of the engineering constants and with the plate aspect ratio, a/b. The value of ΔT depends directly on the square of the inverse of the width-to-thickness ratio, b/t.

The buckling temperature changes from the stress-free temperature are plotted for different width-to-thickness ratios, b/t, as a function of plate aspect ratio, a/b, for high-modulus graphite-epoxy in the top pair of curves in Figure 3-137. The results are the typical festooned buckling-mode-shape-dependent curves. The laminated plates with fibers perpendicular to the restraint direction in Figure 3-137 act as very long

Éléments sous droits d'auteur

plates in comparison to the isotropic plates in Figure 3-93 . That is, the number of axial buckle half-waves, m, increases rapidly for those plates reaching m = 4 to m = 12 by a/b = 2 as compared to m = 5 by a/b = 5 for isotropic plates in Figure 3-93. Thus, the buckling temperature change for laminated plates with fibers perpendicular to the restraint direction is essentially constant at its minimum value for a/b > 2 (and even less than a/b = 2 for plates thinner than b/t = 100).

(3) Symmetric Cross-Ply Laminated Plates under Uniaxial In-Plane Restraint

Let's explore the possibility that a symmetric cross-ply laminated plate can be constructed that cannot buckle at any temperature, i.e., a non-thermal-buckling symmetric cross-ply laminated plate under uniaxial restraint exists. This opportunity arises because the negative α_1 for high-modulus graphite-epoxy leads to (1) cooling causing buckling for a uniaxially restrained unidirectional laminated plate with fibers in the restraint direction and (2) with fibers perpendicular to the restraint direction, heating is required to buckle the plate. Accordingly, the prebuckling equilibrium force in the restraint direction, N_x, must be zero for a certain percentage of 0° layers among the 90° layers of a symmetric cross-ply laminated plate. And, with only uniaxial restraint, $N_y = 0$. Of course, with no prebuckling equilibrium forces on the laminated plate, no buckling can occur. A cross-ply laminate is made up of 0° layers and 90° layers with total thicknesses of $t_{0°}$ and $t_{90°}$, respectively. The 0° and 90° layers can be arranged in any order (stacking sequence) because the resulting laminate extensional stiffnesses are identical for all stacking sequences for which $t_{0°}$ and $t_{90°}$ are identical.

High-modulus graphite-epoxy has a negative α_1 and a positive α_2, so it can be used to construct a non-thermal-buckling symmetric cross-ply laminated plate with $t_{0°}/t = .448$ or 45% 0° layers. Thus, every high-modulus graphite-epoxy symmetric cross-ply laminated plate with more than 45% 0° layers in the restraint direction must be cooled, not heated, to buckle. Conversely, with fewer than 45% 0° layers, the plate must be heated to buckle. The buckling results for three-layered $[0°_{t_1}/90°_{t_2}/0°_{t_1}]$ square plates are displayed as a percentage of 0° layers in the laminate in Figure 3-138. Indeed, at 45% 0° layers in the laminate, the buckling temperature change is infinite. Apparently, there is a singularity in the buckling results at 45% 0° layers as predicted. Note that the magnitude of the buckling results depends on the order of the layers in the laminate stacking sequence because of the dependence on the laminate bending stiffnesses. In contrast, the non-thermal-buckling laminate extensional stiffnesses, which determine the non-thermal-buckling laminate percentage of 0° layers, are independent of the order of the layers in the stacking sequence (the laminate extensional stiffnesses, A_{ij}, do not depend on the manner in which the 0° and 90° layers are distributed, but only on their respective percentages). Thus, for the cross-ply stacking sequence $[90°_{t_2/2}/0°_{2t_1}/90°_{t_2/2}]$, which has the same percentages of 0° and 90° layers as the previous stacking sequence, the buckling temperature changes are lower in absolute value than the results in Figure 3-138.

Éléments sous droits d'auteur

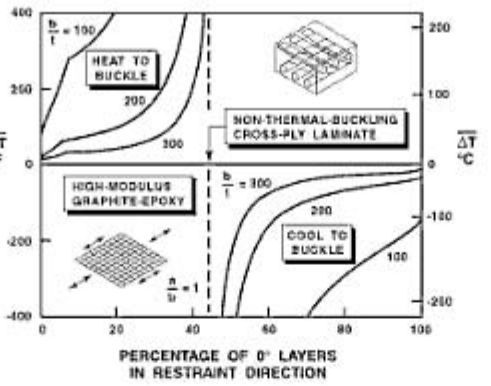


Figure 3-138 Thermal Buckling of Square Uniaxially In-Plane Restrained High-Modulus Graphite-Epoxy Symmetric Cross-Ply Laminated Composite Plates *(After Jones [3-114])*

Because the nature of the prebuckling equilibrium state depends only on the in-plane laminate stiffnesses, A_{11}, A_{12}, A_{22}, and A_{66}, and not on the laminate bending stiffnesses, D_{ij}, the actual order of the layers in the laminate stacking sequence is immaterial (except that the laminate must be symmetric about its middle surface). Thus, the conclusion that cooling causes buckling applies to all high-modulus graphite-epoxy symmetric cross-ply laminated plates with more than 45% 0° layers. However, the specific values of the buckling temperature changes differ for different cross-ply laminates because buckling depends on the laminate bending stiffnesses, D_{ij}, which, in turn, depend strongly on the specific cross-ply laminate stacking sequence. Below 45% 0° layers, the laminate must be heated to buckle. Irrespective of the percentage of 0° layers, the buckling temperature changes are much lower in absolute value for thin plates (b/t = 300) than for thicker plates (b/t = 100) in Figure 3-138. Obviously, the temperature changes required to buckle some laminated plates seem (unrealistically) high. Surely the material must yield and/or have diminished properties because of elevated temperatures. Of course, as the temperature increases, the lamina material properties decrease, especially the matrix-dominated properties and to a lesser extent the fiber-dominated properties. Thus, the pertinent A_{ij} change their relative values and the lamina material properties change in a non-uniform manner. Accordingly, the precise percentage of 0° layers to achieve a non-thermal-buckling symmetric cross-ply laminated plate depends on the operating temperature.

Whitney and Ashton addressed thermal buckling of symmetric $\pm\theta$ angle-ply laminated rectangular plates clamped on two opposite edges and free on the other two edges [3-51]. They found that for θ in the range $0 \leq \theta \leq 17.5°$ cooling, not heating, is required to buckle a plate made of high-modulus graphite-epoxy. And, at $\theta = 17.5°$, the symmetric angle-ply

Éléments sous droits d'auteur

laminated plate does not buckle at all irrespective of whether it is heated or cooled. Their results for symmetric angle-ply laminated plates are analogous to the present symmetric cross-ply laminated plate results.

In summary, anomalous results for thermal buckling of simple fiber-reinforced composite plates include (1) unidirectionally laminated plates that actually buckle upon cooling instead of heating and (2) symmetric cross-ply laminated plates that do not buckle irrespective of whether they are heated or cooled (non-thermal-buckling symmetric cross-ply laminates). Those anomalous situations are unusual, yet intriguing in their design application possibilities.

CHAPTER 3 REFERENCES

3-1 G. H. Bryan, On the Stability of a Plane Plate under Thrusts in Its own Plane, with Applications to the "Buckling" of the Sides of a Ship, *Proceedings of the London Mathematical Society*, Volume 22, from November 1890 to November 1891 (read 11 December 1890), pp. 54–67.

3-2 R. Courant and D. Hilbert, *Methods of Mathematical Physics*, Volume I, Interscience, New York, 1953, p. 190.

3-3 I. S. Sokolnikoff and R. M. Redheffer, *Mathematics of Physics and Modern Engineering*, McGraw-Hill, New York, 1958, pp. 391–395.

3-4 G. Kirchhoff, Über das Gleichgewicht und die Bewegung einer elastischen Scheibe, *Journal für die reine und angewandte Mathematik* (also known as *Crelle's Journal* and *Borchardt's Journal für Mathematik*), Volume 40, Number 1, pp. 51–88, 1850.

3-5 Theodore von Kármán, Festigkeitsprobleme im Maschinenbau, *Encyklopädie der Mathematischen Wissenschaften*, Volume IV, pp. 311–385, 1910. Reprinted on pp. 141–207 in *Collected Works of Theodore von Kármán*, Volume I, 1902–1913, Butterworths Scientific Publications, London, 1956.

3-6 B. O. Almroth, Influence of Edge Conditions on the Stability of Axially Compressed Cylindrical Shells, *AIAA Journal*, Volume 4, Number 1, January 1966, pp. 134–140.

3-7 E. Trefftz, Zur Theorie der Stabilität des elastischen Gleichgewichts, *Zeitschrift für angewandte Mathematik und Mechanik*, Volume 13, Number 2, April 1933, pp. 160–165.

3-8 S. P. Timoshenko and James M. Gere, *Theory of Elastic Stability*, 2nd Edition, McGraw-Hill, New York, 1961.

3-9 Georgi P. Tolstov, *Fourier Series*, translated by Richard A. Silverman, Dover, New York, 1976.

3-10 James Ward Brown and Ruel V. Churchill, *Fourier Series and Boundary Value Problems*, 5th edition, McGraw-Hill, New York, 1993.

3-11 S. P. Timoshenko, Stability of Rectangular Plates under Compression, *Bulletin of the Polytechnic Institute of Kiev*, 1907.

3-12 James H. Johnson, Jr. and Robert G. Noel, Critical Bending Stress for Flat Rectangular Plates Supported Along All Edges and Elastically Restrained Against Rotation Along the Unloaded Compression Edge, *Journal of the Aeronautical Sciences*, Volume 20, Number 8, August 1953, pp. 535–540.

3-13 Manuel Stein and John Neff, *Buckling Stresses of Simply Supported Rectangular Flat Plates in Shear*, NACA Technical Note 1222, National Advisory Committee for Aeronautics, Washington, D.C., March 1947.

3-14 Bernard Budiansky and Robert W. Connor, *Buckling Stresses of Clamped Rectangular Flat Plates in Shear*, NACA Technical Note 1559, National Advisory Committee for Aeronautics, Washington, D.C., May 1948.

3-15 S. P. Timoshenko, Einige Stabilitätsprobleme der Elastizitätstheorie, *Zeitschrift für Mathematik und Physik*, Volume 58, Number 4, pp. 337–385, 1910. Reprinted on pp. 1–50 in *The Collected Papers of Stephen P. Timoshenko*, McGraw-Hill, New York, 1953.

3-16 J. N. Reddy, *Theory and Analysis of Elastic Plates*, Taylor & Francis, Philadelphia, 1999.

Éléments sous droits d'auteur

3-17 J. Singer, J. Arbocz, and T. Weller, *Buckling Experiments: Experimental Methods in Buckling of Thin-Walled Structures, Basic Concepts, Columns, Beams and Plates – Volume 1*, Wiley, Chichester, England, 1998, Chapter 8. Also, *Volume 2, Shells, Built-up Structures and Additional Topics*, 2002, Wiley, New York.

3-18 Manuel Stein, *Loads and Deformations of Buckled Rectangular Plates*, NASA Technical Report R-40, National Aeronautics and Space Administration, Washington, D.C., 1959.

3-19 James Rhodes and James M. Harvey, Examination of Plate Post-Buckling Behavior, *Journal of the Engineering Mechanics Division of the American Society of Civil Engineers*, Volume 103, Number EM3, June 1977, pp. 461–478.

3-20 J. Rhodes and J. M. Harvey, Plates in Uniaxial Compression with Various Support Conditions at the Unloaded Boundaries, *International Journal of Mechanical Sciences*, Volume 13, Number 9, September 1971, pp. 787–802.

3-21 J. Rhodes, J. M. Harvey, and W. C. Fok, The Load-Carrying Capacity of Initially Imperfect Eccentrically Loaded Plates, *International Journal of Mechanical Sciences*, Volume 17, Number 3, March 1975, pp. 161–175.

3-22 A. C. Walker, Thin-Walled Structural Forms under Eccentric Compressive Load Actions, thesis presented to the University of Glascow at Glascow, Scotland in 1964 in partial fulfillment of the requirements for the degree of Doctor of Philosophy.

3-23 Pai C. Hu, Eugene E. Lundquist, and S. B. Batdorf, *Effect of Small Deviations from Flatness on Effective Width and Buckling of Plates in Compression*, NACA Technical Note 1124, National Advisory Committee for Aeronautics, Washington, D.C., September 1946.

3-24 Masuji Uemura and O-Il Byon, Secondary Buckling of a Flat Plate under Uniaxial Compression, Part 2, Analysis of Clamped Plate by F. E. M. and Comparison with Experiments, *International Journal of Non-Linear Mechanics*, Volume 13, Number 1, 1979, pp. 1–14.

3-25 Samuel Levy, *Bending of Rectangular Plates with Large Deflections*, NACA Report 737, National Advisory Committee on Aeronautics, Washington, D. C., 1942.

3-26 N. J. Hoff, Bruno A. Boley, and John M. Coan, The Development of a Technique for Testing Stiff Panels in Edgewise Compression, *Proceedings of the Society for Experimental Stress Analysis*, Volume 5, Number 2, 1948, pp. 14–24.

3-27 Robert M. Jones, *Mechanics of Composite Materials*, 2nd Edition, Taylor & Francis, Philadelphia, 1999.

3-28 James M. Whitney, *Structural Analysis of Laminated Anisotropic Plates*, Technomic, Lancaster, Pennsylvania, 1987. See also J. E. Ashton and J. M. Whitney, *Theory of Laminated Plates*, Technomic, Westport, Connecticut, 1970.

3-29 Jack R. Vinson and Robert L. Sierakowski, *The Behavior of Structures Composed of Composite Materials*, 2nd Edition, Kluwer, Dordrecht, The Netherlands, 2002.

3-30 Valery V. Vasiliev (Robert M. Jones, English Edition Editor), *Mechanics of Composite Structures*, Taylor & Francis, Washington, 1993. A revised, expanded version of *Mechanics of Structures Made of Composite Materials*, Mashinostroenie, Moscow, 1988.

3-31 J. N. Reddy, *Mechanics of Laminated Composite Plates: Theory and Analysis*, CRC Press, Boca Raton, Florida, 1997.

3-32 S. A. Ambartsumyan, *Theory of Anisotropic Shells*, (in Russian, State Publishing House for Physical and Mathematical Literature, Moscow, 1961), NASA Technical Translation TT F-118, National Aeronautics and Space Administration, Washington, D. C., May 1964. Also *Theory of Anisotropic Plates*, first Russian edition, 1967. Second edition (English Edition Editor, Isaak Kunin), Hemisphere Publishing (Taylor & Francis), Washington, 1991.

3-33 K. S. Pister and S. B. Dong, Elastic Bending of Layered Plates, *Journal of the Engineering Mechanics Division*, American Society of Civil Engineers, Volume 85, Number EM 4, October 1959, pp. 1–10.

3-34 E. Reissner and Y. Stavsky, Bending and Stretching of Certain Types of Heterogeneous Aeolotropic Elastic Plates, *Journal of Applied Mechanics*, Volume 28, Series E, Number 3, September 1961, pp. 402–408.

3-35 Robert M. Jones and Jose C. F. Hennemann, Effect of Prebuckling Deformations on Buckling of Laminated Composite Circular Cylindrical Shells, *AIAA Journal*, Volume 18, Number 1, January 1980, pp. 110–115.

Éléments sous droits d'auteur

3-36 S. P. Timoshenko and S. Woinowsky-Krieger, *Theory of Plates and Shells*, McGraw-Hill, New York, 1959.
3-37 James Ting-shun Wang, On the Solution of Plates of Composite Materials, *Journal of Composite Materials*, Volume 3, July 1969, pp. 590–592.
3-38 J. E. Ashton and M. E. Waddoups, Analysis of Anisotropic Plates, *Journal of Composite Materials*, Volume 3, January 1969, pp. 148–165.
3-39 C. C. Chamis, *Thermostructural Response, Structural and Material Optimization of Particulate Composite Plates*, Case Western Reserve University, Report Number SMSMOD 21, Cleveland, Ohio, June 1968.
3-40 John F. Mandell, *Experimental Investigation of the Buckling of Anisotropic Fiber Reinforced Plastic Plates*, M. S. Thesis, Case Western Reserve University, Cleveland, Ohio, January 1968. Also Air Force Materials Laboratory, Wright-Patterson AFB, Ohio, Technical Report AFML-TR-68-281, October 1968.
3-41 J. E. Ashton, An Analogy for Certain Anisotropic Plates, *Journal of Composite Materials*, Volume 3, April 1969, pp. 355–358.
3-42 Robert M. Jones, Buckling and Vibration of Unsymmetrically Laminated Cross-Ply Rectangular Plates, *AIAA Journal*, Volume 11, Number 12, December 1973, pp. 1626–1632.
3-43 Robert M. Jones, Plastic Buckling of Eccentrically Stiffened Multilayered Circular Cylindrical Shells, *AIAA Journal*, Volume 8, Number 2, February 1970, pp. 262–270.
3-44 James Martin Whitney, *A Study of the Effects of Coupling Between Bending and Stretching on the Mechanical Behavior of Layered Anisotropic Composite Materials*, Ph.D thesis, Department of Engineering Mechanics, The Ohio State University, Columbus, Ohio, 1968. (Available from University Microfilms, Inc., Ann Arbor, Michigan, as No. 69-5000.)
3-45 J. M. Whitney, Bending-Extension Coupling in Laminated Plates Under Transverse Loading, *Journal of Composite Materials*, Volume 3, January 1969, pp. 20–28.
3-46 Robert M. Jones, Harold S. Morgan, and James M. Whitney, Buckling and Vibration of Antisymmetrically Laminated Angle-Ply Rectangular Plates, *Journal of Applied Mechanics*, Volume 40, Series E, Number 4, December 1973, pp. 1143–1144.
3-47 Robert M. Jones and Harold S. Morgan, Deflection of Unsymmetrically Laminated Cross-Ply Rectangular Plates, *Proceedings of the 12th Annual Meeting of the Society of Engineering Science*, 20–22 October 1975, Austin, Texas, pp. 155–167.
3-48 Zafer Gürdal and R. Olmedo, In-Plane Response of Laminates with Spatially Varying Fiber Orientations: Variable-Stiffness Concept, *AIAA Journal*, Volume 31, Number 4, April 1993, pp. 751–758.
3-49 K. Chauncey Wu, Zafer Gürdal, and James H. Starnes, Jr., Structural Response of Compression-Loaded, Tow-Placed, Variable-Stiffness Panels, AIAA Paper 2002-1512, *Proceedings of the AIAA/ASME/ASCE/AHS/ASC 43rd Structures, Structural Dynamics and Materials Conference*, Denver, Colorado, 22–25 April 2002, AIAA, Reston, Virginia.
3-50 G. J. Turvey and I. H. Marshall, Editors, *Buckling and Postbuckling of Composite Plates*, Chapman & Hall, London, 1995.
3-51 J. M. Whitney and J. E. Ashton, Effect of Environment on the Elastic Response of Layered Composite Plates, *AIAA Journal*, Volume 9, Number 9, September 1971, pp. 1708–1713.
3-52 Arthur W. Leissa, *Buckling of Laminated Composite Plates and Shell Panels*, Air Force Wright Aeronautical Laboratories, Wright-Patterson AFB, Ohio, Technical Report AFWAL-TR-85-3069, June 1985.
3-53 Alexander E. Bogdanovich and Robert L. Sierakowski, Composite Materials and Structures: A Compendium of Books, Review Papers, and Other Sources of Information, *Applied Mechanics Reviews*, Volume 52, Number 12, Part 1, December 1999, pp. 351–366.
3-54 E. W. Parkes, Panels under Thermal Stress, The Behavior of a Panel Restrained against Expansion in one Direction and Loaded in the other Direction when Subjected to Kinetic Heating, *Aircraft Engineering*, Volume 28, Number 328, June 1956, pp. 180–186.
3-55 N. J. Hoff, Buckling at High Temperature, *Journal of the Royal Aeronautical Society*, Volume 61, Number 563, November 1957, pp. 756–774.
3-56 David Burgreen, *Elements of Thermal Stress Analysis*, C. P. Press, Jamaica, New York, 1971.

Éléments sous droits d'auteur

3-57 Bruno A. Boley and Jerome H. Weiner, *Theory of Thermal Stresses*, Wiley, New York, 1960.

3-58 Marion W. Wilcox and Lewis E. Clemmer, Large Deflection Analysis of Heated Plates, *Journal of the Engineering Mechanics Division, Proceedings of the American Society of Civil Engineers*, Volume 90, Number EM 6, December 1964, pp. 165–189.

3-59 Michael P. Nemeth, Buckling Behavior of Long Anisotropic Plates Subjected to Restrained Thermal Expansion and Mechanical Loads, AIAA Paper 99-1229, *Proceedings of the 40th AIAA/ASME/ASCE/AHS/ASC Structures, Structural Dynamics and Materials Conference*, 12-15 April 1999, St. Louis, Missouri, AIAA, Reston, Virginia. Also *Journal of Thermal Stresses*, Volume 23, Number 9, December 2000, pp. 873–916.

3-60 Earl A. Thornton, *Thermal Structures for Aerospace Applications*, American Institute of Aeronautics and Astronautics, Reston, Virginia, 1996.

3-61 Michael P. Nemeth, Buckling Behavior of Long Anisotropic Plates Subjected to Fully Restrained Thermal Expansion, AIAA Paper 2001-1330, *Proceedings of the 42nd AIAA/ASME/ASCE/AHS/ASC Structures, Structural Dynamics and Materials Conference*, 16-19 April 2001, Seattle, Washington, AIAA, Reston, Virginia. Also, in somewhat expanded form as NASA TP-2003-212131, National Aeronautics and Space Administration, Langley Research Center, Hampton, Virginia, February 2003.

3-62 Robert M. Jones, Buckling of Simply Supported Rectangular Plates under Uniform Thermal and Mechanical Loading, *Problems of Mechanics of Thin Deformable Bodies, Devoted to the 80th Anniversary of Acadamician S. A. Ambartsumian*, Institute of Mechanics, National Academy of Sciences of Armenia, Yerevan, 2002, pp. 178–194.

3-63 Robert M. Jones, Buckling of Simply Supported Rectangular Plates under Uniform Thermal and Mechanical Loading, *Proceedings of the 5th International Congress on Thermal Stresses and Related Problems, TS2003*, Virginia Polytechnic Institute and State University, Blacksburg, Virginia, 8–11 June 2003, pp. TM-5-4-1–TM-5-4-4.

3-64 J. M. Klosner and M. J. Forray, Buckling of Simply Supported Plates Under Arbitrary Symmetrical Temperature Distributions, *Journal of the Aeronautical Sciences*, Volume 25, Number 3, March 1958, pp. 181–184.

3-65 Richard R. Heldenfels and William M. Roberts, *Experimental and Theoretical Determination of Thermal Stresses in a Flat Plate*, NACA Technical Note 2769, National Advisory Committee for Aeronautics, Washington, D. C., August 1952.

3-66 S. P. Timoshenko and J. N. Goodier, *Theory of Elasticity*, 3rd Edition, McGraw-Hill, New York, 1970.

3-67 Myron L. Gossard, Paul Seide, and William M. Roberts, *Thermal Buckling of Plates*, NACA Technical Note 2771, National Advisory Committee for Aeronautics, Washington, D. C., August 1952.

3-68 Alfred M. Freudenthal, On Inelastic Thermal Stresses in Flight Structures, *Journal of the Aeronautical Sciences*, Volume 21, Number 11, November 1954, pp. 772–776.

3-69 H. H. Hilton, Thermal Stresses in Bodies Exhibiting Temperature-Dependent Elastic Properties, *Journal of Applied Mechanics*, Volume 19, Number 3, September 1952, pp. 350–354.

3-70 Eldon E. Mathauser and William A. Brooks, Jr., *An Investigation of the Creep Lifetime of 75S-T6 Aluminum-Alloy Columns*, NACA Technical Note 3204, National Advisory Committee for Aeronautics, Washington, D. C., July 1954.

3-71 Robert M. Jones, Plastic Thermal Buckling of Uniformly Heated Rectangular Plates with Temperature-Dependent Material Properties, AIAA Paper 2005-1935, *Proceedings of the 46th AIAA/ASME/ASCE/AHS/ASC Structures, Structural Dynamics and Materials Conference*, 18-21 April 2005, Austin, Texas, AIAA, Reston, Virginia.

3-72 Earl A. Thornton, Thermal Buckling of Plates and Shells, *Applied Mechanics Reviews*, Volume 46, Number 10, October 1993, pp. 485–506.

3-73 Theodore R. Tauchert, Thermally Induced Flexure, Buckling, and Vibration of Plates, *Applied Mechanics Reviews*, Volume 44, Number 8, August 1991, pp. 347–360.

3-74 P. M. Ogibalov and V. F. Gribanov, *Thermal Stability of Plates and Shells*, Moscow State University, Moscow, 1968. Partial translation (introduction, chapter 4 on shell buckling experiments, and non-Russian references) available as FTD-HC-23-724-71, Foreign Technology Division, Air Force Systems Command, Wright-Patterson AFB, Ohio, AD 734918, N72-19943.

Éléments sous droits d'auteur

3-75 Michael P. Nemeth, Buckling Behavior of Long Symmetrically Laminated Plates Subjected to Combined Loadings, NASA TP-3195, National Aeronautics and Space Administration, Washington, May 1992.
3-76 Michael P. Nemeth, Buckling Behavior of Long Symmetrically Laminated Plates Subjected to Compression, Shear, and Inplane Bending Loads, *AIAA Journal*, Volume 30, Number 12, December 1992, pp. 2959–2965.
3-77 Michael P. Nemeth, Buckling Behavior of Long Anisotropic Plates Subjected to Combined Loadings, NASA TP-3568, National Aeronautics and Space Administration, Langley Research Center, Hampton, Virginia, November 1995.
3-78 Michael P. Nemeth, Buckling Behavior of Long Symmetrically Laminated Plates Subjected to Shear and Linearly Varying Axial Edge Loads, NASA TP-3659, National Aeronautics and Space Administration, Langley Research Center, Hampton, Virginia, July 1997.
3-79 Michael P. Nemeth, Importance of Anisotropy on Buckling of Compression-Loaded Symmetric Composite Plates, *AIAA Journal*, Volume 24, Number 11, November 1986, pp. 1831–1835.
3-80 A. Nadai, *Theory of Flow and Fracture of Solids*, Volume I, McGraw-Hill, New York, 1950.
3-81 Robert M Jones, *Plasticity*, Bull Ridge Publishing, Blacksburg, Virginia, 2006.
3-82 Bernard Budiansky, A Reassessment of Deformation Theories of Plasticity, *Journal of Applied Mechanics*, Volume 26, Series E, Number 2, June 1959, pp. 259–264.
3-83 Robert M. Jones, Plastic Buckling of Eccentrically Stiffened Circular Cylindrical Shells, *AIAA Journal*, Volume 5, Number 6, June 1967, pp. 1147–1152.
3-84 Elbridge Z. Stowell, *A Unified Theory of Plastic Buckling of Columns and Plates*, NACA Report 898, National Advisory Committee on Aeronautics, Washington, D.C., 1948.
3-85 A. A. Ilyushin, *The Elasto-Plastic Stability of Plates*, NACA Technical Memorandum 1188, National Advisory Committee on Aeronautics, Washington, D.C., December 1947. Originally published as Uprugo-Plasticheskaya Ustoichivost Plasteen, *Prikladnaya Matematika i Mekhanika X*, 1946, pp. 623–638.
3-86 F. R. Shanley, Inelastic Column Theory, *Journal of the Aeronautical Sciences*, Volume 14, Number 5, May 1947, pp. 261–268, including discussion by Theodore von Kármán.
3-87 M. E. Lunchick, Plasticity Research on Submarine Pressure Hulls at the David Taylor Model Basin, *Plasticity, Proceedings of the Second Symposium on Naval Structural Mechanics*, Brown University, Providence, Rhode Island, 5–7 April 1960, edited by E. H. Lee and P. S. Symonds, Pergamon Press, Oxford, 1960, pp. 347–368.
3-88 George Gerard and Sorrel Wildhorn, *A Study of Poisson's Ratio in the Yield Region*, NACA Technical Note 2561, National Advisory Committee on Aeronautics, Washington, D.C., January 1952.
3-89 Robert M. Jones, *Plastic Buckling of Eccentrically Stiffened Circular Cylindrical Shells*, Aerospace Corporation Report Number TR-0158(S3316-72)-1, San Bernardino, California, December 1967. Available only from the Clearinghouse CFSTI, United States Department of Commerce.
3-90 J. L. Holmquist and A. Nadai, A Theoretical and Experimental Approach to the Problem of Deep-Well Casing, *Drilling Production Practice*, 1939, American Petroleum Institute, 1940, pp. 392–420.
3-91 Richard A. Pride and George J. Heimerl, *Plastic Buckling of Simply Supported Compressed Plates*, NACA Technical Note 1817, National Advisory Committee for Aeronautics, Washington, D. C., April 1949.
3-92 Stephen W. Tsai, *Composites Design 1986*, Think Composites, Dayton, Ohio, 1986.
3-93 Lucien A. Schmit, The Structural Synthesis Concept and Its Potential Role in Design with Composites, in *Mechanics of Composite Materials, Proceedings of the 5th Symposium on Naval Structural Mechanics*, Edited by F. W. Wendt, H. Liebowitz, and N. Perrone, Philadelphia, Pennsylvania, 8–10 May 1967, Pergamon, New York, 1970, pp. 553–562.
3-94 Zafer Gürdal, Raphael T. Haftka, and Prabhat Hajela, *Design and Optimization of Laminated Composite Materials*, Wiley Interscience, New York, 1999.
3-95 Stephen W. Tsai and Nicholas J. Pagano, Invariant Properties of Composite Materials, in *Composite Materials Workshop*, Edited by S. W. Tsai, J. C. Halpin, and

Éléments sous droits d'auteur

Nicholas J. Pagano, St. Louis, Missouri, 13–21 July 1967, Technomic, Stamford, Connecticut, 1968, pp. 233–253.
3-96 Stephen W. Tsai and Nicholas J. Pagano, *Invariant Properties of Composite Materials*, Air Force Materials Laboratory, Wright-Patterson AFB, Ohio, Technical Report AFML-TR-67-379, March 1968.
3-97 Stephen W. Tsai, *Strength Characteristics of Composite Materials*, NASA Contractor Report CR-224, National Aeronautics and Space Administration, Washington, D. C., April 1965.
3-98 *Webster's New World Dictionary*, Second College Edition, David B. Guralnik, Editor in Chief, Prentice Hall Press, 1984, p. 582.
3-99 Charles Darwin, *On the Origin of Species*, John Murray, London, 1859.
3-100 Walter F. Cannon, foreword in Peter J. Vorzimmer, *Charles Darwin: The Years of Controversy*, Temple University Press, Philadelphia, 1970.
3-101 Kelvin J. Callahan and George E. Weeks, Optimum Design of Composite Laminates using Genetic Algorithms, *Composites Engineering*, Volume 2, No. 3, April 1992, pp. 149–160.
3-102 Rodolphe Le Riche and Raphael T. Haftka, Optimization of Laminate Stacking Sequence for Buckling Load Maximization by Genetic Algorithm, 33rd AIAA/ASME/ASCE/AHS/ASC Structures, Structural Dynamics and Materials Conference, 13–15 April 1992, Dallas, Texas, AIAA, Reston, Virginia. *AIAA Journal*, May 1993, Volume 31, No. 4, pp.951–956.
3-103 Grant Soremekun, Zafer Gürdal, Christos Kassapoglu, and Darryl Toni, Stacking Sequence Blending of Multiple Composite Laminates using Genetic Algorithms, AIAA Paper 2001-1203, 42nd AIAA/ASME/ASCE/AHS/ASC Structures, Structural Dynamics and Materials Conference, 16-19 April 2001, Seattle, Washington, AIAA, Reston, Virginia. Also *Composite Structures*, Volume 56, Number 1, April 2002, pp. 53–62.
3-104 W. Jefferson Stroud and Melvin S. Anderson, PASCO: Structural Panel Analysis and Sizing Code, Capability and Analytical Foundations, NASA Technical Memorandum 80181, National Aeronautics and Space Administration, Washington, D. C., January 1980.
3-105 W. H. Wittrick and F. W. Williams, "Buckling and Vibration of Anisotropic or Isotropic Plate Assemblies Under Combined Loadings", *International Journal of Mechanical Science*, April 1974, pp. 209-239.
3-106 Garret N. Vanderplaats, *CONMIN—a FORTRAN Program for Constrained Function Minimization*, NASA TM X-62-282, version updated in March 1975, NASA Ames Research Center, Moffett Field, California, August 1973.
3-107 C. M. Wang, J. N. Reddy, and K. H. Lee, *Shear Deformable Beams and Plates*, Elsevier Science, Amsterdam, 2000.
3-108 Rudolph Szilard, *Theory and Analysis of Plates, Classical and Numerical Methods*, Prentice-Hall, 1974.
3-109 P. S. Bulson, *The Stability of Flat Plates*, American Elsevier, 1975.
3-110 H. G. Allen and P. S. Bulson, *Background to Buckling*, McGraw Hill, Maidenhead, Berkshire, England, 1980.
3-111 Frederick Bloom and Douglas Coffin, *Handbook of Thin Plate Buckling and Postbuckling*, Chapman & Hall/CRC, Coca Raton, Florida, 2001.
3-112 R. H. Gallagher, *Buckling Strength of Structural Plates, NASA Space Vehicle Design Criteria (Structures)*, NASA SP-8058, National Aeronautics and Space Administration, Washington, D. C., June 1971.
3-113 Harold S. Morgan and Robert M. Jones, Buckling of Cross-Ply Laminated Rectangular Plates with Nonlinear Stress-Strain Behavior, *Journal of Applied Mechanics*, Volume 46, Number 3, September 1979, pp. 637–643.
3-114 Robert M. Jones, Thermal Buckling of Uniformly Heated Unidirectional and Symmetric Cross-Ply Laminated Fiber-Reinforced Composite Uniaxial In-Plane Restrained Simply Supported Rectangular Plates, *Composites, Part A: Applied Science and Manufacturing*, Volume 36, Issue 10, October 2005, pp.1355–1367.

Éléments sous droits d'auteur

Chapter 4

BUCKLING OF CIRCULAR CYLINDRICAL SHELLS

4.1 INTRODUCTION

Motivation for the study of shell buckling and the proper evaluation of shell buckling loads has increased exponentially since the 1930s. The first major impetus for the use of shells was the advent of the Douglas DC-2 stressed-skin airplane with shell elements as in Figure 4-1. Later, missiles and reentry vehicles provided further challenges and applications for shells. More recently, off-shore oil drilling platforms have been developed with giant support systems, major elements of which are shells as in Figure 4-1. Some of the most rapid growth in shell analysis capability has occurred since 1960.

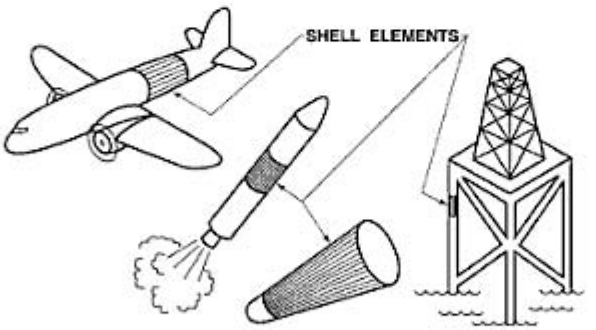


Figure 4-1 Applications of Shells as Structural Elements

Éléments sous droits d'auteur

A representative member of the family of shells that buckle is the circular cylindrical shell. That simple shell exhibits many of the important features of shell buckling, yet is mathematically attractive for study in a first course on buckling. The geometrical parameters, radius, r, thickness, t, and length, L, for a circular cylindrical shell are shown in Figure 4-2. A shell is said to be thin if its radius-to-thickness ratio, r/t, is large and to be long if its length-to-radius ratio, L/r, is large. The coordinate system is x,y,z (axial, circumferential, and radially outward transverse to the shell surface), and the corresponding displacements u,v,w are measured from a reference surface in the middle of the shell (i.e., at half the thickness of the shell), although other locations can be used.

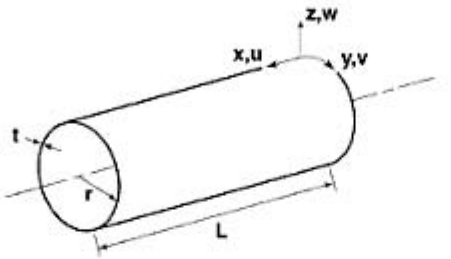


Figure 4-2 Circular Cylindrical Shell Geometry

The forces and moments on a shell element are defined in Figures 4-3 and 4-4, respectively. Actually, we will use forces per unit length and moments per unit length in our analyses (as we did for plates in Chapter 3), but we will simply call them forces and moments for convenience. We will have little need to refer to the Kirchhoff shear forces, K_x and K_y, shown in Figure 4-3, but they are displayed for completeness.

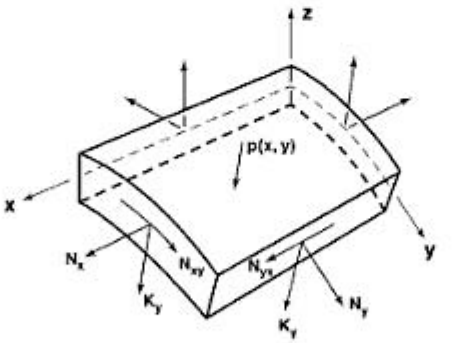


Figure 4-3 Circular Cylindrical Shell Forces

Éléments sous droits d'auteur

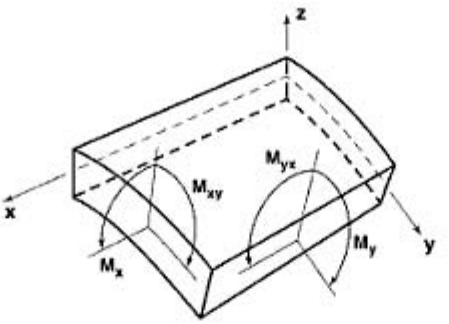


Figure 4-4 Circular Cylindrical Shell Moments

The stresses that are calculated in this section for the applied loadings in Figure 4-5 are valid for shells that are thin enough to have a uniform stress distribution through the shell thickness. Those stresses and the loadings from which they come are described in the following.

Axial compression is a load P in the axial direction of the circular cylindrical shell that produces compressive in-surface force (and force per unit width) and hence compressive stress in the axial direction,

$$N_x = -\frac{P}{2\pi r} \qquad \sigma_x = -\frac{P}{2\pi rt} \tag{4.1}$$

and can come either from P or from N_x applied directly along the edge as in Figure 4-5. Axial tension does not lead to buckling, but could lessen the tendency of an externally pressurized shell to buckle.

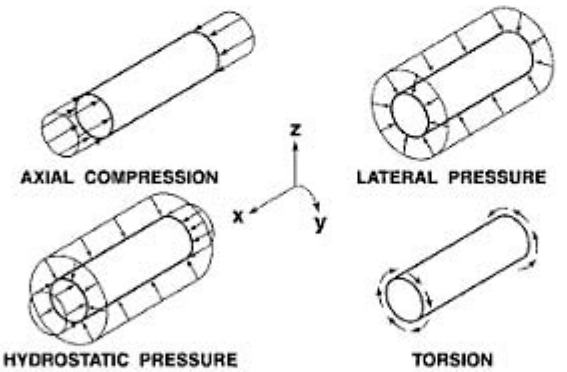


Figure 4-5 Axial Compression, Lateral Pressure, Hydrostatic Pressure, and Torsion on a Circular Cylindrical Shell

Éléments sous droits d'auteur

Lateral pressure is an external pressure loading only in the radially inward (– z) direction on the circumference of the circular cylindrical shell in Figure 4-5 producing a circumferential in-surface force and stress:

$$N_y = -pr \qquad \sigma_y = -\frac{pr}{t} \tag{4.2}$$

No loading exists in the x-direction. Internal pressure does not lead to buckling, but, in fact, stabilizes a shell against buckling! This stabilization concept was used to design the Atlas missile in the 1950s.

Hydrostatic pressure is uniform all-around inward pressure on the circular cylindrical shell in Figure 4-5 producing both circumferential and axial in-surface forces and stresses that are compressive:

$$N_x = -\frac{pr}{2} \quad N_y = -pr \qquad \sigma_x = -\frac{pr}{2t} \quad \sigma_y = -\frac{pr}{t} \tag{4.3}$$

Torsional loading on the circular cylindrical shell shown in Figure 4-5 produces in-surface shearing force and stress:

$$N_{xy} = \frac{T}{2\pi r} \qquad \tau_{xy} = \frac{T}{2\pi rt} \tag{4.4}$$

if the shell is thin enough to be able to ignore the usual mechanics of materials parabolic shear stress variation through the thickness.

In this Chapter, the fundamental differential equations of equilibrium and buckling are derived under certain simplifying conditions. These equations and their associated boundary conditions, as with those for plates, are consistently derived with an energy approach in Section 4.2. These equations will be displayed in various forms, including those due to Donnell [4-1] and Batdorf [4-2]. Classical solutions due to Batdorf et al. for axial compression, lateral pressure, and hydrostatic pressure are obtained for several boundary conditions in Section 4.3 to lay a foundation for more complicated shell buckling problems. The classical solutions are often referred to as Euler buckling loads even though Euler did not address shells. Nevertheless, the same type of theory as he used for bars is extended to shells. Then, the nature of postbuckling response is examined in Section 4.4 in order to assess the physical significance of the Euler buckling loads. Prior to buckling, the classical solutions inherently have an equilibrium state that corresponds to no local bending of the shell. However, the actual shell-edge support conditions cause bending with generally lower buckling loads than are obtained with the classical solution. These effects of prebuckling deformations on shell buckling loads are investigated in Section 4.5. The effects of initial geometric imperfections on buckling are treated in Section 4.6. Then, the contemporary problem of the effect of eccentric stiffeners on shell buckling loads is studied in Section 4.7. The even more contemporary problem of shells laminated of fiber-reinforced composite materials is addressed in Section 4.8. Next, the effect of restrained thermal expansion on shell buckling is examined in Section 4.9. Then, the influence of plastic deformation on buckling loads of single-layered and multilayered shells is assessed in Section 4.10. Finally, design of shells is introduced in Section 4.11, and other interesting areas of shells are briefly touched upon in Section 4.12.

Éléments sous droits d'auteur

4.2 DERIVATION OF EQUILIBRIUM AND BUCKLING EQUATIONS PLUS ASSOCIATED BOUNDARY CONDITIONS

In deriving the shell equilibrium equations and buckling equations, we will rely heavily on the general variational approach developed in the discussion on plates in Chapter 3. That is, we need only derive the total potential energy for a circular cylindrical shell, and then we can directly obtain the equilibrium differential equations and the buckling differential equations by use of the general variational equations. All results are for thin shells, i.e., shells whose thickness is small compared to the radius.

4.2.1 Equilibrium Differential Equations for Moderately Large Deflections

The work presented here is the circular cylindrical shells analogue of von Kármán large-deflection plate theory [4-3]. Apparently, Donnell [4-1] first derived this type of theory in the early 1930s. The essence of the theory is that the lateral displacement w is large enough that the in-surface forces and displacements must be considered in their nonlinear form. The strain-displacement relations for the shell middle surface are

$$\begin{aligned} \bar{\varepsilon}_x &= u_x + \frac{1}{2} w_x^2 \\ \bar{\varepsilon}_y &= v_y + \frac{w}{r} + \frac{1}{2} w_y^2 \\ \bar{\gamma}_{xy} &= v_x + u_y + w_x w_y \end{aligned} \tag{4.5}$$

in which subscripts on displacements denote partial differentiation.

The circumferential strain in Equation (4.5) has a new term in comparison to ε_y for plates. This term, w/r, arises from a larger circumference of the shell caused by a uniform radial expansion w. The diameter before deformation is 2r and after deformation is 2(r + w). Thus, the circumferential strain is

$$\varepsilon_y = \frac{\Delta\text{circumference}}{\text{circumference}} = \frac{2\pi(r+w) - 2\pi r}{2\pi r} = \frac{w}{r} \tag{4.6}$$

and is *not* accompanied by circumferential displacement v.

The Kirchhoff-Love hypothesis is now invoked as developed by A. E. H. Love (1863–1940) for shells [4-4] as a natural extension of Kirchhoff's hypothesis for plates [4-5]. The hypothesis consists of two somewhat contradictory, but extremely useful and effective approximations. First, the stresses σ_x, σ_y, and τ_{xy} acting in the shell surface (the x-y surface) are presumed to dominate the shell behavior. The stress state in which σ_z, τ_{xz}, and τ_{yz} are ignored is therefore an approximate state of plane stress. Second, the transverse shearing strains, γ_{xz} and γ_{yz}, and the transverse normal stress, ε_z, are neglected whereupon the normals to the shell reference surface remain normal and inextensional during deformation as in Figure 4-6. The contradiction arises because having ε_z as well as γ_{xz} and γ_{yz} be zero implies a state of a plane strain, not plane stress as in the first part of the Kirchhoff-Love hypothesis. The presumption of zero transverse shearing strains, γ_{xz} and γ_{yz}, does lead

Éléments sous droits d'auteur

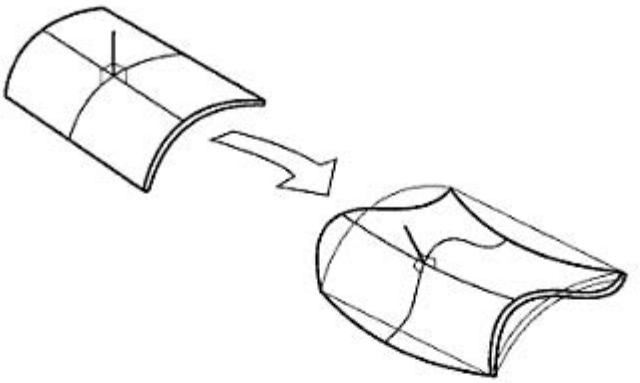


Figure 4-6 Deformation of a Shell Reference Surface Element

to zero transverse shearing stresses, τ_{xz} and τ_{yz} in a consistent manner, so the two presumptions are interrelated. The principal result of the Kirchhoff-Love hypothesis is that the strains vary linearly through the shell thickness:

$$\begin{aligned} \varepsilon_x &= \bar{\varepsilon}_x + z\kappa_x \\ \varepsilon_y &= \bar{\varepsilon}_y + z\kappa_y \\ \gamma_{xy} &= \bar{\gamma}_{xy} + z\kappa_{xy} \end{aligned} \tag{4.7}$$

in which ε_x, ε_y, and γ_{xy} are the strains at any point in the shell; $\bar{\varepsilon}_x$, $\bar{\varepsilon}_y$, and $\bar{\gamma}_{xy}$ are the middle surface strains; z is the thickness coordinate measured from the middle surface; and κ_x, κ_y, and κ_{xy} are the middle surface changes in curvature:

$$\begin{aligned} \kappa_x &= -w_{,xx} \\ \kappa_y &= -w_{,yy} \\ \kappa_{xy} &= -2w_{,xy} \end{aligned} \tag{4.8}$$

That is, the original curvatures of the shell are zero in the x-direction, 1/r in the circumferential direction, and zero twist curvature. After deformation of the shell, the curvatures *change* by the amounts in Equation (4.8).

Stresses are related to strains in an isotropic elastic material by

$$\begin{aligned} \sigma_x &= \frac{E}{1-\nu^2}(\varepsilon_x + \nu\varepsilon_y) \\ \sigma_y &= \frac{E}{1-\nu^2}(\varepsilon_y + \nu\varepsilon_x) \\ \tau_{xy} &= \frac{E}{2(1+\nu)}\gamma_{xy} \end{aligned} \tag{4.9}$$

in which E is the elastic Young's modulus and ν is Poisson's ratio.

Éléments sous droits d'auteur

By definition, the strain energy for an isotropic elastic material with $\sigma_z = 0$, $\tau_{xz} = 0$, and $\tau_{yz} = 0$ is

$$U = \frac{1}{2E}\iint\left[\int_{-t/2}^{t/2}\left[\sigma_x^2 + \sigma_y^2 - 2\nu\sigma_x\sigma_y + 2(1+\nu)\tau_{xy}^2\right]dz\right]dxdy \qquad (4.10)$$

in which Equations (4.7), (4.8), and (4.9) can be substituted and the resulting expression integrated through the thickness to obtain

$$U = U_m + U_b \qquad (4.11)$$

in which U_m is the membrane strain energy,

$$U_m = \frac{Et}{2(1-\nu^2)}\iint\left[\bar{\varepsilon}_x^2 + \bar{\varepsilon}_y^2 + 2\nu\bar{\varepsilon}_x\bar{\varepsilon}_y + \frac{1-\nu}{2}\bar{\gamma}_{xy}^2\right]dxdy \qquad (4.12)$$

and U_b is the bending strain energy,

$$U_b = \frac{Et^3}{24(1-\nu^2)}\iint\left[w_{xx}^2 + w_{yy}^2 + 2\nu w_{xx}w_{yy} + 2(1-\nu)w_{xy}^2\right]dxdy \qquad (4.13)$$

A technically significant difference between plate and shell equation derivations results from different sign conventions. For both two-dimensional structural elements, the coordinates are in consonance with the right-hand screw rule. However, plate coordinates have z positive downward as the most commonly used terminology. Therefore, Green's theorem boundary integrations must be performed in a clockwise manner when looking in the positive z-direction [4-6]. On the other hand, shell coordinates ordinarily have z positive outward as shown in Figure 4-2. Accordingly, Green's theorem boundary integrations must be performed in a counterclockwise manner when looking in the negative z-direction. Although there is no conflict in the foregoing statements, boundary integrations must obviously be performed in opposite directions when viewing a plate versus a shell in a 'natural' manner, i.e., natural relative to the respective chosen coordinate systems and their orientation.

To perform boundary integration for a multiply-connected region such as a circular cylindrical shell, introduce a cut in the integration region to define a closed curve C. The resulting counterclockwise integration path is indicated in Figure 4-7. Note that the integrals along the two sides of the cut cancel because they are of opposite sign. Also, no corner forces can arise because the circumferential location of the cut is arbitrary.

In order to utilize the results given in Chapter 3, Buckling of Plates, for deriving shell equilibrium and buckling equations, all boundary integrations for shells must be regarded as being taken in the counterclockwise direction. Then, the correct boundary conditions for a shell are obtained by proper combination of the integrations of Chapter 3 with the following shell potential energy of external forces integrals.

Éléments sous droits d'auteur

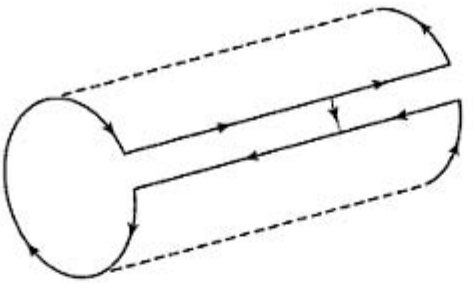


Figure 4-7 Circular Cylindrical Shell Boundary Integration

The potential energy of external forces consists of that due to lateral pressure, p, (also called transverse pressure) over the shell surface:

$$\Omega_p = + \iint p\, w\, dx\, dy \tag{4.14}$$

that due to in-surface forces, $\bar{N}_x$ and $\bar{N}_y$, along the shell edge at the end:

$$\Omega_F = - \int (\bar{N}_x u + \bar{N}_{xy} v)\, dy \tag{4.15}$$

that due to an edge moment, $\bar{M}_x$, along the shell edge at the end:

$$\Omega_M = + \int \bar{M}_x w_{,x}\, dy \tag{4.16}$$

and that due to the Kirchhoff shearing force (as defined in Section 3.2.2):

$$\Omega_k = - \int \bar{K}_x w\, dy \tag{4.17}$$

Note that the forces and moments per unit width are applied only along lines x = constant with the exception of the lateral pressure.

Next, substitute the strain-displacement relations, Equation (4.5), in the strain energy, Equation (4.11), and identify F in Equation (3.5) on page 230 of Section 3.2.1 as

$$\begin{aligned} F = \frac{A}{2} \Bigg[& \left(u_x + \frac{1}{2} w_x^2\right)^2 + \left(v_y + \frac{w}{r} + \frac{1}{2} w_y^2\right)^2 \\ & + 2\nu \left(u_x + \frac{1}{2} w_x^2\right)\left(v_y + \frac{w}{r} + \frac{1}{2} w_y^2\right) + \frac{1-\nu}{2} \left(v_x + u_y + w_x w_y\right)^2 \Bigg] \\ & + \frac{D}{2} \left[w_{xx}^2 + w_{yy}^2 + 2\nu w_{xx} w_{yy} + 2(1-\nu) w_{xy}^2 \right] + pw \end{aligned} \tag{4.18}$$

in which the shell extensional stiffness is

Éléments sous droits d'auteur

$$A = \frac{Et}{1-\nu^2} \tag{4.19}$$

and the shell bending stiffness is

$$D = \frac{Et^3}{12(1-\nu^2)} \tag{4.20}$$

Note that F is a quartic function of w_x and w_y and that only Ω_p contributes to F. The following derivatives of F are required:

$$\begin{aligned}
\frac{\partial F}{\partial u_x} &= \frac{A}{2}\left[2\left(u_x + \frac{1}{2}w_x^2\right) + 2\nu\left(v_y + \frac{w}{r} + \frac{1}{2}w_y^2\right)\right] \\
\frac{\partial F}{\partial u_y} &= \frac{A}{2}\left[(1-\nu)(v_x + u_y + w_x w_y)\right] \\
\frac{\partial F}{\partial v_x} &= \frac{A}{2}\left[(1-\nu)(v_x + u_y + w_x w_y)\right] \\
\frac{\partial F}{\partial v_y} &= \frac{A}{2}\left[2\left(v_y + \frac{w}{r} + \frac{1}{2}w_y^2\right) + 2\nu\left(u_x + \frac{1}{2}w_x^2\right)\right] \\
\frac{\partial F}{\partial w} &= \frac{A}{2}\left[2\left(v_y + \frac{w}{r} + \frac{1}{2}w_y^2\right)/r + 2\nu\left(u_x + \frac{1}{2}w_x^2\right)/r\right] + p \\
\frac{\partial F}{\partial w_x} &= \frac{A}{2}\left[2w_x\left(u_x + \frac{1}{2}w_x^2\right)\right. \\
&\qquad \left. + 2\nu w_x\left(v_y + \frac{w}{r} + \frac{1}{2}w_y^2\right) + (1-\nu)w_y(v_x + u_y + w_x w_y)\right] \\
\frac{\partial F}{\partial w_y} &= \frac{A}{2}\left[2w_y\left(v_y + \frac{w}{r} + \frac{1}{2}w_y^2\right)\right. \\
&\qquad \left. + 2\nu w_y\left(u_x + \frac{1}{2}w_x^2\right) + (1-\nu)w_x(v_x + u_y + w_x w_y)\right] \\
\frac{\partial F}{\partial w_{xx}} &= \frac{D}{2}(2w_{xx} + 2\nu w_{yy}) \\
\frac{\partial F}{\partial w_{xy}} &= \frac{D}{2}\left[4(1-\nu)w_{xy}\right] \\
\frac{\partial F}{\partial w_{yy}} &= \frac{D}{2}(2w_{yy} + 2\nu w_{xx})
\end{aligned} \tag{4.21}$$

Note that the first derivatives of F are more complicated for shells than for plates because of the w/r term in the circumferential strain.

Upon substitution of the first partial derivatives of F from Equation (4.21) in the Euler equations and boundary conditions of Section 3.2.2 on pages 234–237, the equilibrium equations are

$$\frac{\partial}{\partial x}\left[\left(u_x + \frac{1}{2}w_x^2\right) + \nu\left(v_y + \frac{w}{r} + \frac{1}{2}w_y^2\right)\right] + \frac{1-\nu}{2}\frac{\partial}{\partial y}(v_x + u_y + w_x w_y) = 0 \tag{4.22}$$

$$\frac{1-\nu}{2}\frac{\partial}{\partial x}(v_x + u_y + w_x w_y) + \frac{\partial}{\partial y}\left[\left(v_y + \frac{w}{r} + \frac{1}{2}w_y^2\right) + \nu\left(u_x + \frac{1}{2}w_x^2\right)\right] = 0 \tag{4.23}$$

Éléments sous droits d'auteur

$$
\begin{aligned}
&A\left[(v_y + \frac{w}{r} + \frac{1}{2}w_y^2) + \nu(u_x + \frac{1}{2}w_x^2)\right]/r + p \\
&\quad - A\frac{\partial}{\partial x}\left[w_x\left[(u_x + \frac{1}{2}w_x^2) + \nu(v_y + \frac{w}{r} + \frac{1}{2}w_y^2)\right]\right. \\
&\qquad \left. + \frac{1-\nu}{2}w_y(v_x + u_y + w_x w_y)\right] \\
&\quad - A\frac{\partial}{\partial y}\left[w_y\left[(v_y + \frac{w}{r} + \frac{1}{2}w_y^2) + \nu(u_x + \frac{1}{2}w_x^2)\right]\right. \\
&\qquad \left. + \frac{1-\nu}{2}w_x(v_x + u_y + w_x w_y)\right] \\
&\quad + D\left[\frac{\partial^2}{\partial x^2}(w_{xx} + \nu w_{yy}) + 2(1-\nu)\frac{\partial^2}{\partial x \partial y}w_{xy} + \frac{\partial^2}{\partial y^2}(w_{yy} + \nu w_{xx})\right] = 0
\end{aligned}
\tag{4.24}
$$

and the boundary conditions at the shell edges are

$$u = 0 \quad \text{or} \quad A\left[(u_x + \frac{1}{2}w_x^2) + \nu(v_y + \frac{w}{r} + \frac{1}{2}w_y^2)\right] = \tilde{N}_x \tag{4.25}$$

$$v = 0 \quad \text{or} \quad \frac{1-\nu}{2}A(v_x + u_y + w_x w_y) = \tilde{N}_{xy} \tag{4.26}$$

$$
\begin{aligned}
w = 0 \quad \text{or} \quad &A\left[w_x\left[(u_x + \frac{1}{2}w_x^2)\right.\right. \\
&\left.\left. + \nu(v_y + \frac{w}{r} + \frac{1}{2}w_y^2)\right] + \frac{1-\nu}{2}w_y(v_x + u_y + w_x w_y)\right] \\
&- D\left[\frac{\partial}{\partial x}(w_{xx} + \nu w_{yy}) + \frac{\partial}{\partial y}[2(1-\nu)w_{xy}]\right] = \tilde{K}_x
\end{aligned}
\tag{4.27}
$$

$$w_x = 0 \quad \text{or} \quad -D(w_{xx} + \nu w_{yy}) = \tilde{M}_x \tag{4.28}$$

in which the tildes denote applied forces and moments at the edges.

Note here the careful distinction between *edge* boundary conditions and *end* boundary conditions. A circular cylindrical shell has two ends, and at each end of the shell surface there is an edge. The shell surface has edge conditions whereas the shell axis has end conditions. The boundary conditions in Equations (4.25)–(4.28) are for the edges. We have not stipulated the net conditions on the end of the shell except implicitly as an integral along the edge of the edge boundary conditions (because, for example, N_x integrates to P). This distinction can be perceived better with the aid of Figure 4-8. There, each end is regarded as clamped in some manner because the shell axis cannot rotate at the ends when the shell is regarded as a beam supporting load P. However, the shell reference surface can rotate at each end. Hence, the ends are clamped, yet the edges are simply supported. We will speak of *end* conditions for beams or columns (one-dimensional structural elements) and of *both end* and *edge* conditions for plates and shells (two-dimensional structural elements).

Éléments sous droits d'auteur

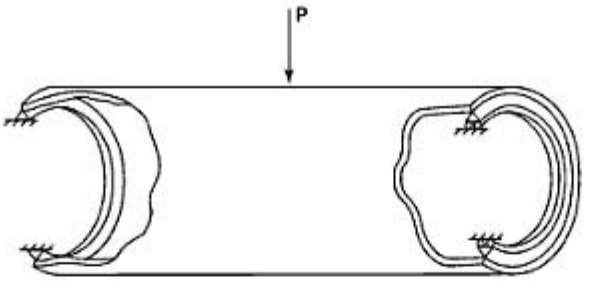


Figure 4-8 Schematic View of Edge and End Support Conditions for a Circular Cylindrical Shell

The equilibrium equations and boundary conditions can be simplified considerably by substitution of the force-strain and moment-curvature relations that are obtained by integrating the stresses, Equation (4.9), in terms of the strain variations, Equation (4.7) and (4.8):

$$\begin{aligned} N_x &= \int_{-t/2}^{t/2} \sigma_x \, dz = A(\bar{\varepsilon}_x + \nu\bar{\varepsilon}_y) \\ N_y &= \int_{-t/2}^{t/2} \sigma_y \, dz = A(\bar{\varepsilon}_y + \nu\bar{\varepsilon}_x) \\ N_{xy} &= \int_{-t/2}^{t/2} \tau_{xy} \, dz = \frac{1-\nu}{2} A\bar{\gamma}_{xy} \end{aligned} \tag{4.29}$$

$$\begin{aligned} M_x &= \int_{-t/2}^{t/2} \sigma_x \, z \, dz = D(\kappa_x + \nu\kappa_y) \\ M_y &= \int_{-t/2}^{t/2} \sigma_y \, z \, dz = D(\kappa_y + \nu\kappa_x) \\ M_{xy} &= \int_{-t/2}^{t/2} \tau_{xy} \, z \, dz = \frac{1-\nu}{2} D\,\kappa_{xy} \end{aligned} \tag{4.30}$$

Note in Equations (4.29) and (4.30) that approximations to the in-surface forces and moments are made in the manner of Donnell shallow shell theory. Actually, more accurate integral expressions due to Flügge [4-7] and Novozhilov [4-8] are typified by stress resultants such as

$$N_x = \int_{-t/2}^{t/2} \sigma_x \left(1 - \frac{z}{r}\right) dz \tag{4.31}$$

Upon substitution of the strain-displacement relations, Equation (4.5), and the curvature-displacement relations, Equation (4.8), Equations (4.29) and (4.30) become

Éléments sous droits d'auteur

$$N_x = A\left[(u_x + \frac{1}{2}w_x^2) + \nu(v_y + \frac{w}{r} + \frac{1}{2}w_y^2)\right]$$
$$N_y = A\left[(v_y + \frac{w}{r} + \frac{1}{2}w_y^2) + \nu(u_x + \frac{1}{2}w_x^2)\right] \quad (4.32)$$
$$N_{xy} = \frac{1-\nu}{2}A(v_x + u_y + w_x w_y)$$

$$M_x = -D(w_{xx} + \nu w_{yy})$$
$$M_y = -D(w_{yy} + \nu w_{xx}) \quad (4.33)$$
$$M_{xy} = -(1-\nu)Dw_{xy}$$

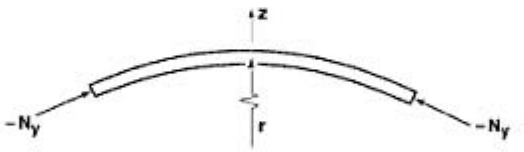
whereupon the equilibrium equations, Equations (4.22), (4.23), and (4.24), become

$$\frac{\partial N_x}{\partial x} + \frac{\partial N_{xy}}{\partial y} = 0 \quad (4.34)$$

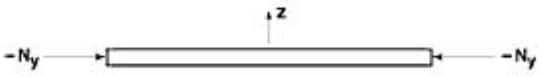
$$\frac{\partial N_{xy}}{\partial x} + \frac{\partial N_y}{\partial y} = 0 \quad (4.35)$$

$$\frac{\partial^2 M_x}{\partial x^2} + 2\frac{\partial^2 M_{xy}}{\partial x \partial y} + \frac{\partial^2 M_y}{\partial y^2} + N_x w_{xx} + N_y w_{yy} + 2N_{xy}w_{xy} - \frac{N_y}{r} = p \quad (4.36)$$

Equation (4.36) reduces to the von Kármán large-deflection plate equilibrium equations when the shell curvature, 1/r, goes to zero [4-3]. Note especially that these equations are *not buckling equations*. The appearance of the curvature and circumferential force per unit width term, N_y/r, in Equation (4.36) is further rationalized by examination of a differential shell element in Figure 4-9a. There, N_y has a component in the z-direction whereas for plates, as in Figure 4-9b, there is no such component.



a Shell Element



b Plate Element

Figure 4-9 Shell and Plate Elements

Éléments sous droits d'auteur

Equations (4.34)–(4.36), when expressed in terms of displacements u, v, and w (via the force-strain-displacement relations [Equations (4.29) and (4.5)] and the moment-curvature-displacement relations [Equations (4.30) and (4.8)]), are three coupled partial differential equations. Recall that the two coupled plate equilibrium equations due to in-plane loading are decoupled from the plate equilibrium equation for deflection under transverse loading. Thus, the shell equilibrium problem always involves bending-extension coupling, so is automatically more complicated than the plate equilibrium problem.

The boundary conditions on displacements, forces, and moments (and their derivatives) for circular cylindrical shells in Equations (4.25–4.28, with tildes to indicate the applied value at the boundary, become

$$\begin{aligned} u &= \tilde{u} \quad \text{or} \quad N_x = \tilde{N}_x \\ v &= \tilde{v} \quad \text{or} \quad N_{xy} = \tilde{N}_{xy} \\ w &= \tilde{w} \quad \text{or} \quad M_{x,x} + M_{xy,y} + N_x w_x + N_{xy} w_y = \tilde{K}_x \\ w_x &= \tilde{w}_x \quad \text{or} \quad M_x = \tilde{M}_x \end{aligned} \tag{4.37}$$

in which $\tilde{K}_x$ is the applied value of the Kirchhoff shear force [see Equations (3.55)–(3.57) and [4-5]]. Note that the displacement-related boundary conditions are actually applied only at the shell reference surface, not over the entire thickness of the edge as we might imagine. Similarly, the forces and moment are applied at the shell reference surface. The forces (positive in tension), moment, and displacements for the edge of shells that are either simply supported or clamped, but not free (so the Kirchhoff shear force is not active), are shown in Figure 4-10.

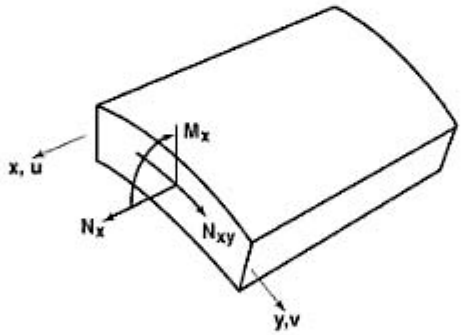


Figure 4-10 Forces, Moment, and Displacements on a Shell Edge

Sobel [4-9] suggested a set of notation for the eight edge boundary conditions of a circular cylindrical shell that buckles from a membrane prebuckling equilibrium state. That set was revised and expanded by Almroth [4-10] in his treatment of the eight boundary conditions for accurate prebuckling deformation in addition to the eight boundary conditions for buckling from the actual prebuckling state. For the common

Éléments sous droits d'auteur

practical cases of simply supported edges and clamped edges, the shell equilibrium boundary conditions in Almroth's notation [4-10] are:

Simply Supported Edges:

$$\begin{array}{llllll} \text{S1:} & w=0 & M_x=0 & u=0 & v=0 \\ \text{S2:} & w=0 & M_x=0 & N_x=\tilde{N}_x & v=0 \\ \text{S3:} & w=0 & M_x=0 & u=0 & N_{xy}=\tilde{N}_{xy} \\ \text{S4:} & w=0 & M_x=0 & N_x=\tilde{N}_x & N_{xy}=\tilde{N}_{xy} \end{array} \tag{4.38}$$

Clamped Edges:

$$\begin{array}{llllll} \text{C1:} & w=0 & w_{,x}=0 & u=0 & v=0 \\ \text{C2:} & w=0 & w_{,x}=0 & N_x=\tilde{N}_x & v=0 \\ \text{C3:} & w=0 & w_{,x}=0 & u=0 & N_{xy}=\tilde{N}_{xy} \\ \text{C4:} & w=0 & w_{,x}=0 & N_x=\tilde{N}_x & N_{xy}=\tilde{N}_{xy} \end{array} \tag{4.39}$$

in which the prescribed forces $\tilde{N}_x$ (again, positive in tension for the equilibrium problem) and $\tilde{N}_{xy}$ might be zero but, of course, not if those forces are the applied loading on the shell. A prescribed moment $\tilde{M}_x$ is not of interest in this book because it does not lead to a classical buckling problem. The edge displacements u and v could be prescribed at the edge as in structural ground-settlement problems.

A shell can be characterized as having any one of the eight conditions in Equations (4.38) and (4.39) on each of its two edges (lines of constant x in Figure 4-2 or Figure 4-10). The range of possibilities is, therefore, quite large (twelve possible conditions on each of the two edges if the free-edge conditions as well as simply supported and clamped-edge conditions are included). The simplest cases to analyze naturally involve like types of boundary conditions on opposite edges. The emphasis in this book is on shells with two simply supported edges, so cases are chosen from those in Equation (4.38). Note that simply supported edges have no rotational restraint, but when this simplified terminology of simply supported edges is used, the specific in-surface conditions are not determined. Obviously, the totality of boundary conditions including in-surface conditions must be specified by stating, for example, that a solution is obtained for S1 boundary conditions.

The shell edge boundary conditions are quite similar to the plate edge boundary conditions discussed in Chapter 3. In fact, we will depict the shell edge boundary conditions in a manner similar to that of the plate edge boundary conditions because both sets of boundary conditions apply in the x-y surface which is flat for plates and curved for a shell.

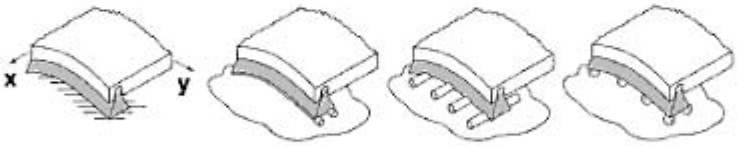
To better appreciate the four possible simply supported edge boundary conditions, consider the support systems for the edge of a shell illustrated in Figure 4-11 in near-physical terms with mechanisms that the reader can easily understand. View the elements in Figure 4-11 as a small segment of a circumferential strip around the end of the shell to constitute the end of the shell. Note that the support mechanisms de-

Éléments sous droits d'auteur

picted are only for understanding how the various supports *could* work. Only the reader can decide what support conditions are applicable to a specific structure of interest. For a simply supported shell edge, the principal support mechanism in Figure 4-11 is a curved triangular prism with a circular-cross-section prismatic protrudance (pivot) on the top as a realistic mechanism for the usual so-called knife-edge support for free rotation about the shell middle surface, i.e., $M_x = 0$. The end view of the curved triangular prism looks similar to the usual beam support, but with more realistic mechanisms that permit the movement(s) required. For a shell, the protrudance is a bearing that permits (limited) rotation about the y-axis through the center of the protrudance which is located at the middle surface of the shell (but not precisely at the edge of the shell). The protrudance fits in a cavity in the shell such that rotation around the y-axis is possible (of course, it is difficult to imagine how a curved surface can rotate except perhaps locally!), but movement transverse to the shell surface is prevented ($w = 0$) and translation along the y-axis of the curved triangular prism is not permitted.

The four manners of supporting the curved triangular prism are:

(1) For the S1 condition, the curved triangular prism is fastened to a curved surface such that the prism cannot translate in either the x- or y-directions. Thus, $u = 0$ and $v = 0$ and forces N_x and N_{xy} exist.
(2) For the S2 condition, the curved triangular prism is supported on partially embedded y-direction roller bearings that permit translation in the x-direction, but translation in the y-direction cannot occur, so $u \neq 0$ and $v = 0$. Hence, force N_x must be zero, but N_{xy} must exist.
(3) For the S3 condition, the curved triangular prism is supported on partially embedded x-direction roller bearings that permit translation in the y-direction, but translation in the x-direction cannot occur, so $u = 0$ and $v \neq 0$. Hence, force N_x must exist, but N_{xy} must be zero.
(4) For the S4 condition, the curved triangular prism is supported on partially embedded spherical bearings that permit translation in any direction in the x-y surface. Thus, $u \neq 0$ and $v \neq 0$, so both forces N_x and N_{xy} must be zero.

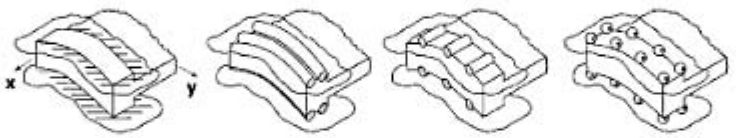


S1	S2	S3	S4
$w = 0$	$w = 0$	$w = 0$	$w = 0$
$M_x = 0$	$M_x = 0$	$M_x = 0$	$M_x = 0$
$u = 0$	$N_x = 0$	$u = 0$	$N_x = 0$
$v = 0$	$v = 0$	$N_{xy} = 0$	$N_{xy} = 0$

Figure 4-11 Simply Supported Edge Equilibrium Boundary Conditions

Éléments sous droits d'auteur

The analogous four boundary conditions for clamped edges are somewhat more difficult to perceive. The first impression for what constitutes a clamped edge might be the C1 condition of no displacements, u, v, and w, and no rotation, $\partial w/\partial x$. However, a clamped edge is commonly interpreted to mean only that the transverse displacement, w, and the edge rotation, $\partial w/\partial x$, are both zero *without specifying any in-plane displacement conditions.* Accordingly, the curved boxy mass that constitutes the clamping fixture in Figure 4-12 restrains both transverse displacement, w, and edge rotation, $\partial w/\partial x$. The way the clamping fixture is itself supported determines the in-surface boundary conditions. Thus, if the clamping fixture cannot move in the x-y surface, then u = 0 and v = 0 for the C1 boundary condition. Only the C1 condition is truly clamped in every respect. The other clamped-edge conditions all have some form of in-surface movement permitted by virtue of the presence of various rollers. That is, the clamped-edge condition is interpreted to mean only that all boundaries have complete restraint of edge rotation and that no displacement can occur transverse to the shell surface. If the clamping fixture can roll in the x-direction, then $N_x = 0$, but v = 0 because no displacement occurs in the y-direction for the C2 boundary condition. Next, if the clamping fixture can roll in the y-direction but not in the x-direction, then $N_{xy} = 0$ and u = 0. Finally, if the clamping fixture can roll in both the x- and y-directions as if supported on frictionless balls, then the in-surface forces must be zero, i.e., $N_x = 0$ and $N_{xy} = 0$.



C1	C2	C3	C4
$w = 0$	$w = 0$	$w = 0$	$w = 0$
$w_{,x} = 0$	$w_{,x} = 0$	$w_{,x} = 0$	$w_{,x} = 0$
$u = 0$	$N_x = 0$	$u = 0$	$N_x = 0$
$v = 0$	$v = 0$	$N_{xy} = 0$	$N_{xy} = 0$

Figure 4-12 Clamped-Edge Equilibrium Boundary Conditions

4.2.2 Buckling Differential Equations and Energy Expressions for Lateral Pressure, Axial Compression, and In-Surface Shear

We begin with the same stress-strain-displacement relations as in the preceding section and use the same total potential energy expression except that we disregard all potential energy of external forces terms except those due to lateral pressure, axial compression, and in-surface shear. These loads that cause buckling are depicted in Figure 4-13. The applied loads $\bar{N}_x$, $\bar{N}_{xy}$, and p do not appear explicitly in the expression for $\delta^2 V$ because $\delta^2 \Omega = 0$. Instead, the loads enter the buckling problem through the solution for the prebuckling equilibrium state.

Éléments sous droits d'auteur

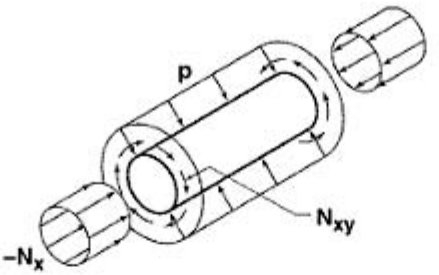


Figure 4-13 Circular Cylindrical Shell with Various Loads

The following nonzero second partial derivatives of F are obtained from Equation (4.21):

$$\frac{\partial^2 F}{\partial u_x^2} = A \quad \frac{\partial^2 F}{\partial u_x \partial w} = \nu A/r \quad \frac{\partial^2 F}{\partial u_x \partial w_y} = \nu A w_y \quad \frac{\partial^2 F}{\partial u_x \partial v_y} = \nu A \quad \frac{\partial^2 F}{\partial u_x \partial w_x} = A w_x$$

$$\frac{\partial^2 F}{\partial u_y^2} = \frac{1-\nu}{2} A \quad \frac{\partial^2 F}{\partial u_y \partial v_x} = \frac{1-\nu}{2} A \quad \frac{\partial^2 F}{\partial u_y \partial w_x} = \frac{1-\nu}{2} A w_y$$

$$\frac{\partial^2 F}{\partial u_y \partial w_y} = \frac{1-\nu}{2} A w_x \quad \frac{\partial^2 F}{\partial v_x^2} = \frac{1-\nu}{2} A \quad \frac{\partial^2 F}{\partial v_x \partial w_x} = \frac{1-\nu}{2} A w_y$$

$$\frac{\partial^2 F}{\partial v_x \partial w_y} = \frac{1-\nu}{2} A w_x \quad \frac{\partial^2 F}{\partial v_y^2} = A \quad \frac{\partial^2 F}{\partial v_y \partial w} = A/r \quad \frac{\partial^2 F}{\partial v_y \partial w_x} = \nu A w_x$$

$$\frac{\partial^2 F}{\partial v_y \partial w_y} = A w_y \quad \frac{\partial^2 F}{\partial w^2} = A/r^2 \quad \frac{\partial^2 F}{\partial w \partial w_x} = \nu A w_x/r \quad \frac{\partial^2 F}{\partial w \partial w_y} = A w_y/r$$

$$\frac{\partial^2 F}{\partial w_x^2} = A\left[(u_x + \frac{1}{2} w_x^2) + w_x^2 + \nu(v_y + \frac{w}{r} + \frac{1}{2} w_y^2) + \frac{1-\nu}{2} w_y^2\right] \tag{4.40}$$

$$\frac{\partial^2 F}{\partial w_x \partial w_y} = A\left[\nu w_x w_y + \frac{1-\nu}{2}(v_x + u_y + w_x w_y) + \frac{1-\nu}{2} w_y w_x\right]$$

$$\frac{\partial^2 F}{\partial w_y^2} = A\left[(v_y + \frac{w}{r} + \frac{1}{2} w_y^2) + w_y^2 + \nu(u_x + \frac{1}{2} w_x^2) + \frac{1-\nu}{2} w_x^2\right]$$

$$\frac{\partial^2 F}{\partial w_{xx}^2} = D \quad \frac{\partial^2 F}{\partial w_{xx} \partial w_{yy}} = \nu D \quad \frac{\partial^2 F}{\partial w_{yy}^2} = D \quad \frac{\partial^2 F}{\partial w_{xy}^2} = 2(1-\nu)D$$

Upon substitution of the second partial derivatives of F, Equation (4.40), in the expression for the second variation of the total potential energy, Equation (3.95) on pages 250–252 in Section 3.2.4, we get

Éléments sous droits d'auteur

$$\begin{aligned}\bar{\delta}^2V = A\iint\Bigg[&\bar{u}_x^2 + \frac{1-\nu}{2}\bar{u}_y^2 + \frac{1-\nu}{2}\bar{v}_x^2 + \bar{v}_y^2 + \frac{\bar{w}^2}{r^2} \\ &+ \left[(u_x + \frac{1}{2}w_x^2) + w_x^2 + \nu(v_y + \frac{w}{r} + \frac{1}{2}w_y^2) + \frac{1-\nu}{2}w_y^2\right]\bar{w}_x^2 \\ &+ \left[(v_y + \frac{w}{r} + \frac{1}{2}w_y^2) + w_y^2 + \nu(u_x + \frac{1}{2}w_x^2) + \frac{1-\nu}{2}w_x^2\right]\bar{w}_y^2\Bigg]\,dxdy \\ &+ D\iint\left[\bar{w}_{xx}^2 + 2(1-\nu)\bar{w}_{xy}^2 + \bar{w}_{yy}^2 + 2\nu\bar{w}_{xx}\bar{w}_{yy}\right]dxdy \\ &+ 2A\iint\Bigg[\left[\frac{1-\nu}{2}(v_x + u_y) + w_xw_y\right]\bar{w}_x\bar{w}_y + \nu\bar{u}_x\bar{v}_y + \frac{1-\nu}{2}\bar{u}_y\bar{v}_x \\ &\quad + w_x\bar{u}_x\bar{w}_x + \nu w_y\bar{u}_x\bar{w}_y + \frac{1-\nu}{2}w_y\bar{u}_y\bar{w}_x + \frac{1-\nu}{2}w_x\bar{u}_y\bar{w}_y \\ &\quad + \frac{1-\nu}{2}w_y\bar{v}_x\bar{w}_x + \frac{1-\nu}{2}w_x\bar{v}_x\bar{w}_y + \nu w_x\bar{v}_y\bar{w}_x + w_y\bar{v}_y\bar{w}_y \\ &\quad + (\nu\bar{u}_x\bar{w} + \bar{v}_y\bar{w} + \nu w_x\bar{w}\,\bar{w}_x + w_y\bar{w}\,\bar{w}_y)/r \\ &\quad + \nu w_x\bar{v}_y\bar{w}_x + w_y\bar{v}_y\bar{w}_y\Big]\,dxdy \end{aligned} \tag{4.41}$$

in which $\bar{u}_x$, $\bar{u}_y$, etc. are actually δu_x, δu_y, etc. (i.e., the derivatives of the variational displacements from the equilibrium state). All quantities with variational symbols or overbars take place during buckling. These variations have no relation to what happens in the equilibrium state leading up to the buckling load. Also, u_x, u_y, etc. are the derivatives of the displacements of the equilibrium state.

Rewrite Equation (4.41) as

$$\bar{\delta}^2V = \bar{\delta}^2U_{m_1} + \bar{\delta}^2U_{m_2} + \bar{\delta}^2U_b \tag{4.42}$$

in which

$$\begin{aligned}\bar{\delta}^2U_{m_1} = A\iint\Bigg[&\left[\bar{u}_x^2 + w_x^2\bar{w}_x^2 + 2\bar{u}_xw_x\bar{w}_x\right] \\ &+ \left[\bar{v}_y^2 + \bar{w}^2/r^2 + w_y^2\bar{w}_y^2 + 2(\bar{v}_y\bar{w}/r + \bar{v}_yw_y\bar{w}_y + \bar{w}w_y\bar{w}_y/r)\right] \\ &+ 2\nu\left[\bar{u}_x\bar{v}_y + \bar{u}_x\bar{w}/r + \bar{u}_xw_y\bar{w}_y + w_x\bar{w}_x\bar{v}_y + w_x\bar{w}_x\bar{w}/r + w_x\bar{w}_xw_y\bar{w}_y\right] \\ &+ \frac{1-\nu}{2}\Big[\bar{v}_x^2 + \bar{u}_y^2 + w_x^2\bar{w}_y^2 + w_y^2\bar{w}_x^2 + 2(\bar{v}_x\bar{u}_y + \bar{v}_xw_x\bar{w}_y + \bar{v}_xw_y\bar{w}_x \\ &\quad + \bar{u}_yw_x\bar{w}_y + \bar{u}_yw_y\bar{w}_x + w_xw_y\bar{w}_y\bar{w}_x)\Big]\Bigg]\,dxdy \end{aligned} \tag{4.43}$$

$$\begin{aligned}\bar{\delta}^2U_{m_2} = A\iint\Bigg[&\left[(u_x + \frac{1}{2}w_x^2) + \nu(v_y + \frac{w}{r} + \frac{1}{2}w_y^2)\right]\bar{w}_x^2 \\ &+ \left[(v_y + \frac{w}{r} + \frac{1}{2}w_y^2) + \nu(u_x + \frac{1}{2}w_x^2)\right]\bar{w}_y^2 \\ &+ (1-\nu)(v_x + u_y + w_xw_y)\bar{w}_x\bar{w}_y\Big]\,dxdy \end{aligned} \tag{4.44}$$

Éléments sous droits d'auteur

$$\bar{\delta}^2 U_b = D\iint\left[\bar{w}_{xx}^2 + \bar{w}_{yy}^2 + 2\nu\bar{w}_{xx}\bar{w}_{yy} + 2(1-\nu)\bar{w}_{xy}^2\right] dxdy \tag{4.45}$$

A practically important alternative form of Equation (4.42) is

$$\bar{\delta}^2 V = \bar{\delta}^2 U_{m_1} + \bar{\delta}^2 U_{m_2} + \bar{\delta}^2 U_{m_3} + \bar{\delta}^2 U_{m_4} + \bar{\delta}^2 U_b \tag{4.46}$$

in which

$$\bar{\delta}^2 U_{m_1} = A\iint\left[\bar{u}_x^2 + \bar{v}_y^2 + \bar{w}^2/r^2 + 2\bar{v}_y\bar{w}/r + 2\nu(\bar{u}_x\bar{v}_y + \bar{u}_x\bar{w}/r) + \frac{1-\nu}{2}(\bar{v}_x^2 + \bar{u}_y^2)\right] dxdy \tag{4.47}$$

$$\bar{\delta}^2 U_{m_2} = A\iint\left[\left[u_x + \nu\left(v_y + \frac{w}{r}\right)\right]\bar{w}_x^2 + \left[\left(v_y + \frac{w}{r}\right) + \nu u_x\right]\bar{w}_y^2 + (1-\nu)(v_x + u_y)\bar{w}_x\bar{w}_y\right] dxdy \tag{4.48}$$

$$\bar{\delta}^2 U_{m_3} = 2A\iint\left[\left[\bar{u}_x + \nu\left(\bar{v}_y + \frac{\bar{w}}{r}\right)\right]w_x\bar{w}_x + \left[\left(\bar{v}_y + \frac{\bar{w}}{r}\right) + \nu\bar{u}_x\right]w_y\bar{w}_y + \frac{1-\nu}{2}(\bar{v}_x + \bar{u}_y)(w_y\bar{w}_x + w_x\bar{w}_y)\right] dxdy \tag{4.49}$$

$$\bar{\delta}^2 U_{m_4} = \frac{A}{2}\iint(3w_x^2\bar{w}_x^2 + 3w_y^2\bar{w}_y^2 + w_x^2\bar{w}_y^2 + \bar{w}_x^2 w_y^2 + 4w_x w_y\bar{w}_x\bar{w}_y)\, dxdy \tag{4.50}$$

$$\bar{\delta}^2 U_b = D\iint\left[\bar{w}_{xx}^2 + \bar{w}_{yy}^2 + 2\nu\bar{w}_{xx}\bar{w}_{yy} + 2(1-\nu)\bar{w}_{xy}^2\right] dxdy \tag{4.51}$$

The motivation for the two alternative forms for $\delta^2 V$, Equations (4.42) and (4.46), is that Equation (4.42) is complete and apparently simple, yet Equation (4.46) is more obviously modified to account for a simple prebuckled shape. For classical shell buckling theory, a membrane prebuckled shape is the equilibrium state. That is, the shell simply contracts and/or expands in the axial and circumferential directions as a membrane under load prior to buckling, but never bends. Then, the prebuckling rotations, w_x and w_y, are zero, and Equations (4.49) and (4.50) vanish identically. However, more rigorous prebuckling shapes require consideration of Equations (4.49) and (4.50) as we will see in Section 4.5. For a classical bifurcation buckling problem, the prebuckled shape is axisymmetric if the loading is axisymmetric; thus, $w_y = 0$.

Upon substitution of the second partial derivatives of F in the general form of the Euler equations for buckling, Equations (3.111), (3.112), and (3.113) on page 254, we get

$$\frac{\partial}{\partial x}\left[\bar{u}_x + w_x\bar{w}_x + \nu\left(\bar{v}_y + \frac{\bar{w}}{r} + w_y\bar{w}_y\right)\right] + \frac{1-\nu}{2}\frac{\partial}{\partial y}(\bar{u}_y + \bar{v}_x + w_y\bar{w}_x + w_x\bar{w}_y) = 0 \tag{4.52}$$

$$\frac{1-\nu}{2}\frac{\partial}{\partial x}(\bar{u}_y + \bar{v}_x + w_y\bar{w}_x + w_x\bar{w}_y) + \frac{\partial}{\partial y}\left[\bar{v}_y + \frac{\bar{w}}{r} + w_y\bar{w}_y + \nu(\bar{u}_x + w_x\bar{w}_x)\right] = 0 \tag{4.53}$$

Éléments sous droits d'auteur

$$
\begin{aligned}
&A\left[\bar{v}_y + \frac{\bar{w}}{r} + w_y\bar{w}_y + \nu(\bar{u}_x + w_x\bar{w}_x)\right]/r \\
&- A\frac{\partial}{\partial x}\left[\left[\bar{u}_x + \nu(\bar{v}_y + \frac{\bar{w}}{r})\right]w_x + \frac{1-\nu}{2}(\bar{u}_y + \bar{v}_x)w_y\right. \\
&\qquad + \left[(u_x + \frac{1}{2}w_x^2) + \nu(v_y + \frac{w}{r} + \frac{1}{2}w_y^2) + w_x^2 + \frac{1-\nu}{2}w_y^2\right]\bar{w}_x \\
&\qquad \left. + \left[\frac{1-\nu}{2}(v_x + u_y + w_xw_y) + \frac{1+\nu}{2}w_xw_y\right]\bar{w}_y\right] \\
&- A\frac{\partial}{\partial y}\left[(\bar{v}_y + \frac{\bar{w}}{r} + \nu\bar{u}_x)w_y + \frac{1-\nu}{2}(\bar{u}_y + \bar{v}_x)w_x\right. \\
&\qquad + \left[\frac{1-\nu}{2}(v_x + u_y + w_xw_y) + \frac{1+\nu}{2}w_xw_y\right]\bar{w}_x \\
&\qquad \left. + \left[(v_y + \frac{w}{r} + \frac{1}{2}w_y^2) + \nu(u_x + \frac{1}{2}w_x^2) + w_y^2 + \frac{1-\nu}{2}w_x^2\right]\bar{w}_y\right] \\
&+ D\nabla^4\bar{w} = 0
\end{aligned}
\tag{4.54}
$$

The first two buckling differential equations, Equations (4.52) and (4.53), seem simple enough, but Equation (4.54) can be considerably simplified and put into a form that is more easily interpreted. First, rewrite Equation (4.54) in the form

$$
\begin{aligned}
&A\left[\bar{v}_y + \frac{\bar{w}}{r} + w_y\bar{w}_y + \nu(\bar{u}_x + w_x\bar{w}_x)\right]/r + D\nabla^4\bar{w} \\
&- A\frac{\partial}{\partial x}\left[\left[\bar{u}_x + w_x\bar{w}_x + \nu(\bar{v}_y + \frac{\bar{w}}{r} + w_y\bar{w}_y)\right]w_x\right. \\
&\qquad + \frac{1-\nu}{2}(\bar{u}_y + \bar{v}_x + w_x\bar{w}_y + w_y\bar{w}_x)w_y + \left[(u_x + \frac{1}{2}w_x^2)\right. \\
&\qquad \left.\left. + \nu(v_y + \frac{w}{r} + \frac{1}{2}w_y^2)\right]\bar{w}_x + \frac{1-\nu}{2}(v_x + u_y + w_xw_y)\bar{w}_y\right] \\
&- A\frac{\partial}{\partial y}\left[\left[\bar{v}_y + \frac{\bar{w}}{r} + w_y\bar{w}_y + \nu(\bar{u}_x + w_x\bar{w}_x)\right]w_y\right. \\
&\qquad + \frac{1-\nu}{2}(\bar{u}_y + \bar{v}_x + w_x\bar{w}_y + w_y\bar{w}_x)w_x + \frac{1-\nu}{2}(v_x + u_y + w_xw_y)\bar{w}_x \\
&\qquad \left. + \left[(v_y + \frac{w}{r} + \frac{1}{2}w_y^2) + \nu(u_x + \frac{1}{2}w_x^2)\right]\bar{w}_y\right] = 0
\end{aligned}
\tag{4.55}
$$

If the indicated differentiation is performed on the coefficients of w_x and w_y and the first two buckling differential equations, Equations (4.52) and (4.53), are utilized for simplification of the results, Equation (4.55) can be shown to be

Éléments sous droits d'auteur

$$
\begin{aligned}
&A\left[\bar{v}_y + \frac{\bar{w}}{r} + w_y\bar{w}_y + \nu(\bar{u}_x + w_x\bar{w}_x)\right]/r + D\nabla^4\bar{w} \\
&- A\left[(\bar{u}_x + w_x\bar{w}_x) + \nu(\bar{v}_y + \frac{\bar{w}}{r} + w_y\bar{w}_y)\right]w_{xx} \\
&- (1-\nu)A(\bar{u}_y + \bar{v}_x + w_x\bar{w}_y + w_y\bar{w}_x)w_{xy} \\
&- A\left[\bar{v}_y + \frac{\bar{w}}{r} + w_y\bar{w}_y + \nu(\bar{u}_x + w_x\bar{w}_x)\right]w_{yy} \\
&- A\frac{\partial}{\partial x}\left[\left[(u_x + \frac{1}{2}w_x^2) + \nu(v_y + \frac{w}{r} + \frac{1}{2}w_y^2)\right]\bar{w}_x + \frac{1-\nu}{2}(v_x + u_y + w_xw_y)\bar{w}_y\right] \\
&- A\frac{\partial}{\partial y}\left[\frac{1-\nu}{2}(v_x + u_y + w_xw_y)\bar{w}_x\right. \\
&\qquad \left. + \left[(v_y + \frac{w}{r} + \frac{1}{2}w_y^2) + \nu(u_x + \frac{1}{2}w_x^2)\right]\bar{w}_y\right] = 0
\end{aligned}
\tag{4.56}
$$

Next, perform the indicated differentiation on the coefficients of $\bar{w}_x$ and $\bar{w}_y$ and use the first two equilibrium differential equations, Equations (4.22) and (4.23), to obtain the simplified result

$$
\begin{aligned}
&A\left[\bar{v}_y + \frac{\bar{w}}{r} + w_y\bar{w}_y + \nu(\bar{u}_x + w_x\bar{w}_x)\right]\text{bigslashr} + D\nabla^4\bar{w} \\
&- A\left[\bar{u}_x + w_x\bar{w}_x + \nu(\bar{v}_y + \frac{\bar{w}}{r} + w_y\bar{w}_y)\right]w_{xx} \\
&- A(1-\nu)(\bar{u}_y + \bar{v}_x + w_x\bar{w}_y + w_y\bar{w}_x)w_{xy} \\
&- A\left[\bar{v}_y + \frac{\bar{w}}{r} + w_y\bar{w}_y + \nu(\bar{u}_x + w_x\bar{w}_x)\right]w_{yy} \\
&- A\left[(u_x + \frac{1}{2}w_x^2) + \nu(v_y + \frac{w}{r} + \frac{1}{2}w_y^2)\right]\bar{w}_{xx} \\
&- A(1-\nu)(v_x + u_y + w_xw_y)\bar{w}_{xy} \\
&- A\left[(v_y + \frac{w}{r} + \frac{1}{2}w_y^2) + \nu(u_x + \frac{1}{2}w_x^2)\right]\bar{w}_{yy} = 0
\end{aligned}
\tag{4.57}
$$

Equations (4.52), (4.53), and (4.57) are the three buckling differential equations in simplest general form for circular cylindrical shells. An alternative form can be obtained by substituting the force-displacement relations, Equation (4.32), and their variations

$$
\begin{aligned}
\delta N_x &= A\left[(\bar{u}_x + w_x\bar{w}_x) + \nu(\bar{v}_y + \frac{w}{r} + w_y\bar{w}_y)\right] \\
\delta N_y &= A\left[(\bar{v}_y + \frac{\bar{w}}{r} + w_y\bar{w}_y) + \nu(\bar{u}_x + w_x\bar{w}_x)\right] \\
\delta N_{xy} &= \frac{1-\nu}{2}A(\bar{v}_x + \bar{u}_y + w_x\bar{w}_y + w_y\bar{w}_x)
\end{aligned}
\tag{4.58}
$$

along with the moment-displacement relations, Equation (4.33), and their variations

Éléments sous droits d'auteur

$$\begin{aligned} \delta M_x &= -D(\overline{w}_{xx} + \nu \overline{w}_{yy}) \\ \delta M_y &= -D(\overline{w}_{yy} + \nu \overline{w}_{xx}) \\ \delta M_{xy} &= -(1-\nu) D \overline{w}_{xy} \end{aligned} \tag{4.59}$$

in Equations (4.52), (4.53), and (4.57) to obtain

$$\frac{\partial}{\partial x}(\delta N_x) + \frac{\partial}{\partial y}(\delta N_{xy}) = 0 \tag{4.60}$$

$$\frac{\partial}{\partial x}(\delta N_{xy}) + \frac{\partial}{\partial y}(\delta N_y) = 0 \tag{4.61}$$

$$\begin{aligned} \frac{\partial^2(\delta M_x)}{\partial x^2} + 2\frac{\partial^2(\delta M_{xy})}{\partial x \partial y} + \frac{\partial^2(\delta M_y)}{\partial y^2} + \delta N_x w_{xx} + 2\delta N_{xy} w_{xy} + \delta N_y w_{yy} \\ + N_x \overline{w}_{xx} + 2N_{xy}\overline{w}_{xy} + N_y \overline{w}_{yy} - \delta N_y / r = 0 \end{aligned} \tag{4.62}$$

The associated buckling boundary conditions are $\bar{u} = 0$ or $\delta N_x = 0$, etc. as in Chapter 3, Equations (3.158) and (3.159) on page 260. All the complexities of a rigorous prebuckling solution are present in Equations (4.60), (4.61), and (4.62), i.e., the terms w_{xx}, w_{xy}, w_{yy}, N_x, N_{xy}, and N_y must be determined from the prebuckling equilibrium state. Note especially that N_x and N_y are defined to be positive in tension. The boundary conditions during buckling can be written in Almroth's notation [4-10] as

Simply Supported Edges:

$$\begin{array}{llllll} \text{S1:} & \delta w = 0 & \delta M_x = 0 & \delta u = 0 & \delta v = 0 \\ \text{S2:} & \delta w = 0 & \delta M_x = 0 & \delta N_x = 0 & \delta v = 0 \\ \text{S3:} & \delta w = 0 & \delta M_x = 0 & \delta u = 0 & \delta N_{xy} = 0 \\ \text{S4:} & \delta w = 0 & \delta M_x = 0 & \delta N_x = 0 & \delta N_{xy} = 0 \end{array} \tag{4.63}$$

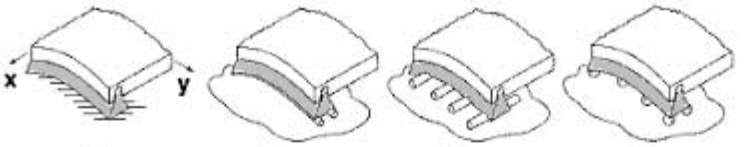
Clamped Edges:

$$\begin{array}{llllll} \text{C1:} & \delta w = 0 & \delta w_{,x} = 0 & \delta u = 0 & \delta v = 0 \\ \text{C2:} & \delta w = 0 & \delta w_{,x} = 0 & \delta N_x = 0 & \delta v = 0 \\ \text{C3:} & \delta w = 0 & \delta w_{,x} = 0 & \delta u = 0 & \delta N_{xy} = 0 \\ \text{C4:} & \delta w = 0 & \delta w_{,x} = 0 & \delta N_x = 0 & \delta N_{xy} = 0 \end{array} \tag{4.64}$$

with visual interpretations in Figures 4-14 and 4-15 with physical descriptions previously on pages 477 and 478.

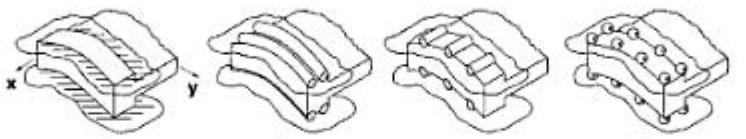
The buckling boundary conditions are somewhat similar to the equilibrium boundary conditions, but in a possibly deceptive manner. In both the buckling boundary conditions S2 and S4 for simply supported edges, the term $\delta N_x = 0$ appears. In the equilibrium boundary conditions, the seemingly analogous term $N_x = 0$ appears and signifies that no force exists in the x-direction at the edge. In contrast for buckling, $\delta N_x = 0$ signifies that a force N_x *can exist*, but that *it does not change (vary) at the buckling load!* Similar statements can be made about the other boundary condition differences between equilibrium and buckling.

Éléments sous droits d'auteur



S1	S2	S3	S4
$\delta w = 0$	$\delta w = 0$	$\delta w = 0$	$\delta w = 0$
$\delta M_x = 0$	$\delta M_x = 0$	$\delta M_x = 0$	$\delta M_x = 0$
$\delta u = 0$	$\delta N_x = 0$	$\delta u = 0$	$\delta N_x = 0$
$\delta v = 0$	$\delta v = 0$	$\delta N_{xy} = 0$	$\delta N_{xy} = 0$

Figure 4-14 Simply Supported Edge Buckling Boundary Conditions



C1	C2	C3	C4
$\delta w = 0$	$\delta w = 0$	$\delta w = 0$	$\delta w = 0$
$\delta w_{,x} = 0$	$\delta w_{,x} = 0$	$\delta w_{,x} = 0$	$\delta w_{,x} = 0$
$\delta u = 0$	$\delta N_x = 0$	$\delta u = 0$	$\delta N_x = 0$
$\delta v = 0$	$\delta v = 0$	$\delta N_{xy} = 0$	$\delta N_{xy} = 0$

Figure 4-15 Clamped-Edge Buckling Boundary Conditions

A significant simplification of the shell buckling equations occurs when the loading is axisymmetric and hence the prebuckling deformations are axisymmetric. Then, $w_y = w_{xy} = w_{yy} = 0$ and $v = 0$ as well as $\partial/\partial y = 0$ which reduces the number of terms in Equation (4.62) directly, but even more terms are eliminated from Equations (4.32), (4.33), and (4.58) which become

$$\begin{aligned} N_x &= A\left[(u_x + \frac{1}{2} w_x^2) + \nu(\frac{w}{r}) \right] \\ N_y &= A\left[\frac{w}{r} + \nu(u_x + \frac{1}{2} w_x^2) \right] \\ N_{xy} &= 0 \end{aligned} \tag{4.65}$$

$$\begin{aligned} M_x &= -Dw_{xx} \\ M_y &= -\nu Dw_{xx} \\ M_{xy} &= 0 \end{aligned} \tag{4.66}$$

Éléments sous droits d'auteur

$$\delta N_x = A\left[(\bar{u}_x + w_x\bar{w}_x) + \nu(\bar{v}_y + \frac{\bar{w}}{r})\right]$$
$$\delta N_y = A\left[(\bar{v}_y + \frac{\bar{w}}{r}) + (\bar{u}_x + w_x\bar{w}_x)\right] \qquad (4.67)$$
$$\delta N_{xy} = \frac{1-\nu}{2} A(\bar{v}_x + \bar{u}_y + w_x\bar{w}_y)$$

Equations (4.60), (4.61), and (4.62), supplemented by the definitions in Equations (4.65), (4.66), and (4.67) and the boundary conditions in Equations (4.63) and (4.64), constitute equations that govern the buckling of circular cylindrical shells under axisymmetric load with accurate prebuckling deformations. The nonlinear prebuckled equilibrium state is often linearized by elimination of w_x from Equations (4.65) and (4.67).

Another significant simplification results from the use of classical buckling theory, i.e., a membrane prebuckled shape. Prior to buckling, the shell is presumed to have *no* boundary conditions and is therefore free to contract or expand as a membrane, e.g., the axially compressed shell in Figure 4-16 shortens axially and expands radially in a uniform manner because of a Poisson effect. The prebuckling stress state involves, as you would expect from the name, only in-surface forces (often called membrane forces) and, of course, no bending moments. During buckling, the shell edges are restrained as a simply supported, clamped, or elastically restrained edge according to the specification of the problem. Thus, *the boundary conditions of the two parts of classical buckling theory are inconsistent.* The lack of a rigorous prebuckled shape in classical buckling theory leads to inaccuracies in calculated axial compression buckling loads as will be seen in subsequent sections.

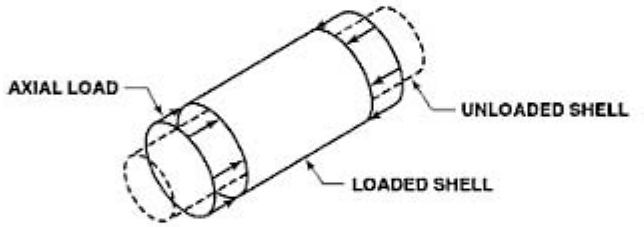


Figure 4-16 Exaggerated Membrane Deformation

A more rigorous approach than classical buckling theory involves the use of the same boundary conditions both prior to and during buckling. The inclusion of a rigorous and consistent prebuckling shape leads to deformations prior to buckling as shown in Figure 4-17 along with the membrane solution for comparison. Obviously, the rigorous prebuckling solution has an 'edge effect' similar to boundary-layer problems. That is, the primary deformation effects are seen in a small boundary layer near the ends of the shell with degeneration to the membrane solution away from the end. The importance of the rigorous prebuckling solution will be discussed later in Section 4.5. We will first examine classical buckling theory in detail along with many solutions in Section 4.3.

Éléments sous droits d'auteur

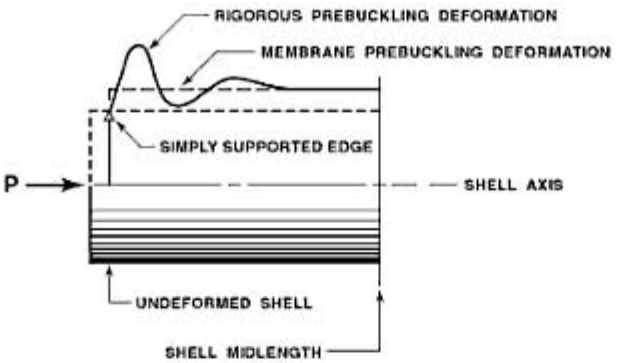


Figure 4-17 Membrane Versus Rigorous Prebuckling Shell Deformations

The simplifications caused by use of the membrane prebuckling shape in classical buckling theory come primarily from the fact that the transverse deflection, w, is constant over all the shell. As a consequence, all terms in w_x and w_y vanish from Equations (4.32) and (4.58). Also, the terms in w_{xx}, w_{xy}, and w_{yy} vanish from Equation (4.33) leaving

$$N_x = A\left[u_x + \nu\left(v_y + \frac{w}{r}\right)\right]$$

$$N_y = A\left(v_y + \frac{w}{r} + \nu u_x\right) \tag{4.68}$$

$$N_{xy} = \frac{1-\nu}{2} A(v_x + u_y)$$

$$M_x = M_y = M_{xy} = 0 \tag{4.69}$$

$$\delta N_x = A\left[\bar{u}_x + \nu\left(\bar{v}_y + \frac{\bar{w}}{r}\right)\right]$$

$$\delta N_y = A\left[\left(\bar{v}_y + \frac{\bar{w}}{r}\right) + \nu \bar{u}_x\right] \tag{4.70}$$

$$\delta N_{xy} = \frac{1-\nu}{2} A(\bar{v}_x + \bar{u}_y)$$

along with Equation (4.59) for δM_x, δM_y, and δM_{xy}. Then, the buckling differential equations in terms of prebuckling forces and variations in forces and moments during buckling can be written as

$$\frac{\partial}{\partial x}(\delta N_x) + \frac{\partial}{\partial y}(\delta N_{xy}) = 0 \tag{4.71}$$

$$\frac{\partial}{\partial x}(\delta N_{xy}) + \frac{\partial}{\partial y}(\delta N_y) = 0 \tag{4.72}$$

$$\frac{\partial^2(\delta M_x)}{\partial x^2} + 2\frac{\partial^2(\delta M_{xy})}{\partial x \partial y} + \frac{\partial^2(\delta M_y)}{\partial y^2} - \bar{N}_x \bar{w}_{xx} - 2\bar{N}_{xy}\bar{w}_{xy} - \bar{N}_y \bar{w}_{yy} - \delta N_y / r = 0 \tag{4.73}$$

Éléments sous droits d'auteur

in which the compressive buckling loads, $\bar{N}_x$, $\bar{N}_{xy}$, and $\bar{N}_y$, are defined as $\bar{N}_x = -N_x$ and $\bar{N}_y = -N_y = -pr$ to get positive values for the buckling loads throughout the rest of the book. That is, the buckling loads are defined as positive in compression for convenience. Alternatively, the three differential equations governing buckling from a membrane prebuckled state (defined in terms of the prebuckling deformations u, v, and w) can be written in terms of the displacements, u, v, w, their variations during buckling, $\bar{u}$, $\bar{v}$, $\bar{w}$, and their derivatives as:

$$\frac{\partial}{\partial x}\left[\bar{u}_x + + \nu\left(\bar{v}_y + \frac{\bar{w}}{r}\right)\right] + \frac{1-\nu}{2}\frac{\partial}{\partial y}(\bar{u}_y + \bar{v}_x) = 0 \tag{4.74}$$

$$\frac{1-\nu}{2}\frac{\partial}{\partial x}(\bar{u}_y + \bar{v}_x) + \frac{\partial}{\partial y}\left[\bar{v}_y + \frac{\bar{w}}{r} + + \nu\bar{u}_x\right] = 0 \tag{4.75}$$

$$D\nabla^4\bar{w} - A\left[u_x + \nu\left(v_y + \frac{w}{r}\right)\right]\bar{w}_{xx} - A(1-\nu)(v_x + u_y)\bar{w}_{xy} - A\left[\left(v_y + \frac{w}{r}\right) + \nu u_x\right]w_{yy} + A\left[\bar{v}_y + \frac{\bar{w}}{r} + \nu\bar{u}_x\right]/r = 0 \tag{4.76}$$

Note that Equation (4.76) reduces to the single plate buckling differential equation, Equation (3.162) when the shell radius, r, goes to infinity (because a plate has zero curvature) eliminating the w/r terms and the entire last term. Also, the first two equations, Equations (4.74) and (4.75) are then decoupled from Equation (4.76). Often, we will write these equations with δu, δv, and δw instead of $\bar{u}$, $\bar{v}$, and $\bar{w}$. Other forms of the preceding equations and their solutions are treated in the following sections.

The variations in displacements $\bar{u}$, $\bar{v}$, and $\bar{w}$ or their derivatives appear implicitly in all three buckling differential equations, Equations (4.71), (4.72), and (4.73) and explicitly in the alternative set of buckling differential equations, Equations (4.74), (4.75), and (4.76). Thus, bending-extension coupling inherently exists during shell buckling, so one of the two sets of three buckling differential equations must be solved simultaneously. This coupling between the equations should be contrasted with the situation for plates wherein the third buckling differential equation in $\bar{w}$ was uncoupled from the first two in $\bar{u}$ and $\bar{v}$. One of the first attempts to solve the coupled equations was made by Donnell [4-1] who noted that the terms involving $\bar{u}$ and $\bar{v}$ could be eliminated from the third buckling differential equation by an involved process of differentiation resulting in

$$r\nabla^4\bar{u} = -\nu\frac{\partial^3\bar{w}}{\partial x^3} + \frac{\partial^3\bar{w}}{\partial x\partial y^2} \tag{4.77}$$

$$r\nabla^4\bar{v} = -(2+\nu)\frac{\partial^3\bar{w}}{\partial x^2\partial y} - \frac{\partial^3\bar{w}}{\partial y^3} \tag{4.78}$$

$$D\nabla^8\bar{w} + \frac{Et}{r^2}\frac{\partial^4\bar{w}}{\partial x^4} - \nabla^4(N_x\bar{w}_{xx} + 2N_{xy}\bar{w}_{xy} + N_y\bar{w}_{yy}) = 0 \tag{4.79}$$

Accordingly, $\bar{w}$ (or δw) is found from Equation (4.79), and the implied $\bar{u}$ (or δu) and $\bar{v}$ (or δv) are found from Equations (4.77) and (4.78). This

Éléments sous droits d'auteur

approach has the disadvantage of our not being able to specify the boundary conditions on $\bar{u}$ and $\bar{v}$ independently of those on $\bar{w}$.

Later, Batdorf [4-2] observed that the eighth-order derivatives in Donnell's approach lead to difficulties such as divergent trigonometric series when shells with clamped edges are treated. He suggested the following version of the third buckling differential equation that is known as Batdorf's Modified Donnell Equation:

$$D\nabla^4\bar{w} + \frac{Et}{r^2}\nabla^{-4}\frac{\partial^4\bar{w}}{\partial x^4} - N_x\bar{w}_{xx} - 2N_{xy}\bar{w}_{xy} - N_y\bar{w}_{yy} = 0 \qquad (4.80)$$

with $\bar{u}$ and $\bar{v}$ being obtained from Equations (4.77) and (4.78). More physical significance can be attached to Batdorf's equation than to Donnell's: the first term in Batdorf's equation is the bending and twisting resistance, the second term is the extensional resistance, and the last terms are the loading. The functions to which the operator ∇^{-4} is applied are the buckling deflections of a shell with obvious boundary conditions. Thus, the operator ∇^{-4} might not be definable in general terms.

Solutions for $\bar{w}$ or δw in Batdorf's formulation, as in Donnell's formulation, imply certain boundary conditions on δu and δv, and on the variations in forces and moments. For many years, those implied boundary conditions were ignored because suitable computational techniques were not available to deal with the necessarily numerical solution of the equations other than Donnell's or Batdorf's. Shell edges were treated as simply supported or clamped, just as in classical bar and plate buckling theory. However, Stein [4-11] and Almroth [4-10] focused attention on *all* the applicable shell boundary conditions, in and out of plane, in order to distinguish between the different buckling loads obtained for seemingly identical boundary conditions.

We now turn to a variety of solutions to the buckling differential equations in Section 4.3. Those solutions are focused on the classical shell buckling theory, namely with a membrane prebuckled state.

Problem Set 4.2

4.2.1 Derive the moderately large-deflection equilibrium equations in terms of displacements, Equations (4.22)–(4.24), according to the hints given in the text. Obtain the equivalent equations in terms of forces and moments, Equations (4.34)–(4.36).

4.2.2 Derive the special second variation of the total potential energy, Equation (4.41).

4.2.3 Derive the buckling differential equations, Equations (4.52)–(4.54). Then, simplify Equation (4.54) according to the hints in the text to obtain Equation (4.57).

4.2.4 Reexpress the buckling differential equations, Equations (4.52), (4.53), and (4.57) in terms of variations in forces and moments, i.e., obtain Equations (4.60)–(4.62).

4.2.5 Specialize the buckling differential equations, Equations (4.60)–(4.62), for axisymmetric loading according to the hints in the text. Express the results both in terms of variations in displacements and in terms of variations in forces and moments.

4.2.6 Specialize the buckling differential equations, Equations (4.60)–(4.62), for a membrane prebuckling state, i.e., derive Equations (4.71)–(4.73) and the equivalent form in terms of variations in displacements.

4.2.7 Derive Donnell's Equation in δw, Equation (4.79), and what it implies for δu and δv, Equations (4.77) and (4.78), respectively.

4.2.8 Derive Batdorf's Modified Donnell Equation, Equation (4.80). What conditions are associated with δu and δv?

Éléments sous droits d'auteur

4.3 CLASSICAL BUCKLING THEORY SOLUTIONS

4.3.1 Introduction

Classical buckling theory solutions are applicable for shells that deform essentially as a membrane (i.e., without bending—only in-surface contraction and/or stretching in the axial and circumferential directions exists) prior to buckling, are subjected to various loads, and have various boundary conditions. That is, we ignore all boundary conditions in the equilibrium state prior to buckling. Eight possible simply supported edge and clamped-edge boundary conditions exist during buckling along each edge at each end of a circular cylindrical shell as described in Section 4.2.2. For a single buckling equation such as Equation (4.76) or (4.77), the inherent bending-extension coupling during buckling is masked because the in-surface displacements, δu and δv, are implied, not explicit.

For shells with simply supported edges, i.e., the class in which $\delta w = \delta M_x = 0$, either Donnell's equation, Equation (4.79), or Batdorf's equation, Equation (4.80), can be used to verify that the buckle deflection

$$\delta w = \bar{w} = \tilde{w} \sin \frac{m\pi x}{L} \sin \frac{ny}{r} \tag{4.81}$$

(or $\cos ny/r$) is an exact solution to the governing differential equation. By use of Equations (4.77) and (4.78), we can show that Equation (4.81) leads to $\delta N_x = \delta v = 0$ and therefore corresponds to buckling boundary condition S2. However, as with bars and plates, the shell buckle deflection amplitude, $\tilde{w}$, is indeterminate in all eigenvalue problems. Solutions for the other boundary conditions are obtained for Batdorf's equation or the three coupled buckling differential equations by use of various approximate techniques such as Galerkin's Method or finite differences. Approaches such as the Rayleigh-Ritz Method or finite elements are based directly on the energy expressions in Equation (4.46).

The term $\sin(m\pi x/L)$ in Equation (4.81) is quite similar to, and fully analogous to, the term $\sin(m\pi x/a)$ in plate buckling solutions; m is the number of buckle half waves in the x-direction over length L for a shell and over side length a for a plate. However, the term $\sin(n/r)$ in Equation (4.81) has a significent difference from the term $\sin(n\pi y/b)$ in plate buckling solutions. First, we can recast the argument of the sin term to be expressed in terms of some quantity over the length of the object, in this case the circumference, $2\pi r$, of the shell, namely,

$$\sin \frac{ny}{r} = \sin \frac{2\pi ny}{2\pi r} = \sin \frac{2n\pi y}{2\pi r} = \sin \frac{n'\pi y}{2\pi r}$$

from which form we conclude that n' is the number of buckle half waves in the y-direction, so n is the number of buckle *full* waves in the y-direction, quite unlike n in plate buckling solutions. Often, n is referred to as the number of buckle waves in the circumferential direction without specification that a wave is two half waves. There must be an integer number of buckle waves, and hence an even integer number of buckle half waves, in the circumferential direction in order to maintain continuity of the buckling displacement, w, and its derivatives at $y = 0$ and $y = 2\pi r$. In

Éléments sous droits d'auteur

contrast, a plate can have an odd integer number of buckle half waves (e.g., n = 3 for some plates corresponding to n = 3/2 for a shell) because there is no periodicity requirement for plates (as there is none for shells in the x-direction). The circumferential periodicity requirement also applies to the in-surface buckling displacements, $\bar{u}$ and $\bar{v}$. Note that n = 1 for a shell could correspond to a lateral translation of the entire cross section such as would occur if the shell buckled as a bar-like object between its ends. Plot the function $\bar{w} = \tilde{w}\sin(y/r)$ to convince yourself of that possibility (although the full description of the buckle requires $\bar{u}$, $\bar{v}$, and $\bar{w}$). Thus, we restrict our attention to $n \geq 2$.

Not all shells buckle with the mode shapes in Equation (4.81). Many have far more complicated geometries, and some are not amenable to any convenient geometric description. We will first concentrate on those shells for which Equation (4.81) and similar forms are applicable.

The solution for the S2 buckling boundary condition on both edges is obtained for axial compression, lateral pressure, and hydrostatic pressure in Section 4.3.2. The solution for the C3 and C1 buckling boundary conditions are obtained by Galerkin's method for axial compression in Sections 4.3.3 and 4.3.4, respectively. Note that the S2 boundary condition provides the least resistance to buckling of the eight boundary conditions whereas the C1 boundary condition provides the most resistance to buckling. In design, the S2 boundary condition is commonly used as a lower bound to all edge condition results. Thus, the S2 buckling boundary condition is emphasized in subsequent sections.

4.3.2 Batdorf's Classical Results

In the 1940s, Samuel B. Batdorf and his associates, Manuel Stein and Murry Schildcrout, at NACA Langley Aeronautical Laboratory in Hampton, Virginia (now NASA Langley Research Center) solved shell buckling problems for many loading and boundary conditions within the restrictions of classical buckling theory. For shells with simply supported edge buckling boundary condition S2, Batdorf published buckling results for axial compression, lateral pressure, and hydrostatic pressure in a now classical report [4-2]. In that report, he presented his modification of Donnell's equation and some solutions to Donnell's equation (recall that the two equations are equivalent for simply supported edges). The solutions will be rederived in the following.

4.3.2.1 Axial Compression

For axial compression loading, $N_x = -\bar{N}_x$, Equation (4.79) reduces to

$$D\nabla^8\bar{w} + \frac{Et}{r^2}\frac{\partial^4\bar{w}}{\partial x^4} + \bar{N}_x\nabla^4\frac{\partial^2\bar{w}}{\partial x^2} = 0 \tag{4.82}$$

If Equation (4.82) is divided by D, we get

$$\nabla^8\bar{w} + \frac{12Z^2}{L^4}\frac{\partial^4\bar{w}}{\partial x^4} + k_x\frac{\pi^2}{L^2}\nabla^4\frac{\partial^2\bar{w}}{\partial x^2} = 0 \tag{4.83}$$

Éléments sous droits d'auteur

in which $\bar{w}$ is the buckling displacement δw,

$$k_x = \frac{\bar{N}_x L^2}{\pi^2 D} \tag{4.84}$$

and

$$Z = \frac{L^2}{rt}\sqrt{1-\nu^2} \tag{4.85}$$

The quantity k_x is an axial loading parameter with both geometric and material properties, and Z is now known as the Batdorf curvature parameter. Note that Z is primarily a geometrical factor but has a mild effect of a material property, namely Poisson's ratio. Because the governing buckling differential equation has k_x and Z as characteristic parameters, so will the solution. Consequently, we are very interested in the physical significance of Z. The infinitely varied types of shells that can be represented with a single fixed value of Z are depicted in Figure 4-18. There, if L is constant, the shell varies from thick with a small radius to thin with a large radius. Or, if r is constant, the shell varies from thick and long to thin and short. Finally, for constant t, the shell varies from large L and r to small L and r.

The buckling displacement (with indeterminate amplitude, $\tilde{w}$),

$$\delta w = \bar{w} = \tilde{w} \sin \frac{m\pi x}{L} \sin \frac{ny}{r} \tag{4.86}$$

satisfies the S2 buckling boundary conditions and also satisfies the differential equation governing buckling, Equation (4.83), if

$$k_x = \frac{(m^2+\beta^2)^2}{m^2} + \frac{12Z^2m^2}{\pi^4(m^2+\beta^2)^2} \tag{4.87}$$

in which

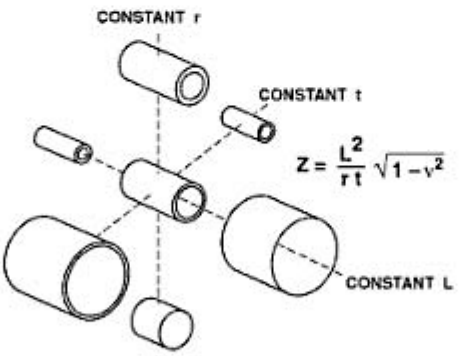


Figure 4-18 Representative Circular Cylindrical Shells Corresponding to the Same Value of Z (Z about 155) *(After Batdorf [4-2])*

Éléments sous droits d'auteur

$$\beta = \frac{nL}{\pi r} \tag{4.88}$$

The lowest buckling load or lowest value of k_x from Equation (4.87) is sought. First, we find a stationary value of Equation (4.87) by noting that it can be differentiated with respect to $(m^2+\beta^2)^2/m^2$ *(assuming this factor can take on continuous values which, in fact, it cannot)* to obtain

$$\frac{\partial k_x}{\partial\left[\dfrac{(m^2+\beta^2)^2}{m^2}\right]} = 1 - \frac{12Z^2}{\pi^4}\left[\frac{(m^2+\beta^2)^2}{m^2}\right]^{-2} = 0 \tag{4.89}$$

whereupon

$$\frac{(m^2+\beta^2)^2}{m^2} = \left[\frac{12Z^2}{\pi^4}\right]^{1/2} \tag{4.90}$$

at which value the second derivative of k_x with respect to $(m^2+\beta^2)^2/m^2$ is positive, so Equation (4.90) provides a minimum to Equation (4.87) of

$$k_x = \frac{4\sqrt{3}}{\pi^2} Z = .702\, Z \tag{4.91}$$

which, if $\nu = .27$, is the familiar, and widely used, axial buckling stress

$$\sigma_x = .6Et/r \tag{4.92}$$

However, we must investigate the range of validity of the foregoing result. Solve Equation (4.90) for β:

$$\beta = \left[\left[\frac{12Z^2}{\pi^4}\right]^{1/4} m - m^2\right]^{1/2} \tag{4.93}$$

The minimum value of the number of axial buckle half-waves, m, is one, so to get real values of β and hence real values of n,

$$Z \geq \frac{\pi^2}{12^{1/2}} \geq 2.85 \tag{4.94}$$

Thus, Equation (4.91) applies for $Z > 2.85$, a moderately long shell.

For values of $Z < 2.85$, the only possible buckled shape is integer buckle wave numbers, $m = 1$ and $\beta = 0$ $(n = 0)$, so from Equation (4.87),

$$k_x = 1 + \frac{12Z^2}{\pi^4} \tag{4.95}$$

which result can be interpreted as representing a short circular cylindrical shell (low Z). As Z goes to zero, k_x in Equation (4.95) goes to one. One interpretation of $Z = 0$ is a very short axially compressed shell that can be 'unrolled' to be viewed as a long flat plate in transverse compression with the long edges simply supported as in Figure 4-19 (the boundary conditions on the two short edges have essentially no effect on the buckling load).

Éléments sous droits d'auteur

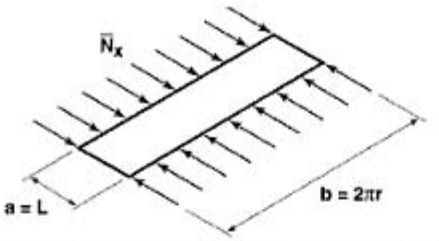


Figure 4-19 'Unrolled' Short Shell under Axial Compression

For the axially compressed simply supported edge plate solution in Equation (3.183) on page 267, divide both sides by $\pi^2 D/a^2$ to get

$$\frac{\bar{N}_x a^2}{\pi^2 D} = \frac{a^4}{m^2}\left[\left[\frac{m}{a}\right]^2 + \left[\frac{n}{b}\right]^2\right]^2 = \frac{1}{m^2}\left[m^2 + \left[\frac{a}{b}\right]^2 n^2\right]^2 \qquad (4.96)$$

For a long flat plate in the y-direction, $a/b \to 0$ and $m \to 1$, so Equation (4.96) becomes $k_x = \bar{N}_x a^2/\pi^2 D = 1$. If we interpret plate length, a, as shell length, L, then $k_x = \bar{N}_x L^2/\pi^2 D = 1$. Thus, an axially compressed circular cylindrical shell with $Z = 0$ can be interpreted as a long flat plate that has been unrolled from the shell or a wide column with simply supported ends, both with axial load.

The k-Z buckling results for all values of Z up to 10^4 are shown in Figure 4-20. Note that very long circular cylindrical shells buckle as Euler bars or columns if r/t is small enough (the horizontal lines labeled 10 and 20). In contrast, if $Z = 0$, the shell buckles as a wide plate with $k_x = 1$.

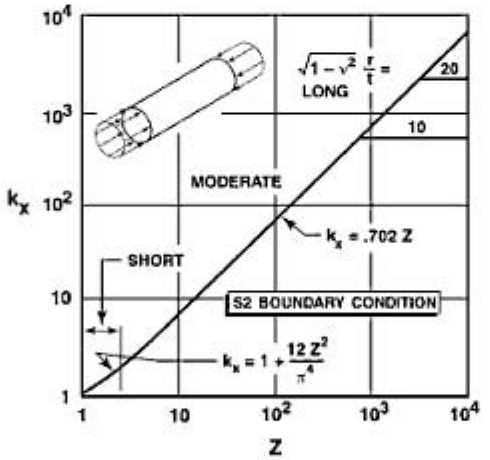


Figure 4-20 Axial Compression Buckling Coefficient k_x for Simply Supported Circular Cylindrical Shells *(After Batdorf [4-2])*

Éléments sous droits d'auteur

The representation of the buckling results as a single k_x-Z curve is a simplification of the actual situation. We assumed k_x to be a continuous function of $(m^2+\beta^2)/m^2$ when we found a stationary value of Equation (4.87). However, m and n (n is contained in β, Equation (4.88)) can take on only integer values because only an integer number of buckle half waves can occur along the length or around the circumference. Otherwise, the axial boundary conditions could not be satisfied nor could circumferential displacement continuity (periodicity). Thus, for a particular shell, i.e., particular values of L, r, and t, the k_x-Z results are scalloped curves *above* the result $k_x = .702Z$ given in Equation (4.89) as in the exaggerated sketch of Figure 4-21. The cusps are caused by a (discrete) change in the buckle mode shape as Z varies just as in plate results as a function of plate aspect ratio. The peaks of the scallops do not differ substantially from the line $k_x = .702Z$. For other values of L, r, and t, the scallops shift along the line $k_x = .702Z$, and their points of tangency are different from those shown in Figure 4-21. Thus, *the line* $k_x = .702Z$ is the locus of the tangent points of all scallops and therefore *represents all shells to the degree just discussed.* In fact, the k-Z curve is a lower bound on the actual buckling results as is easily seen in Figure 4-21.

The k-Z representation of buckling results enables the presentation of theories and experimental data for wide ranges of geometric parameters. For example, Z varies over four orders of magnitude in Figure 4-20. This advantage comes at the expense of distortions associated with the log-log scales used. That is, curves or data that appear close on a log-log plot might actually differ by amounts of substantial engineering concern. This disadvantage might or might not be important in some engineering applications. The same k-Z results can, of course, be plotted on linear scales over much smaller ranges of the geometric parameters. These observations on the nature of log-log k-Z plots are especially important when we examine experimental data for shell buckling.

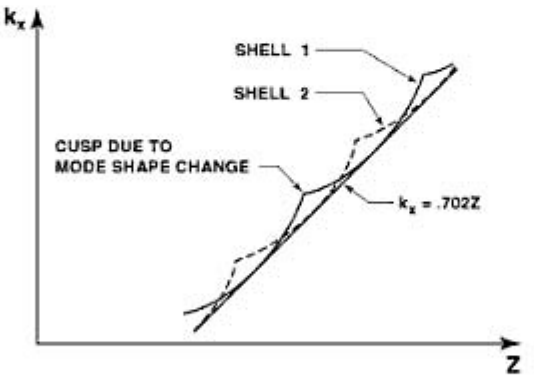


Figure 4-21 Exaggerated Schematic Representation of Actual k_x-Z Results for Two Shells

Éléments sous droits d'auteur

Experimental buckling data for simply supported shells under axial compression from a variety of sources are plotted in the form of buckling stress as a fraction of the Euler buckling stress versus the radius-to-thickness ratio in Figure 4-22. These data were gathered and first presented in this form by Donnell and Wan who cite each specific data source [4-12]. See also Figure 4-119 on page 658 for further experimental results and Singer, Arbocz, and Weller [4-13]. The data for a variety of materials, configurations, and shell support conditions occupy sometimes overlapping regions of the plot. Although most of the data are for shells with supposedly simply supported edges, some shells have somewhat more support tending toward edge fixity. Note that Batdorf's theoretical result is consistently well above the measured buckling loads. This discrepancy cannot be simply data scatter because if it were, then some results would be above the theory and some below. This discrepancy is an indication that the theory lacks at least one, if not more, essential feature to describe the actual physical behavior. Obvious conclusions from Figure 4-22 are (1) the data are always significantly lower than the Euler load, ranging from 40% to 90% lower and (2) the discrepancy is consistently higher for thin shells (high r/t values) than for thick shells (low r/t values). Thus, we cannot claim that the Batdorf result is a reasonable predictive tool for design of isotropic circular cylindrical shells subjected to axial compression.

These experimental data provide us with the essential mystery of shells buckling under axial compression, namely, why is there so much discrepancy between the data and the Euler buckling load? The reason for the discrepancy is not as simple as was the case for bars or columns. Recall from Section 2.9 that early bar buckling experiments were performed on relatively short, thick columns typical of pre-steel construction

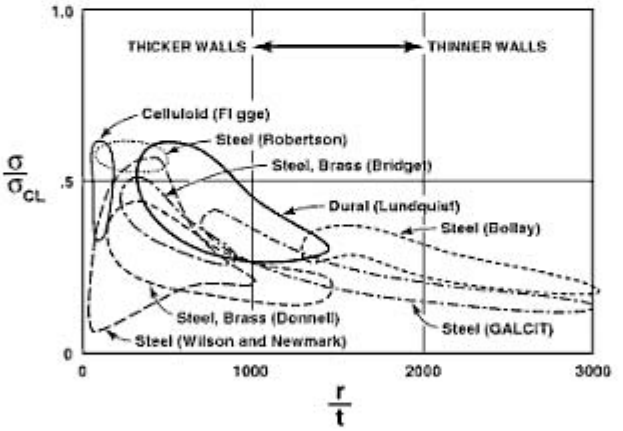


Figure 4-22 Axial Compression Buckling Data for Simply Supported Circular Cylindrical Shells *(After Donnell and Wan [4-12])*

Éléments sous droits d'auteur

which actually buckled, if at all, plastically, a material behavior not accounted for in Euler's bar buckling theory or perhaps recognized in those days (the 1700s). As noted in Section 2.9 on plastic buckling of bars, once plastic buckling was addressed, the agreement with experiments became quite good. And, when longer, thinner bars began to be used in practice (typically made of steel), prediction of their buckling load with (elastic and plastic) Euler theory was quite good. However, shell buckling data present a very different characteristic. The buckling loads for very thin shells for which plastic buckling would *not* occur are far less well predicted than are thicker shells for which plastic buckling *could* influence (and decrease from the elastic Euler buckling load)! Thus, the fundamental nature of the results for the shell buckling problem is quite different from those for the bar or column buckling problem.

The typical diamond-shaped buckles for an axially compressed circular cylindrical shell are shown in Figure 4-23. Such buckles are *not* described with the sine-sine deformation formulation of Equation (4.81). Moreover, the shell edges are not simply supported, but are encapsulated or 'potted' in a soft metal compound to enable good contact with the load-frame platens (the edges must be flat, parallel to each other, and perpendicular to the shell axis). The potted edge provides some moment restraint, i.e., resistance to edge rotation, as well as translational restraint in the plane of the platen because of friction.

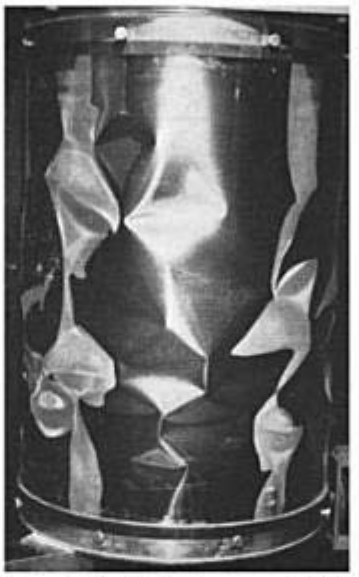


Figure 4-23 Axially Compressed Shell *(After Harris, Suer, and Skene [4-14])*

Many reasons for the discrepancy between theory and experiment for axially loaded shells have been proposed. First, because the discrepancy in Figure 4-22 is noticeably greater for thin shells than for thick shells, the presence of initial geometric imperfections in the shell because of unavoidable defects in the manufacturing process seems a likely reason for the discrepancy. That is, a thin shell is much harder to make "perfectly" than a thick shell. Any manufacturing defect would be a higher percentage of the shell thickness for a thin shell than for a thick shell. Other reasons have been suggested and investigated, among them the effect of boundary conditions at the ends of the shell, a different mechanism for shell buckling than for bar or plate buckling, etc. These potential reasons for, or causes of, the discrepancy between theory and experiment will be discussed in subsequent sections.

Éléments sous droits d'auteur

4.3.2.2 Lateral Pressure

Lateral pressure loading results in circumferential force, $N_y = -\bar{N}_y$, on the shell, and Equation (4.79) reduces to

$$D\nabla^8\bar{w} + \frac{Et}{r^2}\frac{\partial^4\bar{w}}{\partial x^4} + \bar{N}_y\nabla^4\frac{\partial^2\bar{w}}{\partial y^2} = 0 \tag{4.97}$$

wherein by statics $\bar{N}_y = \sigma_y t = pr$. Divide Equation (4.97) by D to get

$$\nabla^8\bar{w} + \frac{12Z^2}{L^4}\frac{\partial^4\bar{w}}{\partial x^4} + k_y\frac{\pi^2}{L^2}\nabla^4\frac{\partial^2\bar{w}}{\partial y^2} = 0 \tag{4.98}$$

in which

$$k_y = \frac{\bar{N}_y L^2}{\pi^2 D} = \frac{pr L^2}{\pi^2 D} \tag{4.99}$$

and

$$Z = \frac{L^2}{rt}\sqrt{1-\nu^2} \tag{4.100}$$

in which k_y is a lateral pressure loading parameter (with both geometric and material properties as does k_x) and Z is the Batdorf curvature parameter as discussed in Section 4.3.2.1.

The buckling displacement (with indeterminate amplitude, $\tilde{w}$),

$$\delta w = \bar{w} = \tilde{w}\sin\frac{m\pi x}{L}\sin\frac{ny}{r} \tag{4.101}$$

satisfies the S2 buckling boundary conditions and also satisfies the differential equation governing buckling, Equation (4.98), if

$$k_y = \frac{(m^2+\beta^2)^2}{\beta^2} + \frac{12Z^2}{\pi^4}\frac{m^4}{\beta^2(m^2+\beta^2)^2} \tag{4.102}$$

in which

$$\beta = \frac{nL}{\pi r} \tag{4.103}$$

Divide the numerator and denominator of the second term in Equation (4.102) by m^4 to obtain

$$k_y = \frac{(m^2+\beta^2)^2}{\beta^2} + \frac{12Z^2}{\pi^4}\frac{1}{\beta^2(1+\beta^2/m^2)^2} \tag{4.104}$$

which takes on a minimum value only for m = 1, i.e., shells under external pressure buckle with one axial half-wave because any higher value of m would cause a greater k_y. Thus, Equation (4.104) becomes

$$k_y = \frac{(1+\beta^2)^2}{\beta^2} + \frac{12Z^2}{\pi^4}\frac{1}{\beta^2(1+\beta^2)^2} \tag{4.105}$$

Éléments sous droits d'auteur

For *short circular cylindrical shells*, Z approaches zero, so that, in the limit of Z = 0, Equation (4.105) becomes

$$k_y = \left[\frac{1}{\beta} + \beta\right]^2 \tag{4.106}$$

which is the the same as the solution for a long rectangular plate in axial compression in Section 3.3.2. Note that the circumferential direction of this short circular cylindrical shell corresponds to the long dimension of the axially loaded flat rectangular plate as for the transversely loaded long plate in Figure 4-19 on page *32. For continuous β, the minimum k_y in Equation (4.106) is $\bar{N}_y L^2/\pi^2 D = 4$ as in Section 3.3.2 with the x- and y-directions interchanged and L replacing b.

For *moderate-length circular cylindrical shells*, $\beta^2 >> 1$, so Equation (4.105) becomes

$$k_y = \beta^2 + \frac{12Z^2}{\pi^4}\frac{1}{\beta^6} \tag{4.107}$$

which is easily minimized to obtain

$$k_y = 1.0396Z^{1/2} \tag{4.108}$$

For *long circular cylindrical shells*, the number of circumferential half-waves decreases to 2 as Z increases. The n = 2 or elliptical shape shown in Figure 4-24 occurs for long circular cylindrical shells whereupon Equation (4.107) becomes $k_y = \beta^2$ (because $1/\beta^6 \rightarrow 0$) which upon substitution of $\beta = 2L/\pi r$ becomes

$$k_y = \frac{4}{\pi^2\sqrt{1-\nu^2}} Z\frac{t}{r} \tag{4.109}$$

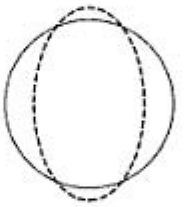


Figure 4-24 Cross-Sectional View of n = 2 Buckling Mode

However, the Donnell shell theory used is not accurate for n = 2 or even somewhat higher. Because a long circular cylindrical shell buckles like a ring, we can show that

$$k_y = \frac{3}{\pi^2\sqrt{1-\nu^2}} Z\frac{t}{r} \tag{4.110}$$

Thus, the result in Equation (4.109) is too high by more than 30%.

The k_y-Z results for short, moderate-length, and long circular cylindrical shells are plotted in Figure 4-25. There, shells exhibit distinctly different regions of buckling behavior as Z increases, ranging from plate-like behavior to ring-like behavior.

Experimental buckling data for simply supported aluminum shells under lateral pressure from Sturm [4-15] are plotted as normalized buck-

Éléments sous droits d'auteur

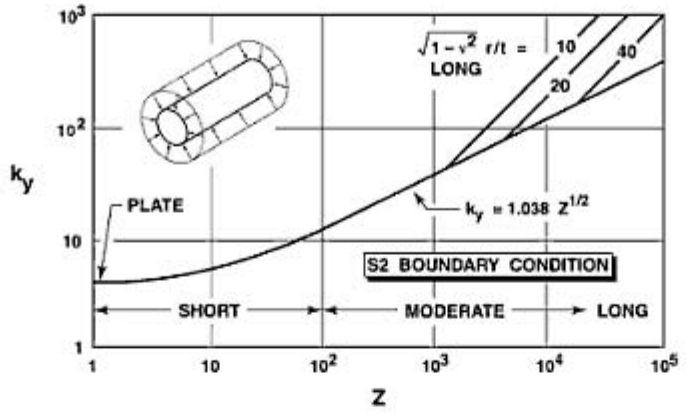


Figure 4-25 Lateral Pressure Buckling Coefficient k_y for Simply Supported Circular Cylindrical Shells *(After Batdorf [4-2])*

ling stress parameter, k_y versus the Batdorf shell parameter, Z, in Figure 4-26. Also shown is the Batdorf theoretical result studied in this subsection for the S2 buckling boundary condition. Some of the shells have a somewhat higher fixity edge condition than simple support because of experimental difficulties in achieving an actual simple support. Some of the data fall above the theoretical result and some below lending confidence to the theory as a practical predictive tool for design of isotropic circular cylindrical shells subjected to lateral pressure.

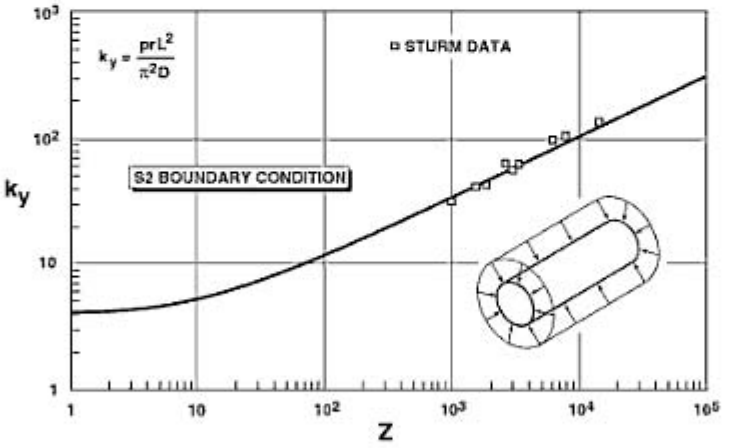


Figure 4-26 Lateral Pressure Buckling Data for Circular Cylindrical Shells

Éléments sous droits d'auteur

The typical buckling deformation for a circular cylindrical shell subject to lateral pressure is shown in Figure 2-27. The buckling mode is $m = 1$ with about ten buckles in the circumferential direction, i.e., $n \cong 10$. Thus, the theoretical buckling deformation of sine-sine form in Equation (4.100) is quite reasonable. However, the clamping bands visible at the top and bottom of the shell impose more like a clamped edge than a simply supported edge. Actually, the shell in Figure 4-27 is subjected to hydrostatic pressure, but the buckling deformations are essentially the same for both lateral and hydrostatic pressure if the shell is long enough (short shells under hydrostatic pressure are dominated by axial compression).



Figure 4-27 Lateral Pressure Buckling of Circular Cylindrical Shells
(After Harris, Suer, and Skene [4-14])

4.3.2.3 Hydrostatic Pressure

For hydrostatic pressure loading, Equation (4.79) reduces to

$$D\nabla^8 \bar{w} + \frac{Et}{r^2}\frac{\partial^4 \bar{w}}{\partial x^4} + \bar{N}_y \nabla^4 \left[\frac{1}{2}\frac{\partial^2 \bar{w}}{\partial x^2} + \frac{\partial^2 \bar{w}}{\partial y^2} \right] = 0 \qquad (4.111)$$

because $\bar{N}_y = pr$ and $\bar{N}_x = pr/2$. Divide Equation (4.111) by D to get

$$\nabla^8 \bar{w} + \frac{12Z^2}{L^4}\frac{\partial^4 \bar{w}}{\partial x^4} + c_p \frac{\pi^2}{L^2}\nabla^4 \left[\frac{1}{2}\frac{\partial^2 \bar{w}}{\partial x^2} + \frac{\partial^2 \bar{w}}{\partial y^2} \right] = 0 \qquad (4.112)$$

in which c_p is a hydrostatic pressure loading parameter

$$c_p = \frac{pr L^2}{\pi^2 D} \qquad (4.113)$$

and

$$Z = \frac{L^2}{rt}\sqrt{1 - \nu^2} \qquad (4.114)$$

Éléments sous droits d'auteur

The buckling displacement (with indeterminate amplitude, $\tilde{w}$),

$$\delta w = \bar{w} = \tilde{w} \sin \frac{m\pi x}{L} \sin \frac{ny}{r} \tag{4.115}$$

satisfies the S2 buckling boundary conditions and also satisfies the differential equation governing buckling, Equation (4.112), if

$$c_p = \frac{(m^2+\beta^2)^2}{\frac{m^2}{2}+\beta^2} + \frac{12Z^2}{\pi^4} \frac{m^4}{(m^2+\beta^2)^2\left[\frac{m^2}{2}+\beta^2\right]} \tag{4.116}$$

The minimum value of c_p can be shown to occur for $m = 1$ in Equation (4.116). The c_p-Z results are similar to those for lateral pressure and are shown in Figure 4-28. Again, short, moderate, and long regions of behavior are evident, ranging from plate-like behavior to ring-like behavior. The typical buckling deformation for a circular cylindrical shell under hydrostatic pressure is shown in Figure 4-27, although the figure is labeled lateral pressure. Discussion of experimental results is postponed until the next subsection.

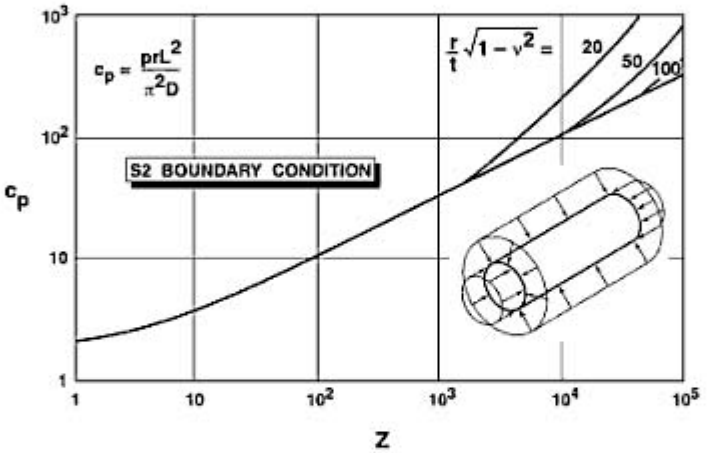


Figure 4-28 Hydrostatic Pressure Buckling Coefficient c_p for Simply Supported Circular Cylindrical Shells *(After Batdorf [4-2])*

4.3.2.4 Comparison of Results for Axial Compression, Lateral Pressure, and Hydrostatic Pressure

The results for axial compression, lateral pressure, and hydrostatic pressure for the S2 boundary condition can all be plotted in Figure 4-29 if we realize that by statics $c_p = 2k_x$. Note that, for increasing Z (above 100), the axial pressure component of hydrostatic pressure has no effect. On the other hand, for low Z, the axial pressure component dominates. This behavior is explained by observing that at large values of Z, the axial

Éléments sous droits d'auteur

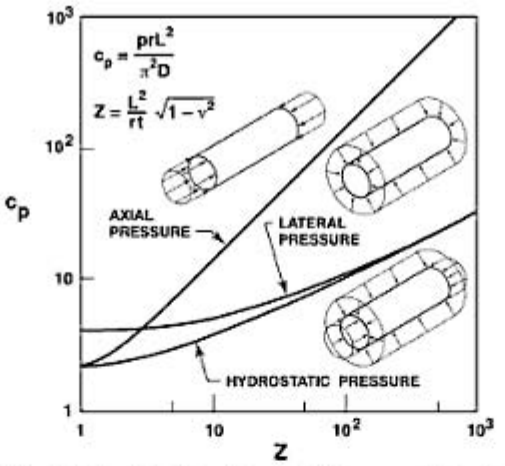


Figure 4-29 Buckling Coefficients for Axial Pressure, Lateral Pressure, and Hydrostatic Pressure on Simply Supported Circular Cylindrical Shells *(After Batdorf [4-2])*

stress to cause buckling is many times the required circumferential stress so the circumferential stress governs buckling because, moreover, the circumferential stress is twice as large as the axial stress. At low Z, the axial stress coefficient required for buckling is much less than k_y.

Note that the so-called Batdorf curvature parameter is common to the differential equations for all three loading conditions. That is, Z is a combined geometric and material parameter that is characteristic to the buckling differential equation, i.e., a so-called characteristic parameter.

Experimental buckling data for simply supported steel and aluminum shells under hydrostatic pressure are plotted as normalized buckling stress parameter, c_p versus the Batdorf shell parameter, Z, in Figure 4-30. There, the aluminum shell data are from Sturm [4-15], whereas the steel shell data are from Windenburg and Trilling [4-16]. Also shown is the Batdorf theoretical result studied in this subsection for the S2 buckling boundary condition. Some of the shells have a somewhat higher fixity edge condition than simple support because of experimental difficulties in achieving an actual simple support along the edge of a shell. The data fall both below and above the theoretical result in most cases for shells with $Z > 100$ lending confidence to the theory as a practical predictive tool. However, for shells with low Z, i.e., $Z < 100$, the data seem to be well below the theoretical result. That this situation would occur (i.e., of varied accuracy over the range of shells studied with the largest difference being for low Z shells) is perfectly logical when we realize that axial compression begins to dominate the hydrostatic pressure loading as Z decreases below 100 in Figure 4-29. Thus, for design of isotropic circular cylindrical shells under hydrostatic pressure, we have a realistic predictive tool in the form of the Batdorf result only for $Z > 100$.

Éléments sous droits d'auteur

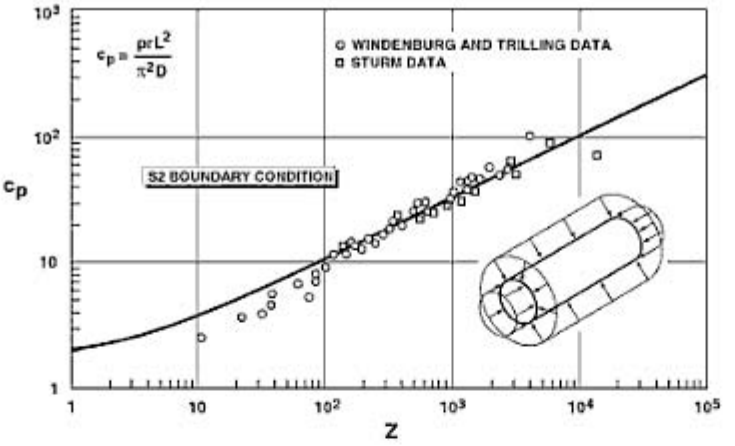


Figure 4-30 Hydrostatic Pressure Buckling Data for Circular Cylindrical Shells

The k-Z plot format in Figure 4-30 masks the actual difference between an experimental data point and the theoretical curve. The log-log plot format shrinks the actual difference to a shadow of its former self. Thus, although we might think the data appear close to the curve, the actual percentage difference might be quite large, and in fact, beyond what we would be willing to accept in design.

4.3.2.5 Torsion

For torsional loading on the shell ends, Equation (4.79) reduces to

$$D\nabla^8(\delta w) + \frac{Et}{r^2}\frac{\partial^4(\delta w)}{\partial x^4} + 2\bar{N}_{xy}\nabla^4\frac{\partial^2(\delta w)}{\partial x \partial y} = 0 \qquad (4.117)$$

Alternatively, Batdorf, Stein, and Schildcrout [4-17] start from the Batdorf equation, Equation (4.80):

$$D\nabla^4(\delta w) + \frac{Et}{r^2}\nabla^{-4}\frac{\partial^4(\delta w)}{\partial x^4} + 2\bar{N}_{xy}\delta w_{xy} = 0 \qquad (4.118)$$

If Equation (4.118) is divided by D, we get

$$\nabla^4\delta w + \frac{12Z^2}{L^4}\nabla^{-4}\frac{\partial^4\delta w}{\partial x^4} + 2k_s\frac{\pi^2}{L^2}\frac{\partial^2\delta w}{\partial x \partial y} = 0 \qquad (4.119)$$

in which

$$k_s = \frac{\bar{N}_{xy}L^2}{\pi^2 D} = \frac{\tau_{cr}tL^2}{\pi^2 D} \qquad (4.120)$$

and

Éléments sous droits d'auteur

$$Z = \frac{L^2}{rt}\sqrt{1-\nu^2} \tag{4.121}$$

As before, the quantity k_s is a torsional loading parameter with both geometric and material properties, and Z is the Batdorf curvature parameter depicted in various manners in Figure 4-18 on page 492. Then, the buckling equation, Equation (4.119), can be expressed as

$$Q(\delta w) = 0 \tag{4.122}$$

in which Q is the operator defined as

$$Q = \nabla^4 + \frac{12Z^2}{L^4}\nabla^{-4}\frac{\partial^4}{\partial x^4} + 2k_s\frac{\pi^2}{L^2}\frac{\partial^2}{\partial x \partial y} \tag{4.123}$$

The solution of Equation (4.122) proceeds by the Galerkin method[1] [4-18] as follows. The approximate buckling displacement δw is:

$$\delta w = \sum_{m=0}^{j} \tilde{v}_m V_m + \sum_{m=0}^{j} \tilde{w}_m W_m \tag{4.124}$$

in which the deflection functions, V_m and W_m, need not satisfy the differential equation governing buckling, but must satisfy the boundary conditions on δw. The approximate buckling displacement, e.g., Equation (4.124), is substituted in the buckling equation, Equation (4.122). Because the approximate δw does not satisfy the buckling equation (unless we 'chose' the exact solution), we 'weight' the buckling equation by multiplying by the functions involved in the displacement approximation. Thus, we substitute δw from Equation (4.124) in the buckling differential equation, Equation (4.122), multiply by V_m once and then separately by W_m, and integrate over the region of the shell to obtain

$$\begin{aligned} &\int_0^{2\pi r}\int_0^{L} V_n Q(\delta w)\, dx dy = 0 \\ &\qquad\qquad n = 0, 1, 2, \ldots, j \\ &\int_0^{2\pi r}\int_0^{L} W_n Q(\delta w)\, dx dy = 0 \end{aligned} \tag{4.125}$$

Equation (4.125) is a set of homogeneous, linear, algebraic equations in which the number of unknowns and equations equals the number of terms taken in Equation (4.124). With those equations, we 'minimize' the residual that occurs when we substitute an approximate displacement solution in the differential equation governing buckling (twice).

The Batdorf, Stein, and Schildcrout solution for shells of short and medium length with simply supported edges with the S2 buckling boundary condition is based on the buckling deflection:

$$\delta w = \sin\frac{ny}{r}\sum_{m=1}^{\infty}\tilde{v}_m \sin\frac{m\pi x}{L} + \cos\frac{ny}{r}\sum_{m=1}^{\infty}\tilde{w}_m \sin\frac{m\pi x}{L} \tag{4.126}$$

in which we identify [in comparison to Equation (4.125)]

[1] The Galerkin method is perhaps more accurately referred to as the Bubnov-Galerkin method. A. S. Volmir [4-19] states that the method was developed by Bubnov [4-20, 4-21] and applied by Galerkin [4-22]. Some Russian authors refer to it as the Bubnov method.

Éléments sous droits d'auteur

$$V_n = \sin\frac{ny}{r}\sin\frac{n\pi x}{L}$$
$$W_n = \cos\frac{ny}{r}\sin\frac{n\pi x}{L} \tag{4.127}$$

If Equations (4.126) and (4.127) are substituted in Equation (4.125) and the indicated integration is performed, then

$$\tilde{v}_n\left[(n^2+\beta^2)^2 + \frac{12Z^2n^4}{\pi^4(n^2+\beta^2)^2}\right] - \frac{8k_s\beta}{\pi}\sum_{m=1}^{\infty}\tilde{w}_m\frac{mn}{n^2-m^2} = 0$$
$$\tilde{w}_n\left[(n^2+\beta^2)^2 + \frac{12Z^2n^4}{\pi^4(n^2+\beta^2)^2}\right] - \frac{8k_s\beta}{\pi}\sum_{m=1}^{\infty}\tilde{v}_m\frac{mn}{n^2-m^2} = 0 \tag{4.128}$$

in which

$$\beta = \frac{nL}{\pi r} \qquad n = 1,2,3,\ldots \tag{4.129}$$

and $m \pm n$ is odd.

Equations (4.128) have a nontrivial solution if the infinite determinant in Equation (4.130) on the facing page vanishes. That determinant was obtained from an intermediate determinant by rearranging rows and columns and factoring into two equivalent subdeterminants, one of which is Equation (4.130). Also,

$$M_n = \frac{\pi}{8\beta}\left[\left(n^2+\beta^2\right)^2 + \frac{12Z^2n^4}{\pi^4(n^2+\beta^2)^2}\right] \tag{4.131}$$

The first approximation to the solution of Equation (4.130) is obtained by taking terms up through $n = 2$, i.e., the second-order determinant in Equation (4.130):

$$k_s^2 = \left[\frac{3}{2}\right]^2 M_1 M_2 \tag{4.132}$$

The second approximation (from the third-order determinant) is

$$k_s^2 = \frac{M_1 M_2 M_3}{\left[\frac{6}{5}\right]^2 M_1 + \left[\frac{2}{3}\right]^2 M_3} \tag{4.133}$$

For a specific value of the curvature parameter, Z, the buckling load depends on the buckle wavelength, 2λ. We are, of course, interested in the lowest buckling load, so k_s is minimized with respect to wavelength by substituting values of β in each of the various approximation equations until we find the minimum k_s on a plot of k_s versus β. Such a procedure is valid only when $\beta > 2L/\pi L$, i.e., $n > 2$. Batdorf, Stein, and Schildcrout show that the solution for the second approximation is barely distinguishable from that of the third approximation on the usual k_s versus Z plot. Thus, we consider the third approximation as sufficiently valid for this approach. Note that the buckle wave amplitudes, $\tilde{v}$ and $\tilde{w}$, are, as usual, indeterminate.

Éléments sous droits d'auteur

$$
\begin{array}{c|cccccc|c|cccccc|c}
 & \tilde{v}_1 & \tilde{w}_2 & \tilde{v}_3 & \tilde{w}_4 & \tilde{v}_5 & \tilde{w}_6 & \cdots & \tilde{w}_1 & \tilde{v}_2 & \tilde{w}_3 & \tilde{v}_4 & \tilde{w}_5 & \tilde{v}_6 & \cdots \\
\hline
n=1 & \frac{M_1}{k_s} & \frac{2}{3} & 0 & \frac{4}{15} & 0 & \frac{6}{35} & \cdots & 0 & 0 & 0 & 0 & 0 & 0 & \cdots \\
n=2 & \frac{2}{3} & \frac{M_2}{k_s} & \frac{-6}{5} & 0 & \frac{-10}{21} & 0 & \cdots & 0 & 0 & 0 & 0 & 0 & 0 & \cdots \\
n=3 & 0 & -\frac{6}{5} & \frac{M_3}{k_s} & \frac{12}{7} & 0 & \frac{2}{3} & \cdots & 0 & 0 & 0 & 0 & 0 & 0 & \cdots \\
n=4 & \frac{4}{15} & 0 & \frac{12}{7} & \frac{M_4}{k_s} & \frac{-20}{9} & 0 & \cdots & 0 & 0 & 0 & 0 & 0 & 0 & \cdots \\
n=5 & 0 & \frac{-10}{21} & 0 & \frac{-20}{9} & \frac{M_5}{k_s} & \frac{30}{11} & \cdots & 0 & 0 & 0 & 0 & 0 & 0 & \cdots \\
n=6 & \frac{6}{35} & 0 & \frac{2}{3} & 0 & \frac{30}{11} & \frac{M_6}{k_s} & \cdots & 0 & 0 & 0 & 0 & 0 & 0 & \cdots \\
\vdots & \vdots & \vdots & \vdots & \vdots & \vdots & \vdots & & \vdots & \vdots & \vdots & \vdots & \vdots & \vdots & \vdots \\
\hline
n=1 & 0 & 0 & 0 & 0 & 0 & 0 & \cdots & \frac{M_1}{k_s} & \frac{-2}{3} & 0 & \frac{-4}{15} & 0 & \frac{-6}{35} & \cdots \\
n=2 & 0 & 0 & 0 & 0 & 0 & 0 & \cdots & \frac{-2}{3} & \frac{M_2}{k_s} & \frac{6}{5} & 0 & \frac{10}{21} & 0 & \cdots \\
n=3 & 0 & 0 & 0 & 0 & 0 & 0 & \cdots & 0 & \frac{6}{5} & \frac{M_3}{k_s} & \frac{-12}{7} & 0 & \frac{-2}{3} & \cdots \\
n=4 & 0 & 0 & 0 & 0 & 0 & 0 & \cdots & \frac{-4}{15} & 0 & \frac{-12}{7} & \frac{M_4}{k_s} & \frac{20}{9} & 0 & \cdots \\
n=5 & 0 & 0 & 0 & 0 & 0 & 0 & \cdots & 0 & \frac{10}{21} & 0 & \frac{20}{9} & \frac{M_5}{k_s} & \frac{-30}{11} & \cdots \\
n=6 & 0 & 0 & 0 & 0 & 0 & 0 & \cdots & \frac{-6}{35} & 0 & \frac{-2}{3} & 0 & \frac{-30}{11} & \frac{M_6}{k_s} & \cdots \\
\vdots & \vdots & \vdots & \vdots & \vdots & \vdots & \vdots & \vdots & \vdots & \vdots & \vdots & \vdots & \vdots & \vdots & \vdots
\end{array}
= 0
$$

(4.130)

The final k_s versus Z results are shown along with experimental results in Figure 4-31 for shells of various materials (aluminum, steel, and brass). There, the present theoretical results are lower than Donnell's solution [4-1] (not shown) and therefore closer to the experimental results. Batdorf, Stein, and Schildcrout found "More than 80 percent of the test points are within 20 percent of the values corresponding to [the Batdorf, Stein, and Schildcrout solution], and all points are within 35 percent of the values corresponding to the [theoretical] curve" [4-17]. A typical torsional buckling deformation is shown in Figure 1-19b on page 16.

Éléments sous droits d'auteur

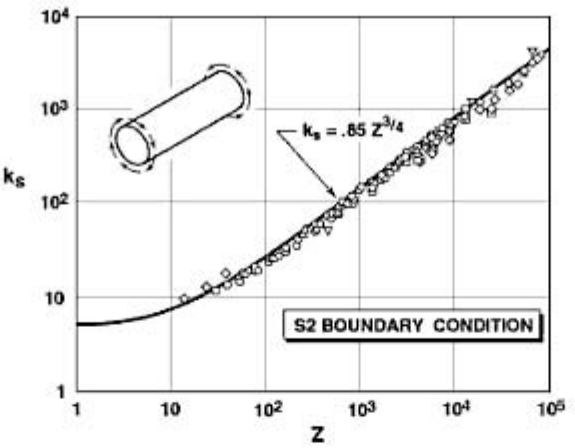


Figure 4-31 Torsional Buckling Coefficient k_s for Simply Supported Circular Cylindrical Shells *(After Batdorf, Stein, and Schildcrout [4-17])*

Batdorf, Stein, and Schildcrout also obtain results for long shells for which the only boundary condition is $\delta w = 0$ and for short and medium-length shells with clamped-edge buckling boundary condition C3. Yamaki [4-23] obtained results for simply supported shells with the S1 buckling boundary condition and for clamped shells with the C1 buckling boundary condition.

4.3.3 Use of Batdorf's Modified Donnell Equation for Axially Compressed Circular Cylindrical Shells with Clamped-Edge Buckling Boundary Condition C3

Batdorf, Schildcrout, and Stein [4-24] considered the buckling displacement (with indeterminate amplitudes $\tilde{w}_m$)

$$\delta w = \sin\frac{ny}{r}\sum_{m=1}^{\infty}\tilde{w}_m\left[\cos\frac{(m-1)\pi x}{L} - \cos\frac{(m+1)\pi x}{L}\right] \tag{4.134}$$

which satisfies the geometric boundary conditions

$$\delta w = 0 \tag{4.135}$$

$$\delta w_x = 0 \tag{4.136}$$

at $x = 0$ and $x = L$. Through the use of Equations (4.77) and (4.78), we can show that the foregoing displacement approximation leads to

$$\delta u = 0 \tag{4.137}$$

$$\delta N_{xy} = 0 \tag{4.138}$$

Éléments sous droits d'auteur

at $x = 0$ and $x = L$. Thus, we are dealing with clamped-edge buckling boundary condition C3.

For this loading condition, Batdorf's Modified Donnell Equation, Equation (4.80), becomes

$$D\nabla^4(\delta w) + \frac{Et}{r^2}\nabla^{-4}\frac{\partial^4(\delta w)}{\partial x^4} + \bar{N}_x\frac{\partial^2(\delta w)}{\partial x^2} = 0 \tag{4.139}$$

which upon division by D is

$$\nabla^4(\delta w) + \frac{12Z^2}{L^4}\nabla^{-4}\frac{\partial^4(\delta w)}{\partial x^4} + k_x\frac{\pi^2}{L^2}\frac{\partial^2(\delta w)}{\partial x^2} = 0 \tag{4.140}$$

in which, as usual,

$$Z = \frac{L^2}{rt}\sqrt{1-\nu^2} \tag{4.141}$$

and

$$k_x = \frac{\bar{N}_x L^2}{\pi^2 D} \tag{4.142}$$

Thus, the buckling equation, Equation (4.140), can be expressed as

$$Q(\delta w) = 0 \tag{4.143}$$

in which Q is the operator defined as

$$Q = \nabla^4 + \frac{12Z^2}{L^4}\nabla^{-4}\frac{\partial^4}{\partial x^4} + k_x\frac{\pi^2}{L^2}\frac{\partial^4}{\partial x^2} \tag{4.144}$$

The solution of Equation (4.143) proceeds via the Galerkin (or Bubnov-Galerkin) method [4-18] as follows. The approximate buckling displacement, e.g., Equation (4.134), is substituted in the buckling equation, Equation (4.143). Because the approximate δw does not satisfy the buckling equation (unless we 'chose' the exact solution), we 'weight' the buckling equation by multiplying by the functions involved in the displacement approximation, i.e., if

$$\delta w = \sum_{m=1}^{\infty}\tilde{w}_m W_m \tag{4.145}$$

in which the W_m need not satisfy the differential equation governing buckling but must satisfy the boundary conditions on δw (and the $\tilde{w}_m$ are the indeterminate amplitudes). Then, we substitute δw from Equation (4.145) in the buckling differential equation, Equation (4.143), multiply by W_m, and integrate over the region of the shell:

$$\int_0^{2\pi r}\int_0^L W_m Q(\delta w)\,dx\,dy = 0 \tag{4.146}$$

Equation (4.146) is a set of homogeneous, linear, algebraic equations in which the number of unknowns and equations equals the number of

Éléments sous droits d'auteur

terms taken in Equation (4.145). With those equations, we 'minimize' the residual (i.e., the non-zero remainder) that occurs when we substitute an approximate displacement solution in the buckling differential equation.

If the indicated operations are performed, we find that

$$\begin{aligned}
&\text{for } m = 1: && \tilde{w}_1(2M_1 + M_3) - \tilde{w}_3 M_3 = 0 \\
&\text{for } m = 2: && \tilde{w}_2(M_2 + M_4) - \tilde{w}_4 M_4 = 0 \\
&\text{for } m = 3,4,5,\ldots: && \tilde{w}_m(M_m + M_{m+2}) - \tilde{w}_{m-2} M_m - \tilde{w}_{m+2} M_{m+2} = 0
\end{aligned} \tag{4.147}$$

in which

$$M_m = \left[(m-1)^2 + \beta^2\right]^2 + \frac{12Z^2}{\pi^4} \frac{(m-1)^4}{\left[(m-1)^2 + \beta^2\right]^2} - (m-1)^2 k_x \tag{4.148}$$

A nontrivial solution exists for the $\tilde{w}_i$ if the determinant of the coefficients of the a_i is zero, i.e.,

$$\begin{vmatrix}
2M_1 + M_3 & 0 & -M_3 & 0 & 0 & 0 & \cdots \\
0 & M_2 + M_4 & 0 & -M_4 & 0 & 0 & \cdots \\
-M_3 & 0 & M_3 + M_5 & 0 & -M_5 & 0 & \cdots \\
0 & -M_4 & 0 & M_4 + M_6 & 0 & -M_6 & \cdots \\
0 & 0 & -M_5 & 0 & M_5 + M_7 & 0 & \cdots \\
0 & 0 & 0 & -M_6 & 0 & M_6 + M_8 & \cdots \\
0 & 0 & 0 & 0 & -M_7 & 0 & \cdots \\
\vdots & \vdots & \vdots & \vdots & \vdots & \vdots & \vdots
\end{vmatrix} = 0 \tag{4.149}$$

Note in the determinant of Equation (4.149) that the odd-subscripted terms do not appear in the same equations as the even-subscripted terms. Thus, Equation (4.149) can be rewritten as in Equation (4.150).

Éléments sous droits d'auteur

$$
\begin{array}{l|cccccccc|l}
m=1: & 2M_1+M_3 & -M_3 & 0 & \cdots & 0 & 0 & 0 & \cdots & \\
m=3: & -M_3 & M_3+M_5 & -M_5 & \cdots & 0 & 0 & 0 & \cdots & \\
m=5: & 0 & -M_5 & M_5+M_7 & \cdots & 0 & 0 & 0 & \cdots & \\
m=7: & 0 & 0 & -M_7 & \cdots & 0 & 0 & 0 & \cdots & \\
\vdots & \vdots & \vdots & \vdots & \cdots & \vdots & \vdots & \vdots & \vdots & = 0 \\
m=2: & 0 & 0 & 0 & \cdots & M_2+M_4 & -M_4 & 0 & \cdots & \\
m=4: & 0 & 0 & 0 & \cdots & -M_4 & M_4+M_6 & -M_6 & \cdots & \\
m=6: & 0 & 0 & 0 & \cdots & 0 & -M_6 & M_6+M_8 & \cdots & \\
m=8: & 0 & 0 & 0 & \cdots & 0 & 0 & -M_8 & \cdots & \\
\vdots & \vdots & \vdots & \vdots & \vdots & \vdots & \vdots & \vdots & \vdots &
\end{array}
\tag{4.150}
$$

The infinite subdeterminant that involves terms with odd subscripts corresponds to a buckling configuration that is symmetrical about the middle (mid-length) of the shell. Similarly, the other subdeterminant corresponds to buckling deformations that are antisymmetric about the middle. By theorems in matrix algebra, we can show that *one or the other subdeterminant must vanish.* The buckling load (and mode shape) corresponds to whichever subdeterminant vanishes at the lowest load. However, the buckle wave amplitude components, $\bar{w}_i$, are indeterminate.

Equation (4.150) represents an infinite number of equations, so we are naturally interested in taking a finite number of the equations to obtain a practical solution. Thus, various numbers of terms are taken to obtain various approximations. The first approximation is one term:

(odd determinant): $2M_1 + M_3 = 0$ (4.151)

(even determinant): $M_2 + M_4 = 0$ (4.152)

and the second approximation consists of a 2 x 2 determinant:

(odd determinant): $2M_1(M_3 + M_5) + M_3M_5 = 0$ (4.153)

(even determinant): $M_2(M_4 + M_6) + M_4M_6 = 0$ (4.154)

Éléments sous droits d'auteur

and so on. For a given Z, the lower of the two values of k_x obtained from Equations (4.151) and (4.152) is the first approximation to the buckling load. Similarly, the lower of the two values of k_x from Equations (4.153) and (4.154) is the second approximation. Higher order approximations are obtained by taking more terms. The second approximation is shown in Figure 4-32 along with the solution for simply supported edge buckling boundary condition S2. There, the actual boundary conditions appear not to be important for moderately long shells, i.e., Z > 10, but are crucial for short shells.

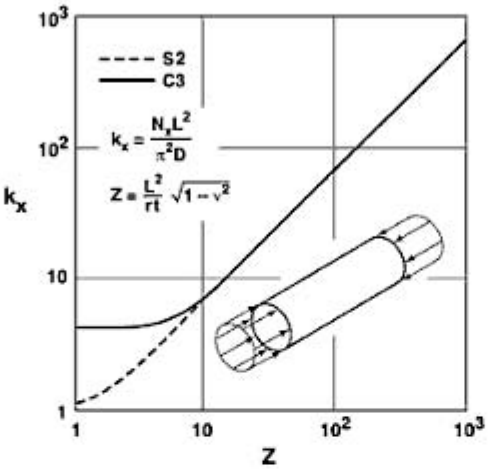


Figure 4-32 Buckling of Axially Compressed Circular Cylindrical Shells with Various Edge Conditions *(After Batdorf [4-2])*

4.3.4 Use of All Three Buckling Differential Equations for Axially Compressed Circular Cylindrical Shells with Clamped-Edge Buckling Boundary Condition C1

Card and Jones [4-25] consider the buckling displacements with indeterminate amplitudes $\tilde{u}_i$, $\tilde{v}_i$, $\tilde{w}_i$:

$$\delta u = \sum_i \tilde{u}_i U_i = \cos\frac{ny}{r}\sum_{i=1}^{\infty}\tilde{u}_i \sin\frac{i\pi x}{L}$$

$$\delta v = \sum_i \tilde{v}_i V_i = \sin\frac{ny}{r}\sum_{i=1}^{\infty}\tilde{v}_i \sin\frac{i\pi x}{L} \qquad (4.155)$$

$$\delta w = \sum_i \tilde{w}_i W_i = \cos\frac{ny}{r}\sum_{i=1}^{\infty}\tilde{w}_i\left[\cos(i-1)\frac{\pi x}{L} - \cos(i+1)\frac{\pi x}{L}\right]$$

that satisfy the geometric boundary conditions

Éléments sous droits d'auteur

$$\delta w = 0 \qquad \delta w_x = 0 \qquad \delta u = 0 \qquad \delta v = 0 \tag{4.156}$$

at x = 0 and x = L which constitute the C1 buckling boundary condition.

The buckling differential equations, Equations (4.74), (4.75), and (4.76), can be written in displacement form and specialized for axial compression as:

$$\delta u_{xx} + \nu(\delta v_{xy} + \delta w_x/r) + \frac{1-\nu}{2}(\delta v_{xy} + \delta u_{yy}) = 0 \tag{4.157}$$

$$\frac{1-\nu}{2}(\delta v_{xx} + \delta u_{xy}) + \delta v_{yy} + \delta w_y/r + \nu \delta u_{xy} = 0 \tag{4.158}$$

$$D\nabla^4(\delta w) + A(\delta v_y + \delta w/r + \nu \delta u_x)/r + \bar{N}_x \delta w_{xx} = 0 \tag{4.159}$$

In the generalized Bubnov-Galerkin procedure [4-18], the following equations must be satisfied:

$$\int_0^{2\pi r}\int_0^L U_i Q_x(\delta u, \delta v, \delta w)\, dxdy = 0 \tag{4.160}$$

$$\int_0^{2\pi r}\int_0^L V_i Q_y(\delta u, \delta v, \delta w)\, dxdy = 0 \tag{4.161}$$

$$\int_0^{2\pi r}\int_0^L W_i Q_z(\delta u, \delta v, \delta w)\, dxdy = 0 \tag{4.162}$$

in which Q_x, Q_y, and Q_z are the left-hand sides of Equations (4.157), (4.158), and (4.159), respectively, with the series expressions, Equations (4.155), substituted for δu, δv, and δw. If k terms are taken in each of the series in Equations (4.155), then Equations (4.160)–(4.162) are a set of 3k symmetric, linear, homogeneous, algebraic equations in 3k unknowns. With those equations, we 'minimize' the residual that occurs when an approximate displacement solution is substituted in the differential equations governing buckling. The residual is the actual value of each of the integrals in Equations (4.160)–(4.162) when the approximate solution is substituted.

Examination of the algebraic equations reveals that those equations with $\bar{u}_i$(i odd), $\bar{v}_i$(i even), and $\bar{w}_i$(i even) are not coupled with those that involve $\bar{u}_i$(i even), $\bar{v}_i$(i odd), and $\bar{w}_i$(i odd). Thus, just as in the last section, two independent sets of simultaneous equations exist, one of which (i odd in $\bar{w}_i$) corresponds to a symmetric δw deformation about the middle of the shell and the other (i even in $\bar{w}_i$) an antisymmetric δw deformation also about the middle of the shell. Both sets can be written as

$$\bar{A}\,X = \bar{B}\,X \tag{4.163}$$

in which

Éléments sous droits d'auteur

$$\bar{A} = \begin{bmatrix} A_{11} & & B_{11} & B_{12} & \cdots & C_{11} & C_{12} & \cdots \\ & A_{22} & B_{21} & B_{22} & \cdots & C_{21} & C_{22} & \cdots \\ & & & & \vdots & \vdots & \vdots & \vdots \\ & & D_{11} & & & E_{11} & E_{12} & \cdots \\ & & & D_{22} & & E_{21} & E_{22} & \cdots \\ & & & & & & \vdots & \vdots \\ & \text{(symmetric about} & & & & F_{11} & F_{12} & \\ & \text{main diagonal)} & & & & & F_{22} & \end{bmatrix} \tag{4.164}$$

$$\bar{B} = \begin{bmatrix} & \text{(zero)} & & \text{(zero)} & & & \text{(zero)} \\ & & & \text{(zero)} & & & \text{(zero)} \\ & \text{(symmetric about} & & & & P_{11} & P_{12} \\ & \text{main diagonal)} & & & & & P_{22} \end{bmatrix} \tag{4.165}$$

and

$$X_{\text{symmetric}} = \begin{bmatrix} \bar{u}_2 \\ \bar{u}_4 \\ \vdots \\ \bar{v}_1 \\ \bar{v}_3 \\ \vdots \\ \bar{w}_1 \\ \bar{w}_3 \\ \vdots \end{bmatrix} \qquad X_{\text{antisymmetric}} = \begin{bmatrix} \bar{u}_1 \\ \bar{u}_3 \\ \vdots \\ \bar{v}_2 \\ \bar{v}_4 \\ \vdots \\ \bar{w}_2 \\ \bar{w}_4 \\ \vdots \end{bmatrix} \tag{4.166}$$

For the symmetric case, the elements of the submatrices in Equations (4.164) and (4.165) are

Éléments sous droits d'auteur

$$A_{ij} = A\left[(2j)^2\left[\frac{\pi}{L}\right]^2 + \frac{1-\nu}{2}\left[\frac{n}{r}\right]^2\right] \qquad (i=j)$$

$$B_{ij} = -\frac{1+\nu}{2} A \frac{8}{L}\frac{n}{r}\frac{i(2j-1)}{(2i)^2-(2j-1)^2}$$

$$C_{ij} = -\frac{\nu A}{r}(2j)\frac{\pi}{L} \qquad (i=j)$$

$$C_{ij} = \frac{\nu A}{r}(2j-2)\frac{\pi}{L} \qquad (i=j-1)$$

$$C_{ij} = 0 \qquad (i=j+1)$$

$$D_{ij} = A\left[\left[\frac{n}{r}\right]^2 + \frac{1-\nu}{2}(2j-1)^2\left[\frac{\pi}{L}\right]^2\right] \qquad (i=j)$$

$$E_{ij} = \frac{4}{\pi}(2i-1)\left[\frac{1}{(2i-1)^2-(2j-2)^2} - \frac{1}{(2i-1)^2-(2j)^2}\right]A\frac{n}{r^2} \qquad (4.167)$$

$$F_{11} = 16\Lambda_1 + 4\Lambda_2 + 3\Lambda_3$$

$$F_{ij} = \left[(2j-2)^4 + (2j)^4\right]\Lambda_1 + \left[(2j-2)^2 + (2j)^2\right]\Lambda_2 + 2\Lambda_3 \qquad (i=j\neq 1)$$

$$F_{ij} = -\left[(2j-2)^4\Lambda_1 + (2j-2)^2\Lambda_2 + \Lambda_3\right] \qquad (i=j-1)$$

$$P_{11} = 4\left[\frac{\pi}{L}\right]^2 N_x$$

$$P_{ij} = \left[(2j-2)^2 + (2j)^2\right]\left[\frac{\pi}{L}\right]^2 N_x \qquad (i=j\neq 1)$$

$$P_{ij} = -(2j-2)^2\left[\frac{\pi}{L}\right]^2 N_x \qquad (i=j-1)$$

in which

$$\Lambda_1 = \left[\frac{\pi}{L}\right]^2 D \quad \Lambda_2 = 2\left[\frac{\pi}{L}\right]^2\left[\frac{n}{r}\right]^2 D \quad \Lambda_3 = \left[\frac{n}{r}\right]^4 D + \frac{A}{r^2} \qquad (4.168)$$

For the antisymmetric case, the elements of the submatrices in Equations (4.164) and (4.165) are

$$A_{ij} = A\left[(2j-1)^2\left[\frac{\pi}{L}\right]^2 + \frac{1-\nu}{2}\left[\frac{n}{r}\right]^2\right] \qquad (i=j)$$

$$B_{ij} = -\frac{1+\nu}{2} A \frac{8}{L}\frac{n}{r}\frac{(2i-1)j}{(2i-1)^2-(2j)^2}$$

$$C_{ij} = \frac{\nu A}{r}(2j-1)\frac{\pi}{L} \qquad (i=j)$$

$$C_{ij} = 0 \qquad (i=j-1)$$

$$C_{ij} = -\frac{\nu A}{r}(2j+1)\frac{\pi}{L} \qquad (i=j+1)$$

$$D_{ij} = A\left[\left[\frac{n}{r}\right]^2 + \frac{1-\nu}{2}(2j)^2\left[\frac{\pi}{L}\right]^2\right] \qquad (i=j)$$

(4.169, continued)

Éléments sous droits d'auteur

$$E_{ij} = \frac{8i}{\pi}\left[\frac{1}{(2i)^2-(2j-1)^2} - \frac{1}{(2i)^2-(2j+1)^2}\right]A\frac{n}{r^2}$$

$$F_{ij} = \left[(2j-1)^4 + (2j+1)^4\right]\Lambda_1 + \left[(2j-1)^2 + (2j+1)^2\right]\Lambda_2 + 2\Lambda_3 \qquad (i = j+1)$$

$$F_{ij} = -\left[(2j-1)^4\Lambda_1 + (2j-1)^2\Lambda_2 + \Lambda_3\right] \qquad (i = j-1)$$

$$P_{ij} = \left[(2j-1)^2 + (2j+1)^2\right]\left[\frac{\pi}{L}\right]^2\bar{N}_x \qquad (i = j)$$

$$P_{ij} = -(2j-1)^2\left[\frac{\pi}{L}\right]^2\bar{N}_x \qquad (i = j-1)$$

(4.169, concluded)

Now, abbreviate Equation (4.163) as

$$\begin{bmatrix} A & B & C \\ B^T & D & E \\ C^T & E^T & F \end{bmatrix}\begin{bmatrix} \bar{u} \\ \bar{v} \\ \bar{w} \end{bmatrix} = \begin{bmatrix} 0 & 0 & 0 \\ 0 & 0 & 0 \\ 0 & 0 & P \end{bmatrix}\begin{bmatrix} \bar{u} \\ \bar{v} \\ \bar{w} \end{bmatrix} \qquad (4.170)$$

in which the superscript T denotes the matrix transpose. Because of the zeros on the right-hand side of Equation (4.170), the following buckling equation can be obtained by matrix operations:

$$\left[[F] - \left[C^T \mid E^T\right]\cdot\begin{bmatrix} A & B \\ B^T & D \end{bmatrix}^{-1}\cdot\begin{bmatrix} C \\ E \end{bmatrix}\right]\{C\} = [P]\{C\} \qquad (4.171)$$

in which the superscript −1 denotes the matrix inverse. The left-hand side of Equation (4.171) can be shown to be symmetric upon consideration of the symmetry properties of matrices A, B, C, etc.

The buckling load can be obtained from the buckling equation, Equation (4.171), in the following manner. When the number of terms in the series expansions of the displacements as well as the number of buckle waves, n, in the circumferential direction are specified, the lowest eigenvalue can be extracted from Equation (4.171) by standard eigenvalue computational routines. The number n is varied over some range until an absolute minimum eigenvalue is found. In the preceding step, several relative minima can be obtained. Thus, a wide range of n must be investigated before an absolute minimum is reasonably assured. For a given problem, the buckling load is the lowest eigenvalue of the two absolute minima obtained for the symmetric and antisymmetric modes. Of course, the buckle wave component amplitudes, $\bar{u}_i$, $\bar{v}_i$, and $\bar{w}_i$, are indeterminate.

Numerical values were obtained by use of a computer program. Convergence of the solutions was assured to an arbitrary accuracy by comparison of solutions with different numbers of terms in the series expansions of the buckling displacements. The number of terms necessary for convergence to an accuracy of three significant figures varied from three to eight as the shell length increased.

Éléments sous droits d'auteur

The buckling results for the C1 buckling boundary condition are plotted in Figure 4-33 as a function of Z along with results from the last section for the C3 buckling boundary condition. The only difference between C3 and C1 buckling boundary conditions is $\delta N_{xy} = 0$ as opposed to $\delta v = 0$, and the latter condition provides more circumferential restraint against buckling than does $N_{xy} = 0$. From comparison of the results for the C3 and C1 buckling boundary conditions, circumferential restraint apparently plays an important role in buckling under axial compression for fairly short shells. However, if Z = 0, a plate, there is no difference between the C3 and C1 results because in-plane effects do not govern buckling of a plate. For moderate-length or long shells (Z > 50), again the shell circumferential restraint plays no significant role.

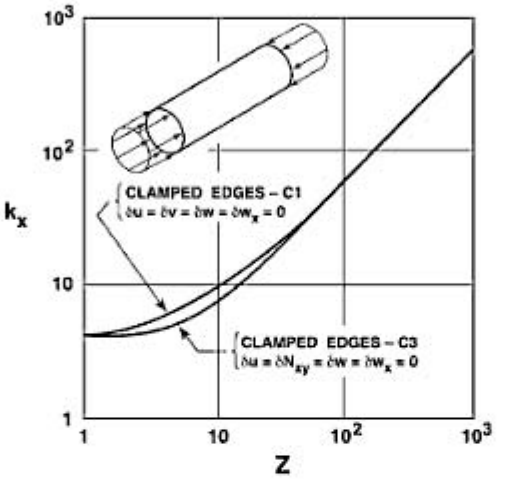


Figure 4-33 Buckling of Axially Compressed Circular Cylindrical Shells with C3 and C1 Clamped-Edge Buckling Boundary Conditions *(After Card and Jones [4-25])*

4.3.5 Summary for Classical Buckling Results

A significant problem with *some* of the classical buckling results presented in this section is the fact that axially compressed circular cylindrical shells buckle at loads well below the Euler load, as the classical buckling results are called. However, for buckling under lateral pressure, hydrostatic pressure, and torsion, the Euler loads are a reasonable representation of the measured buckling results with one exception. Those shells of low Z for which the axial pressure part of hydrostatic pressure dominates have significantly reduced buckling loads. Thus, the classical buckling results are generally accepted by the technical community except for cases in which axial compression plays a dominant role. More

Éléments sous droits d'auteur

definitive descriptions of pertinent experimental results than discussed in this section can be found in Singer, Arbocz, and Weller [4-13].

Shell shapes other than circular cylindrical have, of course, been addressed. For example, Kempner and Chen [4-26] treated cylindrical shells of elliptical or oval cross section (recall that 'cylindrical' means a surface with parallel generatrix, so the cross section perpendicular to the generatrix can be any shape, even square!) and found that the classical buckling stress under axial compression is less than that of a circular cross-section shell by a factor related to the out-of-roundness of the oval. Moreover, that oval cylindrical shell buckling stress corresponds to the buckling stress of a circular cross-section shell with radius equal to the maximum radius of curvature of the oval cross-section shell as a lower bound to the actual buckling stress. For example, if the ratio of the major-axis dimension of the ellipse to the minor-axis dimension is 1.4, then the buckling stress can be as much as 50% less than that of the circular cross-section shell with the same circumference. Analogous results were obtained for buckling of elliptical cylindrical shells under lateral pressure by Yao and Jenkins [4-27].

We will next examine several possible approaches to both (1) better understanding the process of buckling of circular cylindrical shells under axial load and (2) more accurate results. Those approaches include exploring the role of the postbuckling behavior in Section 4.4, the effect of prebuckling deformations in Section 4.5, and the significance of initial geometric imperfections in Section 4.6. Observing the postbuckling behavior should help us understand and evaluate the proper role of the Euler buckling load in the design process for shells as we have seen that it does for both bars and plates. We should suspect that the inclusion of prebuckling deformations will alter the predicted buckling load to some degree. Of course, the presence of initial geometric imperfections will alter and affect the importance and interpretation of the Euler buckling load.

Problem Set 4.3

4.3.1 Verify that the variation in displacement given in Equation (4.81) is associated with the S2 buckling boundary condition for both Donnell's equation and Batdorf's modified Donnell equation.

4.3.2 Derive the general expression for k_x in Equation (4.87).

4.3.3 Specialize the expression for k_x in Equation (4.87) for moderately long shells to obtain Equation (4.91).

4.3.4 Derive Equation (4.92) from Equation (4.91). How sensitive to the value of Poisson's ratio is the final result in Equation (4.92)?

4.3.5 Derive the general expression for k_y in Equation (4.103).

4.3.6 Specialize the expression for k_y in Equation (4.103) for moderate-length shells to obtain Equation (4.107).

4.3.7 Derive the general expression for c_0 in Equation (4.116).

4.3.8 Verify that the variation in displacement given in Equation (4.134) is associated with the C3 buckling boundary condition for both Donnell's equation and Batdorf's modified Donnell equation.

4.3.9 Substitute the variation in displacement given in Equation (4.134) in the buckling differential equation, Equation (4.140), to obtain the explicit form of $Q(\delta w) = 0$.

4.3.10 Integrate Equation (4.146) when $Q(\delta w)$ is known from Exercise 4.3.9 to obtain the homogenous, linear, algebraic equations in Equation (4.147).

Éléments sous droits d'auteur

4.4 POSTBUCKLING BEHAVIOR

Predicted classical bar and plate buckling loads have been shown to be reasonably accurate, even when imperfections and postbuckling behavior are considered. We just found that the influence of various boundary conditions was not sufficient to explain the large discrepancy between classical shell buckling loads and measured results for axial compression. Thus, we investigate the postbuckling response to gain an appreciation of the significance of classical buckling results in Section 4.3 and, to some extent, the more rigorous results in Section 4.5 that are based on analysis of prebuckling deformations. Von Kármán and Tsien [4-28] were among the first to study the postbuckling behavior of axially compressed circular cylindrical shells. They observed that, aside from the unbuckled state, *additional equilibrium states exist for a shell at stresses below the classical Euler buckling stress* as in Figure 4-34. The classical Euler buckling stress occurs for both axisymmetric (sinusoidal only in the axial direction) and chessboard (sinusoidal in both the axial and circumferential directions) buckle modes shown schematically in Figure 4-34. However, the postbuckling configurations usually involve inward-deforming diamond-shaped buckles also shown in Figure 4-34. There, the minimum stress in the buckled state (called the minimum postbuckling stress) is about 10% of the Euler stress. Experimental results also fall at about 10% of the Euler stress, but their deflections do not necessarily correspond to the deflection at the minimum postbuckling stress. Thus, *the minimum postbuckling stress is not a buckling stress.*

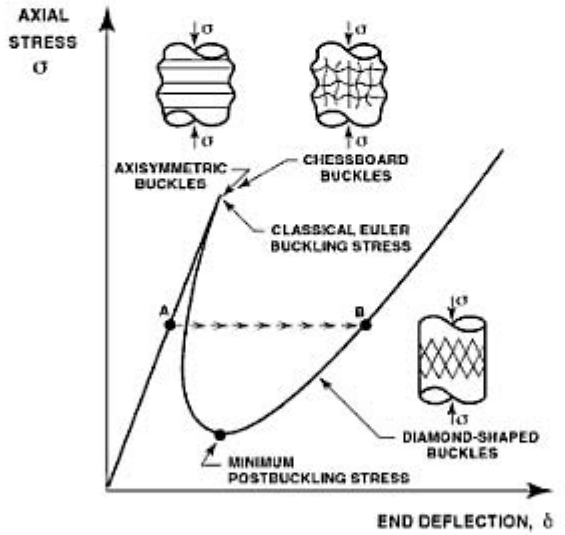


Figure 4-34 Schematic Representation of Postbuckling Behavior of Axially Compressed Circular Cylindrical Shells

Éléments sous droits d'auteur

although the minimum postbuckling stress is the lower bound on the buckling stress (if initial geometric imperfections are ignored) because no equilibrium state other than the unbuckled state exists below the minimum postbuckling stress.

The type of behavior in Figure 4-34 is characterized as unsymmetric in the Koiter sense as described in Section 1.3. Only the falling (unstable) portion of Figure 1-22b on page 20 is applicable, and the slope is very steep, so the behavior is highly unstable and therefore highly susceptible to the influence of imperfections. Thus, initial geometric imperfections of the shell are generally regarded as being responsible for the low actual buckling stresses. However, the postbuckling behavior must be examined to assess the likelihood that initial geometric imperfections cause lower buckling stresses. That is, the lower the minimum postbuckling stress relative to the Euler buckling stress, the more likely that initial geometric imperfections will decrease actual buckling stresses.

The possibility of getting to the postbuckled equilibrium states from the prebuckled equilibrium state for perfect shells is related to the actual buckling stress by the relative energies of the prebuckled and postbuckled equilibrium states. That is, without initial geometric imperfections, the shell could snap through from A to B in Figure 4-34 at some value of axial stress less than the Euler stress. This snap-through buckling stress will be evaluated on the basis of the energy at A versus the energy at B. Tsien [4-29] proposed that the shell buckles when the energy at A is equal to the energy at B (The Tsien equal-energy buckling criterion).

The general von Kármán and Tsien approach, as modified and extended for more accurate results by Almroth [4-30] and Jones [4-31], will be used in this section to study the energy during the buckling process. A higher state of energy than either at A or B will be shown to exist *between* A and B. Thus, an 'energy hump' must be surmounted during buckling, so the Tsien equal-energy buckling criterion cannot be valid (Tsien actually withdrew his criterion in 1947 [4-32], but many engineers still use the criterion despite the fact that Tsien himself disowned it).

The basic theme of examining postbuckling behavior is the definition and comparison of the energies in the various equilibrium configurations that are possible. We restrict our attention to a shell of infinite length, so, because the buckles are periodic over the shell length, we need be concerned only with a single axial wavelength, L_x, of the buckled shape as shown in Figure 4-35. There, circumferential buckles are not shown strictly for convenience of illustration. Also, shell-edge boundary condi-

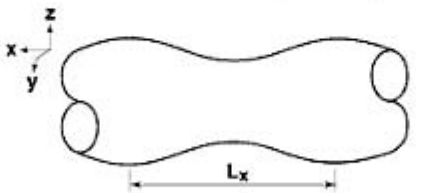


Figure 4-35 Infinitely Long Circular Cylindrical Shell with Exaggerated Periodic Buckles of Wavelength L_x

Éléments sous droits d'auteur

tions are irrelevant because of the infinite shell length. Donnell-type moderately large-deflection strain-displacement relations in Equation (4.5) on page 467 are used to obtain the total potential energy of a shell segment L_x long under axial compression:

$$V = \frac{Et}{2}\int_0^{L_x}\int_0^{2\pi r}\left[(\sigma_x+\sigma_y)^2 - 2(1+\nu)(\sigma_x\sigma_y - \tau_{xy}^2)\right]dxdy$$
$$+ \frac{Et^3}{24(1-\nu^2)}\int_0^{L_x}\int_0^{2\pi r}\left[(w_{xx}+w_{yy})^2 - 2(1-\nu)(w_{xx}w_{yy} - w_{xy}^2)\right]dxdy$$
$$- Et\int_0^{2\pi r}(\sigma_x)_{x=L_x}\left[\int_0^{L_x} u_x\,dx\right]dy \qquad (4.172)$$

in which all stresses and displacements are dimensionless.

The axial displacement of the shell can be written as

$$u = \int_0^{L_x} u_x\,dx \qquad (4.173)$$

for which we will obtain u_x by a relation between strains so that u_x is consistent with the approximation for the radial deflection w. Also, σ_x in Equation (4.172) need not be constant over the end of the shell segment. In fact, the axial stress can be shown to be the sum of an average value σ and some variation in the circumferential direction.

The total potential energy can be reexpressed in terms of the displacements u, v, and w, the three dependent variables comprising the displacement vector, and the loading parameter σ. Then, upon application of the principle of stationary potential energy and reconversion to a stress-based formulation, we obtain three equilibrium equations:

$$\frac{\partial\sigma_x}{\partial x} + \frac{\partial\tau_{xy}}{\partial y} = 0 \qquad (4.174)$$

$$\frac{\partial\tau_{xy}}{\partial x} + \frac{\partial\sigma_y}{\partial y} = 0 \qquad (4.175)$$

$$\nabla^4 w - \frac{12(1-\nu)^2}{Et^2}\left[\sigma_x w_{xx} + \sigma_y\left(w_{yy} - \frac{1}{r}\right) + 2\tau_{xy}w_{xy}\right] = 0 \qquad (4.176)$$

Note that the loading parameter σ does not appear in the equilibrium equations but instead enters the problem through the boundary conditions (this is a moderately large-deflection equilibrium problem, i.e., a boundary value problem). The first two equilibrium equations, Equations (4.174) and (4.175), are necessary and sufficient conditions for the existence of a stress function F defined by

$$F_{xx} = \sigma_y \quad F_{yy} = \sigma_x \quad F_{xy} = -\tau_{xy} \qquad (4.177)$$

Éléments sous droits d'auteur

Because a stress function was introduced, a compatibility equation is required and can be obtained from Equation (4.177), the stress-strain relations, and the strain-displacement relations as

$$\nabla^4 F = E\left[w_{xy}^2 - w_{xx}w_{yy} - \frac{w_{xx}}{r} \right] \tag{4.178}$$

The first step in the solution procedure is the approximation of the radial deflection w with a double cosine series

$$w = \sum_{i=0}^{\infty} \sum_{j=0}^{\infty} a_{ij} \cos \frac{i\pi x}{L_x} \cos \frac{j\pi y}{L_y} \tag{4.179}$$

in which the sum i + j is always even. This series is a representation of the diamond-shaped buckles observed when shells buckle as in Figure 4-34 on page 519 and Figure 4-23 on page 497. These buckles are much harder to represent mathematically than are chessboard (sinusoidal) buckles. At this point, we must recall that we are describing the total deformation state of the shell, not just the displacements that occur during buckling. When the deflection approximation, Equation (4.179), is substituted in the compatibility equation, Equation (4.178), the stress function can be determined in terms of the parameters in Equation (4.179).

Next, the stress function must be substituted in the total potential energy expression, Equation (4.172). However, the integral

$$\iint (w_{xx}w_{yy} - w_{xy}^2)\, dxdy \tag{4.180}$$

can be shown to be identically zero for the orthogonal functions chosen for the radial deflection approximation [4-33]. Moreover, the integral

$$\iint (\sigma_x\sigma_y - \tau_{xy}^2)\, dxdy \tag{4.181}$$

can also be shown to be identically zero when a stress function exists [4-33]. Thus, Equation (4.172) can be simplified considerably.

Upon substitution of the stress function (in terms of the deflection approximation parameters) in the simplified total potential energy integral and integration, we get an explicit function, $V(L_x, L_y, a_{ij}, \sigma, E, \nu)$. Then, if the generalized coordinates L_x, L_y, and the a_{ij} are represented by x_i, the principle of stationary potential energy can be expressed as

$$\frac{\partial V}{\partial x_i} = 0 \tag{4.182}$$

The fact that the energy is made stationary relative to L_x is consistent with the stipulation that the shell is infinitely long. That is, L_x is a continuous variable for an infinite shell. However, because of circumferential continuity, L_y cannot be regarded as a continuous variable as implied in Equation (4.182). That is, $n = r\pi/L_y$ must be an integer, so stationary values of V must be sought for discrete values of L_y. This approach allows study of the energy in the various equilibrium configurations that a shell can assume. In addition, Hoff, Madsen, and Mayers [4-34] showed that if L_y is regarded as a continuous variable rather than having discrete

Éléments sous droits d'auteur

values depending on the value of integer n, the Yoshimura buckled configuration [4-35] is obtained for which the minimum postbuckling stress is zero. If, however, the discreteness of L_y is accounted for, Madsen and Hoff [4-36] showed that the minimum postbuckling stress is finite. At any rate, solution of the simultaneous nonlinear algebraic equations represented by Equation (4.182) is accomplished by use of the Newton-Raphson technique as described by Korn and Korn [4-37].

Because of practical computational limitations, naturally only a finite number of terms can be retained in the radial deflection approximation, Equation (4.179). Jones [4-31] used

$$w = a_{00} + a_{20}\cos 2\alpha x + a_{11}\cos \alpha x \cos \beta y + a_{02}\cos 2\beta y + a_{22}\cos 2\alpha x \cos 2\beta y + a_{33}\cos 3\alpha x \cos 3\beta y + a_{40}\cos 4\alpha x \tag{4.183}$$

in which $\alpha = \pi/L_x$ and $\beta = \pi/L_y = n/r$. The terms in Equation (4.183) are sufficient to achieve agreement with the experimental values of the minimum postbuckling stress (.10 to .25σ_{CL}) obtained by Thielemann [4-38]. Almroth [4-30] obtained .108 σ_{CL} with two more terms than in Equation (4.183). He and Jones obtained .112 σ_{CL} for Equation (4.183) as did Madsen and Hoff (see Figure 4 of [4-36]) for r/t = 787 and n = 7. Thus, both the practicality and validity of the present nonlinear equilibrium analysis are demonstrated.

Solution of the moderately large-displacement equilibrium equations, Equation (4.182), yields an axial stress versus axial shortening per unit length curve (equilibrium curve) for all values of n^2t/r in which n is the number of circumferential waves in the deformed (buckled) shell. A consistent family of such postbuckling equilibrium curves is obtained for a shell with a specific r/t when a variety of integer n values is specified. A typical family of equilibrium curves for r/t = 787 is displayed for $n \geq 7$ in Figure 4-36 and for $n \leq 7$ in Figure 4-37 in which the axial stress is normalized by the Euler buckling stress,

$$\sigma_{CL} = \frac{Et}{r}\frac{1}{\sqrt{3(1-\nu^2)}} \tag{4.184}$$

(which is .6 Et/r for $\nu = .27$) and the axial shortening per unit length is normalized by the end shortening at the Euler buckling stress.

Because the position of the present equilibrium curves is determined with the parameter n^2t/r, any specific curve can be interpreted as being associated with various sets of n and t/r. For example, the lowest equilibrium curve has a lower n for thick shells than for thin shells. We expect, intuitively, that thick shells will buckle into a configuration with fewer circumferential waves than do thin shells. For shells with r/t = 200, the curve for n = 4 lies just above Almroth's curve in Figure 4-37, whereas the curve for n = 5 lies between the curves for n = 9 and n = 10 when r/t = 787. The other n curves for r/t = 200 are similarly spread out upward from Almroth's curve. For thinner shells, the curves are crowded together, and the lowest curve has a higher n than for r/t = 787.

Éléments sous droits d'auteur

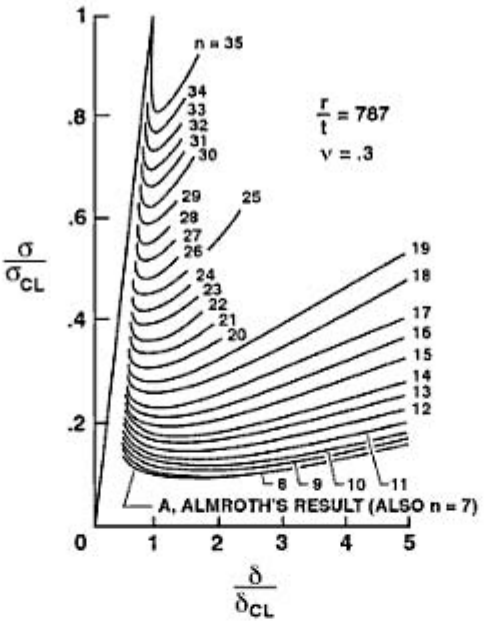


Figure 4-36 Postbuckling Equilibrium Curves for n ≥ 7 *(After Jones [4-31])*

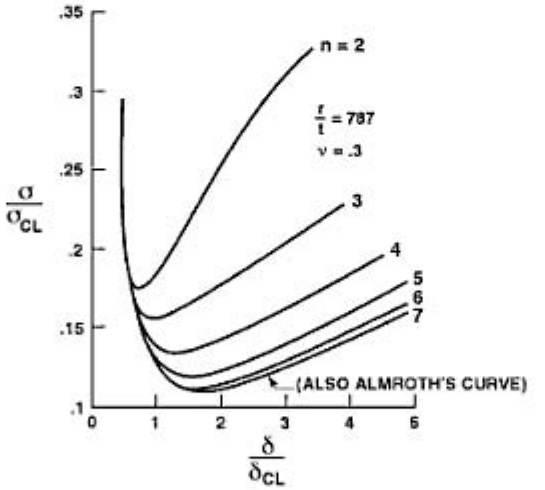


Figure 4-37 Postbuckling Equilibrium Curves for n ≤ 7 *(After Jones [4-31])*

Éléments sous droits d'auteur

The present theoretical postbuckling equilibrium curves for infinite-length shells are shown along with Thielemann's experimental results for finite-length shells [4-38] in Figure 4-38. The agreement between the theoretical and experimental minimum equilibrium stress in the buckled state is excellent; both values are .11 σ_{CL}. The theoretical postbuckling n for the lowest equilibrium curve is lower than the experimental n as might be expected when infinite-length shell results and finite-length shell results are compared because more restraint exists for finite-length shells than for infinite-length shells. Many more experimental results are displayed and discussed by Singer, Arbocz, and Weller [4-13].

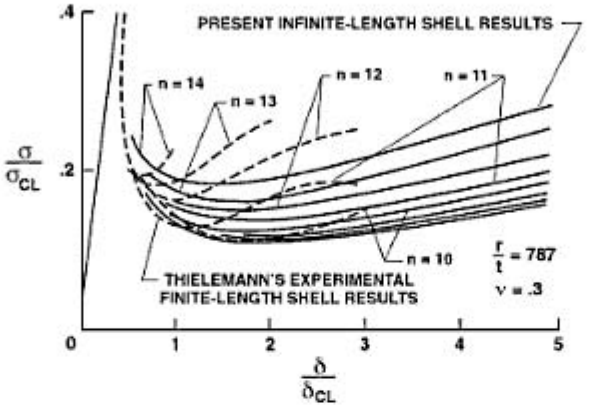
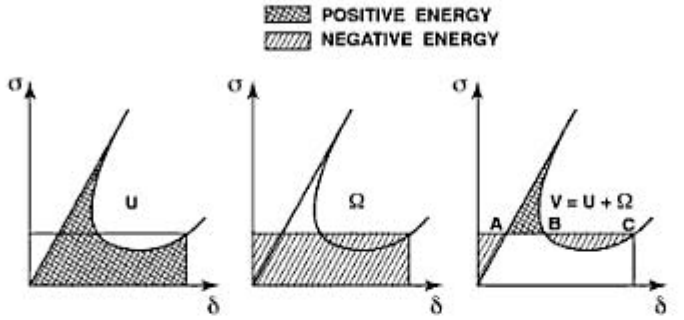


Figure 4-38 Postbuckling Equilibrium Curves for Finite- and Infinite-Length Shells *(After Jones [4-31])*

The total potential energy must be examined to gain insight into the so-called snap-through buckling phenomenon. The total potential energy, V, is shown as the sum of its parts U and Ω in Figure 4-39 in a graphical definition. Results for $\sigma/\sigma_{CL} = .170$ of the energy in the various configurations cut by a constant-stress line ($\sigma/\sigma_{CL} = .170$) in Figures 4-36 and 4-37 are shown in Figure 4-40. Each of the points shown represents a stationary value of V. Moreover, δ is a generalized coordinate, so $\partial V/\partial\delta = 0$. Hence, V must have a horizontal tangent at each discrete number of circumferential buckle waves for a specific r/t. However, for other r/t values, the positions of the horizontal tangent points change. Thus, the locus of values of V for all values of r/t is shown. Based on observation of high-speed movies of the buckling process by Almroth, Holmes, and Brush [4-39], first higher then lower numbers of circumferential buckle waves appear. Thus, we can conclude that the upper branch in Figure 4-40 is realized physically. Loci of the upper branch of V values for various σ/σ_{CL} are shown in Figure 4-41 for which the energy barrier, which is the magnitude of the energy hump, is defined in Figure 4-40. The energy barrier as a percentage of the unbuckled energy is

Éléments sous droits d'auteur

plotted for various σ/σ_{CL} in Figure 4-42. There, we observe that the percentage energy barrier decreases quite rapidly as σ/σ_{CL} goes to one where, of course, the barrier vanishes. The energy barrier can be reasonably correlated with the energy of small disturbances applied to shell experiments. Examples of small disturbances are blowing on the shell or squeezing it radially by hand. Thus, the energy-barrier approach is yet another possible explanation of the discrepancy between theory and experiment for buckling of axially loaded circular cylindrical shells.



a Positive Energy b Negative Energy c Total Energy

Figure 4-39 Change in Total Potential Energy during Constant-Stress Buckling *(After Jones [4-31])*

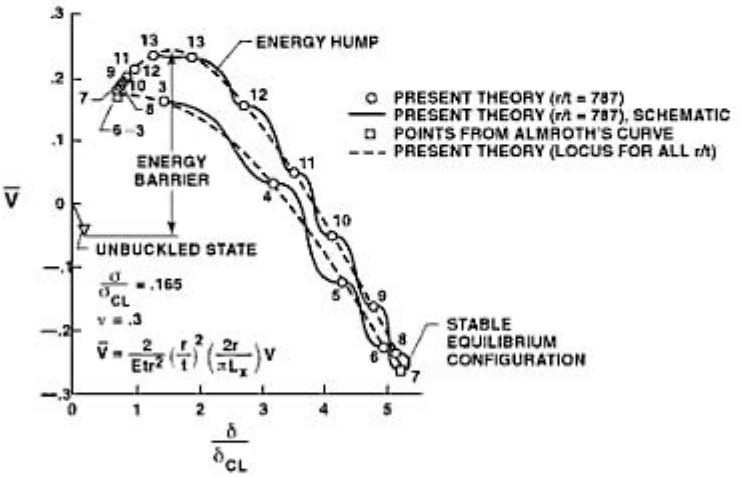


Figure 4-40 Schematic Curve of Energy Values for Discrete Equilibrium Configurations *(After Jones [4-31])*

Éléments sous droits d'auteur

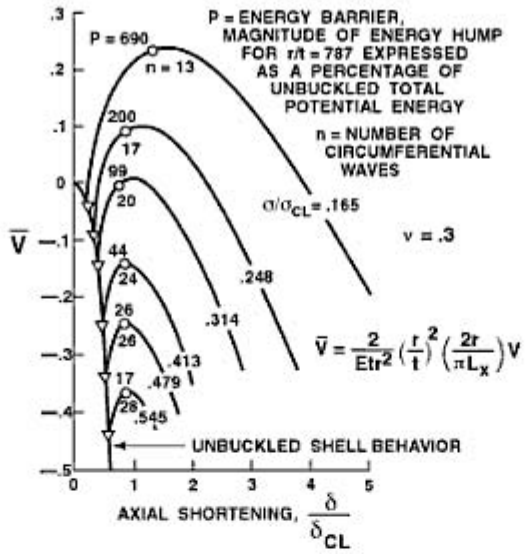


Figure 4-41 Loci of Energy Values *(After Jones [4-31])*

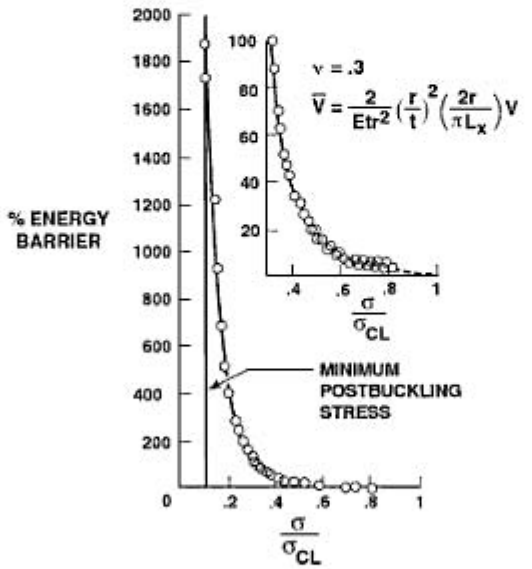


Figure 4-42 Energy Hump versus Stress Ratio *(After Jones [4-31])*

Éléments sous droits d'auteur

For other loading conditions, the postbuckling equilibrium curve is much higher relative to the classical Euler buckling stress than for axial compression. For example, a shell subjected to torsion (N_{xy}) has a load-strain behavior similar to that represented in Figure 4-43. There, the minimum postbuckling stress is about 70% of the Euler stress. Shells subjected to lateral pressure have very nearly no drop in the equilibrium stress after buckling below the Euler stress as shown in Figure 4-44.

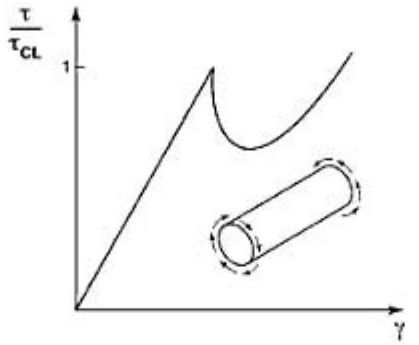


Figure 4-43 Schematic Equilibrium Curve for a Shell under Torsion

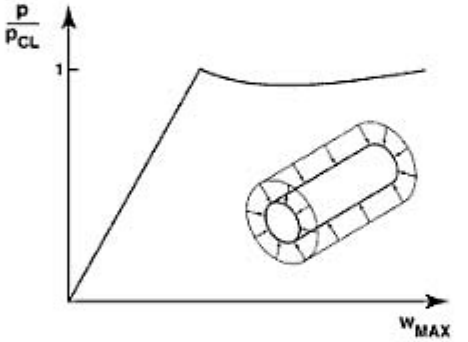


Figure 4-44 Schematic Equilibrium Curve for a Shell under Lateral Pressure

Problem Set 4.4

4.4.1 Express u_x in terms of stresses σ_x and σ_y and the lateral deflection w and its derivatives in order to evaluate Equation (4.173).

4.4.2 Derive the compatibility equation, Equation (4.178), in terms of the stress function and the lateral deflection.

4.4.3 Verify that the integral of the stress functional $\sigma_x\sigma_y - \tau_{xy}^2$ vanishes. Also demonstrate that the integral contributes nothing to the equilibrium equations.

4.4.4 Verify that the integral of the curvature functional $w_{xx}w_{yy} - w_{xy}^2$ vanishes. Also demonstrate that the integral contributes nothing to the equilibrium equations.

Éléments sous droits d'auteur

4.5 EFFECT OF PREBUCKLING DEFORMATIONS ON BUCKLING UNDER AXIAL COMPRESSION

The solutions in Section 4.3 are for classical buckling theory, i.e., a buckling theory in which a membrane prebuckled state is the basis for the simplifications that make the theory so tractable. Prior to about 1960, classical buckling theory was tacitly assumed to be correct, and the large discrepancy between theoretical predictions and corresponding experimental results was blamed entirely on the effect of initial geometric imperfections. In the 1960s, Stein [4-40], Almroth [4-10], and others began a series of investigations into another plausible reason for the discrepancy—the membrane prebuckling state inherent to classical buckling theory is not a sufficiently rigorous description of the equilibrium state prior to buckling. The objective of the various investigations was to obtain a more rigorous prebuckling deformation solution than in classical buckling theory. The key to the new prebuckling solutions is enforcement of consistent boundary conditions on both the prebuckling equilibrium solution and the buckling solution. In contrast, there are no boundary conditions on the membrane prebuckling equilibrium solution in classical buckling theory, i.e., the edges are free of constraint and move both axially and radially under axial load. These two equilibrium states are displayed in Figure 4-45 for a shell with simply supported edges.

The equilibrium differential equations for axisymmetric prebuckling deformations are obtained from Equations (4.22), (4.23), and (4.24) by equating to zero all derivatives with respect to y, the circumferential coordinate, and all terms in v, the circumferential displacement:

$$\frac{\partial}{\partial x}\left[u_x + \frac{1}{2}w_x^2 + \nu\frac{w}{r}\right] = 0 \tag{4.165}$$

$$\frac{A}{r}\left[\frac{w}{r} + \nu\left(u_x + \frac{1}{2}w_x^2\right)\right] - A\frac{\partial}{\partial x}\left[w_x\left[u_x + \frac{1}{2}w_x^2 + \nu\frac{w}{r}\right]\right] + Dw_{xxxx} + p = 0 \tag{4.166}$$

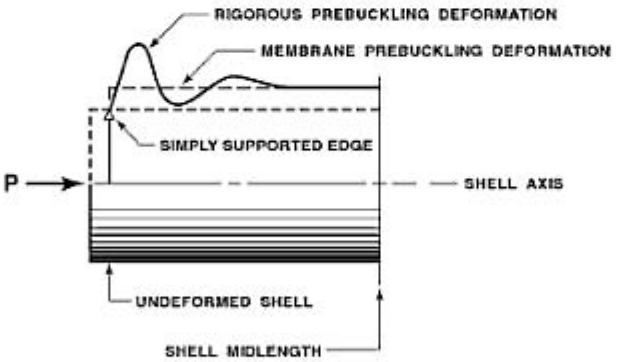


Figure 4-45 Membrane versus Rigorous Prebuckling Deformation

Éléments sous droits d'auteur

Equation (4.186) can be differentiated and then Equation (4.185) substituted to yield a single equilibrium differential equation

$$Dw_{xxxx} + Nw_{xx} + \frac{Et}{r^2} w - \left(\frac{\nu N}{r} - p \right) = 0 \tag{4.187}$$

if we realize that (1) N_x is constant because of Equation (4.185) and thus always equal to $-N$, the axial load per unit width of the edge and (2)

$$N_y = \frac{Et}{r} w - \nu N \tag{4.188}$$

which is obtained from solution of the load-strain relations in Equation (4.65) on page 485 once we know that $N_x = -N$. Those moderately large-deflection load-strain (actually load-displacement) relations are

$$\begin{aligned} N_x &= A\left[\left(u_x + \frac{1}{2} w_x^2 \right) + \nu \frac{w}{r} \right] \\ N_y &= A\left[\frac{w}{r} + \nu \left(u_x + \frac{1}{2} w_x^2 \right) \right] \\ N_{xy} &= 0 \end{aligned} \tag{4.189}$$

The governing equilibrium differential equation, Equation (4.187), is a function of w only and has the general solution

$$w = \frac{r^2}{Et} \left(\frac{\nu N}{r} - p \right) (1 + A_1 \sin a_1 x \sinh a_2 x + A_2 \cos a_1 x \cosh a_2 x) \tag{4.190}$$

in which two of the constants of integration vanish because of boundary condition symmetry about the shell mid-length, the constant term is the membrane prebuckling deformation, and

$$a_1 = \frac{1}{2L} \sqrt{4\sqrt{3}\, Z + \frac{NL^2}{D}} \qquad a_2 = \frac{1}{2L} \sqrt{4\sqrt{3}\, Z - \frac{NL^2}{D}} \tag{4.191}$$

[Z is Batdorf's Z defined in Equation (4.85) on page 492] and for simply supported edges, $w = 0$ and $w_{xx} = 0$ at $x = \pm L/2$ (origin in middle of shell) so

$$\begin{aligned} A_1 &= -\frac{\left(a_2^2 - a_1^2 \right) \cos \frac{a_1 L}{2} \cosh \frac{a_2 L}{2} + 2a_1 a_2 \sin \frac{a_1 L}{2} \sinh \frac{a_2 L}{2}}{2a_1 a_2 \left[\cosh^2 \frac{a_2 L}{2} - \sin^2 \frac{a_1 L}{2} \right]} \\ A_2 &= -\frac{2a_1 a_2 \cos \frac{a_1 L}{2} \cosh \frac{a_2 L}{2} + \left(a_2^2 - a_1^2 \right) \sin \frac{a_1 L}{2} \sinh \frac{a_2 L}{2}}{2a_1 a_2 \left[\cosh^2 \frac{a_2 L}{2} - \sin^2 \frac{a_1 L}{2} \right]} \end{aligned} \tag{4.192}$$

whereas for clamped edges, $w = 0$ and $w_x = 0$ at $x = \pm L/2$, so

$$A_1 = -2 \frac{a_2 \cos \frac{a_1 L}{2} \sinh \frac{a_2 L}{2} - a_1 \sin \frac{a_1 L}{2} \cosh \frac{a_2 L}{2}}{a_1 \sinh a_{2L} + a_2 \sin a_1 L} \tag{4.193a}$$

Éléments sous droits d'auteur

$$A_2 = -2\,\frac{a_2 \sin\dfrac{a_1 L}{2}\cosh\dfrac{a_2 L}{2} + a_1 \cos\dfrac{a_1 L}{2}\sinh\dfrac{a_2 L}{2}}{a_1 \sinh a_2 L + a_2 \sin a_1 L} \tag{4.193b}$$

The eight common choices of boundary conditions in the prebuckling equilibrium state are analogous to the boundary conditions during buckling noted in Equations (4.63) and (4.64) on page 484:

Simply Supported Edges:

$$\begin{array}{llllll} \text{S1:} & \delta w = 0 & \delta M_x = 0 & \delta u = 0 & \delta v = 0 \\ \text{S2:} & \delta w = 0 & \delta M_x = 0 & \delta N_x = 0 & \delta v = 0 \\ \text{S3:} & \delta w = 0 & \delta M_x = 0 & \delta u = 0 & \delta N_{xy} = 0 \\ \text{S4:} & \delta w = 0 & \delta M_x = 0 & \delta N_x = 0 & \delta N_{xy} = 0 \end{array} \tag{4.194}$$

Clamped Edges:

$$\begin{array}{llllll} \text{C1:} & \delta w = 0 & \delta w_{,x} = 0 & \delta u = 0 & \delta v = 0 \\ \text{C2:} & \delta w = 0 & \delta w_{,x} = 0 & \delta N_x = 0 & \delta v = 0 \\ \text{C3:} & \delta w = 0 & \delta w_{,x} = 0 & \delta u = 0 & \delta N_{xy} = 0 \\ \text{C4:} & \delta w = 0 & \delta w_{,x} = 0 & \delta N_x = 0 & \delta N_{xy} = 0 \end{array} \tag{4.195}$$

The terminology 'consistent boundary conditions' then is a reference to the fact that *the same type or class of boundary condition is used in the prebuckling equilibrium solution as in the buckling solution.* Actually, however, some of the foregoing boundary conditions do not make a great deal of sense for an axially loaded shell. For example, S2, S4, C2, and C4 all have $N_x = 0$ at the edges, but this condition is not possible when N_x is the only applied edge load. During buckling, however, we can meaningfully apply the boundary condition $\delta N_x = 0$, i.e., the load remains *constant* at buckling. Other possible inconsistencies arise when we realize that $v = 0$ in the axisymmetric equilibrium state and that hence

$$v_{,x} = 0 \tag{4.196}$$

Also because of axial symmetry,

$$u_{,y} = 0 \qquad w_{,y} = 0 \tag{4.197}$$

Thus, by use of the force-displacement relation for N_{xy} in Equation (4.32),

$$N_{xy} = 0 \tag{4.198}$$

Apparently, we believed that $v = 0$ and $N_{xy} = 0$ were *alternative* boundary conditions, but here we see that they can happen simultaneously and without contradiction for axisymmetric deformation.

The only obvious conclusion that can be made about the prebuckling equilibrium state is that we have either a clamped shell or a simply supported shell, i.e., that either $w_{,x} = 0$ or $w_{,xx} = 0$ in addition to $w = 0$. The true importance of the prebuckling boundary conditions is related to their effect on the radial deformation, w, prior to buckling. During buckling, the boundary conditions become wider in scope, and we can then meaningfully speak of $\delta N_x = 0$ for an axially loaded shell because then the axial load is constant during buckling (hence, its variation is zero).

Éléments sous droits d'auteur

The next step in the problem is to use the rigorous prebuckling equilibrium solution in the solution of the buckling equations, Equations (4.60), (4.61), and (4.62) supplemented by the simplifications of prebuckling axisymmetry in Equations (4.65), (4.66) and (4.67) on pages 484–486, or

$$\frac{\partial}{\partial x}(\delta N_x) + \frac{\partial}{\partial y}(\delta N_{xy}) = 0 \tag{4.199}$$

$$\frac{\partial}{\partial x}(\delta N_{xy}) + \frac{\partial}{\partial y}(\delta N_y) = 0 \tag{4.200}$$

$$-\frac{\partial^2}{\partial x^2}(\delta M_x) - 2\frac{\partial^2}{\partial x \partial y}(\delta M_{xy}) - \frac{\partial^2}{\partial y^2}(\delta M_y) - \delta N_x w_{xx} + N_x \delta w_{xx} + N_y \delta w_{yy} + \delta N_y / r = 0 \tag{4.201}$$

$$N_x = A\left[(u_x + \frac{1}{2}w_x^2) + \nu\frac{w}{r}\right] = N$$
$$N_y = A\left[\frac{w}{r} + \nu(u_x + \frac{1}{2}w_x^2)\right] = -\left[\frac{Et}{r}w - \nu N\right] \tag{4.202}$$

$$\delta N_x = A[(\delta u_x + w_x \delta w_x) + \nu(\delta v_y + \delta w/r)]$$
$$\delta N_y = A[(\delta v_y + \delta w/r) + \nu(\delta u_x + w_x \delta w_x)] \tag{4.203}$$
$$\delta N_{xy} = \frac{1-\nu}{2} A(\delta v_x + \delta u_y + w_x \delta w_y)$$

$$\delta M_x = -D(\delta w_{xx} + \nu \delta w_{yy})$$
$$\delta M_y = -D(\delta w_{yy} + \nu \delta w_{xx}) \tag{4.204}$$
$$\delta M_{xy} = -(1-\nu)D\delta w_{xy}$$

Note at this point that N_x and N_y are known from the prebuckling equilibrium solution as are w and its derivatives. Note also that N_x is constant over the shell, but that w, and hence N_y, varies with position. Thus, the buckling differential equations, Equations (4.199), (4.200), and (4.201), are linear partial differential equations with *nonconstant coefficients*.

If the variables are separated as

$$\delta u = \bar{u}(x)\sin\frac{ny}{r}$$
$$\delta v = \bar{v}(x)\cos\frac{ny}{r} \tag{4.205}$$
$$\delta w = \bar{w}(x)\sin\frac{ny}{r}$$

(note that circumferential continuity (periodicity) is satisfied by stipulating that n be an integer), then Equations (4.199), (4.200), and (4.201) are reduced from partial to ordinary differential equations (but still have variable coefficients). The solution of the equations was obtained by Stein [4-40] for the S3 prebuckling and buckling boundary condition and by Almroth [4-10] for all eight boundary conditions. In both papers, the solution is obtained by applying a finite difference technique to the ordinary differential equations with known variable coefficients.

Éléments sous droits d'auteur

Almroth's results for various Batdorf's curvature parameter Z (and sometimes different values of r/t for a given Z) for shells under combined axial load and lateral pressure for the four clamped-edge boundary conditions are shown in Figure 4-46 and for the four simply supported edge boundary conditions in Figure 4-47. The results are normalized relative to the classical Euler buckling load, $\sigma_{cl} = .6Et/r$. For axial compression only, *all the rigorous-prebuckling-solution clamped-edge shell buckling loads are less than the classical buckling load!* However, as expected, all rigorous-prebuckling-solution simply supported edge buckling loads are less than the corresponding clamped-edge shell buckling loads, i.e., $\sigma_{Si} < \sigma_{Ci} < \sigma_{cl}$ (i = 1,4). Note especially that *the clamped-edge shell buckling loads are only slightly higher than the simply supported edge shell buckling loads for the same in-surface boundary conditions.* Various conclusions can be drawn for the effect of the individual in-surface boundary conditions. First, freeing the edges in the circumferential direction has a tremendous effect for simply supported edge shells (S3 and S4) for unpressurized loading situations (σ_{cr} is about half of σ_{cl}!). For clamped-edge shells, $\delta N_{xy} = 0$ has no effect because results for edge condition C1 are the same as for C3 and for C2 as for C4. Because $\delta N_{xy} = 0$ is not of practical significance, we have still not found the reason for disagreement between theory and experiment—initial geometric imperfections still are the most likely reason for the disagreement. The more reasonable boundary condition $\delta v = 0$ does not lead to the much lower buckling loads generally found in experiments.

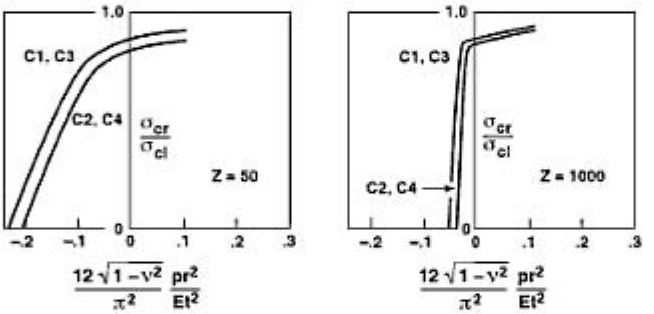
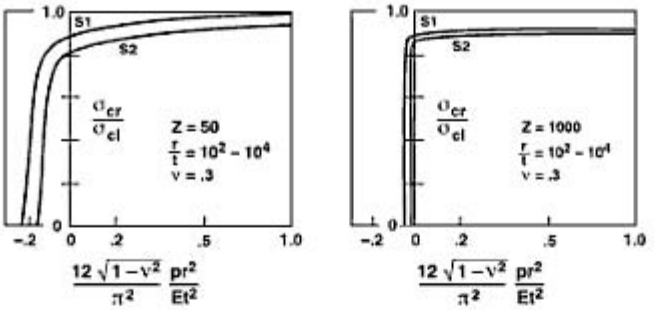


Figure 4-46 Interaction Curves for Clamped-Edge Shells *(After Almroth [4-10])*

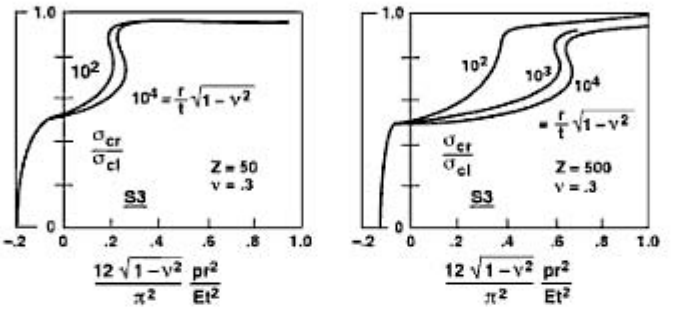
Problem Set 4.5

4.5.1 Derive the equilibrium differential equations, Equations (4.185) and (4.186).
4.5.2 Derive the single equilibrium differential equation, Equation (4.187).
4.5.3 Obtain the solution to the prebuckling equilibrium equation, Equation (4.187), i.e., solve the differential equation to obtain Equation (4.190).
4.5.4 Evaluate the constants of integration in Equation (4.190) for circular cylindrical shells with simply supported edges, i.e., derive Equations (4.192).
4.5.5 Evaluate the constants of integration in Equation (4.190) for circular cylindrical shells with clamped edges, i.e., derive Equations (4.193).
4.5.6 Use the technique of separation of variables, Equation (4.205), to derive the ordinary differential equations that must be solved to determine the buckling load.

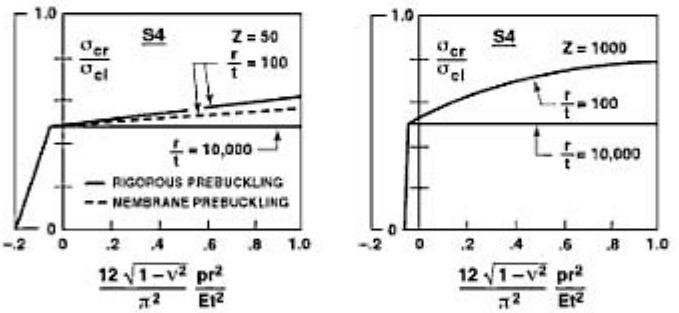
Éléments sous droits d'auteur



a Buckling Interaction Curves for S1 versus S2



b Buckling Interaction Curves for S3



c Buckling Interaction Curves for S4

Figure 4-47 Buckling Interaction Curves for Simply Supported-Edge Shells *(After Almroth [4-10])*

Éléments sous droits d'auteur

4.6 EFFECT OF INITIAL GEOMETRIC IMPERFECTIONS

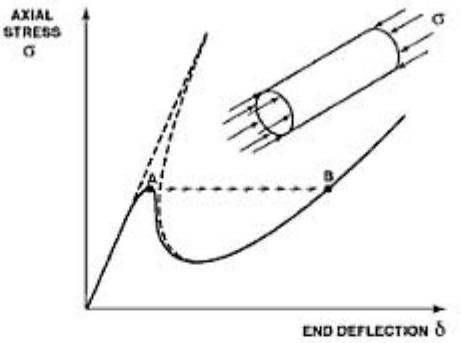


Figure 4-48 Behavior under Axial Load of Imperfect Circular Cylindrical Shells

The sharply peaked stress-(load-)-versus-end-deflection curve depicted with the dashed curve in Figure 4-48 for an axially loaded circular cylindrical shell is generally not realistic because it can occur only for perfectly shaped shells. Actual behavior is more like the schematic representation with a solid line in Figure 4-48 of a shell with surface geometric imperfections, e.g., surface ripples or out-of-roundness caused by inevitable manufacturing errors or variations. Under a constant axial load, the shell will snap through from A to B when the load reaches level A where A is the maximum point on the stress-deflection curve. The value of stress at point A depends on the type and magnitude as well as location of the geometric imperfections.

The quest for the perfect shell to test buckling theories and to understand the buckling process led Tennyson to spin-cast nearly perfect shells of photoelastic plastic [4-41]. Those clamped-edge shells buckled at 10–14% below the classical buckling stress, σ_{cl}, and only a few percent below the rigorous-prebuckling-solution clamped-edge shell buckling stresses calculated by Almroth's approach [4-10]. Recall that the rigorous-prebuckling-solution clamped-edge shell buckling stress is less than the classical buckling stress as noted in Section 4.5. Thus, it is reasonable to conclude that the calculated buckling stresses for perfect shells are probably correct, a fact that is encouraging to know, but not very useful because obviously it is impractical to make perfect shells. Thus, we investigate geometrically imperfect shells as a practical approach.

The importance of initial geometric imperfections for shells was discussed by Donnell in 1934 [4-42]. However, significant numerical results were not obtained until 1950 for axially loaded shells by Donnell and Wan [4-12] and until 1956 for shells under external pressure by Donnell [4-43]. Those numerical results were obtained largely because of the work of von Kármán and Tsien [4-28] who, as noted in Section 4.5 on postbuckling behavior, were the first to demonstrate that equilibrium states other than the prebuckled state exist at stresses below the Euler stress. Their work required Donnell's moderately large-deflection theory [4-42].

The essence of Donnell's approach to the study of initial geometric imperfections is that he assumed the imperfections to be of the same shape as the mode into which the perfect shell buckled. Such geometric imperfections presumably would seem to be the most damaging to the

Éléments sous droits d'auteur

shell. Accordingly, Donnell's approach must lead to an overestimate of the effect of initial geometric imperfections on buckling. That is, using the most damaging kind of geometric imperfections must lead to an upper bound on their effect. Thus, if the shell is to deform into the mode shape used by von Kármán and Tsien [4-28],

$$w = at\left(\cos\frac{m\pi x}{r}\cos\frac{ny}{r} + b\cos\frac{2m\pi x}{r} + c\cos\frac{2ny}{r} + d\right) \qquad (4.206)$$

then the worst-case initial radial geometric imperfection, w_0, is

$$w_0 = a_0 t\left(\cos\frac{m\pi x}{r}\cos\frac{ny}{r} + b\cos\frac{2m\pi x}{r} + c\cos\frac{2ny}{r} + d\right) \qquad (4.207)$$

In this manner, the compatibility equation, which can be shown to be

$$\nabla^4 F = EK(w_{xy}^2 - w_{xx}w_{yy}) - \frac{E}{r}w_{xx} \qquad (4.208)$$

in which $K = 1 + 2w_0/w$, can be solved because K is a constant. It seems obvious that initial geometric imperfections are the most disruptive if they have the same shape as the shape into which the shell is attempting to buckle. However, at the same time, we must realize that such a situation is not very representative of actual geometric imperfections. Moreover, actual geometric imperfections would appear to be extremely difficult to characterize, much less account for in a theoretical approach.

The stress function in Equation (4.208) can be determined by solution of the compatibility equation. Next, the energy of the shell can be found in the manner of Section 4.5 on postbuckling behavior. The coefficients a, b, c, and d in the deflection approximation, Equations (4.206) and (4.207), are then determined by application of the principle of stationary potential energy. Donnell and Wan [4-12] rationalized that the dimensionless coefficient a_0 in the initial geometric imperfection, w_0, should have the form

$$a_0 = \frac{U}{\pi^2}\frac{L_x^{1.5}L_y^{.5}}{t^2} \qquad (4.209)$$

in which U is an unevenness parameter, L_x is the axial buckle half-wave length, and L_y is the circumferential buckle half-wave length. The exponents on the buckle half-wave lengths are somewhat arbitrary (although restricted by dimensional considerations). Stress versus end-deflection results are shown for several values of the unevenness parameter U in Figure 4-49. With small geometric imperfections, a shell tends to buckle quite suddenly from a sharp peak such as seen in Figure 4-49. Obviously, the higher the degree of geometric imperfection, the less susceptible a shell is to buckling in the classical sense. Instead, an imperfect shell merely deforms much more easily than a perfect shell from the time of first loading, i.e., with the application of the smallest amount of load. However, determining a value for U for an actual shell is very difficult. Thus, the practical utility of this approach is severely limited.

For shells subjected to external pressure, the influence of initial geometric imperfections would be expected to be small because the minimum postbuckling stress is quite close to the classical Euler buckling

Éléments sous droits d'auteur

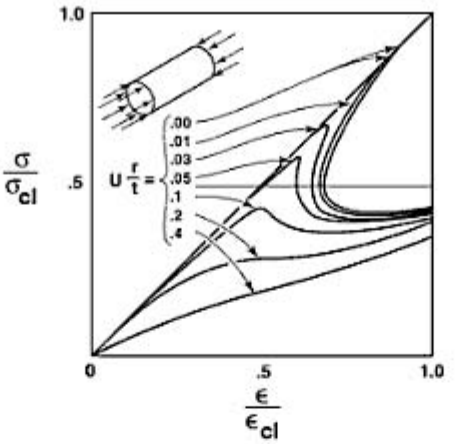


Figure 4-49 Effect of Initial Geometric Imperfections on Behavior of Axially Compressed Imperfect Circular Cylindrical Shells *(After Donnell and Wan [4-12])*

stress as in Figure 4-44 on page 528. Donnell obtained results for circular cylindrical shells with simply supported edges [4-43] and clamped edges [4-44]. He expressed the results in terms of a pressure parameter

$$\bar{p} = \frac{r^{3/2} L p}{t^{5/2} E} \tag{4.210}$$

a volume-change parameter

$$V = \frac{\text{volume decrease}}{(r\,t)^{3/2}} \tag{4.211}$$

and a shell geometry parameter

$$\bar{L} = \frac{L}{\sqrt{r\,t}} \tag{4.212}$$

(the square of Batdorf's curvature parameter Z when $\nu = 0$). The foregoing parameters plus the initial geometric imperfection parameter

$$\frac{Ur}{t} = \frac{\pi^2 a_0 r\,t}{L_x^{3/2} L_y^{1/2}} \tag{4.213}$$

are related to one another in Figure 4-50. There, the pressure parameter is plotted versus the volume-change parameter for four values of the geometry parameter and four values of the initial geometric imperfection parameter. Note that the geometry parameter values 3.1, 5.5, 9.7, and 17.3 correspond to Batdorf curvature values of 9.2, 28.9, 94.8, and 290.5 when $\nu = .3$. Thus, the results in Figure 4-50 are for very short shells through very long shells. The susceptibility of shells to imperfections in-

Éléments sous droits d'auteur

creases as $\bar{L}$ or Z increases. As would be expected, shells with clamped edges buckle at higher pressures than those with simply supported edges (no results are available for simply supported edge shells with $\bar{L} = 17.3$). Moreover, shells with simply supported edges are more susceptible to the effects of geometric imperfections than are shells with clamped edges.

More recent work on the initial geometric imperfection problem includes Koiter's study of the influence of axisymmetric imperfections [4-45] and precise measurement of actual imperfections by Arbocz and Babcock which are described in Section 4.11.5.1 on pages 464–465 [4-46].

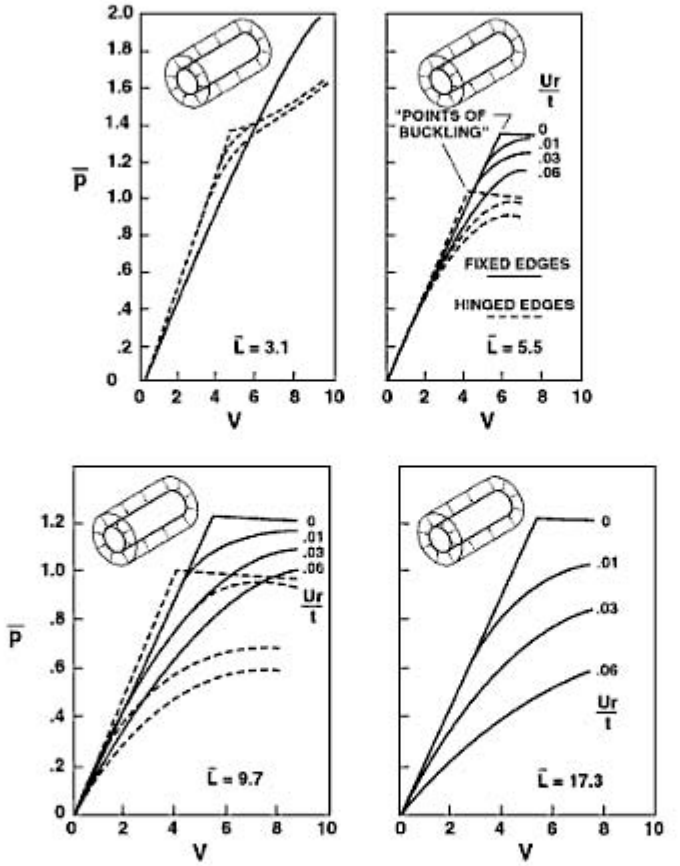


Figure 4-50 Effect of Initial Geometric Imperfections on Behavior of Externally Pressurized Imperfect Circular Cylindrical Shells *(After Donnell [4-44])*

Éléments sous droits d'auteur

The logical extension of work on the influence of initial geometric imperfections on shell buckling must include loadings other than axial compression. For example, both torsional loading and lateral pressure loading have postbuckling equilibrium curves that are much closer to the Euler buckling stress for a perfect shell than is the curve for axial compression loading in Figure 4-48 on page 535. Those two effects are shown in Figures 4-43 and 4-44, respectively, on page 528 and are repeated here in Figures 4-51 and 4-52 along with the load-deformation curves for imperfect shells. Obviously, initial imperfections result in only somewhat lower buckling loads than the Euler buckling load for torsional and lateral pressure loading. Accordingly, the design buckling load for torsional buckling must be reduced about thirty percent from the calculated Euler buckling load. In contrast, the design buckling load for lateral pressure loading can essentially be the (unreduced) Euler buckling load.

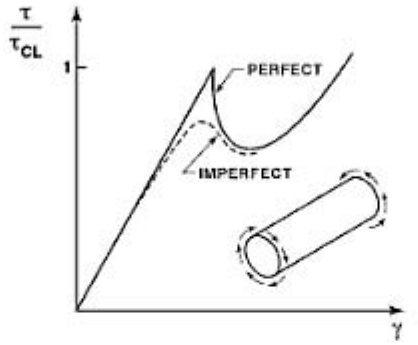


Figure 4-51 Schematic Equilibrium Curves for Perfect and Imperfect Shells under Torsion

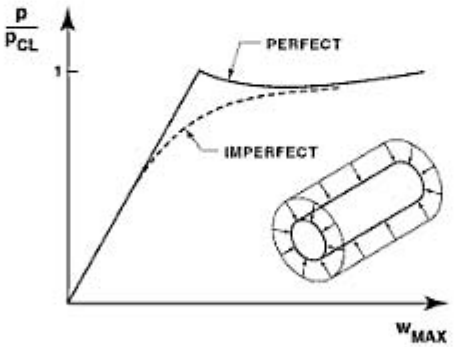


Figure 4-52 Schematic Equilibrium Curves for Perfect and Imperfect Shells under Lateral Pressure

Éléments sous droits d'auteur

4.7 EFFECT OF ECCENTRIC STIFFENERS

4.7.1 Introduction

Stiffeners are fastened to shells (and plates) to give the required design bending and buckling resistance at less weight than shells of uniform thickness, i.e., monocoque shells. Stiffeners also enable the shell to be tailored to the directional nature of the loading environment. For example, rings, also called frames, are added instead of increasing the shell thickness when the predominant loading is external pressure so that unneeded axial stiffness is not provided. Similarly, axial stiffeners (usually called stringers, but sometimes called longerons) are used for predominantly axial compression loading, and both rings and stringers are used for mixing load conditions. Possible stiffener cross sections are depicted in Figure 4-53. The basic objective of the various stiffener shapes is to get as much material as possible as far away as possible from the shell middle surface (i.e., to increase the moment of inertia of the stiffener about its own centroidal axis and to increase the parallel-axis theorem stiffness contributions relative to the shell reference surface).

Stiffeners can be mounted on shells in several different orientations relative to the shell axes. Stiffeners that are mounted in the axial and circumferential directions shown in Figure 4-54 are the most common and will be the prime concern of this section. In Figure 4-54, sections A-A and B-B are used to define the ring spacing a, the stringer spacing b, the distance from the shell middle surface to the ring centroid $\bar{z}_r$ (the ring eccentricity), and the distance from the shell middle surface to the stringer centroid $\bar{z}_s$ (the stringer eccentricity) in addition to the usual shell length, radius, and thickness. Note the use of subscripts r and s to denote ring and stringer, respectively. Spirally oriented or helically oriented stiffeners studied by Soong [4-47] and by Vasiliev et al. [4-48] are depicted in Figure 4-55. Such spiral stiffeners can even be used without a shell in a grid form called a lattice to carry very high axial loads as in a missile interstage structure. That and other applications of lattice structures are surveyed by Vasiliev, Barynin, and Rasin [4-49].

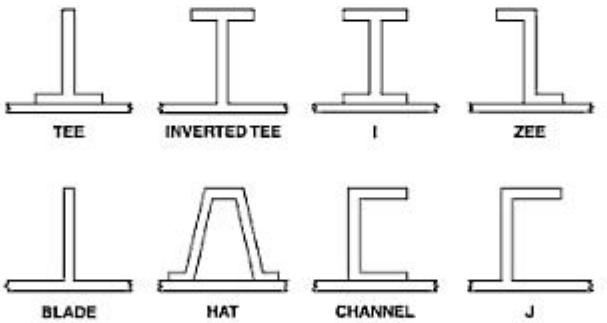


Figure 4-53 Typical Stiffener Cross Sections

Éléments sous droits d'auteur

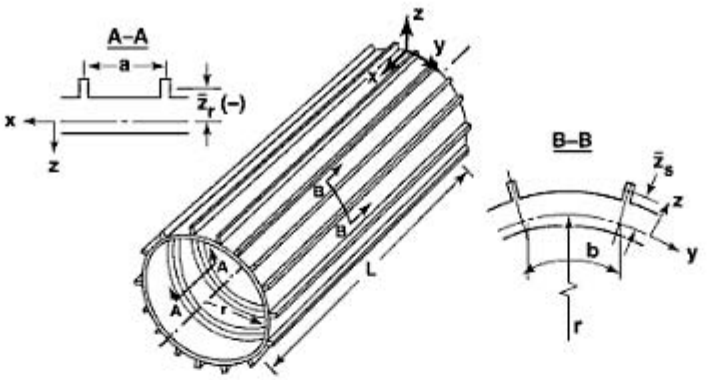


Figure 4-54 Orthogonally Stiffened Circular Cylindrical Shell

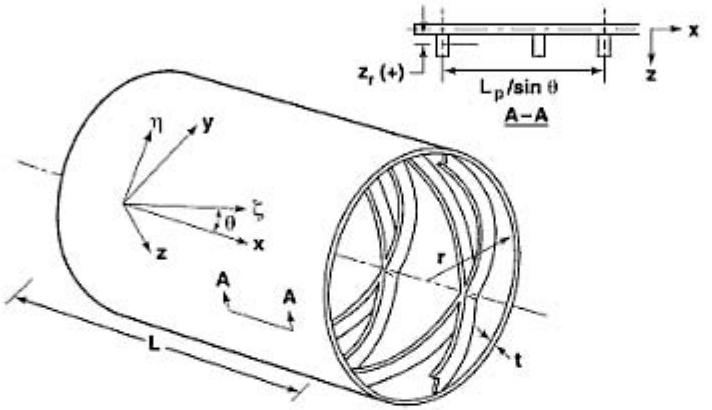


Figure 4-55 Helically Stiffened Circular Cylindrical Shell

For many years, the buckling resistance of stiffened shells was calculated without consideration of whether the stiffeners were located on the inside or outside surface of the shell. That is, the asymmetric or eccentric location of the stiffeners relative to the shell reference surface was ignored (except for the absolute value of the eccentricity in calculation of the stiffened shell bending stiffnesses). Actually, the bending stiffness of the stiffened shell was calculated about an axis through the centroid of a stiffened shell segment centered about one stiffener as shown in Figure 4-56. That bending stiffness was then used as the middle surface stiffness in an orthotropic stiffness shell buckling theory (orthotropy is required to treat different amounts of stiffening in different directions). Thus, no account was taken of the inherent stiffener eccentricity (the sign of $\bar{z}_r$ or $\bar{z}_s$ in Figure 4-54 nor was any account taken of the essentially uniaxial character of the stiffeners.

Éléments sous droits d'auteur

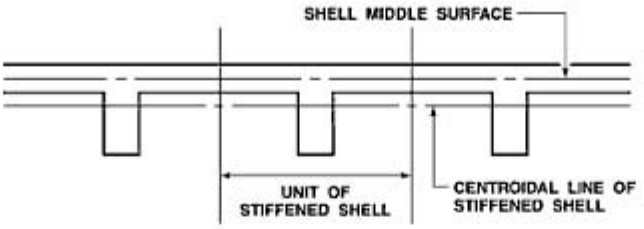


Figure 4-56 Stiffened Shell Segment Geometry

In 1947, van der Neut [4-50] discovered a striking difference of up to a factor of three between the theoretical buckling loads for internally versus externally stiffened shells under axial compression. However, this fact did not become well known and verified by experiments until the early 1960s. Then, important theoretical work on stiffened shells was performed by Baruch and Singer [4-51], Hedgepeth and Hall [4-52], Block, Card, and Mikulas [4-53], and McElman, Mikulas, and Stein [4-54]. The first definitive experiments were performed by Card [4-55] and were compared with theoretical predictions by Card and Jones [4-25]. The effect of initial geometric imperfections was considered by Hutchinson and Amazigo [4-56]. Block [4-57] treated discrete ring spacing, prebuckling deformation, and load eccentricity. Finally, plastic buckling was discussed by Jones [4-58] and is described in Section 4.10.

A derivation of the governing buckling differential equations and solutions for a set of simply supported edge boundary conditions and a set of clamped-edge boundary conditions will be studied along with comparison to the pertinent experiments. Several new problem-solving characteristics are presented in addition to the 'new' physical phenomenon of coupling between bending and extension (this phenomenon also occurs for laminates of different materials such as the common household thermostat and for laminated fiber-reinforced structural elements).

4.7.2 Derivation of Buckling Criterion

Classical Euler buckling theory, by which is implied a membrane prebuckled shape, is applied for the eccentrically stiffened circular cylindrical shell in Figure 4-54. We first use the stress-strain relations to find the variations in stresses that arise during buckling. Then, we integrate those variations in stresses to get the variations in forces and moments during buckling. Both the essentially uniaxial character of the stiffeners and their eccentricity in placement relative to the shell middle surface are accounted for in the manner of Block, Card, and Mikulas [4-53] and McElman, Mikulas, and Stein [4-54]. Next, the variations in forces and moments are substituted in the Donnell-type shell buckling equations to get the buckling differential equations. The buckling differential equations, in turn, are solved exactly to get a buckling criterion (characteristic equation) for S2 simply supported edge buckling boundary conditions. A similar solution for C1 clamped-edge buckling boundary conditions is obtained in the manner of Section 4.3.4.

Éléments sous droits d'auteur

4.7.2.1 Variation of Stresses and Strains during Buckling

The first step in the derivation of the buckling criterion is to establish the stress-strain relations:

$$\begin{aligned}\sigma_x &= \frac{E}{1-\nu^2}(\varepsilon_x + \nu\varepsilon_y)\\ \sigma_y &= \frac{E}{1-\nu^2}(\varepsilon_y + \nu\varepsilon_x)\\ \tau_{xy} &= \frac{E}{2(1+\nu)}\gamma_{xy}\end{aligned} \tag{4.214}$$

Then, during buckling, the stresses take variations

$$\begin{aligned}\delta\sigma_x &= \frac{E}{1-\nu^2}(\delta\varepsilon_x + \nu\delta\varepsilon_y)\\ \delta\sigma_y &= \frac{E}{1-\nu^2}(\delta\varepsilon_y + \nu\delta\varepsilon_x)\\ \delta\tau_{xy} &= \frac{E}{2(1+\nu)}\delta\gamma_{xy}\end{aligned} \tag{4.215}$$

in which $\delta\varepsilon_x$, $\delta\varepsilon_y$, and $\delta\gamma_{xy}$ denote the corresponding variations in the strains and, because of the Kirchhoff-Love hypothesis [4-4], are

$$\begin{aligned}\delta\varepsilon_x &= \delta\varepsilon_x^{\circ} + z\delta\kappa_x\\ \delta\varepsilon_y &= \delta\varepsilon_y^{\circ} + z\delta\kappa_x\\ \delta\gamma_{xy} &= \delta\gamma_{xy}^{\circ} + z\delta\kappa_{xy}\end{aligned} \tag{4.216}$$

in which z is the distance from the shell middle surface, $\delta\varepsilon_x^{\circ}$, $\delta\varepsilon_y^{\circ}$, and $\delta\gamma_{xy}^{\circ}$ are the variations of the middle-surface strains

$$\begin{aligned}\delta\varepsilon_x^{\circ} &= \delta u_{,x}\\ \delta\varepsilon_y^{\circ} &= \delta v_{,y} + \delta w/r\\ \delta\gamma_{xy}^{\circ} &= \delta u_{,y} + \delta v_{,x}\end{aligned} \tag{4.217}$$

and $\delta\kappa_x$, $\delta\kappa_y$, and $\delta\kappa_{xy}$ are the variations of the middle-surface curvatures

$$\begin{aligned}\delta\kappa_x &= -\delta w_{,xx}\\ \delta\kappa_y &= -\delta w_{,yy}\\ \delta\kappa_{xy} &= -2\delta w_{,xy}\end{aligned} \tag{4.218}$$

Thus, the variations of stresses can be written as

$$\begin{aligned}\delta\sigma_x &= \frac{E}{1-\nu^2}\left[(\delta\varepsilon_x^{\circ} + z\delta\kappa_x) + \nu(\delta\varepsilon_y^{\circ} + z\delta\kappa_y)\right]\\ \delta\sigma_y &= \frac{E}{1-\nu^2}\left[(\delta\varepsilon_y^{\circ} + z\delta\kappa_y) + \nu(\delta\varepsilon_x^{\circ} + z\delta\kappa_x)\right]\\ \delta\tau_{xy} &= \frac{E}{2(1+\nu)}(\delta\gamma_{xy}^{\circ} + z\delta\kappa_{xy})\end{aligned} \tag{4.219}$$

Éléments sous droits d'auteur

4.7.2.2 Variation of Forces and Moments during Buckling

The variations of the forces and moments can be obtained by integrating the biaxial stress variations in Equation (4.219) through the shell thickness and by integrating the uniaxial stress variations

$$\delta\sigma_x = E_s\delta\varepsilon_x \qquad \delta\sigma_y = E_r\delta\varepsilon_y \tag{4.220}$$

over the stiffeners as follows:

$$\begin{aligned}
\delta N_x &= \int_{-t/2}^{t/2} \delta\sigma_x\, dz + \frac{1}{b}\int_{A_s} \delta\sigma_x\, dA_s \\
\delta N_y &= \int_{-t/2}^{t/2} \delta\sigma_y\, dz + \frac{1}{a}\int_{A_r} \delta\sigma_y\, dA_r \\
\delta N_{xy} &= \int_{-t/2}^{t/2} \delta\tau_{xy}\, dz
\end{aligned} \tag{4.221}$$

$$\begin{aligned}
\delta M_x &= \int_{-t/2}^{t/2} \delta\sigma_x\, z\, dz + \frac{1}{b}\int_{A_s} \delta\sigma_x\, z\, dA_s \\
\delta M_y &= \int_{-t/2}^{t/2} \delta\sigma_y\, z\, dz + \frac{1}{a}\int_{A_r} \delta\sigma_y\, z\, dA_r \\
\delta M_{xy} &= -\int_{-t/2}^{t/2} \delta\tau_{xy}\, z\, dz - \frac{G_sJ_s}{2b}\delta\kappa_{xy} \\
\delta M_{yx} &= \int_{-t/2}^{t/2} \delta\tau_{xy}\, z\, dz + \frac{G_rJ_r}{2a}\delta\kappa_{xy}
\end{aligned} \tag{4.222}$$

in which the stiffener effects are averaged or 'smeared out' over the respective stiffener spacing (no discrete stiffener effects are treated). The indicated integrations lead to

$$\begin{aligned}
\delta N_x &= (A + E_sA_s/b)\delta\varepsilon_x^\circ + \nu A\delta\varepsilon_y^\circ + (\bar{z}_sE_sA_s/b)\delta\kappa_x \\
\delta N_y &= \nu A\delta\varepsilon_x^\circ + (A + E_rA_r/a)\delta\varepsilon_y^\circ + (\bar{z}_rE_rA_r/a)\delta\kappa_y \\
\delta N_{xy} &= \frac{1-\nu}{2} D\delta\gamma_{xy}^\circ
\end{aligned} \tag{4.223}$$

$$\begin{aligned}
\delta M_x &= (\bar{z}_sE_sA_s/b)\delta\varepsilon_x^\circ + (D + \bar{z}_s^2E_sA_s/b + E_sI_s/b)\delta\kappa_x + \nu D\delta\kappa_y \\
\delta M_y &= (\bar{z}_rE_rA_r/a)\delta\varepsilon_y^\circ + \nu D\delta\kappa_x + (D + \bar{z}_r^2E_rA_r/a + E_rI_r/a)\delta\kappa_y \\
\delta M_{xy} &= -\left[\frac{1-\nu}{2} D + G_sJ_s/2b\right]\delta\kappa_{xy} \\
\delta M_{yx} &= \left[\frac{1-\nu}{2} D + G_rJ_r/2a\right]\delta\kappa_{xy}
\end{aligned} \tag{4.224}$$

in which we note that bending-extension coupling from the eccentric stiffeners exists by virtue of the appearance of variations of curvatures

Éléments sous droits d'auteur

in the force terms and variations of strains in the moment terms. Also, the shell extensional and bending stiffnesses, respectively, are

$$A = \frac{Et}{1-\nu^2} \qquad D = \frac{Et^3}{12(1-\nu^2)} \tag{4.225}$$

4.7.2.3 Buckling Differential Equations

The Donnell-type shell buckling differential equations for combinations of axial compression and lateral pressure from Equations (4.71)–(4.73) on page 487 with an alternative formulation involving both variations in twisting moments, δM_{xy} and δM_{yx}, can be written as

$$\begin{aligned}
&\delta N_{x,x} + \delta N_{xy,y} = 0 \\
&\delta N_{xy,x} + \delta N_{y,y} = 0 \\
&-\delta M_{x,xx} + \delta M_{xy,xy} - \delta M_{yx,xy} - \delta M_{y,yy} + \delta N_y/r + \bar{N}_x \delta w_{,xx} + \bar{N}_y \delta w_{,yy} = 0
\end{aligned} \tag{4.226}$$

Upon substitution of the variations in forces and moments, the buckling differential equations in terms of buckling displacements become

$$\begin{aligned}
&(A + E_s A_s/b)\delta u_{,xx} + \nu A(\delta v_{,xy} + \delta w_{,x}/r) \\
&\quad + \frac{1-\nu}{2} A(\delta u_{,yy} + \delta v_{,xy}) - (\bar{z}_s E_s A_s/b)\delta w_{,xxx} = 0 \\
&\nu A \delta u_{,xy} + (A + E_r A_r/a)(\delta v_{,yy} + \delta w_{,y}/r) \\
&\quad + \frac{1-\nu}{2} A(\delta u_{,xy} + \delta v_{,xx}) - (\bar{z}_r E_r A_r/a)\delta w_{,yyy} = 0 \\
&(\nu A/r)\delta u_{,x} - (\bar{z}_s E_s A_s/b)\delta u_{,xxx} + (1/r)(A + E_r A_r/a)(\delta v_{,y} + \delta w/r) \\
&\quad + (\bar{z}_r E_r A_r/a)\delta v_{,yyy} + (2/r)(\bar{z}_r E_r A_r/a)\delta w_{,yy} \\
&\quad + (D + \bar{z}_s^2 E_s A_s/b + E_s I_s/b)\delta w_{,xxxx} + (2D + G_s J_s/b + G_r J_r/a)\delta w_{,xxyy} \\
&\quad + (D + \bar{z}_r^2 E_r A_r/a + E_r I_r/a)\delta w_{,yyyy} + \bar{N}_x \delta w_{,xx} + \bar{N}_y \delta w_{,yy} = 0
\end{aligned} \tag{4.227}$$

4.7.2.4 Buckling Criterion

An exact solution to the buckling differential equations can be obtained for the S2 buckling boundary conditions in Equation (4.63) on page 484, i.e., $\delta N_x = \delta v = \delta w = \delta M_x = 0$, by use of the buckling displacements

$$\begin{aligned}
\delta u &= \tilde{u} \cos\frac{m\pi x}{L} \cos\frac{ny}{r} \\
\delta v &= \tilde{v} \sin\frac{m\pi x}{L} \sin\frac{ny}{r} \\
\delta w &= \tilde{w} \sin\frac{m\pi x}{L} \cos\frac{ny}{r}
\end{aligned} \tag{4.228}$$

(or equivalently δu, δv, and δw could be cosine-sine, sine-cosine, and sine-sine functions, respectively, if the coordinates are rotated 90°) in which $\tilde{u}$, $\tilde{v}$, and $\tilde{w}$ are the (indeterminate) amplitudes of the buckling displacements. If the buckling displacements in Equation (4.228) are

Éléments sous droits d'auteur

substituted in the buckling differential equations, Equation (4.227), a homogeneous set of equations in $\tilde{u}$, $\tilde{v}$, and $\tilde{w}$ results. In order that a nontrivial solution for $\tilde{u}$, $\tilde{v}$, and $\tilde{w}$ exist, the determinant of the coefficients of $\tilde{u}$, $\tilde{v}$, and $\tilde{w}$ must be zero, and the following buckling criterion results:

$$\bar{N}_x\left[\frac{m\pi}{L}\right]^2 + \bar{N}_y\left[\frac{n}{r}\right]^2 = T_{33} + \frac{2T_{12}T_{13}T_{23} - T_{11}T_{23}^2 - T_{22}T_{13}^2}{T_{11}T_{22} - T_{12}^2} \tag{4.229}$$

in which

$$\begin{aligned}
T_{11} &= (A + E_sA_s/b)(m\pi/L)^2 + \frac{1-\nu}{2}A(n/r)^2 \\
T_{12} &= \frac{1+\nu}{2}A(m\pi/L)(n/r) \\
T_{13} &= (\nu A/r)(m\pi/L) + (z_sE_sA_s/b)(m\pi/L)^3 \\
T_{23} &= (1/r)(A + E_rA_r/a)(n/r) + (z_rE_rA_r/a)(n/r)^3 \\
T_{22} &= \frac{1-\nu}{2}A(m\pi/L)^2 + (A + E_rA_r/a)(n/r)^2 \\
T_{33} &= (D + E_sI_s/b + \bar{z}_s^2E_sA_s/b)(m\pi/L)^4 + (2D + G_sJ_s/b + G_rJ_r/a)(m\pi/L)^2(n/r)^2 \\
&\quad + (D + E_rA_r/a + \bar{z}_r^2E_rA_r/a)(n/r)^4 + (2/r)(\bar{z}_rE_rA_r/a)(n/r)^2 + (1/r^2)(A + E_rA_r/a)
\end{aligned} \tag{4.230}$$

and I is the moment of inertia of a stiffener about its centroidal axis that is parallel to the shell surface, A with a subscript is the area of a stiffener, and r and s subscripts denote ring and stringer, respectively. In addition, J is the torsional constant for a stiffener cross section.

The applied in-surface forces, $\bar{N}_x$ and $\bar{N}_y$, can be related to a positive number λ according to

$$\bar{N}_x = k_1\lambda \qquad \bar{N}_y = k_2\lambda \tag{4.231}$$

Then, the left-hand side of Equation (4.229) can be written as

$$\bar{N}_x\left[\frac{m\pi}{L}\right]^2 + \bar{N}_y\left[\frac{n}{r}\right]^2 = \lambda\left[k_1\left[\frac{m\pi}{L}\right]^2 + k_2\left[\frac{n}{r}\right]^2\right] \tag{4.232}$$

The special loading cases of axial compression, lateral pressure, and hydrostatic pressure are obtained with $k_1 = -1$, $k_2 = 0$; $k_1 = 0$, $k_2 = -1$; and $k_1 = -1/2$, $k_2 = -1$, respectively. More general cases of biaxial loading are obtained by specifying other values of k_1 and k_2 including cases in which one of k_1 or k_2 is positive (thereby inducing tensile forces that inhibit buckling).

For the special case of a shell with stringers only, T_{12}, T_{22}, and T_{23} in Equation (4.230) are functions of the properties of the shell itself (without stringers). For a positive $\bar{z}_s$ (external stringers) in Equation (4.230), T_{13} is larger in the positive sense than for a negative $\bar{z}_s$ (internal stringers). Then, in Equation (4.229), the term $2T_{12}T_{13}T_{23}$ is larger and the term $T_{22}T_{13}^2$ is larger (but it is always negative). The denominator in Equation (4.229) is constant irrespective of stringer location. The term T_{33} (as are T_{11}, T_{12}, and T_{22}) remains constant irrespective of stiffener placement (as long as the stiffener eccentricities are equal in absolute

Éléments sous droits d'auteur

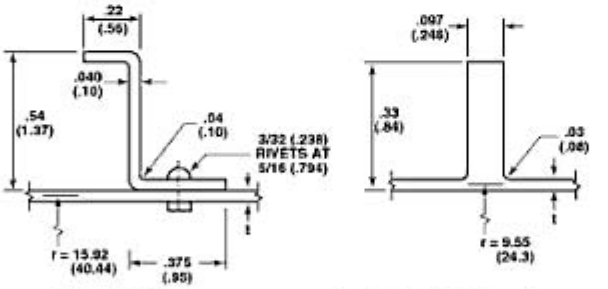
value). Even with the foregoing relative value assessments, the net effect on the buckling load is not obvious without some rather messy algebra or numerical results. The final result is that the term $2T_{12}T_{13}T_{23}$ is always greater than the term $T_{22}T_{13}^2$, so $\bar{N}_x$ is greater for external stringers than for internal stringers.

The solution of the buckling criterion for simply supported edge buckling boundary condition S2, Equation (4.409), was obtained by Block, Card, and Mikulas [4-53]. The absolute minimum buckling load for a specified range of discrete values of the buckling mode parameters m and n is found by the minimization procedure due to Jones [4-59]. See Appendix B for a generic description of a search procedure for how to find the absolute minimum buckling load for some range of integer values of m and n.

The buckling criterion for clamped-edge boundary condition C1 on an eccentrically stiffened shell was solved by Card and Jones [4-25] in the manner of Section 4.3.3 with appropriate stiffener terms added. That is, the same buckling displacements, Equation (4.155), lead to buckling differential equations similar to Equations (4.157–4.159). The same numerical solution procedure using the generalized Galerkin procedure [4-18] leads to the numerical results in the following sub-section.

4.7.3 Numerical and Experimental Results

Twelve longitudinally stiffened shells were made and loaded to buckling. Four specimens of about 9.55-in (24.26-cm) radius and about .0279-in (.0709-cm) thickness employed integral rectangular cross-section stiffeners of width .097 in (.246 cm) and height .302 in (.767 cm) spaced at 1.00 in (2.54 cm). The material is 2024-T351 aluminum with $E = 10.5 \times 10^6$ psi (72,400 MPa) and $\nu = .32$. Eight specimens of about 15.92-in (40.44-cm) radius and about .0399-in (.1013-cm) thickness had z cross-section stiffeners that were riveted to the shells. The z-stiffener dimensions are shown in Figure 4-57. The material is 7075-T6 aluminum with $E = 10.5 \times 10^6$ psi (72,400 MPa) and $\nu = .32$.



a Riveted Z-Stiffener

b Integral Rectangular Cross-Section Stiffener

Figure 4-57 Stiffener Cross Sections with Dimensions in in (cm) *(After Card and Jones [4-25])*

Éléments sous droits d'auteur

Both types of shell were made flat, wrapped into a circular cylindrical shape, and fastened with riveted doubler plates. All specimens were designed with stiffeners that are closely spaced in the circumferential direction to preclude local buckling of the shells. The shell ends were potted in a soft low-temperature alloy and then ground flat to ensure uniform bearing of the shell ends on the load-frame platens. Further construction details are given by Card and Jones [4-25].

A typical buckling mode for a shell with externally mounted integral stiffeners is shown in Figure 4-58. Note the staggered rows of inward-deforming diamond-shaped buckles, the flat bearing on the bottom load-frame platen, and the device for measuring end shortening under load.



Figure 4-58 Buckled Integrally Stiffened Circular Cylindrical Shell *(After Card and Jones [4-25])*

Numerical results for the S2 simply supported edge buckling boundary conditions are shown along with a clamped-edge solution and experimental results for integrally stiffened and Z-stiffened shells in Figures 4-59 and 4-60. The solution of the buckling differential equations, Equation (4.227), for C1 clamped-edge buckling boundary conditions was obtained by Card and Jones [4-25] in the manner of Section 4.3.4 with, of course, stiffener terms added. Note that the two buckling boundary conditions, C1 and S2, bound the experimental results from above and below, respectively. This situation should be expected for experimental conditions of soft-metal-potted edges that are not completely fixed nor obviously are they simply supported. The experimental results range from 70 to 100% of the theoretical values for stiffened shells with clamped edges. Furthermore, the ratio of the buckling load for externally stiffened shells to that for internally stiffened shells is about two for all length-to-radius ratios examined in Figure 4-61, both by theoretical prediction and experimental verification. Thus, a simple theory is readily available for prediction of the important stiffening effects.

Éléments sous droits d'auteur

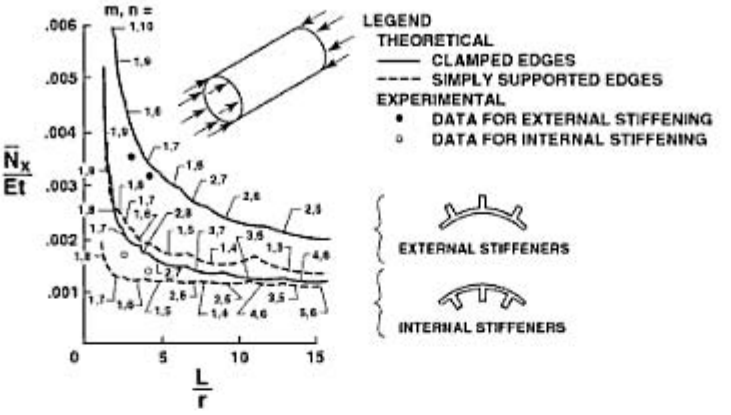


Figure 4-59 Buckling of Integrally Stiffened Circular Cylindrical Shells under Axial Compression *(After Card and Jones [4-25])*

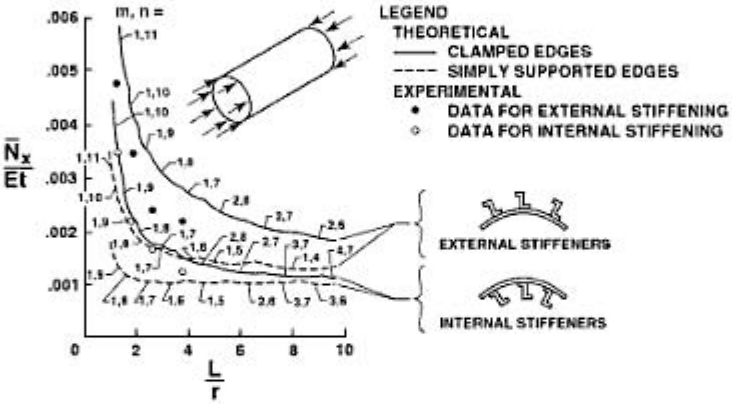


Figure 4-60 Buckling of Z-stiffened Circular Cylindrical Shells under Axial Compression *(After Card and Jones [4-25])*

Note that the experimental results for internally z-stiffened shells are much closer to the clamped-edge solution than are externally z-stiffened shells in Figure 4-61. This observation might be explained with the following three-step logic: (1) the z-stiffener protrudes a substantial distance from the basic shell, (2) shells always tend to buckle *inward*, not outward, (3) thus, internally placed z-stiffeners would tend to restrain the buckling deformation by fully contacting the loading platens of the load frame as in the left-hand side of Figure 4-62. In contrast, externally placed z-stiff-

Éléments sous droits d'auteur

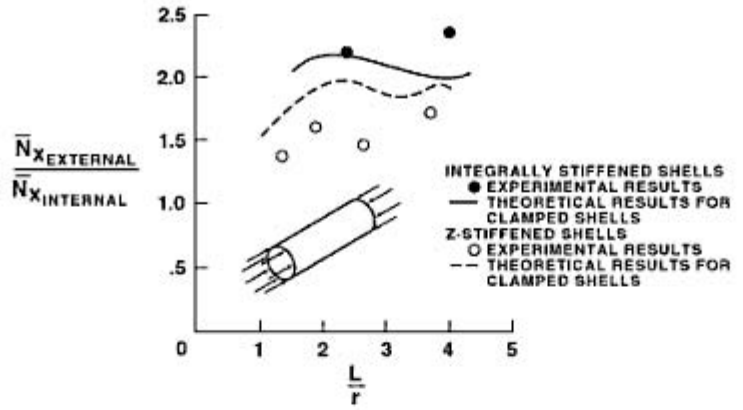


Figure 4-61 Effect of Stiffener Eccentricity on Axial Compression Buckling Load *(After Card and Jones [4-25])*

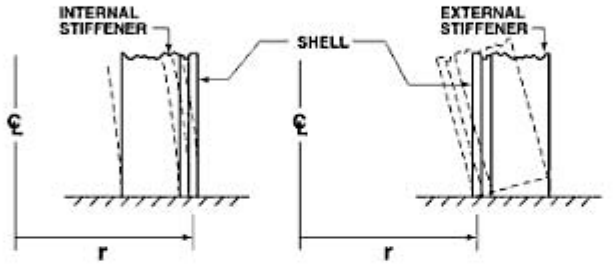


Figure 4-62 Different Restraint Mechanisms for Internally and Externally Stiffened Shells

eners would provide no such restraint because their outside edge would tend to lift off the loading platens, and thus the external stiffener would rotate away from contact as in the right-hand side of Figure 4-62. This effect does not appear to exist for the integrally stiffened shells perhaps because the stiffener protrusion from the basic shell is too small to activate the aforementioned edge support mechanism.

4.7.4 The Stiffener Eccentricity Effect

A simplistic explanation of the physical reasons for the stiffener eccentricity effect involves portions of stiffened shells. As loads are introduced in the shells, interaction between the shell and the stiffeners has two kinds of effects on buckling: (1) the direct effect and (2) the Poisson effect. We merely look at the forces acting *from* the shell *on* the stiffener caused by the necessary deformations of the shell from the applied load.

Éléments sous droits d'auteur

In the direct effect, the stiffeners are aligned with the principal loading as depicted in Figure 4-63. Shear forces are induced along the surface between the shell and stiffener because of the tendency of the shell to contract in the direction of the load. These shear forces are applied from the shell to the bottom of the stiffeners (hence, eccentrically relative to the stiffener centroid) causing bending of the stiffeners away from the shell, as well as contraction. The shear forces are shown on a curved line that is projected downward from the bottom of the stiffener in Figure 4-63. For deformation compatibility of the two structural elements, the shell must bend toward the stiffeners. Thus, because all shells tend to buckle inward toward the shell axis, externally stringer-stiffened shells have higher buckling resistance under axial compression than internally stringer-stiffened shells. This result was verified both theoretically and experimentally in the foregoing sub-section. Similar reasoning leads to the conclusion that, for ring-stiffened circular cylindrical shells under lateral pressure, shells with external rings have higher buckling resistance than shells with internal rings.

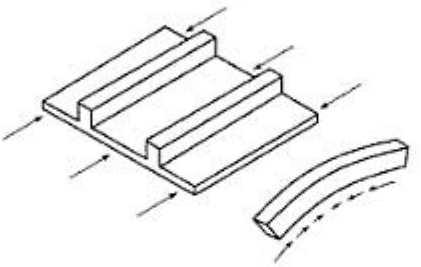


Figure 4-63 Direct Effect for Stiffened Shells

In the Poisson effect, the stiffeners are perpendicular to the principal loading as depicted in Figure 4-64. Shear forces are developed along the stiffener because of the expansion of the shell perpendicular to the applied compressive load (hence, the name Poisson effect). These shear forces are applied from the shell to the bottom of the stiffeners (hence, eccentrically relative to the stiffener centroid) causing bending of the stiffeners toward the shell as well as extension. As in the direct effect, the shear forces are shown on a curved line that is projected downward from the bottom of the stiffener in Figure 4-64. For deformation compatibility of the two structural elements, the shell must bend away from the stiffeners. Thus, the stiffened shell must bend away from the stiffeners. Accordingly, when the Poisson effect governs, internal stiffeners provide more buckling resistance than external stiffeners. Apparently, ring-stiffened shells under axial compression have more buckling resistance with internal rings than with external rings. Similarly, internal stringers provide more buckling resistance than external stringers for stringer-stiffened shells under lateral pressure.

Éléments sous droits d'auteur

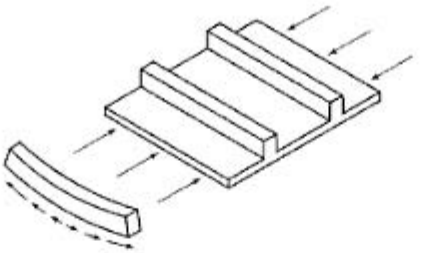


Figure 4-64 Poisson Effect for Stiffened Shells

Whether the direct effect or the Poisson effect dominates depends on the shell geometry and type of loading. For the uniaxial loadings discussed in the preceding paragraphs, the conclusions are clear. However, for biaxial loading such as hydrostatic pressure on ring-stiffened shells, ranges of geometry exist for which external rings provide more buckling resistance than internal rings and still other ranges in which the opposite is true as in Figure 4-65. There, the results for many ring-stiffened shells are depicted schematically with a range over which the basic conclusion about stiffener effectiveness changes. For high values of Z, the lateral pressure component of hydrostatic pressure dominates the loading as in Figure 4-66. Thus, the direct effect governs, and external rings provide more buckling resistance than internal rings. However, for low values of Z, the axial compression component of hydrostatic pressure dominates the loading as in Figure 4-66. Thus, the Poisson effect governs, and internal rings provide more buckling resistance than external rings. Accordingly, for a specific shell and loading, a brief parametric study is necessary to determine the most effective stiffener placement.

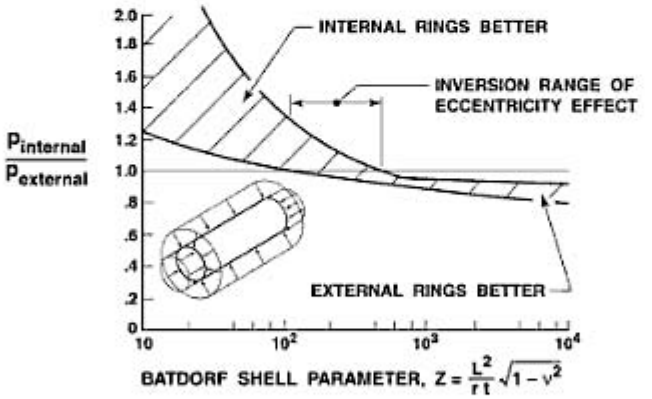


Figure 4-65 Inversion of the Stiffener Eccentricity Effect for Ring-Stiffened Circular Cylindrical Shells under Hydrostatic Pressure *(After Singer, Baruch, and Harari [4-161])*

Éléments sous droits d'auteur

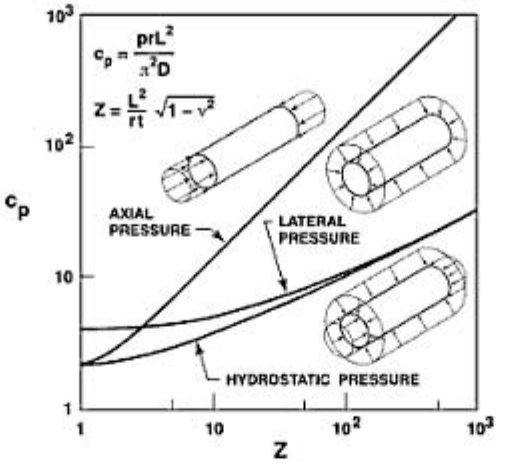


Figure 4-66 Buckling of Circular Cylindrical Shells under Axial, Lateral, and Hydrostatic Pressure *(After Batdorf [4-2])*

Two other significant points for buckling of stiffened shells involve the torsional stiffness of the stiffeners and the definitions of panel and general instability. First, Card and Jones [4-25] noted that the buckling loads in Figure 4-59 and 4-60 were about ten to twenty percent lower if the stiffener torsional stiffness G_sJ_s is ignored. Thus, the torsional stiffness term must be retained in stiffened shell theory. The other important aspect of stiffened shell theory and design is the distinction between panel and general instability.

Panel instability is defined as buckling between rings (or stringers) in which the stiffeners do not participate, even to the point of twisting (remember the torsional stiffness) as in Figure 4-67. The prediction of panel instability is usually accomplished by use of monocoque shell theory for a shell segment as long as the ring spacing (or as wide as the stringer spacing) with appropriate edge boundary conditions.



PANEL INSTABILITY



GENERAL INSTABILITY

Figure 4-67 Panel and General Instability of a Longitudinal Section of a Ring-Stiffened Circular Cylindrical Shell

Éléments sous droits d'auteur

General instability is defined as buckling in which some or all of the stiffeners participate (i.e., twist and/or deflect) as in Figure 4-67. Naturally, general instability predictions require the use of stiffened shell theory. If the rings are not closely spaced, then discrete ring theory such as Block's [4-57] must be used instead of the smeared-out ring stiffnesses used in the foregoing derivation.

The usual objective in designing a ring-stiffened shell is to make the panel instability buckling load approximately equal to the general instability buckling load. In this manner, a so-called balanced design is obtained with apparently maximum efficiency of material usage. Obviously, such an objective might be difficult to achieve.

4.7.5 Summary

The stiffener eccentricity effect actually does exist as seen from experimental results and can be predicted well, as has been confirmed by comparison of theoretical and experimental results. The influence of edge clamping is apparently quite significant from observation of the measured behavior, as is the importance of stiffener torsional stiffness in the calculated buckling loads. To obtain the highest buckling load of orthogonally stiffened circular cylindrical shells under axial compression, the stiffeners in the load direction must be placed on the outside of the shell and those stiffeners perpendicular to the load direction must be placed on the inside of the shell. For biaxial loading or nonorthogonally stiffened shells, a brief parametric study is necessary to determine the optimum placement (internal or external) of the stiffeners from the point of view of maximum buckling resistance. Apparently, prebuckling deformations and initial geometric imperfections do not play a significant role in the buckling of eccentrically stiffened circular cylindrical shells, even under axial compression. That is, Euler buckling loads with a membrane prebuckled state seem to be quite representative of actual shell behavior, unlike unstiffened shells. Suppose the stiffener placement must be fixed for specific design reasons. For example, on a missile, all stiffeners must be placed internally to avoid the obvious aerodynamic drag associated with external stiffeners. Then, the present approach still leads to more accurate analyses than were possible with previous approaches. The stiffener eccentricity effect is an example of coupling between bending and extension of a structural element such as occurs for the ordinary bonded bimetallic strip used as a household thermostat (the two metals have different coefficients of thermal expansion, so they bend when heated or cooled instead of merely expanding or contracting). Coupling between bending and extension was examined for laminated plates in Section 3.6 and is studied for laminated shells in the next section.

Problem Set 4.7

4.7.1 Verify that the variations in forces and moments in Equations (4.223) and (4.224), respectively, are correct.

4.7.2 Verify that the buckling differential equations in terms of variations in displacements, Equations (4.227), are correct.

4.7.3 Verify that the variations in displacements in Equation (4.228) satisfy the S2 buckling boundary conditions and the governing buckling differential equations, Equations (4.227), i.e., derive the buckling criterion in Equation (4.229).

Éléments sous droits d'auteur

4.8 EFFECT OF MULTIPLE FIBER-REINFORCED LAYERS

4.8.1 Introduction

The contemporary topic of structures made with laminated fiber-reinforced composite materials cannot escape attention. This field has grown explosively since 1960. Cross-ply laminated circular cylindrical shells as in Figure 4-68 are sometimes found in the aerospace industry, although angle-ply shells are far more common. The advent of advanced fiber-reinforced materials such as graphite-epoxy with their high weight savings because of their high stiffness-to-weight and strength-to-weight ratios has resulted in a significant increase in the use of laminated shells. Therefore, general knowledge of their behavior sheds light on the behavior of more complex laminates such as angle-plys and laminates of mixed laminae orientations. See Appendix C for an introduction to the mechanics of composite materials and Jones [4-60].

An important step in learning how to properly laminate shells is to understand the influence of lamination asymmetries about the shell middle surface. Those asymmmetries cause coupling between bending and extension of the laminate. This phenomenon is evidenced by *bending* of a laminate that is subjected to only in-plane or in-surface forces or *extension* of a laminate that is bent by the application of moments alone. Another example is bending of a laminate that is subjected to a uniform temperature rise; this is the principle by which the common household thermostat works, i.e., an ordinary bonded bimetallic strip in which the two metals have different coefficients of thermal expansion, so they bend when heated or cooled instead of merely expanding or contracting. For unsymmetrically laminated plates, the coupling results in significantly decreased buckling loads (see Section 3.6 and Jones [4-60]). Bending effects for symmetrically laminated plates are uncoupled from extensional effects. In contrast, for symmetrically laminated or even isotropic shells, bending effects are always coupled to extension effects. However, that inherent coupling is quite small if the shell is flat enough (nearly a plate). For unsymmetrically laminated shells, we seek to organize the results in an understandable manner, realizing that the effect of bending-extension coupling is to lower the buckling loads from those of shells with symmetrically laminated construction.

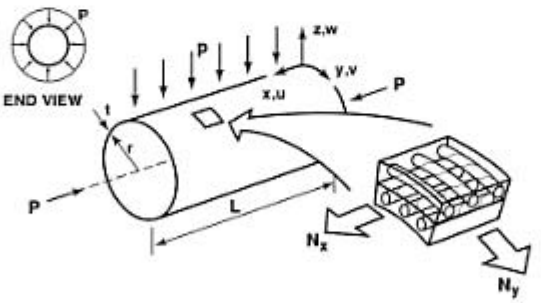


Figure 4-68 Cross-Ply Laminated Shell Geometry and Loading

Éléments sous droits d'auteur

The object of the present section is to extend previous theories to buckling of circular cylindrical shells with multiple orthotropic layers as in Figure 4-68. Attention here is restricted to cross-ply laminates, i.e., laminates with laminae (sometimes called plies) that have their principal material directions (one being the fiber direction) aligned with the axial and circumferential coordinates of the shell. That is, the fibers in one layer are aligned in the axial direction whereas, in the next layer, the fibers might be aligned in the circumferential direction. Any sequence of 0° (axial) or 90° (circumferential) layers can be considered. Note that angle-ply laminates (nonaligned laminae) cannot be treated with this theory. Classical buckling theory, which implies a membrane prebuckling deformed shape, is used for the S2 simply supported edge buckling boundary conditions. $\delta N_x = \delta v = \delta w = \delta M_x = 0$. The present theory enables the study of coupling between bending and extension due to the presence of different layers in the shell. A buckling criterion will be derived and applied to a specific numerical example. Then, the results will be generalized for antisymmetrically laminated shells to the k-Z format that is so useful for classical shell buckling theories. Finally, unsymmetrically laminated shell behavior will be addressed.

Further description of the differences between the various classifications of cross-ply laminates is appropriate because of the similarity of the adjectives used to designate each class. First, the adjective 'regular' is suggested to describe laminates with all equal-thickness laminae as in the top half of Figure 4-69. Irregular or nonregular laminates have laminae of arbitrary, different thicknesses. Hereafter, dropping the adjective 'regular' implies that the laminae are of unequal thickness, i.e., the term 'irregular' will not be explicitly used, but is the default adjective. Also shown in Figure 4-69 are examples of symmetric, antisymmetric, and unsymmetric laminates. Symmetric laminates have both geometric and material property symmetry about the middle surface of the laminate. Antisymmetric laminates have geometric symmetry and material property antisymmetry. Unsymmetric laminates could have geometric symmetry, but do not have material property symmetry or antisymmetry.

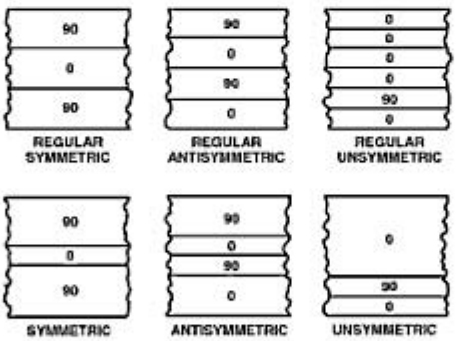


Figure 4-69 Contrast between Regular and 'Irregular' Symmetric, Antisymmetric, and Unsymmetric Cross-Ply Laminates

Éléments sous droits d'auteur

The behavior of laminates that are symmetric, antisymmetric, or unsymmetric about the shell middle surface is studied in this section. Symmetrically laminated shells can be treated with conventional orthotropic shell theory. Antisymmetrically laminated shells have a simple form of coupling between bending and extension and therefore require a more complicated shell theory than symmetrically laminated shells. Unsymmetrically laminated shells have even more complicated coupling between bending and extension than antisymmetrically laminated shells.

4.8.2 Derivation of Buckling Criterion

Expressions are obtained for the variations of stresses during buckling in the k^{th} layer of a multilayered shell in terms of the variations of strains during buckling. Subsequently, the variations of stresses are integrated through the shell thickness to obtain expressions for the variations in forces and moments during buckling. Finally, the variations in forces and moments are substituted in Donnell-type buckling differential equations which are then solved to yield a closed-form buckling criterion in terms of the geometric and material properties of the multilayered circular cylindrical shell. The following derivation is quite similar to the classical work in the 1940s and 1950s by Ambartsumyan [4-61] and further work by Pister and Dong [4-62] and Reissner and Stavsky [4-63] for plates and by Dong, Pister, and Taylor [4-64] for shells.

4.8.2.1 Orthotropic Stress-Strain Relations

The stress-strain relations for an orthotropic material in principal material directions are described by Jones [4-60] and can be written as:

$$\begin{aligned}\sigma_1^k &= Q_{11}^k \varepsilon_1 + Q_{12}^k \varepsilon_2 \\ \sigma_2^k &= Q_{12}^k \varepsilon_1 + Q_{22}^k \varepsilon_2 \\ \tau_{12}^k &= Q_{66}^k \gamma_{12}\end{aligned} \tag{4.233}$$

in which

$$\begin{aligned} Q_{11}^k &= \frac{E_1^k}{1 - \nu_{12}^k \nu_{21}^k} & Q_{22}^k &= \frac{E_2^k}{1 - \nu_{12}^k \nu_{21}^k} \\ Q_{12}^k &= \frac{\nu_{12}^k E_1^k}{1 - \nu_{12}^k \nu_{21}^k} & Q_{66}^k &= G_{12}^k \end{aligned} \tag{4.234}$$

and the superscript k denotes the k^{th} layer of a laminate. The quantity E_1^k is Young's modulus in the 1-direction, E_2^k is the Young's modulus in the 2-direction, G_{12}^k is the shear modulus between the 1- and 2-axes in the 1-2 plane, and $\nu_{12}^k(\nu_{21}^k)$ is the Poisson's ratio for contraction in the 2(1)-direction due to tension in the 1(2)-direction. Apparently five material constants are required per layer; however, because of the reciprocal relations ($\nu_{12}^k E_1^k = \nu_{21}^k E_2^k$), actually only four constants are independent.

Éléments sous droits d'auteur

The orthotropic layers can be placed in the shell with their 1-direction either in the axial (x) or circumferential (y) direction. Thus, the 2-direction is either in the y- or the x-direction, respectively. For a unidirectionally reinforced layer, the 1-direction is the fiber direction and the 2-direction is transverse to the fibers. In what follows, the shell coordinates (x,y) are used, and the values of the material properties E_1, E_2, ν_{12}, and G_{12} are interpreted in accordance with the actual orientation of each layer relative to the x-y coordinates of the shell.

4.8.2.2 Variations of Stresses and Strains during Buckling

During buckling, the shell stresses vary from their prebuckling values [4-65]. Let the variation be denoted by δ; then, from Equation (4.233)

$$\begin{aligned}\delta\sigma_x^k &= Q_{11}^k\delta\varepsilon_x + Q_{12}^k\delta\varepsilon_y\\ \delta\sigma_y^k &= Q_{12}^k\delta\varepsilon_x + Q_{22}^k\delta\varepsilon_y\\ \delta\tau_{xy}^k &= Q_{66}^k\delta\gamma_{xy}\end{aligned} \tag{4.235}$$

in which $\delta\varepsilon_x$, $\delta\varepsilon_y$, and $\delta\gamma_{xy}$ denote the corresponding variations in the strains during buckling. Note that the elastic material properties do not vary during buckling (the material properties will, however, vary when we consider plastic buckling in Section 4.10). Because of the Kirchhoff-Love hypothesis [4-4], the variations in strains during buckling are linear:

$$\begin{aligned}\delta\varepsilon_x &= \delta\varepsilon_x^o + z\delta\kappa_x\\ \delta\varepsilon_y &= \delta\varepsilon_y^o + z\delta\kappa_y\\ \delta\gamma_{xy} &= \delta\gamma_{xy}^o + z\delta\kappa_{xy}\end{aligned} \tag{4.236}$$

The z-coordinate is measured from an arbitrary reference surface at Δ from the inside of the shell as in Figure 4-70. In Equation (4.236), $\delta\varepsilon_x^o$, $\delta\varepsilon_y^o$, and $\delta\gamma_{xy}^o$ are the variations of the reference-surface strains

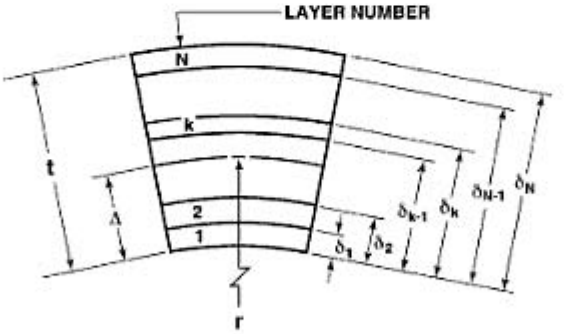


Figure 4-70 Partial Cross Section of an N-Layered Shell

Éléments sous droits d'auteur

$$\begin{aligned}\delta\varepsilon_x^o &= \delta u_{,x}\\ \delta\varepsilon_y^o &= \delta v_{,y} + \delta w/r\\ \delta\gamma_{xy}^o &= \delta u_{,y} + \delta v_{,x}\end{aligned} \tag{4.237}$$

and $\delta\kappa_x$, $\delta\kappa_y$, and $\delta\kappa_{xy}$ are variations of the reference-surface curvatures

$$\begin{aligned}\delta\kappa_x &= -\delta w_{,xx}\\ \delta\kappa_y &= -\delta w_{,yy}\\ \delta\kappa_{xy} &= -2\delta w_{,xy}\end{aligned} \tag{4.238}$$

Upon substitution of Equation (4.236), the linear variations in stresses in the k^{th} layer can be written as

$$\begin{aligned}\delta\sigma_x^k &= Q_{11}^k(\delta\varepsilon_x^o + z\delta\kappa_x) + Q_{12}^k(\delta\varepsilon_y^o + z\delta\kappa_y)\\ \delta\sigma_y^k &= Q_{12}^k(\delta\varepsilon_x^o + z\delta\kappa_x) + Q_{22}^k(\delta\varepsilon_y^o + z\delta\kappa_y)\\ \delta\tau_{xy}^k &= Q_{66}^k(\delta\gamma_{xy}^o + z\delta\kappa_{xy})\end{aligned} \tag{4.239}$$

The variations in stresses are piecewise linear through the laminate.

4.8.2.3 Variations of Forces and Moments during Buckling

The variations of forces and moments during buckling are obtained by integration of the variations of stresses through each of the shell layers, i.e., through the multilayered shell thickness as the summation of the integration through each layer with a common origin for z in Figure 4-70:

$$\delta N_x = \sum_{k=1}^{N}\int_{t_k}\delta\sigma_x^k\,dz \qquad \delta N_y = \sum_{k=1}^{N}\int_{t_k}\delta\sigma_y^k\,dz \qquad \delta N_{xy} = \sum_{k=1}^{N}\int_{t_k}\delta\tau_{xy}^k\,dz \tag{4.240}$$

$$\begin{aligned}\delta M_x &= \sum_{k=1}^{N}\int_{t_k}\delta\sigma_x^k\,z\,dz \qquad & \delta M_{xy} &= -\sum_{k=1}^{N}\int_{t_k}\delta\tau_{xy}^k\,z\,dz\\ \delta M_y &= \sum_{k=1}^{N}\int_{t_k}\delta\sigma_y^k\,z\,dz \qquad & \delta M_{yx} &= \sum_{k=1}^{N}\int_{t_k}\delta\tau_{xy}^k\,z\,dz\end{aligned} \tag{4.241}$$

in which t_k is the thickness of the k^{th} layer and N is the number of layers. Because the variations in reference surface strains and curvatures in Equations (4.237) and (4.238) are constant relative to the through-the-thickness integration, the integrations in Equations (4.240) and (4.241) yield

$$\begin{aligned}\delta N_x &= A_{11}\delta\varepsilon_x^o + A_{12}\delta\varepsilon_y^o + B_{11}\delta\kappa_x + B_{12}\delta\kappa_y\\ \delta N_y &= A_{12}\delta\varepsilon_x^o + A_{22}\delta\varepsilon_y^o + B_{12}\delta\kappa_x + B_{22}\delta\kappa_y\\ \delta N_{xy} &= A_{66}\delta\gamma_{xy}^o + B_{66}\kappa_{xy}\end{aligned} \tag{4.242}$$

Éléments sous droits d'auteur

$$\begin{aligned}
\delta M_x &= B_{11}\delta\varepsilon_x^o + B_{12}\delta\varepsilon_y^o + D_{11}\delta\kappa_x + D_{12}\delta\kappa_y \\
\delta M_y &= B_{12}\delta\varepsilon_x^o + B_{22}\delta\varepsilon_y^o + D_{12}\delta\kappa_x + D_{22}\delta\kappa_y \\
\delta M_{xy} &= -B_{66}\delta\gamma_{xy}^o - D_{66}\delta\kappa_{xy} \\
\delta M_{yx} &= B_{66}\delta\gamma_{xy}^o + D_{66}\delta\kappa_{xy}
\end{aligned} \tag{4.243}$$

in which

$$\begin{aligned}
A_{ij} &= \sum_{k=1}^{N} Q_{ij}^k(\delta_k - \delta_{k-1}) \\
B_{ij} &= \frac{1}{2}\sum_{k=1}^{N} Q_{ij}^k\left[(\delta_k^2 - \delta_{k-1}^2) - 2\Delta(\delta_k - \delta_{k-1})\right] \\
D_{ij} &= \frac{1}{3}\sum_{k=1}^{N} Q_{ij}^k\left[(\delta_k^3 - \delta_{k-1}^3) - 3\Delta(\delta_k^2 - \delta_{k-1}^2) + 3\Delta^2(\delta_k - \delta_{k-1})\right]
\end{aligned} \tag{4.244}$$

The stiffnesses in Equation (4.244) are due to Ambartsumyan [4-61] and depend on the location of the reference surface which is located a distance Δ measured from the shell inner surface. The reference surface can be changed by varying Δ in order to address different loadings and boundary conditions. The most-common location for the reference surface is the shell middle surface.

4.8.2.4 Buckling Differential Equations

The Donnell-type buckling differential equations for circular cylindrical shells subjected to combinations of axial compression and lateral pressure are, from an alternative to Equations (4.71)–(4.73) on page 487,

$$\begin{aligned}
&\delta N_{x,x} + \delta N_{xy,y} = 0 \\
&\delta N_{xy,x} + \delta N_{y,y} = 0 \\
&-\delta M_{x,xx} + \delta M_{xy,xy} - \delta M_{yx,xy} - \delta M_{y,yy} + \frac{\delta N_y}{r} + \overline{N}_x\delta w_{,xx} + \overline{N}_y\delta w_{,yy} = 0
\end{aligned} \tag{4.245}$$

and the force and geometric boundary buckling conditions at $x = 0$ and L are chosen from the following sixteen possibilities (any set of four alternatives in the following pairs constitutes a set of boundary conditions):

$$\begin{aligned}
\delta N_x = 0 \quad &\text{or} \quad \delta u = 0 \\
\delta N_{xy} = 0 \quad &\text{or} \quad \delta v = 0 \\
\delta M_{x,x} + \delta M_{yx,y} + \overline{N}_x\delta w_{,x} = 0 \quad &\text{or} \quad \delta w = 0 \\
\delta M_x = 0 \quad &\text{or} \quad \delta w_{,x} = 0
\end{aligned} \tag{4.246}$$

from which the usual buckling boundary condition sets S1–S4, C1–C4, etc. are collected after Almroth [4-10].

Éléments sous droits d'auteur

Upon substitution of the expressions for the variations of forces and moments during buckling, Equations (4.242) and (4.243), and the variations of reference surface strains and curvatures, Equations (4.237) and (4.238), the buckling differential equations become

$$\begin{aligned}
&A_{11}\delta u_{,xx} + A_{12}(\delta v_{,xy} + \delta w_{,x}/r) + A_{66}(\delta u_{,yy} + \delta v_{,xy}) \\
&\quad - B_{11}\delta w_{,xxx} - (B_{12} + 2B_{66})\delta w_{,xyy} = 0 \\
&A_{12}\delta u_{,xy} + A_{22}(\delta v_{,yy} + \delta w_{,y}/r) + A_{66}(\delta u_{,xy} + \delta v_{,xx}) \\
&\quad - (B_{12} + 2B_{66})\delta w_{,xxy} - B_{22}\delta w_{,yyy} = 0 \\
&(A_{12}/r)\delta u_{,x} - B_{11}\delta u_{,xxx} - (B_{12} + 2B_{66})(\delta u_{,xyy} + \delta v_{,xxy}) \\
&\quad + (1/r)A_{22}(\delta v_{,y} + \delta w/r) + B_{22}\delta v_{,yyy} - (2B_{12}/r)\delta w_{,xx} \\
&\quad + (2/r)B_{22}\delta w_{,yy} + D_{11}\delta w_{,xxxx} + (4D_{66} + 2D_{12})\delta w_{,xxyy} \\
&\quad + D_{22}\delta w_{,yyyy} + \bar{N}_x\delta w_{,xx} + \bar{N}_y\delta w_{,yy} = 0
\end{aligned} \tag{4.247}$$

Note that lamination-induced bending-extension coupling exists whenever the B_{ij} in Equation (4.247) are nonzero. Of course, some bending-extension coupling always exists for shells.

4.8.2.5 Buckling Criterion

We desire to find the solution to the buckling differential equations for the S2 simply supported edge buckling boundary conditions

$$\delta N_x = \delta v = \delta w = \delta M_x = 0 \tag{4.248}$$

The following buckling displacements satisfy the buckling boundary conditions of Equation (4.248):

$$\begin{aligned}
\delta u &= \tilde{u}\cos\frac{m\pi x}{L}\cos\frac{ny}{r} \\
\delta v &= \tilde{v}\sin\frac{m\pi x}{L}\sin\frac{ny}{r} \\
\delta w &= \tilde{w}\sin\frac{m\pi x}{L}\cos\frac{ny}{r}
\end{aligned} \tag{4.249}$$

(or equivalently δu, δv, and δw could be cosine-sine, sine-cosine, and sine-sine finctions, respectively, if the coordinates are rotated 90°) [in which $\tilde{u}$, $\tilde{v}$, and $\tilde{w}$ are the (indeterminate) amplitudes of the buckling displacements] and are substituted in the buckling differential equations, Equation (4.247). In order to obtain the (exact) nontrivial solution to the resulting equations, the determinant of the coefficients of $\tilde{u}$, $\tilde{v}$, and $\tilde{w}$ must be zero, and the following buckling criterion results:

$$\bar{N}_x(m\pi/L)^2 + \bar{N}_y(n/r)^2 = T_{33} + \frac{2T_{12}T_{13}T_{23} - T_{11}T_{23}^2 - T_{22}T_{13}^2}{T_{11}T_{22} - T_{12}^2} \tag{4.250}$$

in which

Éléments sous droits d'auteur

$$
\begin{aligned}
T_{11} &= A_{11}(m\pi/L)^2 + A_{66}(n/r)^2 \\
T_{12} &= (A_{12} + A_{66})(m\pi/L)(n/r) \\
T_{13} &= (A_{12}/r)(m\pi/L) + B_{11}(m\pi/L)^3 + (B_{12} + 2B_{66})(m\pi/L)(n/r)^2 \\
T_{22} &= A_{66}(m\pi/L)^2 + A_{22}(n/r)^2 \\
T_{23} &= (B_{12} + 2B_{66})(m\pi/L)^2(n/r) + (1/r)(A_{22})(n/r) + B_{22}(n/r)^3 \\
T_{33} &= D_{11}(m\pi/L)^4 + (2D_{12} + 4D_{66})(m\pi/L)^2(n/r)^2 + D_{22}(n/r)^4 \\
&\quad + (2B_{12}/r)(m\pi/L)^2 + (2/r)B_{22}(n/r)^2 + (1/r)^2 A_{22}
\end{aligned}
\tag{4.251}
$$

The solution represented by Equation (4.250) reduces to the solution of Batdorf, Schildcrout, and Stein [4-24] for single-layered isotropic circular cylindrical shells. The buckling load under axial compression is obtained from Equation (4.250) by equating N_y to zero and solving for N_x. Similarly, the buckling load under lateral pressure is obtained by equating N_x to zero and solving for $N_y (N_y = pr)$. Finally, the buckling load under hydrostatic pressure is obtained by equating N_x to $N_y/2$ and solving for N_y. In addition, if $N_x(N_y)$ is fixed, the critical values of $N_y(N_x)$ can be found. The value of N_x can be varied to obtain an interaction curve between axial compression and lateral pressure.

Because of the numerous parameters in Equation (4.250) and the need to investigate a large range of buckling modes to determine the lowest buckling load, from a practical standpoint a digital computer must be used for numerical work. In the computer program for integer numbers of axial halfwaves, m, and circumferential waves, n, in the buckled shape, the appropriate buckling load is found. See Appendix B for a generic description of a search procedure for how to find the absolute minimum buckling load for some range of integer values of m and n.

4.8.3 Numerical Example

Because of the many geometrical properties in the theory, meaningful general results are difficult, if not impossible, to present. Thus, a specific numerical example is given to illustrate application of the theory. The results are compared with results of previous approaches.

For this example, the buckling of a ring-stiffened circular cylindrical shell unsymmetrically laminated with two isotropic layers under hydrostatic pressure is considered. The properties of the layers are

$E_1 = 44 \times 10^6$ psi (300 GPa)	$E_2 = 2 \times 10^6$ psi (14 GPa)
$\nu_1 = 0$	$\nu_2 = .4$
$t_1 = .04$ in (.10 cm)	$t_2 = .3$ in (.76 cm)

The shell has a length of 12 inches (30.5 cm) and a radius of 6 inches (15.2 cm) to the middle surface of layer one (which, in this case, is also the reference surface). The rings are of rectangular cross section with a height of .25 in (.64 cm) and a thickness of .06 in (.15 cm). The rings are fastened to the inner surface of layer one, and have the same material properties as layer one. In order to treat the rings, appropriate stiffener terms must be added to the variations in forces and moments during buckling and thus to the buckling criterion as in Section 4.7.

Éléments sous droits d'auteur

The hydrostatic buckling pressure of the subject configuration is shown as the solid line in Figure 4-71 as a function of ring spacing. The results shown are for general instability (buckling in which the rings participate as in Section 4.7.4). The buckling pressures for panel instability (buckling between rings) are much higher and, hence, do not govern the buckling of the present configuration. Other failure criteria, e.g., yielding, are ignored for the purposes of this illustration of the present analysis technique. The dashed curve in Figure 4-71 represents an orthotropic stiffness approach to the problem (e.g., Block, Card, and Mikulas [4-53]) and is from 3 to 9 percent lower than the results from the present theory. These lower results are caused by neglect of coupling between bending and extension of the layered shell and of the eccentric stiffeners in the orthotropic stiffness approach. The dashed curve with a single dot represents a stiffened shell with a single equivalent Poisson's ratio for bending ($\nu_D = .311$) used in both layers by Jones and Klein [4-66] and is from 7 to 11 percent lower than the results of the present theory. Finally, the dashed curve with two dots represents a stiffened shell with a single equivalent Poisson's ratio for extension ($\nu_B = .115$) used in both layers [4-66] and is from 14 to 18 percent lower than the results of the present theory. The lower results for ν_D and ν_B are caused by neglect of coupling between bending and extension of the two shell layers and of the eccentric stiffeners in the orthotropic stiffness approach. Note that all approaches previous to the present theory are conservative for this example, i.e., they yield lower buckling pressures than can actually be realized by the stiffened shell. For other problems, the previous approaches can yield *unconservative* results [4-66]. Thus, the importance of bending-extension coupling should not be overlooked.

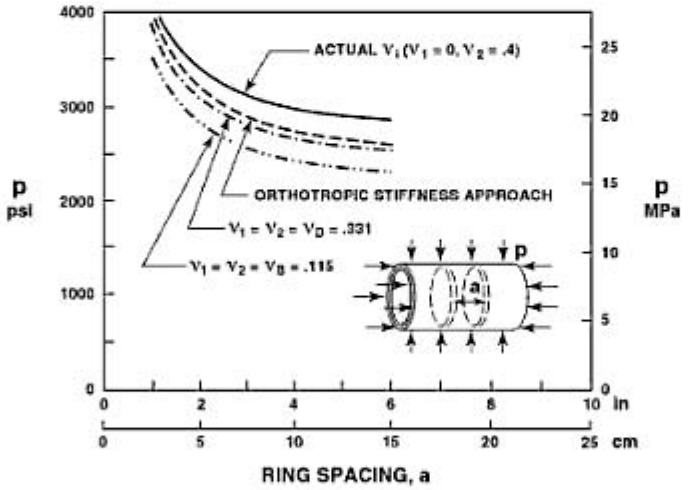


Figure 4-71 Buckling under Hydrostatic Pressure of a Ring-Stiffened, Two-Layered Circular Cylindrical Shell *(After Jones [4-65])*

Éléments sous droits d'auteur

4.8.4 General k-Z Results for Antisymmetric Cross-Ply Laminates

Rather than continue with numerical results for specific individual shells, it will be more helpful to present more general results in a k-Z format. That is, a normalized loading parameter versus a modification of the Batdorf shell curvature parameter format can be adopted for laminated shell results. This format has the advantage of far more general ability for interpretation of results than do the results for specific individual shells. The shells studied are cross-ply laminated as in Figure 4-69, and are antisymmetric about the middle surface of the shell. The objective of this section is to present extensive numerical results for buckling of laminated shells as depicted in Figure 4-68.

Normalized analysis results are presented for buckling of antisymmetrically laminated regular cross-ply circular cylindrical shells after the familiar Batdorf k-Z normalization is attained [4-2]. For antisymmetric cross-ply laminates, $A_{11} = A_{22}$, $B_{11} = -B_{22}$, $B_{12} = B_{66} = 0$, and $D_{11} = D_{22}$ as in Appendix C.

4.8.4.1 Axial Compression

For axial compression, the buckling criterion, Equation (4.250) can be rearranged for regular alternating layers as

$$
\begin{aligned}
k_x &= \frac{\bar{N}_x L^2}{\pi^2 D_{11}} \\
&= m^2\left[1+4\left[\frac{D_{66}}{D_{11}}+\frac{\nu_{12}F}{(1+F)}\right]\left[\frac{nL}{m\pi r}\right]^2+\left[\frac{nL}{m\pi r}\right]^4\right]+\frac{12Z^2}{m^2\pi^4 A} \\
&\quad -\frac{B_{11}^2}{A_{11}D_{11}}\left[1+\frac{A_{11}}{A_{66}}\left[\frac{nL}{m\pi r}\right]^2+2\left[\frac{2\nu_{12}F}{1+F}+1\right]\left[\frac{nL}{m\pi r}\right]^4\right. \\
&\quad \left.+\frac{A_{11}}{A_{66}}\left[\frac{nL}{m\pi r}\right]^6+\left[\frac{nL}{m\pi r}\right]^8\right]\frac{m^2}{A} \\
&\quad +4\left[\frac{L^2}{r}\right]\left[\frac{B_{11}}{D_{11}}\right]\left[\frac{\nu_{12}F}{1+F}\right]\frac{\left[\left[\frac{nL}{m\pi r}\right]^4+1\right]}{\pi^2 A}
\end{aligned}
\tag{4.252}
$$

in which the orthotropy ratio, F, is defined as

$$F = \frac{E_2}{E_1} \tag{4.253}$$

(the ratio of the modulus of an orthotropic layer in the transverse to the fibers direction to the modulus in the fiber direction) and the modified Batdorf shell curvature parameter, Z, is

Éléments sous droits d'auteur

$$Z = \left[\frac{L^2}{rt}\right]\left[1 - \frac{4\nu_{12}^2 F^2}{(1+F)^2}\right]^{1/2} \tag{4.254}$$

which reduces to the well-known Batdorf shell curvature parameter when $F = 1$ and $\nu_{12} = \nu$ for isotropy with physical interpretation in Figure 4-72, and

$$A = 1 + \left[\frac{A_{11}}{A_{66}}\left[1 - \frac{4\nu_{12}^2 F^2}{(1+F)^2}\right] - \frac{4\nu_{12}F}{(1+F)}\right]\left[\frac{nL}{m\pi r}\right]^2 + \left[\frac{nL}{m\pi r}\right]^4 \tag{4.255}$$

The expression for k_x, Equation (4.252) has four terms: (1) an orthotropic plate bending contribution; (2) a shell curvature component; (3) a contribution of lamination effects (bending-extension coupling); and (4) coupling between lamination effects and curvature effects. Terms (1) and (2) are found in classical shell theory. Terms (1) and (3) are found in classical laminated plate theory. Thus, the fourth term has a new character that has not been discussed before.

The coefficient on the lamination effects term can be shown to be

$$\frac{B_{11}^2}{A_{11}D_{11}} = 3\frac{(F-1)^2}{\left[(NL)^2(1+F)^2\right]} \tag{4.256}$$

in which NL is the number of layers in the laminate. Thus, as the number of layers in the laminate increases, the lamination effects term decreases rapidly. The rapid decrease of this term is responsible for the rapid approach of laminated plate buckling loads to the orthotropic plate results determined by Whitney and Leissa [4-67].

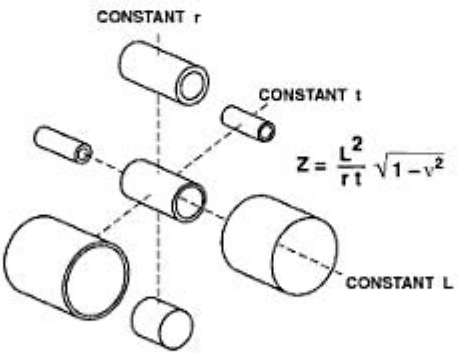


Figure 4-72 Representative Circular Cylindrical Shells Corresponding to the Same Value of Z (Z About 150) *(After Batdorf [4-2])*

Éléments sous droits d'auteur

The lamination-curvature coupling effects coefficient reduces to

$$\frac{L^2}{r}\frac{B_{11}}{D_{11}} = \frac{6(F-1)}{(NL)(1+F)}\frac{L^2}{rt} \tag{4.257}$$

This coefficient approaches zero only as the inverse of NL as opposed to the inverse of $(NL)^2$ for the lamination effects coefficient in Equation (4.256). Note that the component L^2/rt is the Batdorf shell curvature parameter if all association with material properties is removed.

Axial compression $k_x - Z$ results for antisymmetrically laminated graphite-epoxy shells for 2, 4, and an infinite number of layers are shown in Figure 4-73. The results for an infinite number of layers are the same as the orthotropic solution in which all bending-extension coupling is ignored (then, B_{11}, the only bending-extension coupling coefficient for an antisymmetric cross-ply laminate, is zero). Because of the log-log format in Figure 4-73, the large percentage differences between the buckling loads for laminates with different numbers of layers are obscured. The well-known large coupling effects for plates are detected by observing that all curves are far apart for $Z = 1$. For $Z > 20$, $k_x - Z$ results for various numbers of layers have the same slope so have a constant relation to one another. However, the effect of bending-extension coupling is less for a long shell ($Z > 20$) than for a plate. The orthotropic approximation ($B_{11} = 0$) is too high at $Z = 100$ by 67% for two-layered shells and by 9% for four-layered shells. For more than four layers, the coupling effect is negligible. Thus, the effect of bending-extension coupling rapidly dies out as the number of layers increases.

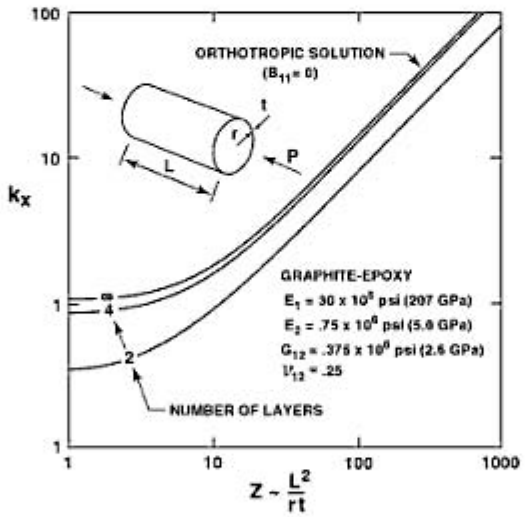


Figure 4-73 Normalized Axial Compression Buckling Loads for Antisymmetric Cross-Ply Laminated Graphite-Epoxy Shells *(After Jones and Morgan [4-68])*

Éléments sous droits d'auteur

For other composite materials, when the shell length, radius, and thickness are fixed, the buckling loads depend essentially on the modulus ratio, E_1/E_2. Values of G_{12}/E_2 and ν_{12} are constant in this study because their influence on the buckling load is small compared to that of E_1/E_2. The buckling loads relative to the buckling load of an orthotropic shell (for which $B_{11} = 0$) when $Z = 300$ are plotted as a function of E_1/E_2 for various numbers of layers in Figure 4-74. The curves plotted are actually envelopes to the segmented curves with cusps (caused by buckle mode shape changes) that exist for a specific shell geometry. For other L, r, and t for $Z = 300$, the curves vary so as to fit above the envelopes plotted (as in Figure 4-21 on page 495). At any rate, the specific numerical values are not as important as the general influence of the modulus ratio. The relative buckling loads decrease with increasing E_1/E_2. For a boron-epoxy shell (for which $E_1/E_2 = 10$), the effect of bending-extension coupling is not quite as striking as for the graphite-epoxy ($E_1/E_2 = 40$) shells already discussed. However, the effect of bending-extension coupling is still substantial for low numbers of layers.

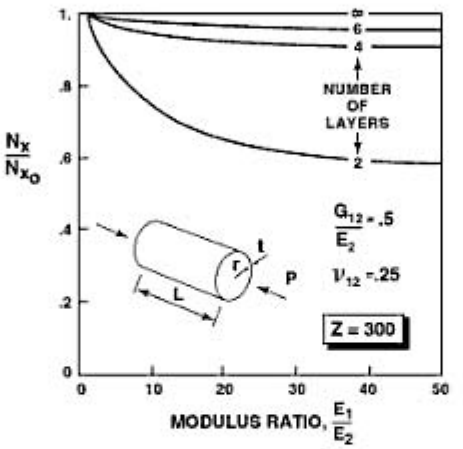


Figure 4-74 Relative Axial Compression Buckling Loads for Antisymmetric Cross-Ply Laminated Shells *(After Jones and Morgan [4-68])*

4.8.4.2 Lateral Pressure

For lateral pressure, the buckling criterion, Equation (4.250), can be written as

$$k_y = \frac{\bar{N}_y L^2}{\pi^2 D_{11}} = \left[\frac{m\pi r}{nL}\right]^2 k_x \qquad (4.258)$$

Éléments sous droits d'auteur

and thus has the same four components (orthotropic plate bending, etc.) as the normalized axial compression buckling load. For long shells, $nL/m\pi r$ is much greater than one so Equation (4.258) has minimum value

$$k_y = CZ^{1/2} \tag{4.259}$$

in which C is a function of the lamination properties including the number of layers. For isotropic shells, $C = 4/\sqrt{3}$. For 2 layers, the value of C is less than for 4 layers which in turn is less than for 6 layers and so on. Thus, the $k_y - Z$ results for long graphite-epoxy shells in Figure 4-75 are not parallel but rather divergent for large values of Z. That is, the effect of coupling between bending and extension increases with increasing Z. For example, the orthotropic approximation to the two-layered shell buckling load is about 120% too high at Z = 100 and about 140% too high at Z = 10,000. Generally, however, the effect of coupling dies out rapidly with increasing number of layers for all shells.

The lateral pressure buckling loads normalized relative to orthotropic shell buckling loads are plotted for various modulus ratios, E_1/E_2, in Figure 4-76. Again, E_1/E_2 is used to display the essence of the behavior of various composite materials whereas G_{12}/E_2 and ν_{12} are fixed because their effect is far less important. As for axial compression, only the envelopes of the actual curves are plotted. The effect of coupling for a two-layered shell is much greater than for axial compression. Even for a boron-epoxy shell ($E_1/E_2 = 10$), the actual buckling load is only 60% of the predicted value for orthotropic shells (for which coupling doesn't exist). The orthotropic approximation is too high by 67% for boron-epoxy shells and by 127% for graphite-epoxy shells. These overestimates of buckling resistance die out rapidly as the number of layers increases.

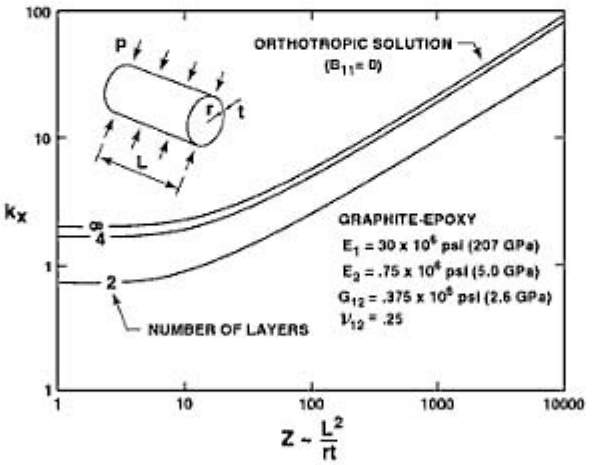


Figure 4-75 Normalized Lateral Pressure Buckling Loads for Antisymmetric Cross-Ply Laminated Graphite-Epoxy Shells *(After Jones and Morgan [4-68])*

Éléments sous droits d'auteur

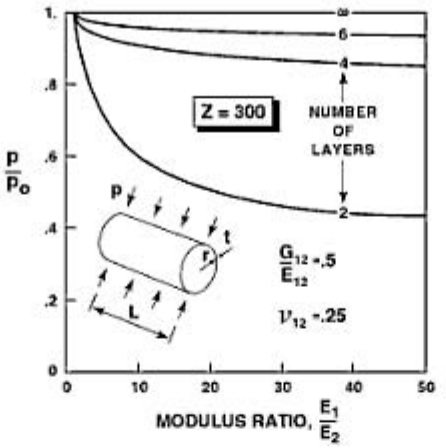


Figure 4-76 Relative Lateral Pressure Buckling Loads for Antisymmetric Cross-Ply Laminated Shells *(After Jones and Morgan [4-68])*

4.8.4.3 Summary for Antisymmetric Cross-Ply Laminates

For buckling of antisymmetrically laminated cross-ply shells, the effect of coupling between bending and extension dies out rapidly as the number of layers increases. For shells under lateral pressure, the effect of coupling is larger for long shells than for moderate length shells. For axial compression of long shells, the effect of coupling is essentially constant with increasing Z, the modified Batdorf curvature parameter.

For buckling problems, switching the layer stacking sequence from [0°/90°/ ...] to [90°/0°/ ...] does not change the buckling loads. For a two-layered shell, a large difference might be expected when an analogy is made with the stiffener eccentricity effect in Section 4.7 which is another form of bending-extension coupling [4-25]. Both the lamination effect and the stiffener eccentricity effect have terms that (1) change sign depending on either lamination sequence or stiffener placement (on the outside or the inside of the shell) and (2) occupy the same positions in the buckling differential equation and its solution [4-65]. For an axially compressed circular cylindrical shell with longitudinal stiffeners (stringers), the buckling load for externally placed stringers can be twice or even three times the buckling load for internal stringers (see Section 4.7). For the same loading, higher buckling loads are obtained for shells with internal rings than for shells with external rings. For [0°/90°/ ...] shells versus [90°/0°/ ...] shells, there is no difference in buckling loads because a laminated shell is actually analogous to a shell with simultaneous ring and stringer stiffening (same stiffener sizes and spacings) on the same side of the shell. That is, a laminate is inherently a two-dimensional element whereas a stiffener is idealized as a one-dimensional element. Thus, a laminate has effects that are mutually counteracting.

Éléments sous droits d'auteur

4.8.5 Results for Unsymmetric Cross-Ply Laminates

Because of the infinite complexity of the class of unsymmetric laminates, general results are impossible to obtain. Instead, consider the cross sections of the contrived, but representative unsymmetric laminate example in Figure 4-77. There, the fibers in the second layer from the bottom are oriented at 90° and the fibers in all other layers are oriented at 0° to the shell x-axis which runs horizontally from left to right in the figure. That is, the laminate has predominately layers with axial fibers, but one layer has circumferential fibers. Thus, as the number of layers increases for a constant-thickness laminate, the 90° layer gets thinner and moves toward the bottom of the laminate. The laminates must be of constant thickness so we can compare laminates of the same weight in order to concentrate on how the laminae orientations in the laminate alone influence the buckling load, i.e., without extraneous effects. As mentioned previously, this example is contrived (i.e., probably not ever encountered in engineering practice), but it is a simple, straightforward example of unsymmetric laminates that is amenable to rather comprehensive theoretical parametric study with the objective of better understanding unsymmetric laminates.

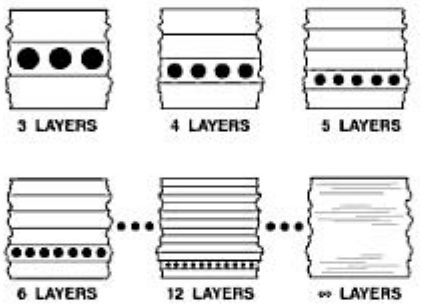


Figure 4-77 Unsymmetric Laminate Example *(After Jones and Morgan [4-68])*

4.8.5.1 Axial Compression

Normalized axial compression buckling loads for an unsymmetrically laminated graphite-epoxy shell as a function of the number of layers are shown in Figure 4-78. The shell has all 0° layers except for one 90° layer and a length, radius, and thickness such that $Z = 1000$. One of the baseline comparison values is the buckling load for a shell with all 0° layers. The other comparison case is an unsymmetrically laminated shell for which coupling between bending and extension is ignored ($B_{ij} = 0$). Results for the actual unsymmetrically laminated shell, for which coupling between bending and extension is considered, are labeled exact solution in Figure 4-78.

Éléments sous droits d'auteur

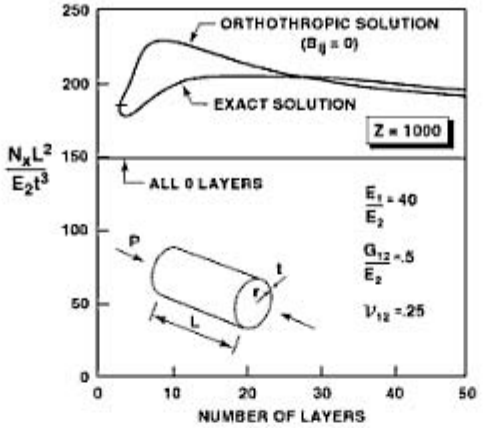


Figure 4-78 Normalized Axial Compression Buckling Loads of Unsymmetric Cross-Ply Laminated Graphite-Epoxy Shells *(After Jones and Morgan [4-68])*

The actual laminate has, not surprisingly, less buckling resistance than a laminate with $B_{ij} = 0$ except when the laminate has a large number of layers (more than about thirty). However, the actual laminate always has more buckling resistance than a laminate with all 0° layers. The reason for this curious result is related to the relative values of the stiffnesses in the x- and y-directions and as well to the shell parameters. As will be seen subsequently, D_{11} is decreased somewhat by the presence of a 90° layer, but D_{22} is most easily examined for a three-layered shell which is, of course, symmetric. Thus, the exact solution corresponds to the orthotropic solution ($B_{ij} = 0$)., e.g., see the horizontal hash mark at three layers in Figure 4-78 where the two curves coincide. At that point, the solution for an orthotropic plate which buckles into the $m = 1$, $n = 1$ mode is

$$\bar{N}_x L^2 = \pi^2 \left[\frac{D_{11}}{4} + 2(D_{12} + 2D_{66}) + 4D_{22} \right] \tag{4.260}$$

which is readily obtained from Equation (4.250). For a graphite-epoxy laminate, the term in Equation (4.260) involving D_{11} decreases by less than 4% when the actual laminate is considered as opposed to the all-0°-layer laminate. However, the term involving D_{22} is 2 1/2 times as big for the actual laminate as it is for the all-0°-layer laminate. The net result is a 33% bigger buckling load for the actual laminate than for the all-0°-layer laminate.

The differences between the exact and orthotropic predictions for graphite-epoxy laminates in Figure 4-78 range from 18% less than the orthotropic solution ($B_{ij} = 0$) at 6 layers to 12% less at 10 layers to 2% more at 50 layers. In addition, the exact results range from about 38%

Éléments sous droits d'auteur

more than the all-0°-laminate results at 20 layers to about 30% more at 50 layers. Such differences are well within the consideration of usual engineering design practice. However, the differences exist for many more layers than bending-extension coupling was previously believed to be important. That belief was established on the basis of extrapolating antisymmetric cross-ply results. Obviously, such extrapolation is invalid.

As an aid to understanding the buckling behavior illustrated in Figure 4-78, the extensional, coupling, and bending stiffnesses are plotted versus the number of layers in Figure 4-79 for graphite-epoxy. The stiffnesses in the x-direction (with which most fibers are aligned), A_{11}, and D_{11}, are nearly independent of the number of layers. However, the 90° layer causes the stiffnesses in the y-direction, A_{22} and D_{22}, to deviate by up to an order of magnitude from the value for all 0° layers (which is the same as the value for an infinite number of layers). These discrepancies die out very slowly as the number of layers increases. Moreover, the normalized stiffness for bending-extension coupling, which can be shown to be

$$\frac{B_{11}}{Q_{11}t^2} = \frac{NL-3}{2(NL)^2}\left[1-\frac{E_2}{E_1}\right] \tag{4.261}$$

(in which NL is number of layers) and which appears in Equation (4.250) and thereby enables stiffnesses A_{22} and D_{22} to influence the buckling load, also dies out slowly. The maximum coupling occurs for this unsymmetric laminate when NL = 6. The magnitudes of, for example, D_{22} and $B_{11}/Q_{11}t^2$, cannot be compared quantitatively. They do not have the

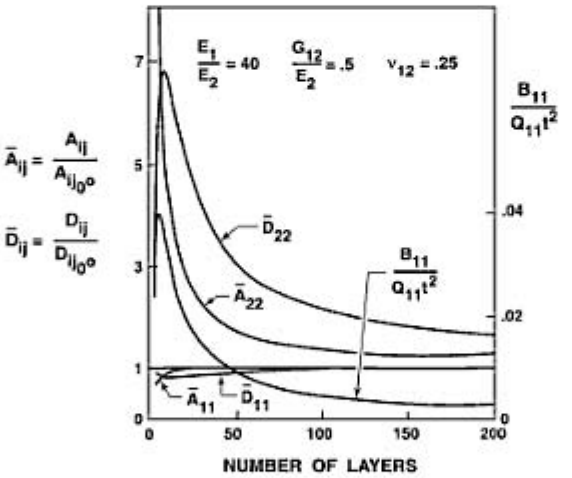


Figure 4-79 Normalized Stiffnesses of Example Unsymmetric Cross-Ply Graphite-Epoxy Laminate *(After Jones and Morgan [4-66])*

Éléments sous droits d'auteur

same base for normalization (B_{11} cannot be normalized relative to its value for all 0° layers because there its value is zero). Thus, it is easy to see why the effect of a single unsymmetrically placed 90° layer on the buckling load dies out slowly as the number of layers increases.

For unsymmetric cross-ply laminates wherein each layer is of the same material but of different orientation (either 0° or 90°, but not necessarily alternating), B_{12} and B_{66} can easily be shown to be zero. Also, B_{11} and B_{22} are not of equal value but opposite sign as for antisymmetric cross-ply laminates. However, for general unsymmetric laminates of different materials, all coupling stiffnesses can occur. The present theory is applicable to the general lamination case if the principal material directions of each layer are aligned with the shell coordinate directions.

4.8.5.2 Lateral Pressure

Normalized lateral pressure buckling loads for an unsymmetrically laminated graphite-epoxy shell are shown in Figure 4-80 as a function of the number of layers. The shell has all 0° layers except for one 90° layer and a length, radius, and thickness such that Z = 1000. The exact, orthotropic, and all-0°-layer solutions are identified as was done in the axial compression results. The differences between the exact and orthotropic predictions in Figure 4-80 range from 56% less than the orthotropic solution at 6 layers to 38% less at 20 layers to 17% less at 50 layers. In addition, the exact results range from 79% more than the all-0°-layer solution at 10 layers to 78% more at 50 layers. These are the largest differences attributed to bending-extension coupling of unsymmetrically laminated plates and shells known to the author, and they persist for a large number of layers.

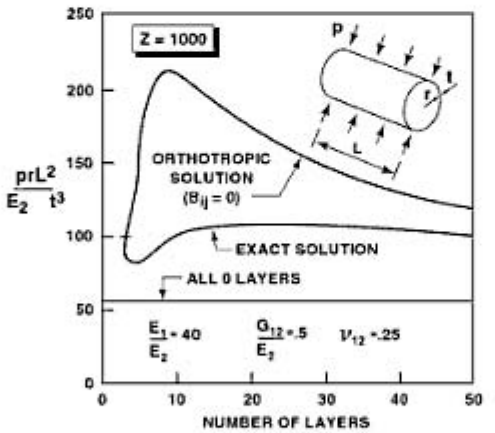


Figure 4-80 Normalized Lateral Pressure Buckling Loads for Unsymmetric Cross-Ply Laminated Graphite-Epoxy Shells *(After Jones and Morgan [4-68])*

Éléments sous droits d'auteur

4.8.5.3 Summary for Unsymmetrically Laminated Shells

Bending-extension coupling has a large effect on the buckling loads of the example unsymmetric cross-ply laminated circular cylindrical shell. This conclusion is valid when the laminate has mostly 0° layers with a single 90° layer. However, when the laminate has mostly 90° layers with a single 0° layer, the exact results are nearly identical to the orthotropic solution (in which coupling is ignored). Thus, there is an interaction between the lamination sequence and the loading that affects whether bending-extension coupling is important. Moreover, if the single 90° layer (out of many 0° layers) is moved within the laminate, as in the 20-layer laminate of Figure 4-81, then the amount of bending-extension coupling varies. Thus, for example, the exact normalized lateral pressure buckling loads for a 20-layer laminated shell range in Figure 4-82 from

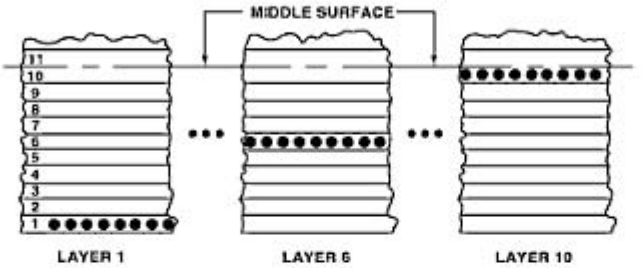


Figure 4-81 Position of 90° Layer in a 20-Layer Unsymmetric Laminate

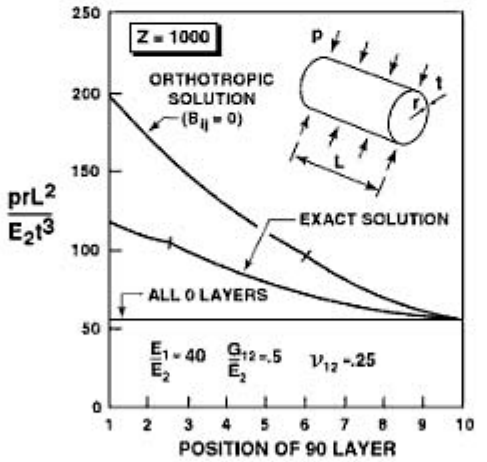


Figure 4-82 Effect of 90° Layer Position on Lateral Pressure Buckling Loads for 20-Layer Unsymmetric Cross-Ply Laminated Graphite-Epoxy Shells *(After Jones and Morgan [4-68])*

Éléments sous droits d'auteur

41% less than the orthotropic solution when the 90° layer is the first layer to 38% less at the second layer position to 26% less at the sixth layer position to, of course, nearly the same value when the 90° layer is next to the middle of the laminate. Of course, the 90° layer cannot be placed with its middle surface coincident with the laminate middle surface because the number of layers is even. Accordingly, even larger effects of bending-extension coupling than shown in Figures 4-78 and 4-80 are possible. Obviously, smaller effects of bending-extension coupling can also exist. Designers must, therefore, include bending-extension coupling in all analyses to be able to account for all reasonable possibilities.

4.8.6 Summary for Laminated Shells

An 'exact' theory for buckling of symmetrically, antisymmetrically, and unsymmetrically laminated cross-ply circular cylindrical shells is presented and discussed. The shells can be subjected to arbitrary combinations of axial compression and lateral pressure to cause buckling. Classical laminated shell theory including the Kirchhoff-Love hypothesis of nondeformable normals [4-4] is used for S2 type simply supported edge buckling boundary conditions and a membrane prebuckled shape. Thus, the present solution can be regarded as a lower bound on results for practical shells if initial geometric imperfections and prebuckling deformations are ignored. Initial geometric imperfections usually have a much smaller effect on lowering the buckling loads of laminated composite shells than on metal shells. The influence of prebuckling deformations is mentioned later in this summary. Numerical examples for common graphite-epoxy composite materials are used to display results of the theory. Both antisymmetric laminates and the more general case of unsymmetric laminates are addressed in the examples. The primary new factor introduced with laminate asymmetry is bending-extension coupling

A numerical example is given to illustrate the effect of bending-extension coupling caused by the presence of different layers in laminated shells. The present theory is compared with previous approaches such as use of a single 'equivalent' Poisson's ratio in all layers of a layered shell. The buckling predictions of the previous approaches, in which bending-extension coupling is neglected, are seen to be erratic in that they are sometimes conservative and sometimes unconservative for the analysis of an example stiffened shell with two isotropic layers. Thus, the importance of bending-extension coupling must not be overlooked.

For antisymmetrically laminated cross-ply circular cylindrical shells, buckling results are presented in a generalized Batdorf k-Z form in which bending-extension coupling causes buckling loads that are lower than orthotropic predictions by 65% for long graphite-epoxy shells. Conversely, the orthotropic predictions are too high by about 186%. Somewhat smaller differences occur for boron-epoxy shells. For buckling of antisymmetrically laminated cross-ply shells, the effect of bending-extension coupling dies out rapidly as the number of layers increases to the point where, for many practical laminates, the effect is unimportant.

For unsymmetrically laminated cross-ply circular cylindrical shells, a very contrived example is used to illustrate what can happen if bending-extension coupling is ignored. The special example is necessary be-

Éléments sous droits d'auteur

cause general results cannot be presented for a class of laminates with infinite variety. For buckling problems, the effect of bending-extension coupling decreases very *slowly* with an increasing number of layers in contrast to the rapid decrease for antisymmetrically laminated shells. Even for a laminate with as many as *forty* layers, the effect of bending-extension coupling is about 20%! Another specific laminate example was used to demonstrate that the effect of bending-extension coupling can be even higher or much lower depending on the distribution of layers in the laminate. Thus, designers will have to account for bending-extension coupling in *all* practical unsymmetric laminates. This conclusion was reached by use of a simple counterexample argument. That is, we found a class of unsymmetric laminates which, even for many layers, exhibits large differences from orthotropic solutions for buckling loads because of bending-extension coupling. Accordingly, the *possibility* of bending-extension coupling being important for general unsymmetric laminates has been clearly established. That is, the existance of the possibility means that we must consider and analyze bending-extension coupling for *all* unsymmetric laminates.

The effect of rigorously determined prebuckling deformations on buckling loads was found in the manner of Almroth [4-10] by Jones and Hennemann [4-69] for antisymmetric cross-ply laminated circular cylindrical shells with S2 simply supported edge buckling boundary conditions. The calculated buckling loads are not numerically very different from the classical buckling loads in which prebuckling effects are ignored. This situation is quite different from isotropic monocoque shells for which prebuckling effects can lead to buckling loads up to 20% lower than classical buckling loads for S2 buckling boundary conditions. Thus, the inclusion of prebuckling effects in design analysis of cross-ply laminated circular cylindrical shells is probably not warranted for S2 buckling boundary conditions. The same claim cannot be made for other buckling boundary conditions. In fact, Booton and Tennyson [4-70] obtain results for the effect of prebuckling deformations on buckling of axially compressed glass-epoxy circular cylindrical shells with clamped edges. For a $[\theta/-\theta]$ laminated shell with $L^2/rt = 200$, the actual buckling loads (with rigorous prebuckling deformations) range from a few percent higher than the classical loads at $\theta = 0°$ and $\theta = 90°$ to as much as 15% lower than the classical buckling loads at $\theta = 15°$. Thus, investigation of the full set of possible buckling boundary conditions appears warranted.

Recent books with additional composite shell results include that by Vinson and Sierakowski [4-71] and by Vasiliev [4-72] who also addresses shells of revolution including pressure vessels. Also consult the extensive compendium of composite materials and structures books, review papers, conference proceedings, ASTM STPs, and journals by Bogdanovich and Sierakowski [4-73].

Problem Set 4.8

4.8.1 Derive the variations in forces as a function of the variations in middle-surface strains and curvatures, Equation (4.242).
4.8.2 Derive the buckling differential equations, Equation (4.247).
4.8.3 Derive the buckling criterion, Equation (4.250).

Éléments sous droits d'auteur

4.9 EFFECT OF RESTRAINED THERMAL EXPANSION

4.9.1 Introduction

Our objective in this section is to determine the influence that thermal expansion caused by spatially uniform temperature change has on the stress state of a circular cylindrical shell that has suitable restraint against thermal expansion and, further, what effect that stress state has on shell buckling. The shell thermal buckling problem is much more general than that restricted problem, and we will describe some features of the more general problem. The reader should review both bar thermal buckling in Section 2.9 and plate thermal buckling in Section 3.7 before addressing the present treatment of shell thermal buckling. Even if you do review those sections, you will often find yourself going back to those topics for results and analogies to help you understand the mechanics of shell thermal buckling.

Recall some of the fundamental origins of thermal stresses and of thermal strains that are discussed in Section 2.9.2 prior to treating thermal buckling of bars. The stresses that we call thermal stresses are actually *thermally induced stresses* because a stress is just a stress irrespective of its origin (and *all* stresses are a figment of our imagination as well!). However, for the sake of convenience in this book, we refer to thermally induced stresses as simply thermal stresses. Recall that one-dimensional bars must have axial restraint in order to develop thermal stresses under uniform through-the-thickness thermal loading. Two-dimensional plates develop thermal stresses if restrained in their plane, e.g., between two opposite boundaries of a rectangular plate. However, two-dimensional plates do *not* require external or boundary restraint to develop thermal stresses. Similarly, circular cylindrical shells develop thermal stresses if restrained axially or even radially at their ends. That is, the edges at each end are the only place we can control the deformation unless we apply some kind of surface restraint between the ends. Shells, like plates, do *not* require external or boundary restraint to develop thermal stresses. Various temperature-change distributions can lead to thermal stresses high enough to cause buckling.

Shells, just like plates, can, under certain circumstances, *self-impose* thermal stresses by means of inherent internal elastic restraints. For example, if a locally concentrated temperature increase (a hot spot) is imposed on a plate or shell, then the surrounding colder regions of the plate or shell provide elastic restraint against expansion of the hotter region (just as the bar with a nonlinear temperature gradient in Section 2.9.2 develops thermal stresses and thermal strains). Note that the thermal stresses must be self-equilibrating if no external restraint is provided. The compressive thermal stresses in the hot region of a plate or shell could get high enough to cause thermal buckling. The tensile thermal stresses in the cold region do not suppress buckling, but, in fact, drive buckling by inducing compressive thermal stresses when the cold region 'declines' to expand as much as the hot region 'wants' it to. Such problems are not simple because the prebuckling equilibrium stress state

Éléments sous droits d'auteur

is highly nonuniform (a significant thermoelasticity problem by itself), and the buckling differential equation therefore has nonconstant coefficients, so must be solved with numerical techniques. We will address only the simpler boundary restraints that cause thermal buckling under uniform heating in this section and leave the internal restraints and self-equilibrating stress fields to further study.

Just as axial restraint and in-plane boundary restraint were the key factors in determining the prebuckling equilibrium stresses for uniformly heated bars and plates, respectively, in-surface edge restraints are the key factor for determining the prebuckling stresses for uniformly heated shells. The specific nature of the prebuckling in-surface restraint to free thermal expansion must be clearly identified. Out-of-surface restraint by itself does not cause in-surface stresses that lead to buckling. If there is no restraint, then a spatially uniform increase in temperature merely leads to free thermal expansion with no accompanying stresses in an isotropic shell, and no thermal buckling can occur. However, with in-surface restraint, thermal forces that can cause buckling do develop. Thus, we will address a simply supported shell almost in the 'usual' sense except for considerable focus on the nature of the in-surface restraint.

For bars, plates, and shells, rotational restraints at the ends or edges do not affect the prebuckling forces, but do strongly influence the bar, plate, or shell buckling loads. Recall from Section 2.9 that for a bar, axial restraint at the bar ends determines whether thermal load can be developed (and without axial restraint, there is no thermal load), but rotational restraint (or lack thereof) at the bar end determines how high the thermal load can get until buckling occurs. For example, the thermal load is $E\alpha\Delta TA$ for both pinned-pinned bars and fixed-fixed bars that have both ends perfectly restrained against axial movement. However, that thermal load grows only to the value π^2EI/L^2 for pinned-pinned bars before buckling whereas the thermal load can grow to $4\pi^2EI/L^2$ for fixed-fixed bars with a ΔT four times higher than that for pinned-pinned bars. For a plate, the in-plane restraint at the plate edges determines whether the uniform thermal load can be developed in the direction perpendicular to the in-plane restraint (and without that restraint there is no thermal load), but the rotational restraint (or lack thereof) at each plate edge determines how high the thermal load can get until buckling occurs. In addition to the simply supported shell we address, we could treat a clamped-edge shell, but with a variety of in-surface restraint conditions. For the same in-surface restraint, the clamped-edge shell has a higher thermal buckling load than the simply supported shell because of the higher out-of-surface deformation resistance of the clamped-edge shell.

Shells are two-dimensional in character (we effectively eliminate the dimension perpendicular to the shell surface by using the Kirchhoff-Love hypothesis [4-4]), so the *possibility* of combined thermal and mechanical loading exists. How the combined loading can occur depends on the restraint conditions possible for each structural element. Bars can be restrained only in the axial direction to create conditions that lead to buckling, so combined thermal and mechanical loading can occur only in the axial direction under conditions of screw-type loading as described

Éléments sous droits d'auteur

in Section 2.9.4. The plate problem is more complicated than the bar problem because of the two-dimensional nature of a plate. Plates can have in-plane restraint in either or both of the two perpendicular directions relative to the (rectangular) plate edges (with additional complications because of the Poisson effect). Thus, in-plane boundary condition restraint-compatibility conditions arise at the plate corners, as discussed in Section 3.7.3 (and simultaneous thermal and mechanical loading can be applied in a single direction if the mechanical loading is applied in a screw-type load frame). In contrast, shells can be restrained only in the axial direction (unless out-of-surface restraints are applied), so no adjacent-edge restraint-compatibility conditions exist for circular cylindrical shells. You are advised to review the discussion of plates with biaxial mechanical loads in Section 3.3.3 before addressing problems of shells with combined mechanical and thermal load. For shells, both thermal buckling and buckling caused by mechanical loads can occur under certain circumstances. For example, axial edge restraint of heated shells causes axial thermal stresses, but mechanical axial loading can also occur simultaneously with screw-type loading as depicted in Figure 3-78 on page 366. Also, heating with axial restraint and lateral pressure loading leads to a combined thermal and mechanical buckling problem.

Thermal buckling of shells parallels that of plates because both involve inherently two-dimensional prebuckling stress states (with three-dimensional deformation states after buckling). However, the simple flat prebuckling deformation state of plates has no analogy in the more complex prebuckling deformation state of circular cylindrical shells. For shells, we must take certain liberties of approximations to gain some solutions with varying degrees of accuracy. Boundary conditions, as in all buckling problems (but especially thermal buckling problems), play a significant and crucial role. For classical buckling analysis of a shell, we imagine the prebuckling deformations of a circular cylindrical shell under axial load to be merely an axial contraction and a uniform radial expansion that constitutes a membrane, i.e., another circular cylindrical surface of constant curvature in the circumferential direction with larger radius than in the undeformed (unloaded) state, as in Figure 4-83. Thus, the shell edge boundary conditions permit both axial and radial movement in the prebuckling equilibrium state. Another way of stating the situation is that prior to buckling there are no boundary conditions! We must attempt to achieve that membrane prebuckling deformation state for a uniformly

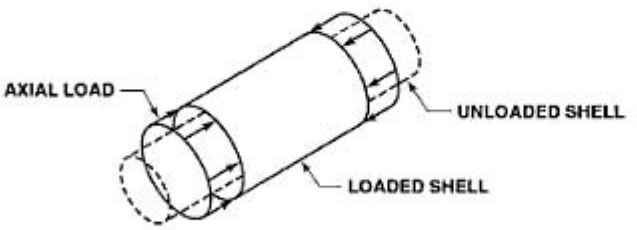


Figure 4-83 Exaggerated Membrane Prebuckling Deformation

Éléments sous droits d'auteur

heated shell in order to construct a classical shell thermal buckling analysis in analogy to classical buckling under mechanical loading.

In actuality, the shell, if restrained at each end prior to buckling by a ring-like simple support that cannot move in the axial direction must deform as the curve labeled 'rigorous prebuckling deformation' in Figure 4-84 as in Section 4.5. That is, the circumference of the shell must be restrained at the support (by restraining the radial deformation at the edge), so the equilibrium radial deformation under load has quite a pronounced variation near the edge, but dies out quite rapidly to the membrane prebuckling deformation as in Figure 4-84. The complexity of retaining the actual equilibrium deformation in Figure 4-84 is treated by Almroth [4-10] for isotropic shells. However, his solution constitutes a second-order theory of buckling that is not appropriate for the first-order (classical) thermal buckling theory treated in this section. Accordingly, the prebuckling deformation is considerably simplified relative to the physical reality of some kind of immoveable support system. Prior to buckling, the shell is considered to be a membrane with no curvature in the axial direction and a slightly decreased (but constant over the shell surface) curvature in the circumferential direction because of movement during the application of a change in temperature.

In this section, we first examine the fundamental thermoelastic relations in Section 4.9.2. Then, the in-surface loading and edge restraint conditions needed to solve structural mechanics problems of thermal buckling of shells are described in Section 4.9.3. Next, the Equivalent Mechanical Load Concept that was introduced for plates in Section 3.7.4 is addressed for shells in Section 4.9.4. Subsequently, two simple thermal buckling problems for shells are solved. First, an axially restrained shell under uniform heating is treated in Section 4.9.5. Then, uniform heating and lateral pressure are simultaneously applied to an axially restrained shell in Section 4.9.6. Finally, we summarize our accomplishments and then explore the nature of some more complicated shell thermal buckling problems in Section 4.9.7.

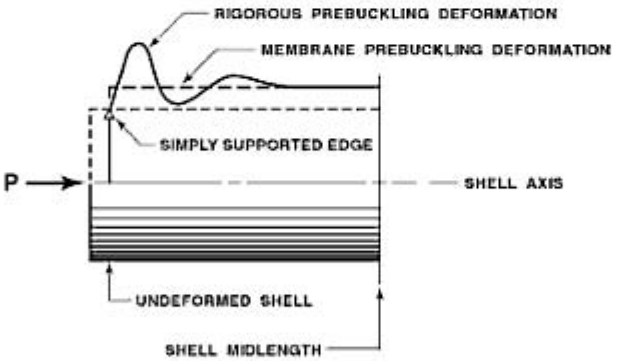


Figure 4-84 Membrane versus Rigorous Prebuckling Deformation

Éléments sous droits d'auteur

4.9.2 Fundamental Thermoelastic Relations

For an isotropic elastic shell subjected to a biaxial state of (plane) stress and some form of temperature-change distribution over the shell volume, the two-dimensional thermoelastic strain-stress relations are

$$\begin{aligned} \varepsilon_x &= \frac{\sigma_x}{E} - \frac{\nu}{E}\sigma_y + \alpha\,\Delta T \\ \varepsilon_y &= -\frac{\nu}{E}\sigma_x + \frac{\sigma_y}{E} + \alpha\,\Delta T \\ \gamma_{xy} &= \frac{\tau_{xy}}{G} \end{aligned} \tag{4.262}$$

in which (1) ε_x, ε_y, and γ_{xy} are the total strains, (2) σ_x/E, σ_y/E, and τ_{xy}/G are mechanical strains and (3) $\alpha\,\Delta T$ is the free thermal strain resulting from the temperature change at any point in the plate volume as a function of time, namely $\Delta T = T(x,y,z,t) - T_{ref}$, where T_{ref} is the arbitrary and convenient reference temperature at which no strain is observed in a baseline configuration of 'zero strain' or zero thermal stress. We will not address the time dependence of the temperature change in this section except in Section 4.9.7. Note that an isotropic body only expands (contracts) upon heating (cooling) and does not exhibit any shearing deformation caused solely by thermal loading. In contrast, heating or cooling of an orthotropic body does induce shearing deformations.

The corresponding two-dimensional thermoelastic stress-strain relations are, by inversion of Equation (4.262),

$$\begin{aligned} \sigma_x &= \frac{E}{1-\nu^2}(\varepsilon_x - \alpha\Delta T) + \frac{\nu E}{1-\nu^2}(\varepsilon_y - \alpha\Delta T) \\ \sigma_y &= \frac{\nu E}{1-\nu^2}(\varepsilon_x - \alpha\Delta T) + \frac{E}{1-\nu^2}(\varepsilon_y - \alpha\Delta T) \\ \tau_{xy} &= G\gamma_{xy} \end{aligned} \tag{4.263}$$

in which ε_x, ε_y, and γ_{xy} are the total strains, $\alpha\Delta T$ is the free thermal strain, and $\varepsilon_x - \alpha\Delta T$ and $\varepsilon_y - \alpha\Delta T$ are apparently the mechanical strains.

In a typical structural mechanics problem, we impose conditions (1) on the total strain (such as, e.g., $\varepsilon_x = 0$ on a heated bar between two immovable walls as in Figure 4-85a) which can be regarded as a displacement-type boundary condition, e.g., $u = 0$ at the ends of the bar or (2) on the stress (such as, e.g., $\sigma_x = 0$ on the free end of a heated cantilever bar as in Figure 4-85b), i.e., a stress-type boundary condition. Shell support conditions will be addressed in more detail in Section 4.9.3 where we will see conditions analogous to those for bars in Figure 4-85.



a Bar between Walls b Cantilever Bar

Figure 4-85 Two Bar Support Conditions

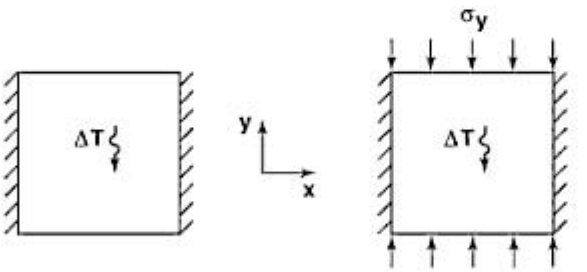
Éléments sous droits d'auteur

Consider the plate that is restrained from in-plane movement in the x-direction but not restrained in the y-direction in Figure 4-86. If only thermal loading is applied as in Figure 4-86a, then the total strains are $\varepsilon_x = 0$ and $\varepsilon_y \neq 0$ [see if you can prove that $\varepsilon_y = (1 - \nu)\alpha\Delta T$] whereas the stresses are $\sigma_x = -E\alpha\Delta T$ and $\sigma_y = 0$. Obviously, σ_x is a thermal stress (a stress of thermal origin) and there is no mechanical stress. If both thermal and mechanical loading are applied as in Figure 4-86b, then the total strains are $\varepsilon_x = 0$ because of the perfect restraint and $\varepsilon_y \neq 0$ because mechanical load σ_y is applied as well as ΔT. The resulting stresses are somewhat involved. First, σ_x has one component caused by restraint of thermal expansion and another component caused by restraint of the Poisson expansion. Thus, σ_x is both a thermal and a mechanical stress. Also, σ_y is a mechanical stress. However, both stresses have the same symbol, σ, i.e., are indistinguishable from each other in the stress-strain relations, Equation (4.263). Thus, unlike strains, *stresses cannot necessarily be simply labeled as mechanical or thermal stresses because their specific identity depends on the support and loading conditions.*

By the Kirchhoff-Love shell deformation hypothesis [4-4], lines originally normal to the undeformed middle surface remain normal after deformation and do not change length as in Figure 4-6 on page 468, i.e.,

$$\gamma_{xz} = \gamma_{yz} = 0 \qquad \varepsilon_z = 0 \tag{4.264}$$

which is a state of plane strain. We have implied a state of plane stress and simultaneously a state of plane strain, an unacceptable fundamental contradiction of elasticity theory. However, ordinary shell theory is not elasticity theory but is a mechanics of materials approach in which vastly simplifying presumptions are made based on apparent physical reasons related to the nature of the behavior (e.g., we say plane sections remain plane for beams because we can see from lines drawn on the side of a beam before bending that those lines remain straight in Figure 2-44 on page 107 after deformation *to the resolution level of our naked eye!*) and are simply part of the necessarily approximate and imperfect problem-solving process. Of course, with heating or cooling, the shell thickness changes (hence, there actually is a transverse strain, ε_z), but we do not address that out-of-plane behavior in this book.



a Uniform Thermal Load b Uniform Thermal and Mechanical Load

Figure 4-86 Plate Restrained in the x-Direction

Éléments sous droits d'auteur

Consequently, the total strains are observed to vary in an approximately linear manner through the shell thickness:

$$\begin{aligned} \varepsilon_x &= \bar{\varepsilon}_x + z\,\kappa_x \\ \varepsilon_y &= \bar{\varepsilon}_y + z\,\kappa_y \\ \gamma_{xy} &= \bar{\gamma}_{xy} + z\,\kappa_{xy} \end{aligned} \tag{4.265}$$

in which the terms $\bar{\varepsilon}_x$, $\bar{\varepsilon}_y$, and $\bar{\gamma}_{xy}$ are nonlinear moderately large-deflection middle-surface strains in the manner of von Kármán [4-3]:

$$\begin{aligned} \bar{\varepsilon}_x &= \frac{\partial u_o}{\partial x} + \frac{1}{2}\left[\frac{\partial w_o}{\partial x}\right]^2 \\ \bar{\varepsilon}_y &= \frac{\partial v_o}{\partial y} + \frac{w_o}{r} + \frac{1}{2}\left[\frac{\partial w_o}{\partial y}\right]^2 \\ \bar{\gamma}_{xy} &= \frac{\partial u_o}{\partial y} + \frac{\partial v_o}{\partial x} + \frac{\partial w_o}{\partial x}\frac{\partial w_o}{\partial y} \end{aligned} \tag{4.266}$$

in which u_o and v_o are in-surface displacements of the shell middle surface, w_o is the transverse deflection of the shell middle surface, z is the through-the-thickness coordinate from the middle surface, and κ_x, κ_y, and κ_{xy} are the middle-surface curvatures:

$$\kappa_x = -\frac{\partial^2 w_o}{\partial x^2} \qquad \kappa_y = -\frac{\partial^2 w_o}{\partial y^2} \qquad \kappa_{xy} = -2\frac{\partial^2 w_o}{\partial x \partial y} \tag{4.267}$$

However, we presume $\varepsilon_z = 0$, so w_o cannot be distinguished from w at any point through the thickness. Thus, we will use w in the following derivations instead of w_o as well as simply u and v, and for all such symbols we mean middle-surface values.

The Kirchhoff-Love hypothesis is applicable only to strains from pure bending, i.e., the only loading is moments M_x and M_y as in Figure 4-4 on page 465. To account for the free thermal expansion of a shell, we merely add the free thermal expansion to the mechanical strains to get the total strains and invert the result to get the stress-strain relations

$$\begin{aligned} \sigma_x &= \frac{E}{1-\nu^2}(\bar{\varepsilon}_x - z\,w_{xx} - \alpha\Delta T) + \frac{\nu E}{1-\nu^2}(\bar{\varepsilon}_y - z\,w_{yy} - \alpha\Delta T) \\ &= \frac{E}{1-\nu^2}\left[(\bar{\varepsilon}_x - \nu\bar{\varepsilon}_y) - z(w_{xx} + \nu w_{yy}) - (1+\nu)\alpha\Delta T\right] \\ \sigma_y &= \frac{\nu E}{1-\nu^2}(\bar{\varepsilon}_x - z\,w_{xx} - \alpha\Delta T) + \frac{E}{1-\nu^2}(\bar{\varepsilon}_y - z\,w_{yy} - \alpha\Delta T) \\ &= \frac{E}{1-\nu^2}\left[(\bar{\varepsilon}_y - \nu\bar{\varepsilon}_x) - z(w_{yy} + \nu w_{xx}) - (1+\nu)\alpha\Delta T\right] \\ \tau_{xy} &= G\bar{\gamma}_{xy} \end{aligned} \tag{4.268}$$

Éléments sous droits d'auteur

in which $\bar{\varepsilon}_x$, $\bar{\varepsilon}_y$, and $\bar{\gamma}_{xy}$ contain in Equation (4.266) nonlinear terms that are essential for buckling analysis, but we will keep those nonlinear terms within the middle-surface strains, $\bar{\varepsilon}_x$, $\bar{\varepsilon}_y$, and $\bar{\gamma}_{xy}$, for a few steps.

The in-surface forces (per unit width by convention used throughout this book) on a shell element are

$$N_x = \int \sigma_x \, dz = \frac{E}{1-\nu^2} \int (\bar{\varepsilon}_x + \nu \bar{\varepsilon}_y) \, dz - \frac{E(1+\nu)}{1-\nu^2} \int \alpha \, \Delta T \, dz$$

$$= \frac{E}{1-\nu^2} \int (\bar{\varepsilon}_x + \nu \bar{\varepsilon}_y) \, dz - \frac{E}{1-\nu^2} \int (w_{xx} + \nu w_{yy}) \, z \, dz - \frac{E}{1-\nu} \int \alpha \, \Delta T \, dz$$

$$= \frac{E}{1-\nu^2} (\bar{\varepsilon}_x + \nu \bar{\varepsilon}_y) \int dz - \frac{E}{1-\nu^2} (w_{xx} + \nu w_{yy}) \int z \, dz - \frac{E}{1-\nu} \int \alpha \, \Delta T \, dz$$

$$= \frac{E\,t}{1-\nu^2} (\bar{\varepsilon}_x + \nu \bar{\varepsilon}_y) - \frac{E}{1-\nu} \int \alpha \, \Delta T \, dz = A(\bar{\varepsilon}_x + \nu \bar{\varepsilon}_y) - N^T$$

$$N_y = \frac{E\,t}{1-\nu^2} (\bar{\varepsilon}_y + \nu \bar{\varepsilon}_x) - \frac{E}{1-\nu} \int \alpha \, \Delta T \, dz = A(\bar{\varepsilon}_y + \nu \bar{\varepsilon}_x) - N^T$$

$$N_{xy} = G\,t\,\bar{\gamma}_{xy} = \frac{1-\nu}{2} A \bar{\gamma}_{xy} \tag{4.269}$$

in which the extensional stiffness is $A = Et/(1-\nu^2)$ as defined on page 242 and we define the thermal force (per unit width) as

$$N^T = \frac{E}{1-\nu} \int \alpha \, \Delta T \, dz \tag{4.270}$$

which depends on how the temperature change, ΔT, and coefficient of thermal expansion, α, vary through the shell thickness.

The moments (per unit width) on a shell element are

$$M_x = \int \sigma_x \, z \, dz = \frac{E}{1-\nu^2} \int (\bar{\varepsilon}_x + \nu \bar{\varepsilon}_y) \, z \, dz - \frac{E(1+\nu)}{1-\nu^2} \int \alpha \, \Delta T \, z \, dz$$

$$= \frac{E}{1-\nu^2} \left[\int (\bar{\varepsilon}_x + \nu \bar{\varepsilon}_y) \, z \, dz - \int (w_{xx} + \nu w_{yy}) \, z^2 \, dz \right] - \frac{E}{1-\nu} \int \alpha \, \Delta T \, z \, dz$$

$$= \frac{E}{1-\nu^2} \left[(\bar{\varepsilon}_x + \nu \bar{\varepsilon}_y) \int z \, dz - (w_{xx} + \nu w_{yy}) \int z^2 \, dz \right] - \frac{E}{1-\nu} \int \alpha \, \Delta T \, z \, dz$$

$$= -\frac{E\,t^3}{12(1-\nu^2)} (w_{xx} + \nu w_{yy}) - \frac{E}{1-\nu} \int \alpha \, \Delta T \, z \, dz = -D(w_{xx} + \nu w_{yy}) - M^T$$

$$M_y = -\frac{E\,t^3}{12(1-\nu^2)} (w_{yy} + \nu w_{xx}) - \frac{E}{1-\nu} \int \alpha \, \Delta T \, z \, dz = -D(w_{yy} + \nu w_{xx}) - M^T$$

$$M_{xy} = -G \frac{t^3}{6} w_{xy} = -\frac{E}{1+\nu} \frac{t^3}{12} w_{xy} = -(1-\nu) D w_{xy} \tag{4.271}$$

Éléments sous droits d'auteur

in which the bending stiffness is $D = Et^3/\left[12(1-\nu^2)\right]$ as defined on page 242, and we define the thermal moment (per unit width) as

$$M^T = \frac{E}{1-\nu}\int \alpha\,\Delta T\, z\, dz \tag{4.272}$$

which depends on how the moment of the temperature change, ΔT, and coefficient of thermal expansion, α, vary through the shell thickness.

The in-surface forces (per unit width) with explicit nonlinear terms are

$$N_x = \frac{Et}{1-\nu^2}\left[\left[\frac{\partial u_o}{\partial x}+\frac{1}{2}\left[\frac{\partial w}{\partial x}\right]^2\right]+\nu\left[\frac{\partial v_o}{\partial y}+\frac{w}{r}+\frac{1}{2}\left[\frac{\partial w}{\partial y}\right]^2\right]\right]-N^T$$

$$N_y = \frac{Et}{1-\nu^2}\left[\left[\frac{\partial v_o}{\partial y}+\frac{w}{r}+\frac{1}{2}\left[\frac{\partial w}{\partial y}\right]^2\right]+\nu\left[\frac{\partial u_o}{\partial x}+\frac{1}{2}\left[\frac{\partial w}{\partial x}\right]^2\right]\right]-N^T$$

$$N_{xy} = \frac{Et}{1+\nu}\left[\frac{\partial u_o}{\partial y}+\frac{\partial v_o}{\partial x}+\frac{\partial w}{\partial x}\frac{\partial w}{\partial y}\right] \tag{4.273}$$

or in more compact notation, upon realizing that all terms exist only on the shell middle surface,

$$\begin{aligned} N_x &= A\left[(u_x+\frac{1}{2}w_x^2)+\nu(v_y+\frac{w}{r}+\frac{1}{2}w_y^2)\right]-N^T \\ N_y &= A\left[(v_y+\frac{w}{r}+\frac{1}{2}w_y^2)+\nu(u_x+\frac{1}{2}w_x^2)\right]-N^T \\ N_{xy} &= (1-\nu)A(u_y+v_x+w_xw_y) \end{aligned} \tag{4.274}$$

The moderately large-deflection equilibrium differential equations and associated boundary conditions as well as the buckling differential equations and associated boundary conditions can be derived in the manner of the fundamental energy approach used in Section 4.2. Simply include the thermal effects in the strain energy density expression (strain energy per unit volume) by subtracting the free thermal strains from the total strains to get the mechanical strains that cause energy to be stored:

$$\begin{aligned} U_o &= \frac{E}{2(1-\nu^2)}\left[(\varepsilon_x-\alpha\Delta T)^2+(\varepsilon_y-\alpha\Delta T)^2\right. \\ &\qquad \left.+2\nu(\varepsilon_x-\alpha\Delta T)(\varepsilon_y-\alpha\Delta T)+\frac{1-\nu}{2}\gamma_{xy}^2\right] \\ &= \frac{E}{2(1-\nu^2)}\left[\varepsilon_x^2-2\varepsilon_x\alpha\Delta T+(\alpha\Delta T)^2+\varepsilon_y^2-2\varepsilon_y\alpha\Delta T+(\alpha\Delta T)^2\right. \\ &\qquad \left.+2\nu\varepsilon_x\varepsilon_y-2\nu\varepsilon_x\alpha\Delta T-2\nu\varepsilon_y\alpha\Delta T+2\nu(\alpha\Delta T)^2+\frac{1-\nu}{2}\gamma_{xy}^2\right] \\ &= \frac{E}{2(1-\nu^2)}\left[(\varepsilon_x^2+\varepsilon_y^2+2\nu\varepsilon_x\varepsilon_y+\frac{1-\nu}{2}\gamma_{xy}^2)\right. \\ &\qquad \left.-2(1+\nu)(\varepsilon_x+\varepsilon_y)\alpha\Delta T+2(1+\nu)(\alpha\Delta T)^2\right] \end{aligned} \tag{4.275}$$

Éléments sous droits d'auteur

[which reduces to the strain energy density for a bar, Equation (2.553) on page 168, if $\varepsilon_y = 0$, $\gamma_{xy} = 0$, and $\nu = 0$ and is identical to the strain energy density of a plate] in which the sum of the quadratic terms in the strains constitutes the mechanical strain energy density, the sum of the linear terms in the strain and in ΔT constitutes the coupling between the mechanical and thermal effects portion of the strain energy density, and the quadratic term in ΔT is the constant thermal term that is irrelevant in the subsequent variational process when the principle of stationary potential energy is applied [because $\delta(\text{constant}) = 0$]. Thus, the only relevant additional term in the strain energy density expression beyond the mechanical effects is

$$(U_o)_T = -\frac{E}{(1-\nu)}\alpha\,\Delta T\,(\varepsilon_x + \varepsilon_y) \tag{4.276}$$

in which ΔT can be a function of x, y, and z (and time). The results of the variational process lead to the nonlinear equilibrium differential equations and linear buckling differential equations and their associated boundary conditions just as in Section 4.2. Here, we show only the results and leave verification to exercises in Problem Set 4.9.

The moderately large-deflection nonlinear circular cylindrical shell equilibrium equations with thermal effects are

$$\frac{\partial}{\partial x}\left[A\left[u_x + \frac{1}{2}w_x^2 + \nu\left(v_y + \frac{w}{r} + \frac{1}{2}w_y^2\right)\right] - N^T\right] + \frac{1-\nu}{2}A\frac{\partial}{\partial y}(v_x + u_y + w_x w_y) = 0$$

$$\frac{1-\nu}{2}A\frac{\partial}{\partial x}(v_x + u_y + w_x w_y) + \frac{\partial}{\partial y}\left[A\left[v_y + \frac{w}{r} + \frac{1}{2}w_y^2 + \nu\left(u_x + \frac{1}{2}w_x^2\right)\right] - N^T\right] = 0$$

$$\left[A\left[\left(v_y + \frac{w}{r} + \frac{1}{2}w_y^2\right) + \nu\left(u_x + \frac{1}{2}w_x^2\right)\right] - N^T\right]\Big/r$$
$$-\frac{\partial}{\partial x}\left[w_x\left[A\left[u_x + \frac{1}{2}w_x^2 + \nu\left(v_y + \frac{w}{r} + \frac{1}{2}w_y^2\right)\right] - N^T\right] + \frac{1-\nu}{2}Aw_y(v_x + u_y + w_x w_y)\right]$$
$$-\frac{\partial}{\partial y}\left[w_y\left[A\left[v_y + \frac{w}{r} + \frac{1}{2}w_y^2 + \nu\left(u_x + \frac{1}{2}w_x^2\right)\right] - N^T\right] + \frac{1-\nu}{2}Aw_x(v_x + u_y + w_x w_y)\right]$$
$$+D\left[\frac{\partial^2}{\partial x^2}(w_{xx} + \nu w_{yy}) + 2(1-\nu)\frac{\partial^2}{\partial x \partial y}w_{xy} + \frac{\partial^2}{\partial y^2}(w_{yy} + \nu w_{xx})\right] + \nabla^2 M^T = -p \tag{4.277}$$

and the associated boundary conditions on edges $x = 0, L$ are

$$u = 0 \quad \text{or} \quad A\left[\left(u_x + \frac{1}{2}w_x^2\right) + \nu\left(v_y + \frac{w}{r} + \frac{1}{2}w_y^2\right)\right] - N^T = \bar{N}_x$$

$$v = 0 \quad \text{or} \quad \frac{1-\nu}{2}A(v_x + u_y + w_x w_y) = \bar{N}_{xy}$$

$$w = 0 \quad \text{or} \quad w_x\left[A\left[u_x + \frac{1}{2}w_x^2 + \nu\left(v_y + \frac{w}{r} + \frac{1}{2}w_y^2\right)\right] - N^T\right] + \frac{1-\nu}{2}Aw_y(v_x + u_y + w_x w_y)$$
$$-\left[D\frac{\partial}{\partial x}(w_{xx} + \nu w_{yy}) + M^T + D\frac{\partial}{\partial y}[2(1-\nu)w_{xy}]\right] = \bar{K}_x$$

$$w_x = 0 \quad \text{or} \quad -D(w_{xx} + \nu w_{yy}) - M^T = \bar{M}_x \tag{4.278}$$

Éléments sous droits d'auteur

We now turn our attention from the thermoelastic equilibrium problem to the thermoelastic buckling problem of a circular cylindrical shell. We must determine the variations in forces and moments that occur during buckling in terms of the variations in stresses. Then, we use the variational process to find the differential equations governing buckling.

The variations in forces and moments during buckling are

$$\delta N_x = \int \delta\sigma_x \, dz \qquad \delta N_y = \int \delta\sigma_y \, dz \qquad \delta N_{xy} = \int \delta\tau_{xy} \, dz \tag{4.279}$$

$$\delta M_x = \int \delta\sigma_x \, z \, dz \qquad \delta M_y = \int \delta\sigma_y \, z \, dz \qquad \delta M_{xy} = \int \delta\tau_{xy} \, z \, dz \tag{4.280}$$

in which the variations in stresses during buckling are

$$\begin{aligned} \delta\sigma_x &= \frac{E}{1-\nu^2}(\delta\varepsilon_x + \nu\delta\varepsilon_y) \\ \delta\sigma_y &= \frac{E}{1-\nu^2}(\delta\varepsilon_y + \nu\delta\varepsilon_x) \\ \delta\tau_{xy} &= \frac{E}{2(1+\nu)}\delta\gamma_{xy} \end{aligned} \tag{4.281}$$

Note that the $\alpha\,\Delta T$ terms in the thermoelastic stress-strain relations, Equation (4.263), *do not have a variation*, i.e., both α and ΔT are constant during buckling, just as is the mechanical load when the displacements are varied. Thus, all variations of thermal forces and thermal moments are zero because these thermal loadings, like the mechanical loadings, are constant in the variational process.

The variations in strains are

$$\begin{aligned} \delta\varepsilon_x &= \delta\bar{\varepsilon}_x + z\,\delta\kappa_x \\ \delta\varepsilon_y &= \delta\bar{\varepsilon}_y + z\,\delta\kappa_y \\ \delta\gamma_{xy} &= \delta\bar{\gamma}_{xy} + z\,\delta\kappa_{xy} \end{aligned} \tag{4.282}$$

Then, after elimination of the subscript zero for the middle surface, the variations in middle-surface strains are

$$\begin{aligned} \delta\bar{\varepsilon}_x &= \delta u_x + w_x\delta w_x \\ \delta\bar{\varepsilon}_y &= \delta v_y + \frac{\delta w}{r} + w_y\delta w_y \\ \delta\bar{\gamma}_{xy} &= \delta v_x + \delta u_y + w_x\delta w_y + w_y\delta w_x \end{aligned} \tag{4.283}$$

which for an initially membrane-shaped shell with $w_x = w_y = 0$ become

$$\begin{aligned} \delta\bar{\varepsilon}_x &= \delta u_x \\ \delta\bar{\varepsilon}_y &= \delta v_y + \frac{\delta w}{r} \\ \delta\bar{\gamma}_{xy} &= (\delta v_x + \delta u_y) \end{aligned} \tag{4.284}$$

Also, the variations in middle-surface curvatures are

$$\delta\kappa_x = -\delta w_{xx} \qquad \delta\kappa_y = -\delta w_{yy} \qquad \delta\kappa_{xy} = -2\delta w_{xy} \tag{4.285}$$

Éléments sous droits d'auteur

Thus, the variations in in-surface forces on a shell element are

$$\delta N_x = \int \sigma_x \, dz = \frac{E}{1-\nu^2} \int (\delta\bar{\varepsilon}_x + \nu\delta\bar{\varepsilon}_y) \, dz$$

$$= \frac{E}{1-\nu^2} \int (\delta\bar{\varepsilon}_x + \nu\delta\bar{\varepsilon}_y) \, dz - \frac{E}{1-\nu^2} \int (\delta w_{xx} + \nu\delta w_{yy}) \, z \, dz$$

$$= \frac{E}{1-\nu^2} (\delta\bar{\varepsilon}_x + \nu\delta\bar{\varepsilon}_y) \int dz - \frac{E}{1-\nu^2} (\delta w_{xx} + \nu\delta w_{yy}) \int z \, dz$$

$$= \frac{E\,t}{1-\nu^2} (\delta\bar{\varepsilon}_x + \nu\delta\bar{\varepsilon}_y) = A(\delta\bar{\varepsilon}_x + \nu\delta\bar{\varepsilon}_y) = A\left[\delta u_x + \nu\left(\delta v_y + \frac{\delta w}{r}\right)\right]$$

$$\delta N_y = \frac{E\,t}{1-\nu^2} (\delta\bar{\varepsilon}_y + \nu\delta\bar{\varepsilon}_x) = A(\delta v_y + \frac{\delta w}{r} + \nu\delta u_x)$$

$$\delta N_{xy} = G\,t\,\delta\gamma_{xy} = \frac{1-\nu}{2} A\delta\gamma_{xy} = \frac{1-\nu}{2} A(\delta u_y + \delta v_x) \tag{4.286}$$

and the variations in moments are

$$\delta M_x = \int \delta\sigma_x \, z \, dz = \frac{E}{1-\nu^2} \int (\delta\varepsilon_x + \nu\delta\varepsilon_y) \, z \, dz$$

$$= \frac{E}{1-\nu^2} \left[\int (\delta\bar{\varepsilon}_x + \nu\delta\bar{\varepsilon}_y) \, z \, dz - \int (\delta w_{xx} + \nu\delta w_{yy}) \, z^2 \, dz \right]$$

$$= \frac{E}{1-\nu^2} \left[(\delta\bar{\varepsilon}_x + \nu\delta\bar{\varepsilon}_y) \int z \, dz - (\delta w_{xx} + \nu\delta w_{yy}) \int z^2 \, dz \right]$$

$$= -\frac{E\,t^3}{12(1-\nu^2)} (\delta w_{xx} + \nu\delta w_{yy}) = -D(\delta w_{xx} + \nu\delta w_{yy})$$

$$\delta M_y = -\frac{E\,t^3}{12(1-\nu^2)} (\delta w_{yy} + \nu\delta w_{xx}) = -D(\delta w_{yy} + \nu\delta w_{xx})$$

$$\delta M_{xy} = -G\,\frac{t^3}{6}\,\delta w_{xy} = -\frac{E}{1+\nu}\,\frac{t^3}{12}\,\delta w_{xy} = -(1-\nu)D\delta w_{xy} \tag{4.287}$$

The in-surface forces for a shell that is membrane-shaped before buckling (so $w_x = 0$ and $w_y = 0$) become

$$N_x = A\left[u_x + \nu\left(v_y + \frac{w}{r}\right)\right] - N^T$$

$$N_y = A\left(v_y + \frac{w}{r} + \nu u_x\right) - N^T \tag{4.288}$$

$$N_{xy} = Gt(u_y + v_x) = \frac{1-\nu}{2} A(u_y + v_x)$$

Éléments sous droits d'auteur

The compressive in-surface forces at buckling are $\bar{N}_x$, $\bar{N}_y$, and $\bar{N}_{xy}$:

$$\begin{aligned}\bar{N}_x &= -N_x = -A\left[u_x + \nu\left(v_y + \frac{w}{r}\right)\right] + N^T \\ \bar{N}_y &= -N_y = -A\left(v_y + \frac{w}{r} + \nu u_x\right) + N^T \\ \bar{N}_{xy} &= -N_{xy} = -\frac{1-\nu}{2}A(u_y + v_x)\end{aligned} \tag{4.289}$$

Note that the moments do not appear in the buckling equations, only the *variations in moments during buckling* which have been shown to be

$$\begin{aligned}\delta M_x &= -D(\delta w_{xx} + \nu\delta w_{yy}) \\ \delta M_y &= -D(\delta w_{yy} + \nu\delta w_{xx}) \\ \delta M_{xy} &= -(1-\nu)D\delta w_{xy}\end{aligned} \tag{4.290}$$

The variations in in-surface forces during buckling from a membrane prebuckled state are shown in Equation (4.70) on page 487 to be

$$\begin{aligned}\delta N_x &= A\left[\delta u_x + \nu\left(\delta v_y + \frac{\delta w}{r}\right)\right] \\ \delta N_y &= A\left[\delta v_y + \frac{\delta w}{r} + \nu\delta u_x\right] \\ \delta N_{xy} &= \frac{1-\nu}{2}A(\delta v_x + \delta u_y)\end{aligned} \tag{4.291}$$

in which we note that $\delta N^T = 0$ by inspection of the expression for N^T in Equation (4.270) because α and ΔT are constant during buckling.

The process of making the second variation in strain energy stationary can be used to get the buckling differential equations and boundary conditions as was done in Section 4.2. Specifically, we supplement the second variation in energy integrals, Equations (3.164), (3.165), and (3.166) on page 263, with

$$\delta^2 U_T = -\iint N^T(\delta w_x^2 + \delta w_y^2)dxdy \tag{4.292}$$

which can easily be shown to come from varying the integral of the strain energy density of the coupled mechanical and thermal terms, Equation (4.276), over the area of the shell.

The shell buckling equations (without body forces) are identical to the equations for mechanical loading from Section 4.2.2, i.e., Equations (4.71)–(4.73) on page 487:

$$\delta N_{x,x} + \delta N_{xy,y} = 0 \tag{4.293}$$

$$\delta N_{xy,x} + \delta N_{y,y} = 0 \tag{4.294}$$

$$\delta M_{x,xx} + 2\delta M_{xy,xy} + \delta M_{y,yy} - \bar{N}_x\delta w_{xx} - 2\bar{N}_{xy}\delta w_{xy} - \bar{N}_y\delta w_{yy} - \delta N_y/r = 0 \tag{4.295}$$

or

$$D\nabla^4\delta w + \bar{N}_x\delta w_{xx} + 2\bar{N}_{xy}\delta w_{xy} + \bar{N}_y\delta w_{yy} + \delta N_y/r = 0 \tag{4.296}$$

Éléments sous droits d'auteur

in which we seek the values of the applied compressive in-surface mechanical and thermal forces at buckling, $\bar{N}_x$, $\bar{N}_y$, and $\bar{N}_{xy}$ that yield a solution to Equations (4.293), (4.294), and (4.295) or (4.296). The nature (distribution) of those forces is obtained from the prebuckling equilibrium solution to the shell problem. Note that the first variations of the thermal forces and thermal moments are zero. The thermal force, N^T, is implicitly included in $\bar{N}_x$ and/or $\bar{N}_y$ to account for the thermal loading. Note that the thermal moment, M^T, does not appear in the buckling equation because such a moment would cause the shell to bend immediately upon imposition of the slightest ΔT rather than buckle at an elevated ΔT. That is, those loadings that create a thermal moment do not cause buckling.

The associated buckling boundary conditions for the buckling problem analogous to those for the equilibrium problem in Almroth's notation [4-10] for shells are:

Simply Supported Edges:

$$\begin{array}{llllll} \text{S1:} & \delta w = 0 & \delta M_x = 0 & \delta u = 0 & \delta v = 0 \\ \text{S2:} & \delta w = 0 & \delta M_x = 0 & \delta N_x = 0 & \delta v = 0 \\ \text{S3:} & \delta w = 0 & \delta M_x = 0 & \delta u = 0 & \delta N_{xy} = 0 \\ \text{S4:} & \delta w = 0 & \delta M_x = 0 & \delta N_x = 0 & \delta N_{xy} = 0 \end{array} \tag{4.297}$$

Clamped Edges:

$$\begin{array}{llllll} \text{C1:} & \delta w = 0 & \delta w_{,x} = 0 & \delta u = 0 & \delta v = 0 \\ \text{C2:} & \delta w = 0 & \delta w_{,x} = 0 & \delta N_x = 0 & \delta v = 0 \\ \text{C3:} & \delta w = 0 & \delta w_{,x} = 0 & \delta u = 0 & \delta N_{xy} = 0 \\ \text{C4:} & \delta w = 0 & \delta w_{,x} = 0 & \delta N_x = 0 & \delta N_{xy} = 0 \end{array} \tag{4.298}$$

in which δM_x and δN_x do not include M^T or N^T variations because they are zero. Note that these boundary conditions are on the *variations* in forces and variations in moments, not on the forces and moments, so the prebuckling boundary conditions have nothing to do with the buckling boundary conditions. Observe the graphic depiction of the simply supported edge buckling boundary conditions in Figure 4-14 on page 485 as well as for clamped edges in Figure 4-15 on page 485. Equations (4.293), (4.294), and (4.295) (or 4.296) are homogeneous differential equations with homogeneous boundary conditions in Equations (4.297) or, alternatively, (4.298). Thus, they constitute an eigenvalue problem and are solved accordingly. The eigenvalue is the value of $\bar{N}_x$ ($\bar{N}_y$), i.e., the buckling load, or within $\bar{N}_x$ ($\bar{N}_y$) the value of $\overline{\Delta T}$, the thermal buckling load. The eigenvector is the shape of the buckled shell.

The three buckling differential equations, Equations (4.293), (4.294), and (4.295) or (4.296) can be reformulated into either Donnell's equation or Batdorf's modified Donnell equation as in Section 4.2. We will use these fundamental thermoelastic relations in problems involving buckling after we have further explored the issue of shell support conditions as related to in-surface loading and restraint in Section 4.9.3.

Éléments sous droits d'auteur

4.9.3 In-Surface Loading and Restraint Conditions for Shells

Only the *change in temperature* from some reference state affects the buckling load, although absolute temperature determines the properties of the material involved. And that change in temperature, if uniform throughout the volume, must take place while some form of appropriate restraint exists on bar, plate, or shell movement. That is, the uniformly distributed temperature could increase from a low temperature for some time while the bar, plate, or shell is not restrained in any manner, so only free thermal expansion would take place. Then, if some type of in-plane restraint were introduced, the amount of temperature change to cause buckling would be sought. However, that temperature change does not include the temperature at any time prior to application of the restraint condition, but only the change in temperature from the instant the restraint was imposed. In addition, the temperature change need not be constant over the volume of the structural element. Thus, we are concerned with how a structural element develops thermal forces from variously distributed thermal loadings under various deformation restraint conditions. We will also describe how thermal buckling can occur without restraint but with spatially nonuniform changes in temperature.

Some combinations of in-surface edge restraint and distributions of temperature change produce shell buckling when a certain level of temperature change is reached. For example, if the temperature change is constant through the thickness of a shell, buckling occurs from the membrane state at a specific temperature change (long after the first increment of temperature change is applied). However, other combinations of in-surface edge restraint and temperature change distributions produce only bending, bowing, or curling from the instant that the first increment of temperature change is applied. If the temperature change distribution varies through the thickness of a shell in a manner that is not symmetric about the shell middle surface, then the shell will not remain in a membrane state as the temperature change is increased in amplitude, i.e., the shell will bend, bow, or curl at the instant when the first increment of temperature change is imposed, i.e., no buckling occurs unless into a different mode at a higher ΔT. The simplest case of thermal loading for us to consider is a spatially uniform temperature change distribution, and we will concentrate on that case in this book. However, we will also address some nonuniform temperature change distributions.

4.9.3.1 What In-Surface Boundary Conditions Can Result in Thermal and/or Mechanical Buckling of a Shell?

The principal in-surface restraint necessary in order for thermal buckling to occur under a *spatially uniform or nonuniform temperature change* distribution is on the in-surface displacement normal to the edge on *two opposite edges* (at the ends) of a circular cylindrical shell. That normal in-surface displacement must be restrained in some manner to resist free thermal expansion of the shell in order to develop in-surface compressive forces that cause thermal buckling to occur when a sufficiently high temperature change is reached. Also realize that full restraint

Éléments sous droits d'auteur

of the in-surface displacement normal to the shell edge on two opposite edges permits no mechanical forces to be applied in the in-surface direction perpendicular to those two opposite edges because in-surface movement under load cannot occur; thus, buckling under mechanical loading cannot take place (except as in the next subsection). The in-surface displacement tangential to a shell edge can also be restrained to not allow free thermal expansion along the edge and, hence, the restraint would cause thermal stresses that in turn could cause thermal buckling if the stresses are high enough. The alternative to buckling is bowing, curling, or bending that begins at the first instant that temperature change is applied, i.e., no (sudden) buckling event occurs. Loading and support conditions in engineering laboratories and in engineering practice are contrasted in the following to address their influence on buckling under both thermal and mechanical loading.

4.9.3.2 Load Versus Displacement Application in the Laboratory

If a displacement, in contrast to a load, is mechanically applied, then a structural element has axial or in-plane boundary restraint in addition to a mechanical load in the direction of the displacement. Displacements can be applied with a screw-type loading machine whereas loads are applied by dead-weight loading or hydraulic loading machines. Turning the screws on a screw-type loading machine or load frame as in Figure 4-87 moves the head to a new position and the screws keep the head in that position (which is why this form of loading is called displacement loading or displacement control). The head compresses the object, straining it, thereby stressing it, and thus introducing mechanical load. When the screws stop turning, the applied displacement is held relatively constant by the position of the loading head on the screws. Most load frames currently in laboratories are hydraulically operated with very sophisticated programmable load-application controls. Those controls are capable of applying load, displacement, or strain. Although displacements can be applied, many current loading machines are not stiff enough to remain perfectly in position when a thermal load is applied in addition to the mechanical load that is being held (these machines have a large load capacity, but relatively small stiffness). That is, heating the specimen could move the supposedly "fixed" head. A load frame with four screws (two on each side of the plate) is typically stiffer than one with only two screws. That enhanced stiffness is important for plate and shell thermal buckling experiments. Machines with lesser stiffness have a tendency for the heads to move when a thermal load is applied.

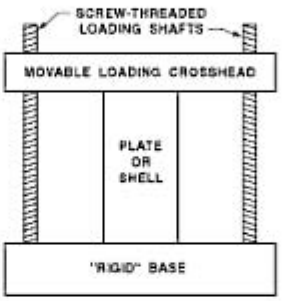


Figure 4-87 Screw-type Load Frame

Éléments sous droits d'auteur

For a shell, edge displacement can be applied with a loading machine that has at least two threaded screw shafts as in Figure 4-87. Applying a thermal loading to an object as big in diameter and as stiff as a shell can be quite difficult. If only a bar is being loaded, then a very small heating box can be placed around the bar so the heat is not applied to the load frame. The heating box encloses the specimen and has heating coils to apply heat to the specimen and, unavoidably, also applies heat to the load frame to some extent. However, the heating box for a shell must be much larger than for a bar, and the inevitable larger heat loss to the load frame must be accounted for. Heating the load frame usually results in diminished mechanical loading because the load frame tends to expand and therefore release some of the mechanical load by movement of the loading head.

After a displacement has been applied and held, a temperature change can be applied and if it *and* the load corresponding to the applied displacement are high enough, the shell will buckle. That is, the buckling load can be composed of a mechanical component as well as a thermal component in a wide variety of possible proportions of the two components. If the mechanical load is small, the thermal load causing buckling is large and vice versa. The complex methods of ensuring that various types of simply supported or clamped edges are effectively modeled on shells in the laboratory is left to the descriptions of experimental work in Singer, Arbocz, and Weller [4-13].

4.9.3.3 Loading and Restraint Conditions in Engineering Practice

Whether the loading and restraint conditions available in the engineering laboratory are specifically applicable in engineering practice is questionable and a matter of engineering judgement. The important issue is to recognize the types of restraint that are possible and their effects and then to be able to identify the actual restraint conditions that exist in engineering practice. For example, consider the set of frames, spars, stringers, and ribs of different stiffnesses in different directions on a wing panel for an aircraft wing or in a stiffened fuselage panel in Figure 4-88. The biaxially stiffened plate is fastened to unequal-stiffness stiffeners in the two directions at the plate edges. One set of stiffeners is called 'heavy' and the other 'light' in Figure 4-88. The heavy stiffeners do not respond quickly in the y-direction to temperature change. Thus, the heavy stiffeners (nearly) prevent thermal expansion of the panel in the y-direction. The light stiffeners have so little stiffness that the panel expands (almost) freely in the x-direction. Mechanical load can be accepted in the x-direction because movement can take place in the x-direction. In this case, the frames in one direction, the y-direction, are so stiff as to be approximated by rigid restraint but in the perpendicular x-direction, the restraint is so small as to be negligible. Such approximations are always necessary in engineering practice unless analyses for more precise evaluations are available *and* the actual stiffnesses are known to some degree of precision or accuracy.

Éléments sous droits d'auteur

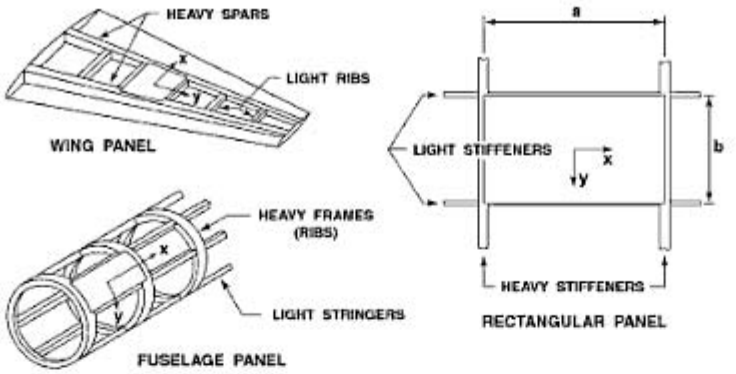


Figure 4-88 Mechanically and Thermally Loaded Panel and Shell Examples *(Inspired by Parkes [4-74])*

Examples of this type of loading and restraint include aircraft wing panels and fuselage panels as in Figure 4-88. Wing panels react wing bending moments by y-direction forces (compression in the top panels and tension in the bottom panels or vice versa). Fuselage panels react body bending moments by variable x-direction forces. Simultaneously, the heavy spars in wings and the heavy frames (also called ribs) in fuselage structures prevent thermal expansion in the y-direction. The thermal loading comes from heating during supersonic aircraft flight, reentry of spacecraft into the atmosphere, or movement of spacecraft in and out of the sun. Mechanical loading is caused by wing and fuselage bending and twisting in addition to fuselage pressurization. Hoff [4-75] reviews motivations for treating thermal buckling.

4.9.3.4 Elastic In-Surface Edge Restraint

The restraint of normal-to-the-edge displacement could be complete, i.e., fixed to be zero, or partial, e.g., elastic restraint in which the restraining force is proportional in some manner to the normal displacement of the edge. For example, if some linear translational springs are placed normal to the edge of the shell in its surface to restrain the edge as in Figure 4-89, then the re-

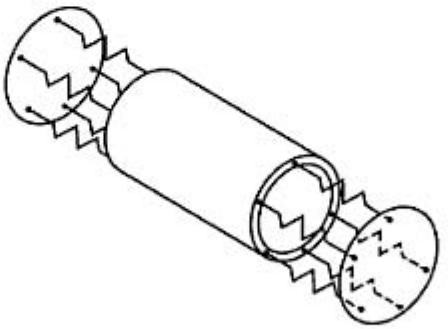


Figure 4-89 Shell with In-Surface Spring Restraint

Éléments sous droits d'auteur

straining force is linearly proportional to the normal displacement of the edge. More complex load-deformation characteristics of the in-surface springs (elastic restraints) result in a nonlinear relationship between the restraining force and the edge normal displacement. The thermal buckling load is highest for 'rigid' in-surface springs and decreases as the in-surface, normal-to-the-edge springs decrease in stiffness until, in the limit of zero-stiffness in-surface springs, no restraint exists and thus thermal buckling cannot occur. Rotational-edge-restraint springs are also possible (in addition to essential in-plane restraint of some type to develop thermal forces) as shown in the simple side view of a bar in Figure 3-81 on page 369. The 'infinitely stiff' limit for the rotational springs leads to the usual clamped-edge condition with a high ΔT. Successively decreasing the stiffness of the rotational springs leads to the lower simply supported edge shell value of ΔT for zero-stiffness rotational springs. The in-surface translational springs affect the nature and magnitude of the prebuckling thermal load, whereas the rotational springs have no effect on the prebuckling thermal load, but do affect the level of the thermal buckling load.

4.9.3.5 Thermal Buckling without In-Surface Edge Restraint

Thermal buckling can occur for a *spatially nonuniform temperature change* even in the absence of restraint of the in-surface displacement normal (or tangential) to the edge. That is, no edge restraints whatever are needed for thermal buckling to occur if the temperature distribution is nonuniform because then self-equilibrating tensile and *compressive stresses will develop* inside the shell area even without boundary restraint. Thus, a central 'hot spot' in a shell could cause buckling in the following manner. The hot spot tends to expand, but is restrained by deformation compatibility with the surrounding colder region that tends to expand less leading to a complex self-equilibrating stress field of compressive stresses in the hot spot and tensile stresses in the colder region. If the temperature change is uniform through the thickness, then at some level of temperature change, as the hot spot gets hotter, the compressive stresses in the hot spot cause the region of the hot spot to buckle. If the temperature change is not uniform through the thickness, then the hot spot will simply bulge or bow from the very first instant that the temperature change is applied.

A spatially uniform temperature change is the most common situation in engineering practice. Yes, spatial temperature gradients do exist in many practical problems because of heat conduction that occurs at different rates for different materials. Also, spatial temperature gradients exist for aerodynamic problems such as airflow over a wing leading to panels with nonuniform in-plane temperature distributions. Of course, spatial temperature distributions are the most complicated and interesting to treat, but they are out of the scope of this book (except for the through-the-thickness temperature variation for a bar in Section 2.9.5). However, the nature of some spatial temperature distribution problems is addressed for the shell thermal buckling summary in Section 4.9.7.

Éléments sous droits d'auteur

4.9.4 Equivalent Mechanical Load Concept

In *some* thermal loading problems, a mechanical load that is equivalent in action caused to the prescribed thermal load can be found, i.e., causes the same prebuckling equilibrium stresses. This *equivalent mechanical load concept* can be used to thoughtfully extend the applicability of some problems of buckling under mechanical loading to buckling under thermal loading. For many simple thermal loading problems, this process has long been used implicitly, i.e., without a name and without a general description of its applicability and only on a case-by-case basis for a very few cases.[1] In this subsection, we will describe and develop the *equivalent mechanical load concept* for thermal buckling problems.

We implicitly made use of the equivalent mechanical load concept in our study of thermal buckling of bars in Section 2.9. There, we immediately visualized an axially restrained bar as having an end mechanical force that arose from restraint of thermal expansion in the axial direction (see Figure 2-73 on page 174). We found the logic of a mechanical force needed to 'push back' the free thermal expansion compellingly obvious and easy to understand. The general situation for thermally loaded bars was fairly simple: (1) either a mechanical force or a thermal force could exist (at the ends), although both could exist under certain conditions; (2) either an end was restrained or it was free to move; (3) the bar could be subjected to uniform ΔT or one that varied along the length of the bar (if ΔT varied through the bar thickness in a manner not symmetric about the bar axis, we found that a thermal moment develops causing bending, curling, or bowing, not thermal buckling).

For plates and shells, the equivalent mechanical load concept is more involved than for bars because there are potentially two forces or loadings, one in each perpendicular direction of a rectangular plate or a circular cylindrical shell. For example, uniform temperature change on an unrestrained plate causes free thermal expansion in *both* the x- and y-directions. Restraint can be in one or the other or both directions in the simplest cases. However, recall that a force applied in one direction on a two-dimensional object to eliminate the deformation in that direction to simulate restraint actually causes a change in dimension of the object in the perpendicular direction because of the Poisson effect. Thus, although temperature change causes free thermal expansion in two directions, how each of those two directions is, or is not, restrained can lead to somewhat complicated equations for the in-plane forces in a plate or the in-surface forces in a shell. We must include the Poisson effect in any analysis by use of the two-dimensional strain-displacement relations and the stress-strain-change-in-temperature relations.

The process of establishing an equivalent mechanical load is centered on identifying the stresses in the prebuckling equilibrium state of a thermally loaded plate or shell and then hopefully finding a mechanically loaded plate or shell with the same stresses. That is, the key element in the process is the prebuckling equilibrium stresses because if the

[1] For example, Burgreen addresses how an equivalent mechanical stress problem can be developed for a three-dimensional thermal stress equilibrium problem with specializations for two-dimensional and one-dimensional problems [4-76].

Éléments sous droits d'auteur

prebuckling stresses in two problems are identical, then the buckling loads are identical because the origin of the prebuckling stresses in a buckling problem is immaterial. By 'stresses' is meant the entire prebuckling stress distribution within the plate or shell and on its boundary.

Are the prebuckling deformations the same for the thermal loading problem as for the equivalent mechanical loading problem? No. Recall that *deformation restraint* is essential to develop thermal force whereas *deformation* is essential to develop or accept mechanical load. For thermal buckling of bars, axial restraint forced the axial deflection to be zero to develop an axial thermal force whereas, in contrast, axial deflection must exist to develop and accept mechanical load. For thermal loading of plates or shells, required in-plane or in-surface restraint causes at least one in-plane deflection to be zero to develop an in-plane thermal force whereas in-plane deflection must be non-zero in one direction to have a mechanical loading. However, those deflections are quite small in comparison to the major structural element dimensions, namely the bar length or the plate length and width or the shell diameter and length.

To find the prebuckling stresses from the thermal loading, we must first consider the deformation restraints, if any, on the plate or shell edges because these restraints are irretrievably associated with the development of thermal stresses on the plate or shell boundary. However, thermal stresses can develop wholly within the plate or shell without any stresses existing on the boundary; in this class of thermal buckling problems, no equivalent mechanical load exists. That is, without deformation restraints on the boundary, there is no distribution of prebuckling stresses on the boundary, and we know of no *simple* buckling problem for mechanical loading without prebuckling boundary stresses, i.e., load on the boundary.

To find the equivalent mechanical loading for any structural element, we must simultaneously consider the three conditions of

- stress-strain-change-in-temperature (σ-ϵ-ΔT) relations
- equilibrium in the prebuckled state
- boundary support conditions

The boundary support conditions, especially (1) along the axis of a bar at the end or (2) in the plane of a rectangular plate at the edges or (3) in the surface of a circular cylindrical shell along the edges at each end, are crucial to the (proper) determination of the prebuckling thermal forces and hence to the definition of the equivalent mechanical loads and finally to the proper solution of thermal buckling problems.

The equivalent mechanical load concept will be developed for two straightforward thermal buckling of simply supported shells problems in the process of solving those problems in the next two sub-sections. Both problems involve uniform temperature change and axial restraint boundary support conditions, but lateral pressure also exists in the second problem, i.e., combined uniform temperature change and mechanical loading is addressed in which an axial in-surface mechanical force develops because of the Poisson effect and the one-dimensional in-surface deformation restraint.

Éléments sous droits d'auteur

4.9.5 Buckling of an Axially Restrained Circular Cylindrical Shell under Uniform Temperature Change

Suppose we heat a circular cylindrical shell with a uniform temperature change, ΔT, throughout its volume so that it both lengthens and increases in circumference. Of course, the thickness also increases, but the thickness change is quite small in comparison to the axial lengthening and circumference increase (although all are of the same percentage increase), and is therefore a neglected higher order effect). The movement restraint that we apply at the edges is in the axial direction only, i.e., no restraint is applied in the radial or circumferential directions. Thus, an axial thermal force is developed that is analogous to an axial mechanical force—both can cause buckling if large enough.

The shell is simply supported at each end with effectively a radial expanding, but axially 'rigid', circular disk mounted on an 'immovable' support. This imaginary disk is subjected to the same temperature change field as the shell. Thus, the disk provides almost an S1 equilibrium boundary condition ($w = 0$, $M_x = 0$, $u = 0$, $v = 0$) to the shell at each end as shown in cross-sectional view in Figure 4-90. Note that the coefficient of thermal expansion of the disk material must be the same as that of the shell so the disk expands radially the same amount as the shell when heat is applied, i.e., w of the shell equals w of the support. Accordingly, the boundary condition $w = 0$ is *not* provided. Thus, we approximate the real problem by one in which the shell expands uniformly as a membrane prior to buckling, but is restrained against axial growth. The prebuckling deformation is axisymmetric as shown as the membrane prebuckling deformation in Figure 4-84 on page 580.

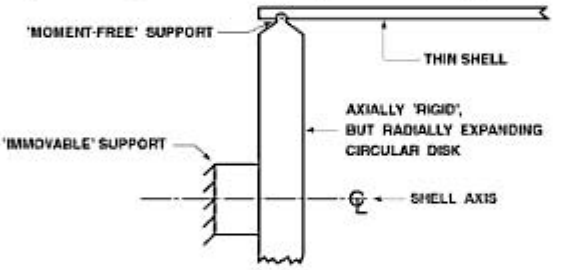


Figure 4-90 Schematic of Hypothetical Expanding Disk Providing the S1 Equilibrium Boundary Condition

Another way of providing the effective restraint is the hard-to-implement hypothetical support depicted in Figure 4-91. The rollers that permit radial movement must be very short in order to always act radially. Also, a point on the edge must be fixed to prevent rigid-body translation. Axial deformation of the shell is prevented by the 'immovable' support. The net result is the membrane deformation in Figure 4-91. However, the moment-free edge that can freely translate in the radial direction seems unlikely to be physically possible (except in our imagination).

Éléments sous droits d'auteur

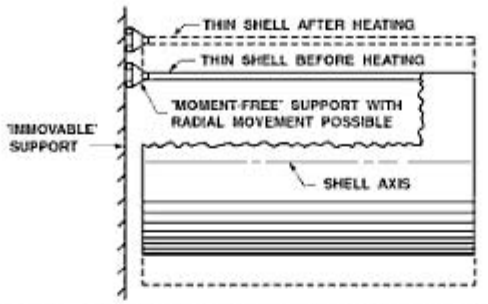


Figure 4-91 Exaggerated Schematic of Hypothetical Support Providing the S1 Equilibrium Boundary Condition

4.9.5.1 Prebuckling Equilibrium Solution

The prebuckling equilibrium solution for shells is more complicated than for plates because of the coupled interaction between deformations in and out of the shell surface. Thus, we must derive the prebuckling equilibrium state from the equilibrium equations. With a uniform temperature change on the axially restrained shell in either Figure 4-90 or 4-91, we expect the prebuckling deformations to be axisymmetric and hopefully membrane in nature. Thus, the displacements depend only on the axial coordinate, x, i.e., not on the circumferential coordinate, y. Moreover, the circumferential displacement, v, must be zero. Hence, we seek the prebuckling displacement solution in the form

$$u = 0 \qquad v = 0 \qquad w = w(x) \tag{4.299}$$

and expect that w(x) = constant is the solution (a requirement for classical shell buckling theory). Thus, the linearized prebuckling in-surface forces (per unit width, as usual) from Equation (4.32) on page 474, with thermal terms added, i.e., Equation (4.288) on page 588, reduce to

$$\begin{aligned} N_x &= \frac{E\,t}{1-\nu^2}\left[\nu\,\frac{w}{r}\right] - N^T \\ N_y &= \frac{E\,t}{1-\nu^2}\,\frac{w}{r} - N^T \end{aligned} \tag{4.300}$$

(because u = 0 implies $u_x = 0$ and v = 0 implies $v_y = 0$) in which

$$N^T = \frac{E\,\alpha}{1-\nu}\int_{-t/2}^{t/2} \Delta T\,dz = \frac{E\,\alpha\,t}{1-\nu}\,\Delta T \tag{4.301}$$

The linearized prebuckling equilibrium differential equations are (see Equations (4.34)–(4.36) on page 474 or (4.277) on page 586)

$$\frac{\partial N_x}{\partial x} + \frac{\partial N_{xy}}{\partial y} = 0 \tag{4.302}$$

Éléments sous droits d'auteur

$$\frac{\partial N_{xy}}{\partial x} + \frac{\partial N_y}{\partial y} = 0 \tag{4.303}$$

$$D\nabla^4 w + \frac{N_y}{r} = -p \tag{4.304}$$

in which the forces do not vary with circumferential coordinate, y. From the first prebuckling equilibrium differential equation, Equation (4.302), because the in-surface shear force, N_{xy}, must be independent of y (and in fact zero), we see that

$$\frac{\partial N_x}{\partial x} = 0 \tag{4.305}$$

Hence, N_x is constant throughout the shell. The second prebuckling equilibrium differential equation, Equation (4.303), is automatically satisfied because of the axisymmetric geometry, load, stress, and deformation state ($N_{xy} = 0$ and N_y is independent of y). Finally, the third prebuckling equilibrium differential equation, Equation (4.304), reduces to

$$D\frac{d^4 w}{dx^4} + \frac{N_y}{r} = 0 \tag{4.306}$$

which with the circumferential force N_y, Equation (4.300), becomes

$$D\frac{d^4 w}{dx^4} + \frac{1}{r}\left[\frac{E\,t}{1-\nu^2}\frac{w}{r} - \frac{E\,\alpha\,t}{1-\nu}\Delta T\right] = 0 \tag{4.307}$$

However, solution of this differential equation leads to w(x) that is not the membrane prebuckling deformation in Figure 4-84, but is instead the rigorous prebuckling deformation. Thus, to avoid significant complication resulting from variable radial deflection (namely, nonconstant coefficients in the buckling differential equations as noted by Almroth [4-10]), we consider only a constant radial deflection, w, corresponding to a membrane prebuckling deformation (that we have carefully contrived an edge support condition to achieve in either Figure 4-90 or 4-91). Thus, if w is *constant* consistent with classical buckling theory, then from the third prebuckling equilibrium differential equation, Equation (4.306), $N_y = 0$ and that condition with the second of Equations (4.300) implies

$$N_y = \frac{E\,t}{1-\nu^2}\frac{w}{r} - \frac{E\,\alpha\,t}{1-\nu}\Delta T = 0 \tag{4.308}$$

whereupon the corresponding membrane deflection is

$$w = (1+\nu)\,r\,\alpha\,\Delta T \tag{4.309}$$

Thus, the membrane (in-surface) axial force is (from Equations (4.300) and (4.309))

$$N_x = \frac{E\,t}{1-\nu^2}\left[\nu\frac{(1+\nu)\,r\,\alpha\,\Delta T}{r}\right] - \frac{E\,\alpha\,t}{1-\nu}\Delta T = -E\,t\,\alpha\,\Delta T \tag{4.310}$$

in which N_x is the restraining in-surface force that, when large enough, causes buckling.

Éléments sous droits d'auteur

4.9.5.2 Buckling Solution

The Donnell shell buckling differential equation is, from Equation (4.79) with the axial prebuckling force, N_x, from Equation (4.310),

$$D\nabla^8\delta w + \frac{E\,t}{r^2}\,\delta w_{,xxxx} + E\,t\,\alpha\,\overline{\Delta T}\,\nabla^4\delta w_{,xx} = 0 \tag{4.311}$$

which can be divided by D to get

$$\nabla^8\delta w + \frac{12\,Z^2}{L^4}\,\delta w_{,xxxx} + k_x^T\,\frac{\pi^2}{L^2}\,\nabla^4\delta w_{,xx} = 0 \tag{4.312}$$

in which, as usual, the Batdorf curvature parameter is

$$Z = \frac{L^2}{r\,t}\sqrt{1-\nu^2} \tag{4.313}$$

and we introduce the axial thermal loading parameter

$$k_x^T = \frac{12}{\pi^2}\,(1-\nu^2)\,\frac{L^2}{t^2}\,\alpha\,\overline{\Delta T} \tag{4.314}$$

which is obtained by recognizing that the prebuckling force is

$$\overline{N}_x = E\,t\,\alpha\,\overline{\Delta T} \tag{4.315}$$

in the expression for the axial loading parameter, k_x, of the axial compression buckling problem in Section 4.3.2.1:

$$k_x = \frac{\overline{N}_x L^2}{\pi^2 D} \tag{4.316}$$

Note that k_x has both geometric and material properties studied in Section 4.3.2.1, and k_x^T is a thermal loading parameter also with both geometric and material properties, although independent of E. The Batdorf curvature parameter is primarily a geometrical factor but has a mild secondary effect of a material property, namely Poisson's ratio. Because the governing buckling differential equation has k_x^T (or k_x) and Z as characteristic parameters, so will the solution. Consequently, we are very interested in the physical significance of Z. The infinitely varied types of shells that can be represented with a fixed value of Z are depicted in Figure 4-18 on page 492 and discussed in Section 4.3.2.1.

The variation-in-displacement buckling boundary conditions for the buckling differential equation are

$$\delta w(0) = \delta w(L) = 0 \tag{4.317}$$

(the radial displacement at the edges, w, prior to buckling does grow with ΔT, but the buckling radial displacement, δw, must be zero at the edges) and the variation-in-moment buckling boundary conditions reduce to

$$\delta w_{,xx}(0) = \delta w_{,xx}(L) = 0 \tag{4.318}$$

The buckling displacement (with indeterminate amplitude, $\tilde{w}$)

$$\delta w = \tilde{w}\,\sin\frac{m\pi x}{L}\,\sin\frac{ny}{r} \tag{4.319}$$

Éléments sous droits d'auteur

is claimed in Section 4.3.1 to correspond to the S2 buckling boundary condition ($\delta w = 0$, $\delta M_x = 0$, $\delta u = 0$, $\delta v = 0$) (see Problem 4.3.1 on page 518). Stop! We were considering S1 equilibrium boundary conditions, so why the change from S1 to S2? Realize that *the buckling boundary conditions need not be identical to the equilibrium boundary conditions.* For example, the condition $u = 0$ in the equilibrium boundary conditions is responsible for the development of the axial restraining force in the prebuckling equilibrium state. However, that force does not change during buckling, so the buckling boundary condition S2 involving $\delta N_x = 0$ is both feasible and reasonable. That is, we need not insist that $\delta u = 0$ as in the S1 buckling boundary condition. Moreover, by the Equivalent Mechanical Load Concept in Section 4.9.4, we need only identify a prebuckling stress state from the ΔT and a corresponding mechanical loading problem with the same prebuckling stress state, plus, of course, an assurance that the *buckling* boundary conditions in both problems are appropriate. In the spirit of the Equivalent Mechanical Load Concept, the now-established axial prebuckling load does not change during buckling because ΔT is constant, i.e., $\delta N_x = 0$ along with $\delta v = 0$, $\delta M_x = 0$, and $\delta w = 0$ constitutes the S2 buckling boundary condition. Thus, we get at least an approximate solution for the buckling problem if we recognize that the buckling displacement in Equation (4.319) is the exact solution of the (approximate) buckling differential equation, Equation (4.312), for S2 buckling boundary conditions if, as in Section 4.3.2.1,

$$k_x^T = \frac{(m^2 + \beta^2)^2}{m^2} + \frac{12Z^2 m^2}{\pi^4 (m^2 + \beta^2)^2} \tag{4.320}$$

in which

$$\beta = \frac{nL}{\pi r} \tag{4.321}$$

The value of k_x^T is different for each set of buckling mode shape values, m and n. The buckling temperature occurs when k_x^T achieves its least value as a function of integer values of m and n (which, by inspection of the form of Equation (4.320) are *not* $m = 1$ and $n = 1$). We addressed this problem for mechanical loading in Section 4.3.2.1, i.e., k_x instead of k_x^T in Equation (4.320) (the right-hand side of Equation (4.320) is identical to that of Equation (4.87) in Section 4.3.2.1). Recall that we could not simply 'minimize' k_x by use of differential calculus, but had to account for the integer nature of m and n.

In parallel to the development in Section 4.3.2.1, we easily see that for moderate-length shells, i.e., for $Z > 2.85$ as shown in Section 4.3.2.1, the lowest value of k_x^T is

$$k_x^T = \frac{4\sqrt{3}}{\pi^2} Z = .702\, Z \tag{4.322}$$

which, if $\nu = .27$, is the familiar, and widely used, axial buckling stress

$$\sigma_x = .6\, E\, t/r \tag{4.323}$$

or because

Éléments sous droits d'auteur

$$\sigma_x t = \bar{N}_x = E \alpha \bar{\Delta T} t \tag{4.324}$$

implies

$$\alpha \bar{\Delta T} = .6 \frac{t}{r} \tag{4.325}$$

which is independent of the shell Young's modulus and is also independent of the shell length, L (subject to the restriction $Z \geq 2.85$). For shorter shells, i.e., for $Z < 2.85$, the value of k_x^T is somewhat higher:

$$k_x^T = 1 + \frac{12 Z^2}{\pi^4} \tag{4.326}$$

Very long shells buckle as Euler bars if r/t is small enough. In contrast, if $Z = 0$, the shell becomes a plate for which $k_x^T = 1$ in analogy to the short shell solution for axial compression in Section 4.3.2.1, i.e., the shell effectively unrolls into a long plate with compression transverse to the long edges for which $k_x = 1$ as demonstrated in Section 4.3.2.1.

4.9.5.3 Thermal Buckling Results

The thermal buckling results for $Z = 1$ to $Z = 10^4$ obtained from Equations (4.322) and (4.326) are shown in Figure 4-92 where we have simply relabeled Figure 4-20 on page 494 with the appropriate parameter for k_x^T and noted the appropriate shell end boundary conditions. The inset sketch is meant to suggest the boundary conditions in either Figure 4-90 or 4-91. We should expect that these thermal buckling results for axially restrained shells are just as affected (degraded) by initial geometric imperfections as those for shells under axial mechanical loading because the buckling mechanism is the same.

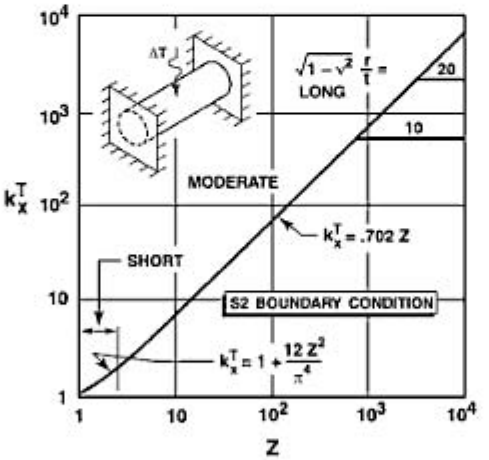


Figure 4-92 Thermal Buckling of an Axially Restrained Circular Cylindrical Shell under Uniform Temperature Change

Éléments sous droits d'auteur

As a numerical example, consider 7075-T6 aluminum shells with $Z > 2.85$ so that from Equation (4.325)

$$\overline{\Delta T} = .6\,\frac{1}{\alpha}\,\frac{t}{r} \tag{4.327}$$

in which $\alpha = 13.1\text{x}10^{-6}/°\text{F}$ $(23.6\text{x}10^{-6}/°\text{C})$. Numerical results are displayed to three-significant-figure accuracy in the following even though the accuracy of the input data do not warrant such high implied accuracy. The corresponding thermal buckling temperature change $\overline{\Delta T}$ is plotted against r/t in Figure 4-93 for all $Z > 2.85$. At $r/t = 10$, $\overline{\Delta T} = 4{,}580°\text{F}$ (2540°C). At $r/t = 100$, $\overline{\Delta T} = 458°\text{F}$ (254°C). At $r/t = 300$, $\overline{\Delta T} = 153°\text{F}$ (85°C). At $r/t = 1000$, $\overline{\Delta T} = 46°\text{F}$ (26°C). These results are plausible for large r/t. If the shell has r = 10 in. with variable t and L, we can calculate an approximate L by ignoring ν in Equation (4.85) on page 492, i.e.,

$$Z_{\text{approximate}} \cong \frac{L^2}{rt} \tag{4.328}$$

after we specify Z (which must exceed 2.85 for Equation (4.322) to be valid). For $Z = 1000$, then at $r/t = 100$, $L \cong 30$ in. and $L/r \cong 3$. At $r/t = 1000$, $L \cong 10$ in. and $L/r \cong 1$. For $Z = 100$, then at $r/t = 100$, $L \cong 10$ in. and $L/r \cong 1$. At $r/t = 1000$, $L \cong 3$ in. and $L/r \cong 1/3$. Such calculations give us a feel for the size and shape of the shells we address. In this range of interest, the shells are fairly short, i.e., have medium to small L/r.

However, two concerns are bothersome. First, the shell must yield by when $E\alpha\overline{\Delta T}$ reaches σ_y, i.e., for room-temperature material properties

$$\overline{\Delta T_y} = \frac{\sigma_y}{E\alpha} = \frac{55\text{x}10^3\,\text{psi}}{(10.5\text{x}10^6\,\text{psi})(13.1\text{x}10^{-6}/°\text{F})} = 400°\text{F}\ (222°\text{C}) \tag{4.329}$$

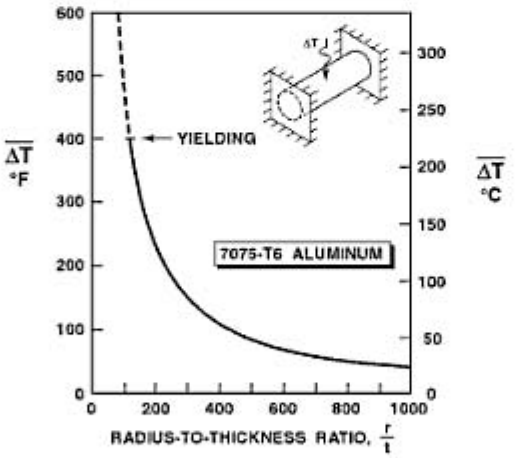


Figure 4-93 Thermal Buckling of an Axially Restrained Circular Cylindrical Shell under Uniform Temperature Change for all $Z > 2.85$

Éléments sous droits d'auteur

so at r/t = 100, the shell would yield before it buckles. Thus, a plastic shell buckling analysis as in Section 4.10 is required. The behavior curve in Figure 4-93 is dashed above $\Delta T = 400°F$ (222°C) to indicate that at least yielding has taken place, so the results cannot be accurate. The second bothersome issue is that a temperature change of more than 400°F (222°C) surely must have changed the aluminum material properties including α, E, and σ_y as well as significantly increased the stress-strain curve nonlinearity. Thus, ΔT_y would be affected as would all ΔT for r/t below about r/t = 115 and even higher. In fact, Mathauser and Brooks measured nonlinear stress-strain curves for 7075-T6 aluminum from room temperature to 600°F (316°C) [4-77] as displayed in Figure 3-106 on page 406. As temperature increases, E and σ_y decrease, and the nonlinearity increases very significantly. Jones considered the effects of temperature-dependent material properties on plastic thermal buckling of a uniformly heated bar [4-78] and of a uniformly heated plate [4-79], and similar results could be obtained for plastic thermal buckling of shells. Generally, the behavior curve in Figure 4-93 should be lower and yield at a higher r/t when all temperature-dependent and nonlinear stress-strain curve effects are considered.

The likelihood of a thin shell with r/t = 1000 being drastically affected by initial imperfections is quite high. Thus, the predicted ΔT of 46°F (26°C) is probably not going to be reached without buckling at a lower temperature change. In contrast, although a relatively thick shell with r/t = 10 might not be as highly affected by initial imperfections, the predicted ΔT of 4,568°F (2,540°C) is a ridiculously high temperature change over which to expect the material properties not to be highly degraded (in fact, the aluminum would melt well below that temperature change!). Thus, we must carefully examine each calculated buckling result to test for flaws in the analysis process and in the material properties used which affect the credibility of the answer presented.

Our awareness of the buckling mode shape in our calculations is suppressed by the use of the k-Z parameters which lead to a lower-bound envelope of results above which lie the results for specific shells with various mode shape numbers as in Figure 4-21 on page 495. Thornton calculated ΔT from Equation (4.320) for a specific shell with r/t = 100 and varied the shell length [4-80]. He found mode shape indistinctness at a specific buckling load, i.e., several buckling modes for the same shell led to the same buckling temperature change value identical to four significant figures. However, no such buckling mode shape indistinctness was found in the present investigation. Nevertheless, most of the solution in this subsection is due to Thornton (except for the k-Z format equation and results).

4.9.5.4 Correlation with Measured Buckling Temperature Change

We now compare our thermal buckling predictions with measured buckling temperature changes. The many complications inherent to shell buckling under heating with realistic boundary conditions are discussed by Ross, Hoff, and Horton [4-81] with more details in their report [4-82].

Éléments sous droits d'auteur

Their shells consist of two sets, one of AISI Type 304 stainless steel and the other of AISI Type 1006 cold-rolled steel. Both sets are 48.0 in. long (121.9 cm.) and of radius 5.187 in. (13.17 cm). The stainless steel shells are .0155 in. (.0393 cm.) thick whereas the cold-rolled steel shells are .0179-in. (.0455 cm.) thick. The coefficients of thermal expansion over the temperature range of interest are 9.6×10^{-6}/°F (5.3×10^{-6}/°C) for stainless steel and 7.85×10^{-6}/°F (4.36×10^{-6}/°C) for cold-rolled steel. The shell ends are restrained both axially (by a central shaft that is unavoidably heated and expands by up to 4%) and radially (by circumferential bands that capture the ends). Shell axial stress is inferred from strain-gage measurements on the central shaft. Twelve axially oriented tubular infared quartz lamps are equally spaced around the inner circumference of the shell to provide uniform heating both axially and circumferentially. The sounds of buckling are detected with a microphone (a 'significant distortion of the signal' is heard during snap-through buckling).

The clamped edge with both axial and radial restraint necessarily has non-membrane prebuckling equilibrium deformations. The shell generators do not remain straight during prebuckling deformation, so the prebuckling axial stresses are not $E\alpha\Delta T$, but are some lesser amount because of the generators bending. If the generators remained straight, then the axial stresses would be higher for a specified ΔT. The radial restraint should lead to a lower buckling load and hence lower buckling temperature change than for a shell with no radial restraint. A clamped edge, per se, should have a higher buckling load, hence higher buckling temperature change, than a simply supported edge. However, the experimental shells are quite long, so the effect of edge clamping over simply supported edges should be small.

The clamped edge has axial restraint, so the predictions of this subsection should be related in some manner to Ross, Hoff, and Horton's experimental results. If we use Equation (4.327) to evaluate the buckling temperature change for classical thermal buckling theory with axial restraint and a membrane prebuckled shape, we get ΔT = 187°F (104°C) for stainless steel and ΔT = 264°F (147°C) for cold-rolled steel. The corresponding experimental values (as averages of six stainless steel shells and five cold-rolled steel shells) are 121°F (67°C) and 174°F (97°C), respectively [4-81].

Predictions with Equation (4.327) are not strictly valid for the support conditions of the experimental shells. However, the prebuckling deformations are known to reduce the buckling load from our experience in Section 4.5. There, we saw reductions of 15-20% because of the prebuckling deformations. Moreover, the clamped edges should increase the buckling temperature change, although not significantly because of the great length of the shells (large L/r) and the results in Section 4.5. The net result is that the theoretical predictions should be higher than the measured buckling temperature changes, and they are. However, we cannot evaluate how much higher they should be because all the arguments are strictly qualitative. This 'correlation' of theory and experiment is by no means comprehensive, accurate, or satisfying, but is a display of some of the difficulties inherent in such a complex endeavor.

Éléments sous droits d'auteur

4.9.6 Buckling of an Axially Restrained Circular Cylindrical Shell under Uniform Temperature Change and Lateral Pressure

We now imagine the circular cylindrical shell to be heated or cooled with a uniform temperature change, ΔT, throughout its volume so that both its length and circumference change. Of course, the thickness also changes, but the thickness change is small in comparison to the length and circumference changes (although all dimensional changes are of the same percentage), and is therefore a neglected higher order effect. In addition, we apply a lateral pressure to the external or internal surface of the shell. The restraint that we apply is in the axial direction only, i.e., no restraint is applied in the radial or circumferential directions. Thus, when the shell is heated, an axial thermal compressive force is developed that is analogous to an axial mechanical force—both can cause buckling if large enough. If the shell is cooled, the shell is reinforced against buckling with an axial tension unless the shell 'lifts off' the axial restraint, i.e., unless the axial restraint is engaged only in compression. Of course, the lateral pressure can also cause buckling if it is applied externally to the shell, but reinforces the shell against buckling if applied internally to the shell by creating circumferential tension. We are interested in the combined effect of heating or cooling and internal or external lateral pressure on buckling.

Suppose the shell is simply supported at each end with the radially expanding, axially 'rigid' circular disk mounted on an 'immovable' support as in Figure 4-90 on page 598. The 'expanding disk' is satisfactory for the thermal-loading-only problem to maintain a membrane prebuckling shape, but the introduction of lateral pressure causes the shell to have a variable w(x) especially near the supported edge. Thus, the support mechanism in Figure 4-90 does not allow a true membrane prebuckling state of deformation. However, the hypothetical support system in Figure 4-91 on page 599 does allow a simple radial expansion or contraction with lateral pressure as well as with change in temperature. Thus, a membrane prebuckling deformation exists as in Figure 4-84 on page 580, and we can expect the simplest first-order solution to the buckling problem. However, we must recognize that the support system in Figure 4-91 is unlikely to be implemented in a practical situation. Having tiny rollers on the edge of a thin shell is virtually impossible. Most axially loaded shells have their edges 'potted' in a soft metal so that the shell ends can be machined to be flat, parallel to each other, and perpendicular to the shell axis. Such potted edges are also unlikely to to move in the radial direction because of frictional resistance. Nevertheless, we use this hypothetical edge support in Figure 4-91 as an approximate boundary condition to obtain a classical buckling theory solution to the problem.

4.9.6.1 Prebuckling Equilibrium Solution

The prebuckling equilibrium solution for shells is more complicated than for plates because of the coupled interaction between deformations in and out of the shell surface. Thus, we must actually derive the prebuckling equilibrium state and make certain approximations.

Éléments sous droits d'auteur

With uniform temperature change and lateral pressure, we expect the prebuckling deformations to be axially symmetric because of the support condition in Figure 4-91 on page 599. Thus, the displacements depend only on the axial coordinate, x, i.e., not on the circumferential coordinate, y. Moreover, the circumferential displacement, v, must be zero. Hence, we seek the prebuckling displacement solution in the form

$$u = 0 \qquad v = 0 \qquad w = w(x) \tag{4.330}$$

with the expectation (a requirement for classical shell buckling theory) that w is a constant, and we seek that constant. Thus, the linearized prebuckling membrane forces (per unit width, as usual) from Equation (4.32), with thermal terms added in Equation (4.288), reduce to

$$\begin{aligned} N_x &= \frac{E\,t}{1-\nu^2}\left[\nu\,\frac{w}{r}\right] - N^T \\ N_y &= \frac{E\,t}{1-\nu^2}\,\frac{w}{r} - N^T \end{aligned} \tag{4.331}$$

in which

$$N^T = \frac{E\,\alpha}{1-\nu}\int_{-t/2}^{t/2}\Delta T\,dz = \frac{E\,\alpha\,t}{1-\nu}\,\Delta T \tag{4.332}$$

The linearized prebuckling equilibrium differential equations are (see Equations (4.34)–(4.36))

$$\frac{\partial N_x}{\partial x} + \frac{\partial N_{xy}}{\partial y} = 0 \tag{4.333}$$

$$\frac{\partial N_{xy}}{\partial x} + \frac{\partial N_y}{\partial y} = 0 \tag{4.334}$$

$$D\nabla^4 w + \frac{N_y}{r} = -p \tag{4.335}$$

in which the forces do not vary with circumferential coordinate, y. From the first prebuckling equilibrium differential equation, Equation (4.333), because the in-surface shear force, N_{xy}, must be independent of y (and in fact zero), we see that

$$\frac{\partial N_x}{\partial x} = 0 \tag{4.336}$$

Hence, N_x is constant throughout the shell. The second prebuckling equilibrium differential equation, Equation (4.334), is automatically satisfied because of the axisymmetric geometry, load, stress, and deformation state ($N_{xy} = 0$ and N_y is independent of y). Finally, the third prebuckling equilibrium differential equation, Equation (4.335), reduces to

$$D\,\frac{d^4 w}{dx^4} + \frac{N_y}{r} = -p \tag{4.337}$$

in which we could substitute the circumferential force N_y from Equation (4.331) to get

Éléments sous droits d'auteur

$$D\frac{d^4w}{dx^4}+\frac{1}{r}\left[\frac{Et}{1-\nu^2}\frac{w}{r}-\frac{E\alpha t}{1-\nu}\Delta T\right]=-p \tag{4.338}$$

However, solution of this differential equation leads to w(x) that is not the membrane prebuckling deformation solution of Figure 4-84 on page 580, but instead the rigorous prebuckling equilibrium solution noted there. Thus, to avoid significant complication resulting from a variable radial deflection (namely, nonconstant coefficients in the buckling differential equations as described by Almroth [4-10]), we consider only a constant radial deflection, w. Thus, if w is constant, then from the third prebuckling equilibrium differential equation, Equation (4.337),

$$N_y=-pr \tag{4.339}$$

and that condition applied to the second of Equations (4.331) implies

$$N_y=\frac{Et}{1-\nu^2}\frac{w}{r}-\frac{E\alpha t}{1-\nu}\Delta T=-pr \tag{4.340}$$

whereupon the corresponding membrane prebuckling deflection is

$$w=-\frac{1-\nu^2}{Et}pr^2+(1+\nu)r\alpha\Delta T \tag{4.341}$$

i.e., the sum of the inward (outward) deformation caused by the external (internal) lateral pressure and the outward (inward) deformation caused by heating (cooling). Thus, the in-surface axial force is (from Equations (4.331) and (4.341))

$$\begin{aligned}N_x&=\frac{Et}{1-\nu^2}\left[\frac{\nu}{r}\left[-\frac{1-\nu^2}{Et}pr^2+(1+\nu)r\alpha\Delta T\right]\right]-\frac{E\alpha t}{1-\nu}\Delta T\\&=-\nu pr-Et\alpha\Delta T\end{aligned} \tag{4.342}$$

in which N_x is the compressive restraining force that, when large enough, causes buckling. Thus, both ΔT and **p** can cause buckling as we would expect. Moreover, because of the axial restraint and the corresponding Poisson effect term, $-\nu pr$, the lateral pressure actually increases the restraining axial force that can cause buckling. There is no such term in the ordinary lateral pressure buckling problem of Section 4.3.2.2. We faced a similar situation in the thermal and mechanical loading of a plate in Section 3.7.7.

4.9.6.2 Buckling Solution

The Donnell shell buckling differential equation is, from Equation (4.79) on page 488 with the axial force, N_x, identified as in Equation (4.342),

$$D\nabla^8\delta w+\frac{Et}{r^2}\delta w_{,xxxx}+\left[\nu pr+Et\alpha\Delta T\right]\nabla^4\delta w_{,xx}+pr\nabla^4\delta w_{,yy}=0 \tag{4.343}$$

which can be divided by D to get

Éléments sous droits d'auteur

$$\nabla^8 \delta w + \frac{12 Z^2}{L^4} \delta w_{,xxxx} + (k_x^T + k_x^p) \frac{\pi^2}{L^2} \nabla^4 \delta w_{,xx} + k_y \frac{\pi^2}{L^2} \nabla^4 \delta w_{,yy} = 0 \quad (4.344)$$

in which, as usual, the Batdorf curvature parameter is

$$Z = \frac{L^2}{rt} \sqrt{1 - \nu^2} \quad (4.345)$$

and we introduce the axial thermal loading parameter

$$k_x^T = \frac{12}{\pi^2} (1 - \nu^2) \frac{L^2}{t^2} \alpha \overline{\Delta T} \quad (4.346)$$

which is the same definition as in Section 4.9.5 and is obtained by recognizing that

$$\overline{N}_x = E t \alpha \overline{\Delta T} \quad (4.347)$$

in the expression for the axial loading parameter of the axial compression buckling problem in Section 4.3.2.1:

$$k_x = \frac{\overline{N}_x L^2}{\pi^2 D} \quad (4.348)$$

The quantity k_x^p is an axial loading parameter caused by the lateral pressure through the Poisson effect and the axial restraint:

$$k_x^p = \frac{\overline{N}_x^p L^2}{\pi^2 D} = \frac{\nu \overline{p} r L^2}{\pi^2 D} \quad (4.349)$$

and has both material and geometric properties. The quantity k_y is the usual lateral loading parameter with both geometric and material properties studied in Section 4.3.2.2:

$$k_y = \frac{\overline{N}_y L^2}{\pi^2 D} = \frac{\overline{p} r L^2}{\pi^2 D} \quad (4.350)$$

so we have two loading parameters, p and ΔT or, alternatively, we could choose k_x^T and k_y plus k_x^p (although the latter three are not independent because k_y and k_x^p both depend on $\overline{p}$). The Batdorf curvature parameter is primarily a geometrical factor but has a mild effect of a material property, namely Poisson's ratio. Because the governing buckling differential equation has k_x^T (or k_x), k_y, k_x^p, and Z as characteristic parameters, so will the solution. Consequently, we are very interested in the physical significance of Z. The infinitely varied types of shells that can be represented with a fixed value of Z are depicted in Figure 4-18 on page 492 and discussed in Section 4.3.2.1.

The variation-in-displacement buckling boundary conditions for the buckling differential equation are

$$\delta w(0) = \delta w(L) = 0 \quad (4.351)$$

and the variation-in-moment buckling boundary conditions reduce to

Éléments sous droits d'auteur

$$\delta w_{,xx}(0) = \delta w_{,xx}(L) = 0 \tag{4.352}$$

The buckling displacement (with indeterminate amplitude, $\bar{w}$)

$$\delta w = \bar{w} = \bar{\bar{w}} \sin \frac{m\pi x}{L} \sin \frac{ny}{r} \tag{4.353}$$

is the exact solution of the (approximate) buckling differential equation, Equation (4.344), for S2 boundary conditions (as in Section 4.9.5, appropriate for the support condition imagined). Rather than proceed in the usual manner, we can take advantage of the fact that under axial and circumferential forces, Equation (4.79) can be written in the form

$$D\nabla^8 \bar{w} + \frac{Et}{r^2} \frac{\partial^4 w}{\partial x^4} + \bar{N}_x \nabla^4 \bar{w}_{xx} + \bar{N}_y \nabla^4 \bar{w}_{yy} = 0 \tag{4.354}$$

i.e., that we have a general problem of combined axial and circumferential forces. Divide Equation (4.354) by D to get

$$\nabla^8 \bar{w} + 12 \frac{Z^2}{L^4} \frac{\partial^4 \bar{w}}{\partial x^4} + k_x \frac{\pi^2}{L^2} \nabla^4 \bar{w}_{xx} + k_y \frac{\pi^2}{L^2} \nabla^4 \bar{w}_{yy} = 0 \tag{4.355}$$

which has solution

$$k_x m^2 + k_y \beta^2 = (m^2 + \beta^2)^2 + \frac{12Z^2}{\pi^4} \frac{m^4}{(m^2 + \beta^2)^2} \tag{4.356}$$

in which

$$\beta = \frac{nL}{\pi r} \tag{4.357}$$

Equation (4.356) is a complex relation between three variables as contrasted with the two variables in each of the axial compression, lateral pressure, and hydrostatic pressure buckling problems. In some regions of k_x versus k_y, m must be one, but in other regions m is larger, so the simplifications for lateral and hydrostatic pressure do not apply in general. Also, the expression cannot be 'minimized' as was the k_x expression in terms of Z. By the equivalent mechanical load concept, we can reformulate the combined $\bar{N}_x$ and $\bar{N}_y$ problem in terms of the present problem of thermal loading and lateral pressure loading on an axially restrained shell, i.e.,

$$k_x = k_x^T + k_x^p \tag{4.358}$$

and Equation (4.356) becomes

$$(k_x^T + k_x^p)m^2 + k_y \beta^2 = (m^2 + \beta^2)^2 + \frac{12Z^2}{\pi^4} \frac{m^4}{(m^2 + \beta^2)^2} \tag{4.359}$$

The relation between k_x^T, k_x^p, k_y, and Z could be plotted as k_x^T versus k_y for a specific Z, e.g., for plots of low, medium, and high Z.

Alternatively, we can revert to the three Donnell-type shell buckling differential equations for combinations of axial compression and lateral pressure:

Éléments sous droits d'auteur

$$\begin{aligned}
&\delta N_{x,x} + \delta N_{xy,y} = 0 \\
&\delta N_{xy,x} + \delta N_{y,y} = 0 \\
&-\delta M_{x,xx} + \delta M_{xy,xy} - \delta M_{yx,xy} - \delta M_{y,yy} + \delta N_y/r + \bar{N}_x \delta w_{,xx} + \bar{N}_y \delta w_{,yy} = 0
\end{aligned} \tag{4.360}$$

Upon substitution of the usual variations in forces and moments in Equations (4.70) and (4.59) on pages 487 and 485, respectively, the buckling differential equations in terms of buckling displacements become

$$\begin{aligned}
&A[\delta u_{,xx} + \nu(\delta v_{,xy} + \delta w_{,x}/r)] + \frac{1-\nu}{2} A(\delta u_{,yy} + \delta v_{,xy}) = 0 \\
&\frac{1-\nu}{2} A(\delta u_{,xy} + \delta v_{,xx}) + A[(\delta v_{,yy} + \delta w_{,y}/r) + \nu \delta u_{,xy}] = 0 \\
&D\nabla^4(\delta w) + A[(\delta v_{,y} + \delta w/r) + \nu \delta u_{,x}]/r + \bar{N}_x \delta w_{,xx} + \bar{N}_y \delta w_{,yy} = 0
\end{aligned} \tag{4.361}$$

An exact solution to the buckling differential equations can be obtained for the S2 buckling boundary conditions in Equation (4.63), i.e., $\delta N_x = \delta v = \delta w = \delta M_x = 0$, by use of the buckling displacements

$$\begin{aligned}
\delta u &= \tilde{u} \cos \frac{m\pi x}{L} \cos \frac{ny}{r} \\
\delta v &= \tilde{v} \sin \frac{m\pi x}{L} \sin \frac{ny}{r} \\
\delta w &= \tilde{w} \sin \frac{m\pi x}{L} \cos \frac{ny}{r}
\end{aligned} \tag{4.362}$$

(or equivalently δu, δv, and δw could be cosine-sine, sine-cosine, and sine-sine functions, respectively, if the coordinates are rotated 90°) in which $\tilde{u}$, $\tilde{v}$, and $\tilde{w}$ are the (indeterminate) amplitudes of the buckling displacements. If the buckling displacements in Equation (4.362) are substituted in the buckling differential equations, Equation (4.361), a homogeneous set of equations in $\tilde{u}$, $\tilde{v}$, and $\tilde{w}$ results. In order that a nontrivial solution for $\tilde{u}$, $\tilde{v}$, and $\tilde{w}$ exist, the determinant of the coefficients of $\tilde{u}$, $\tilde{v}$, and $\tilde{w}$ must be zero, and the following buckling criterion results:

$$\bar{N}_x \left[\frac{m\pi}{L}\right]^2 + \bar{N}_y \left[\frac{n}{r}\right]^2 = T_{33} + \frac{2T_{12}T_{13}T_{23} - T_{11}T_{23}^2 - T_{22}T_{13}^2}{T_{11}T_{22} - T_{12}^2} \tag{4.363}$$

in which

$$\begin{aligned}
T_{11} &= A(m\pi/L)^2 + \frac{1-\nu}{2} A(n/r)^2 \\
T_{12} &= \frac{1+\nu}{2} A(m\pi/L)(n/r) \\
T_{13} &= (\nu A/r)(m\pi/L) \\
T_{23} &= (1/r)A(n/r) \\
T_{22} &= \frac{1-\nu}{2} A(m\pi/L)^2 + A(n/r)^2 \\
T_{33} &= D\left[(m\pi/L)^4 + 2(m\pi/L)^2(n/r)^2 + (n/r)^4\right] + A/r^2
\end{aligned} \tag{4.364}$$

Éléments sous droits d'auteur

Again, we reformulate the problem by use of the equivalent mechanical load concept to express $\bar{N}_x$ and $\bar{N}_y$ in terms of the temperature change and the lateral pressure when the shell is axially restrained, i.e.,

$$\begin{aligned} \bar{N}_x &= E\alpha t\Delta\bar{T} + \nu\bar{p}_{AR}r \\ \bar{N}_y &= \bar{p}_{AR}r \end{aligned} \tag{4.365}$$

in which $\bar{p}_{AR}$ is the lateral pressure buckling load when the shell is axially restrained (a lower lateral pressure buckling value than when the shell is not axially restrained as in Section 4.3.2.2).

Thus, the buckling solution to the present combined thermal and mechanically loaded circular cylindrical shell is

$$E\alpha t\Delta\bar{T}(m\pi/L)^2 + \nu\bar{p}_{AR}r(m\pi/L)^2 + \bar{p}_{AR}r(n/r)^2 = RHS \tag{4.366}$$

in which 'RHS' is the terms on the right-hand side of Equation (4.363).

4.9.6.3 Thermal Buckling Results

The general nature of the buckling results from Equation (4.366) is shown as the typical interaction curve between buckling temperature change, $\Delta\bar{T}$, and lateral pressure, $\bar{p}$, in Figure 4-94. There, the buckling boundary is the dividing line between the region in which buckling does not occur and the region in which buckling does occur. Also, buckling mode shape changes take place at solid circles on the buckling boundary. The buckling results occur in the first three quadrants of Figure 4-94, but buckling does not occur in the fourth quadrant because neither cooling nor internal pressure cause compressive forces that can cause buckling of the shell. In the second quadrant, the usual interaction be-

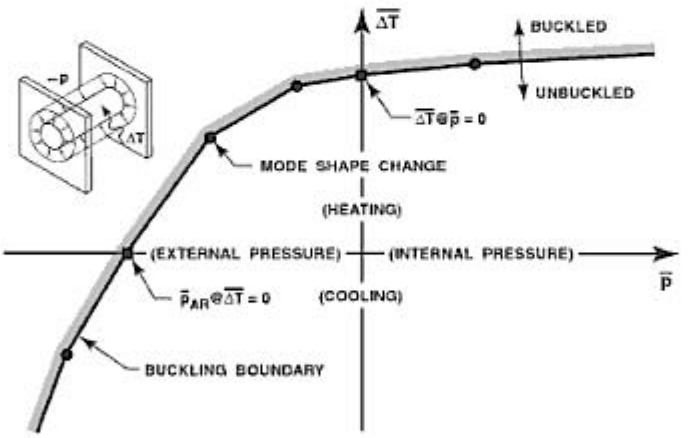


Figure 4-94 Schematic View of Thermal and Mechanical Buckling of an Axially Restrained Circular Cylindrical Shell under Uniform Temperature Change and Lateral Pressure

Éléments sous droits d'auteur

tween heating and external pressure occurs. In the first quadrant, the pressure of internal pressure permits the $\Delta\bar{T}$ to exceed the value for zero pressure, i.e., internal pressure allows a higher buckling temperature change. Similarly, in the third quadrant, the presence of cooling permits the $\bar{p}$ to exceed the value for no temperature change. The magnitudes of these effects depend on the specific shell geometry.

Numerical thermal and mechanical buckling results are obtained in the following manner. First, the external lateral pressure buckling pressure with axial restraint, $\bar{p}_{AR}$, is calculated by solving for $\bar{p}$ when $\Delta\bar{T} = 0$. Note that $\bar{p}_{AR}$ is less than $\bar{p}$ in Section 4.3.2.2 when the axial restraint is removed. Then, the thermal buckling temperature change, ΔT, is calculated by solving for $\Delta\bar{T}$ when no lateral pressure is applied, i.e., when $\bar{p} = 0$ (the same result as in Section 4.9.5 must, of course, be obtained). Then, in the first and second quadrants in Figure 4-94, lateral pressures, $\bar{p}$, are specified and the corresponding $\Delta\bar{T}$ is calculated from

$$E\alpha\Delta\bar{T}(m\pi/L)^2 = -\nu\bar{p}r(m\pi/L)^2 - \bar{p}r(n/r)^2 + RHS \qquad (4.367)$$

Solutions to Equation (4.367) are obtained for a range of specified lateral pressure, $\bar{p}$, until the quadrants are full, i.e., a complete buckling boundary is obtained in the first and second quadrants. In all these buckling calculations, the lowest buckling load (or temperature change) is sought for an integer number of axial buckle half-waves, m, and circumferential buckle waves, n, by use of Subroutine MINIMA in Appendix B for a specified range of values of m and n. In the third quadrant of Figure 4-94, $\bar{p} < \bar{p}_{AR}$ (actually, the external pressure is higher in absolute value than $\bar{p}_{AR}$), and for fixed values of $\bar{p}$ the buckling temperature change is calculated from Equation (4.367) for a range of specified lateral pressure, $\bar{p}$, values until the buckling boundary is defined. However, in contrast to calculations in the first and second quadrants, all positive values of $\Delta\bar{T}$ for various m and n are inadmissible in the third quadrant because they lead to solutions outside the buckling boundary. That is, $\Delta\bar{T}$ must be negative (cooling) if $\bar{p} < \bar{p}_{AR}$. Of the $\Delta\bar{T}$ that are negative, only the largest defines the buckling boundary (the others are outside the buckling boundary). Thus, $\Delta\bar{T}$ is inverted and then Subroutine MINIMA is used to find the smallest of the inverses of the $\Delta\bar{T}$ and hence to identify the largest $\Delta\bar{T}$. Note that in the second quadrant of Figure 4-94, the buckling boundary is concave toward the origin, but in the first and third quadrants the buckling boundary always expands with an 'open end'. Of course, buckling is not possible in the fourth quadrant because no compressive forces are developed under conditions of internal pressure and cooling. The population and character of the various quadrants would change dramatically for those fiber-reinforced composite materials with negative coefficients of thermal expansion because Jones showed that thermal buckling occurs under cooling, not heating, for some unidirectional laminates and some cross-ply laminates [4-83] (see Section 3.10).

The buckling interaction curve between applied temperature and lateral pressure is shown for a specific 7075-T6 aluminum circular cylindrical shell with axial restraint in Figure 4-95. The pertinent material properties are $\alpha = 13.1 \times 10^{-6}$ /°F (23.6×10^{-6} /°C), $E = 10.5 \times 10^{6}$ psi

Éléments sous droits d'auteur

(72.4 GPa), $\nu = .3$, and $\sigma_y = 55$ ksi (379 MPa). The shell dimensions are shown on the figure along with the mode shapes, (m,n), into which the shell buckles. Mode shape transition points are indicated with solid circles. The $\overline{\Delta T}$ with no lateral pressure is 231°F (128.3°C), and the external lateral pressure buckling pressure with axial restraint is $\bar{p}_{AR} = -16.9$ psi (-116.5 kPa). The buckling boundary, i.e., the boundary between loading conditions corresponding to buckling and those corresponding to no buckling, is denoted with the shaded line. Inside the shaded line, the shell is subjected to loads that do not cause buckling. In the third quadrant, cooling the shell enables the external pressure to exceed $\bar{p}_{AR}$ by a significant amount. In the first quadrant, applying internal pressure causes an insignificant increase in $\overline{\Delta T}$. From results not shown, only for small Z of 50 or less does a significant increase in ΔT occur for applied internal pressure.

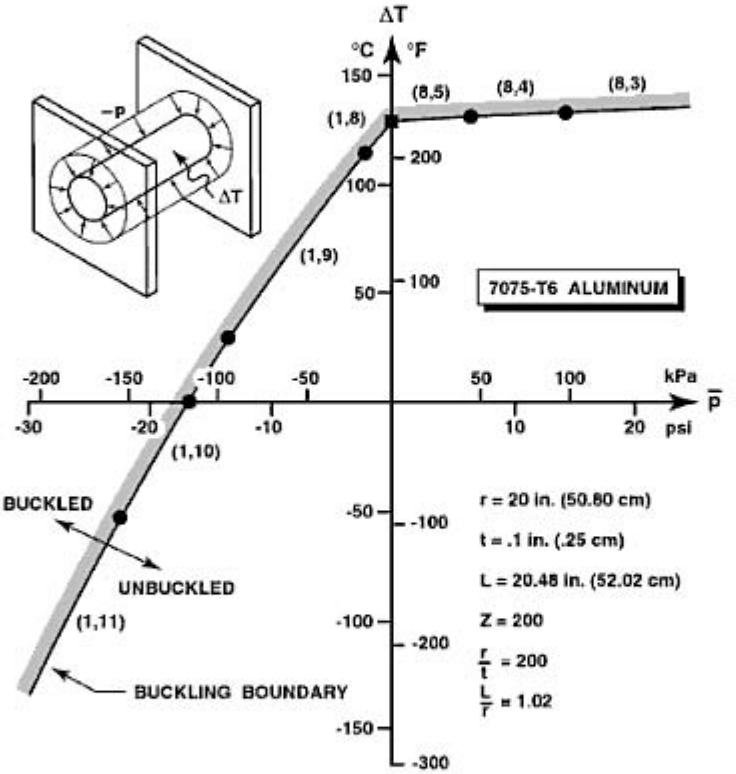


Figure 4-95 Thermal and Mechanical Buckling of an Axially Restrained Circular Cylindrical Shell under Uniform Temperature Change and Lateral Pressure

Éléments sous droits d'auteur

Let us consider the level of the calculated buckling temperatures and stresses obtained for the shell of Figure 4-95. The pure thermal buckling temperature change of 231°F (128°C), i.e., without any lateral pressure, corresponds to a temperature of 300°F (149°C) which has a stress-strain curve as shown in Figure 3-106 on page 406. There, the yield stress is 36 ksi (248 MPa) and the Young's modulus is 9.2×10^6 psi (63.4 GPa). The axial stress developed at thermal buckling is

$$\begin{aligned}\sigma_x &= -\frac{\bar{N}_x}{t} = -\frac{E\alpha\overline{\Delta T}t}{t} = -E\alpha\overline{\Delta T} \\ &= -(9.2 \times 10^6 \text{ psi}) \times (13.1 \times 10^{-6}/°\text{F}) \times (231°\text{F}) \\ &= -27{,}800 \text{ psi } (192 \text{ Gpa})\end{aligned} \tag{4.368}$$

Thus, the developed stress is somewhat close to the yield stress at the corresponding actual shell temperature [ΔT + 70°F (21°C)]. The circumferential stress developed at thermal buckling when only lateral pressure acts (at p_{AR}) is

$$\begin{aligned}\sigma_y &= -\frac{\bar{N}_y}{t} = -\frac{pr}{t} \\ &= -\frac{(16.9 \text{ psi}) \times (20 \text{ in.})}{.1 \text{ in.}} = -3{,}380 \text{ psi } (23.3 \text{ GPa})\end{aligned} \tag{4.369}$$

The Poisson-effect-induced axial stress because of the axial restraint when lateral pressure acts is

$$\sigma_x^p = -\nu pr = -.3 \times (16.9 \text{ psi}) \times (20.0 \text{ in.}) = -101 \text{ psi } (.7 \text{ GPa}) \tag{4.370}$$

Thus, the compressive stresses generated by the lateral pressure alone (including the Poisson-effect-induced axial stress) are well below the yield stress irrespective of the yield criterion used.

The combinations of $\overline{\Delta T}$ and $\bar{p}_{AR}$ in the second quadrant seem not to cause yielding. The material properties are somewhat higher in the second quadrant because the temperature is lower than at pure thermal buckling. Only when the $\overline{\Delta T}$ rises above about 300°F (167°C) in the first quadrant or goes below -300°F (-167°C) in the third quadrant does yielding become possible. The effect of nonlinear temperature-dependent material properties is small for this shell. Thicker shells could have a very pronounced effect of nonlinear temperature-dependent material properties because of higher buckling temperatures. Thinner shells might not have any noticeable effect of nonlinear temperature-dependent material properties because of lower buckling temperatures.

4.9.7 Summary and Other Topics in Thermal Buckling of Shells

The prebuckling and buckling boundary conditions addressed in Sections 4.9.5 and 4.9.6 are not 'practical' boundary conditions because they are enormously difficult, if not impossible, to implement for a real shell. However, use of those boundary conditions enables us to study the general nature of shell thermal buckling to first-order effects (classical shell buckling theory). Such simple solutions are consistent with the

Éléments sous droits d'auteur

objectives of this book, namely to introduce the basic concepts and tweak the reader's interest to pursue more advanced topics. Comparison of these theoretical results with experimental results would not be fully realistic because of the inherent differences between the theoretical and actual boundary conditions.

We made great effort to contrive support conditions that permit only a membrane prebuckling equilibrium deformation state to achieve our objective of simplicity. However, the fact remains that actual, practical support conditions generally do not allow a membrane prebuckling deformation state to exist. Moreover, a membrane prebuckled state cannot exist for a shell with an axial or circumferential variation in temperature distribution. Thus, the prebuckling stress analysis must be more complicated in order to properly account for the axial and/or circumferential distributions of displacements and stresses. Accordingly, more rigorous treatment of prebuckling boundary conditions and deformation in the manner of Almroth [4-10] is essential. Other practical considerations must be recognized: heating a shell and simultaneously restraining its axial deformation is extremely difficult because heat is lost from the shell to the axial support which event would naturally cause the support to move as seen in Ross, Hoff, and Horton's experiments [4-81]. There, the central shaft was unavoidably exposed to the heating and expanded by up to 4%. *Any* mechanism that restrains radial movement of an edge inherently leads to a non-membrane prebuckling deformation because the rest of the shell away from the edges tends to expand with ΔT in the radial direction (also observed in Ross, Hoff, and Horton's experiments). Without the membrane prebuckled shape, the buckling differential equation has nonconstant coefficients and is therefore more difficult to solve than for constant coefficients because numerical solution techniques are required.

Many other shell thermal and mechanical buckling problems exist, and the level of their complexity is not even hinted at in the previous sections. Several other topics were described for plate thermal buckling in Section 3.7.9 and are equally applicable for shells, so need not be repeated here. Those topics include various edge support conditions, nonuniform heating, time-dependent temperature distributions, limitations of the linear elastic material model, temperature-dependent material properties, nonlinear stress-strain behavior, and the analogy between temperature and moisture effects.

One of the topics discussed in Section 3.7.9.2 for plates deserves additional attention for shells, namely the type of temperature-change distribution over the volume of the shell. We treated the extraordinarily simple, yet common, case of uniform temperature-change distribution over the shell volume in this section. Another thermal loading possibility is a through-the-thickness temperature-change variation that would introduce thermal moments prior to buckling that would, as in the bar thermal bending problem in Section 2.9.4, cause immediate bending of the shell wall and not a classical Euler bucking response. However, as the average temperature change in the shell increases, the shell behavior approaches the buckling load that occurs if no through-the-thickness

Éléments sous droits d'auteur

ΔT variation exists, just as is true for the bar thermal bending problem in Section 2.9.4. Other non-uniform thermal loading situations can lead to an axial, areal, or volumetric ΔT distribution. Obviously, many physical situations lead to a variety of temperature-change distributions. Hoff and his associates treated various types of thermal loading of shells including axially varying circumferential stresses [4-84], circumferentially varying thermal gradients [4-85], heating along an axial strip [4-86], as well as uniform heating [4-81].

Some thermal buckling investigators have claimed that if a very large buckling temperature is predicted, say thousands of degrees, then the shell will not buckle. However, that rather *curious* view is incomplete and misleading. Obviously, the validity of the linear elastic model has been far exceeded. Even more obviously, inelastic material behavior and even melting occur well below the predicted temperatures. Thus, there is no basis for their conclusion that the shell does not buckle. *Something* must happen to the shell at a temperature much lower than the incorrectly predicted outrageously high temperature. Just because the predicted elastic ΔT is large does not mean the shell won't buckle—inelastic and temperature-dependent material properties are all the more important! Their effects will lower the calculated buckling load greatly, although not necesarily to a realizeable ΔT. Those more complicated calculations must be made to determine whether the shell will buckle thermally.

Some of the most comprehensive correlations of thermal buckling predictions with experimental results were undertaken by Bushnell [4-87], [4-88], [4-89], and [4-90] with summary discussion in [4-91]. He demonstrated the importance of several theoretical considerations beyond those used in this book essential to gain the correlation. Those considerations involve boundary conditions including actual prebuckling deformations and rotations as well as non-uniform heating. Other experimental and theory-experiment correlation efforts are described by Singer, Arbocz, and Weller [4-13] and should be given great attention.

More shell thermal buckling and thermal bending problems are summarized by Thornton in a very comprehensive review paper [4-92] and in his thermal structures book [4-80]. He reviews work on plates, curved panels, circular cylindrical shells, and circular conical shells. Also of significant interest is the thermal buckling of plates and shells book by Ogibalov and Gribanov [4-93].

Problem Set 4.9

4.9.1 Demonstrate that the thermal force per unit width of a shell is

$$N_x^T = -\frac{E\,\alpha}{1-\nu}\int_{-t/2}^{t/2}\Delta T\,dz$$

by using the plane stress condition $\sigma_z = 0$ in the three-dimensional stress-strain relations including thermal expansion terms.

4.9.2 Use variational techniques to derive the moderately large-deflection equilibrium differential equations and their associated boundary conditions for a shell with thermal effects. Be sure to clarify precisely where the thermal effects enter the problem.

4.9.3 Use variational techniques to derive the buckling differential equations and their associated boundary conditions for a shell with thermal effects. Be sure to clarify precisely where the thermal effects enter the problem.

Éléments sous droits d'auteur

4.10 EFFECT OF PLASTIC DEFORMATION

4.10.1 Introduction

Plastic deformation generally reduces buckling loads as we have seen in previous chapters. Here, the configuration treated is a ring- and stringer-stiffened isotropic circular cylindrical shell as shown in Figure 4-96 (we will also treat multilayered shells). The loading is arbitrary combinations of axial force and lateral pressure and is high enough to cause plastic deformation before buckling. Both the essentially uniaxial character of the stiffeners and their eccentricity in placement relative to the shell middle surface is accounted for in the manner of Section 4.7. That is, the stiffeners are 'smeared out' or averaged over their spacing in the shell rather than being treated as discrete stiffeners. Classical buckling theory, by which is implied a membrane prebuckled shape, is used for the S2 buckling boundary condition $\delta N_x = \delta v = \delta w = \delta M_x = 0$.

Simple J_2 deformation theory of plasticity (also called maximum octahedral shear stress theory, maximum energy of distortion theory, etc.) as described by Nadai [4-94] and Jones [4-95] is used in spite of the fact that incremental theory is more valid for general loading histories. Incremental and deformation theories lead to identical results for proportional loading equilibrium problems because, for that class of problems, deformation theory is merely incremental theory integrated along a single straight load path. However, Budiansky [4-96] shows that deformation theory is consistent with accepted incremental theory conditions even for a range of nonproportional loading about the proportional loading condition. The permissible bounds on the degree of nonproportionality of loading are not necessarily satisfied by the deformations *during* buckling. However, experimental bar, plate, and shell buckling results are in good agreement with deformation theory predictions whereas predictions with incremental theory are well above measured buckling loads. Nevertheless, more experimental evidence is required to fully substantiate the applicability of deformation theory to plastic buckling problems.

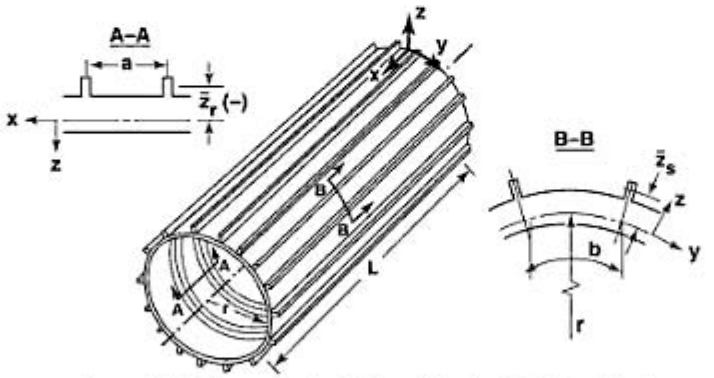


Figure 4-96 Geometry of a Stiffened Circular Cylindrical Shell

Éléments sous droits d'auteur

The present solutions by Jones for both stiffened single-layered shells [4-58] in Section 4.10.2 and for stiffened multilayered shells [4-59] in Section 4.10.5 are an extension of plates work by Stowell [4-97] and Ilyushin [4-98] and plates and shells work by Gerard [4-99] (who did not treat the essentially uniaxial character and eccentricity of the stiffeners). Stowell, like Shanley [4-100], presumed that unloading does not occur during buckling. In contrast to the constant Poisson's ratio ($\nu = 1/2$) employed by Stowell and Ilyushin, a variable Poisson's ratio here provides a smooth transition from the elastic compressible state to the plastic incompressible state with increasing stresses. The present secant-modulus theory for a biaxial configuration, i.e., a plate or shell, reduces to tangent-modulus theory when the biaxial terms are reduced to uniaxial terms in a consistent manner. Donnell-type buckling differential equations are used to derive a transcendental buckling criterion in terms of the geometry and material properties *at buckling*. The technique for solving this type of buckling criterion is discussed, and numerical examples are given to illustrate application of the theory.

4.10.2 Derivation of Single-Layered Shells Buckling Criterion

By use of simple J_2 deformation theory of plasticity, expressions are obtained for the variations of the biaxial stresses during buckling in terms of the variations of strains and material properties during buckling of a stiffened circular cylindrical shell. The variations in biaxial stresses are integrated over the shell thickness and the variations in uniaxial stresses are integrated over the stiffeners to obtain expressions for the variations in forces and moments during buckling. Finally, the variations in forces and moments are substituted in Donnell-type shell buckling differential equations to obtain a transcendental buckling criterion in terms of the geometry and nonlinear material properties of the stiffened shell *at buckling*. The criterion is applicable for arbitrary combinations of axial force and lateral pressure, and is solved in a subsequent subsection.

4.10.2.1 Fundamental Relations in J_2 Deformation Theory

The fundamental definitions in the J_2 deformation theory of plasticity for isotropic materials (see Nadai [4-94] and Jones [4-95]) are the stress intensity, σ_i, ($\sigma_i = 3\tau_o/\sqrt{2}$ in which τ_o is the octahedral shear stress):

$$\sigma_i = \sqrt{\sigma_x^2 + \sigma_y^2 - \sigma_x\sigma_y + 3\tau_{xy}^2} \tag{4.371}$$

the strain intensity, ε_i, ($\varepsilon_i = 3\gamma_o/[2\sqrt{2}\,(1+\nu)]$ in which γ_o is the octrahedral shear strain):

$$\varepsilon_i = \frac{1}{1-\nu^2}\sqrt{(1-\nu+\nu^2)(\varepsilon_x^2+\varepsilon_y^2) - (1-4\nu+\nu^2)\varepsilon_x\varepsilon_y + \frac{3}{4}(1-\nu)^2\gamma_{xy}^2} \tag{4.372}$$

(This strain intensity expression is apparently due to Lunchick [4-101] and is a continuous function of ν, so ν varies from the elastic value to the plastic value of 1/2 rather than being restricted to 1/2 at all stress levels as is the expression by Ilyushin [4-98]—set $\nu = 1/2$ in Equation (4.372)),

Éléments sous droits d'auteur

and the stress-strain relations, with general nonlinear material properties, E_{sec} and ν,

$$\sigma_x = \frac{E_{sec}}{1-\nu^2}(\varepsilon_x + \nu\varepsilon_y)$$
$$\sigma_y = \frac{E_{sec}}{1-\nu^2}(\varepsilon_y + \nu\varepsilon_x) \qquad (4.373)$$
$$\tau_{xy} = \frac{E_{sec}}{2(1+\nu)}\gamma_{xy}$$

that relate the stress intensity to the strain intensity, i.e., $\sigma_i = E_{sec}\varepsilon_i$. In addition, certain material properties are defined in terms of the stress and strain intensities on a stress-intensity versus strain-intensity curve. However, the problem is enormously simplified by the following result. For a uniaxial stress state (σ_x plus ε_x and $\varepsilon_y = -\nu\varepsilon_x$), the stress intensity is simply $\sigma_i = \sigma_x$ and the strain intensity can be shown to be $\varepsilon_i = \varepsilon_x$ (see Problem 3.8.1 on page 421). Thus, *the stress-intensity versus strain-intensity curve is simply the uniaxial stress-strain curve for an isotropic material.* This powerful identity enables us to directly use the usual uniaxial stress-strain curve as the stress-intensity versus strain-intensity curve, so no special stress-intensity versus strain-intensity curve need be measured. Thus, we define three variable material properties on the *nonlinear uniaxial stress-strain curve* in Figure 4-97. First, the secant modulus, E_{sec}, is the slope of a line from the origin of the stress-strain curve to the active stress point (the stress level being considered):

$$E_{sec} = \frac{\sigma_i}{\varepsilon_i} = \frac{\sigma}{\varepsilon} \qquad (4.374)$$

Second, the tangent modulus, E_{tan}, is the stress-strain curve slope at the active stress point:

$$E_{tan} = \frac{d\sigma_i}{d\varepsilon_i} = \frac{d\sigma}{d\varepsilon} \qquad (4.375)$$

Third, Poisson's ratio, ν, is

$$\nu = -\frac{\varepsilon_y}{\varepsilon_x} \qquad (4.376)$$

for an applied uniaxial σ_x and is derived by Gerard and Wildhorn [4-102] to be

$$\nu = \frac{1}{2} - \left(\frac{1}{2} - \nu_e\right)\frac{E_{sec}}{E} \qquad (4.377)$$

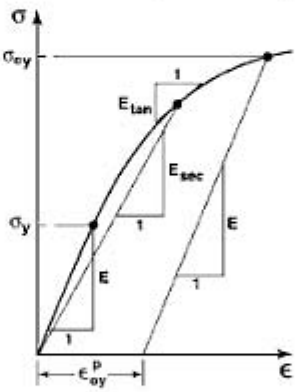


Figure 4-97 Nonlinear Stress-Strain Curve

in which ν_e is the elastic Poisson's ratio and E is the elastic Young's modulus. Thus, a smooth transition is provided between the elastic compressible state and the plastic incompressible state of the material as opposed to Stowell's and Ilyushin's assumption that ν is always the plastically incompressible state Poisson's ratio ($\nu = \nu_e = \nu_p = 1/2$).

Éléments sous droits d'auteur

4.10.2.2 Variations of Strains during Buckling

During buckling, the strains vary from their prebuckling values. Let the variation be denoted by δ. Then,

$$\begin{aligned}\delta\varepsilon_x &= \delta\varepsilon_x^o + z\delta\kappa_x\\ \delta\varepsilon_y &= \delta\varepsilon_y^o + z\delta\kappa_y\\ \delta\gamma_{xy} &= \delta\gamma_{xy}^o + z\delta\kappa_{xy}\end{aligned} \tag{4.378}$$

in which z is the distance from the shell reference surface in Figure 4-96; $\delta\varepsilon_x^o$, $\delta\varepsilon_y^o$, and $\delta\gamma_{xy}^o$ are the variations of the reference-surface strains,

$$\begin{aligned}\delta\varepsilon_x^o &= \delta u_{,x}\\ \delta\varepsilon_y^o &= \delta v_{,y} + \frac{\delta w}{r}\\ \delta\gamma_{xy}^o &= \delta u_{,y} + \delta v_{,x}\end{aligned} \tag{4.379}$$

$\delta\kappa_x$, $\delta\kappa_y$, and $\delta\kappa_{xy}$ are the variations of the reference-surface curvatures,

$$\begin{aligned}\delta\kappa_x &= -\delta w_{,xx}\\ \delta\kappa_y &= -\delta w_{,yy}\\ \delta\kappa_{xy} &= -2\delta w_{,xy}\end{aligned} \tag{4.380}$$

and δu, δv, and δw are the variations in the reference-surface displacements that occur during buckling.

4.10.2.3 Variations of Stresses during Buckling

During buckling, the stresses and the nonlinear material properties, E_{sec} and ν, in Equation (4.373) vary from their prebuckling values, e.g.,

$$\begin{aligned}\delta\sigma_x = {} & \frac{E_{sec}}{1-\nu^2}(\delta\varepsilon_x + \nu\delta\varepsilon_y) + (\varepsilon_x + \nu\varepsilon_y)\frac{\delta E_{sec}}{1-\nu^2}\\ & + \varepsilon_x E_{sec}\delta\left[\frac{1}{1-\nu^2}\right] + \varepsilon_y E_{sec}\delta\left[\frac{\nu}{1-\nu^2}\right]\end{aligned} \tag{4.381}$$

Accordingly, the following variations are required:

$$\delta E_{sec} = -\frac{E_{sec}^2}{\sigma_i}\left[1 - \frac{E_{tan}}{E_{sec}}\right]\delta\varepsilon_i \tag{4.382}$$

$$\delta\left[\frac{1}{1-\nu^2}\right] = \frac{2\nu}{(1-\nu^2)^2}\delta\nu \tag{4.383}$$

$$\delta\left[\frac{\nu}{1-\nu^2}\right] = \frac{1+\nu^2}{(1-\nu^2)^2}\delta\nu \tag{4.384}$$

From the fundamental relation for Poisson's ratio, Equation (4.377), and the variation in E_{sec}, Equation (4.382),

$$\delta\nu = (1-2\nu)\frac{E_{sec}}{2\sigma_i}\left[1 - \frac{E_{tan}}{E_{sec}}\right]\delta\varepsilon_i \tag{4.385}$$

Éléments sous droits d'auteur

so that all variations of the material parameters are expressed in terms of $\delta\varepsilon_i$ which, in turn, can be obtained from ε_i [Equation (4.372)] as

$$\delta\varepsilon_i = \frac{1}{2H\sigma_i(1-\nu^2)}\left[[(2-\nu)\sigma_x - (1-2\nu)\sigma_y]\delta\varepsilon_x + [(2-\nu)\sigma_y - (1-2\nu)\sigma_x]\delta\varepsilon_y + 3(1-\nu)\tau_{xy}\delta\gamma_{xy}\right] \quad (4.386)$$

in which

$$H = 1 - \frac{1-2\nu}{2(1-\nu^2)}\left[1 - \frac{E_{tan}}{E_{sec}}\right] \times \left[2\nu + \frac{1}{2\sigma_i^2}\left[-(1+2\nu)(\sigma_x^2+\sigma_y^2) + 2(2+\nu)\sigma_x\sigma_y - 6(1+\nu)\tau_{xy}^2\right]\right] \quad (4.387)$$

For the present loading condition of only combinations of axial compression and lateral pressure, $\tau_{xy} = 0$, so the stress variations simplify from Jones' more general treatment [4-58]:

$$\delta\sigma_x = \frac{E_{sec}}{1-\nu^2}(K_{11}\delta\varepsilon_x + \nu K_{12}\delta\varepsilon_y)$$
$$\delta\sigma_y = \frac{E_{sec}}{1-\nu^2}(\nu K_{12}\delta\varepsilon_x + K_{22}\delta\varepsilon_y) \quad (4.388)$$
$$\delta\tau_{xy} = \frac{E_{sec}}{1-\nu^2}K_{33}\delta\gamma_{xy}$$

in which

$$K_{11} = 1 - \frac{K}{4(1-\nu^2)}[(2-\nu)\sigma_x - (1-2\nu)\sigma_y]^2$$
$$K_{12} = 1 - \frac{K}{4\nu(1-\nu^2)}[(2-\nu)\sigma_y - (1-2\nu)\sigma_x][(2-\nu)\sigma_x - (1-2\nu)\sigma_y] \quad (4.389)$$
$$K_{22} = 1 - \frac{K}{4(1-\nu^2)}[(2-\nu)\sigma_y - (1-2\nu)\sigma_x]^2$$
$$K_{33} = (1-\nu)/2$$

in which

$$K = \frac{1}{H\sigma_i^2}\left[1 - \frac{E_{tan}}{E_{sec}}\right] \quad (4.390)$$

For the elastic case, $E_{sec} = E$ and $K = 0$, so the K_{ij} reduce to unity (except for K_{33}), and the variations of stresses, Equation (4.388), are identical to the variations in elastic stresses.

The variations of the stiffener stresses during buckling from a membrane prebuckled shape are obtained by varying the uniaxial normal stresses

$$\sigma_{x_s} = E_{sec_s}\varepsilon_{x_s} \qquad \sigma_{y_t} = E_{sec_t}\varepsilon_{y_t} \quad (4.391)$$

and the last of Equation (4.373) to get:

Éléments sous droits d'auteur

$$\delta\sigma_{x_s} = E_{tan_s}\delta\varepsilon_{x_s} \qquad \delta\sigma_{y_r} = E_{tan_r}\delta\varepsilon_{y_r}$$
$$\delta\tau_{xy_s} = G_{sec_s}\delta\gamma_{xy_s} \qquad \delta\tau_{xy_r} = G_{sec_r}\delta\gamma_{xy_r} \tag{4.392}$$

Note that the variations of shear stress are not obtained from uniaxial relations in parallel to Equation (4.391) because such relations do not apply when no shear strain exists prior to buckling.

4.10.2.4 Variations of Forces and Moments during Buckling

The variations of forces and moments during buckling are obtained by integration of the variations of stresses through the shell thickness and over the stiffeners for the variations of forces, e.g.,

$$\delta N_x = \int_{-t/2}^{t/2} \delta\sigma_x \, dz + \frac{1}{b}\int_{A_s} \delta\sigma_{x_s} \, dA_s \tag{4.393}$$

in which the axial stiffener effect is averaged over its spacing, b, so

$$\begin{aligned}
\delta N_x &= (A_{11} + E_{tan_s}A_s/b)\delta\varepsilon_x + A_{12}\delta\varepsilon_y + (\bar{z}_s E_{tan_s}A_s/b)\delta\kappa_x \\
\delta N_y &= A_{12}\delta\varepsilon_x + (A_{22} + E_{tan_r}A_r/a)\delta\varepsilon_y + (z_r E_{tan_r}A_r/a)\delta\kappa_y \\
\delta N_{xy} &= A_{33}\delta\gamma_{xy}
\end{aligned} \tag{4.394}$$

The moments of the variations of stresses are similarly integrated to get the variations of moments:

$$\begin{aligned}
\delta M_x &= (\bar{z}_s E_{tan_s}A_s/b)\delta\varepsilon_x + (D_{11} + \bar{z}_s^2 E_{tan_s}A_s/b + E_{tan_s}I_s/b)\delta\kappa_x + D_{12}\delta\kappa_y \\
\delta M_y &= (\bar{z}_r E_{tan_r}A_r/a)\delta\varepsilon_y + D_{12}\delta\kappa_x + (D_{22} + \bar{z}_r^2 E_{tan_r}A_r/a + E_{tan_r}I_r/a)\delta\kappa_y \\
\delta M_{xy} &= -(D_{33} + G_{sec_s}J_s/2b)\delta\kappa_{xy} \\
\delta M_{yx} &= (D_{33} + G_{sec_r}J_r/2a)\delta\kappa_{xy}
\end{aligned} \tag{4.395}$$

in which

$$A_{ij} = \frac{K_{ij}E_{sec}t}{1-\nu^2} \qquad D_{ij} = \frac{K_{ij}E_{sec}t^3}{12(1-\nu^2)} \tag{4.396}$$

and the stiffener quantities are defined in Section 4.7. Note that A_{ij} and D_{ij} are plastic buckling extensional and bending stiffnesses, respectively. The elastic versions of the extensional and bending stiffnesses, A_{ij} and D_{ij}, are obtained from Equation (4.396) by using elastic values of K_{ij} [$K_{11} = K_{22} = K_{12} = 1$ and $K_{33} = (1-\nu)/2$], elastic moduli, and the elastic Poisson's ratio in Equations (4.391) and (4.396). The plastic versions of the prebuckling extensional and bending stiffnesses, $\bar{A}_{ij}$ and $\bar{D}_{ij}$, are obtained by using the elastic values of K_{ij}, plastic secant modulus, and plastic Poisson's ratio in Equations (4.391) and (4.396).

4.10.2.5 Buckling Criterion

The Donnell-type buckling differential equations for circular cylindrical shells under combined axial compression and lateral pressure are, from Equations (4.71)–(4.73) on page 487,

Éléments sous droits d'auteur

$$\begin{aligned}
&\delta N_{x,x} + \delta N_{xy,y} = 0\\
&\delta N_{xy,x} + \delta N_{y,y} = 0\\
&-\delta M_{x,xx} + \delta M_{xy,xy} - \delta M_{yx,xy} - \delta M_{y,yy} + \frac{\delta N_y}{r} + \bar{N}_x \delta w_{,xx} + \bar{N}_y \delta w_{,yy} = 0
\end{aligned} \tag{4.397}$$

The buckling displacements (δu, δv, and δw could equivalently be cosine-sine, sine-cosine, and sine-sine functions, respectively)

$$\begin{aligned}
\delta u &= \tilde{u} \cos \frac{m\pi x}{L} \cos \frac{ny}{r}\\
\delta v &= \tilde{v} \sin \frac{m\pi x}{L} \sin \frac{ny}{r}\\
\delta w &= \tilde{w} \sin \frac{m\pi x}{L} \cos \frac{ny}{r}
\end{aligned} \tag{4.398}$$

satisfy the usual S2 simply supported edge buckling boundary conditions $\delta N_x = \delta v = \delta w = \delta M_x = 0$ and are substituted in the variations in forces and moments, Equations (49.25) and (49.26), which are subsequently substituted in the buckling differential equations. In order for a nontrivial solution to exist for the resulting homogeneous equations in $\tilde{u}$, $\tilde{v}$, and $\tilde{w}$, the (indeterminate) buckling amplitudes, the determinant of the coefficients of $\tilde{u}$, $\tilde{v}$, and $\tilde{w}$ must vanish which leads to the buckling criterion

$$\bar{N}_x \left[\frac{m\pi}{L} \right]^2 + \bar{N}_y \left[\frac{n}{r} \right]^2 = T_{33} + \frac{2T_{12}T_{13}T_{23} - T_{11}T_{23}^2 - T_{22}T_{13}^2}{T_{11}T_{22} - T_{12}^2} \tag{4.399}$$

in which

$$\begin{aligned}
T_{11} &= (A_{11} + E_{tan_s} A_s/b)(m\pi/L)^2 + A_{33}(n/r)^2\\
T_{12} &= (A_{12} + A_{33})(m\pi/L)(n/r)\\
T_{13} &= (A_{12}/r)(m\pi/L) + (z_s E_{tan_s} A_s/b)(m\pi/L)^3\\
T_{22} &= A_{33}(m\pi/L)^2 + (A_{22} + E_{tan_r} A_r/a)(n/r)^2\\
T_{23} &= (1/r)(A_{22} + E_{tan_r} A_r/a)(n/r) + (z_r E_{tan_r} A_r/a)(n/r)^3\\
T_{33} &= (D_{11} + E_{tan_s} I_s/b + \bar{z}_s^2 E_{tan_s} A_s/b)(m\pi/L)^4\\
&\quad + (4D_{33} + 2D_{12} + G_{sec_s} J_s/b + G_{sec_r} J_r/a)(m\pi/L)^2 (n/r)^2\\
&\quad + (D_{22} + E_{tan_r} I_r/a + \bar{z}_r^2 E_{tan_r} A_r/a)(n/r)^4\\
&\quad + (2/r)(z_r E_{tan_r} A_r/a)(n/r)^2 + (1/r)^2 (A_{22} + E_{tan_r} A_r/a)
\end{aligned} \tag{4.400}$$

Equation (4.399) is a transcendental expression for the buckling forces, N_x and N_y, in terms of the material properties at N_x and N_y, the geometry, and the buckling mode numbers m and n. This buckling criterion reduces to Lunchick's solution [4-101] for unstiffened plastic circular cylindrical shells: Block, Card, and Mikulas' solution [4-53] for stiffened elastic circular cylindrical shells; and to the classical 'Euler solution' for unstiffened elastic circular cylindrical shells. This buckling criterion was obtained by Jones [4-58], and the solution procedure [4-103] is described in the following sub-section.

Éléments sous droits d'auteur

4.10.3 Solution of Single-Layered Shells Buckling Criterion

Because the buckling criterion is a transcendental expression, a direct solution is not possible. A logical scheme must be developed to find the buckling load by some form of trial-and-error method that converges to the correct load. The basis of the logic is that a buckling load is estimated and then corresponding material properties are found with the last step being the use of the material properties to calculate a buckling load. At each stage, the calculated load is minimized with respect to discrete m and n as in Sections 4.7–4.9 and Appendix B. If the estimated load is too low, the calculated buckling load is too high and vice versa. Thus, we have an ideal test by which we determine whether the estimated load is above or below the exact solution. A sequence of four estimated loads with the four corresponding calculated loads is shown in Figure 4-98. The search for the exact solution proceeds by increments up the load-deformation curve and stops when $\lambda_{calc} < \lambda_{est}$. Then, the last increment is investigated by an interval-halving technique to obtain the exact solution to a specified accuracy by the most efficient process.

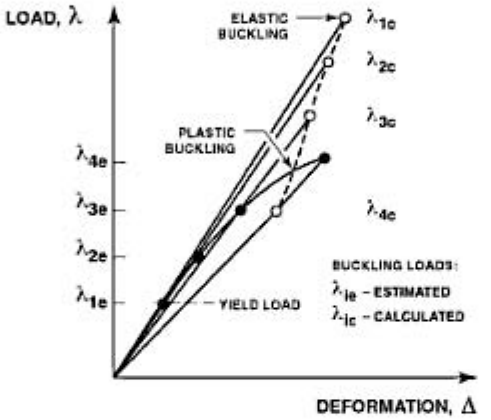


Figure 4-98 Estimated versus Calculated Buckling Loads

To obtain the load-deformation curve, the shell and stiffener materials (they need not be the same material) are represented with the Nadai stress-strain curve [4-104]:

$$\sigma_i \le \sigma_y: \quad \varepsilon_i = \frac{\sigma_i}{E}$$

$$\sigma_i > \sigma_y: \quad \varepsilon_i = \frac{\sigma_i}{E} + .002\left[\frac{\sigma_i - \sigma_y}{\sigma_{oy} - \sigma_y}\right]^n \tag{4.401}$$

in which σ_i is the stress intensity, ε_i is the strain intensity, σ_y is the yield stress, σ_{oy} is the offset yield stress (at .2% strain), and n is a material parameter that determines the shape of the stress-strain curve.

Éléments sous droits d'auteur

The buckling load calculated from Equation (4.399) must coincide with the estimated load for which the material properties in Equation (4.399) apply in order for the plastic buckling solution to have been found. If the estimated load, λ_e, is too low, the calculated load, λ_c, is too high because the material properties are too high. Conversely, if λ_e is too high, λ_c is too low. Thus, the special relation of λ_e to λ_c is an ideal criterion for use in a numerical technique to determine where λ_c equals λ_e to a prescribed accuracy.

Various load estimates, λ_{ie}, are made in Figure 4-98 on the load-deformation curve, and the corresponding absolute minimum calculated buckling loads are obtained by procedures discussed previously. The first load estimate, λ_{1e}, is the previously determined yield load for which the corresponding λ_{1c} is too high in Figure 4-98 because the material properties are too high. Successive load increments, $\Delta\lambda$, of one-tenth the yield load are added until λ_{ic} is less than λ_{ie}, e.g., $\lambda_{4c} < \lambda_{4e}$ in Figure 4-98. At this point, the estimated load is reduced by $\Delta\lambda/2$. The new λ_{ie} is compared to the corresponding λ_{ic} whereupon λ_{ie} is increased by $\Delta\lambda/4$ or decreased by $\Delta\lambda/2$ according to whether $\lambda_{ic} > \lambda_{ie}$ or $\lambda_{ic} < \lambda_{ie}$ as in Figure 4-99. The load increment is halved at essentially each step until $\lambda_{ic} = \lambda_{ie}$ to a prescribed accuracy. This interval-halving search procedure converges by virtue of the relation of λ_e to λ_c and can be shown to be the most efficient search procedure. The iteration procedures attempted for the determination of where $\lambda_e = \lambda_c$ did not converge.

All these elements just described are put together in a computer program [4-103] for efficiency in performing the calculations and in achieving convergence of the transcendental procedure. Also, the step-by-step minimization of the buckling loads with respect to integer values of m and n, the buckle mode shape numbers, (see Appendix B, subroutine MINIMA) is performed in the program.

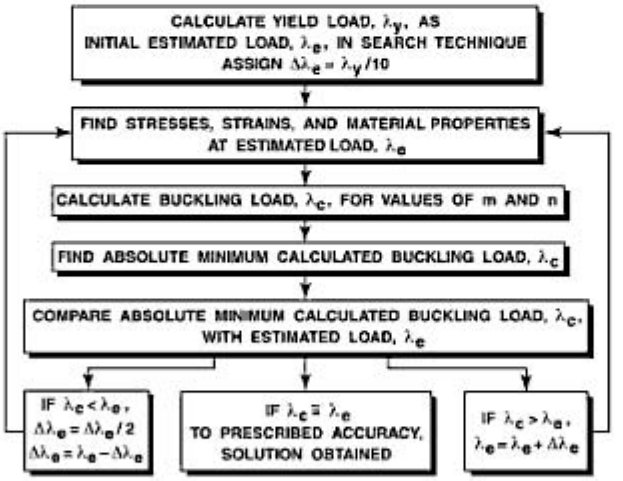


Figure 4-99 Buckling Criterion Solution Procedure *(After Jones [4-59]*

Éléments sous droits d'auteur

4.10.4 Numerical Results for Single-Layered Shells

The numerous geometrical and material parameters in the present investigation cannot be nondimensionalized in a meaningful fashion, i.e., general results cannot be presented. Accordingly, two numerical examples are given in order to illustrate application of the present theory. The first example is a single-layered shell subjected to hydrostatic pressure. The second example goes beyond the concept of a simple shell to that of a stiffened shell as developed in Section 4.7. The second example is a re-examination of a ring-and stringer-stiffened shell that is representative of current large-diameter missile-interstage structures. Buckling of the latter shell under axial compression was studied by Jones [4-58 & 4-59] and is examined in order to illustrate the capability of the present theory to treat negative loading components, e.g., internal pressurization of axially compressed shells or axial tension on a shell subjected to lateral pressure.

4.10.4.1 Single-Layered Circular Cylindrical Shell under Hydrostatic Pressure

Consider shells made of 7075-T6 aluminum for which the stress-strain curve is shown in Figure 4-100. That curve has the following characteristics when represented with a Nadai stress-strain curve model in Equation (4.401) on page 626 [4-104]:

$\sigma_y = 55$ ksi (380 MPa) $\quad E = 10.5 \times 10^3$ ksi (72.4GPa)
$\sigma_{oy} = 72$ ksi (500 MPa) $\quad n = 2.16$

for which the measured stress-strain curve points used to determine n are ($\sigma_1 = 63.5$ ksi (438 MPa), $\varepsilon_1 = .00649$) and ($\sigma_2 = 72$ ksi (500 MPa), $\varepsilon_2 = .00883$).

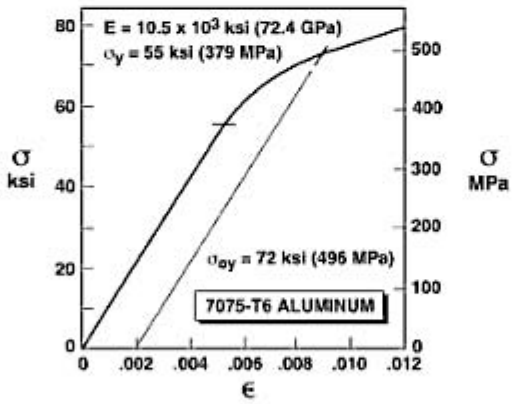


Figure 4-100 Stress-Strain Curve for 7075-T6 Aluminum

Éléments sous droits d'auteur

For a shell of thickness t = .2 in (.51 cm), R = 10 in (25 cm), and variable length, the elastic and plastic buckling pressures are shown in Figure 4-101. The yield pressure is 1.54 ksi (10.6 MPa) and corresponds to an axial stress of 31.75 ksi (219 MPa) with a circumferential stress of 63.5 ksi (438 MPa). Note that the circumferential stress itself is well above the uniaxial yield stress when the shell yields. In fact, this perhaps surprising situation is proper as can be verified by substitution of the axial and circumferential stresses in Equation (4.371) for the stress intensity which is indeed found to be 55 ksi (380 MPa). If the shell is longer than L/r = .52, the buckling is elastic. Below that L/r, very large reductions from elastic to plastic buckling pressures are observed. In addition, some cusps are observed at the tick marks that are perpendicular to the curves; the cusps are caused by changes in buckle mode shape as a function of shell length. The shell buckles into m = 1 (one axial half-wave) with a variable n (number of circumferential buckle waves).

If a thick shell is considered, plastic action influences the shell behavior to higher values of L/r than for the thin shell in Figure 4-101. For example, if t = .4 in (1.02 cm), the boundary between elastic and plastic buckling occurs at L/r = 1.36 as in Figure 4-102. That is, generally the influence of plasticity is felt most for thick and/or short shells.

Definitive plastic versus elastic buckling experiments are difficult to perform with shells. Experimentally representing the simply supported edge boundary conditions to which the present theory applies is quite difficult, if not impossible, under conditions of hydrostatic pressure. Under axial compression between the platens of a loading machine, the real boundary conditions of an actual shell are someplace in between simply supported and fixed edges. Hydrostatic pressure, however, must be applied as a fluid pressure to be realistic, and thus, supporting the shell is quite difficult. Certainly, in any real loading situation, the theoretical approximations to the actual boundary conditions can be quite crude.

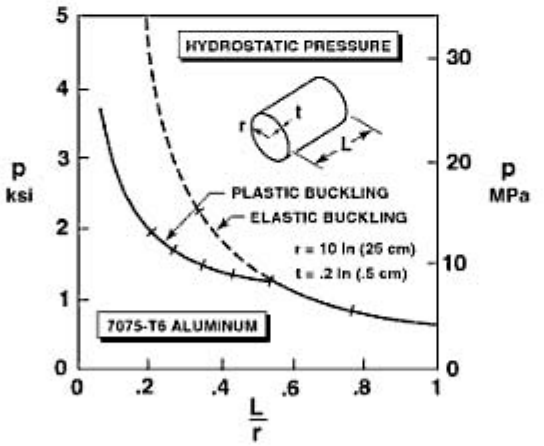


Figure 4-101 Plastic Buckling of Shells [t = .2" (.51 cm)]

Éléments sous droits d'auteur

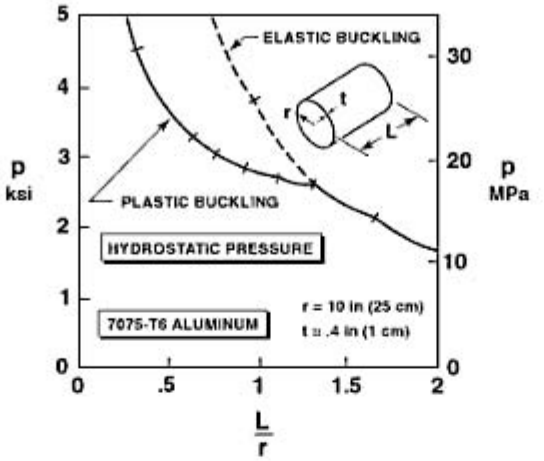


Figure 4-102 Plastic Buckling of Shells [t = .4" (1.02 cm)]

A solution for the plastic buckling of circular cylindrical shells is derived by use of a deformation theory of plasticity for the S2 simply supported edge buckling boundary conditions $\delta N_x = \delta v = \delta w = \delta M_x = 0$. Comparison of theoretical buckling loads with experimental buckling loads is difficult without a solution for clamped edges because shells used in experiments have some degree of edge clamping. Card and Jones [4-25] obtained an elastic clamped-edge solution and compared it to an elastic simply supported edge solution and to experimental data. Edge clamping was found to be important for elastic buckling [4-25] and might be as important for plastic buckling. The present simply supported edge plastic buckling solution can be regarded as a lower bound on the true solution if initial geometric imperfections and prebuckling deformations are ignored. However, additional experimental substantiation of the applicability to plastic buckling problems of the deformation theory as opposed to the incremental theory of plasticity is required.

4.10.4.2 Stiffened Large-Diameter Missile-Interstage Shell under Biaxial Loading

A ring- and stringer-stiffened shell that is representative of a large-diameter missile-interstage structure such as the Saturn V "moon rocket" is subjected to axial compression and then to biaxial loading including axial tension and internal pressure. The shell has a radius of 135 in (343 cm), a length of 135 in (343 cm), and a thickness of .10 in (.25 cm). The ring and stringer cross sections are shown in Figure 4-103. The stringer spacing is 2 in (5.1 cm) for all cases. The material is 7075-T6 aluminum for which a stress-strain curve is shown in Figure 4-100. Parameters to represent this aluminum with a Nadai stress-strain curve are given in Section 4.10.4.1.

Éléments sous droits d'auteur

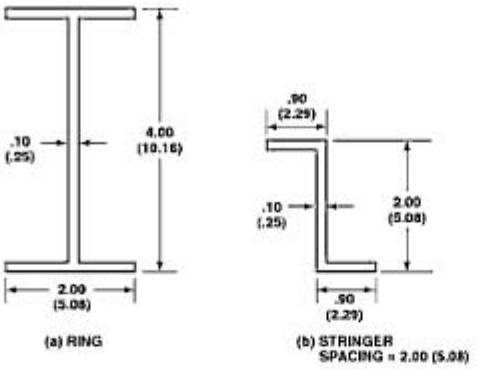


Figure 4-103 Stiffener Dimensions in Inches (cm) *(After Jones [4-58])*

General instability buckling stresses, i.e., buckling in which both rings and stringers participate as defined in Figure 4-67 on page 553, are displayed in Figure 4-104 for a range of ring spacings. The increase in buckling stress obtained by placing stringers externally as opposed to internally is seen to be considerably lessened for small ring spacings in this example when plastic results are compared to elastic results.

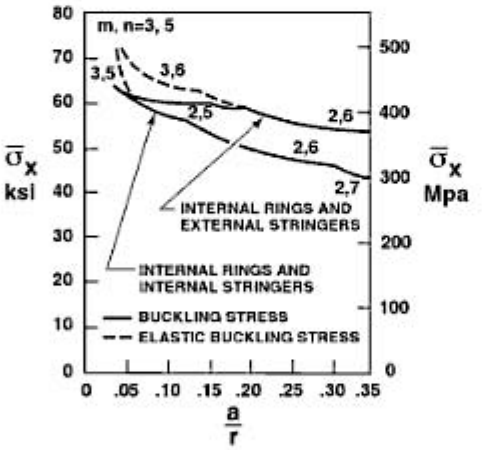


Figure 4-104 General Instability under Axial Compression of a Large-Diameter Missile-Interstage Structure *(After Jones [4-58])*

Éléments sous droits d'auteur

For panel instability, i.e., buckling in which only stringers participate because buckling occurs between rings as shown in Figure 4-67 on page 553, buckling stresses are shown in Figure 4-105 for a range of ring spacings. Large effects of plastic deformation are seen for small ring spacings. However, only for large ring spacings are the panel instability stresses lower than the general instability stresses. The effects of eccentricity are seen to decrease with increasing plastic deformation.

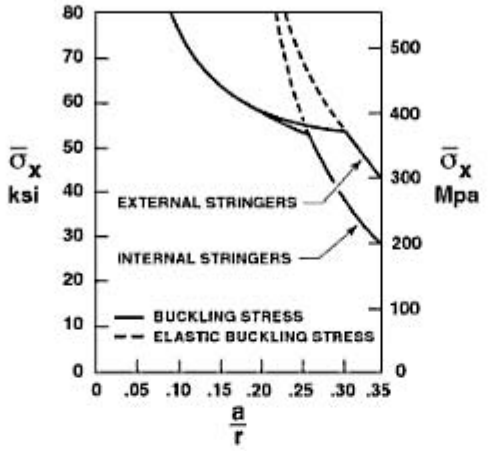


Figure 4-105 Panel Instability under Axial Compression of a Large-Diameter Missile-Interstage Structure *(After Jones [4-58])*

General instability results for the large-diameter missile-interstage structure under biaxial loading are displayed in Figure 4-106. The yield curve, which is denoted by a dashed line with intermittent dots, separates the regions of elastic and plastic behavior. Substantial reductions, especially at large axial tension or large internal pressure, from the elastic results (dashed curve) are noted for plastic results (solid curve).

For missiles, it is sometimes desired to increase the resistance to buckling under axial compression by use of internal pressurization, e.g., the Atlas missile of the 1950s. In the present example, the net axial buckling force decreases with internal pressurization due to effects of plastic deformation on the buckling resistance. When this result is compared with the prediction of increasing net axial buckling force with internal pressurization under elastic conditions, it is obvious that substantial modification must be made to the usual conclusion that internal pressurization increases the buckling resistance of missiles. Although some benefit is obtained by use of internal pressurization, the elastic approach would result in an overestimate of the axial buckling load by 30% at 100-psi (689 kPa) internal pressure. Similar results are obtained for the use of axial tension to increase the buckling resistance under lateral pressure.

Éléments sous droits d'auteur

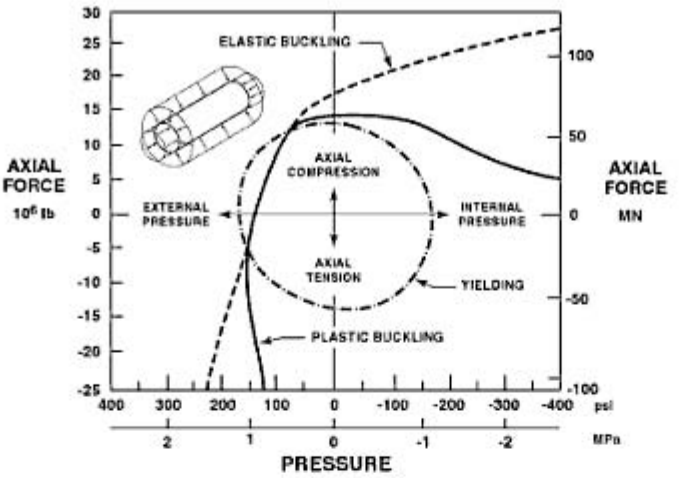


Figure 4-106 A Large-Diameter Missile-Interstage Structure under Biaxial Loading *(After Jones [4-59])*

4.10.5 Derivation of Multilayered Shells Buckling Criterion

4.10.5.1 Introduction

For plastic buckling, if we expand our attention from single-layered to multilayered plates and shells, then we must add several levels of analytical and numerical complexity to address the multiple layers and how they interact with one another. This sub-section is a merger of the nature of the analysis of multilayered plates and shells with the resulting complexities of the nonlinear analysis for plastic deformation, as well as the intricacies of stiffeners for shells.

By use of simple J_2 deformation theory of plasticity, expressions are obtained for the variation of biaxial stresses during buckling in terms of the variations of strains and material properties during buckling of a stiffened multilayered circular cylindrical shell. The variations in biaxial stresses are integrated over the shell layers and the variations in uniaxial stresses are integrated over the stiffeners to obtain expressions for the variations in forces and moments during buckling. Finally, the variations in forces and moments are substituted in Donnell-type shell buckling differential equations for shells with an S2 buckling boundary condition to obtain a transcendental buckling criterion in terms of the geometry and nonlinear material properties of the stiffened multilayered shell. The transcendental buckling criterion involves the complexity of (1) layer strain compatibility, (2) layer equilibrium, and (3) layer stress-strain relations that must be treated with various iterative techniques. The criterion is applicable for arbitrary combinations of axial and lateral pressure, and is solved in a subsequent subsection.

Éléments sous droits d'auteur

4.10.5.2 Fundamental Relations in J_2 Deformation Theory

The fundamental quantities in the J_2 deformation theory of plasticity for the k^{th} layer of a multilayered shell made of isotropic materials (see Nadai [4-94] and Jones [4-95]) are the stress intensity, σ_i^k, ($\sigma_i = 3\,\tau_o/\sqrt{2}$ in which τ_o is the octahedral shear stress):

$$\sigma_i^k = \sqrt{(\sigma_x^k)^2 + (\sigma_y^k)^2 - \sigma_x^k\sigma_y^k + 3(\tau_{xy}^k)^2} \tag{4.402}$$

the strain intensity, ε_i^k, ($\varepsilon_i = 3\gamma_o/[2\sqrt{2}\,(1+\nu)]$ in which γ_o is the octrahedral shear strain):

$$\bar{\varepsilon}_i^k = \frac{1}{1-\nu_k^2}\sqrt{\begin{aligned}&(1-\nu_k+\nu_k^2)((\bar{\varepsilon}_x^k)^2 + (\bar{\varepsilon}_y^k)^2)\\ &-(1-4\nu_k+\nu_k^2)\bar{\varepsilon}_x^k\bar{\varepsilon}_y^k + \frac{3}{4}(1-\nu_k)^2(\gamma_{xy}^k)^2\end{aligned}} \tag{4.403}$$

and the stress-strain relations for each layer:

$$\begin{aligned}\sigma_x^k &= \frac{E_{sec}^k}{1-\nu_k^2}(\bar{\varepsilon}_x^k + \nu_k\bar{\varepsilon}_y^k)\\ \sigma_y^k &= \frac{E_{sec}^k}{1-\nu_k^2}(\bar{\varepsilon}_y^k + \nu_k\bar{\varepsilon}_x^k)\\ \tau_{xy}^k &= \frac{E_{sec}^k}{2(1+\nu_k)}\gamma_{xy}^k\end{aligned} \tag{4.404}$$

that relate the stress intensity to the strain intensity. In addition, certain material properties are defined in terms of the stress and strain intensities: First, the secant modulus, E_{sec}^k, is the slope of a line from the origin of the stress-strain curve for the material in the k^{th} layer to the active stress point as in Figure 4-107. Recall that the stress-intensity versus strain-intensity curve can be shown to be identical to the uniaxial stress-strain curve for an isotropic material.

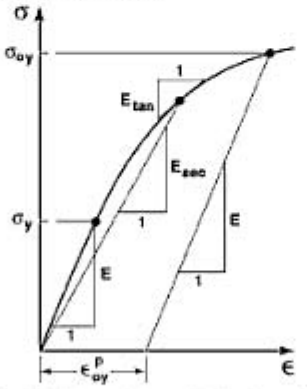


Figure 4-107 Nonlinear Stress-Strain Curve for each Layer

Éléments sous droits d'auteur

$$E^k_{sec} = \frac{\sigma^k_i}{\varepsilon^k_i} \tag{4.405}$$

The tangent modulus, E^k_{tan}, is the local slope at the active stress point:

$$E^k_{tan} = \frac{d\sigma^k_i}{d\varepsilon^k_i} \tag{4.406}$$

Third, Poisson's ratio, ν_k, is defined as

$$\nu_k = -\frac{\varepsilon^k_y}{\varepsilon^k_x} \tag{4.407}$$

for an applied uniaxial σ_x. For elastic-plastic isotropic materials, Poisson's ratio is further derived by Gerard and Wildhorn [4-102] to be

$$\nu_k = \frac{1}{2} - \left(\frac{1}{2} - \nu^e_k\right)\frac{E^k_{sec}}{E^k} \tag{4.408}$$

in which ν^e_k is the elastic Poisson's ratio and E^k is the elastic Young's modulus in the k^{th} layer. By use of Equation (4.408), a smooth transition is provided between the elastic compressible state and the plastic incompressible state of the material. Note that $E > E_{sec} > E_{tan}$ for all layers.

4.10.5.3 Variations of Strains during Buckling

As with eccentrically stiffened shells in Section 4.7, the Kirchhoff-Love hypothesis [4-4] leads to the variations in strains

$$\begin{aligned}
\delta\varepsilon_x &= \delta\varepsilon^o_x + z\delta\kappa_x \\
\delta\varepsilon_y &= \delta\varepsilon^o_y + z\delta\kappa_y \\
\delta\gamma_{xy} &= \delta\gamma^o_{xy} + z\delta\kappa_{xy}
\end{aligned} \tag{4.409}$$

The z-coordinate is measured from an arbitrary reference surface at Δ from the inside of the shell (here the middle surface) as in Figure 4-108. In Equation (4.409), $\delta\varepsilon^o_x$, $\delta\varepsilon^o_y$, and $\delta\gamma^o_{xy}$ are the variations of the reference-surface strains

$$\begin{aligned}
\delta\varepsilon^o_x &= \delta u_{,x} \\
\delta\varepsilon^o_y &= \delta v_{,y} + \frac{\delta w}{r} \\
\delta\gamma^o_{xy} &= \delta u_{,y} + \delta v_{,x}
\end{aligned} \tag{4.410}$$

and $\delta\kappa_x$, $\delta\kappa_y$, and $\delta\kappa_{xy}$ are variations of the reference-surface curvatures

$$\begin{aligned}
\delta\kappa_x &= -\delta w_{,xx} \\
\delta\kappa_y &= -\delta w_{,yy} \\
\delta\kappa_{xy} &= -2\delta w_{,xy}
\end{aligned} \tag{4.411}$$

Éléments sous droits d'auteur

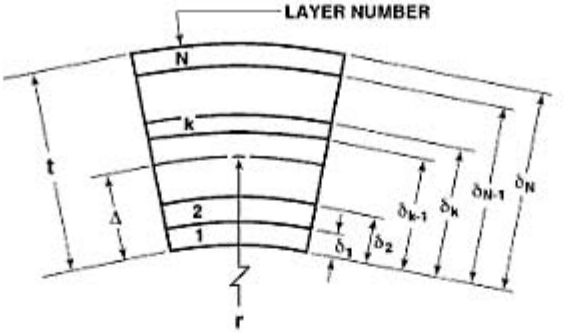


Figure 4-108 Partial Cross Section of an N-Layered Shell

4.10.5.4 Variations of Stresses during Buckling

During buckling, the stresses and the nonlinear material properties, E_{sec} and ν, in Equation (4.404) vary from their prebuckling values, e.g.,

$$\delta\sigma_x^k = \frac{E_{sec}^k}{1-\nu_k^2}\left(\delta\varepsilon_x^k + \nu_k\delta\varepsilon_y^k\right) + \left(\varepsilon_x^k + \nu_k\varepsilon_y^k\right)\frac{\delta E_{sec}^k}{1-\nu_k^2} + \varepsilon_x^k E_{sec}^k\,\delta\left[\frac{1}{1-\nu_k^2}\right] + \varepsilon_y^k E_{sec}^k\,\delta\left[\frac{\nu_k}{1-\nu_k^2}\right] \tag{4.412}$$

Accordingly, the following variations are required:

$$\delta E_{sec}^k = -\frac{(E_{sec}^k)^2}{\sigma_i^k}\left[1-\frac{E_{tan}^k}{E_{sec}^k}\right]\delta\varepsilon_i^k \tag{4.413}$$

$$\delta\left[\frac{1}{1-\nu_k^2}\right] = \frac{2\nu_k}{(1-\nu_k^2)^2}\,\delta\nu_k \tag{4.414}$$

$$\delta\left[\frac{\nu_k}{1-\nu_k^2}\right] = \frac{1+\nu_k^2}{(1-\nu_k^2)^2}\,\delta\nu_k \tag{4.415}$$

From the fundamental relation for Poisson's ratio, Equation (4.408), and the variation in E_{sec}, Equation (4.413),

$$\delta\nu_k = (1-2\nu_k)\frac{E_{sec}^k}{2\sigma_i^k}\left[1-\frac{E_{tan}^k}{E_{sec}^k}\right]\delta\varepsilon_i^k \tag{4.416}$$

so that all variations of the material parameters are expressed in terms of $\delta\varepsilon_i^k$ which, in turn, can be obtained from ε_i^k [Equation (4.403)] as

Éléments sous droits d'auteur

$$\delta\varepsilon_i^k = \frac{1}{2H^k\sigma_i^k(1-\nu_k^2)}\left[\left[(2-\nu_k)\sigma_x^k-(1-2\nu_k)\sigma_y^k\right]\delta\varepsilon_x^k + \left[(2-\nu_k)\sigma_y^k-(1-2\nu_k)\sigma_x^k\right]\delta\varepsilon_y^k + 3(1-\nu_k)\tau_{xy}^k\delta\gamma_{xy}^k\right] \tag{4.417}$$

in which

$$H^k = 1-\frac{1-2\nu_k}{2(1-\nu_k^2)}\left[1-\frac{E_{tan}^k}{E_{sec}^k}\right] \times\left[2\nu_k+\frac{1}{2(\sigma_i^k)^2}\left[-(1+2\nu_k)\left[(\sigma_x^k)^2+(\sigma_y^k)^2\right] + 2(2+\nu_k)\sigma_x^k\sigma_y^k-6(1+\nu_k)(\tau_{xy}^k)^2\right]\right] \tag{4.418}$$

For the present loading condition of only combinations of axial compression and lateral pressure, $\tau_{xy}=0$, the stress variations are

$$\begin{aligned}\delta\sigma_x^k &= \frac{E_{sec}^k}{1-\nu_k^2}\left(K_{11}^k\delta\varepsilon_x^k+\nu_kK_{12}^k\delta\varepsilon_y^k\right)\\ \delta\sigma_y^k &= \frac{E_{sec}^k}{1-\nu_k^2}\left(\nu_kK_{12}^k\delta\varepsilon_x^k+K_{22}^k\delta\varepsilon_y^k\right)\\ \delta\tau_{xy}^k &= \frac{E_{sec}^k}{1-\nu_k^2}K_{33}^k\delta\gamma_{xy}^k\end{aligned} \tag{4.419}$$

in which

$$\begin{aligned}K_{11}^k &= 1-\frac{K^k}{4(1-\nu_k^2)}\left[(2-\nu_k)\sigma_x^k-(1-2\nu_k)\sigma_y^k\right]^2\\ K_{12}^k &= 1-\frac{K^k}{4\nu_k(1-\nu_k^2)}\left[(2-\nu_k)\sigma_y^k-(1-2\nu_k)\sigma_x^k\right]\left[(2-\nu_k)\sigma_x^k-(1-2\nu_k)\sigma_y^k\right]\\ K_{22}^k &= 1-\frac{K^k}{4(1-\nu_k^2)}\left[(2-\nu_k)\sigma_y^k-(1-2\nu_k)\sigma_x^k\right]^2\\ K_{33}^k &= (1-\nu_k)/2\end{aligned} \tag{4.420}$$

in which

$$K^k = \frac{1}{H^k(\sigma_i^k)^2}\left[1-\frac{E_{tan}^k}{E_{sec}^k}\right] \tag{4.421}$$

Éléments sous droits d'auteur

For the elastic case, $E^k_{sec} = E^k$ and $K^k = 0$, so the K^k_{ij} reduce to unity, and the variations of stresses, Equation (4.419), are identical to the variations in elastic stresses.

The variations of the stiffener stresses during buckling from a membrane prebuckled shape are obtained by varying the uniaxial normal stresses

$$\sigma_{x_s} = E_{sec_s}\varepsilon_{x_s} \qquad \sigma_{y_r} = E_{sec_r}\varepsilon_{y_r} \tag{4.422}$$

and the last of Equation (4.404) to get:

$$\begin{aligned} \delta\sigma_{x_s} &= E_{tan_s}\delta\varepsilon_{x_s} & \delta\sigma_{y_r} &= E_{tan_r}\delta\varepsilon_{y_r} \\ \delta\tau_{xy_s} &= G_{sec_s}\delta\gamma_{xy_s} & \delta\tau_{xy_r} &= G_{sec_r}\delta\gamma_{xy_r} \end{aligned} \tag{4.423}$$

Note that the variations of shear stress are not obtained from uniaxial relations in parallel to Equation (4.422) because such relations do not apply when no shear strain exists prior to buckling.

4.10.5.5 Variations of Forces and Moments during Buckling

The variations of forces and moments during buckling are obtained by integration of the variations of stresses over all the layers through the shell thickness and over the stiffeners for the variations of forces, e.g.,

$$\delta N_x = \sum_{k=1}^{N} \int_{t_k} \delta\sigma_x^k \, dz + \frac{1}{b}\int_{A_s} \delta\sigma_{x_s} \, dA_s \tag{4.424}$$

in which the effect of the axial stiffener is averaged over its spacing, b.

$$\begin{aligned} \delta N_x &= (A_{11} + E_{tan_s}A_s/b)\delta\varepsilon_x + A_{12}\delta\varepsilon_y + (B_{11} + \bar{z}_s E_{tan_s}A_s/b)\delta\kappa_x + B_{12}\delta\kappa_y \\ \delta N_y &= A_{12}\delta\varepsilon_x + (A_{22} + E_{tan_r}A_r/a)\delta\varepsilon_y + B_{12}\delta\kappa_x + (B_{22} + z_r E_{tan_r}A_r/a)\delta\kappa_y \\ \delta N_{xy} &= A_{33}\delta\gamma_{xy} + B_{33}\delta\kappa_{xy} \end{aligned} \tag{4.425}$$

The moments of the variations of stresses are similarly integrated to get the variations of moments.

$$\begin{aligned} \delta M_x &= (B_{11} + \bar{z}_s E_{tan_s}A_s/b)\delta\varepsilon_x + B_{12}\delta\varepsilon_y \\ &\quad + (D_{11} + \bar{z}_s^2 E_{tan_s}A_s/b + E_{tan_s}I_s/b)\delta\kappa_x + D_{12}\delta\kappa_y \\ \delta M_y &= B_{12}\delta\varepsilon_x + (B_{22} + \bar{z}_r E_{tan_r}A_r/a)\delta\varepsilon_y \\ &\quad + D_{12}\delta\kappa_x + (D_{22} + \bar{z}_r^2 E_{tan_r}A_r/a + E_{tan_r}I_r/a)\delta\kappa_y \\ \delta M_{xy} &= -B_{33}\delta\gamma_{xy} - (D_{33} + G_{sec_s}J_s/2b)\delta\kappa_{xy} \\ \delta M_{yx} &= B_{33}\delta\gamma_{xy} + (D_{33} + G_{sec_r}J_r/2a)\delta\kappa_{xy} \end{aligned} \tag{4.426}$$

in which

Éléments sous droits d'auteur

$$A_{ij} = \sum_{k=1}^{N} K_{ij}^{k} \frac{E_{sec}^{k}}{1-\nu_k^2}(\delta_k - \delta_{k-1})$$

$$B_{ij} = \frac{1}{2}\sum_{k=1}^{N} K_{ij}^{k} \frac{E_{sec}^{k}}{1-\nu_k^2}\left[(\delta_k^2 - \delta_{k-1}^2) - 2\Delta(\delta_k - \delta_{k-1})\right] \tag{4.427}$$

$$D_{ij} = \frac{1}{3}\sum_{k=1}^{N} K_{ij}^{k} \frac{E_{sec}^{k}}{1-\nu_k^2}\left[(\delta_k^3 - \delta_{k-1}^3) - 3\Delta(\delta_k^2 - \delta_{k-1}^2) + 3\Delta^2(\delta_k - \delta_{k-1})\right]$$

in which N is the number of layers, δ_k is the distance from the inner surface of the layered shell to the outer surface of the k^{th} layer, Δ is the distance from the inner surface of the layered shell to the reference surface (usually the middle surface), and the stiffener quantities are defined in Section 4.7 on stiffened shells. The stiffnesses in Equation (4.427) are due to Ambartsumyan [4-61] and depend on the location of the reference surface. Note that A_{ij} and D_{ij} are plastic buckling extensional and bending stiffnesses, respectively, whereas the B_{ij} are the plastic bending-extension coupling stiffnesses studied in their elastic version in Section 4.8 on laminated shells. The elastic versions of the extensional, bending-extension coupling, and bending stiffnesses, A_{ij}, B_{ij}, and D_{ij}, are obtained from Equation (4.427) by using elastic values of K_{ij} [$K_{11} = K_{22} = K_{12} = 1$ and $K_{33} = (1-\nu)/2$], elastic moduli, and elastic Poisson's ratios in Equations (4.422) and (4.427). The plastic versions of the prebuckling extensional, bending-extension coupling, and bending stiffnesses, A_{ij}, B_{ij}, and D_{ij}, are obtained by using the elastic values of K_{ij}, plastic secant moduli, and plastic Poisson's ratios in Equations (4.422) and (4.427).

4.10.5.6 Buckling Criterion

The Donnell-type buckling differential equations for circular cylindrical shells under combined axial compression and lateral pressure are, from Equations (4.71)–(4.73) on page 487,

$$\begin{aligned}
&\delta N_{x,x} + \delta N_{xy,y} = 0\\
&\delta N_{xy,x} + \delta N_{y,y} = 0\\
&-\delta M_{x,xx} + \delta M_{xy,xy} - \delta M_{yx,xy} - \delta M_{y,yy} + \frac{\delta N_y}{r} + \bar{N}_x \delta w_{,xx} + \bar{N}_y \delta w_{,yy} = 0
\end{aligned} \tag{4.428}$$

The buckling displacements (with indeterminate amplitudes, $\tilde{u}$, $\tilde{v}$, and $\tilde{w}$)

$$\begin{aligned}
\delta u &= \tilde{u}\cos\frac{m\pi x}{L}\cos\frac{ny}{r}\\
\delta v &= \tilde{v}\sin\frac{m\pi x}{L}\sin\frac{ny}{r}\\
\delta w &= \tilde{w}\sin\frac{m\pi x}{L}\cos\frac{ny}{r}
\end{aligned} \tag{4.429}$$

Éléments sous droits d'auteur

satisfy the S2 simply supported edge buckling boundary conditions $\delta N_x = \delta v = \delta w = \delta M_x = 0$ and are substituted in the variations in forces and moments, Equations (4.425) and (4.426), in terms of the variations in reference-surface strains and changes in curvature, Equations (4.410) and (4.411), which are subsequently substituted in the buckling differential equations, Equation (4.428). In order for a nontrivial solution to exist for the resulting homogeneous equations in $\tilde{u}$, $\tilde{v}$, and $\tilde{w}$, the determinant of the coefficients of $\tilde{u}$, $\tilde{v}$, and $\tilde{w}$ must vanish which condition leads to the buckling criterion

$$\bar{N}_x\left[\frac{m\pi}{L}\right]^2 + \bar{N}_y\left[\frac{n}{r}\right]^2 = T_{33} + \frac{2T_{12}T_{13}T_{23} - T_{11}T_{23}^2 - T_{22}T_{13}^2}{T_{11}T_{22} - T_{12}^2} \tag{4.430}$$

in which

$$\begin{aligned}
T_{11} &= (A_{11} + E_{tan_s}A_s/b)(m\pi/L)^2 + A_{33}(n/r)^2 \\
T_{12} &= (A_{12} + A_{33})(m\pi/L)(n/r) \\
T_{13} &= (A_{12}/r)(m\pi/L) + (B_{11} + \bar{z}_s E_{tan_s}A_s/b)(m\pi/L)^3 + (B_{12} + 2B_{33})(m\pi/L)(n/r)^2 \\
T_{22} &= A_{33}(m\pi/L)^2 + (A_{22} + E_{tan_r}A_r/a)(n/r)^2 \\
T_{23} &= (B_{12} + 2B_{33})(m\pi/L)^2(n/r) + (1/r)(A_{22} + E_{tan_r}A_r/a)(n/r) \\
&\quad + (B_{22} + \bar{z}_r E_{tan_r}A_r/a)(n/r)^3 \\
T_{33} &= (D_{11} + E_{tan_s}I_s/b + \bar{z}_s^2 E_{tan_s}A_s/b)(m\pi/L)^4 \\
&\quad + (4D_{33} + 2D_{12} + G_{sec_s}J_s/b + G_{sec_r}J_r/a)(m\pi/L)^2(n/r)^2 \\
&\quad + (D_{22} + E_{tan_r}I_r/a + \bar{z}_r^2 E_{tan_r}A_r/a)(n/r)^4 \\
&\quad + (2/r)(B_{22} + \bar{z}_r E_{tan_r}A_r/a)(n/r)^2 + (1/r)^2(A_{22} + E_{tan_r}A_r/a)
\end{aligned} \tag{4.431}$$

Equation (4.430) is a transcendental expression for the buckling forces, $\bar{N}_x$ and $\bar{N}_y$, in terms of the material properties at the buckling forces $\bar{N}_x$ and $\bar{N}_y$ and in terms of the geometry and the buckling mode numbers m and n. This buckling criterion was obtained by Jones [4-59] and reduces to Jones' solution for plastic buckling of stiffened single-layered circular cylindrical shells [4-58] (also shown in Section 4.10.2); Jones' solution for elastic buckling of stiffened multilayered circular cylindrical shells [4-65]; Block, Card, and Mikulas' solution [4-53] for elastic buckling of stiffened single-layered circular cylindrical shells; and the classical 'Euler solution' for unstiffened elastic circular cylindrical shells. The solution procedure for the transcendental buckling criterion, Equation (4.430), for the lowest of the many buckling loads is discussed in the next sub-section.

Éléments sous droits d'auteur

4.10.6 Solution of Multilayered Shells Buckling Criterion

4.10.6.1 Introduction

The buckling load calculated from a buckling criterion such as Equation (4.430) for shells depends on the geometry, buckling mode parameters, m and n, and the nonlinear material properties. However, for plastic buckling, the material properties are a function of the buckling load. Thus, the buckling criterion is a transcendental expression and because of this fact and the numerous geometric and material properties, a computer program [4-105] is essential to the practical calculation of buckling loads. Actually, the major portion of the effort in analysis of plastic buckling of plates and shells is in the solution of the transcendental buckling criterion. However, little, if any, discussion of the solution procedure is published. Description of the solution procedure is especially important for multilayered shells because of required new techniques.

The solution procedure is displayed schematically in Figure 4-109 and is outlined in the following sections. The objective of the solution procedure is to logically estimate a succession of loads to search for the load at which the stiffened multilayered shell buckles according to the transcendental stability criterion. The first step is to calculate the yield load, λ_y, to determine the boundary between elastic and plastic behavior (λ_y is the basis for a decision at a later step). The second step is to determine the layer and stiffener stresses, strains, and, hence, material properties at an estimated load by a succession of numerical techniques (with the exception that at the first estimated load, λ_y, the material properties are elastic so the stresses and strains can be determined directly).

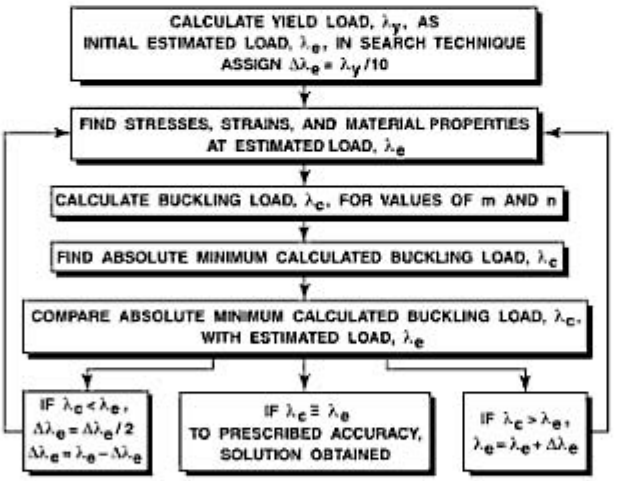


Figure 4-109 Buckling Criterion Solution Procedure *(After Jones [4-59])*

Éléments sous droits d'auteur

The third step is to calculate the buckling load for each value of m and n at the material properties corresponding to the estimated load and to select the absolute minimum calculated buckling load from among values for a prescribed range of m and n. The fourth and final step is to compare the absolute minimum calculated buckling load with the estimated buckling load to determine whether the solution has been obtained. For the first estimated buckling load, λ_y, if the absolute minimum calculated buckling load is less than the yield load, buckling is elastic and the solution has been obtained. If it is greater than the yield load, a searching technique is developed herein for choosing a succession of estimated loads and repeating steps two through four until the estimated plastic buckling load is the same as the absolute minimum calculated plastic buckling load to a prescribed accuracy. The searching technique is displayed in Figure 4-109 and described in this section.

The stiffened multilayered shell is represented by its geometry and by nonlinear stress-strain curves for each layer and stiffener. The Nadai stress-strain curve for a .2% offset yield stress [4-104] is used for the purposes of illustration:

$$\sigma_i \le \sigma_y: \quad \varepsilon_i = \frac{\sigma_i}{E}$$
$$\sigma_i > \sigma_y: \quad \varepsilon_i = \frac{\sigma_i}{E} + .002\left[\frac{\sigma_i - \sigma_y}{\sigma_{oy} - \sigma_y}\right]^n \tag{4.432}$$

in which σ_i is the stress intensity, ε_i is the strain intensity, σ_y is the yield stress, σ_{oy} is the offset yield stress (at .2% strain), and n is a material parameter that determines the shape of the stress-strain curve. Any other nonlinear stress-strain relations can be used if desired. The stiffeners and each layer can have different values of E, ν, σ_y, σ_{oy}, and n in the author's computer program [4-105].

4.10.6.2 Determination of the Yield Load

We must first find the yield load for the multilayered shell (perhaps only one layer yields, but more than one layer could yield simultaneously) in order to start the analysis process. In the axisymmetric elastic membrane prebuckled state, the force-strain relations are given by

$$\bar{N}_x = \left[\bar{A}_{11} + \frac{E_s A_s}{b}\right]\bar{\varepsilon}_x + \bar{A}_{12}\bar{\varepsilon}_y$$
$$\bar{N}_y = \bar{A}_{12}\bar{\varepsilon}_x + \left[\bar{A}_{22} + \frac{E_r A_r}{a}\right]\bar{\varepsilon}_y \tag{4.433}$$

Let N_x and N_y be related to a positive number λ that represents the level of loading in the following manner.

$$\bar{N}_x = k_1\lambda \qquad \bar{N}_y = k_2\lambda \tag{4.434}$$

in which k_1 and/or k_2 can be negative, although it is to be noted that buckling occurs only when either k_1 or k_2 is positive. The objective of this

Éléments sous droits d'auteur

section is to find the value of λ that will cause yielding in at least one layer of the shell or in the stiffeners. To this end, let

$$AA = \bar{A}_{11} + \frac{E_s A_s}{b} \qquad BB = \bar{A}_{12}$$
$$CC = \bar{A}_{22} + \frac{E_r A_r}{a} \tag{4.435}$$

Equations (4.433–4.435) can be written as

$$k_1\lambda = AA\,\bar{\varepsilon}_x + BB\,\bar{\varepsilon}_y \qquad k_2\lambda = BB\,\bar{\varepsilon}_x + CC\,\bar{\varepsilon}_y \tag{4.436}$$

Solve Equation (4.436) for $\bar{\varepsilon}_x$

$$\bar{\varepsilon}_x = \left[\frac{BB\,k_2 - CC\,k_1}{BB^2 - AA\,CC}\right]\lambda = \bar{A}\,\lambda \tag{4.437}$$

Similarly,

$$\bar{\varepsilon}_y = \left[\frac{k_1 - AA\,\bar{A}}{BB}\right]\lambda = \bar{B}\,\lambda \tag{4.438}$$

so the membrane strains are known in terms of the applied loads. Upon substitution of the membrane strains in the expression for the strain intensity in the k^{th} layer

$$e_{ik} = \frac{1}{1-\nu_k^2}\left[(1-\nu_k+\nu_k^2)(\bar{A}^2+\bar{B}^2) - (1-4\nu_k+\nu_k^2)\bar{A}\,\bar{B}\right]^{1/2}\lambda \tag{4.439}$$

and conversion to the stress intensity in the k^{th} layer by use of Equation (4.405), the load causing yielding in the layered shell is the smallest of

$$\lambda_{yk} = \frac{\sigma_{yk}}{E^k \bar{C}_k} \tag{4.440}$$

in which $\bar{C}_k$ is the coefficient of λ in Equation (4.439). For the rings, the load that causes yielding is

$$\lambda_{yr} = \left|\frac{\sigma_{yr}}{E_r \bar{B}}\right| \tag{4.441}$$

whereas for the stringers, the load that causes yielding is

$$\lambda_{ys} = \left|\frac{\sigma_{ys}}{E_s \bar{A}}\right| \tag{4.442}$$

The yield load for the stiffened shell is the smallest of the λ in Equations (4.440–4.442). The yield load, of course, separates the elastic behavior of the shell from the nonlinear behavior. The stresses and strains at the yield load are obtained by substitution of the smallest λ in Equations (4.437), (4.438), and (4.404) successively.

Éléments sous droits d'auteur

4.10.6.3 Determination of Layer and Stiffener Stresses, Strains, and Material Properties at an Estimated Buckling Load

In order to determine the layer and stiffness stresses, strains, and material properties at an estimated buckling load, the load-deformation behavior of the stiffened multilayered plate or shell must first be found. For single-layered plates and shells in a membrane prebuckling equilibrium state, the load-deformation behavior is merely a scaling constant times the stress-strain behavior. However, multilayered plates and shells, even in a membrane prebuckling equilibrium state, exhibit much more complex behavior because no such scaling constant exists. Although the axial, as well as the lateral or circumferential, strain is the same in each layer, the strain intensity, Equation (4.403), is not the same because the Poisson's ratio is different in each layer.

Actually, at this stage in the solution, only a portion of the load-deformation behavior is required, namely, the determination of the deformation at the estimated buckling load. At each such required determination in the search for the buckling load, the necessary steps are shown in Figure 4-110 and described as follows. The associated numerical techniques are explained in more detail in the following paragraphs. First, the load-deformation curve is extrapolated from a known point to the new estimated load, λ_{cl}, at which the strains are calculated using the material properties of the known point. The second step is to calculate the layer and stiffener stresses and material properties at the strains calculated in the first step. The third step is to calculate the actual load from the layer and stiffener stresses at the calculated strains and compare it to the desired load. If the calculated load is not equal to the desired load, a new (smaller) load increment is determined by the difference between the calculated and desired loads. The steps are repeated

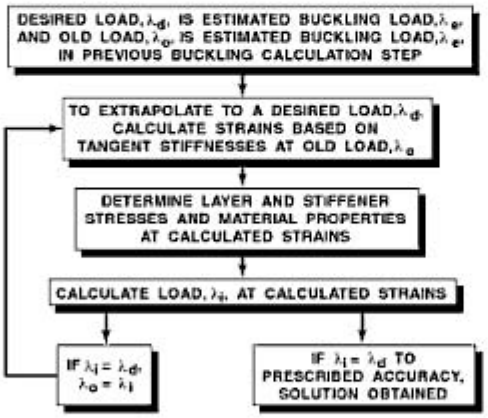


Figure 4-110 Procedure for Determination of Layer and Stiffener Stresses, Strains, and Material Properties at the Estimated Buckling Load *(After Jones [4-59])*

Éléments sous droits d'auteur

until the calculated load is the same as the desired load to a prescribed accuracy. Three broad classes of iteration are noted in Figures 4-109 and 4-110: 1) load estimates; 2) strain estimates; and 3) layer and stiffener stress estimates. The number of iterations, subiterations, and subsubiterations that must be undergone is highly dependent on the degree of nonlinearity of the stress-strain curves and on the geometry of the configuration. The number of iterations, etc., for a particular case are given in the numerical example in Section 4.10.7.

The extrapolation procedure, or tangent predictor technique, can best be explained by reference to Figure 4-111 in the following discussion. In Figure 4-111, λ is the load and Δ is a characteristic deformation. The tangent extensional stiffnesses, A_{ij}, are used to extrapolate from the old load, λ_o, at the previous known deformation (starting with the yield deformation and load at the beginning of the entire procedure to solve the buckling criterion) to the desired load, λ_d, at which the deformation is to be determined. If an increment in λ is formed in the manner of Equation (4.434), the prebuckling force-strain relations

$$\begin{aligned} \bar{N}_x &= \left[\hat{A}_{11} + \frac{E_{sec_s} A_s}{b} \right] \bar{\varepsilon}_x + \hat{A}_{12} \bar{\varepsilon}_y \\ \bar{N}_y &= \hat{A}_{12} \bar{\varepsilon}_x + \left[\hat{A}_{22} + \frac{E_{sec_r} A_r}{a} \right] \bar{\varepsilon}_y \end{aligned} \tag{4.443}$$

can be written in incremental form

$$\begin{aligned} \Delta \bar{N}_x &= \left[A_{11} + \frac{E_{tan_s} A_s}{b} \right] \Delta \bar{\varepsilon}_x + A_{12} \Delta \bar{\varepsilon}_y \\ \Delta \bar{N}_y &= A_{12} \Delta \bar{\varepsilon}_x + \left[A_{22} + \frac{E_{tan_r} A_r}{a} \right] \Delta \bar{\varepsilon}_y \end{aligned} \tag{4.444}$$

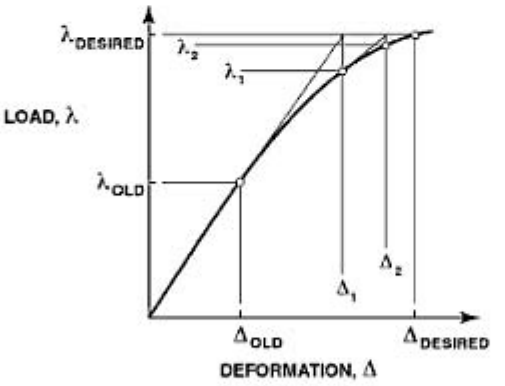


Figure 4-111 Tangent Predictor Technique for Obtaining Load-Deformation Curve *(After Jones [4-59])*

Éléments sous droits d'auteur

The increments in strain determined for Equation (4.444) when added to the old strains constitute an approximation to the strains (or deformation, Δ_1) at the desired λ_d. The question remains to determine the actual λ_1 that corresponds to Δ_1. A procedure is described in the next two paragraphs for determining the layer and stiffener stresses and material properties at the strains calculated from Equation (4.444) corresponding to Δ_1. After the actual λ_1 is determined, another trial value, Δ_2, of the strains at the desired λ_d is obtained and the procedure is repeated until λ_i agrees with λ_d to a prescribed accuracy. In Figure 4-111, only two approximations are shown because further approximations are so close to the desired solution as to be indistinguishable at the scale of Figure 4-111.

A set of strains for the layered shell is determined in the preceding paragraph. Because of the membrane prebuckled equilibrium state, the strains are equal in all layers so the strains in each layer are known *a priori*. However, the material properties, and hence the stresses, are not known in each layer. The stresses are determined for each layer by forming e_{ips_k}:

$$e_{ips_k} = \frac{1}{(1-\nu_k^2)}\left[(1-\nu_k+\nu_k^2)(\bar{\varepsilon}_x^2+\bar{\varepsilon}_y^2)-(1-4\nu_k+\nu_k^2)\bar{\varepsilon}_x\bar{\varepsilon}_y\right]^{1/2} \qquad (4.445)$$

the strain intensity determined by the prescribed strains and material properties at a given stress intensity, and searching by an interval-halving technique for the stress intensity with a corresponding strain intensity, e_{i_k}, that agrees with e_{ips_k} to a prescribed degree of accuracy. A schematic indication of the aforementioned procedure in given for a single layer in Figure 4-112. There, note that $e_{ips_1} > e_{i_1}$ so the stress intensity is increased by $\Delta\sigma_i$ to σ_{i_2}. At σ_{i_2}, $e_{ips_2} < e_{i_2}$ so σ_i is decreased by $\Delta\sigma_i/2$ to σ_{i_3} where $e_{ips_3} > e_{i_3}$. Then, σ_i is increased by $\Delta\sigma_i/4$ to σ_{i_4} at which point $e_{ips_4} < e_{i_4}$. The interval halving is repeated to continually bound the correct solution closer from above and below until $e_{ips} = e_i$ to the desired accuracy. The last step is to calculate the stresses from Equation (4.404) when the material properties are obtained from the Nadai stress-strain curve for the determined stress intensity.

The stress in the stiffeners is found by use of the tangent predictor technique for determining uniaxial stress at a prescribed uniaxial strain as illustrated schematically in Figure 4-113. The ring stress, for example is given an increment

$$\Delta\sigma_y = E_{tan_r}\Delta\varepsilon_{y_r} \qquad (4.446)$$

in which $\Delta\varepsilon_{y_r}$ is initially the difference between the prescribed strain and some convenient initial value of strain, saythe value at the previous load (at which E_{tan_r} is also evaluated). The new strain, ε_{y_r}, corresponding to the new stress is calculated by use of the Nadai stress-strain relation for

Éléments sous droits d'auteur

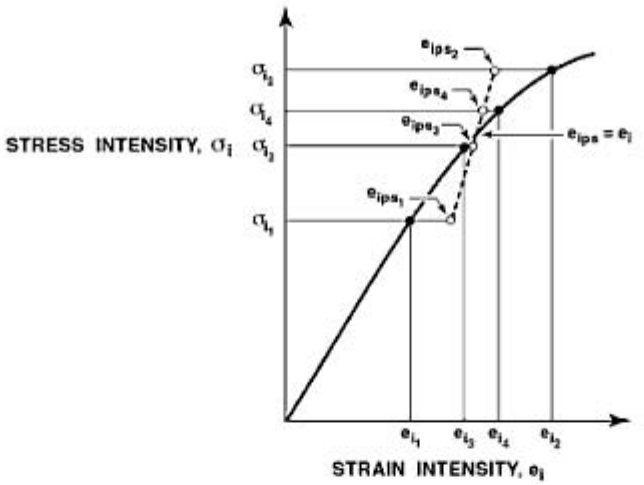


Figure 4-112 Determination of Stress Intensity and Strain Intensity for Given $\bar{\epsilon}_x$ and $\bar{\epsilon}_y$ *(After Jones [4-59])*

the stiffener. Because the new strain does not agree with the prescribed strain, their difference is used in Equation (4.446) to obtain a new stress and strain. The procedure is repeated until the new strain agrees with the prescribed strain to the desired accuracy thereby determining the stress and material properties of the stiffener at the prescribed strain. This relatively simple procedure is unsuitable for the determination of stress in a layered shell because the prescribed strains do not determine a unique strain intensity from which to calculate incremental strain. Accordingly, in that case the search for a solution would be somewhat like a cat chasing its tail and never catching it.

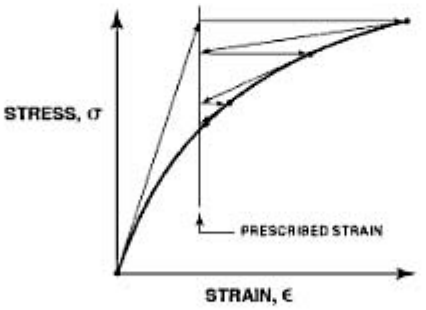


Figure 4-113 Tangent Predictor Technique for Determining Uniaxial Stress at a Prescribed Uniaxial Strain *(After Jones [4-59])*

Éléments sous droits d'auteur

4.10.6.4 Calculation of the Absolute Minimum Buckling Load at an Estimated Load

See Appendix B for an explanation of this procedure.

4.10.6.5 Comparison of Estimated Buckling Load and Absolute Minimum Calculated Buckling Load

The buckling load that is calculated from Equation (4.430) must coincide with the estimated load for which the material properties in Equation (4.430) apply in order for the plastic buckling solution to have been found. If the estimated load, λ_e, is too low, the calculated load, λ_c, is too high because the material properties are too high. Conversely, if λ_e is too high, λ_c is too low. Thus, the special relation of λ_e to λ_c is an ideal criterion for use in a numerical technique to determine where λ_c equals λ_e to a prescribed accuracy.

Various load estimates, λ_{ie}, are made in Figure 4-114 on the load-deformation curve and corresponding absolute minimum calculated buckling loads are obtained by procedures discussed previously. The first load estimate, λ_{1e}, is the previously determined yield load for which the corresponding λ_{1c} is too high in Figure 4-114 because the material properties are too high. Successive load increments, $\Delta\lambda$, of one-tenth the yield load are added until λ_{ic} is less than λ_{ie}, e.g., $\lambda_{4c} < \lambda_{4e}$ in Figure 4-114. At this point, the estimated load is reduced by $\Delta\lambda/2$. The new λ_{ie} is compared to the corresponding λ_{ic} whereupon λ_{ie} is increased by $\Delta\lambda/4$ or decreased by $\Delta\lambda/2$ according to whether $\lambda_{ic} > \lambda_{ie}$ or $\lambda_{ic} < \lambda_{ie}$ as in Figure 4-109. The load increment is halved at essentially each step until $\lambda_{ic} = \lambda_{ie}$ to a prescribed accuracy. This interval-halving search procedure converges by virtue of the relation of λ_e to λ_c and can be shown to be the most efficient search procedure. The iteration procedures that were attempted to find where λ_e equals λ_c did not converge.

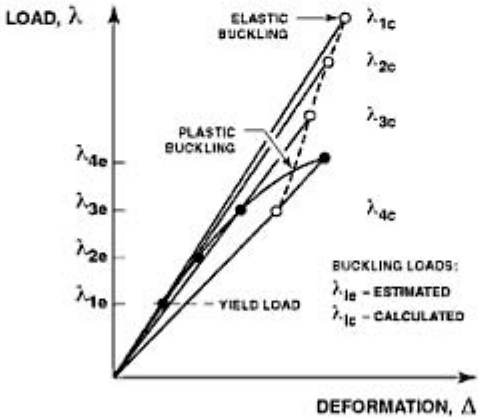


Figure 4-114 Estimated versus Calculated Buckling Loads

Éléments sous droits d'auteur

4.10.7 Numerical Results for Multilayered Shells

The third numerical example is illustrative of the capability represented by the present theory in that plastic buckling of a ring-stiffened, four-layered shell under hydrostatic pressure is solved [4-59]. A ring-stiffened four-layered shell is examined as, for example, a simulation of configurations with in-surface material properties that vary in the radial direction due to thermal degradation. Contrived material properties given in Table 4-1 are used in order to simplify the illustration. The corresponding stress-strain curves are shown in Figure 4-115. The rings are of the same material as the first layer and are .25 in (.64 cm) high, .06 in (.15 cm) thick, and have a spacing that is varied in the present example. The basic shell is 12 in (30.5 cm) long, has a radius of 6 in (15.2 cm) to the reference surface which is chosen to be the center of the innermost layer, and has four layers of unequal thickness [t_1 = .040 in (.10 cm), t_2 = .030 in (.08 cm), t_3 = .020 in (.05 cm), and t_4 = .010 in (.03 cm)].

Table 4-1 Material Properties of a Four-Layered Configuration*

Layer	E, psi (GPa)	ν_ε	c	σ_y, psi (MPa)	σ_{0Y}, psi (MPa)
1	10×10^6 (69)	.20	2.0	20×10^3 (140)	30×10^3 (207)
2	6×10^6 (41)	.25	3.0	9×10^3 (62)	13.5×10^3 (93)
3	4×10^6 (28)	.30	4.0	4×10^3 (28)	6×10^3 (41)
4	2×10^6 (14)	.35	5.0	1×10^3 (7)	1.5×10^3 (10)

After Jones [4-59]

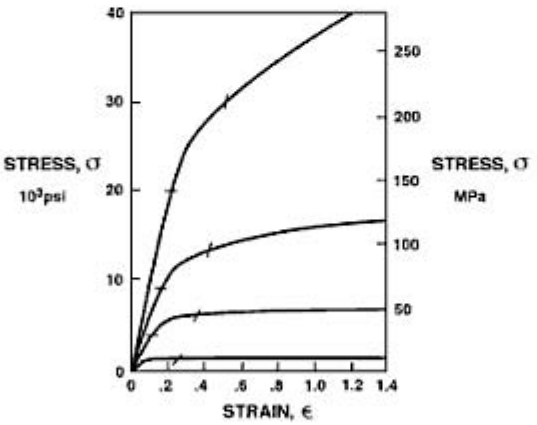


Figure 4-115 Stress-Strain Curves for Four Contrived Materials *(After Jones [4-59])*

Éléments sous droits d'auteur

General instability (i.e., buckling in which the rings participate) results for a varying ring spacing are shown in Figure 4-116 in which plastic buckling is denoted by the solid curve and elastic buckling is denoted by the dashed curve. Panel instability (i.e., buckling between rings) results are shown in Figure 4-117 with the same notation as in Figure 4-116. In both Figures 4-116 and 4-117, cusps are noted at ring spacings at which a layer (or ring) yields or at which the buckling mode shape changes. A typical load-deformation curve is shown in Figure 4-118 (for a = 1.5 in (3.8 cm)) wherein elastic behavior is denoted by a dashed line and plastic behavior is denoted by a solid curve. The results for Figure 4-118 require about 1.4 sec of CDC 6600 central processor time (an IBM 360/65 FORTRAN G system takes about three times as long). During that time, there are 38 load estimates, 2-3 strain estimates per load estimate, 15-25 layer stress intensity estimates per strain estimate, and 1-3 stiffener stress estimates per strain estimate. Of course, all calculations would be performed much faster on current computers, but the relative times should be approximately correct.

If a balance between general and panel instability were sought for the elastic case in Figures 4-116 and 4-117, the 'optimum' ring spacing is 7 in (17.8 cm) at a buckling pressure of 180 psi (1.24 MPa). However, when plastic effects are accounted for, the 'optimum' ring spacing is 5 in (12.7 cm) at a buckling pressure of 175 psi (1.21 MPa). Perhaps more important is the fact that at a ring spacing of 7 in (17.8 cm), the elastic buckling pressure is 26% higher than the plastic buckling pressure.

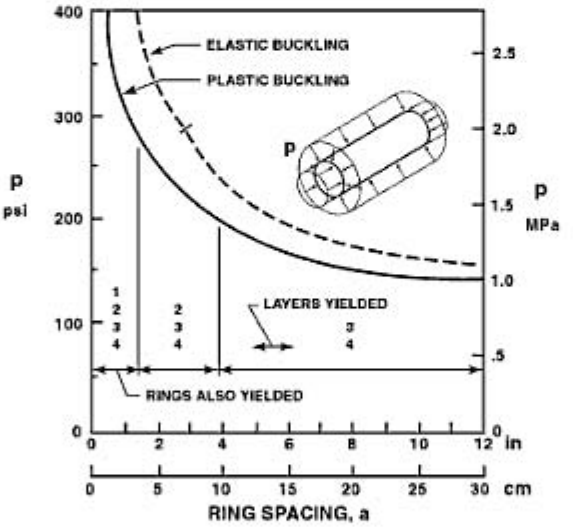


Figure 4-116 General Instability under Hydrostatic Pressure of a Ring-Stiffened, Four-Layered Circular Cylindrical Shell *(After Jones [4-59])*

Éléments sous droits d'auteur

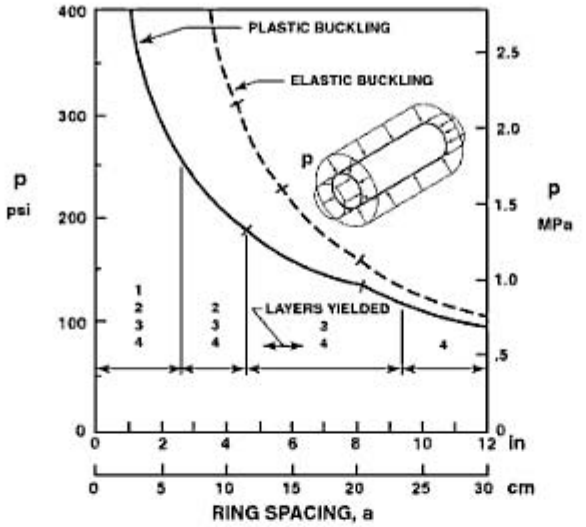


Figure 4-117 Panel Instability under Hydrostatic Pressure of a Ring-Stiffened, Four-Layered Circular Cylindrical Shell *(After Jones [4-59])*

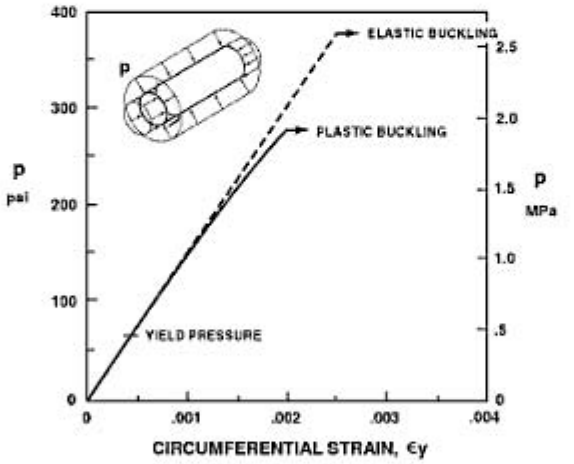


Figure 4-118 Load-Deformation Behavior under Hydrostatic Pressure of a Ring-Stiffened, Four-Layered Circular Cylindrical Shell *(After Jones [4-59])*

Éléments sous droits d'auteur

From an analysis, rather than a design, viewpoint, the neglect of plastic effects in the present example results in the buckling pressure being overestimated by from 20% to 90% as the ring spacing varies over the practical range from 4 in (10.2 cm) to .5 in (1.27 cm). In addition, it can be noted by comparison of Figures 4-116 and 4-117 that the general and panel instability results are much closer to each other for the plastic case than for the elastic case.

A configuration like the aforementioned example except with four layers, each .020-in (.05 cm) thick, yields slightly different results. The optimum ring spacing changes from 3.5 in (8.9 cm) in the elastic case to about 1 in (2.5 cm) in the plastic case. A striking observation is the fact that, due to plastic effects, panel instability governs over nearly the entire range of stiffener spacings in contrast to the elastic case for which general instability governs over a wide range of stiffener spacings. Thus, had we used only elastic buckling analysis, we would have calculated the wrong value of stiffener spacing for 'optimum design', i.e., equal panel and general instability loads. In addition, the rings of the equal thickness four-layered shell yield at a ring spacing noticeably different from the ring spacing at which the innermost layer (to which the rings are fastened) yields.

4.10.8 Summary

Transcendental buckling criteria are derived for plastic buckling of eccentrically stiffened circular cylindrical shells (1) with a single isotropic layer and, more generally, (2) with multiple isotropic layers under combinations of axial and lateral pressure (including one component of pressure that causes tension). The deformation theory of plasticity is utilized in conjunction with classical buckling theory, which implies a membrane prebuckled shape, for a set of simply supported edge buckling boundary conditions for each criterion. The technique of applying this type of buckling criterion is discussed and includes new procedures required to address the many complexities of multi-layered shells.

The numerous geometrical and material parameters in the present investigation cannot be nondimensionalized in a meaningful fashion, i.e., general results cannot be presented. Accordingly, three numerical examples are given to illustrate application of the derived theory. The first example is an unstiffened single-layered 7075-T6 aluminum circular cylindrical shell under hydrostatic pressure with the nonlinear aluminum behavior modeled with the Nadai stress-strain curve [4-104]. For fixed shell radius and thickness, a short shell buckles plastically whereas a long shell buckles elastically, as we would expect. If the shell is made thicker, but with the same radius, then the length at which plastic buckling occurs is higher than for a thinner shell, i.e., plastic effects are more broadly applicable and influential for short, thick shells than for long, thin shells. The second numerical example involves a ring- and stringer-stiffened 7075-T6 aluminum shell that is representative of a large-diameter missile-interstage structure (the Saturn V "moon rocket") subjected to biaxial loading (including axial tension or internal pressure

Éléments sous droits d'auteur

as well as axial compression and external pressure that are know to cause shell buckling). Because of plastic effects, the benefit of internally pressurizing an axially compressed shell is substantially reduced. Similar results occur when axial tension is used to stabilize an externally pressurized shell. In addition, the stiffener eccentricity effect studied in Section 4.7 (i.e., large differences in buckling loads between internally and externally stiffened shells) seems to decrease with increasing plastic behavior. The third example is a ring-stiffened four-layered shell under hydrostatic pressure. Each shell layer has different contrived (i.e., not representative of any specific material) nonlinear isotropic material properties. For one case, plastic effects result in a decrease of the optimum ring spacing, elastic results are from 20-90% too high. In another case, plastic effects result in panel instability governing over a much wider range of ring spacings than under elastic conditions.

Comparison of theoretical and measured buckling loads is difficult without a solution for clamped edges because experimental shells nearly always have some degree of edge clamping. Card and Jones [4-25] obtained an elastic clamped-edge solution and compared it to an elastic simply supported edge solution and to experimental results (see Section 4.7). Edge clamping was found to be important for elastic buckling and might be as important for plastic buckling.

Other modifications such as truly nonlinear independent non-isotropic stress-strain curve behavior typical of laminated composite materials [i.e., all stress-strain curves in the principal material directions (see Appendix C) are independent of each other so that some are more nonlinear than others] in the form of plates are treated by Morgan and Jones [4-106]. They found that the influence of the nonlinearity in the transverse-to-the-fibers direction for boron-epoxy and graphite-epoxy, materials with only a single stress-strain curve nonlinearity (except for shear), is approximately ten to twenty percent. In contrast, for boron-aluminum, a material with nonlinearities in all principal material direction stress-strain curves, the effect of the multiple nonlinearities can be as high as eighty percent (although this prediction does not include processing stresses and is not yet substantiated by experiments). Similar results are expected for laminated composite circular cylindrical shells.

Problem Set 4.10

4.10.0 Verify that the stress-intensity versus strain-intensity curve in Figure 4-97 is identical to the uniaxial stress-strain curve for an isotropic material.

4.10.1 Verify the variation in axial stress, $\delta\sigma_x$, in Equation (4.412).

4.10.2 Verify the variations in stresses in Equation (4.419).

4.10.3 Verify the variations in forces and moments in Equations (4.425) and (4.426).

4.10.4 Verify the buckling criterion in Equation (4.430).

4.10.5 Demonstrate that the buckling criterion for single-layered circular cylindrical shells, Equation (4.430), reduces to Lunchick's solution [4-101] for unstiffened plastic circular cylindrical shells.

4.10.6 Demonstrate that the buckling criterion for single-layered circular cylindrical shells, Equation (4.430), reduces to Block, Card, and Mikulas' solution [4-53] for stiffened elastic circular cylindrical shells.

4.10.7 Demonstrate that the buckling criterion for single-layered circular cylindrical shells, Equation (4.430), reduces to the classical Euler load for elastic (unstiffened) circular cylindrical shells.

Éléments sous droits d'auteur

4.11 ASPECTS OF DESIGN OF SHELLS AGAINST BUCKLING

4.11.1 Introduction

We know that the calculated classical Euler buckling stress for geometrically perfect, simply supported, axially compressed isotropic circular cylindrical shells with a membrane prebuckled shape, i.e.,

$$\overline{\sigma}_E = Et/(r(3(1-\nu^2))^{1/2}) \tag{4.447}$$

is not a practically useful value because shells simply cannot be manufactured, supported, and loaded accurately enough to achieve this high a buckling stress. Thus, we must look for adequate methods to predict shell buckling stresses suitable for use in the design process.

A special consideration for design of shells is the absolute requirement to account for the obviously very different physical significance of the buckling load calculations for different loadings. Certainly, the axially loaded shell buckling load calculation is far overstated in comparison to experimental measurements (see Figure 4-22 on page 496). However, the calculated buckling load for a shell under lateral pressure is reasonably accurate (see Figure 4-26 on page 500). The accuracy of the hydrostatic pressure case lies in between the axial compression and the lateral pressure cases: (1) for long shells, the accuracy is high because the loading depends strongly on the importance of the lateral pressure component of hydrostatic pressure and (2) for short shells, the accuracy is much lower because the loading depends strongly on the importance of the axial compression component of hydrostatic pressure (see Figure 4-30 on page 504). With these remarks in mind, we will concentrate on the biggest problem, namely the axially compressed shell.

Another special consideration for shells is that when they buckle, they typically undergo fairly large deformations, so the act of buckling must be regarded as a catastrophic event in comparison to the more benign buckling of plates and the simple situation that the Euler buckling load of a bar is the largest load that can be practically carried without really large deflections. In fact, axially loaded shells buckle well below the Euler load whereas bars buckle at the Euler buckling load and plates can carry significant load above the Euler buckling load as we have seen in Chapters 2, 3, and 4. For each of the three structural elements, an appropriate factor of safety must be used, and that factor depends on the use of the structure as well as its type and loading. More will be described on the concept of the factor of safety in Chapter 5.

Some readers might wonder about the seeming obsession of most buckling researchers and designers with simply supported edge boundary conditions for shells. We usually consider a simply supported shell for two reasons. The most important reason is that the buckling load for a simply supported structural member is a lower bound on the buckling loads for all other support conditions except an edge without any support, i.e., a free edge. The second reason is that the effort to calculate the buckling load by classical analysis techniques for a simply supported structural member is nearly always less than the calculation for another edge condition. However, that second reason is not active when shell

Éléments sous droits d'auteur

buckling calculations are made with numerical techniques such as finite element programs because any boundary condition can be treated with equal ease. Nevertheless, a calculation based on simply supported edges would seem to be the conservative approach to most designs.

Refined shell buckling analysis is a highly complex subject that requires tremendously deep background to properly perform. The level of knowledge and experience required to truly control such complicated shell analysis computer programs such as BOSOR [4-107] and STAGS [4-108] is far beyond the capabilities of the ordinary B.S. graduate. No, we ought not 'train' students to manipulate advanced structural analysis computer programs. Instead, we must *educate* them to prepare them to take on self-study and advanced courses to learn more about structural analysis to the point where they can reasonably consider using such refined techniques. We will study a specific, noteworthy example of incorrect and somewhat blind use of nonlinear shell analysis computer programs in Section 5.6. That example is an illustration of both the difficulties that can be encountered and a glimpse of the breadth of knowledge required to analyze shell buckling behavior.

The design of shells against buckling is even more intimidating than shell buckling analysis as evidenced by David Bushnell's formidable and comprehensive paper 'Buckling of Shells—Pitfall for Designers' [4-109]. The educational and practical knowledge required to intelligently design shells against buckling is a post-post-graduate course at a minimum. In Bushnell's landmark paper, he describes many situations in which buckling of actual structures occured, but was totally unexpected by their designers. They didn't even realize that their shells could buckle, i.e., they did not expect buckling as a possible failure mode, so they did nothing to design against buckling. Bushnell also describes the effects of many factors on buckling including combined effects of large deformations, initial geometric imperfections, plastic deformation, transverse shear, laminated composite materials, stiffening, geometric nonlinearities, boundary conditions, and load eccentricity. All in all, there's a tremendous amount to learn from his very extensive paper. And, it's really not possible to truly appreciate all of his points without a strong background in the fundamentals of shell buckling! The buckling analyses addressed in this book are quite simplistic in comparison to what Bushnell has to offer. He went on to write his own book, *Computerized Buckling Analysis of Shells* [4-91], an advanced reference on shell buckling that, like his paper, should be addressed by those already intimately familiar with the basic characteristics and nuances of shell buckling.

There is obviously tremendous power in being able to make very sophisticated calculations such as CFD (computational fluid dynamics) representations of air flow around aircraft wings and even around various bombs and rockets hung beneath those wings. However, we must use those calculations intelligently and realistically. Are they confirmed by appropriate measurements? In Bushnell's case, there is a high degree of correlation between his sophisticated calculations and the measured response [4-109]. We must ensure that correlation also occurs for every advanced analysis capability we use.

Éléments sous droits d'auteur

We start this section on design by describing the importance of experimental investigations to develop effective shell buckling analyses and design procedures, i.e., to ensure that adequate correlation exists between our calculations and reality. Next, the 'knock-down' design procedure for axially loaded shells based on accumulated experimental data is described along with the implied penalties for its use. Then, we briefly examine Nemeth and Starnes' discussion of the topics that must be addressed to analyze, measure, and design shells with contemporary construction concepts and the detail essential to treat the concepts in a rational and accurate manner [4-110]. Next, we address high-fidelity analysis and design of shells as being the trend to take now that we are able to accurately measure initial geometric imperfections and to include them in analyses that are highly accurate and reliable as long as the imperfections are considered simultaneously with the nuances of support and loading. Finally, we briefly address design against buckling of stiffened isotropic shells and laminated composite shells.

4.11.2 The Importance of Experiments in the Development of Shell Buckling Analysis and Design

We expect to use experiments to verify our theories as demonstrated by Jones in a paper *Reflections on the Importance of Experimental Results to All Mechanicists, Especially Theoreticians* [4-111]. He uses two examples from composite material mechanics to demonstrate very good correlation between theoretical predictions and experimental measurements. However, there is absolute need for experimental investigations to go beyond mere verification of theory. Moreover, theory must be used to extend the domain of usefulness of experimental results that obviously cannot be obtained for every conceivable circumstance, i.e., every combination of the pertinent variables of the problem.

Experiments will always be an essential part of the analysis and design of shells to resist buckling. We simply cannot rely on theory alone to claim we know the behavior of shells well enough to reliably design them. The reader is referred to Section 1.4 to review the importance of experimental results in the development of theories. Especially note there that experimental results are used more than 'just' to verify theory. Moreover, observations from experimental results are the very basis of all theoretical models! Those comments, again a part of Jones' *Reflections* paper, are of particularly high importance for shell buckling.

Because of its specific applicability to shell buckling, the following list is repeated from Chapter One. Josef Singer described eight motives for shell buckling experiments in 1980 [4-112] and 1982 [4-113]:

"(A) Better understanding of buckling and postbuckling behavior and the primary factors affecting it.
(B) To find new phenomena.
(C) To obtain better inputs for computations.
(D) To obtain correlation factors between analysis and test and for materials effects.
(E) To build confidence in multipurpose computer programs.

Éléments sous droits d'auteur

(F) To test novel ideas of construction or very complicated elements of a structure.
(G) For buckling under dynamic loading and in fluid-structure interaction problems.
(H) For certification tests of full-scale structures."

Singer, Arbocz, and Weller, go on to explain each of the motives in their extensive and very comprehensive book *Buckling Experiments: Experimental Methods in Buckling of Thin-Walled Structures* [4-13].

4.11.3 Knockdown Approach to Buckling-Critical Shell Design

Until the early 2000s, the generally accepted approach to design of axially compressed isotropic circular cylindrical shells against buckling was to examine all experimental results for shells with the same radius-to-thickness ratio, r/t, and *expect the shell to withstand only the smallest load that any previous shell withstood.* This approach is called *knockdown design* or *knockdown-factor design* because all experimental evidence is lower than the classical buckling result of $\bar{\sigma}_E = Et/(r(3(1-\nu^2))^{1/2})$. The knockdown factor is the ratio of the lowest experimental result with the same radius-to-thickness ratio, r/t, to the classical buckling result. Of course, all experimental results are affected by initial geometric imperfections, so this important effect is automatically taken into account in the knockdown-factor-design approach. Unfortunately, the lowest experimental result corresponds to the worst possible initial imperfections, the worst boundary conditions, and the worst loading conditions, so all advantages of better construction, etc., are lost or ignored.

For axial compression loading, many of the shell buckling results obtained since 1928 are plotted in Figure 4-119. The results were obtained by Robertson [4-114]; Lundquist [4-115]; Bridget, Jerome, and Vosseller [4-116]; Ballerstedt and Wagner [4-117]; Lo, Crate, and Schwartz [4-118]; Harris, Suer, Skene, and Benjamin [4-119]; Weingarten, Morgan, and Seide [4-120]; Arbocz and Babcock [4-46]; Esslinger and Geier [4-121]; and Doup [4-122]. The results were first assembled in this form by Weingarten, Morgan, and Seide [4-120] with even more experimental results than in Figure 4-119. An equation for the curve representing the lower bound on all buckling results is used as the design equation along with an appropriate factor of safety as recommended in the shell design monograph NASA SP-8007 [4-123]:

$$\frac{P}{\bar{P}_{classical}} = 1 - .901\left[1 - e^{-\frac{1}{16}\sqrt{\frac{r}{t}}}\right] \qquad \frac{r}{t} \le 1500 \qquad (4.448)$$

Obviously, the shell analysis and statistical evaluation is based only on r/t, not length, because only r and t appear in the buckling stress equation, Equation (4.447), and in the equation for the lower-bound curve, Equation (4.448). Thus, boundary conditions and length effects are ignored in both equations. As r/t increases, the shell becomes thinner and hence naturally more susceptible to the degrading influence of initial geometric imperfections; hence, the knockdown factor decreases.

Éléments sous droits d'auteur

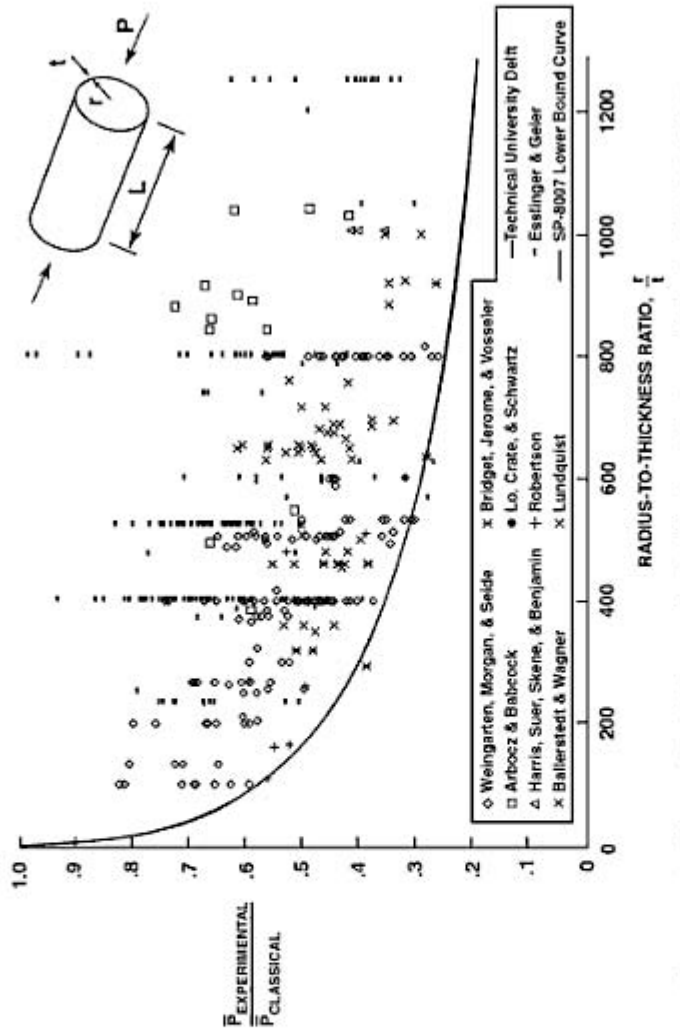


Figure 4-119 Measured Axial Compression Buckling Loads for Isotropic Circular Cylindrical Shells

Éléments sous droits d'auteur

The buckling results in Figure 4-119 are obtained from many sources and were measured over many years under a wide variety of manufacturing, loading, and boundary conditions. Hence, the scatter is tremendous. Some of the experimental results obtained since the 1920s have unknown boundary and loading conditions. Thus, we cannot use all of the results in the overall data base for knockdown-factor design without unfairly and unrealistically compromising the data base because some of the results simply might not belong to the same group. Moreover, we have no information on the nature of the initial geometrical imperfections for most of the data points because no one analyzed the effect of initial geometric imperfections on shell buckling before about 1950. People such as Donnell in 1934 [4-1] and later von Kármán and Tsien [4-28] speculated about the significance of imperfections, but no one had analyzed a shell with imperfections, much less measured actual imperfections and correlated them with buckling. Accordingly, use of Equation (4-448) is overly conservative in that all shells are automatically considered to have the worst imperfections and the most unfavorable boundary conditions of all shells in Figure 4-119. Thus, we see a review of the basic precepts of the knockdown factor approach in the next sub-section and how shell design against buckling could be improved.

The fundamental problem or disadvantage with knockdown design based on the lower-bound curve in Figure 4-119 is that we always design assuming that the worst-possible initial geometric imperfections, boundary conditions, prebuckling deformations, etc., are active for our shell. Obviously, many shells are not so drastically affected as evidenced by the vast multitude of data points well above the lower-bound curve in Figure 4-119! That is, many shells are far better performers than those near the lower-bound curve, but we have no way to identify them based only on the calculations leading to Figure 4-119 [the classical shell buckling equation, Equation (4.447)]. Somehow we must move beyond such a strangling limitation that typically leads to inefficient shell design.

Suppose we view the data in Figure 4-119 as an extensive collection of the effects of various initial geometric imperfections, boundary conditions, prebuckling conditions, etc. We can readily imagine that if we were to somehow take those factors into account, we could raise the lower-bound curve for a specific class of shells (those for which we accounted for the foregoing factors). That is, we could decrease the extreme scatter of the data by more carefully and more specifically analyzing each class of shells. A class might consist of a group of shells all manufactured under the same conditions, e.g., shells rolled from plate stock and joined by riveting along a longitudinal joint as opposed to shells that are electroformed over a mold in their final shape. Thus, there would be a different curve for each specific class of shells, all but one curve being above the lower-bound curve in Figure 4-119. Accordingly, we would thereby gain the capability to design shells with more realistic factors relating actual to theoretical performance. Hence, more efficient structures would be designed than are now possible with knockdown design based only on the lower-bound curve. Such concepts are the basis for the current changes in procedures for design of shells against buckling.

Éléments sous droits d'auteur

4.11.4 Review of the NASA Shell Design Monographs

The various NASA monographs on recommendations for design of buckling-critical shells date from the late 1960s [4-123, 4-124, 4-125]. The primary configuration treated is thin-walled isotropic metal shells under axial compression, lateral pressure, hydrostatic pressure, torsion, or bending, or combinations thereof. Thus, many contemporary structural concepts such as laminated fiber-reinforced composite materials are not addressed, so designers are at a serious disadvantage. Moreover, the monographs were developed for preliminary design of launch vehicles and spacecraft, so topics such as shells with stiffeners or cutouts that arise in intermediate or final design stages are not included.

Nemeth and Starnes reviewed the NASA monographs in 1997 to assess what topics and procedures must be added to reflect current design needs [4-110]. The following is a brief synopsis of their views along with some of the author's views on design. Suggestions are divided into three categories: (1) enhanced shell analysis capabilities, (2) sophisticated, comprehensive experimental measurements, and (3) design.

4.11.4.1 Enhanced Shell Analysis Capabilities

Many shell analysis capabilities have been dramatically enhanced since the 1960s in response to the development of new structural concepts such as laminated fiber-reinforced composite material construction and in response to the identification of problem areas such as boundary conditions and initial geometric imperfections. Finite element techniques and, to a lesser extent, finite difference techniques have enabled accurate and definitive treatment of the topics listed in Table 4-2 that are not addressed satisfactorily, if at all, in the NASA shell design monographs.

Table 4-2 Pertinent Shell Analysis Topics
(After Nemeth and Starnes [4-110])

- Initial Geometric Imperfections
- Nonlinear Prebuckling Deformations
- Cutouts
- Joints
- Boundary Conditions
- Load Introduction Effects
- Thickness Variations
- Variations in Material Properties
- Stiffener Geometry and Spacing
- Local Reinforcement
- Combined Loads
- Variations of Loads with Time
- Small Vibrations
- Laminated Wall Construction
- Transverse Shear Deformation
- Sandwich Construction
- Inelasticity
- Damage
- Local Eccentricities

Currently, the topics in Table 4-2 can indeed be quantitatively addressed in rational analyses, although many require detailed technical expertise and experience not found in the fresh college graduate. However, the design of sophisticated, high-performance structures, whether for space exploration or everyday automobiles, requires sophisticated analysis and design procedures. Without such procedures, complicated structures simply cannot be designed rationally and without excessive conservatism. Although some conservatism is essential, excessive conservatism

Éléments sous droits d'auteur

can render a design unbuildable or too expensive. Today's highly complex structures are required to perform many different tasks in a safe manner. Analyses on the level of simple beam analysis ($\sigma = P/A \pm Mc/I$) are nowhere close to adequate. Sophisticated modeling is required to represent the structure in an analysis at many levels, namely modeling of material behaviors, variations of structural geometry from nominal dimensions, and structural behavior effects such as nonlinear prebuckling deformations. Those and other topics can be treated in either deterministic or probabilistic approaches, although it is easy to lose sight of the objectives and the "engineer's feel for the problem" with probabilistic approaches. Starnes, Nemeth, Hilburger, and associates have had great success in using the Lockheed computer program STAGS (STructural Analysis of General Shells) [4-108] to treat many complex shell problems.

4.11.4.2 Sophisticated Experimental Measurements

The shell buckling results for axial compression in Figure 4-119 on page 658 were obtained by many different investigators over a long period of time and under many different experimental conditions. The experimental conditions of past years were not recorded to the level that we require today to perform an adequate analysis of each shell. Actual initial geometric imperfections were simply not measured in a realistic manner until the late 1960s. Boundary conditions at the shell edges were typically not well described or often the simply supported edge boundary condition was not well approximated. Other reporting and experimental inadequacies (to today's standards) are common. Accordingly, many of the reported data points should not be compared with one another (the proverbial comparison of apples and oranges). In all fairness, the engineers who measured shell buckling loads in the 1930s and even the 1950s simply were not aware of many important behavioral effects because those phenomena hadn't yet even been discovered!

Today, the sophistication of the shell analysis must be matched by the sophistication of the shell buckling experiment. Without a match, we cannot hope to develop rational design procedures. For example, initial geometric imperfections must be measured over the surface of the shell so they can be incorporated in the accompanying analysis. Also, each of the dimensions and the material properties and their variations over the shell must be carefully measured. Boundary conditions and manners of load introduction must be carefully described so they can be accurately modeled. During the experiments, behavioral information, e.g., deformations and strains, must be measured at sufficient locations with sufficient accuracy and in sufficiently small time steps to enable reasonable comparison with the predicted behavior. Such 'testing' details as loading rates, flatness and parallelness of loading frame platens, insulation of heated shells, thermal expansion and insulation characteristics of parts in contact with the shell can be very important in either current modeling efforts or in future efforts so that the experiments need not be unnecessarily repeated to capture a detail that is not foreseen now. Many other factors are mentioned by Nemeth and Starnes [4-110].

Éléments sous droits d'auteur

4.11.4.3 Integration of Sophisticated Analysis and Sophisticated Experiments in the Design Process

With a very sophisticated analysis capability and a correspondingly sophisticated experimental capability, we are in a strong position to rationally design complicated structures. That is, design is not merely the specification of shell and stiffener dimensions to take a particular load or set of loads, although that is a formidable task. We must be able to demonstrate that a complex structure will actually perform well under its intended loading. Of course, not all in-service loadings can be simulated in a 'testing' facility. For example, the aerodynamic forces and heating on a vehicle reentering the atmosphere from space are beyond the capabilities of ground-based simulation facilities. However, we still try to simulate certain loadings to ensure that a structure performs in a manner that is consistent with the objectives we strive to meet.

The design process must involve the predictive analysis capability in a manner that enables the selection of pertinent dimensions and materials of the desired structure. Obviously, this process is iterative because there is no simple analysis equation that can be inverted to solve for the shell dimensions that are required to attain the desired load-carrying capability. The *logic* that 'drives' the changes in dimensions toward the best design in the iterative design process, sometimes called optimization, is all-important. Without the logic to determine how dimensions must be changed, we have no rational design process. Presuming that logic is developed, we proceed to design the structure.

After designing a structure, we must demonstrate that the structure will actually perform as designed. Thus, the need for experiments that might be called a proof test. If those experiments are performed in a comprehensive manner as described earlier (or more comprehensively by Nemeth and Starnes [4-110]), then we have a firm basis for comparing experiment with theory to a high level of fidelity. Reasonable agreement of theoretically predicted behavior with measured behavior would add considerable confidence to our assessment of the designed structure.

4.11.4.4 Summary and What's to Come

Soon after Nemeth and Starnes suggested the foregoing improvements in the analysis and design of buckling-resistant shells in a session honoring the late Manuel Stein at the 38th AIAA/ASME/ASCE/AHS/ASC Structures, Structural Dynamics, and Materials Conference (SDM Conference) held in Orlando, Florida during 7–10 April 1997 [4-110], contributions began to be made. The new area was termed 'high-fidelity analysis and design' by Nemeth and Starnes. The contributions, divided into high-fidelity analysis and high-fidelity design, have been offered in the annual SDM Conferences starting in 1998, although not with titles explicitly involving 'high-fidelity' until 2001 when even the sessions were entitled 'high-fidelity analysis and design'. This emerging area has not fully matured, but its promise as well as the progress to date justify including some description in this book. The next sub-section is devoted to an overview of the current status of high-fidelity analysis and design.

Éléments sous droits d'auteur

4.11.5 High-Fidelity Analysis and Design of Buckling-Critical Shells

The objective of the development of high-fidelity analysis and design of shell structures against buckling is to reduce our dependence on the empiricism and over-conservative nature of knockdown-factor design that was discussed in Sections 4.11.3 and 4.11.4. That is, we will ultimately attempt to use more accurate buckling prediction techniques in both the analysis process and the design process than are currently used in practice. Two steps are required to achieve that lofty, but realistic goal:

1. develop high-fidelity analyses that are
   - *comprehensive* in that all applicable performance factors such as geometric imperfections and boundary conditions are treated.
   - *accurate* in that correlation with actual shell behavior is both highly successful and dependable.
2. develop probabilistic design procedures to establish a shell with characteristics of geometry and material properties, even if those characteristics are perturbed with the statistical variations inherent to all manufacturing processes, that can carry the load required with virtually no possibility of buckling before the design load is reached.

The first step has been nearly achieved, but we cannot yet implement the second step, although some progress has been made.

Prior to high-fidelity analysis, we must have high-fidelity measurements of individual as-manufactured shells, classes of manufactured shells, and of experiments as actually conducted. We first address those measurements, then high-fidelity analysis, and finally high-fidelity design.

4.11.5.1 High-Fidelity Measurements and Experimental Procedures

There are two phases to High-Fidelity Measurements and Experimental Procedures. First, the as-manufactured state of the shell must be precisely measured, i.e., imperfections of all natures must be quantified. Second, when the shell is buckled in an experiment, the loading environment must be carefully and completely characterized to be able to properly analyze the behavior and compare it with the measured buckling load. The first phase is essential to analyze a necessarily imperfect shell, and the second phase is essential in any high-fidelity correlation between theory and experiment. In addition, the imperfections that are characteristic of specific manufacturing processes must be known before shells can be designed to be made by those processes.

High-Fidelity Prebuckling Measurements

The imperfection shape that is most damaging or disadvantageous to the buckling load is one that corresponds to the lowest buckling load of a perfect shell, i.e., an eigenvector or eigen-mode (buckling mode) imperfection. Suppose we were to assume that the manufacturing process creates an imperfection with the shape of one of the eigenvectors of the linearized buckling problem. Then, we would nearly always get a buckling load well below what occurs with most manufacturing processes. That is, such an assumption is clearly a worst-case scenario and

Éléments sous droits d'auteur

also not a likely occurence. However, that worst-case scenario was used in analyses of the effect of imperfections for many years mainly because of its worst-case status, but also because it was part of a tractable solution procedure for those times with more severe computer limitations than exist now. That is, the use of a geometric imperfection with the known shape of an eigenvector was a straightforward mathematical process (for a simple structural configuration such as a bar, plate, or shell). In contrast, the description of a general imperfection requires a much more complicated mathematical process. Importantly, most imperfections are far less damaging, and hence lead to higher buckling loads, than an imperfection in the shape of an eigenvector.

To analyze a buckling-critical shell, we must carefully and completely measure the actual imperfections. To design a buckling-critical shell, we must identify the more likely imperfections that result from the usual manufacturing processes, namely the manufacturing imperfection signature. The *manufacturing imperfection signature* is the residue of the effect of the manufacturing process on the shell, namely the statistical representation of the geometric imperfections in the shape of the shell which are characteristic of a specific manufacturing process. However, in the case of fiber-reinforced laminated composite shells, the manufacturing imperfection signature also includes characteristic gaps between in-layer-adjacent pieces of tape (called lamina ply gaps or just ply gaps) leading to thickness, stiffness, and strength changes or anomalies. The problem is to identify a realistic imperfection shape that is clearly associated with a specific manufacturing imperfection signature characteristic of the proposed construction. For example, different manufacturing imperfection signatures occur for roll-formed shells, than electroplated shells, than machined metallic shells, etc. For fiber-reinforced laminated composite shells, manufacturing imperfection signatures are different for filament-wound as opposed to tape-layed composite shells. Note that these different manufacturing imperfection signatures are discussed as if they exist, but, in fact, they have not been definitively characterized. That significant set of tasks remains to be done as of this writing.

The surface imperfections of a specific shell (isotropic electroformed copper shell as measured by Arbocz and Babcock [4-46]) can be a very complicated shape such as shown for the infamous shell A8 in Figure 4-120 and therefore quite complicated to deal with in an analysis setting. There, the imperfection, w, is normalized by the shell thickness, t. The imperfection appears to be dominated by an $n = 2$ mode (a shape with two full waves in the circumferential direction) at the top of the figure with about five shell thicknesses between the trough and the crests of the imperfection waves. The appearance is quite different at the bottom of the figure. Obviously higher modes are superimposed, including some variation in the axial direction. A manufacturing imperfection signature is typically even more complex than for the single shell in Figure 4-120 because the signature is the superposition of many imperfections for many shells (but all made by the same manufacturing process). Thus, we must consider the separation between first-order effects and higher order effects in any manufacturing signature. For example, any gross

Éléments sous droits d'auteur

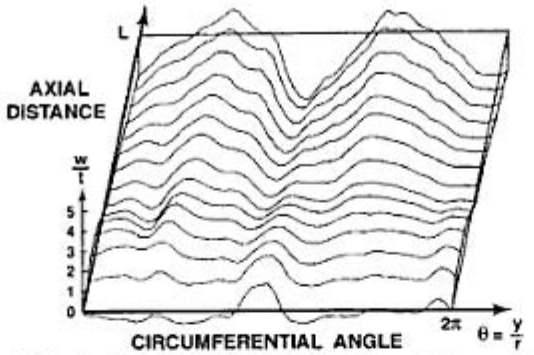


Figure 4-120 Surface Imperfections of Electroformed Copper Shell A8
(After Arbocz and Babcock [4-46])

imperfections that cause an overall n = 2 shape are obviously of first order. Any effects that cause slight imperfections that oscillate over the n = 2 shape at very high frequency (or vary with very short wavelength) are in the noise level of the manufacturing imperfection signature and are therefore of higher order. The first-order effects should be characteristic of the manufacturing process, and the higher order effects characteristic of the variations within the manufacturing process. Perhaps only by use of Fourier Series Analysis with identification of the significant coefficients and the insignificant coefficients can we begin to identify the first-order effects as opposed to the higher order effects. However, we must be very careful because some small imperfections can grow during prebuckling loading and have a significant effect on the buckling load.

Arbocz has persisted over many years in developing more accurate measurement and analysis capabilities that account for the inherent flaws in manufactured shells. His Ph.D. thesis under Babcock is the acknowledged landmark work on shell imperfection measurement [4-46]. He and Singer were the prime movers in the establishment of imperfection data bases to aid in design [4-126, 127, 128, & Chapter Ten of 4-13].

High-Fidelity Buckling Measurements and Experimental Procedures

For measurement of shell deformations during and after buckling, high-speed motion pictures have given way to digital photography for accurate recording. Another aspect of the high-fidelity measurement procedures is the characterization of the experimental environment in which the buckling load of the actual shell is measured. For example, the out-of-flatness and the non-parallelness of the loading platens and their relation to one another during the loading process often must be taken into account to achieve good agreement between predictions and measurements. Moreover, any edge restraint such as a typical potting block (to protect the edges from damage) must be included in the boundary conditions. Other factors are listed by Nemeth and Starnes in Table 4-2 on page 660, and some are discussed in Section 4.11.4.2.

Éléments sous droits d'auteur

4.11.5.2 Development of High-Fidelity Analyses

High-fidelity analyses have several heretofore unusual characteristics. First, very robust modeling techniques are used to achieve the required accuracy of buckling load prediction. Initial geometric imperfections, including both surface waviness and thickness variations, must be accurately measured and then numerically simulated to precisely represent actual shells whose performance can be predicted and compared with their measured behavior. Finally, we want to model contemporary structural configurations to a high degree of realism including cutouts, joints, and other discontinuities, plus, of course, all the specific manufacturing anomalies associated with laminated fiber-reinforced composite materials. Thus, the analysis tools would be extended from the preliminary design capability for simple configurations in the NASA design monographs to applicability to more complex structural configurations typically considered in intermediate and final design stages.

The motivation for treating shell geometries with enhanced accuracy is related to the previous characteristic of knockdown-factor design—we want to eliminate all causes of inaccuracy in buckling load predictions so we can design more efficient shell structures. The causes of discrepancies between current predictions and measurements as well as extensive scatter in experimental results are:

1. initial geometric imperfections
2. boundary conditions on the shell edges
3. nontraditional imperfections such as in the boundary geometry
4. inelastic effects

Each of these causes must be evaluated and accounted for in order to establish the accuracy of any analysis. Moreover, many of these causes have statistical variations that must be addressed in the analysis process, especially initial imperfections. These causes are in addition to the enhanced treatment of complicated structural configurations.

Many experimental shell buckling results obtained since the 1920s have unknown conditions (e.g., specific boundary conditions and initial geometric imperfections), so we cannot use them in the overall data base for knockdown-factor design without unfairly and unrealistically compromising the data base because some of the results simply do not belong together. We must try to develop a suitable experimental results data base with data about which we know all essential qualifications so we know *the data are realistic and suitable for our design application.* For example, the data base for metal shells must be entirely separate from the data base for laminated composite shells because the nature of the imperfections is quite different. Even those two data bases must have many separate sub-bases to account for different manufacturing processes, e.g., filament-wound versus tape-layed composite shells.

The ultimate use of high-fidelity analysis is in design, but much work remains until that goal is achieved. First, we must show beyond a reasonable doubt that high-fidelity analyses are reliable enough to be used in design. The qualification process has the following steps:

Éléments sous droits d'auteur

1. an accurate, comprehensive analysis method must be identified
2. geometry and material analysis input must be highly accurate
3. the analysis with input must be accurately correlated with measured performance of exceptionally well-characterized shells

High-fidelity analysis has two purposes with a different level of sophistication characteristic of each purpose.

1. For correlating analysis with experiment, the as-manufactured imperfections of a specific shell are used in conjunction with a very sophisticated finite element model of the shell and loading environment to predict the behavior. This step must be performed to have confidence in the analysis tools and in the imperfection and load measurement techniques. Without such confidence, the tools and techniques are of little use in design.

2. In design, high-fidelity analysis would be used to iteratively cycle in on the final configuration and dimensions of the structure. To do so reliably, the manufacturing imperfection signature must be used with some statistical variation to effectively work with a lower bound on the buckling load (but of course a much higher lower bound than from the data of Figure 4-119). That is, the as-manufactured state for a single specific shell (its specific imperfections) would not be used. The full robust modeling capabilities of a program such as STAGS would be used only in the final design-analysis stages (with the appropriate manufacturing imperfection signature) because of the high cost of a sophisticated model. Before those stages, the model for STAGS would be much more approximate, i.e., cruder.

Hierarchical Analysis

Arbocz, Starnes, and Nemeth suggest a hierarchical approach to high-fidelity shell buckling analysis with three types or levels of analysis to progressively refine the estimated buckling load [4-129]:

- Level 1 analysis: classical shell buckling analysis with a membrane prebuckled state (hence no prebuckling boundary conditions) and simply supported edge buckling boundary conditions.

- Level 2 analysis: actual prebuckling boundary conditions are enforced to yield the effect of prebuckling deformations and boundary conditions on the buckling load.

- Level 3 analysis: refined analysis taking into account all geometric and material property details and distributions and capable of treating geometric imperfections as well as boundary displacement and/or stiffness variations that affect the buckling load.

Level 3 analyses are the most accurate and comprehensive and, at the same time, the most difficult and expensive to implement. Typically, finite element and finite difference approaches are in this category. One

Éléments sous droits d'auteur

of the issues in level 3 analysis is the number of finite difference mesh points or finite elements that are used. Obviously, the more elements or mesh points, the higher the accuracy. However, the affordability of the analysis must be considered. Thus, the least number of elements that will enable reasonable accuracy must be used. For example, Arbocz and Starnes recommend that we use at least 5 meshpoints per half wave in the buckle to accurately represent buckles (which requires us to have a good idea of how many buckles to expect or to redo the analysis with a finer mesh) [4-130]. An example of a level 3 analysis is the Lockheed finite element program STAGS that was developed originally by Bo Almroth and Frank Brogan in the 1960s [4-108].

Arbocz uses all three levels of analysis in the program DISDECO (Delft Interactive Shell DEsign COde) to allow an analyst to explore the quantitative nature of the many effects in an ever-increasingly complex and sophisticated set of analyses, i.e., hierarchical analyses. DISDECO was developed at Delft Institute of Technology [4-131]. Each level can be used to evaluate various Koiter imperfection sensitivity schemes [4-132], some of which require actual measured imperfections in the root-mean-square sense as opposed to the actual distribution of imperfections. The root-mean-square approach yields upper and lower bounds that are rather far apart and not well suited to high-fidelity correlation. Only with actual imperfections modeled precisely throughout the shell can we make high-fidelity buckling calculations.

The imperfection sensitivity analyses of and after Koiter have been used by some over the years to attempt to account for initial geometric imperfections. Koiter's approaches include both axisymmetric and asymmetric imperfections. Many actual shell imperfections are not axisymmetric, e.g., CalTech A8 in Figure 4-120, but vary somewhat circumferentially (mainly $n = 2$) and far less axially (usually not very much). Thus, imperfection sensitivity approaches based only on assumed axisymmetric imperfections cannot reflect reality. Only those approaches based on asymmetric imperfections can be expected to give results that are close to reality. Moreover, the Koiter approach is limited to the determination of *sensitivity* to buckling as opposed to the determination of an actual buckling load. Upper and lower bounds can sometimes be found with the Koiter approach, but those bounds are often so far apart that they make no practical impact on design of buckling-critical shells. Moreover, the use of Koiter imperfection sensitivity approaches in design is far more complicated than the vast majority of designers are willing to cope with. Most designers are not prepared to use the Koiter approaches. Even if they were adequately prepared, they would not be satisfied with bounds on the buckling load that are not at all close.

Some of the initial searching for a shell that is a viable candidate for a design being considered (i.e., can carry the required loads without buckling) would usually be done iteratively with classical shell buckling analysis (level 1). Refinements by use of level 2 analysis would not have a significant effect on the make-up or nature of the configuration (that could not be expected by virtue of the known small effect of prebuckling boundary conditions on the buckling load). Thus, level 2 analysis seems

Éléments sous droits d'auteur

unlikely to be performed by designers. Level 3 analysis is where the detailed configuration is considered, probably first without cutouts and then later with cutouts and specially stiffened regions if such configurations are an issue. Thus, the major effort in the hierarchical approach is in level 3 analysis which might itself have several levels of complexity.

A viable and more likely alternative to the hierarchical approach is to be aware of the classical shell buckling result (level 1 in the hierarchical approach) and proceed directly to the various levels of modeling in a robust finite element program such as STAGS. The actual imperfections for a specific shell or the actual manufacturing imperfection signature for the appropriate class of shells would be used with statistical variations instead of Koiter's imperfection sensitivity analyses. Even though the computational demands are high, most designers can at least appreciate something like a STAGS analysis in which actual measured imperfections, or some generalized imperfections, are used.

Correlation of High-Fidelity Analysis and Measured Buckling Loads

Hilburger, Starnes, and Nemeth began a realistic and sophisticated high-fidelity shell nonlinear response and buckling analysis approach in 1999 with an ASTM presentation [4-133]. Hilburger and Starnes continued with AIAA/ASME/ASCE/AHS/ASC Structures, Structural Dynamics, and Materials Conference papers in 2000 [4-134] and 2001 [4-135]. Their most successful and most comprehensive correlation between theory and experiment was published in 2002 [4-136]. All those works cited were about unstiffened, laminated, fiber-reinforced composite shells under axial compression, i.e., shells of strong contemporary interest subjected to a loading for which various imperfections play a significant role. Following is an overview of the landmark 2002 paper because the results exemplify the depth of the high-fidelity analysis required to gain a robust and accurate predictive technique.

A typical shell and its finite element model are shown in Figure 4-121. There, the ends are potted in an aluminum-filled epoxy resin to reduce the possibility of crushing the somewhat fragile edges as load is

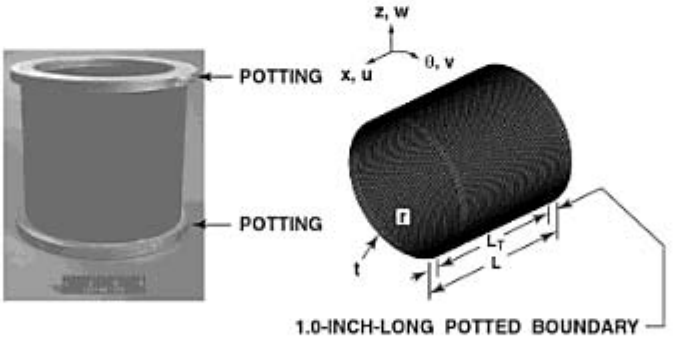


Figure 4-121 Typical Specimen and Finite Element Geometry
(After Hilburger and Starnes [4-136])

Éléments sous droits d'auteur

applied through the load-frame platens at each end. The stiffness of the potted ends is accounted for in the finite element analysis with the widely used STAGS program [4-108]. Moreover, the initial out-of-flatness of the movable platen as well as the subsequent deflections and rotations at three points of the platen are input to the finite element analysis.

Three lamination stacking sequences for the shell were addressed: (1) C1, an axially stiff $[\mp 45/0_2]_2$ laminate; (2) C2, a circumferentially stiff $[\mp 45/90_2]_2$ laminate; and (3) C3, a quasi-isotropic $[\mp 45/0/90]_2$ laminate. Each shell of nominal length 16.0 in (40.6 cm) and radius 8.0 in (20.3 cm) was fabricated from eight layers of .005-in (.013 cm) thick AS4-3502 graphite-epoxy unidirectional tape laid by hand on a mandrel and cured in an autoclave.

The traditional inner-surface and outer-surface imperfections were measured for each shell to determine their initial middle-surface imperfection shapes as well as their thickness distributions. The resulting middle-surface imperfection contours are normalized by the average shell wall thickness and shown for shell C3 in Figure 4-122. There, that shell has two fairly distinct circumferential waves over all its surface with little variation in the axial direction with amplitude variation from $+1.34\ t_{avg.}$ to $-1.54\ t_{avg.}$, a fairly representative result for all three shells.

Of the nontraditional imperfections, the shell wall thicknesses varied from .93 to 1.32 times $t_{avg.}$, a fairly large variation over a short distance. Most of that variation is attributed to resin variations caused by the fabrication process. Also, small gaps [some as big as .1 in (.25 cm)] occur between in-layer-adjacent tapes in some layers. For example, if each in-layer-adjacent 0° tape just touches during layup, then the heat during curing causes circumferential expansion of the steel mandrel that exceeds that of the tapes, necessarily causing an in-layer gap to develop between each tape. (Recall that steel has a higher coefficient of thermal expansion than graphite-epoxy, even in the resin-dominated transverse-to-the-fiber direction). Ply-gaps also occur between 90° tapes in the axial direction and between 45° tapes in both the axial and circumferential directions. Thus, in effect, the 8-layer laminate can have only 7 layers or

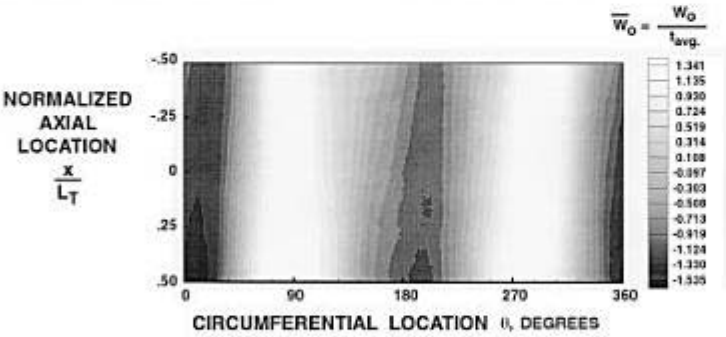


Figure 4-122 Measured Inner Surface Imperfection Shape for Quasi-Isotropic Shell C3 *(After Hilburger and Starnes [4-136])*

Éléments sous droits d'auteur

even only 6 layers (where ply-gaps in two separate layers of the same fiber orientation intersect) in very localized banded regions of a shell. The practice of deliberately overlapping in-layer-adjacent tapes during layup on the mandrel might avoid the occurrence of gaps. However, leaving a permanent ridge is also possible because the overlap regions might not get pulled apart perfectly during heating. The net result of ply-gaps is to induce middle-surface eccentricity (locally creating bending-extension coupling) and reduced laminate stiffnesses. Those effects were accounted for in the finite element analysis.

The shells were analyzed with the STAGS program that has already been described [4-108]. Notable is the fact that the model had about 100,000 degrees of freedom. Geometrically perfect shells were modeled with nominal geometry, material properties, and boundary conditions. Geometrically imperfect shells were modeled with actual dimensional variations including traditional initial middle-surface imperfections and nontraditional thickness variations, ply-gaps, thickness-adjusted laminate properties, elastic boundary conditions (caused by the end potting), end geometric imperfections, and non-uniform end loading.

All load versus end-shortening results for the geometrically perfect shells are normalized by the linear bifurcation buckling load of quasi-isotropic shell C3 [42,590 lb (189.5 kN)] and the nominal shell laminate thickness [.04 in (.102 cm)] in Figure 4-123. Normalized buckling loads calculated with STAGS including the effects of prebuckling deformations are .707, .868, and .979 for shells C1, C2, and C3, respectively, with different prebuckling load versus end-shortening curve slopes for each shell because of different axial stiffnesses. Buckling under controlled shortening (not controlled load, i.e., deadweight loading) was followed by rapid load decrease to a stable postbuckling normalized load level of .403, .218, and .286 for C1, C2, and C3, respectively. The dynamic behavior between the buckling load and the postbuckling load is described in the paper [4-136]. Note that, although shell C1 has the lowest buckling load of all three shells, it has the highest postbuckling load. Thus, laminate stacking sequence plays an important role in the response.

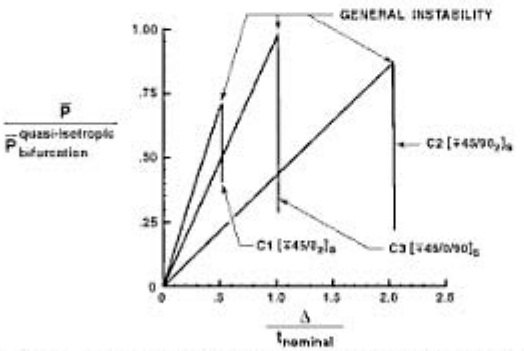


Figure 4-123 Normalized Load versus End Shortening Response *(After Hilburger and Starnes [4-136])*

Éléments sous droits d'auteur

Ply-Gaps A parametric study was performed for variable ply-gap orientation angle (0°, 90°, -45°, and +45°), width [.1 in (.25 cm) and .2 in (.50 cm), and depth (1/2 and one lamina thickness) for quasi-isotropic shell C3. Ply-gaps in 0° layers have a miniscule effect irrespective of their width and depth. Ply-gaps in 90° layers cause the biggest reductions in buckling load. The effect is about 10% for a full lamina thickness depth and width of .2 in (.50 cm). The width of .2 in (.50 cm) is probably on the large side of what would be expected, and in fact is out of specification for most manufacturing processes. If the ply-gap is only .1 in (.25 cm) wide, the reduction is about 4%. Ply-gaps in -45° layers caused buckling load reductions of 4 to 6%. Finally, ply-gaps in +45° layers caused buckling load reductions of 2 to 4%. For shells C1 and C2, ply-gaps caused a maximum of 1 to 2% reduction in the buckling load.

Predicted versus Measured Response Non-linear analysis results were obtained for measured initial middle-surface imperfections, measured thickness imperfections, thickness-adjusted material property variations, ply-gaps, measured loading variations, elastic radial support conditions, and selected specimen parameter uncertainties (such as inaccuracies in thickness measurement, fiber-volume fraction, and loading). Upper and lower bounds on response were obtained based on 'traditional combinatorial analysis'. Both predicted and measured load versus end-shortening response curves are shown in Figure 4-124. All loads are normalized by the linear bifurcation buckling load of quasi-isotropic shell C3. The measured results are .652, .749, and .803 for shells C1, C2, and C3, respectively, are 7.8%, 13.7%, and 18.0% lower than the predicted buckling loads. Note that the predicted lower bounds are quite close to the measured results.

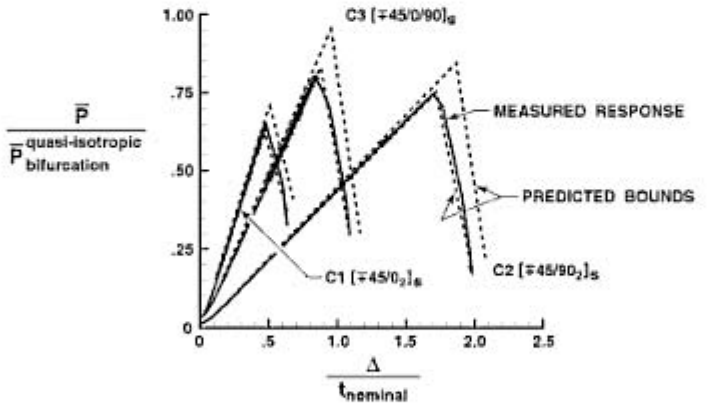


Figure 4-124 Predicted and Measured C1, C2, and C3 Normalized Load versus End-Shortening Response with Upper and Lower Bounds on Predicted Response *(After Hilburger and Starnes [4-136])*

Éléments sous droits d'auteur

Design Implications Various results are shown in the normalized load versus end-shortening curves of Figure 4-125 to put the high-fidelity approach in perspective. The linear bifurcation buckling result for the geometrically perfect quasi-isotropic shell C3 is implied at $\bar{P}/\bar{P}_{bif} = 1$ whereas its modified calculation is labeled Geometrically Perfect (with the dot-dashed line). The predicted bounds from the combinatorial analysis are shown as the short-dashed lines. The measured response is the solid line. Finally, the NASA SP-8007 knockdown factor of .47 is calculated from Equation (4.448) for the nominal shell $r/t = 200$ (without calculating the knockdown factor using the composite laminate characteristics in NASA SP-8007). The lower of the two bounds is about 4% higher than the measured buckling load, a very good correlation (but with the somewhat inspecific lower bound). Both the measured buckling load (.803) and the lower bound (.832) are well above (70–80% above) the NASA SP-8007 recommended design result. Thus, there is strong motivation to use high-fidelity analysis to achieve lighter, more efficient buckling-critical shell structures than can be obtained with the knockdown-factor approach.

Summary Remarks on High-Fidelity Analysis

Both the heirarchical and high-fidelity analyses are but a single step in the far more complicated actual design process. High-fidelity analysis must be used to rationally and accurately evaluate the buckling resistance of a specific shell. However, that shell is merely one candidate design in the overall design process. That is, we must expect to change the design variables (dimensions and laminate stacking sequence) of a candidate design to create a new candidate design until all design requirements are met with the desired safety factor and presumably the 'best' shell ('best' meaning lowest weight, lowest cost, or some other merit function). The design process is examined in the next section.

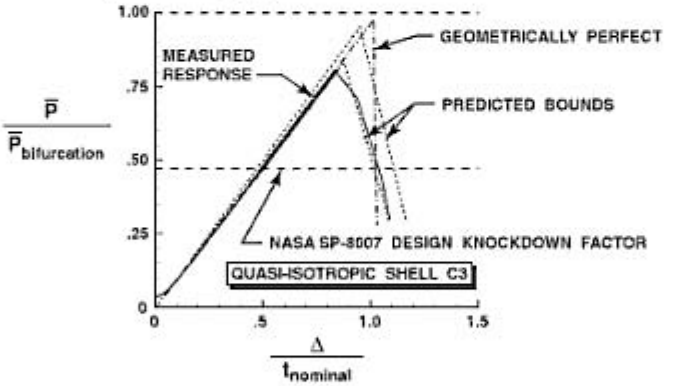


Figure 4-125 Predicted and Measured Quasi-Isotropic Shell C3 Normalized Load versus End-Shortening Response with Upper and Lower Bounds on Predicted Response with NASA SP-8007 Prescribed Knockdown
(After Hilburger and Starnes [4-136])

Éléments sous droits d'auteur

4.11.5.3 High-Fidelity Design Procedure

Now that high-fidelity analyses have been shown to have the requisite accuracy and reliability for buckling load prediction, the corresponding high-fidelity design procedure must be developed as follows:

1. The design loads are established as objectives for a shell to achieve.
2. The manufacturing procedure selected must have its inherent associated imperfections accurately characterized in a probabilistic manner as input to the design procedure. That is, the nature of the shell that we make must be known (predicted, not measured because we will *use* the shell, not 'test it' unless as a 'proof test') based on its associated manufacturing process.
3. Then, the geometrical and material characteristics of the shell must be determined—this process is not simply the inverse of the high-fidelity analysis procedure, but is a process in which the nominal characteristics of the shell are established such that the design loading can be successfully carried with at least the specified factor of safety. Those nominal characteristics are obviously established with the knowledge that statistical variations are inherent and must be accounted for. Moreover, the fundamental nature of the design process is iterative or searching because no equations can be directly solved for the design variables. That is, the design process is actually optimization which involves a rational process of changing or evolving the design variables until the best design is obtained. Thus, in addition to the analysis element, e.g., STAGS, a design program must have an optimization element as well as the logic necessary to decide how to change the design variables and by how much.
4. The design procedure must be capable of creating (designing) or establishing a nominal shell design that has load-carrying capability sufficient to satisfy the objectives with the associated inevitable statistical variations and the desired factor of safety.

If we were to analyze the designed shell with high-fidelity analysis procedures, we would have to get a load-carrying prediction in excess of the requirements. If we take into account the probable statistical variations of the shell properties, then no predicted buckling load (with its own probability of variation) would be under the assigned probability of the required load-carrying capacity with the desired safety factor.

We must model the various manufacturing processes for shells in order to define and characterize the nature of the various imperfections that occur in practice. Recall the preliminary discussion of manufacturing imperfection signatures in Section 4.11.5.1 (more will be addressed in the present section). We must take care to determine the kinds of manufacturing operations that would lead to imperfections or other characteristics of shells that would affect their buckling loads. For example, shell buckling is more sensitive to short wavelength imperfections in the circumferential direction than to long wavelength imperfections because buckling often occurs with a high number of waves (hence short wavelength). Thus, processes that inherently tend to create shells with

Éléments sous droits d'auteur

short wavelength imperfections must either be avoided or very well characterized in their manufacturing imperfection signatures. The intrinsic uncertainties of each and every design parameter must be accounted for with probabilistic methods to achieve a realistic design.

Understand that we want to control the factor of safety that is obtained with the final design. That is, the minimum factor of safety is specified before the design proceeds is started. The only way we can achieve that goal is by analyzing the performance characteristics of the shell by the most accurate means possible, i.e., high-fidelity analysis. Hilburger and Starnes [4-136] have shown that high-fidelity analysis of composite shells has agreed with the measured buckling behavior to within a few percent, which is obviously within our goal. However, that accuracy cannot be achieved when a manufacturing imperfection signature with its inherent statistical variations is used to design a shell. In design, we must accept the fact that an upper bound and a lower bound to the predicted shell performance exist, and those bounds are farther apart than a few percent because the details of a specific shell are no longer relevant. That is, the normal variation of the properties of shells manufactured with a specific process spreads the characteristic bounds farther apart than those that exist for a single shell. Moreover, we must accept a modeling of the loading conditions that is only nominal, rather than the very accurate model used in Section 4.11.5.2. That is, when designing a shell, we must consider a very general and inspecific model of the loading conditions because we cannot characterize them with the essential details before the shell is built and loaded. Our factor of safety must be based on the lower-bound performance because that bound has been shown to be below the actual performance, but we cannot know by how much. The point is that the buckling behavior can be reasonably predicted if the actual state of the shell is both known and accurately accounted for in the high-fidelity analysis. The more general state characterized with the manufacturing imperfection signature for imperfections is used for design. The old knockdown-factor approach simply is so imprecise that it, by default, cannot help but be overly conservative in the main, but very seldom correct. If, however, incorrect or incomplete information about the manufacturing imperfection signature is used, even in high-fidelity design, then the design validity is, of course, negated.

Development of a Manufacturing Imperfection Signature

The basic premise is that each different shell manufacturing process, e.g., roll-forming, filament winding, electroplating, etc., produces shells with essentially similar and unique initial geometric imperfection shapes that can be characterized statistically. Those statistically characterized shapes are called manufacturing imperfection signatures. To develop a manufacturing imperfection signature for a specific class of shells that are all manufactured by the same technique, we must measure the surface imperfections of a group of shells representative of that class and calculate their mean imperfection signature. Hilburger, Nemeth, and Starnes determined the manufacturing imperfection signature of a group of six laminated fiber-reinforced composite shells [4-137]. The six shells

Éléments sous droits d'auteur

were the three eight-layered shells, C1, C2, and C3, used in the correlation of the high-fidelity analysis with experimental results [4-136] in the preceding sub-section plus their sixteen-layered shell counterparts, C4, C5, and C6. The first approximation to the mean signature is shown in Figure 4-126, in which n is about 2 (two circumferential buckle waves) and not much variation occurs in the axial direction. Then, the standard deviation of the mean imperfection signature as in Figure 4-127 must be calculated along with some of the higher deviations to obtain a complete statistical representation of the imperfections and their range for the specific class of shells. The standard deviation also has little variation in the axial direction. The shell population of six is not adequate for more than an approximate single standard deviation. That is, much larger shell populations must be characterized before design with more than a single standard deviation can be attempted.

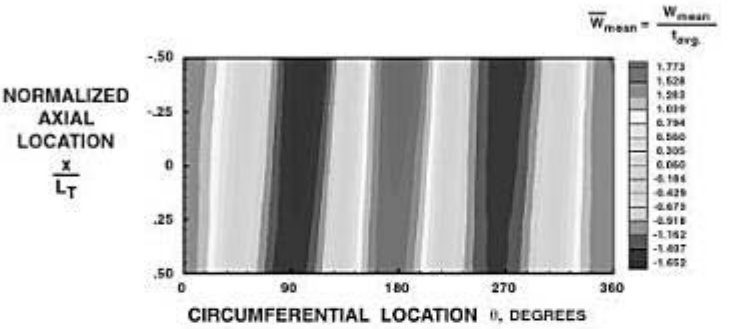


Figure 4-126 Calculated "First-Approximation" Mean Imperfection Signature *(After Hilburger, Nemeth, and Starnes [4-137])*

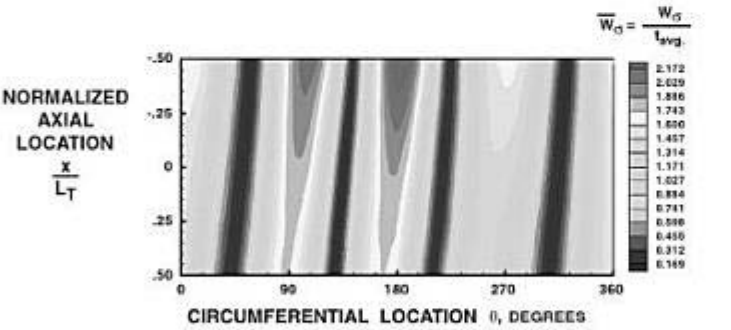


Figure 4-127 Calculated Standard Deviation to the Mean Imperfection Signature in Figure 4-126 *(After Hilburger, Nemeth, and Starnes [4-137])*

Éléments sous droits d'auteur

Use of a Manufacturing Imperfection Signature to Predict Buckling

The manufacturing imperfection signature for a specific manufacturing process is of far more use in design than the actual imperfections for an individual shell made with that process. Hilburger, Nemeth, and Starnes found that the mean imperfection distribution plus one standard deviation (i.e., generally larger imperfections than with only the mean imperfections), when used in a high-fidelity analysis, typically gave an approximate lower bound on the predicted axial compression buckling load for a shell with the actual imperfections [4-137]. Also, the mean imperfection distribution minus a standard deviation (i.e., generally smaller imperfections) usually was an upper bound on the predicted buckling load for a shell with the actual imperfections. The numerical results are predicted with STAGS and the model shown in Figure 4-121. All four predicted results with various imperfections (lower bound, mean imperfections, upper bound, and as-measured imperfections of quasi-isotropic shell C3) are shown in Figure 4-128. Note first that the buckling load of this composite shell is not significantly below that of a perfect composite shell. Note further that the postbuckling behavior, especially the postbuckling load level, is not sensitive to the various imperfections addressed. The imperfections of a specific shell lead to very good agreement between the calculated and measured buckling loads if the full rigor of high-fidelity analysis is applied. Such treatment of the statistics of the measured imperfections to create a manufacturing imperfection signature should be quite useful in design, given that we certainly don't know the actual imperfections of a specific shell before we manufacture it. For two of the three shells whose buckling loads are reported, the buckling load for the mean imperfection distribution plus one standard deviation is still above the measured buckling load. Thus, the single standard deviation is not sufficient to give a true lower bound. Obviously, the sample size of six shells to obtain the manufacturing imperfection signature is not adequate to address the necessary statistics.

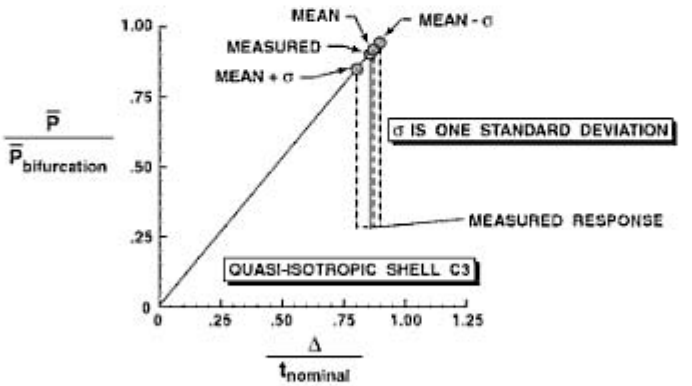


Figure 4-128 Use of a Manufacturing Signature to Predict Buckling Loads *(After Hilburger, Nemeth, and Starnes [4-137])*

Éléments sous droits d'auteur

Manufacturing Imperfection Signature Approach to Design

The essence of the relation of the manufacturing imperfection signature approach to other possible approaches to shell design for combined axial compression and torsion is depicted in Figure 4-129 for specific quasi-isotropic shell C3 from the set of six fiber-reinforced laminated composite shells for which the manufacturing imperfection signature was measured. There, Hilburger, Nemeth, and Starnes [4-137] obtained the buckling behavior for five approaches to shell design:

1. A geometrically perfect shell with classical buckling analysis.
2. A specific shell with its actual measured surface imperfections.
3. The buckling load for the mean manufacturing imperfection signature for a specific class of composite shells [which includes the specific shell in (2)] plus one standard deviation from the mean. Note that the buckling load curve for the mean manufacturing imperfection signature *minus* one standard deviation is an upper bound on the results for the actual imperfections whereas the lower bound is the manufacturing imperfection signature *plus* one standard deviation. *We are far more interested in lower bounds than in upper bounds!*
4. A shell with an imperfection in the shape of the buckling mode for the lowest buckling load calculated with classical buckling analysis (the eigen-mode imperfection). Use of this form of imperfection was the standard approach to analysis of the effect of imperfections for many years and is also known as the worst-case imperfection approach.
5. an imperfect shell with behavior assumed to be predicted with a knockdown factor from the lower-bound curve of NASA SP-8007, Figure 4-119 and Equation (4.448), by using only the r/t of the composite shell, i.e., the NASA SP-8007 approach [4-123].

Also shown is the measured axial compression buckling load for the specific quasi-isotropic shell C3 in Figure 4-129.

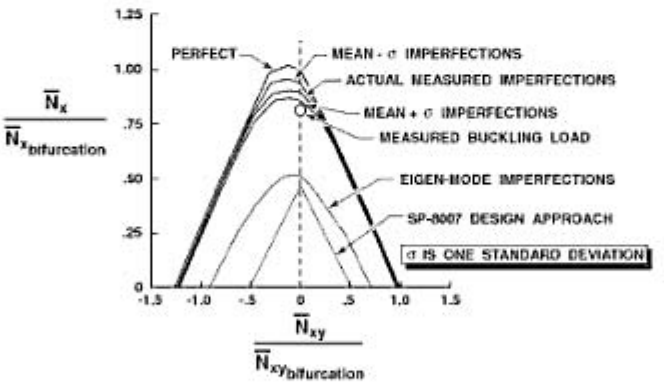


Figure 4-129 Five Approaches to Shell Design for Quasi-Isotropic Shell C3 *(After Hilburger, Nemeth, and Starnes [4-137])*

Éléments sous droits d'auteur

As expected, and why we must go further than classical buckling analysis, the predicted perfect shell behavior (Approach 1) is significantly above the actual shell behavior for quasi-isotropic shell C3. Moreover, the predicted behavior of the specific shell with its actual measured imperfections (Approach 2) is above the measured buckling load because not all effects necessary to properly correlate the analysis with experiment are considered (i.e., only a limited high-fidelity analysis was performed). For the same reason, the predicted behavior with the manufacturing imperfection signature plus one standard deviation (Approach 3), a lower bound on the manufacturing imperfection signature, is above the measured buckling load. However, note how much lower the predicted behavior with an imperfection that is the shape of the mode for the lowest buckling load (the worst-case or eigen-mode imperfection with an amplitude of 1/2 the nominal thickness, Approach 4) is than the measured buckling load. Moreover, the predicted behavior using the NASA SP-8007 lower-bound equation, Equation (4.448), (Approach 5) is even lower than the worst-case imperfection approach. Thus, the dramatically overly conservative nature of both Approaches 4 and 5 is quite evident.

The buckling behavior in Figure 4-129 is actually for combined axial compression and torsion which generates in-plane shearing force N_{xy}. The lack of symmetry of the curve in Figure 4-129 about the vertical line $N_{xy} = 0$ is caused by the presence of a $-45°$ layer on the outer surface of the specific laminated composite shell (C3) and its different reaction to positive and negative torsional loading. Such an interaction curve for an isotropic shell would be symmetric. Note also that the curves in Figure 4-129 for mixed axial compression and torsion rapidly approach those for a perfect shell, i.e., imperfections are much less important for torsional loading than for axial compression loading.

The lower-bound mean manufacturing imperfection signature plus one standard deviation (mean + σ) approach does not represent the best prediction by high-fidelity analysis because such shell-specific effects as thickness variations, material property variations because of ply gaps, and loading imperfections are not taken into account. That is, we are trying to display a design approach in which the specific characteristics of a given shell are decidedly unknown and, indeed, out of scope of the design process because they are not known until the shell is manufactured. However, the *general* statistical character of the manufacturing imperfection signature is, of course, known or else we would not be attempting high-fidelity design. Such characteristics are peculiar to the fabrication of each individual shell and to each set of loading conditions, both of which are unknown at the design stage. Those effects are difficult to include in the manufacturing imperfection signature. If imperfections caused by representative ply-gaps (causing thickness variations) could be included in the manufacturing imperfection signature, they would lead to predicted buckling loads on the order of 5–10% lower than if only the surface imperfections are addressed according to Hilburger and Starnes [4-137]. Moreover, the statistics for the manufacturing imperfection signature should be extensive enough that more than one standard deviation can be calculated, i.e., the shell sample size must far

Éléments sous droits d'auteur

exceed the six shells for this study in order to obtain a realistic and robust manufacturing imperfection signature suitable for design use.

Under combined axial compression and torsion in Figure 4-130, note that the measured shell buckling load for axially stiff shell C1 is actually on the lower-bound curve for the imperfections. Of course, the results for individual shells have a statistical spread relative to the result plotted for the mean. That is, an individual shell can have a buckling load that is outside the mean plus one standard deviation. A single standard deviation from the mean cannot be expected to encompass all measured results, so we must expect to use more than a single standard deviation, and the size of the data population must justify those higher deviations.

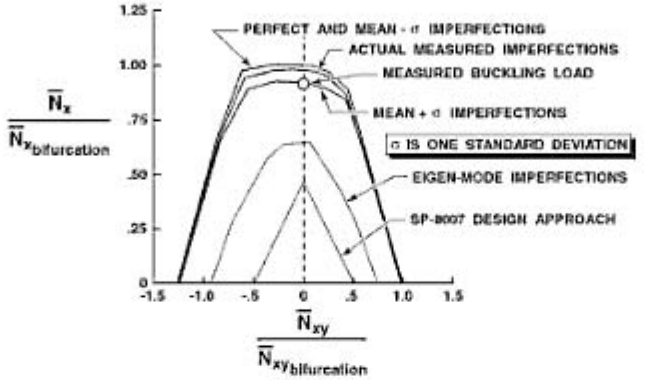


Figure 4-130 Five Approaches to Shell Design for Axially Stiff Shell C1 *(After Hilburger, Nemeth, and Starnes [4-137])*

The measured axial compression buckling load for circumferentially stiff shell C2 is somewhat below the lower-bound curve for the imperfections in Figure 4-131. For both C1 and C2, the buckling results for the geometrically perfect shells are virtually identical to the upper-bound results for imperfections. This observation only reinforces the position that the upper-bound results are not of much use in design. Note that the combined loading behavior near pure axial compression loading is quite peaked for shell C2 in Figure 4-131, much less peaked for shell C3 in Figure 4-129, and quite broad for shell C1 in Figure 4-130. That is, all three shells are sensitive to initial imperfections, but the degree of sensitivity changes as torsional loading varies depending on the laminate stacking sequence.

The manufacturing imperfection signatures approach has been successfully demonstrated in a 'bare bones' fashion by use of a very small sample size. The number of samples in the signature must be perhaps an order of magnitude larger to justify calculation of the statistics permitting prediction of buckling loads for the mean plus *several* standard deviations which are necessary to actually bound all the measured shell buckling behavior. Nevertheless, we can reach an obvious conclusion.

Éléments sous droits d'auteur

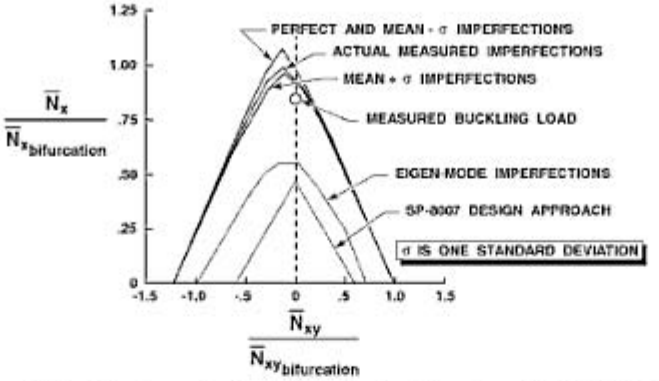


Figure 4-131 Five Approaches to Shell Design for Circumferentially Stiff Shell C2 *(After Hilburger, Nemeth, and Starnes [4-137])*

From Figures 4-129, 4-130, and 4-131, it is readily apparent that each of the three shells can actually carry quite a bit more axial load (from 70% to 80% more) without buckling than if their capacity were evaluated by the overly conservative lower-bound on all the old data knockdown-factor approach of NASA SP-8007. The design implication of that statement is that shells evaluated with the high-fidelity approach using the manufacturing imperfection signature will result in shell designs that are far lighter than previously possible with the NASA SP-8007 approach. In addition, the use of eigen-mode imperfections with amplitude of 1/2 the nominal thickness also leads to overly conservative designs, although not by as large a margin as the knockdown-factor approach. However, we are getting ahead of ourselves in the design situation. *We've been evaluating specific designs, not designing a shell to take a certain prescribed design load.*

Comments on Manufacturing Signatures Approach to Shell Design

Let's examine what was just accomplished in the context of the following two definitions:

1. Analysis is determining the theoretical behavior of a specific configuration (i.e., with specific values of design variables) with accuracy ranging from crude to highly sophisticated to gain correlation with measured behavior.
2. Design is the process of changing the design variables of a configuration until it has the desired load-carrying capability with the desired safety factor for all load cases, usually with some objective or merit function such as minimum weight, least cost, etc.

The high-fidelity analysis with the manufacturing imperfection signatures is performed to assess the actual buckling resistance (establish a new so-called knockdown factor) for each of the candidate design shells

Éléments sous droits d'auteur

considered. Those high-fidelity analysis results are estimated to be within 10% of measured buckling loads. However, in the context of the two definitions, the work done by Hilburger, Nemeth, and Starnes is a refined analysis of a single candidate design. Note that the shells were 'pre-designed' in that their lamination sequence and geometry was already selected for each shell. Thus, with the new knockdown factor found for each shell, the next step is to see whether each shell, with its current buckling resistance now well evaluated, satisfies the design requirements (which might consist of multiple loading conditions) with the appropriate safety factor. If a candidate shell does not meet the design requirements, then it must be reconfigured (redesigned), i.e., the dimensions and/or laminate stacking sequence changed, and a new, revised knockdown factor found for the new candidate shell by using the manufacturing imperfection signature again. This iterative or search process, which is truly high-fidelity design, must be repeated until the shell has been reconfigured to meet the design requirements. At that stage, a sample shell might be loaded until it buckles as a proof test of the designed shell. That is, the design is not complete until the design requirements are met both theoretically and actually.

A high-fidelity design computer program to accomplish the foregoing iterative design procedure must have three fundamental elements:

1. *a high-fidelity analysis tool* capable of determining the buckling load of a candidate shell design to a high degree of accuracy.
2. *an optimization tool* to select the 'best' (minimum weight, lowest cost, etc.) design among the many candidate designs investigated.
3. *logic* to determine or decide how a new candidate design is selected or configured, i.e., just what design variables (such as dimensions or laminate stacking sequence) change and by how much? In other words, how do we control the evolution of the design variables from those of the first candidate design until we reach the 'best' design?

It should be obvious that the computer resources of time and space are enormous if one analysis iteration of the design process takes 100,000 degrees of freedom (as was the case for each of the three shells)! Perhaps some of the investigation of possible candidate designs could, and should, be performed with cruder numerical representations than the finite element model used for the three shells.

As this high-fidelity approach to buckling-critical shell design matures, more information will become available on various manufacturing imperfection signatures and behavior under various combined loadings.

Other Approaches to Design

Various attempts have been made to develop a probabilistic approach to buckling-critical shell design. See, for example, the papers by Arbocz, Starnes, and Nemeth [4-138] and Elishakoff and Starnes [4-139] and the book by Elishakoff, Li, and Starnes [4-140]. That approach will take some time to mature and come to the point where it is both appreciated and accepted by designers.

Éléments sous droits d'auteur

4.11.6 Design of Buckling-Critical Stiffened Isotropic Metal Shells

Shells are stiffened to increase their bending resistance and hence their buckling load with less added weight than by merely increasing the shell thickness. Stiffening concepts for two-dimensional structures are briefly described in Section 4.7. The stiffening generally causes stiffened shells to be less affected by initial geometric imperfections than are unstiffened shells. Both plates and shells are two-dimensional structural elements and thus have many common design characteristics. Thus, design of stiffened isotropic shells could be a combination of the techniques for stiffened plates in Section 3.9.3.3 and the shell buckling design concepts using the knockdown factor approach in Section 4.11.3 or the high-fidelity design concepts in Section 4.11.5. However, there is no firm knockdown-factor design procedure for stiffened isotropic shells, even though such a procedure is described in NASA SP-8007 [4-123]. The treatment of stiffened shells as orthotropic has no firm, rational basis for use with the available measured shell buckling load data. The main problem is that the experimental data underlying the approach in NASA SP-8007 are obtained primarily on unstiffened isotropic metal shells, and there is no logical extrapolation of those data to stiffened shells.

A prominent example of a stiffened shell design computer program is PANDA (PANel Design Analysis) developed by Bushnell. PANDA is an interactive program for minimum-weight design based on embedded closed-form solutions to some stiffened panel and shell buckling problems [4-141]. Those closed-form solutions are exploited in an optimization routine, CONMIN [4-142 and 4-143], developed by Vanderplatts to obtain the configuration of the panel or shell with least weight. The design variables include the stiffener properties and spacing as well as the overall shell dimensions. Specifically, composite, elastic-plastic (if isotropic or a unidirectional stiffener), stiffened, geometrically perfect, circular cylindrical panels and shells can be treated in PANDA. In contrast, PANDA2 [4-144] is a much more general optimization program than PANDA with more arbitrary configurations treated by means of an analysis element (consisting of subroutines from the shell of revolution analysis program BOSOR4 which discretize only in the circumferential direction) that is exploited in the optimization routine, ADS [4-145 and 4-146], developed by Vanderplaats. PANDA2 treats imperfections with a shape of a known buckling mode, an approach known to be more conservative than necessary for unstiffened shells. A major complication is that imperfections in stiffened shells cause redistribution of stress between the skin and stiffeners that changes the stress and buckling constraints unlike for unstiffened shells. The difference between PANDA and PANDA2 represents the trend in optimization program to far more capable analysis elements as well as optimization elements that are enabled by advancing computer technology. Bushnell developed and used PANDA and PANDA2 to treat a very wide variety of stiffened, laminated composite panel and shell problems [4-147]–[4-149]. In his most recent comprehensive and revealing contribution, 'Difficulties in Optimization of Imperfect Stiffened Cylindrical Shells' [4-150], he and Rankin investigate an extraordinary number of stiffener conditions and shell wall constructions and describe an interface with STAGS.

Éléments sous droits d'auteur

4.11.7 Design of Buckling-Critical Laminated Composite Shells

Laminated shells must be designed with the same nondeterministic approach as laminated plates in Section 3.9 insofar as lamination selection is concerned. However, the physical nature of the Euler buckling load is enormously different for plates than for shells, so certain design adjustments must be made for that crucial difference. Still, genetic algorithm approaches to laminate design are equally applicable to shells as to plates. Also, initial geometric imperfections do not affect laminated composite shells as strongly as for isotropic metal shells. However, initial geometric imperfections still must be considered. In fact, the high-fidelity analysis and design concepts examples in Section 4.11.5 are for laminated composite shells. However, there was no attempt made in that work to let the lamination scheme be a variable, i.e., the three laminates were preselected, so no actual laminate design was performed.

There is no firm knockdown-factor design procedure for laminated composite shells, even though such a procedure is described in NASA SP-8007 [4-123]. That is, the procedure described has no firm, rational basis for use. Besides, we are aware from the high-fidelity analysis and design discussions in Section 4.11.5 that the knockdown-factor approach for composite shells is overly conservative. The main problem is that the experimental data underlying the approach in NASA SP-8007 are obtained primarily on unstiffened isotropic metal shells, and there is no logical extrapolation of those data to laminated composite shells.

The concepts of laminate design discussed in Section 3.9 on plate design are generally applicable to laminated shells with obvious modifications and extensions to treat shell curvature as well as the differences associated with the various types of loadings. PANDA2 (see Section 4.11.6) is certainly appropriate for design of laminated composite shells against buckling because the design variables include lamina thicknesses and layup angles with possible linking between them to preserve laminate symmetry or a balanced laminate, if desired. Optimum design procedures are also addressed in books by Gürdal, Haftka, and Hajela [4-151] and Vasiliev and Gürdal [4-152].

4.11.8 Summary Remarks on Shell Design Against Buckling

Design of a shell to resist buckling is very challenging, complicated by the more natural susceptibility of shells to buckling than bars or certainly plates. The contrast between the buckling behavior of the three structural elements, bars, plates, and shells, is quite dramatic. Proper assessment of shell buckling behavior has taken many more years than for bars or even plates. The major difficulty has been in understanding in a quantitative manner the effects of various behavioral factors, many of which have no parallel in bar or plate behavior or do not affect them as much (e.g., initial geometric imperfections). Thus, understanding of shell buckling behavior has advanced slowly, although more rapidly since the 1960s when we began to employ sophisticated numerical techniques that were possible only because of advances in computer technology.

Éléments sous droits d'auteur

4.12 BUCKLING OF SHELLS SUMMARY

The fundamental basis for analyzing shell buckling to first-order effects has been developed in this chapter. An energy approach was used to derive the equilibrium differential equations and their boundary conditions as precursors to the buckling differential equations and their boundary conditions. As a useful alternative, energy integrals were derived and left in that form to be used in Rayleigh-Ritz, finite element, etc., approaches. Also, the postbuckling equations were developed and used.

The wide range of classical shell buckling solutions in which only membrane prebuckling effects are considered were explored first and led to the traditional Euler buckling load. Then, more contemporary issues of special significance were addressed. The postbuckling behavior of circular cylindrical shells was investigated in order to gain an appreciation for the practical significance of the Euler buckling load. The real behavior in the postbuckling range is well below the Euler buckling load in the case of axial compression loading. Thus, the Euler buckling load should not be used to assess the capability of a shell unless other loading conditions prevail. The influence of actual prebuckling deformations was investigated and found to be far more rational than the classical approach. Initial geometric imperfections were also treated, although not in a fully satisfying manner, and found to reduce the effective buckling resistance of a shell. The eccentricity of unidirectional stiffening was found to have a profound influence on the buckling resistance of shells. *The buckling load can be a factor of two or even three higher for externally as opposed to internally stiffened shells under some loading conditions!* Fiber-reinforced composite structures are the primary motivation for studying multilayered shells. The bending-extension coupling that can exist because of laminate asymmetry is actually the same phenomenon that was investigated for eccentric stiffening. However, the differences in buckling loads caused by laminate stacking sequence changes are not as great as those caused by changing stiffeners from inside the shell to outside. Next, the effect of restrained thermal expansion on buckling loads was treated. The thermal buckling load was found for two simple cases. Finally, the influence of plastic deformation on the buckling load was addressed. The deformation theory of plasticity was used to develop expressions for prediction of buckling loads with a nonlinear relationship between stress and strain in the prebuckling and buckling regime. The degree of reduction of the buckling load from elastic behavior depends on the degree of nonlinearity of the stress-strain curve and on the level of loading (hence, how much of the nonlinearity is excited).

These behavioral aspects all lead toward a multi-faceted appreciation of the buckling behavior of an important class of structural elements, namely shells. Shells with more complex curvature than circular cylindrical shells exhibit similar behavior, but demonstration of that contention is left to the technical literature. A prominent means of analyzing the buckling behavior of shells of revolution is with the Lockheed-Martin computer program BOSOR4 (Buckling Of Shells Of Revolution) [4-107]. For more general shells, the Lockheed-Martin computer program STAGS

Éléments sous droits d'auteur

(STructural Analysis of General Shells) [4-108] and the MSC Software computer program NASTRAN (NASA STRuctural ANalysis) [4-153] are used to treat many complex shell buckling problems.

Predicted buckling loads are generally closer to measured buckling loads for laminated composite and/or stiffened shells than for isotropic shells. That is, geometric imperfections seem to have a lesser influence on laminated composite and/or stiffened shells than on isotropic shells. Nevertheless, the influence is still large enough to address. Treating those imperfections in a rational and complete manner is the subject of the high-fidelity analysis and design effort that is underway at the NASA Langley Research Center as of the writing of this book with a summary of progress to date in Section 4.11.5. That effort has great promise to enable more efficient buckling-critical shell structures to be built in a rational manner than is possible with current design techniques.

Singer, Arbocz, and Weller's book on experimental results for bar, plate, and shell buckling is a remarkably rich compilation and discussion of an extraordinary collection of information [4-13] and must be consulted by any serious student of buckling. That book is more than worthy of the many mentions of it throughout this book.

Some readers might wonder about the seeming obsession of most classical buckling researchers with the simply supported edge buckling boundary condition for shells. We most often consider a simply supported shell because of two factors. The most important factor is that the buckling load for a simply supported shell is a lower bound on the buckling loads for all other support conditions except an edge without any support, i.e., a free edge. The second factor is that calculating the buckling load for a simply supported shell is nearly always easier than the calculation for another edge condition. In the modern world of shell buckling analysis by use of computer programs, consideration of different boundary conditions is quite easy *in principle*. However, *understanding* the various boundary conditions and how they are physically implemented are the weak links in the analysis chain.

Other shell buckling effects that can be considered include shells made of materials that have different stress-strain behavior under tensile loading than under compressive loading. Such behavior exists for most composite materials, whether fiber-reinforced or granular. The first-order model of such behavior is represented with the bilinear stress-strain curve of Figure 4-132. Note that the bilinear approximation involves a discontinuous modulus at the origin of the stress-strain curve. In contrast, the actual behavior is a more realistic continuous variation from a tensile modulus to a compressive modulus over some range of stress and strain in a transition region around the origin. Thus, to obtain a first-order approximation to the complex tension-compression phenomenon, the usual continuous modulus variation at the origin of the stress-strain curve is replaced with a discontinuous modulus, i.e., a modulus jump. The measurement of strains near zero stress is difficult to perform accurately, but the obviously nonlinear behavior in Figure 4-132 is realistic. However, for most materials, the mechanical property data on which to base the more complex model are inadequate.

Éléments sous droits d'auteur

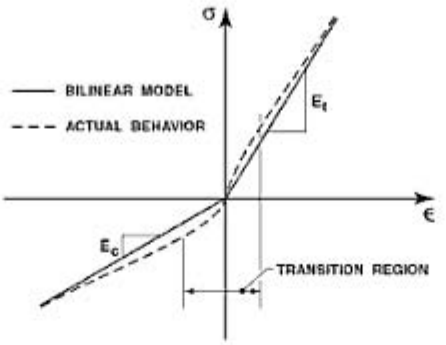


Figure 4-132 Stress-Strain Curve for a Material with Different Behavior in Tension and Compression

Ambartsumyan [4-154] studied such bimodular stress-strain behavior first followed by Jones [4-155] and Bert and Reddy [4-156]. In the models by Ambartsumyan and Jones, the Young's modulus in a particular direction is presumed to depend on the sign of the stress in that direction. For example, if a tensile stress exists in a specific direction, then the modulus in that direction is E_t as in Figure 4-132. Alternatively, if a compressive stress exists in a specific direction, then the modulus in that direction is E_c. To make such decisions, the stresses must be normal stresses in a principal stress state, i.e., without shearing stresses that would complicate the decision. For example, if σ_x is in tension and σ_y is in compression, the strain-stress relations are

$$\begin{aligned} \varepsilon_x &= \frac{1}{E_t}\sigma_x - \frac{\nu_c}{E_c}\sigma_y \\ \varepsilon_y &= -\frac{\nu_t}{E_t}\sigma_x + \frac{1}{E_c}\sigma_y \\ \gamma_{xy} &= 0 \end{aligned} \tag{4.449}$$

in which x and y are principal stress coordinates. Note that the reciprocal relation, $\nu_c/E_c = \nu_t/E_t$ must be satisfied [4-155]. Because of the different moduli in tension and compression, the strain-stress relations in Equation (4.449) are of the same form as those for orthotropic materials. Alternatively to the stress sign determining the modulus value, Bert [4-156] suggests that the modulus value be determined on the basis of the sign of the strain instead of on the sign of the stress. In any event, the formerly isotropic material becomes effectively orthotropic when subjected to a state of mixed stresses (or strains). Extension to actual orthotropic multimodulus materials was made by Jones [4-157] and Ambartsumyan [4-158] with improvements to both extensions by Jones [4-159].

If a circular cylindrical shell is subjected only to combinations of external pressure and axial compression, then all stresses are compressive, so no bimodulus effect enters the behavior. However, if either

Éléments sous droits d'auteur

internal pressure is applied with axial compression or if axial tension is applied with external pressure, then a mixed state of tension and compression exists. Thus, in those latter cases, the bimodular effect enters the buckling behavior. Of course, combinations of axial tension and internal pressure do not cause buckling.

Jones used classical buckling theory, by which is implied a membrane prebuckled shape as in Section 4.3, for simply supported edge conditions during buckling [4-155]. Thus, the prebuckling stress state is determinate for all loading conditions. Accordingly, with the knowledge of the stresses, including their signs, the appropriate material properties are assigned. The resulting buckling criterion is valid for all combinations of axial force and lateral pressure. The criterion can be expressed in terms of the generalized biaxial loading parameters k_x and k_y defined as

$$k_x = \frac{\bar{N}_x L^2}{\pi^2 D_{11}} = \frac{P L^2}{2\pi^3 R D_{11}} \qquad k_y = \frac{\bar{N}_y L^2}{\pi^2 D_{22}} = \frac{p r L^2}{\pi^2 D_{22}} \tag{4.450}$$

in which k_x is related to axial load, P, (positive in compression) and k_y to lateral pressure, p, (positive when external pressure).

The implication of a drastic change in Young's modulus when transitioning from tension to compression is quite evident in the buckling of shells. For example, consider shells with an abbreviated form of Batdorf's curvature parameter Z = 100 [in which Z is defined as L^2/rt instead of Equation (4.85) on page 492 modified for bimodular materials [4-155]]

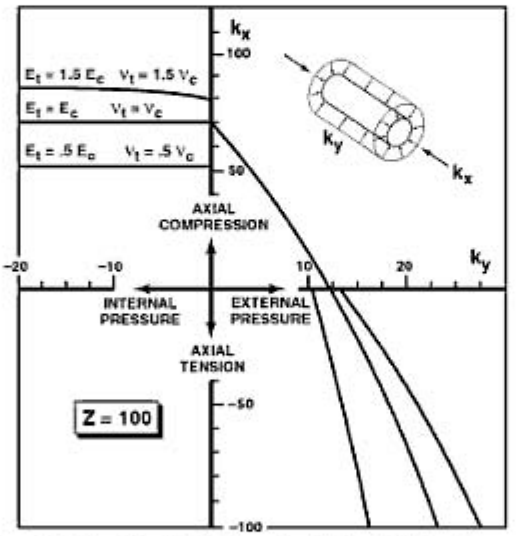


Figure 4-133 Biaxial Buckling Results for Shells with Different Moduli in Tension and Compression *(after Jones [4-155])*

Éléments sous droits d'auteur

under biaxial loading parameters in Figure 4-133. The introduction of a slight amount of compression can cause the buckling load to rise or drop, depending on whether the compression modulus is higher or lower than the tensile modulus. That is, a result of two different moduli determined as a function of stress sign is that the buckling load jumps when the loading state changes from slight compression to slight tension in the direction perpendicular to the main loading as in Figure 4-133. The jumps are more dramatic as E_t changes from E_c.

The most striking observation that can be made about Figure 4-133 is that for $E_t < E_c$ there is a sharp drop in buckling load on passing from the axial compression – external pressure quadrant to either the axial tension – external pressure quadrant (26%) or the axial compression – internal pressure quadrant (17%). Conversely, a somewhat less sharp rise occurs for $E_t > E_c$ (13% and 10%, respectively). Those changes occur for a 50% rise or drop in E_t relative to E_c, amounts that are somewhat high for many fiber-reinforced composite materials, but low for carbon-carbon. These discontinuities arise because the moduli change in a discontinuous fashion upon passing from a biaxial compression state to a stress state involving both tension and compression. In turn, the discontinuities in moduli occur because of the slope discontinuity in the stress-strain curve model. Then, note that, at an unstressed point (the origin), the variation in stress can have two different signs and two different moduli. Such an unstressed point occurs, for example, in the axial direction in a shell loaded by external pressure or in the circumferential direction in a shell loaded by axial compression. Thus, only as the slightest amount of tension is applied does the shell 'know' it has (significantly) different moduli in tension and compression. The resulting step change in the moduli causes a large change in buckling load essentially at a point. That is, the bimodular model implies that the shell is either more or less stiff and, hence, either more or less buckling resistant in one direction or another depending on the loading.

The sharp drop or rise in buckling load around pure external pressure or pure axial compression would be eliminated if the bimodular model with its inherent slope discontinuity were replaced by a continuous stress-strain curve as indicated with the dashed line in Figure 4-132. However, only the portion of the present results that would be affected occurs around the discontinuities. The remainder of the present results are valid and would be approached by the more accurate model after the discontinuities were smoothed out. Away from the 'controversial' region of significant rise or drop, under internal pressure, the curves are parallel, i.e., maintain the same position relative to one another. And, under axial tension, the curves diverge from one another so that the percentage differences increase as axial tension increases.

This approach was extended to stiffened multilayered circular cylindrical shells with different orthotropic moduli in tension and compression by Jones [4-157]. For the predicted behavior of circular cylindrical shells made of laminated fiber-reinforced composite materials with different moduli in tension and compression, see Jones and Morgan [4-160].

Many other shell buckling topics of interest remain. However, they are left for literatures searches when you find a need.

Éléments sous droits d'auteur

CHAPTER 4 REFERENCES

4-1 L. H. Donnell, *Stability of Thin-Walled Tubes under Torsion*, NACA Report 479, National Advisory Committee on Aeronautics, Washington, D.C., 1933. Also, A New Theory for the Buckling of Thin Cylinders Under Axial Compression and Bending, *Transactions of the American Society of Mechanical Engineers*, Volume 56, November 1934, pp. 795–806.

4-2 S. B. Batdorf, *A Simplified Method of Elastic-Stability Analysis for Thin Cylindrical Shells*, NACA Report 874, National Advisory Committee on Aeronautics, Washington, D.C., 1947.

4-3 Theodore von Kármán, Festigkeitsprobleme im Maschinenbau, *Encyklopädie der Mathematischen Wissenschaften*, Volume IV, pp. 311–385, 1910. Reprinted on pp. 141–207 in *Collected Works of Theodore von Kármán*, Volume I, 1902–1913, Butterworths Scientific Publications, London, 1956.

4-4 A. E. H. Love, The Small Free Vibrations and Deformation of a Thin Elastic Shell, *Philosophical Transactions of the Royal Society of London, A*, Volume 179, 1888, pp. 491–546.

4-5 G. Kirchhoff, Über das Gleichgewicht und die Bewegung einer elastischen Scheibe, *Journal für die reine und angewandte Mathematik* (also known as *Crelle's Journal* and *Borchardt's Journal für Mathematik*), Volume 40, Number 1, 1850, pp. 51–88.

4-6 I. S. Sokolnikoff and R. M. Redheffer, *Mathematics of Physics and Modern Engineering*, McGraw-Hill, New York, 1958, pp. 391–395.

4-7 Wilhelm Flügge, *Stresses in Shells*, 2nd Edition, Springer-Verlag, New York, 1973.

4-8 V. V. Novozhilov, *The Theory of Thin Shells*, P. Noordhoff, Groningen, The Netherlands, 1959 (translation of 1951 Russian Edition).

4-9 L. H. Sobel, Effects of Boundary Conditions on the Stability of Cylinders Subject to Lateral and Axial Pressure, *AIAA Journal*, Volume 2, Number 8, August 1964, pp. 1437–1440.

4-10 B. O. Almroth, Influence of Edge Conditions on the Stability of Axially Compressed Cylindrical Shells, *AIAA Journal*, Volume 4, Number 1, January 1966, pp. 134–140.

4-11 Manuel Stein, The Effect on Buckling of Perfect Cylinders of Prebuckling Deformations and Stresses Induced by Edge Support, in *Collected Papers on Instability of Shell Structures*, Technical Note D-1510, National Aeronautics and Space Administration, Washington, D.C., December 1962, pp. 217–227.

4-12 L. H. Donnell and C. C. Wan, Effect of Imperfections on Buckling of Thin Cylinders and Columns Under Axial Compression, *Journal of Applied Mechanics*, Volume 17, March 1950, pp. 73–83.

4-13 J. Singer, J. Arbocz, and T. Weller, *Buckling Experiments: Experimental Methods in Buckling of Thin-Walled Structures, Volume 1, Basic Concepts, Columns, Beams and Plates*, 1998, Wiley, Chichester, England, *Volume 2, Shells, Built-up Structures and Additional Topics*, 2002, Wiley, New York.

4-14 L. A. Harris, H. S. Suer, and W. T. Skene, Modal Investigations of Unstiffened and Stiffened Circular Shells, *Experimental Mechanics (Proceedings of the Society for Experimental Stress Analysis)*, Volume 18, Number 2, July 1961, pp. 1–9. See also Leonard A. Harris, Herbert S. Suer, William T. Skene, and Roland J. Benjamin, The Stability of Thin-Walled Unstiffened Circular Cylinders under Axial Compression Including the Effects of Internal Pressure, *Journal of the Aeronautical Sciences*, Volume 24, Number 8, August 1957, pp. 587–596.

4-15 Rolland G. Sturm, *A Study of the Collapsing Pressure of Thin-Walled Cylinders*, Bulletin 329, Engineering Experiment Station, University of Illinois, Urbana, Illinois, 11 November 1941.

4-16 Dwight F. Windenburg and Charles Trilling, Collapse by Instability of Thin Cylindrical Shells under External Pressure, *Transactions of the American Society for Mechanical Engineers*, New York, Volume 56, No. 11, November 1934, pp. 819–825.

4-17 S. B. Batdorf, Manuel Stein, and Murry Schildcrout, *Critical Stress of Thin-Walled Cylinders in Torsion*, NACA Technical Note 1344, National Advisory Committee on Aeronautics, Washington, D.C., June 1947.

4-18 R. A. Frazer, W. J. Duncan, and A. R. Collar, *Elementary Matrices*, Cambridge University Press, 1955, pp. 224–228.

4-19 A. S. Volmir, *Flexible Plates and Shells*, translated by Department of Engineering Science and Mechanics, University of Florida, Air Force Flight Dynamics Laboratory

Éléments sous droits d'auteur

Technical Report AFFDL-TR-66-216, April 1967, Wright-Patterson Air Force Base, Ohio.

4-20 I. G. Bubnov, *Review of the Papers of Professor Timoshenko*, St. Petersburg, 1913.

4-21 I. G. Bubnov, *Theory of Structures of Ships*, St. Petersburg, 1914.

4-22 B. G. Galerkin, *Beams and Plates*, Vestnik Tekhnologov, 1915.

4-23 N. Yamaki, *Elastic Stability of Circular Cylindrical Shells*, North-Holland, Amsterdam, 1984, pp. 35–42.

4-24 S. B. Batdorf, Murry Schildcrout, and Manuel Stein, *Critical Stress of Thin-Walled Cylinders in Axial Compression*, NACA Report 887, National Advisory Committee on Aeronautics, Washington, D.C., 1947.

4-25 Michael F. Card and Robert M. Jones, *Experimental and Theoretical Results for Buckling of Eccentrically Stiffened Cylinders*, NASA Technical Note D-3639, National Aeronautics and Space Administration, Washington, D.C., October 1966.

4-26 Joseph Kempner and Youl-Nan Chen, Buckling and Postbuckling of an Axially Compressed Oval Cylindrical Shell, in *Proceedings - Symposium on the Theory of Shells to Honor Lloyd Hamilton Donnell*, 4–6 April 1966, Edited by D. Muster, University of Houston, 1967, McCutchan Publishing Corp., pp. 141–183.

4-27 John C. Yao and William C. Jenkins, Buckling of Elliptic Cylinders under Normal Pressure, *AIAA Journal*, Volume 8, Number 1, January 1970, pp. 22–27.

4-28 Theodore von Kármán and Hsue-Shen Tsien, The Buckling of Thin Cylindrical Shells under Axial Compression, *Journal of the Aeronautical Sciences*, Volume 8, Number 8, June 1941, pp. 303–312.

4-29 Hsue-Shen Tsien, A Theory for the Buckling of Thin Shells, *Journal of the Aeronautical Sciences*, Volume 9, Number 10, August 1942, pp. 373–384.

4-30 B. O. Almroth, Postbuckling Behavior of Axially Compressed Circular Cylinders, *AIAA Journal*, Volume 1, Number 3, March 1963, pp. 630–633.

4-31 Robert M. Jones, Toward a New Snap-Through Buckling Criterion for Axially Compressed Circular Cylindrical Shells, *AIAA Journal*, Volume 4, Number 9, September 1966, pp. 1526–1530.

4-32 Hsue-Shen Tsien, Lower Buckling Load in the Nonlinear Buckling Theory for Thin Shells, *Quarterly of Applied Mathematics*, Volume V, Number 2, July 1947, pp. 236–237.

4-33 Robert M. Jones, *On Exact Simplifications of the Strain Energy Expression for Plates and Circular Cylindrical Shells*, The Aerospace Corporation, San Bernardino, California, TDR-469 (S5810-12)-3, May 1965. Available only from the Clearinghouse CFSTI, United States Department of Commerce.

4-34 Nicholas J. Hoff, Wayne A. Madsen, and J. Mayers, Postbuckling Equilibrium of Axially Compressed Circular Cylindrical Shells, *AIAA Journal*, Volume 4, Number 1, January 1966, pp. 126–133.

4-35 Y. Yoshimura, On the Mechanism of Buckling of a Circular Cylindrical Shell Under Axial Compression, *Reports of the Institute of Science and Technology*, Volume 5, University of Tokyo, Tokyo, Japan, November 1951 (in Japanese). Also NACA Technical Memorandum 1390, National Advisory Committee on Aeronautics, Washington, D.C., 1955.

4-36 Wayne A. Madsen and Nicholas J. Hoff, *The Snap-Through and Postbuckling Equilibrium Behavior of Circular Cylindrical Shells Under Axial Load*, SUDAER 227, Stanford University, Stanford, California, April 1965.

4-37 Granino A. Korn and Theresa M. Korn, *Mathematical Handbook for Scientists and Engineers*, Section 20.2-2, 2nd Edition, McGraw-Hill, New York, 1968.

4-38 W. F. Thielemann, On the Postbuckling Behavior of Thin Cylindrical Shells, *Collected Papers on Instability of Shell Structures—1962*, NASA Technical Note D-1510, National Aeronautics and Space Administration, Washington, D.C., December 1962, pp. 203-216.

4-39 B. O. Almroth, A. M. C. Holmes, and D. O. Brush, An Experimental Study of the Buckling of Cylinders Under Axial Compression, *Experimental Mechanics*, Volume 4, Number 9, September 1964, pp. 263–270.

4-40 Manuel Stein, *The Influence of Prebuckling Deformations and Stresses on the Buckling of Perfect Cylinders*, NASA Technical Report R-190, National Aeronautics and Space Administration, Washington, D.C., February 1964.

4-41 R. C. Tennyson, Buckling Modes of Circular Cylindrical Shells under Axial Compression, *AIAA Journal*, Volume 7, Number 8, August 1969, pp. 1481–1487.

Éléments sous droits d'auteur

4-42 L. H. Donnell, A New Theory for the Buckling of Thin Cylinders Under Axial Compression and Bending, *Transactions of the American Society of Mechanical Engineers*, Volume 56, Number 11, November 1934, pp. 795–806.
4-43 L. H. Donnell, Effect of Imperfections on Buckling of Thin Cylinders Under External Pressure, *Journal of Applied Mechanics*, Volume 23, Number 4, December 1956, pp. 569–575.
4-44 L. H. Donnell, Effect of Imperfections on Buckling of Thin Cylinders with Fixed Edges Under External Pressure, *Proceedings of the 3rd U.S. National Congress of Applied Mechanics*, 11–14 June 1958, Providence, Rhode Island, American Society of Mechanical Engineers, New York, pp. 305–311.
4-45 W. T. Koiter, *The Effect of Axisymmetric Imperfections on the Buckling of Cylindrical Shells Under Axial Compression*, Report 6-90-63-86, Lockheed Missiles and Space Co., Sunnyvale, California, August 1963. Also published in *Proceedings of the Koninklijke Nederlandse Akademie van Wetenschappen B66*, 1963, pp. 265–279.
4-46 Johann Arbocz and Charles D. Babcock, Jr., The Effect of General Imperfections on the Buckling of Cylindrical Shells, *Journal of Applied Mechanics*, Volume 36, Series E, Number 1, March 1969, pp. 28–38.
4-47 Tsai-Chen Soong, Buckling of Cylindrical Shells with Eccentric Spiral-Type Stiffeners, *AIAA Journal*, Volume 7, Number 1, January 1969, pp. 65–72.
4-48 V. V. Vasiliev and G. P. Pichkhadze, Composite Shells and Plates with Spatial Reinforcement, in *Design, Analysis, and Testing of Composite Structures*, Central Aerohydrodynamics Institute (TSAGI), Moscow, Volume 9, 1982, pp. 83–90. See also V. A. Bunakov and V. D. Protasov, Lattice Composite Cylindrical Shells, *Mechanics of Composite Materials*, 1989, Number 6, pp. 1046–1053. See also Valery V. Vasiliev (Robert M. Jones, English Edition Editor), *Mechanics of Composite Structures*, Taylor & Francis, Washington, 1993. A revised, expanded version of *Mechanics of Structures Made of Composite Materials*, Mashinostroenie, Moscow, 1988. See also V. A. Bunakov, Design of Axially Compressed Composite Cylindrical Shells, in *Optimal Design*, V. V. Vasiliev and Z. Gurdal, Editors, Technomic, 1999, pp. 207–246.
4-49 V. V. Vasiliev, V. A. Barynin, and A. F. Rasin, Anisogrid Lattice Structures – Survey of Development and Application, *Composite Structures*, Volume 54, Issues 2–3, November-December 2001, pp. 361–370.
4-50 Arie van der Neut, *The General Instability of Stiffened Cylindrical Shells Under Axial Compression*, Report S. 314, National Aeronautical Research Institute, Amsterdam, The Netherlands, 1947.
4-51 M. Baruch and J. Singer, Effect of Eccentricity of Stiffeners on the General Instability of Stiffened Cylindrical Shells Under Hydrostatic Pressure, *The Journal of Mechanical Engineering Science*, Volume 5, Number 1, March 1963, pp. 23–27.
4-52 John M. Hedgepeth and David B. Hall, Stability of Stiffened Cylinders, *AIAA Journal*, Volume 3, Number 12, December 1965, pp. 2275–2286.
4-53 David L. Block, Michael F. Card, and Martin M. Mikulas, Jr., *Buckling of Eccentrically Stiffened Orthotropic Cylinders*, NASA Technical Note D-2960, National Aeronautics and Space Administration, Washington, D.C., August 1965.
4-54 J. A. McElman, M. M. Mikulas, Jr., and M. Stein, Static and Dynamic Effects of Eccentric Stiffening of Plates and Cylindrical Shells, *AIAA Journal*, Volume 4, Number 5, May 1966, pp. 887–894.
4-55 Michael F. Card, *Preliminary Results of Compression Tests on Cylinders with Eccentric Longitudinal Stiffeners*, NASA Technical Memorandum X-1004, National Aeronautics and Space Administration, Washington, D.C., September 1964.
4-56 John W. Hutchinson and John C. Amazigo, Imperfection Sensitivity of Eccentrically Stiffened Cylindrical Shells, *AIAA Journal*, Volume 5, Number 3, March 1967, pp. 392–401.
4-57 David L. Block, Influence of Prebuckling Deformations, Ring Stiffeners, and Load Eccentricity on the Buckling of Stiffened Cylinders, *Proceedings of the AIAA/ASME 8th Structures, Structural Dynamics & Materials Conference*, Palm Springs, California, March 1967, pp. 597–607. Also, NASA Technical Note D-4263, National Aeronautics and Space Administration, Washington, D.C., January 1968.
4-58 Robert M. Jones, Plastic Buckling of Eccentrically Stiffened Circular Cylindrical Shells, *AIAA Journal*, Volume 5, Number 6, June 1967, pp. 1147–1152.

Éléments sous droits d'auteur

4-59 Robert M. Jones, Plastic Buckling of Eccentrically Stiffened Multilayered Circular Cylindrical Shells, *AIAA Journal*, Volume 8, Number 2, February 1970, pp. 262–270.
4-60 Robert M. Jones, *Mechanics of Composite Materials*, 2nd Edition, Taylor & Francis, Philadelphia, 1999.
4-61 S. A. Ambartsumyan, *Theory of Anisotropic Shells*, (*Teoriya Anizotropnykh Obolochek*, in Russian, State Publishing House for Physical and Mathematical Literature, Moscow, 1961). Also NASA Technical Translation TT F-118, National Aeronautics and Space Administration, Washington, D.C., May 1964.
4-62 K. S. Pister and S. B. Dong, Elastic Bending of Layered Plates, *Journal of the Engineering Mechanics Division*, ASCE, Volume 85, Number EM 4, October 1959, pp. 1–10.
4-63 E. Reissner and Y. Stavsky, Bending and Stretching of Certain Types of Heterogeneous Aeolotropic Elastic Plates, *Journal of Applied Mechanics*, Volume 28, Series E, Number 3, September 1961, pp. 402–408.
4-64 S. B. Dong, K. S. Pister, and R. L. Taylor, On the Theory of Laminated Anisotropic Shells and Plates, *Journal of the Aerospace Sciences*, Volume 29, Number 8, August 1962, pp. 969–975.
4-65 Robert M. Jones, Buckling of Circular Cylindrical Shells with Multiple Orthotropic Layers and Eccentric Stiffeners, *AIAA Journal*, Volume 6, Number 12, December 1968, pp. 2301–2305. Errata, Volume 7, Number 10, October 1969, p. 2048.
4-66 Robert M. Jones and Stanley Klein, Equivalence Between Single-Layered and Certain Multilayered Shells, *AIAA Journal*, Volume 6, Number 12, December 1968, pp. 2295–2300.
4-67 J. M. Whitney and A. W. Leissa, Analysis of Heterogeneous Anisotropic Plates, *Journal of Applied Mechanics*, Volume 36, Series E, Number 2, June 1969, pp. 261–266.
4-68 Robert M. Jones and Harold S. Morgan, Buckling and Vibration of Cross-Ply Laminated Circular Cylindrical Shells, *AIAA Journal*, Volume 13, Number 5, May 1975, pp. 664–671.
4-69 Robert M. Jones and Jose C. F. Hennemann, Effect of Prebuckling Deformations on Buckling of Laminated Composite Circular Cylindrical Shells, *AIAA Journal*, Volume 18, Number 1, January 1980, pp. 110–115.
4-70 M. Booton and R. C. Tennyson, Buckling of Imperfect Anisotropic Circular Cylinders Under Combined Loading, *AIAA Journal*, Volume 17, Number 3, March 1979, pp. 278–287.
4-71 Jack R. Vinson and Robert L. Sierakowski, *The Behavior of Structures Composed of Composite Materials*, 2nd Edition, Kluwer, Dordrecht, The Netherlands, 2002.
4-72 Valery V. Vasiliev (Robert M. Jones, English Edition Editor), *Mechanics of Composite Structures*, Taylor & Francis, Washington, 1993. A revised, expanded version of *Mechanics of Structures Made of Composite Materials*, Mashinostroenie, Moscow, 1988.
4-73 Alexander E. Bogdanovich and Robert L. Sierakowski, Composite Materials and Structures: A Compendium of Books, Review Papers, and Other Sources of Information, *Applied Mechanics Reviews*, Volume 52, Number 12, Part 1, December 1999, pp. 351–366.
4-74 E. W. Parkes, Panels under Thermal Stress. The Behavior of a Panel Restrained against Expansion in one Direction and Loaded in the other Direction when Subjected to Kinetic Heating, *Aircraft Engineering*, Volume 28, Number 328, June 1956, pp. 180–186.
4-75 N. J. Hoff, Buckling at High Temperature, *Journal of the Royal Aeronautical Society*, Volume 61, Number 563, November 1957, pp. 756–774.
4-76 David Burgreen, *Elements of Thermal Stress Analysis*, C. P. Press, Jamaica, New York, 1971.
4-77 Eldon E. Mathauser and William A. Brooks, Jr., *An Investigation of the Creep Lifetime of 75S-T6 Aluminum-Alloy Columns*, NACA Technical Note 3204, National Advisory Committee for Aeronautics, Washington, D. C., July 1954.
4-78 Robert M. Jones, Plastic Thermal Buckling of Uniformly Heated Bars with Temperature-Dependent Material Properties, AIAA Paper 2004-1709, *Proceedings of the 45th AIAA/ASME/ASCE/ AHS/ASC Structures, Structural Dynamics and Materials Conference*, 19–22 April 2004, Palm Springs, California, AIAA, Reston, Virginia.

Éléments sous droits d'auteur

4-79 Robert M. Jones, Plastic Thermal Buckling of Uniformly Heated Plates with Temperature-Dependent Material Properties, AIAA Paper 2005-1935, *Proceedings of the 46th AIAA/ASME/ASCE/ AHS/ASC Structures, Structural Dynamics and Materials Conference*, 18–21 April 2005, Austin, Texas, AIAA, Reston, Virginia.

4-80 Earl A. Thornton, *Thermal Structures for Aerospace Applications*, American Institute of Aeronautics and Astronautics, Reston, Virginia, 1996.

4-81 B. Ross, N. J. Hoff, and W. H. Horton, The Buckling Behavior of Uniformly Heated Thin Circular Cylindrical Shells, *Experimental Mechanics*, Volume 6, Number 11, November 1966, pp.529–537.

4-82 Bernard Ross, Nicholas J. Hoff, and Wilfred H. Horton, *The Buckling Behavior of Uniformly Heated Thin Circular Cylindrical Shells*, Department of Aeronautics and Astronautics, Stanford University, Stanford, California, SUDAER Number 225, April 1965.

4-83 Robert M. Jones, Thermal Buckling of Uniformly Heated Unidirectional and Symmetric Cross-Ply Laminated Fiber-Reinforced Composite Uniaxial In-Plane Restrained Simply Supported Rectangular Plates, *Composites, Part A: Applied Science and Manufacturing*, Volume 36, Issue 10, October 2005, pp.1355–1367.

4-84 N. J. Hoff, Buckling of Thin Cylindrical Shell Under Hoop Stresses Varying in Axial Direction, *Journal of Applied Mechanics*, Volume 24, Number 3, September 1957, pp. 405–412.

4-85 David Abir and S. V. Nardo, Thermal Buckling of Circular Cylindrical Shells Under Circumferential Temperature Gradients, *Journal of the Aerospace Sciences*, Volume 26, Number 12, December 1959, pp. 803–808.

4-86 N. J. Hoff, C. Chao, and W. A. Madsen, Buckling of a Thin-Walled Circular Cylindrical Shell Heated Along an Axial Strip, *Journal of Applied Mechanics*, Volume 31, Number 2, June 1964, pp. 253–258.

4-87 David Bushnell, Analysis of Ring-Stiffened Shells of Revolution under Combined Thermal and Mechanical Loading, *AIAA Journal*, Volume 9, Number 3, March 1971, pp. 401–410.

4-88 David Bushnell, Effect of Ring Out-of-Plane Bending Stiffness on Thermal Buckling Prediction for Ring-Stiffened Cylinders, *AIAA Journal*, Volume 9, Number 8, August 1971, pp. 1653–1654.

4-89 David Bushnell and Strether Smith, Stress and Buckling of Nonuniformly Heated Cylindrical and Conical Shells, *AIAA Journal*, Volume 9, Number 12, December 1971, pp. 2314–2321.

4-90 David Bushnell, Nonsymmetric Buckling of Cylinders with Axisymmetric Thermal Discontinuities, *AIAA Journal*, Volume 11, Number 9, September 1973, pp. 1292–1295.

4-91 D. Bushnell, *Computerized Buckling Analysis of Shells*, Martinus Nijhoff, Kluwer, Dordrecht, 1985, pp. 168–179.

4-92 Earl A. Thornton, Thermal Buckling of Plates and Shells, *Applied Mechanics Reviews*, Volume 46, Number 10, October 1993, pp. 485–506.

4-93 P. M. Ogibalov and V. F. Gribanov, *Thermal Stability of Plates and Shells*, Moscow State University, Moscow, 1968. Partial translation (introduction, chapter 4 on shell buckling experiments, and non-Russian references) available as FTD-HC-23-724-71, Foreign Technology Division, Air Force Systems Command, Wright-Patterson AFB, Ohio, AD 734918, N72-19943.

4-94 A. Nadai, *Theory of Flow and Fracture of Solids*, Volume I, McGraw-Hill, New York, 1950.

4-95 Robert M. Jones, *Plasticity*, Bull Ridge Publishing, Blacksburg, Virginia, 2006.

4-96 Bernard Budiansky, A Reassessment of Deformation Theories of Plasticity, *Journal of Applied Mechanics*, Volume 26, Series E, Number 2, June 1959, pp. 259–264.

4-97 Elbridge Z. Stowell, *A Unified Theory of Plastic Buckling of Columns and Plates*, NACA Report 898, National Advisory Committee on Aeronautics, Washington, D.C., 1948.

4-98 A. A. Ilyushin, *The Elasto-Plastic Stability of Plates*, NACA Technical Memorandum 1188, National Advisory Committee on Aeronautics, Washington, D.C., December 1947. Translated from Uprugo-Plasticheskaya Ustoichivost Plasteen, *Prikladnaya Matematika i Mekhanika X*, 1946, pp. 623–638.

4-99 G. Gerard, Plastic Stability Theory of Geometrically Orthotropic Plates and Cylindrical Shells, *Journal of the Aeronautical Sciences*, Volume 28, Number 8, August 1962, pp. 956–962.

Éléments sous droits d'auteur

4-100 F. R. Shanley, Inelastic Column Theory, *Journal of the Aeronautical Sciences*, Volume 14, Number 5, May 1947, pp. 261–268, discussion by Theodore von Kármán.

4-101 M. E. Lunchick, Plasticity Research on Submarine Pressure Hulls at the David Taylor Model Basin, *Plasticity, Proceedings of the Second Symposium on Naval Structural Mechanics*, Brown University, Providence, Rhode Island, 5–7 April 1960, Edited by E. H. Lee and P. S. Symonds, Pergamon Press, New York, 1960, pp. 347–368.

4-102 George Gerard and Sorrel Wildhorn, *A Study of Poisson's Ratio in the Yield Region*, NACA Technical Note 2561, National Advisory Committee on Aeronautics, Washington, D.C., January 1952.

4-103 Robert M. Jones, *Plastic Buckling of Eccentrically Stiffened Circular Cylindrical Shells*, TR-0158(S3816-72)-1, December 1967, Aerospace Corporation, San Bernardino, California, available only from the Clearinghouse CFSTI, United States Department of Commerce.

4-104 J. L. Holmquist and A. Nadai, A Theoretical and Experimental Approach to the Problem of Deep-Well Casing, *Drilling Production Practice*, 1939, American Petroleum Institute, 1940, pp. 392–420.

4-105 Robert M. Jones, *Plastic Buckling of Eccentrically Stiffened Multilayered Circular Cylindrical Shells*, TR-0200(S4816-75)-1, February 1969, The Aerospace Corporation, San Bernardino, California, available only from the Clearinghouse CFSTI, United States Department of Commerce.

4-106 Harold S. Morgan and Robert M. Jones, Buckling of Rectangular Cross-Ply Laminated Plates with Nonlinear Stress-Strain Behavior, *Journal of Applied Mechanics*, Volume 46, Number 3, September 1979, pp. 637–643.

4-107 David Bushnell, BOSOR4: Program for Stress, Buckling, and Vibration of Complex Shells of Revolution, *Structural Mechanics Software Series - Volume 1*, edited by N. Perrone and W. Pilkey, University Press of Virginia, Charlottesville, Virginia, 1977, pp. 11–131.

4-108 Charles C. Rankin, Frank A. Brogan, William A. Loden, and Harold D. Cabiness, *STAGS Users Manual, Version 5.0*, Report LMSC P032594, Lockheed-Martin Missiles & Space Co., Inc., Advanced Technology Center, Palo Alto, California, March 2003.

4-109 David Bushnell, Buckling of Shells—Pitfall for Designers, *AIAA Journal*, Volume 19, Number 9, September 1981, pp. 1183–1226. Also, Paper 80-0665, *Proceedings of the 21st AIAA/ASME/ASCE/AHS Structures, Structural Dynamics, and Materials Conference*, Seattle, Washington, 12–14 May 1980, AIAA, Reston, Virginia, 1980, pp. 1–56.

4-110 Michael P. Nemeth and James H. Starnes, Jr., *The NASA Monographs on Shell Stability Design Recommendations, A Review and Suggested Improvements*, AIAA paper 1997-1302, *Proceedings of the 38th AIAA/ASME/ASCE/AHS/ASC Structures, Structural Dynamics, and Materials Conference*, Kissammee, Florida, 7–10 April 1997, AIAA, Reston, Virginia, 1997. Also, NASA Technical Publication TP-1998-206290, National Aeronautics and Space Administration, Washington, D.C., January 1998. Also, pp. 371–384 in *Stability Analysis of Plates and Shells, A Collection of Papers in Honor of Dr. Manuel Stein*, Compiled by Norman F. Knight, Jr. and Michael P. Nemeth, NASA CP-1998-206280, National Aeronautics and Space Administration, Washington, D.C., January 1998.

4-111 Robert M. Jones, Reflections on the Importance of Experimental Results to All Mechanicists, Especially Theoreticians, *Recent Advances in Experimental Mechanics – In Honor of Isaac M. Daniel*, Kluwer Academic Publishers, Amsterdam, 2002, pp. 537-550.

4-112 J. Singer, The Status of Experimental Buckling Investigations of Shells, *Buckling of Shells*, Proceedings of a State-of-the-Art Colloquium, 6–7 May 1982, Universität Stuttgart, edited by E. Ramm, Springer-Verlag, Berlin, Heidelberg, and New York, 1982, pp. 501–533.

4-113 J. Singer, Buckling Experiments on Shells—a Review of Recent Developments, Euromech Colloquium Number 128, *Stability, Buckling and Postbuckling Behavior; Foundations and Analysis*, Delft, 30 March – 2 April 1980, *Solid Mechanics Archives*, Volume 7, Issue 3, Martinus Nijhoff, The Hague, 1982, pp. 213–313.

4-114 Andrew Robertson, The Strength of Tubular Struts, *Proceedings of the Royal Society of London, Series A, Containing Papers of a Mathematical and Physical Character*, Volume 121, Issue 788, 1 December 1928, pp. 558–585.

Éléments sous droits d'auteur

4-115 Eugene E. Lundquist, *Strength Tests of Thin-Walled Duralumin Cylinders in Compression*, NACA Technical Report 473, National Advisory Committee on Aeronautics, Washington, D. C., 1934.

4-116 F. J. Bridget, C. C. Jerome, and A. B. Vosseller, Some New Experiments on Buckling of Thin-Walled Construction, *Transactions of the American Society of Mechanical Engineers*, APM-56-6, Volume 56, Number 8, August 1934, pp. 569–578.

4-117 W. Ballerstedt and H. Wagner, Versuche über die Festigkeit dünner unversteifter Zylinder unter Schub- und Längskräften, *Luftfahrtforschung*, Volume 13, Number 9, 20 September 1936, pp. 309–312.

4-118 Hsu Lo, Harold Crate, and Edward B. Schwartz, *Buckling of Thin-Walled Cylinder under Axial Compression and Internal Pressure*, NACA Technical Note 2021, National Advisory Committee on Aeronautics, Washington, D.C., January 1950. See also NACA Report 1027, National Advisory Committee on Aeronautics, Washington, D.C., 1951.

4-119 Leonard A. Harris, Herbert S. Suer, William T. Skene, and Roland J. Benjamin, The Stability of Thin-Walled Unstiffened Circular Cylinders Under Axial Compression Including the Effects of Internal Pressure, *Journal of the Aeronautical Sciences*, Volume 24, Number 8, August 1957, pp. 587–596.

4-120 V. I. Weingarten, E. J. Morgan, and P. Seide, *Final Report on Development of Design Criteria for Elastic Stability of Thin Shell Structures*, STL/TR-60-0000-19425, Space Technology Laboratories, Inc., Los Angeles, California, AFBMD-TR-61-7, Air Force Ballistic Missile Division, Inglewood, California, 31 December 1960. Also, Elastic Stability of Thin-Walled Cylindrical and Conical Shells under Axial Compression, *AIAA Journal*, Volume 3, Number 3, March 1965, pp. 500–505.

4-121 M. Esslinger and B. Geier, Comments on "Some Complements to the ECCS Design Code Concerning Isotropic Cylinders" given in the "Preliminary Report" for the Liege Colloquium, Internor bericht IB-152-77/06, Deutsche Forschungs- und Versuchsan- stalt für Luft- und Raumfarht, Institut für Strukturmechanik, April 1977.

4-122 M. R. Doup, Probabilistic Analysis of the Buckling of Thin-Walled Shells, M.Sc. thesis, Memorandum M-808, Faculty of Aerospace Engineering, Delft University of Technology, The Netherlands, August 1997.

4-123 V. I. Weingarten, P. Seide, and J. P. Peterson, *Buckling of Thin-Walled Circular Cylinders, NASA Space Vehicle Design Criteria (Structures)*, NASA Special Publication SP-8007, September 1965, Revised August 1968, National Aeronautics and Space Administration, Washington, D.C.

4-124 P. Seide and V. I. Weingarten, *Buckling of Thin-Walled Truncated Cones, NASA Space Vehicle Design Criteria (Structures)*, NASA Special Publication SP- 8019, September 1968. National Aeronautics and Space Administration, Washington, D.C.

4-125 V. I. Weingarten and P. Seide, *Buckling of Thin-Walled Doubly Curved Shells, NASA Space Vehicle Design Criteria (Structures)*, NASA Special Publication SP-8032, August 1969. National Aeronautics and Space Administration, Washington, D.C.

4-126 J. Arbocz and J. H. Abramovich, *The Initial Imperfection Database at the Delft University of Technolgy*, Report LR-290, Faculty of Aerospace Engineering, Delft University of Technology, The Netherlands, December 1979.

4-127 J. Arbocz, The Imperfection Data Bank, A Means to Obtain Realistic Buckling Loads, *Buckling of Shells*, Proceedings of a State-of-the-Art Colloquium, 6–7 May 1982, Universität Stuttgart, edited by E. Ramm, Springer-Verlag, Berlin, Heidelberg, and New York, 1982, pp. 535–567.

4-128 Josef Singer and Haim Abramovich, The Development of Shell Imperfection Measurement Techniques, *Thin-Walled Structures*, Volume 23, Issues 1–4, 1995, pp. 379–398.

4-129 Johann Arbocz, James H. Starnes, Jr., and Michael P. Nemeth, A Hierarchical Approach to Buckling Load Calculations, AIAA Paper 1999-1232, *Proceedings of the 40th AIAA/ASME/ASCE/AHS/ASC Structures, Structural Dynamics, and Materials Conference*, St. Louis, Missouri, 12–15 April 1999, AIAA, Reston, Virginia.

4-130 Johann Arbocz and James H. Starnes, A Heirarchical High-Fidelity Analysis Procedure for Buckling Critical Structures, AIAA paper 2003-1844, *Proceedings of the 44th AIAA/ASME/ASCE/AHS/ASC Structures, Structural Dynamics, and Materials Conference*, Norfolk, Virginia, 7–10 April 2003, AIAA, Reston, Virginia. Also, Hierarchical High-Fidelity Methodology for Buckling Critical Structures, *Journal of Aerospace Engineering*, Volume 18, No. 3, July 2005, pp. 168–178.

Éléments sous droits d'auteur

4-131 J. Arbocz and J. M. A. M. Hol, Shell Stability Analysis in a Computer-Aided Engineering (CAE) Environment, *Proceedings of the 34th AIAA/ASME/ASCE/AHS/ASC Structures, Structural Dynamics, and Materials Conference*, La Jolla, California, 19–22 April 1993, AIAA, Reston, Virginia, pp. 300–314.

4-132 Warner Tjardus Koiter, *On the Stability of Elastic Equilibrium*, Ph.D. thesis (in Dutch), Technical High School – Delft, The Netherlands, 1945, H. J. Paris, Amsterdam. Also English translation: NASA TT F-10, National Aeronautics and Space Administration, Washington, D.C., March 1967. Also English translation: AFFDL-TR-70- 25, Air Force Flight Dynamics Laboratory, Wright-Patterson Air Force Base, Ohio, February 1970.

4-133 James H. Starnes, Jr., Mark W. Hilburger, and Michael P. Nemeth, The Effects of Initial Imperfections on the Buckling of Composite Cylindrical Shells, *Composite Structures: Theory and Practice, ASTM STP 1383*, edited by Peter Grant and Charles Q. Rousseau, presented at the ASTM Symposium Composite Structures: Theory and Practice, 17–18 May 1999, Seattle, Washington, American Society for Testing and Materials, West Conshohocken, Pennsylvania, 2000, pp. 529–550.

4-134 Mark W. Hilburger and James H. Starnes, Jr., Effects of Imperfections on the Buckling Response of Compression-Loaded Composite Shells, AIAA Paper 2000-1387, *Proceedings of the 41st AIAA/ASME/ASCE/AHS/ASC Structures, Structural Dynamics, and Materials Conference*, Atlanta, Georgia, 3–6 April 2000, AIAA, Reston, Virginia.

4-135 Mark W. Hilburger and James H. Starnes, Jr., High-Fidelity Nonlinear Analysis of Compression-Loaded Composite Shells, AIAA paper 2001-1394, *Proceedings of the 42nd AIAA/ASME/ASCE/AHS/ASC Structures, Structural Dynamics, and Materials Conference*, Seattle, Washington, 16–19 April 2001, AIAA, Reston, Virginia.

4-136 Mark W. Hilburger and James H. Starnes, Jr., Effects of Imperfections on the Buckling Response of Compression-Loaded Composite Shells, *International Journal of Non-Linear Mechanics*, Volume 37, Issues 4-5, June 2002, pp. 623–643.

4-137 Mark W. Hilburger, Michael P. Nemeth, and James H. Starnes, Jr., Shell Buckling Design Criteria Based on Manufacturing Imperfection Signatures, AIAA paper 2003-1843, *Proceedings of the 44th AIAA/ASME/ASCE/AHS/ASC Structures, Structural Dynamics, and Materials Conference*, Norfolk, Virginia, 7–10 April 2003, AIAA, Reston, Virginia. Also, NASA TM-2004-212659, May 2004. Also *AIAA Journal*, Volume 44, Number 3, March 2006, pp. 654–663.

4-138 Johann Arbocz, James H. Starnes, and Michael P. Nemeth, Towards a Probabilistic Criterion for Preliminary Shell Design, AIAA Paper 1998-2051, *Proceedings of the 39th AIAA/ASME/ASCE/AHS/ASC Structures, Structural Dynamics, and Materials Conference*, Long Beach, California, 20–23 April 1998, AIAA, Reston, Virginia.

4-139 Isaac Elishakoff and James H. Starnes, Jr. Safety Factor and the Non-Deterministic Approaches, AIAA Paper 1999-1614, *Proceedings of the 40th AIAA/ASME/ASCE/AHS/ASC Structures, Structural Dynamics, and Materials Conference*, St. Louis, Missouri, 12–15 April 1999, AIAA, Reston, Virginia.

4-140 Isaac Elishakoff, Yiwei Li, and James H. Starnes, Jr., *Non-Classical Problems in the Theory of Elastic Stability*, Cambridge University Press, New York, 2001.

4-141 David Bushnell, PANDA—Interactive Program for Minimun Weight Design of Stiffened Cylindrical Panels and Shells, *Computers & Structures*, Volume 16, Number 1–4, 1983, pp. 167–185.

4-142 Garret N. Vanderplaats, *CONMIN—a FORTRAN Program for Constrained Function Minimization*, NASA TM X-62-282, version updated in March 1975, NASA Ames Research Center, Moffett Field, California, August 1973.

4-143 Garret N. Vanderplaats and Fred Moses, Structural Optimization by Method of Feasible Directions, *Computers & Structures*, Volume 3, Number 4, July 1973, pp. 739–755.

4-144 David Bushnell, PANDA2 - Program for Minimun Weight Design of Stiffened, Composite, Locally Buckled Panels, *Computers & Structures*, Volume 25, Number 4, 1987, pp. 469–605.

4-145 Garret N. Vanderplaats, *ADS—a FORTRAN Program for Automated Design Synthesis, Version 2.01*, Engineering Design Optimization, Inc., Santa Barbara, California, January 1987.

Éléments sous droits d'auteur

4-146 Garret N. Vanderplaats and Hiroyuki Sugimoto, A General-Purpose Optimization Program for Engineering Design, *Computers & Structures*, Volume 24, Number 1, 1986, pp. 13–21.

4-147 David Bushnell, Theoretical Basis of the PANDA Computer Program for Preliminary Design of Stiffened Panels under Combined In-Plane Loads, *Computers & Structures*, Volume 27, Number 4, 1987, pp. 541–563.

4-148 David Bushnell, Optimization of Composite, Stiffened, Imperfect Panels under Combined In-Plane Loads for Service in the Postbuckling Regime, *Computer Methods in Applied Mechanics and Engineering*, Volume 103, Issues 1–2, March 1993, pp. 43–114.

4-149 David Bushnell and Charles Rankin, Optimization of Perfect and Imperfect Ring and Stringer Stiffened Cylindrical Shells with PANDA2 and Evaluation of the Optimum Designs with STAGS, AIAA paper 2002-1408, *Proceedings of the 43rd AIAA/ASME/ASCE/AHS/ASC Structures, Structural Dynamics, and Materials Conference*, Denver, Colorado, 20–24 April 2002, AIAA, Reston, Virginia.

4-150 David Bushnell and Charles Rankin, Difficulties in Optimization of Imperfect Stiffened Cylindrical Shells, AIAA paper 2006-1943, *Proceedings of the 47th AIAA/ASME/ASCE/AHS/ASC Structures, Structural Dynamics, and Materials Conference*, Newport, Rhode Island, 1–4 April 2006, AIAA, Reston, Virginia

4-151 Zafer Gürdal, Raphael T. Haftka, and Prabhat Hajela, *Design and Optimization of Laminated Composite Materials*, John Wiley & Sons, New York, 1999.

4-152 Valery Vasiliev and Zafer Gürdal, *Optimal Design - Theory and Applications to Materials and Structures*, Technomic, Lancaster, Pennsylvania, 1999.

4-153 NASTRAN Users' Manual, NASA SP-222(06), National Aeronautics and Space Administration, Washington, D. C., June 1986.

4-154 S. A. Ambartsumyan, The Axisymmetric Problem of a Circular Cylindrical Shell Made of Material with Different Stiffness in Tension and Compression, *Izvestiya Akademii Nauk SSSR, Mekhanika*, Number 4, 1965, pp. 77–85. Translation available from STAR as N69-11070.

4-155 Robert M. Jones, Buckling of Circular Cylindrical Shells with Different Moduli in Tension and Compression, *AIAA Journal*, Volume 9, Number 1, January 1971, pp. 53–61.

4-156 C. W. Bert, Models for Fibrous Composites with Different Properties in Tension and Compression, *Journal of Engineering Materials and Technology, Transactions ASME*, Volume 99, Series H, Number 4, October 1977, pp. 344–349. See also C. W. Bert and J. N. Reddy, Mechanics of Bimodular Composite Structures, in *Mechanics of Composite Materials – Recent Advances*, Proceedings of the IUTAM Symposium on Mechanics of Composite Materials, Virginia Polytechnic Institute and State University, Blacksburg, Virginia, 16–19 August 1982. Edited by Zvi Hashin and Carl T. Herakovich, Pergamon Press, New York, pp. 323–337.

4-157 Robert M. Jones, Buckling of Stiffened Multilayered Circular Cylindrical Shells with Different Orthotropic Moduli in Tension and Compression, *AIAA Journal*, Volume 9, Number 5, May 1971, pp. 917–923.

4-158 S. A. Ambartsumyan, Basic Equations and Relations in the Theory of Elasticity of Anisotropic Bodies with Differing Moduli in Tension and Compression, *Inzhenernyi Zhurnal, Mekhanika Tverdogo Tela*, Number 3, 1969, pp. 51–61. Translation available as LRG-70-T-1 from The Aerospace Corporation, El Segundo, California, 1970.

4-159 Robert M. Jones, Stress-Strain Relations for Materials with Different Moduli in Tension and Compression, *AIAA Journal*, Volume 15, Number 1, January 1977, pp. 16–23.

4-160 Robert M. Jones and Harold S. Morgan, Buckling of Laminated Composite Circular Cylindrical Shells with Different Moduli in Tension and Compression, *Proceedings of the 1975 International Conference on Composite Materials*, Geneva, Switzerland and Boston, Massachusetts, 7-18 April 1975, The Metallurgical Society of AIME, New York, 1976, Volume 2, pp. 318–343.

4-161 J. Singer, M. Baruch, and O. Harari, *Further Remarks on the Effect of Eccentricity of Stiffeners on the General Instability of Stiffened Cylindrical Shells*, TAE Report No. 42, Department of Aeronautical Engineering, Technion – Israel Institute of Technology, Haifa, Israel, August 1965. See also Inversion of the Eccentricity Effect in Stiffened Cylindrical Shells Buckling under External Pressure, *Journal of Mechanical Engineering Science*, Volume 8, Number 4, 1966, pp. 363–373.

Éléments sous droits d'auteur

Chapter 5

SUMMARY AND OTHER TOPICS

5.1 INTRODUCTION

The purpose of this summary is threefold: (1) to impart some additional practical design-related perspective on the topics covered in this book, (2) to direct the reader's attention to other buckling topics that might be of interest, and (3) to relate this fundamental theoretical study to the numerical computational aspects of current engineering practice. The perspective on the topics in this book hopefully will be advanced by study and discussion of Section 5.2, Design-Related Perspective on Contrast Between Bar, Plate, and Shell Behavior. Some other classical buckling problems that could be considered essentially parallel to the treatment in this book are briefly discussed in Section 5.3, Further Classical Buckling Topics. Then, topics that are more advanced than any in this book are described in Section 5.4, Advanced Buckling Topics. Next, how this book relates to currently available and widely used numerical analysis procedures such as the finite element method is addressed in Section 5.5, On the Transition to Computational Approaches. Finally, in Section 5.6, a common panel buckling benchmark problem is used to illustrate some of the possible pitfalls of numerical analysis as well as the often-overlooked communication tools in engineering problem solving. An abbreviated outline of this chapter is shown in Figure 5-1.

- **DESIGN-RELATED PERSPECTIVE**
- **FURTHER CLASSICAL BUCKLING TOPICS**
- **ADVANCED BUCKLING TOPICS**
- **ON THE TRANSITION TO COMPUTATIONAL APPROACHES**
- **PITFALLS IN NUMERICAL ANALYSIS AND COMMUNICATIONS**

Figure 5-1 Outline of Chapter Five

Éléments sous droits d'auteur

5.2 DESIGN-RELATED PERSPECTIVE ON CONTRAST BETWEEN BAR, PLATE, AND SHELL BUCKLING BEHAVIOR

5.2.1 General Response

By examining the postbuckling portion of the load-deflection behavior of each fundamental structural element including the effect of initial geometric imperfections, we determine the practical design significance of the classical Euler buckling load for bars, plates, and shells. The load-deflection behavior of perfect bars, plates, or shells is denoted with solid lines and curves in Figure 5-2, whereas the behavior of the corresponding imperfect structural element is denoted with a dashed curve.

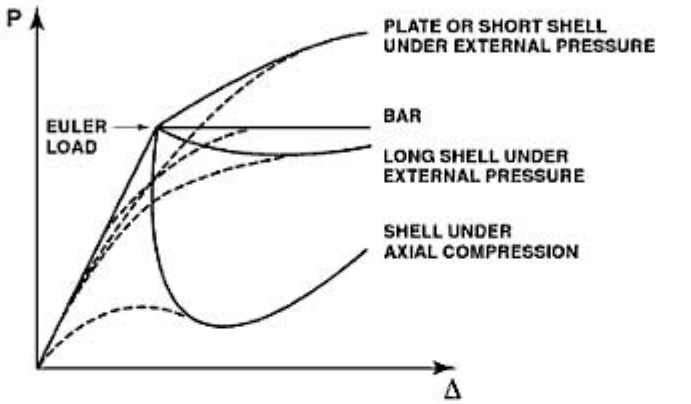


Figure 5-2 Contrast Between Bar, Plate, and Shell Behavior

For perfect bars under axial load, P, the load P neither increases nor decreases beyond the Euler buckling load in Figure 5-2 with increasing *axial* deformation, Δ, because no lateral stresses can be developed to resist or assist lateral deformation. The effect of initial geometric imperfections on bar deformation behavior shown in Figure 5-2 as well as in the form of load versus *transverse-to-the-bar* deformation in Figure 5-3 is to cause slightly larger deflections than would occur for a perfect bar at a given load. A perfect bar can buckle with equal probability either to the left or to the right (when viewed from the side so that you can see the profile of the bar as in Figure 2-2 on page 50) (path A^+ or A^- in Figure 5-3). However, an imperfect bar tends to buckle in the direction of the imperfection if the gross nature of the imperfection is of 'suitable' form (i.e., predominating in one direction transverse to the bar as in Figure 2-63 on page 158). Thus, the Euler buckling load is the practical maximum load-carrying capacity for all axially loaded bars, both perfect and imperfect.

For perfect plates under in-plane load, P, the load P can actually increase above the Euler buckling load with increasing axial deformation,

Éléments sous droits d'auteur

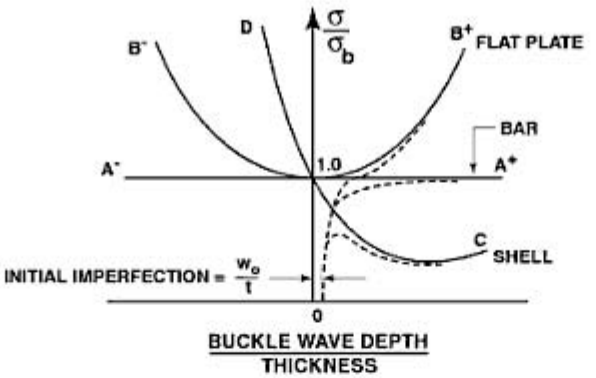


Figure 5-3 Buckling Stress Versus Buckle Wave Depth for Axially Compressed Bars, Plates, and Circular Cylindrical Shells

Δ, as shown in Figures 5-2 and 5-3. This increase is caused by tensile in-plane reactive forces that are transverse to the axial in-plane load and that develop after buckling to restrain the lateral displacement of the plate because of the lateral supports of the plate (if there were no lateral supports, then the plate would actually be a bar or wide column). This action occurs irrespective of the direction of the buckle as shown in Figure 5-3 because the direction of buckling for a plate (upward or downward, i.e., path B^+ or B^- in Figure 5-3) is, by symmetry, immaterial. The effect of initial geometric imperfections is to cause slightly larger displacements than for a perfect plate at a given load. Thus, for all plates, both perfect and imperfect, the Euler buckling load is merely a load at which the plate becomes less stiff. That is, a plate can carry more load than the Euler buckling load, but the axial deflections increase more rapidly with increasing load above the Euler buckling load than below it.

For shells under various loadings, the Euler buckling load can be either a very conservative or a very unconservative limit on the maximum load depending on the shell geometry and the loading. By use of the Batdorf curvature parameter (see Section 4.3), we easily recognize that a shell can be so 'short' as to approach a plate. In such a situation, the Euler buckling load is a conservative estimate of maximum load in accordance with plate results. For 'long' shells, the curvature becomes important and, hence, plate behavior is not at all approximated. Then, the specific loading that causes buckling must be examined. Obviously, axial compression results in postbuckling loads well below the Euler buckling load. Therefore, the Euler buckling load is not a good measure of the maximum load-carrying capacity for a shell subjected to axial compression. Note that a shell cannot buckle in the outward-from-the-shell direction (because, in that situation, the shell would have to stretch, not compress!), so path D in Figure 5-3 is not possible. Instead, an

Éléments sous droits d'auteur

axially loaded shell buckles along path C in Figure 5-3. Under external pressure, the postbuckling loads of a short shell exceed the Euler buckling load because those shells approach a plate. The postbuckling loads of a long shell in Figure 5-2 are not much below the Euler buckling load. Therefore, the Euler buckling load is a reasonable practical estimate of the maximum load-carrying capacity for a long shell subject to external pressure and an overly conservative estimate of the maximum load-carrying capacity for a short shell subjected to external pressure. Apparently, many factors must be taken into account before the Euler buckling load can be used as a design-analysis tool for shells.

5.2.2 Design Considerations and Factor of Safety

The schematic postbuckling behavior of perfect bars, plates, and shells shown in Figure 5-4 is the basis for some observations on design against buckling. Given that bar buckling is a relatively catastrophic event (i.e., the bar deflects seemingly without limit as in Figure 5-4), the factor of safety against bar buckling must necessarily be quite high. In contrast, plate buckling is a relatively benign event (the plate stiffness in the loaded direction merely becomes somewhat smaller as in Figure 5-4). Thus, the factor of safety against buckling for plates need not be anywhere near as high as that for bars. In fact, some panels in highly maneuverable military aircraft are designed to operate in the postbuckling regime at up to perhaps eight times the Euler buckling load! In yet another contrast, thin shells cannot be loaded in axial compression to more than about ten or twenty percent of the Euler load without buckling! Thus, shell buckling under axial load is ultra-catastrophic relative to the Euler load in Figure 5-4. For other loadings such as lateral pressure, thin shells typically buckle somewhat near the Euler load with rather pronounced buckling deformation. Thus, the appropriate design factor of safety for shells is highly dependent upon the type of loading.

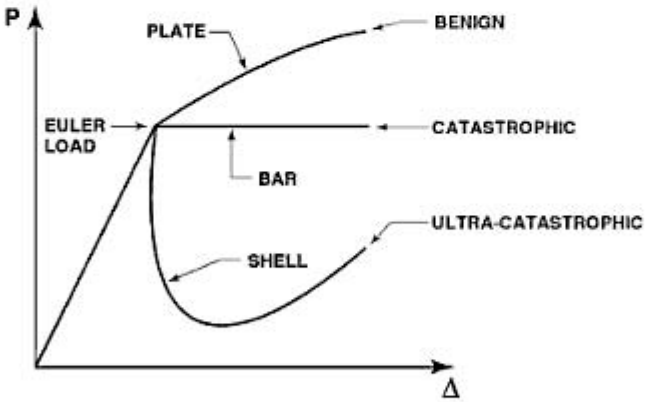


Figure 5-4 Relative Nature of the Buckling Event

Éléments sous droits d'auteur

The buckling equations are dominated by bending stiffnesses, so design against buckling is similar to design against transverse loading which causes bending. That is, the bending stiffnesses are the main parameters in the design process. However, for some laminated plates and all shells, the extensional stiffnesses also enter the design process because bending and extension are inherently coupled to each other.

We establish the factor of safety to use in design by assessing the danger that buckling of a structural element would pose. This assessment is based on the nature of the prebuckling versus the postbuckling behavior. Thus, an engineer must learn the fundamentals of structural behavior before attempting to design a structure so he can deal with the aspects of behavior that affect the design. To determine the factor of safety, we are concerned with the friendliness or the danger of the buckling event for a structural member. Is buckling a benign or a catastrophic event? Of course, the factor of safety must be far higher against a catastrophic event than against a benign event. Moreover, man-rated structures always require a higher factor of safety than unmanned structures. Thus, we recall from Section 2.4 that when a bar buckles, it can carry very little higher load after buckling, but it can still carry the buckling load. However, buckling is accompanied by substantial transverse deformation in addition to increased axial deformation as in Figure 5-4. Thus, bar buckling is generally a catastrophic event that is to be avoided at all costs, hence the need for a 'high' factor of safety.

In contrast, plate buckling is a rather gentle, but still quite audible and visual development of transverse buckles at a particular (specific) load. After buckling, the plate can accept much higher load than the Euler buckling load as shown in Figure 5-4. The axial deformation increases at a somewhat higher rate with added load than occurred below the Euler buckling load because the axial extensional stiffness has decreased. As the load increases, additional buckling from one buckling mode into another can occur, further lowering the axial stiffness with accompanying increased axial deformation per unit of applied axial load. Thus, plate buckling is somewhat benign (i.e., certainly not catastrophic), so the factor of safety against plate buckling need not be as high as that for bar buckling. In fact, some fighter aircraft panels are actually designed to operate under very high-g maneuvering conditions (definitely not normal level-flight conditions), in the postbuckling regime at loads in the vicinity of eight times the Euler buckling load!

For shells, the design significance of the Euler buckling load is, or can be, quite different from that of bars and plates as seen in Figures 5-2 and 5-4. A shell with nearly zero curvature behaves similarly to a plate. However, a shell with high curvature can act quite differently from a plate. The load-carrying capacity of a perfect circular cylindrical shell under axial compression drops off dramatically once the Euler buckling load is reached. An unstiffened imperfect metal shell can never be loaded to the Euler buckling load (because there is no such beast as a perfect shell when made with ordinary manufacturing processes), but the shell instead achieves a significantly lower maximum load followed by buckling. Thus, the Euler load itself is of little practical significance for actual behavior and design of an unstiffened metal shell. Instead, 'knockdown factors' are usually used in design to account for the factors

Éléments sous droits d'auteur

that cause the actual buckling load to be quite a bit less than the Euler buckling load as in Section 4.11. A stiffened metal shell achieves a maximum load quite near the Euler buckling load as seen in Section 4.7. An imperfect unstiffened laminated composite shell can be loaded before buckling to a much higher percentage of the Euler load than can an imperfect metal circular cylindrical shell. And, a stiffened composite circular cylindrical shell can be loaded to nearly the Euler buckling load before buckling. Thus, the Euler load is significant in the design sense for the latter shells. Snap-through buckling (sudden movement of the shell under dead-weight loading into a buckled equilibrium configuration with much larger axial and transverse deformations than in the unbuckled equilibrium state) can occur well below the Euler load. Thus, shell buckling is far worse than catastrophic if the Euler load is used as a predictive tool because the Euler load cannot be reached. That is, the nature of shell buckling at that load has no meaning, so buckling at the Euler load is not catastrophic, but *has already happened at a much lower load!* Accordingly, the factor of safety for shells can be quite variable depending on the type of shell involved and on the loading. Hence, shell buckling at the Euler load is termed ultra-catastrophic.

5.2.3 Comparison with Experimental Results

Comparison of predicted load-deformation behavior with well-measured experimental results is absolutely essential to the assessment of the prediction techniques presented in this book before those techniques can be used in design of buckling-critical structures. Moreover, experimental evidence must always be used as a guide to the development of theoretical analyses. For example, recall that experimental observations were essential to the choice of a deflection function and, as well, to the determination of the 'deformation path' in configuration space for the analysis of postbuckling behavior of a circular cylindrical shell under axial compression (see Section 4.4). Perhaps the strongest example of evidence guiding theory is the classical Bernoulli-Euler observation that plane sections of a beam remain plane under beam bending based on what we can actually see with our own eyes of the deformation of lines on the side of a beam as in Figure 2-44 on page 107. Of course, that observation is valid only to first approximation and is replaced with higher order evidence in elasticity theories.

The premier reference for study of experimental observations on buckling is the two-volume book by Singer, Arbocz, and Weller [5-1]. Aside from the attractive content, one of their major points is that experimental and theoretical work are essential adjuncts to one another. I strongly echo their thought adding that *every theory must be guided by experiment* in order to correctly make the inevitable approximations and assumptions so essential to fruitful problem solving. That is, there must be a well-thought-out definitive reason why we make a specific approximation or assumption. In fact, the word 'assumption' should be *'presumption'* because presumption implies both the hypothesis of an assumption (which might or might not be true) and an accompanying *reason* that makes us think the assumption is true. And that reason can only be based on experimental observations!

Éléments sous droits d'auteur

5.3 FURTHER CLASSICAL BUCKLING TOPICS

5.3.1 History of Buckling

Stephen P. Timoshenko offers the unique perspective of one who lived much of the history of buckling (and indeed of mechanics in general) in two books, one a serious, comprehensive history of strength of materials [5-2] and the other a very personal recollection of experiences [5-3]. Another pioneer who engagingly relates his memories and experiences is Theodore von Kármán [5-4]. Both of these mechanics giants contributed greatly to the development of what we have discussed. All the books are very interesting and informative reading, and they will expand your perspectives on mechanics in general. See also Langhaar's abbreviated review of the history of buckling with many references [5-5].

5.3.2 Comments on Theoretical Derivations in this Book

Some authors say they used small-deflection theory to obtain buckling loads. Instead, in this book, we show that the consistent application of energy principles, including both equilibrium and buckling theory, leads to rational buckling differential equations to find eigenvalues (buckling loads) only from a base of large (or moderately large) deflection theory. Small-deflection theory does not, in fact, lead to the equations that describe buckling. Only through the misinterpretation of certain steps in the derivation of buckling differential equations do many people fall into the trap of identifying parts of the equations as 'small-deflection-theory terms'. Other parts of the equations or energy expressions are then rationalized in various inconsistent, and of course unacceptable, ways. Such attempts at what amounts to black magic, although certainly well intended, serve to confuse students of buckling. In many cases, the right equations are used for the wrong reasons. Properly understanding the correct reasoning is essential to understanding buckling. The approach in this book should build a firm foundation for understanding the phenomenon of buckling as well as for further study of buckling concepts.

5.3.3 Other Structural Elements and Structures

In this book, we do not discuss buckling of structural elements such as beam-columns, frames and arches, lateral buckling of beams, etc. that are so well described by Timoshenko and Gere [5-6], Bleich [5-7], etc. Those topics are regarded as involving logical extensions and modifications of bar buckling theory and are therefore left to the option of the interested reader. Similarly, there are many studies on plates that are not rectangular, e.g., circular, oval, annular, etc., which are not addressed in this book. And, of course, circular cylindrical shells only scratch the surface of the various kinds of shells that have been treated in the literature, many with essentially an Euler approach. For example, shells of revolution have wide practical application, and they can suffer from susceptibility to buckling. Many more general shells are not susceptible to buckling, but some are. For example, Galletly showed that toroidal shells of elliptical cross section buckle under *internal* pressure [5-8].

Éléments sous droits d'auteur

5.3.4 Solution Procedures for Buckling Problems

Specific solution procedures for eigenvalue problems have only been alluded to in this book. We have concentrated on closed-form solutions in order to study the fundamental buckling problem instead of the associated applied mathematics. Of course, any practical problem will involve mathematics beyond most of that discussed in this book. Certainly, the finite element and finite difference techniques must receive considerable attention because they are the most prominent and most practical among currently used numerical solution techniques as is admirably demonstrated by Bushnell [5-9]. Some of these ideas are expressed in Section 5.5, On the Transition to Computational Approaches.

5.3.5 Other Structural Configurations

The overall shape of a structural element is the first step in classification of the type of structural element. The nature of the structural element perpendicular to the surface determining its shape determines the structural configuration, the second step in classification. That is, how is the structural element constructed through the thickness of, say, a bar? Is it a single layer, multiple layers as in a composite bar, multiple layers as in a sandwich beam, stiffened in some special manner (with, for example, cover plates), etc.? Similarly, how are plates and shells constructed through their thickness? We will very briefly address here two structural configurations: (1) sandwich construction and (2) laminated fiber-reinforced composite structures.

5.3.5.1 Sandwich Construction

For beams, plates, and shells in which bending resistance is of prime design importance, sandwich construction is often used. Bending stiffness determines buckling resistance, so sandwich construction is natural for buckling-critical applications. The term 'sandwich' is used as an analogy to the everyday sandwich that might be eaten for lunch. The luncheon sandwich consists of two pieces of bread surrounding some form of meat (or cheese, etc.). In the analogous structural sandwich, the two pieces of bread are the 'face layers' or 'face sheets' and the meat is the 'core'. The mechanism for achieving enhanced bending resistance (stiffness) over that provided by monocoque (single-layer) construction is to separate the two relatively thin 'face layers' or 'face sheets' by inserting a thick layer called the 'core'. The core does not provide much bending resistance and must have low density to be structurally effective (unlike what we expect for lunch!). Perhaps more layers actually constitute each face layer if the 'bread' is a laminated composite material as described in Appendix C. Of course, the core layer of 'meat' could also be more complicated with layers of meat, cheese, lettuce, special sauce, etc., but our analogy is with the simple sandwich. A typical honeycomb sandwich panel consists of face sheets or layers with thickness t_{face} and a core with thickness t_{core} as seen in Figure 5-5. The face sheets are generally bonded with adhesive to the core, although compatible metal face sheets and metal core could be welded.

Éléments sous droits d'auteur

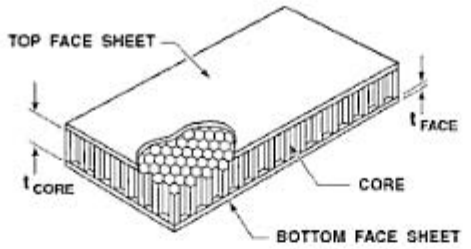


Figure 5-5 Typical Honeycomb Sandwich Panel Construction

The two face sheets serve as the primary mechanism for carrying in-plane loads *and bending moments*. Thus, the face sheets must be made of high-strength and usually high-stiffness materials, at least relative to the core. If the face sheets are adjacent to one another, but bonded, then they effectively constitute a monocoque panel. However, if the face sheets are separated in some manner (by the core), then the bending stiffness increases dramatically, although, of course, the in-plane stiffness is unchanged. The purpose of the face sheets is like that of the flanges in an I-beam, i.e., to provide the largest possible contribution to the bending resistance and virtually the entire extensional resistance. The core, like the web of an I-beam, separates the two face sheets to enable them to provide larger bending resistance by application of the parallel-axis theorem (as when calculating beam cross-section moments of inertia) than if they were placed next to one another. The two face sheets are often identical, but they can be different if the need arises in an application, e.g., one-sided heating might lead to the need for different face sheets with different temperature-resistance capabilities.

The main purpose of the core layer is to cause the two face sheets as a pair to carry a couple (moment) of magnitude dependent upon the face-sheet-separation distance. That distance between the face-sheet centroids is the core thickness plus twice the half-face-sheet thickness. The core simply separates, but also connects, the two face sheets and takes up space while weighing very little (quite unlike the luncheon sandwich with its low-density bread and high-density meat). The face sheets have a large inherent in-plane stress-carrying capability, but a small bending resistance capability because of their thinness. However, if the two face sheets are separated, but still connected by a core layer so they act together, then their combined bending resistance as a pair depends mainly on their physical separation distance squared! Again, because of the parallel-axis theorem. Thus, sandwich panels can have several hundred times the bending stiffness of a monocoque panel and, hence, far higher buckling loads at far less weight, i.e., significant structural weight savings are enabled by using sandwich construction. However, the in-plane stiffness is essentially identical for the two types of panels. The secondary purpose of the core is to support any shear loading imposed on the structural element.

Éléments sous droits d'auteur

Sandwich panel core layers are typically light-weight honeycomb-core panels (with the honeycomb cell axis perpendicular to the sandwich panel surface) as in Figure 5-5 or light-weight solids such as balsa wood or foams that need not be depicted to be imagined. Or, the core could be some form of truss or struts between the face sheets. The main purpose of the core is to take up space between the face sheets without adding significant weight and without providing a premature failure mechanism. The main attribute of the core is that it is shear-deformable and yet shear-resistant. Thus, the core has a far lower modulus than the face sheets. A possible disadvantage of some core materials is the potential to absorb or capture water in, for example, the pores of a foam or in the honeycomb cells. Such moisture 'take-up' is both a weight-increasing mechanism and simultaneously a possible strength-lowering mechanism. The water can also degrade the bond between the core and the face sheets. The key to good design of sandwich construction is to 'balance' all the requirements and use materials for the core and face sheets that 'work together' to achieve a viable combination.

Sandwich panels can be flat to serve as beams or plates, or they can be curved to serve as curved panels or shells. Note that sandwich construction has no advantage in extensional resistance over monocoque construction, so is not used in extensional applications. Moreover, a cost disadvantage would prohibit use for no structural advantage.

The principal analysis feature of sandwich construction is the higher order differential equations than for 'solid' plates or laminates. The principal design feature of sandwich construction is the essential requirement for more design variables with special attention to the vastly different characteristics of the core material from the face sheet material. For example, that disparity between the properties of the two sandwich constituents, the face sheets and the core, leads to the possibility of local buckling of a face sheet away from the core. Debonding of the face sheets from the core is also a possibility. Such additional failure modes complicate the analysis and design of sandwich construction relative to single-layer construction.

Plantema [5-10] was one of the first to write a book on sandwich concepts to achieve more bending- and buckling-resistant structures than are possible with monocoque construction. He was soon followed by Allen [5-11]. Karl-Axel Olsson [5-12] of the Royal Institute of Technology (KTH) in Stockholm, Sweden is responsible for developing much of the composite sandwich technology over the years leading to extensive application in Swedish naval vessels whose hulls do not set off magnetic mines. Zenkert of KTH later formalized, clarified, and extended the concepts of sandwich construction [5-13]. Isotropic and composite sandwich plates and shells were treated more recently by Vinson [5-14].

5.3.5.2 Laminated Fiber-Reinforced Composite Structures

The very high structural efficiency of fiber-reinforced composite materials demonstrated in the form of high strength-to-weight and high stiffness-to-weight ratios motivates their widespread use in weight-sensi-

Éléments sous droits d'auteur

tive applications such as aircraft, spacecraft, cars, etc. Some of these motives are briefly described in Appendix C, but are far more completely discussed by Jones [5-15]. Because of the current strong interest in composite materials, especially in laminated fiber-reinforced form, interest has resurged in many of the classical plate and shell theories. Many fascinating problems arise in the analysis of laminated plates and shells as we have seen in our sampling of buckling problems in Sections 3.6 and 4.8. Extensions and reinterpretations of classical theory are necessary to accommodate the special behavior and characteristics of laminated composite materials. Discussion of laminated plate problems is found in Ashton and Whitney [5-16], Whitney [5-17], Reddy [5-18], and Jones [5-15]. Laminated shells are treated in many recent papers in the *Journal of Composite Materials*, the *Journal of Composite Materials and Structures*, and the *AIAA Journal*, and in books such as those by Vinson and Sierakowski [5-19] and Vasiliev [5-20].

Note that these fiber-reinforced composite laminates can be used as 'face sheets' in the sandwich construction of Section 5.3.5.1 as in Figure 5-6 and have been used on many highly contoured fuselage sections of the latest military and commercial aircraft. One of the most active areas of concentration recently is far more involved and extensive use of fiber-reinforced laminated composite stiffeners on plates and shells than is seen in Section 4.7 on stiffened shells. Some additional composite construction techniques are shown in Figure 5-6. There, we see, in addition to the traditional fiber-reinforced laminate, (1) a laminate with hat stiffeners, (2) a sandwich-core laminate with hat stiffeners, and finally a laminate with reinforcement around a cutout.

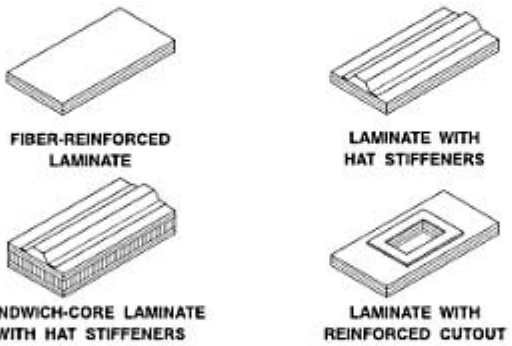


Figure 5-6 Possible Laminated Fiber-Reinforced Composite Construction

Many concepts and even philosophies of buckling exist that are far more extensive, advanced, and complicated than those addressed in this book. Moreover, there are vastly more complicated fundamental equations that lead to less workable theories than those described in this book. We briefly examine some advanced buckling concepts in the next section to point the way to other topics of possible interest.

Éléments sous droits d'auteur

5.4 ADVANCED BUCKLING TOPICS

5.4.1 Introduction

The classical Euler approach to buckling involves idealizations that include a perfectly elastic material in the structure, loads that are independent of time and constant in direction, and linearized differential equations. Many practical problems challenge or violate one or more of those idealizations. For shell buckling, the much lower buckling loads than predicted with an Euler approach were discovered by von Kármán and Tsien [5-21] to be predicted with nonlinear strain-displacement relations that lead to nonlinear differential equations (in reality a nonlinear equilibrium approach rather than a buckling load prediction as shown in Section 4.4). For materials that are not elastic, Shanley [5-22] resolved a long-standing controversy over the proper approach to finding the plastic buckling load. Moreover, Hoff [5-23] addressed the actual loading conditions present in a typical laboratory load frame environment in which buckling loads are determined to compare with theoretical predictions as opposed to Euler's idealizations of load behavior.

These departures from the strict idealizations of Euler are but a start at extending buckling theory to be able to treat problems that are more realistic than can be addressed within the limitations of Euler buckling theory. That is, buckling is sometimes far more complicated than we can realize by studying the Euler approach in this book, even with the inclusion of prebuckling deformations of shells in Section 4.5. One of the most common complications is nonlinearities. Another common complication is that we often must treat buckling or stability from a dynamic or kinetic sense as opposed to the far more restrictive static sense that we used in prior chapters. Ziegler shows us the way.

5.4.2 Ziegler's Classification of Stability Problems

Ziegler approaches stability problems from a very broad point of view in his *Principles of Structural Stability* [5-24]. He classifies more complicated forms of structural response including buckling in his classical papers [5-25] and [5-26]. The first classification distinction he makes is between conservative and nonconservative mechanical systems. *A conservative mechanical system is one for which the work done is zero when the forces on the mechanical system move through kinematically admissible displacements over a closed path in the possible deformations of the system.* The starting point of the path is identical to the finishing point and therefore the path is called closed. *A nonconservative mechanical system is one for which the work done is not zero when the forces on the mechanical system move through kinematically admissible displacements over a closed path in the possible deformations of the system.* An alternative to the closed-path argument is that the work done when the mechanical system moves from one configuration to another configuration is independent of the path chosen from point to point if the system is conservative. Of course, the work done is dependent on the path if the mechanical system is nonconservative.

Éléments sous droits d'auteur

Mechanical systems have two types of external forces, *active forces* or *loads* and *reactive forces* or *reactions*. The loads are known functions of the generalized coordinates (q_k), generalized velocities ($\dot{q}_k$), and time (t). In contrast, the reactions are not known until the differential equations of motion are solved for the problem addressed. However, the *type* of reaction can be determined before that solution. That is, the reactions at supports can be *nonworking* for which the work done is zero (e.g., normal force or static dry friction) or *dissipative* for which the work done is negative (e.g., kinetic dry friction). Hence, nonworking reactions are conservative, and dissipative reactions are nonconservative.

Loads are classified by Ziegler with the first breakdown being instationary versus stationary loads in Figure 5-7 [5-24]. *Instationary loads* depend explicitly on time, such as pulsating loads [$F(q_k, \dot{q}_k, t)$], and are not conservative. *Stationary loads* do not depend on time and are further broken down into velocity-dependent [$F(q_k, \dot{q}_k)$] and velocity-independent [$F(q_k)$] loads, some of which are conservative and some of which are nonconservative. *Velocity-dependent loads* are either gyroscopic or dissipative. *Gyroscopic loads* do no work during motion, so are conservative (such as Coriolis forces, Lorentz forces, and gyroscopic moments). *Dissipative loads* do negative work, so are nonconservative. *Velocity-independent loads* are either noncirculatory or circulatory. *Noncirculatory loads* can be derived from a stationary, single-valued potential function, and thus are conservative (such as all the loads in the previous chapters). *Circulatory loads* cannot be derived from a stationary, single-valued potential function, so they are nonconservative. Circulatory loads do work on bodies that cyclically move through the same position such as power-transmitting devices (cranks, shafts, pulleys, etc.).

The various types of loads and reactions can be combined to obtain mechanical systems with different characteristics. If only one type of load is present, the five fundamental mechanical systems are depicted in Figure 5-8. More complicated combinations of possible loads and reactions are possible to achieve more complex mechanical systems.

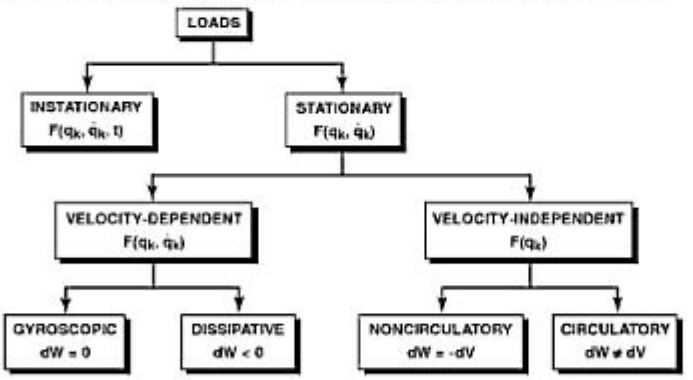


Figure 5-7 Ziegler's Classification of Loads *(After Ziegler [5-24])*

Éléments sous droits d'auteur

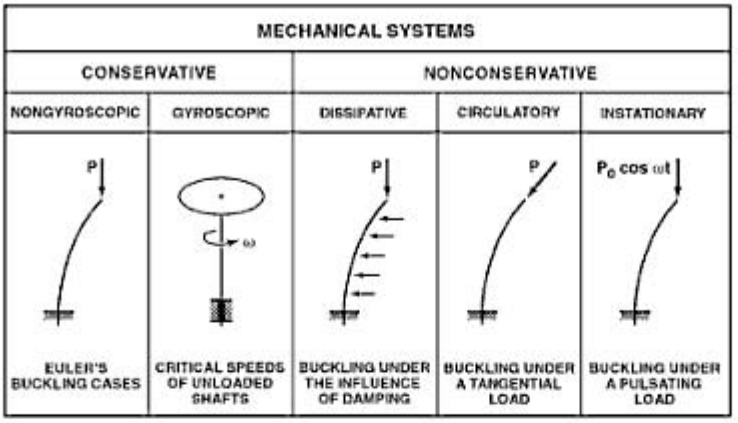


Figure 5-8 Ziegler's Classification of Mechanical Systems *(After Ziegler [5-24])*

For conservative mechanical systems, we must distinguish between nongyroscopic and gyroscopic systems. *Nongyroscopic mechanical systems* have no motion, i.e., are static systems with very slow movement to accomplish a change in configuration. All problems in previous chapters are examples of this static concept of stability, instability, and buckling. The loads are constant in magnitude and direction. In contrast, *gyroscopic mechanical systems* move, but the work done during the motion is always zero. Thus, the work done, of which there is none, obviously is independent of the path of the motion, so the system is conservative. A typical problem is to find the critical speed of a rotating, but unloaded shaft.

For nonconservative mechanical systems, we must distinguish between dissipative, circulatory, and instationary mechanical systems. *Dissipative mechanical systems* lose (dissipate) energy with motion over time by, for example, the result of the action of fluid friction during motion of a structure in water, oil, or air. In the case of fluid friction in which the fluid is air, we usually call the effect aerodynamic drag. Also, internal friction in a body is dissipative. Dissipative forces always do negative work, so energy is not conserved. *Circulatory mechanical systems* have velocity-independent forces that are nonconservative. For example, the tangential load in Figure 5-8 changes in direction during buckling (see the next section), so a potential function does not exist. Instationary mechanical systems have loads that vary with time, so are always nonconservative. For example, a fixed-end column is subjected to an always vertical, sinusoidally varying load in the right-most panel of Figure 5-4.

Many mechanical systems are combinations of the types in Figure 5-8. Dissipative forces exist in virtually every mechanical system in addition to various other forces. Note that all reactions and loads must be conservative for a mechanical system to be conservative. If only one reaction or load is nonconservative, then the system is nonconservative.

Éléments sous droits d'auteur

5.4.3 Nonconservative Systems

Bolotin amplifies the discussion of buckling of nonconservative systems in his book *Nonconservative Problems of the Theory of Elastic Stability* [5-27]. A prominent example of a nonconservative system of the circulatory type in Figure 5-8 is the bar loaded by a force that always remains tangent to the centerline or axis of the bar (called a follower force because it 'follows' the action of the deforming bar) as in Figure 5-9. Such forces have been thought to arise, for example, as the thrust of a non-gimbaled rocket engine (non-swiveling) relative to the flexible rocket itself (more on this contention later, but such forces do arise as a component of the system of forces on a pipe conveying fluid). This seemingly modest change in the manner of loading, specifically in the direction of loading, from the Euler cases in this book results in enormously different behavior. To treat this problem requires that we address the now unconservative nature of the loading instead of the conservative nature that predominates in this book. Classical static buckling concepts, in which the nonconservative nature of the load (the work done is dependent on the path taken in configuration space) is ignored, lead to an obviously unacceptable infinite buckling load. However, when the nonconservative nature of the load is accounted for as was done by Beck [5-28], the bar is predicted to buckle at a finite load, namely

$$\bar{P} \equiv 20.05 \frac{EI}{L^2} \equiv 2.031\pi^2 \frac{EI}{L^2} \tag{5.1}$$

which is about eight times the buckling load if the load were to remain vertical at all times ($\pi^2 EI/4L^2$). More on the buckling of nonconservative systems can be found in Herrmann's *Applied Mechanics Review* survey article [5-29] and in the proceedings of a conference on dynamic stability of structures edited by Herrmann [5-30].



Figure 5-9 Buckling of a Bar Loaded by a Follower Force

The existence or non-existence of the follower force in Beck's problem has been discussed for many years by many buckling luminaries as well as others. Elishakoff examined several hundred papers on the controversial follower-force problem in a very extensive, superbly documented *Applied Mechanics Reviews* article [5-31]. He noted that Koiter addressed 'unrealistic follower forces' in 1996 [5-32] (some 44 years after Beck's work) whereas Sugiyama, Langthjem, and Ryu defended 'realistic

Éléments sous droits d'auteur

follower forces' [5-33] just two years later. Many other researchers weigh in on one side or the other of the argument. Much of the controversy stems from fundamental difficulties in experimentally simulating or creating Beck's column. Additional difficulty arises when the influence of the necessarily occuring structural damping is considered. Many feel that Beck's column is an unattainable, oversimplified model of a problem with nonconservative forces. Moreover, the oversimplification and the inability to experimentally model the problem lead some to trivialize Beck's problem. Perhaps the definition of Beck's column is itself unstable.

5.4.4 Stochastic Excitation

A stochastic process involves random variables with an associated need for probability analysis. For a structure, we are typically interested in the random nature of excitation or loading and subsequent response, i.e., stochastic excitation has both time and spatial variations. A well-known and well-studied example of a stochastic excitation is the wind gusts that caused the Tacoma Narrows bridge to oscillate dramatically and then collapse in November 1940. Potapov studies the stability of both conservative and nonconservative, elastic and viscoelastic systems under stochastic excitation, including rods and plates [5-34]. Elishakoff, Li, and Starnes addressed stochastic buckling of bars and shells [5-35].

5.4.5 Dynamic Buckling

Dynamic buckling under a time-varying load is an instationary, nonconservative mechanical system in Ziegler's classification. Definitive work appears in Bolotin's *The Dynamic Stability of Elastic Systems* [5-36] and in the proceedings of an international conference on dynamic stability of structures [5-30], especially a paper by Hoff [5-37].

5.4.6 Chaos

One of the most recently addressed topics in advanced buckling is chaos. Chaotic buckling is a mixture of the elements of chaotic behavior and the dynamic buckling of a nonconservative mechanical system with instationary forces. The nonlinear differential equations governing the behavior must be integrated over time, and the most notable characteristic of the problem is that small changes in the initial conditions rapidly lead to vastly different solutions. This type of response is termed chaotic behavior. Chaos is popularly exemplified by the random effect of a butterfly flapping its wings one way or the other in Indonesia causing perturbations in the weather system as it flows across the globe to accumulate in such a manner that perhaps a tornado results in Kansas some days or weeks later. In fact, chaotic behavior was discovered by Edward Lorenz of MIT, a mathematician and meteorologist, while investigating weather forecasting [5-38]. James Gleick, then a *New York Times* science editor and reporter, wrote a very nice best-selling book on the general nature of chaos [5-39]. Gilmore focused more on science and engineering applications [5-40]. El Naschie concentrated on applications of chaos in structural engineering, specifically buckling [5-41].

Éléments sous droits d'auteur

5.5 ON THE TRANSITION TO COMPUTATIONAL APPROACHES

The next step after learning the fundamental buckling behavior of the three basic structural elements, bars, plates, and shells, in this book is to progress to more complicated structural elements and structures. That step requires a computational approach as opposed to the closed-form solutions and other relatively simple solution techniques studied so far. This advance in complexity cannot be taken lightly. There are both promises and pitfalls in the road ahead, and each are described for the following pertinent issues:

- how to learn complex buckling behavior
- simple analytical approaches versus numerical approaches
- computational tools available
- replacement of measured behavior
- designing structures

5.5.1 How to Learn Complex Buckling Behavior

The obvious promise is to learn more about buckling phenomena than is possible with the relatively simple solutions in this book. The pitfalls are many. Often, the results and procedure are so complex that gleaning a general truism about buckling is difficult. If the mechanism for examining new results is a closed-form solution, then often the solution itself enables a general conclusion to be drawn because the effect of the variables in the solution is readily apparent. In contrast, if the mechanism for examining new buckling results is numerical, many different results usually must be examined before a general result becomes obvious because the trend in the numbers must be determined. Thus, accumulating new knowledge about buckling is not easy after we have exhausted the available closed-form solutions.

The specific buckling problems addressed in this book are simple in nature by deliberate design or plan. The point is to learn fundamental buckling behavior in the most direct manner. Complications of difficult numerical procedures are avoided in favor of straight-forward analytical techniques where possible. However, you might say, the 'real world' is not solely composed of simple problems; there are many complex problems, too. Obviously, that statement is painfully true! So, how do we address those more complex problems in a rational, revealing manner?

We have no business starting with difficult problems when we do not understand fundamental buckling behavior. That is, our 'first day on the job' should not consist of the boss telling us to use NASTRAN [5-42] to calculate the buckling load of the complexly stiffened and partitioned mid-fuselage of the new X-55 rocket plane! Even if we knew quite a bit about buckling load calculation, we would probably not have the training or the education to use NASTRAN to solve such a problem. Note the difference between training and education: universities necessarily attempt to provide an education, and other types of organizations train people to do things without necessarily educating them (although education is not excluded). We must first understand the fundamental buckling behavior of structural elements whose aspects we can firmly grasp by rigorous study of this book, i.e., become educated in buckling theory.

Éléments sous droits d'auteur

Then, based on that knowledge and understanding, we can begin to approach more difficult problems via perhaps the finite element method (for finite element, read finite difference if you like). Obviously, the finite element method is extremely powerful, but that power can easily deceive us into thinking we have the correct answer when we actually do not. See Section 5.6 for a problem that many thought was solved correctly, but it was not.

It is not at all obvious whether the numbers on a computer printout or screen are right or wrong. My friend Jack Martinelli said the common acronym GIGO does not mean just 'Garbage In, Garbage Out', but really means 'Garbage In, Gospel Out' because many young engineers (as well as some who are not necessarily supposed to know better) tend to *bless* any results that come from a computer even if the input and the understanding are garbage [5-43]. Note that Jack made that comment more than twenty years before publication of this book! Some other individuals have similar low levels of understanding computer programs. I once took a printout of a simple addition and subtraction result from an absolutely trivial FORTRAN program to a bank official to demonstrate that the escrow account for my home mortgage account had too high a minimum balance, and I requested a refund. The official took one look at the computer output and was absolutely snowed. He said: "I'll give you a refund, but please don't show this program to your neighbors because our bank has their mortgages, too." Such lack of understanding of computer programs (and unethical behavior) is, unfortunately, not limited to nonengineers! Too many engineers are quite willing to believe the computer results without giving sufficient attention to making certain that they *understand and believe* those results! Moreover, those results must be evaluated relative to known simpler results.

An ordinary engineer is not going to learn buckling by running computer programs developed by someone else. It takes a lot of perspective to begin to draw conclusions about buckling behavior by merely running a computer program and getting lengthy numerical results. The process is not information gathering, but knowledge accumulation. That is, information is not knowledge, *seek knowledge!* Information can often be obtained with a Google search. Knowledge is far more difficult to obtain. Seemingly, in the computer age, independent thinking has been often replaced by double clicking! Life is just not that easy!

Understanding buckling behavior is built on a foundation of simple problems. That foundation enables us to next move to more complex problems as we proceed from the foundation to the building we're constructing. However, we must always return to the foundation to correctly interpret results at a 'higher' level. We must know some bounding behavior from simple problems to make certain our more complicated problem is being addressed correctly. We must know some approximate results from simple problems to get an idea of what answer we should expect for the more complicated problem. Another good friend, Dr. James G. Crose, said in May 1987: "If you don't know the answer to within 20% *without* the computer, then you're in never-never land *with* the computer" [5-44]. The bottom line is that we must have a firm grasp on the principles underlying every computer program and understand what must 'come out' to be able to intelligently use computer programs.

Éléments sous droits d'auteur

5.5.2 Simple Analytical Approaches versus Numerical Approaches

The promise of comparing simple analytical approaches with more complex numerical approaches is that you can hopefully find the best way to solve your specific problem. Moreover, you can use the simple analytical approaches to complement the numerical approaches by providing a basis of understanding of approximate behavior. Thus, you extend your confidence in the numerical approaches which are otherwise difficult to evaluate. The pitfalls have two extremes. First, some simple approaches by their very nature oversimplify the problem, i.e., leave out essential phenomena. At the other end of the spectrum, some approaches are more complicated than you're willing to endure.

Some of the general characteristics of both simple analytical approaches (e.g., solutions to differential equations) and numerical approaches (e.g., finite element programs) are listed in Figure 5-10. The analytical approaches are typically much simpler and less comprehensive, although quite easy to obtain (when they're already available), evaluate, and understand. However, the more complicated numerical approaches are always the only way to work really tough problems, but are often difficult to interpret.

ANALYTICAL APPROACHES E.G., SOLUTIONS TO DIFF. EQUATIONS	NUMERICAL APPROACHES E.G., FINITE ELEMENTS
• LIMITED TO PROBLEMS WITH SIMPLE GEOMETRY AND LOADING	• VALID FOR PROBLEMS WITH COMPLEX GEOMETRY AND LOADING
• EASY TO UNDERSTAND	• HARD TO UNDERSTAND UNLESS FAMILIAR WITH SIMPLE PROBLEMS
• VALIDITY OBVIOUS	• MUST BE VALIDATED BY SOLVING MANY SIMPLE PROBLEMS
• USUALLY INEXPENSIVE BECAUSE ALREADY AVAILABLE	• OFTEN EXPENSIVE
• LITTLE TIME NEEDED	• OFTEN TIME-CONSUMING
• ESSENTIAL BASIS FOR VALIDATION OF ALL NUMERICAL APPROACHES	• ONLY WAY TO WORK REALLY TOUGH PROBLEMS
• BEST WAY TO LEARN BEHAVIOR	• NOT A LEARNING TOOL FOR BASIC BEHAVIOR

Figure 5-10 Analytical versus Numerical Approaches

With a numerical approach, you get only a number, but how do you know that number is anywhere near correct? Only by some extension of your basic understanding of buckling behavior from simple analytical approaches to the more complex problem you're trying to solve! That extension requires firm and comprehensive understanding of fundamental buckling behavior that can be learned only with simple solutions. Moreover, you must have an approximate solution with which you can compare the results of a numerical approach. Again, as Dr. James G. Crose said in May 1987: "If you don't know the answer to within 20% *without* the computer, then you're in never-never land *with* the computer" [5-44]. Merely attempting to appreciate the numerical results directly is fraught with terrible pitfalls that will bedevil you (and your boss!).

Éléments sous droits d'auteur

5.5.3 Computational Tools Available

The promise of computational tools is that 'seek and ye shall find' a computer program that will do everything you need it to do. The pitfalls are that often the program is not easy to use and also the results and their implications can be difficult to understand.

After engineers have been thoroughly educated in the basic principles and concepts of a topic, e.g., buckling, then it is time to address problems that are more complex from a geometric and/or loading point of view. Any good engineer with a firm grasp of the basic concepts should be able to teach himself, *given enough time*, to use a numerical procedure such as a finite element computer program to execute the more complex problems. However, he must always keep in mind the extrapolation he is making from the basic concepts to the new, inherently more complicated problem. New phenomena in the more complicated problem provide a challenge to be understood.

Computational tools have become ever more popular and powerful, so we need to appreciate what they can do for us. It is helpful to know something about how such programs are developed in order to understand their capabilities as well as their limitations. The development of complex finite element programs (I helped develop a widely used finite element program, so I've had to do much of the following [5-45]) is based on an apparently general solution technique that supposedly can solve problems of broad complexity. Thus, a program must be thoroughly tested to make certain that it actually solves the problems it is advertised to solve. The testing of a general program must involve demonstration with good test cases that the correct answers to simple problems are obtained. If those simple problems are not solved correctly, then the program is just plain wrong! If those simple problems are solved correctly, then the finite element program *might* be right. That is, correct solution of simple problems is a *necessary, but not sufficient condition* for the finite element program to be correct. However, correctly solved simple problems give us more confidence that the finite element program *might* be correct. We are in the uncomfortable position of not being able to definitively prove that a computer program is right (because there is no such 'theorem' to prove), but we can, with just one simple counterexample, prove that a computer program is wrong. Thus, demonstration of supposed correctness of a computer program is not even possible.

Does the more complex problem exhibit the nature of the behavior we know it must based on our knowledge of simpler problems? We don't learn those simple problems just so we can forever after solve simple problems! We study simple problems to *build up our knowledge* so we can extrapolate our knowledge to more and more complex problems as we proceed through our professional life.

Engineers are supposed to use ingenuity and basic knowledge to solve problems. That knowledge is best used in a building-block fashion, i.e., solve and understand simple problems, then progress to more complex problems with the background of the simple problems to rely on, and finally solve the most complicated problems by using all information at their disposal. Engineers must always prove that what they are doing is

Éléments sous droits d'auteur

correct, so they must demonstrate that they understand all aspects of a problem. Part of that demonstration is proper use of fundamental behavior in a manner that can be extrapolated to more complex problems. Failure to use the basic fundamentals usually leads to serious mistakes, failures, and sometimes loss of lives. We cannot afford to 'cut corners' by assuming that a finite element program actually works as it is advertised! Or that we have 'operated' the program correctly. Too many failures have occurred because engineers have blindly depended on the unevaluated results of a misused finite element program. All such programs must be used in an intelligent, discerning manner.

You will need your analysis ability to create and understand computer programs that 'automate' the analysis of a complex structure. Without that ability, you will merely be training to use a 'black box' in the worst sense of the term. Education is far more important than training in the world of engineering practice. I am not saying, by any means, that all finite element program users are merely trained and not educated—that is false and misleading. I am saying that you can't put off education and hope that training to use a computer program will make up for the lack of education. I both developed and used finite element programs for complex problems. However, I had an extensive analytical background that prepared me to be able to understand the program and the results I obtained with the program. Thus, I often knew whether the results were reasonable. That someone would simply believe the output of a computer program without doing a few check calculations 'on the side' is absolutely wrong and certainly incredible (as well as less than intelligent and responsible). Nevertheless, too few computer program users take the time to make such meaningful checks on their work.

When using any computer program, ask yourself these questions:

- Do you actually know what you're doing, or are you just feeding a black box?
- Do you understand the principles on which the black box is based?
- Do you have any 'feel' for what results you should obtain? Or, are you 'in the dark'?
- Can you tell if the results you get are meaningful?

Yet another time, as Dr. James G. Crose said in May 1987: "If you don't know the answer to within 20% *without* the computer, then you're in never-never land *with* the computer" [5-44].

Many special-purpose and general-purpose finite element and finite difference computer programs that treat buckling exist. The list includes BOSOR, STAGS, ABAQUS, MARC, NASTRAN, ADINA, ANSYS, etc. Rather than give you citations that might change, I encourage you to simply Google those program names for the latest information.

Singer, Arbocz, and Weller [5-1, page 111] said: "One should not expect that complicated structural stability problems involving thin-walled plate and shell components, where nonlinear effects play an important role, can be solved routinely without much effort and thought by any of the many codes that are currently available. A thorough understanding of the shell and stability theory involved supplemented by a good working

Éléments sous droits d'auteur

knowledge of the computational algorithms used are the prerequisites the analyst must possess in order to be able to arrive at the appropriate solutions. Otherwise the chances are high that incorrect or unreliable solutions will be obtained." After presenting some BOSOR4 and PANDA2 results, Dr. Charles Rankin was asked how easy it is to use those programs. He responded [5-46]: "I think you have to learn the fundamentals." You have to get "the feel for it" ... "I don't see a way to make it easier" ... "difficult phenomenon" ... "will get worse with optimization." Those words are from a guru of STAGS who is quite familiar with BOSOR and PANDA2 and makes presentations on results from all those programs.

5.5.4 Replacement of Measured Behavior by Computer Simulation

The promise of 'replacement of measured behavior' by computer simulation is that computer simulation would be sufficiently accurate and comprehensive to allow it to reliably replace actual measured behavior of a structure or object. However, the pitfalls are numerous.

Simulation of behavior is primarily based on what we have already seen, not what we will see in the future, i.e., new behavior that has not yet been observed. For example, realize that carbon nanotubes were not observed until the 1990s. Thus, how could we have simulated them before that time? To be sure, particle physics has theoretical simulations of particles that have not yet been observed, but mechanics is not quite as esoteric as particle physics.

Let us hope that computational approaches which are claimed by too many to be capable of totally replacing experimental approaches do not achieve this false god status. In fact, as discussed in Section 1.4, Singer noted that experiments are always necessary to develop, motivate, and refine theories. Thus, the concept of *in silico*[1] prediction of structural behavior is fallacious. Let us temper those objectives of a totally computational approach with a heavy dose of reality!

Computer simulations of vehicle or structural performance might become accurate enough and sufficiently comprehensive that they could be used to *reduce, but not eliminate,* the number of proof tests of a structure or object before it is used. To be sure, we often find structural applications for which we cannot fully simulate the environment they will experience, e.g., many aerospace applications. In those situations, we must do the best we can to computationally simulate what the structure will experience. However, for many earth-bound applications, we can simulate the environment mechanically as opposed to computationally. Who would want to ride in a vehicle that has not been proof tested? OK, there are many Evel Knievels out there, but when we responsibly design and construct vehicles for the general public, we must take reasonable care to prevent accidents. The conclusion is that we must proof test vehicles, by actual mechanical means, not by more computer simulation.

[1] *in vivo* (that which is alive), *in vitro* (in glass, e.g., in a test tube), and *in silico* (in silicon, i.e., on a computer).

Éléments sous droits d'auteur

5.5.5 Designing Structures

The promise of designing structures is to be able to use rational, mathematics-based means to design a structure that is 'best' by some measure(s) of efficiency. Those measures, called 'merit functions', could include least cost, least weight, longest life, fastest aircraft, etc. with possible combinations. The pitfalls are mainly the multiple complexities of the design problem related to the ability to analyze, to model, and to optimize, all of which strongly depend on computer capabilities.

Before optimization, design was based on 'seat-of-the-pants' intuition with some feedback from very approximate analysis of the 'designed' structure. That intuition was based on the ability to construct or manufacture as well as on perceived behavior. Ideally, changes in the 'design' would be made to push toward the most efficient design based on what constituted efficient for the object, i.e., the merit function(s). However, the ability to realistically analyze was quite limited and very slow, so only a few changes to the design were made unless the object failed. That is, most designs were certainly not the 'best'—they merely 'worked', but were typically overweight and over strength.

With the advent of computer-based analysis and the rapid advances in computer capability, the ability to analyze structures has increased amazingly. The ability to design structures has also increased, although optimum design is still not at the same level as analysis. Actually, the term 'optimum design' is somewhat redundant. Design is the overall process of creating a structure on paper, and when we seek the 'best' design, we generally need optimization concepts to help us. Optimization is a mathematics-based set of algorithms to make choices about which (design) variables to change and by how much in order to achieve a design for which some merit function or functions are minimized. Thus, optimization concepts are just as important to develop as are analysis approaches. That is, the structure could grow to be so complicated (yet analyzible) that we cannot understand how to change the design variables to achieve an optimum design without using optimization concepts.

The analysis and design process can be thought of as consisting of a triad of characteristics: (1) analysis capability or complexity; (2) model complexity; and (3) optimization complexity. These three characteristics are represented schematically in Figure 5-11. The distance along each axis represents the ill-defined degree of complexity with some point, P, in the three-space to define a particular analysis-model-optimization situation. Analysis complexity can be thought of as those behavioral aspects of a structure that are considered. For example, the analysis axis might be labeled with the following sequence of increasing capability or complexity: elastic with small deformations; elastic with large deformations; and plastic with large deformations. In contrast, model complexity is the accuracy with which we pursue the analysis, e.g., how many finite elements or degrees of freedom are used to represent the structure. Of course, optimization complexity is the degree to which, and the manner in which, we pursue the goal of 'best' structure in a logical mathematics-based manner. Computer time and storage requirements go up as all

Éléments sous droits d'auteur

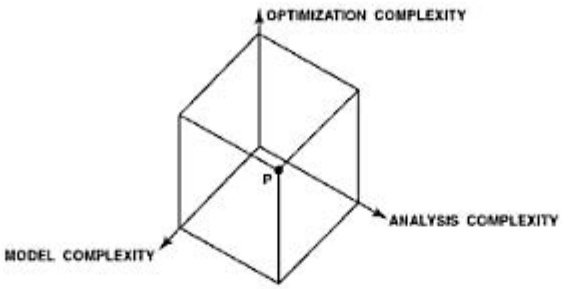


Figure 5-11 The Design Triad

three complexities increase. Note that if analysis and optimization approaches to design do not include all possible failure modes, than that approach is doomed to 'create' faulty designs, just as is the human who neglects a possible failure mode. Of course, that failure mode might not govern for a specific object, but for other ranges of the design variables, the neglected failure mode could govern and cause a failure.

There is no point in pursuing any design approach that is not balanced, i.e., one in which the three sides of the triad box to point P in Figure 5-11 are not approximately equal, presuming we can overcome the lack of precise definition of degree of complexity. For example, a crude model coupled to superior analysis and optimization capabilities is obviously not desirable. Also, a highly accurate model with a superior analysis along with a very limited optimization capability is of little value. An example of the last situation is a model with many hundreds of thousands of degrees of freedom in an analysis with the ability to treat large plastic deformation, but with little ability to change the design variables in the optimization process. Such an example is unfortunately characteristic of how some analyses are so complicated that some people think they represent reality and forget the real objective of design. However, that example is but one small step in the necessarily complicated design process and is therefore of little value by itself! Unless coupled to a correspondingly capable optimization program, that model and analysis provide little information in the actual design process. *The design variables must be changed for design to take place!* Thus, those who think that a complex finite element analysis is the 'be all and end all' in structural design are sadly misinformed (although that claim could be correct in the *structural analysis* phase). To obtain the best advantage of complex finite element analyses, we must use correspondingly comprehensive optimization capabilities. Although many have pushed the analysis element in design too far for the 'times' (i.e., relative to other capabilities), the optimization element has always lagged behind in accomplishment of the overall design objective. To increase the optimization capability requires both advances in computer capability and conceptual optimization techniques. Venkataraman and Haftka reviewed the progress of optimization techniques up to 2002 with particular emphasis on the influence of computer advances over time [5-47].

Éléments sous droits d'auteur

5.6 THE INCORRECT BENCHMARK PANEL BUCKLING SOLUTION AND COMPUTER PROBLEM-SOLVING LESSONS LEARNED

5.6.1 Introduction

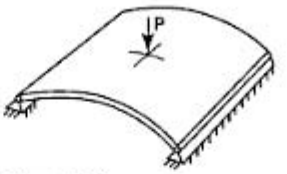


Figure 5-12
Circular Cylindrical Panel with a Centrally Applied Point Load

The highly nonlinear load-deformation response of a centrally loaded thin square isotropic circular cylindrical panel (a segment in the circumferential direction of a circular cylindrical shell as shown in Figure 5-12) is studied with two objectives: (1) to determine the response character and (2) to demonstrate that some approaches to determining the response have been flawed, so we can learn from those mistakes. The panel spans, and is supported on, two straight axial edges with pinned fixtures that cannot move, i.e., hinges that allow rotation, but no translation. The panel is free on the two curved circumferential edges which have a mid-span height called the 'rise'. The central point load, P, is initially downward as shown on the initially concave-downward panel, but can be applied either downward or upward as necessary to maintain equilibrium during large deformations of the panel. Geometric nonlinearities and only unlimited linear elastic stress-strain behavior are treated in this section, i.e., we do not consider nonlinear material behavior or material failure caused by excessive stresses. We address the essential behavior of the panel without equations or numbers and concentrate on the qualitative nature of the results that were obtained by others.

Sabir and Lock [5-48] studied the behavior of a circular cylindrical panel with fixed span, length, and rise, but varying thickness, in 1972 as an example of their numerical shell analysis procedure. Their thinnest panel had a peculiar behavior that seemed to be a good example for others to emulate. The problem has since been used many times as a benchmark solution with which the results of other computer programs were compared. That is, the accuracy of various techniques for highly nonlinear load-deformation analysis was determined relative to the benchmark solution. However, the Sabir and Lock solution will be shown to be incorrect, so the benchmarking efforts have been misdirected and have as much demonstrated a lack of fundamental shell buckling understanding as they have sophisticated analysis capabilities.

First, the types of load-deflection behavior of a circular cylindrical panel are described along with common types of loading. Then, the characteristics of the Sabir and Lock incorrect benchmark solution are described in general terms. Next, the characteristics of the correct solution to the benchmark panel load-deformation response obtained by Wardle [5-49] are discussed. Finally, some common difficulties in engineering problem solving with computer techniques are identified, and improvements are suggested. This section stemmed from extensive discussions with Dr. Brian Wardle of the Massachusetts Institute of Technology who determined that the benchmark problem is incorrectly solved by obtaining the correct solution and performing related experiments.

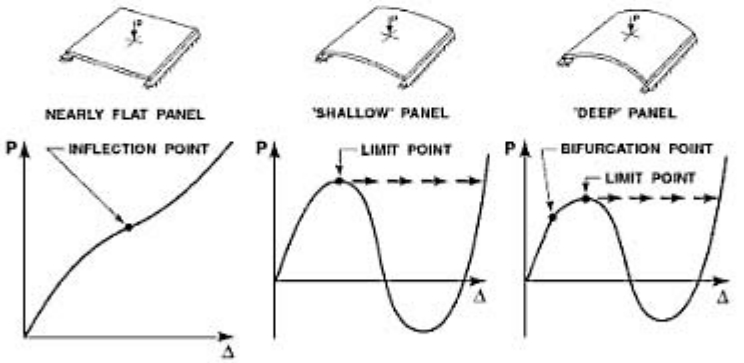
Éléments sous droits d'auteur

5.6.2 General Characteristics of the Panel Buckling Problem

The panel span, length (along the supports), thickness, and mid-span height ('rise') plus the loading determine the nature of the panel behavior. The amount of rise for a fixed thickness, length, and span is used to distinguish between classes of panels as rise goes from zero (flat panels) to 'small' rise ('shallow' panels) to 'larger' rise ('deep' panels) in this study. In contrast, Sabir and Lock decreased the thickness and fixed the other panel dimensions to achieve the same goal.

The behavioral events and their order of occurrence in the load-deflection response of a curved panel depend on the type of loading. Some loading devices are load controlled, i.e., load always increases or remains constant as deformation increases, but load cannot decrease (sometimes called dead-weight loading). Other loading devices are deflection controlled, i.e., deflection always increases or remains constant regardless of accompanying load increase or decrease, but deflection cannot decrease (as in screw-driven load frames). In yet other loading devices (as well as in many real structures), a combination of both load and deformation can be applied under highly controlled circumstances.

Three types of panel response exist as shown in load, P, versus center deflection, Δ, plots in Figure 5-13. First, if the rise is nearly zero, i.e., the panel is nearly flat, then the panel has a simple increasing load and center deflection but with an inflection point between the concave-downward portion (softening) and the concave-upward secondary portion (stiffening) in Figure 5-13a. The deformation is always symmetric about the panel mid-span, and the behavior is stable at all points of the curve. This nonlinear equilibrium problem has no buckling and is called *inflection-point response*. Second, if the rise is 'small', the panel exhibits limit-point behavior as in Figure 5-13b with deformations that are also always symmetric about the panel mid-span. Behavior at the limit point is defined in Figure 1-9 on page 5 with a jump under constant load con-



a Inflection-Point Response

b Limit-Point Response

c Bifurcation and Limit-Point Response

Figure 5-13 Possible Load versus Center Deflection, Δ, Behaviors of Central-Point-Loaded Circular Cylindrical Panels

Éléments sous droits d'auteur

ditions to a much higher deflection as shown with the arrows in Figure 5-13b. The load can become negative for some deflections as shown in Figure 5-13b or can remain always positive depending on the panel geometry. Whether the response is stable or unstable depends on the type of loading as just described. Such panels are termed 'shallow', and the behavior is called *limit-point response*. Third, if the rise is 'large enough', then the panel bifurcates (i.e., buckles) from the symmetric prebuckling deformation state to an asymmetric deformation state and can subsequently exhibit limit-point behavior as in Figure 5-13c. The asymmetric deformation mode after bifurcation has both symmetric and antisymmetric components that each can grow or shrink with increasing load or deformation. That is, deformations are first symmetric about the panel mid-span, then an antisymmetric component enters at bifurcation and initially grows as the response progresses. Later, the deformations become dominated again by a symmetric component at large loads and deflections. These panels are not shallow and are the focus of attention in this section. For these 'deep' ('non-shallow') panels, bifurcation means only a mild transition from symmetric response to asymmetric response, i.e., no dramatic deformation change. This behavior is called *bifurcation and limit-point response*. As with limit-point response, the loads in bifurcation and limit-point response can be always positive or sometimes negative for various panel geometries. For deeper (or thinner) panels, the limit point and bifurcation point can move toward each other to coincide, so deformation after bifurcation occurs with decreasing load in deflection control as in Figure 5-14 (or the response is unstable if load is controlled). Such behavior is a subclass of the bifurcation and limit-load behavior shown in Figure 5-13c. Note that both flat panels and initially concave-upward panels never buckle, but always have monotonically increasing load-deflection curves.

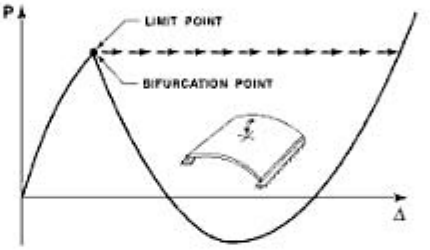


Figure 5-14 Load-Deflection Behavior of 'Deeper' Point-Loaded Circular Cylindrical Panels

5.6.3 Characteristics of the Incorrect Benchmark Solution

Regardless of the manner of loading (load-controlled, or deflection-controlled, etc.), the deformation response of the curved panel begins at low loads as a deflection shape that is symmetrical about the mid-span of the panel with a 'dimple' (a locally concave region) under the load as in Figure 5-15. There, the view is of a cut made through the center of the panel in the

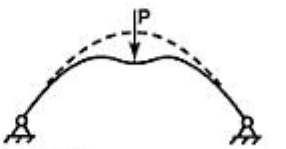


Figure 5-15 Symmetrical Panel Deformation at Low Load Levels

Éléments sous droits d'auteur

span-wise direction. The deformation shown is essentially what would be obtained with small-deflection theory for a panel or an arch. That symmetric deformation grows with load until some event occurs to modify the nonlinear deformation growth.

For many years, that first event in the Sabir and Lock benchmark deformation and buckling problem was assumed by the benchmark users to be a 'load-limit point' which is a point above which the load cannot be increased, i.e., a local maximum height on the initial portion of the load-deflection curve in Figure 5-16. A (load-) limit point is defined on a load-deflection curve in Figure 5-13b (and in Figure 1-9 on page 5 along with typical behavior). If the loading is load-controlled, then the panel dynamically snaps *across* from the 'load-limit point' to the highly deformed region at the right of Figure 5-16. There, the center deflection is about twice the panel rise, i.e., the deformed panel is now concave upward. That behavior is usually called 'snap-through buckling', but the term 'snap-across buckling' is suggested because of the direction of snapping on the load-deflection curve of Figure 5-16 (and the next definition). Of course, the term 'snapping' is used because of the sharp snapping noise that accompanies snap-across buckling. In contrast, if the loading is not load-controlled after the load-limit point, then, at higher deformations, a 'deflection-limit point' is encountered where deflection achieves an initial local maximum and then begins to decrease if the loading is not deflection-controlled. If the loading is deflection-controlled, then the panel dynamically snaps *down* from the 'deflection-limit point' to the same value of deflection at a much lower load (which can even be negative). The 'down' in 'snap-down buckling' is a reference to the direction of snapping on the load-deflection curve of Figure 5-16. Irrespective of the manner of loading, the panel response eventually reaches the monotonically increasing (stiffening) behavior on the right-hand side of Figure 5-16 where the deformed panel is concave upward, e.g., Point F.

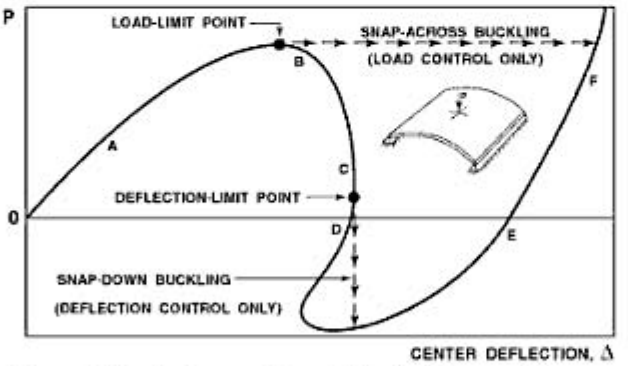


Figure 5-16 Load versus Center Deflection Response for the Benchmark Square Circular Cylindrical Panel Analyzed Only for Symmetric Behavior *(After Wardle, Lagace, and Tudela [5-50])*

Éléments sous droits d'auteur

The presence of a 'load-limit point' and a 'deflection-limit point', i.e., points of load-magnitude reversal or deflection-magnitude reversal, are distinct challenges for numerical analysis procedures for highly nonlinear shell response. That type of behavior can be calculated with the use of arc-length or path-parameter analysis techniques such as the Riks arc-length method [5-52]. Those techniques are available with the STAGS (STructural Analysis of General Shells) finite element program [5-53] that is widely used. The load-deflection behavior shown in Figure 5-16 can be measured only in a loading device wherein both load and deflection are simultaneously varied without either remaining constant. However, as we will show in the next sub-section, the response shown in Figure 5-16 does not actually occur for the benchmark panel, but is the result of incorrect calculation. That is, those researchers calculating the benchmark solution, starting with Sabir and Lock, did not investigate the possibility of a bifurcation in the load-deflection response of Figure 5-16 despite ample evidence that bifurcation into an asymmetric deformation mode is possible for panels if they are 'deep enough'.

Panel deformation progresses with load as in Figure 5-17. There, the unloaded shape and the deformations are greatly enlarged in the vertical direction so the deformations are easily distinguished from one another. The slight deformation with a 'dimple' at the point of load application at loads below the load-limit point is Curve A (similar to Figure 5-15). Each curve with a letter in Figure 5-17 corresponds to a point with the same letter on the load-deflection curve of Figure 5-16. The deformation increases substantially to the shape in Curve B just after the load-limit point so that the point of application of the force, P, has reached the vicinity of the level of the pinned supports. That is, the center deflection is approximately the panel rise. As the load approaches the deflection-limit point with Curve C, the point of application of the force, P, has gone below the level of the pinned supports, i.e., the center

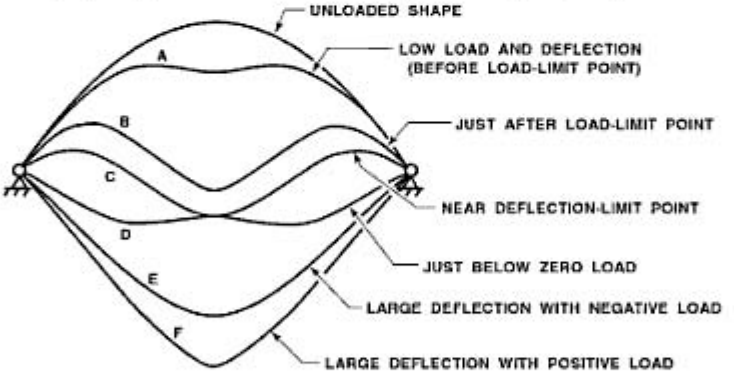


Figure 5-17 Deformations at Various Load Levels for the Benchmark Square Circular Cylindrical Panel Analyzed for Only Symmetric Behavior *(After Wardle [5-51])*

Éléments sous droits d'auteur

deflection exceeds the panel rise. Just after zero load, the load acts upward, so the 'dimple' in Curve D is upward. As the center deflection again increases (from the lowest local value), but with negative (upward acting) load, the panel exhibits the large deformation in Curve E. Finally, as the center deflection continues to increase, the load changes back to positive (downward acting), and the panel continues to deform in the manner of Curve F with substantial stretching of the concave-upward panel. Note that there is no 'dimple' under the load in either Curve E or F.

The load- and deflection-limit-point behavior with symmetric deformation into the highly nonlinear region obtained by Sabir and Lock [5-48] and shown in Figure 5-16 has long been used as a benchmark solution to validate many computer-based numerical approaches to nonlinear shell analysis with samples of references given by Wardle [5-49]. That so-called benchmark solution was apparently accepted as realistic by all. The sole objective was to make certain that all computer programs for highly nonlinear shell response would predict the behavior shown in Figure 5-16. However, the behavior shown in Figure 5-16 is, unfortunately, *incorrect!* That is, the computer programs were all compared with each other but without reference to the reality of actual panel behavior. The (incorrect) solution is merely a fancy analysis of an unstable equilibrium configuration that is, of course, never realized by the panel.

5.6.4 Characteristics of the Correct Panel Buckling Solution

Wardle identified a significant and definitive event that occurs at a lower load than the load-limit point of the benchmark solution, namely bifurcation from the symmetric deformation configuration into an asymmetric deformation configuration as in Figure 5-18 [5-49]. At the bifurcation point, the panel response bifurcates, i.e., one of the two possible load paths is chosen. One path is unstable, of higher energy, and in-

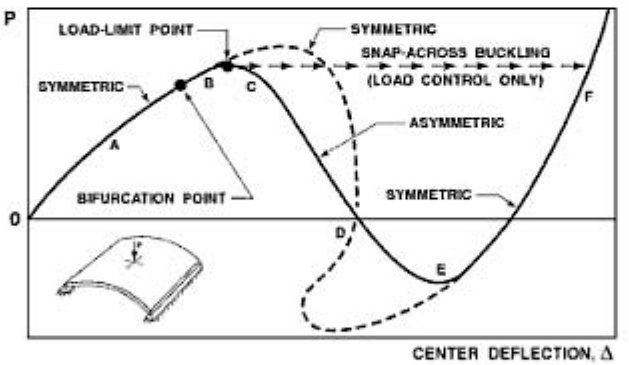


Figure 5-18 Load versus Center Deflection Response for the Benchmark Square Circular Cylindrical Panel Analyzed for Both Symmetric and Asymmetric Behavior *(After Wardle, Lagace, and Tudela [5-50])*

Éléments sous droits d'auteur

volves deformation that continues to be symmetric about the mid-span of the panel (the incorrect panel buckling benchmark solution). The other path is stable, of lower energy, and involves deformation that is asymmetric about the panel mid-span. Thus, the panel can be said to have buckled from a symmetric deformation state to an asymmetric deformation state. However, the panel in its asymmetric deformation state can continue to accept more load (just as a plate accepts more load after buckling) until a load-limit point is encountered as in Figure 5-13c (for other panel geometries, the behavior after bifurcation might be as in Figure 5-14). The behavior beyond the load-limit point depends on the nature of the loading, i.e., whether load-controlled, deflection-controlled, or more general loading. Note that no 'deflection-limit point', and hence no snap-down buckling, occurs in the (correct) asymmetric response. That is, the correct load-deflection curve never bends back upon itself as does the curve of the incorrect solution in Figure 5-16. Wardle discovered the incorrectly calculated Sabir and Lock benchmark response (i.e., the missed bifucation buckling) while addressing buckling of a point-loaded, fiber-reinforced composite, circular cylindrical panel from both a theoretical and experimental standpoint. He analyzed the isotropic circular cylindrical panel of Sabir and Lock [5-48] as a simpler case of the more complex composite panel response and found that the bifurcation versus load-limit point argument is the same in both cases.

It is more than unfortunate that a long string of previous researchers did not recognize that the behavior of the circular cylindrical panel is analogous to the behavior of a simple arch. That is, the arch, if thin enough and not shallow, also bifurcates from a symmetric deformation configuration into an asymmetric deformation configuration at a lower load than at which it would achieve a load-limit point with a symmetric deformation configuration. That behavior has long been known from the classic work of Fung and Kaplan [5-54]. Timoshenko and Gere also show asymmetric deformation of an arch [5-55, p. 297]. Sabir and Lock supposedly also used their numerical approach for arches, yet made no mention of any asymmetric response of a panel after bifurcation buckling. Moreover, it is especially disturbing that no one who used the benchmark solution until Wardle thought to perform an experiment to determine the actual behavior of the circular cylindrical panel to see whether the unusual behavior in Figure 5-16 is even realized. (Johnson, Hyer, and Carper performed similar experiments on narrow fiber-reinforced composite curved panels [5-56] and found bifurcation, but were not involved in the benchmark usage). Wardle's experiments prompted him to further investigate the theoretical behavior and uncover the real behavior, namely bifurcation into an asymmetric deformation configuration with subsequent diminishing of the asymmetry of the deformation until the deformation again becomes symmetric as in Figure 5-18. There, the unrealized symmetric deformation up to its load-limit point and beyond is shown as a dashed line to emphasize that it is not realized. From both the unrealized load-limit point on the symmetric deformation curve and the realized load-limit point on the asymmetric deformation curve, it is

Éléments sous droits d'auteur

possible to have 'snap-across buckling' if the panel is loaded with load control. However, no 'snap-down buckling exists in the correct solution.

At bifurcation, the specific load-deflection behavior is difficult to perceive at the scale of Figure 5-18, so we enlarge the load-deflection response in the neighborhood of the bifurcation point in Figure 5-19. At the bifurcation point, the deformation behavior changes from symmetric response to asymmetric response, as for many, but not all, bifurcation situations (e.g., perfect bars go from straight to symmetric or asymmetric deformations depending on the boundary conditions). We observe deflection continuity and slope discontinuity at bifurcation in Figure 5-19. That is, there is no change in deflection, unlike the drastic change in deflection for a perfectly straight, axially compressed bar in Chapter Two and like the 'no change' for a perfectly flat, in-plane compressed plate in Chapter Three. Moreover, there is a small change in slope of the load-deflection response, unlike a perfect plate which has a significant change in slope and a perfect bar which has a drastic change in slope (to zero). There is no drastic change in deformation shape at bifurcation as we see in Curve B of Figure 5-20, which is analogous to the deformation behavior versus load level curve of Figure 5-17 (again, the deformation in the vertical direction is enlarged). The asymmetry is quite mild initially relative to the prebuckling symmetric deformation that still dominates the deformation shape. The major problem is establishing the bifurcation point in an analysis, and this topic is addressed shortly. For a geometrically perfect panel, bifurcation might occur with a noticeable popping noise. However, for a geometrically imperfect panel, the transition from a symmetric panel with imperfections to an asymmetric panel (with the same imperfections) typically occurs without any noise. Note that experiments performed on necessarily imperfect panels have no noise accompanying bifurcation (if, in fact, bifurcation even occurs). In contrast, any snapping-type buckling always has significant associated noise.

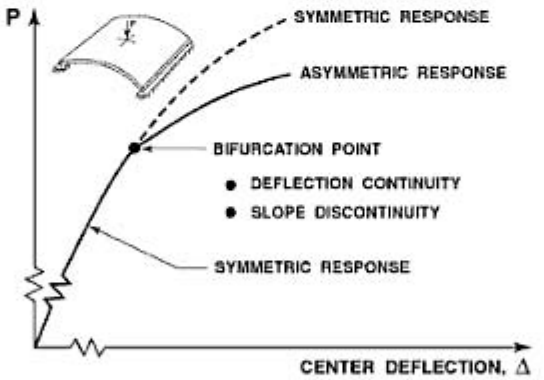


Figure 5-19 Enlarged Load-Deflection Response for the Benchmark Square Circular Cylindrical Panel in the Neighborhood of the Bifurcation Point

Éléments sous droits d'auteur

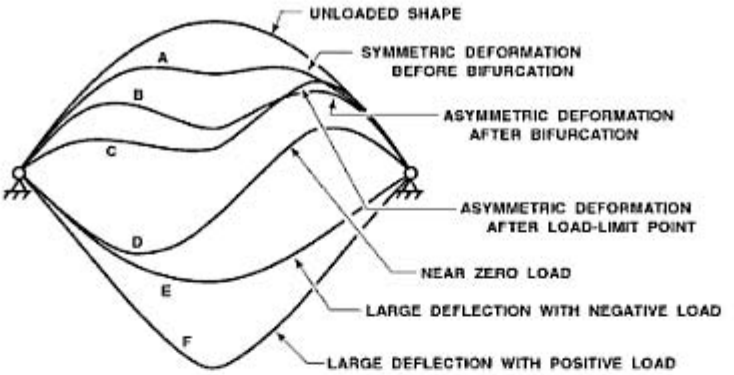


Figure 5-20 Deformations at Various Load Levels for the Benchmark Square Circular Cylindrical Panel Analyzed for Both Symmetric and Asymmetric Behavior *(After Wardle [5-51])*

The panel deformation with the (correct) asymmetric behavior analyzed takes on many different characters as the load-deflection curve is traversed. After load is applied, the initial symmetric deformation with a 'dimple' is seen (Curve A in Figure 5-20 which is identical to Curve A in Figure 5-17) until bifurcation occurs. Each curve in Figure 5-20 labeled with a letter corresponds to a point with the same letter on the load-deflection curve in Figure 5-18. After bifurcation, asymmetric deformation occurs that is similar to two buckle waves, one down and the other up, but sometimes with a 'dimple' under the load (Curve B). The deformation becomes ever more asymmetric as the load-limit point is passed and the load decreases (Curve C). Near the zero-load condition, the deformation is highly asymmetric—almost purely antisymmetric (Curve D). As the load decreases into the negative range and subsequently increases above zero, the deformation asymmetry decreases considerably (Curve E). When the load again becomes large (and positive), the deformation is again symmetric (Curve F) with substantial stretching of the now concave-upward panel as load increases. The antisymmetric deformation component of the overall deformation has simply diminished, leaving the symmetric component to dominate at large downward deflection where essentially membrane stretching occurs. Note that the asymmetric deformations shown could just as easily have happened in a manner reflected about the vertical centerline, i.e., higher waves on the left than on the right, just as a perfect vertical bar of circular cross section can buckle in any direction with equal probability.

The deformation response after bifurcation can be thought of as being composed of superimposed symmetric and antisymmetric shapes with each shape having different amplitudes at different loading stages. Thus, the asymmetric deformation after bifurcation buckling is not of a

Éléments sous droits d'auteur

constant shape as the center deflection increases. The 'degree' of asymmetry changes with load in the nonlinear deformation problem, first increasing (Curve C), next achieving near antisymmetry (near Point D represented with Curve D), then decreasing (Curve E), and finally disappearing (Curve F). That is, at large center deflections, the deformation shape is again symmetric (Curve F) because the panel is being stretched by large membrane forces and essentially behaves like a symmetric membrane (without any bending that would lead to asymmetry).

Wardle measured symmetric response of a fiber-reinforced composite circular cylindrical panel under deflection-controlled loading up to the bifurcation load and then found asymmetric response until the load decreased to zero in Figure 5-21. There, the center deflection, Δ, is normalized by the panel thickness, t. Note the similarity to the behavior in Figure 5-14. He measured center deflection and full-field deformation shapes with a non-contacting, traversing laser displacement transducer. His measured response agreed very well both qualitatively and quantitatively with the predicted behavior involving bifurcation buckling and subsequent asymmetric response calculated with the STAGS program [5-53]. The bifurcation load was indeed far lower than the composite panel equivalent of the incorrect symmetric benchmark solution calculated with STAGS. He was unable to continue measurements into the negative load regime because his load applicator could provide only downward load. His analysis and experiments (including measured deformation shapes, the presence of which establishes the bifurcation buckling experimentally because of their asymmetry) are further described in papers by Wardle, Lagace, and Tudela [5-57 and 5-50].

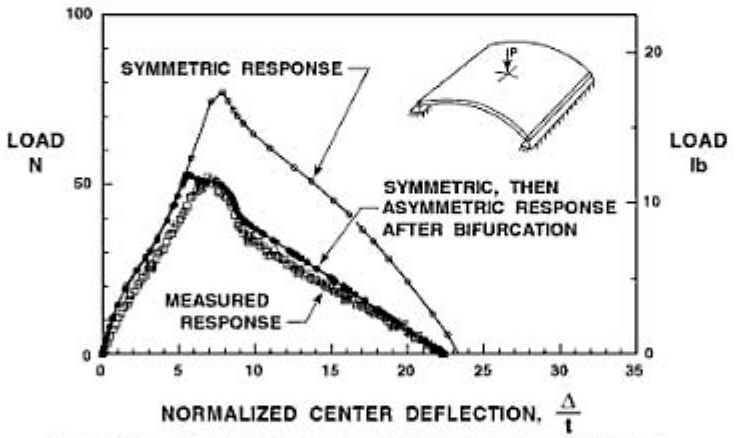


Figure 5-21 Wardle's Square Circular Cylindrical Composite Panel Analyzed for Both Symmetric and Asymmetric Behavior with Experimental Results
(After Wardle, Lagace, and Tudela [5-50])

Éléments sous droits d'auteur

5.6.5 Common Difficulties in Engineering Problem Solving

The load-deflection response in Figures 5-16, 5-18, and 5-21 and the deformations in Figures 5-17 and 5-20 were calculated with the STAGS finite element program [5-53]. A symmetric finite element model of the entire panel was analyzed to obtain the symmetric response comprising the so-called (incorrect) benchmark solution. Note that if the symmetry of the actual panel is 'built-in' to the finite element model by modeling only one half or one quarter of the panel (as was done in the benchmark solution), then the model cannot respond with any deformation that is not symmetric (unless some antisymmetry boundary condition is prescribed). Programs such as STAGS can traverse the bifurcation point and calculate the associated correct post-bifurcation response that is asymmetric about the mid-span of the panel only if (1) the full panel is modeled and (2) bifurcation is suitably triggered in some manner. (The bifurcation load and mode can be calculated with *either* a quarter-panel or full-panel finite element model *if you simply look for them!*). Such triggering is usually accomplished by introducing loading imperfections such as small moments in the load vector or geometric imperfections in the stiffness matrix. Both methods require considerable experience to perform correctly and consistently. Wardle used the conventional methods for triggering a bifurcation and also an asymmetric meshing technique (AMT) in his dissertation [5-51] (described briefly in [5-50]). In AMT, he simply put a different number of elements in the left half of the panel (when observed in the axial direction in Figure 5-15 as an arch) than in the right half. That method does not require experience (just innovation!) and leads readily to the desired (and correct) asymmetric response. All three methods are tricking STAGS (or any other numerical analysis program, e.g., a finite difference mesh could also be made asymmetric). That is, STAGS and other programs must be 'tricked' to yield the correct solution. However, the engineer must first realize that he must perform that tricking! Usually, you get only what you look for with numerical analyses. If you 'take advantage' of the original geometric symmetry of a structure by modeling it based on the lines of symmetry, then in many cases the calculated deformation is forced to be symmetric, the asymmetric deformation modes having been excluded from consideration.

The other obvious failure during the development of the incorrect benchmark problem solution is in communications. Communications can be written or oral, e.g., books, articles, email, telephone calls, conversations, etc. Books and articles are passive forms of communication. Email, telephone calls, and conversations are active forms. Of course, we are all responsible for 'searching the literature' to gain background for the problem we address. That more or less passive act is enormously enhanced by Google searches, among others. Still, the history of a problem is best sought by asking a known expert in the area for some tips or short cuts. That active act is just as valuable as Google, if not more so. In addition, trying to explain a difficulty with a problem to a colleague forces us to be more logical than we might be while 'conversing with ourself'. While trying to logically explain such a difficulty to a

Éléments sous droits d'auteur

colleague, I have often answered my own question without my colleague even responding! That result happened because I naturally tried to be more logical when talking to someone else than when 'conversing with myself'. Of course, I have more often benefited from the advice and counsel of a colleague. Never be afraid or too aloof to ask someone about a difficulty or to review your logic!

The incorrect and correct benchmark solutions to the curved panel buckling problem lead to several common difficulties in both nonlinear shell analysis and general engineering problem solving being identified:

- Not realizing that other structural problems are analogous to a problem being investigated and would therefore be helpful in understanding new problems.
- Not realizing that simple experiments, if properly conducted, can open your eyes to the real behavior of a loaded structure.
- Some numerical approaches to structures that are physically symmetric will yield only symmetric response solutions when, in fact, the response can be asymmetric. That is, just because a structure is symmetric does not mean it will respond symmetrically!
- Some numerical approaches to structural analysis must be adjusted or tricked in some manner to ensure that proper response behavior is obtained. If not tricked, some proper behavior is not necessarily predicted and might, in fact, be excluded.
- With as rich a literature as exists, it is truly hard to be familiar with all the results that are available. Hence, consulting a colleague, near or far, is often quite helpful. That is, *communications* might reveal another possible solution or pertinent experimental result. However, some engineers seem to try to 'go it alone'. Good engineers have learned to talk with those who might give them a different perspective on a problem rather than seeking out similar and/or reinforcing opinions.

5.6.6 Summary

Engineering Experience is the key factor to properly perceiving, understanding, and coping with all the common shell analysis difficulties that were identified. Indeed, those difficulties are part of the overall engineering problem-solving process. Certainly it is not possible to simply 'feed computer programs' and be assured that the proper solution to a structures problem has been obtained. Computer programs must be intelligently used as but one of many tools in the search for answers to problems. Certainly, Crose's comment ("If you don't know the answer to within 20% *without* the computer, then you're in never-never land *with* the computer") [5-44] and Martinelli's observation ("Garbage in, gospel out") [5-43] are most applicable. Martinelli's caution against blessing whatever comes out of the computer absolutely must be heeded.

In all problem-solving situations, we must expect to discuss our results with colleagues to gain perspective on the problem we address. That is, not just our difficulties in solving a problem, but the significance of what we have done. Those direct, active communications are essential in our quest for the 'correct solution' to a problem.

Éléments sous droits d'auteur

5.7 SUMMARY REMARKS

There will be times when you become overwhelmed with the numerical aspects of the solution to a buckling problem. At those times, you must never lose sight of the fundamental principles of buckling that you learned in this book for the three basic structural elements: bars, plates, and shells. Always come back to the fundamentals! When you get new results, try to discover an explanation that is consistent with the fundamentals (such as the discussion of the stiffener eccentricity effect in Section 4.7). Never merely accept numerical results without comparing them to known results. And the known results are the available classical solutions and other published results. However, be very cautious about whether the 'known results' are correct because they might not be (recall the follower force problem in Section 5.4.3 and the incorrect benchmark solution for buckling of a centrally loaded circular cylindrical panel in Section 5.6). Moreover, note the important role that experiments play in both the follower-force problem and the panel buckling problem.

CHAPTER 5 REFERENCES

5-1 J. Singer, J. Arbocz, and T. Weller, *Buckling Experiments: Experimental Methods in Buckling of Thin-Walled Structures, Volume 1, Basic Concepts, Columns, Beams and Plates*, Wiley, Chichester, England, 1998, *Volume 2, Shells, Built-up Structures and Additional Topics*, Wiley, New York, 2001.

5-2 Stephen P. Timoshenko, *History of Strength of Materials*, McGraw-Hill, New York, 1953. Reprinted by Dover Publications, New York, 1983.

5-3 Stephen P. Timoshenko, *As I Remember; the Autobiography of Stephen P. Timoshenko*, translated from Russian by Robert Addis, Van Nostrand, Princeton, New Jersey, 1968.

5-4 Theodore von Kármán with Lee Edson, *The Wind and Beyond; Theodore von Kármán, Pioneer in Aviation and Pathfinder in Space*, Little, Brown and Company, Boston, 1967.

5-5 H. L. Langhaar, General Theory of Buckling, *Applied Mechanics Reviews*, Volume 11, Number 11, November 1958, pp. 585–588.

5-6 Stephen P. Timoshenko and James M. Gere, *Theory of Elastic Stability*, 2nd Edition, McGraw-Hill, New York, 1961.

5-7 Friedrich Bleich, *Buckling Strength of Metal Structures*, McGraw-Hill, New York, 1952.

5-8 G. D. Galletly, Elastic Buckling of Complete Toroidal Shells of Revolution of Elliptical Cross-Section Subjected to Uniform Internal Pressure, *Thin-Walled Structures*, Volume 30, Numbers 1–4, 4 January 1998, pp. 23–34.

5-9 D. Bushnell, *Computerized Buckling Analysis of Shells*, Nijhoff (Kluewer), Dordrecht, The Netherlands, 1985.

5-10 Frederick J. Plantema, *Sandwich Construction - The Bending and Buckling of Sandwich Beams, Plates, and Shells*, Wiley, New York, 1966.

5-11 Howard G. Allen, *Analysis and Design of Structural Sandwich Panels*, Pergamon Press, Oxford, 1969.

5-12 *Sandwich Constructions I—Proceedings of the First International Conference on Sandwich Construction*, Stockholm, Sweden, 19–21 June 1989, edited by K-A. Olsson and R. P. Reichard, EMAS Publications, United Kingdom, 1989.

5-13 Dan Zenkert, *An Introduction to Sandwich Construction*, Engineering Materials Advisory Services, Ltd., Cradley Heath, West Midlands, England, 1995.

5-14 Jack Vinson, *The Behavior of Sandwich Structures of Isotropic and Composite Materials*, Technomic, Lancaster, Pennsylvania, 1999.

5-15 Robert M. Jones, *Mechanics of Composite Materials*, 2nd Edition, Taylor & Francis, Philadelphia, 1999.

Éléments sous droits d'auteur

5-16 J. E. Ashton and J. M. Whitney, *Theory of Laminated Plates*, Technomic, Stamford, Connecticut, 1970.
5-17 James M. Whitney, *Structural Analysis of Laminated Anisotropic Plates*, Technomic, Lancaster, Pennsylvania, 1987.
5-18 J. N. Reddy, *Mechanics of Laminated Composite Plates: Theory and Analysis*, CRC Press, Boca Raton, Florida, 1997.
5-19 Jack Vinson and Robert W. Sierakowski, *The Behavior of Structures Composed of Composite Materials*, Nijhoff, Dordrecht, The Netherlands, 1986.
5-20 Valery V. Vasiliev (Robert M. Jones, English Edition Editor), *Mechanics of Composite Structures*, Taylor & Francis, Washington, D. C., 1993.
5-21 Theodore von Kármán and Hsue-Shen Tsien, The Buckling of Thin Cylindrical Shells under Axial Compression, *Journal of the Aeronautical Sciences*, Volume 8, Number 8, June 1941, pp. 303–312.
5-22 F. R. Shanley, Inelastic Column Theory, *Journal of the Aeronautical Sciences*, Volume 14, Number 5, May 1947, pp. 261–268, including discussion by Theodore von Kármán.
5-23 N. J. Hoff, Buckling and Stability, The Forty-First Wilbur Wright Memorial Lecture, Fourth Anglo-American Aeronautical Conference, London, 14 September 1953, *Journal of the Royal Aeronautical Society*, Volume 58, Number 517, January 1954, pp. 3–52.
5-24 Hans Ziegler, *Principles of Structural Stability*, Blaisdell, Waltham, Massachusetts, 1968. 2nd Edition, Birkhauser, Basel, 1977.
5-25 Hans Ziegler, Linear Elastic Stability, *Zeitschrift für Angewandte Mathematik und Physik*, 1953, First Part, Volume IV, Number 2, pp. 89–121. Second Part, Volume IV, Number 3, pp. 167–185.
5-26 Hans Ziegler, On the Concept of Elastic Stability, *Advances in Applied Mechanics*, edited by H. L. Dryden and T. von Kármán, Volume IV, 1956, Academic Press, New York, pp. 351–403.
5-27 V. V. Bolotin, *Nonconservative Problems of the Theory of Elastic Stability*, Pergamon Press, Macmillan, New York, 1963.
5-28 Max Beck, Die Knicklast des Einseitig Eingespannten, Tangential Gedrückten Stabes, *Zeitschrift für Angewandte Mathematik und Physik*, Volume 3, No. 3, 1952, pp. 225–228. Erratum, pp. 476–477.
5-29 George Herrmann, Stability of Equilibrium of Elastic Systems Subjected to Nonconservative Forces, *Applied Mechanics Reviews*, Volume 20, Number 2, February 1967, pp. 103-108.
5-30 George Herrmann, Editor, *Dynamic Stability of Structures*, Proceedings of the International Conference on Dynamic Stability of Structures, Northwestern University, Evanston, Illinois, 18–20 October 1965, Pergamon, Oxford, 1967.
5-31 Isaac Elishakoff, Controversy Associated with the So-Called "Follower Forces": Critical Overview, *Applied Mechanics Reviews*, Volume 58, March 2005, pp. 117–142.
5-32 W. T. Koiter, Unrealistic Follower Forces, *Journal of Sound and Vibration*, Volume 194, Issue 4, 25 July 1996, pp. 636–628.
5-33 Y. Sugiyama, M. A. Langthjem, and B. -J. Ryu, Realistic Follower Forces, *Journal of Sound and Vibration*, Volume 225, Issue 4, 26 August 1998, pp. 779–782.
5-34 V. D. Potapov, *Stability of Stochastic Elastic and Viscoelastic Systems*, Wiley, Chichester, England, 1999.
5-35 Isaac Elishakoff, Yiwei Li, and James H. Starnes, Jr., *Non-Classical Problems in the Theory of Elastic Stability*, Cambridge University Press, New York, 2001.
5-36 V. V. Bolotin, *The Dynamic Stability of Elastic Systems*, Holden-Day, San Francisco, 1964.
5-37 Nicholas J. Hoff, Dynamic Stability of Structures, in *Dynamic Stability of Structures*, Edited by George Herrmann, Proceedings of the International Conference on Dynamic Stability of Structures, Northwestern University, Evanston, Illinois, 18–20 October 1965, Pergamon, Oxford, 1967, pp. 7–41.
5-38 Edward N. Lorenz, Deterministic Nonperiodic Flow, *Journal of the Atmospheric Sciences*, Volume 20, Number 2, March 1963, pp. 130–141.
5-39 James Gleick, *Chaos: Making a New Science*, Viking Penguin, New York, 1987.
5-40 Robert Gilmore, *Catastrophe Theory for Scientists and Engineers*, John Wiley & Sons, New York, 1981. Reprinted by Dover Publications, New York, 1993.

Éléments sous droits d'auteur

5-41 M. S. El Naschie, *Stress, Stability, and Chaos in Structural Engineering: An Energy Approach*, McGraw-Hill, London, 1990.
5-42 *NASTRAN User's Manual*, NASA SP-222(08), Volume 2, National Aeronautics and Space Administration, Washington, D. C., June 1986.
5-43 Jack Martinelli, personal communication, May 1984.
5-44 James G. Crose, personal communication, May 1987.
5-45 Robert M. Jones, Effective Development, Documentation, and Distribution of Computer Programs, *Computers & Structures*, Volume 2, Issues 5-6, December 1972, pp. 1089–1095.
5-46 Charles Rankin, response to question during the 43rd AIAA/ASME/ASCE/AHS/ASC Structures, Structural Dynamics, and Materials Conference, Denver, Colorado, 23 April 2002.
5-47 Satchi Venkataraman and Raphael T. Haftka, Structural Optimization: What Has Moore's Law Done For Us? *Proceedings of the 43rd AIAA/ASME/ASCE/AHS/ASC Structures, Structural Dynamics, and Materials Conference*, 22–25 April 2002, Denver, Colorado, AIAA Paper No. 2002-1342, AIAA, Reston, Virginia.
5-48 A. B. Sabir and A. C. Lock, The Application of Finite Elements to the Large Deflection Geometrically Non-linear Behaviour of Cylindrical Shells, In *Variational Methods in Engineering: Proceedings of an International Conference*, edited by C. A. Brebbia and H. Tottenham, 25 September 1972. Volume 2, Southhampton University Press, Surrey, United Kingdom, 1973, pp. 7/66–7/75.
5-49 Brian L. Wardle, The Incorrect Benchmark Shell Buckling Solution, *Proceedings of the 47th AIAA/ASME/ASCE/AHS/ASC Structures, Structural Dynamics, and Materials Conference*, 1–4 May 2006, Newport, Rhode Island, AIAA Paper No. 2006-2026, AIAA, Reston, Virginia.
5-50 Brian L. Wardle, Paul A. Lagace, and Mark A. Tudela, Buckling Response of Transversely Loaded Composite Shells, Part II: Numerical Analysis, *AIAA Journal*, Volume 42, Number 7, July 2004, pp. 1465–1473.
5-51 Brian L. Wardle, *Buckling and Damage Resistance of Transversely-Loaded Composite Shells*, Ph. D. Dissertation, Technology Laboratory for Advanced Composites, TELAC Report 98-7, Department of Aeronautics and Astronautics, Massachusetts Institute of Technology, Cambridge, Massachusetts, June 1998.
5-52 E. Riks, Some Computational Aspects of the Stability Analysis of Nonlinear Structures, *Computer Methods in Applied Mechanics and Engineering*, Volume 47, Number 3, December 1984, pp. 219–259.
5-53 Charles C. Rankin, Frank A. Brogan, William A. Loden, and Harold D. Cabiness, *STAGS Users Manual, Version 5.0*, Report LMSC P032594, Lockheed-Martin Missiles & Space Co., Inc., Advanced Technology Center, Palo Alto, California, March 2003.
5-54 Y. C. Fung and A. Kaplan, *Buckling of Low Arches or Curved Beams of Small Curvature*, NACA TN 2840, National Advisory Committee for Aeronautics, Washington, D. C., November 1952.
5-55 Stephen P. Timoshenko and James M. Gere, *Theory of Elastic Stability*, Second Edition, McGraw-Hill, New York, 1961, p. 297.
5-56 Eric R. Johnson, Michael W. Hyer, and Douglas M. Carper, Response of Composite Material Shallow Arch to Concentrated Load, *AIAA Journal*, Volume 23, Number 6, June 1985, pp. 529–536.
5-57 Mark A. Tudela, Paul A. Lagace, and Brian L. Wardle, Buckling Response of Transversely Loaded Composite Shells, Part I: Experiments, *AIAA Journal*, Volume 42, Number 7, July 2004, pp. 1457–1464.

Éléments sous droits d'auteur

Appendix A

MAXIMA AND MINIMA OF FUNCTIONS OF A SINGLE VARIABLE

Most engineering students are well aware that the first derivative of a continuous function is zero at a maximum or minimum of the function. Fewer recall that the sign of the second derivative signifies whether the stationary value determined by a zero first derivative is a maximum or a minimum. Even fewer are aware of what to do if the second derivative happens to be zero. Thus, this appendix is presented to put finding relative maxima and minima of a function on a firm foundation.

Consider a function V of a single variable x, V(x), for which a stationary value occurs at the ith value of x, $x = x_i$, i.e.,

$$\left.\frac{dV}{dx}\right|_{x=x_i} = 0 \qquad \text{(A.1)}$$

Such a stationary value of V can be a relative maximum, a relative minimum, a neutral point, or an inflection point as shown in Figure A-1. There, Equation (A.1) is satisfied at points i = 1, 2, 3, 4, and 5. By inspection, the function V(x) has a relative minimum at points 1 and 4, a relative maximum at point 3, and an inflection point at point 2. Also shown in Figure A-1 at position 5 is a succession of neutral points for which all derivatives of V(x) vanish. A simple physical example of such stationary values is a bead on a wire shaped as in Figure A-1. That is, a minimum of V(x) (the total potential energy of the bead) corresponds to stable equilibrium, a maximum or inflection point to unstable equilibrium, and a neutral point to neutral equilibrium.

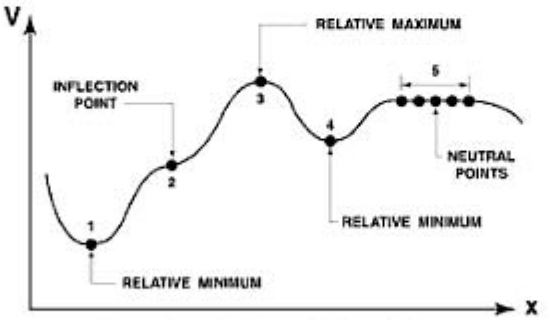


Figure A-1 Stationary Values of V(x)

Éléments sous droits d'auteur

To determine the specific character of a stationary point, first expand V(x) in a Taylor series about the stationary point $x = x_1$:

$$V(x_1 + h) = V(x_1) + h \left.\frac{dV}{dx}\right|_{x=x_1} + \frac{h^2}{2!} \left.\frac{d^2V}{dx^2}\right|_{x=x_1} + \frac{h^3}{3!} \left.\frac{d^3V}{dx^3}\right|_{x=x_1} + \cdots \quad \text{(A.2)}$$

in which h is the expansion parameter about x_1, as shown in Figure A-2.

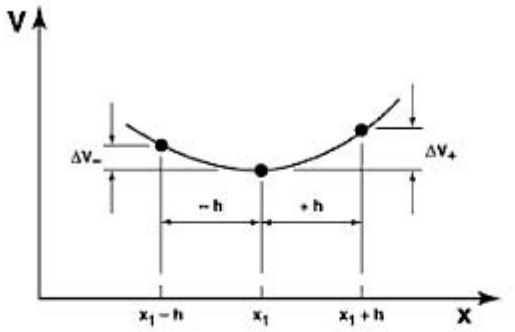


Figure A-2 Taylor Series Expansion of V(x) about $x = x_1$

Then, the change in V, ΔV, is

$$\Delta V = h \left.\frac{dV}{dx}\right|_{x=x_1} + \frac{h^2}{2!} \left.\frac{d^2V}{dx^2}\right|_{x=x_1} + \frac{h^3}{3!} \left.\frac{d^3V}{dx^3}\right|_{x=x_1} + \cdots \quad \text{(A.3)}$$

However, in accordance with the definition of a stationary point, Equation (A.1), the first term in Equation (A.3) for ΔV vanishes irrespective of the value or size of h so that

$$\Delta V = \frac{h^2}{2!} \left.\frac{d^2V}{dx^2}\right|_{x=x_1} + \frac{h^3}{3!} \left.\frac{d^3V}{dx^3}\right|_{x=x_1} + \frac{h^4}{4!} \left.\frac{d^4V}{dx^4}\right|_{x=x_1} + \cdots \quad \text{(A.4)}$$

The character of ΔV will determine the type of stationary value at $x = x_1$. Specifically, the dominant term in the Taylor series for ΔV must be examined in order to determine whether ΔV is always positive (a relative minimum), always negative (a relative maximum), sometimes negative and sometimes positive (an inflection point), or always zero (a neutral point). For ΔV to be positive, the leading term in the Taylor series, Equation (A.4), which is by inspection the largest term because h is a very small number, must be positive, i.e.,

$$\frac{h^2}{2!} \left.\frac{d^2V}{dx^2}\right|_{x=x_1} > 0 \quad \text{(A.5)}$$

Éléments sous droits d'auteur

But, even though h can have positive or negative values, because h is squared,

$$\left.\frac{d^2V}{dx^2}\right|_{x=x_1} > 0 \tag{A.6}$$

is sufficient for a minimum of V(x) at $x = x_1$. Similar reasoning leads to

$$\left.\frac{d^2V}{dx^2}\right|_{x=x_1} < 0 \tag{A.7}$$

as sufficient for a maximum of V(x) at $x = x_1$. However, if

$$\left.\frac{d^2V}{dx^2}\right|_{x=x_1} = 0 \tag{A.8}$$

then the second-derivative term in the Taylor series is no longer the dominant term.

Accordingly, the next term in the Taylor series

$$\left.\frac{h^3}{3!}\frac{d^3V}{dx^3}\right|_{x=x_1} \tag{A.9}$$

must be examined. Obviously, because h can have positive or negative values and is cubed, the term in Equation (A.9) can be positive or negative irrespective of the (nonzero) value of the third derivative. Thus, a nonzero third derivative of V(x) at $x = x_1$ corresponds to an inflection point of V(x) because ΔV can be either positive or negative.

If the term involving the third derivative, Equation (A.9) in the Taylor series, is zero, then the next higher term

$$\left.\frac{h^4}{4!}\frac{d^4V}{dx^4}\right|_{x=x_1} \tag{A.10}$$

is the dominant term. Of course, the second derivative must also be zero in order for us to need to consider the third-derivative term at all. Obviously, the conclusions reached for the second-derivative term are also valid for the fourth-derivative term, Equation (A.10).

Thus, by mathematical induction, the rules for determining the character of a stationary value of V(x) at $x = x_1$ are

(1) If the first nonzero derivative evaluated at $x = x_1$ is even and greater than zero, then $V(x_1)$ is a relative minimum.
(2) If the first nonzero derivative evaluated at $x = x_1$ is even and less than zero, then $V(x_1)$ is a relative maximum.
(3) If the first nonzero derivative evaluated at $x = x_1$ is odd, then $V(x_1)$ is an inflection point.
(4) If all derivatives are zero, then $V(x_1)$ is a neutral point.

These rules are schematically depicted in Figure A-3.

Éléments sous droits d'auteur

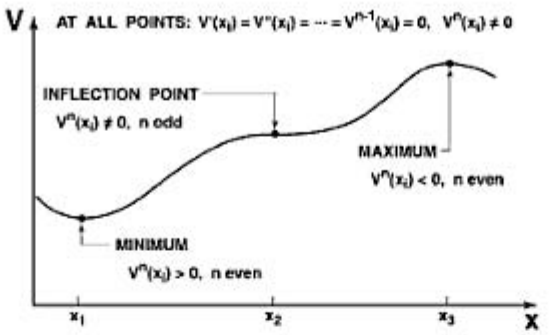


Figure A-3 Maxima, Minima, and Inflection Points of a Function of a Single Variable

The following simple examples are useful aids to understanding the foregoing rules.

(1) $V = x^2$ (plotted in Figure A-4)

$V' = 2x$

$V' = 0$ at $x = 0$

$V''\Big|_{x=0} = 2$

$\therefore$ V(0) is a relative minimum

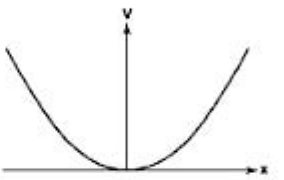


Figure A-4 $V = x^2$

(2) $V = x^3$ (plotted in Figure A-5)

$V' = 3x^2$

$V' = 0$ at $x = 0$

$V''\Big|_{x=0} = 6x\Big|_{x=0} = 0$

$V'''\Big|_{x=0} = 6$

$\therefore$ V(0) is an inflection point

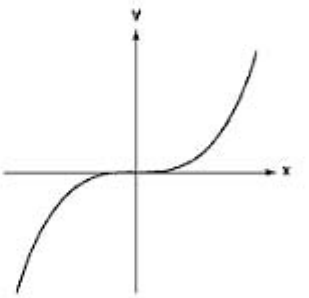


Figure A-5 $V = x^3$

Éléments sous droits d'auteur

(3) $V = x^4$ (plotted in Figure A-6)

$V' = 4x^3$

$V' = 0$ at $x = 0$

$V''\Big|_{x=0} = 12x^2\Big|_{x=0} = 0$

$V'''\Big|_{x=0} = 24x\Big|_{x=0} = 0$

$V''''\Big|_{x=0} = 24$

$\therefore$ V(0) is a minimum

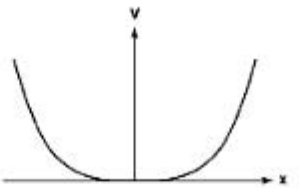


Figure A-6 $V = x^4$

(4) $V = x^{10}$ (plotted in Figure A-7)

$V' = 10x^9$

$V' = 0$ at $x = 0$

By mathematical induction,

$V''\Big|_{x=0} = 0$

$\vdots$

$V^{IX}\Big|_{x=0} = 0$

$V^{X}\Big|_{x=0} = 10!$

$\therefore$ V(0) is a minimum

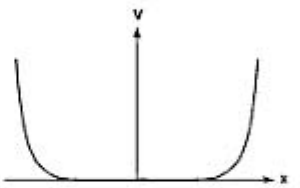


Figure A-7 $V = x^{10}$

If V is a function of more than one variable, then more complex criteria for determining maxima and minima are obtained. Generally, but not always, the second partial derivatives of the function with respect to all its variables are sufficient to determine the character of a stationary value of V. For such functions, the theory of quadratic forms as described by Langhaar [A-1] should be examined.

APPENDIX A REFERENCE

A-1 Henry L. Langhaar, *Energy Methods in Applied Mechanics*, Wiley, New York, 1962, pp. 308–328. (Also Krieger Publishing, Malabar, Florida, 1982.)

Éléments sous droits d'auteur

Appendix B

ABSOLUTE MINIMUM OF A FUNCTION OF TWO INTEGER VARIABLES

Consider a function λ of two variables m and n

$$\lambda = \lambda(m, n) \tag{B.1}$$

for which we seek the minimum. The quantity λ is just a name, in this case, for an eigenvalue (buckling load) that we seek. We could use differential calculus to find a minimum of the function in Equation (B.1), but that use would inherently presume that λ is a continuous function of m and n. Unfortunately, λ is a top.continuous function function of only integer values of m and n, so differential calculus cannot be employed. That is, the number of buckle half-waves in each of the x- and y-directions, m and n, can only be an integer and satisfy the boundary conditions at the edges of the plate or, for a shell, at the edges and in the circumferential direction (for continuity). Thus, we must use a technique suited to that condition of integer values of m and n.

The application of the title problem in buckling is to determine the minimum buckling load for a plate or shell from the general expression

$$\lambda = T_{33} + T_{ij}(m, n, a, b) \tag{B.2}$$

in which the T_{ij} are functions of the buckle mode shape numbers m and n, the number of buckle waves in the x and y directions, respectively. The buckle mode shape for a plate with m = 2 and n = 1 is shown in Figure B-1. Obviously, m = 2.5 is not physically possible.

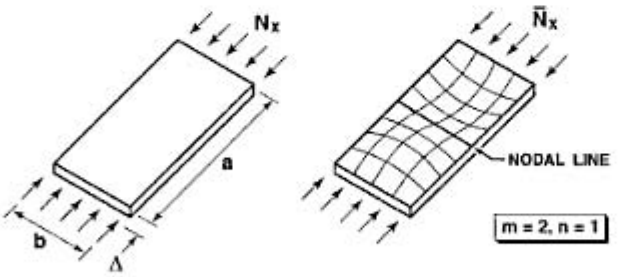


Figure B-1 In-Plane Loaded Plate Before Buckling and Typical Buckling Mode

Éléments sous droits d'auteur

Because T_{11}, T_{12}, and T_{22} are functions of both m and n, no simple conclusion can be drawn about the value of n at buckling as could be done for ordinary isotropic plates for which n was determined to be one. Instead, Equation (B.2) is a complicated function of both m and n that generally does not achieve a minimum for m = 1 and n = 1.

If the number of buckle waves is quite large, λ can be treated as a continuous function of m and the minimum of λ is obtained from the stationary value condition of differential calculus

$$\frac{\partial \lambda}{\partial m} = 0 \tag{B.3}$$

subject to the condition for a minimum that

$$\left.\frac{\partial^2 \lambda}{\partial m^2}\right|_{\frac{\partial \lambda}{\partial m}=0} > 0 \tag{B.4}$$

If m and n are small, the minimum λ must be found for *discrete* (integer) values of m. The following reasoning is offered in support of the preceding contention. Consider a hypothetical plot of λ versus m in which λ has values only at integer values of m in Figure B-2. Actually, $\lambda = \sigma_{f_{cr}}$ is the buckling stress of a fiber that is embedded in a surrounding matrix material that provides lateral support to the fiber, hence forces high buckling mode numbers. Strictly speaking, there must be an integer number of buckle half waves to satisfy fiber or bar end conditions. The buckling load for the indicated lowest minimum at m = 2.7 does not physically exist and deviates substantially in value from the physical minimum at m = 3 because the mode number is squared in the buckling expression. However, the buckling load for the second minimum at m = 37.5, although it does not physically exist, is a reasonably close approximation to the actual minimum because the percentage difference between the buckling load for m = 37.5 and that for m = 37 or 38 is negligible. The physical problem for which this rather surprising result occurs is described by Jones [B-1] who points to significant experimental evidence by Dow and Rosen [B-2] that such large numbers of buckle waves do actually occur.

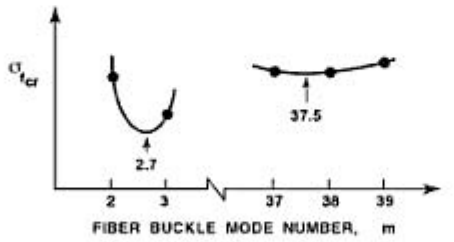


Figure B-2 Hypothetical Relative Minima of $\sigma_{f_{cr}}$

Éléments sous droits d'auteur

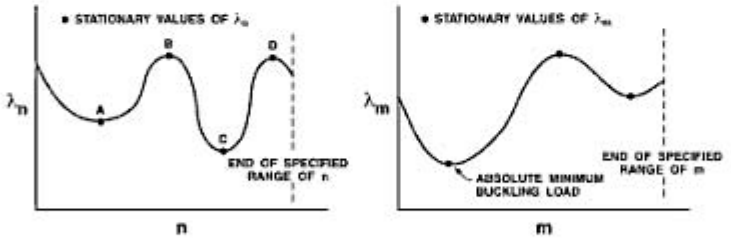
We have already seen that plates buckle with a small number of buckles (just not necessarily m = 1 and n = 1). Consequently, the lowest buckling load must be found in Equation (B.2) by a searching procedure due to Jones involving *integer* values of m and n [B-1] and *not* by equating to zero the first partial derivatives of $\bar{N}_x$ with respect to m and n (stationarization by differential calculus).

One of the major complications in the plate or shell buckling solution is the need to investigate the influence of buckle mode shape on the buckling load itself. That is, the plate or shell buckling load in Equation (B.2) is a function of the buckling mode shape parameters m and n as well as the laminated plate or shell wall stiffnesses. In contrast, the bar buckling load can, of course, be expressed in terms of the buckle mode shape parameter m, i.e.,

$$\bar{P} = m^2 \pi^2 \frac{EI}{L^2} \tag{B.5}$$

However, because we are usually interested only in the lowest buckling load for a bar, m is always one and never noninteger. For plates and shells, both m and n enter the buckling equation as well as the plate aspect ratio, a/b, or an equivalent shell parameter in a complex manner, so the lowest buckling load does not typically occur for m = 1 and n = 1. Thus, we must find the absolute minimum of the values of the buckling load, $\bar{N}_x$, or more generally, λ, for a potentially wide range of m and n values.

First, the relative minima of λ for a series of fixed values of m are found by varying n over a prescribed range, as in Figure B-3a. The absolute minima of the λ for each value of m are then compared to find the absolute minimum λ for all m and n in Figure B-3b. The actual buckling load versus m and n space is a three-dimensional space with m and n as two horizontal axes and the buckling load as the vertical axis. We slice through the three-space parallel to the m-axis to get Figure B-3a. Then, we slice through the three-space parallel to the n-axis to get Figure B-3b. We treat each slice separately in a two-dimensional sense rather than trying to approach the three-dimensional problem all at once. The



a Values of λ for Each Value of n when m is Fixed

b Absolute Minimum Values of λ_m for Each Value of m

Figure B-3 Determination of the Absolute Minimum Buckling Load

Éléments sous droits d'auteur

aforementioned procedure of searching for an absolute minimum λ for discrete values of m and n is necessary because of the possibility of more than one relative minimum for plates as in Figure B-3b. In such cases, the ordinary procedures of determining a stationary value of λ by differentiating λ with respect to m and n and equating the results to zero are both totally inadequate and misleading. Those procedures depend on the buckling load being a continuous function of m and n, and obviously that function is not continuous. Moreover, more than one minimum of λ can occur.

The sign of the second derivative of λ with respect to m and n must be examined in order to determine whether a minimum, maximum, or inflection point is obtained by the stationary value procedure that many erroneously call 'minimization.' Actually, the determination of such derivatives and the associated logic for selection of the absolute minimum would result in noninteger values of m and n that are physically unrealistic (incompatible with the plate or shell boundary conditions) and indeed impossible. Moreover, that inappropriate procedure would take about the same computational effort as the present more-suitable procedure.

The present search procedure obviates the need for determining any derivatives of λ, but is subject to the limitation that a sufficiently wide range of values of m and n must be prescribed before starting the solution. Otherwise, the absolute minimum λ can be missed, i.e., the prescribed range of values of m and n must include the values for the true absolute minimum and cannot be truncated below that range without overestimating the buckling load. Two factors ease the difficulty in deciding on the range of values of m and n to be investigated: (1) practical experience and (2) behavior such as a decreasing λ as the end of a range of n (or m) is approached as in Figure B-3a is noted by the computer program developed by Jones [B-3]. A message is printed that the range of n (or m) should be increased to see if a lower λ is found. Such a procedure is obviously not infallible. For example, if the range of n investigated stopped after C but before D in Figure B-3a, no message would be printed, whereas the minimum after D could be lower than the minimum at C. Practical experience with this computational aid should lead to reasonable assurance that no relative minimum that might be the absolute minimum is missed.

The following FORTRAN subroutine, MINIMA, is used to find the absolute minimum buckling load within a prescribed range of m and n. The type font has proportional letters, so the columns do not line up vertically as is so important for FORTRAN. In the terminology of a computer program, the number n is varied in an inner FORTRAN DO loop for a fixed m until all relative minima of the buckling load are found within a given range of values of n in the manner of Jones [B-3]. The number m is then varied in an outer DO loop so that all relative minima are found. Finally, the absolute minimum buckling load is selected from the collection of relative minima. Note that many variables are passed to and from the subroutine in the COMMON statement. Also, the largest range of 100 relative minima should be more than sufficient. See Jones [B-4] for an implementation of the essence of MINIMA in a buckling problem.

Éléments sous droits d'auteur

```
      SUBROUTINE MINIMA(ORDN)
C*****************************************************************
C  THE RELATIVE MINIMA AND ABSOLUTE MINIMUM EIGENVALUES ARE DETERMINED
C*****************************************************************
C  COMMON STATEMENT
C*****************************************************************
      COMMON M,MI,MF,MINCNT,N,NF,MABS,ABSMIN,NABS,AMOFM1,ORDNM1,ORDNM2,
     1MREL(100),RELMIN(100),NREL(100),NI,NOLD
C*****************************************************************
C  FORMAT STATEMENTS
C*****************************************************************
 1000 FORMAT(//38H *** EQUAL OR NEAR EQUAL ORDINATES ***/10XI4,8H ORDNM1=
     1E16.8,10XI4/10XI4,8H   ORDN=E16.8,10XI4//)
 1001 FORMAT(//93H *** THE ORDINATE IS DECREASING SO THE RANGE ON N IS I
     1NSUFFICIENT TO DETERMINE ALL MINIMA ***//10X,31H THE RELATIVE MINI
     2MA SO FAR ARE//20X,1HM,10X,3HORD,10X,1HN)
 1002 FORMAT(18XI3,3XE17.8,5XI3)
 1003 FORMAT(//110H *** THE RELATIVE MINIMA ARE DECREASING SO THE RANGE
     1ON M IS INSUFFICIENT TO DETERMINE AN ABSOLUTE MINIMUM ***//)
 1004 FORMAT(//43H *** NO RELATIVE MINIMA HAVE BEEN FOUND ***//)
C*****************************************************************
C  TEST FOR CHANGE OF SIGN OF ORDN
C*****************************************************************
      IF(ORDNM1.GT.0..AND.ORDN.GT.0.) GO TO 100
C
C  SKIP ORDN IF NEGATIVE FOR N = NI
C
      IF(N.EQ.NI) GO TO 150
C
C SAVE THE SOLE POSITIVE VALUE OF ORDN
C
      IF(N.EQ.2.AND.ORDNM1.NE..8E+35) GO TO 130
      IF(N.EQ.NI+1.AND.ORDNM1.NE..8E+35) GO TO 130
C
C  SKIP THE ARTIFICIAL ORDNM1
C
      IF(N.EQ.2.AND.ORDNM1.EQ..8E+35) GO TO 150
      IF(N.EQ.NI+1.AND.ORDNM1.EQ..8E+35) GO TO 150
C
C  SAVE THE LAST POSITIVE VALUE OF ORDN IF ORDN IS DECREASING
C
      IF(ORDNM2.GT.ORDNM1) GO TO 130
C
C  SKIP ALL REMAINING NEGATIVE VALUES OF ORDN
C
      GO TO 150
C*****************************************************************
C  BEGIN TEST FOR RELATIVE MINIMA AND ABSOLUTE MINIMUM
C*****************************************************************
C
C  ORDNM1 IS THE ORDINATE AT ABSCISSA N-1
C  ORDNM2 IS THE ORDINATE AT ABSCISSA N-2
C
C  TEST FOR EQUAL OR NEAR EQUAL ORDINATES
C
  100 IF(ABS(2.*(ORDN-ORDNM1)/(ORDN+ORDNM1)).GT..1E-4) GO TO 110
C
C  ORDINATES ARE CLOSE ENOUGH TO CAUSE TROUBLE IN RELATIVE MINIMA SEARCH
C
      NM1=NOLD
      WRITE(6,1000) M,ORDNM1,NM1,M,ORDN,N
      GO TO 150
C
C  TEST TO SEE WHETHER ORDN IS INCREASING OR DECREASING
C
  110 IF(ORDN.GT.ORDNM1) GO TO 120
C
C  ORDN DECREASING
C
```

Éléments sous droits d'auteur

```
      IF(N.NE.NF) GO TO 150
      IF(MINCNT.EQ.0) WRITE(6,1004)
      WRITE(6,1001)
      WRITE(6,1002) (MREL(I),RELMIN(I),NREL(I),I=1,MINCNT)
      RETURN
C
C  ORDN INCREASING
C
  120 IF(ORDNM2.GT.ORDNM1) GO TO 130
C
C  NO RELATIVE MINIMUM
C
      GO TO 150
C*****************************************************************
C  TEST FOR ABSOLUTE MINIMUM
C*****************************************************************
C
C  AMOFM1 IS THE ABSOLUTE MINIMUM VALUE OF ORDN IN THE MF-1 LOOP
C
  130 IF(M.EQ.MF-1.AND.ORDNM1.LT.AMOFM1) AMOFM1=ORDNM1
      IF(M.EQ.MF.AND.MI.NE.MF.AND.ORDNM1.LT.AMOFM1) WRITE(6,1003)
      IF(ORDNM1.GT.ABSMIN) GO TO 140
C
C  NEW ABSOLUTE MINIMUM FOUND
C
      ABSMIN=ORDNM1
      MABS=M
      NABS=NOLD
C
C  STORE ALL RELATIVE MINIMA
C
  140 MINCNT=MINCNT+1
      MREL(MINCNT)=M
      RELMIN(MINCNT)=ORDNM1
      NREL(MINCNT)=NOLD
C
  150 ORDNM2=ORDNM1
      IF(ORDN.GT.0.) ORDNM1=ORDN
      IF(ORDN.GT.0.) NOLD=N
      RETURN
      END
```

APPENDIX B REFERENCES

B-1 Robert M. Jones, *Mechanics of Composite Materials*, 2nd Edition, Taylor & Francis, Philadelphia, 1999.

B-2 Norris F. Dow and B. Walter Rosen, *Evaluations of Filament-Reinforced Composites for Aerospace Structural Applications*, NASA Contractor Report CR-31, National Aeronautics and Space Administration, Washington, D. C., April 1964.

B-3 Robert M. Jones, Plastic Buckling of Eccentrically Stiffened Multilayered Circular Cylindrical Shells, *AIAA Journal*, Volume 8, Number 2, February 1970, pp. 262–270.

B-4 Robert M. Jones, *Plastic Buckling of Eccentrically Stiffened Multilayered Circular Cylindrical Shells*, Technical Report TR-0200(S4816-75)-1, February 1969, The Aerospace Corporation, San Bernardino, California, available only from the Clearinghouse CFSTI, United States Department of Commerce.

Éléments sous droits d'auteur

Appendix C

BEHAVIOR OF FIBER-REINFORCED LAMINATED COMPOSITE MATERIALS AND STRUCTURAL ELEMENTS

C.1 INTRODUCTION

Fiber-reinforced laminated composite materials are the high-profile structural efficiency phenomenon of the 1960s through the 1990s, and their applications will continue to grow with time. These structural materials are defined, laminae (layers of material) through laminates, and their advantages related to structural efficiencies and other design advantages are described. Then, we focus on laminate behavior with the basic questions of laminate analysis in Figure C-1 being (1) what are the conditions that a collection of laminae must meet in order to be considered a laminate? and (2) how, i.e., in what deformation modes, will a laminate respond to loading with imposed forces and moments?

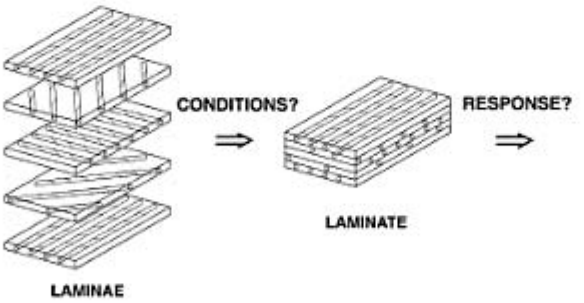
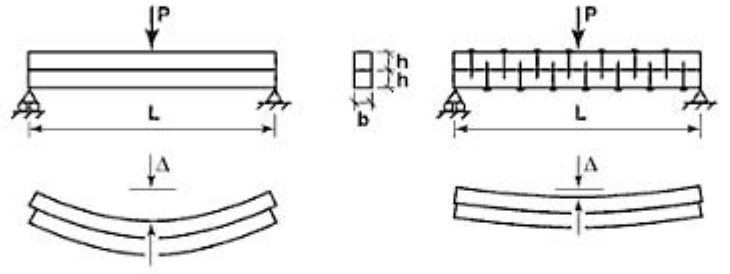


Figure C-1 The Basic Questions of Laminate Analysis

Éléments sous droits d'auteur

The combination of high-stiffness, high-strength fibers with low-weight matrix materials leads to laminated composite materials with directionally oriented properties of extraordinary structural efficiency. That efficiency depends on how we construct a laminate. A laminate is two or more laminae (layers) bonded together to act as an integral structural element as in Figure C-1. The reason laminae are combined to create a laminate is to achieve the largest possible bending stiffness for the materials used. Recall the 'two-beam' problem from basic mechanics of materials. First, consider the two beams as not fastened together and loaded at midspan by a concentrated force as in Figure C-2a. In contrast, the same two beams could be fastened together by nails, screws, or bonding as in Figure C-2b. The deflection is less for the bonded beams than the unbonded beams by a factor of four! Thus, bonding laminae together results in a large increase in bending resistance that compells their use.



$$\Delta = \frac{PL^3}{48EI} = \frac{PL^3}{48E(2)\frac{1}{12}bh^3} = \frac{PL^3}{8Ebh^3} \qquad \Delta = \frac{PL^3}{48EI} = \frac{PL^3}{48E\frac{1}{12}b(2h)^3} = \frac{PL^3}{32Ebh^3}$$

$$\Delta_{unbonded} = 4\Delta_{bonded}$$

a Unbonded Beams b Bonded Beams

Figure C-2 Reason for Lamination: The Two-Beam Problem

To describe laminae and laminates, we use the concept of principal material directions (PMD), i.e., directions that are parallel to the intersections of the three orthogonal planes of material property symmetry of an orthotropic material (the most complex state of the usual lamina). More complicated materials have less symmetry, if any. Isotropic materials have an infinite number of planes of material property symmetry. Principal material coordinates (PMC) are the set of axes in the principal material directions. The various laminae of a laminate are oriented with (local) principal material directions at different angles to the global laminate axes to produce a structural element capable of resisting load in several directions. The stiffnesses of such a composite material structural configuration are obtained from the properties of the constituent laminae by procedures derived in this appendix. Those procedures enable analysis of laminates that have individual laminae with principal material directions oriented at arbitrary angles to the global laminate axes.

Éléments sous droits d'auteur

The stiffness characteristics of laminated plates and shells must be known in order to determine their buckling loads. Thus, we develop laminate stiffnesses in a multi-step procedure. First, we define a composite material, a lamina, and a laminate, and then we discuss the structural efficiency advantages of laminates in Section C.2. Next, we address an anisotropic body and an orthotropic body in Section C.3. Then, we analyze the stress-strain relations for an orthotropic lamina under plane stress (the usual loading for a lamina) in principal (characteristic) material directions in Section C.4. Next, we determine the stress-strain relations for an orthotropic lamina in non-principal material directions in Section C.5. Then, we develop the laminate stiffnesses via Classical Lamination Theory in Section C.6. Finally, we learn from a collection of special cases what to expect from loading a laminate in Section C.7. For a far more comprehensive and informative treatment of the subject, please consult the author's *Mechanics of Composite Materials* [C-1].

C.2 LAMINATED FIBER-REINFORCED COMPOSITE MATERIALS

C.2.1 Introduction

The word *composite* in the term *composite material* signifies that two or more materials are combined on a macroscopic scale to form a useful third material. The fundamental advantage of composite materials is that, if well designed, they usually exhibit the best qualities of their constituents and often some qualities that neither constituent possesses. Some of the properties that can be improved by forming a composite material are listed in Figure C-3. Naturally, *not all of these properties are improved at the same time nor is there usually any requirement to do so.* In fact, some of the properties are in conflict with one another, e.g., thermal insulation versus thermal conductivity. The *objective* is merely to create a material that has only the characteristics needed to perform the design task at hand with due consideration given to project cost.

- strength
- stiffness
- corrosion resistance
- wear resistance
- appearance
- weight
- fatigue life
- temperature-dependent behavior
- thermal insulation
- thermal conductivity
- acoustical insulation
- acoustical conductivity

Figure C-3 Material Properties of Interest

We specialize our attention in this appendix to layered or laminated fiber-reinforced composite materials among all the other forms of composite materials that exist such as reinforced concrete which consists of gravel, sand, cement, water, and reinforcing bars. The basic terminology of fiber-reinforced composite laminates will be introduced in this section. For a lamina, the configurations and functions of the constituent materials, the fibers and matrix, will be described. Next, a laminate is defined. Finally, some of the advantages of fiber-reinforced composite laminates are discussed.

Éléments sous droits d'auteur

C.2.2 Laminae

The basic building block of a laminate is a *lamina* which is a flat (although sometimes curved as in a shell) arrangement of unidirectional fibers or woven fibers in a matrix. Two typical flat laminae along with their principal material axes that are parallel and perpendicular to the fiber direction are shown in Figure C-4. The fibers have a high length-to-diameter ratio as well as near crystal-sized diameter. The fibers are often special high-strength and high-stiffness materials such as carbon or graphite, boron, plus special glasses, and aramids. The fibers are the principal reinforcing or load-carrying agent and are typically strong and stiff. The matrix can be organic, metallic, ceramic, or carbon. Often, the matrix is a low-density polymer such as epoxy. Metals are used as matrix material for higher temperature applications that epoxies can tolerate. The function of the matrix is to support and protect the fibers and to distribute load among, and transmit load between, the fibers (especially when, as so often happens, one or more fibers break).

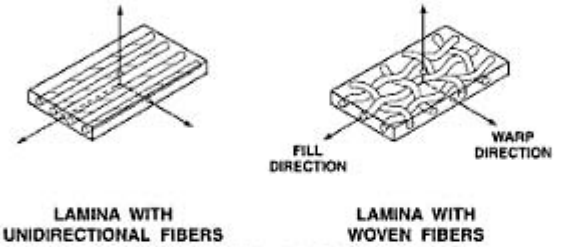


Figure C-4 Two Principal Types of Laminae

C.2.3 Laminates

A *laminate* is a bonded stack of laminae with various orientations of principal material directions in the laminae as in Figure C-1 where both unbonded laminae and a (bonded) laminate are depicted. Note that the fiber orientations of the various layers in Figure C-1 are not symmetric about the middle surface of the laminate. The layers of a laminate are usually bonded together by the same matrix material that is used in the individual laminae. That is, some of the matrix material in a lamina coats the surfaces of a lamina and is used to bond each lamina to its adjacent laminae without the addition of more matrix material. Laminates can be composed of layers of different materials or, in the present context, fiber-reinforced laminae. A laminated circular cylindrical shell can be made by winding resin-coated fibers on a removable core structure called a mandrel first with one orientation to the shell axis, then another, and so on until the desired thickness is achieved.

A major purpose of lamination is to tailor the directional dependence of strength and stiffness of a composite structure to match the usually directional nature of the loading environment on the structural element. Laminates are uniquely suited to this objective because the principal ma-

Éléments sous droits d'auteur

terial directions of each layer can be oriented according to design need. For example, the five layers of the laminate in Figure C-1 are two in the 0° direction, one at 90°, and one each at – 45° and at + 45°. We will see that such a laminate has its highest bending stiffness in the 0° direction. Moreover, the laminae are not arranged symmetrically about the middle surface of the laminate, so the stiffnesses have coupling between bending and extension, and we will discuss that interesting phenomenon later.

C.2.4 Advantages of Laminates

Consider the very high strength and stiffness advantages of fiber-reinforced composite materials. We often express those strength and stiffness properties in relative terms by dividing them by the density to express the efficiency of the material as to what it can do per unit weight. Those strength-to-density and stiffness-to-density quotients are simply a manner of expressing what we call specific strength and specific modulus or specific stiffness that are particularly attractive when weight-sensitive structures such as aircraft or spacecraft are addressed.

First, we examine how the properties of the composite material constituents, fiber and matrix, generally contribute to the lamina properties and, subsequently, how lamina properties influence the laminate properties. We plot the strength vertically and the stiffness or modulus horizontally in Figure C-5 on translation from constituent properties of the composite material to the lamina level and then finally to the laminate level. Typical fibers used in advanced composite materials are very high in strength and often very high in modulus. Next, we put those fibers in a matrix material that is typically low in strength and stiffness to create a unidirectionally reinforced lamina. Such a lamina has substantially different strengths and stiffnesses in different directions. The strength and stiffness in the fiber direction are the highest properties. However, perpendicular to the fibers, that is, at 90°, the lowest properties exist with some variation in between as the angle varies from 0° to 90°. At 90°, the lamina stiffness and strength are closer to the matrix properties than the fiber properties, whereas, at 0° to the fiber direction, the properties are fiber dominated.

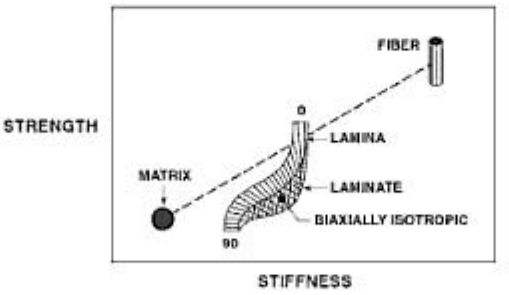


Figure C-5 Translation from Constituent Properties to Lamina to Laminate Properties

Éléments sous droits d'auteur

A laminate is a bonded mixture of variously angled laminae as in Figure C-1. We expect the laminate properties to be not as high as those of the 0° lamina nor as low as those of the 90° lamina, but some values in between. The zone marked laminate in Figure C-5 must include both the 0° and the 90° cases because we can make a laminate, if we so choose, with all 0° or all 90° fibers. At some place in the laminate zone, a so-called biaxially isotropic laminate exists with equal in-plane stiffness and strength properties in at least two directions. The biaxially isotropic laminate is an artificial (impractical) laminate that is simply used as a basis for comparison of one composite laminate to another or of a composite material to a metal. The type of properties plot in Figure C-5 is the basic scheme that we will use to compare many different materials.

The strength and stiffness of many materials on the basis of effectiveness per unit weight are represented in Figure C-6. The properties of common structural metals in bulk form are denoted by open squares. Various composite material forms are denoted by three types of circles: fibers alone are represented with open circles; laminae with unidirectional fibers (a unidirectional lamina) are shown as circles with a vertical line in them; and laminates with equal numbers of fibers in two perpendicular directions (a biaxially isotropic laminate) are shown with circles with both a horizontal and a vertical line in them. All laminae and laminates have an epoxy matrix in Figure C-6. The most effective material obviously lies in the upper right-hand corner of Figure C-6. Fibers alone are stiffer and stronger than when placed in a matrix. However, fibers are not used without a matrix because of the important advantages of the combination of fibers in a matrix (see Jones [C-1]. Also, unidirectional laminae are stiffer and stronger in the fiber direction than biaxially isotropic laminates in either of the two directions. Practical laminates lie somewhere between unidirectional and biaxially isotropic configurations.

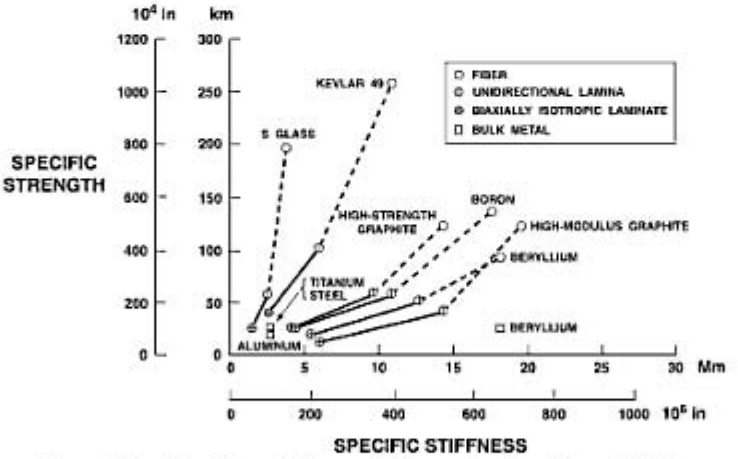


Figure C-6 Strength and Stiffness of Composite Materials and Metals

Éléments sous droits d'auteur

Let's compare various forms of specific composite materials with structural grade metals. Metals have no constituents, and there are no orientation aspects, so only a square is necessary to represent their stiffness and, simultaneously, their strength on the specific strength versus specific stiffness curve in Figure C-6. The bulk metals considered for structural applications are steel, titanium, and aluminum in the lower left-hand corner of Figure C-6 and, not so commonly, beryllium in the lower right-hand corner. Now, contrast those bulk metal properties with the properties of a high-modulus graphite fiber which is plotted as an open circle up and to the right about as far as possible in Figure C-6. Observe that the graphite looks wonderful at first glance. However, we cannot use graphite in strictly a fiber form. We must drop back from the capabilities of the fiber form to the unidirectional laminate form (a unidirectional laminate is merely bonded unidirectional laminae) at least, if not back more toward the biaxially isotropic laminate. And the real practical application is between these two simple composite laminates. Still, high-modulus graphite-epoxy is both stiffer and stronger than the usual structural metals. The primary advantage is stiffness.

A unidirectional laminate can be used in certain special applications. For example, all the fibers can be aligned in the axial direction of a strut or column to take advantage of every possible capability of a graphite-epoxy composite material in that uniaxial loading environment. In contrast, for aircraft wings, all the fibers cannot be oriented in one direction. Multiple fiber orientations must be used to achieve the proper balance of strength and stiffness necessary to accommodate loads from various directions. Certainly the loads are larger in one direction than another, and we would then prejudice the fiber system to accommodate the higher load levels. We simply cannot do that prejudicing of directional properties with a metal structure. We must accept uniform all-around properties with a metal structure unless we add stiffeners (as is often done).

A wide selection of materials is depicted in Figure C-6, e.g., both high-strength graphite-epoxy and high-modulus graphite-epoxy which is naturally further to the right on the figure than is high-strength graphite-epoxy. Generally, high-modulus graphite-epoxy is obtained by a higher graphitization temperature of the graphite fibers than high-strength graphite. Boron falls fairly close to high-strength graphite. Beryllium is over to the right in fiber form and much lower on the chart in bulk metal form. The fiber form of beryllium is much stronger, i.e., up higher in the figure, than the bulk form of beryllium because of fewer imperfections in the fiber form. Thus, a beryllium-fiber composite material has a significant advantage over bulk beryllium in strength. Beryllium fibers in a composite form lead to loss in stiffness to some extent because we have had to use a less-stiff matrix material to surround the beryllium fibers, but we still have a considerable strength advantage. In contrast, we see fiberglass (S glass) to the left in the figure, which is extremely strong, but not very stiff. When we put the glass fibers in a usable form, namely a unidirectional composite material, we get the same specific stiffness as ordinary structural metals, but fiberglass does have a higher specific strength. Fiberglass in the biaxially isotropic form has about the same specific strength as steel or titanium, but higher than aluminum. However, fiberglass has a lower specific modulus than any of the conven-

Éléments sous droits d'auteur

tional metals. Kevlar 49®-epoxy fits between the set of lines for S-glass-epoxy and the high-strength graphite-epoxy in Figure C-6. Thus, we would typically use glass or Kevlar 49® in a strength-critical application whereas any of the graphites, even the high-strength graphites, would be used in stiffness-critical applications. For a certain balance of strength and stiffness, you might want a material some place in the Kevlar to high-strength graphite region of materials rather than to go all the way to a fiberglass or all the way to a high-modulus graphite, for example. That is, you must look at your specific design requirements to determine what material you need.

For example, we might make a strength-critical pressure vessel with glass-epoxy. We would wind the fibers so that they are not unidirectional, but resist the variously oriented pressure vessel stresses. A pressure vessel has a biaxial state of stress, so we must do more than just circumferential fiber winding. In some cases, some axial windings are necessary, and we might also wind some fibers at $\pm 45°$ or other angles. We can find the angle to optimize the strength of this highly biaxially loaded structure. Some pressure vessels are made of graphite-epoxy as well as of fiberglass or Kevlar-epoxy.

The duality of the plot in Figure C-6 is very important. That is, *stiffness is often equally important and sometimes even more important than strength in many structures.* Some people tend to say strength when they actually mean stiffness. We must carefully and completely distinguish between these two very different physical concepts.

Not all of the strength and stiffness advantages of fiber-reinforced composite materials can be transformed directly into structural advantages. Prominent among the reasons for this statement is the fact that the joints for members made of composite materials are typically more bulky than those for metal parts. These relative inefficiencies are being studied because they obviously affect the cost trade-offs for application of composite materials. Other laminated structures advantages include manufacturing cost and weight as discussed by Jones [C-1]. Raw material cost comparisons are probably not valid by themselves because many factors influence cost beyond raw material cost.

C.3 STRESS-STRAIN RELATIONS FOR ANISOTROPIC AND ORTHOTROPIC MATERIALS

Suppose stresses are applied on a three-dimensional element of a body in Figure C-7. We must determine the corresponding strains.

Anisotropy means total lack of isotropy, so an anisotropic body has different material properties in all directions. Moreover, there are no principal material directions about which material property symmetry exists. The strains can be shown to be related to the stresses by the compliances, S_{ij}, (see Jones [C-1]) as

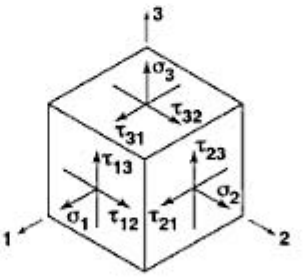


Figure C-7 Stresses on an Element

Éléments sous droits d'auteur

$$\begin{aligned}\varepsilon_1 &= S_{11}\sigma_1 + S_{12}\sigma_2 + S_{13}\sigma_3 + S_{14}\tau_{23} + S_{15}\tau_{31} + S_{16}\tau_{12}\\ &\vdots\\ \gamma_{12} &= S_{16}\sigma_1 + S_{26}\sigma_2 + S_{36}\sigma_3 + S_{46}\tau_{23} + S_{56}\tau_{31} + S_{66}\tau_{12}\end{aligned} \tag{C.1}$$

Thus, for an applied uniaxial stress $\sigma_1 = \sigma$ (all other stresses are zero):

$$\begin{aligned}\varepsilon_1 &= S_{11}\sigma \qquad \varepsilon_2 = S_{12}\sigma \qquad \varepsilon_3 = S_{13}\sigma\\ \gamma_{23} &= S_{14}\sigma \qquad \gamma_{31} = S_{15}\sigma \qquad \gamma_{12} = S_{16}\sigma\end{aligned} \tag{C.2}$$

A major objective of studying the strain-stress relations is to be able to conclude what deformation response occurs because of a given applied stress. The physical interpretation of these strains is that an originally equal-sided cube of anisotropic material has many deformations. Specifically, every non-parallel cube side deforms in length differently from every other non-parallel cube side (because $S_{11} \neq S_{12} \neq S_{13}$), and every non-parallel cube side undergoes different shearing deformation (because $S_{14} \neq S_{15} \neq S_{16}$), as depicted imperfectly in Figure C-8, where the dashed lines represent the undeformed cube and the solid lines represent the deformed cube. Imagine yourself in a room that undergoes these deformations! In contrast, a material that is isotropic would have the same change in side length in the 2- and 3-directions (because $S_{12} = S_{13}$), but less than in the 1-direction (because of the Poisson effect) and no shearing deformation of any cube side (because $S_{14} = S_{15} = S_{16} = 0$). Thus, for an anisotropic material, significant coupling occurs between the applied stress and the various strain responses, unlike the simpler response for an isotropic material.

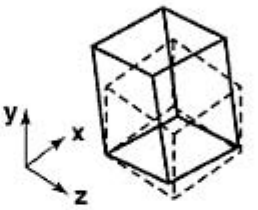


Figure C-8 Deformation of an Anisotropic Cube under σ_y

Those various couplings are shown for an arbitrarily stressed body in Figure C-9 where the physical significance of each compliance is labeled. There, the terms S_{11}, S_{22}, and S_{33} each govern extensional response to an individual applied stress, σ_1, σ_2, and σ_3, respectively, *in the same direction*. The terms S_{44}, S_{55}, and S_{66} govern shear strain response to an applied shear stress *in the same plane*. The terms S_{12}, S_{13}, and S_{23} govern coupling between dissimilar normal stresses and normal strains (*extension-extension coupling* more commonly known as the Poisson effect). The terms S_{14}, S_{15}, S_{16}, S_{24}, S_{25}, S_{26}, S_{34}, S_{35}, and S_{36} govern normal strain response to applied shear stress in a more complex manner than for the preceding compliances (*shear-extension coupling*). Finally, the terms S_{45}, S_{46}, and S_{56} govern shear strain response to shear stress applied in another plane (*shear-shear coupling*). In contrast, the only coupling that exists for an isotropic material is extension-extension coupling. Thus, the deformation response of an anisotropic material even to simple stress states can literally be in every direction and in every plane. We will see in Section C.5 that orthotropic materials can exhibit apparent anisotropy when stressed in nonprincipal material coordinates. Moreover, we will see that S_{11}, S_{22}, and

Éléments sous droits d'auteur

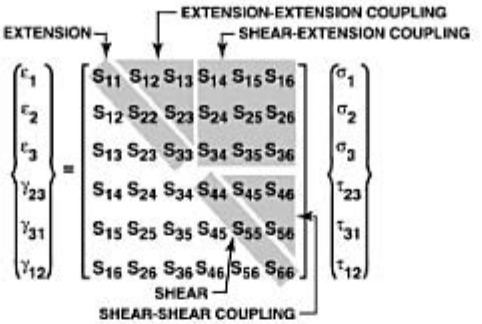


Figure C-9 Physical Significance of the Anisotropic Strain-Stress Relations

S_{33} are related to the Young's moduli in the 1-, 2-, and 3-directions, respectively. Also, S_{12}, S_{13}, and S_{14} will be related to the Poisson's ratios and Young's moduli. Finally, S_{44}, S_{55}, and S_{66} will be related to shear moduli in the 2-3, 3-1, and 1-2 planes, respectively. In summary, because of the various couplings between stresses and strains noted in Figure C-9, an applied normal stress on an anisotropic body results in

1. Normal strain in the direction of the applied stress
2. Normal strains in the directions perpendicular to the applied stress (extension-extension coupling)
3. Shear strain in the three planes (shear-extension coupling)

Moreover, an applied shear stress in one plane results in

1. Shear strain in the plane of the applied stress
2. Shear strains in the other planes (shear-shear coupling)
3. Normal strains in the three directions (shear-extension coupling)

The strain-stress relations can be inverted to obtain the stress-strain relations as related by the stiffnesses, C_{ij}:

$$\begin{Bmatrix} \sigma_1 \\ \sigma_2 \\ \sigma_3 \\ \tau_{23} \\ \tau_{31} \\ \tau_{12} \end{Bmatrix} = \begin{bmatrix} C_{11} & C_{12} & C_{13} & C_{14} & C_{15} & C_{16} \\ C_{12} & C_{22} & C_{23} & C_{24} & C_{25} & C_{26} \\ C_{13} & C_{23} & C_{33} & C_{34} & C_{35} & C_{36} \\ C_{14} & C_{24} & C_{34} & C_{44} & C_{45} & C_{46} \\ C_{15} & C_{25} & C_{35} & C_{45} & C_{55} & C_{56} \\ C_{16} & C_{26} & C_{36} & C_{46} & C_{56} & C_{66} \end{bmatrix} \begin{Bmatrix} \varepsilon_1 \\ \varepsilon_2 \\ \varepsilon_3 \\ \gamma_{23} \\ \gamma_{31} \\ \gamma_{12} \end{Bmatrix} \tag{C.3}$$

Éléments sous droits d'auteur

For an orthotropic material (a material for which three mutually orthogonal planes of material property symmetry exist, such as a fiber-reinforced composite material with different fibers in three perpendicular directions), the stress-strain relations in principal material directions are:

$$\begin{bmatrix} \sigma_1 \\ \sigma_2 \\ \sigma_3 \\ \tau_{23} \\ \tau_{31} \\ \tau_{12} \end{bmatrix} = \begin{bmatrix} C_{11} & C_{12} & C_{13} & 0 & 0 & 0 \\ C_{12} & C_{22} & C_{23} & 0 & 0 & 0 \\ C_{13} & C_{23} & C_{33} & 0 & 0 & 0 \\ 0 & 0 & 0 & C_{44} & 0 & 0 \\ 0 & 0 & 0 & 0 & C_{55} & 0 \\ 0 & 0 & 0 & 0 & 0 & C_{66} \end{bmatrix} \begin{bmatrix} \varepsilon_1 \\ \varepsilon_2 \\ \varepsilon_3 \\ \gamma_{23} \\ \gamma_{31} \\ \gamma_{12} \end{bmatrix} \tag{C.4}$$

and the strain-stress relations are

$$\begin{bmatrix} \varepsilon_1 \\ \varepsilon_2 \\ \varepsilon_3 \\ \gamma_{23} \\ \gamma_{31} \\ \gamma_{12} \end{bmatrix} = \begin{bmatrix} S_{11} & S_{12} & S_{13} & 0 & 0 & 0 \\ S_{12} & S_{22} & S_{23} & 0 & 0 & 0 \\ S_{13} & S_{23} & S_{33} & 0 & 0 & 0 \\ 0 & 0 & 0 & S_{44} & 0 & 0 \\ 0 & 0 & 0 & 0 & S_{55} & 0 \\ 0 & 0 & 0 & 0 & 0 & S_{66} \end{bmatrix} \begin{bmatrix} \sigma_1 \\ \sigma_2 \\ \sigma_3 \\ \tau_{23} \\ \tau_{31} \\ \tau_{12} \end{bmatrix} \tag{C.5}$$

Thus, no shear-extension coupling or shear-shear coupling exists for orthotropic materials that are loaded in principal material directions, a crucial restriction that is not always satisfied.

The foregoing stress-strain and strain-stress relations are elegant and compact. However, they are mainly conceptual and somewhat impractical to use in the context of the usual engineering measurements of material behavior. A more everyday approach is addressed next.

Most simple material characterization or property measurements are performed with a known applied load or, conceptually, stress. The resulting displacement and strain are then measured. The engineering constants are generally the slope of a stress-strain curve (e.g., $E = \sigma/\varepsilon$) or the slope of a strain-strain curve (e.g., $\nu = -\varepsilon_y/\varepsilon_x$ for $\sigma_x = \sigma$ and all other stresses are zero). Thus, the components of the compliance (S_{ij}) matrix are determined more directly than those of the stiffness (C_{ij}) matrix. For an orthotropic material that is stressed in principal material coordinates (the 1,2,3 coordinates), the compliance matrix components in terms of the engineering constants are expressed in matrix form as

Éléments sous droits d'auteur

$$[S_{ij}] = \begin{bmatrix} \frac{1}{E_1} & -\frac{\nu_{21}}{E_2} & -\frac{\nu_{31}}{E_3} & 0 & 0 & 0 \\ -\frac{\nu_{12}}{E_1} & \frac{1}{E_2} & -\frac{\nu_{32}}{E_3} & 0 & 0 & 0 \\ -\frac{\nu_{13}}{E_1} & -\frac{\nu_{23}}{E_2} & \frac{1}{E_3} & 0 & 0 & 0 \\ 0 & 0 & 0 & \frac{1}{G_{23}} & 0 & 0 \\ 0 & 0 & 0 & 0 & \frac{1}{G_{31}} & 0 \\ 0 & 0 & 0 & 0 & 0 & \frac{1}{G_{12}} \end{bmatrix} \tag{C.6}$$

in which

E_1, E_2, E_3 = Young's extensional moduli in the 1-, 2-, and 3-directions

ν_{ij} = Poisson's ratio (extension-extension coupling coefficient), i.e., the negative of the transverse strain in the j-direction over the strain in the i-direction when stress is applied in the i-direction, i.e.,

$$\nu_{ij} = -\frac{\varepsilon_j}{\varepsilon_i} \tag{C.7}$$

for $\sigma_i = \sigma$ and all other stresses are zero

G_{23}, G_{31}, G_{12} = shear moduli in the 2-3, 3-1 (= 1-3), and 1-2 planes

Note that an orthotropic material that is stressed in principal material coordinates (the 1, 2, and 3 coordinates) does not exhibit either shear-extension or shear-shear coupling. Recall that an orthotropic material has nine independent constants because

$$S_{ij} = S_{ji} \tag{C.8}$$

and the compliance matrix is the inverse of the stiffness (C_{ij}) matrix that can be shown to be symmetric. When engineering constants are substituted in Equation (C.8),

$$\frac{\nu_{ij}}{E_i} = \frac{\nu_{ji}}{E_j} \qquad i, j = 1, 2, 3 \qquad i \neq j \tag{C.9}$$

Thus, three reciprocal relations must be satisfied for an orthotropic material. Moreover, only ν_{12}, ν_{13}, and ν_{23} need be further considered because ν_{21}, ν_{31}, and ν_{32} can be expressed in terms of the first-mentioned group of Poisson's ratios and the Young's moduli. The latter group of Poisson's ratios must not be forgotten, however, because for some tests they are what is actually measured, not ν_{12}, ν_{13}, and ν_{23}.

Éléments sous droits d'auteur

C.4 STRESS-STRAIN RELATIONS FOR PLANE STRESS ON AN ORTHOTROPIC MATERIAL

For a unidirectionally reinforced lamina in the 1-2 plane as shown in Figure C-10 or a woven lamina in the 1-2 plane as in Figure C-4, a plane stress state is defined by setting

$$\sigma_3 = 0 \qquad \tau_{23} = 0 \qquad \tau_{31} = 0 \tag{C.10}$$

so that

$$\sigma_1 \neq 0 \qquad \sigma_2 \neq 0 \qquad \tau_{12} \neq 0 \tag{C.11}$$

in the three-dimensional stress-strain relations given in Equations (C.3) and (C.4) for anisotropic or orthotropic materials. Note that a plane stress state on a lamina is not merely an idealization of reality, but instead is a practical and achievable objective of how we must use a lamina with fibers only in its plane. After all, the lamina cannot withstand high stresses in any direction other than that of the fibers, so why would we subject it to unnatural stresses such as σ_3? That is, we expect to load a lamina *only* in plane stress because carrying in-plane stresses is its fundamental capability. A unidirectionally reinforced lamina would need 'help' carrying in-plane stress perpendicular to its fibers, but that help can be provided in the plane by other (parallel) layers that have their fibers in the direction of the stress. Thus, a laminate is needed to carry variously oriented stresses, but we concentrate on the characteristics of a lamina in this section. Note that any stress applied perpendicular to the plane must be quite limited because of lower stiffness and strength in that direction for a lamina. Practical examples of primarily in-plane loaded structural elements are most car body panels, aircraft wings and fuselages, etc.

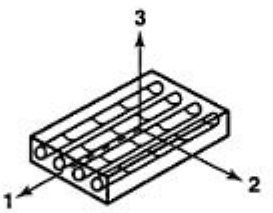


Figure C-10 Unidirectionally Reinforced Lamina

For orthotropic materials, imposing a state of plane stress results in implied out-of-plane strains of

$$\varepsilon_3 = S_{13}\sigma_1 + S_{23}\sigma_2 \qquad \gamma_{23} = 0 \qquad \gamma_{31} = 0 \tag{C.12}$$

in which the compliances S_{ij} are

$$S_{13} = -\frac{\nu_{13}}{E_1} = -\frac{\nu_{31}}{E_3} \qquad S_{23} = -\frac{\nu_{23}}{E_2} = -\frac{\nu_{32}}{E_3} \tag{C.13}$$

Moreover, the strain-stress relations in Equation (C.5) reduce to

Éléments sous droits d'auteur

$$\begin{bmatrix} \varepsilon_1 \\ \varepsilon_2 \\ \gamma_{12} \end{bmatrix} = \begin{bmatrix} S_{11} & S_{12} & 0 \\ S_{12} & S_{22} & 0 \\ 0 & 0 & S_{66} \end{bmatrix} \begin{bmatrix} \sigma_1 \\ \sigma_2 \\ \tau_{12} \end{bmatrix} \tag{C.14}$$

supplemented by Equation (C.12) in which

$$S_{11} = \frac{1}{E_1} \qquad S_{12} = -\frac{\nu_{12}}{E_1} = -\frac{\nu_{21}}{E_2} \qquad S_{22} = \frac{1}{E_2} \qquad S_{66} = \frac{1}{G_{12}} \tag{C.15}$$

Note that in order to determine ε_3 in Equation (C.12), ν_{13} and ν_{23} must be known in addition to the engineering constants in Equation (C.15). That is, ν_{13} and ν_{23} arise from S_{13} and S_{23} in Equation (C.12).

The strain-stress relations in Equation (C.14) can be inverted to obtain the stress-strain relations

$$\begin{bmatrix} \sigma_1 \\ \sigma_2 \\ \tau_{12} \end{bmatrix} = \begin{bmatrix} Q_{11} & Q_{12} & 0 \\ Q_{12} & Q_{22} & 0 \\ 0 & 0 & Q_{66} \end{bmatrix} \begin{bmatrix} \varepsilon_1 \\ \varepsilon_2 \\ \gamma_{12} \end{bmatrix} \tag{C.16}$$

in which the Q_{ij} are the so-called *reduced stiffnesses* for a plane stress state in the 1-2 plane which are determined either (1) as the components of the inverted compliance matrix in Equation (C.14) or (2) from the C_{ij} (stiffnesses) directly by applying the condition $\sigma_3 = 0$ to the strain-stress relations to get an expression for ε_3 and simplifying the results to get

$$Q_{ij} = C_{ij} - \frac{C_{i3}C_{j3}}{C_{33}} \qquad i,j = 1, 2, 6 \tag{C.17}$$

The term C_{63} is zero because no shear-extension coupling exists for an orthotropic lamina in principal material coordinates. For the orthotropic lamina, the Q_{ij} are

$$\begin{aligned} Q_{11} &= \frac{S_{22}}{S_{11}S_{22} - S_{12}^2} & Q_{22} &= \frac{S_{11}}{S_{11}S_{22} - S_{12}^2} \\ Q_{12} &= \frac{S_{12}}{S_{11}S_{22} - S_{12}^2} & Q_{66} &= \frac{1}{S_{66}} \end{aligned} \tag{C.18}$$

or, in terms of the engineering constants,

$$\begin{aligned} Q_{11} &= \frac{E_1}{1 - \nu_{12}\nu_{21}} & Q_{22} &= \frac{E_2}{1 - \nu_{12}\nu_{21}} \\ Q_{12} &= \frac{\nu_{12}E_2}{1 - \nu_{12}\nu_{21}} = \frac{\nu_{21}E_1}{1 - \nu_{12}\nu_{21}} & Q_{66} &= G_{12} \end{aligned} \tag{C.19}$$

Note that four independent material properties, E_1, E_2, ν_{12}, and G_{12}, exist in Equations (C.14) and (C.16) if Equations (C.15) and (C.19) are considered in addition to the reciprocal relation, Equation (C.9):

Éléments sous droits d'auteur

$$\frac{\nu_{12}}{E_1} = \frac{\nu_{21}}{E_2} \tag{C.20}$$

The preceding stress-strain and strain-stress relations are the basis for stiffness and stress analysis of a lamina subjected to stresses in its plane. Thus, the relations are indispensable in laminate analysis.

C.5 STRESS-STRAIN RELATIONS FOR A LAMINA OF ARBITRARY ORIENTATION

In Section C.4, the stresses and strains were defined in the principal material coordinates for an orthotropic material. However, the principal directions of orthotropy often do not coincide with coordinate directions that are geometrically natural to the solution of the problem. For example, consider the helically wound fiber-reinforced circular cylindrical shell in Figure C-11. There, the coordinates natural to the solution of the shell problem are the shell coordinates x, y, z, whereas the principal material coordinates are x', y', z' in the shell surface. The directions normal to the surface, z and z', are identical. The filament-winding angle is defined by $\cos(y', y) = \cos\alpha$. Other examples include laminated plates with different laminae at different orientations. Thus, a relation is needed between the stresses and strains in the principal material coordinates and those in the body coordinates. Accordingly, a method of transforming stress-strain relations from one coordinate system to another is also needed.

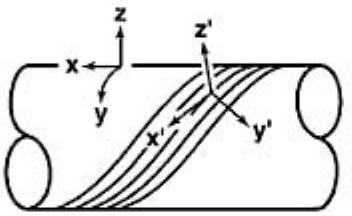


Figure C-11 Helically Wound Fiber-Reinforced Circular Cylindrical Shell

At this point, we recall from elementary mechanics of materials the transformation equations for expressing stresses in an x-y coordinate system in terms of stresses in a 1-2 coordinate system,

$$\begin{bmatrix} \sigma_x \\ \sigma_y \\ \tau_{xy} \end{bmatrix} = \begin{bmatrix} \cos^2\theta & \sin^2\theta & -2\sin\theta\cos\theta \\ \sin^2\theta & \cos^2\theta & 2\sin\theta\cos\theta \\ \sin\theta\cos\theta & -\sin\theta\cos\theta & \cos^2\theta - \sin^2\theta \end{bmatrix} \begin{bmatrix} \sigma_1 \\ \sigma_2 \\ \tau_{12} \end{bmatrix} \tag{C.21}$$

in which θ is the angle *from* the x-axis *to* the 1-axis (see Figure C-12). Note especially that the transformation has nothing to do with the material properties but is merely a rotation of stress directions. Also, the *direction* of rotation is crucial.

Éléments sous droits d'auteur

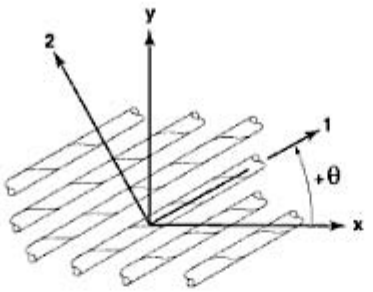


Figure C-12 Positive Rotation of Principal Material Axes from x-y Axes

Similarly, the strain-transformation equations for the strains in x-y coordinates (body coordinates) in terms of the strains in 1-2 coordinates (principal material direction coordinates) are

$$\begin{bmatrix} \varepsilon_x \\ \varepsilon_y \\ \dfrac{\gamma_{xy}}{2} \end{bmatrix} = \begin{bmatrix} \cos^2\theta & \sin^2\theta & -2\sin\theta\cos\theta \\ \sin^2\theta & \cos^2\theta & 2\sin\theta\cos\theta \\ \sin\theta\cos\theta & -\sin\theta\cos\theta & \cos^2\theta - \sin^2\theta \end{bmatrix} \begin{bmatrix} \varepsilon_1 \\ \varepsilon_2 \\ \dfrac{\gamma_{12}}{2} \end{bmatrix} \quad \text{(C.22)}$$

in which we observe that strains do transform with the same transformation as do stresses in Equation (C.21) if the tensor definition of shear strain is used (which is equivalent to dividing the engineering shear strain by two). The difference between the tensor definition of strain, ε_{12}, and the engineering definition, γ_{12}, has an often troublesome factor of two. That factor of two will be treated shortly with an innovative approach by Reuter [C-2].

The two transformations are commonly written as

$$\begin{bmatrix} \sigma_x \\ \sigma_y \\ \tau_{xy} \end{bmatrix} = [T]^{-1} \begin{bmatrix} \sigma_1 \\ \sigma_2 \\ \tau_{12} \end{bmatrix} \quad \text{(C.23)}$$

$$\begin{bmatrix} \varepsilon_x \\ \varepsilon_y \\ \dfrac{\gamma_{xy}}{2} \end{bmatrix} = [T]^{-1} \begin{bmatrix} \varepsilon_1 \\ \varepsilon_2 \\ \dfrac{\gamma_{12}}{2} \end{bmatrix} \quad \text{(C.24)}$$

in which the superscript –1 on a matrix denotes the matrix inverse and the transformation matrix, T, is

Éléments sous droits d'auteur

$$[T] = \begin{bmatrix} \cos^2\theta & \sin^2\theta & 2\sin\theta\cos\theta \\ \sin^2\theta & \cos^2\theta & -2\sin\theta\cos\theta \\ -\sin\theta\cos\theta & \sin\theta\cos\theta & \cos^2\theta - \sin^2\theta \end{bmatrix} \tag{C.25}$$

However, if the simple matrix

$$[R] = \begin{bmatrix} 1 & 0 & 0 \\ 0 & 1 & 0 \\ 0 & 0 & 2 \end{bmatrix} \tag{C.26}$$

suggested by Reuter [C-2] is introduced to take care of the factor of two, then the engineering strain vectors (one-dimensional matrices)

$$\begin{bmatrix} \varepsilon_1 \\ \varepsilon_2 \\ \gamma_{12} \end{bmatrix} = [R] \begin{bmatrix} \varepsilon_1 \\ \varepsilon_2 \\ \dfrac{\gamma_{12}}{2} \end{bmatrix} \tag{C.27}$$

$$\begin{bmatrix} \varepsilon_x \\ \varepsilon_y \\ \gamma_{xy} \end{bmatrix} = [R] \begin{bmatrix} \varepsilon_x \\ \varepsilon_y \\ \dfrac{\gamma_{xy}}{2} \end{bmatrix} \tag{C.28}$$

can be used instead of the tensor strain vectors in the strain transformations as well as in stress-strain law transformations. The beauty of Reuter's transformation is that concise matrix notation can then be used. Thus, the usual expressions for stiffness and compliance matrices with awkward factors of 1/2 and 2 in various rows and columns are avoided.

A so-called *specially orthotropic lamina* is an orthotropic lamina whose principal material axes are aligned with the natural body axes:

$$\begin{bmatrix} \sigma_x \\ \sigma_y \\ \tau_{xy} \end{bmatrix} = \begin{bmatrix} \sigma_1 \\ \sigma_2 \\ \tau_{12} \end{bmatrix} = \begin{bmatrix} Q_{11} & Q_{12} & 0 \\ Q_{12} & Q_{22} & 0 \\ 0 & 0 & Q_{66} \end{bmatrix} \begin{bmatrix} \varepsilon_1 \\ \varepsilon_2 \\ \gamma_{12} \end{bmatrix} \tag{C.29}$$

for which the principal material axes are shown in Figure C-10. These stress-strain relations were introduced in Section C.4 and apply when the principal material directions of an orthotropic lamina are used as coordinates.

However, as mentioned previously, orthotropic laminae are often constructed in such a manner that the principal material coordinates do not coincide with the natural coordinates of the body. This statement is not to be interpreted as meaning that the material itself is no longer orthotropic; instead, we are just looking at an orthotropic material in a

Éléments sous droits d'auteur

somewhat unnatural manner, i.e., in a coordinate system that is oriented at some angle to the principal material coordinate system. Then, the basic question is: given the stress-strain relations in the principal material coordinates, what are the stress-strain relations in x-y coordinates?

Accordingly, we use the stress and strain transformations of Equations (C.23) and (C.24) along with Reuter's matrix, Equation (C.26), after abbreviating Equation (C.29) as

$$\begin{bmatrix} \sigma_1 \\ \sigma_2 \\ \tau_{12} \end{bmatrix} = [Q] \begin{bmatrix} \varepsilon_1 \\ \varepsilon_2 \\ \gamma_{12} \end{bmatrix} \tag{C.30}$$

to obtain

$$\begin{bmatrix} \sigma_x \\ \sigma_y \\ \tau_{xy} \end{bmatrix} = [T]^{-1} \begin{bmatrix} \sigma_1 \\ \sigma_2 \\ \tau_{12} \end{bmatrix} = [T]^{-1}[Q][R][T][R]^{-1} \begin{bmatrix} \varepsilon_x \\ \varepsilon_y \\ \gamma_{xy} \end{bmatrix} \tag{C.31}$$

However, $[R][T][R]^{-1}$ can be shown to be $[T]^{-T}$ where the superscript T denotes the matrix transpose. Then, if we use the abbreviation

$$[\bar{Q}] = [T]^{-1}[Q][T]^{-T} \tag{C.32}$$

the stress-strain relations in x-y coordinates are

$$\begin{bmatrix} \sigma_x \\ \sigma_y \\ \tau_{xy} \end{bmatrix} = [\bar{Q}] \begin{bmatrix} \varepsilon_x \\ \varepsilon_y \\ \gamma_{xy} \end{bmatrix} = \begin{bmatrix} \bar{Q}_{11} & \bar{Q}_{12} & \bar{Q}_{16} \\ \bar{Q}_{12} & \bar{Q}_{22} & \bar{Q}_{26} \\ \bar{Q}_{16} & \bar{Q}_{26} & \bar{Q}_{66} \end{bmatrix} \begin{bmatrix} \varepsilon_x \\ \varepsilon_y \\ \gamma_{xy} \end{bmatrix} \tag{C.33}$$

in which

$$\begin{aligned}
\bar{Q}_{11} &= Q_{11}\cos^4\theta + 2(Q_{12} + 2Q_{66})\sin^2\theta\cos^2\theta + Q_{22}\sin^4\theta \\
\bar{Q}_{12} &= (Q_{11} + Q_{22} - 4Q_{66})\sin^2\theta\cos^2\theta + Q_{12}(\sin^4\theta + \cos^4\theta) \\
\bar{Q}_{22} &= Q_{11}\sin^4\theta + 2(Q_{12} + 2Q_{66})\sin^2\theta\cos^2\theta + Q_{22}\cos^4\theta \\
\bar{Q}_{16} &= (Q_{11} - Q_{12} - 2Q_{66})\sin\theta\cos^3\theta + (Q_{12} - Q_{22} + 2Q_{66})\sin^3\theta\cos\theta \\
\bar{Q}_{26} &= (Q_{11} - Q_{12} - 2Q_{66})\sin^3\theta\cos\theta + (Q_{12} - Q_{22} + 2Q_{66})\sin\theta\cos^3\theta \\
\bar{Q}_{66} &= (Q_{11} + Q_{22} - 2Q_{12} - 2Q_{66})\sin^2\theta\cos^2\theta + Q_{66}(\sin^4\theta + \cos^4\theta)
\end{aligned} \tag{C.34}$$

in which the bar over the $\bar{Q}_{ij}$ matrix denotes that we are dealing with the *transformed reduced stiffnesses* instead of the reduced stiffnesses, Q_{ij}.

Éléments sous droits d'auteur

Note that the transformed reduced stiffness matrix $\overline{Q}_{ij}$ has terms in all nine positions in contrast to the presence of zeros in the reduced stiffness matrix Q_{ij} in Equation (C.29). However, there are still only *four* independent material constants because the lamina is orthotropic. In the general case with body coordinates x and y, there is coupling between shear strain and normal stresses and between shear stress and normal strains, i.e., shear-extension coupling exists. Thus, in body coordinates, even an orthotropic lamina appears to be anisotropic. However, because such a lamina does have orthotropic characteristics in principal material coordinates, it is called a *generally orthotropic lamina* because it can be represented by the stress-strain relations in Equation (C.33). That is, a *generally orthotropic lamina* is an orthotropic lamina whose principal material axes are not aligned with the natural body axes.

The only advantage associated with generally orthotropic laminae as opposed to anisotropic laminae is that generally orthotropic laminae are simpler to characterize experimentally (and are more natural and more common). However, if we do not realize that principal material axes exist, then a generally orthotropic lamina is indistinguishable from an anisotropic lamina. That is, we cannot take away the inherent orthotropic character of a lamina, but we can orient the lamina in such a manner as to make that character quite difficult to recognize.

C.6 CLASSICAL LAMINATION THEORY

Classical lamination theory consists of a collection of mechanics-of-materials type of stress and deformation hypotheses that are described in this appendix. By use of this theory, we can consistently proceed directly from the basic building block, the lamina, to the end result, a structural laminate. The whole process is one of finding effective and reasonably accurate simplifying presumptions that enable us to reduce our attention from a complicated three-dimensional elasticity problem to a solvable two-dimensional mechanics of deformable bodies problem.

Actually, because of the stress and deformation hypotheses that are an inseparable part of classical lamination theory, a more correct name would be classical thin lamination theory, or in structural applications even classical laminated plate or shell theory. We will use the common term classical lamination theory, but recognize that it is a convenient oversimplification of the rigorous nomenclature. In the composite materials literature, classical lamination theory is often abbreviated as CLT.

First, the stress-strain behavior of an individual lamina is reviewed in Section C.6.1, and expressed in equation form for the k^{th} lamina of a laminate. Then, the variations of stress and strain through the thickness of the laminate are determined in Section C.6.2. Finally, the relation of the laminate forces and moments to the strains and curvatures is found in Section C.6.3 where the laminate stiffnesses are the link from the forces and moments to the strains and curvatures. The derivations in this section are quite similar to the pioneering work in the 1940s and 1950s by Ambartsumyan [C-3] and further work by Pister and Dong [C-4] as well as by Reissner and Stavsky [C-5].

Éléments sous droits d'auteur

C.6.1 Lamina Stress-Strain Behavior

The stress-strain relations in principal material coordinates for a lamina of an orthotropic material under plane stress are

$$\begin{bmatrix} \sigma_1 \\ \sigma_2 \\ \tau_{12} \end{bmatrix} = \begin{bmatrix} Q_{11} & Q_{12} & 0 \\ Q_{12} & Q_{22} & 0 \\ 0 & 0 & Q_{66} \end{bmatrix} \begin{bmatrix} \varepsilon_1 \\ \varepsilon_2 \\ \gamma_{12} \end{bmatrix} \tag{C.35}$$

The reduced stiffnesses, Q_{ij}, are defined in terms of the engineering constants in Equation (C.19). In any other coordinate system in the plane of the lamina, the stresses are

$$\begin{bmatrix} \sigma_x \\ \sigma_y \\ \tau_{xy} \end{bmatrix} = \begin{bmatrix} \overline{Q}_{11} & \overline{Q}_{12} & \overline{Q}_{16} \\ \overline{Q}_{12} & \overline{Q}_{22} & \overline{Q}_{26} \\ \overline{Q}_{16} & \overline{Q}_{26} & \overline{Q}_{66} \end{bmatrix} \begin{bmatrix} \varepsilon_x \\ \varepsilon_y \\ \gamma_{xy} \end{bmatrix} \tag{C.36}$$

in which the transformed reduced stiffnesses, $\overline{Q}_{ij}$, are given in terms of the reduced stiffnesses, Q_{ij}, in Equation (C.34).

The stress-strain relations in arbitrary in-plane coordinates, namely Equation (C.36), are useful in the definition of the laminate stiffnesses because of the arbitrary orientation of the constituent laminae of a laminate. Both Equations (C.35) and (C.36) can be thought of as stress-strain relations for the k^{th} layer of a multilayered laminate. Thus, Equation (C.36) can be written compactly as

$$\{\sigma\}_k = [\overline{Q}]_k \{\varepsilon\}_k \tag{C.37}$$

Most laminae have either unidirectional fibers or orthotropic-weave fabric as in Figure C-4, so their material properties are well-represented with Equation (C.35). Very few actual anisotropic laminae exist. To be anisotropic, they require multi-directional fibers in their plane at other than 90° to each other. Merely having unidirectional fibers at some angle to the load axes does not qualify a lamina to be called anisotropic.

We will proceed in the next section to define the strain and stress variations through the thickness of a laminate. The resultant forces and moments on a laminate will then be obtained in Section C.6.3 by integrating the stress-strain relations for each layer, Equation (C.37), through the laminate thickness subject to the stress and strain variations determined in Section C.6.2.

C.6.2 Strain and Stress Variation in a Laminate

Knowledge of the how the stresses and strains vary through the laminate thickness is essential to the definition of the various stiffnesses of a laminate that is to be used as a structural element. The most significant condition imposed on the laminate behavior is that the laminate

Éléments sous droits d'auteur

is presumed to consist of perfectly bonded laminae.[1] That is, the displacements are continuous across lamina boundaries so that no lamina can slip relative to any adjacent laminae. Moreover, the bonds are presumed to be infinitesimally thin so they are non-shear-deformable. Thus, the laminate acts as a single layer with very *special properties* that later we will see constitute a *structural element*.

Accordingly, if the laminate is thin, a line originally straight and perpendicular to the middle surface of the laminate, i.e., a normal to the middle surface, is presumed to remain straight and perpendicular to the middle surface when the laminate is deformed, e.g., bent, extended, contracted, sheared, or twisted. Requiring the normal to the middle surface to remain straight and normal under deformation is equivalent to ignoring the shearing strains in planes perpendicular to the middle surface, that is, $\gamma_{xz} = \gamma_{yz} = 0$ where z is the direction of the normal to the middle surface in Figure C-13 (note that γ_{xz} and γ_{yz} are the angles that a *deformed* normal would make with the deformed middle surface). In addition, the normals are presumed to have constant length so that the strain perpendicular to the middle surface is ignored as well, that is, $\varepsilon_z = 0$. The foregoing collection of presumptions of the behavior of the single layer that represents the laminate constitutes the familiar Kirchhoff hypothesis for plates and the Kirchhoff-Love hypothesis for shells (and

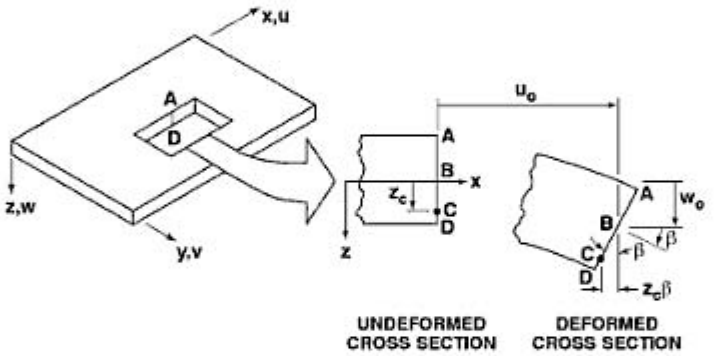


Figure C-13 Geometry of Deformation in the x-z Plane

[1]That the layers are perfectly bonded is *not* an idealization that cannot be realized in a practical sense. In fact, tests exist to determine whether layers are bonded to one another. Those tests are an integral part of current manufacturing technology for composite structures. One such test is the simple coin tap that anyone can perform. The noise from tapping a coin on a laminate changes pitch from regions of perfect bonding to regions where disbonds exist. Accordingly, effective bonds between laminae are *ensured by suitable inspection*. Thus, the usual (correct) perception that bonds between fiber and matrix at the microscopic level are never perfect has no analog at the (macroscopic) laminate level. Laminates that are not completely bonded will likely be rejected (or repaired, if possible) in usual manufacturing practice. The reason for this insistence on good bonds is that nearly perfect bonds are *required* in all laminates to ensure that the laminae work together as a *unit* instead of separately (If the laminae are not bonded, then we do not have a laminate!).

Éléments sous droits d'auteur

is the two-dimensional analog of the ordinary one-dimensional beam theory presumption that plane sections, i.e., sections normal to the beam axis, remain plane after bending (the Euler-Bernoulli hypothesis)—thus, the physical justification of the collection of presumptions should be obvious). Note that no restriction has been made to flat laminates; the laminates can, in fact, be curved or shell-like.

The implications of the Kirchhoff hypothesis on the laminate displacements u, v, and w in the x-, y-, and z-directions are derived by use of the laminate cross section in the x-z plane shown in Figure C-13. The displacement in the x-direction of point B from the undeformed middle surface to the deformed middle surface is u_o (the symbol 'nought' (^{o}) is used to designate middle-surface values of a variable). Because line ABCD remains straight under deformation of the laminate, the displacement at point C is

$$u_c = u_o - z_c \beta \tag{C.38}$$

But because line ABCD, under deformation, further remains perpendicular to the middle surface, β is the slope of the laminate middle surface in the x-direction, that is,

$$\beta = \frac{\partial w_o}{\partial x} \tag{C.39}$$

Then, the displacement, u, in the x-direction at any point z through the laminate thickness is

$$u = u_o - z \frac{\partial w_o}{\partial x} \tag{C.40}$$

By similar reasoning, the displacement, v, in the y-direction at any point z through the laminate thickness is

$$v = v_o - z \frac{\partial w_o}{\partial y} \tag{C.41}$$

The laminate strains have been reduced to ε_x, ε_y, and γ_{xy} by virtue of the Kirchhoff hypothesis. That is, $\varepsilon_z = \gamma_{xz} = \gamma_{yz} = 0$. For small strains (linear elasticity), the remaining strains are defined in terms of (derivatives of) displacements as

$$\begin{aligned} \varepsilon_x &= \frac{\partial u}{\partial x} \\ \varepsilon_y &= \frac{\partial v}{\partial y} \\ \gamma_{xy} &= \frac{\partial u}{\partial y} + \frac{\partial v}{\partial x} \end{aligned} \tag{C.42}$$

Thus, for the derived displacements u and v in Equations (C.40) and (C.41), the strains are

Éléments sous droits d'auteur

$$\varepsilon_x = \frac{\partial u_o}{\partial x} - z\frac{\partial^2 w_o}{\partial x^2}$$

$$\varepsilon_y = \frac{\partial v_o}{\partial y} - z\frac{\partial^2 w_o}{\partial y^2} \qquad \text{(C.43)}$$

$$\gamma_{xy} = \frac{\partial u_o}{\partial y} + \frac{\partial v_o}{\partial x} - 2z\frac{\partial^2 w_o}{\partial x \partial y}$$

or

$$\begin{bmatrix} \varepsilon_x \\ \varepsilon_y \\ \gamma_{xy} \end{bmatrix} = \begin{bmatrix} \varepsilon_x^o \\ \varepsilon_y^o \\ \gamma_{xy}^o \end{bmatrix} + z \begin{bmatrix} \kappa_x \\ \kappa_y \\ \kappa_{xy} \end{bmatrix} \qquad \text{(C.44)}$$

in which the middle-surface strains are

$$\begin{bmatrix} \varepsilon_x^o \\ \varepsilon_y^o \\ \gamma_{xy}^o \end{bmatrix} = \begin{bmatrix} \dfrac{\partial u_o}{\partial x} \\ \dfrac{\partial v_o}{\partial y} \\ \dfrac{\partial u_o}{\partial y} + \dfrac{\partial v_o}{\partial x} \end{bmatrix} \qquad \text{(C.45)}$$

and the middle-surface curvatures are

$$\begin{bmatrix} \kappa_x \\ \kappa_y \\ \kappa_{xy} \end{bmatrix} = - \begin{bmatrix} \dfrac{\partial^2 w_o}{\partial x^2} \\ \dfrac{\partial^2 w_o}{\partial y^2} \\ 2\dfrac{\partial^2 w_o}{\partial x \partial y} \end{bmatrix} \qquad \text{(C.46)}$$

(The last term in Equation (C.46) is the twist curvature of the middle surface.) We refer only to curvatures of the middle surface as a reference surface and not of any other surface, so nought superscripts are not needed on κ_x, κ_y, and κ_{xy}. Thus, the Kirchhoff hypothesis has been readily verified to imply a linear variation of strain through the laminate thickness because the strains in Equation (C.44) have the form of a straight line, i.e., $y = mx + b$. The foregoing strain analysis is valid only

Éléments sous droits d'auteur

for plates because of the nature of the strain-displacement relations in Equation (C.42). For circular cylindrical shells, the ε_y term in Equation (C.42) must be supplemented by w_o/r where r is the shell radius; other shells have more complicated strain-displacement relations.

Substitute the linear strain variation through the thickness, Equation (C.44), in the stress-strain relations, Equation (C.37). Thus, the stresses in the k^{th} layer can be expressed in terms of the laminate middle-surface strains and curvatures as

$$\begin{bmatrix} \sigma_x \\ \sigma_y \\ \tau_{xy} \end{bmatrix}_k = \begin{bmatrix} \bar{Q}_{11} & \bar{Q}_{12} & \bar{Q}_{16} \\ \bar{Q}_{12} & \bar{Q}_{22} & \bar{Q}_{26} \\ \bar{Q}_{16} & \bar{Q}_{26} & \bar{Q}_{66} \end{bmatrix}_k \left[\begin{bmatrix} \varepsilon_x^o \\ \varepsilon_y^o \\ \gamma_{xy}^o \end{bmatrix} + z \begin{bmatrix} \kappa_x \\ \kappa_y \\ \kappa_{xy} \end{bmatrix} \right] \tag{C.47}$$

The $\bar{Q}_{ij}$ can be different for each layer of the laminate, so the stress variation through the laminate thickness is not necessarily linear (a straight line as in ordinary isotropic plate theory), even though the strain variation is linear through the laminate thickness. Instead, typical strain and stress variations are shown in Figure C-14 where the stresses are *piecewise linear* (i.e., linear in each layer, but discontinuous at boundaries between laminae because the stiffnesses (moduli) are different in each adjacent layer).

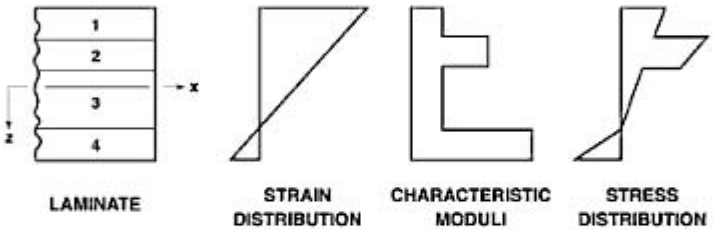


Figure C-14 Hypothetical Variation of Strain and Stress through the Laminate Thickness

C.6.3 Resultant Laminate Forces and Moments

The resultant forces and moments acting on a laminate are obtained by integration of the stresses in each layer or lamina through the laminate thickness, for example,

$$N_x = \int_{-t/2}^{t/2} \sigma_x \, dz \qquad M_x = \int_{-t/2}^{t/2} \sigma_x \, z \, dz \tag{C.48}$$

Note in Figure C-14 that the stresses vary within each lamina as well as from lamina to lamina, so the integration is not trivial. Actually, N_x is a force per unit width of the cross section of the laminate as shown in Figure C-15.

Éléments sous droits d'auteur

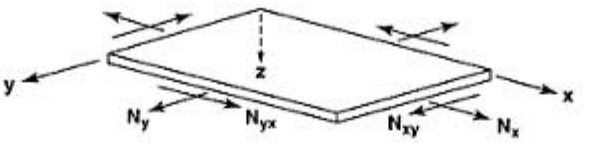


Figure C-15 In-Plane Forces on a Flat Laminate

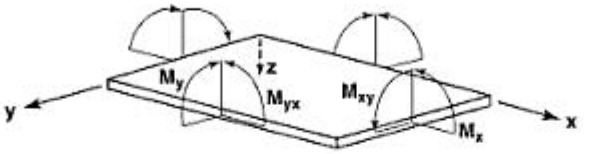


Figure C-16 Moments on a Flat Laminate

Similarly, M_x is a moment per unit width as shown in Figure C-16. However, N_x, etc., and M_x, etc., will be referred to as forces and moments with the stipulation of 'per unit width' being dropped for convenience. The entire collection of force and moment resultants for an N-layered laminate is depicted in Figures C-15 and C-16 and is defined as

$$\begin{bmatrix} N_x \\ N_y \\ N_{xy} \end{bmatrix} = \int_{-t/2}^{t/2} \begin{bmatrix} \sigma_x \\ \sigma_y \\ \tau_{xy} \end{bmatrix} dz = \sum_{k=1}^{N} \int_{z_{k-1}}^{z_k} \begin{bmatrix} \sigma_x \\ \sigma_y \\ \tau_{xy} \end{bmatrix}_k dz \qquad (C.49)$$

and

$$\begin{bmatrix} M_x \\ M_y \\ M_{xy} \end{bmatrix} = \int_{-t/2}^{t/2} \begin{bmatrix} \sigma_x \\ \sigma_y \\ \tau_{xy} \end{bmatrix} z\, dz = \sum_{k=1}^{N} \int_{z_{k-1}}^{z_k} \begin{bmatrix} \sigma_x \\ \sigma_y \\ \tau_{xy} \end{bmatrix}_k z\, dz \qquad (C.50)$$

in which z_k and z_{k-1} are defined in the laminate through-the-thickness geometry of Figure C-17. Note there that the z_i are directed distances (coordinates) in accordance with the convention that z is positive downward from the middle surface. That is, z_k is the directed distance to the bottom of the k^{th} layer, and z_{k-1} is the directed distance to the top of the k^{th} layer. Moreover, $z_0 = -t/2$, $z_1 = -t/2 + t_1$, etc., whereas $z_N = +t/2$, $z_{N-1} = +t/2 - t_N$, etc. These force and moment resultants do not depend on z after integration, but are functions of x and y, the coordinates in the plane of the laminate middle surface.

Éléments sous droits d'auteur

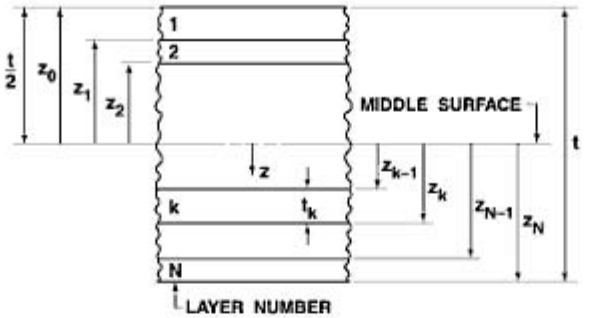


Figure C-17 Through-the-Thickness Geometry of an N-Layered Laminate

Equations (C.49) and (C.50) can be rearranged to take advantage of the fact that the stiffness matrix for a lamina is often constant within the lamina (unless the lamina has temperature-dependent or moisture-dependent properties and a temperature gradient or a moisture gradient exists across the lamina). If the elevated temperature or moisture is constant through the thickness of the lamina (a 'soaked' condition), then the values of the $[\overline{Q}_{ij}]_k$ are constant in the layer but are likely degraded because of the presence of temperature and/or moisture. Thus, the stiffness matrix goes outside the integration over each layer, but is within the summation of force and moment resultants for each layer. When the lamina stress-strain relations, Equation (C.47), are substituted, the forces and moments become

$$\begin{bmatrix} N_x \\ N_y \\ N_{xy} \end{bmatrix} = \sum_{k=1}^{N} \begin{bmatrix} \overline{Q}_{11} & \overline{Q}_{12} & \overline{Q}_{16} \\ \overline{Q}_{12} & \overline{Q}_{22} & \overline{Q}_{26} \\ \overline{Q}_{16} & \overline{Q}_{26} & \overline{Q}_{66} \end{bmatrix}_k \left[\int_{z_{k-1}}^{z_k} \begin{bmatrix} \varepsilon_x^\circ \\ \varepsilon_y^\circ \\ \gamma_{xy}^\circ \end{bmatrix} dz + \int_{z_{k-1}}^{z_k} \begin{bmatrix} \kappa_x \\ \kappa_y \\ \kappa_{xy} \end{bmatrix} z\, dz \right] \quad \text{(C.51)}$$

$$\begin{bmatrix} M_x \\ M_y \\ M_{xy} \end{bmatrix} = \sum_{k=1}^{N} \begin{bmatrix} \overline{Q}_{11} & \overline{Q}_{12} & \overline{Q}_{16} \\ \overline{Q}_{12} & \overline{Q}_{22} & \overline{Q}_{26} \\ \overline{Q}_{16} & \overline{Q}_{26} & \overline{Q}_{66} \end{bmatrix}_k \left[\int_{z_{k-1}}^{z_k} \begin{bmatrix} \varepsilon_x^\circ \\ \varepsilon_y^\circ \\ \gamma_{xy}^\circ \end{bmatrix} z\, dz + \int_{z_{k-1}}^{z_k} \begin{bmatrix} \kappa_x \\ \kappa_y \\ \kappa_{xy} \end{bmatrix} z^2\, dz \right] \quad \text{(C.52)}$$

Sometimes the stiffness matrix for a lamina, $[\overline{Q}_{ij}]_k$, is not constant through the thickness of the lamina. For example, if a temperature gradient or moisture gradient exists in the lamina and the lamina material properties are temperature dependent and/or moisture dependent, then $[\overline{Q}_{ij}]_k$ is a function of z and must be left inside the integral. In such cases,

Éléments sous droits d'auteur

the laminate is nonhomogeneous within each layer, so a more complicated numerical integration solution is required than is addressed here.

We now recall that ε_x^o, ε_y^o, γ_{xy}^o, κ_x, κ_y, and κ_{xy} are not functions of z, but are middle-surface values so they can be removed from within the summation signs. Thus, Equations (C.51) and (C.52) can be written as

$$\begin{bmatrix} N_x \\ N_y \\ N_{xy} \end{bmatrix} = \begin{bmatrix} A_{11} & A_{12} & A_{16} \\ A_{12} & A_{22} & A_{26} \\ A_{16} & A_{26} & A_{66} \end{bmatrix} \begin{bmatrix} \varepsilon_x^o \\ \varepsilon_y^o \\ \gamma_{xy}^o \end{bmatrix} + \begin{bmatrix} B_{11} & B_{12} & B_{16} \\ B_{12} & B_{22} & B_{26} \\ B_{16} & B_{26} & B_{66} \end{bmatrix} \begin{bmatrix} \kappa_x \\ \kappa_y \\ \kappa_{xy} \end{bmatrix} \tag{C.53}$$

$$\begin{bmatrix} M_x \\ M_y \\ M_{xy} \end{bmatrix} = \begin{bmatrix} B_{11} & B_{12} & B_{16} \\ B_{12} & B_{22} & B_{26} \\ B_{16} & B_{26} & B_{66} \end{bmatrix} \begin{bmatrix} \varepsilon_x^o \\ \varepsilon_y^o \\ \gamma_{xy}^o \end{bmatrix} + \begin{bmatrix} D_{11} & D_{12} & D_{16} \\ D_{12} & D_{22} & D_{26} \\ D_{16} & D_{26} & D_{66} \end{bmatrix} \begin{bmatrix} \kappa_x \\ \kappa_y \\ \kappa_{xy} \end{bmatrix} \tag{C.54}$$

in which

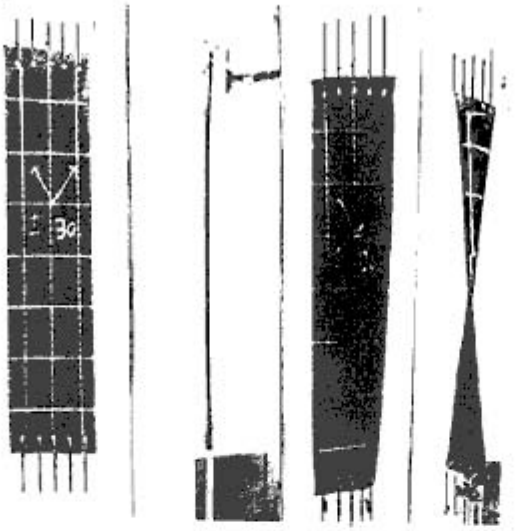
$$\begin{aligned} A_{ij} &= \sum_{k=1}^{N} (\bar{Q}_{ij})_k (z_k - z_{k-1}) \\ B_{ij} &= \frac{1}{2} \sum_{k=1}^{N} (\bar{Q}_{ij})_k (z_k^2 - z_{k-1}^2) \\ D_{ij} &= \frac{1}{3} \sum_{k=1}^{N} (\bar{Q}_{ij})_k (z_k^3 - z_{k-1}^3) \end{aligned} \tag{C.55}$$

In Equations (C.53), (C.54), and (C.55), the A_{ij} are extensional stiffnesses, the B_{ij} are bending-extension coupling stiffnesses, and the D_{ij} are bending stiffnesses. The mere presence of the B_{ij} implies coupling between bending and extension of a laminate [because both forces and curvatures as well as moments and strains simultaneously exist in Equations (C.53) and (C.54)]. Thus, it is impossible to pull on a laminate that has B_{ij} terms without at the same time bending and/or twisting the laminate. That is, an extensional force results in not only extensional deformations, but bending and/or twisting of the laminate. Also, such a laminate cannot be subjected to moment without at the same time suffering extension of the middle surface. The first observation is borne out for the two-layered, nylon-reinforced rubber laminate depicted in Figure C-18. Without load, the laminate is flat as in Figure C-18a. Subject the laminate to the force resultant N_x and, because of the manner of support and loading, $N_y = N_{xy} = M_x = M_{xy} = 0$. When the principal material directions of the two laminae are oriented at $+\alpha$ and $-\alpha$, respectively, to the laminate x-axis, we can show that the general expression for N_x is specialized to

$$N_x = A_{11}\varepsilon_x^o + A_{12}\varepsilon_y^o + B_{16}\kappa_{xy} \tag{C.56}$$

Éléments sous droits d'auteur

Thus, the force resultant N_x produces twisting of the laminate as evidenced by the κ_{xy} term in addition to the usual normal strains ε_x° (extension) and ε_y° (contraction) as readily seen in Figure C-18b.



a Unloaded b Loaded with N_x

Figure C-18 Twisting of a Two-Layered Antisymmetric Laminate under Tension *(After Ashton, Halpin, and Petit [C-6])*

C.6.4 Summary

Classical lamination theory consists of a comprehensive set of deformation hypotheses leading to the force-strain-curvature and moment-strain-curvature relations of Equations (C.53) and (C.54) shown in Figure C-19 where the physical significances of the A_{ij}, B_{ij}, and D_{ij} are labeled. There, A_{16} and A_{26} represent shear-extension coupling at the laminate level analogous to that found for a single lamina in Section C.5. Of course, the B_{ij} represent coupling between bending and extension, a phenomenon not found at the lamina level. Finally, D_{16} and D_{26} represent bend-twist coupling. Bend-twist coupling is illustrated by bending a fiber-reinforced rubber beam that has unidirectional nylon fibers at some angle to the spanwise direction in the horizontal plane as in Figure C-20b. There, the beam not only bends in the spanwise direction, but it also twists about its spanwise axis as outlined with white ink on the black rubber body of the beam such that two diagonally opposite corners of the beam actually lift off the supports at each end of the beam. If the same beam is rotated 90° about its spanwise axis (so the fibers are at some angle to the spanwise axis in the *vertical* plane) and bent as in Figure C-20a, then no twisting occurs! A plate with fibers at an angle to the spanwise direction behaves in a similar manner as shown in Figure C-21.

Éléments sous droits d'auteur

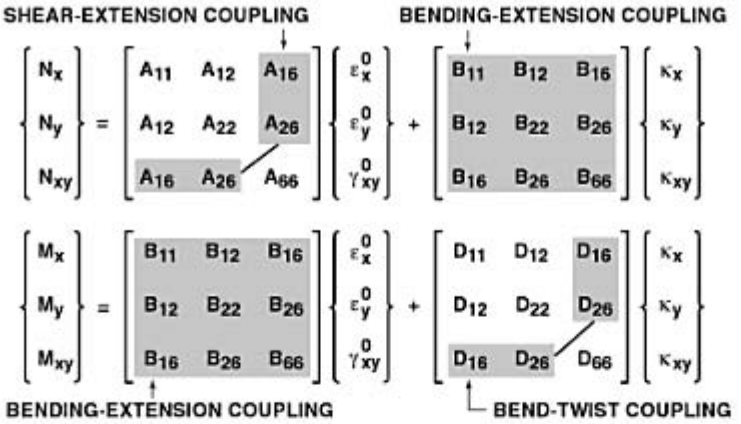
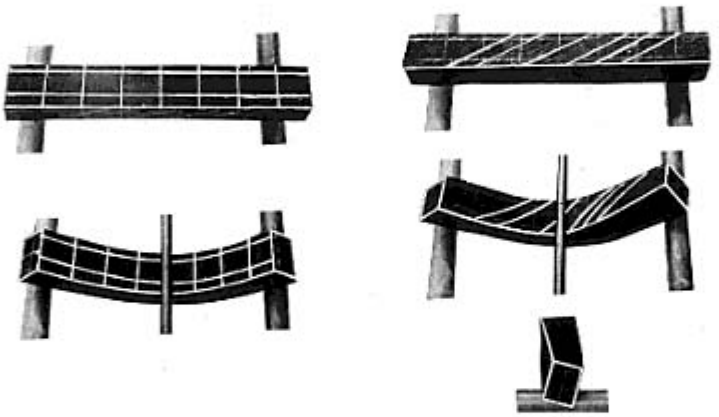


Figure C-19 Physical Significance of Stiffness Terms in Force and Moment Resultants



a Aligned Orthotropy b Non-Aligned Orthotropy

Figure C-20 Effect of Bend-Twist Coupling on Beam Bending *(After Ashton, Halpin, and Petit [C-6])*

The behaviors studied so far include isotropic materials, orthotropic materials (often called specially orthotropic if loaded in principal material directions), generally orthotropic materials (merely an orthotropic material loaded in non-principal material directions), and laminates. Each configuration is shown in Figure C-22 along with its deformation response to

Éléments sous droits d'auteur

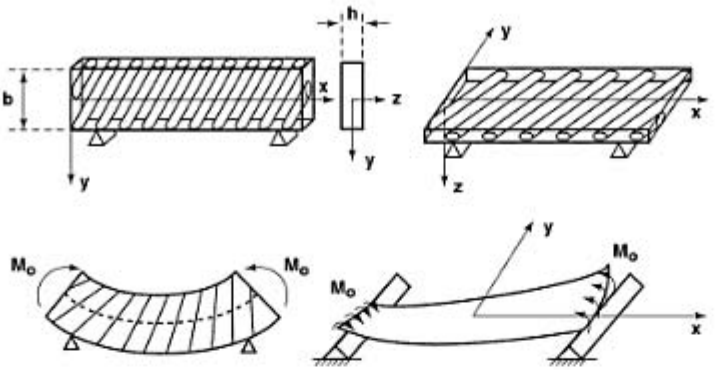


Figure C-21 Effect of Bend-Twist Coupling on Plate Bending
(After Ashton, Halpin, and Petit [C-6])

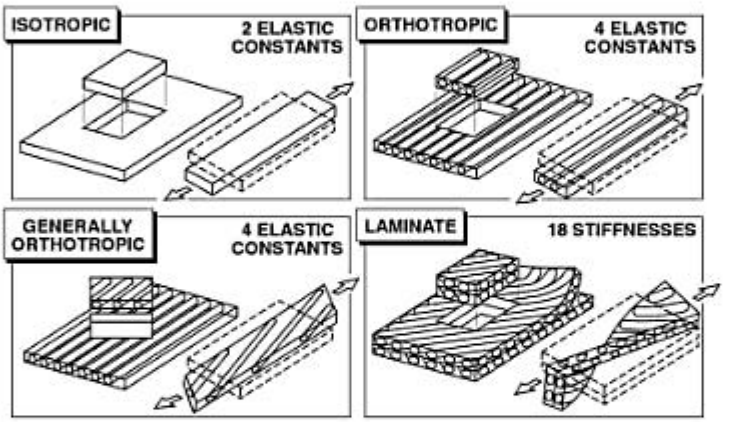


Figure C-22 Material and Structural Forms
(After Ashton, Halpin, and Petit [C-6])

axial loading. Note that shear-extension coupling does not occur for orthotropic materials loaded in principal material directions, but does occur if the loading is not in those directions. Moreover, a laminate can twist when pulled in the axial direction. Also shown is the number of independent elastic constants for each material class (two for isotropic materials and four for orthotropic materials). Note especially that a laminate has a maximum of 18 stiffnesses (six each of A_{ij}, B_{ij}, and D_{ij}). *The stiffnesses are not elastic constants, but are a combination of elastic constants and geometric terms. Thus, a laminate is a structural element,*

Éléments sous droits d'auteur

not a material. The number of elastic constants for a laminate made of orthotropic laminae is a maximum of four per layer, but if the laminate is made of the same orthotropic material in each layer, then the laminate has only four elastic constants.

Some engineers have tried to characterize laminates with effective laminate stiffnesses, E_x, E_y, ν_{xy}, and G_{xy}, and indeed such properties can be determined for a laminate by the usual measurements. However, it is crucial to recognize that with an effective laminate stiffness approach

- shear-extension coupling is ignored
- all bending response is ignored
  (including, of course, bend-twist coupling)
- coupling between bending and extension is ignored
  (many laminates are symmetric, but many others are not)

Again, we must realize that *a laminate is not a material, but instead is a structural element with essential features of both material properties and geometry that cannot be ignored.* Thus, an effective laminate stiffness approach is fatally flawed in most practical applications (although not for the special case of a laminate that is symmetric about the middle surface and subjected only to extensional loading). Accordingly, *we must characterize laminates with the essential extension, bending-extension coupling, and bending stiffnesses of Equation (C.55).*

In conclusion, classical lamination theory enables us to calculate forces and moments if we know the strains and curvatures of the middle surface (or vice versa). Then, we can calculate the laminae stresses in laminate coordinates. Next, we can transform the laminae stresses from laminate coordinates to lamina principal material directions. Finally, we would expect to apply a failure criterion to each lamina in its own principal material directions. This process seems straightforward in principle, but the force-strain-curvature and moment-strain-curvature relations in Equations (C.53) and (C.54) are difficult to completely understand. Thus, we attempt some simplifications in the next section in order to enhance our understanding of classical lamination theory.

C.7 SPECIAL CASES OF LAMINATE STIFFNESSES

This section is devoted to those special cases of laminates for which the stiffnesses take on certain simplified values as opposed to the general form in Equation (C.55). The general force-moment-strain-curvature relations in Equations (C.53) and (C.54) are far too comprehensive to easily understand. Thus, we build up our understanding of laminate behavior from the simplest cases to more complicated cases. Some of the cases are almost trivial, others are more specialized, some do not occur often in practice, but the point is that *all* are contributions to the understanding of the concept of laminate stiffnesses. Many of the cases result from the common practice of constructing laminates from laminae that have the same material properties and thickness, but have different orientations of the principal material directions relative to one another and relative to the laminate axes. More general cases are also examined.

Éléments sous droits d'auteur

Stiffnesses for single-layered configurations are treated first to provide a baseline for subsequent discussion. Such stiffnesses should be recognizable in terms of concepts previously encountered by the reader in his study of plates and shells. Next, laminates that are symmetric about their middle surface are discussed and classified. Then, laminates with laminae that are antisymmetrically arranged about their middle surface are described. Finally, laminates with a complete lack of middle-surface symmetry, i.e., unsymmetric laminates, are discussed. For all laminates, the question of laminae thicknesses arises. *Regular laminates* have equal-thickness laminae, and *irregular laminates* have non-equal-thickness laminae. Finally, a convenient laminate stacking-sequence notation is described along with the concept of hybrid laminates.

C.7.1 Single-Layered Configurations

The special single-layered configurations treated in this section are isotropic, specially orthotropic, generally orthotropic, and anisotropic. The generally orthotropic configuration cannot, of course, be distinguished from an anisotropic layer from the analysis point of view, but does have only the four independent material properties of an orthotropic material instead of the six for an anisotropic material.

Single Isotropic Layer

For a single isotropic layer with material properties, E and ν, and thickness, t, the laminate stiffnesses of Equation (C.55) reduce to

$$\begin{aligned}
A_{11} &= \frac{E\,t}{1-\nu^2} = A & & & D_{11} &= \frac{E\,t^3}{12(1-\nu^2)} = D \\
A_{12} &= \nu A & & & D_{12} &= \nu D \\
A_{22} &= A & B_{ij} &= 0 & D_{22} &= D \\
A_{16} &= 0 & & & D_{16} &= 0 \\
A_{26} &= 0 & & & D_{26} &= 0 \\
A_{66} &= \frac{E\,t}{2(1+\nu)} = \frac{1-\nu}{2}A & & & D_{66} &= \frac{E\,t^3}{24(1+\nu)} = \frac{1-\nu}{2}D
\end{aligned} \qquad \text{(C.57)}$$

in which A is the extensional stiffness and D the bending stiffness of an isotropic layer. The resultant forces depend only on the in-plane strains of the laminate middle surface, and the resultant moments depend only on the curvatures of the middle surface:

$$\begin{bmatrix} N_x \\ N_y \\ N_{xy} \end{bmatrix} = \begin{bmatrix} A & \nu A & 0 \\ \nu A & A & 0 \\ 0 & 0 & \frac{1-\nu}{2}A \end{bmatrix} \begin{bmatrix} \varepsilon_x^\circ \\ \varepsilon_y^\circ \\ \gamma_{xy}^\circ \end{bmatrix} \qquad \text{(C.58)}$$

Éléments sous droits d'auteur

$$\begin{bmatrix} M_x \\ M_y \\ M_{xy} \end{bmatrix} = \begin{bmatrix} D & \nu D & 0 \\ \nu D & D & 0 \\ 0 & 0 & \dfrac{1-\nu}{2} D \end{bmatrix} \begin{bmatrix} \kappa_x \\ \kappa_y \\ \kappa_{xy} \end{bmatrix} \tag{C.59}$$

Thus, there is no coupling between bending and extension of a single isotropic layer. Also note the special relation between A and D:

$$D = \frac{A t^2}{12} \tag{C.60}$$

Single Specially Orthotropic Layer

For a single specially orthotropic layer of thickness, t, and lamina stiffnesses, Q_{ij}, given in Equation (C.14), the laminate stiffnesses are

$$\begin{aligned} A_{11} &= Q_{11} t & & & D_{11} &= \frac{Q_{11} t^3}{12} \\ A_{12} &= Q_{12} t & & & D_{12} &= \frac{Q_{12} t^3}{12} \\ A_{22} &= Q_{22} t & B_{ij} &= 0 & D_{22} &= \frac{Q_{22} t^3}{12} \\ A_{16} &= 0 & & & D_{16} &= 0 \\ A_{26} &= 0 & & & D_{26} &= 0 \\ A_{66} &= Q_{66} t & & & D_{66} &= \frac{Q_{66} t^3}{12} \end{aligned} \tag{C.61}$$

in which $D_{ij} = A_{ij}^2/12$ similar to Equation (C.60). Thus, as with a single isotropic layer, the resultant forces depend only on the in-plane strains, and the resultant moments depend only on the curvatures:

$$\begin{bmatrix} N_x \\ N_y \\ N_{xy} \end{bmatrix} = \begin{bmatrix} A_{11} & A_{12} & 0 \\ A_{12} & A_{22} & 0 \\ 0 & 0 & A_{66} \end{bmatrix} \begin{bmatrix} \varepsilon_x^\circ \\ \varepsilon_y^\circ \\ \gamma_{xy}^\circ \end{bmatrix} \tag{C.62}$$

$$\begin{bmatrix} M_x \\ M_y \\ M_{xy} \end{bmatrix} = \begin{bmatrix} D_{11} & D_{12} & 0 \\ D_{12} & D_{22} & 0 \\ 0 & 0 & D_{66} \end{bmatrix} \begin{bmatrix} \kappa_x \\ \kappa_y \\ \kappa_{xy} \end{bmatrix} \tag{C.63}$$

Single Generally Orthotropic Layer

For a single generally orthotropic layer of thickness, t, and lamina stiffnesses, Q_{ij}, given in Equation (C.29), the laminate stiffnesses are

Éléments sous droits d'auteur

$$A_{ij} = \bar{Q}_{ij}\, t \qquad B_{ij} = 0 \qquad D_{ij} = \frac{\bar{Q}_{ij}\, t^3}{12} \tag{C.64}$$

Again, there is no coupling between bending and extension, so the force and moment resultants are

$$\begin{bmatrix} N_x \\ N_y \\ N_{xy} \end{bmatrix} = \begin{bmatrix} A_{11} & A_{12} & A_{16} \\ A_{12} & A_{22} & A_{26} \\ A_{16} & A_{26} & A_{66} \end{bmatrix} \begin{bmatrix} \varepsilon_x^\circ \\ \varepsilon_y^\circ \\ \gamma_{xy}^\circ \end{bmatrix} \tag{C.65}$$

$$\begin{bmatrix} M_x \\ M_y \\ M_{xy} \end{bmatrix} = \begin{bmatrix} D_{11} & D_{12} & D_{16} \\ D_{12} & D_{22} & D_{26} \\ D_{16} & D_{26} & D_{66} \end{bmatrix} \begin{bmatrix} \kappa_x \\ \kappa_y \\ \kappa_{xy} \end{bmatrix} \tag{C.66}$$

Note that, in contrast to both an isotropic layer and a specially orthotropic layer, extensional forces depend on shearing strain as well as on extensional strain. Also, the resultant shearing force, N_{xy}, depends on the extensional strains, ε_x° and ε_y°, as well as on the shear strain, γ_{xy}°. Similarly, the moment resultants all depend on both the bending curvatures, κ_x and κ_y, and on the twist curvature, κ_{xy}. Thus, both shear-extension and bend-twist coupling occur.

Single Anisotropic Layer

The only difference between a single generally orthotropic layer and an anisotropic layer is that the latter has lamina stiffnesses, Q_{ij}, defined implicitly in Equation (C.33) with six independent material properties whereas the generally orthotropic layer has stiffnesses, Q_{ij}, defined in Equation (C.29) with only four independent properties. The laminate stiffnesses are

$$A_{ij} = Q_{ij}\, t \qquad B_{ij} = 0 \qquad D_{ij} = \frac{Q_{ij}\, t^3}{12} \tag{C.67}$$

and the force and moment resultants are Equations (C.65) and (C.66).

C.7.2 Symmetric Laminates

If laminates are symmetric in *both geometry and material properties* about the middle surface, then the general stiffness equations, Equation (C.55), simplify greatly. To achieve that symmetry, for each pair of equal-thickness laminae: (1) both laminae must have the same material properties and principal material direction orientations, i.e., both laminae have the same $[\bar{Q}_{ij}]_k$; and (2) if one lamina is a certain distance above the middle surface, then the other lamina is the same distance *below* the middle surface. A single layer that straddles the middle surface is inherently symmetric about the middle surface).

Éléments sous droits d'auteur

Because of the symmetry of the $[\bar{Q}_{ij}]_k$ and the thicknesses t_k about the middle surface of the laminate, all of the bending-extension coupling stiffnesses, the B_{ij}, are zero. The elimination of the B_{ij} has two important practical ramifications. First, such laminates are usually much easier to analyze than laminates with bending-extension coupling. Second, symmetric laminates do not have a tendency to bend or twist from the inevitable thermally induced contractions that occur during cooling following an elevated-temperature curing process. For example, an unsymmetric cross-ply laminate that was laid up from individual layers on a flat steel plate and enclosed top and bottom with flat steel plates during curing in a hot press is shown in Figure C-23 after being removed from the plates and the hot press. What a shock to see such a *highly curved laminate* come *out* of the curing process after you put *in* a set of *flat* laminae between *flat* steel plates in a *flat* hot press! Consequently, symmetric laminates are commonly used unless special circumstances require an unsymmetric laminate. For example, part of the function of a laminate might be to serve as a heat shield, but the heat comes from only one side; thus, an unsymmetric laminate must be used (or will result anyway!) The force and moment resultants for a symmetric laminate are

$$\begin{bmatrix} N_x \\ N_y \\ N_{xy} \end{bmatrix} = \begin{bmatrix} A_{11} & A_{12} & A_{16} \\ A_{12} & A_{22} & A_{26} \\ A_{16} & A_{26} & A_{66} \end{bmatrix} \begin{bmatrix} \varepsilon_x^o \\ \varepsilon_y^o \\ \gamma_{xy}^o \end{bmatrix} \tag{C.68}$$

$$\begin{bmatrix} M_x \\ M_y \\ M_{xy} \end{bmatrix} = \begin{bmatrix} D_{11} & D_{12} & D_{16} \\ D_{12} & D_{22} & D_{26} \\ D_{16} & D_{26} & D_{66} \end{bmatrix} \begin{bmatrix} \kappa_x \\ \kappa_y \\ \kappa_{xy} \end{bmatrix} \tag{C.69}$$

Special cases of symmetric laminates will be described in the following subsections. In each case, the A_{ij} and D_{ij} in Equations (C.68) and (C.69) take on different values, and some will even vanish.

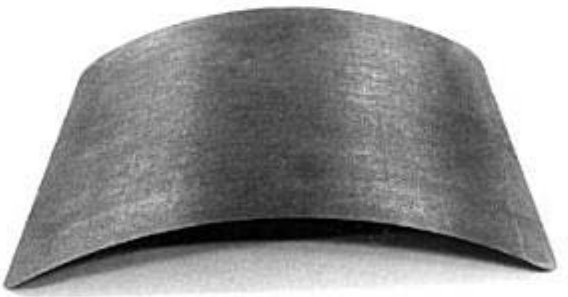


Figure C-23 An Unsymmetric Laminate after Curing

Éléments sous droits d'auteur

Even a laminate that is made symmetrically about the middle surface can have coupling between bending and extension! If the laminae have temperature-dependent material properties and a through-the-thickness thermal gradient is applied (recall the heat shield example on the preceding page), then the premises on which Equations (C.51) and (C.52) are based are no longer applicable. The stiffnesses are far more complicated than in Equation (C.55). The temperature gradient actually changes the material properties differently through the thickness and, hence, destroys the original laminate symmetry.

Symmetric Laminates with Multiple Isotropic Layers

If multiple isotropic layers of various thicknesses are arranged symmetrically about a middle surface from both a geometric and a material property standpoint, then the resulting laminate does not exhibit coupling between bending and extension. A simple example of a symmetric laminate with three isotropic layers (which occurs with auto safety glass) is shown in Figure C-24. There, the two types of symmetry, material property and geometric, are quite evident. A more complicated example of a symmetric laminate with six isotropic layers of different elastic properties and thicknesses is given in Table C-1. There also, the geometric and material property symmetry are both obvious. Note that layers 3 and 4 in Table C-1 could together be regarded as a single layer of thickness 6t without changing the stiffness characteristics.

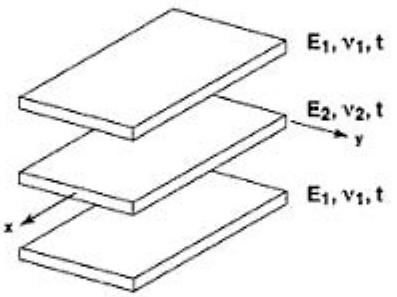


Figure C-24 Unbonded View of a Three-Layered Symmetric Laminate with Isotropic Layers

Table C-1 Symmetric Laminate with Six Multiple Isotropic Layers

Layer	Material Properties	Layer Thickness
1	E_1, ν_1	t
2	E_2, ν_2	2t
3	E_3, ν_3	3t
4	E_3, ν_3	3t
5	E_2, ν_2	2t
6	E_1, ν_1	t

Éléments sous droits d'auteur

The extensional and bending stiffnesses for the general case are calculated from Equation (C.55) wherein for the k^{th} layer

$$(\bar{Q}_{11})_k = (\bar{Q}_{22})_k = \frac{E_k}{1-\nu_k^2} \qquad (\bar{Q}_{16})_k = (\bar{Q}_{26})_k = 0$$
$$(\bar{Q}_{12})_k = \frac{\nu_k E_k}{1-\nu_k^2} \qquad (\bar{Q}_{66})_k = \frac{E_k}{2(1-\nu_k)} \tag{C.70}$$

The force and moment resultants take the simplified form

$$\begin{bmatrix} N_x \\ N_y \\ N_{xy} \end{bmatrix} = \begin{bmatrix} A_{11} & A_{12} & 0 \\ A_{12} & A_{22} & 0 \\ 0 & 0 & A_{66} \end{bmatrix} \begin{bmatrix} \varepsilon_x^o \\ \varepsilon_y^o \\ \gamma_{xy}^o \end{bmatrix} \tag{C.71}$$

$$\begin{bmatrix} M_x \\ M_y \\ M_{xy} \end{bmatrix} = \begin{bmatrix} D_{11} & D_{12} & 0 \\ D_{12} & D_{22} & 0 \\ 0 & 0 & D_{66} \end{bmatrix} \begin{bmatrix} \kappa_x \\ \kappa_y \\ \kappa_{xy} \end{bmatrix} \tag{C.72}$$

wherein, for isotropic layers, $A_{11} = A_{22}$ and $D_{11} = D_{22}$ because of the first condition of Equation (C.70). The specific form of the A_{ij} and D_{ij} can be somewhat involved, as can easily be verified by examining some simple examples. Note that no shear-extension or bend-twist coupling exists.

Symmetric Laminates with Multiple Specially Orthotropic Layers

Because of the behavioral and analytical complications from the stiffnesses A_{16}, A_{26}, D_{16}, and D_{26}, a laminate is often desired that does not have these stiffnesses. Laminates can be made with orthotropic layers that have principal material directions aligned with the laminate axes. If the thicknesses, locations, and material properties of the laminae are symmetric about the middle surface of the laminate, there is no coupling between bending and extension. A general example is shown in Table C-2. Note that the material property symmetry requires equal $[\bar{Q}_{ij}]_k$ of the two layers that are placed at the same distance above and below the middle surface. Thus, both the orthotropic material properties,

Table C-2 Symmetric Laminate with Five Specially Orthotropic Layers

Layer	Material Properties				Orientation	Thickness
	Q_{11}	Q_{12}	Q_{22}	Q_{66}		
1	F_1	F_2	F_3	F_4	0°	t
2	G_1	G_2	G_3	G_4	90°	2t
3	H_1	H_2	H_3	H_4	90°	4t
4	G_1	G_2	G_3	G_4	90°	2t
5	F_1	F_2	F_3	F_4	0°	t

Éléments sous droits d'auteur

$[Q_{ij}]_k$, of the layers *and* the angle of the principal material directions to the laminate axes (i.e., the orientation of each layer) must be identical.

The extensional and bending stiffnesses are calculated from Equation (C.55) wherein for the k^{th} layer

$$(\bar{Q}_{11})_k = \frac{E_1^k}{1 - \nu_{12}^k \nu_{21}^k} \qquad (\bar{Q}_{12})_k = \frac{\nu_{12}^k E_1^k}{1 - \nu_{12}^k \nu_{21}^k} \qquad (\bar{Q}_{22})_k = \frac{E_2^k}{1 - \nu_{12}^k \nu_{21}^k}$$

$$(\bar{Q}_{16})_k = 0 \qquad (\bar{Q}_{26})_k = 0 \qquad (\bar{Q}_{66})_k = G_{12}^k \qquad \text{(C.73)}$$

The $(\bar{Q}_{16})_k$ and $(\bar{Q}_{26})_k$ are zero, so the stiffnesses A_{16}, A_{26}, D_{16}, and D_{26} vanish. Also, the bending-extension coupling stiffnesses B_{ij} are zero because of laminate symmetry. This type of laminate could therefore be called a specially orthotropic laminate in analogy to a specially orthotropic lamina. However, *a laminate should not be called by a material property characterization name because laminates are not materials, but instead are structural elements* (Jones [C-7]). The force and moment resultants take the form of Equations (C.71) and (C.72), respectively, except that $A_{11} \neq A_{22}$ and $D_{11} \neq D_{22}$ for a laminate with specially orthotropic layers.

A very common special case of symmetric laminates with multiple specially orthotropic layers occurs when the laminae are all of the same thickness and material properties, but have their major principal material directions alternating at 0° and 90° to the laminate axes, for example, 0°/90°/0°. Such laminates are called *regular symmetric cross-ply laminates* (*regular* because the laminae thicknesses are the same, symmetric because both the geometry and material properties are symmetric about the laminate middle surface, and *cross-ply* because the fibers in adjacent layers are at 90° to one another). A simple example of a regular symmetric cross-ply laminate with three layers of equal thickness and properties is shown in Figure C-25. The laminate must have an odd number of layers to satisfy the symmetry requirement by which coupling between bending and extension is eliminated (unless the layers do not alternate in fiber direction, in which case effectively thicker layers are created, so the laminate is not regular).

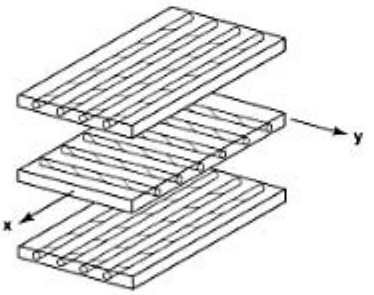


Figure C-25 Unbonded View of a Three-Layered Regular Symmetric Cross-Ply Laminate

Éléments sous droits d'auteur

The logic to establish the various stiffnesses will be traced to illustrate the general procedures. First, consider the extensional stiffnesses

$$A_{ij} = \sum_{k=1}^{N} (\bar{Q}_{ij})_k (z_k - z_{k-1}) \tag{C.74}$$

The A_{ij} are the sum of the product of the individual laminae $\bar{Q}_{ij}$ and the laminae thicknesses. Thus, the only ways to obtain a zero individual A_{ij} are for all $\bar{Q}_{ij}$ to be zero or for some $\bar{Q}_{ij}$ to be negative and some positive so that their products with their respective thicknesses sum to zero. From the expressions for the transformed lamina stiffnesses, $\bar{Q}_{ij}$, in Equation (C.29), apparently $\bar{Q}_{11}$, $\bar{Q}_{12}$, $\bar{Q}_{22}$, and $\bar{Q}_{66}$ are positive-definite because all trigonometric functions appear to even powers. Thus, A_{11}, A_{12}, A_{22}, and A_{66} are positive-definite because the thicknesses are, of course, always positive. However, $\bar{Q}_{16}$ and $\bar{Q}_{26}$ are zero for lamina orientations of 0° and 90° to the laminate axes. Thus, A_{16} and A_{26} are zero for laminates of orthotropic laminae oriented at either 0° or 90° to the laminate axes, so no shear-extension coupling exists.

Second, consider the bending-extension coupling stiffnesses

$$B_{ij} = \frac{1}{2} \sum_{k=1}^{N} (\bar{Q}_{ij})_k (z_k^2 - z_{k-1}^2) \tag{C.75}$$

If the cross-ply laminate is symmetric about the middle surface in both material properties and geometry, then the B_{ij} all vanish.

Finally, consider the bending stiffnesses

$$D_{ij} = \frac{1}{3} \sum_{k=1}^{N} (\bar{Q}_{ij})_k (z_k^3 - z_{k-1}^3) \tag{C.76}$$

The various D_{ij} are sums of the product of the individual laminae $\bar{Q}_{ij}$ and the term $(z_k^3 - z_{k-1}^3)$. Because $\bar{Q}_{11}$, $\bar{Q}_{12}$, $\bar{Q}_{22}$, and $\bar{Q}_{66}$ are positive-definite and the geometric term is positive-definite, then D_{11}, D_{12}, D_{22}, and D_{66} are positive-definite. Also, $\bar{Q}_{16}$ and $\bar{Q}_{26}$ are zero for lamina principal material property orientations of 0° and 90° to the laminate coordinate axes. Thus, D_{16} and D_{26} are zero, so no bending-extension coupling exists. Accordingly, we have achieved a symmetric laminate with neither shear-extension coupling nor bending-extension coupling.

Symmetric Laminates with Multiple Generally Orthotropic Layers

A laminate of multiple generally orthotropic layers that are symmetrically arranged about the middle surface exhibits no coupling between bending and extension; that is, the B_{ij} are zero. Therefore, the force and moment resultants are represented by Equations (C.68) and (C.69), respectively. There, all the A_{ij} and D_{ij} are required because of coupling between normal forces and shearing strain, shearing force and normal strains, normal moments and twist, and twisting moment and normal curvatures. Such coupling is evidenced by the A_{16}, A_{26}, D_{16}, and D_{26} stiffnesses, i.e., both shear-extension coupling and bending-extension coupling exist.

Éléments sous droits d'auteur

A special subclass of this class of symmetric laminates is the *regular symmetric angle-ply laminate* (*angle-ply* because the adjacent laminae are at $+\alpha$ and $-\alpha$ to the axial direction of the laminate). Such laminates have orthotropic laminae of equal thicknesses. The adjacent laminae have opposite signs of the angle of orientation of the principal material properties with respect to the laminate axes, e.g., $[+\alpha/-\alpha/+\alpha]$. Thus, for symmetry, there must be an odd number of layers. A simple example of a three-layered regular symmetric angle-ply laminate is shown in Figure C-26. A more complicated example of a symmetric laminate with generally orthotropic layers is given in Table C-3. Note that the laminae orthotropic material properties, orientations, and thicknesses are all symmetric about the laminate middle surface.

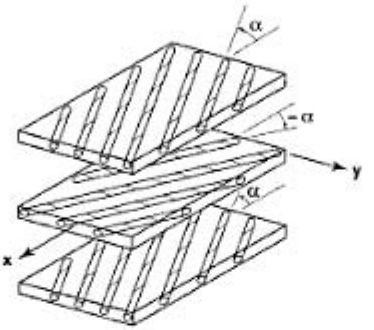


Figure C-26 Unbonded View of a Three-Layered Regular Symmetric Angle-Ply Laminate

Table C-3 Symmetric Laminate with Five Generally Orthotropic Layers

Layer	Material Properties				Orientation	Thickness
	Q_{11}	Q_{12}	Q_{22}	Q_{66}		
1	F_1	F_2	F_3	F_4	+30°	t
2	G_1	G_2	G_3	G_4	−60°	3t
3	H_1	H_2	H_3	H_4	+10°	5t
4	G_1	G_2	G_3	G_4	−60°	3t
5	F_1	F_2	F_3	F_4	+30°	t

The aforementioned coupling that involves A_{16}, A_{26}, D_{16}, and D_{26} takes on a special form for symmetric angle-ply laminates. Those stiffnesses can be shown to be largest when $N = 3$ (the lowest N for which this class of laminates exists) and decrease in proportion to 1/N as N increases (see Jones' Section 4.4.4 [C-1]). Actually, in the expressions for the extensional and bending stiffnesses A_{16} and D_{16},

$$A_{16} = \sum_{k=1}^{N} (\bar{Q}_{16})_k (z_k - z_{k-1}) \tag{C.77}$$

Éléments sous droits d'auteur

$$D_{16} = \frac{1}{3}\sum_{k=1}^{N}(\bar{Q}_{16})_k(z_k^3 - z_{k-1}^3) \tag{C.78}$$

Obviously, A_{16} and D_{16} are sums of terms of alternating signs because

$$(\bar{Q}_{16})_{+\alpha} = -(\bar{Q}_{16})_{-\alpha} \tag{C.79}$$

as can be concluded from Equation (C.34). Thus, for many-layered symmetric angle-ply laminates, the values of A_{16}, A_{26}, D_{16}, and D_{26} can be quite small when compared to the other A_{ij} and D_{ij}, respectively.

When the always-present advantage of zero B_{ij} because of symmetry is considered in addition to the low A_{16}, A_{26}, D_{16}, and D_{26}, many-layered symmetric angle-ply laminates can offer significant, practically advantageous simplifications over some more general laminates. In addition, symmetric angle-ply laminates offer more shear stiffness than do the simpler cross-ply laminates, so are used more often. However, knowledge of the effect of A_{16}, A_{26}, D_{16}, and D_{16} on the individual class of problems being considered by an analyst or designer is essential because even a small A_{16} or D_{16} might cause significantly different response results from cases in which those stiffnesses are exactly zero. Only in the situation where A_{16}, A_{26}, D_{16}, and D_{26} are exactly zero can they be ignored without further thought or analysis.

C.7.3 Antisymmetric Laminates

Symmetry of the material properties and geometry about the laminate middle surface is often desirable to avoid coupling between bending and extension and the resulting bending after elevated-temperature curing in Figure C-23. However, many physical applications of laminated composite materials require unsymmetric laminates to achieve their design requirements. For example, some form of coupling is necessary to make jet turbine fan blades with pretwist without using a complex mold. As a further example, if the shear stiffness of a laminate made of laminae with unidirectional fibers must be increased, one way to achieve this requirement is to position layers at some angle to the laminate axes. To stay within weight and cost requirements, an even number of such layers might be necessary at orientations that alternate from layer to layer, e.g., $[+\alpha/-\alpha/+\alpha/-\alpha]$. Therefore, symmetry about the middle surface is destroyed, and the behavioral characteristics of the laminate can be substantially changed from the symmetric case. Although the example laminate is not symmetric, it is antisymmetric about the middle surface, and certain stiffness simplifications are possible.

Antisymmetry of a laminate requires (1) symmetry about the middle surface of geometry (i.e., consider a pair of equal-thickness laminae, one some distance above the middle surface and the other *the same distance below the middle surface*), but (2) some kind of a *'reversal' or mirror image of the material properties* $[Q_{ij}]_k$. In fact, the orthotropic material properties $[Q_{ij}]_k$ are symmetric, but *the orientations of the laminae principal material directions are not symmetric about the middle surface.* Those orientations are reversed from 0° to 90° (or vice versa) or from

Éléments sous droits d'auteur

$+\alpha$ to $-\alpha$ (a mirror image about the laminate x-axis). Because the $[\bar{Q}_{ij}]_k$ are not symmetric, bending-extension coupling exists.

Antisymmetric laminates must have an even number of layers if adjacent laminae also have alternating signs of the principal material property directions with respect to the laminate axes. If adjacent laminae do not have alternating signs, then the number of layers need not be even.

The stiffnesses of an antisymmetric laminate of anisotropic laminae do not simplify from those presented in Equations (C.53) and (C.54). However, as a consequence of antisymmetry of material properties of generally orthotropic laminae,[2] but symmetry of their thicknesses, the shear-extension coupling stiffness A_{16},

$$A_{16} = \sum_{k=1}^{N} (\bar{Q}_{16})_k (z_k - z_{k-1}) \tag{C.80}$$

is easily seen to be zero because, from Equation (C.34),

$$(\bar{Q}_{16})_{+\alpha} = -(\bar{Q}_{16})_{-\alpha} \tag{C.81}$$

and layers symmetric about the middle surface have equal thickness and hence the same value of the geometric term multiplying $(\bar{Q}_{16})_k$. Similarly, A_{26} is zero as is the bend-twist coupling stiffness D_{16}.

$$D_{16} = \frac{1}{3} \sum_{k=1}^{N} (\bar{Q}_{16})_k (z_k^3 - z_{k-1}^3) \tag{C.82}$$

because again Equation (C.81) holds, and the geometric term multiplying $(Q_{16})_k$ is the same for two layers symmetric about the middle surface. The preceding reasoning applies also for D_{26}.

The bending-extension coupling stiffnesses, B_{ij}, vary for different classes of antisymmetric laminates of generally orthotropic laminae, and, in fact, no general representation exists other than in the following force and moment resultants:

$$\begin{bmatrix} N_x \\ N_y \\ N_{xy} \end{bmatrix} = \begin{bmatrix} A_{11} & A_{12} & 0 \\ A_{12} & A_{22} & 0 \\ 0 & 0 & A_{66} \end{bmatrix} \begin{bmatrix} \varepsilon_x^0 \\ \varepsilon_y^0 \\ \gamma_{xy}^0 \end{bmatrix} + \begin{bmatrix} B_{11} & B_{12} & B_{16} \\ B_{12} & B_{22} & B_{26} \\ B_{16} & B_{26} & B_{66} \end{bmatrix} \begin{bmatrix} \kappa_x \\ \kappa_y \\ \kappa_{xy} \end{bmatrix} \tag{C.83}$$

$$\begin{bmatrix} M_x \\ M_y \\ M_{xy} \end{bmatrix} = \begin{bmatrix} B_{11} & B_{12} & B_{16} \\ B_{12} & B_{22} & B_{26} \\ B_{16} & B_{26} & B_{66} \end{bmatrix} \begin{bmatrix} \varepsilon_x^0 \\ \varepsilon_y^0 \\ \gamma_{xy}^0 \end{bmatrix} + \begin{bmatrix} D_{11} & D_{12} & 0 \\ D_{12} & D_{22} & 0 \\ 0 & 0 & D_{66} \end{bmatrix} \begin{bmatrix} \kappa_x \\ \kappa_y \\ \kappa_{xy} \end{bmatrix} \tag{C.84}$$

[2]Because of the existence of bending-extension coupling, the terminology 'generally orthotropic' and 'specially orthotropic' have meaning only with reference to an individual layer and not to a laminate. See Jones on laminate terminology [C-7].

Éléments sous droits d'auteur

The purpose of the remainder of this section is to discuss two important classes of antisymmetric laminates, the antisymmetric cross-ply laminate and the antisymmetric angle-ply laminate. Neither laminate is used much in practice, but both add to our fundamental understanding of how laminates behave.

Antisymmetric Cross-Ply Laminates

An antisymmetric cross-ply laminate consists of an even number of orthotropic laminae laid on each other with principal material directions alternating at 0° and 90° to the laminate axes as in the simple example of Figure C-27. A more complicated example is given in Table C-4 (where the adjacent layers do not always have the sequence 0°, then 90°, then 0°, etc.). Such laminates do not have A_{16}, A_{26}, D_{16}, and D_{26} (because both the Q_{16} and Q_{26} are zero for each lamina), but do have bending-extension coupling. For the same reason, B_{16} and B_{26} are zero. Moreover, B_{12} and B_{26} are zero, but $B_{11} = B_{22}$ are not zero. Thus, the coupling is such that the force and moment resultants are

$$\begin{bmatrix} N_x \\ N_y \\ N_{xy} \end{bmatrix} = \begin{bmatrix} A_{11} & A_{12} & 0 \\ A_{12} & A_{22} & 0 \\ 0 & 0 & A_{66} \end{bmatrix} \begin{bmatrix} \varepsilon_x^\circ \\ \varepsilon_y^\circ \\ \gamma_{xy}^\circ \end{bmatrix} + \begin{bmatrix} B_{11} & 0 & 0 \\ 0 & -B_{11} & 0 \\ 0 & 0 & 0 \end{bmatrix} \begin{bmatrix} \kappa_x \\ \kappa_y \\ \kappa_{xy} \end{bmatrix} \tag{C.85}$$

$$\begin{bmatrix} M_x \\ M_y \\ M_{xy} \end{bmatrix} = \begin{bmatrix} B_{11} & 0 & 0 \\ 0 & -B_{11} & 0 \\ 0 & 0 & 0 \end{bmatrix} \begin{bmatrix} \varepsilon_x^\circ \\ \varepsilon_y^\circ \\ \gamma_{xy}^\circ \end{bmatrix} + \begin{bmatrix} D_{11} & D_{12} & 0 \\ D_{12} & D_{22} & 0 \\ 0 & 0 & D_{66} \end{bmatrix} \begin{bmatrix} \kappa_x \\ \kappa_y \\ \kappa_{xy} \end{bmatrix} \tag{C.86}$$

A *regular antisymmetric cross-ply laminate* is defined to have laminae all of equal thickness and is common because of simplicity of fabrication. As the number of layers increases, the bending-extension coupling stiffness B_{11} can be shown to approach zero.

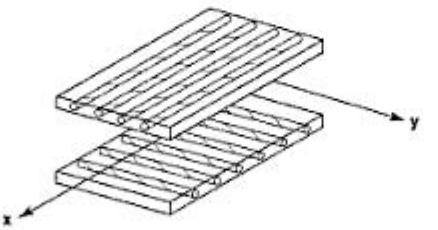


Figure C-27 Unbonded View of a Two-Layered Regular Antisymmetric Cross-Ply Laminate

Éléments sous droits d'auteur

Table C-4 Antisymmetric Laminate with Six Specially Orthotropic Layers

Layer	Material Properties				Orientation	Thickness
	Q_{11}	Q_{12}	Q_{22}	Q_{66}		
1	F_1	F_2	F_3	F_4	0°	t
2	G_1	G_2	G_3	G_4	90°	3t
3	H_1	H_2	H_3	H_4	90°	2t
4	H_1	H_2	H_3	H_4	0°	2t
5	G_1	G_2	G_3	G_4	0°	3t
6	F_1	F_2	F_3	F_4	90°	t

Antisymmetric Angle-Ply Laminates

An antisymmetric angle-ply laminate has laminae oriented at $+\alpha$ degrees to the laminate coordinate axes on one side of the middle surface and corresponding equal-thickness laminae oriented at $-\alpha$ degrees on the other side at the same distance from the middle surface. A simple example of a two-layered antisymmetric angle-ply laminate is shown in Figure C-28. A more complicated example with mixed materials and lamination angles is given in Table C-5.



Figure C-28 Unbonded View of a Two-Layered Regular Antisymmetric Angle-Ply Laminate

Table C-5 Six-Layered Antisymmetric Angle-Ply Laminate

Layer	Material Properties				Orientation	Thickness
	Q_{11}	Q_{12}	Q_{22}	Q_{66}		
1	F_1	F_2	F_3	F_4	−45°	t
2	G_1	G_2	G_3	G_4	+30°	2t
3	H_1	H_2	H_3	H_4	0°	3t
4	H_1	H_2	H_3	H_4	0°	3t
5	G_1	G_2	G_3	G_4	−30°	2t
6	F_1	F_2	F_3	F_4	+45°	t

A *regular antisymmetric angle-ply laminate* has laminae all of the same material and thickness for ease of fabrication. This class of laminates can be further restricted to have a single value of α as opposed to the several orientations, materials, and thicknesses in Table C-5.

Éléments sous droits d'auteur

The force and moment resultants for an antisymmetric angle-ply laminate are

$$\begin{bmatrix} N_x \\ N_y \\ N_{xy} \end{bmatrix} = \begin{bmatrix} A_{11} & A_{12} & 0 \\ A_{12} & A_{22} & 0 \\ 0 & 0 & A_{66} \end{bmatrix} \begin{bmatrix} \varepsilon_x^\circ \\ \varepsilon_y^\circ \\ \gamma_{xy}^\circ \end{bmatrix} + \begin{bmatrix} 0 & 0 & B_{16} \\ 0 & 0 & B_{26} \\ B_{16} & B_{26} & 0 \end{bmatrix} \begin{bmatrix} \kappa_x \\ \kappa_y \\ \kappa_{xy} \end{bmatrix} \tag{C.87}$$

$$\begin{bmatrix} M_x \\ M_y \\ M_{xy} \end{bmatrix} = \begin{bmatrix} 0 & 0 & B_{16} \\ 0 & 0 & B_{26} \\ B_{16} & B_{26} & 0 \end{bmatrix} \begin{bmatrix} \varepsilon_x^\circ \\ \varepsilon_y^\circ \\ \gamma_{xy}^\circ \end{bmatrix} + \begin{bmatrix} D_{11} & D_{12} & 0 \\ D_{12} & D_{22} & 0 \\ 0 & 0 & D_{66} \end{bmatrix} \begin{bmatrix} \kappa_x \\ \kappa_y \\ \kappa_{xy} \end{bmatrix} \tag{C.88}$$

The bending-extension coupling stiffnesses B_{16} and B_{26} can be shown to go to zero as the number of layers in the laminate increases for a fixed laminate thickness.

C.7.4 Unsymmetric Laminates

Unsymmetric or nonsymmetric or asymmetric laminates are the most general class of laminate. Lack of symmetry can occur by design as in deliberately constructing a laminate that is not symmetric about the middle surface. Or, a symmetric laminate could be built but subjected in service to heating from one side so that the resulting thermal gradient acting on the temperature-dependent material properties renders the laminate unsymmetric. We will briefly address unsymmetric laminates with multiple isotropic, specially orthotropic, generally orthotropic, and anisotropic layers.

For the general case of multiple isotropic layers of thickness t_k and material properties E_k and ν_k, the extensional, bending-extension coupling, and bending stiffnesses are given by Equation (C.55) wherein

$$\begin{aligned} (\bar{Q}_{11})_k &= (\bar{Q}_{22})_k = \frac{E_k}{1-\nu_k^2} & (\bar{Q}_{16})_k &= (\bar{Q}_{26})_k = 0 \\ (\bar{Q}_{12})_k &= \frac{\nu_k E_k}{1-\nu_k^2} & (\bar{Q}_{66})_k &= \frac{E_k}{2(1+\nu_k)} \end{aligned} \tag{C.89}$$

No special reduction of the stiffnesses is possible when t_k is arbitrary. That is, coupling between bending and extension can be obtained by unsymmetric arrangement about the middle surface of isotropic layers with different material properties and possibly (but not necessarily) different thicknesses. Thus, coupling between bending and extension is *not* a result of material orthotropy but rather of laminate heterogeneity; that is, a combination of *both* geometric and material properties. The force and moment resultants are

Éléments sous droits d'auteur

$$\begin{bmatrix} N_x \\ N_y \\ N_{xy} \end{bmatrix} = \begin{bmatrix} A_{11} & A_{12} & 0 \\ A_{12} & A_{11} & 0 \\ 0 & 0 & A_{66} \end{bmatrix} \begin{bmatrix} \varepsilon_x^\circ \\ \varepsilon_y^\circ \\ \gamma_{xy}^\circ \end{bmatrix} + \begin{bmatrix} B_{11} & B_{12} & 0 \\ B_{12} & B_{11} & 0 \\ 0 & 0 & B_{66} \end{bmatrix} \begin{bmatrix} \kappa_x \\ \kappa_y \\ \kappa_{xy} \end{bmatrix} \tag{C.90}$$

$$\begin{bmatrix} M_x \\ M_y \\ M_{xy} \end{bmatrix} = \begin{bmatrix} B_{11} & B_{12} & 0 \\ B_{12} & B_{11} & 0 \\ 0 & 0 & B_{66} \end{bmatrix} \begin{bmatrix} \varepsilon_x^\circ \\ \varepsilon_y^\circ \\ \gamma_{xy}^\circ \end{bmatrix} + \begin{bmatrix} D_{11} & D_{12} & 0 \\ D_{12} & D_{11} & 0 \\ 0 & 0 & D_{66} \end{bmatrix} \begin{bmatrix} \kappa_x \\ \kappa_y \\ \kappa_{xy} \end{bmatrix} \tag{C.91}$$

Unsymmetric laminates with multiple specially orthotropic layers can be shown to have the force and moment resultants in Equations (C.90) and (C.91) but with different A_{22}, B_{22}, and D_{22} from A_{11}, B_{11}, and D_{11}, respectively. That is, there are no shear-extension coupling terms nor any bend-twist coupling terms, so the solution of problems with this kind of lamination is about as easy as with isotropic layers.

Unsymmetric laminates with multiple generally orthotropic layers or with multiple anisotropic layers have force and moment resultants no simpler than Equations (C.53) and (C.54). All stiffnesses are present. Hence, configurations with either of those two laminae are much more difficult to analyze than configurations with either multiple isotropic layers or multiple specially orthotropic layers.

C.7.5 Stacking-Sequence Notation

The manner of describing a laminate by use of individual layer thicknesses, principal material property orientations, and overall stacking sequence could be quite involved. However, fortunately, all pertinent parameters are represented in a simple, concise fashion by use of the following stacking-sequence terminology. For regular (equal-thickness layers) laminates with all laminae of the same material,[1] a listing of the layers and their orientations suffices, for example, [0°/90°/45°]. Note that only the principal material direction orientations need be given along with a note of the lamina thickness and material. Many different laminates could be made with the same layers, i.e., [90°/0°/45°]. For irregular (layers do not have the same thickness) laminates, a notation of layer thicknesses must be appended to the previous notation, for example, $[0^\circ_t/90^\circ_{2t}/45^\circ_{3t}]$ or [0°@t/90°@2t/45°@3t] in addition to a note of the material. Finally, for symmetric laminates, the laminate with full specification [0°/90°/45°/45°/90°/0°] can be represented as $[0^\circ/90^\circ/45^\circ]_{\text{symmetric}}$ or $[0^\circ/90^\circ/45^\circ]_{\text{sym}}$ or $[0^\circ/90^\circ/45^\circ]_S$. If multiple laminae occur at the same angle, then subscripts are used to designate the number of such multiple layers, e.g., $[0^\circ/0^\circ/0^\circ/90^\circ/90^\circ] = [0^\circ_3/90^\circ_2]$. If sequences of laminae are repeated, then those multiple-layers sequences are grouped with a sub-

[1] For laminates with laminae of different materials, see Section C.7.7, Hybrid Laminates.

Éléments sous droits d'auteur

script to indicate the number of sequence repetitions, e.g., the representations $[0°/90°/45°/0°/90°/45°] = [0°/90°/45°]_2$. If one layer is equally split by the middle surface, then a bar is put over the split layer, e.g., $[0°/90°/0°] = [0°/\overline{90°}]_S$. Finally, if all the laminae are specified in the stacking sequence shown and no implications of symmetry, repeated sequences, etc., are desired nor can any ambiguity be tolerated, then a subscript T is used to indicate complete or total specification for emphasis, e.g., $[0°/90°/45°/-45°/0°/90°]_T$, i.e., no symmetry or repeated sequence is desired. This notation is used widely in laminated fiber-reinforced composite structures practice.

C.7.6 Balanced Laminates

Although the word 'balanced' is ambiguous and not definitive, the common meaning in practice for a *balanced laminate* is a laminate in which all equal-thickness laminae at angles θ other than $0°$ and $90°$ to the reference axis occur only in $\pm\theta$ pairs. The individual $+\theta$ and $-\theta$ layers are not necessarily adjacent to each other. Note also that balanced laminates are required to be symmetric about the laminate middle surface, so there must be two $+\theta$ laminae and two $-\theta$ laminae for each $\pm\theta$ pair. The behavioral characteristics of a balanced laminate are that shear-extension coupling does not exist, nor does bending-extension coupling exist. However, bend-twist coupling does exist (see the result of bend-twist coupling in Figure C-20 on page 777), although it can be small if the number of $\pm\theta$ pairs is high enough. See Jones for further comments on fiber-reinforced composite laminate terminology [C-7].

C.7.7 Hybrid Laminates

A *hybrid laminate* is a mixture of two or more material systems to form a laminate. For example, graphite-epoxy laminae are used with Kevlar-49®-epoxy laminae to create wing-to-body fairings for the Boeing 757 and 767. Note that the two epoxies in the two different types of laminae must have compatible curing conditions in order to achieve a functioning laminate. Thus, although different fiber systems are often mixed in hybrid laminates, not many different matrix systems can be mixed. An example of a graphite-epoxy laminate surrounded by layers of boron-epoxy could be written as $[0^\circ_B/\pm45^\circ_{Gr}/90^\circ_{Gr}]_S$. At first glance, this laminate might appear to be quasi-isotropic (isotropic in extensional stiffnesses—the same in all in-plane directions—but not in bending stiffnesses—obviously not a situation of *material* isotropy, hence the prefix 'quasi'). However, this laminate is *not* quasi-isotropic because the laminae, although of the correct angular orientation for a $\pi/4$ laminate, are of two different material systems. See Jones' *Mechanics of Composite Materials* for a more complete definition of a quasi-isotropic laminate and a $\pi/4$ laminate [C-1] and Jones' paper on fiber-reinforced composite laminate terminology [C-7].

Éléments sous droits d'auteur

C.8 SUMMARY REMARKS

The nature, characteristics, and advantages of laminae and laminates made of fiber-reinforced composite materials, as well as other materials, are summarized. Next, the pertinent stress-strain relations for various kinds of laminae are addressed, and the type needed for the usual fiber-reinforced lamina is focused upon. Then, classical lamination theory is described, special cases of the resulting laminate stiffnesses are studied, and needed special laminate definitions are introduced.

For most structures, the general practicality of the cross-ply and angle-ply laminates studied in this Appendix is somewhat limited because the laminates are so 'simple'. However, cross-ply laminates are used for plywood (in irregular thickness form with thin veneer surface layers that have attractive grain and thicker inner layers to provide stiffness and strength), and angle-ply laminates are used for tires, often in hybrid laminate form. The annual monetary production value of these two everyday applications is quite high. And, study of both types of laminates is a good first step toward understanding more general laminates, e.g., those used in contemporary vehicle and aerospace structures which have relatively low, but growing, annual production statistics. Of course, Jones' *Mechanics of Composite Materials* [C-1] has a far more comprehensive treatment of composite materials and structures, their uses, and their analysis, as well as their design, than we have been able to address in this brief Appendix.

APPENDIX C REFERENCES

C-1 Robert M. Jones, *Mechanics of Composite Materials*, 2nd Edition, Taylor & Francis, Philadelphia, 1999.

C-2 Robert C. Reuter, Jr., Concise Property Transformation Relations for an Anisotropic Lamina, *Journal of Composite Materials*, Volume 5, April 1971, pp. 270–272.

C-3 S. A. Ambartsumyan, *Theory of Anisotropic Shells*, (in Russian, State Publishing House for Physical and Mathematical Literature, Moscow, 1961), NASA Technical Translation TT F-118, National Aeronautics and Space Administration, Washington, D. C., May 1964.

C-4 K. S. Pister and S. B. Dong, Elastic Bending of Layered Plates, *Journal of the Engineering Mechanics Division*, American Society of Civil Engineers, Volume 85, No. EM 4, October 1959, pp. 1–10.

C-5 E. Reissner and Y. Stavsky, Bending and Stretching of Certain Types of Heterogeneous Aeolotropic Elastic Plates, *Journal of Applied Mechanics*, Volume 28, Series E, Number 3, September 1961, pp. 402–408.

C-6 J. E. Ashton, J. C. Halpin, and P. H. Petit, *Primer on Composite Materials: Analysis*, Technomic, Westport, Connecticut, 1969. See also J. C. Halpin, *Revised Primer on Composite Materials: Analysis*, Technomic, Lancaster, Pennsylvania, 1984.

C-7 Robert M. Jones, Fiber-Reinforced Composite Laminate Terminology: 'Understood' but Misused — Suggestions for Improvement, Paper Number 31, Proceedings of the 20th Annual Technical Conference, 7–9 September 2005, Philadelphia, American Society for Composites, Dayton, Ohio.

Éléments sous droits d'auteur

Appendix D

ELEMENTS OF DESIGN PHILOSOPHY

D.1 INTRODUCTION

Many issues in this appendix were raised previously by Henry Petroski [D-1] and [D-2], and I have expanded upon them in greater detail, adding some of my own interpretations and examples. Petroski emphasizes that failures of past structures play an undeniably important role in the proper design of new structures. Thus, studying case histories of actual failures yields valuable information on how to appropriately modify the design process to achieve safe structures. Moreover, studying those failures should also alert all of us to the dangers of designing with our eyes closed. Petroski [D-1, p. 188] observes that

> "Failure analysis is as easy as Monday-morning quarterbacking; design is more akin to coaching. However, the design engineer must do better than any coach, for he is expected to win every game he plays. That is a tough assignment when one mistake can often mean a loss. And when defeat occurs, all one can hope is to analyze the game films and learn from the mistakes so that they are less likely to be repeated the next time out."

The Game Film for structural engineers is that of the 1940 Tacoma Narrows Bridge failure near Tacoma, Washington.[1] That film has been shown to innumerable civil engineering students and others since it was made. Viewing that film in the late 1950s is forever etched on my brain! The first message of the film is that the bridge oscillated wildly and with ever-increasing amplitude until the deck (along with the dog) crashed into the water. Such aerodynamically excited motion had not previously been seen in suspension bridges. The second message is that, more generally, we must be extremely cautious when extrapolating previously successful designs to designs with 'significant' changes in dimensions or materials because previously inactive, but existant (i.e., possible) failure mechanisms or modes can show up and cause major problems. More case histories of important failures are available in various forms and quite instructive, although not all failures are captured on film.

[1] More information on this bridge failure is available in Petroski [D-1, pp. 163–168] and [D-2, pp. 156–162] and in Levy and Salvadori [D-3, pp. 109–120].

Éléments sous droits d'auteur

The most notable and disasterous structural failure is that of the World Trade Center Twin Towers after they were struck by terrorists flying Boeing 767 aircraft loaded with jet fuel into the upper floors of each tower. Most of the people in the world have seen the videotape of that cowardly attack and the subsequent collapse of the buildings, and many even watched live on television. The collapses were caused by progressive floor-by-floor buckling of the structural steel columns triggered in turn by melting of the columns in the aircraft strike zones such that those columns could no longer support the weight of the floors above the aircraft strike zone. Then, the columns below the strike zone buckled successively because they were unable to withstand the dynamic loading from the collapsing floors above them. Of course, many might not interpret the Twin Towers collapse as a structural failure or as a failure of the design process, but, clearly, the Twin Towers did suffer a structural failure because of an event that was not considered in the design process. Yes, designing a tall building to be able to withstand such a heretofore unthinkable attack is possible, but certain consequences are unavoidable. The tall building would necessarily have an enormously expensive and well-protected structural frame as well as few windows. Thus, Petroski thinks that single event is likely responsible for very tall buildings never again being built [D-4].

We will describe the nature of engineering design and how to differentiate it from other forms of design. Then, the various approaches through the ages to ensuring good designs are addressed. Next, how failures play an undeniable role in both understanding and improving design practice is considered. Finally, identifying all possible failure modes for a structure is emphasized as being essential in design.

D.2 WHAT IS ENGINEERING DESIGN?

The objective of engineering design is to anticipate all possible failures and then to design against them in the creation of a structure or device. Obviously, you can't prevent something from causing damage unless you know what it is! Thus, engineers must be quite imaginative about what might happen to a structure or device during its entire service life. Overlooking a rare, but possible, event can only increase the likelihood of structural failure. By searching for possible failure modes, a design engineer is not being pessimistic, he's being responsible!

Design is a form of *behavior modification*. And, you must know the behavior before you can modify it. That is, a structural designer must be intimately familiar with structural analysis and how structures behave in order to rationally control or even approach the design process. He must be able to modify the structural behavior in order to make the structure achieve certain design goals usually expressed in terms of strength, stiffness, and life.

Establishing suitable design failure criteria is a difficult task, yet fundamental to the design process. The concept of design failure criteria is much more complicated and involved than just the issue of gross failure of a specific structural element because we must ask *how* the *structure*

Éléments sous droits d'auteur

fails. What does failure mean in the context of that specific design? Failure basically means that the structure cannot fulfill some design requirement(s). All failure really means then is that we have designed a structure or object to do a particular job, and that structure cannot do its job. Obviously, nothing was mentioned about the structure breaking or falling down. That is, failure means far more than just fracture.

Design requirements are simply a collection of statements of what we ask the structure being designed to do. What is the required performance? Those requirements can be expressed in terms of structural response or, alternatively, in terms of system performance.

Consider an example involving several design requirements. For a beam overhead above the ceiling of a room, what we want the beam to do most importantly is to hold up the ceiling so it does not fall on our heads. That requirement is a *strength issue*. We also do not want that ceiling beam to deflect very much so it stays well above our head, and deflection is a *stiffness issue*. Another problem with a ceiling beam deflecting too much is if the ceiling is plaster, then the plaster will crack as in Figure D-1, and that cracking is obviously unsightly. If you were paying for a nice, new building, you certainly would not want cracked plaster, so obviously a stiffness requirement exists. There is also a stiffness requirement because we do not want people who are in the building to perceive that the floor above them is sagging so much that they get scared. Thus, we are faced with two very clear issues, i.e., strength and stiffness. Another issue is that the ceiling beam must withstand whatever loads are imposed on it over the *lifetime* of the structure such as intermittant snow loads, a lot of walking around, or moving equipment around, etc. That collection of circumstances is a *life issue*. Thus, we have identified three different structural issues in the design of a ceiling beam, namely **strength, stiffness,** and **life.** Failure of the beam is not failure from the standpoint of simply breaking apart, i.e., fracture, although obviously that is the essence of the first issue, strength. After that simplistic concern, other significant issues must be addressed, namely stiffness and life just to list two such issues. Many other issues exist beyond strength, stiffness, and life, and we now identify some of them.

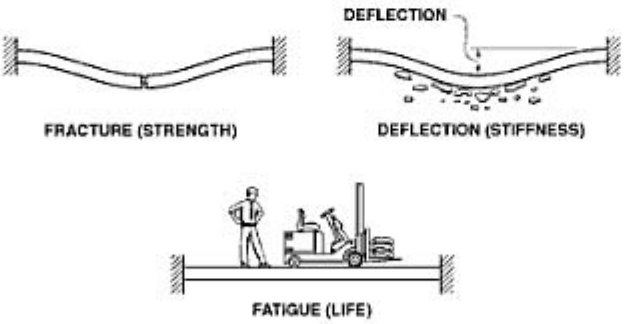


Figure D-1 Ceiling Beam Design Requirements

Éléments sous droits d'auteur

We can go through that same kind of problem analysis for many different structures, and, in the process, design requirements could be expressed for each of them. The most common design requirements are expressed in some manner in terms of strength, stiffness, and life, but there are many other issues as well. Whether the material will corrode, for example. Whether it will provide the proper insulation or just the opposite, sufficient conductivity, and so on. There are many, many different types of tasks that we ask a structure to perform.

Failure has many meanings or interpretations in the context of the structural design process. The main meaning is that failure is the inability of the structure to perform up to its design requirements. Those requirements can be expressed simplistically in terms of the following functional issues, some beyond those already described:

1. strength — the material will have limits of stress or strain that cannot be exceeded without fracture
2. stiffness — the structure will be designed to deform a specific amount or perhaps be limited to a specific deformation without vibrating excessively or buckling.
3. life — the structure might have a specified service-life span
4. energy — the structure might have to absorb specified amounts of energy and still remain functional
5. weight — the structure might have to weigh less than a specified amount for the configuration to be a feasible design
6. cost — the structure might have to cost less than a specified amount or else a configuration that works in every other respect must be redesigned
7. manufacturing — if the structure cannot be built, then the configuration is unacceptable

If these or other specific design criteria cannot be met, then the design is a failure, and the structure must be redesigned to meet the requirements. Thus, design is an iterative process coupled with analysis and testing activities to assess the success or failure of a structure. All design activities must be accompanied by an evaluation program to assess the structure's characteristics relative to each of the goals and the progress toward satisfaction of the goals. Accordingly, each of *the goals or design criteria must be clearly defineable and readily measureable.* Otherwise, they are not achievable in any specific sense.

Besides structural designers, many other professionals or quasi-professionals call themselves designers. For example, architects are also regarded as designers. Their main concerns are form and, to some extent, function. However, architects are not able to control the performance or behavior of their structures sufficiently to avoid structural failure (the most common reason for lawsuits against architectural firms). To control and create safe structures, architects must appeal to structural engineers to perform this structural design task. An exception to that 'rule' is the diminishing ranks of the architectural engineer, i.e., a combination of the educations of an architect and an engineer.

Éléments sous droits d'auteur

I am personally familiar with how structural analysis is studied and valued in one architecture curriculum. Three courses are supposed to be taken in a specific order from the basic to the advanced. However, even though each successive course had the previous lower-level course as a prerequisite, some students were allowed to take the three courses in *precisely reverse order!* That is, first the advanced course, then the intermediate course, and finally the basic course. Obviously, structural analysis is not regarded as important in that curriculum! With such an attitude on the part of the architecture faculty, their graduates are not assured of having the requisite knowledge to understand structural analysis and its role in building a safe structure. Such unfortunate, improper, and irresponsible situations might exist elsewhere.

Artists, in particular commercial artists, design artwork, advertising layouts, etc. with the sole concern being appeal to the observer's eye, especially the customer's. They know well the use of color, various font sizes and styles, and open space to make their work eye-catching.

Dress designers understand how various materials drape over the human form and how to take advantage of that behavior to create a stunning result. Moreover, color and texture play important roles in their work. Note that all their activities are qualitative, not quantitative in nature. In the limit, anyone handy with thread, a needle, and scissors can create a respectable dress. Safety of the dress is not an issue; no one ever lost her (in most cases) life because a dress was improperly designed! A dress failure might have exposed a part of their anatomy, but that situation involves only embarassment (or not!).

In contrast, structural engineers who are designers employ *quantitative rationale* based on *mechanistic relationships* between

- material properties
- structural elements
- structures

The quantitative rationale and the mechanistic relationships have no parallel in the 'other' fields involving design (except in other branches of engineering where analogous quantitative relationships exist). Design of structures requires design-analysts who are well-rounded in interdisciplinary activities and well-versed in materials, analysis, design, and construction. Obvious changes can be made in the foregoing remarks or activities to describe someone who designs devices.

D.3 PHILOSOPHIES OVER THE AGES OF HOW TO ENSURE SAFE DESIGNS

Governments or society and the public have always been concerned that those who design and build structures for public or private use be held responsible for their actions (unless political lobbiests enter the debate, and then no one is held responsible!). That holding-responsible process might have begun almost four thousand years ago with the Babylonian Code of Hammurabi:

Éléments sous droits d'auteur

"If a builder build a house for a man and do not make its construction firm, and the house which he has built collapse and cause the death of the owner of the house, that builder shall be put to death.

If it cause the death of the son of the owner of the house, they shall put to death a son of that builder.

If it cause the death of a slave of the owner of the house, he shall give to the owner of the house a slave of equal value.

If it destroy property, he shall restore whatever it destroyed, and because he did not make the house which he built firm and it collapsed, he shall rebuild the house which collapsed from his own property.

If a builder build a house for a man and do not make its construction meet the requirements and a wall fall in, that builder shall strengthen the wall at his expense." [D-1, p. 3].

Later, in czarist times, Russian bridge builders and designers huddled with their families under a bridge they designed just as the first traffic went over the bridge. Then, if the bridge failed, the builder and his family were the first to die. In more recent times (the 1980s), designers and consultants for a failed bridge near Riga, Latvia (then a Soviet Republic) were dismissed from their university leadership positions, a far more benign response to charges of improper design than occurred under the czar. However, just a few years ago, Chinese aerospace bureaucrats who had responsibility for converting the country's various airlines' computer systems for the Y2K changeover were required to be in the air on one of their planes at midnight on 31 December 1999. Again, a philosophy of immediate retribution against those who didn't do their jobs properly. Incidently, nothing happened on any of the flights. Recent practice of retribution for failure to design and build safe structures generally has been limited to monetary damages and loss of professional licenses rather than the previous 'an eye for an eye' philosophy.

D.4 THE ROLE OF PAST FAILURES IN UNDERSTANDING AND IMPROVING DESIGN PRACTICE

Studying and publicizing structural failures is educational to all engineers so that they don't repeat the mistakes of their predecessors. Confucious said: 'If you wish to control the future, study the past'. Isn't design (hopefully) controlling the future? Isn't failure of designs the past? Failure is how we find our limits whether for structures or for the personal behavior of individuals. That is, we learn from failures the behavioral nature of a structure or device over a certain range of structural and loading parameters. Outside that range, we really don't know anything about the structure or device. As we extrapolate designs and design concepts that worked in the past to bigger, longer, taller, etc. measures than have prevously been built, at some point we will encounter a failure mode that was inherent to the structure before, but was not active (i.e., not governing) for previous structures. Thus, merely looking at and emulating an existing structural design because it was successful, but ex-

Éléments sous droits d'auteur

trapolating its dimensions beyond what was successfully built before *will someday lead to failure!* Historically, such extrapolation-related failures have always happened sooner or later (see Section D.6).

Design has one clear ethical distinction from research. Whereas copying others' work in research is clearly plagerism (because research must be original, otherwise it has no value except as confirmation), taking advantage of the characteristics of others' successfully built structures is only common sense. We rely upon the base of proven experience of others to lend confidence to our design. Only when we clearly exceed the range of previous design variables do we encounter trouble. Unfortunately, that simple lesson all too often eludes us.

D.4.1 de Havilland Comet Fatigue Failures

Most structural failures are dramatic such as the crashes of the British de Havilland Comet jetliner that introduced us to fatigue failure in airplanes in the early 1950s.[2] The Comets had one of the first pressurized fuselages (to facilitate passenger comfort at high altitudes), and, of course, a relatively early all-metal fuselage, as it turns out, a dangerous combination. Two Comets crashed for initially unexplained reasons in the first two years of service (between 1952 and 1954 during which four other Comets crashed for reasons that were understood) [D-5]. At first, many suspected sabotage of some nature or overall design error. However, extensive investigation including retrieving a fallen Comet from its watery grave in a shallow part of the Tyrrhenian Sea near the island of Elba (where Napoleon was imprisoned—just not when the Comets flew) on a flight from Rome to London led to the discovery that fatigue cracks initiated at the only slightly rounded corners of the rectangular passenger windows and other windows (which were only lightly reinforced) in the fuselage. Any engineer knows to expect cracks at a stress concentration[3] if the load is high enough (now, passenger window corners are quite rounded, not sharp, as well as reinforced, but pilots' windows have sharp corners with heavy reinforcement around them). That crack initiation plus the cyclic loading of the fuselage (which was gradually pressurized after take-off before cruising altitude was reached and then gradually depressurized as the plane loses altitude in preparation for landing in each flight, hence stressed and then unstressed repeatedly) lead to identification of fatigue failure. After the cracks became large enough in the plane that crashed near Elba, the fuselage exploded with enough force to leave the imprint of a coin and of a newspaper on the tail! The occurrence of fatigue failure for aircraft was the theme of Nevil Shute's (his real name was Nevil Shute Norway, and he started his aircraft engineering career at de Havilland) popular novel *No Highway* [D-6] that was

[2]More information on this aircraft failure is available in Petroski [D-1, pp. 176–188], Levy and Salvadori [D-3, pp. 120–126], and Dempster [D-5].

[3]At stress concentrations (small regions of very high stress because of sudden geometry changes or force introductions), maximum stresses were forced into the plastic range of behavior, so repeated stresses were always causing more plastic deformation. Thus, fatigue failure occurred rapidly at a relatively low number of cycles.

Éléments sous droits d'auteur

published in 1948 as the Comet was being designed. Some speculate that Shute was actually predicting that the Comet would fail in fatigue! After all, he named his fictitious aircraft the 'Reindeer' and the first reindeer of the team that pulls Santa Claus' sleigh is 'Comet'! Rudolph had not yet been created.

D.4.2 Hyatt Regency Hotel Skywalk Failure

The failure of the Hyatt Regency Hotel suspended walkways or skywalks (a form of small bridge) in Kansas City on 17 July 1981 is a classic example of design error as well as misunderstanding.[4] Not an error *per se* in the original design, but in the modified design after it was determined that the original design could not be built (another category of design error—after all, a design that cannot be built is worthless—no design at all!). That is, the original design was effectively in error because it was unbuildable! The essential misunderstanding, as we will see, hinges upon the use of the word 'reviewed' by the structural engineers who designed the walkways. The walkways connect the tower building where sleeping rooms are located to a shorter 'function building' in which restaurants and meeting rooms are located. The walkways enable guests to transit from one wing to another without going through the ground-floor level thereby avoiding traffic jams, as evident in Figure D-2.

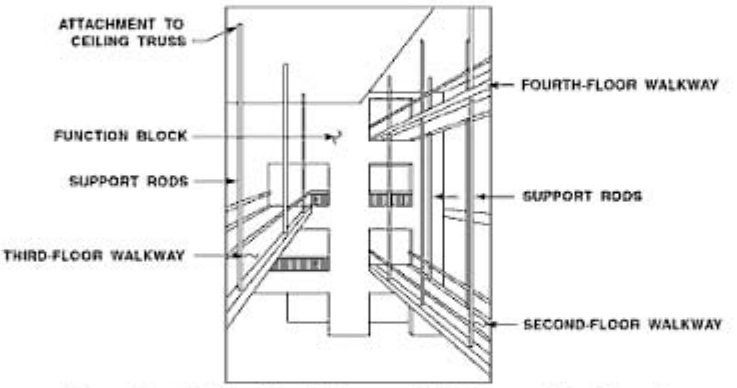


Figure D-2 Atrium of Hyatt Regency Hotel, Kansas City, Missouri
(After Marshall et al. [D-7])

The usual relationship between the architect, structural engineer, and building contractor for a large project is that the architect is the team leader responsible for coordinating the specialized efforts of all team members. Each member of the team is separately licensed in their own

[4]More information on this building failure is available in Petroski [D-1, pp. 85–93 & 102–104] and [D-2, pp. 58–62], in Levy and Salvadori [D-3, pp. 221–230], and in the National Bureau of Standards investigative report [D-7].

Éléments sous droits d'auteur

specialities. If the building fails and the architect did not use the services of a structural engineer (which often occurs for houses and other small projects), then the architect is at fault. If the building fails and the building contractor did not use the prescribed materials in the prescribed manner, then the builder is at fault unless it can be shown that the design was flawed in the area of the failure. In that event, the structural engineer is clearly at fault.

The as-designed suspended walkways depicted in Figure D-2 featured a single long continuous vertical support rod from the bottom of the second-floor walkway support beam through the fourth-floor walkway support beam and on up to fasten to the ceiling truss as shown in Figure D-3. There was no third-floor walkway between the second- and fourth-floor walkways. The third-floor walkway on the other side of the atrium in Figure D-2 is fastened directly to the ceiling with vertical support rods. The original working drawings were prepared by the structural engineers and submitted to the contractor and the architects. All either can do is accept or reject, but not approve. The as-built walkway was the result of the contractor modifying the original design by replacing each long continous support rod with two shorter rods, one from the bottom of the second-floor walkway support beam to the top of the fourth-floor walkway support beam and the other from the bottom of the fourth-floor walkway support beam to the ceiling truss with the fourth-floor walkway and two versions of its connection to the support rod shown in Figure D-3. The shop drawings for the 'as-built' walkway were submitted by the contractor to the architects and the structural engineers, The architects stamped 'approved' on the shop drawings, and the structural engineers stamped 'reviewed' on the same shop drawings. Note that structural engineers are often advised by their attorneys never to stamp 'approved' on the contractor's shop drawings in order to avoid liability for the actions of others. We will revisit that unfortunate advice later.

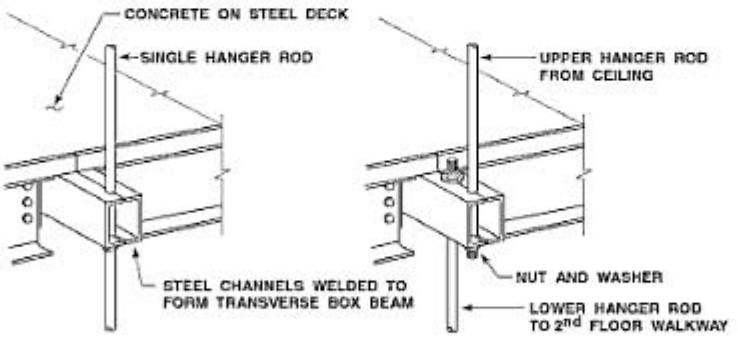


Figure D-3 Hyatt Regency Hotel Skywalk Design Details
(After Marshall et al. [D-7])

Éléments sous droits d'auteur

The key issue is what is the meaning and significance of the word 'reviewed'? The dictionary definition of 'review' as a verb is [D-8]:

1. (now rare) to view, or look at, again
2. to look back on; view in retrospect
3. to survey in thought, speech, or writing; make or give a survey of
4. to examine or inspect; specifically to inspect (troops, etc.) formally
5. to give or write a critical report and evaluation of (a recent book, etc.)
6. to reexamine; specifically to reexamine judicially (a lower court's decision)
7. to go over (lessons, a subject, etc.) again, as in study or recitation

Any layman, indeed any rational individual, would think that if structural engineers 'reviewed' a redesign[5], then they would have tried to identify any feature of the contractor's shop drawings that might cause a problem, e.g., a violation of the building codes or, worse, a failure in consonance with definitions 4 and 5. Perhaps the structural engineers had intended to subject the 'redesign' in the shop drawings to suitable analysis and failure evaluation in addition to checking for building code violations. However, *none of that activity took place for the walkway support system! Or, the activity took place, but was not done properly.* Thus, the faulty 'redesign' was built, and it failed with the loss of 114 lives along with more than 200 injured (and many of the 200 were maimed).

If the structural engineers were not willing to 'approve' the contractor's shop drawings, but were advised to use the word 'reviewed' by their attorneys, then the question would be: *what precisely does 'reviewed' mean?* Clearly, the structural engineers did not do what they were obliged to do according to their professional code of ethics (namely check the 'redesign' thoroughly for errors and building code compliance). Others, namely the contractor and the architects, assumed the structural engineers had critically evaluated the changes represented by the shop drawings and did not object to the replacement of the long rod with two shorter rods. Thus, the misinterpretation of the word 'reviewed' led directly to tragic loss of lives and injuries.

Let's review what occurred during the building design process that led up to the collapse. Building contractors cannot design a structure! *Just because someone* **draws** *a part or all of a building on a piece of paper doesn't mean the building has been designed!* Whether a drawing is a design depends on the criterion or criteria of the beholder. To an artist, a drawing on a piece of paper is a design because it looks right and he can show it to people. To an architect, a drawing on a piece of paper is a design because it looks right and he can present it to a client. To a building contractor, a drawing on a piece of paper is a design because it looks right and he can use it to build a building. However, to a

[5]The contractor's shop drawings cannot be called a re-design because a contractor is not competent to design a structure, nor is an architect! Neither has the education necessary to design a structure. Yes, one of them can build a designed structure, and the other can make the structure serve the owner's needs and look beautiful, but neither can make certain the structure will function as required, much less make certain that it will not fail.

Éléments sous droits d'auteur

structural engineer, a mere piece of paper with a drawing on it is essentially meaningless! Or, at most, a crude beginning. To engineer a structure requires effort far beyond the artistic aspect of how something looks! Structural engineers are concerned with loads, stresses, deformations, bearing areas, stress concentrations, and a myriad of other technical pursuits that require far more than a drawing and are all beyond the educational background of artists, architects, and contractors. If that statement seems somewhat pretentious, too bad, because it's absolutely true. Professionals are licensed to perform certain tasks, and those without the license cannot do the work! Yes, architects are licensed, and they do 'design' buildings, but the structural aspects of the building must be certified by a licensed professional structural engineer.

The structural engineers obviously overlooked the fact that the shear load on the as-built beam supporting the fourth-floor walkway was twice what they had designed the connection to hold (even their original design was inadequate [D-7]!). Thus, the skywalk support beam for the fourth floor in the modified design *should* fail under design loads. Actually, the modified design did well to stand up under loadings less than design loads. In fact, workmen avoided the skywalks when wheeling heavy wheelbarrows from point to point in the building after the skywalks uncomfortably wobbled during a first pass. That the connection (the ability of the flanges of the back-to-back welded channel sections to carry load) was insufficient is clear from the sketch of the failure in Figure D-4. The upper rod, which held the weight of *two walkways* simply pulled out of the flanges of the fourth-floor support beam because the flanges could not carry that much load.

The National Bureau of Standards investigation team did not assign blame for the collapse (because that is not their function), but they clearly portrayed the structural engineers as bearing the main responsibility [D-7]. Subsequently, the structural engineers lost their Missouri professional licenses. Obviously, reliance of the structural engineers on the word 'reviewed' instead of 'approved' is faulty advice from their lawyers. That word change did not allow the structural engineers to escape re-

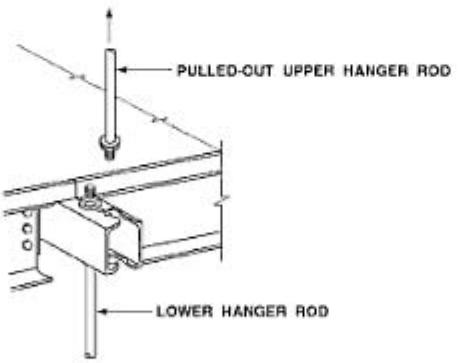


Figure D-4 Upper Hanger Rod Pulled Out From Box Beam
(After Marshall, et al. [D-7])

Éléments sous droits d'auteur

sponsibility for their actions and their inactions. More importantly, use of the word 'reviewed' allowed the building to be built, and then part of the building fell down.

Two possible meanings of 'reviewed' exist for this circumstance. If reviewed really means carefully went over and evaluated any modifications (definitions 4 & 5), then 'reviewed' should suffice. If reviewed really means only 'looked at' (definition 2 or 1), then 'reviewed' is not sufficient. The public deserves the definitive and unambiguous 'approved' by structural engineers on a set of shop drawings before a building is built. We know what we demand of the structural design process, but we must never allow ambiguous words to jeopardize our goal of safe structures.

If a structural engineer is not willing to approve the shop drawings, merely on the advice of his attorney, then we have not gotten full professional value and should not pay the structural engineer. The structural engineer's attorney is just trying to weasel out of an ethical obligation of the engineer. However, it is unethical not to discharge such an obvious obligation. If the structural engineer has specific concerns about the adequacy or correctness of the shop drawings, then he must make those concerns known to the architect and require correction. Certainly, we have every reason to expect the structural engineer to carefully examine all the details of the design and construction process. Of course, we also deserve the full attention and committment to safe design of the structural engineer no matter how he labels his effort when he examines the shop drawings presented to him.

D.5 FAILURE MODES IN DESIGN

The role or possible roles of various failure modes for a design can be illustrated by use of the simple load-deformation curve for a structure. We suppose that several (actually many) modes of failure are possible and attempt to understand the circumstances under which each mode might govern the structural behavior. The *shape* of the load-deformation curve for a simple structure in Figure D-5 is determined by the (variable) stiffness characteristics of the material and structure, as well as on the various behavioral events that occur during loading of the structure (such as, e.g., benign buckling events). Of course, many different loads and deformations are necessary to portray the behavior of a complex structure with correspondingly many different load-deformation curves. However, to illustrate this part of the design process, we concentrate on only one representative load, P, and one representative deformation or deflection, Δ, in Figure D-5.

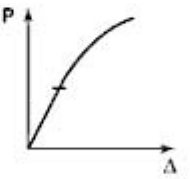


Figure D-5 Load-Deformation Curve for a Simple Structure

The *'end' of the curve,* i.e., the distance along the curve from the origin (where the structure is not loaded at all) to the point at which failure

Éléments sous droits d'auteur

occurs in some manner, depends on the *type* and *mode* of failure. The type is elastic or plastic. The mode is one of

1. fracture because of high stresses or
2. instability of the structure
   - buckling
   - torsional instability
   - aerodynamic instability

   or
3. fatigue, i.e., strength under cyclic loading or
4. other failure modes whatever they might be

whichever failure event or mode occurs first as the structure is loaded along its load-deformation curve.

Many failure modes are possible to end the load-deformation curve of the structure, so many failure scenerios are possible with a few shown schematically in Figure D-6. That is, for variations on the design of a structure, different failure modes can occur. Whether plastic behavior occurs or not depends on the level of stresses relative to the load achieved. Buckling can occur in the elastic range or in the plastic range of the load-deformation behavior as can many other failure modes.

The key to successful engineering design is to identify and understand *all* the various modes in which the structure can fail. Only then with that information are we able to design against failure! After all, if we are not aware of a failure mode that could occur, then we will automatically leave it out of our failure calculations and therefore endanger the structure because that just might be the actual failure mode of the

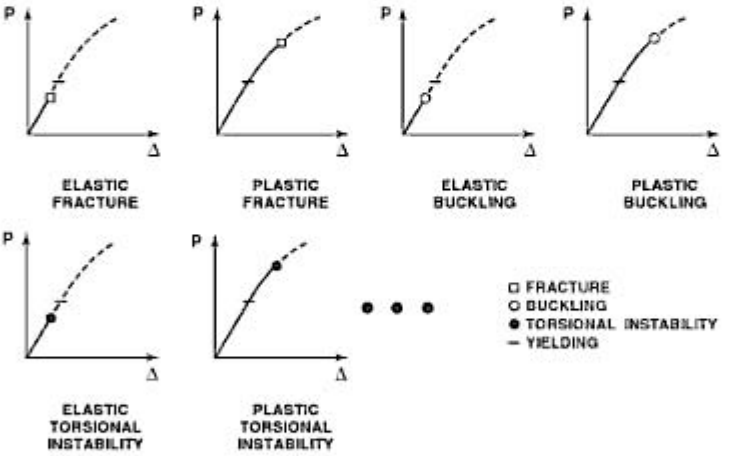


Figure D-6 Some of the Different Structural Failure Modes Relative to Where They Occur on the Load-Deformation Curve

Éléments sous droits d'auteur

structure. Or, more typically, that unknown mode of failure might not govern over a wide range of structural parameters such as load, dimensions, or materials, so within that range *we seem to be 'in control'* of how the structure behaves. However, that unknown mode for certain thinner structural members or longer bridges might just be the dominant failure mode! In that range, the structural behavior is surprising or even shocking because it is not what we expect (on the basis of our limited experience with previous bridges or buildings in this class of structure), and that might just be why the structure fails. That is, *beyond the familiar range of experience, we no longer 'control' how the structure behaves.*

If buckling is the dominant failure mode, then we restrain or stiffen the structure so that buckling mode cannot be realized. However, then we must look for another failure mode that might not be buckling, and the failure load for the new mode might not be much higher than the buckling load we just prevented. That is, there is often some control possible over how a structure will buckle, but that control is not without its problems. Some structures buckle into different modes at the same load. Many buckle into the next highest mode at very high margins over the lowest buckling load. Only in the latter situation will forcing a change in the buckling mode lead to increased design allowable loads for the structure.

The shape of the load-deflection curve also depends on the type of structural element. For example, a plate can buckle several times as in Figure 1-12 on page 8 with a corresponding load-deflection curve that has lower and lower slope with each buckling event. That type of buckling can occur below yielding of the plate as in Figure D-7. Or, yielding could occur between the two buckling loads shown in Figure D-7 with accompanying nonlinearity of the load-deflection curve after yielding. That is, the plate can carry load above buckling (even above two buckling events!) as well as above yielding of a material with a nonlinear stress-strain curve (such as aluminum). Above a buckling load or above yielding, the deformation increases more rapidly than before those events. At some point, the deformation might be the limiting factor in the design rather than the load. Again, *failure doesn't always mean fracture!*

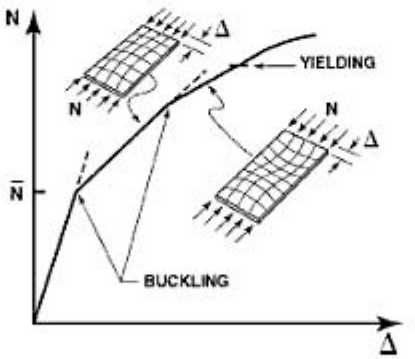


Figure D-7 Load-Deformation Curve for a Plate

Éléments sous droits d'auteur

Another failure mechanism is creep or creep rupture. Creep is the characteristic of a material with increased deformation under constant stress with time. Creep rupture is the characteristic of a material which has first increased deformation under constant stress with time and then fractures at a stress well below the static strength. Such behavior is typical of most plastics as well as some metals under elevated temperatures. For example, if the support cables or rods are made of a material that creeps, then for small loads the weight W in Figure D-8 will lower for some time and then stop. If the amount of lowering (the deflection of weight W) is acceptable, then the design is acceptable. If the deflection is not acceptable, the system fails because of excessive deformation. If the load W is high enough, the cable will creep for a while and then rupture allowing the weight to fall.

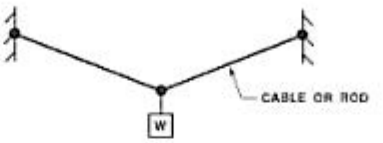


Figure D-8 Behavior of a Cable System Made of a Material that Creeps

D.6 SUMMARY REMARKS

I strongly encourage, even implore, the reader to seriously study Henry Petroski's *Design Paradigms: Case Histories of Error and Judgment in Engineering* [D-2] to be able to begin to put into proper engineering perspective (nay, even to learn about what proper engineering perspective is!) why he even addresses buckling of structural elements at all! Indeed, we must study buckling because structures can and have failed by buckling (or some other form of instability) throughout the centuries that we have attempted to design useful and safe structures. Only by studying what has happened, especially what seems periodically to be neglected in engineering analysis, can we hope to avoid failures. After all, the purpose of engineering design is to avoid failure! Another most suitable study selection is Petroski's earlier book, *To Engineer is Human: The Role of Failure in Successful Design* [D-1], which is a rich source of understanding the point of its subtitle. Also, Levy and Salvadori's *Why Buildings Fall Down* [D-3] has many tales of unsuccessful structures along with reasons for the failures.

Petroski calls to our attention [D-2, pp. 166–169] the fact that Sibly and Walker [D-9] identified an approximately thirty-year cycle over a 150-year timespan of important and differently designed bridge failures that were caused by over-extrapolation of preceding designs in which a specific failure mode did not govern to designs in which that failure mode dominates the design and hence causes 'unexpected' and often dramatic failures. Indeed, as this book goes to press, we are at the end of a thirty-year period from the 1970 failure of the Milford Haven bridge in Wales which followed the 1940 failure of the Tacoma Narrows bridge near Tacoma, Washington. Actually, the numeric progression of the failures over 150 years works out so that 2004 "should" be the next failure, and it will be a cable-stayed bridge if that progression, a statistical

Éléments sous droits d'auteur

phenomenon (but *not necessarily a method of prediction!*), holds true. Of course, my confidence in 'predicting' that bridge failure is equal to or higher than my wife's confidence in my stock market purchases.

Development of engineering thinking and engineering judgment will not happen via the study of mathematics and mechanics alone for they are a means to an end, taken up to see how to progress to that end. However, identification of the 'end' is far more important and indeed even essential to the progression of engineering applications. And that identification process is part of engineering judgment, not mechanics.

Engineering is not just applying equations, but includes applying engineering judgment to solve problems. The development of engineering judgment transcends the ages and even the various advances in analytical and computational techniques because it is the *soul* of engineering, the framework around which we address a problem, and the context in which we evaluate our 'solution' or design.

That is, we must learn to think like engineers in analyzing design problems with which we are faced to be able to creatively *treat all essential aspects of a design* so that we can be assured of having 'covered all the bases' or addressed all the potential problems that a structure or device might presumably experience. Engineering judgment is a pulling together of all the bits and pieces that we know in order to gain control over the structure or device we are designing. That control is the essence of the design process.

Case histories of both failures and successes are a most suitable, even essential, way to educate students about how to properly design a structure. Indeed, Henry Petroski is noted and acclaimed for his structures case history course at Duke. All engineering professors would do well to seriously consider emulating Henry Petroski!

APPENDIX D REFERENCES

D-1 Henry Petroski, *To Engineer is Human: The Role of Failure in Successful Design*, St. Martin's Press, New York, 1985.

D-2 Henry Petroski, *Design Paradigms: Case Histories of Error and Judgment in Engineering*, Cambridge University Press, New York, 1994.

D-3 Matthys Levy and Mario Salvadori, *Why Buildings Fall Down*, W. W. Norton & Company, New York, 1992, pp. 221–230.

D-4 Henry Petroski, The Fall of Skyscrapers, *American Scientist*, Volume 90, Number 1, January-February 2002, pp. 16–20.

D-5 Derek D. Dempster, *The Tale of the Comet*, David McKay, New York, 1959.

D-6 Nevil Shute, *No Highway*, William Morrow & Co., New York, 1948.

D-7 R. D. Marshall, E. O. Pfrang, E. V. Leyendecker, K. A. Woodward, R. P. Reed, M. B. Kasen, and T. R. Shives, *Investigation of the Kansas City Hyatt Regency Walkways Collapse*, NBS Building Science Series 143, National Bureau of Standards, U. S. Dept. of Commerce, Washington, D. C., May 1982.

D-8 *Webster's New World Dictionary*, Second College Edition, David B. Guralnik, Editor in Chief, Prentice Hall Press, 1984.

D-9 P. G. Sibly and A. C. Walker, Structural Accidents and Their Causes, *Proceedings of the Institution of Civil Engineers, Part 1, Design and Construction*, Volume 62, May 1977, pp. 191–208.

Éléments sous droits d'auteur

Index

A

Adjacent equilibrium method 98
Alfutov, Nicolai A. 223
Allen, Howard G. 448, 709
Almroth, Bo O. 31, 223, 246, 260, 327, 364, 475-476, 484, 489, 520, 523, 525, 529, 532-535, 560, 576, 580, 590, 600, 609, 617, 668
Amazigo, John C. 21, 542
Ambartsumyan, S. A. 320, 557, 560, 639, 687, 767
Anderson, Melvin S. 447
Arbocz, Johann 30, 223, 301, 319, 367, 448-451, 496, 518, 525, 538, 657, 664-665, 667-668, 682, 686, 704, 719
Ashton, James E. 213, 338, 351, 407, 454, 709, 776-778
Assumption 33
Asymptotic analysis 21

B

Babcock, Charles D., Jr. 538, 657, 664-665
Ballerstedt, W. 657
Bars
  alternative buckling differential equation 67-78
  buckling 6-7, 10, 12-14
  definition 49
  differential equation by rigorous energy approach 106
  effective-length concept 76-77
  elastic restraint 60
  fixed-fixed 57, 71-72
  fixed-free 58, 72-73, 79-133
  fixed-free under own weight 138-140
  fixed-free with change in cross section 140-142
  fixed-guided 73-74
  fixed-pinned 56, 70
  lateral buckling 222
  pinned with mid-span spring 62-66, 142-143
  pinned-free with elastic restraint 59-61
  pinned-guided 75
  pinned-pinned 50-55, 69, 127-130, 174-177
  plastic buckling 187-201
  the elastica 79-91
  thermal buckling 161-186
Baruch, M. 542
Barynin, V. A. 540
Batdorf curvature parameter 492, 503, 505, 565
Baldorf's Modified Donnell Equation 489-490, 509, 518
Batdorf, Samuel Burbridge 12, 313, 317-318, 466, 489, 491-492, 494, 496, 500, 502-508, 512, 553, 562, 565, 701
Beck, Max 713-714
Bend-twist coupling 321, 337-338, 346
Bending strain energy
  variation-in-moment 154
Bending strain energy integral
  variation-in-curvature 121
  variation-in-moment 122
Bending-extension coupling 320-321, 339
Benjamin, Roland T. 657
Bernoulli-Euler hypothesis
  See Euler-Bernoulli hypothesis
Bert, C. W. 687
Bifurcation 7, 333
Bifurcation buckling load 7, 8, 18, 19, 24
Bleich, Friedrich 86, 705
Block, David L. 542, 547, 554, 563, 640
Bloom, Frederick 448
Bogdanovich, Alexander E. 351, 576
Boley, Bruno A. 319, 381, 385, 451
Bolotin, Vladimir V. 713-714
Booton, M. 576
BOSOR 655, 685, 719-720
Boundary conditions
  derivation 100, 106
  geometric 68, 105, 110, 113, 117
  natural 68, 105, 110, 113, 117

Éléments sous droits d'auteur

plate buckling 258-262, 331-332
plate equilibrium 243-248, 326-329
shell buckling 484-489
shell equilibrium 472-476
Bridget, F. J. 657
Brogan, Frank A. 668, 719-720, 727, 732-733
Brooks, William A. 405-406
Brown, D. M. 79
Brown, James Ward 136, 266, 280
Browning, C. E. 213
Brush, Don O. 31, 223, 525
Bryan, G. H. 12, 228, 264, 415
Bubnov-Galerkin method
See Galerkin's method
Bubnov, I. G. 505
Buckling
advanced buckling topics 710-714
attributes 8
bar differential equation from non-straight prebuckling shape 115
bar differential equation from straight prebuckling shape 111
bars 6-7, 10, 12-14, 49-226
bars - design against 202-221
classification of 18
computational approaches 715-735
definition of buckling load 5
deflection 51
dynamic 714
factors affecting 27
further classical topics 705-709
nonconservative systems 710-714
plates 8, 10, 14, 227-462
plates - design against 422-447
shells 10, 15-17, 463-698
shells-design against 654-684
snap-across 726, 728, 730
snap-down 726, 729
snap-through 17, 704, 726
stochastic 714
Buckling criteria 97-99, 111, 115
adjacent equilibrium method 98, 111, 114, 115
neutral equilibrium method 98, 114
Trefftz buckling criterion 99, 111, 114-115
Buckling deflection function
approximate 119, 123, 125
multiple degree of freedom 135
single degree of freedom 119
Buckling equations
bars 50-55, 67-78, 111-118
plates 249-263
shells 478-489
Buckling load 5-9, 14
definition of 5
Buckling mode 12-17, 19
diamond-shaped 16
sinusoidal 12-14, 490
Budiansky, Bernard 290, 408, 618
Bulson, P. S. 448
Bunakov, Vladimir A. 540
Bushnell, David 655, 683, 706, 719-720
Byon, O-Il 314, 319, 451

C

Cabiness, Harold D. 719-720, 727, 732-733
Calculus of variations 92, 100, 104, 109, 111, 115
fundamental lemma 104, 109
special second variation 111, 115
Callahan, Kelvin J. 446
Cannon, Walter F. 442
Card, Michael F. 512-517, 542, 547-550, 553, 563, 569, 630, 640, 653
Carper, Douglas M. 729
Castigliano's theorem 151
Chajes, Alexander 223
Chamis, C. C. 338
Chaos 714
Characteristic equation 53, 56
transcendental 56
Characteristic value 51
Chen, Youl-Nan 518
Churchill, Ruel V. 136, 266, 280
Classical lamination theory 767-779
bending-extension coupling 775-776
laminate forces and moments 772-776
strain and stress variation 768-772
Clemmer, Lewis E. 382
Coan, John M. 319, 451
Coefficient of thermal expansion 102
Coffin, Douglas 448
Collar, A. R. 505, 509, 513
Columns
See Bars
Composite materials
advantages of 751
definition of 751
tailoring of 752
Computational approaches 11-12, 332, 715-735
Configuration 2-4, 6-8, 10, 18
Confucious 602
Connor, Robert 290
Conservative mechanical system 2, 5
Conservative mechanical systems 710-714
Considère, A. 190
Constraint 2, 9, 13
Coupling
bend-twist 321, 337-338, 346, 775-779, 787-790

Éléments sous droits d'auteur

bending-extension 320-321, 339-342, 346, 542, 554-576, 685, 775-779, 783, 789-796
shear-extension 320-321, 337, 767, 779, 782, 787-789
stiffnesses 320, 775
Courant, R. 104, 109, 230
Crate, Harold 657
Creep 811
Critical buckling load 14
Crose, James G. 11, 716-717, 719, 734

D

Darwin, Charles 442, 444
de Havilland Comet 803
Deformation
excessive 9-10
inelastic 9-10
mode 8
plastic 9-10
prebuckling 15
Degrees of freedom
definition 119
Dempster, Derek D. 803
Design
See also Optimization
bars 202-221
codes 215
constraints 433
cost 206
definition 203
design drivers 429-430
design requirements
life 798-800
stiffness 798-800
strength 798-800
deterministic 423, 426, 433
driver 206
effect of creep 211
effect of earthquakes 212
environmental effects 213
factor of safety 654, 657, 673-675, 681
failure criteria 798, 800
failure modes 206
general concepts 9, 700-704, 721-722
genetic algorithm 442-447
isotropic plates 425-430
iteration 203
knockdown factor 703
laminated plates 431-447
life-cycle cost 422
load and resistance factor design 220
mechanistic relations 204
merit function 433
nondeterministic 204, 426, 432-433
objectives 422, 435
optimization techniques 434
overdesign 423-424, 434, 442
philosophy 204, 797-812
requirements 203, 422-424
shells 654-684
high-fidelity analysis and design 662-682
knockdown factor 657-659, 663, 666, 673, 676, 681, 683-684
stiffness-sensitive 429
structural reconfiguration 423-424
trade-offs 206
underdesign 423-424
variables 9, 203, 423
versus analysis 202-206
weight 206
weight-sensitive 429
Direct energy methods 119-144
DISDECO 668
Displacement 2
Dong, Stanley B. 320, 557, 767
Donnell shallow shell theory 473, 489
Donnell's Equation 486-490, 518
Donnell, Lloyd Hamilton 12, 223, 466-467, 488-489, 507, 535-538, 659
Doup, M. R. 657
Dow, Norris F. 744
Drucker, Daniel C. 29
Duncan, W. J. 505, 509, 513
Dym, Clive L. 92
Dynamic buckling 714

E

Eccentric stiffening 540-554, 685
Effective-length concept 76-77, 202
Eigenvalue 18-19, 51
equation 53
Eigenvector 19, 51
El Naschie, M. S. 714
Elastic limit 10
Elastica 79-91
Elishakoff, Isaac 682, 713-714
Ellis, C. A. 79
Emde, Fritz 82
Energy concepts 49, 92-95, 705
bending strain energy 468
direct energy methods 119-144
energy principles 46
inflection point 738-741, 746
maxima 746
maxima and minima of functions of a single variable 738-742
membrane strain energy 469
metastable 4
minima 742-746

Éléments sous droits d'auteur

minimum of a function of two integer variables 743-748
minimum potential energy 4, 738
minimax 4
neutral point 739-740
potential energy 4
potential energy of external forces 92, 469
principle of minimum potential energy 94, 738
principle of stationary potential energy 93, 738
relative maxima 738-742
relative minima 738-742
saddle point 4
stationary potential energy 738
stationary value 744, 746
stationary value (of potential energy) 738-740, 742
strain energy 92, 469
total potential energy 4-5, 92
variational calculus 46
Engesser, Friedrich 190, 191
Engineering constants 759-760, 768
Environmental effects 213
Equilibrium
character 93
configuration 3-4, 6-8, 10, 18, 51
neutral 93, 97
path 3, 8
prebuckling configuration 10
stable 2, 4-6, 10, 93-94, 96-97
state 2
types 93
unstable 3-6, 93, 96-97
Equilibrium equations
bars 110
large-deflection for bar 110
plates 230-248
shells 467-478
Equivalent mechanical load concept 377-378, 596-597
Esslinger, M. 657
Euler buckling load 7-8, 12-14, 17-18, 91, 145-160, 202-205, 466, 654, 700-704, 710, 713
practical significance for bars 91
Euler column or bar equation 50-60
Euler equation 235, 471
Euler-Bernoulli hypothesis 38, 79, 107, 166, 322, 704
Euler, Leonhard 7, 21, 50, 79, 187, 204, 221
Expansional strains 213
Experimental results
See also theory versus experiment under Bars, Plates, and Shells
basis for theoretical models 30
comparison with theory 26, 704
importance of 26-32
motives for 29, 656
validation of theory 26

F

Factor of safety 9, 19, 216, 219, 425-428, 434, 439, 441, 447, 654, 657, 673-675, 681, 702-704
Failure
analysis 797
creep 811
modes 9
modes or mechanisms 798, 808-809
structural 797-812
Fiber-reinforced laminated composite materials 633-652
Finite difference method 332, 490
Finite element method 11, 332, 490, 715-735
Finite theory of stability 4
Flügge, W. 473
Fok, W. G. 310
Follower force 713-714
Forray, M. J. 401
Fourier series analysis 665
Fourier sine series 135
Frazier, R. A. 505, 509, 513
Free thermal strain 161
Friedrichs, Kurt O. 7
Frisch-Fay, R. 66
Fung, Y. C. 229

G

Galambos, Theodore V. 221
Galerkin method 338
Galerkin's method 332, 338, 490, 505, 509, 513, 547
Galerkin, B. G. 505
Gallagher, Richard H. 448
Galletly, G. D. 705
Gaylord, Charles N. 215
Gaylord, Edwin H., Jr. 215
Geier, Bodo 657
Genetic algorithm 442-447
Gerard, George 66, 410, 620-621, 635
Gere, James M. 11, 93-94, 138, 223, 257, 263, 284-285, 289, 296-297, 301, 333, 705, 729
GIGO 12, 716
Gilmore, Robert 714
Glass-transition temperature 213
Gleich, James 714
Goodier, J. N. 148, 151
Gossard, Myron L. 402-403
Grashof, F. 66

Éléments sous droits d'auteur

Green's theorem 233, 469
Greenhill, A. G. 136
Gribanov, V. F. 407, 618
Gürdal, Zafer 350, 434, 446, 684

H

Haftka, Raphael T. 434, 446, 684, 722
Hajela, Prabhat 434, 446, 684
Hall, David H. 542
Halpin, John C. 776-778
Hammurabi, Code of 801
Harris, Leonard A. 16, 497, 501, 657
Hartman, E. C. 199-200
Harvey, James M. 309-313, 319, 449-450
Hedgepeth, John M. 542
Heldenfels, Richard R. 401-402
Hennemann, Jose C. F. 323, 329, 576
Herrmann, George 713
High-fidelity shell analysis and design 662-682
Hilbert, D. 104, 109, 230
Hilburger, Mark W. 661, 669-682
Hoff, Nicholas J. 7, 211, 223, 319, 451, 522-523, 710, 714
Holmes, A. M. C. 31, 525
Holmquist, J. L. 196, 417, 626
Holt, M. 199-200
Hu, Pai C. 313, 317-318
Husman, G. E. 213
Hutchinson, John W. 21, 542
Hyatt Regency Hotel skywalk 44, 604-608
Hyer, Michael W. 729

I

Ilyushin, A. A. 408-410
Inelastic deformation 10
Infinitesimal theory of stability 4, 93, 97
Inflection point 738-741, 745
Initial geometric imperfections 8, 17, 22-23, 25
  bars 156-160
  general 700-701
  plates 308-319, 334
  shells 535-539
Instability 3-5
  definition of 3
  metastable 4
  unstable mechanical system 3
  unstable stable in the large 4
  unstable structural element 4

J

Jahnke, Eugene 82
Jasinski, F. S. 190
Jenkins, William C. 516
Jerome, C. C. 657
Johnson, Eric R. 729
Johnson, James H. 280
Jones, Robert M. 11, 29, 33, 175, 212, 320, 323, 329, 339-349, 406, 409-409, 415-417, 420-421, 434, 452-454, 512-517, 520-527, 542, 547-550, 553, 555-576, 605, 614, 619-653, 656, 687-689, 709, 718, 744-745, 751, 754, 756, 766, 788, 790, 795-796
Jump 5-6

K

Kaplan, Abner 729
Kármán large-deflection plate equilibrium equations 474
Kármán large-deflection plate theory 467
Kármán, Theodore von 12, 190, 199, 222, 240, 245, 302, 310, 317, 325, 467, 474, 519-520, 535-536, 659, 705, 710
Kasen, M. B. 604-605, 807
Kassapoglu, Christos 446
Kempner, Joseph 518
Kirchhoff free-edge condition 326
Kirchhoff hypothesis 41, 240, 324, 353, 356, 467, 769-772
Kirchhoff plate theory 42
Kirchhoff shear force 228, 239, 464, 470, 475
Kirchhoff-Love hypothesis 467-468, 543, 558, 575, 578, 582, 769-772
Kirchhoff, G. 239, 324
Klein, Stanley 563
Klosner, J. M. 401
Knockdown factor 657-659, 663, 666, 673, 675, 681, 683-684, 703
Koiter, Warner Tjardus 21, 25, 520, 536, 668-669, 713
Kollbrunner, Curt Fritz 451
Korn, Granino A. 138, 523
Korn, Teresa M. 138, 523
Kraus, Harry 211

Éléments sous droits d'auteur

L

Lagace, Paul A. 37, 39, 726, 728, 732
Lagrange, J. L. 79
Lamina
  definition of 752
  generally orthotropic 767
  specially orthotropic 765
  stress-strain behavior 761-767, 768
  unidirectionally reinforced 752, 753-754
  woven 752
Laminate
  advantages of 753-756
  angle-ply 788-789, 792-793
  antisymmetric 789-796
  balanced 795
  behavior 775-779
  cross-ply 783, 786-787, 789, 791-792
  curing 783
  definition of 752
  environmental effects 213
  forces and moments 772-776
  hybrid 795
  purpose of 752
  reason for 750
  regular 780, 786-788, 791-792, 794
  specially orthotropic 790
  stacking sequence notation 794-795
  stiffnesses 775
  strain and stress variation 768-772
  symmetric 782-788
  temperature-dependent properties of 774
  unidirectional 755
  unsymmetric 783, 789, 793-794
Laminated fiber-reinforced composite materials 17, 708-709, 749-796
Laminated plates 320-351
  angle-ply
    antisymmetric 342-345
    symmetric 337-338
  behavior 435, 436, 451, 452
    brittle 435
    ductile 435
    energy absorption 435
    fatigue 436
    load-deflection behavior 436
    nonlinear stress-strain 451-452
  behavioral restrictions and presumptions 322-325
  bending 325-329, 346
  boundary conditions
    buckling 331-332
    equilibrium 326-329
  buckling 320-351, 451-452
  buckling equations 329-332
  coupling stiffnesses
    bend-twist 321, 337-338, 346
    bending-extension 320-321, 339-342, 346
    shear-extension 320-321, 337
  cross-ply
    antisymmetric 339-342
    specially orthotropic 335-337
    symmetric 335-337
    unsymmetric 346-348
  design 431-447
  design problem 433, 436
  equilibrium equations 325-329
  first-ply failure load 438
  initial geometric imperfections 334
  Kirchhoff hypothesis 324
  life-prediction techniques 437
  maximum strain failure criterion 439
  nonlinear stress-strain behavior 451-452
  optimization 442-447
  quasi-isotropic 434
  solution techniques 332
  stacking sequence 436
  stiffnesses 340-349
  strength analysis procedure 437
  thermal buckling 453-457
Laminated shells 555-577
  cross-ply 555-577
    antisymmetric 564-569
    unsymmetric 570-575
  plastic buckling 633-652
Lang, H. A. 122, 130
Langhaar, Henry L. 46, 92, 705, 742
Langthjem, M. A. 713
Lateral buckling of a bar 222
Layer
  See Lamina
Le Riche, Rodolphe 446
Least-cost structures 206
Least-weight structures 206
Lee, K. H. 448
Lehrer, Tom 221
Leissa, Arthur W. 351, 565
Levy, Matthys 797, 803-804
Levy, Samuel 318
Leyendecker, E. V. 804-805, 807
Li, Yiwei 682, 714
Liebowitz, Harold 451
Limit of stability 97
Limit point 5-6, 724
  deflection-limit point 726-729
  load-limit point 5-6, 724, 726-731
Lloyd Hamilton Donnell 498
Lo, Hsu 657
Load-carrying capacity 9, 14, 18, 20-23, 25, 49, 709-704
Load-deformation behavior 3, 5-6, 10, 13-14, 16, 18, 20, 700-704
  jump 5-6
Lobachevski, Nicolai Ivanovich 221
Lock, A. C. 723-724, 726-729
Loden, William A. 710-720, 727, 732-733

Éléments sous droits d'auteur

Lorenz, Edward N. 714
Love, A. E. H. 467
Lunchick, Myron E. 409
Lundquist, Eugene E. 223, 313, 317-318, 657

M

Madsen, W. A. 522-523
Mandell, John F. 336
Manufacturing imperfection signature 664
Margin of safety
  See Factor of safety
Marguerre, Karl 107
Marshall, I. H. 351
Marshall, R. D. 804-805, 807
Martin, James R. 212
Martinelli, Jack 716, 734
Massonnet, C. E. 221
Material properties
  temperature-dependent 161, 404-406
Mathauser, Eldon E. 405-406
Maxima 746
Maxima and minima of functions of a single variable 738-742
Maximum load 9
Mayers, J. 522
McElman, John A. 542
Mechanistic relationships 204
Metastable 4
Metastable point 94
Michell, A. G. M. 222
Mikulas, Martin M., Jr. 542, 547, 563, 640
Miller, Robert E. 92
Minima 743-746
Minimum of a function of two integer variables 743-748
Minimum potential energy 4, 738
Minmax 4
Moisture absorption 213
Moment of inertia
  See Second moment of the cross-sectional area
Monocoque construction 706
Morgan, E. J. 657
Morgan, Harold S. 345-346, 452, 566-575, 653, 689
Moscow Hotel 42-43
Murphy's law 46

N

Nadal stress-strain curve 196-198, 417, 628
Nadai, A. 196, 408-409, 417, 619-620, 626, 634
NASA design monographs 657, 660-662, 666, 673, 678-681, 683-684
NASTRAN 686
Neff, John 289-291
Nemeth, Michael P. 83-86, 382, 385, 400, 407, 656, 660-669, 676-682
Neutral equilibrium buckling criterion 114
Neutral equilibrium method 98
Neutral point 738-740
Neutral stability 24
Newton-Raphson method 528
Nodal circle 15
Nodal line 14-15, 333
Nodal point 12, 14-15, 54
Noel, Robert G. 280
Nonconservative mechanical systems 710-714
Nonlinear equilibrium problem 1
Nonlinear strain-displacement relation 106, 166
Nonlinear stress-strain behavior 17
Novozhilov, V. V. 473

O

Ogibalov, P. M. 407, 618
Oldfather, W. A. 79
Olmedo, R. 350
Olsen, Karl-Axel 708
Optimization 422, 447, 721-722
  brute-force search 432
  constraints 433
  laminate 431
  merit function 433
  Tsai's laminate ranking procedure 432
Orthotropic modulus ratio 342, 345
Orthotropy 325
Orthotropy ratio 564
Osgood, William R. 197

Éléments sous droits d'auteur

P

Pagano, Nicholas J. 434
PANDA 683-684, 720
Panel versus General Instability 553-554
Parkes, E. W. 366, 381, 385, 594
Perrone, Nicholas 461
Peterson, James P. 657
Petit, P. H. 776-778
Petroski, Henry 46, 797-798, 803-804, 811-812
Pflüger, A. 98
Pfrang, E. O. 804-805, 807
Pichkhadze, G. P. 540
Pister, Karl S. 320, 557, 767
Pitarresi, James M. 148
Planlema, Frederick J. 708
Plastic buckling
  deformation theory 408-409, 619-620
  nonlinear stress-strain curve 410, 621
  plates 408-421
  secant-modulus theory 409
  shells 619-653
  strain intensity 409-410, 620-621
  stress intensity 409-410, 620-621
  tangent-modulus theory 409
Plastic buckling of bars 187-201
  governing equation 191-193
  reduced-modulus theory 189-190
  tangent-modulus theory 191-201
  theory versus experiment 199-200
Plastic buckling of plates 408-421
  buckling criterion 414-415
  solution strategy 415-416
  theory vs. experiment 419-421
Plastic buckling of shells 619-653
  buckling criterion 624-625
  laminated shells 633-652
  numerical results 628-633, 649-652
  solution strategy 626-627
Plastic deformation 10
Plate buckling
  secondary 307
  strain-reversal method 315, 319
  top-of-the-knee method 315-316, 319
Plates
  aspect ratio 227, 323
  boundary conditions
    buckling 258-262, 331-332
    equilibrium 243-248, 326-329
  buckling 6, 10, 14
  classical buckling solutions (see table of contents) 264-301
  definition 227
  design 422-447
  initial geometric imperfections 308-319, 334
  plastic buckling 408-421
  postbuckling behavior 302-307
  skew 338
  solution techniques 332
  thermal buckling 352-407
Poisson's ratios 750
Popov, E. P. 91
Postbuckling behavior 8, 17, 18-25
  bars 21, 25, 79-91
  classification of 18
  degree of stability 24-25
  general 700-704
  imperfect structures 22-25
  initial 21
  initial slope 21
  neutral 20, 22
  perfect structures 20-21
  plates 21, 25, 302-307
  shells 21, 25, 519-528
  stable 18
  symmetric stable 21-23
  symmetric unstable 21-23
  unsymmetric 21-23
Potapov, V. D. 714
Potential energy 4
Potential energy of external forces 92
Prandtl, Ludwig 222
Prebuckling deformations 15
  shells 486-487, 526-534
Prebuckling geometry 9
Presumption 33
Principal material directions
  definition of 750
  nonalignment with body coordinates 783
Principle of minimum potential energy 94, 738
Principle of stationary potential energy 93, 738
  stationary value 93
Problem solving: lessons learned and communication 733
Prolasov, Victor D. 540

R

Radiation 213
Radius of gyration 54-55
Ramberg-Osgood stress-strain curve 197
Ramberg, Walter 197
Rankin, Charles C. 719-720, 727, 732-733
Rasin, Alexander F. 540
Rayleigh method 116-135, 151, 154-155
Rayleigh-Ritz Method 135-138, 332, 338, 490
Rayleigh, Lord (John William Strutt) 119

Éléments sous droits d'auteur

Reddy, J. N. 92, 301, 320, 333, 448, 667, 709
Redhefter, R. M. 233
Reduced-modulus theory 189-190
Reed, R. P. 804-805, 807
Reissner, Eric 320, 557, 767
Relative maxima 738-742
Relative minima 738-742
Restriction 40
Router, Robert C. 764-765
Rhodes, James 308-313, 319, 449-450
Riks, Eduard 727
Ritz, Walther 119, 135
Roberts, William M. 401-403
Robertson, Andrew 657
Roorda, J. 223
Rosen, B. Walter 744
Ryu, B.-J. 713

S

Sabir, A. B. 723-724, 726-729
Saddle point 4
Safety
  See Factor of safety
Salvadori, Mario 797, 803-804
Sandwich construction 706-709
Schildcrout, Murry 401, 504-508, 562
Schmit, Lucien A. 434
Schwartz, Edward B. 657
Second moment of the cross-sectional area 52, 146, 202, 205
Secondary buckling 307
Seide, Paul 402-403, 657
Separation of variables 332
Shames, Irving H. 92, 148
Shanley, Francis R. 190-192, 201, 408, 620, 710
Shear moduli 758-760
Shear stiffness effect 145-155
Shear-extension coupling 320-321, 337
Shells
  buckling 10, 15-17
  buckling equations and boundary conditions 478-489
  classical buckling solutions (see table of contents) 490-518
  definition 464-466
  design 654-684
  different moduli in tension and compression 586-589
  eccentrically stiffened 540-554
  equilibrium equations and boundary conditions 467-478
  incorrect benchmark panel buckling solution 723-734
  initial geometric imperfections 535-539
  k-Z representation 492, 495, 504, 556, 564-569
  laminated 555-577
  membrane prebuckled shape 486-487
  plastic buckling 619-653
  postbuckling behavior 519-528
  prebuckling deformations 486-487, 529-534
  Problem solving: lessons learned and communication 734
  stiffened 540-554
  theory versus experiment
    axial compression 496, 547-550
    hydrostatic pressure 503-504
    lateral pressure 499-500
    torsion 507-508
  thermal buckling 577-618
Shen, M. K. 89
Shives, T. R. 804-805, 807
Shute, Nevil 803
Sibly, P. G. 811
Sierakowski, Robert L. 320, 351, 576, 709
Simitses, George J. 223
Singer, Josef 29, 223, 301, 319, 367, 449-451, 496, 518, 525, 542, 656-657, 665, 686, 704, 719
Skene, William T. 16, 497, 501, 657
Skew plates 338
Sobel, L. H. 475
Sokolnikoff, I. S. 233
Solution techniques 332
  finite differences 332
  finite elements 332
  Galerkin's method 332
  Rayleigh-Ritz method 332
  separation of variables 332
Soong, T.-C. 540
Soremekun, Grant 446
Southwell plot 319
Southwell, R. V. 223
Space effects 213
Sparaco, Pierre 46
Special second variation 111, 115, 120, 136-137
Specially orthotropic laminate 321, 335-337
Specific stiffness 753-756
Specific strength 753-756
Stability
  definition of 2
  degree of 24-25
  finite theory of 4
  infinitesimal theory of 4
  metastable 4
  neutral 24
  stable in the small 4
  stable mechanical system 2
  stable structural element 2
Stable equilibrium 2, 4, 10

Éléments sous droits d'auteur

Stable equilibrium configuration 66
Stable in the small 4
Stable mechanical system 2
Stable structural element 2
STAGS 655, 667-671, 685, 719-720, 727, 732-733
Stallmeyer, James E. 215
Starnes, James H., Jr. 350, 656, 660-662, 714
Stationary potential energy 738
Stationary value 744, 746
Stationary value (of potential energy) 93, 736-740, 742
Stavsky, Y. 320, 557, 767
Stein, Manuel 289-291, 302-308, 311, 318, 450-451, 489, 491, 504-508, 529, 532, 542, 562, 662
Stiffeners 540-554
  eccentricity effect 550-554
  embedded stiffening strap 442
  manufacturing 430
  optimum design 442
  types 430
Stiffness 751, 753-756
Stiffnesses
  bending 775-776
  bending-extension 775
  extensional 775-776
  for anisotropic materials 758
  for bending-extension coupling 776
  for orthotropic materials 759
  laminate 776
  of anisotropic layer 782
  of generally orthotropic layer 781-782
  of isotropic layer 780-781
  of specially orthotropic layer 781
  reduced 762, 768
  special cases for 779-786
  transformed reduced 766, 768
Stochastic excitation 714
Stowell, Elbridge Z. 408-410, 415, 620
Strain energy 92
Strains
  engineering shear strain 764
  tensor shear strain 764
Strength 751, 753-756
Stress-strain relations
  for a generally orthotropic lamina 767
  for a lamina of arbitrary orientation 783-787
  for a specially orthotropic lamina 765
  for anisotropic and orthotropic materials 756-760
  plane stress (orthotropic) 761-763
  transformed 763
Stroud, W. Jefferson 447
Structural design process 422
Structural reconfiguration 423-424
Sturm, Rolland G. 199-200, 499-500, 503-504
Suer, Herbert S. 16, 497, 501, 557
Sugiyama, Y. 713
Szilard, Rudolph 448

T

Tacoma Narrows Bridge 714, 797
Tail, Lambert 216-217, 219, 220
Tangent-modulus theory 191-201
Tauchert, T. R. 407
Taylor series 94, 97, 120, 739-740
Taylor, R. L. 557
Temperature effects 213
Templin, R. L. 199-200
Tennyson, Rod C. 535, 576
the Elastica 79-91
Thermal bending of bars
  pinned-pinned 178-184
Thermal buckling of bars
  pinned-pinned 174-177
  support conditions 171-173
  thermoelastic relations 165-170
Thermal buckling of plates 352-407
  cross-ply laminated composites 453-457
  equivalent mechanical load concept 377-378
  loading and restraint conditions 365-376
  moisture effects 406-407
  nonlinear stress-strain behavior 404-406
  nonuniform heating 401-403
  temperature-dependent material properties 404-406
  thermoelastic relations 355-364
  time-dependent temperature distributions 403-404
Thermal buckling of shells 577-618
  equivalent mechanical load concept 596-597
  in-surface loading and restraint 591-595
  nonlinear stress-strain behavior 618
  temperature-change distribution 617-618
  temperature-dependent material properties 618
  theory versus experiment 618
  thermoelastic relations 581-590
Thermal effects
  free thermal strain 161-163, 355, 578, 581
  restrained expansion 161, 352-407, 577-618
  self-equilibrating thermal stress 164

Éléments sous droits d'auteur

self-equilibrating thermal stresses 352, 577
self-imposed thermal stresses 352, 577
thermal force 167, 584
thermal moment 167, 585
thermal stress 161-164
thermoelastic relations 355-364, 581-590
Thielemann, W. F. 523, 525
Thornton, Earl A. 163-164, 176, 178-180, 385, 407, 618
Timoshenko, Stephen P. 7, 11-12, 79, 83-84, 114, 136, 148, 151, 222-223, 257, 263, 280, 284-285, 289, 292, 296-297, 301, 326, 333, 705, 729
Tolstov, Georgi P. 136, 266, 280
Toni, Darryl 446
Total potential energy 4-5, 92, 95, 111, 116
special second variation 111, 115, 120, 136-137
Transverse shear stiffness effect 145-155
Trefftz buckling criterion 99, 111, 114-115
Trefftz, E. 99, 253
Trilling, Charles 503-504
Trivial solution 53
Tsai, Stephen W. 432, 434, 436
Tsien, Hsue-Shen 12, 519-520, 535-536, 659, 710
Tudela, Mark A. 726, 728, 732
Turvey, G. J. 351

U

Uemura, Masuji 314, 319, 451
Unstable equilibrium 3-5
Unstable in the large 4
Unstable mechanical system 3
Unstable structural element 4

V

van der Neut, Arie 542
Vanderplaats, Garret N. 447, 683
Variational calculus 46
Vasiliev, Valery V. 43, 320, 540, 576, 664, 709
Venkataraman, Satchi 722
Vibration 346
Vinson, Jack R. 320, 576, 708-709
Volmir, A. S. 505
Vorzimmer, Peter J. 442
Vosseller, A. B. 657

W

Waddoups, Max E. 338
Wagner, H. 657
Walker, A. C. 313, 319, 811
Wan, C. C. 498, 535-537
Wang, C. M. 448
Wang, James Ting-shun 332
Wardle, Brian L. 723, 726-729, 731-733
Weeks, George E. 446
Weiner, Jerome H. 381, 385
Weingarten, Victor I. 657
Weller, Tanchum 30, 223, 301, 319, 367, 449-451, 490, 518, 525, 657, 665, 666, 704, 719
Wendt, F. W. 461
Whitney, James M. 213, 320, 333, 336, 343, 345, 351, 407, 454, 565, 709
Wilcox, Marion W. 382
Wildhorn, Sorrel 410, 621, 635
Williams, F. W. 447
Windenburg, Dwight F. 503-504
Wittrick, W. H. 447
Woinowsky-Krieger, S. 326
Woodward, K. A. 804-805, 807
World Trade Center Twin Towers 798
Wu, K. Chauncey 350

Y

Yamaki, N. 508
Yao, John C. 518
Yoshimura, Y. 523
Young's moduli 756, 760
Young, D. H. 148

Z

Zenkert, Dan 708
Ziegler, Hans 710, 712, 714

Éléments sous droits d'auteur

FIGURE AND TABLE REPRODUCTION ACKNOWLEDGEMENTS

I sincerely appreciate the efforts of Ms. Heather Brennan of the American Institute of Aeronautics and Astronautics for carefully explaining the circumstances that do and do not require getting permission to reproduce figures. All figures, photos, and tables are referenced where they appear. I am also pleased to acknowledge written permission from the following 'special' sources of figures, tables, and photographs:

Springer Science and Business Media "kindly gave permission" to reproduce the photographs used in Figure 1-19, p. 16; Figure 4-23, p. 497; Figure 4-27, p. 501; Figure 5-7, p. 711; and Figure 5-8, p. 712.

McGraw-Hill for Table 2-2, p. 83; Figure 2-26, p. 84; Table 3-1, p. 284; Table 3-3, p. 296; and Table 3-4, p. 297 from *Theory of Elastic Stability*, 2nd edition, by Stephen P. Timoshenko and James M. Gere, copyright 1961 by the McGraw-Hill Book Company, Inc. As indicated below each table and figure, the material is reproduced with permission (of The McGraw-Hill Companies).

Alcoa for permission to use Figure 2-69, p. 200 from *Column Strength of Various Aluminum Alloys*, by R. L. Templin, R. G. Sturm, E. C. Hartmann, and M. Holt, Aluminum Research Laboratories Technical Paper No. 1, copyright 1938 by Aluminum Company of America, Pittsburgh.

Elsevier for Figure 3-41, p. 310; Figure 3-44, p. 314; Figure 3-137, p. 454; Figure 3-138, p. 456; Figure 4-121, p. 669; Figure 4-122, p. 670; Figure 4-123, p. 671; Figure 4-124, p. 672; and Figure 4-125, p. 673.

Taylor and Francis for Figure 3-62, p. 336 and Figure 3-70, p. 345. Both figures are copyrighted 1999 from *Mechanics of Composite Materials*, Second Edition, by Robert M. Jones. Also, for Figure C-18, p. 776; Figure C-20, p. 776; Figure C-21, p. 776; and Figure C-22, p. 776, all copyrighted 1969 from *Primer on Composite Materials: Analysis*, by J. E. Ashton, J. C. Halpin, and P. H. Petit. Reproduced by permission of Routledge/Taylor and Francis Group, LLC.

The American Society of Mechanical Engineers for Figure 3-69, p. 345; Figure 3-136, p. 452; Figure 4-22, p. 496; Figure 4-49, p. 537; Figure 4-50, p. 538; and Figure 4-120, p. 665.

I am unhappy that some greedy publishers would grant permission to use their copyrighted material only upon payment of an outrageous fee (sometimes in the neighborhood of $100 for a single figure!). Needless to say, I substituted alternative material to avoid any copyright violations. Still, I credited the original authors for the essence of their contributions. After all, they created the work, not the publishers!

Éléments sous droits d'auteur

About the Book...

Buckling of structural elements has intrigued structural mechanicists for nearly three centuries. First, Euler studied bar buckling in the mid-eighteenth century. Then, Bryan treated plate buckling in the late nineteenth century. Finally, shell buckling was a twentieth-century pursuit of Timoshenko, Donnell, Flugge, von Karman, Tsien, Batdorf, Hoff, Gerard, van der Neut, Thielemann, Koiter, Volmir, Feodosiev, Singer, Geier, Esslinger, Stein, Almroth, Tennyson, Alfutov, Bushnell, Arbocz, Starnes, and many others.

This graduate text and reference book is addressed to practically oriented structural mechanicists in civil, mechanical, aerospace, and ocean engineering as well as engineering mechanics. Fundamental buckling behavior is studied for three basic structural elements: one-dimensional bars, two-dimensional plates, and three-dimensional shells. The approach features a consistent energy-based formulation after Langhaar. Emphasized are the differences between the three principal sets of equations governing (1) *behavior prior to buckling* (equilibrium equations), (2) *the onset of buckling* (buckling equations), and (3) *behavior after buckling occurs* (large-deflection equilibrium equations). Euler bifurcation buckling loads are found for bars, plates, and shells as well as postbuckling behavior to determine the practical significance of the Euler load. Also treated are the contemporary buckling behavior topics of the effects of prebuckling deformations, initial imperfections, thermal expansion and constraint, eccentric stiffening, plastic deformation, and, causing renewed interest in buckling problems, laminated composite materials. The final topic in each of the chapters on bars, plates, and shells is an introduction to the essence of design for each structural element.

About the Author...

Robert M. Jones, Ph.D., is Professor Emeritus of Engineering Science and Mechanics at Virginia Polytechnic Institute and State University (Virginia Tech) in Blacksburg, Virginia. Since the 1960s, Dr. Jones has authored *Mechanics of Composite Materials* (1st edition, 1975, and 2nd edition, 1999), edited Valery V. Vasiliev's *Mechanics of Composite Structures*, collaborated on Irving H. Shames' *Engineering Mechanics*, and written thirty-five reports and papers on buckling. He is a Fellow and former Chairman of the Structures Technical Committee of the American Institute of Aeronautics and Astronautics; a Fellow of the American Society of Mechanical Engineers; a Founder Member, Fellow, and former President of the American Society for Composites; and a Founder Member of the American Academy of Mechanics.

For information and ordering, contact:

Bull Ridge Publishing
Box 10698
Blacksburg, VA 24062-0698
BullRidgePublishing.com

ISBN 0-9787223-0-2
9 780978 722302 90000

Éléments sous droits d'auteur